Abstracts / Extended Papers of Lectures

Unsupervised discovery of intraparticle communication in Al6061 alloy by Reflectance Microscopy

R. Li, T. Galochkina**, J-F. Lemineur*, F. Kanoufi*, V. Shkirskiy**

**Université Paris Cité, ITODYS, CNRS, 75013 Paris, France*

***Université Paris Cité, INSERM, BIGR, 75015 Paris, France*

viacheslav.shkirskiy@cnrs.fr

Recent developments in optical microscopies have pushed their application beyond microscale visual inspection to *operando* nanoscale quantification of corrosion events.[1–3] Employed in a reflection mode, also known as Reflectance Microscopy (RM), optical models provide means for the conversion of light intensity fluctuations into variations in roughness, thickness of surface films and even chemical composition. RM approach is a wide-field (mm×mm) technique, highly resolved in space (~200 nm) and time (~kHz) providing a wealth of unstructured but valuable corrosion information collected in a single experiment. The high dimensionality of optical datasets poses a daunting challenge on data extraction that cannot be addressed with conventional data treatment tools.[4] In this work, we developed machine vision procedures with the focus on unsupervised machine learning to automatize data extraction from optical movies of the degradation of Al6061 in acid environment as an example system. The interest of unsupervised algorithms is to speed up extraction of local corrosion events triggered by intermetallic particles while removing any human bias in pattern recognition that can obscure the discovery of novel corrosion mechanisms. In our case, analysis of over 2000 regions of interest revealed that certain areas of single intermetallic particles can communicate with each other, presumably through the exchange of produced OH^- ions. Finite element simulations were undertaken to describe the flow of fluxes over these particles and rationalize the experimental data.

1. Pfaff, S. *et al.* Operando Reflectance Microscopy on Polycrystalline Surfaces in Thermal Catalysis, Electrocatalysis, and Corrosion. *ACS Appl. Mater. Interfaces* **13**, 19530–19540 (2021).
2. Olgiati, M., Denissen, P. J. & Garcia, S. J. When all intermetallics dealloy in AA2024-T3: Quantifying early stage intermetallic corrosion kinetics under immersion. *Corros. Sci.* **192**, 109836 (2021).
3. Godeffroy, L., Derouich, S., Kanoufi, F. & Shkirskiy, V. Imaging and quantifying the chemical communication between single particles in metal alloy. *ChemRxiv* (2022) doi:10.26434/chemrxiv-2022-rn77b.
4. Godeffroy, L. *et al.* Bridging the Gap between Single Nanoparticle Imaging and Global Electrochemical Response by Correlative Microscopy Assisted By Machine Vision. *Small Methods* **6**, 2200659 (2022).

Azole free, biodegradable yellow metal Corrosion Inhibitor for Cooling water Systems

Michael Urschey, Philipp Schmidt, Rainer Haug

Kurita Europe GmbH, Mannheim, Germany

For many decades, azoles like Benzotriazole and Tolyltriazole have been the most widely used chemicals in water treatment to protect copper and copper-based alloys from corrosion. This chemistry´s striking feature is its extremely high efficiency at low inhibitor concentration. On the other hand, due to their extremely low biodegradability and high aquatic toxicity, azoles are persistent in the aquatic environment and cause increasing environmental concerns. Therefore, regulatory pressure to substitute these chemicals by more environmentally friendly compounds is increasing and azole use in open cooling systems has already been banned in specific locations in Europe. Further restrictions of triazole use in water systems are to be expected in the near to midterm.

In order to satisfy this need, Kurita has launched a development program to find adequate substitutes combining a high yellow metal corrosion inhibition efficiency with a better environmental profile. Efficient screening protocols utilizing very harsh corrosion conditions in highly saline water qualities were established. This enabled rapid yet systematic testing of a large pool of candidate chemistries including amino and carboxylic acids, amines, imidazole and other azole compounds, nitrogen containing heterocycles, azo compounds as well as metal based and inorganic inhibitors. In total, more than 50 individual compounds belonging to more than 12 chemical classes have been screened. Promising candidates have been further evaluated in circulation test devices for periods of 14 days while simulating water cycles (evaporation and makeup), heat load and use of non-oxidizing and oxidizing biocides.

These efforts resulted in the development of a new group of azole free corrosion inhibitors for copper and yellow metal alloys. The new products reach corrosion

inhibition levels comparable to those achieved with Benzotriazole / Tolyltriazole while being readily biodegradable. Microbiological control of the water circuit is possible using either type of biocide in line with current cooling water treatment practices. Bioaccumulation of the active compounds will not occur, leading to an environmentally sustainable treatment program. All relevant regulatory demands including REACH compliance are met.

While the main use case is for open cooling systems with direct or indirect discharge to surface water bodies, the new product group can also be applied in closed systems, geothermal wells etc. A combination with other Kurita technologies e. g. for scale control as well as online cleaning is possible. Currently, the product group is rolled out for industrial use.

Research and development work as well as the methods employed are presented and the ecological profile of the new product group is compared to that of traditional triazoles.

Eco-friendly (H-&S-free) and effectively performing inhibitors for multi-metal and temporary protection in waterborne systems

Dr. Jan Johan Zwinselman[1], Dr. Andreas Heyn[2]

([1]AloxX GmbH, Zürich, CH, [2]Otto-von-Guericke University Magdeburg, D)

Corrosion is one of the major problems when metal items get in contact with air and humidity and/or aqueous systems. Complex systems of corrosion inhibitors are often the only effective way to prohibit the corrosion process. However, “corrosion” is a very general word that implies many different complex processes that most of the times cannot be tackled by one single chemical. Effective passivators and/or corrosion inhibitors, however, do carry mostly minimum H- and/or S-phrases, in many cases even hazardous symbols. These chemicals are many times not only harmful for man but also harmful for the environment. For this reason, the industry is seeking for corrosion inhibitors that do not carry any harmful symbols nor any H- and/or/ S-phrases but are also show effective corrosion inhibiting properties for various metal surfaces. These preferred properties are mostly not in line with each other. A very good example is the copper passivator based on triazole. Copper can only be passivated effectively when the medium contains a triazole based chemical (BTA or TTA), but these chemicals are known as cancer initiator for man and extremely harmful for the environment. Since no other chemical is known to act as effective copper passivator, the triazole based chemical is still widely used in the industry.

In the presentation, we introduce an effectively performing alternative to the dangerous triazoles that provides multi-metal protection in neutral aqueous systems. This means that steel-based materials as well as copper, aluminum and zinc show high positive inhibitor protection values. This has been achieved thanks to statistically planned and optimally matched mixtures of metal gluconates and organic zinc salts, which were investigated using electrochemical methods and long-term immersion tests. The optimized compositions exhibit both anodic inhibition (film formation) and cathodic inhibition (suppression of oxygen reduction). In addition, an extremely effective and environmentally friendly formulation for temporary corrosion protection was found, which forms very thin barrier films after only short contact times with the metal and whose use is also likely to find application in coatings and emulsion films.

Electrochemistry in a microdroplet: investigation of ionic liquids as potential corrosion inhibitors

Samantha M. Gateman[1], Oumaïma Gharbi[2], Mireille Turmine[2], Vincent Vivier[2]

[1]The University of Western Ontario, London, Canada

[2]CNRS, Laboratoire de Réactivité de Surface, Sorbonne Université, Paris, France

Surface heterogeneities such as grain orientation, roughness or chemical composition are known to influence the electrochemical reactivity of metals and alloys. Conventionally, corrosion tests are made on mm to cm scale samples, often causing inappropriate approximations when corrosion mechanisms are investigated. Indeed, although useful, global electrochemical measurements do not depict the complexity of some alloy systems when localized corrosion mechanisms are involved.

Microelectrochemical analysis is a routine tool used to investigate corrosion initiation mechanisms of metals and alloys. It has been shown that electrochemical characterization can be realized to investigate the effect of surface composition on the corrosion reaction mechanisms.

In this work, the microdroplet techniques will be used to investigate the inhibition mechanism of several ionic liquids used as corrosion inhibitors for pure Al and Fe as well as Al alloy systems. Several electrochemical techniques such as potentiodynamic polarization curves or electrochemical impedance spectroscopy will be performed, coupled with wettability measurements using a setup recently devised by our group [1]. The surfaces will be subsequently analyzed by SEM, XPS and Raman spectroscopy to correlate passive film formation and corrosion products to the local reactivity.

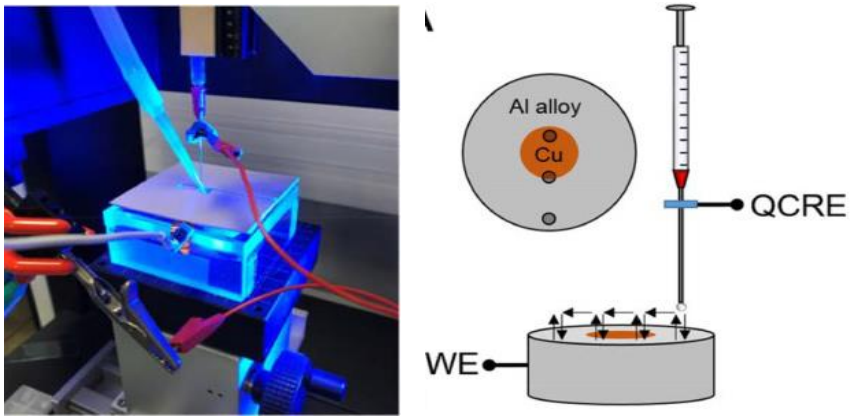

Figure 1: Schematic of the microelectrochemical set up coupled wettability measurement from [1]

[1] S.M Gateman, O. Gharbi, M. Turmine, V. Vivier, Electrochimica Acta, 399, 2021

Corrosion-inhibiting oil for potential application as float coat for temporary protection of mild steel

Ivan Stojanović[1], Vesna Alar[2], Marin Kurtela[3], Boris. A. Mikšić[4], Ivana Radić Boršić[5]

[1]Faculty of Mechanical Engineering and Naval Architecture, Zagreb, Croatia

[2]Faculty of Mechanical Engineering and Naval Architecture, Zagreb, Croatia

[3]Faculty of Mechanical Engineering and Naval Architecture, Zagreb, Croatia

[4]Cortec Corporation, FNACE, St. Paul, MN, USA

[5]Cortec Corporation Europe, Zagreb, Croatia

Abstract: Oil tanks are often made from mild steel, and as such, they are subject to corrosion damage that can cause leaks which pose a danger to public health and safety and to the environment. Critical parts of the above ground storage tank such as the bottom plate, the lower part of the shell and the roof are often protected with protective coatings, while the other surfaces in contact with oil are not permanently protected. Special attention should be addressed to such bare surfaces when mild steel is in direct contact with water such as during hydrostatic testing. One possible solution is application of a corrosion inhibiting oil which floats on the surface of the water and, in contact with tank walls, forms a protective layer.

Electrochemical testing of mild steel samples protected by corrosion-inhibiting oil in natural sea water at elevated temperature (30±2) °C was performed. The three test mixtures were pure sea water, sea water inhibited by oxygen scavenger, and sea water inhibited by oxygen scavenger and treated with biocide. The study included determination of corrosion potential, metal resistance and corrosion rate. The tested corrosion-inhibiting oil showed significant prevention of general corrosion of the mild steel samples.

Key words: corrosion-inhibiting oil, float coat, temporary protection, mild steel, sea water

Introduction

The cost of corrosion influences many industries and brings the need for development of corrosion resistant materials and improvement of corrosion protection measures in focus. It is estimated that the annual cost of corrosion reaches 3-4% of GDP in developed countries [1]. In the oil, gas and chemical industry alone, corrosion is one of the most challenging tasks and is estimated to cost 170 billion USD annually [2,3]. In addition to high costs of corrosion, it also concerns the health and environmental issues connected with the possible failure of oil and gas equipment, production line and storage tanks. Therefore, effective corrosion prevention has a high economic and ecological impact [4].

Storage tanks are an integral part of all industries. They serve to store various liquids including crude oil, oil derivatives, wastewater, chemicals, food products and many others. Tanks are most often made of non-alloyed carbon steel, and as such are subject to corrosion damage that can cause leaking and thereby endanger public health, the environment and safety.

There are basically eight types of tanks used to store liquids: tanks with a fixed roof, external floating roof tanks, internal floating roof tanks, external floating roof tanks with a dome, horizontal containers, pressure tanks, tanks with variable steam space, LNG (liquefied natural gas) tanks [5].

The above ground storage tank (AST) is placed on the ground, so it can have a larger volume to meet the needs of oil storage, while the construction technology is simpler and more practical, which can reduce the construction cost. In addition, increasingly strict environmental protection requirements require more attention to be paid to the safety of oil storage, and an above-ground oil storage tank makes it possible to avoid the stored oil leaking into the ground. Aboveground storage tanks in the petroleum industry come in a wide variety of sizes, ranging from sizes of 200 m^3 up to storage volumes more than 100,000 m^3 [6].

Corrosion is the primary reason of the deterioration of steel storage tanks and therefore, control and prevention of tank corrosion is of prime importance for efficient plant economics and safety [7]. If not repaired in a timely manner, corrosion damage will gradually reduce wall thickness, which can weaken or destroy tank components resulting in pits, reduced structural capacity, and tank failure.

The corrosion intensity is greatly influenced by several factors including environmental conditions, tank material and construction (joints, insulation, etc.), length of exposure of unprotected steel to moisture, chemical properties of the liquid, and undesirable temperature ranges.

Figure 1 shows damage to the ground plate of the product storage tank after 6 years in operation, due to microbiologically induced corrosion by sulphate-reducing bacteria (SRBs). The insulation in the tank pad below the tank was found to be contaminated with sulphate. In combination with the high groundwater level, this led to the growth of sulphate-reducing bacteria. The resultant sulphide attacked the steel. Remedy is to raise the pad so that the tank no longer stands in the groundwater and use sulphate-free insulation [8].

Figure 1. Microbiologically induced corrosion of product storage tank bottom plate after 6 years (CASE HISTORY 01.11.17.01) [8]

Figure 2 shows the damage to the tank floor in the zone of the welded joint which was exposed to contaminated water that settles out with solids on the bottom of the tank. The heat-affected zone dissolved electrolytically because this zone was less noble in relation to the rest of the plate. Attack by aggressive water in bottom sediment can be prevented by application of a coating to the bottom. In this case, no measures have been taken because the lowest bottom plate was still intact, so there was no danger of leakage [8].

Figure 2. Bottom plate weld corrosion of crude oil storage tank after 5 years (CASE HISTORY 01.11.02.05) [8]

The corrosion of the tanks could be external and internal. The occurrence of internal corrosion of a storage tank depends on the aggressiveness of the stored product and the material of which the tank is constructed. In some cases, it is necessary to use linings (coatings) that are more resistant to the corrosive properties of the stored fluid than are the tank construction materials. In some particularly corrosive services, it may be necessary to construct the tanks of a corrosion resistant material [9]. This paper deals with internal corrosion and corrosion prevention of crude oil tanks.

The internal corrosion could occur in permanent use due to accumulation of water at the bottom of storage tanks but also during hydrostatic testing with fresh water and in some cases with sea water. That is the reason why corrosion inhibitors are often used for corrosion mitigation of bare carbon steel tank surfaces. These treatment systems have proven to be effective for short-term exposure. However, for such applications, possible solution is corrosion-inhibiting oil as float coat which requires much less material vs treating a very large tank body with water, and possible use of seawater, which itself can be huge saving at places where there is no fresh water.

The float coat, being a hydrocarbon-based product, floats on the surface of the water, allowing for a unique application using a much smaller volume of product than typical chemical/inhibiting additives. The vessel floor and initial meter of wall height is sprayed with a layer of the float coat before any water is added to the system. Water is slowly added, until a point just below the initial spray treatment. The remainder of the float coat is applied to the top of the water layer. Hydrotesting is then carried out as normal

with care to fill the system at such a rate that the float coat layer on the water's surface is not disturbed. As the hydrotest proceeds, the walls of the vessel are coated with the float coat and further recoated as the vessel is drained [10].

Experimental study

In this paper, corrosion-inhibiting oil M645 for potential application as float coat for temporary protection of mild steel during hydrotesting with seawater was studied. In this study three types of corrosion protection of carbon steel in natural seawater at 30 °C were tested, that is:

1. Carbon steel protected with M-645.
2. Carbon steel protected with M-645 and addition of 100 ppm oxygen scavenger S7 in natural seawater.
3. Carbon steel protected with M-645 and addition of 100 ppm oxygen scavenger S7 and 1% biocide Izosan G (chlorine solution) in natural seawater.

The carbon steel samples DIN C10 (0.08 %C, 0.2 %Si, 0.41 %Mn, P < 0.045 %, S < 0.045 %) were prepared by sandpaper granulation 220-600, washed with water and degreased in ethanol. M-645 was applied on prepared samples by immersion, hold for two hours, drained, and then immersed in testing solution. S7 and biocide were dosed into testing solution before immersion of testing sample.

To evaluate corrosion inhibiting performance, electrochemical polarisation study of mild steel samples protected by corrosion-inhibiting oil in natural sea water at elevated temperature (30±2) °C was performed.

The study included determination of corrosion potential, metal resistance and corrosion rate. The testing was conducted in a standard three electrode test cell in relation to the reference saturated calomel electrode (SCE), using a Potentiostat/Galvanostat device, Model VersaSTAT 3 (Princeton applied research AMETEK). Polarization curves were registered after 1000 seconds of exposure to the testing solution to allow corrosion potential (E_{corr}) stabilization. Polarization resistance (R_p) was determined in a ± 20 mV potential range around the corrosion potential. During the potentiodynamic measurements, the working electrode was polarized to the potential of ± 250 mV relative to the corrosion potential and the current (I_{corr}) response was measured.

For interpretation of the obtained data, the ZSimpWin Version 3.2 software was used. Besides electrochemistry, gravimetric method for determination of weight loss was performed, whereas assessment of surface after corrosion testing was conducted using microscope.

Results

Testing electrochemical polarization results of blank sample – carbon steel in seawater are shown in Table 1 and Figures 3 and 4.

Table 1. Polarization test results of unprotected carbon steel after 24 hours in natural seawater

Electrolyte	Natural seawater
Temperature	(30±2) °C
Testing material	Carbon steel, DIN C10, **blank sample**
Corrosion potential, E_{corr} **vs. SCE**	-726.281 mV
Metal resistance, R_p	0.351 kΩ/cm^2
Corrosion current, I_{corr}	16.044 µA
Corrosion rate, v_{corr}	0.18678 mmpy
Tafel slope, $ß_a$	58.357 mV
Tafel slope, $ß_c$	224.697 mV

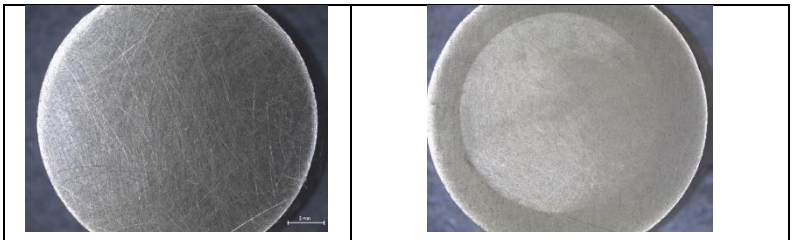

Before testing	After 24 h immersion in seawater

Figure 3. Carbon steel sample view before and after polarization testing in seawater

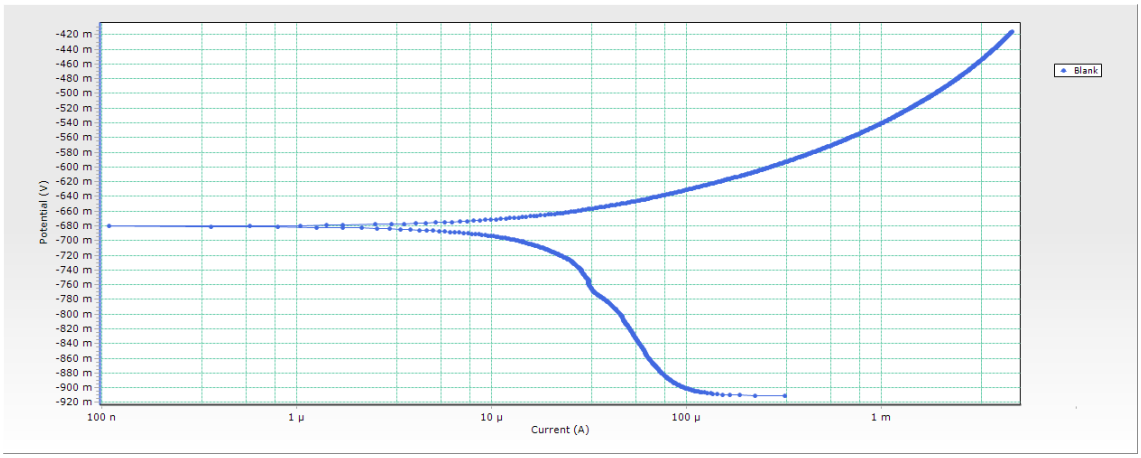

Figure 4. Tafel plot of blank sample after 24 h testing in seawater

Polarization test results and gravimetric test results of protected carbon steel tested in natural seawater after 1- and 3-days immersion are presented in Table 2.

Table 2. Polarization test results of carbon steel in natural seawater

Immersion time (days)		Δm [g]	Corrosion potential, E_{corr} vs. SCE (mV)	Corrosion current, I_{corr} (µA)	Corrosion rate, v_{corr} (mmpy)	ß$_A$ (mV)	ß$_K$ (mV)
M-645	1	0.0013	-328.789	0.45158	0.0052571	20.701	74.836
	3	0.0010	-501.465	0.578	0.0067255	28.302	94.172
M-645 + S7	1	0.0005	-368.661	0.138341	0.0016105	31.401	98.996
	3	0.0015	-218.988	0.567963	0.006612	58.516	228.675
M-645 + S7 + B	1	0.0019	-223.909	0.975162	0.011352	110.194	110.194
	3	0.0011	-142.312	0.35307	0.0041103	95.209	56.785

Overlapped Tafel diagrams after 1 and 3 days immersions in natural seawater are shown in Figures 5 and 6.

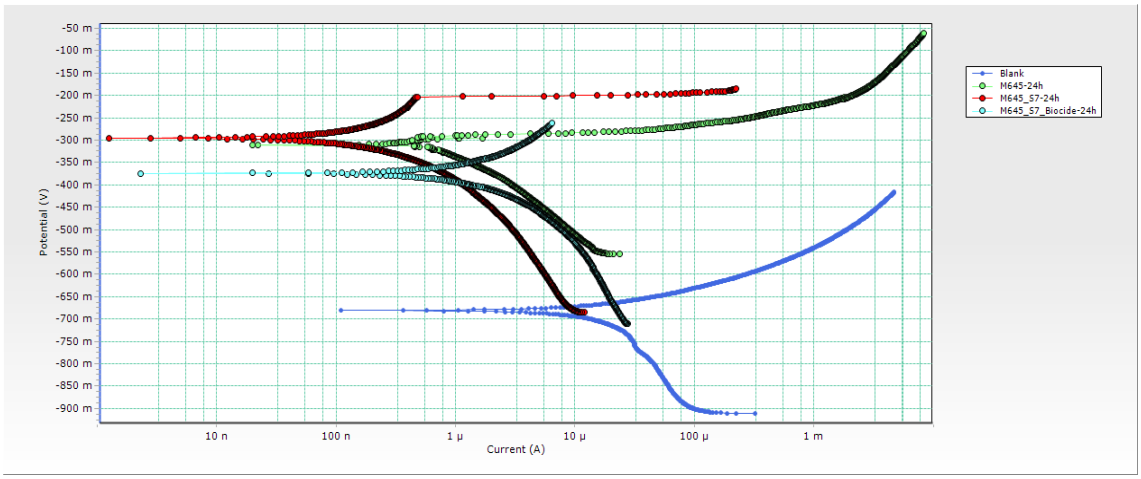

Figure 5. Tafel plots for all types of corrosion protection after 24 h in seawater

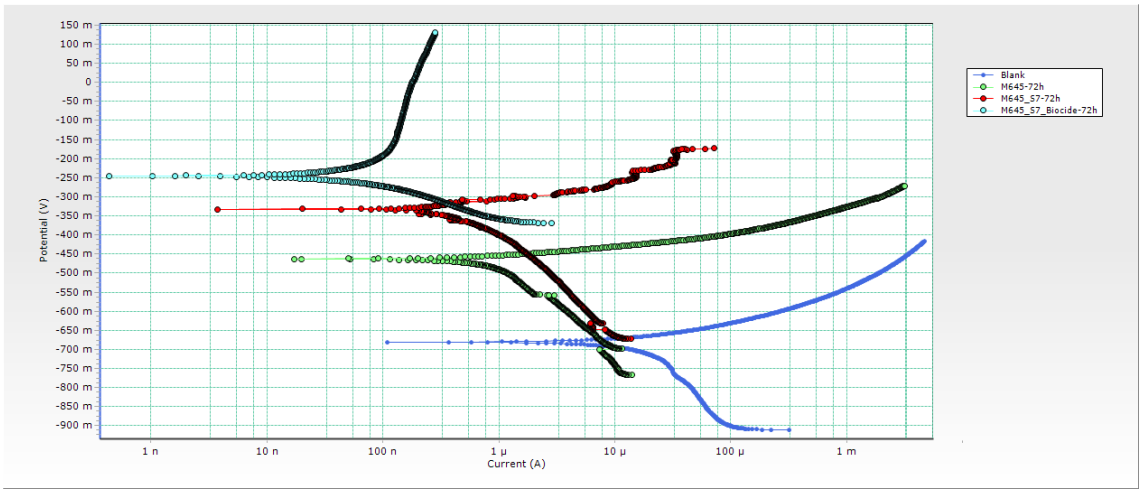

Figure 6. Tafel plots for all types of corrosion protection after 72 h in seawater

From the obtained research results the lowest corrosion rate of carbon steel after 72 hours in the natural seawater was achieved by third method of corrosion protection by application of M-645 on test coupons and adding the 100 ppm of S7 and 1% of chlorine-based biocide in solution (Figure 7).

It should be considered that this result refers to uniform or general corrosion, which represents a uniform loss of metal over the entire surface. Visual examination of samples showed localized pitting initiation on testing samples after polarization testing, possible due to local cracking of protective film in chlorine environment.

Before testing	After 72 hours of immersion in seawater
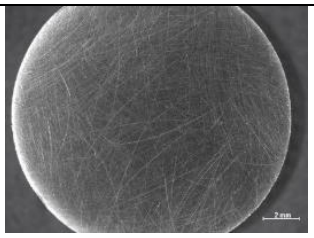	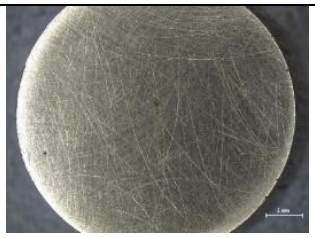
Grinding traces on the surface	Spot damage visible at intersection of the grinding traces

Figure 7. Sample view before and after 72 hours of immersion in sea water and Tafel extrapolation testing, sample protection by M-645 + S7 + BIOCIDE

Conclusion

Based on the conducted electrochemical testing at elevated temperature after 1 and 3 days in natural seawater on carbon steel samples protected by M-645 float coating, with and without addition of S7 and biocide, the following may be concluded:

1. All tested corrosion protection solutions showed lower general corrosion rate compared to unprotected carbon steel in natural seawater at elevated temperature.
2. All tested corrosion protection solutions shift corrosion potential to more positive values, meaning that they exhibit anodic inhibitor behaviour.
3. Additive S7 slows down the cathodic reaction of the redox process and directly affects the reduction of the corrosion rate. The corrosion rate values of mild steel treated with M645+S7 are slightly lower than the sample treated only with M645.
4. The lowest general corrosion rate after 3 days of testing in natural seawater was achieved by application of M645+S7+biocide.
5. Weight loss measurement showed the approximately same results provided by electrochemical polarisation testing.
6. The general corrosion is effectively suppressed but pitting prevention should be additionally addressed in a future study.

Reference

1. F. U. Renner , A. Stierle , H. Dosch , D. M. Kolb , T. L. Lee and J. Zegenhagen , *Nature*, 2006, 707 —710.
2. S. D. Cramer and B. S. Covino , *Corrosion: fundamentals, testing and protection* , ASM International Handbook, 2003, vol. 13A.
3. F. M. Song , D. W. Kirk , J. W. Graydon and D. E. Cormack , *Corrosion*, 2004, **60** , 736 —748.
4. D. Dwivedi, K. Lepková, T. Becker: Carbon steel corrosion: a review of key surface properties and characterization methods, RSC Advances, 2017, 7, 4580.
5. Stewart, Maurice. Surface Production Operations: Volume 5: Pressure Vessels, Heat Exchangers, and Aboveground Storage Tanks: Design, Construction, Inspection, and Testing. First Edition. Boston: Gulf Professional Publishing; 2021.
6. G.H. Stilt, *Petroleum Engineering Handbook,* Chapter 13, “Oil Storage” (Richardson, TX: SPE International), pp. 505-523
7. Mohamed Abdelgawad Gebril , Farag Shuaeib: Recent Advances in Protective Coating of Crude Oil Storage Tanks, The 6th Libyan Corrosion Conference, 2007, Pp 460-472.
8. During Evert D.D. Corrosion Atlas. 3rd Edition. Amsterdam: Elsevier Science; 2018.
9. API Recommended practice 575, "Inspection of Atmospheric and Low Pressure Storage Tanks, American Petroleum Institute, First Edition, 1995.
10. J. WuLterkens, C. Heurung, H. Sabry: Using a Float Coat for Preservation of Large-Volume Storage Systems, MATERIALS PERFORMANCE, 2017, 1-13.

Corrosion and inhibition of carbon steel XC38 in a standardized reconstituted geothermal water (SRGW) in the absence or presence of formulated biodegradable biosourced inhibitors

Chahinez HELALI[1,2], Romain VALENTIN[2], Stéphanie BETELU[1], Sophie THIEBAUD-ROUX[2] and Ioannis IGNATIADIS[1], [1]BRGM, ORLEANS/FRANCE; [2]INPT, TOULOUSE/FRANCE2

Several countries are moving towards the development of low-carbon energies. The geothermal energy is a good alternative to fossil fuels that will address this challenge. By 2030, the French Energy Transition Act provides growth of 33% in the heat of renewable origin consumed in France. The progressive use of geothermal energy requires maintenance that is well adapted to the operating system, but also to the circular economy, using bio-sourced, biodegradable and non-toxic corrosion inhibitors and as efficient as possible against corrosion. Organic surfactants are widely used in the corrosion inhibition of carbon steels, especially in the geothermal sector, where they are essentially petro-sourced. In the Paris Basin (France), corrosion and iron sulfide scale are encountered as a problematic of the geothermal energy, sanctioning it by economical prejudice and industrial and technological challenges. The vector of corrosion is the presence in the water of corrosive agents such as Cl-, HCO_3^-, SO_4^{2-}, HS^- and gases H_2S and CO_2. In these anoxic and acidic waters, H_2S/HS- content can attain several decades of mg/L depending on the well place and flowrate, but also on the microbiological activities.

The study consist of comparing the effectiveness of new bio-sourced surfactants (BSS) between more than 22 candidates, with those of petro-sourced ones in inhibiting carbon steel corrosion when immersed in a SRGW. The electrochemical behaviors of carbon steel immersed in the SRGW, in the absence and in the presence of BSS, permit the selection of 6 BSS for their biodegradability and their anti-corrosive action. One BSS among the previous 6 has engendered by synthesis an original BSS family, represented by 4 alkylated oxazoline congeners, that each one has been tested successfully. They also formulated with two BSS among the 5 and successfully tested. The formulations require only a single injection to achieve both a synergistic effect and an enhanced inhibition. Their anticorrosion action, which is similar to that of petro-sourced inhibitors at the same low concentration dosage, is discussed in terms of chain length, nature and action of BSSs present in formulations.

Next Generation Boiler Water Treatment in Food & Beverage Industry

Julia Jasper, Duygu Disci, Philipp Schmidt, Andre de Bache

An increasing awareness of protecting the environment can be observed in many industrial applications. In addition, higher regulations are required in the food and beverage industry where the steam has direct or indirect contact to food and therefore its purity must be ensured.

Therefore, this industry segment is especially challenging to keep the operational and functional and regulatory key performance indicators in the desired framework.

Kurita's next generation Cetamine® technology was especially designed to overcome those challenges in food and beverage industry. While the treated system is well protected against corrosion and scale formation, customers benefit from economical savings due to reduced carbon dioxide emission and less water and energy consumptions. Cetamine® FB products can be safely applied in boiler systems where the generated steam has either direct or indirect contact to food.

Electrochemical investigation on the corrosion inhibition of a silicate – alginate blend in a dynamic aqueous chlorine environment

Elias De Ketelaere[1], David Moed[2], Marjolein Vanoppen[3], Arne R.D. Verliefde[3], Kim Verbeken[1], Tom Depover[1]

[1]Ghent University, Department of Materials, Textiles and Chemical Engineering, Research Group Sustainable Materials Science, Zwijnaarde, Belgium, Elias.Deketelaere@UGent.be; Tom.Depover@UGent.be; Kim.Verbeken@UGent.be
[2]Evides Industriewater, Rotterdam, The Netherlands, D.Moed@Evides.nl
[3]Ghent University, Department of Green Chemistry and Technology, Research Group Particle and Interfacial Technology, Ghent, Belgium, Marjolein.Vanoppen@UGent.be; Arne.Verliefde@UGent.be

Abstract

An often used strategy to limit corrosion in industrial cooling water system is the addition of corrosion inhibitors to the cooling water stream. As some amount of the chemicals added for inhibition end up in the surface water, sustainable green corrosion inhibitors are investigated within cooling water applications. In this work, the corrosion inhibition behavior for a mixture of sodium silicate (SS) and -alginate (SA) is studied.

Different blends of SA and SS are evaluated on their inhibition efficiency for S235 carbon steel within a 3wt% NaCl environment under dynamic conditions. To assess the inhibition behavior of different SASS-blends, electrochemical impedance spectroscopy (EIS) as well as potentiodynamic scans (PDS) are executed in a rotating cylinder electrode (RCE) setup, which allows for a precise temperature and flow rate control. In different concentrations, EIS and PDS showed that a synergistic blend was achieved between SS and SA within a dynamic regime. More efficiently inhibiting SASS-blends were found within compositions containing more than 1mM SS. It is proposed that sufficient SS is necessary to ensure an insulating SS network near the steel surface. A more protective film was formed by incorporation of SA within the film structure. In conclusion, the combined inhibition of SA and SS is an ecological organic-inorganic blend that provides good protection against corrosion by improving the insulating behavior of the formed, protective SASS film.

Keywords

Carbon Steel; Green corrosion inhibitors; Cooling water; Electrochemical Impedance Spectroscopy; Potentiodynamic Polarization

Introduction

The consequences of material degradation are often a weak link in the reliability of industrial cooling water systems. An often used strategy to limit corrosion in these systems is the addition of corrosion inhibitors to the cooling water stream. In the past, chromate- and nitrate based inhibitors were a frequently made choice due to their good inhibition behaviour. Although due to their inherent toxicity, environmental restrictions were put on these products. [1,2] In the light of this finding, research towards the development of new green corrosion inhibitors received increased attention.

In previous works [3-6], sodium silicate (SS) was identified as a performant corrosion inhibitor, forming a silicate network structure on the metal surface. However, SS is also known to be less effective in water containing too much dissolved Mg and Ca or in low pH water. [4] Another group of eco-friendly inhibitors can be found within the organic inhibitors. Especially organic compounds containing electron-rich hetero-atoms (i.e. O, N, S and/or P) excel in limiting corrosion. Alginates are a lesser known bio-polymer that is known to show good corrosion inhibition behaviour [7,8] by adsorbing to the metal surface. Environmental factors were shown to have a major influence on this inhibition behaviour. [9]

In the search for new sustainable green corrosion inhibitors, this work aims to investigate a silicate-alginate inhibitor blend in a dynamic salt water environment. For this, electrochemical tests such as electrochemical impedance spectroscopy and potentiodynamic scans were performed on S235 steel in a dynamic 3wt.% NaCl environment with different proportions and concentrations of alginate and silicate added as corrosion inhibitor.

Materials

Dynamic electrochemical tests are performed on S235 carbon steel, for which the composition is given in Table 1. The steel samples are prepared to be ring-shaped and before each measurement these carbon steel samples are polished (until emery 2000 grade), cleaned with distilled water and dried.

Table 1: Composition of S235JR steel - Maximum concentrations given in wt.%

C	Mn	P	S	Si	Fe
0.22%	1.60%	0.05%	0.05%	0.05%	Balance.

After the sample preparation, the steel rings are attached to a rotating working electrode within a salt water environment. To simulate extreme water conditions, a 3 wt.% NaCl dynamic water environment containing the tested corrosion inhibitors is opted for. In order to simulate flowing water conditions, a rotating cylinder electrode setup was used in combination with a water-jacketed electrochemical cell attached to an external heating bath. In this configuration, electrochemical measurements can be done under precise temperature- and flow rate control (0.5m/s rotation speed at the sample surface).

Different quantities of sodium alginate (SA) and sodium silicate (SS) are combined to test both the individual inhibitors and different blends between SA and SS ('SASS'-blends). Concentrations of 1 g/L SA and 1 mM SS were considered in this work. To guarantee a reproduceable and homogeneous solution before each measurement, after adding the selected inhibitor, the solution is stirred for 1 hour.

Electrochemical tests are performed with a Gamry interface 1010 potentiostat attached to a typical three-electrode setup. Here, the steel ring represents the working electrode, platina is used as a counter electrode and Ag/AgCl is used a reference electrode. Electrochemical impedance spectroscopy (EIS) and potentiodynamic scans (PDS) are performed after a 12h open circuit potential (OCP) period to reach a stable OCP value. PDS scans are performed in a

-0.5V to 1.5V range w.r.t. the measured OCP at a speed of 1mV/s. [1,3,10] Tafel-extrapolation is done on the measured polarization curves to obtain the corrosion current density (J_{corr}) and the corrosion potential (E_{corr}) via the anodic- and cathodic Tafel lines. EIS scans are performed within potentiostatic regulations, starting at the measured OCP. The system is excited within the 10 kHz to 10mHz frequency range with 10 points per decade by applying a 10 mV_{rms} sinusoidal potential w.r.t. the measured OCP. The generated spectra are validated with Kramers-Kronig and fit via the Aftermath software.

Results and Discussion

Polarization curves for SA,SS and a 1-1 SASS blend are given in Figure 1, the corresponding corrosion current density (J_{corr}) and corrosion potential (E_{corr}) are given in Table 2. Additionally, the inhibition efficiency (IE) is calculated based on the measured J_{corr} as given in Equation 1:

$$IE\ (\%) = \frac{J_{corr,0} - J_{corr,i}}{J_{corr,0}} * 100\% \quad (1)$$

With $J_{corr,0}$ and $J_{corr,I}$ the corrosion current densities of the uninhibited and the sample inhibited by SA, SS or SASS respectively. A synergism parameter (S) is also calculated to evaluate in which degree the inhibitors act in a synergistic fashion, as given in following Equation 2:

$$S = \frac{1 - \theta_{1+2}}{1 - \theta'_{1+2}} \quad (2)$$

With $\theta_{1+2} = (\theta_1+\theta_2) - (\theta_1 \cdot \theta_2)$ and θ_1, θ_2 and θ'_{1+2} the surface coverage of SA, SS and the SASS blend, respectively, under the estimation that the surface coverage is related to the IE. [2,11] By this definition of S, an S>1 implies that the combination of compounds provides a better inhibition behaviour than the sum of the individual inhibitors' inhibition behaviour. Such blends are referred to as synergistic blends, blends for which S<1 are indicated as antagonistic blends.

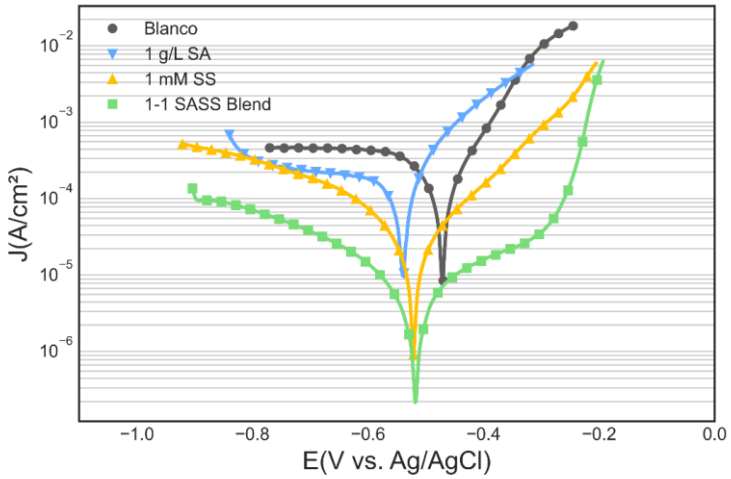

Figure 1: Comparison of polarization curves in dynamic salt water environment inhibited by SA, SS and SASS; T=25°C; rotation speed = 0.5m/s at sample surface

Table 2: Tafel Parameters corresponding with the polarization curves for S235 steel in a dynamic salt water environment inhibited by SA, SS and SASS; T=25°C; rotation speed = 0.5m/s at sample surface

SA (g/L)	SS (mM)	E_{corr}(mV vs. Ag/AgCl)	J_{corr} (mA/cm²)	IE (%)	S (-)
0	0	-430	0.258	-	-
0	1	-511	0.024	90.61%	-
1	0	-556	0.148	42.75%	-
1	1	-522	0.005	98.00%	2.68

From the polarization curves (Figure 1) it is observed that the measured current density is drastically decreased by blending the SA and SS. This can also be seen in Table 1, where a significant decrease in J_{corr} is achieved by adding SA and SS. Consequently, a higher IE (98%) is also calculated as compared with the moderate and good corrosion IE reported for SA (42.75%) and SS (90.61%), respectively. As a result of the fact that a large improvement in inhibition is achieved by the co-addition of SA and SS, the 1-1 SASS blend can also be seen as a very synergistic blend (S=2.68). When comparing the E_{corr}, SA,SS and SASS all three show a more cathodic potential than the uninhibited sample.

Concerning the EIS measurements, the spectra for SS, SA and a SASS blend are given in Figure 2. The spectra were fit with a Modified Randles circuit, as provided in this figure. The corresponding parameters are given in Table 3. Additionally, an IE is calculated as defined by the following Equation 3 :

$$IE\ (\%) = \frac{R_{p,i} - R_{p,0}}{R_{p,i}} * 100\% \qquad (3)$$

With the polarization resistance $R_{p,i}$ and $R_{p,0}$ the sum of the film resistance (R_f) and the charge transfer resistance (R_{ct}) of the inhibited and unprotected steel samples, respectively. On the other hand, in the Modified Randles circuit R_s respresents the solution resistance, and C_f and C_{dl} are the film- and double layer capacitance, respectively. The synergism parameter was also calculated according to Equation 2.

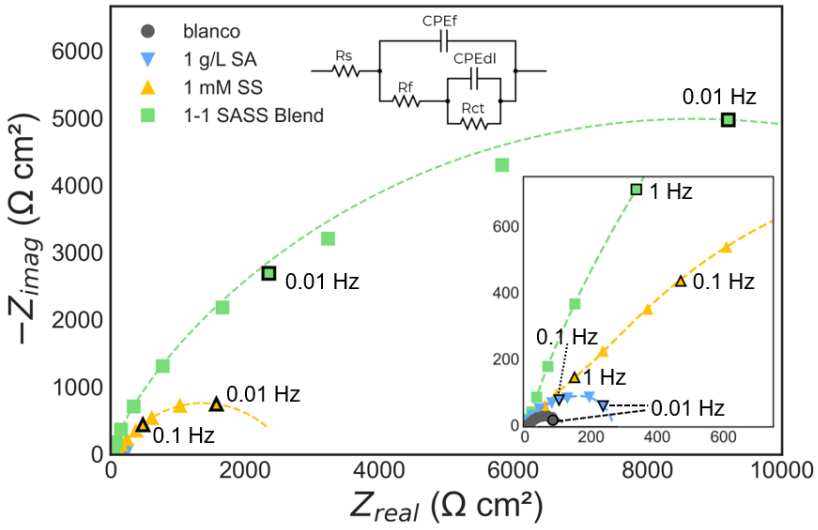

Figure 2: Comparison of the EIS spectra measured within a dynamic salt water environment inhibited by SA,SS and SASS; T=25°C; rotation speed = 0.5m/s at sample surface ; Modified Randles circuit selected as an equivalent circuit for fitting

Table 3:Fitting parameters corresponding with the measured EIS spectra for S235 steel in a dynamic salt water environment inhibited by SA, SS and SASS; T=25°C; rotation speed = 0.5m/s at sample surface

SA (g/L)	SS (mM)	R_s (Ω cm²)	R_f (Ω cm²)	R_{ct} (Ω cm²)	C_f (mF)	C_{dl} (mF)	R_p (Ω cm²)	IE (%)	S (-)
0	0	8	13	103	1.13	3.60	116	-	-
0	1	10	596	2054	0.96	1.72	2650	95.62%	-
1	0	8	125	77	6.09	1.09	201	42.37%	-
1	1	7	5760	10043	0.30	0.89	15803	99.27%	2.69

When looking at the Nyquist plots in Figure 2, it is observed that a the impedance magnitude increases when the SA and SS inhibitors are blended. Here, an integration of SA within the SS film produces a more resistive film as seen by the increase in R_f and R_{ct}, which is also reflected in the increase of IE and the spotted synergistic behaviour (S=2.69). This observation is in agreement with the decreased J_{corr} measured in the PDS curves (Figure 1). On the other hand, the addition of SA has a drastic impact on the film resistance, which takes a more prominent role in the measured polarization resistance. Moreover, the addition of SA to the structured SS film decreased both the capacitance at the film-solution interface and the metal-film interface, which might be the result of a better silica attachment at the base of the film and a more homogenous film surface.

Conclusion

In the present study, sodium silicate (SS) and sodium alginate (SA) were added and combined as corrosion inhibitors. EIS and PDS indicated that SA showed moderate inhibition (~42%), while SS showed good corrosion inhibition (~93%). The SASS blend showed synergistic characteristics with a very good inhibition efficiency (IE=98-99%). This beneficial behaviour was linked to the formation of a more resistive film by integration of SA within the SS network, which was also visible in the decreased interfacial capacitances.

References

1. B. Zhang, C. He, X. Chen, Z. Tian, and F. Li, "The synergistic effect of polyamidoamine dendrimers and sodium silicate on the corrosion of carbon steel in soft water," Corrosion Science, vol. 90, pp. 585–596, 1 2015.
2. M. Salasi, T. Shahrabi, E. Roayaei, and M. Aliofkhazraei, "The electrochemical behaviour of environment-friendly inhibitors of silicate and phosphonate in corrosion control of carbon steel in soft water media," Materials Chemistry and Physics, vol. 104, pp. 183–190, 7 2007.
3. E. De Ketelaere, D. Moed, M. Vanoppen, A. R.D. Verliefde, K. Verbeken, and T. Depover, "Sodium silicate corrosion inhibition behaviour for carbon steel in a dynamic salt water environment," Corrosion Science, vol. 217, p. 111119, 6 2023.
4. N. Asrar, A. U. Malik, and S. Ahmed, "Corrosion prevention with sodium silicate," Saline Water Conversion Corporation, Tech. Rep., 7 1998.
5. Jiann-Ruey Chen, Huei-Yun Chao, Yuh-Lin Lin, Iua-Jou Yang, Jung-Chou Oung, & Fu-Ming Pan, "Studies on carbon steel corrosion in molybdate and silicate solutions as corrosion inhibitors. ", Surface Science, 247(2), 352–359, 2 1991.
6. H. Gao, Q. Li, F. N. Chen, Y. Dai, F. Luo, and L. Q. Li, "Study of the corrosion inhibition effect of sodium silicate on az91d magnesium alloy," Corrosion Science, vol. 53, pp. 1401–1407, 4 2011.
7. I. B. Obot, I. B. Onyeachu, and A. Kumar, "Sodium alginate: A promising biopolymer for corrosion protection of api x60 high strength carbon steel in saline medium," Carbohydrate Polymers, vol. 178, pp. 200–208, 2017.
8. N. Dang, Y. H. Wei, L. F. Hou, Y. G. Li, and C. L. Guo, "Investigation of the inhibition effect of the environmentally friendly inhibitor sodium alginate on magnesium alloy in sodium chloride solution," Materials and Corrosion, vol. 66, pp. 1354–1362, 11 2015.
9. C. Wang, J. Chen, B. Hu, Z. Liu, C. Wang, J. Han, M. Su, Y. Li, and C. Li, "Modified chitosan-oligosaccharide and sodium silicate as efficient sustainable inhibitor for carbon steel against chloride-induced corrosion," Journal of Cleaner Production, vol. 238, p. 117823, 11 2019.

10. W. Zhang, H. J. Li, L. Chen, J. Sun, X. Ma, Y. Li, C. Liu, X. Han, B. Pang, and Y. C. Wu, “Performance and mechanism of a composite scaling–corrosion inhibitor used in seawater: 10-methylacridinium iodide and sodium citrate,” Desalination, vol. 486, p. 114482, 7 2020.
11. F. Ivusic, O. Lahodny-Sarc, H. O. Curkovic, and V. Alar, “Synergistic inhibition of carbon steel corrosion in seawater by cerium chloride and sodium gluconate,” Corrosion Science, vol. 98, pp. 88–97, 9 2015.

The impact of different parameters on silica redissolution in mixed aqueous/non-aqueous media (MEG and engine coolants) in the absence or presence of chemical additives.

Georgia Skordalou,[(a)] *Konstantinos D. Demadis,*[(a)] *Sander Clerick,*[(b)] *Guy Buytaert*[(b)]

[(a)] *Crystal Engineering, Growth and Design Laboratory, Department of Chemistry, University of Crete, Voutes Campus, Heraklion, Crete, GR-71003, Greece*

[(b)] *Arteco NV, Sint-Denijs-Westrem, Belgium*

Silicate polycondensation is an intensively-studied process in aqueous media. The silica chemistry and behavior in non-aqueous or mixed aqueous/non-aqueous media has recently been the focus of ongoing studies in our research group, within the scope of engine coolant technology.[1] Several experimental parameters have been found to influence the silicate polycondensation process in non-aqueous media, like monoethylene glycol (MEG). For example,the working pH as well as the % MEG in the MEG/water mixtures, plays a significant role in the polycondensation reaction. The silicate autocondensation reaction is faster in MEG compared to the pure aqueous system, exhibiting the highest polymerization degree at pH ~ 8. The enhancement of polymerization is even more profound in engine coolants, where other components are also present.

The presence of active silicate in an engine coolant is necessary for corrosion protection of engine components.[2] This can be achieved by dissolution of the polymerized silicate. Its dissolution, in the absence of any chemical additives, was observed when high temperatures were applied. The addition of water (dilution of the pure MEG or coolant) has an immediate impact on the dissolution effect, resulting in systematically higher active silicate levels as the % water is increased. Addition of certain chemical additives (silicate stabilizers) can increase the amount of active silicates recovered. Interestingly, in the presence of certain metal ions (even at low concentration) the influence of the chemical additives on silica dissolution is inhibited. More specifically, the amount of active silicates recovered due to dilution and heat

drastically drops in the presence of aluminum, even with a silicate stabilizer present. Therefore, taking advantage of the affinity of certain chemical additives for aluminum ions, a study was conducted in the absence and presence of silicate stabilizers in an attempt to sequesterand inactivate aluminum ions present in the solution.

References

1. Skordalou, G.; Clerick, S.; Buytaert, G.; Verlent, I.; Lievens, S.; Demadis, K. D.*ACS Omega***2022**,*submitted*.
2. Coelho, L.B.; Lukaczynska-Anderson, M.; Clerick, S.; Buytaert, G.; Lievens, S.; Terryn, H.A. *Corr. Sci.***2022**, *199*, 110188.

“Two birds with one stone”: Phosphonates as multifunctional inhibitors for scale and corrosion control under geothermal stresses

Stefania Liakaki-Stavropoulou,[#] Konstantinos D. Demadis,[#] Michaela Kamaratou,[#] Duygu Disci,[§] Argyro Spinthaki,[§] and Hermann Kempen.[§]*

[#] Crystal Engineering, Growth and Design Laboratory, Department of Chemistry, University of Crete, Voutes Campus, Heraklion, Crete, GR-71003, Greece

[§] Kurita Europe GmbH, Theodor-Heuss-Anlage 2, DE-68165, Mannheim, Germany

Scale and corrosion can be described as a two-prong problem in geothermal systems, as they cause problems that lead to reduced efficiency, increased energy consumption, and equipment failure. High temperatures, as well as geothermal fluid composition enhance the aggressiveness of scale formation and deposition, as well as corrosion initiation and corrosion product(s) build-up.

Among the various methods employed in order to delay (and ideally eliminate) these processes, one stands out, ie. the utilization of designed chemical additives that act as antiscalants and/or corrosion inhibitors. Therefore, an attractive and novel strategy is to discover efficient chemical additives that possess the highly desirable feature of controlling both scaling and corrosion issues.

Polyphosphonic acids and derivatives are organophosphorus additives with attractive attributes. They contain stable C-P bonds in their structure, which endow them with resistance to high thermal and hydrolytic stresses. Furthermore, they display several acidic phosphonate moieties (-PO_3H_2) that become deprotonated (singly or doubly, depending on solution pH), thus becoming anionic and being able to strongly complex metal ions present in the brine system. In addition, phosphonates demonstrate high affinity for the metal oxide layer on the metal surfaces in contact with the brine fluid.

Phosphonic acids have proven to be effective inhibitors against the formation and deposition of various scales, such as metal carbonates, sulfates and silicates. Moreover, they are efficient corrosion inhibitors for carbon steel, especially in brines

with high ion concentrations, since they can function synergistically with the metal ions present in the fluid.

In this article, comparative results from combined scale and corrosion experiments in the presence of phosphonates under several conditions, are presented. Their inhibitory performance was used to understand their optimum dual-function performance and to correlate structure with efficiency.

Factors that influence silica scale formation: Know thy “enemy”

Konstantinos D. Demadis

Crystal Engineering, Growth and Design Laboratory, Department of Chemistry, University of Crete, Voutes Campus, Heraklion, Crete, GR-71003, Greece

“Silica scale” is an expression that is often used to describe the formation, precipitation and deposition of miscellaneous forms of silicon dioxide (SiO_2, amorphous, colloidal, hydrous, metal cation-impregnated, ect.) in various water systems. Silica stands out from the commonly-observed mineral scales due to the unique way it forms. The mechanism of its formation can be described as an auto/poly-condensation process (in contrast to mineral scales that form by cation-anion association, nucleation and crystal growth processes). Silicate monomers react with each other at appropriate pH regions (usually 7.0-8.5) to initially form a di-silicic acid dimer, then a trimer, then oligomers and small silica “polymers”. The eventual formation of silica nanoparticles and colloids drive the entire process thermodynamically. When silica forms on a surface it creates silica deposits onto critical system equipment surfaces that create the same problems as mineral scale deposits.

In this presentation we present how several factors influence the chemistry of amorphous silica formation. These include: (a) pH, (b) temperature, (c) presence of certain metal ions (eg. Mg^{2+}, Al^{3+}, Fe^{2+}, Fe^{3+}), (d) supersaturation, etc. We also present mitigation strategies based on carefully-designed chemical additives and we attempt to delineate possible control mechanisms that could be applied in practical applications in the field.

Geothermal iron sulfide precipitates: Physicochemical characterization, and control strategies based on scale inhibition and dispersion

M. Kamaratou,[#] Konstantinos D. Demadis[#,*] Argyro Spinthaki,[§] Duygu Disci,[§] Hermann Kempen[§]

[#] Crystal Engineering, Growth and Design Laboratory, Department of Chemistry, University of Crete, Voutes Campus, Heraklion, Crete, GR-71003, Greece

[§] Kurita Europe GmbH, Theodor-Heuss-Anlage 2, DE-68165 Mannheim, Germany

Abstract

One of the significant problems in modern geothermal industry is the deposition of inorganic precipitates (crystalline or amorphous) on critical equipment parts that come in contact with hot geochemical fluids. The most common precipitates/deposits are metal sulfides, amorphous silica and metal silicates, depending on the brine chemistry. The case of metal sulfides is intriguing. Usually, deposits that contain Fe and S are referred to as "iron sulfide", revealing very little about its true identity.

This research is focused on efforts to reveal the true nature of the so-called "iron-sulfide". A series of iron sulfide synthesis experiments were carried out under various conditions that take into account iron and sulfide concentrations (at the supersaturation regime), solution pH and temperature. Complete physiochemical characterization of the formed precipitates reveals that they are solids that share several characteristics with amorphous Fe-oxide/hydroxide particles, most likely "doped" with S^{2-} anions. Another goal of this study was targeted towards the control of iron sulfide formation with the use of chemical additives as inhibitors and dispersants. Possible mechanisms and structure/function relationships will be discussed.

Keywords: sulfide, iron, iron sulfide, scale inhibitors, dispersants, geothermal systems

Corrosion inhibitor persistency in aqueous CO_2-containing environments

Ryan Abou-Shakra[1], Joshua Owen[1], Richard Woollam[1], William Durnie[2], Richard Barker[1]

[1]Institute of Functional Surfaces, School of Mechanical Engineering, University of Leeds, Leeds, LS2 9JT, United Kingdom

[2]bp Australia, 240 St Georges Terrace, Perth, Western Australia, Australia

Corrosion inhibitors are commonly employed to protect carbon steel infrastructure in aqueous carbon dioxide (CO_2)-saturated environments such as those encountered in oil and gas production and geothermal operation. However, unexpected events can occur that lead to periods where corrosion inhibitor addition ceases completely, or the quantity of inhibitor added falls short of the typical concentration required for the desired level of corrosion mitigation. In these instances, there is limited understanding on the persistency of the corrosion inhibitor and the subsequent effects on the corrosion rate of carbon steel. This study presents a combined numerical and experimental approach with the goal of developing an improved understanding of how short-term changes (order of hours to days) in corrosion inhibitor concentration influence uniform corrosion protection in corrosive CO_2-containing systems. Initially, a combination of first and mixed first/second order adsorption/desorption kinetic models are assessed in their ability to model the transient response between the uninhibited corrosion rate and the inhibited corrosion rate for benzyldimethyl-tetradecylammonium chloride in rotating cylinder electrode experiments, at concentrations spanning above and below the critical micelle concentration. The kinetic models are used to derive adsorption kinetic constants, as well as theoretical desorption kinetic constants to provide a theoretical understanding of inhibitor persistency, assuming complete reversibility of the adsorption process. Subsequently, a series of laboratory methodologies/experiments are trialled to ascertain the most suitable approach to represent such transitions in inhibitor concentration observed in a field scenario. A critical assessment of the methodologies employed and a comparison with the theoretical model are provided.

Investigation of black tea extract as corrosion inhibitor for mild steel under CO_2 condition

Ghada Shaban[1], Martin Andersson[2], Rajan Ambat[1]

[1] *Section of Material and Surface Engineering, Department of Civil and Mechanical Engineering, Technical University of Denmark, Produktionstorvet 425, Kongens Lyngby, 2800 Denmark*

[2]Department of Chemical Engineering, Technical University of Denmark, Produktionstorvet 229, Kongens Lyngby, 2800 Denmark

Abstract

Use of corrosion inhibitor is one of the possible ways of controlling CO2 corrosion in oil and gas and presently in connection with CO2 capture and storage application. Many commercial inhibitors used today have toxic constituents and overall composition is not environmental friendly. Hence, there is significant interest to explore green inhibitor chemistries that can provide comparable inhibitor efficiency similar to presently used molecules. In this study, the inhibition ability of black tea extract (BTE) on the corrosion behavior of 1Cr carbon steel was investigated in detail. An important step is the identification of the appropriate extraction method to produce the inhibition chemistry, which was explored and produced solid extract through molecular distillation process. Different filtering process was also investigated as a part of this and connection to inhibition efficiency. For corrosion investigation, tests were conducted at atmospheric pressure in a 1wt.% NaCl solution saturated with CO_2 at 40 and 60 ^oC with different inhibitor concentrations (from 50 to 4000 ppm). Linear Polarization Resistance (LPR) and electrochemical impedance spectroscopy(EIS) were used to study the electrochemical behavior. Scanning Electron Microscopy (SEM) and Energy Dispersive X-Ray Spectroscopy (EDS) were utilized to analyze the phase composition and morphology of the film formed. Results showed changing the morphology and properties of the formed corrosion layers as a result of materials protection from corrosion by BTE. Moreover, extract synthesis approach found to affect the inhibitor efficiency. Increase in temperature found to increase inhibitor efficiency.

Keywords

Inhibitor; Carbon steel; CO2 corrosion; Tea ; EIS; LPR; SEM

Industrial routes to low-aquatoxic and biodegradable corrosion inhibitors suitable for Oilfield use

Per-Erik Hellberg, Hans Oskarsson and Zahra Taleat,
Nouryon Performance Formulations, Stenungsund, Sweden

Ever increasing requirements from society and regulatory bodies call for the development of more environmentally acceptable oilfield chemicals, including corrosion inhibitors. Two current examples of such requirements are a) the globally spreading deployment of OSPAR or OSPAR-like regulations and b), the recently increasing regulatory pressure on certain types of imidazolines within the REACH area. As one way of offering the market “green” products, “natural extracts” originating e.g. from various parts of plants, like leaves, fruits, roots etc are regularly suggested to be utilized as corrosion inhibitors, e.g. for HCl. It may in theory look appealing to use substances which comes directly from nature, which seemingly should guarantee a use free of risk for man and environment. Although this approach certainly should not be disregarded, it is also linked to several issues when it comes to aspects connected to large-scale use of such extracts. This includes e.g. characterization, regulatory and scale-up challenges.

This paper will briefly discuss these challenges, but mainly address the approach from a global chemical vendor perspective to develop new substances by a structured and future-proof methodology. Specific examples will be given, including two low-aquatoxic and biodegradable corrosion inhibitors suitable for Oilfield use, their properties and performance. The inhibitors mentioned are primarily intended for fighting sweet (CO_2) and sour (H_2S) corrosion.

Corrosion Inhibition Batch Treatment for Water Supply Wells

S.A Mutairi, Research Center, Saudi Arabia, samotairi9@gmail.com

N.A Rasheedi, Research Center, Saudi Arabia, Rashna0c@gmail.com

W. A. Ghamdi, Research Center, Saudi Arabia, ghamwa0f@aramco.com

Keywords: Electrochemical, polarization, Batch, Squeezed, Wells.

Water supply wells' downhole corrosion inhibition program is considered to maintain the downhole components integrity and the fluid corrosively below 5 MPY. Batch treatment is currently used as a method to inject the oil field chemical. This work is a case study consists of analytical procedures used to optimize the frequency of the corrosion inhibition treatments of the wells. During the study a corrosion cell which fitted with special three-electrode configuration for electrochemical measurements, electrochemical linear polarization, corrosion monitoring, and microbial analysis were conducted. The study revealed that the current practice is not adequate to mitigate the material of the downhole system for more than three months.

Corrosion and surface deposition of sulphide scales on steel in H_2S – containing environments

Olawale Frank, Olujide Sanni, Richard Barker and Frederick Pessu

Institute of Functional Surfaces, School of Mechanical Engineering, University of Leeds, Leeds, LS2 9JT, United Kingdom.

Corrosion products can facilitate surface deposition of scale, by serving as the heterogeneous sites for scale nucleation or by contributing directly to heavy deposition as a major component. The challenges in managing both scaling and corrosion failures (especially localised corrosion) in oilfields and geothermal energy environments are enormous, and there is no evidence that this has been previously investigated, particularly in combined H_2S-containing environments, where pitting corrosion of carbon steel is considered to be a common occurrence. The deposition of sulphide scale poses a major challenge in oil and gas, and geothermal energy industries, where flow assurance issues can result in significant operating costs and production downtime. These two phenomena occur simultaneously at equipment surface, as interwoven processes, therefore the need for both processes to be investigated concomitantly, especially as FeS, ZnS, and PbS are often considered to be among the most challenging sulphide scales to inhibit.

Dissolved sulphide species and the kinetics of iron sulphide formation from corrosion in 10%H_2S – 90%CO_2 environments is expected to influence interactions with transition cations; Zn^{2+}/Pb^{2+}/Fe^{2+} in brine chemistries at temperatures up to 80°C. It is hypothesised that in a combined scale and corrosion environment, co-precipitation of Zn, Pb & Fe sulphides scale with and without corrosion induced-FeS could occur at the surface. This project will investigate the effect of the Zn^{2+}/Pb^{2+}/Fe^{2+} within the bulk chemistry and from corrosion, on the evolution and surface deposition of sulphide scales; ZnS, PbS and FeS at 30^{o}C & 80^{o}C. The effect of surface deposited sulphide scales and/or corrosion product on corrosion behaviour of interface will be investigated over 48hours. Composition and morphology of sulphide scales and corrosion product will be analysed using SEM- EDX and XRD, while the extent of pitting corrosion damage on the metal surface will be investigated using white light interferometer.

Corrosion inhibitory potential of selected flavonoid derivatives: Electrochemical, molecular···Zn surface interactions and quantum chemical approaches

T. Sithuba,[1] N.D. Masia,[2] J. Moema,[2] Lutendo C. Murulana[1], Gift Masuku[1], Indra Bahadur[3], Mwadham M Kabanda[1]

[1]University of Venda, South Africa.
[2]Mintek, South Africa
[3]North-West University, South Africa.

Zinc metal corrosion inhibitor potential of some flavonoid derivatives, namely, naringenin (NRNG), morin hydrate (MNHD) and 6-hydroxyflavone (6-HFN) were investigated by measuring their inhibitory activities, determining their thermodynamic and kinetic adsorption mechanistic properties as well as comparing their molecular···Zn metal surface interaction strengths. The inhibition efficiencies were evaluated in 1.5 M hydrochloric acid (HCl) environment using gravimetric and various electrochemical methods. The molecular···metal surface interactions were determined using the density function theory method by using the GGA/RPBE/DNP approach. Electrochemical studies show that 6-HFN and NRNG are the most and least effective corrosion inhibitors, respectively. Atomic absorption spectroscopy technique was used to compare the concentration of the zinc ions that remained in solution after gravimetric analysis, in the absence and presence of the inhibitors at 30 °C; it was found that the inhibited solution contained less concentrations of zinc ions as compared to the uninhibited solution. Surface morphology techniques (e.g., 3D microscope) suggest that localised type of corrosion took place on the metals and the corrosion damage was minimal in the presence of the inhibitors. FT-IR showed a strong adsorption of the functional groups found in the inhibitor compounds, with C=C functional group being strongly retained by all the three inhibitors. The flavonoid inhibitor compounds were found to absorb chemically at low temperature and physically at high temperatures. Langmuir adsorption isotherm was obeyed. The trend for molecular···metal surface interaction strengths follows the trend obtained from experimental findings on inhibition efficiency. Overall, the results suggest that all the molecules investigated are good

corrosion inhibitors with preference for those compounds in which there exist extended electron delocalization through the aromatic rings and in which there are minimal electron withdrawing groups on the aromatic rings.

Keywords: Chemical adsorption; molecular-surface interactions; surface morphology analysis; 6-Hydroxyflavone

The influence of Mo on the oxidation behavior of Cr-rich Cr-xMo-8Si (at.%) refractory metal alloys at 1200°C

Lisa Koliotassis, Emma M. H. White, Mathias C. Galetz

DECHEMA-Research Institute, Frankfurt am Main / Germany

Due to their high melting points and high strength, refractory metal alloys are potential materials for structural applications at service temperatures above 1100°C (current limit of state-of-the-art Ni-based superalloys). Among the refractory metals, chromium is a promising base material candidate due to its relatively low density and high availability. The challenges of structural bulk Cr, such as fast nitridation of pure Cr at high temperatures in air, can be addressed by alloying suitable elements.

An addition of 5-13 at.% Si results in a precipitation-hardenable Cr solid solution matrix (A2) with intermetallic Cr_3Si (A15) precipitates. This microstructure is beneficial for mechanical properties, as well as corrosion behavior, since the A15 phase shows high creep and oxidation/nitridation resistance, while the A2 phase offers some ductility and fracture toughness. Molybdenum, as a third alloying element, shows a refining effect on the microstructure and elevates the creep resistance of the A15 phase further, while leading to solid solution hardening and improving the nitridation resistance of the A2 phase.

This study investigates the influence of Mo content (10-40 at.%) in arc melted Cr-xMo-8Si (at.%) alloys on the oxidation behavior in air at 1200°C. The ‘as cast’ and post-annealed state microstructures are also analyzed and compared. The most promising composition range is then discussed with insights towards manufacturing larger specimens via powder metallurgy. The outlook for performing high temperature mechanical testing of the developed alloy and a potential application window is considered.

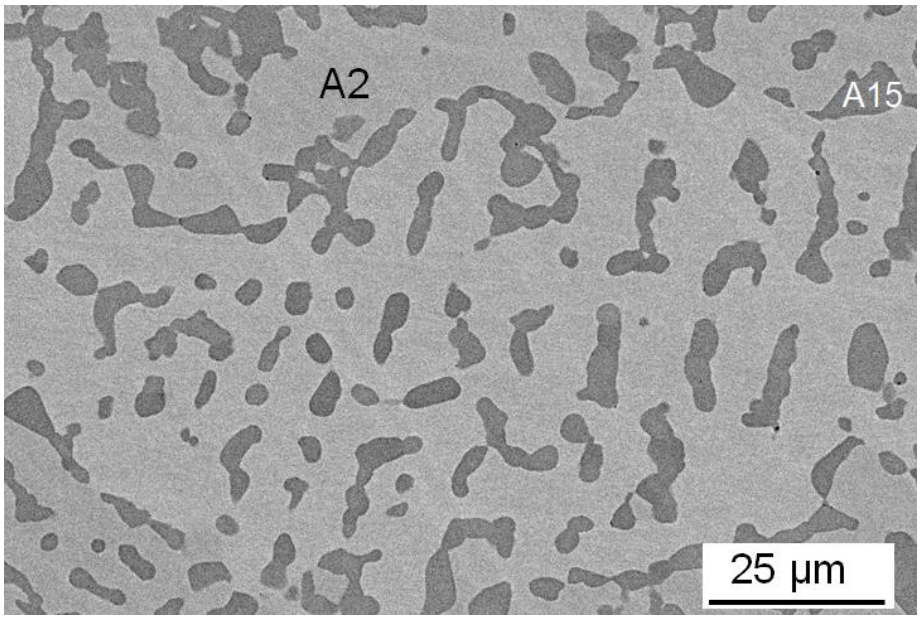

Figure 1. Two phase matrix of $(Cr,Mo,Si)_{ss}$ and intermetallic $(Cr,Mo)_3Si$

The effect of small halide additions on the high-temperature corrosivity and melting behavior of a synthetic deposit

Juho Lehmusto, Abo Akademi University, Turku/Finland
Jan-Erik Eriksson, Abo Akademi University, Turku/Finland
Meheretu Dirbeba, Abo Akademi University, Turku/Finland
Linus Silvander, Abo Akademi University, Turku/Finland
Daniel Lindberg, Aalto University, Espoo/Finland
Leena Hupa, Abo Akademi University, Turku/Finland

There is a great interest in using renewable biomasses and waste-derived materials as sustainable substitutes for fossil fuels. However, in firing these kinds of low-grade fuels with complex chemical compositions and the risk of high-temperature corrosion, the maximum steam temperatures in superheaters of CHP plants have to be kept significantly lower than in a coal-fired boiler. Regarding agricultural and forest biomass, potassium and chlorine have so far been identified as the main cause of high-temperature corrosion. More recently, new alternatives for renewable fuels have emerged to the side of nature-based fuels. These include, among others, solid recovered fuels (SRFs), brominated flame retardants (BFRs), and high-performance plastics known as fluoropolymers, which can be found in various commodities. Therefore, Br and F are found more often in modern-day feedstocks. However, their possible role in high-temperature corrosion has not been widely addressed.

In this study, three differently alloyed commercial steels; low-alloyed 10CrMo9-10, stainless AISI 347, and high-alloyed Sanicro 28, were studied. The samples were exposed in a tube furnace to a K_2SO_4+Na_2SO_4 mixture containing 0.85 mol% KCl, KBr, or KF at 500, 550, and 600 °C for 168 hours. After the experiments, the morphology, thickness, and composition of the formed oxide scale were characterized with SEM-EDS. Additionally, the melting behavior of the salt mixtures was studied with TG-DTA and modelled thermodynamically (Figure 1).

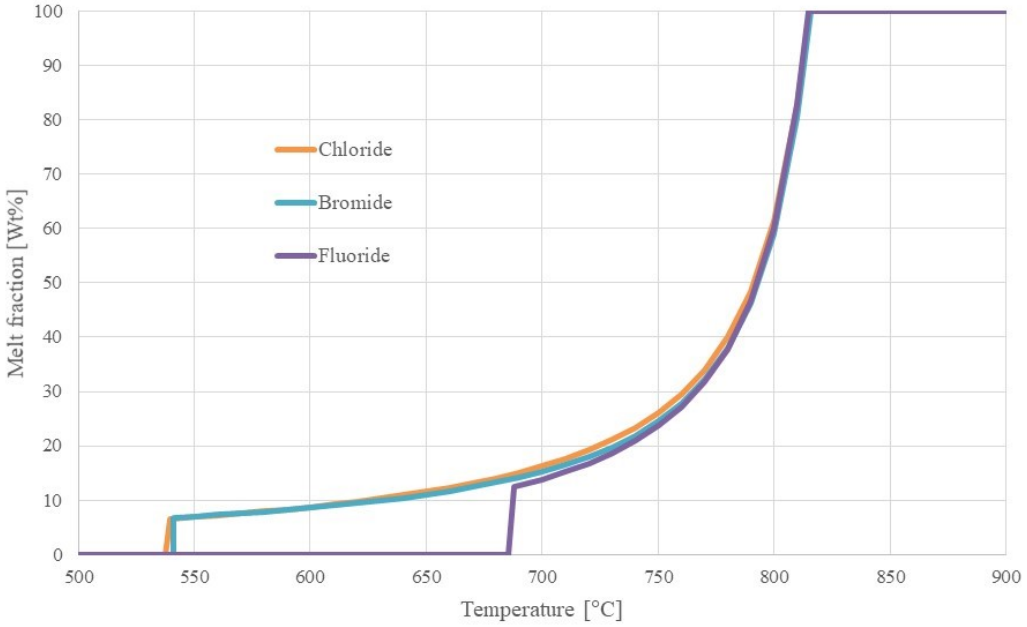

CALCULATED	MEASURED
K_2SO_4/Na_2SO_4: $T_0 = 834$ °C	K_2SO_4/Na_2SO_4: $T_0 = 838$ °C
$K_2SO_4/Na_2SO_4 + KCl$: $T_0 = 537$ °C	$K_2SO_4/Na_2SO_4 + KCl$: $T_0 = 524$ °C
$K_2SO_4/Na_2SO_4 + KBr$: $T_0 = 541$ °C	$K_2SO_4/Na_2SO_4 + KBr$: $T_0 = 549$ °C
$K_2SO_4/Na_2SO_4 + KF$: $T_0 = 686$ °C	$K_2SO_4/Na_2SO_4 + KF$: $T_0 = 698$ °C

Figure 1. The predicted melting behavior of the K_2SO_4+Na_2SO_4 mixture with an addition of either KCl, KBr, or KF as a function of temperature. Below the figure, the calculated and measured first melting temperature (T_0) are given.

Based on the measured mass losses of the studied alloys, the corrosivity of the salts increased in order K_2SO_4+Na_2SO_4+KF < K_2SO_4+Na_2SO_4+KBr < K_2SO_4+Na_2SO_4+KCl. Similarly, the corrosion resistance of the studied alloys grew in series 10CrMo9-10 < AISI 347 < Sanicro 28. The most notable outcome of the study was that already small amounts of corrosive impurities in an otherwise inert synthetic deposit altered significantly the corrosivity and melting behavior of the deposit. This can be significant in practical applications such as modern-day biomass- and waste-fired CHP boilers, whose feedstock contains growing amounts of side streams with a high chemical complexity.

HIGH TEMPERATURE CORROSION RESISTANCE OF HEAT RESISTANT STAINLESS STEELS IN SIMULATED WASTE INCINERATOR CONDITIONS

Novello F.[1], Masalskas M. B.[1], Cissé S.[2], Robin E.[2], Le Manchet S.[2]

[1] CRM Centre for Research in Metallurgy (frederic.novello@crmgroup.be, murilo.borges@crmgroup.be)

[2] Industeel ArcelorMittal, Le Creusot Materials Research Center (sarata.cisse@arcelormittal.com , emilie.robin@arcelormittal.com , sandra.le-manchet@arcelormittal.com)

Abstract

Due to increasingly stringent requirements in terms of energy recovery from waste incineration units, equipment is susceptible of new high temperature corrosion problematics.

A similar situation exists for new recycling processes and new energy storage units for which the hot corrosion mechanisms are directly linked with the chemical composition of the corrosive atmosphere that can differ considerably from one plant to another.

It is, thus, essential to precisely evaluate the corrosion rate under conditions close to each specific application.

Material selection in these stringent operating conditions is of first importance. In waste incineration units conditions, main heat resistant stainless steels are candidates, from austenitic stainless steels to Ni based alloys including Si enriched grades, Rare Earth Metals enriched grades, etc … In order to guide the selection of the most appropriate material, the present study is dedicated to assess the corrosion behavior of four stainless steels (UNS S31009, S30815, N08811, N08120) in simulated waste

incineration environments at four temperatures: 500, 600, 700 and 800°C during 1000h. Tests carried out and related procedures are developed in order to faithfully reproduce waste incinerator operating conditions.

The paper presents the testing equipment and the obtained results including visual examinations of the samples, metallographic and chemical evaluation of sub-surface and surface oxide layers, corrosion rates and their monitoring during the time.

Keywords: High temperature corrosion testing, Waste incinerator, Stainless Steels, Heat Resistant grades

Analysis of sulphur ingress along carbide phase boundaries under type II hot corrosion conditions

Andrew Potter, Cranfield University, Cranfield, UK
Nigel Simms, Cranfield University, Cranfield, UK
Kristopher Bramley, Cranfield University, Cranfield, UK
Stefano Mori, Cranfield University, Cranfield, UK
Joy Sumner, Cranfield University, Cranfield, UK

Abstract

Modern gas turbines require advanced materials, referred to as superalloys, that can withstand their high temperatures, pressures and mechanical loads. Precipitation hardening is one method by which the mechanical properties of the superalloys may be improved. This is achieved through the formation of refractory metal carbide phases within the superalloy matrix.

Refractory metal carbide phases at the surface of the alloy are known to rapidly oxidize in turbine operating atmospheres [1]. The remains of these carbide phases could possibly act as sites of nucleation for hot corrosion degradation, often associated with gas turbines [2]. It is therefore possible that the operational lifetime of certain turbine components may be limited by the presence of carbide phases. By improving understanding of this phenomena, industrial gas turbine materials selection can be better informed.

This research investigates hot corrosion degradation localized around the remains of refractory metal carbide precipitates on samples of PWA 1483 and MarM 509. To induce hot corrosion degradation, samples were corroded over time periods of 100, 200 and 500 hours in an atmosphere of 300 ppm SO_2 in air with an 80% Na_2SO_4, 20% K_2SO_4 depsoit at a flux of 1.5 µg/cm²/h applied cyclicly every 50 hours.

Changes in morphology were analysed using a scanning electron microscope outfitted with energy dispersive X-ray capabilities. A focused ion beam milling was used to

observe the ingress of deleterios species along the phase boundry between the superalloy matrix and carbide phases.

[1] A. Potter, J. Sumner, N. J. Simms, and J. E. Oakey, “Hot corrosion in the next generation of industrial gas turbines,” Conference. Eurocorr 2014, 2014.

[2] A. Potter, J. Sumner, and N. J. Simms, “The role of superalloy precipitates on the early stages of oxidation and type II hot corrosion,” Mater. High Temp., vol. 3409, pp. 1–7, 2018.

Influence of Protective Coatings on the Hot Corrosion Resistance of Mo-based Systems

Katharina Beck[1], Frauke Hinrichs[2], Martin Heilmaier[2], Till König[1], Ceyhun Oskay[1], Mathias Christian Galetz[1]

[1] DECHEMA-Forschungsinstitut, High Temperature Materials, Frankfurt am Main, Germany

[2] Karlsruher Institut für Technologie, Institut für Angewandte Materialien-Werkstoffkunde, Karlsruhe, Germany

Currently used high-temperature materials, e.g. Ni-base alloys reach their limit beyond 1150 °C and new material systems are needed. Due to their high melting point and their high mechanical strength at elevated temperatures, refractory metals and their alloys are possible candidates for applications such as internal combustion engines, where corrosion processes involving salts, such as sulphates and alkali metal salts occur and are known to cause hot corrosion. For Ni-based alloys, a distinction between Type I and Type II hot corrosion, depending on the temperature range and the occurring impairment, is well described. The behavior of refractory systems in hot corrosion conditions on the other hand is not well understood. One reason is, that the temperature range (700-950°C) relevant for hot corrosion itself poses a real challenge for such pesting-prone systems even without the deposits. To counteract these attack mechanisms, the formation of protective oxide scales is necessary. In this work Mo-Si-Ti alloys were exposed in a type II hot corrosion environment at 700 °C. Since α-Al_2O_3 and Cr_2O_3 scales are known to increase the resistance in oxidizing and hot corrosion environments, the effect of Al_2O_3- and Cr_2O_3-forming diffusion coatings was investigated additionally. Using an in situ chemical vapor deposition process (pack cementation), Al-coatings (up to 60 µm) and Cr-coatings (up to 20 µm) were successfully applied to recently developed Mo-Si-Ti alloys (eutectic Mo-20.0Si-52.8Ti and eutectoid Mo-21.0-34.0Ti).[1] The mechanism of hot corrosion for Mo-Si-Ti is discussed and compared to oxidation in air at 700°C. It is demonstrated, that the Al_2O_3 and Cr_2O_3 forming coatings resulted in a substantially decreased degradation in comparison to the uncoated substrates.

[1] Schliephake, Daniel, et al. "Constitution, oxidation and creep of eutectic and eutectoid Mo-Si-Ti alloys." Intermetallics 104 (2019): 133-142.

High Temperature Corrosion Resistance of INCONEL alloy 740H in high efficiency and green energy technologies

Stephen McCoy, Special Metals Corporation, Hereford, UK

John deBarbadillo, Special Metals Corporation, Huntington, WV, USA

Brian Baker, Special Metals Corporation, Huntington, WV, USA

Abstract

Nickel superalloys are of increasing interest in new and emerging energy production applications for their high temperature mechanical and creep strength, stability, durability and corrosion resistance. The precipitation hardenable Ni-Co-Cr superalloy 740H(R) has been developed for high pressure- high temperature environments and is an ASME code approved material up to 800ºC. New applications for the material in emerging green energy technologies include concentrated solar power receiver tubes due its very high creep and fatigue resistance in the temperature range from 600ºC to 760ºC. The solar receiver tubes contain a heat transfer medium of molten salts used to transfer and store the solar energy. Solar receiver technology is also being combined with new supercritical carbon dioxide power cycles which have the potential advantages of high efficiency and reduced demand for water in desert environments. The paper includes molten salt corrosion testing of alloy 625, N06230 and 740H in Nitrate salts at 600C for exposure periods up to 400hours and also candidate chloride salts with protective additives, where temperatures of 700C are required for higher efficiency.

The alloy 740H is also fabricable and is available in a wide range of product forms including heavy wall seamless and seam -welded pipes and thin-walled welded receiver tubes designed for strength and heat transfer. The properties of the materials in the various product forms and fabrications schedules are shown to comply with the pressure code requirements. New data has also been generated to demonstrate the performance of solution annealed and age hardened welds in high temperature applications within the creep range.

In power applications using a sCO2 power cycle high efficiency compact heat exchangers and recuperators operate at temperatures up to 800C and require a material with high strength, fatigue resistance and corrosion resistance in the hot gas.

Studies on corrosion resistance have shown negligible corrosion loss of the Nickel base superalloys compared with stainless steels at temperatures up to 800C.

$CaCl_2$-induced corrosion during the combustion of carbon-neutral fuels

Hanna Kinnunen, Valmet Technologies Oy, Finland; Jaakko Tamminen, Valmet Technologies Oy, Finland

Energy production is experiencing a transition in a pathway to decarbonisation by moving from fossil fuels to carbon-neutral alternatives. With circular economy principles, only the non-recyclable rest fractions shall be utilised in combustion. One example is the pulp and paper mill rejects and sludges. They are known to increase the probability of ash-related problems, but it is an attractive way to reduce and utilise potential mill side streams.

Sludges typically have high ash content and calcium concentration. Calcium is known to capture sulphur during combustion, thus promoting the formation of alkali chlorides instead of non-corrosive alkali sulphate. However, if there is a surplus of calcium compared to sulphur, $CaCl_2$ formation is known to happen at least in the cooler flue gas temperatures from CaO or $CaCO_3$ in the presence of HCl. Alkali chloride corrosion is well-known and studied phenomenon in power boilers. Lately, $CaCl_2$ has been shown to be corrosive in the cold end of the boiler, e.g. in the air preheater area, but the effect on the hot side is not widely published [1]. These investigations aimed to study the formation and corrosivity of $CaCl_2$ during the combustion of sludge and rejects.

Experimental

Superheater and deposit samples were taken from a CFB (circulating fluidised bed) boiler combusting paper processing rejects and sludge for detailed SEM-EDS (scanning electron microscope and energy dispersive X-ray spectroscopy) analyses. The purpose was to find a reason for the corrosion of the superheaters. The analyses showed the presence of $CaCl_2$ and calcium chromate ($CaCrO_4$) in the tertiary superheater deposits, Figure 1. Typically, corrosion of austenitic stainless steel in high-temperature superheaters is caused by alkali chlorides via alkali chromate formation (K_2CrO_4 or Na_2CrO_4).

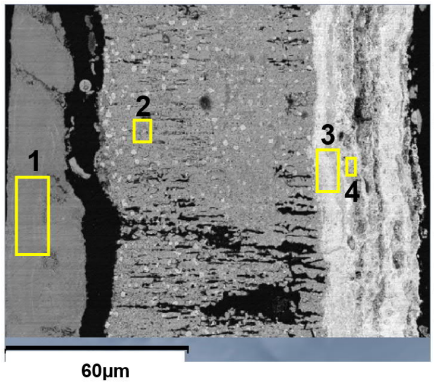

Analysis point	O	Na	Cl	K	Ca	Al	Si	Cr	Fe	Ni	Possible compounds
	atomic-%										
1	68.2		1.6		25.5	2.0	2.8				$CaO/CaCO_3$, $CaCl_2$, aluminium silicate
2		41.2	53.8	2.9	2.1						NaCl, KCl, $CaCl_2$
3	60.8				7.3			6.4	22.9	2.6	$CaCrO_4$, Fe-Ni-oxide
4	63.4				17.8			17.9	0.8		$CaCrO_4$

Figure 1. *Deposit composition taken from the tertiary superheater. The analysis is made with SEM-EDS, and possible compounds are evaluated based on the atomic-% compositions.*

Karlsson et al. studied the corrosivity of $CaCl_2$ in the laboratory test set-up and noticed the $CaCrO_4$ formation [2]. $CaCl_2$ was found to be less corrosive than alkali chlorides (KCl or NaCl) due to the rapid oxidation of $CaCl_2$ to CaO. However, the findings from the boiler showed the importance of understanding calcium behaviour and the formation of $CaCl_2$ during combustion. It might have a more significant role in corrosion not only at the cold end of the boiler but also in the superheater area. During suitable conditions, the formation of NaCl-$CaCl_2$ melt could be possible according to the phase diagram [3]. The results of the investigations handled in this work give more information about the corrosivity and relevance of $CaCl_2$ during the combustion of carbon-neutral fuels.

References

1. E. Vainio, N. DeMartini, L. Hupa, L-E. Åmand, T. Richards, M. Hupa. *Hygroscopic Properties of Calcium Chloride and Its Role on Cold-End Corrosion in Biomass Combustion*, Energy Fuels 33 (11913–11922), 2019. https://doi.org/10.1021/acs.energyfuels.9b02731

2. S. Karlsson, J. Liske, L-G Johansson, J-E Svensson. *Alkali Induced High-Temperature Corrosion of Stainless Steel: The Influence of NaCl, KCl and CaCl2*, Oxidation of Metals 78 (83-102), 2012. http://dx.doi.org/10.1007/s11085-012-9293-7

3. Phase diagram for binary NaCl-$CaCl_2$ solution. http://www.factsage.cn/fact/documentation/ftsalt/CaCl2-NaCl.jpg accessed 16th of Jan, 2023.

Understanding the molten salt corrosion mechanisms using EIS equivalent circuits based on distribution relaxation times methodology

Angel G. Fernández, University of the Basque Country, San Sebastián/Spain

Mikel Alberro, University of the Basque Country, San Sebastián/Spain

Jalel Labidi, University of the Basque Country, San Sebastián/Spain

Abstract

Thermal energy storage (TES) has become as one of the main important development for the energy industry, since it has the potential to overcome the existing mismatch between energy production and demand for discontinuous energy sources, especially for solar thermal at high temperature.

Molten salt technology using nitrate salts in tubular external receivers is the current state-of-the-art in concentrated solar power (CSP) technology [1] but new molten salts chemistry, using carbonates and chloride salts, have been proposed in order to increase the TES temperature and improve the turbine block efficiency [2]. The selection of a high-temperature molten-salt chemistry is needed, as well as the need to understand its impact on containment materials, to achieve acceptable strength, durability, and cost targets at these high temperatures. In this direction, the corrosion mechanisms for the main storage media proposed in CSP plants working at temperatures from 300-720°C have been studied in this work, through electrochemical impedance spectroscopy tests (EIS).

Different authors [3,4] proposed equivalent circuits that match to the main corrosion processes obtained in a molten salt environment at high temperature, obtaining different case scenarios, a localize corrosion model, porous layer or protective layer model. These models are common for molten salt corrosion at high temperature and in our opinion, these models must be optimized depending the molten salt chemistry involved during the corrosion process.

The aim of this work is the development of specific equivalent circuits model (ECM) that can be proposed for a better understanding of nitrate, carbonate and chloride molten salt corrosion, taking into account the number of polarization processes

involved in the distributed relaxation times (DRT) methodology applied. The corrosion tests were carried out in an electrochemical cell, especially designed for corrosion monitorization analysis, which can work at static/dynamic conditions or at inert atmosphere, to avoid the oxygen content, especially in chloride molten salt tests.

It was found a better match between the EIS results and the ECM proposed according the DRT methodology, so new equivalent circuits were proposed for each molten salt chemistry to identify the protective/non-protective superficial behaviour of the layers formed in the different materials and temperature tested (Table 1).

Table1. Testing conditions of the electrochemical tests to define the equivalent circuit models.

Material	**Molten salt**	**Temperature (ºC)**	**Type of immersion conditions**	**Exposure Time (h)**
A516	60%$NaNO_3$+40%KNO_3	390	Dynamic	150
304	60%$NaNO_3$+40%KNO_3	390	Dynamic	150
HR233	32%K_2CO_3+35% Li_2CO_3+ 33%Na_2CO_3	650	Static	500
HR233	20.4%KCl+55.1%$MgCl_2$+24.5%NaCl	720	Static-Inert atmosphere	150
HR242	32%K_2CO_3+35% Li_2CO_3+ 33%Na_2CO_3	650	Static	500
HR242	20.4%KCl+55.1%$MgCl_2$+24.5%NaCl	720	Static-Inert atmosphere	150

References:

1. A.G. Fernandez, J. Gomez-vidal, E. Oro, A. Kruizenga, A. Sole, L. F. Cabeza. Mainstreaming commercial CSP systems: A technology review. Renewable Energy, 2019, 140, pp: 152-176
2. M. Mehos, C. Turchi, J. Vidal, M. Wagner, Z. Ma, C. Ho, W. Kolb, C. Andraka, and A. Kruizenga, *Concentrating Solar Power Gen3 Demonstration Roadmap.* Technical Report, NREL/TP-5500-67464, 2017.
3. Zeng, C.L., W. Wang, and W.T. Wu, Electrochemical impedance models for molten salt corrosion. Corrosion Science, 2001, 43: p. 787-801.
4. A. Anderko, N. Sridhar, L.T. Yang, S.L. Grise, B.J. Saldanha, M.H. Dorsey, Validation of localized corrosion model using real time corrosion monitoring in a chemical plant. Corrosion Engineering, Science and Technology 40, 2005, 33-42.

Acknowledgements

Dr. Angel G. Fernández wants to acknowledgement the financial support from RyC 2020-28787-I funded by MCIN/AEI /10.13039/501100011033 and ESF “Investing in your future”.

Effect of composition on processability, microstructure, and early-stage oxidation of Co-Cr-Cu-Fe-Mn-Ni complex concentrated alloys

Jonathan Apell[1,2], *Robert Wonneberger*[2], *Stephanie Lippmann*[1], *Andreas Undisz*[2]

[1] *Friedrich Schiller University Jena, Jena, Germany*

[2] *Chemnitz University of Technology, Chemnitz, Germany*

Complex concentrated alloys (CCAs) are a focal point of research towards novel materials with improved mechanical and functional properties. Recently, Cu has been shown to enhance mechanical properties and wear resistance of Co-Cr-Fe-Mn-Ni CCAs, aiming for high-temperature applications. The variety of microstructures reported for Co-Cr-Cu-Fe-Mn-Ni CCAs is expected to strongly affect oxidation behavior. However, details of the impact of composition and processing on microstructure and oxidation behavior in this system remain to be assessed.

In this systematic study, melting, processing and oxidation behavior are presented for equiatomic CoCrCuFeMnNi and its six sub-alloys, obtained by omitting one element each. Microstructure and oxidation for 1 h at 800 °C in air were investigated using scanning and transmission electron microscopy and X-ray diffraction.

The Co-free and Ni-free CCAs displayed an inhomogeneous microstructure caused by liquid phase separation and were unsuitable for further processing. The other investigated alloys were successfully processed into sheets by annealing and cold rolling. CoCrCuFeMnNi, the Cr-free and Fe-free CCAs, all containing Mn and Cu, had a two-phase microstructure with a Cu/Mn-rich interdendritic phase. This phase was susceptible to preferential oxidation, forming porous, Mn-rich oxides that spalled off. The Mn-free CCA exhibited a two-phase microstructure, containing a Cu-rich and a Cu-lean phase. Whereas the Cu-lean phase formed a thin protective oxide, the Cu-rich phase was preferentially oxidized, forming thick oxides. The Cu-free (‘Cantor’) alloy was single-phase FCC and formed a multi-layered oxide, consisting of outer Mn_3O_4, intermediate Cr_2O_3 and inner $MnCr_2O_4$. Despite the formation of a thin Cr_2O_3 layer, outward diffusion and depletion of Mn in the alloy was observed. It is concluded that the Cu-rich phase is decisive for high-temperature application of Co-Cr-Cu-Fe-Mn-Ni CCAs and should be avoided. Further research should address the according limits of Cu and Mn contents to avoid formation of the Cu-rich phase.

Laboratory-scale method for high-temperature deposit and corrosion studies – first results with $PbCl_2$

Jonne Niemi, Juho Lehmusto, Leena Hupa

Johan Gadolin Process Chemistry Centre, Åbo Akademi University, Turku, Finland

High-temperature corrosion is one of the key challenges limiting the efficiency and availability of waste-firing boilers. The corrosion issues in boilers are often connected to the ash composition of the fuel. Waste fractions, such as recovered waste wood, often include elevated amounts of heavy metals and chlorine that cause severe corrosion to the heat exchangers. High-temperature corrosion relating to ash deposit-induced corrosion has been studied extensively. However, most of the detailed laboratory studies have been conducted in isothermal conditions with a pre-applied deposit on the steel sample. This study aims to develop and test a novel experimental set-up considering the temperature gradient effects on high-temperature corrosion. While experimental set-ups that consider the temperature gradient have been utilized before, they have mainly utilized pre-applied deposits. In this work, the studied material is deposited on top of the steel surface during the experiment via nucleation. Additionally, the study aims to shed light on corrosion issues related to $PbCl_2$ and alkali salt-containing environments, e.g., heat exchanger corrosion of certain waste-fired boilers.

The experimental set-up (see Fig. 1) consists of an air-cooled probe equipped with a detachable steel sample piece at the end. The sample is situated so that the tested surface is vertical. The probe is inserted into a hot furnace, resulting in a temperature difference between the surrounding atmosphere (~650 °C) and the cooled steel sample (350–400 °C). The temperature profile mimics the boiler heat exchanger application. Deposit-forming compounds are volatilized in the same furnace and then condense onto the steel surface from the surrounding furnace gases/atmosphere. After exposure, the steel sample and the deposited material are analyzed with SEM/EDX.

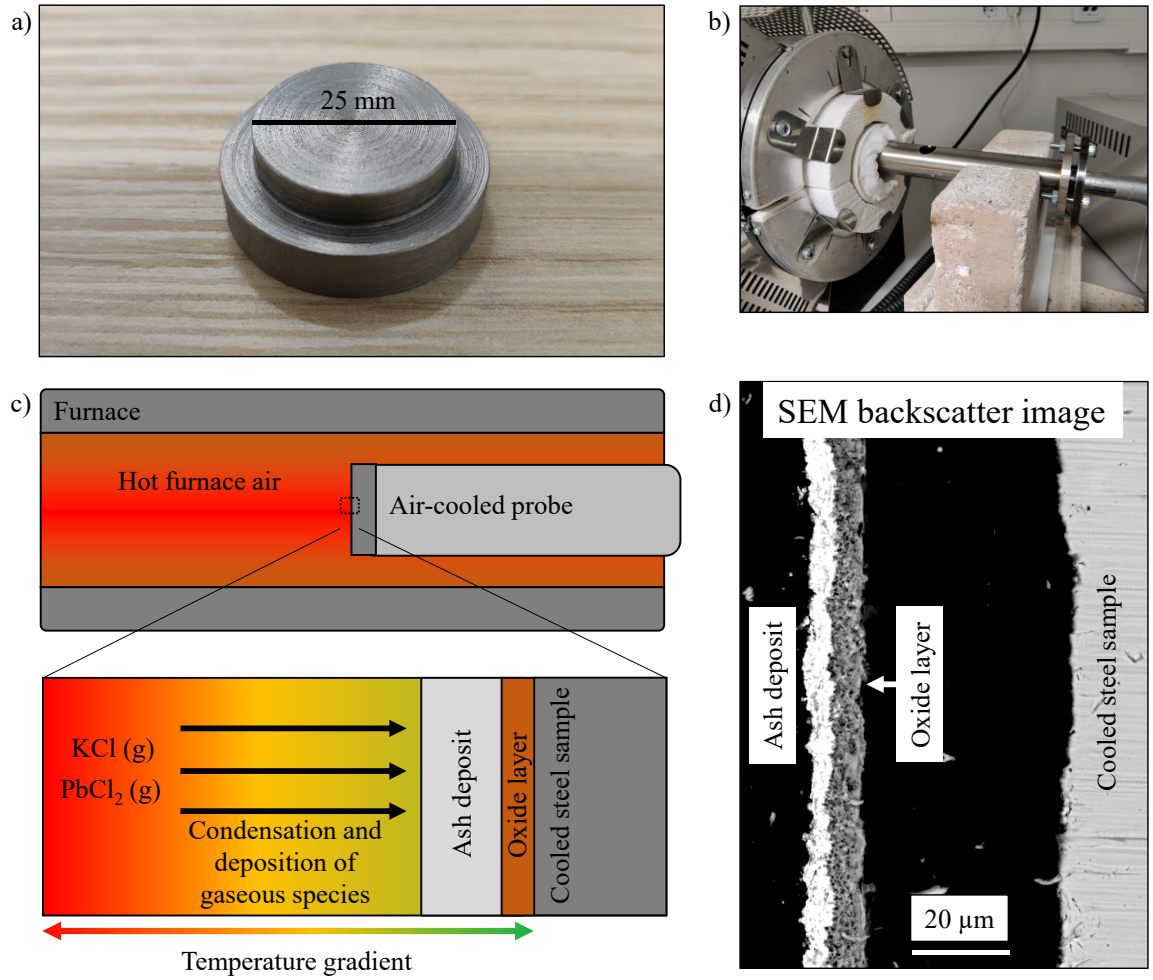

Fig. 1. a) The steel sample piece, b) a picture of the probe during an experiment, c) a schematic visualization of the experimental set-up, and d) post-exposure cross-sectional SEM backscatter image of the steel sample with oxide layer and $PbCl_2$ deposit.

Significant amounts of $PbCl_2$ were analyzed on the steel samples after exposure to an atmosphere containing the volatilized lead salt. Even at the relatively low material temperatures of 350 °C, compared to the surrounding atmosphere temperature of ~650 °C, the carbon steel samples were heavily corroded when exposed to $PbCl_2$ containing atmosphere. The SEM backscatter images showed an average deposit thickness of ~10 µm after four hours of exposure. The novel temperature gradient set-up was found practical for high-temperature corrosion studies. The method accounted for the desired temperature gradient and allowed studying deposition and corrosion simultaneously. Thus, the deposit formation method will offer new insights into the corrosion mechanisms in boilers and other high-temperature processes and applications.

Role of Mn on oxidation behavior on Chromium steel

Gurkirt Singh[a], PC Yadav[a], M. I. Khan[b] and H.K. Mehtani[a*]

[a] Mechanical Engineering Department, Thapar Institute of Engineering and Technology, Patiala 147004.

[b] CITE, Titan Company, Hosur -635126

Abstract: -

The quality of steel is affected by surface defects and oxidation kinetics. Oxidation depends on grain size, texture, surface roughness, and alloying. In the present work, we investigate the influence of Mn in ultra-low carbon Cr steel (Fe-20wt%Cr) by keeping all other parameters the same. The alloys (Fe-20wt% Cr and Fe-18wt%Cr-2wt%Mn) were prepared in a vacuum arc melting furnace. To keep all the parameters like grain size, texture and surface roughness the same, these alloys went under thermomechanical processing. This behavior of the material was investigated in both ways, isochronal as well as isothermal (773K and 973K). These temperatures (isothermal) were chosen below and above the eutectoid transformation of iron and oxygen. In both temperatures, parabolic kinetics were observed for both alloys. This study showed significant improvement in oxidation resistance by replacing Cr (Fe-20Cr) with Mn (Fe-18Cr-2Mn). Parallelly, Fe-18Cr-2Mn also showed better corrosion resistance when tested under the industrial condition of sulphuric acid (H_2SO_4) with 0.5M strength. Oxide microstructure analysis was done with the help of SEM-EDS and EBSD. The phase analysis of the oxide scale was done with XRD and Raman spectroscopy. There was a clear sign of Mn and Cr oxide particles on the surface. The presence of Mn, Cr oxide appeared to correlate with improved oxidation resistance.

Keywords: Iron, Chromium, Manganese, Oxide, Texture, EBSD (Electron Backscattered Diffraction)

High temperature oxidation and corrosion behaviour of novel Cr-Si slurry diffusion coatings

M.Kerbstadt[A], E. White[A], M.C. Galetz[A], [A] DECHEMA-Forschungsinstitut, Materials and Corrosion, Theodor-Heuss-Allee 25, 60486 Frankfurt am Main, Germany

Diffusion coatings are widely used in high temperature applications to enhance the oxidation and corrosion resistance of metals and alloys. Commonly Al, Cr, and/or Si are enriched at the surface in order to provide chemical reservoirs to form protective oxide scales during exposures at high temperatures. Commercially Al, Cr and Si-based diffusion coatings are mostly achieved by pack cementation, where the deposition occurs via a gas diffusion process. For pack cementation the parts/substrates are usually fully embedded into a powder mixture which is energy- and labor-intensive, requiring large furnaces with extensive fixturing to be heated-up to high temperatures for the diffusion process to occur.

Alternatively, slurry-based coatings do not require embedding into and heating up a big powder bed, nor such large furnaces (as more localized heat treatments can be used), and are thus a much more economical option. For an Al diffusion coating, the slurry process has been well established, where the slurry is sprayed onto the metallic surfaces by an air brush. The coating is then formed during a subsequent heat treatment by interdiffusion between the metallic particles from the slurry and the substrate. For sufficient diffusion rates during the heat treatment, the existence of a liquid phase at the interface of the substrate surface and the slurry particles is necessary.

Because of the high melting point of Cr, the deposition of Cr-based diffusion coatings by the slurry technique has been challenging. Cr-Si slurry coatings have recently been successfully developed by the Dechema-Forschungsinstitut. These newly developed slurry coatings are applied using an aqueous suspension where distilled water is used as the solvent. Higher Cr-activities, due to the partial liquid state, enable higher coating thicknesses when compared to similar coatings applied by

pack cementation. This creates a larger reservoir (up to 200 µm) of the protective oxide-forming elements Cr and Si, resulting in longer-lasting protection from the coating.

Within this work the high temperature oxidation and corrosion performance of these novel Cr-Si slurry coatings were investigated with the goal to improve the surfaces of particle receiver of novel concentrating solar thermal power (CSP) systems. Thus, the coating was applied on the austenitic steel Sanicro 25 and the Ni-base alloy Inconel 617b. The enrichment of Cr leads to the formation of a protective Cr_2O_3 scale which minimizes the degradation of the materials during high temperature exposures. For evaluation of the oxidation behaviour, isothermal and cyclic (1h/cycle) exposures in lab air at 900°C for 1000 h were carried out. To determine the weight gain samples were removed after 300 h, 700 h and 1000 h. To obtain an initial impression of the hot corrosion behaviour, a Na_2SO_4 salt of 2.5 mg per cm^2 was deposited via the evaporation of a saturated solution on the samples. Afterwards the samples were exposed at 900° C for 50 h in a gas mixture of synthetic air containing 0.1 % SO_2. Analysis of the samples was performed by XRD, SEM and EPMA to determine the structure and composition of the oxide layers and the degree of attack. Due to the increased amount of protective elements, the slurry coated samples showed significantly reduced attack by oxidation and corrosion during the exposures compared to the bare substrate materials.

Aging effect of the surface oxide layer after early-stage oxidation of 316L

Robert Wonneberger [1], Maximilian Schaal [2], Felix Otto [2], Torsten Fritz [2] and Andreas Undisz [1]

[1] Chemnitz University of Technology, Chemnitz, Germany

[2] Friedrich Schiller University Jena, Jena, Germany

The high temperature oxidation of 316L results in the formation of multicompositional oxide phases of both, corundum-type and spinel-type oxide. The formation of the oxides at the early stages is considered to occur via outward diffusion of the oxide forming elements Cr, Fe and Mn through the growing oxide layer. Accordingly, the path of the oxidizing species, e.g., through the oxide grain volume and / or along oxide grain boundaries are of major importance for understanding the underlying growth mechanism. Commonly, the formation of a Cr-rich oxide is promoted by outward diffusion of Cr^{3+} that can be incorporated into the crystal lattice of the corundum-type as well as the spinel-type oxide phase. Recent studies indicate that the phenomenon of multilayered oxides with a two-layered structure (inner Fe-rich and outer Cr-rich at 400 °C) and Cr-Fe-Cr three-layered structure (≥ 600 °C) are caused by different dominant paths of Cr diffusion with respect to the applied temperature. To the best of our knowledge it has not been considered yet whether the valence state of available Cr ions differs in dependence of the annealing temperature. In order to determine the valence state of Cr ions, samples annealed between 400 °C and 800 °C in ambient air were analyzed using X-ray photoelectron spectroscopy. It is shown that the surface oxide layer formed at 600 °C gets altered when exposed to ambient air. Unexpectedly, after annealing at 600 °C, both, Cr^{3+} and Cr^{6+} species are detected at the direct surface of the oxide. After extended exposure to ambient air, the amount of Cr^{6+} decreased and essentially Cr^{3+} was detected on the same sample. This indicates towards an important contribution of Cr^{6+} regarding the diffusion of Cr during oxide layer growth. This aging effect was not revealed until now, likely due to the reduction of Cr^{6+} to Cr^{3+} within a few days.

Formation of a protective oxide layer on the surface of high temperature alloys

Sergio DIEZ [a,b], *Laure MARTINELLI* [b], *Fabien ROUILLARD* [b]

[a] *Université Paris Sorbonne, Chimie Physique et Chimie Analytique de Paris-Centre (ED-388)*

[b] *Universite Paris-Saclay, CEA, Service de la Corrosion et du Comportement des Matériaux dans leur Environnement, 91190, Gif-sur-Yvette, France*

Understanding the parameters influencing the formation of a fast-growing duplex oxide layer at high temperatures for a range of metallic alloys is crucial in order to minimize or avoid the accelerated degradation of the alloy. Depending on various independent variables (such as alloy composition, surface state, microstructure, temperature, exposure time, and environment composition), a so-called “protective” single-layer or a “non-protective” duplex layer may form. From an industrial point of view, the formation of the latter is not beneficial and it has been studied through various theories and scenarios [1–3]. Research work of CEA Saclay, based in Robertson’s articles [4], has led to the theory known as the Available Space Model [5–7]. This model assumes that the oxidant rapidly penetrates to the metal/oxide interface through short circuits, resulting in the formation of an internal oxide layer. Being observed in the literature for very diverse systems and conditions [1,8–10], a generalization of the model has never been made. The objective of this study is to identify the cases of the duplex scale formation following the “Available Space Model” and to achieve a better understanding of the relevant parameters involved in it.

Firstly, an exhaustive literature work is performed in order to provide a thorough understanding of the existing hypothetical theories or mechanisms explaining the formation of a “duplex” layer. The realisation of a parametric table summarising the experimental conditions of past studies allows identifying the exact conditions of formation of the “non-protective” layer in various environment-alloy couples, providing a theoretical framework for the study.

Oxidation tests are conducted in a Gas-Phase Analysis facility (DRAGONS [11]) allowing the measure of the kinetics of chemical reactions between gases and solids and gas-desorption experiments. The main parameters considered to vary for the different experiments are temperature, alloy composition and environment. The combination of these different variables allow a better understanding about the triggering and proceeding of the “Available Space Model”. Later characterisation of the scales formed, coupled to oxidation tests, allow to assess the presence of the proposed model and to identify the precise conditions on which it happens. The use of model alloys will allow first results and conclusions to be drawn.

---

1. Brückman, A. The mechanism of transport of matter through the scales during oxidation of metals and alloys. *Corros. Sci.* **7**, 51–59 (1967).
2. Whittle, D. P. & Wood, G. C. Complex Scale Formation on an Iron-18% Chromium Alloy. *J. Electrochem. Soc.* **114**, 986 (1967).
3. Maak, F. & Wagner, C. Mindestgehalte von Legierungsbestandteilen für die Bildung von Oxydschichten hoher Schutzwirkung gegen Oxydation bei höheren Temperaturen. *Mater. Corros.* **12**, 273–277 (1961).
4. Robertson, J. & Manning, M. I. Criteria for formation of single layer, duplex, and breakaway scales on steels. *Mater. Sci. Technol. U. K.* **4**, 1064–1071 (1988).
5. Gibbs, G. B. & Hales, R. The influence of metal lattice vacancies on the oxidation of high temperature materials. *Corros. Sci.* **17**, 487–507 (1977).
6. Martinelli, L. *et al.* Oxidation mechanism of an Fe–9Cr–1Mo steel by liquid Pb–Bi eutectic alloy at 470°C (Part II). *Corros. Sci.* **50**, 2537–2548 (2008).
7. Martinelli, L. *et al.* Comparative oxidation behaviour of Fe-9Cr steel in CO2 and H2O at 550°C: Detailed analysis of the inner oxide layer. *Corros. Sci.* **100**, (2015).
8. Dravnieks, A. & Mcdonald, H. J. The Zone of Metal Phase Consumption in Gas-Metal Reactions. (1948) doi:10.1149/1.2773831.
9. Kofstad, P. On the formation of porosity and microchannels in growing scales. *Oxid. Met.* **24**, 265–276 (1985).
10. Atkinson, A. Transport processes during the growth of oxide films at elevated temperature. *Rev. Mod. Phys.* **57**, 437–470 (1985).
11. Rouillard, F. & Young, D. J. Benefits of gas phase analysis facility using isotopically labelled gases for the understanding of gas–solid reactions: Reactivity of iron and mild steel in O2, CO2 and CO2/O2 environments. *Corros. Sci.* **178**, 109092 (2021).

Oxidation of $CrTaO_4$ forming alloys in water vapor at high temperatures

Fabian Lanoy[1], Emma White[1], Björn Schäfer[2], Bronislava Gorr[2], Mathias Galetz[1]

[1] DECHEMA-Forschungsinstitut, Frankfurt am Main, Germany

[2] Institut für Angewandte Materialien – Angewandte Werkstoffphysik, Karlsruher Institut für Technologie (KIT), Karlsruhe, Germany

Introduction

While chromia, silica and alumina are very common protective oxides for high temperature alloys, the role of complex oxides, such as $CrTaO_4$, has only garnered research interest in recent years [1]. It is likely that $CrTaO_4$ layers play an important role in the oxidation resistance of refractory high entropy alloys [2]. Furthermore, it was found that some nickel-based alloys form continuous $CrTaO_4$ layers as part of more complex oxide scales [3]. In this work, the oxidation behavior of different $CrTaO_4$-forming alloys in argon-water atmospheres was investigated to clarify their kinetics and scale morphologies.

Methods

To investigate their oxidation behavior, several refractory alloys and refractory high entropy alloys, which potentially form $CrTaO_4$, were isothermally exposed in an Ar-H_2O atmosphere at temperatures up to 1000°C for durations up to 288 hours. Additionally, the water content and oxygen partial pressures of the atmospheres were varied to study the influence on formation of the oxide scales. The oxidized samples were analyzed by means of XRD, EPMA and SEM.

Results

The first experiments show the formation of a continuous $CrTaO_4$ layer below a Cr_2O_3 layer at an exposure time of 24 and 48 hours for Cr-20at.%Ta, see Figure 1 and Figure 2. Furthermore, the layer not only covers the tantalum-containing Cr_2Ta laves phase, but also the chromium solid solution phase.

The described experiments provide knowledge whether the refractory high entropy alloy CrTaTiAlMo exhibits similar oxidation behavior in water vapor-containing atmospheres.

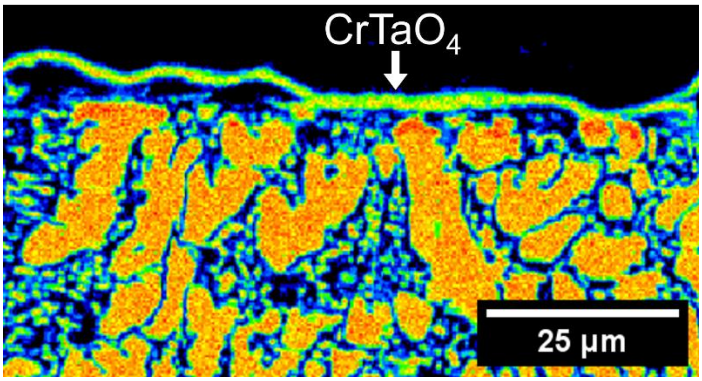

Figure 1: Tantalum signal of an EPMA mapping of a Cr-20at.%Ta sample cross-section, showing a continous $CrTaO_4$ layer after exposure in an Ar-5H_2O atmosphere at 1000°C.

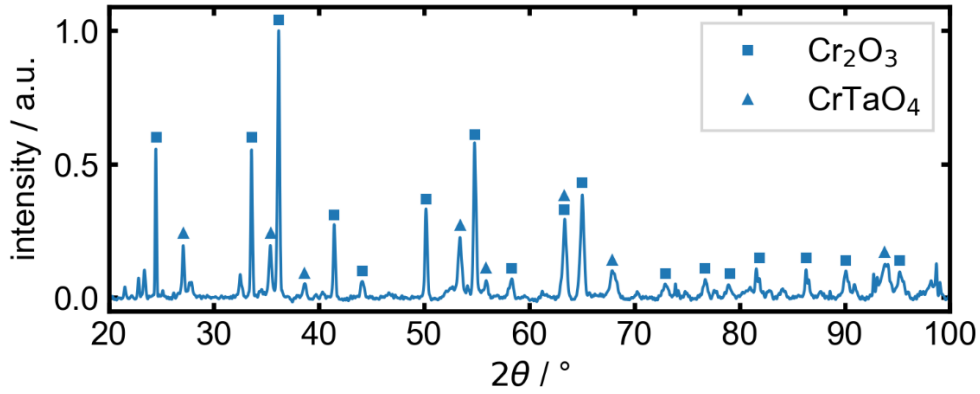

Figure 2: XRD pattern of a Cr-20at.%Ta sample after exposure in an Ar-5H_2O atmosphere at 1000°C showing the formation of both chromium oxide and chromium tantalum oxide.

References

[1] M. P. Brady, P. F. Tortorelli, E. A. Payzant und L. R. Walker, „Oxidation behavior of Cr2N, CrNbN, and CrTaN phase mixtures formed on nitrided Cr and Laves-reinforced Cr alloys," *Oxidation of Metals,* Bd. 5, pp. 379-401, 2004.

[2] K.-C. Lo, Y.-J. Chang, H. Murakami, J.-W. Yeh und A.-C. Yeh, „An oxidation resistant refractory high entropy alloy protected by CrTaO4-based oxide," *Scientific reports,* Bd. 1, pp. 1-12, 2019.

[3] W. Ren, F. Ouyang, B. Ding, Y. Zhong, J. Yu, Z. Ren und L. Zhou, „The influence of CrTaO4 layer on the oxidation behavior of a directionally-solidified nickel-based superalloy at 850--900 C," *Journal of Alloys and Compounds,* pp. 565-574, 2017.

Comparison of the Oxidation Behaviour of Wrought and Additively Manufactured Alloy 625.

Boma Phoebe Norman, Cranfield University, Cranfield, UK

Andrew Potter, Cranfield University, Cranfield, UK

Nigel Simms, Cranfield University, Cranfield, UK

Emily Rose Lewis, University of Birmingham, Birmingham, UK

Sam Cruchley, University of Birmingham, Birmingham, UK

Joy Sumner, Cranfield University, Cranfield, UK

Abstract

Supercritical carbon dioxide (sCO_2) power cycles are promising cycles for cleaner and more sustainable power generation. Some of the components needed for these novel cycles have complex geometries, so there is an interest in the use of novel manufacturing methods such as Powder Bed Fused manufacturing, a type of additive manufacturing (AM). AM has benefits including reducing cost, waste and lead time compared to traditional metal production practices. In indirect-fired cycles, such as the Allam cycle, supercritical fluid temperatures and pressures of >700°C and 300 bar have been suggested, to achieve target efficiencies of 51%-59%. These conditions give rise to material challenges.

This research aims to investigate the difference in materials performance for addictive and traditional techniques of manufacturing. To do so, wrought and additively manufactured Alloy 625 samples have been exposed in a simulated CO_2 environment including contaminants such as H_2O, O_2, N_2 and SO_2. Baseline tests have been carried out on coupons in a laboratory, controlled atmosphere furnace at 800°C and 1 bar.

This study presents quantitative elemental information and surface morphology of the as received and exposed Alloy 625 samples. The AM alloys' microstructure, oxidation behaviours and surface roughnesses/conditions have been compared with a wrought equivalent. The effect of surface roughness on oxidation rate was investigated. Optical microscopy, scanning electron microscopy (SEM) and energy dispersive X-ray (EDX) spectroscopy have provided details on the oxide scale and elemental segregation.

Keywords: sCO_2, Additive manufacturing, Alloy 625, Allam cycle, Oxidation behaviour

Oxidation Behaviour of Austenitic Stainless Steel 304HCu in Advanced Ultra Supercritical Steam

C. Sundaresan[1], Bhagwat Ghule[1], S. Ningshen[2], Dandapani Vijayshankar[1] and V.S. Raja[1]*

[1]Department of Metallurgical Engineering and Materials Science, Indian Institute of Technology Bombay, Mumbai 400076, India

[2]Corrosion Science and Technology Division, Metallurgy and Materials Group, Indira Gandhi Centre for Atomic Research, Kalpakkam 603102, India

**Presenting author; Email: csundar92@gmail.com*

The drive towards lesser emissions and higher operational efficiencies has guided the coal-fired power plants to adopt increasingly higher steam temperatures and pressures. At the current juncture, this has led to the 'Advanced Ultra-Supercritical (AUSC) Power plants' which operate at steam temperatures and pressures as high as 710 ℃ and 31 MPa respectively. Besides a need for enhanced creep strength, AUSC power plants demand alloys with superior steam-side oxidation resistance owing to the hostile working conditions. Austenitic stainless steel 304HCu is one such candidate material for AUSC plants and is limited for usage till 650 ℃. Although there are studies concerning the oxidation of 304HCu in supercritical steam, the oxidation behaviour of the same in AUSC conditions has not been explored. This assumes importance since higher steam pressures in the AUSC regime could potentially influence the oxidation behaviour.

In the present work, the oxidation behaviour of the alloy 304HCu (Fe-18Cr-8.6Ni-3.2Cu-0.8Mn-0.4Nb wt.%) is investigated in a simulated AUSC test loop at 650 ℃ temperature and 31 MPa pressure. Ultrapure feed water with electrical conductivity less than 0.1 µS/cm and dissolved oxygen content less than 10 ppb was used at a flow rate of 20 ml/min. The test was carried out for 100, 300 and 600 hours to develop the mass gain kinetics. Besides gravimetric analysis, X-ray diffraction (XRD), Laser Raman Spectroscopy (LRS) and oxide cross-sectional analysis using Scanning Electron Microscopy (SEM) with Energy Dispersive Spectroscopy (EDS) were employed to understand the nature of oxides formed.

The normalized mass gains after 100 and 300 hours of oxidation were 3.01 and 5.21 mg/cm^2 respectively. In both the cases, an external, porous magnetite (Fe_3O_4) scale and inner dense scale made of $Fe(Cr,Ni)_2O_4$ spinel were observed. Chromium volatilization leads to Cr-depleted spots in the initially formed chromia layer triggering breakaway oxidation. Unprotective magnetite then grows outwards from these regions while Cr-rich spinel grows internally leading to a dual-layered oxide. However, the external oxide suffered spallation upon nearing 600 hours and the mass gain after 600 hours was 4.04 mg/cm^2. The obtained mass gain values are much higher than those reported in the existing literature in which steam pressures were limited to 25 MPa. Higher steam pressure leads to increased equilibrium partial pressure of oxygen (pO_2) in steam and higher density of supercritical water which in turn promotes the adsorption of oxidants on the alloy surface. Besides, chromium volatilization also becomes severe with increasing steam pressures. The detailed oxidation mechanism and the potential effect of steam pressure behind the oxidation in the AUSC environment will be discussed. Notably, the oxidation of alloy 304HCu in the AUSC steam environment is found to be much more severe than expected and probable causes for the same are proposed.

Keywords: Oxidation; Supercritical water; Alloy 304HCu; High temperature and pressure; Advanced Ultra Supercritical (AUSC)

From the Coriou effect to the stress corrosion cracking of stainless steel in nuclear power plants

Damien Féron, Université Paris-Saclay, CEA, Service de recherche en Corrosion et Comportement des Matériaux, 91191 Gif Sur Yvette, France

This overview of stress corrosion cracking (SCC) in water cooled reactors focuses on an historical perspective, from the choice of Alloy 600 in pressurised water reactors (PWRs) to its prohibition and ends with few considerations regarding the SCC of stainless steels in primary PWRs circuits.

The “Coriou effect” named SCC of a nickel alloy (Alloy 600) in pure (or primary) water at high temperature. Henry Coriou (head of CEA’s “corrosion laboratories”) observed and reported the SCC of Alloy 600 at the end of the 1950s during laboratory experiments in pure water at 350 °C. These experiments were more representative of water reactor conditions than any others obtained in boiling magnesium chloride solutions in which Alloy 600 is not susceptible to SCC. Nevertheless, Alloy 600 has been chosen and used extensively in PWRs up to the end of the 80s. We propose to go back to this period, to the choice of the Alloy 600 despite experimental evidences, to the scientific and technical disputes and to the first occurrences of the SCC cracks observed in reactor plants. Finally, the large cracking observed on steam generator tubing lead to the replacement of Alloy 600 by the use of Alloy 690 (or Alloy 800) at the end of the 80s.

The end of the talk includes a short overview on SCC of stainless steels in primary PWR circuits, including a rapid summary of the recent events in French PWRs.

Stress corrosion cracking of Type 304 stainless steel in simulated primary water of pressurized water reactor

Hong Pyo Kim, Jong Yeon Lee, Min Jae Choi, Sung Hwan Cho, Seong Woo Kim, Dong Jin Kim, Seong Sik Hwang, Yun Soo Lim

Korea Atomic Energy Research Institute, Daejeon, Republic of Korea

Stress corrosion cracking (SCC) of cold worked Type 304H stainless steel containing delta ferrite was studied using compact tension (CT) specimen with L-T orientation in simulated primary water of 325^{o}C. Primary water contained 1200 ppm B as H_3BO_3 and 2.2 ppm Li as LiOH and 30 cc H_2 /1kg H_2O. CT specimen was precracked in air and then in SCC test solution. Crack growth rate was measured at stress intensity factor of 30 MPa·m$^{1/2}$ with alternated direct current potential drop. Fracture surface and side surface were observed after SCC test with scanning electron microscope-electron back scattered diffraction (SEM-EBSD). SCC proceeded with both intergranular (IG) and transgranular(TG) SCC mode. In case of IGSCC, most cracked grain boundaries were normal to loading axis. In case of TGSCC, SEM-EBSD analysis showed that crack predominantly propagated along {111} plane and the angles between plane normal to loading axis and cracked {111} plane were varied from 20 to 60^{o}, suggesting that cracked plane had both high resolved shear stress and tensile stress. Effect of δ ferrite on SCC and fractography of TGSCC were discussed.

Influence of Dissolved Hydrogen on the Intergranular Oxidation of Alloys 600 and 690 in Hydrogenated Primary Water

Yun Soo Lim, Dong Jin Kim, Sung Woo Kim, Hong Pyo Kim, Jong Yeon Lee
Korea Atomic Energy Research Institute
1045 Daedeok-daero, Yuseong-gu, Daejeon 34057, Korea

Primary water stress corrosion cracking (PWSCC) of Ni-base Alloys has been a major concern in the primary side of pressurized water reactors (PWRs). Alloys 600 and 690 show noticeable differences in the cracking behavior and resistance owing to their different Cr contents. It is necessary, therefore, to reveal the root causes of the different cracking behavior between Alloys 600 and 690 in PWR primary water to ensure safe service and good performance. Hydrogen is normally added at levels of 25 - 50 cm^3 H_2/kg H_2O to primary water to remove dissolved oxygen, and hydrogen is known to have significant effects on the cracking resistance of Ni-base alloys. The PWSCC susceptibility of Alloy 600 is known to peak near the Ni/NiO transition, and the location of the Ni/NiO transition has been shown to vary with temperature, from 25 cm^3 H_2/kg H_2O at 360 ℃ to 4 cm^3 H_2/kg H_2O at 288 ℃. The aim of the present study was to characterize the surface oxidation layers of Alloys 600 and 690 depending on the hydrogen concentration to obtain clear insight into the different cracking resistance and behavior between Alloys 600 and 690 when exposed to simulated PWR primary water.

The oxidation test of Alloys 600 and 690 was conducted at 325 ℃ in simulated PWR primary water environment. 1200 ppm B (by weight) of H_3BO_3 and 2 ppm Li (by weight) of Li(OH) were added to pure water maintaining a dissolved oxygen content below 5 ppb. The hydrogen contents were 5, 30 and 50 cm^3 H_2/kg H_2O. From the XRD measurements, it was found that Ni was in a metallic state when the hydrogen concentrations were 30 and 50 cm^3 H_2/kg H_2O, whereas pyramidal oxides identified as NiO emerged on the surface when the hydrogen concentration was 5 cm^3 H_2/kg H_2O at which Ni was in an oxidized state. It was revealed from a TEM examination that intergranular (IG) oxidation of Alloy 600 occurred irrespective of hydrogen

concentration. There was Ni enrichment in the oxidized grain boundaries of Alloy 600 when the hydrogen concentration was 30 cm^3 H_2/kg H_2O, whereas Ni-rich oxides emerged in the oxidized grain boundaries when the hydrogen concentration was 5 cm^3 H_2/kg H_2O. These results indicate that the behavior of Ni in Ni-base alloys considerably changes depending on the hydrogen concentration. On the other hand, IG oxidation of Alloy 690 did not occur within a range of hydrogen concentration between 5 and 50 cm^3 H_2/kg H_2O. The continuous band-shaped innermost Cr_2O_3 layer just over the grain boundaries beneath the surface is believed to be responsible for the prevention of oxygen diffusion into the grain boundary and the resultant suppression of IG oxidation. Ni nodules emerged on the surface when the hydrogen concentrations were 30 and 50 cm^3 H_2/kg H_2O. Therefore, it appears that the formation of Ni nodules or Ni enrichment in the oxidized regions is common in Ni-base alloys when Ni is in a metallic state. Diffusion induced grain boundary migration was frequently found in Alloy 690 irrespective of the hydrogen concentration. All the above different oxidation phenomena observed in Alloys 600 and 690 depending on the hydrogen concentration are believed to be caused mainly by the different Cr concentrations in these alloys, and to significantly affect their resistance to PWSCC.

Intergranular oxidation of Alloys 600& 182 exposed PWR primary water: Effect of cold worked and industrial surface finishes

Y. Vidalenc, Framatome Centre Technique, Le Creusot/France

J. Caballero Hinostroza, Framatome, Paris/France

M. Berthaud, Centre Technique, Le Creusot/France

O. Calonne, Framatome Site Ugine, Ugine/France

Several components present in the primary circuit of Pressurized Water Reactors (PWR) were manufactured with alloys 600 and 182. Field experience of the primary circuit of PWRs showed that alloys 600/182 may suffers intergranular stress corrosion cracking (IGSCC). In contrast, the effect of operating factors such as applied tensile stress, surface finish and Stress Relief Heat Treatment (SRHT) still not meet consensus within the nuclear community. Several studies have shown a detrimental effect of Cold Working (CW) on Stress Corrosion Cracking (SCC) initiation, but a common opinion is obviously not available within the literature regarding the influence of surface CW and stress on intergranular oxidation kinetics. While some authors have shown an acceleration of IG oxidation with the CW level, often limited to sample surface with laboratory surface finishes which are not representative of industrial surfaces, an oxidation delaying effect of highly deformed refined microstructure has been reported in nickel base alloys and austenitic stainless steel exposed to PWR primary water.

The main objective of this study is evaluating the effect of industrial-like surface finish on internal oxidation and induced IG embrittlement produced on Alloys 600 and 182. For that, an Alloy 600 in its mill annealed condition and a weld deposit from Alloy 182 stud were both oxidized in nominal primary water at 325°C during 1500 hours with a dissolved hydrogen content below the Ni/NiO equilibrium. The surface grain boundary density, oxide penetration depth and grain boundary weakening by prior oxidation under in situ SEM tensile testing were evaluated on surface finishes as polishing (SiC 1200 and diamond paste 1 µm, known as undeformed references) and severe hand grinding (reproduced as workshop practices using an automatic grinding bench). These results from surface analyses were correlated to microstructure crystallographic features (EBSD) and the local strain distribution from image

correlation (DIC). The comparison of oxidation damages is established with literature results.

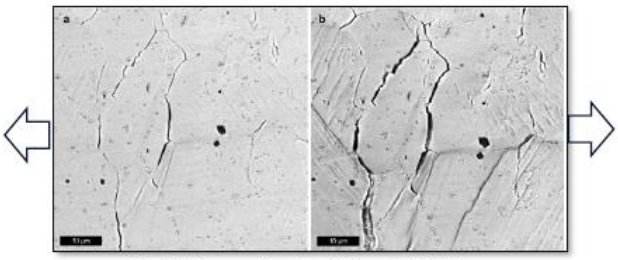

IG oxidation opening at a) 3.9% and b) 12.1%

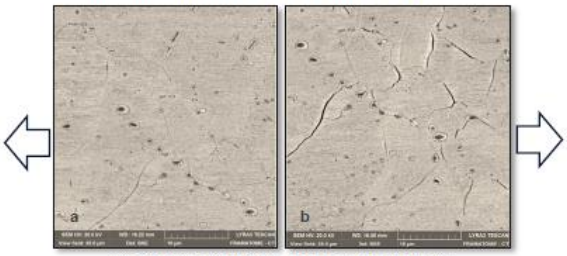

IG oxidation at a) 3.4% and opening at b) 5.4%

This study shows results in a quite agreement with some public papers and it gives a complementary insight on the role of highly deformed surface relatively to oxidation kinetics and induced IG oxidation density under mechanical loading. While a 20% bulk cold working does not show higher IG oxidation density, the degree of oxidation in depth does seem slightly more pronounced than as-received microstructure (forged as received conditions). The Beilby (ultra fine) layer promoted by surface grinding appears much deeply oxidized than polished surface from as received or 20% cold worked conditions. Nevertheless, oxidation depth is never met beyond the ultra-fine layer of 2-3 µm after a period of 1500 hours. On weld deposited material, grinding induces significant change in the oxide's morphology and on the oxide penetration depth. The original presumed beneficial effect of recrystallized sub-layer formed after SRHT does appear to only bring a slight advantage regarding the IG oxidation. More generally, industrial-like surface finish showing a refined microstructure within first micrometers are more favorable to IG oxidation but the depth extension of embrittlement seems reduced for a given post-oxidation deformation. SRHT does not act as a strong oxidation inhibitor and its known beneficial effect in PWSCC resistance is probably associated to a softening impact on microstructure with reduce hardness and residual stress.

Testing modified alternative martensitic stainless steel for fusion applications

Patricia Jovičević-Klug[1], Michael Rohwerder

[1]Group of Corrosion, Department of Interface Chemistry and Surface Engineering, Max-Planck-Institute for Iron Research, Düsseldorf, Germany

Keywords: martensitic stainless steel, fusion, deep cryogenic treatment, microstructure, residual stress, corrosion resistance

Introduction

The simultaneous improvement of known materials and exploration of new alternative material options for applications in high demanding environments, such as fusion, is currently one of the leading research endeavours in engineering[1]. Materials used in fusion applications have to inhibit unique combination of properties with high corrosion resistance, high toughness and strength, while also being machinable. In the last 5 years a novel procedure, dubbed deep cryogenic treatment (DCT), has strongly emerged as an additional step in the heat treatment of different steels, including stainless steels, which provides improvements of various properties[2]. During DCT, steels are subjected to temperatures below 113 K, usually to the temperature of liquid nitrogen (77 K) or liquid helium (4 K)[1]. DCT fundamentally changes steel properties (hardness, toughness, strength, ductility, corrosive and wear resistance etc. [1]) through the leading mechanisms of improved austenite transformation into martensite and increased carbide precipitation[1]. Within this study, the proposed alternative material - martensitic stainless steel (MSS) X17CrNI16-2 is studied for possible fusion applications. The proposed MSS has unique combination of strength, toughness and corrosive resistance. Furthermore, in this study, the effect of DCT on selected MSS in correlation to changed microstructure, residual stressed and corrosive resistance is tested in order to test the potential of DCT also for MSS.

Material and Methods

The chemical composition of selected MSS X17CrNI16-2 is in wt.%15.2 Cr, 1.5 Ni, 0.8 Mn, 0.2 C, 0.02 S, 0.3 Si, 0.1 Mo, 0.1 Cu and Fe as base. The samples were divided into two groups: classical heat treatment (no DCT, hardening (ΔTa= 1323 K / 0.5 h) and 1 cycle of tempering, ΔTt=753 K / 2h) and DCT group (hardening (ΔTa= 1323 K / 0.5 h), DCT (77K / 24 h) and followed by 1 cycle of tempering, ΔTt=753 K / 2h). The

samples were prepared and etched according to[3]. The microstructure was analysed with SEM and the residual stress measurements were conducted with XRD and pulse overlap diffractometer. Corrosion resistance was tested in different corrosive environments (air/nitrogen/oxygen and dry/humid) with SKP and SKPFM.

Results and Discussion

The results indicate a strong modification of the MSS X17CrNI16-2 microstructure after DCT application, resulting from the improved transformation of austenite into martensite, increased precipitation of finer carbides. Additionally, we disclose the suppression of austenite reversion transformation with DCT, which is an important phenomenon to consider for material stability during prolonged exposure in high-demanding environments. Residual stress measurements provide unique insight into the change of tensile stresses to compressive stresses after application of DCT, which depict a complex DCT mechanism within the selected MSS. SKP and SKPFM results indicate the impact of modified microstructure on corrosion resistance and its temporal evolution, where the major role for corrosion progression are primary carbides and grain boundaries that act as weak points. Nevertheless, the increased precipitation and matrix reconstruction with DCT play an additional role in the formation of potentially weak points, which is up to now still in question. As such, the newly obtained MSS microstructure provides higher dimensional stability, which results from the maximal saturation of the material with precipitates. With our conclusions we propose that the modified precipitation has an important role in the prolonged functionally of this MSS in high demanding environments, such as fusion.

Conclusions

To conclude, the research indicates that MSS X17CrNI16-2 is a promising alternative material for applications in high demanding environment such as fusion applications. Additionally, the study shows also that DCT can be used to effectively modify the microstructure and properties of MSS, which can significantly prolong functionally and extend the applicability of MSSs. However, more research is still required to fully test the newly observed phenomena correlated to DCT MSS.

References

1. Knaster et al. *Nature Physics*, 2016.
2. Jovičević-Klug et al. *Metals*, 2020.
3. Jovičević-Klug et al. *Materials Today Communications,* 2021.

Mitigation of stress corrosion cracking in Alloy 182 weld metal by zinc injection into boiling water reactor coolant

Adrianna Mackiewicz, Paul Scherrer Institute (PSI), Villigen/Switzerland, adrianna.mackiewicz@psi.ch

Stefan Ritter, Paul Scherrer Institute (PSI), Villigen/Switzerland

Kai Chen, Paul Scherrer Institute (PSI), Villigen/Switzerland

Hans-Peter Seifert, Paul Scherrer Institute (PSI), Villigen/Switzerland

Sannakaisa Virtanen, Friedrich-Alexander University Erlangen-Nürnberg, Erlangen/Germany

Keywords: zinc water chemistry, SCC mitigation, oxide film, Alloy 182, BWR.

Abstract

At first and up to now, zinc (Zn) injection into boiling water reactor (BWR) coolant has been applied mainly for the radioactive build-up reduction in the primary circuit. Zn forms thermodynamically more stable oxide films on primary circuit components with less neutron-activated Co^{60} isotopes. More recent studies and in-plant experience from BWRs indicated a positive side-effect of the Zn – stress corrosion cracking (SCC) mitigation. This finding has enhanced further research recently on the SCC behaviour of structural materials, like Ni-based alloys or weld metals. Based on only few studies, in some cases even with contradictory results, it is not clear yet, what concentration of Zn is sufficient regarding SCC mitigation effect and what is the mechanism behind. Therefore, further investigations are needed to get more insights on the SCC mitigation efficiency by the Zn injection and its underlying mechanisms.

The impact of Zn injection on the SCC behaviour and oxide film properties of Alloy 182 weld metal exposed to BWR environment have been studied. It was shown that the SCC susceptibility under 40 ppb Zn water chemistry conditions and even down to 15 ppb Zn concentration was reduced. The enhanced protectiveness of the Zn-doped oxide film is believed to be responsible for the reduced SCC initiation susceptibility. The current presentation puts a focus on the oxide layer characteristics formed under BWR hydrogen water chemistry with and without Zn addition. Several microstructural and electrochemical characterisation techniques (e.g., electron microscopy, energy-dispersive X-ray spectroscopy, electrochemical impedance spectroscopy) were used to reveal possible changes in morphology, composition and electrochemical properties

of the oxide film prior to and after the Zn treatment. The results show that Zn is present in the surface oxide film, changing its electrochemical properties and resulting in a thinner but more protective oxide film.

Acknowledgements

The Swiss Federal Nuclear Safety Inspectorate (ENSI), as well as the European Union's Horizon 2020 research and innovation program under the Marie Skłodowska-Curie grant agreement no. 884104 (PSI-FELLOW-III-3i) are gratefully acknowledged for their financial support. Great thanks are expressed to Hans Kottmann, Beat Baumgartner, Roger Schwenold, Elisabeth Müller (all PSI) and to our trainee Zhao-Wei Fu (NTH University, Taiwan) for their excellent experimental support.

Influence of the microstructure and surface state on the release of corrosion products from alloy 690 steam generator tubes of Pressurised Water Reactors

Nathan Ribière, Univ.Toulouse/CIRIMAT, Toulouse/France, Nathalie Engler, Daniel Brimbal, Framatome SAS, Courbevoie/France, Milan Skocic, Framatome SAS, Le Creusot/France, Eric Andrieu, Christine Blanc, Lydia Laffont, Univ.Toulouse/CIRIMAT, Toulouse/France

The release of corrosion products, specifically ^{58}Ni, from the steam generator (SG) tubes of Pressurised Water Reactors (PWRs) is responsible for a significant part of the contamination of the primary and auxiliary circuits. Indeed, in the core of the reactor, the nickel 58 (^{58}Ni) released from the nickel base alloy tubes (Inconel 690) is activated under neutron flux in cobalt 58 (^{58}Co) which is then redeposited on the surface of the circuits. This ^{58}Co contamination has important consequences on the operation of the units. To reduce this activity and hence the radiation exposure during the maintenance and associated operation costs, it is necessary to control and minimise the release.

This study focuses on two industrial SG tubes made of nickel base alloy 690. These tubes were exposed and tested in Framatome “Plateforme d’ETudE du Relâchement” (PETER) loop which reproduces the conditioning and temperature of primary coolant to determine the Ni release. In order to understand the differences in Ni release observed between the two tubes, the inner surfaces of these two as-received 690 SG tubes were studied in terms of roughness, microstructure and chemical composition. These multi-scale characterisations were performed using a stylus profilometer, a white light interferometry (WLI) microscope, SEM-EBSD, TKD-EDS, TEM as well as STEM coupled with EDS. These observations were correlated with the release kinetics and provided a better understanding of the various mechanisms implied in the release of corrosion products.

Studying the Surface Oxidation of Proton-Irradiated and Cold-Worked 304L Stainless Steel in Water at 300°C using *in-situ* Raman Spectroscopy

Vindel S. Ramsundar, Kevin Daub, Mark R. Daymond, Suraj Y. Persaud
Department of Mechanical and Materials Engineering, Queen's University,60 Union St. W, Kingston, Ontario, Canada, K7L 2N8

Several in-core components in nuclear power systems are exposed to high temperature water in the presence of radiation fields. In general, the dynamic effect of radiation and water chemistry on material performance is not well understood partly due to experimental difficulty. Thus, the evolution of metal oxides with time for irradiated materials in high temperature water remains unclear. A novel facility consisting of a high temperature and pressure corrosion loop coupled with *in-situ* Raman spectroscopy and proton irradiation has been commissioned to examine material behaviour in more realistic reactor conditions. The facility enables degradation studies of key nuclear components such as 304L stainless steel (SS) components, pressure tubes (Zr alloys) and proposed fuel cladding (Fe-Cr-Al). The main objective of this study was to evaluate the oxide chemistry and structure evolution on as-received (AR), cold-worked (CW) and proton irradiated SS 304L in water at 300°C via *in-situ* Raman spectroscopy over a 48-hour period. Results indicated that *in-situ* Raman spectroscopy was successful at detecting changes in the metal oxide chemistry and structure with time, and provides a feasible pathway for kinetic studies. The AR and 0.1 dpa SS displayed similar oxidation behaviour across all timespans, indicating that the damage imparted by protons was not sufficient to manifest a detectable change in the oxide. However, changes of the spinel structure and different oxidation kinetics with time were observed for the 3.0 dpa and CW SS, as compared to the AR. As seen in the Raman spectra of Figure 1, the intensity of the spinel peak (~700 cm^{-1}) was the greatest for the 3.0 dpa SS followed by the CW SS over the first 6 hours. However, Figure 2 shows that at 48 hours, the CW SS exhibited the highest oxidation kinetics. These findings suggest that the surface oxidation of irradiated and cold-worked SS is mechanistically different, depending on the type of damage experienced by the base metal.

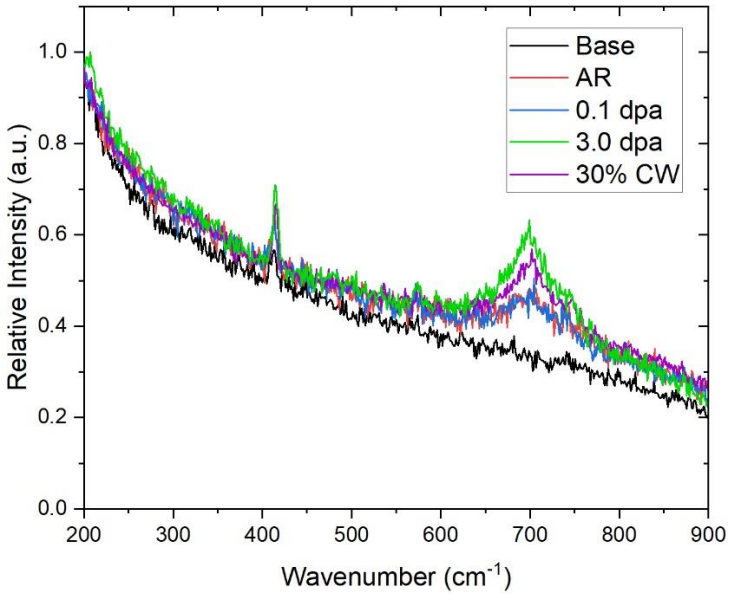

Figure 1. Raman spectra (*in-situ*) of 304L SS foils after 6-hour exposure to water at 300°C with 8 ppm dissolved oxygen

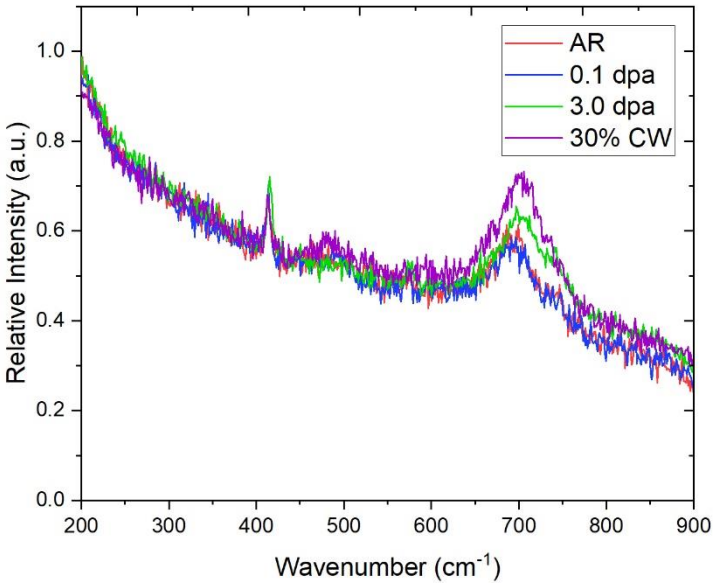

Figure 2. Raman spectra (*in-situ*) of 304L SS foils after 48-hour exposure to water at 300°C with 8 ppm dissolved oxygen

Synchrotron X-ray tomography of in-situ developed stress corrosion cracking on stainless steels

Kuo Yuan, University of Bristol, Bristol, United Kingdom

Ronald Clark, National Nuclear Laboratory, Stonehouse, United Kingdom

Mahmoud Mostafavi, University of Bristol, Bristol, United Kingdom

Nuclear corrosion, stress corrosion cracking, tomography

Spent AGR (advanced gas-cooled reactor) fuel cladding may suffer from stress corrosion cracking (SCC) while stored in cooling ponds. A micromechanical testing method has been developed to study SCC by observing with DIC (digital image correlation) on surrogate materials (thermally sensitised 304 stainless steel). Although DIC is a powerful method, it can only monitor the surface cracking. To compare the cracking behaviours in 2D with that in 3D, an X-ray tomography experiment was then proposed that can develop SCCs and track them in real time with the high intensity of the DIAD beamline at Diamond Light Source. A self-loading tensile rig (Figure 1) was designed and fabricated for the synchrotron experiment, where the load can be applied by turning a bolt on top of the rig. Both thermally sensitised cladding material (20/25/Nb) and 304 stainless steel were tested, and a heated corrosive solution (1000 $mg \cdot L^{-1}$ sodium thiosulphate solution) was circulated in small tube around the sample to accelerate the initiation of SCC. After 7 hours, SCCs successfully developed, and tomography of the specimens was taken at 30 keV. The scanned volume was then reconstructed, and the cracks studied by DVC (digital volume correlation) to identify the difference between SCCs in 3D with SCCs in 2D to infer if SCC from DIC can be representative. Additionally, the tomography of the fuel cladding material can be compared with thermally sensitised 304 stainless steel.

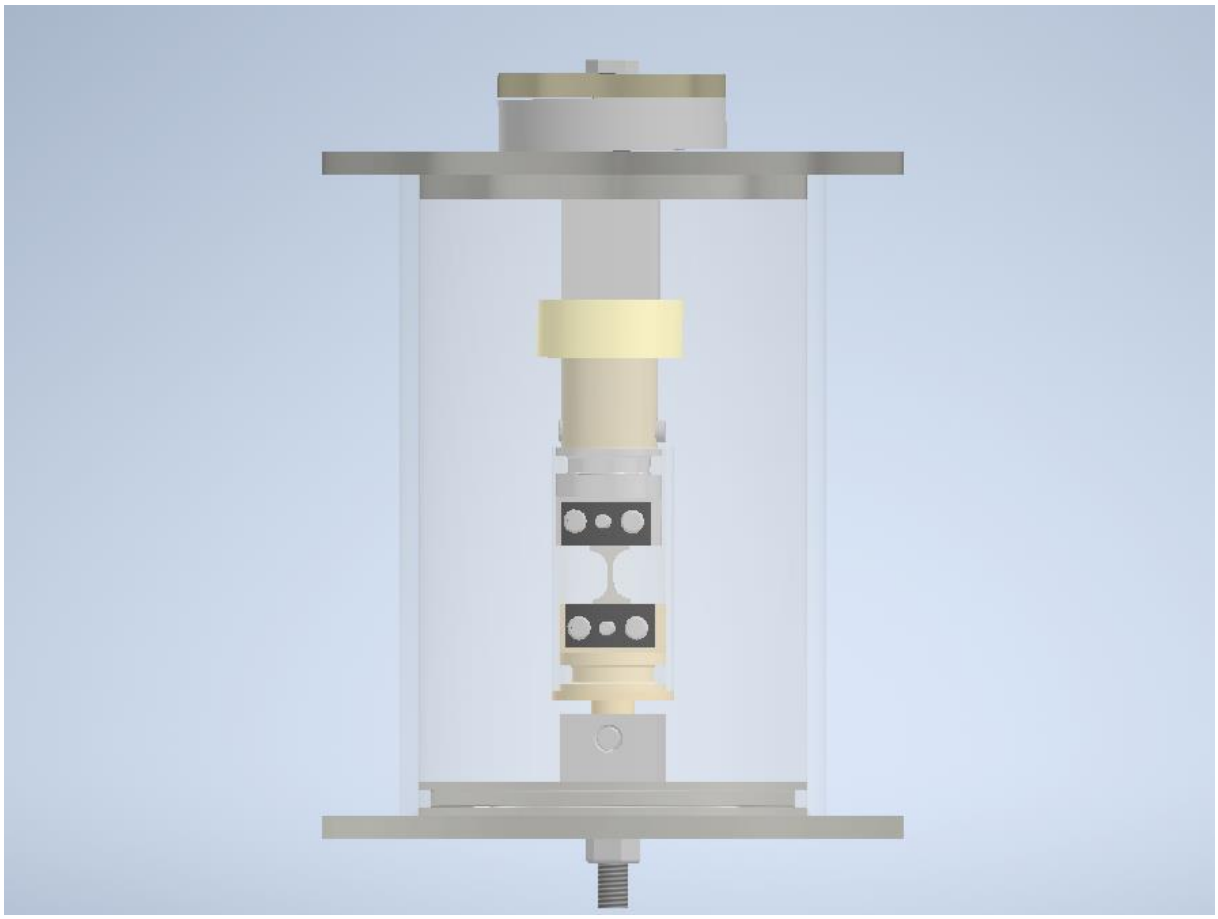

Figure 1 Tensile rig for synchrotron X-ray tomography

Corrosion of CuCrZr alloy under radiation in light water reactor-like environment

J. Lim[1], G. Was[2], G. Fulton[1], E. Prestat[1], P. Wang[2], R. Hanbury[2]

1 United Kingdom Atomic Energy Authority, Culham Science Centre, Abingdon, OX14 3DB, United Kingdom,

2 University of Michigan, Ann Arbor, Michigan, 48109-2104, United States

Subtopic – Nuclear Corrosion (WP4)

Nuclear fusion energy is one of the clean energy sources that many countries are considering in their strategy for low carbon future energy mix. Nuclear fusion reaction do not generate carbon dioxide or other greenhouse gases into the atmosphere. Its major by-product is helium gas. Nuclear fusion reactors aim not to produce high level radioactivity and long-lived nuclear waste. The recent record-breaking 59 megajoules of sustained fusion energy demonstrates potential of fusion to be part of the future energy mix at world-leading Joint European Torus facility, a Tokamak-type fusion reactor design, in Oxford, UK [https://www.euro-fusion.org/news/2022/european-researchers-achieve-fusion-energy-record/]. Like any other thermal power plant, coolant/s will be used to transfer heat energy generated from fusion reactions and converted to electrical energy.

Authors investigated the corrosion behaviour of CuCrZr alloy under DEMO & ITER proposed operating conditions. CuCrZr alloy is a selected material candidate to be used in a proposed water-cooled plasma facing and divertor component designs in a Tokamak-type fusion reactor. This study demonstrates the importance of gaining corrosion behaviour under radiation as radiation introduced radiolysis and influencing the diffusion rate of oxidation-rate dependent alloying elements or species. In this paper, corrosion behaviour of CuCrZr alloy under radiation as a function of temperature and radiation damage will be discussed. The impact of radiation on corrosion behaviour of CuCrZr alloy will also be discussed.

Electrochemical determination of thermodynamic properties of corrosion products in lead-bismuth eutectic cooled nuclear systems

Giacomo Gregori, Alexander Aerts, Jun Lim, SCK CEN The Belgian Nuclear Research Centre, Mol/Belgium; Thomas Doneux, Université Libre de Bruxelles (ULB), Brussels/Belgium

Liquid Pb and Pb-Bi eutectic alloy (LBE) are promising candidates as primary coolants for the GEN IV lead fast reactors (LFRs) and Accelerator Driven Systems (ADSs). The Belgian Nuclear Research Centre (SCK CEN) is active in the development of MYRRHA, a pilot plant for a LBE-cooled ADS. The corrosion of reactor structural steels by liquid Pb-alloys hinders their scalability for industrial applications. Corrosion products, such as Fe, Ni, Cr, and Co, released from steels in the liquid metal can react with dissolved oxygen to form solid oxide particles. These particles can cause fouling in critical flow channels in the core or the heat-exchanger, which can negatively impact the long-term safe operation of these reactors. Understanding the corrosion product chemistry in liquid Pb-alloys is thus essential for the safe and efficient operation of LFRs and ADSs.

In the present study, we designed and validated new electrochemical methodologies enabling the determination of thermodynamic properties of the steel corrosion products expected in LBE from LFR and ADS operating conditions. We developed an electrochemical method, based on the coulometric titration of oxygen, to measure the solubility product of metal oxides and the solubility limit of metal impurities in a liquid metal solvent. After dissolving a metallic element in a liquid metal close to its solubility limit, the metal solute was oxidized by adding a known amount of oxygen in the melt with a coulometric titration, performed with an electrochemical oxygen pump. By measuring and analysing the dynamic evolution of the oxygen concentration during the titration, the solubility product of the metal oxide could be determined. Combining the measured value with thermochemical data of the chemical species involved in the process, such as Sieverts' constant of oxygen and Gibbs free energy of formation of the oxide, the elemental solubility of the metallic element in the liquid could be derived as well.

In this work, we successfully validated the method by determining the solubility product of magnetite (Fe_3O_4) and the Fe solubility in LBE, in the thermal range of 723-826 K. The solubility data obtained in this study are in excellent agreement with the experimental data reported in literature (Figure a), and this method could measure for the first time the Fe solubility in LBE below 823 K. The same methodology was applied for Co: after having characterized cobalt monoxide (CoO) as the resulting oxide forming in LBE, the CoO solubility product and the Co solubility were measured down to 673 K, and further measurements at lower temperatures are still ongoing.

Our methodology, coupled with microstructural analysis, was applied to Ni shedding new light on the formation of Ni oxides and on the identification of Ni-Bi intermetallic compounds. SEM-EDX metallographies of solid Ni inserted in LBE proved the formation of $NiBi_3$ in the thermal range of 496-748 K (Figure b). Subsequently, the dissolution of a controlled amount of Ni in LBE induced the ternary equilibrium $Ni_{(LBE)}$-$NiO_{(s)}$-$NiBi_{3(s)}$. From the measurement of the equilibrium oxygen concentration, the activity of dissolved Ni was obtained in the thermal range of 566-595 K. Combining this value with thermodynamic data from literature, *i.e.* the activity of Bi and the Ni activity coefficient in LBE, the Gibbs free energy of formation of $NiBi_3$ and the Ni solubility could be derived as well.

a)

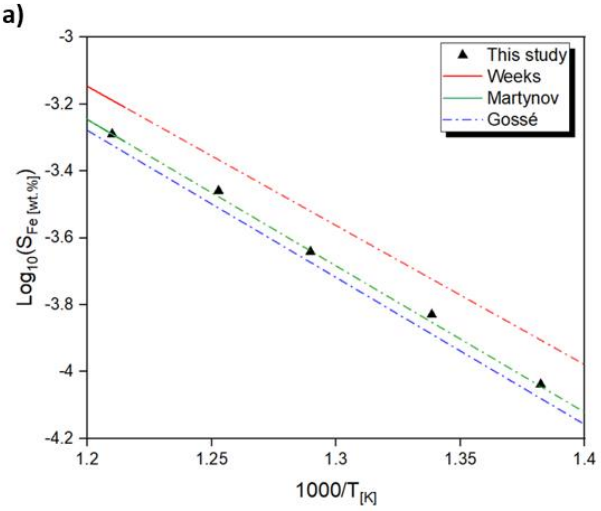

b)

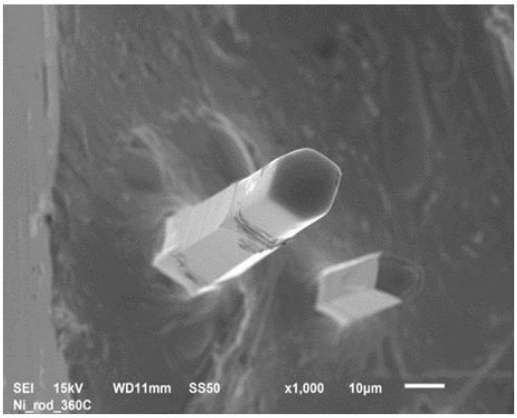

Parametric study of early stages of liquid metal corrosion of austenitic stainless steels 316L in liquid lead-bismuth eutectic (LBE)

Eloa Lopes Maia [1,2], Serguei Gavrilov[2], Valentyn Tsisar[2], Iris De Graeve[1]

[1]Vrije Universiteit Brussel (VUB), Electrochemical and Surface Engineering (SURF), Pleinlaan 2, B-1050, Brussel, Belgium

[2]SCK CEN, Boeretang 200, B-2400, Mol, Belgium

In the past years, many studies have addressed the effect of the parameters that influence liquid metal corrosion (LMC) evolution. However, knowledge of the mechanisms that occur at the early stages of the corrosion process still is not well understood, since most previous studies have focused on long-term exposure tests in order to access corrosion rates and mechanisms of corrosion propagation. Therefore, in this study the early stages of LMC of austenitic stainless steel (ASS) 316L exposed to static liquid lead-bismuth eutectic (LBE) are analyzed at 500 and 400 °C, with dissolved oxygen concentration ranging from 10^{-10} to 10^{-5} wt% in the liquid metal after short exposure (5h) to long exposures (1000h). Additionally, surface preparation (polished and ground surfaces) is also examined since previous studies have shown the relevance of this parameter but some of the findings are controversial. In general, the experimental results indicates that polished surfaces are more susceptible to corrosion degradation than ground surfaces. Furthermore, at 500 °C in static liquid LBE, the mean of corrosion depth increases with the increase of the oxygen concentration in the liquid from 10^{-10} wt% to 10^{-7} wt%. This behavior suggests that two mechanisms takes place near the surface of the solid material: first the dissolution of main elements of the ASS to the liquid LBE and second the reaction of the dissolved elements with the available oxygen. The combination of these two mechanisms results in the continuity of mass transfer in the system stimulating further dissolution of the ASS elements. Finally, as a result of testing the chosen test matrix, it is possible to observe and discuss different modes of corrosion processes, that short exposure tests provide relevant insights into the initial stages of liquid metal corrosion.

Oxidation behavior of Al-alloyed Fe-14Cr-20Ni-2Mn-3Al austenitic steel at 500 °C in static Pb with ~10^{-6} mass% dissolved oxygen for 500 h – effects of surface finishing and *pre*- and *in-situ*- applied tensile stress

Valentyn Tsisar, SCK CEN, Mol/Belgium;
Amke Lescur, University of Ghent, SCK CEN, Mol/Belgium;
Fuentes Solis Noelia, KU Leuven, SCK CEN, Mol/Belgium;
Lopes Maia Eloa, Vrije Universiteit Brussel, SCK CEN, Mol/Belgium;
Kamil Tucek, European Commission, Joint Research Centre, Petten/The Netherlands;
Peter Hähner, European Commission, Joint Research Centre, Petten/The Netherlands;
Serguei Gavrilov, SCK CEN, Mol/Belgium;
Erich Stergar, SCK CEN, Mol/Belgium;

The corrosion behavior of Al-alloyed Fe-14Cr-20Ni-2Mn-3Al austenitic steel in static Pb with ~10^{-6} mass% dissolved oxygen at 500°C for 500 h was investigated depending on the surface finishing (ground or polished) and the deformation state of the samples (reference annealed; pre-strained at 500°C in ArH_2 atmosphere up to ~0.5% of plastic strain; and in-situ strained at 500°C in liquid Pb up to ~0.5% of plastic strain). The oxidation of the samples showed a clear dependence on the type of surface finishing. A polished surface enhanced the oxidation reactivity, irrespective of the deformation state of the samples. A non-protective bi-layer scale consisting of an outer Fe-O layer and inner porous Fe-Cr-O layer was formed. The scale was prone to exfoliation along the inner oxide / steel interface. The ground surfaces showed a better oxidation resistance. Independent of the deformation state (reference, pre-strained, in-situ strained), a very thin (<1 µm) oxide film covered the surface of the samples. However, on a background of this thin oxide film, oxide nodules composed of Fe and O were observed, indicating that the local failure of the protective oxide film resulted in enhanced oxidation. The effect of the deformation state of the samples (reference annealed, pre-strained and in-situ strained) on the corrosion response was not obvious. However, a preferential oxidation of deformation bands reaching the surface during the in-situ straining of samples in liquid Pb was detected on both ground and polished surfaces. The peculiarities of the oxidation are discussed depending on the surface finishing and deformation state of the bulk and the near-surface zone of the samples.

Oxidation Kinetics of Metallic Elements in Liquid Lead Bismuth Eutectic

Daniel Stein [1,2], Jun Lim[1], Serguei Gavrilov [1], Iris De Graeve [2]

[1] SCK CEN The Belgian Nuclear Research Centre, Mol, Belgium;,

[2] Vrije Universiteit Brussel (VUB), Dept. of Materials and Chemistry, Research Group of Electrochemical and Surface Engineering, Brussels, Belgium

The MYRRHA reactor is a novel sub-critical nuclear accelerator driven system (ADS) that uses lead-bismuth eutectic (LBE) as both the spallation target and coolant. Oxygen control in lead and LBE cooled nuclear systems is essential for the safe and reliable operation of the reactor. The oxygen concentration must be kept above the level required to form iron oxide and chromium oxide which form a protective layer that inhibits corrosion, and below the concentration where PbO nucleation may occur, which could cause blockages in narrow channels of either the core or the heat exchanger in the MYRRHA reactor. To maintain the set operational constraints for the MYRRHA reactor an effective oxygen removal system needs to be developed. This study aims to identify suitable metallic elements in terms of oxidation rate and oxygen removal by conducting a comparative assessment of various metallic elements including chromium, vanadium, molybdenum, niobium, tantalum and iron at different temperatures. These pure metallic samples are submerged in LBE at a dissolved oxygen content of $2*10^{-7}$ wt%, which is around the nominal oxygen level in the LBE coolant during the operation of the MYRRHA reactor. The oxygen content is maintained at $2*10^{-7}$ wt% by an electrochemical oxygen pump which compensates for the oxygen consumed by the oxidation of the metallic element. Current tests indicate that pure iron has a significantly faster rate of oxidation at a temperature of 673K at $1.1*10^{-8}$ $kg_O*s^{-1}*m^{-2}$ compared to chromium and molybdenum at $4.0*10^{-10}$ $kg_O*s^{-1}*m^{-2}$ and $2.7*10^{-10}$ $kg_O*s^{-1}*m^{-2}$ respectively. This suggests that iron may be a suitable candidate material as an oxygen removal material in the MYRRHA reactor in the target oxygen range. While a high rate of oxygen consumption for these materials is important other factors such as the total oxygen capacity of the metallic elements and contamination of the LBE by the dispersed oxide particles needs to be considered before proposing a candidate material.

Oxidation kinetics at 450–550 °C for Steel T91 in flowing lead–bismuth eutectic (2 m/s, 10^{-6} % oxygen)

Carsten Schroer, Aleksandr Skrypnik, Olaf Wedemeyer, Karlsruhe Institute of Technology (KIT), Eggenstein-Leopoldshafen, Germany; Valentyn Tsisar, Belgian Nuclear Research Centre (SCK•CEN), Mol, Belgium.

Nuclear Corrosion (WP4)

Proving the compatibility of steels with liquid lead (Pb) alloys has gained in importance especially with the development of fast-neutron or accelerator-driven nuclear reactors. Steel generally dissolves in such liquids, which will be significantly delayed if the solid surface is covered by an oxide scale. While pure Pb or the lead–bismuth eutectic (LBE) allow oxygen to be added to the liquid in order to stabilise such a protective scale, the functionality of plant components designed for heat transfer tends to degrade with oxide growth, i.e., the thickness must be controlled.

Oxygen dissolved in LBE generally makes ferritic/martensitic steel with 9 % chromium (Cr) form a triple-layer oxide scale consisting of an internal oxidation zone (IOZ) in the steel, followed by iron (Fe)–Cr mixed oxide and almost pure Fe oxide (magnetite) at the interface with the liquid metal. While the mixed-oxide seems always present, the IOZ and the magnetite top layer may be absent at relatively low (450 °C) and high temperature (550 °C), respectively. The absence of magnetite at 550 °C is especially observed in flowing LBE.

Kinetic data for oxidation of the steel T91 in flowing LBE (450 °C and 550 °C; 2 m/s; 10^{-6} % dissolved oxygen) is supplemented by recent results from respective experiments at 500 °C. Metallography reveals an oxide scale that is intermediate between the observations at 450 and 550 °C. Analogous to 450 and 550 °C, metal recession in connection with oxidation is reflected by a parabolic rate law. The apparent activation energy (450–550 °C) is 83 kJ/mol. The comparison with 133 kJ/mol (400–550 °C) observed earlier for flowing LBE with ~10^{-7} % oxygen suggests decreasing activation energy with increasing oxygen concentration. The findings will be combined into a predictive equation for consumption of T91 by oxidation in flowing LBE, considering that steady parabolic behaviour may need some time to establish. Feasibility and limitations of including the thickness of oxide layers or transfer of steel elements onto the liquid metal will be outlined.

Active / passive zones on carbon steel in contact with argillites fragment and specific cement grout designed for radioactive waste repository

M. Robineau [a,b], *V. Maillot* [b], *D. Crusset* [b], *M. Jeannin* [a], *Ph. Refait* [a]
[a] *Laboratoire des Sciences de l'Ingénieur pour l'Environnement (LaSIE), UMR 7356 CNRS-Univ. La Rochelle, Bât. Marie Curie, Av. Michel Crépeau, F-17042 La Rochelle cedex 01, France.*
[b] *Andra, Parc de la Croix Blanche, 1/7 rue Jean Monnet, F-92298 Châtenay-Malabry, France.*

In France, it is planned to bury the high-level and intermediate-level radioactive waste packages in an underground site, at a depth of 500 meters corresponding to a Callovo-Oxfordian argillite layer. This stable claystone layer is 145 m thick and has a very low permeability. Within claystone, it is planned to dig galleries and to insert steel casing inside them. The casing will allow the reversibility of the storage as planned in the French program. In this project, a specific cement grout will be injected between the carbon steel casing and the argillite. Despite tunnel cleaning, fragments of argillite will remain in contact with the carbon steel casing. Thus, small zones of the steel surface in contact with argillite should be surrounded by large zones in contact with cement grout. In argillite environment, the various corrosion products can form from steel such as magnetite, siderite, chukanovite, iron silicates and mackinawite [1-5]. In presence of the specific cement grout, iron sulphides (mackinawite and greigite) were mainly identified, together with magnetite [6]. The system constituted by steel areas covered with argillite and steel areas covered with cement grout may favour corrosion cells as it involves heterogeneous corrosion product layers containing various electronic conductors (magnetite and iron sulphides) likely to act as cathodic sites [7,8].

The present study focuses on the behaviour of carbon steel in an aerated solution to simulate the corrosion system just after injection of the grout. For that, a bi-electrode was used, with one zone in contact with an argillite fragment and the second zone in contact with the cement grout. Experimental conditions close to those encountered in the radioactive waste storage environment for 112 days (55 days at 25°C and 57 days at 80°C) were considered. The corrosion processes of each zone of the electrode were studied using various electrochemical methods (voltammetry, linear polarisation resistance measurements) while mixed potential and galvanic current measurements were carried out to investigate possible galvanic effects between the two zones of the bi-electrode.

At the end of the experiment, visual observations revealed the presence of localized corrosion on the zone located under the argillite fragment. In the one hand, the mixed potential measurements showed that the zone covered with argillite was the anode, which led to the formation of a layer of corrosion products at 25°C. The increasing of temperature at 80°C causes an inversion polarity and the zone in contact with the cement grout becomes the anode. On the other hand, the galvanic current measurements between the two zones showed that the intensity of the coupling decreased over time due to the formation of a layer of corrosion products on the surface of both zones of the bi-electrode. µ-Raman spectroscopy analysis revealed that the corrosion product layers were mainly composed of mackinawite and magnetite. These results confirm the risk of localised corrosion processes associated with galvanic coupling, in aerated conditions, between areas covered with fragments of argillite (active zones) and areas covered with cement grout (passive zones).

[1] A. Romaine, M. Jeannin, R. Sabot, S. Necib, P. Refait, Electrochimica Acta, 182 (2015) 1019-1028.
[2] A. Romaine, R. Sabot, M. Jeannin, S. Necib, P. Refait, Electrochimica Acta, 114 (2013) 152-158.
[3] S. Necib, Y. Linard, D. Crusset, N. Michau, S. Daumas, E. Burger, A. Romaine, M.L. Schlegel, Corrosion Science, 111 (2016) 242-258.
[4] M.L. Schlegel, C. Bataillon, C. Blanc, D. Prêt, E. Foy, Environmental Science & Technology, 44 (2010) 1503-1508.
[5] M.L. Schlegel, C. Bataillon, F. Brucker, C. Blanc, D. Prêt, E. Foy, M. Chorro, Applied Geochemistry, 51 (2014) 1-14.
[6] M. Robineau, V. Deydier, D. Crusset, A. Bellefleur, D. Neff, E. Vega, R. Sabot, M. Jeannin, P. Refait, Materials, 14 (2021) 3563.
[7] M. Robineau, A. Romaine, R. Sabot, M. Jeannin, V. Deydier, S. Necib, P. Refait, Electrochimica Acta, 255 (2017) 274-285.
[8] M. Robineau, R. Sabot, M. Jeannin, V. Deydier, D. Crusset, P. Refait, Materials and Corrosion, 72 (2021) 194-210.

Interaction between carbon steel and low-pH bentonitic cement grout in anoxic and heterogeneous conditions at 80°C.

J. Goethals[1], C. Wittebroodt[2], L. De Windt[3], C. A. Abdelouas[1], X. de la Bernardie[1], Y. Morizet[4], B. Zajec[5] and V. Detilleux[6]

[1] Laboratoire Subatech, UMR 6457, Nantes, France

[2] Institute of Radiation Protection and Nuclear Safety (IRSN)/LETIS, BP 17, Fontenay-aux-Roses, France

[3] Mines Paris, PSL University, Centre for Geosciences, 77300 Fontainebleau, France

[4] Laboratoire de Planétologie et de Géosciences (LPG) UMR 6112, Nantes, France

[5]Slovenian National Building and Civil Engineering Institute (ZAG), Ljubljana, Slovenia

[6] BEL V, Anderlecht, Belgium

The French multi-barrier concept for deep geological disposal of high level nuclear waste (HLW) implies large amounts of metallic elements. With such a concept, HLW stainless-steel primary canister would be encapsulated into cylindrical carbon steel overpack and inserted in a carbon steel casing tube within an horizontal micro-tunnel drilled in clay rock. A low pH bentonitic cement-based grout material (pH ≈ 11) would be injected between the steel casing and the host rock in order to (i) neutralize the acidity coming from pyrite oxidation in the clay rock (ii) limit oxygen diffusion and microbial activity and (iii) passivate the steel casing surface [1,2]. In this context, the BACUCE in situ experiments have been designed in the Tournemire underground research laboratory (IRSN, France) to investigate the impact of microbial activity and temperature (80°C) on the anoxic corrosion of steel in contact with such cement grout and/or in presence of spatial heterogeneity (imperfect contact between steel and cement grout) filled by synthetic porewater solution. The present study is based on results coming from the laboratory BACUCE mock-up experiments [3] that have been performed in parallel to these field experiments to better constraint the processes that would occur *in situ*.

In this study, the effect of the surface treatment of steel and the feedback effect of porewater and cement grout evolution on corrosion were also assessed. The steel at contact with cement grout suffered from localized corrosion, particularly at the surface

presenting a mill-scale layer, with pits measuring up to 160 µm within one year of interaction. SEM, XRD and µ-Raman spectroscopy analyses allowed a full characterization of the corrosion sequence. First, the initiation of localized corrosion process is mainly due to the presence of HS^- and residual oxygen, which favor the formation of corrosion cells by producing FeS/FeO(OH) in anodic area and by reducing water/O_2 at the cathodic ones. The formation of magnetite is then favored when the concentration of HS^- drops. Then, formation of iron silicate and of iron sulphides occurred simultaneously, due to the release of silicon from the hydrated silica fume contained in the cement grout and to the diffusion of sulphides aqueous species inside the cement grout. Geochemical simulations support these experimental findings. Eventually, a drop in the mean corrosion rate, as well as a limiting pit depth, are depicted after approximately 250 days of interaction, which is associated to the formation of a protective layer of corrosion products that could limit the ingress of aggressive species from the grout.

Research funding by the ACED/EURAD European Union's H2020 program under grant agreement No 847593 is gratefully acknowledged.

[1] M. Robineau, A. Romaine, R. Sabot, M. Jeannin, V. Deydier, S. Necib, P. Refait, Galvanic corrosion of carbon steel in anoxic conditions at 80 °C associated with a heterogeneous magnetite (Fe3O4)/mackinawite (FeS) layer, Electrochim. Acta. 255 (2017) 274–285. https://doi.org/10.1016/j.electacta.2017.09.183.

[2] J. Bonnet, R. Mosser-Ruck, J. Sterpenich, F. Bourdelle, H. Verron, N. Michau, X. Bourbon, Y. Linard, Chemical and mineralogical characterizations of a low-pH cementitious material designed for the disposal cell of the high-level radioactive waste (HLW), Cem. Concr. Res. 162 (2022) 107013. https://doi.org/10.1016/j.cemconres.2022.107013.

[3] J. Goethals, L. De Windt, C. Wittebroodt, A. Abdelouas, X. de la Bernardie, Y. Morizet, B. Zajec, V. Detilleux, Interaction between carbon steel and low-pH bentonitic cement grout in anoxic, high temperature (80 °C) and spatially heterogeneous conditions, Corros. Sci. 211 (2023) 110852. https://doi.org/10.1016/j.corsci.2022.110852.

Influence of radiation on the passivation of carbon steel in simulated cement porewater solution

James Hesketh[1], Andy Rance[1], Paul Fennell[1], Nick Smart[1], Bharti Reddy[1], Roberto Gaggiano[2], Cristiano Padovani[1]

[1]Jacobs, United Kingdom

[2]Ondraf/Niras, Belgium

The Belgian Agency for Radioactive Waste and Enriched Fissile Materials (ONDRAF/NIRAS) is considering the supercontainer concept as a reference case for the disposal of spent fuel and high level radioactive waste in Belgium. The concept includes a carbon steel overpack, encased in a cementitious buffer and surrounded by a stainless steel envelope, which will be placed in a deep geological disposal facility in a Clay host rock. The overpack's role is to provide primary containment of radionuclides for at least the duration of the thermal phase, after which it is expected that the host rock will provide containment if the overpack has been breached.

To meet the design requirement, the overpack must corrode slowly and predictably, and must exhibit only uniform corrosion for the necessary duration. The presence of the highly alkaline (pH >13) cementitious buffer in an oxygen-free environment leads to passivation of the carbon steel and extremely low corrosion rates. In this environment, pitting is not expected due to the absence of oxidants and low levels of aggressive species such as chlorides and sulphides. Previous long-term corrosion testing has demonstrated the absence of localised corrosion and the presence of passive conditions in simulated porewater solutions over the course of decades. However, a full understanding of the mechanistic processes behind the formation and growth of the passive film is needed to be confident in the corrosion resistance of the steel for even longer periods of time. A key factor in this is the influence of radiation, which is present with an initial dose rate of up to 25 Gy hr^{-1} at the external wall of the overpack and is expected to influence the redox potential for several hundred years.

In this study, carbon steel was exposed to simulated cement porewater to simulate the aqueous phase in the repository. The specimens were tested in the presence and absence of gamma radiation and were analysed after different periods of exposure, between 100 and 10,000 hours, to determine the composition and morphology of the

corrosion product. The results demonstrate the influence of gamma radiation at a dose rate of up to 25 Gy hr^{-1} on the corrosion rate and corrosion rate evolution during early exposure, as well as the influence of radiation on the chemistry of the corrosion product during its initial formation and subsequent growth. These findings are discussed in relation to the anticipated long-term performance of carbon steel as the overpack material in the Belgian supercontainer concept during the deep geological disposal of radioactive waste, and the impact of radiation in corrosion performance assessment.

Influence of the incorporation of ceramic particles in ZnAl Cold Spray coatings on the protection of carbon steel in conditions simulating the deep geological disposal of radioactive waste

A. Martin [a], *V. Maillot* [b], *G. Charrier* [b], *D. Crusset* [b], *F. Gouraud* [c], *C. Verdy* [d], *R. Sabot* [a], *J. Creus* [a], *Ph. Refait* [a]

[a] *Laboratoire des Sciences de l'Ingénieur pour l'Environnement (LaSIE), UMR 7356 CNRS- La Rochelle Université, Av. Michel Crépeau, F-17042 La Rochelle cedex 01, France.*

[b] *Andra, Parc de la Croix Blanche, 1/7 rue Jean Monnet, F-92298 Châtenay-Malabry, France.*

[c] *CITRA, 16 rue Atlantis, Parc ESTER Technopole, F-87068 Limoges, France*

[d] *ICB-PMDM-LERMPS UMR 6303, CNRS, UTBM, Université De Bourgogne Franche-Comté, Belfort, 90010, France*

For high-level and intermediate-level long-lived radioactive waste, the French National Radioactive Waste Management Agency (Andra) is currently developing a 500 m deep geological disposal site, called Cigeo. The vitrified waste in its stainless-steel container will be set in a carbon steel overpack that will be sled inside a carbon steel casing inserted inside the ~horizontal tunnels drilled in stiff clay formation. A specific cement grout (pH > 10) will be injected between the carbon steel casing and the claystone. Due to the radioactivity, a temperature of 50°C is expected at the overpack surface.

A sacrificial coating is envisaged as an additional protection for the carbon steel overpacks. A previous corrosion study, performed in conditions simulating the storage, had shown that ZnAl coatings (with 15 wt. % Al) were more efficient than pure Zn or Al coatings. Unfortunately, electrolyte infiltration occurred and induced oxidation of the boundaries of the particles that composed the coating. To mitigate this phenomenon, the addition of ceramics particles was considered. First, alumina particles were added to the ZnAl15wt% coating. Then, to improve the cohesion of the particles in the coating, heavy ceramic particles were tested (TaC and WC). The composite coatings behaviour was first investigated using voltammetry. Then, the sacrificial properties of the coatings were investigated through 2 extended immersion experiments: immersion of coated samples and immersion of coated samples with a cross defect. OCP, linear polarisation resistance and electrochemical impedance spectroscopy measurements were carried

out to characterize the evolution over time of the samples. After experiments, the corrosion product layers covering the samples were characterized by XRD, SEM-EDS and μ-Raman spectroscopy. The addition of heavy particles led to an improvement of the cohesion in the ZnAl coatings.

Penetration of corrosive species along grain boundaries of copper explored by SIMS-based techniques

Xiaoqi Yue, KTH Royal Institute of Technology, Stockholm, Sweden; Per Malmberg, and Elias Ranjbari, Chalmers University of Technology, Gothenburg, Sweden; Vilma Ratia-Hanby and Elina Huttunen-Saarivirta, VTT, Espoo, Finland;

Jinshan Pan and Christofer Leygraf, KTH Royal Institute of Technology, Stockholm, Sweden;

According to the nuclear waste disposal concept in Sweden and Finland, copper is regarded as the candidate material for use as canister during long-term storage of nuclear waste. A possible scenario that needs to be thoroughly understood is that groundwater may come in direct contact with the copper canister. The groundwater contains corrosive species, such as Cl^- and SO_4^{2-} -ions, and also HS^- -ions from microbiological activity near the canister.

A study has recently been initiated in which copper was exposed to simulated groundwater at room temperature and 60 ^oC, and the penetration of corrosive species containing S, O and Cl investigated with time-of-flight secondary ion mass spectrometry (ToF-SIMS). The study provides clear evidence that corrosive species penetrate significantly into the copper microstructure (1). The penetration occurs locally along certain fast pathways, most likely grain boundaries. After four months of exposure at 60 ^oC, S penetrates around 500 nm along these fast pathways.

To provide further evidence for the possible penetration of corrosive species along grain boundaries of copper, complementary nano-scale resolution investigations are currently underway. For this, copper samples have been prepared through FIB-cutting and investigated with nano-SIMS, to obtain chemical information (including H-distribution) at higher lateral resolution than with ToF-SIMS, and transmission electron microscopy (TEM), to reveal the grain boundary microstructure.

In all, this effort seeks to understand the mechanism of penetration of corrosive species containing S, O, Cl and H, and its possible implications on S-induced stress corrosion cracking (SCC) and H-induced embrittlement of the copper canister. Selected results from these investigations will be presented herein.

References:

1. X. Yue et al, Corrosion Science, 210 (2023) 110833

Risk of microbiologically induced pitting corrosion of 316L stainless steel in DGR environment

Richard Bureš[1], Veronika Hlaváčková[2], David Dobrev[3], Tomáš Basl[1], Jan Stoulil[1]

[1]University of Chemistry and Technology, Prague/Czech Republic;

[2]Technical University, Liberec/Czech Republic

[3]ÚJV a.s., Řež/Czech Republic

This work is focused on synergistic effect of sulphate reducing bacteria (SRB) and radiolysis in deep geological repository (DGR) for spent nuclear fuel. Products of reaction are thiosulphates, which can locally dissolve passive layer on stainless steel surface and cause pitting corrosion. This kind of corrosion is problematically predictable and therefore represents high risk in material lifetime. Stainless steel samples were exposed in synthetic pore bentonite solution and in slurry with Czech bentonite BCV. Different conditions of exposure were tested - temperature up to 50°C, concentration of sulfides up to 1 mmol/l and thiosulphates up to 30 mmol/l, irradiation with ^{60}Co source under dose rate 1 Gy/h. A long term exposure tests were performed. According to gravimetry is corrosion velocity negligible, but the observation shows local breakdown of passive layer. This corrosion defects are formed after exposure with increased temperature even at low thiosulphates concentrations. Defects can be repasivated or continuously start pit propagation. Hence low pH of occluded solution probably facilitates pit propagation, meanwhile thiosulphates deteriorate passive layer. The results show that the risk of pitting corrosion in DGR environment with SRB is evident and mechanism of pit propagation needs further investigation.

Lifetime of stainless steel inner case of canister for DGR

Jan Stoulil, Richard Bureš, University of Chemistry and Technology, Prague/Czech Republic

David Dobrev, Nuclear Research Institute, Rez/Czech Republic

The canister inner case guarantees the main portion of planned lifetime 10^6 years. Electrochemical potentiostatic measurements of 316L stainless steel in deaerated bentonite slurry in the irradiation facility with Co^{60} source and 1 Gy/h dose rate showed very quick reaching of steady state dissolution, which is extremely negligible. Parallel experiments of stainless steel natural dissolution in pore solution showed much slower unforced dissolution and the time necessary for reaching steady state is much longer. Nevertheless, simulations show the inner case lifetime is sufficient to assure required insulation of SNF.

Oxidation of a Pu alloy stabilized in δ–phase: study of Ga alloying element behavior

B. Ravat [1], L. Jolly [1], N. Favart [1], D. Menut [2], B. Oudot [1], F. Delaunay [1], I. Popa [3]

[1]CEA centre de Valduc, 21120 Is-sur-Tille, France
[2] Synchrotron SOLEIL, Ligne de lumière MARS, L'Orme des Merisiers, Saint Aubin – BP 48, 91192 Gif-sur-Yvette, France
[3] ICB UMP 6303 CNRS Univ. Bourgogne Franche-Comté, 9 avenue Savary, 21078 Dijon, France

Introduction

Understanding Plutonium alloy oxidation related to safe and long term storage is essential. Therefore, many studies deal with the reactivity of highly metastable δ-Pu alloy under controlled dry oxygen atmosphere at different temperatures and pressures [1-2].

Oxidation at high temperature under oxygen atmosphere of PuGa alloys leads to the formation of an oxide scale composed by an outer layer of PuO_2 and an inner layer of Pu_2O_3. Furthermore, oxidation leads to a surprising destabilization of the δ phase suggesting that it also modifies the structure of the alloy.

But the precise role played by Ga alloying element during oxidation is not really understood. Does it diffuse out of the oxide scale to be oxidized instead of plutonium atoms limiting the formation of the plutonium oxide scale? Does it stay in the oxide scale and where? Although significant experimental and theoretical results [3-5] were recently published about this topic, several questions remain unanswered.

Experiment and analysis

Thus, the purpose of this work [6] is to bring new insights into Ga behaviour during the oxidation process of δ-Pu alloy. The originality of this study lies in

the combination of GIEXAFS (Grazing Incidence Extended X-ray Absorption Fine structure) experiments performed at SOLEIL synchrotron coupled with EXAFS data analysis using a RMC (Reverse Monte Carlo) method [7] which is an atomistic simulation technique allowing to reconstruct the 3D atomic structure of by minimizing differences between experimental and simulated EXAFS spectra.

Results

The results have highlighted the presence of Ga in the Pu oxide scale. However, no formation of Ga aggregates or Ga oxides was detected. Actually, the RMC analysis of experimental data has evidenced the presence of Ga atoms within the PuO_2 lattice. More precisely, the results showed that Ga atoms may occupy Pu substitutional site or octahedral site. Nevertheless, this incorporation leads to a large local disorder with displacement of Ga atoms from their initial high symmetry crystallographic site. A noteworthy agreement is obtained by DFT calculations when incorporating Ga in Pu substitutional site in PuO_2 lattice. Thus, the calculations highlight that the diffusion of Ga atoms into Pu vacancies in PuO_2 lattice is likely to be the main process responsible for the δ–phase destabilization during oxidation.

References

[1] Stakebake et al., Journal of Less Common Metals, 136(1988) 349-366.
[2] Ravat et al., Corrosion Science, 138 (2018) 66-74.
[3] Donald et al., Corrosion Science, 194 (2022) 109923.
[4] Hernandez et al., Journal of Physical Chemistry, C 120 (2016) 13095 − 13102.
[5] Ao et al., Computational Materials Science 122 (2016) 263 − 271.
[6] Ravat et al., submitted to Corrosion Science (2023).
[7] Timoshenko et al., J. Phys.: Condens. Matter 26 (2014) 055401.

Optimizing pickling procedure to maximize corrosion resistance of stainless steel

Václav Šefl, Mehrdad Zia Hoseinpoor, Kateryna Popova, Tomáš Prošek

Technopark Kralupy of the University of Chemistry and Technology Prague, Kralupy nad Vltavou, Czech Republic

Acid pickling is a chemical process that is used to produce a passive surface film that protects stainless steel by removing iron oxides and enriching the surface with chromium. However, several pickling bath compositions can be found in both standards and research papers, with insufficiently systematic evaluation of the process result, that is, the actual corrosion resistance.

The goal of this paper is to identify key parameters of pickling baths and their effect on the resistance of various grades of stainless steel in corrosive environments. Commonly used mixtures containing between 10 and 25 wt. % HNO_3 and from 2 to 5 wt. % HF are highly aggressive, as shown by an internally developed real-time corrosion monitoring CorrSen system with AISI 304 and 316 sensors. Up to 200 and 25 $g/m^2 \cdot$day of metal is dissolved in a relatively mild mixture of 10 wt. HNO_3 and 2 wt. % HF during picking of AISI 304 and AISI 316, respectively. After just 3 days of pickling in such a bath, the effectivity of the metal removal dropped by nearly 25 % for both materials. Obviously, the pickling time can be optimized to obtain maximal corrosion resistance and minimal material loss. It has been shown that low-frequency electrochemical impedance spectroscopy (EIS) provides useful data for identification of the optimal time delay in a pickling bath. Prolonged pickling results only in material loss with diminishing returns in terms of corrosion resistance. These findings were supported by measurements of the pitting and repassivation potential. The effect of bath parameters such as the initial composition, the level of saturation with Cr, Fe, and Ni, the temperature, and subsequent autopassivation were studied.

The outcome of the study was demonstrated on as-received samples, thermally treated samples simulating welding, and samples exposed to high temperature water simulating the secondary cooling loop using CorrSen sensors and metallic coupons. The paper demonstrates that the new on-line monitoring method can be used for both research and production control. Several examples of efficient pickling procedures are also given.

Damage and Liquid Metal Embrittlement sensibility of a FeCrMnNi alloy in presence of liquid lead-bismuth eutectic

Jorge SALGADO GIAMPAOLI[1], Ingrid PRORIOL SERRE[1], Manon BONVALET ROLLAND[1], Franck BECLIN[1], Anna FRACZKIEWICZ[2]

[1] *Univ. Lille, CNRS, INRAE, Centrale Lille, UMR 8207—UMET—Unité Matériaux Et Transformations, 59 000 Lille, France*

[2] *Mines Saint-Etienne, Univ Lyon, CNRS, UMR 5307 LGF, Centre SMS, 42023 Saint-Etienne, France*

The accelerator driven system and the lead cold fast reactor use liquid lead or lead-bismuth eutectic (LBE) as coolant. One of the main challenges in the development of such reactors is to find appropriate structural materials. Several factors must be taken into account when selecting these materials. Especially the exposure of the structural materials to irradiation, at high temperatures and so the presence of the liquid metal need to be investigated. It includes the analyze of the corrosion resistance and of the modification of the mechanical properties in the presence of liquid metal. A recurring phenomenon in ductile metals is premature fracture in contact with liquid metal, a phenomenon called Liquid Metal Embrittlement (LME). Different studies have analyzed the behavior of steels in contact with liquid lead or liquid LBE at temperatures between 250 and 550 °C. The results show that martensitic and ferritic steels with body centered cubic (BCC) structure present LME between 250 and 450 °C. Then, the best candidates appear to be austenitic materials with face centered cubic (FCC) structure, such as 316L and 15-15Ti because they only present a slight LME at higher temperatures (above 450°C) because of their high ductility. But the austenitic steels are very sensitive to corrosion by Pb and LBE, especially because of the selective dissolution of Ni. Therefore, high entropy alloys or complex composition alloys with a FCC structure, are expected to obtain better corrosion resistance and mechanical characteristics, thanks to their variety of elements and their high concentration, and so their crystallographic structure.

In this communication, the mechanical behavior in presence of LBE of the FCC alloy Y3 FeCr15Mn17Ni22 at.% will be presented. Tensile tests in air and in liquid LBE saturated in oxygen at 300°C, 400°C and 500°C have been carried out at 5.10^{-5} s^{-1}. After the tests, the fracture surfaces and cross sections of the fractured specimens

have been observed employing SEM (scanning electron microscopy) and EDX-SEM (energy dispersive X-ray) to analyze the effects of LBE on the fracture mode, the microstructure and the cracking. In addition, SEM-EBSD (Electron Backscatter Diffraction) allowed analyzing the phases present in the material before and after tests as well as determining the path of cracking.

The material presents whatever the temperature a ductile behavior and ductile fracture at air. The presence of LBE induces no modification of the first part of the tensile curves but a premature fracture. But the material presents a LME sensitivity at all the studied temperatures. A brittle intergranular fracture surface was observed at 400 °C and 500°C and mixed fracture mode at 300°C: a brittle fracture with some small area of ductile fractures with the presence of dimples. Liquid LBE induces intergranular propagation of surface cracks. Moreover, the loss of Mn and Ni was observed with the presence of Fe-Cr particles in the cracks after tests performed in liquid metal.

In conclusion, the FCC material presents LME sensitivity at all the studied temperatures. The highest temperature promotes the LME sensitivity. The liquid metal induces intergranular cracking with the dissolution of Ni and Mn. The LME due to an effect at grain boundaries accompanied by the loss of Ni and Mn could be explained by modeling approach based to thermodynamic-based calculations.

Comprehension of the corrosion of alumina-forming alloy in molten NaCl-$MgCl_2$

L.Pellicot[a, b], L.Martinelli[b], N.Gruet[b], R.Malacarne[b], J.Serp[c]

[a] *Université Paris Sorbonne, Chimie Physique et Chimie Analytique de Paris-Centre (ED-388)*

[b] *Universite Paris-Saclay, CEA, Service de la Corrosion et du Comportement des Materiaux dans leur Environnement, 91190, Gif-sur-Yvette, France*

[c] *CEA, DES, ISEC, DMRC, University of Montpellier, Marcoule, 30207 Bagnols sur Ceze, France*

The molten salt reactor (MSR) is a next-generation reactor design in which the coolant is a molten salt. CEA Saclay is currently studying a MSR that would use NaCl-$MgCl_2$-$PuCl_3$ as a fuel. The salt is both the coolant and the fuel as it contains $PuCl_3$ and possibly UCl_3. This allows renewing the fuel without stopping the plant by changing batches of salt. Moreover, it makes the plant safer as the reactivity coefficient is negative. Indeed, if there is an excess of reactivity, temperature increases and the salt dilates, which increases the distance between plutonium atoms, and reduces the reactivity. The reactor is then self-regulating.

However, NaCl-$MgCl_2$ is a very corrosive medium due to the presence of dissolved impurities as oxide ions, water, oxygen and chlorine in the salt. These impurities are mainly due to its reactivity with oxygen and moisture. Hitherto, no conventional nuclear alloy meets the requirements to make the construction of a MSR possible. This is due to the high chromium and iron solubility limits in the chloride salt. The objectives of this study is to evaluate the resistance of alumina-forming alloy in NaCl-$MgCl_2$ since Al_2O_3 is known to dissolve more slowly than chromium or iron oxides in this medium.

Two Alumina Forming Austenitic (AFA) alloys developed by ORNL have been studied. The compositions of the two alloys are very close and are given in table below:

%wt	Ni	Cr	**Al**	W	Mo	Nb	Si	Mn	Fe
OCL	20	14	**3**	1	2	2.5	0.14	2	Bal.
OC4	25	14	**3.5**	1	2	2.5	0.14	2	Bal.

Two preoxidizing treatments were performed for each alloy. Then samples were immersed at 600°C for 7 days or 21 days in NaCl-$MgCl_2$ purified by electrolyzes. In

order to evaluate the efficiency of cathodic protection on the corrosion rate of the steels, redox potential in the OC 4 salt has been fixed by the $Mg°/Mg^{2+}$ couple. This was achieved by adding Mg° in the solution during the electrolysis.

Results showed that OC4 alloy did not lose mass revealing the very good efficiency of the cathodic protection. On the contrary, OCL preoxidized 4h at 750°C showed a 2µm internal corrosion depth in average after 7 days and a 10µm internal corrosion depth after 21 days. In both cases, a preferential dissolution of chromium and iron occurs. A spinel oxide $MgAl_2O_4$ was also observed nearby the surface of each sample. This could be the result of the reaction between Al_2O_3 at the sample surface and MgO dissolved in the salt. The EDS maps also shown that Nb and Mo did not dissolved.

At the end of the 21 days immersion, the OCL series 2 salts were analyzed by cyclic voltammetry and showed the presence of two peaks that are characteristic of the Cr/Cr^{2+} and Fe/Fe^{2+} couples attesting the selective dissolution as shown by Figure 1. On the contrary, OC4 salts did not show any changes.

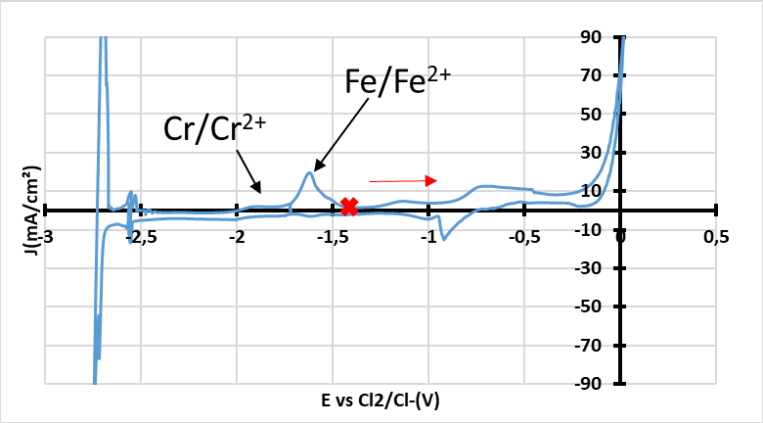

WE and CE : W
Ref : Ag/AgCl
Scan speed : 100mV/s
Eoc= -1.44V

Figure 1 : cyclic voltamogram of NaCl-$MgCl_2$ after 21 days of OCL immersion at 600°C

These immersion tests show that molten chloride salts less corrode OC4 and OCL than other steels that do not contain aluminum. For instance, corrosion depth of Inconel 625 or Hastelloy X and Hastelloy B3 can be of 10 to 20 µm after 5 days in NaCl-$CaCl_2$-$MgCl_2$ [1]. A corrosion mechanism has been built in order to understand the behavior of OCL and OC 4 alloys in liquid NaCl-$MgCl_2$ salt. Cathodic protection as shown its efficiency as expected. These results are promising and show that alumina-forming alloy are materials of interest in the perspective of building a MSR.

[1] B. Liu, X. Wei, W. Wang, J. Lu, et J. Ding, « Corrosion behavior of Ni-based alloys in molten NaCl-CaCl 2 -MgCl 2 eutectic salt for concentrating solar power », *Sol. Energy Mater. Sol. Cells*, vol. 170, p. 77-86, oct. 2017, doi: 10.1016/j.solmat.2017.05.050.

Corrosion rate of Ni and Fe based alloys in molten NaCl-$MgCl_2$ salt

Seong Sik Hwang, Dae Jong Kim, Chang Hwa Lee, Gyeong Hoi Koo

Korea Atomic Energy Research Institute, 989-111 Daedeok-daero,Yuseong, Daejeon, 34057, Korea

Abstract

MSR (Molten salt reactor), which is being developed by more than 15 research institutes around the world, such as ORNL in the US, is known to be more advantageous than conventional large-scale PWR reactors in terms of miniaturization, safety, and economy. Unlike fluorine salt, structural material corrosion studies on chloride-based molten salt reactors are very few worldwide. In this paper, we will discuss the research status of candidate materials for molten salt reactors, corrosion factors of molten salt reactor materials, methods for controlling impurities, methods for reducing electrochemical potential, and methods for increasing corrosion resistance by cladding. Corrosion test results in chloride salts for several candidate materials that can be used in molten salt reactors are introduced. As is known, it was confirmed that $MgCl_2$ reacts very quickly with water (H_2O) and the corrosion of the material is greatly accelerated. In the chloride salt composition used in the experiment, the Ni-based alloy had better corrosion resistance than the Fe-based alloy, and the trend was in the order of Hastelloy N > Alloy 617 >> Alloy 800H > STS 316H (Fig. 1). Most of the damage inside the oxide film progresses rapidly through grain boundaries. It was reconfirmed that the element having the greatest effect on corrosion was Cr, and it was judged that the element Fe had a greater effect on the dissolution rate of metal in an environment containing H_2O. A linear correlation between Cr content and corrosion rate was not observed in this study. It is necessary to develop a process to remove impurities in molten salt and a technology to control redox potential. As a result of performing Ni plating on type 304 material, which is an austenitic stainless steel like 316H material, it was confirmed that the base metal and the plating layer showed very good adhesion (Fig. 2). It is planned to measure the corrosion rate by putting Type 316H material, which has undergone surface treatment of several different techniques such as Ni plating, into the molten salt.

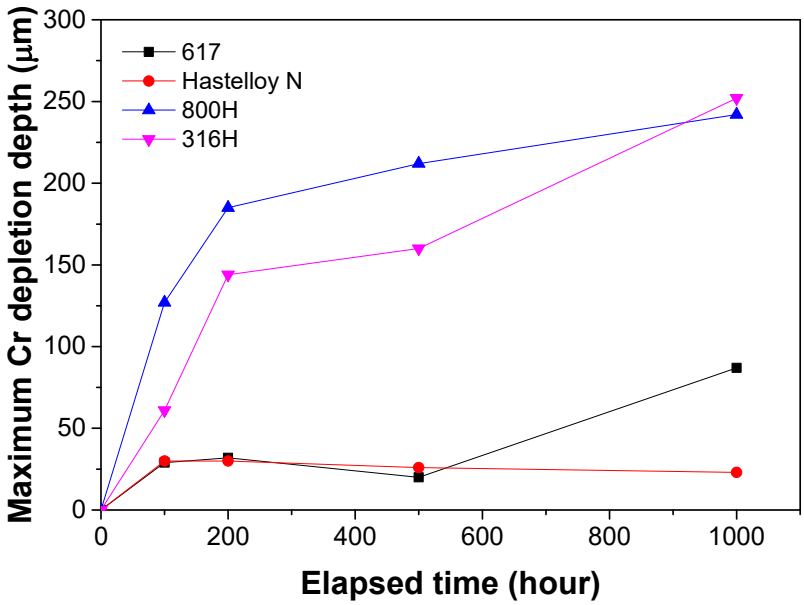

Figure 1. Corrosion rate of Ni and Fe base alloys in molten NaCl-$MgCl_2$ salt

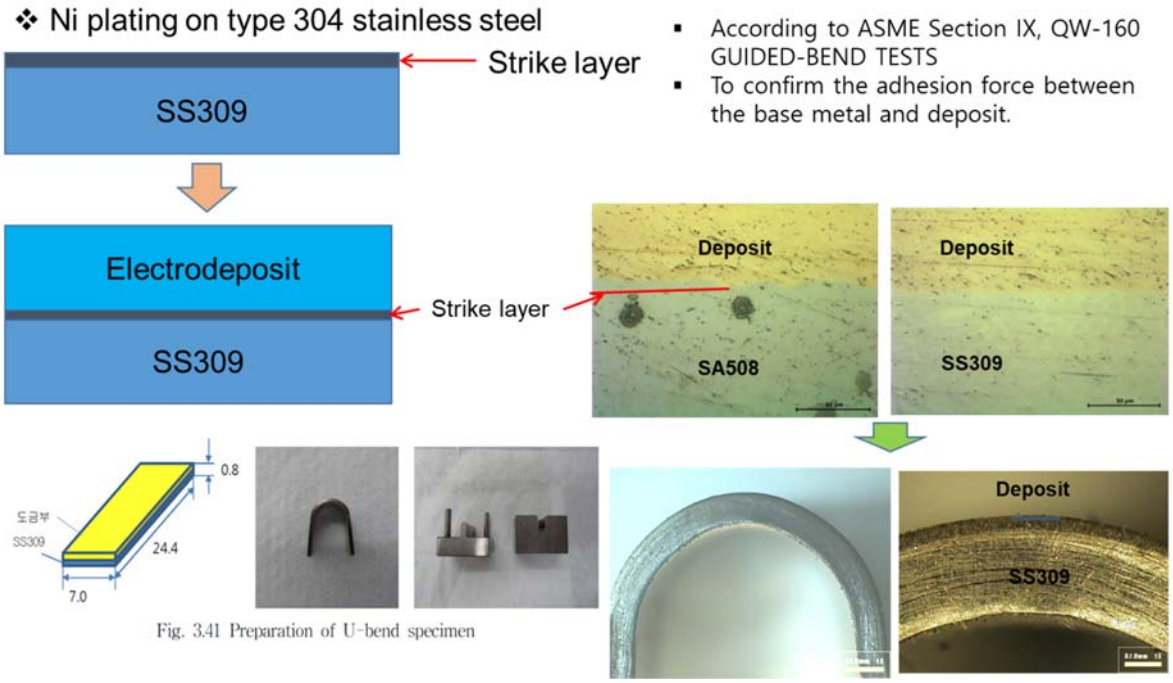

Figure 2. Preliminary study on Ni plating on austenitic stainless steel

Understanding of the corrosion behavior of the candidate materials considered in the Czech SNF disposal package concept

Michaela Matulová[1]; Lucie Hausmannová[1]; Jan Stoulil[2]

[1]Radioactive Waste Repository Authority (SÚRAO), Prague, Czech Republic;

[2]University of Chemistry and Technology, Prague, Czech Republic

Abstract

Deep geological disposal systems rely on a multi-barrier system that comprises the natural geological barrier and so-called engineered barriers that serve to isolate the nuclear waste from the biosphere. The key component of the engineered barrier system concerns the waste disposal package. A comprehensive understanding, and the prediction of the corrosion, of the candidate materials for the waste disposal package for spent nuclear fuel (SNF) considered in the Czech concept are necessary so as to demonstrate its safety and reliability. The research and development of the Czech waste disposal package for SNF has been underway for several years. The main design considerations concern the lifetime of the construction materials and the predictability of both the types and rates of corrosion under deep geological repository (DGR) conditions. Only materials that corrode uniformly under such conditions are being considered. The most suitable design, determined based on a multicriterial evaluation, comprises a double-walled steel-based canister with an outer case made of carbon steel and an inner case made of stainless steel. Stainless steel corrodes very slowly and is able to fulfill the various set lifetime requirements. However, stainless steel can be used only under ambient temperature conditions (between 40 and 50°C) in the DGR environment (according to current knowledge); pitting corrosion may occur above this temperature limit.

Therefore, a carbon steel outer casing was chosen aimed at protecting the inner casing until the DGR environment becomes suitable in terms of the corrosion parameters of the inner stainless steel material. The total lifetime according to all the corrosion models considered has been verified as in excess of 100,000 years, with a preliminary evaluation of up to 1,000,000 years. The aim of the various research projects currently underway is to attempt to imitate as best as possible the conditions under which the SNF disposal package will be emplaced in terms of changes to the materials over time under underground laboratory conditions, and to determine the relevant reliable data.

Effect of gamma ray on anode reactions on the surface of stainless steel in the nitric acid solution

Eriko Irisawa, Chiaki Kato, Naoki Yamashita, Naruto Sano, Susumu Tagami

Japan Atomic Energy Agency, Japan

In spent nuclear fuel reprocessing facilities, nitric acid solutions containing metal components derived from spent fuel are heated and concentrated. This process solution is highly corrosive to stainless steel. According to previous studies, it was shown that the dissolution of oxidizing metal ions causes the cathodic reaction to occur in a higher potential range than in pure nitric acid solutions. And, it has been suggested that the anodic reaction is not sensitive to dissolved metal ion species, but is determined by the concentration of nitric acid and pH. On the other hand, the radiation released from the fuel-derived radionuclides can cause radiolysis of the reprocessing process solution. It is known that nitrous acid is produced by radiolysis of nitric acid media and reaction of nitric acid with radiolysis products. The formation of nitrite is thought to affect the cathodic reaction among the corrosion reactions on the surface of stainless steels.

In this study, the effect of gamma-ray on corrosion rate of stainless steel in the nitric acid solution with and without the oxidizing cation was investigated by the immersion corrosion tests and polarization behaviors.

And in our previous results as shown in Fig. 1, the differences in anodic localization curves of stainless steels in the nitric acid solution with and without gamma irradiation were confirmed. Therefore, in this study the constant potential polarizations of stainless steel in nitric acid solution under gamma irradiation were performed, and the current efficiency was calculated from the weight loss and electric quantity before and after the polarization. The difference in the current efficiency was discussed to determine the difference in anodic reactivity with and without gamma irradiation.

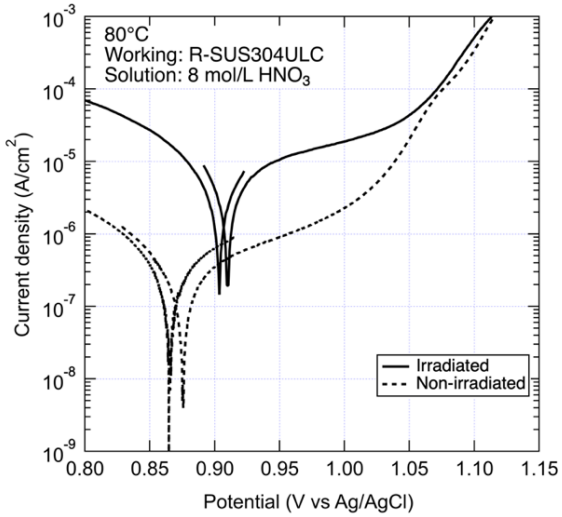

Fig.1 Polarization curves of stainless steel (R-SUS304ULC) in the nitric acid solution with and without gamma-ray irradiation.

Noble Metal Effect on the Hydrothermal Corrosion of FeCrAl Alloys

Liang Yin, T.B. Jurewicz, R.V. Umretiya and R.B. Rebak

General Electric Research, Schenectady, NY, USA

As one of the promising accident tolerant fuel (ATF) concepts, FeCrAl ferritic alloys have been recently studied for using as cladding materials to improve the high temperature steam and water oxidation resistance of traditional uranium oxide based nuclear fuel. Austenitic stainless steels, such as 304SS and 316SS, have been extensively used as internal structural components in light water reactors since the 1960s. In boiling water reactors (BWRs), austenitic steel components may be vulnerable to intergranular stress corrosion cracking (IGSCC). Currently, a majority of worldwide BWRs are implementing IGSCC mitigation strategies that combine feedwater hydrogen injection and noble metal chemical addition. The strategy effectively reduces the electrochemical corrosion potential < -230 mV (vs. standard hydrogen electrode SHE), which is considered as low susceptibility for IGSCC, without using excessive hydrogen that would increase steam line gamma-ray dose rates, due to the formation of radioactive nitrogen-16. The fuel performance of zirconium-based alloy cladding, in term of corrosion and hydrogen pickup, does not seem to be negatively impacted by the noble metal chemistry.

In this study, the effect of noble metal chemical addition on the hydrothermal corrosion of FeCrAl alloys was investigated. Two FeCrAl alloy compositions were selected, FA-SMT and PM-C26M, the compositions were Fe-21.6Cr-5.2Al-3Mo and Fe-12.2Cr-5.7Al-2Mo, respectively. Before exposing to BWR hydrogen water chemistry (HWC) (0.3 ppm hydrogen) at 288°C, and normal water chemistry (NWC) (1 ppm oxygen), the tube coupons were pretreated by an Online NobleChem (OLNC) process to deposit Pt nanoparticles on the tube surface. The short-term immersion up to 6 weeks showed the corrosion behavior of PM-C26M was sensitive to the noble metal pretreatment in the HWC testing, while FA-SMT did not show significant dependence in both HWC and NWC testing. Detailed characterizations will be presented, including Raman spectroscopy, FIB-SEM (focused ion beam – scanning electron microscopy), etc.

Keywords – Nuclear fuel, hydrothermal corrosion, boiling water reactor (BWR), noble metal addition

Hydrothermal Corrosion and Steam Oxidation Behavior of FeCrAl alloys in Multiple Environments

Rajnikant V. Umretiya, Andrew K. Hoffman, Richard Blair, Wanming Zhang, Robert Motyl, Liang Yin, Raul B. Rebak, Evan Dolley

GE Research, Schenectady, NY, 12309, USA

Iron-Chromium-Aluminum (FeCrAl) alloys FeCrAl alloys are considered as lead Accident Tolerant Fuel (ATF) candidate because of their ability to form an effective passive Al film during high temperature exposure above ~800°C. In addition to their accident tolerance, FeCrAl alloys also exhibit good hydrothermal corrosion in light water reactor (LWR) operating conditions due to their Cr content. Since these alloys have been traditionally used for high temperature applications, a significant amount of industrial data is available for use in high temperature environments. However, there is still need of generating data on corrosion performance at relevant lower temperature conditions to understand the behavior of these alloys in a light water nuclear reactor environment. In this study we go through the alloy chemistry optimization being done at General Electric for the development of FeCrAl for LWR applications. The effects of different Cr, Al, and Mo content will be discussed on how these alloys perform in hydrothermal corrosion, lower temperature (400°C) steam, and high temperature steam (≥1000°C). We have shown that each Cr and Al both significantly effect on the oxidation properties of FeCrAl alloys, and Mo has little to no effect on the oxidation/corrosion resistance of this alloy system for relevant environments.

Statement of Impact: The nuclear power industry in the USA and the world has been using the same materials for more than six decades. Many of these electricity generating reactors are being shut down and removed from the grid because they are highly regulated and therefore more expensive to operate than a plant burning inexpensively produced natural gas. In order to maintain nuclear power as a source of clean energy, the newer or innovative proposed materials would allow the existing reactors to operate safely and at a lower cost for longer times (more than 60 years). Since most of the proposed materials were never used in a reactor before in a light water reactor, they need to be fully characterized for this recent intended application.

Simulation of single and two-phase Flow-Accelerated Corrosion (FAC) using Computational Fluid Dynamics (CFD)

Lasseur Théo[a,b], Shkirskiy Viacheslav[a], Kanoufi Frédéric[a] and Mimouni Stéphane[b]

[a]Université Paris Cité, ITODYS, CNRS, 75013 Paris, France

[b]EDF R&D Lab, 78400 Chatou, France

Flow-Accelerated Corrosion, FAC, is one of the most prevalent form of degradation of carbon and low alloy steel pipes exposed to water flow, leading to significant wall thinning, in particular in the primary and secondary coolant systems in nuclear power plants. It is of critical importance to be able to predict regions of local FAC enhancement to avoid any future failure of the pipe systems. CFD alongside experimentations is a relevant tool to determine those locations of a severe attack. The objective of this study is to compare different numerical approaches to estimate the locations and the rates of FAC using CFD. Many theoretical and empirical models have been developed to allow predictions of the FAC rate. The simplest and commonly used prediction of FAC relies on the postulate that the mass transfer is the rate controlling step of the overall corrosion process and that only the hydrodynamic quantities influence locally the rate of degradation. The wall thinning rate in this model is proportional to a mass transfer coefficient and a concentration driving force between the wall and the bulk fluid.[1] With this approach, the prediction of both FAC locations and intensity especially relies on the accuracy of calculation of the mass transfer coefficient distribution. However, some authors have already pointed out discrepancies between experimental results of wall thinning and numerical simulations, peculiarly after separation and reattachment positions of the flow in pipe singularities. This is particularly the case of elbows, a geometry investigated in this study.[2] Because variations in the local chemistry, and consequently the oxide layer, may have been mistakenly neglected, a model based on a coupling of fluid dynamics, water chemistry as well as local electrochemical reactions is considered. Conclusions will seek to determine which approach is the more suitable and accurate to characterize rate and locations of FAC in different configurations.

1. Dooley B. & Lister D. Flow-Accelerated Corrosion in Steam Generating Plants. *PowerPlant Chemistry*, 20(4) (2018).
2. Xiadong Si et al. Investigation of corrosion behavior at elbow by array electrode and computational fluid dynamics simulation. *Materials and Corrosion*, (2020).

Stress corrosion cracking susceptibility of austenitic stainless steels welded joints in chloride containing media

Laura DE LIMA E SILVA, CIRIMAT, Université de Toulouse, CNRS, INP-ENSIACET, Toulouse, France / CETIM, Pôle MMS, Nantes, France; Nadège DUCOMMUN, CETIM, Pôle MMS, Nantes, France; Laurent JUBIN, CETIM, Pôle IDA, Nantes, France; Eric ANDRIEU, CIRIMAT, Université de Toulouse, CNRS, INP-ENSIACET, Toulouse, France; Christine BLANC, CIRIMAT, Université de Toulouse, CNRS, INP-ENSIACET, Toulouse, France

Stress corrosion cracking (SCC) is a fast and local damaging process without significative mass loss or gain and it is also the second type of corrosion that most affects the stainless steels (SS) welded joints, particularly those obtained by arc welding; moreover, it is present in many types of industrial sectors and equipment [1]. In most cases, the failures are found on austenitic stainless steels (ASS) welded joints. Since the SCC susceptibility of a material is dependent on multiple variables linked to the material manufacturing route, the welding process, the environment and the stress state of the workpiece, it is far from being a trivial issue to be studied.

In this work, welded joints of two ASS, 304L (1.4307) and 316L (1.4404), and the respective base metals (BM) were studied. For each ASS, two plates of a same ASS were welded by means of the Gas Tungsten Arc Welding (TIG) technique using a filler metal wire (W19 9L and W19 12 3L for 1.4307 and 1.4404 plates, respectively) varying the heat input (high or “HHI” and low or “LHI”) and the oxygen content for the backing gas (100 ppm or “HO” and 10 000 ppm or “LO”). The microstructure of the BM and welded joints were studied by using optical microscopy (OM), scanning electron microscopy (SEM) and X-ray diffraction (XRD). Their mechanical properties were characterized by means of tensile tests and hardness mapping. To study the full range of ASS weld applications and their SCC susceptibility, three physico-chemical parameters of the environment were varied: the temperature (25, 50 and 80°C), the chloride ion content (0.5 and 1M NaCl) and the pH (4, 6 and 8). Firstly, preliminary electrochemical measurements were done for each weld and BM to evaluate their corrosion behavior in different conditions of chloride contents, pH and temperature. Subsequently, the SCC susceptibility of the materials was tested by means of the four-point bend test (FPB) during 7 days. To determine the load that was applied during the

SCC tests, an approximation of welds lower yield strength (YS_{min}) was done using the results of the hardness mapping. The FPB tests were divided in two stages: a study performed by varying the physico-chemical parameters (pH, temperature and chloride content) for one weld condition, and the rating of all ASS welds SCC susceptibility, done with the most relevant media that were selected with the first stage results. After exposure, the specimen surface and/or the fractured surfaces were analyzed by means of OM and SEM and, for those that were not fractured, residual mechanical properties were measured by tensile tests.

Both 304L and 316L welds presented a characteristic weld structure with four different zones: melted zone (MZ) with dendrites, interfacial zone (IZ) with cellular structure, heat affected zone (HAZ) with grain growth and the BM. The first stage of the FPB tests was done with the 316L-HHI-LO and it enabled the classification of each media from the less aggressive to the more aggressive and, also, a first analysis of the role of each separate variable on the SCC susceptibility. Five media were selected and tested with the 304L-HHI-LO to complement the analysis. Thereafter, two most pertinent media were chosen for the second stage of the SCC susceptibility study. The analyses after tests identified the cracks initiation sites and the propagation path for each case. For the non-fractured specimens, the tensile tests measured the property loss after immersion as well as the differentiation of the fractured surface before and after exposure to the corrosive media. All these results together with the preliminary electrochemical tests allowed the classification of the BM and the welds in terms of their SCC susceptibility, the main location of crack initiation and type of crack propagation. The set of results obtained in this work allows for a better understanding of the influence of each one of the factors that are involved in the susceptibility of SCC of ASS welded joints.

[1] D. le Bras and L. Jubin, “Assemblage par soudage ou brasage - Principaux cas de ruine,” 2013.

An advanced multi-phase-field approach for Electro-chemo-mechanical dissolution applied to Aluminum alloys

Chaitanya Kandekar, Wolfgang E. Weber, Helmut Schmidt University/ University of the Federal Armed Forces Hamburg, Germany;

Aravinth Ravikumar, Daniel Höche, Helmholtz-Zentrum hereon GmbH Geesthacht, Germany

Abstract:

At the microstructural level, failure due to stress corrosion cracking (SCC) is often modelled with multiphysics components such as mechanical, chemical and electrical contributions. In this coupled problem, crack nucleation and propagation are strongly affected by crystal orientation, properties at the grain boundaries, mechanical loading, and aggressive corrosive environment. This results in the competition between intergranular SCC (IGSCC) and transgranular SCC (TGSCC), which has been a trending research topic in the scientific community. Therefore, for the investigation of structural failure by SCC, a comprehensive and detailed modelling technique is needed that tackles the consequences of various phenomena while taking scaling effects in time and space into account and retaining coupled mechanistic interaction. Simulating such a complex coupled processes limits computational capabilities. In this work, a multi-phase-field computational approach is presented, which as an extension of a previous model [1] and recently published works [2, 3], to incorporate anisotropic effects for both elasto-plasticity and material dissolution along the preferential directions. Two separate software environments are used with dedicated solver settings and different time steps to simulate the fracture and dissolution-driven pitting corrosion stages considering the crystal anisotropy in the proposed computational setup. Subsequently, to exchange and interpolate the data, these solvers are coupled in predefined time step using an open-source coupling framework. Both IGSCC and TGSCC are simulated in an efficient manner. The proposed model is illustrated by several numerical examples that forecast the evolution of complicated fracture networks caused by stress corrosion cracking within a 2D polycrystalline model of an aluminum alloy.

Keywords:

Dissolution; Corrosion; Fracture; Stress corrosion cracking (SCC); Anisotropy; Polycrystalline; Phase-Field Modelling.

References:

1. Kandekar, C., Ravikumar, A., Höche, D. & Weber, W. E.: A partitioned computational framework for damage evolution in stress corrosion cracking utilizing phase-field. *Proceedings in Applied Mathematics & Mechanics*,
doi: 10.1002/pamm.202200211, to appear.

2. Cui, C., Ma, R., Martínez−Pañeda, E.: A generalised, multi-phase-field theory for dissolution-driven stress corrosion cracking and hydrogen embrittlement. *Journal of the Mechanics and Physics of Solids* 166, pp. 104951, 2022.

3. Nguyen, Thanh-Tung, Réthoré, Julien, Baietto, Marie-Christine, Bolivar, José, Fregonese, Marion and Bordas, Stéphane P.A.: Modeling of inter- and transgranular stress corrosion crack propagation in polycrystalline material by using phase field method, *Journal of the Mechanical Behavior of Materials*, vol. 26, pp. 181-191, 2017.

Modelling of Downhole H2S, CO2 Environment with High Chloride and Fitness for Purpose Testing of Corrosion Resistant Alloys

Noelle Easter C. Co, Ravi M. Krishnamurthy,
Blade Energy Partners, Houston, TX, USA
Bjørn-Andreas Hugaas, Aker BP, Oslo, Norway;
Ragnar Marcelius Fredriksen, Rishi Ramtahal, Stein Ove Hjelle
Aker BP, Stavanger, Norway

Abstract

ISO 15156 indicates a chloride limit of 120,000 mg/L for super duplex alloys for downhole application. Aker BP is planning to drill four extreme HPHT wells during the first phase of the Valhall PWP – Fenris project, see Figure 1. The four wells will be drilled in a gas / condensate field. The produced fluids are primarily gas condensate with some formation water. The operator anticipates a very high chloride environment in the four wells. The performance of super duplex 25CRW, nickel alloys 2535H and 2550 become questionable at conditions where chloride levels can reach greater than 120,000 mg/L. The objectives of this study are to establish the chemistry inside the wells, to determine the test parameters representative of downhole environment, and to assess if 25CRW, 2535H and 2550 can withstand the high chloride environment. Thermodynamic modeling was used to establish the downhole chemistry based on the estimated production rates of each well. Results show that the chloride in one of the wells can go as high as 308,000 mg/L, and scaling of halite, barite, calcite, and aragonite are predicted at certain depths inside the well. The H2S fugacity was determined to reach 0.025 bar, and the CO2 fugacity was determined to reach 16.6 bar. The fitness-for-purpose testing parameters were selected based on the chloride concentrations with and without halite scaling. Four-point bend tests, crevice corrosion tests and slow strain rate tests were performed to assess the performance of 25CRW, 2535H and 2550 in downhole environment containing H2S, CO2 and high chloride concentration up to 308,000 mg/L. Four-point bent tests and crevice corrosion tests were conducted for 720 hours and 1440 hours at test temperature of 184°C. Slow strain rate tests were conducted using strain rates of 1x10E-6 and 5x10E-7. Results show that there is no cracking on four-point-bend specimens made of 25CRW and 2550. However, one 2535H specimen exhibited a crack at a location outside the inner roller

of the four-point bend jig. The mass loss corrosion rates were estimated to be at 0.18 mpy for 25CRW, 0.23 mpy for 2535H and 0.09 mpy for 2550. Slow strain rate test results show that the 25CRW, 2535H and 2550 failure characteristics tested in inert condition and in downhole high chloride conditions are similar. There is no significant loss in ductility when specimens are tested in downhole high chloride conditions. There is no secondary cracking observed in all the slow strain rate specimens. The overall results of the study indicate that 25CRW, 2535H, 2550 will be able to withstand the high chloride environment predicted inside the wells as long as the H2S partial pressure is below 0.3 bar. The applicability of these austenitic alloys is beyond the specified chloride limits, but require a true reflection of the downhole environment and thus ensure a fit for purpose result.

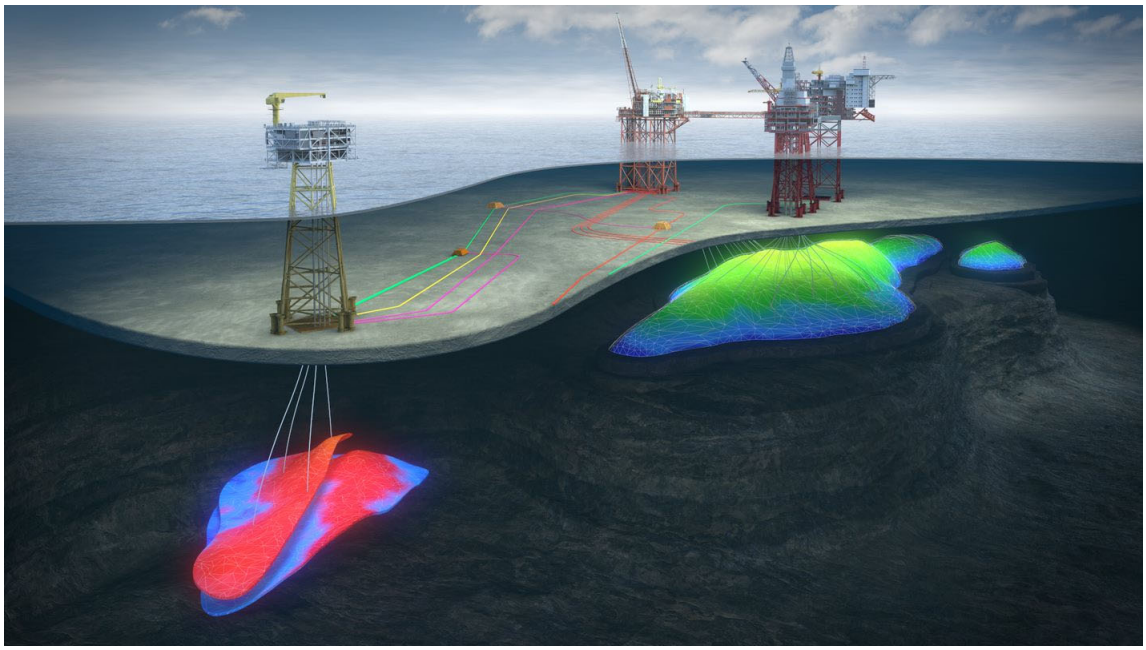

Figure 1

Corrosion fatigue damage mechanism of the AISI 316L stainless steel produced by additive manufacturing

Xavier MAJNONI d'INTIGNANO [1,3], Mohamed EL MAY [1], Nicolas SAINTIER [1], Olivier DEVOS [2], Sébastien MERCIER [3], Charles BIANCHETTI [3], Pascale KANOUTE [3]

[1] *I2M, CNRS, Arts et Métiers Institute of technology, Bordeaux, France*

[2] *I2M, CNRS, University of Bordeaux, Bordeaux, France*

[3] *ONERA, Châtillon, France*

The development of metal additive manufacturing (AM) and progress made over the past decade result in AM alloys with excellent mechanical properties and extend their domain of use. In the case of 316L, it was shown in previous study that this material exhibit excellent fatigue and corrosion properties [1]. However, the case of strongly coupled fatigue-corrosion is not dressed in the literature while having a significant impact on many materials.

The main objective of the present work is to investigate the interaction of cyclic loading, microstructure and corrosion reactions on fatigue damage. For this purpose, the passive film resistance in a corrosion fatigue situation was evaluated.

Laser beam melting (LBM) 316L stainless steel was obtained with a SLM 280HL machine. High cycle fatigue (HCF) tests at 10^6 cycles were carried out in air and in a 3.5 wt.% NaCl aqueous solution with a load ratio R = 0.1. Electrochemical behaviour of passive film was investigated during corrosion fatigue tests by monitoring the free potential (OCP) and *in-situ* electrochemical impedance spectroscopy measurements (EIS). Fatigue crack initiation mechanisms in air and in 3.5 wt% NaCl aqueous solution were investigated. The corrosion fatigue crack initiation was related to the passive film strength under cyclic loading and the presence of AM process defects.

[1] N. Haghdadi, M. Laleh, M. Moyle, S. Primig, Additive manufacturing of steels: a review of achievements and challenges, J. Mater. Sci. (2020). https://doi.org/10.1007/s10853-020-05109-0.

Quantitative study of the roles of bisulfite in the stress corrosion cracking of aluminum alloy in the atmospheric environment

Zhongyu Cui[a,c], *Mingtao Wang*[b], *Liwei Wang*[b], *Wendi Yang*[a], *Yuxi Liu*[b], *Herman Terryn*[c], *Hongzhi Cui*[a]

a School of Materials Science and Engineering, Ocean University of China, Qingdao 266100, China

b College of Mechanical and Electrical Engineering, Qingdao University, Qingdao, 266071, China

c Research Group Electrochemical and Surface Engineering, Vrije Universiteit Brussel, Brussels, 1050, Belgium

Effect of bisulfite (HSO_3^-) on the stress corrosion cracking (SCC) behavior of 7050-T7451 aluminum alloy in the thin electrolyte layer environment in the presence of Cl^- is investigated. Addition of HSO_3^- inhibits the corrosion initiation but promotes the corrosion propagation and hydrogen uptake. With a quantitative calculation, the HSO_3^- is demonstrated to significantly facilitate the synergistic effect between stress, corrosion, and hydrogen during the in-situ tensile test, resulting in the change of the SCC controlling step from corrosion-induced hydrogen to mechanical-electrochemical-hydrogen interactions. The buffer effect of HSO_3^-, which can continuously provide H^+ and support the electrochemical reactions and hydrogen uptake, is the dominant mechanism of the HSO_3^--accelerated SCC deterioration.

Operando synchrotron high-energy XRD study of hydrogen embrittlement of a super duplex stainless steel at high tensile load

***Jinshan Pan*[1]**, *Xiaoqi Yue[1], Cem Örnek[2], Alfred Larsson[3], Ammar Aksoy[2], Andrea Grespi[3], Ulf Kivisäkk[4], Ulrich Lienert[5], Zoltan Hegedüs[5], Edvin Lundgren[3]*

[1]KTH Royal Institute of Technology, Stockholm, Sweden

[2]Istanbul Technical University, Istanbul, Turkey

[3]Lund University, Lund, Sweden

[4]Alleima, Sandviken, Sweden

[5]DESY Photon Science, Hamburg, Germany

Hydrogen embrittlement (HE) of high-strength alloys is a challenge for many applications of the alloys, especially in the transition to hydrogen (H) energy and engineering to reduce carbon emissions. H absorption causes H accumulation at grain/phase boundaries, dislocations, and precipitates, leading to local microstructural deformation that may lead to crack initiation, especially under mechanical stress. HE has been studied extensively, and many mechanisms have been proposed. However, achieving a fundamental understanding of the mechanism of HE requires real-time information on H-microstructure interactions. Previously, we utilized synchrotron high-energy XRD (HEXRD) to study HE of a fine-grain super duplex stainless steel (SDSS) under electrolytic H-charging at a macroscopic strain of ca. 1%. The results show dynamic heterogeneous microscopic strain evolution in the microstructure, but no crack formation [1].

In this work, we performed a similar operando synchrotron HEXRD measurement of a coarse-grain SDSS at high levels of tensile loading (up to 110% of the yield strength) to investigate the strain evolution/localization leading to crack formation. After the HEXRD measurement, we did a microprint test of the sample to visualize H traps and examined the cracks formed in the microstructure using SEM/EDS. Here we report the real-time observation of the heterogeneous strain evolution/localization in the microstructure of the sample under H-charging as a function of stepwise increased tensile strain up to and beyond the yield point, as well as the microstructure features and H traps associated with the crack formation.

1. C. Örnek, T. Müller, U. Kivisäkk, F. Zhang, M. Långberg, U. Lienert, K.H. Hwang, E. Lundgren, J. Pan, *Corros. Sci.*, **2020**, 175, 108899.

The role of Mo in stabilizing passivity of stainless steel and Cr-containing multi-principal element alloys

Vincent Maurice, Xueying Wang, Shova Neupane, Antoine Seyeux, Sandrine Zanna, Dimitri Mercier, Philippe Marcus

PSL University / CNRS - Chimie ParisTech, Institut de Recherche de Chimie Paris (IRCP), Research Group of Physical Chemistry of Surfaces, Paris, France

Stainless steels (SS) and other chromium-containing alloys are widely used in various industrial domains because of the self-protection provided by the passive film formed at the surface, only a few nanometers thick and strongly enriched in Cr(III) (hydr)oxide species. Even though numerous studies have characterized the passivity of such alloys at macroscopic level, only recent surface analytical investigations performed on austenitic SS grades have revealed, at the nanometer scale, the genesis of Cr-depleted weak points of protection in the early stages of growth of the protective surface oxide film. Hence, the inhomogeneous distribution of the chromium enrichment appears as crucial for the barrier properties of the passive film and a key factor for stable passivity at the nanoscale.

In this work, we have examined how molybdenum, when present in the alloy, can reinforce these weak points of protection, and stabilize passivity in aggressive chloride-containing environments. Advanced surface analysis, combining time-of-flight secondary ion mass spectrometry (ToF-SIMS) and X-ray photoelectron spectroscopy (XPS), was applied to 316L SS and Cr- and Mo-containing multi-principal element alloys showing enhanced resistance to Cl-induced passivity breakdown in accelerated tests of initiation of localized corrosion. The results show that the depth distribution of the enrichment of Mo(VI) and Mo(IV) oxidized species in the duplex structure of the passive film is at the origin of the enhancement of passivity. The Mo(VI) species, concentrated in the outer exchange layer, poisons the depth penetration of chlorides in the protecting oxide, while the Mo(IV) species, distributed at the interface with the inner barrier layer but also within the inner layer, combine with oxidized iron species to stabilize the iron-rich weak points of protection.

This project has received funding from the European Research Council (ERC) under the European Union's Horizon 2020 research and innovation program (grant agreement No. 741123, CIMNAS).

Electrochemical Impedance Spectroscopy as a tool to qualify effectiveness of passivation processes and oxides properties of various alloys

Tiphaine SCHOTT[1], Yassine AMCHAYD[1], Lyne THEILLER[1], Françoise LIAUTAUD[1]

[1]CETIM, Mulhouse, France, Tiphaine.schott@cetim.fr

Abstract:
A passive material is able to form a protective oxide layer at its surface. However, the corrosion resistance of this layer may be dependent not only on its nature, but also on its thickness, its resistivity, or other parameters. Their estimation may help in understanding corrosion behavior, which is the aim of this study. First of all, a methodology was developed concerning experimental conditions and data interpretation for oxide layer characterization by electrochemical impedance spectroscopy (EIS). This approach was then applied to stainless steels to evaluate the quality of the oxide layers after various passivation processes. It was demonstrated that the layer thickness estimated by EIS is few nanometers, as expected. However, it does not seem to be the determining factor for corrosion resistance, as illustrated by polarization curves. Instead, the layer composition and resistivity may be the relevant parameters, and EIS does give information on resistivity profile, which follows the power law model for stainless steel. To the contrary, aluminum alloys display a Young resistivity distribution in their passive layers, and the developed methodology could be applied as well to demonstrate a 3 nm aluminum oxide layer immediately formed in air.

Keywords:
passive layer ; electrochemical impedance spectroscopy ; oxide thickness ; resistivity profile

Introduction

A passive material is able to form a protective oxide layer at its surface, and its characterization is of high importance for understanding or predicting corrosion behaviour. Several techniques may be used to estimate the layer thickness such as TEM, XPS or ToF-SIMS. However, the mentioned techniques require expensive equipment, and the thickness estimation is approximate (XPS and ToF-SIMS) or requires a difficult sample preparation (TEM).

Literature works [1-6] suggest that electrochemical impedance spectroscopy (EIS) may be used as an alternative technique to study passive layer of various metallic materials, giving access not only to oxide thickness but also to resistivity profile within the layer, with the "simple use" of a potentiostat. A methodology was developed internally [7] concerning EIS experimental conditions and data interpretation for austenitic stainless steel for a given passivation process, and the results were promising.

The aim of the present study was to investigate how the methodology can be used to discriminate passivation processes from the layer quality point of view, and if other materials can be studied with the same approach. The final objective is to propose a recipe for EIS investigation of passive layers.

Material and methods for data collection

Experimental conditions used for data collection are described in our previous work [7] and completed here.

Electrode preparation

To investigate passive layer of stainless steel, samples were taken from a pure austenitic stainless steel bar (grade 316L) which were machined into circular tablets to be used in a sample holder with a rubber sealing (exposed surface: 0.64 cm^2). The surface of the sample was polished until P1200 SiC abrasive papers to get rather smooth surface. Then, the oxide film was formed in a 14 w% nitric acid solution during 3 hours at room temperature or at 60°C, or by exposition to air for 1 week.

Aluminium oxide passive layers were prepared from magnesium-containing aluminium alloy (series 5000) samples, which were polished and exposed to air for various durations (few minutes to several days). The aluminium samples were either tablets or mounted in epoxy resin.

Electrochemical impedance spectroscopy

A three-electrode cell configuration consisting of the sample as the working electrode, a platinum wire as counter electrode and a reference electrode was placed in a Faraday cage to reduce the influence of external noise.

Electrochemical measurements were performed using a Gamry 3000 potentiostat, at ambient temperature. The experimental protocol was as followed. Once the working electrode was placed in the electrolyte, the open circuit potential (OCP) was monitored 24h or until the potential was stabilized enough. Then, measurements were performed.

For electrochemical impedance spectroscopy (EIS) measurements, the test medium was 0.5M Na_2SO_4, unless specified, and a K_2SO_4-saturated mercurial sulphate electrode (MSE) was used as reference electrode. The reference electrode was placed directly in the electrolyte, as double sintered glass junction makes EIS measurements impossible. EIS was recorded at OCP (except for the study of the degradation level) with 10 measurement points per frequency decade. The potential perturbation was kept small to 5 mV, since no signal improvement was observed for 10 mV perturbation. Various frequency ranges were investigated, the most common one being 100 kHz to 10 mHz. Artefacts were observed at higher frequencies [7] and lower frequencies were only recorded if needed since it involves experiment duration.

For polarization curve measurements, the test medium was 0.5M NaCl, unless specified, and a saturated calomel electrode (SCE) was used as reference electrode. The polarization curves were recorded at 0.1 mV/s until 0.1 mA/cm^2.
The result reproducibility was verified by conducting several identical experiments with newly passivated electrodes. Also, selected EIS measurements were repeated several times to check the result repeatability as well as the stability of the measurements.

Approach for EIS data interpretation

The theory, approach and software used for data interpretation are mostly described in our previous work [7] and completed here with the main step, using the layer model of Figure 1.
In this study, the passive layer at the metallic surface is modeled by a layer with a distribution of resistivity between the position x=0, corresponding to the substrate interface, and x=δ, corresponding to the electrolyte interface. In other words, δ is the passive layer thickness.

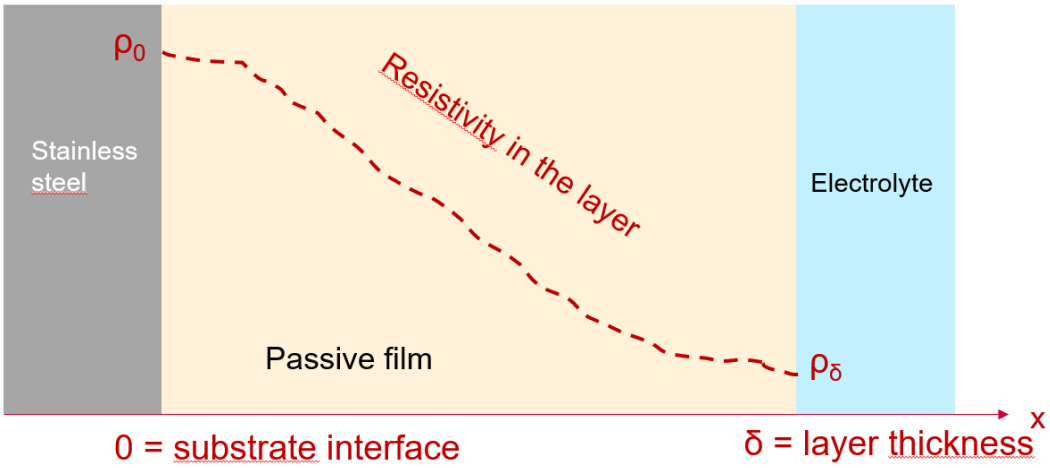

Figure 1. Layer model used in this study

Both graphical interpretation and fitting were used to analysis the data. It should be mentioned at this stage that caution concerning data units should be taken for each change of software.

Graphical extraction of parameters

After normalizing EIS data by sample surface area (not always automatic with potentiostat software) and excluding abherrant points (e.g. by checking Kramers-Kronig relationships), some parameters can be graphically extracted.
First, the electrolyte resistance R_e is determined on Nyquist plot, from the real part at high frequencies (Figure 2). The obtained value can be used to correct the EIS data if needed, or as input data for data fitting.

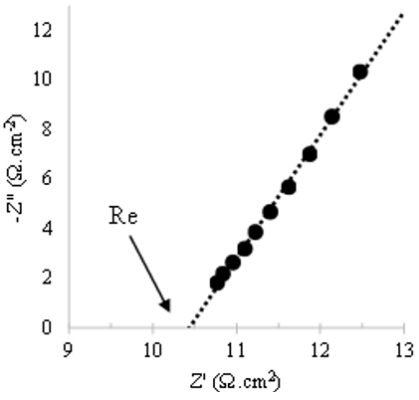

Figure 2. Determination of R_e from Nyquist plot

After R_e-correction, Cole-Cole representation of the EIS data can be done through Gamry software "Echem Analyst" by plotting the imaginary part of the capacitance in function of the real part of the capacitance (Figure 3). At high frequencies, the real part represents the infinite capacitance C∞. If extrapolation to the x-axis is impossible, the C∞ is taken equal to real part of the capacitance at the highest measured frequency.

At this stage, if the layer permittivity ε is known or can be approximated, the layer thickness δ can be accessed through the following relationship using C∞:

$$\delta = \frac{\varepsilon_0 \varepsilon}{C}$$

With ε_0 the vacuum permittivity.

In any case, C∞ can be used as input data for data fitting.

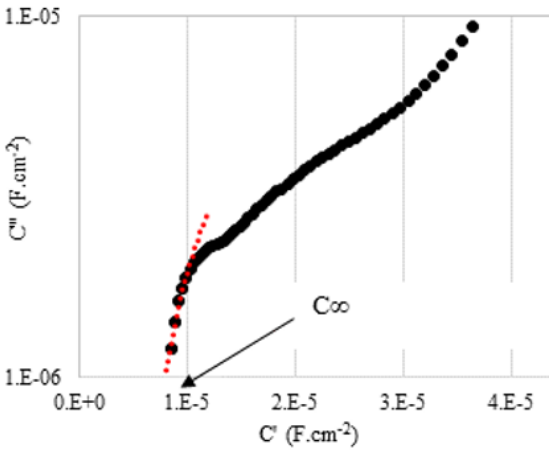

Figure 3. Determination of C∞ from Cole-Cole plot

If the resistivity distribution follows the power law model, as it will be described later, it is also possible to determine the α coefficient from the constant phase element (CPE). Two methodologies can be used (Figure 4).

For the first one, the imaginary part of the raw EIS data is plotted in function of the frequencies. The slope in log-log scale is equal to α.

For the second methodology, the phase of R_e-corrected EIS data is plotted in function of the frequencies (Bode representation). If the power law model is valid, a constant phase should be visible over a large frequency window. Then α can be calculated from the value of the phase on this plateau with:

$$\phi_{adj}(plateau) = -90 * \alpha$$

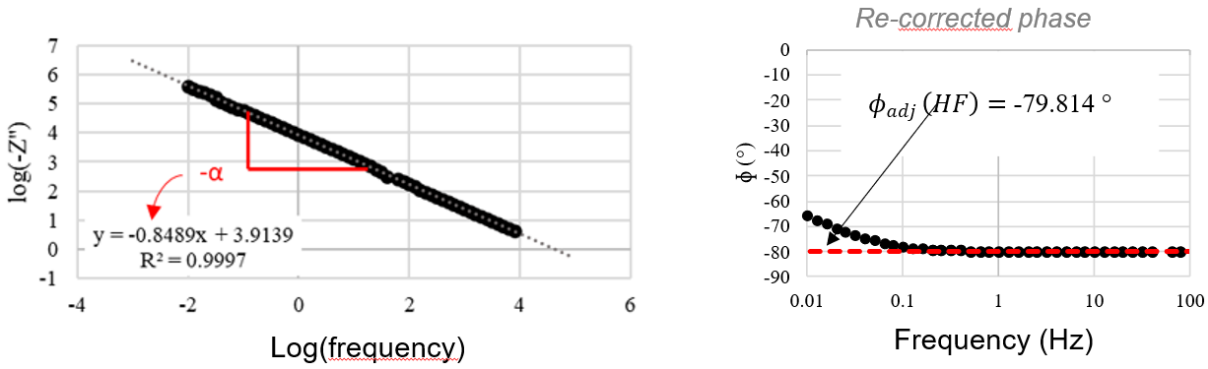

Figure 4. Two methodologies for CPE-coefficient α determination

Finally, it is possible to graphically determine the characteristic frequency f_0, which is related to ρ_0, resistivity at the substrate/oxide interface (x=0):

$$\rho_0 = \frac{1}{2\pi * \varepsilon * \varepsilon_0 * f_0}$$

Indeed, by plotting the imaginary part of the EIS data in function of the frequency, f_0 corresponds to the frequency at the maximum of the imaginary part of the impedance (Figure 5).
In practice, it is however difficult to access to these data since f_0 is a low frequency and thus require EIS measurement duration of several days. For this, it is particularly important to have a stable system. Cl-containing medium should be avoided.
Estimation of f_0 is nevertheless useful when the permittivity is unknown, as it can be used as an input data for data fitting.

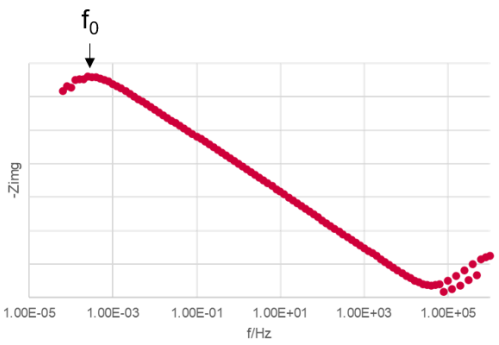

Figure 5. Graphical determination of f_0

Approximation using Voigt elements

This stage was performed with the open-access software Measurement model developed by Orazem and Watson [8].
In this software, EIS data can be fitted with a series of Voigt elements, which are a capacitance in parallel with a resistance. These elements are mathematically valid for all systems.
The optimal number of Voigt elements should be chosen, taking either the software limit or a confidence interval inferior to 20%. In this study, the number of required Voigt elements was between 5 and 9 depending on the samples.
For each element i, the resistance R_i, the capacity C_i and the time constant τ_i are given by the software. Then, the local distance d_i and the local resistivity ρ_i can be calculated with:

$$d_i = \frac{\varepsilon_0 . \varepsilon}{C_i}$$

$$\rho_i = \frac{\tau_i}{\varepsilon_0 . \varepsilon}$$

Then, the layer thickness δ_{MM} (from Measurement Model) is estimated to be the sum of the local distance di, with n the number of Voigt element used for the data fitting:

$$\delta_{MM} = \sum_{i=1}^{n} d_i$$

Besides, by ranking the local resistivity ρ_i from the highest to the lowest, with the corresponding di, it is possible to get a first representation of the resistivity distribution, which is the plot of the resistivity in function of the position in the layer.
Two types of mathematical models can be used to characterize the resistivity distribution within a layer: Young model or Power law model (PLM).
In the PLM, the distribution of resistivity is expressed as:

$$\frac{\rho}{\rho_\delta} = \left(\frac{\rho_\delta}{\rho_0} + \left(1 - \frac{\rho_\delta}{\rho_0}\right)\xi^\gamma\right)^{-1}$$

with the dimensionless position $\xi = \frac{x}{\delta}$ ($\xi = 0$ at the metal/oxide interface, 1 at the oxide/solution interface), ρ_0 and ρ_δ the bounded values of the resistivity of the metal/oxide and oxide/solution interfaces, respectively, and γ a constant characterizing the amount of resistivity variation within the interface.
In the Young model, an exponential relationship exists for the resistivity ρ:

$$\rho(x) = \rho_0 \exp\left(-\frac{x}{\lambda}\right) = \rho_\delta \exp\left(\frac{\delta - x}{\lambda}\right)$$

where ρ_0 is the resistivity at x = 0 (metal/oxide interface), and λ is a characteristic distance of the resistivity profile.

Then, by plotting the resistivity in function of the position in the layer, one may identify the relevant model (Figure 6). A linear correlation in log-log scale plot reveal that the PLM is valid (the case for stainless steel in our work), while a linear correlation in semi-log scale plot suggests a Young model (the case for aluminium alloy in this study).

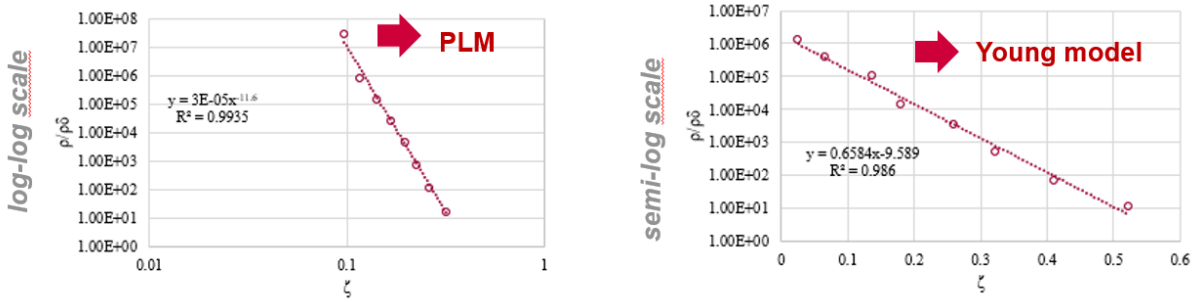

Figure 6. Correlation between resistivity and layer position to determine the relevant model for resistivity distribution.

Then, the appropriate model is used to fit EIS data using LISE software "Simad" in which it is possible to enter analytical equations [9].

Fitting with Power-law model (PLM)

This model is valid for stainless steel samples at OCP in this study. In Simad software, the following equation is used to fit EIS data of this material:

$$Z = Re + Z_{PLM} = Re + \left(1 + 2.88 * \left(\frac{1}{1-\alpha}\right)^{-2.375}\right) * \frac{\frac{\varepsilon_0 \varepsilon}{C} {\rho_\delta}^{1-\alpha}}{({\rho_0}^{-1} + j\omega\varepsilon_0\varepsilon)^\alpha}$$

As many input parameters as possible should be entered. This means all the graphically determined values: Re, C∞, α, and f_0 (related to ρ_0) if possible. If f_0 is unknown, then the permittivity is estimated. Either the theoretical value for chromium oxide is used (15) or other techniques are applied to estimate the layer thickness. For example, XPS was applied to a representative stainless steel sample (not shown here), and from the thickness determined by XPS and the capacity estimated from Cole-Cole plot of EIS data, the oxide permittivity was estimated to 25.

This approach gives only two output parameters, for which the range should be adapted before fitting. Indeed, ρ_0 (if f_0 is unknown) and $\rho\delta$ may be up to 10^{20} ohm.cm, while ε (if f_0 is known) should lie between 0 and 50.

From these fitting results, it is then possible to access to the layer thickness and to the resistivity profile.

Fitting with Young model

This model is valid for aluminium alloy at OCP in this study, and again, as many input parameters as possible (Re, C∞, …) should be used before fitting with Simad. Moreover, the equation should be careful chosen, as adjustement is only working for ρ_δ-related equations. One possible relationship is:

$$Z = Re + Z_Y = Re + \frac{P}{j\omega C}.\ln\left(\frac{1 + j\omega.\tau.\exp\left(\frac{1}{P}\right)}{1 + j\omega.\tau}\right)$$

where the output data, P the relative penetration depth and τ the time constant, are related to the layer thickness and to the resistivity ρ, with:

$$P = \frac{\lambda}{\delta_Y} \text{ and } \rho_\delta = \frac{\tau}{\varepsilon_0 \varepsilon}$$

Results with stainless steel

Influence of the test medium

First of all, it is reasonable to question the pertinence of Na_2SO_4 test medium, while it may be more relevant to study the passive layer in its utilization medium, potentially more aggressive, and follow its evolution over time.

Our previous work demonstrated that EIS measurements in NaCl medium are difficult, especially at low frequencies, due to instabilities of stainless steel in Cl-containing solution [7]. Nevertheless, it was later found that fitting of high frequencies EIS data collected in such medium lead to similar layer parameters than in Na_2SO_4. Then, it why decided to keep Na_2SO_4 in this work to evaluate the possibility of the technique without being perturbed by pitting corrosion or other system instabilities.

Effect of passivation process

The resistance towards localized corrosion of the different stainless-steel samples was investigated by polarization curves measured in NaCl. Indeed, as mentioned above, pitting corrosion is expected to occur on stainless steel in Cl^- containing medium. The obtained curves are displayed in Figure 7. As comparison, a sample polished immediately before measurements was measured as well to highlight the behaviour in absence of a passive layer.

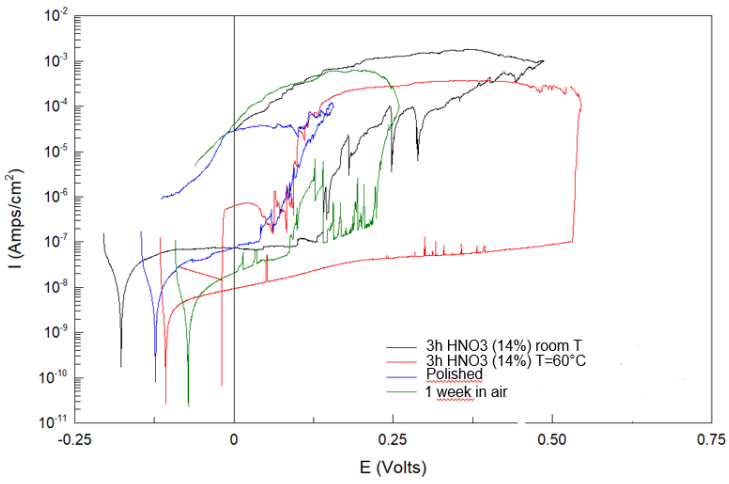

Figure 7. Polarisation curves of stainless steel in NaCl

As expected, the polished sample displays the narrowest passivation domain, while sample passivated in hot nitric acid presents the longest passivation domain (around 700 mV).

For the sample passivated in air, current pits are observed, suggesting the occurrence of metastable pitting, contrary to samples passivated in nitric acid. This demonstrates the importance of performing appropriate passivation process to get optimal protection of stainless steel.

To investigate the oxide properties affecting the corrosion resistance, the samples were studied by EIS in Na_2SO_4 prior to the polarization curves. The obtained data were treated as described above using PLM, and the resulting resistivity profiles are given here (Figure 8).
For all types of passivation process, the resistivity profiles look similar, with (for a permittivity of 15) a small plateau (<0.5 nm) of constant resistivity and a total layer thickness between 1.5 and 4 nm (in the same order of magnitude of XPS or ToF-SIMS results, not shown here). In addition, a lack of reproducibility is observed within a given passivation process, leading to difficult trend identification.

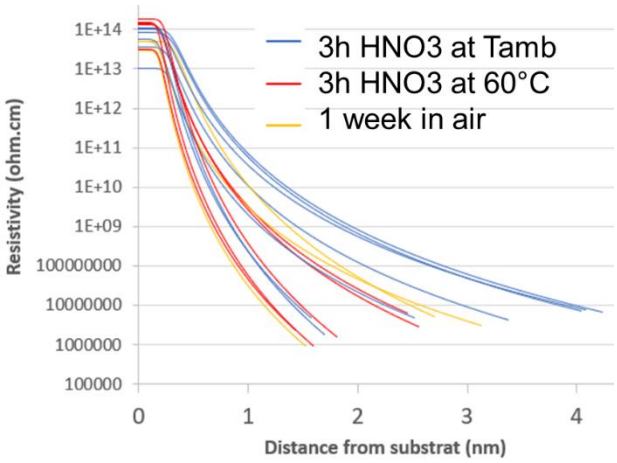

Figure 8. Resistivity profiles estimated from EIS for stainless steel with various passivation processes (ε = 15).

Next step was to find correlations between EIS data and polarization results.
By plotting the depassivation potential, representing the resistance towards localized corrosion, in function of the estimated layer thickness, no relationship could be detected (Figure 9a).
On one hand, the error bars show that thickness estimation by impedance may not be precise enough due to multiple factors such as reproducibility of the experiment itself, sensibility of the technique or approximation during data treatment. In particular, it may be that the permittivity value chosen for data treatment is not identical for all samples (due to e.g. differences in composition), although estimation from low frequency data suggest that they are close.
On the other hand, it can be that the resistance towards localized corrosion of passive material is not (or not only) related to the layer thickness, but to other layer properties.
With this in mind, the depassivation potential was plotted in function of the oxide resistivity (Figure 9b). Despite large errors bars and close resistivity range, a linear correlation between the resistance towards localized corrosion and the resistivity at the substrate/oxide interface seems to exist.

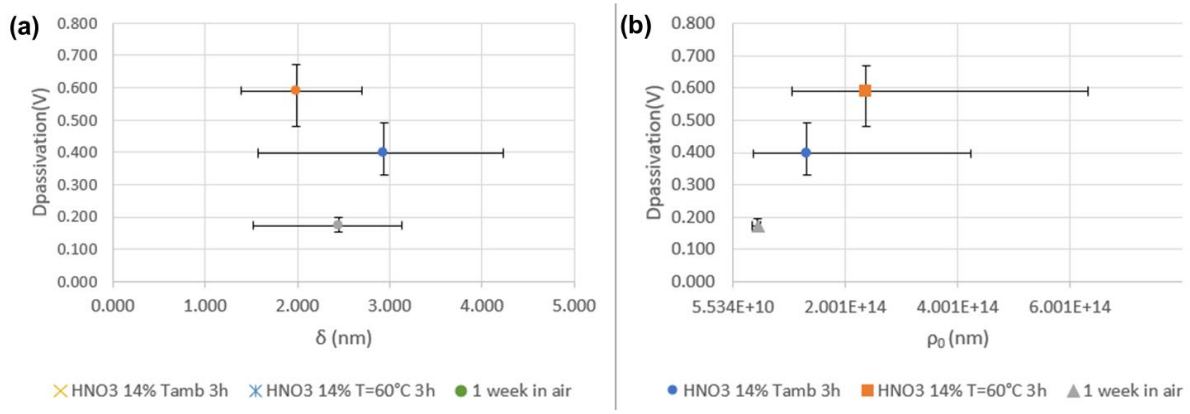

Figure 9. Relationship between (a) layer thickness or (b) resistivity at the substrate interface, and depassivation potential of stainless steel.

Preliminary ToF-SIMS results on these samples confirmed the absence of correlation between oxide thickness and corrosion resistance. Interestingly, the samples passivated in nitric acid

present more chromium in their passive layer than those passivated in air, which may be related to the layer resistivity. Further investigations are under progress.

Effect of degradation level

To investigate evolution of passive layer properties with corrosion, impedance spectra were recorded at different potentials corresponding of the passivation domain or the transpassive region, as illustrated on the polarization curve recorded in Na_2SO_4 (Figure 10a). Each potential was hold for 2 min before recording EIS. Apart from the potential, all other experimental conditions were identical to previous EIS measurements. By applying identical data treatment than other EIS results, the following resistivity profiles were obtained for the different potentials (Figure 10b), showing that EIS is indeed sensitive to changes in the passive layer.

It can be observed that the profile at the beginning of the passivation domain (current density below 10^{-7} A/cm^2 on the polarization curve) is superposed with that at OCP, showing no damages of the passivation layer at this potential. To the contrary, for higher potentials, although still within the passivation domain, some changes in the resistivity profile are observed. Indeed, the resistivity at the oxide/substrate interface gradually decreased with the current densities (from 10^{-7} and 10^{-5} A/cm^2), in agreement with the relationship between this resistivity and the protection toward localized corrosion.

Again, the passive layer thickness seems not to be the determining factor for corrosion since it is not affected by the applied potential within this region, lying around 2 nm for all applied potentials until +0.6V/MSE. For the highest applied potential (+0.9V/MSE), the transpassive region is reached with current densities around 10^{-4} A/cm^2, leading to low resistivity and low thickness, as expected from a damaged layer.

Nevertheless, it should be mentioned that the data treatment at high potentials is not straightforward, as the usual model is not valid over the whole frequency range. It might be due to influence of layer porosities and/or layer of corrosion products which may not have the same resistivity distribution and/or permittivity than the initial passive layer.

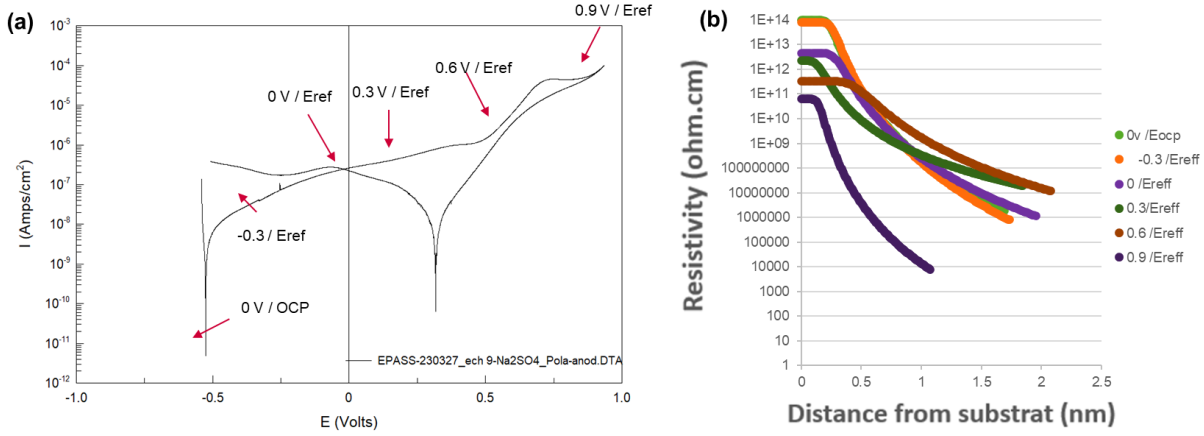

Figure 10. (a) Polarization curves of passivated stainless steel in 0.5M Na_2SO_4 ; (b) resistivity profiles from EIS data at indicated potentials

Results with aluminium alloys

For the aluminium alloys investigated in this study, the resistivity follows a Young distribution. The oxide layer thickness estimated by EIS using this model is about 3 nm, already after only few minutes in air, and displays a linear resistivity profile (Figure 11). This suggests that the oxide is only composed of aluminium oxide, which is very rapidly formed when aluminium is exposed to air. Further investigation on aluminium alloys are under progress.

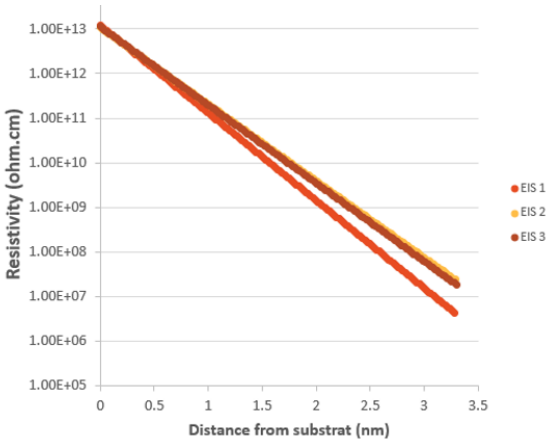

Figure 11. Resistivity profiles of aluminium alloy

Conclusion

A methodology for characterizing passive layer by EIS was described in this study, from data collection to data interpretation. Although this approach is laborious with a lot of data manipulation and use of several softwares, it does not require expensive equipment except a potentiostat.

By applying this approach to stainless steel, it was demonstrated that the layer thickness estimated by this technique is few nanometers, in the same order of magnitude than other techniques. However, oxide thickness does not seem to be the determining factor for corrosion resistance, as it is similar for all studied passivation processes. Instead, the resistivity may be the relevant parameter, and EIS does give information on resistivity values and profile, which follows the power law model for stainless steel. To the contrary, aluminium alloys display a Young resistivity distribution, and investigation will pursue with other aluminium alloys, as well as nickel-base alloys.

Next step will be to correlate the resistivity profiles obtained for different samples by EIS with layer composition obtained by ToF-SIMS and XPS to get a complete picture of the passive layers. Indeed, both the chromium content [10] and the ratio between oxides and hydroxides (as suggested by resistivity profile interpretation [6]) may play a role in the layer quality on stainless steels.

References

1. Benoit et al., Electrochimica Acta, **201** (2016) 340
2. Tribollet et al, “EIS technique in passivity studies: determination of the dielectric properties of passive films”, in Encyclopedia of Interfacial Chemistry (2018) pp. 93–107.
3. Revilla et al, Corrosion Science **167** (2020) 108480.
4. Zhang et al, Electrochimica Acta **353** (2020) 136531.
5. Barroux et al., Corrosion Science **191** (2021) 109750.
6. Marcelin et al, Journal of The Electrochemical Society **168** (2021) 021503.
7. Theiller et al., “Estimation of passivation layer thicknesses: how easily can electrochemical impedance spectroscopy (EIS) be used ?”, in EuroCorr, Berlin (2022).
8. Watson et Orazem, EIS: Measurement Model Program (https://osf.io/2xdhf), 2020.
9. LISE laboratory, UMR 8235 CNRS, Sorbonne University, Paris, France
10. Nonmandatory Appendix E - Passivation procedure qualification, in ASME BPE (2012)

Intergranular corrosion of Q&P processed martensitic stainless steels

Gaojie Li[a], Kees Kwakernaak[a], Ali Smith[b], Marta Muratori[c], Maria Santofimia[a], Yaiza Gonzalez-Garcia[a]

[a]Delft University of Technology, Delft, The Netherlands

[b]RINA Consulting - Centro Sviluppo Materiali SpA, Rome, Italy

[c]Acerinox Europa S.A.U., Los Barrios, Spain

Martensitic stainless steels containing more than 11% Cr are extensively used in automotive industries due to the combination of mechanical properties and moderate corrosion resistance. Driven by the increasing demand for lightweight and energetically sustainable automobile materials, novel high-strength martensitic stainless steels have been developed through the application of the Quenching and Partitioning (Q&P) treatment. Q&P ideally minimise the formation of carbide since all the carbon atoms are partitioned into austenite. Nevertheless, this condition is not always fulfilled and depending on the chemical composition of the alloy, carbides can still precipitate, favouring localised corrosion such as pitting and intergranular corrosion (IGC).

This research aimed to elucidate the susceptibility to localised corrosion of a 0.3C – 3.0Mn – 0.35Si – 13Cr (in wt.%) martensitic stainless steel. By applying different quenching temperatures, Q&P microstructures with different austenite fractions were obtained. Furthermore, microstructure characterisation showed the presence of segregation banding with Cr-content variations. These bands emerge during casting and solidification and are difficult to eliminate via heat treatment. Potentiodynamic polarisation experiments in 3.5wt% NaCl solution showed no indication of pitting corrosion. Post-analysis of the samples confirmed the absence of pits, but grain-boundary attack was detected. The IGC performance of both as-received and Q&P processed microstructures was investigated by double-loop electrochemical potentiokinetic reactivation (DL-EPR) test in a 0.01M H_2SO_4 solution. The DL-EPR test enabled the quantitative analysis of the IGC susceptibility. Further characterisation of the grain boundaries was carried out using scanning electron microscopy (SEM), transmission electron microscopy (TEM) equipped with energy-dispersive X-ray spectroscopy (EDS) and scanning Kelvin probe force microscopy (SKPFM).

This research revealed the interrelation between microstructure and the degree of sensitisation to IGC. The Q&P processed samples showed lower IGC susceptibility than that of the as-received sample. The IGC is attributed to the Cr-carbide precipitation at grain boundaries. Moreover, the higher austenite fraction leads to severer carbon depletion in the martensite, leading to the selective attack of the (martensite-rich, i.e. Cr-poor) segregation bands.

Data-driven analysis of the local current distributions of 316L stainless steel corrosion in NaCl solution

Leonardo B. Coelho, Daniel Torres, Miguel Bernal, Gian M. Paldino, Gianluca Bontempi, Jon Ustarroz, Université Libre de Bruxelles (ULB), Brussels, Belgium

A high throughput approach, based on the Scanning Electrochemical Cell Microscopy (SECCM), was used to collect corrosion activities from randomly probed locations of electropolished 316L. Potentiodynamic polarization in NaCl media drove the development of pitting. Machine learning allowed the estimation of relevant pitting-related descriptors (E_{pass}/j_{pass}, E_{pit}/j_{pit}). The conditional mean of *log(j)* as a function of *E* was generally a poor descriptor of populations of polarization curves. Contrarily, conditional median curves were more representative of the corresponding datasets. Fitting with theoretical functions described conditional *log(j)* distributions as a function of: 1. applied potential; 2. testing aggressiveness (Cl^- concentration and scan rate pairs). Unimodal distributions fitted the *log(j)* at *E* regions before the passivity breakdown, while the uniform distribution was mainly assigned to *E* regions related to stable pitting. The testing aggressiveness was essential for triggering the potential dependent transition between the unimodal and the uniformly random behavior. The conditional variance of *log(j)* as a function of *E* was provided as a metric for the degree of randomness of the underlying distributions, with the uniform function generally providing the highest values of uncertainty. The high randomness associated with pitting increased with *E* and [Cl^-] and decreased with the scan rate.

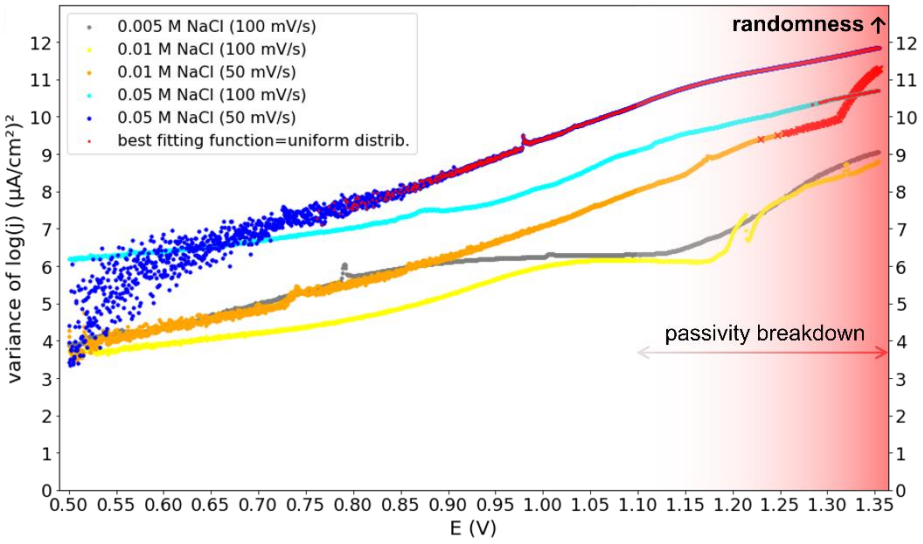

Influence of chlorides and pH on the susceptibility to pitting corrosion of stainless steels with different microstructures and PRENs

Andressa Trentin[1], Ahmad Mardoukhi[2], Mari Lindgren[2], Pekka Pohjanne[1], Elina Huttunen-Saarivirta[1]

[1]VTT Technical Research Centre of Finland Ltd, Espoo/Finland

[2]Metso Outotec Research Centre, Pori/Finland

Stainless steels do not corrode in the same way as ordinary carbon steel due to the presence of a protective chromium-rich oxide film on the surface. In reason of their high corrosion resistance, they are commonly used in industrial assets. However, high temperatures, the presence of chlorides, and/or acidic environments can cause layer breakdown, resulting in corrosion. Understanding the specific conditions that cause localized corrosion of commercial stainless steel (SS), such as grades 1.4404, 1.4162, 1.4539, 1.4462, 1.4547, and 1.4410 with pitting resistance equivalent numbers (PRENs) of 24, 25, 34, 35, 43 and 44, respectively, is critical to ensure safe industrial operations and technological solutions. Although researchers have devoted attention to the effect of operation temperature [1], less is known on how different pH values, chloride contents [Cl^-], and particularly their specific combinations, influence the susceptibility to pitting corrosion of these alloys and how this is related to their microstructure and composition. Our aim is to shed more light on this area.

To elucidate the combination of [Cl^-] and pH value that cause pitting attack in SSs, the specimens were examined using cyclic polarization measurements varying the [Cl^-] from 0 to 5000 mg/L, solution pH (1, 2.5, 4), and the type of acid (sulfuric acid, hydrochloric acid) at elevated temperatures. In addition, the inhibiting effect of sulfates on the pitting corrosion of SSs will be investigated in the sulfuric acid environment. The results will demonstrate the correlation between the operation conditions, susceptibility of materials to pitting corrosion, and the material specifications (PREN, austenitic or duplex microstructure).Mechanistic insights will be provided on the preferential attack in the material (considering microstructure, grain boundaries and composition). Finally,

the summary table built upon the results will support researchers, engineers and industrialists in the field of corrosion toward a proper selection of materials.

Keywords: stainless steel, pitting, chloride, pH, cyclic polarization curve

References

[1] E. Huttunen-Saarivirta, et al. Corrosion of Stainless Steels S31603, S31655, and S32101 in Sulfuric Acid Solutions: Effects of Concentration, Chlorides, and Temperature, Corrosion. 78 (2022) 943–962. https://doi.org/10.5006/4122.

Corrosion mechanisms of a Super-duplex Stainless Steel in Sour Conditions

Wenle He, Raveendra Siriki**, and Anand Rajagopal**,*

Alleima

**Tube R&D; **Strategic Research Laboratories,*

Sandviken/Sweden

Abstract

In a previous study, a temperature-pH domain of stress corrosion cracking (SCC) resistance was provided for a super duplex stainless steel tube material (UNS S32750), by using slow strain rate testing (SSRT) screening in sour conditions containing 50 g/L NaCl, 5 g/L CH_3COONa under 0.5 bar (7.25 psi) H_2S at temperature 23 °C, 50 °C, 80 °C and pH 2.0, 2.8, 3.5, 4.5, 6. Initiation of selective dissolution (SD) and cracking has been identified using Scanning electron microscope (SEM) equipped by energy-dispersive X-ray spectrometer (EDS) analysis and Electron backscatter diffraction (EBSD) measurements. However, it was difficult to differentiate Mo and S found in corroded phase and corrosion products because of SEM-EDS signal overlap of these elements. In this study, Electron Microprobe Analysis (EMPA) has been used for identification of elemental enrichment or depletion in the corrosion and cracking areas. By EBSD characterization, microstructural/micro-texture changes in the material after the testing in the sour conditions have been investigated and compared with the original material matrix. Local misorientation angle (LMO) has been used for a case study where localized corrosion occurred on a specimen shoulder area. Combing EBSD with EMPA analysis on the corrode specimens, the corrosion initiation and progress have been seen in more detail. The possible corrosion mechanisms of the material degradation in different conditions are discussed.

Fast throughput screening of localised corrosion in duplex stainless steel with bipolar electrochemistry

Yiqi Zhou[*1], Dirk Lars Engelberg[2]

1. Beijing Advanced Innovation Center for Materials Genome Engineering, Institute for Advanced Materials and Technology, University of Science and Technology Beijing, Beijing 100083, China

2. Metallurgy and Corrosion, Department of Materials, The University of Manchester, Manchester, M13 9PL, Manchester, UK

Duplex stainless steels (DSS) typically contain a balanced phase fraction of austenite and ferrite, which gives these alloys excellent corrosion performance and stress corrosion cracking resistance. The size, shape and connectivity of both phases influences the overall susceptibility to localised corrosion, and in particular affects pit nucleation propensity, pit lacy cover appearance, and pit propagation pathways. This then affects the associated pit growth mechanism and growth rate.

Bipolar electrochemistry has therefore been applied to assess and measure corrosion kinetics in lean 2101 and standard 2205 DSS with exposure to chloride containing environments. All exposure tests were carried out in ambient temperature, under a wide range of applied electrochemical potentials. This allowed results to be obtained simultaneously on one sample surface, including pit nucleation probabilities, pit growth kinetics, re-passivation performance, and pit shape analysis.

Examples of the application of bipolar electrochemistry for understanding DSS corrosion are provided and discussed. This technique allows to assess the relationship between microstructure and pitting corrosion, revealing a wealth of information.

Enhanced corrosion resistance by engineering crystallography on metals

Xinxin Wei, Bo Zhang, Xiuliang Ma

Bay Area Center for Electron Microscopy, Songshan Lake Materials Laboratory, Dongguan, Guangdong 523808, China

Nanometer-thick passive films usually impart superior corrosion resistance to metals by effectively isolating the metal surface from corrosive media. Nevertheless, the passive films are degraded in long-term service, particularly in acidic environments; they are also susceptible to chloride-induced localized attack, which is one of the major causes of materials failure, with corresponding economic, safety and environmental consequences. Here, by engineering crystallographic configurations upon metal matrices adjacent to their passive films, we obtain a great enhancement of corrosion resistance of FeCr15Ni15 single crystal in sulphuric acid, with activation time up to two orders of magnitude longer than that of the non-engineered counterparts. Meanwhile, the strategy of interface engineering obviously decreases the passive current density and shifts the pitting potential to noble values. Applying anodic polarizations under a transpassivation potential, we make the metal matrices underneath the transpassive films highly uneven where both peaks and valleys feature a geometric configuration of nano-polyhedron (Figure 1). The uneven faceted metal is terminated by the close-packed {111} planes (Figure 2), and it is the as-resultant lowest-energy {111} interface between the metal and transpassive film that is responsible for the enhancement of corrosion resistance. The transpassivation strategy also works in the commercial stainless steels where both grain interior and grain boundaries are rebuilt into the low-energy configurations. Our results suggest that by engineering crystallography at the atomic scale it should be possible to improve the corrosion resistance of metals, and demonstrate a significant technological implication in the pretreatment process of anti-corrosion engineering.

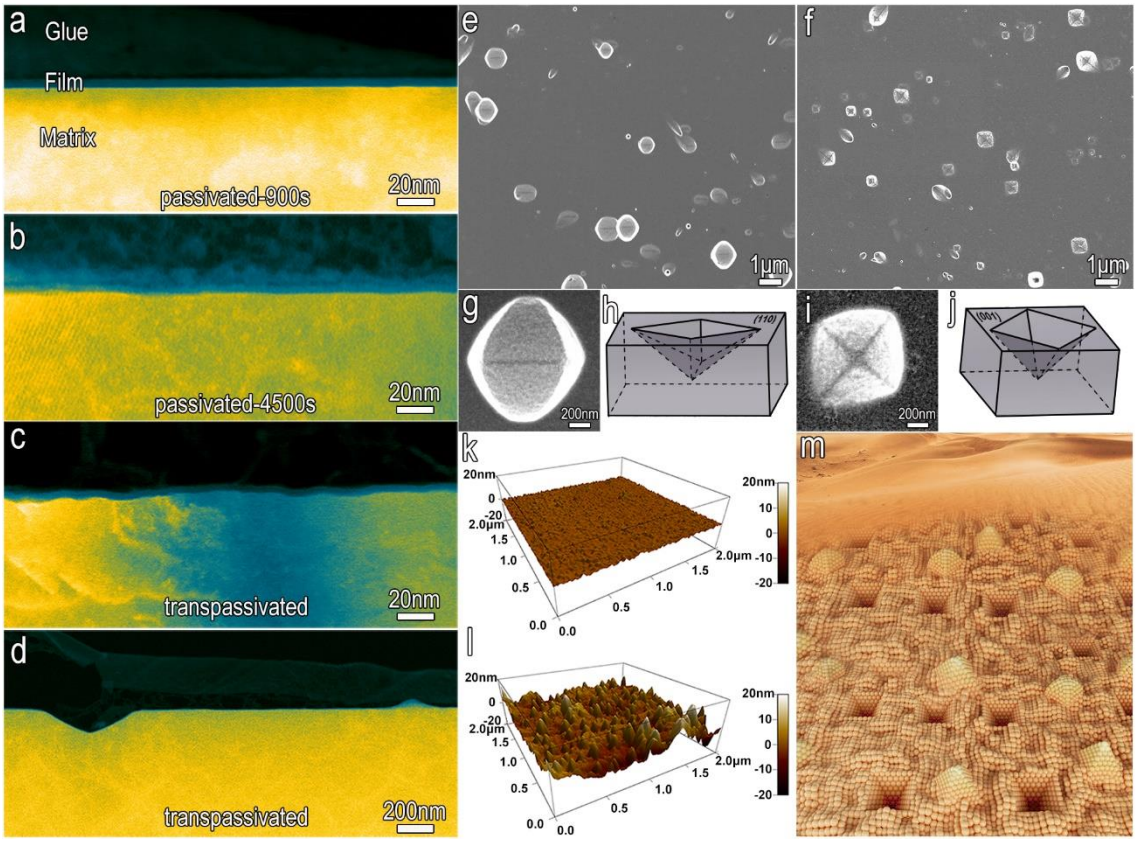

Figure 1 Transpassivation induces undulations at the metal/film interface and roughens the surface of the FeCr15Ni15 alloy. (a-d) HAADF-STEM images revealing sharp and straight interfaces of passive films (a, b) and the undulating interface for transpassive films (c, d). (e-f) SEM images of the transpassivated surface of the (110) (e) and (001) (f) plane, showing the pyramidal-shaped deep concaves enclosed by the {111} planes. (g-j) Zoom-in SEM image and schematic of concaves on (110) and (001) surfaces. (k-l) AFM images of the passivated (k) and transpassivated (l) surfaces confirming that transpassivation roughens the surface. (m) Schematic map illustrating the configuration of the TF/Me interface.

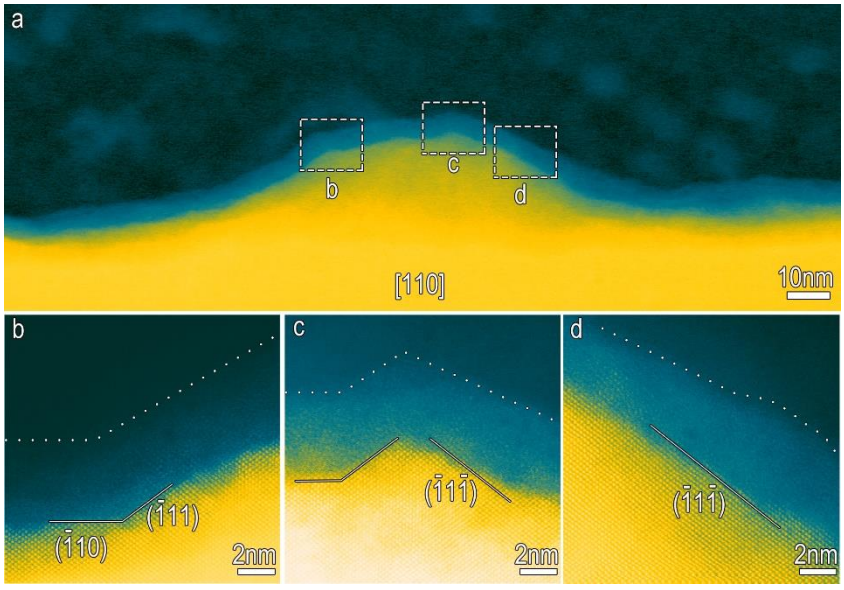

Figure 2. HRHAADF-STEM images showing transpassivation-induced prevalence of the interfaces composed of {111} close packed planes.

Erosion-corrosion resistance of martensitic stainless steels in chlorides environments

M. MONNOT, I. CHARLEUX, S. LE MANCHET
Industeel – ArcelorMittal Group, France

Martensitic stainless are widely used for their good mechanical properties in several applications like hydroelectricity, immersed chains, etc. The targeted environment contains usually moderate concentration of chlorides, but some hard particles could be also present leading to some erosion phenomena at steel surface. These particles are mainly inert terms of chemical reactivity. However, the possible erosion can affect the passive film resistance and so the pitting resistance too.

The present study focuses on the understanding of the erosion-corrosion mechanism on several martensitic stainless grades. Immersion tests and electrochemical measurements have been performed to quantify pitting resistance without erosion effect. The pitting corrosion resistance is compared with standard stainless steels: 304L, 316L and 2202. A new set-up has been developed to characterize the erosion-corrosion performance. The system consists of projecting corrosion solution containing silicon carbides at steel specimen surface. From this set-up the possible synergic effect of erosion and corrosion can be highlighted. An experimental plan has been conducted to quantify the weight of each experimental parameters on the outcomes of the set-up. And erosion-corrosion performance of different martensitic stainless are discussed.

Comparison of three different electrochemical hydrogen charging methodologies on low alloy steels and carbon steels

Luca Paterlini [a], Fabio Maria Bolzoni [a], Luca Casanova [a], Marco Ormellese [a], Giorgio Re [a]

[a] Politecnico di Milano, Milano, Italy

Hydrogen has recently been identified as a versatile energy carrier within the broader framework of the ecological energy conversion. The insertion of a significant amount of gaseous hydrogen within the existing infrastructure dedicated to NG transport and distribution is now a reality that needs to be addressed.

Hydrogen, however, is known to affect the mechanical properties of several categories of materials, including carbon steel and low-alloy steel, major components of the existing NG distribution and transportation networks.

Consequently, the compatibility of these steels with high-pressure gaseous hydrogen requires extensive investigation.

There are several well-established methods capable of reproducing the actual working conditions of pipelines in contact with high-pressure gaseous hydrogen, even on a laboratory scale.

In particular, this paper will focus on ectrochemical hydrogen charging, a versatile method capable of introducing a considerable amount of hydrogen inside the crystal lattice of steel without the necessity of involving high pressures in the process. The advantage of the electrochemical charging method is related to the formation, during cathodic polarization, of atomic hydrogen, the only one that can be absorbed by steel. As a result, it is possible to obtain an even more effective hydrogen charge, in terms of equivalent pressure, than in high-pressure gaseous hydrogen.

Three different solutions (acid and recombination poison) were tested for electrochemical hydrogen charging on carbon and low-alloy steel specimens with ferritic-pearlitic microstructure. Specifically, 20-mm-thick J-integral mechanical test CT specimens, representative of the characteristic dimensions of high-pressure NG transport pipelines, were electrochemically charged with hydrogen.

The solutions that were employed were:

- Acetic acid and sodium sulfide
- Acetic acid and potassium iodide
- Sulfuric acid and arsenic oxide.

The most relevant parameters, such as the amount of recombination poison, charging time and current density will be briefly discussed in order to highlight the advantages and limitations of each solution.

In addition, electrochemical charging tests of varying duration were performed in sulfuric acid and arsenic oxide solution on bulk carbon steel and low alloy steel specimens, in order to study the hydrogen adsorption and desorption behaviour during and after charging.

Localized corrosion resistance properties of 17-4 PH additive manufactured stainless steel specimens

P. Forcellese[1], T. Mancia[2], M. Simoncini[2], M. Kouril[3], T. Bellezze[1]

[1]Department of Materials, Environmental Sciences and Urban Planning, Polytechnic University of Marche, Ancona, Italy

[2]Department of Industrial Engineering and Mathematical Science, Polytechnic University of Marche, Ancona, Italy

[3]Department of Metals and Corrosion Engineering, University of Chemistry and Technology, Prague, Czech Republic

This study evaluates the localized corrosion resistance properties in neutral sodium chloride solutions of 17-4 PH as sintered and heat-treated stainless steel specimens, additive manufactured by Bound Metal Deposition™ (BMD™) in different build-up orientations of 0°, 45° and 90°.

The electrochemical measurements were carried out by means of anodic Cyclic Potentiodynamic Polarization in 0.35% NaCl solution and Open Circuit Potential and Electrochemical Impedance Spectroscopy monitoring as a function of exposure time in 3.5% NaCl solution. Furthermore, morphological and microstructural properties of the specimens were investigated.

The results revealed that after the solubilization and ageing treatments of the as-sintered BMD™ specimens the localized corrosion resistance properties are improved and are more comparable to those of wrought martensitic stainless steel. The presence of micro-porosities affecting the bulk of the examined steel, due to the printing patterns, together with the abundant silica-rich inclusions observed in the microstructure, produce negative effect on the localized corrosion behavior of the additive manufactured specimens. Consequently, these features seem to play a key role in the BMD™ printing of 17-4 PH stainless steel addressed to field applications in corrosive environments containing considerable amounts of chlorides.

Effect of residual stress on additive manufactured metals and their corrosion properties

E. Maria Paschalidou[1], Sara Munktell[1], Konstantin Simonov[1], Jesper Flyg[1], Markus Uhlirsch[1], Nuria Fuertes[1], Hannah Johansson[2], Magnus Grinell[2], Per Waernqvist[3], Pål Efsing[3], Björn Forssgren[3], Mimmi Bäck[4], Mattias Jonsson Coudret[4], Daniel Klint[5], James Shipley[6], Peter Gillberg[7], [1]Swerim AB, 16440 Kista, Sweden; [2]Forsmark, 74294 Östhammar, Sweden; [3]Ringhals, 43285 Väröbacka, Sweden; [4]OKG, 57283 Oskarshamn, Sweden; [5]Alfa Laval, 226 55 Lund, Sweden; [6]Quintus, 721 36 Västerås, Sweden; [7]CURTISS-WRIGHT, 732 47 Arboga, Sweden

Introduction

Stress Corrosion Cracking (SCC) is a well-known degradation mechanism affecting stainless steel (SS) operating in harsh environments. Preventative measures such as rigorous testing/appropriate test standards are in place in the material qualification process. There is a desire in certain industries to replace conventional SS, *e.g.* 316L, with the corresponding additive manufactured (AM) SS material, to shorten the lead time and reduce the cost for special components (such as complex geometries). This desire presents a demand for AM SS to withstand the same operational requirements similarly to conventional materials. The SCC phenomenon is well investigated and controlled for conventional 316L SS but has only partially explored for AM 316L SS [1-5].

Materials and Methods

In the current study, material properties of AM 316L SS, produced by Laser Powder Bed Fusion, are investigated. The effect of post processing, by Hot Isostatic Pressing (HIP) and shot peening, on SCC properties is also explored. Test methods include SCC testing (based on 4-point bend and slow strain rate, SSRT), residual stress measurements (based on X-ray diffraction) and field tests in nuclear reactor environment in the autoclave system at OKG (in reactor “Oskarshamn 3”). The autoclaves are connected to the water cleaning facility for the pressurized water reactor (PWR). The gathered results will further be linked to microstructure and compared SCC resistance of AM 316L SS in relation to conventional 316L SS material.

Results

X-ray measurements showed that HIP reduces internal stresses in AM 316L SS. EBSD analysis of cross sections showed that shot peening introduces significant surface deformation and compressional stress in the surface near region. In this work, the effect of different post-processing steps on AM 316L on the resistance of SCC is evaluated by correlating the residual stress level by XRD after post-processing with the results from SCC testing by SSRT, 4pt bend testing and field exposures.

References

1. Kain, V. Stress corrosion cracking (SCC) in stainless steels. in Stress Corrosion Cracking 199–244 (Elsevier, 2011). doi:10.1533/9780857093769.3.199
2. IAEA. Stress Corrosion Cracking in Light Water Reactors: Good Practices and Lessons Learned. IAEA Nucl. Energy Ser. No. NP-T-3.13 115 (2011).
3. Kong, D., Dong, C., Ni, X. & Li, X. Corrosion of metallic materials fabricated by selective laser melting. npj Mater. Degrad. 3, (2019).
4. Sander, G. et al. Corrosion of additively manufactured alloys: A review. Corrosion 74, 1318–1350 (2018).
5. Örnek, C. Additive manufacturing–a general corrosion perspective. Cor. Eng. Sci. Technol. 53, 531–535 (2018).

In-situ synchrotron X-ray study of evolution of the passive film on nickel alloys in acidic chloride solution

Xiaoqi Yue[1], *Alfred Larsson*[2], *Andrea Grespi*[2], *Josefin Eidhagen*[1,3], *Ulrich Lienert*[4], *Zoltan Hegedüs*[4], *Edvin Lundgren* [2], *and Jinshan Pan* [1]

[1] *KTH Royal Institute of Technology, Division of Surface and Corrosion Science, Stockholm, Sweden*

[2] *Lund University, Division of Synchrotron Radiation Research, Lund, Sweden*

[3]*Alleima (former Sandvik Materials Technology), Sandviken, Sweden*

[4]*DESY Photon Science, Hamburg, Germany*

The evolution of the passive films formed on nickel alloys at elevated anodic potentials in 3 M $MgCl_2$ at low pH was investigated by combining electrochemical methods and synchrotron-based X-ray reflectivity (XRR), X-ray diffraction (XRD), X-ray fluorescence (XRF), and two-dimensional surface optical reflectance (2D-SOR). The results indicated that an increasing current density and reduced impedance of nickel alloys at high applied potentials are associated not only with the dissolution of metal, but also with the evolution of the passive film and the oxygen evolution reaction. A change in density and thickness of the passive film can be detected by XRR from open circuit potential (OCP) to 400 mV above OCP. The 2D-SOR shows violent bubbling at higher applied potentials due to oxygen evolution reaction. As the applied potential increases, the reduction in impedance with inductive characteristics is associated with the enhanced dissolution of Mo, followed by the deposition of corrosion products. The results also suggest the preferential dissolution of the passive film in specific grain orientations of the metal substrate.

Pitting engineering diagrams for stainless steel

Sukanya Hägg Mameng, Lena Wegrelius, Björn Helmersson

Avesta R&D Center, Outokumpu Stainless AB, Avesta, Sweden

Abstract

Stainless steel is one of the most corrosion-resistant materials and is a significant construction material for water applications. The limiting condition for the pitting resistance of stainless steel depends on, among other things, the alloying composition and the service environment. The pitting resistance increases with increasing alloying level, allowing for a rough estimate to be done in terms of the Pitting Resistance Equivalent Number (PREN). For the environmental condition, chloride ion level, temperature, and the open circuit potential (OCP) in a system containing oxidizing species such as chlorine also influence the risk of pitting corrosion which, if raised, would increase the risk of pit initiation.

This paper addresses a new concept of defining limiting conditions of pitting corrosion for different standard austenitic and duplex stainless steel grades in non-chlorinated and chlorinated water systems based on extensive electrochemical testing. The electrochemical tests were performed in chloride-containing environments, with chloride levels corresponding to a range from potable water to seawater and higher. Results are discussed in the current understanding of the critical levels of key parameters for constructing the pitting engineering diagrams.

Keywords

Stainless Steel; pitting engineering diagram, pitting corrosion, chloride, temperature, open circuit potential (OCP) of the water system, non-chlorinated water, chlorinated water

Multimodal *in situ* synchrotron study of the passive film breakdown on a Ni-Cr-Mo industrial alloy

***Alfred Larsson*[1]**, *Andrea Grespi[1], Josefin Eidhagen[2,3], Giuseppe Abbondanza[1], Dorotea Gajdek[4], Konstantin Simonov[5], Xiaoqi Yue[2], Huajie Tang[2,6], Ulrich Lienert[7], Zoltan Hegedüs[7], Mattia Scardamaglia[8], Andrey Shavorskiy[8], Lindsay R. Merte[4], Jinshan Pan[2], and Edvin Lundgren[1]*

[1]*Lund University, Division of Synchrotron Radiation Research, Lund, Sweden*
[2]*KTH Royal Institute of Technology, Division of Surface and Corrosion Science, Stockholm, Sweden*
[3]*Alleima (former Sandvik Materials Technology), Sandviken, Sweden*
[4]*Malmö University, Materials Science and Applied Mathematics, Malmö, Sweden*
[5]*Swerim AB, Department of Materials and Process Development, 164 07 Kista, Sweden*
[6]*University of Science and Technology Beijing, School of Materials Science and Engineering, Beijing, China*
[7]*DESY Photon Science, Hamburg, Germany*
[8]*MAX IV Laboratory, Lund, 221 00, Sweden*

Our current understanding of the structure and chemistry of passive films is primarily based on ex-situ surface analysis using X-ray Photoelectron Spectroscopy (XPS) and Scanning Tunneling Microscopy (STM). The commonly used XPS has traditionally been limited to Ultra High Vacuum (UHV) conditions, so the results do not really represent the true *real-world surface composition*. To be able to observe corrosion initiation and progression and obtain a fundamental understanding of the corrosion mechanisms there is a need for techniques that can combine *in situ* capabilities with detailed chemical and structural information from the surface region. To this end, we have used a combination of Ambient Pressure XPS (AP-XPS), X-ray Reflectivity (XRR), Grazing Incidence X-ray Diffraction (GI-XRD), X-ray Fluorescence (XRF), and X-ray Absorption Near Edge Structure (XANES) to follow the passive film growth and breakdown of a Ni-Cr-Mo alloy in NaCl solution. Growth of the passive film and enrichment of Mo^{6+} oxide was observed in the passive range bellow 800 $mV_{vs\ Ag/AgCl}$, followed by a drastic increase in the electrochemical current coupled with the formation

of a thick hydrous film of MoO_3, and $Cr(OH)_3$, as seen in Figure 1 a). The current increase at potentials above 800 $mV_{vs\ Ag/AgCl}$ coincided with the dissolution of Ni^{2+}, Cr^{3+}, and Mo^{6+}, as seen in Figure 1 b). Quantitative analysis revealed that a substantial part of the measured current was due to oxygen evolution, as shown in Figure 1 c). The experimental techniques and the unique information they provide will be discussed, as well as the role of the oxygen evolution reaction on the passivity breakdown of the Ni-Cr-Mo alloy.

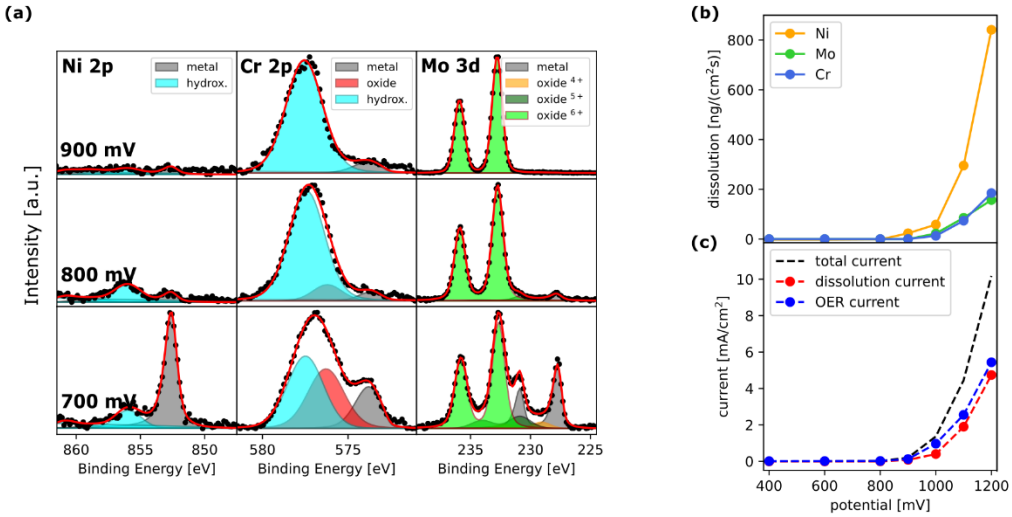

Figure 1: a) AP-XPS data on Ni-Cr-Mo alloy after electrochemical exposure steps. b) in situ XRF dissolutions measurements. c) Total current, dissolution current and oxygen evolution current.

High resolution analysis of passive films with low energy ion scattering reveal new insight into passive film structures and chemistries on steels and high entropy alloys

Matthias Kogler, Lukas Kalchgruber and Markus Valtiner

Vienna University of Technology, Vienna Austria and CEST GmbH, Wienerneustadt, Austria

It is common knowledge that passive film are central to the stability of a wide range of engineering metals and new materials such as high entropy alloys. Many studies focused on characterizing passive films using XPS and other surface sensitive spectroscopies. However, these techniques are not truly surface sensitive, but probe a depth of about 5-10 nm. Therefore, it is not trivial and often error prone, how oxide film characteristics are derived from traditional surface science tools. We utilize a novel low energy ion scattering tool, operando-coupled to an electrochemical cell, to characterize a large range of passive films on steels, galvanized steels and high entropy alloys. Our data allows to characterize quantitatively passive film chemistries with sub nanometer vertical resolution. This also provides access to diffusion gradients of alloying elements across an oxide under varying electrochemical conditions. We will finally compare our data with the current understanding of passive film chemistries, and compare data to AFM topographic evolution, and ICP-MS real time evaluation of metal dissolution across a passive film, for materials ranging from steel to high entropy alloys.[1,2]

References.

1) **Combining AFM imaging and elementally resolved spectroelectrochemistry for understanding stability and quality of passive films formed on Alloy 600**
Dominik Dworschak, Marina Bishara, Hsiu-Wei Cheng, Markus Valtiner, 2022, Materials and Corrosion, https://doi.org/10.1002/maco.202112984

2) **Bottom-up characterization of electrochemical passivity from simple binary alloys to high entropy alloys,** D Dworschak, KK Tseng, JW Yeh, HW Cheng, M Valtiner, Electrochimica Acta 405, 139804

Correlation of corrosion and mechanical properties of Fe-Ni-Cr-Mn alloy synthesized by diffusion multiples

Yasemin Yesilcicek [a], *Annica Wetzel* [a], *Julia Witt* [a], *Matthias Dimper* [a], *Ozlem Ozcan* [a]

[a] *Bundesanstalt für Materialforschung und-prüfung, Berlin, Germany*

Abstract

The efficient exploration of novel alloy compositions is crucial for advancing the development of new materials. One widely utilized approach for creating phase diagrams is the use of diffusion-controlled synthesis for gradient alloys. This method is also an effective means for rapidly identifying potential material combinations.

The present study focusses on the exploration of quaternary multi-principle-element alloys (MPEAs) using diffusion multiples. We established a diffusion system by combining an equimolar ternary alloy (FeNiCr) with single diffusing elements Mn and Mo. Using ThermoCalc simulations, we determined suitable temperature ranges where we can expect the formation of single-phase alloys. Depending on the diffusion constants of the selected metals, diffusion times were adjusted to obtain diffusion zones with a depth of greater than 50 µm. Microstructural and compositional information was gathered via scanning electron microscopy (SEM) and energy dispersive X-ray spectroscopy (EDX) and correlated to local mechanical properties evaluated by means of nanoindentation. Local corrosion properties were examined using Atomic Force Microscopy (AFM) and Scanning Electrochemical Microscopy (SECM).

Our results indicate that the ThermoCalc simulations have a good predictive power for crystallographic phases. However, especially with the Mn-FeNiCr system, formation of Cr-rich secondary phases were observed, which led to Cr-depletion and thus to localized corrosion processes in the matrix at the vicinity of the secondary phases. Based on the results of the local electrochemical tests, we have selected single-phase compositions along the diffusion zone and synthesized these alloys in bulk for corrosion studies by means of potentiodynamic polarization and SECM.

The presentation will summarize our methodology using diffusion couples as an efficient tool for exploring compositional spaces of MPEAs in the search for novel single-phase alloys and the results of our correlative study on the mechanical and corrosion properties of these materials.

Effect of alloying elements on spontaneous repassivation of Cantor-based high entropy alloys: measurement based on atomic emission spectroelectrochemistry

Chenyang Xie [1], Junsoo Han [2], Fan Sun [1], Kevin Ogle [1]

[1] Chimie-ParisTech, PSL University, IRCP-CNRS, 75005 Paris, France;

[2] Sorbonne Université, Laboratoire Interfaces et Systèmes Electrochimiques, LISE, 75005 Paris, France

Cantor alloy is well-known high entropy alloy which containing 20% of Cr; thus, the anticorrosion property is highly depends upon the nature and stability of the Cr rich passive film. Physical attacks such as scratch and abrasion and/or chemical attacks such as pitting and crevice corrosion could remove partial of the film. Therefore, the ability of spontaneous repassivation after the removal of the film is of significant importance. However, it is difficult to measure quantitatively this spontaneous repassivation directly with “conventional” electrochemistry as it occurs at the open circuit potential without any external current or potential perturbation applied to the material.

To this end, we have applied a new methodology to directly monitor the kinetics of spontaneous passivation by using element-resolved electrochemistry (atomic spectroelechemistry, or AESEC) [1-3]. The experimental protocol is to first partially remove the passive film via a potentiostatic hold and then to monitor repassivation after a return to the open circuit potential by following the elemental dissolution rates as a function of time. For example, the passive film may be dissolved in an acidic solution a potential hold in either the cathodic or transpassive potential domain. By monitoring the corrosion rate of each individual alloying element as a function of time during these processes, we obtain a quantitative analysis of dissolution and surface enrichment during the passivation process.

Alloy composition is a major factor in repassivation kinetics, for example, our previous work has shown the benefit of Mo [2] and deterioration from Mn [3]. The chemistry of the alloying elements is interconnected with the chemistry of the electrolyte. In general, dissolved oxygen has a positive effect on repassivation kinetics [3] and the oxygen impoverished occluded zones such as occur during crevice or pitting corrosion serve to accelerate the corrosion process. Likewise, Cl^- ions are frequently present in the environment and also destabilize the passive film. In this presentation we will describe experimental repassivation kinetics measurements for Cantor-based alloy (95 at.% of equimolar CoCrFeNi) with 5% of other alloying elements (Mn, V, Ti, Cu, Al, Mo, W). We will also discuss how the repassivation kinetics are affected by Cl^- and dissolved oxygen in the electrolyte.

1) K Ogle “Atomic emission spectroelectrochemistry: real-time rate measurements of dissolution, corrosion, and passivation”, Corrosion 75 (2019)1398-1419. Open access.

2) X Li, J D Henderson, F P Filice, D Zagidulin, M C Biesinger, F Sun, B Qian, D W Shoesmith, J J Noël, K Ogle, “The contribution of Cr and Mo to the passivation of Ni22Cr and Ni22Cr10Mo alloys in sulfuric acid”, Corrosion Science 176, (2020) 109015.

3) X Li, P Zhou, H Feng, Z Jiang, H Li, K Ogle, “Spontaneous passivation of the CoCrFeMnNi high entropy alloy in sulfuric acid solution: The effects of alloyed nitrogen and dissolved oxygen”, Corrosion Science 196(2022)110016.

Understanding corrosion passivation layers on high entropy alloys using High Sensitivity – Low Energy Ion Scattering Spectroscopy (LEIS)

Matthias Kogler[1,2], *Christian Pichler*[1,2], *Markus Valtiner*[1,2]

[1]*Centre for Electrochemistry and Surface Technology GmbH, Wr. Neustadt/Austria*

[2]*Technical University of Vienna, Vienna/Austria*

Complex metallic materials such as Multi-Principal Alloys (MPEAs) and High Entropy Alloys (HEAs) possess unique material properties, allowing a broad variety of mechanical properties to be achieved by combining 5 or more elements in HEAs. High corrosion resistance is a property of great importance for the application of such materials, which, however, is not yet well understood due to the multi-element nature of the alloys.

Especially with regard to corrosion-protective passivation films, the complex correlations with the corrosion behaviour are fully unclear to date, and require an in-depth atomic level characterisation and rationalisation. However, the precise layer by layer structure of such passive films is particularly challenging to assess, since traditional techniques such as XPS or Auger electron spectroscopy have analysis penetration depths of few nanometres and cannot reach atomic layer resolution. However, to fully understand and quantify the passivation layer structure, such an atomic layer resolution is necessary, due to the complexity of HEAs.

In order to obtain an exact understanding of the atomistic mechanism at the monoatomic layer level, High-Sensitivity - Low Energy Ion Scattering Spectroscopy (HS-LEIS), was applied, which provides the required monolayer sensitive resolution to study the passivation layers of such complex multicomponent alloys. Due to the high resolution achieved by static and sputter depth profile modes, we could determine the exact composition of the HEA passivation layer with resolution on atomic monolayer scale.

This provides the potential to significantly advance the current understanding of the passivation behaviour of MPEAs and HEAs, and the development of novel metallic materials with superior properties. Valuable insights for understanding the corrosion resistance for those highly advanced materials could thereby be generated.

Advanced SMART materials for extreme environments: functionality at nanoscale

A. Litnovsky[1], J. Gonzalez-Julian[1,2], M. Bram[1], I. Povstugar[1], E. Prestat[3], J. Lim[3], D. Nguyen-Manh[3], M. Gilbert[3], D. Sobieraj[4], J.S. Wróbel[4], A. Reuban[1], J. W. Coenen[1,5], Ch. Linsmeier[1].

[1]Forschungszentrum Jülich GmbH, Institut für Energie und Klimaforschung, 52425 Jülich, Germany

[2]Institute of Mineral Engineering, RWTH Aachen University, 52074, Aachen, Germany

[3]CCFE, United Kingdom Atomic Energy Authority, Culham Science Centre, Abingdon, Oxfordshire OX14 3DB, United Kingdom

[4]Faculty of Materials Science and Engineering, Warsaw University of Technology, Wołoska 141, 02-507 Warsaw, Poland

[5]Department of Engineering Physics, University of Wisconsin – Madison, Madison, WI 53706, USA

Subtopic: Surface Science and Mechanisms of Corrosion and Protection (WP6)

Self-passivating Metal Alloys with Reduced Thermo-oxidation (SMART) were initially proposed as a passive safety measure for the fusion power plant. These tungsten-based alloys change their properties depending on environment. During the regular plasma operation of the power plant, the SMART plasma-facing wall features the properties of the pure tungsten, highly advantageous for plasma operation. In case of an accident with a loss of coolant and air ingress into the power plant, the alloying elements in SMART form their own dense oxide scale, protecting tungsten from oxidation and subsequent sublimation into the atmosphere. The most advanced SMART materials contain 11.4 weight percent of Chromium (Cr), 0.6 weight percent of Yttrium (Y) and tungsten (W) constituting the rest.

The functionality of the SMART concept has been demonstrated already. It was shown, that during plasma operation the sputtering resistance to fusion-relevant deuterium plasma is the same for pure tungsten and for SMART. The oxidation resistance of SMART material is outstanding. The SMART features at least 10^4-fold suppression of oxidation rate at 1000^{o}C in air atmosphere containing 70 volume percent of humidity as compared to that of pure tungsten. The sublimation of tungsten oxide is at least 40-fold less for SMART material than that for pure tungsten.

The progress in SMART technology opened the way for its expansion to energy systems outside fusion. Presently studies are started to investigate the SMART as potential material of high-temperature receiver for concentrated solar power stations. Nevertheless, the in-depth physics understanding plays the extremely important role in gaining the full control over the SMART concept. Especially, the role of Yttrium, present in tiny amount in SMART and drastically changing the oxidation behavior is being thoroughly investigated both by modeling and experiments. The processes at nanoscale are playing the crucial role in functionality of the SMART materials.

The first-principles modeling performed for W-Cr-Y system demonstrates that all alloying elements are tending to segregate from each other up to the temperature of 1560^{o}C. The presence of Yttrium was appeared to shift the spinodal decomposition temperature for W-Cr to nearly 1100^{o}C, thus stabilizing SMART at lower temperature already.

The state-of-the-art experiments, involving Atom Probe Tomography (APT) and innovative in-situ oxidation in Transmission Electron Microscope (TEM) are underway. The APT studies have confirmed the formation the perovskite-like $CrYO_3$ oxides as predicted by modeling. Tomography studies show also an outstanding “cleaning” action of the SMART grain boundaries from oxygen stimulated by Yttrium, Figure 1. The absence of O along the grain boundaries is believed to ease the Cr transport needed for maintaining the protective chromia scale.

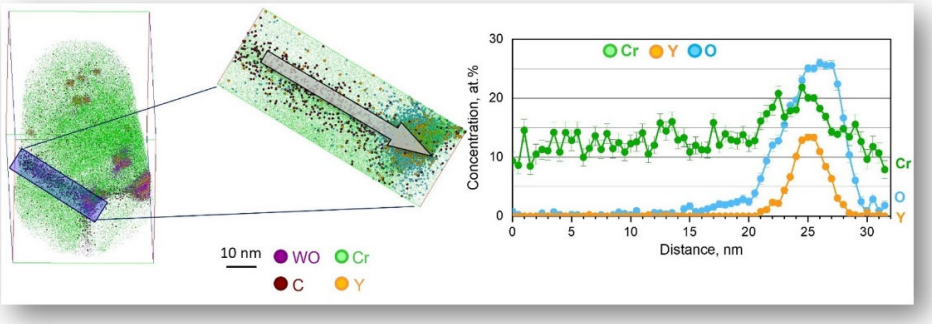

Figure 1. Atom probe tomogram and elemental distribution along the grain boundary demonstrating the “oxygen cleaning” action of yttrium-containing particles

The *in situ* oxidation has revealed another spectacular effect. Despite expectations, the formation of initial protecting scale is not driven by diffusion of alloying elements along grain boundaries. Dense chromia scale is formed first at grains enriched with Cr, then spreading along the surface of the material. Investigations of unique SMART materials will be presented and discussed in the contribution.

Investigation of the influence of iron-rich precipitates on the corrosion of recycled Al6xxx alloys

Alexander Lutz, Group of Electrochemical and Surface Engineering, Vrije Universiteit Brussel, Brussels, Belgium

Wouter Vereycken, Group of Electrochemical and Surface Engineering, Vrije Universiteit Brussel, Brussels, Belgium

Iris De Graeve, Group of Electrochemical and Surface Engineering, Vrije Universiteit Brussel, Brussels, Belgium

Al6xxx alloys gain their main mechanical properties from precipitates containing Mg and Si. However, a significant amount of iron is also present in this alloy series to decrease the gloss of the surface after chemical etching. For alloys produced mainly from end-of-life (EOL) scrap, the content of elements like iron is typically higher, because automated separation is costly. Therefore, it is important to understand under which conditions increased amounts of alloying elements like iron cause undesired effects and under which circumstances their influence is negligible.

We will first show the effects of iron on the corrosion properties of bare alloys, secondly we will discuss the effects on anodized alloys and finally we will look into the effects on conversion coated alloys. We will compare alloys with different iron and recycle content. To give an in-depth understanding of the corrosion mechanisms we will discuss the results of global and local electrochemical techniques and combine them with optical and electron microscopy.

Finally, we would like to comment on the possibility of increasing the recycle content of 6060 type aluminum alloys based on the presented results.

Stabilizing Metal Electrocatalysts with Ionic Liquids

Michael G. Strebl[1], Yunsheng Qiu[2], Juntao Yang[3], Olaf Brummel[3], Jörg Libuda[3], Karl J.J. Mayrhofer[2], Sannakaisa Virtanen[1]

[1]Institute for Surface Science and Corrosion, Friedrich-Alexander Universität Erlangen-Nürnberg (FAU), Erlangen, Germany

[2] Helmholtz-Institute Erlangen-Nürnberg for Renewable Energy, Forschungszentrum Jülich GmbH, Erlangen, Germany

[3]Interface Research and Catalysis, Friedrich-Alexander Universität Erlangen-Nürnberg (FAU), Erlangen, Germany

Suitable electrocatalysts for reactions related to future clean energy conversion technologies such as HER/ HOR, ORR/OER or CO_2 reduction reaction are key for the transition to a more sustainable society. In this context, Pt-Ni alloys are promising candidate materials for the ORR electrocatalyst in fuel cells, since they achieve increased catalytic activity while decreasing the noble metal loading. Further optimization of the catalyst is possible by modification of the electrocatalytic surface with functionalized ionic liquids (ILs) according to the SCILL (solid catalyst with ionic liquid layer) concept. [1] While it was shown that electrochemical SCILLs show increased activity [2] and selectivity [3] of the targeted reactions, little is known about the influence of ILs on the dissolution rate. Hence, the aim of this work is to fundamentally investigate the influence of selected ILs, either added to an aqueous electrolyte (water-miscible ILs) or deposited on the metallic catalyst (water-immiscible ILs), on the corrosion behavior and dissolution rates.

Screening of different ILs on pure Ni was carried out in 0.1 M $HClO_4$ electrolyte by electrochemical characterization with EIS and polarization curves. While some ILs decreased the dissolution rate at the free corrosion potential, other ILs showed a beneficial passivation effect during anodic polarization. Selected ILs were tested on different Pt-Ni alloys with electrochemical scanning flow cell coupled ICP-MS to measure time- and potential-resolved dissolution rates via the amount of dissolved metal cations released into the stream of electrolyte. Slightly accelerated dissolution by adding IL to the electrolyte was found for low Ni content Pt-Ni alloys. However, in

line with the results on pure Ni, IL addition strongly suppressed dissolution rates for Ni-rich alloys. A newly developed high resolution respirometric method was employed to monitor time-dependent corrosion rates based on the amount of evolved H_2 or the amount of consumed O_2. To elucidate the degradation and protection mechanisms at the catalyst/IL interfaces, XPS analysis of the surface films was carried out. Furthermore, electrochemical infrared reflection absorption spectroscopy (EC-IRRAS) was performed to reveal the potential-dependent specific adsorption of the IL-anion on a Ni surface.

In summary, the SCILL concept presents an opportunity to extend the range of possible non-noble metal containing catalyst materials by the stabilizing effect of IL modification.

[1] G.-R. Zhang, B.J.M. Etzold, Adv. Funct. Mater., 31 (2021) 2010977, https://doi.org/10.1002/adfm.202010977
[2] J. Snyder, T. Fujita, M.W. Chen, J. Erlebacher, Nat. Mater., 9 (2010) 904-907, https://doi.org/10.1038/nmat2878
[3] T. Yang, J. Yang, X. Deng, E. Franz, L. Fromm, N. Taccardi, Z. Liu, A. Görling, P. Wasserscheid, O. Brummel, J. Libuda, Angew. Chem. Int. Ed., 61 (2022) 202202957, https://doi.org/10.1002/anie.202202957

EQCM study of early stage of aluminum oxidation kinetics in water based solutions from alkaline to acidic pH range

Olga Guseva, Patrik Schmutz

Laboratory for Joining Technologies and Corrosion,

Empa - Swiss Federal Laboratories for Materials Science and Technology,

Dübendorf CH-8600, Switzerland

Both, thermodynamic and kinetic aspects are necessary for understanding of electrochemical processes related to corrosion. The well-known potential-pH diagrams (Pourbaix diagrams) are used to describe the thermodynamic stability of a metal (usually in pure water) as a function of potential and pH at a given temperature. Regarding Pourbaix diagram for aluminum, three main regions in aqueous media at 25 °C can be distinguished: an alkaline region, typically pH > 10, where aluminum is corroding; a stability "passive" domain, 4 < pH < 10, where a stable oxide/hydroxide film protects the metal surface; and an acidic region, pH < 4, where aluminum is corroding again. The reaction kinetics, i.e. the actual corrosion rate, is much less understood and is dependent on specific environmental parameters, such as temperature, solution composition and the presence of intermediate "solid" reaction limiting layer. In this work, the kinetics of aluminum oxidation, i.e. reaction rates, across these three pH regions is considered using the electrochemical quartz crystal microbalance (EQCM) technique, which is proved to be a very sensitive method for study of interfacial phenomena at the solid-liquid interface.

The measurements are based on specifically coated electrodes, pure aluminum in this work, on both sides of a piezoelectric quartz crystal oscillating at an eigenfrequency in contact with an electrolyte on one side. During the reaction of the electrode with environment, the mass of the coated quartz changes, which results in a frequency shift. For small changes in mass the frequency shift, (ΔF in Hz) is linearly dependent on the mass (Δm is mass per unit area (g cm^{-2})); according to a Sauerbrey equation $\Delta F = -C_f \cdot \Delta m$ where C_f is a constant dependent on material properties of the quartz oscillator. Competing dissolution and "oxide" film formation processes can be better described with EQCM information. The study was complemented by surface analytical (SEM, XPS) characterization of the aluminum surface after the solution exposure.

At alkaline conditions, pH > 10, the expected active dissolution of aluminum substrate happens, dissolution rate depending on solution pH. Based on EQCM data analysis in NaOH solution in a pH range of 10 – 11.5, a surface pre-treatment procedure was proposed aimed to a well-defined removal of the native oxide layer followed by a dissolution of 20 – 25 nm from the upper layer of the aluminum substrate. This alkaline "etching" procedure was then performed prior to all EQCM measurements reported in this work, to ensure the same initial surface conditions for all subsequent experiments.

At weakly acidic conditions, 3 < pH < 5.8, in order to track the anodic oxide film formation/dissolution processes, polarizing in citric acid of pH 3, 4, and 5.8 at 10 V for four hours was performed (see Fig. 1).

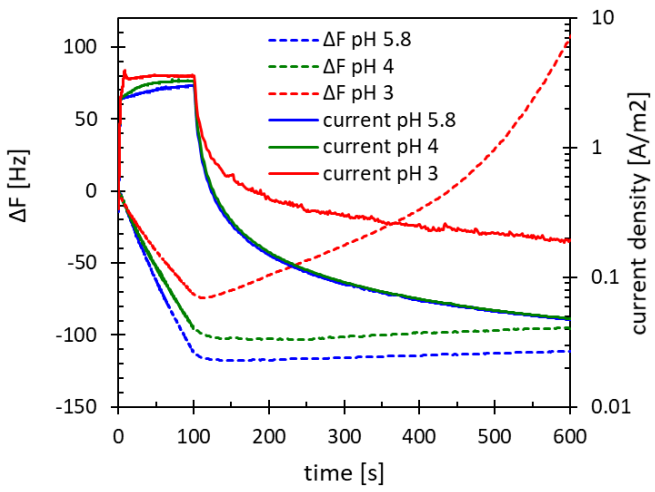

Fig. 1. ΔF variation (dashed lines) and current density (solid lines) vs time during the anodizing of aluminum sample from 0 to 10 V with a scan rate of 100 mV/s. The potential was ramped up during the first 100 s, subsequently keeping a constant 10 V value for 4 h in citric acid of different pH values. (Note, that decrease in ΔF values means film growth).

During the ramp-anodizing time (0 - 100 s), a linear-time-dependent film growth is observed in all solutions up to an estimated total film thickness of 14 nm (assuming density of an amorphous oxide of 3.17 g/cm^3), even in presence of strong chemical dissolution in pH 3. It was also found that, at the end of anodizing ramp (100 s), dissolution of aluminum Al^{3+} ions takes place (8 %) even in non-aggressive solution of pH 5.8. In a pH 3 solution, the dissolution increases up to 27 %. Further keeping of anodizing potential at a constant value of 10 V for 4 hours leads to interplay of electrochemical faradic film growth and dissolution processes.

Additionally, immersion of aluminum in MilliQ water (pH value of 5.7) at open circuit potential (OCP) at room and 50 °C was conducted. Whereas at 25 °C no significant mass change occurred, a rapid hydroxide film formation was obtained at 50 °C.

At a very low pH of 0.4 (immersion at OCP in 0.5 M H_2SO_4), after an initial diffusion-controlled film formation (presumably salt film) during the first hour, a steady slow active dissolution of aluminum substrate was observed with a constant rate.

Correlation between corrosion properties and the stress-induced martensite transformation of a Fe-Mn-Al-Ni-Cr shape memory alloy

Johanna-Maria Frenck[1], *Georg Frenck*[2], *Sebastian Degener*[1,3], *Malte Vollmer*[1], *Thomas Niendorf*[1]

[1] *University of Kassel, Institute of Materials Engineering, Germany*

[2] *Augsburg University, Institute of Mathematics, Germany*

[3] *now at: Bundesanstalt für Materialforschung und -prüfung (BAM) Berlin, Germany*

In recent years, iron-based shape memory alloys have become increasingly attractive for potential applications in civil engineering. The characteristic phase transformation results in high damping capacities, that are of particular interest for buildings in earthquake-prone areas. The Fe-Mn-Al-Ni shape memory alloy is characterized by a reversible phase transformation between the high-temperature α-austenite phase and the low-temperature γ'-martensite phase. While the mechanical properties of this alloy have already been studied comprehensively, it is equally important to thoroughly understand the corrosion behavior. Therefore, electrochemical corrosion tests, i.e. open circuit potential and potentiodynamic polarization, have been conducted on Fe-35Mn-13.5Al-7.5Ni-1.5Cr (at.-%) specimens in a sodium chloride solution. The microstructure of the specimens was characterized by an austenitic matrix with randomly distributed stress-induced martensite plates. During immersion in the electrolytic solution the specimens appeared to form a protective oxide layer on the surface. However, severe pitting corrosion of the γ'-martensite plates led to an unstable passive corrosion behavior. To further investigate the effect of a corrosive environment on the mechanical properties and martensite transformation, incremental strain tests considering different surface conditions were performed. The tested surfaces were characterized by partial surface corrosion, featuring areas of locally severe pitting corrosion. The significant changes of surface quality did not show a negative effect on the mechanical properties. However, it was shown that areas with retained martensite serve as nucleation zones for further corrosion damage. Eventually, stress-induced corrosion cracks develop, which are very detrimental with respect to functional response.

New REACh compliant anodized-impregnated-sealed multilayers system for the corrosion protection of 2618-T851 aluminum alloy: A coupled SEM/XPS diagnosis of the inner chemical interactions.

Celine MIRA[(1)], Jean-Charles DUPIN[(1)], Joffrey TARDELLI[(2)], Laetitia THOMAS[(2)], Jerome FRAYRET[(3)], Virginie BAGUE[(4)], David SINOPOLI[(5)], [(1)]Universite de Pau et des Pays de l'Adour, E2S UPPA, CNRS, IPREM, PAU/France, [(2)] IRT-M2P, DUPPIGHEIM/France, [(3)]Ineosurf, GRABELS/France, [(4)]Safran Aircraft Engines, EVRY/France, [(5)]Airbus Helicopters, MARIGNANE/France

For many years, anodizing and sealing were performed with chromium (VI) compounds such as chromic acid and potassium dichromate on aluminum alloys for corrosion protection [1]. These compounds, classified as CMR (Carcinogenic, Mutagenic and Reprotoxic), have to be substituted according to the European legislation REACh [2]. With the COCA* project, a promising REACh compliant process has been developed as a new alternative in the corrosion protection of 2618-T851 Al alloy. This alloy contains numerous Ni and Fe intermetallic particles [3], which make difficult its anti-corrosion treatment. The aim of this study is to corroborate a mechanistic approach (identification of active chemical species) with the corrosion protection performance.
In its protection concept, the COCA process consists of three steps (Figure 1), the second step corresponds to the impregnation into a conversion solution containing both Cr and Zr species and normally used for TCP ("Trivalent Chromium Process").

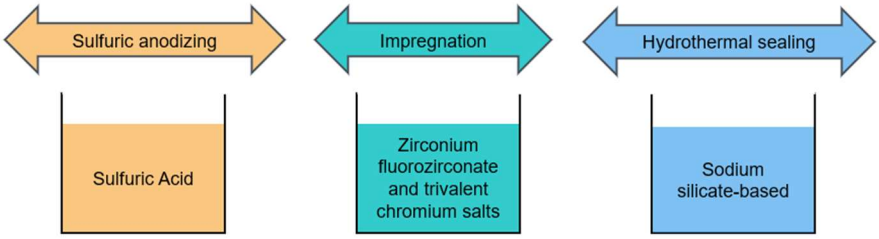

Figure 1: Scheme of the new REACh compliant process

Different anodizing regimes, impregnation solutions and sealing baths were solicited in the study to reach the best anti-corrosion performance. After 2618-T851 Al materials treatments, some scanning electron microscopy (SEM) analyses coupled with a chemical surface investigation, conducted by X-ray photoelectron spectroscopy (XPS), clearly highlighted the formation of $Cr(OH)_3/Cr_2O_3$ and ZrO_2, at the top surface, between the anodic and the sealing layers, but even around the intermetallic particles

present in the anodic layer. With the 3 different Cr/Zr concentration ratios tested, the distribution of these species is similar, but the Zr species diffusion in the anodic layer seems to be dependent of Cr/Zr ratio. The interdependence of Zr and Cr has been demonstrated for the building of the protective layer. In the sealing step, the silicon from the silicates solution forms a thin and dense layer of SiO_2 at the outermost surface as illustrated in Figure 2.

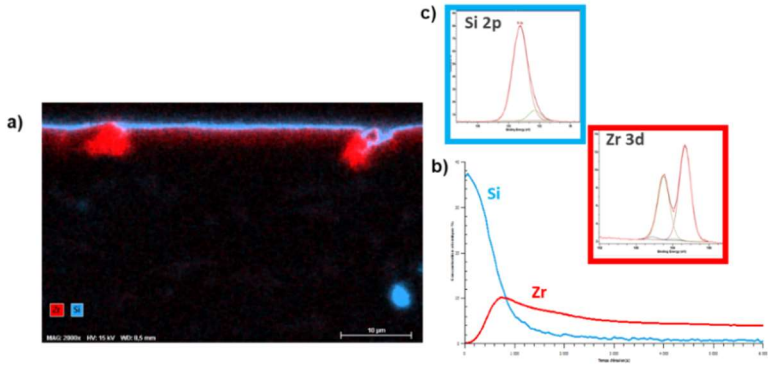

Figure 2: Sample of 2618-T851 anodized- Cr (III)/Zr (IV) impregnated- sodium silicate-based sealed_ a) Micrography MEB-EDX sectional view (Magnitude: 2000, HV:15 kV) b) Profile XPS and c) High Resolution spectra of Zr 3d and Si 2p

Nonetheless, without impregnation, silicon is able to spread in the anodic layer. In both cases, with and without impregnation, the protective chemical entity SiO_2 could be formed. However, Neutral Salt Spray Tests (NSST) put into light the efficiency of impregnation step before sealing one. Besides, according to the NSST results, the hydrothermal sealing was not protective enough against corrosion and the presence of silicates in the sealing bath appears necessary to obtain a high corrosion resistance. Consequently, this research work leads to a better understanding of the corrosion protection thanks to the identification of chemical environments involved in.

** The COCA project (COlmatage Couche Anodisée meaning Sealing Anodic Layer) is financed by ANR (National Research Agency) belonging to the academic, technological and industrial consortium as IPREM, IRT-M2P, Ineosurf, Safran Aircraft Engines, Safran Tech and Airbus Helicopters.*

[1] M. Kendig and R. Buchheit, « Corrosion Inhibition of Aluminum and Aluminum Alloys by Soluble Chromates, Chromate Coatings, and Chromate-Free Coatings », *Corrosion*, vol. 59, mai 2003, doi: 10.5006/1.3277570.
[2] Referred to in « Article 57 of Regulation (EC) No. 1907.2006 », Official Journal of the European Union L136, 2007.
[3] I. N. A. Oguocha, S. Yannacopoulos, and Y. Jin, « The structure of Al FeNi phase in Al-Cu-Mg-Fe-Ni alloy (AA2618) », *Journal of Materials Science*, vol. 31, p. 5615-5621, 1996.

Influential parameters on filament chemistry and electrochemistry in filiform corrosion of Aluminum

Iman Taji, Mats Stensrud Skui, Andreas Erbe

Department of Materials Science and Engineering, Norwegian University of Science and Technology (NTNU), 7491 Trondheim, Norway

Abstract:

Understanding influential parameters in filiform corrosion is a crucial step to design more filiform resistant materials and protection system. Textbooks normally referred filiform mechanism as the formation of an active, anodic head together with the cathodic tail because of different oxygen content at these two sites. However, less attention is paid to the role of other parameters which may affect the nature of the activation and passivation of filiform corrosion. For example, how much would be the contribution of pH reduction in increasing the anodic reaction rate, or how does this pH reduction contribute to the rate of hydrogen evolution reaction, which in turn also affects the pH. It is also important to know, quantitatively, the role of Cl^- concentration on the dissolution kinetics at the head of the filament. The geometry of the anode-cathode is also playing role which needs attention.

Since filiform corrosion is an underpaint phenomena, experimental measurement of local composition is a challenging task. In this work, finite element modelling has been used to simulate a filament. A solution of the Nernst-Planck equation is implemented to model the current distribution while the convection is neglected. The electrochemical dissolution of Al considered as an anodic reaction and two cathodic reactions of oxygen reduction and hydrogen evolution are included. The hydrolysis reaction of Al ions in water is also considered. Na^+ and Cl^- ions in aqueous solution were present in the filament in which the electroneutrality of ions will be maintained. The concentration dependent Butler-Volmer equation together with Nernst equation are used to model the electrochemical reactions.

In addition, polarizations curves using different pHs and chloride concentrations have been measured and a machine learning method was used to obtain the pH/Cl^- dependency of important input parameters for the modelling. The results are used to evaluate the role of pH, Cl^- concentration, hydrogen evolution reaction and cathode to anode ratio on the filiform corrosion of Al.

Elucidating Sweet Corrosion Scales at High Spatial Resolution: Key Components for Protection and Breakdown

Dominic Craske, Michael Dowhyj, Robert Lindsay

University of Manchester, Manchester, UK

Surabhi Agrawal, Mobbassar H. Sk, Stuart M. Clarke

University of Cambridge, UK

Jessica M. Walker, Julia E. Parker

Diamond Light Source, UK

Sweet (CO_2-induced) corrosion of carbon steel is a consequence of the dissolution of gas phase CO_2 in H_2O to form carbonic acid (H_2CO_3). Resulting aqueous phase species stimulate corrosion through supplying reactants for the cathodic process, i.e., $H_2(g)$ evolution; iron dissolution (Fe(s) to $Fe^{2+}(aq)$) occurs at anodic sites. Besides substrate degradation, sweet corrosion can also induce the formation of adherent corrosion products, that may protect the underlying carbon steel substrate. Early work suggested that such scales were simply composed of $FeCO_3$ (siderite) crystallites, but more recent studies have revealed further details. For example, $Fe_2(OH)_2CO_3$ (chukanovite) and Fe_3O_4 (magnetite) have also been observed to be scale components, with the latter being more favoured at higher temperature. Furthermore, several researchers have suggested the formation of bilayer scales, which can vary in phase and/or crystallinity as a function of depth, e.g., an inner layer consisting of nanocrystalline/amorphous $FeCO_3$ underlies micron-size $FeCO_3$ crystallites (see Fig. 1).

Figure 1: Cartoon of a sweet scale displaying an inner nanocrystalline/ amorphous $FeCO_3$ layer, and an outer layer of micron-size $FeCO_3$ crystals.

Given their propensity for complexity, this presentation will provide further insight into the phase composition and crystallinity of sweet corrosion scales through application of nano X-ray diffraction (n-XRD) and nano X-ray absorption near edge spectroscopy (n-XANES). Measurements were performed on the *I14* beam line at the Diamond Light Source (UK), exploiting the < 100 nm X-ray spot size to acquire highly-spatially

resolved n-XRD and Fe *K*-edge n-XANES from scale/substrate cross sections generated using focussed ion beam (FIB) lift-out (see Fig 2). These measurements have allowed variations in scale composition and/or crystallinity to be mapped, both parallel and perpendicular to the scale/carbon steel interface.

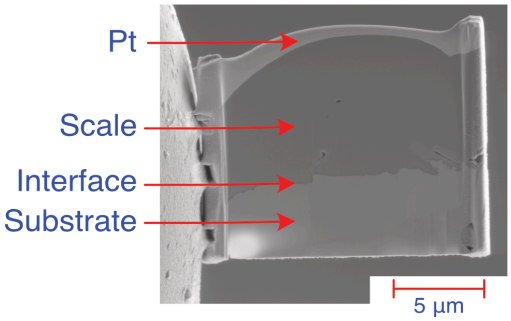

Figure 2: FIB lift-out cross section from a Fe sample that has been exposed to CO_2-saturated solution (pH 6.8, T = 80°C) for 72 hours. Labelling highlights substrate, corrosion scale, their interface, and the Pt coating employed to minimise damage during sample preparation.

Under the current experimental conditions, no evidence of the previously proposed bilayer scales has been found, i.e., there is no distinct interfacial *substrate binding* phase. n-XRD/n-XANES data show that much of the scale is simply composed of micron-sized crystallites of either $FeCO_3$ or $Fe_2(OH)_2CO_3$. Most interestingly, however, local regions within some of the $FeCO_3$ crystals display XANES profiles that are more consistent with amorphous/less well-ordered $FeCO_3$/$Fe_2(OH)_2CO_3$. Consistent with previous studies of sweet scale formation, we argue that this phenomenon is a result of $FeCO_3$ being formed through pathways involving such intermediate phases, and that these regions are trapped remnants of this process. Regarding scale protection, these local phase discontinuities may play a key role, e.g., triggers for scale breakdown due to local stress concentration.

Passivity and corrosion behaviour of 5083 aluminium alloy studied by combined X-ray photoelectron spectroscopy and electrochemical impedance spectroscopy approach

C. Nkoua, Univ. Toulouse/CIRIMAT, Toulouse/France; J. Esvan, Univ. Toulouse/CIRIMAT, Toulouse/France; B. Tribollet, Sorbonne Universités/LISE, Paris/France; R. Basseguy, Univ. Toulouse/LGC, Toulouse/France; C. Blanc, Univ. Toulouse/CIRIMAT, Toulouse/France

The ANR MICOATEC project aims to develop a new anticorrosive coating technology based on a biomimetic strategy for the protection of metals. The material that has been selected for this project is an Al-Mg 5083 alloy, largely used in various fields of application, e.g. marine environments. We have shown in a recently published paper[1] that the corrosion behaviour of this aluminium alloy is significantly improved by an immersion in natural seawater compared to the bare material and to the material pre-exposed to sterilised seawater. This has been attributed to modifications of the sample surface during immersion due to the action of marine micro-organisms, associated in particular to the formation of a few micrometers thick layer. Current studies performed by MICOATEC partners aim to analyse the structure and composition, as well as the anticorrosive properties of this layer. However, for a better understanding of the results, a preliminary study of the corrosion behaviour of the 5083 Al alloy was performed. This was done by using electrochemical impedance spectroscopy (EIS) combined with X-ray photoelectron spectroscopy (XPS) to assess the electrical properties of the passive film formed on the alloy.

A first graphical analysis of the EIS diagrams plotted in chloride-containing sulphate solution revealed that the corrosion behaviour of the 5083 Al alloy was, at least, partly controlled by Mg dissolution at Mg-rich intermetallic coarse particles (IMCs). This was related with the identification by XPS of Mg-rich species inside the passive film, this film showing a bi-layer structure rigorously described using XPS results: in particular a gradient in chemical composition perpendicular to the sample surface was evidenced. Combining all results, the electrochemical behaviour of the 5083 Al alloy was modelled using a model based on the work of Baril et al.[2] developed

to describe the corrosion behaviour of pure Mg. This also allowed to plot the resistivity profiles of the passive films formed on the 5083 Al alloy, which evidenced the double-layer structure of the passive films, and confirmed the gradient in chemical composition in agreement with XPS results.

This work was financially supported by the ANR, in the framework of the MICOATEC project (ANR-19-CE08-0018).

[1]C. Nkoua, C. Josse, A. Proietti, R. Basseguy, C. Blanc, Corrosion behaviour of the microbially modified surface of 5083 aluminium alloy. Corrosion Science, 210, Part 1, 110812 (2023)

[2]G. Baril , G. Galicia, C. Deslouis, N. Pébère, B. Tribollet, V. Vivier, An Impedance Investigation of the Mechanism of Pure Magnesium Corrosion in Sodium Sulfate Solutions, J. Electrochem. Soc. 154 (2007) C108–C113. DOI: 10.1149/1.2401056.

Combined electrochemical and in-situ AP-XPS approach to study corrosion of low-Cr alloy steels

K. Simonov[1], S. Munktell[1], N. Fuertes[1], M. Paschaliodu[1], M. Uhlirsch[1]

J. Y Jonson[2], B. Helmersson[2], D. Orrling[3], U. Bexell[4], A. Shavorskiy[5], T. Ericson[6], R. Lindblad[6]

[1]Swerim AB, Kista, Sweden; [2]Outokumpu Stainless AB, Avesta, Sweden; [3]SSAB EMEA AB, Oxelösund, Sweden; [4]SSAB EMEA AB, Borlänge, Sweden; [5]MAX IV Laboratory, Lund, 221 00, Sweden; [6]Uppsala University, Uppsala, Sweden

Introduction

It is generally accepted that steels containing enough chromium (Cr) exhibit excellent corrosion resistance due to the formation of a protective chromium oxide film. Below 11 wt%, the continuous protective chromium oxide layer cannot form. Nevertheless, electrochemical tests carried out for low-Cr alloys (up to 5 wt% Cr) indicate the positive influence of chromium on the corrosion resistance [1]. One of the explanations suggests that the positive influence of Cr is related to surface enrichment with Cr_2O_3 as corrosion product [2]. In another study, based on thermodynamic diagrams (Fe-Cr-C-O-H), Inaba et al. [3] demonstrated that the increase of corrosion resistance of low-chromium steels in humid CO_2 can be explained by the reduction of the Fe^{2+} stability range and formation of a $Fe_xCr_{3-x}O_4$ spinel. It was also demonstrated that pH of the electrolyte can influence the formation of surface Cr hydroxides for low-Cr steels [4]. The goal of the present work was to test new approach using advanced analytical techniques and to understand how low amounts of Cr affect the oxide film properties formed during anodic polarization of low-Cr steels.

Materials and Methods

In the present work industrial alloys with up to 5 wt% of Cr were tested in 0.01 M NaCl at pH = 7 and pH = 4.2. Combination of synchrotron-based in-situ ambient-pressure XPS (AP-XPS) with electrochemical control and laboratory electrochemical tests was implemented to study changes in the surface oxide chemistry under applied potential in presence of electrolyte. Such an approach was recently tested for stainless steels and Ni-base alloys [5] and provided valuable information about changes in oxide film composition during electrochemical process. The AP-XPS measurements were performed at HIPPIE beamline (MAX IV synchrotron, Lund, Sweden) using dip-and-

pull method, as described in [5], while electrochemical laboratory tests were performed at Swerim AB.

Results

The standard polarization tests and EIS measurements performed at Swerim indicated that steel grades with 1 wt% and 5 wt% of Cr are both prone to corrosion in acidic and neutral 0.01 M NaCl solution. No clear passive region was observed, with the corrosion rate being similar for both materials. However, a lower E_{corr} observed for material with 1 wt% of Cr indicate that it has a lower corrosion resistance in the studied medias. No strong pH effect on the corrosion resistance was observed in laboratory tests. The complementary synchrotron AP-XPS measurements were performed for the same materials to shed light on the role of Cr during anodic dissolution of the oxide film. For 5 wt% Cr material in acidic pH the amount of Cr relative to Fe in oxyhydroxide layer rapidly grew as a function of applied potential. Similarly, but less pronounced this effect was observed for neutral solution. Analysis of high-resolution Cr 2p AP-XPS peaks after immersion in the acidic electrolyte at constant potential allowed to conclude that all Cr present at the surface is already oxidized to the Cr^{3+} state at the low anodic potential applied to the sample. At the same time, according to Fe 2p signal, significant Fe^{0} signal was observed (alongside with Fe^{3+} and Fe^{2+}) at any value of potential (up to OCP + 0.6V). The $I(Fe^{0})/[I(Fe^{2+}) + I(Fe^{3+})]$ ratio was changing for different points of the same sample due to lateral inhomogeneity of the surface reaction. Together with the clear Cr enrichment of the surface these observations point out to the preferential dissolution of Fe oxide, while Cr oxide phases stay on the surface in agreement with [2].

References

[1] A. Łukaszczyk et al. Electrochem, 2, 546 (2021).

[2] Y.F. Cheng, F.R. Steward, Corr. Sci. 46, 2405 (2004).

[3] H. Inaba et al. Corros. Sci. 38, 1449 (1996).

[4] XU Lining et al. Acta Metallurgica Sinica, 56, 677 (2017).

[5] A. Larsson et al. Appl. Surf. Sci. 611, 155714 (2023).

A novel local domain boundary element method for the numerical simulation of corrosion problems

Dimitrios T. Kalovelonis, Department of Mechanical Engineering and Aeronautics, University of Patras, GR-26504, Patras, Greece.

Theodoros V. Gortsas, Department of Mechanical Engineering and Aeronautics, University of Patras, GR-26504, Patras, Greece.

Stephanos V. Tsinopoulos, Department of Mechanical Engineering, University of Peloponnese, Greece, GR-26334, Patras, Greece.

Demosthenes Polyzos, Department of Mechanical Engineering and Aeronautics, University of Patras, GR-26504, Patras, Greece.

Corresponding author: d.kalovelonis@upnet.gr

Abstract

Metals and alloys spontaneously corrode in corrosive environments, such as seawater, soil, concrete etc. Potential gradients and species concentration gradients are significant in the simulation of galvanic and localized corrosion problems. In the last decades, the finite element method (FEM), finite volume method (FVM), finite differences method (FDM), and boundary element method (BEM) have been used extensively to solve corrosion problems. BEM offers the advantage of high solution accuracy on the potential gradients and species concentration gradients. However, BEM can not treat such problems efficiently due to its time-consuming computations and high demand for computer memory.

A novel local domain BEM (LD-BEM) for solving steady state and time domain corrosion problems is proposed, which exhibits the same order of computational complexity as FEM, retaining the above-mentioned BEM advantages. The proposed LD-BEM is applied to both flowing and stationary electrolytes. The numerical results are verified by comparing them with the ones obtained by commercial software packages.

Verification of the passivity condition of cathodically protected carbon steel using in-situ electrochemical and spectroscopic techniques

Luca Casanova, Andrea Brenna, Marco Ormellese - Dipartimento di Chimica, Materiali e Ingegneria Chimica "G. Natta", Politecnico di Milano, Milano
Marco Menegazzo, Gianlorenzo Bussetti - Dipartimento di Fisica, Politecnico di Milano, Milano
Francesco Di Franco, Monica Santamaria - Dipartimento di Ingegneria, Università degli Studi di Palermo, Palermo

Cathodic protection, in conjunction with surface coatings, is a protection technique for carbon steel structures widely consolidated and diffused in multiple sectors. The protection condition is guaranteed upon the circulation of a direct current applied from an anode and the structure to be protected; the current causes the potential of the structure to move cathodically thus decreasing considerably the metal dissolution reaction. The cathodic current is responsible to impart a secondary effect of alkalinization strictly dependent on the level of applied current density, circulating in the cell, and on the kinetics of the diffusive motion of the major species involved in the electrochemical reactions. This has the consequence of influencing the surface state of the metal in agreement with Pourbaix diagram where the alkalinity should favor the formation of passivity conditions. In this paper some laboratory results are collected with the aim of demonstrating the presence of surface films when a protection current is applied. The presence of passive films is demonstrated by electrochemical impedance spectroscopy (EIS), photocurrent spectroscopy tests and in-situ Raman spectroscopy.

Keywords: cathodic protection, carbon steel, EIS, Raman, photocurrent spectroscopy.

INTRODUCTION

Buried carbon steel structures and infrastructures, as like pipelines used for the transport of methane or pressure vessels, are protected from the electrolytic corrosion by a cathodic protection system (impressed current systems or by galvanic anodes) combined with insulating coatings. Based on current legislation, a buried structure can be considered under cathodic protection if the potential of the structure, corrected by the ohmic drop (IR-free potential), has a value below −0.85 V/CSE in aerated soils with medium-low resistivity (CSE, copper/copper sulphate electrode) [1]–[3]. In this condition, the corrosion rate is considered to be negligible, with values below 10 µm/year. A secondary effect caused by the ongoing cathodic reactions is the raise of the pH near the metal surface; cathodic reactions like oxygen reduction and hydrogen evolution are the main processes contributing to this effect. For example, when the pH shift occurs in seawater the precipitation of a magnesium or calcium carbonate deposit may form over the protected surface.
According to the Pourbaix diagram of the iron-water system, the local pH increase may be responsible for provoking the formation of passivity conditions on steel. Even if this chemical effect is widely known and documented there is still a lack of knowledge about the mechanisms and the type of passive layers forming over the structure of interest, thus only now thanks to very sophisticated electrochemical and surface techniques the nature of those surface layers has been partially clarified [4], [5].
In this context the present elaborate has the aim of investigate, using in-situ techniques, the nature of the surface films attended as a consequence of the application of a cathodic potential of −1.1 V/CSE over carbon steel. Furthermore, a better comprehension of the conditions involving surface oxides formation may have an impact on current cathodic protection criteria in presence of continuous non stationary interference [6]. The electrode surface activity is investigated through electrochemical impedance spectroscopy (EIS), in-situ Raman spectroscopy and photocurrent spectroscopy experiments.
The present work derives from a fruitful collaboration between Politecnico di Milano and Università degli Studi di Palermo, the work is financed by APCE (Associazione per la Protezione dalle Corrosioni Elettrolitiche).

MATERIALS AND METHODS

The present research is carried out on cylindrical carbon steel specimens (0.05 %C – 0.264 %Mn – 0.031 %Ni – 0.018 %Cu – 0.012 %Al) having diameter of 10 mm and thickness 1 mm; samples are mirror polished with emery papers and alumina powder.
EIS tests are carried out using a potentiostat/galvanostat Autolab PGSTAT in a three electrode cell of PTFE using a Pt counter and a Ag/AgCl/KCl saturated reference electrode ($SSC_{sat.}$, +0.197 V/SHE). Experiments are carried out in a soil simulating solution having 1000 ppm of SO_4^{2-} held at 21 °C (conductivity = 1207 µS/cm,

pH = 7). EIS analysis are performed at the corrosion potential (E_{corr}) and at the protection potential (−1.1 V/CSE) using a sinusoidal signal with 10 mV_{rms} of amplitude in a frequency window between 10^5 and 10^{-2} Hz collecting 10 points per decade of frequency.
The protection potential is applied for a total of 24 hours measuring protection currents in the order of 500 mA/m^2.
Raman acquisitions are carried out considering a commercial system employing an electrochemical cell, using a green laser (λ=532 nm) with an exposure time of 10 s and an accumulation of 50 spectra, limiting the laser power of the sample to 0.7 mW, thus ensuring to almost eliminate eventual structural artefacts introduced by the radiative source [7].

According to Photocurrent Spectroscopy tests (PCS) it was possible to obtain information about the electronic properties of the surface layers in terms of band-gaps (E_g) and their composition. Photocurrent measurements are registered through an experimental set-up combining a xenon lamp and a monochromator. Based on that it is possible to irradiate the working electrode with a photon flux having variable wavelength, a chopper is used to isolate the photocurrent contribution from the dark one and a lock-in permits to obtain the modulus and phase of the photocurrent.
By registering the photocurrent value for different wavelengths it is possible to estimate the E_g of the passive oxide layers.
Photocurrent spectra are registered immediately after the cathodic polarisation in a solution of 0.1 M ammonium diborate (ABE) at the open circuit potential (U_{ocp}) in order to avoid any modification of the previously formed passive film.
To do that a photoelectrochemical cell with quartz windows is used and a three electrodes configuration adopted with a Pt net as counter and a $SSC_{sat.}$ as reference electrode.

RESULTS
The electrochemical activity of the electrode has been verified by EIS at E_{corr} (~ −0.70 V/CSE) and in protection condition (E = −1.1 V/CSE).

In the first case, Fig. 1a, the spectrum presents a single semicircle which can be simulated according to the circuit highlighted in Fig. 1c. In this case the resistance R_1 describes the polarisation resistance. At E_{corr} R_1 is equivalent to 934 $\Omega \cdot cm^2$ corresponding to a corrosion rate of 313 μm/year. According to the use of the Brug's equation [8] it is possible to extract an effective capacitance associated to the constant phase element used to describe the response of the electrical double layer (EDL) formed at the metal solution interface. Fitting results are collected in Tab. 1 and a value of 93 $\mu F/cm^2$ is attributed to the EDL capacitance.

EIS spectra are strongly modified by application of the protection potential (−1.1 V/CSE). Even from the first hours of polarisation, the semicircle, present in the Nyquist representation, shows a larger diameter synonym of a larger polarisation resistance when the electrode is cathodically polarised with respect to free corrosion conditions. Being the flowing current almost entirely cathodic, it is reasonable to infer the higher observed impedance to the slower kinetics of the cathodic reactions caused by a surface modification of the electrode. Considering the two cathodic reactions (1) and (2) occurring in the present study a sensible pH increase allows to speculate the formation of passive layers according to Pourbaix [9].

$$\frac{1}{2}O_2 + 2H^+ + 2e^- \leftrightarrow H_2O \quad (1)$$

$$2H_2O + 2e^- \leftrightarrow H_2 + 2OH^- \quad (2)$$

Thus it is now necessary to add further elements to the equivalent circuit used to describe EIS data in order to describe the presence of surface films as in Fig. 1d. This circuit is generally used by Orazem *et al.* [10] to describe porous layers on steel.

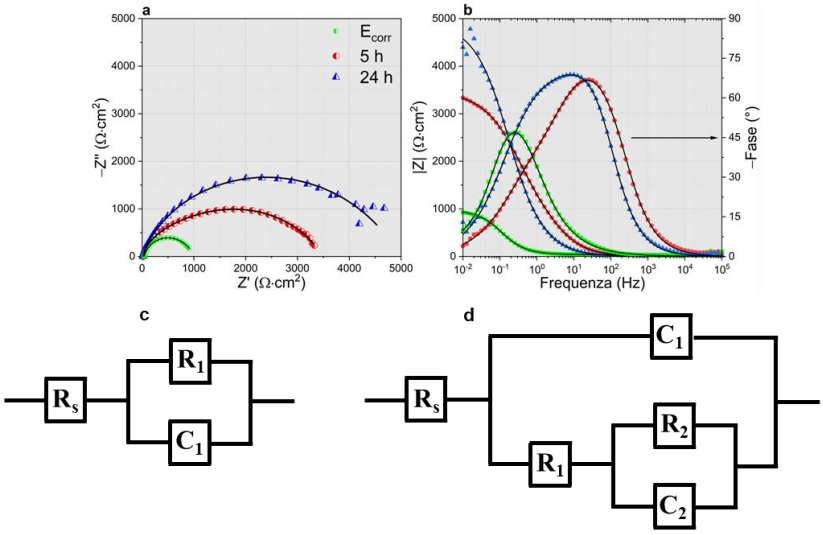

Fig. 1 Nyquist **a** and Bode **b** representations, electrochemical equivalent circuits used for the fitting of the EIS test performed at E_{corr} **c** and in protection **d**.

According to the circuit analysis it is possible to see that the film, under the analysed 24 hours, contributes to the improved protection of the metal diminishing the protection current from 555 to 403 mA/m^2 after 24 h of polarisation at −1.1 V/CSE. However, the lower current may derive also from the consumption of the main cathodic reagent, i.e., oxygen. According to the observation of the phase angle, of the three analysed conditions, it is possible to see that under protection conditions a further time constant forms. However, having the two relaxations similar time scale they are described by a single asymmetric peak.

Tab. 1 EIS parameters extracted using circuits of Fig. 1c and d.

Sample	R_s Ω·cm^2	R_1 Ω·cm^2	C_1 µF/cm^2	n	R_2 Ω·cm^2	C_2 µF/cm^2	n	d_{ox} nm	χ^2
E_{corr}	34.12	934.17	93.72	0.84	/	/	/	/	$6.1\cdot10^{-2}$
5 h	21.38	1064.01	32.42	0.90	2409.74	7.12	0.63	5.4	$7.2\cdot10^{-3}$
24 h	17.12	371.33	90.89	0.95	4596.25	3.96	0.63	10.5	$3.5\cdot10^{-2}$

According to in-situ Raman spectroscopy it is possible to monitor the chemical evolution of the surface, thus providing further confirmation to EIS results. According to that even from the first instants at E_{corr}, the metal is covered by a layer of lepidocrocite (γ-FeOOH) and goethite (α-FeOOH). Their formation is supposed to derive from the corrosion of the first iron layers in contact with the solution forming Fe^{2+} species further oxidized to Fe^{3+} according to the aerobic conditions. Application of the cathodic potential permits evident variation of the Raman spectra to be observed. In particular, the application of the cathodic potential increases the intensity of the Raman lines describing previous observed phases (see Fig. 2a).

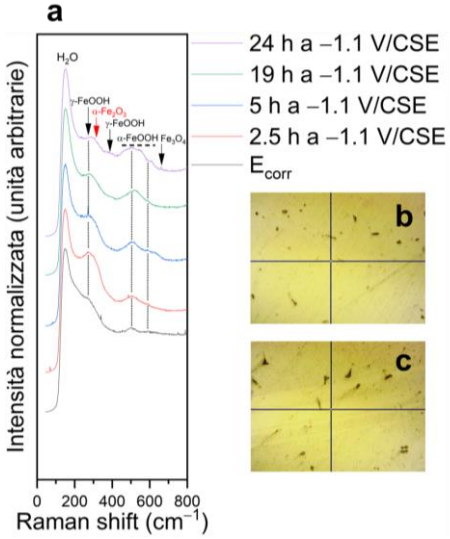

Fig. 2 Raman spectra **a** collected in-situ during electrode polarisation at −1.1 V/CSE and optical microscope images collected at E_{corr} **b** and after 24 h of polarisation **c**.

However, only after 24 hours of polarisation the vibrational modes related to (α-Fe_2O_3) [11] and magnetite (Fe_3O_4) [7] appear, whose formation is probably related to the alkalinity generated by the ongoing electrochemical reactions. Based on those results the surface layer seems to be composed by a multitude of phases presenting Fe^{3+}. Assuming hematite as the principal constituent a dielectric constant of 44 [12] may be inferred. Using the capacitor equation (3) it is possible to estimate the thickness of the dielectric material covering the metal surface

$$d = \frac{\varepsilon_o \varepsilon_{oxide}}{C_{oxide}} \quad (3)$$

corresponding to around 10 nm after 24 h of polarisation at −1.1 V/CSE as shown in Tab. 1.
In Fig. 3 the photocurrent spectra collected in the previously described solution are reported. In this case, the sample prior to photocurrent acquisition is polarised at two different potentials, 0.8 V/CSE and −1.3 V/CSE.

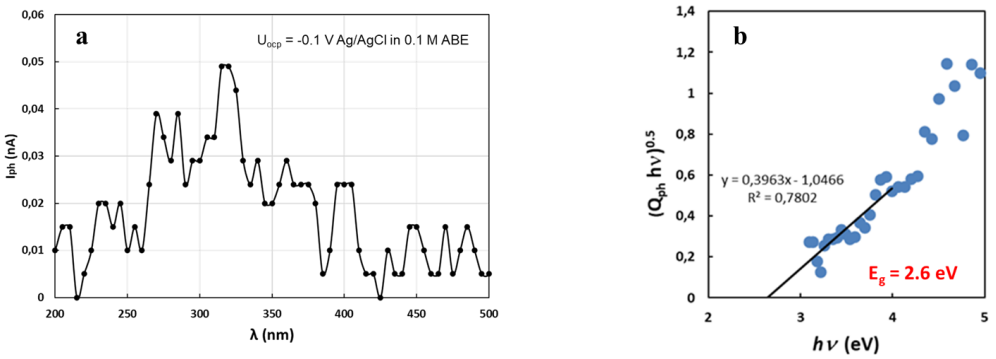

Fig. 3 **a** Photocurrent spectrum collected in 0.1 M ABE at open circuit potential (U_{ocp} = −0.1 V/$SSC_{sat.}$), over a carbon steel sample previously polarised at −0.8 V/CSE for 24 h. **b** Band gap estimation assuming an indirect optical transition.

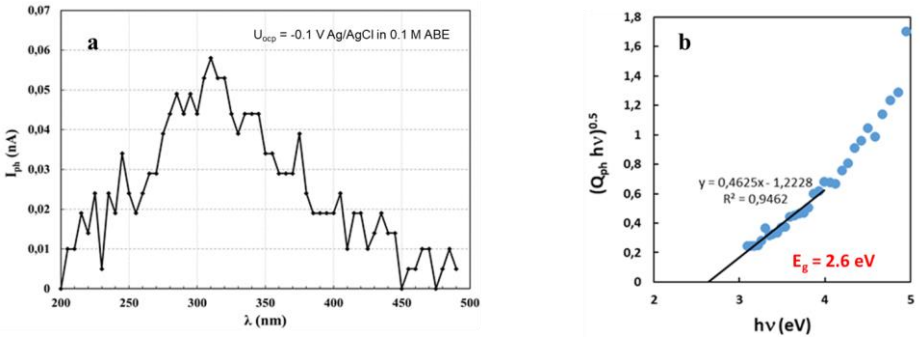

Fig. 4 **a** Photocurrent spectrum collected in 0.1 M ABE at open circuit potential (U_{ocp} = −0.1 V/$SSC_{sat.}$), over a carbon steel sample previously polarised at −1.3 V/CSE for 24 h. **b** Band gap estimation assuming an indirect optical transition.

The photocurrent experiments confirm, in both cases, the presence of photoactive passive films with semiconductive properties. Assuming an indirect optical transition it is possible to obtain the value of E_g according to equation (4):

$$\left(Q_{ph} h\nu\right)^{0.5} = \alpha\left(h\nu - E_g\right) \quad (4)$$

where Q_{ph} is the photocurrent value corrected for the efficiency of the lamp-monochromator system, α is the absorption coefficient, hν the energy of the incident photons and E_g the band gap of the semiconductive material. For both conditions a band gap of 2.6 eV is estimated (see Fig. 3b and 4b), this value corresponds to the value of γ-FeOOH (lepidocrocite) [13], confirming the outcome of the previous in-situ Raman investigation.

CONCLUSIONS

Surface characterisation analysis (EIS, in-situ Raman and photocurrent spectroscopy) applied on carbon steel polarised at −1.1 V/CSE demonstrate the formation of a passive layer composed by iron oxide and oxi-hydroxide with the cation oxidized 3+, having a thickness of around 10 nm after a polarisation of 24 h. The presence of a passive film is confirmed by ex-situ photocurrent spectroscopy acquisitions.

BIBLIOGRAPHY

[1] ISO-15589-EN, International Standard Petroleum, petrochemical and natural of pipeline systems, (2015).

[2] NACE INTERNATIONAL, Control of External Corrosion on Underground or Submerged Metallic Piping Systems., (1969).

[3] P. PEDEFERRI, Cathodic protection and cathodic prevention, (1996).

[4] F. MARTINELLI-ORLANDO, Cathodic protection mechanisms of steel in soil, 2022.

[5] S. S. LEEDS, R. A. COTTIS, An investigation into the influence of surface films on the mechanism of cathodic protection, in *NACExpo*, 2006.

[6] M. ATTARCHI, A. BRENNA, M. ORMELLESE, Cathodic protection and DC non-stationary anodic interference, (2020).

[7] D. L. A. DE FARIA, S. VENÂNCIO SILVA, M. T. DE OLIVEIRA, Raman microspectroscopy of some iron oxides and oxyhydroxides, (1997).

[8] G. . J. BRUG, A. . L. . G. VAN DEN EEDEN, M. SLUYTERS-REHBACH, J. . H. SLUYTERS, The analysis of electrode impedances complicated by the presence of a constant phase element, (1984).

[9] M. POURBAIX, *Atlas of electrochemical equilibria in aqueous solutions*. 1974.

[10] Y.-M. CHEN, N. G. RUDAWSKI, E. LAMBERS, M. E. ORAZEM, Application of Impedance Spectroscopy and Surface Analysis to Obtain Oxide Film Thickness, (2017).

[11] M. HANESCH, Raman spectroscopy of iron oxides and (oxy)hydroxides at low laser power and possible applications in environmental magnetic studies, (2009).

[12] R. A. LUNT, A. J. JACKSON, A. WALSH, Dielectric response of Fe2O3 crystals and thin films, (2013).

[13] G. Tranchida, F. Di Franco, B. Megna, M. Santamaria, Semiconducting properties of passive films and corrosion layers on weathering steel, (2020).

Microelectrochemical study of pit initiation in light metals with high-speed microscopy and acoustic emission

Kaige Wu, Nobu Yatagai, Takayuki Shiraiwa, Manabu Enoki*

Department of Materials Engineering, The University of Tokyo, Tokyo, Japan.

**kaigewu@rme.mm.t.u-tokyo.ac.jp*

Abstract

Pitting corrosion has been studied for decades and a considerable understanding of pit growth has been realized. However, an in-depth description of the early stage of pit initiation, including the earliest stage of passive-film breakdown and the growth of metastable pits, is still lacking due to the small dimensions, short timescale, and random occurrence. In this work, real-time acoustic emission (AE) monitoring, *in-situ* AE signal-driven high-speed microscopic imaging, and microelectrochemical intermittent anodic polarization approach were coupled to study the early stage of a single pit initiation event on AA5083 and $Mg_{89}Zn_4Y_7$ alloy in 3.5 wt.% NaCl solution at room temperature. Attention was focused on the high-speed imaging of the corrosion site between -1 ms and +200 ms of the first AE signal. It was found in both cases that the AE signal was first detected when no visible microscopic changes occurred; subsequently, after a short time delay, corrosion and hydrogen (H_2) bubble evolution became visible with concurrent AE signals. In terms of AE evolution, this finding agrees with the theory classifying the onset of localized corrosion by passive-film breakdown giving rise to the earliest stage of pit nucleation and anodic dissolution and H_2 evolution leading to the early pit initiation. In addition, H_2 bubble dynamics and concurrent AE signals during pit initiation were found to be largely dependent on the involved local microstructure and the dominant mechanisms in terms of trenching or dealloying. This study visualizes the early stage of pitting corrosion initiation for the first time and validates the feasibility of the AE method for process monitoring and mechanistic understanding of pitting corrosion in light metals.

Keywords: Pitting corrosion, passive-film breakdown, hydrogen-bubble evolution, acoustic emission, high-speed imaging, intermittent anodic polarization.

High-Precision *In Situ* 3D Ultrasonic Imaging of Localized Corrosion Processes

Yunda Chen, Fangxin Zou

Department of Aeronautical and Aviation Engineering, The Hong Kong Polytechnic University, Hung Hom, Kowloon, Hong Kong SAR, China

Localized corrosion is one of the primary reasons for the degradation and failure of metallic structures. Understanding the kinetics of localized corrosion is significant to achieving sustainable structural designs. A localized corrosion process would induce time-variant 3D morphological changes on the substrate. Therefore, a straightforward approach to investigating localized corrosion would be to profile substrate morphologies in real time. However, the conventional research techniques in this area are either *ex situ* (e.g., SEM, TEM, etc.), capable of capturing substrate morphologies but requiring corrosion processes to be terminated, or indirect (e.g., WBE, SECM, etc.), necessitating empirical knowledge to deduce substrate morphologies from electrochemical measurements. Recently, advanced *in situ* techniques for imaging substrate morphological changes have been developed from STM, AFM, optical microscopy, etc. Nevertheless, the measurement accuracy of these techniques is often undermined by the presence of corrosion products, which are inevitable in and crucial to corrosion processes.

In this work, we introduced a novel ultrasonic research platform that can image in real time 3D substrate morphological changes during localized corrosion experiments. To establish an experimental setup, the non-working surface of a substrate would be permanently attached on by a 2D multi-element piezoelectric transducer array. During a localized corrosion experiment, the transducer elements would continuously excite ultrasonic shear waves that propagate across the substrate, and capture the reflections off the working surface of the substrate. The reflections would then be processed into a real-time reconstruction of the morphological evolution process of the substrate. The technique has a customizable field of view and lateral resolution. The axial resolution of the technique was found to be at the nanometer level, and the measurement accuracy of the technique was well validated by white light interferometry. What's

more, the measurement accuracy of the technique is insensitive to corrosion products, thanks to the nature of ultrasound.

The proposed technique was used to monitor the localized corrosion processes of carbon steel in weakly acidic to neutral NaCl solutions under constant applied DCs. Transient accelerations and decelerations in corrosion rates were observed. Based on the XRD patterns of the corrosion products obtained and the different features of the ultrasonic signals received, it was deduced that an increase in corrosion rate would have been caused by the transformation of $Fe(OH)_2$ to Fe_3O_4, which is an electron-consuming oxidation process that would have accelerated iron dissolution. As time went on, a solid-state corrosion product layer would have grown on the substrate, giving rise to a barrier that would have slowed down oxygen diffusion and the oxidation of $Fe(OH)_2$ to Fe_3O_4, and hence decelerated iron dissolution. The recovery in corrosion rate would have also been accompanied by the detachment of the corrosion product layer from the substrate.

Electrode reaction kinetics and mechanisms on Fe-based alloys using electrochemical online ICP-OES

A. Fujimura[1)], *S. Shoji*[2)], *Y. Kitagawa*[2)], *Y. Hasegawa*[2)], *T. Doi*[3)], *K. Fushimi*[2)]

[1)]*Graduate School of Chemical Sciences and Engineering Hokkaido Univ., Sapporo/JAPAN*

[2)]*Faculty of Engineering, Hokkaido Univ., Sapporo/JAPAN*

[3)]*Research & Development, Nippon Steel Corporation, Amagasaki/JAPAN*

Introduction

The investigations of the corrosion reaction mechanisms and kinetics are important for considering application and physicochemical properties of materials. Detail reaction step is unclear due to the complexity of the system. Quantification of generated species is effective for understanding the electrode reactions using an analysis technique that is able to quantify the electrochemically inactive species (such as Al^{3+}) is expected to lead the discussion of reaction mechanisms. We have developed and optimized a solution analysis system using inductively coupled plasma-optical emission spectroscopy (ICP-OES) combined with a channel flow-type electrochemical cell. This technique is widely used to obtain the sequential concentration of generated species and has been used to analyze the dissolution mechanisms of metals [1] [2].

In this study, the inherent anodic current of elemental species (i_a) around corrosion potential was obtained from the concentration profiles measured by ICP-OES.

Results

The signal of i_a which was calculated from the concentration of element enables to analyze the Tafel slope and provides 60 mV decade^{-1} for pure Fe material in acidic Na_2SO_4 solution. This implies that a rate determining step of anodic reactions for Fe is different from that in previous study (40 mV decade^{-1}) [3]. The reaction kinetics on the electrode surface were estimated by comparing the numerical calculation results and experiments.

References

[1] K. Ogle and S. Weber, *J. Electrochem. Soc.*, **147**, 1770 (2000).
[2] A. Fujimura, S. Shoji, Y. Kitagawa, Y. Hasegawa, T. Doi, and K. Fushimi, *Electrochim. Acta*, **433**, 141246 (2022).
[3] J. O. M. Bockris, S. Srazic, and A. R. Despic, *Electrochim. Acta*, **4**, 325 (1961).

Acknowledgement

This paper is based on results obtained from a project commissioned by the New Energy and Industrial Technology Development Organization (NEDO).

Title of the presentation:

Decoating of metallic surfaces in the field of corrosion protection, renovation, maintenance, revisions.

Presenter:

M.S. Sergej Retich, Clean-Lasersysteme GmbH , Herzogenrath/ Germany

Dr.-Ing. Uwe Specht, Fraunhofer-Institut für Fertigungstechnik und Angewandte Materialforschung IFAM, Bremen/ Germany

Eckhardt Krebs, Glatt Laser Process Technology GmbH, Binzen / Germany

Abstract

Clean-Lasersysteme GmbH (cleanLASER) developed the laser ablation technology for industrial surface processing and cleaning as well as for decoating more than 25 years ago. The cleanLASER technology was qualified for industrial processes and finds numerous applications in different industries, but mainly in the automotive and supplier industry. Away from these industries, High Power Laser technology has been increasingly establishing itself for a few years as a hand-held laser ablation technology in all areas of industries where corrosion protection is relevant and non-destructive testing of stressed surfaces is mandatory. As a low-emission, safe, relatively quiet and media-free process, the laser offers advantages over conventional abrasive blasting methods.

The lecture will go into the functional principle of laser beam technology and discuss some interesting application examples and technical solutions in typical fields of application of hand-held laser beam surface technology such as partial paint stripping of corrosively damaged areas on structures, as well as spot decoating for performing NDT. In addition, current results from the investigations will be presented.

- general comparison laser de-coating process vs blasting process

- partial de-coating for recoating on special geometries (thin sheets, complex access)

and in nature landscapes

- maintenance of infrastructures in C1 + C3 + C5 areas (landside structures like towers, waterside structures like bridges, coating protection 2-25 years)

- examples from LaserREP project: Laser based local surface preparation of protective coatings in steel construction

- de-coating of metallic structures for non-destructive testing

- removal of CMR coatings for renovations like paint inclusive heavy metals and asbestos

- renovations on objects

Example pictures

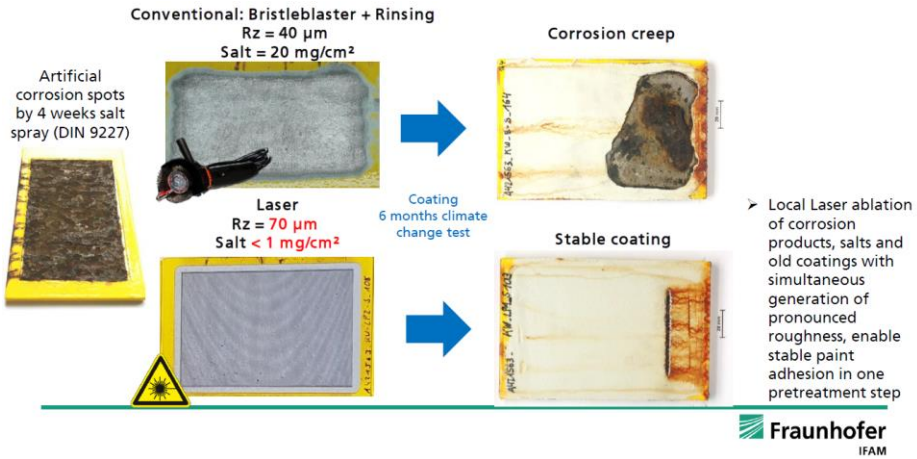

Fraunhofer-Institut für Fertigungstechnik und Angewandte Materialforschung IFAM

Clean-Lasersysteme GmbH, Adapt Laser

Understanding the Passive Behaviour of Low-Chromium High-Strength *Hybrid* Steel in Corrosive Environments

Cem Örnek[1], Beste Payam[1], Andrei Gloskovskii[2], Kürşat Kazmanlı[1], Bora Derin[1], Mustafa Ürgen[1], Burçak Avcı[1], Steve Ooi[3,4]*

[1]Istanbul Technical University, Department of Metallurgical and Materials Engineering, Istanbul, Türkiye

[2]Photon Science, Deutsches Elektronen-Synchrotron DESY, Notkestr. 85, 22607 Hamburg, Germany

[3]Ovako Corporate R&D, Maxwell Centre, JJ Thompson Avenue, Cambridge CB3 0HE, United Kingdom

[4]Ovako Corporate R&D, Building 202, SE-813 82 Hofors, Sweden

**Corresponding author: email: cornek@itu.edu.tr, tel.: +90 212 285 6864*

Modern and tomorrow's engineering applications require high material performance while resistant to harsh environments, sustainable and financially payable. Hybrid steel combines several features compared to traditional steels, such as a high strength-to-weight ratio, improved corrosion resistance in chloride media, and high toughness. Among all material properties, understanding the corrosion in chloride-bearing media has the utmost importance since the service lifetime and efficiency depend on the corrosion resistance of the steel. Our electrochemical tests have shown that 5Cr-6Ni-2Al Hybrid steel offers exceptionally high corrosion resistance in sulfuric acid and chloride solutions.

Therefore, we examined the unusual passive character of Hybrid steel in de-aerated sulfuric acid and aqueous sodium chloride solutions by benchmark corrosion and surface analytical tests in combination with CalPhaD-based thermochemical modelling. The electrochemical potentiodynamic polarization measurements have shown that Hybrid steel possesses all characteristic features of what makes steel stainless, such as passivity, breakdown and pitting, similar to standard low-alloyed

stainless steel. Synchrotron hard X-ray photoelectron spectroscopy (HAXPES) analysis revealed that the stainless nature of Hybrid steel is achieved by a dynamically protective nanometre-sized passive film consisting of Fe, Cr, Ni, and Al oxides. The thermodynamic calculations showed that the surface oxide composition is $Fe_2O_3 \cdot FeCr_2O_4 \cdot NiO \cdot Al_2O_3$, which changes structure, fraction and existence over electrochemical polarization.

It has become understood that the presence of Al and Ni supports Cr in forming a spontaneously passive and hence protective surface, yielding exceptional corrosion resistance in acidic and chloride-containing aqueous solutions. The surface oxide could withstand breakdown and remain passive/repassivated even after transpassing the Cr(III)-to-Cr(VI) redox potential. While Cr is the prime passivating agent, an adverse effect of Cr was seen on grade 304 and 420 stainless steel when Cr(VI) species were released, savaging the passive film due to extensive interfacial pH reduction. However, among all tested stainless steels, Hybrid steel could repassivate due to the remaining and enriching Al and Ni oxides providing superior anodic passivation. Our work demonstrates that delicate alloying and microstructure engineering can design sustainable stainless steel with optimum high-strength properties without needing the well-known Cr threshold concentration of 10.5 per cent.

Identification of resistivity profiles in protective films using EIS and machine learning

B. Wouters, H. Terryn, A. Hubin

Research Group Electrochemical and Surface Engineering, Department of Materials and Chemistry, Vrije Universiteit Brussel, Pleinlaan 2, 1050 Brussels, Belgium

Electrochemical Impedance Spectroscopy (EIS) is a powerful technique for studying corrosion protection systems, such as organic coatings or (anodized) oxide layers. As an example, for organic coatings, using the correct electrical equivalent circuit (EEC) the ion and water uptake can be monitored as a function of time [1, 2]. In this case, the water uptake is linked to finding the correct value for the coating capacitance, and the ion uptake is linked to the coating resistivity profile. In the case of oxide layers, the thickness of the oxide layer can also be identified through its effective capacitance. Unfortunately, typically these protective films display an imperfect capacitance, which is often modeled using a Constant Phase Element (CPE). In this case, the calculation of the effective capacitance from the fitting parameters needs to be estimated using the power law model, which can be non-trivial [3]. A different element that can be used for fitting an imperfect capacitance is a Young impedance, where the effective capacitance can be determined directly via the fitting parameters. Choosing the right element for the fitting of the impedance spectra is critical to obtain a correct value for the capacitance of the protective film under study.

In this research, a new methodology is developed to identify the correct EEC element to use, using the impedance data as an input. In the case of protective films, the difference between a Young impedance and a CPE originates from differences in the resistivity distribution as a function of the distance to the metal interface. This resistivity can resemble an exponential distribution or a power law distribution, respectively. Depending on the resistivity distribution of the layer under study, a different EEC element should be used for the fitting. One way of determining the resistivity distribution is via Voigt element modelling using the measurement model [4], where a linear relationship can be found in either a logarithmic or semilogarithmic plot of modelled resistivity versus distance. However, this method often does not provide very clear results, especially if the number of datapoints that can be fitted accurately is low. Therefore, a new methodology using machine learning might provide a more reliable

method. As input data, an extensive number of impedance spectra of organic coatings and oxide layers is simulated, with a known effective capacitance and resistivity distribution. The machine learning model is then trained to identify the resistivity distribution in the data. Initial results are promising, as an initial accuracy of 96% was obtained. The results of this study provide a step to improve the accuracy of effective capacitance determination of protective films via EIS measurements.

[1] B. Wouters *et al.*, Monitoring initial contact of UV-cured organic coatings with aqueous solutions using odd random phase multisine electrochemical impedance spectroscopy. Corrosion Science 190 (2021) 109713
[2] N. Madelat *et al.*, Differentiating between the diffusion of water and ions from aqueous electrolytes in organic coatings using an integrated spectro-electrochemical technique. Corrosion Science 212 (2023) 110919
[3] B. Hirschorn *et al.*, Constant-phase-element behavior caused by resistivity distributions in films, Journal of the Electrochemical Society 157 (2010) C452
[4] Y.-M. Chen *et al.*, Identification of resistivity distributions in dielectric layers by measurement model analysis of impedance spectroscopy. Electrochimica Acta 219 (2016) 312

Corrosion mechanism of spheroidal graphite cast iron GGG40 in saturated Wyoming bentonite

Andrés G. Muñoz, GRS gGmbH, Braunschweig/Germany;
Dieter Schild, Karlsruhe Institute of Technology, Eggenstein-Leopoldshafen/Germany

The overpack of the Pollux® 10 container, taken as a reference for the storage of fuel elements in different types of host rocks, is manufactured from spheroidal graphite carbon steel (GGG 40 / 0.7040) [1]. The near field environment after emplacement is constituted by bentonite, which turns moisty, warm, and anaerobic after some decades because of the decay of the heat generation and the consumption of oxygen by reaction with the container wall, microbes, and minerals [2]. Thus, the corrosion mechanism of metal containers in these conditions is an essential issue for the design of repository concepts of radioactive waste.

In this work, we followed two experimental approaches. In one of them, samples of GGG40 steel were left in contact with light compacted Wyoming bentonite in equilibrium with artificial pore water at 30°C and 50°C. The corrosion was monitored by polarizations and impedance spectroscopy for a period of 3 months. The surface chemistry and morphological changes were investigated by local XPS, SEM-EDX and TEM. This experiment was complemented with corrosion studies performed in pore water under different temperatures, hydrostatic pressures, pH and, with and without dissolved oxygen.

In these systems, the rate of iron dissolution is controlled by its coupling with the reduction of water. The presence of dissolved oxygen seems to play a secondary role in the dissolution mechanism. The oxidation of the silicon contained in the alloy, however, plays a more fundamental role in the activation of cathodic elements localized in the graphite spheres. The morphology of the surface after the corrosion in near neutral pore water shows the formation of series of precipitated iron silicates containing Al, Mg and Cr (figure 1). The significance of the formation of silicates is evident in the surface analysis of samples after long-term experiments in contact with saturated bentonite. TEM pictures of a cross sectional lamella including part of graphite sphere shows the formation of a silicate film covering the corroding surface with an

irregular adherence (figure 2). The accumulation of silicates at the surface creates an additional barrier for the metal dissolution, which may favor a crevice type of corrosion.

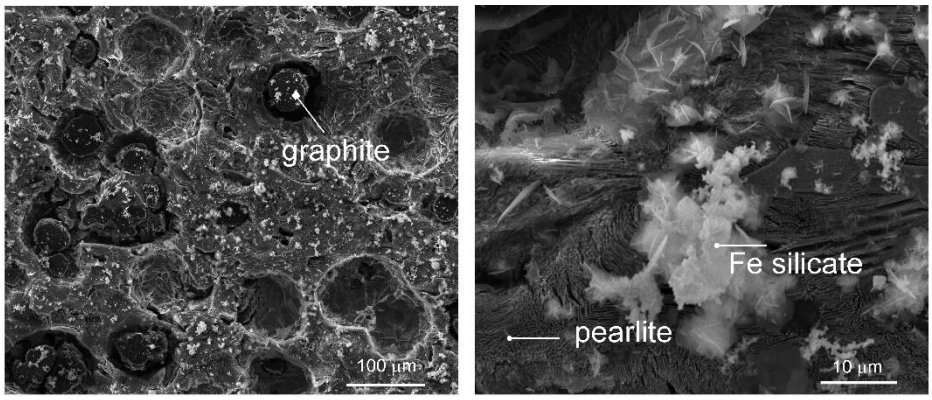

Figure 1: SEM pictures of the surface of GGG40 after corrosion during 48 h in anoxic pore water at 30°C and p: 5 atm.

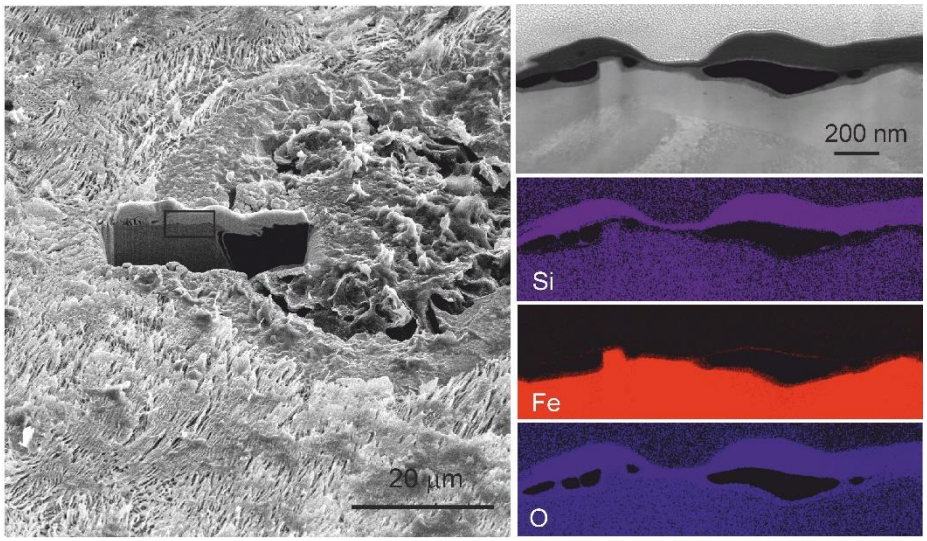

Figure 2: Left: SEM picture showing the surface of GGG40 after 3 months corrosion in contact with saturated Wyoming bentonite at 30°C. Right: STEM-HAADF of a cross section lamella obtained as indicated in the left figure and the corresponding EDX analysis.

[1] T. Hassel, A. Köhler, Ö.S. Kurt, Das ENCON-Behälterkonzept – Generische Behältermodelle zur Einlagerung radioaktiver Reststoffe für den interdisziplinären Optionsvergleich, ENTRIA-Arbeitsbericht-16, Institut für Werkstoffe, Leibniz-Universität Hannover (2019), Hannover, Germany.

[2] F. King, C. Padovani, Corros. Eng. Sci. Technol. 46 (2011), 82-90.

Effect of grain size on the corrosion of AZ91 alloys

Noémie Ott[1,2], Xinyi Hao[3], Christopher Gourlay[4], Qianqian Li[3]

[1] Institute for Microtechnology and Photonics, OST – Eastern Switzerland University of Applied Sciences, Buchs, Switzerland

[2] Laboratory for Joining Technologies and Corrosion, Empa, Dübendorf, Switzerland

[3] Department of Aeronautics, Imperial College London, London, United Kingdom

[4] Department of Materials, Imperial College London, London, United Kingdom

Among various magnesium-based alloys, Mg-Al alloys are the most common in commerce, accounting for about 43% of the total magnesium alloys used [1], and Mg-9wt.%Al-1wt.%Zn (AZ91) alloy has one of the best overall performances in castability, mechanical strength and corrosion resistance for lightweight applications. However, due to the limited number of independent slip systems in the hexagonal close-packed (HCP) crystal structure, unreinforced magnesium alloys would inevitably have poor ductility and workability.

In recent years, different strategies have been implemented to further improve their mechanical properties. Amongst them, grain refinement is considered as one of the most effective approaches that can simultaneously increase the strength, ductility and formability and reduce casting segregation and porosity of a given casting alloy. But its effect on the corrosion resistance of these alloys has received little attention.

In this study, we investigate the effect of gain size on the corrosion mechanisms of AZ91 alloys. Electrochemical impedance spectroscopy (EIS) combined with environmental scanning Kelvin probe force microscopy (AFM/SKPFM) and microscopic analysis was used to elucidate the fundamental correlation between the microstructure and surface reactivity of the alloys. As expected, all samples are very active in 0.1 M NaCl. Increasing the grain size seems however to lead to a more active dissolution.

References:

[1] D. S., Kumar et al., Am. J. Mater. Sci. Technol, 2015, 4(1), 12-30.

Effect of deformation on the corrosion behavior of Ni-coated steels

Arash Azimi Dastgerdi, Delft University of Technology, Netherlands, Ricardo Bouwer, Tata steel, Netherlands, Yaiza Gonzalez-Garcia, Delft University of Technology, Netherlands

Abstract

Nickel coatings are extensively used for their good corrosion performance and wear resistance. Based on their final application, Ni-coated steel may undergo some forming processes such as deep drawing and wall ironing, to produce a can shape. These cans are usually used as food storage containers or battery cases in which the corrosion performance plays an important role. In this research, we study the corrosion mechanism of electroplated Ni-coated steel after temper rolling conditions, deep drawing, and wall ironing. Two groups of Ni-coated steels with different coating thickness were evaluated. The microstructure and surface characteristics were assessed by optical microscopy, and SEM/EDS analysis. The results revealed that the deformation leads to a heterogenous thickness profile of the coating as well as the creation of cracks on it. This anisotropy in coating leads to different corrosion responses of the material in different parts of the can wall (i.e., top, middle, and bottom) and both outside and inside of the can, as well. Electrochemical evaluation of the coating by potentiodynamic polarization and EIS experiments showed that the corrosion resistance of the deformed specimens dropped considerably compared to undeformed ones by promoting localized corrosion mechanisms. This also confirmed the variability of the susceptibility to corrosion due to the heterogenous thickness and microstructural changes of the coating across the can. The experiments were carried out in conventional Cl-containing solution, and alkaline electrolyte typically used in battery applications.

Keyword

Nickel coating, deformation, polarization method, corrosion, microstructure

Interpretation of electrochemical impedance spectra of magnesium in corrosive environment

Linqian Wang[a], Darya Snihirova[a], Min Deng[a], Sviatlana V. Lamaka[a], Mikhail L. Zheludkevich[a,b]

[a] Institute of Surface Science, Helmholtz-Zentrum Hereon, Geesthacht, Germany

[b]Institute of Materials Science, Faculty of Engineering, Kiel University, Kiel, Germany

The Electrochemical Impedance Spectroscopy (EIS) is widely used to study corrosion behavior of different bare and coated metallic materials. EIS has been actively applied to study the corrosion properties of Mg and its alloys as well. However, the analysis and interpretation of EIS results for Mg are still controversial. Assignment of the observed time constants to the specific processes at electrode electrolyte interface is still debated. Diverse equivalent circuits are used by different researchers to fit the similar impedance spectra. Generally the impedance spectra of Mg evidences two time constants at high and middle frequencies often followed by a low frequency inductive response.

In this work, we report a systematic study involving number of complementary techniques in order to contribute towards more precise understanding of the impedance spectra of magnesium. The assignment of the high frequency relaxation process is confirmed through investigation of the oxide/hydroxide films formed at Mg surface in electrolytes with different pH values. The detailed characterization of the interface using TEM confirms the assignment of the high-frequency time constant to resistance and capacitance of the thin native MgO film present at the metal surface [1]. Moreover, the tribo-electrochemical impedance spectroscopy (Tribo-EIS) measurements was performed under different rotation speeds. The obtained results allowed assigning the middle frequency time constant to the response from the charge transfer process [2].

Additionally, a systematic EIS study of corrosion of several Mg-based materials in number of electrolytes was performed in order to find a clear pattern between the appearance of low-frequency “inductive loop” and the applied conditions. Different features can be identified at different corrosion stages. The “inductive loop” is more prominent in the case of systems which experience a fast transition during the

measurements in such a way that linearity and stability conditions are hard to be preserved. The spectra are influenced by the internal non-stationarity of Mg-medium system and the external non-stationarity induced by EIS measurement. Accordingly, the potential origin of inductive behavior of Mg-based materials is discussed.

References:

1. Linqian Wang, Darya Snihirova, Min Deng, Cheng Wang, Bahram Vaghefinazari, Gert Wiese, Mark Langridge, Daniel Höche, Sviatlana V. Lamaka, Mikhail L. Zheludkevich, Insight into physical interpretation of high frequency time constant in electrochemical impedance spectra of Mg, Corrosion Science, 187, 2021, 109501.

2. Linqian Wang, Darya Snihirova, Min Deng, Bahram Vaghefinazari, Daniel Höche, Sviatlana V. Lamaka, Mikhail L. Zheludkevich, Revealing physical interpretation of time constants in electrochemical impedance spectra of Mg via Tribo-EIS measurements, Electrochimica Acta, 404, 2022, 139582.

Investigation of the influence of Nb addition on the corrosion product formation and hydrogen uptake of tempered martensitic steel in H_2S environment

Elien Wallaert[1], Kim Verbeken[1], Tom Depover[1]

[1]Ghent University, Department of Materials, Textiles and Chemical Engineering, Research Group Sustainable Materials Science, Zwijnaarde, Belgium, Elien.Wallaert@Ugent.be, Kim.Verbeken@Ugent.be, Tom.Depover@Ugent.be

Abstract

The use of niobium as micro-alloying element in high strength OCTG (Oil Country Tubular Goods) steel has a significant influence on the SSC (Sulphide Stress Cracking) resistance. Niobium addition will influence the microstructure, introducing finer grains and small precipitates which can act as H-trapping sites.

In this study, two tempered martensitic materials, one without Nb and one with 0.029w% of Nb, were placed into a cell containing and aqueous solution with 0.5w% acetic acid and 5w% NaCl, saturated with H_2S at room temperature. The samples were left under these conditions for 3, 7, 14, 21 and 28 days. As a function of time, the corrosion surface layers and their evolution were investigated, using EPMA, XRD and XPS, and the influence of the corrosion products on the hydrogen uptake inside the material was evaluated using hot/melt extraction.

A clear difference in corrosion product formation was observed between the two materials. The addition of Nb to the base metal caused a significant reduction in the amount of FeS corrosion products present after the test. This was due to the formation of a much thicker Cr_2FeO_4 layer between the base material and the FeS corrosion products. This layer was brittle, had a lot of vertical cracks over the whole thickness, was not very adherent and caused the FeS to spall of the surface more easily.

The lack of a thick layer of FeS corrosion product on most of the metal surface caused the corrosion, and as such the hydrogen production, to take place close to the metal surface. As such, after the material was saturated, no drop in the diffusible hydrogen content was observed as was the case for the Mo containing material.

In summary, the niobium addition had a positive effect on the corrosion rate and the initial amount of diffusible hydrogen. However, on the long term, the amount of hydrogen in the material remains at a constant high value and no decrease was observed, as was the case for the material without Nb. As such, although the corrosion was slower for the Nb containing material, hydrogen embrittlement could be more problematic.

Keywords

Sour corrosion, OCTG steel, hydrogen uptake, Niobium addition

Introduction

The use of niobium as micro-alloying element in high strength OCTG (Oil Country Tubular Goods) steel is a commonly used strategy to improve the SSC resistance [1].

The addition of niobium will result in a finer grained microstructure after austenitization. The Nb(C,N) particles in the material will pin the grain boundaries, which prevents grain growth and results in a finer grained microstructure. Research has indicated that the coarser the prior austenite grain size (PAGS), the more susceptible the material becomes to SSC cracking. The PAGS should not exceed 5-10 µm, as such, a proper austenitization is required to prevent or minimize detrimental grain growth [2]. The refinement of prior austenite grains will induce a refinement of the eventual martensite structure, which explains the positive influence [3]. The refinement of the microstructure with Nb is often combined with specific heat treatments, such as accelerated cooling after rolling and induction hardening to obtain ultra-fine grains.

Niobium addition will also have a beneficial effect on the strength because of the precipitation hardening by the niobium precipitates [4]. However, the higher the strength level of the material, the more prone the material is mentioned to be to hydrogen embrittlement. That is why the hydrogen trapping by the niobium carbonitrides is also of great importance.
The materials were austenitized for one hour at 890 °C and were quenched in water. The low Mo material was tempered for one hour at 670 °C. To investigate the influence of Nb addition, the low Mo material was compared to the Nb-alloy. The main difference between these two materials is the addition of Nb (Table 1) and as a result of the pinning effect of the Nb precipitates, the tempering temperature of the Nb-alloy was higher, 697°C for the Nb-alloy and 670°C for the low Mo material.

Material	C (wt%)	Mo (wt%)	Cr (wt%)	Mn (wt%)	Nb (wt%)	Other elements
Low Mo	Max 0.35	0.43	0.89	Max 1.2	-	Si, P, S
Nb-alloy	Max 0.35	0.48	0.96	Max 1.2	0.029	Si, P, S

Table 1: Composition of the materials.

Cross-section analysis

SEM was used to examine the development of the corrosion products that formed on the materials' surfaces. After three days, both materials look very similar, only small nanocrystals are visible on the surface. After 14 days submersion, a difference between the two materials is observed. On the low Mo material, 14 days contact time with the test solution clearly resulted in crystal growth of the corrosion products on the alloy surface . However, for the Nb-alloy, no large crystals are observed. There is a cracked corrosion layer on this surface, but apparently, the corrosion products do not generate large crystals. This can either be attributed to diminished or lack of corrosion or to the early removal or bad adherence of the corrosion products. Also after 28 days of submersion, no thick layer of corrosion products was observed for the Nb-alloy, only on some distinct spots a larger crystal has grown.

The lack of corrosion products is evident when examining the cross-sections of the corroded materials. In Figure 1 a and b, SEM images of the cross-section of the Nb-alloy are shown. After 14 days, a significant part of the surface is corrosion product free, only on some sites some corrosion products are present. After 28 days, some regions are covered with corrosion product, but this layer is not as thick as for the low Mo material. Also, no double layer, as seen on the low Mo in Figure 1 c, is visually detected in the corrosion products.

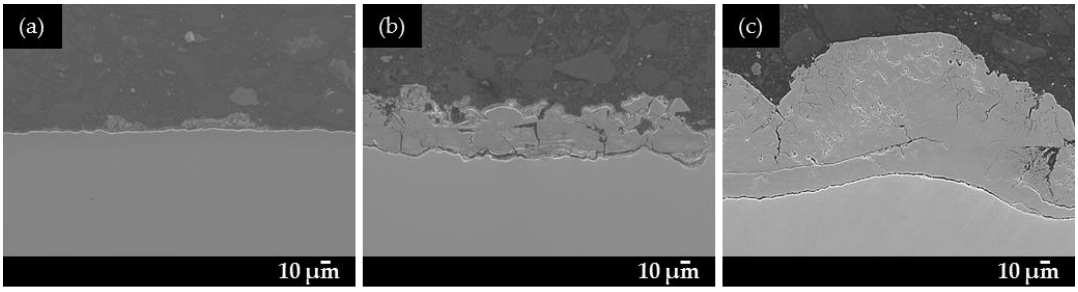

Figure 1: Scanning electron microscopy (SEM) images of the cross-sections of the Nb-alloy after (a) 14 days, (b) 28 days and of the low Mo material after (c) 28 days.

The elemental distribution in the corrosion product layers was examined by performing EPMA measurements. Therefore, a distinct region with a lot of corrosion products was selected, this region was not representative for the complete surface, since, as previously mentioned, the

corrosion products are lacking on most places. Although the double layer was not clearly visible in the SEM image, on the elemental mappings two distinct layers are visualized in the corrosion products. The upper layer consisted mainly of Fe and S enriched with Mo, while the inner layer consisted of Fe, O and Cr. The Cr and Fe rich oxide layer between the FeS and the base material is much thicker than for the low Mo material. A schematic view of the corrosion product layers on both materials is shown in Figure 2.

The thicker oxide layer could be attributed to the presence of Nb carbides in the material. NbC is known to be electrochemically quite noble [5] and contact between these stable carbides and more oxidation prone matrix causes the creation of local micro-galvanic cells causing the accelerated oxidation of the matrix. The local enrichment of Cr and Fe at the surface, due to the accelerated oxidation, causes the formation of more Fe_2CrO_4, rather than FeS, and as such a thicker oxide layer is present compared to the low Mo material. This process is also further assisted by the grain refinement of the martensitic microstructure caused by the Nb addition. The grain refinement offers better conditions to form a thicker passive film and larger amount of grain boundaries generates more diffusion paths for chromium to enrich the passive film, causing the formation of a more stable film [6, 7]. The thicker oxide layer however, appeared to be quite brittle and many vertical cracks were observed over the complete layer thickness . As such, this oxide layer will show a lower adherence to the base material and the delamination of the corrosion products will occur faster for the Nb material than for the low Mo material due to the higher oxide thickness. The original sample surface can also no longer be identified for the Nb material, while it is still visible for the low Mo material. This is further proof that heavier delamination of the corrosion product occurs when the material is alloyed with Nb. Local precipitation on the surface of the sample is what creates the FeS layer on top of the oxide.

Hydrogen uptake

The amount of diffusible hydrogen present in the samples was measured as a function of the test duration in order to assess the impact of the corrosion layer on the hydrogen uptake. The results are shown in Figure 2. Both materials show a rapid initial increase in hydrogen content, but after reaching an initial peak, the low Mo material shows a declining hydrogen content, while the Nb-alloy remains at constant levels. The difference in maximum value of both curves is also notable. This difference can be attributed to the various amount of dislocations, caused by the difference in tempering temperature of both materials. Additionally, the Nb-alloy contains many small Nb precipitates that serve as hydrogen traps and may contribute to the lower initial diffusible hydrogen. Consequently, Figure 2 also provides a schematic overview of the difference between the corrosion product formation and the influence of this corrosion product on the hydrogen content inside the metal of the two different alloys.

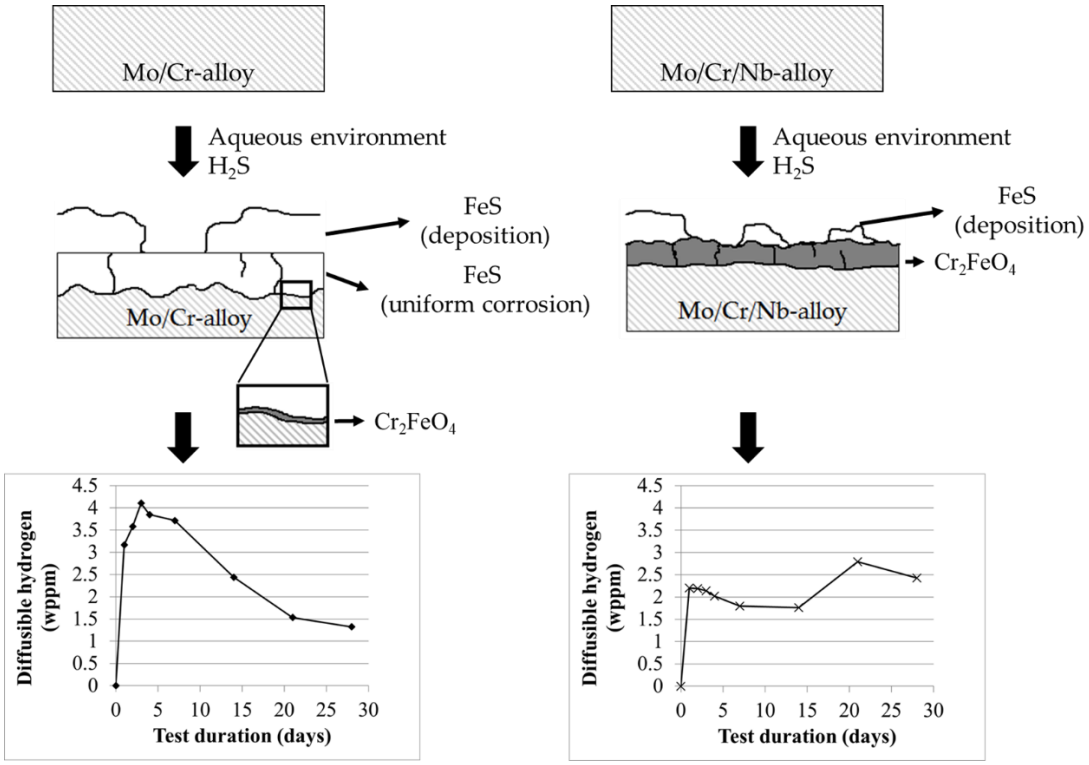

Figure 2: Schematic overview of the difference between the corrosion product formation and the influence of this corrosion product on the hydrogen content inside the metal of the two different alloys.

Conclusion

The addition of Nb results the development of local galvanic cells, generating a larger enrichment of Fe and Cr close to the surface and, consequently, generating a thicker Cr_2FeO_4 layer. A decrease in the grain size of the metal, because of the grain refinement effect of Nb, facilitates the diffusion of Cr to the surface and accelerates the oxide layer growth. As a result, the Cr_2O_4 layer is much ticker when Nb is added. However, this oxide layer is quite brittle, has multiple cracks, and spalls off the surface quite easily. Therefore, the FeS corrosion and deposition products are lacking on most of the surface and the corrosion process takes place near the base material. The material is saturated with hydrogen and no decrease is observed, since no thick sulfide layer is covering the material, as is the case for the material without Nb.

References

[1] Komizo, Y; Kushida, T; Miyata, K; Omura, T;, "Niobium in high strength steels for oil country tubular goods," in *International Symposium Niobium 2001*, 2001.

[2] A. Schino, "Metallurgical design and development of C125 grade for mild sour service applications," in *Corrosion NACE expo 2006*, 2006.

[3] Zhang, C; Wang, Q; Ren, J; Li, R; Wang, M; Zhang, F; Sun, K, "Effect of martensitic morphology on mechanical properties of an as-quenched and tempered 25CrMo48V steel," *Materials Science and Engineering A*, no. 534, pp. 39-346, 2012.

[4] Vervynckt, S; Verbeken, K; Lopez, B; Jonas, JJ, "Modern HSLA steels and role of non-recrystallization temperature," *International Materials Reviews*, vol. 57, no. 4, pp. 187-207, 2012.

[5] Messner, M; Walczyk, DJ; Palazzo, BG; Norris, ZA; Taylor, G; Carroll, J; Pham, TX; Hettinger, JD; Yu, L, "Electrochemical oxidation of metal carbides in aqueous solutions," *Journal of the electrochemical society*, vol. 165, no. 4, pp. H3107-H3114, 2018.

[6] Wu, SQ; Zhang, CH; Zhang, S; Wang, Q; Liu, Y; Abdullah, AO, "Effect of Nb addition on microstructure and corrosion resistance of novel stainless steels fabricated by direct laser metal deposition," *Materials Research Express*, vol. 5, no. 3, p. Art n° 036524, 2018.

[7] Fattah-Alhosseini, A; Vafaeian, S, "Comparison of electrochemical behavior between coarse-grained and fine-grained AISI 430 ferritic steel by Mott-Schottky analysis and EIS measurements," *Journal of Alloys and Compounds*, vol. 639, pp. 301-307, 2015.

Quantitative measurement of hydrogen intruded in steel sheet by channel flow double electrode with Devanath-Stachurski cell

Koji Fushimi, Yuya Mizushiri, Sunao Shoji, Yuichi Kitagawa, Yasuchika Hasegawa,
Hokkaido University, Sapporo/Japan

From the viewpoint of energy conservation, the use of high-strength steel as a structural material for transportation equipment is becoming more important. However, there is concern that high-strength steels have relatively high susceptibility to hydrogen embrittlement due to atmospheric corrosion. Electrochemical hydrogen permeation tests with Devanathan-Stachurski (DS) cell [1] have been used as a method to evaluate the hydrogen embrittlement resistance of steel sheets. For example, the hydrogen diffusion coefficient has been measured by analyzing the transfer function of the anodic current flowing to the hydrogen withdrawal electrode behind the steel sheet with in relation to the cathodic current flowing to the hydrogen entry electrode. A method to derive the amount of hydrogen trapped in a steel sheet from the analysis of the transfer function has been reported [2], but it is semi-quantitative and has many accuracy problems.

Here, we combined a channel flow double electrode with a DS cell and attempted in-situ measurement of non-intrusion hydrogen in a hydrogen permeation test using the DS cell. By taking into account the mass balance of hydrogen during the test, we were able to quantitatively evaluate the amount of hydrogen that intruded into the steel sheet and estimate the amount of trapped hydrogen.

[1] M. A. V. Devanathan, Z. Stachurski, “The adsorption and diffusion of electrolytic hydrogen in palladium”, Proc. R. Soc. (London), A, 270 (1962) 90-102.

[2] A. McNabb, P. K. Foster, "A new analysis of the diffusion of hydrogen in iron and ferritic steels", Trans. Metall. Soc. AIME, 227 (1963) 618–627.

Corrosion and Hydrogen absorption in high strength steels exposed to sweet and sour environments: the effect of microstructure and corrosion layer

Shabnam Karimi [a], Iman Taji [a] Tarlan Hajilou [a], Simona Palencsár [b], Arne Dugstad [b], Afrooz Barnoush [a,c], Kim Verbeken [d], Tom Depover [d], Roy Johnsen [a]

[a] Department of Mechanical and Industrial Engineering, Norwegian University of Science and Technology (NTNU), N-7491 Trondheim, Norway

[b] Institute for Energy Technology (IFE), P.O. Box 40, NO-2027, Kjeller, Norway

[c] Qatar Environment and Energy Research Institute (QEERI), Hamad Bin Khalifa University (HBKU), P.O. Box 34110, Doha, Qatar

[d] Department of Materials, Textiles and Chemical Engineering, Ghent University (UGent), Technologiepark 46, B-9052 Ghent, Belgium

Keywords:

High strength steels, CO_2/H_2S environment, Hydrogen absorption, thermal desorption spectroscopy, Focused ion beam

Abstract:

High strength carbon steels are among the materials which have massive application in oil and gas industries because of their excellent mechanical and cost-effective properties. However, they may experience severe environmental conditions due to the presence of corrosive species and reactions together with mechanical loading during service. In this work three kinds of high strength steels with 0.62, 0.65 and 0.83 wt.% carbon which are used as armor wires in flexible pipelines have been investigated under the CO_2 and CO_2/H_2S conditions. The corrosion rate of the alloys in these environments have been monitored with weight loss and linear polarization resistance (LPR) techniques and the effect scale formation on the corrosion rate has been studied. In addition, the role of the cementite morphology on the corrosion products formation has been evaluated by careful microstructural analysis of the base material and cross-sectional images of the corrosion layer using scanning electron microscope (SEM) and focused ion beam (FIB). After 21 days of exposure in corrosive

environment, the hydrogen absorption of the samples was measured by thermal desorption spectroscopy (TDS) to investigate the role of microstructure and corrosion layer on hydrogen absorption capability of the alloys. Detailed TDS analysis was also carried out under laboratory cathodic charging to reveal the H-microstructure interaction in different alloys of this study. The present study shows that the corrosion layer formed in CO_2/H_2S environment acts as a corrosion barrier while it can not prevent H atoms to absorb in the material. Under the conditions of CO_2 purging on the electrolyte, a thick, porous corrosion layer is formed which was not protective against corrosion. In this specific condition, the corrosion rate was mostly controlled by the morphology of the alloy's microstructure rather than the corrosion layer. However, the thick corrosion product formed in CO_2 environment delays the H desorption since H needs to pass through a tortuous corrosion layer containing remaining Fe_3C partially filled with corrosion products. In the studied alloys, the pearlite/ferrite or pearlite/pearlite interfaces were found to be a strong irreversible trap in pearlitic microstructures.

Electrochemical Impedance Spectroscopy of parylene coated magnesium stents in organic solvent

V. Roche[a], M. Diaz-Ramos[a], R. Song[b], H. Fan[b], C. Bureau[c], JC. Lepretre[a]

a Univ. Grenoble Alpes, Univ. Savoie Mont Blanc, CNRS, Grenoble INP+, LEPMI, 38000 Grenoble, France
b Sino Medical Sciences Technology Inc., #5 4th St.TEDA Tianjin, China
c Alchimedics, 28 Cours Albert 1er, 75008 Paris France

Parylene layers on stents of Mg-Nd-Zn-Zr alloy were studied by electrochemical techniques in an organic electrolyte. As a novelty this article reported the electrochemical impedance spectroscopy characterization in an organic based electrolyte : TetraButylAmmonium Perchlorate dissolved in Dimethylformamide. Additionally in this work, a methodology of EIS data treatment is proposed based both on the use of the Measurement Model [1] and power law model to fit the resistivity distribution of the layers which is rarely reported in the literature. The results show a constant-phase element (CPE) behavior, which was attributed to the layers on stent surface, as well as diffusion impedance associated with Mg2+ ions diffusion. Power law model was suggested to characterize electrical properties of the layers. Additionally, samples with oxide layers presented a high-frequency distribution which was well described by complex ohmic impedance. Compared with bare and plasma pre-treated stents, the parylene coatings showed lower capacitances values, associated with a thicker layer which is maintained after crimping and expansion

[1] H. Liao, W. Watson, A. Dizon, B. Tribollet, V. Vivier, M.E. Orazem, Electrochim. Acta. 354 (2020) 136747. https://doi.org/10.1016/j.electacta.2020.136747

Effect of droplets on inhibitor performance for steel and galvanized steel

C Samarawickrama[1], Xiao-Bo Chen[1], Paul White[1], Patrick Keil [1 2], Ivan Cole[1]

[1] RMIT University, Melbourne VIC 3001, Australia

[2] BASF Coatings GmbH, Glasuritstrasse 1, 48165 Muenster, Germany

Corrosion prevention of steel and galvanized steel has become a crucial aspect of sustainability. Each year, an extensive amount of steel is being produced for the automotive and construction industry, creating a significant carbon footprint. Corrosion protection of these metals are most commonly achieved through protective coatings and/or corrosion inhibitors. Most inhibitor studies have been conducted utilizing the bulk volume of electrolyte, only a limited amount of research has been done in understanding the corrosion protection mechanism associated with droplet volume.

Atmospheric corrosion is defined as material destruction due to aerosols or droplets deposition, and it is crucial to focus on minute volumes to represent such situations. In comparison to a bulk electrolyte environment, by utilizing a droplet volume, many factors such as electrolyte evaporation, pH gradients, secondary spreading, oxygen diffusion gradients, droplet volumes and shapes should be taken into consideration. Therefore, this study focuses on establishing an electrochemical testing method to accommodate droplet volumes as well as bulk volume and thereby screen a range of inhibitors to determine the effects of droplet volume on the inhibitor effectiveness. This test method is a rapid screening technique that can be used to test a wide a range of inhibitors rapidly and this allows to determine the most effective or ineffective inhibitor functional groups for droplet and bulk corrosion. The results obtained via this technique has discovered significant differences in the effectiveness of inhibitors in droplet and bulk volumes. These results display a clear indication of the importance of understanding corrosion mechanism under droplets as some well-known effective inhibitors may not be effective against droplet corrosion. The influence of droplet volume, pH gradients and other parameters on the inhibitor performance for a wide range of inhibiting compounds will be discussed in-depth with

the utilization of electrochemical and surface analytical techniques to further understand the corrosion protection process under droplet and bulk volumes.

Unravelling the buried hybrid interfacial influences on the onset of corrosion of coated metals in situ by a combined spectro-electrochemical approach

T. Hauffman, N. Madelat, B. Wouters, A. Hubin, H. Terryn,
Research group Electrochemical and Surface Engineering, Dept. Materials and Chemistry, Vrije Universiteit Brussel, Brussels, Belgium

The stability and durability of organic coated structures, used in a wide variety of applications such as packaging, automotive, aerospace,…. is governed by a plethora of factors. Indeed, the (dynamic) environment, the coating components, the surface pre-treatment, type of oxide, metal microstructure and the interplay between all components and their variation as a function of exposure time, influence the to be optimized lifetime. One of the most crucial aspects is the hybrid buried interface between the protective coating and the pre-treated metal. This hidden zone provides the second barrier to potential dissolution of the metal by providing organic-inorganic bonds which inhibit electrochemical reactions. The mechanistic understanding of reactions at this area is thus key for the understanding of the total (electro)chemical behaviour of the hybrid structure.

The main challenge is that this nanometer interface/interphase is buried between two micro- to millimeter thick phases. Therefore, it is very hard to analyze its response to a corrosive environment in situ in a non-destructive way. In order to analyze the influence of the uptake of environmental species (such as water and ions) through the coating and their subsequent action on the interface, we present a spectro-electrochemical approach.

By employing a combination of odd random phase multisine electrochemical impedance spectroscopy and infrared spectroscopy in the Kretschmann geometry, we can benefit from two techniques that simultaneously measure the overall electrochemical behaviour of the system under study, while probing the direct spectroscopic response of the buried interface/interphase. This occurs in the same time frame, and in such a way that even fast dynamic changes are captured.

The technique is validated on model samples, comprising pre-treated aluminium oxides coated with ultrathin polyacrylic acid or polymethyl metacrylate coatings [1].

Here, we could clearly unravel the influence of the interfacial changes on the impedance behaviour. Furthermore, the mechanistic insights obtained were supported by ambient pressure X-ray photoelectron spectroscopy measurements [2-3]. In a next stage, the coating complexity was enhanced, by increasing the thickness of the layer to >100 micrometer, and by including pigments. An EIS data treatment will be proposed in this presentation, where the uptake of water and sions throughout the coating can be followed up separately [4]. The arrival of ions at the interface could be linked to a change in electrochemical behaviour as observed by EIS [5]. The spectroscopic and EIS data interpretation was supported by secondary ion mass spectrometry analysis, where the diffusion profiles of the electrolyte ions were determined by ion gas cluster sputtering and compared to the EIS results.

The spectro-electrochemical approach presented in this work has shown to be a very valuable tool to understand the influence of localized areas of the hybrid structure to the overall behaviour of the system. It provides in situ insights in the optimization strategy of the interfacial interactions between organic coatings and metallic substrates.

[1] Pletincx S. et al., An in situ spectro-electrochemical monitoring of aqueous effects on polymer/metal oxide interfaces, Journal of Electroanalytical Chemistry 848 (2019).
[2] Pletincx S. et al., Unravelling the chemical influence of water on the PMMA/aluminium oxide hybrid interface in situ, Scientific Reports 7:13341 (2017).
[3] Pletincx S. et al., In situ characterization of the initial effect of water on molecular interactions at the interface of organic/inorganic hybrid systems, Scientific Reports 7:45123 (2017).
[4] Wouters B. et al., Monitoring initial contact of UV-cured organic coatings with aqueous solutions using odd random phase multisine electrochemical impedance spectroscopy, Corrosion Science 190 (2021).
[5] Madelat N. et al., Differentiating between the diffusion of water and ions from aqueous electrolytes in organic coatings using an integrated spectro-electrochemical technique, Corrosion Science accepted (2022).

Microscale and nanoscale infrared spectroscopy studies of initial SO_2 induced atmospheric corrosion of ZnAlMg coated steel in humid air.

D. Persson, RISE, Sweden; A. Wärnheim, RISE Sweden; S. Sainas, RISE Sweden; D.Thierry, RISE Sweden; and N. Lebozec, Institut de la Corrosion, France

Abstract

Hot dipped zinc coated steel alloyed with small amount of aluminium and magnesium is used increasingly for application in automotive industry and coil coated steel. as an alternative to conventional hot dipped zinc coated steel. The alloyed zinc coatings have improved properties compared to HDG, such as improved formability and better corrosion resistance. The ZnAlMg coatings show better corrosion properties compared to hot dipped galvanized steel and electro plated steel in salt spray, cyclic corrosion testing as well as during various field exposures. However, it has been observed that ZnAlMg coated steel exposed in humid atmosphere containing SO_2 under laboratory conditions show an increased formation of sulphate containing corrosion products compared to pure zinc coated steel and zinc [1]. Here, the initial formation of sulphite and sulphate containing corrosion products on ZnAlMg coating surfaces and how this is related to the microstructure of the alloy was investigated. The initial corrosion product formation was studied with FTIR-ATR focal plane array imaging, SEM-EDS and nanoscale AFM-IR. While FTIR-ATR provide chemical information in the micrometer scale AFM-IR gives information about the corrosion product formation with a nanometric /submicron lateral resolution. Initial corrosion formation of sulphite and sulphate containing products were formed initially mainly in the eutectic areas on the surface. Formation of submicron /nanoscale corrosion product clusters was observed in the eutectic areas as determined by AFM-IR.

1. D. Persson, T. Prosek, N. Lebozec, D. Thierry and G. Luckender, Corr. Sci 90 (2015), 276-283

Effect of cerium salts in the cut edge of zinc-based sacrificial coatings: influence of Al and Mg alloying elements on galvanic corrosion

T. T. Nguyen, University of Mons, Mons/Belgium and Institute of Tropical technology/Vietnam (Hanoï); S. Akbarzadeh, University of Mons/Belgium; T. T. Thai, Institute of Tropical technology/Vietnam (Hanoï); A. T. Trinh, Institute of Tropical technology/Vietnam (Hanoï); M.-G. Olivier, University of Mons, Mons/Belgium

Zinc sacrificial coatings alloyed with Al and Mg for sacrificial protection of steel have been developed during the last decades and improved significantly the performance of steel against corrosion compared to pure zinc coating [1]. Despite the significant reinforcement achieved by this sacrificial coating, the cut edges or the appearance of scratches reaching the steel are the major problems due to the formation of galvanic coupling between steel and zinc-based coating. Therefore, it required supplementary active protection for galvanic coupled metallic materials.

In previous work [2], cerium chloride has been reported as a promising corrosion inhibitor on the top surface of electro-galvanized steel. Thus, this study aims at investigating the protective properties of cerium salts for the cut edge of zinc-based sacrificial layers.

Four types of the sacrificial coating were employed in this study: pure zinc coating on steel (fabricated by electrodeposition), Hot Dip Galvanized steel (HDG), ZA (9 wt. % Al), and ZAM (7 wt. % Al and 4 wt. % Mg). A galvanic corrosion prediction was established through the potentiodynamic polarization curves performed on the top surface of sacrificial coatings and steel in 0.1 M NaCl + 5.10^{-3} M cerium salts. Then, a local electrochemical technique (Scanning Vibrating Electrode Technique) was conducted on the cross-section of Zn-based coated steel in 0.015 M NaCl + 5.10^{-3} M inhibitor. In addition, cross-section characterizations of all substrates after 24 h of immersion in the electrolyte solution without and with inhibitor were analyzed by Scanning Electron Microscopy coupled with Energy Dispersive X-Ray Spectroscopy.

References:

[1] P. Volovitch, T.N. Vu, C. Allély, A. Abdel Aal, K. Ogle, Corrosion Science, **2011**, 53, 2437–2445

[2] C. Arrighi, T.T. Nguyen, Y. Paint, C. Savall, L.B. Coelho, J. Creus, M.-G. Olivier, Corrosion Science, **2022**, 200, 110249

Acknowledgments

This work is carried out in the framework of the Research project (PRD2020) “Renforcement de l’expertise environnementale du centre de compétences en protection contre la corrosion et en électrochimie” between Institute of Tropical technology (ITT-VAST, Vietnam) and Materials Science Department, UMONS, Belgium

Roll of zinc ions supply layer on corrosion of carbon steel in model fresh water

M. Sakairi and Li Li, Hokkaido University, Sapporo/Japan

Introduction

Carbon steels are widely used in structural materials such as vehicles, bridges and buildings. Corrosion Inhibitors are a common method to protect steels used in aqueous environments from corrosion. However, this method has some disadvantages, a high cost and destruction of the environment. It is desired to develop an environmentally friendly, non-toxic, low-cost, and simple-to-handle corrosion prevention techniques. One possible way is using metal cations. There are reports that the metal cations, especially zinc ions, can inhibit the corrosion of metals in aqueous solutions.

In this study, zinc ions supply layer was formed on carbon steel by electrodeposition and heat treatment. The corrosion protective activity of formed layers was investigated by immersion and electrochemical tests.

Experimental

Sheets of carbon steel were used as specimens. The sheets were cut into 10 × 10 mm, and polished. Electrodeposition was carried out with constant current density of 20 mA/cm^2 in 100 g $ZnSO_4$ / $7H_2O$ + 20 g H_3BO_3 at 298 K. The electrodeposition time was changed form 70 s to 300 s. Specimens with zinc layer were heated at 673 K.

The immersion corrosion tests were carried out in 10 mM NaCl for 86.4, 172.8, and 259.2 ks. After each immersion period, the Electrochemical Impedance Spectroscopy (EIS) measurements were carried out at OCP with a modulation amplitude of 10 mV in the frequency range from 10 kHz to 10 mHz.

Surface observation and analysis were carried out by XRD,SEM-EDS, Auger Electron Spectroscopy (AES) and X-ray Photoelectron Spectroscopy (XPS).

Results and discussion

The electrodeposition and successive heat treatment make it possible to form zinc-iron layer with Fe_4Zn_9 structure on the specimens. From the EIS tests, charge transfer resistance of specimens with zinc-iron layer showed a higher value than only zinc layer formed specimen immersed after 259.2 ks. From the immersion tests results also exhibited zinc-iron layer has good corrosion resistance.

Organic Coating/Metal Interfacial Degradation Kinetics Study by Using Combined Novel Hydrogen Permeation Potentiometry & Electrochemical Impedance Spectroscopy Technique

Rasmi Ranjan Tripathy, Dandapani Vijayshankar,*
Department of Metallurgical Engineering and Materials Science, Indian Institute of Technology (IIT), Bombay, Mumbai - 400076

Organic coatings applied to protect metal surfaces tend to fail prematurely due to false estimation of its corrosion rate owing to the inaccessible (buried) nature of the metal/polymer interface. Cathodic disbondment by which majority of polymer coated iron and zinc-based alloys fail is still governed by the initial rate of electrochemical oxygen reduction reaction (ORR) [1]. Challenges in its quantification arise when conventional electrochemical techniques such as cyclic voltammetry that primary rely on ion transfer through the coating, cannot compensate for the high Ohmic resistance of the protective coating. Although sophisticated methods/techniques for probing such buried interfaces exist, they are still limited in their ability to provide quantitative reaction kinetic data for industrially useful polymer/metal buried interfaces, non-destructively. Previously, the novel hydrogen potentiometry (HP) technique for the quantification of cathodic delamination by oxygen reduction reaction (ORR) at various intact metal/polymer interfaces has been introduced by Vijayshankar et. al [2]. This technique works by sending in nascent hydrogen (H) by galvanostatic charging from the back side of an electrochemical double cell to combine with molecular oxygen (saturated) on the front side to undergo a coupled redox reaction that achieves equilibrium at dynamic conditions. The open circuit potential thus established between hydrogen oxidation and oxygen reduction at the front cell, is used to plot the current-potential ie., I(U) curve for the ORR kinetics by considering the hydrogen reduction current from the back cell as a proxy for the ORR current. I(U) curves derived for bare palladium as well as for physisorbed poly-vinylbutyral organic coating showed potential of this technique not only for quantification of ORR kinetics but also for exploring the water uptake kinetics through such polymer coatings. Here in this work, the use of electrochemical impedance spectroscopy (EIS) as a tool for capturing real-time interface degradation controlling factors during initial stages of cathodic disbondment enabled by hydrogen potentiometry is introduced. By simultaneously

measurement of the charge transfer resistance (R_{ct}) for ORR and pore resistance (R_{pore}) of the polymer coating using EIS on the front side upon stepwise galvanostatic H charging, the protection ability of the coating can be evaluated. Proof of concept shown on a bare palladium membrane immersed in a saturated oxygen containing alkaline environment shows a steep decrease in the charge transfer resistance with increase in the amount of hydrogen for oxygen reduction. Further study of a model poly-methyl-methacrylate (PMMA)/Pd interface reveals 60 mV (1 pH unit) cathodic shift pointing to inhibited ORR kinetics due to physisorbed coating interface. Co-related EIS data shows two-time constants corresponding to ORR kinetics and another to pore diffusion for the PMMA coating. 30-fold decrease in R_{CT} value for identical H charging conditions as compared to bare Pd, proves that only ORR rate can be measured. In order to exclusively find the sensitivity of this technique, a self-assembled monolayer of octane thiol used as an inhibitor for ORR deposited on Pd with the model PMMA as a top coat shows a 5-fold increase in R_{CT} value along with a cathodic shift of around -193 mV (3 pH units) compared to model PMMA coated Pd at a charging current of -25 µA/cm^2. This indicates inhibited ORR kinetics due to alkalinization at the interface.

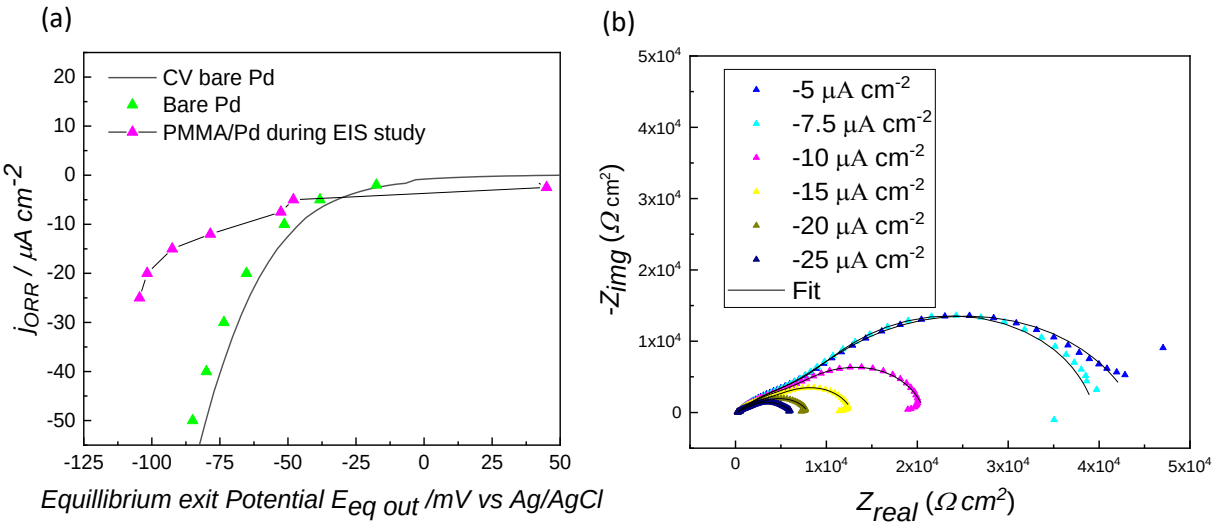

Fig: (a) I(U) curve from Hydrogen Potentiometry (HP) and (b) Nyquist plot from (EIS) for PMMA/Pd interface

References:

1. A. Leng, H. Streckel, M. Stratmann, *Corros. Sci.* 41 (1999) 579-597

2. D. Vijayshankar, A. Altin, C. Merola, A.Bashir, E.Heinen, M. Rohwerder, *J. Electrochem. Soc.* 2016, 163, C778-783

Modeling of intergranular corrosion inhibition of copper using DFT

Fatah Chiter, Dominique Costa, Vincent Maurice, Philippe Marcus
PSL University, CNRS-Chimie ParisTech, Institut de Recherche de Chimie Paris, Research Group Physical Chemistry of Surfaces, Paris (France)

Inhibition of the initiation of intergranular corrosion of copper was modeled at the atomic scale for 2-mercaptobenzothiazole (MBT), using dispersion corrected density functional theory (DFT-D). The modeled copper surface and grain boundary was a (110)-oriented copper bi-crystal exposing an emergent Σ9 coincident site lattice (CSL) grain boundary (GB). Isolated molecule and full monolayer coverages were investigated.

It was found that in both cases the molecule adsorbed on the grain surface and on grain boundary sites is perpendicular or tilted whereas no parallel orientation to the surface is obtained.

Chemical bonding of the thione and thiolate conformers involves both endocyclic and exocyclic S atoms, or the exocyclic S and the nitrogen atoms. A net energy gain (per surface area) is calculated for the dense (full) monolayer, but at the cost of a significant molecule deformation.

The adsorption of 2-MBT enhances the Cu vacancy formation energy at the grain and GB sites, revealing that MBT also inhibits Cu dissolution for the more susceptible GBs with an efficiency depending on the atomic density at the GB emergence.

A final discussion will integrate the above findings with recent experimental data obtained by in situ electrochemical scanning tunneling microscopy.

RMIT Classification: Trusted

Advances in the design of corrosion inhibitors on active metals

Ivan Cole[1], Patrick Keil[2], Pablo Ordejon[3], Ernane De Freitas Martins[1,3], Jose Castillo Robles[1,3], Steffen Jeschke[1], Rou Jun Toh[1], Jim Jose[1] Qiushi Deng[1], Paul White[1], Xiaobo Chen[1], Chathumini Samarawickrama[1], Philip Eiden[4], Milan Patel[1]

[1] RMIT University, Melbourne, Australia；

[2] BASF Coatings GmbH, Muenster, Germany

[3] ICN2, Barcelona, Spain

[4] BASF SE, Ludwigshafen, Germany

EXTENDED ABSTRACT: “Inverse Design” is a grand challenge for the design of materials systems in general and corrosion inhibitors. In inverse design, the particular features that render a material system functionally effective are identified and then databases of materials are searched for materials with these features. In the particular case of the use of small molecules as corrosion inhibitors, molecular forms and properties (molecular attributes) that give rise to good inhibition properties are selected by statistical, Quantitative Structure-Activity Relationships (QSAR) or machine learning. Having identified these attributes, molecular databases are searched to extract promising inhibitor candidates. This approach is particularly promising as not only can it be used to sort through the tens of thousands of possible inhibitors, but it can virtually explore new families not previously considered as candidates.

However, there are a number of challenges limiting the successful application of inverse design to corrosion inhibitor selection. In many works, the selection of molecular attributes does not appear to model the observed variation in inhibitor efficiency in a robust way so that while reasonable test models can be developed their predictive capability is limited. Secondary very large databases of both molecular attributes and electrochemical properties are required to drive current QSAR models and these are expensive and time-consuming to build. Lastly, there are some fundamental limits to our understanding of small molecular

surface interactions in aqueous media particularly when the surface is charged. This paper will present recent work on modelling the double layer or electrified interface in aqueous systems, the development of robotic electrochemistry to help build large databases and recent large data studies that have refined the definition of molecular attributes.

To address some of the above problems with the QSAR approach we are addressing the possibilities that arise when “evolutionary algorithms” are combined with robotic experimentation. In this approach rather than construct large data bases, one begins with a constrained selection of possible inhibitors that are tested via robotic electrochemistry and then a refined set of molecules is derived by “mutating” the original selection based on this testing results and the mutated selection is then tested and the process continues until an optimum selection of inhibitors is obtained.

Are NHCs potential corrosion inhibitors?
NHC interaction with metallic and oxidized Al surfaces explored by DFT

D. COSTA,[1] F. CHITER,[1] D. MERCIER,[1] S. ZANNA,[1] L. FENSTERBANK,[2] F. RIBOT,[3] P. MARCUS[1]

[1] PSL Research University, Chimie ParisTech-CNRS, Institut de Recherche de Chimie Paris (IRCP), Research Group Physical Chemistry of Surfaces, 75005 Paris, France

[2] Institut Parisien de Chimie Moléculaire, Sorbonne Université, 4 Place Jussieu, 75252 Paris cedex 5 France

[3] Sorbonne-Université, CNRS, Laboratoire de Chimie de la Matière Condensée de Paris (LCMCP), 75252 Paris cedex 5 France

ABSTRACT

Localized corrosion by chlorides on Al and Al alloys is a major problem, and green corrosion inhibitors are a cheap and environmentally friendly solution for Cr(VI) replacement. In the search for corrosion inhibition candidates, Density Functional Theory (DFT) calculations provide insights into molecule/surface interactions. Nitrogen Heterocyclic Carbene (NHC) molecules are possible candidates for corrosion inhibition. An efficient inhibitor must adsorb on the metal and oxidized/hydroxylated surface. Therefore, the adsorption of 1,3-dimethylbenzimidazol-2-ylidene, a model of NHC molecule, on Al, metallic and oxidized/hydroxylated, was investigated by means of periodic DFT including van der Waals forces.

The NHC molecule adsorbs on Al metal in an on top position, with an adsorption energy of E_{ads}=-1.28 eV. On dry oxidized Al, adsorption occurs on a Al(III) surface ion, in a Lewis acid-base reaction, forming a NHC-Al adduct, with an adsorption energy of E_{ads} =-2.43 eV. On the hydroxylated surface, NHC can either substitute an OH group (E_{subst} =-1.18 eV) to form the NHC-Al adduct, or react and form oxygenated adducts, (NHC-OH-Al) (E_{react} =-0.86 eV) or (NHC-O-Al)(E_{react} =-1.39 eV) adduct. The main results are i) NHC adsorbs on the metal, oxide and hydroxylated surfaces, ii) adsorption is in all cases exothermic, iii) on the hydroxylated surface, it does not require OH desorption. All these trends suggest that NHC are promising candidates for Al corrosion inhibition.

Synergistic inhibition effect between 2-amino-4-methylthiazole and 2-methylthiol-imidazole on galvanised steel corrosion in NaCl solution

Qiushi Deng[1], Steffen Jeschke[1], Paul White[1], Sabine Hirth[2], Philipp Eiden[2], Jan N. Gorges[2], Xiao-Bo Chen[1], Patrick Keil[1,3], Ivan Cole[1]

[1]School of Engineering, RMIT University, Melbourne, VIC 3000, Australia
[2]BASF SE, Carl-Bosch-Strasse 38, Ludwigshafen am Rhein 67056, Germany
[3]BASF Coatings GmbH, Glasuritstrasse 1, Münster 48165, Germany

The use of corrosion inhibitors is one of the most practical means to tackle metal corrosion. Whilst a large number of studies focus on discovering novel and high-efficient corrosion inhibitors, great endeavours have been contributed to exploring effective inhibitor mixtures within a variety of corrosion inhibitors. To date, attempts to combine inhibitors of different categories (e.g., organic and inorganic regimes), inhibiting effects, and molecular structures have been conducted to determine the feasible formulations. However, challenges remain, given the exponentially increased combinations by diverse candidates, which leaves the synergy study a “cherry-picking” process.

The presented work demonstrated a synergistic inhibition strategy using inhibitor candidates with particular inhibitory behaviours to achieve superior and sustainable corrosion protection for electro-galvanised steel (ZE) in a neutral NaCl solution. The subtle formulation design outperforms in a fashion by taking advantage of each inhibitor individual. Specifically, binary inhibitor systems of 2-amino-4-methylthiazole (2AT-Me) and 2-methylthio-imidazole (I-2MT) of different molar ratios were prepared. Electrochemical results have revealed that the formulated mixtures at a 1:1 and 1:4 (2AT-Me: I-2MT) molar ratios displayed a synergistic effect, in which at a molar ratio of 1:1, the inhibitor mixture rendered sustainable corrosion protection of ZE and the inhibitory efficiency remains 96% after 7-day immersion. The analytical investigation of the surface and the electrolyte chemistry revealed that the growth dynamic of the protective layer is a two-step process reflecting the sequential responses of each

inhibitor's characteristic mode-of-action. This synergistic inhibition formulation also shows promises to modify post-corroded ZE surface.

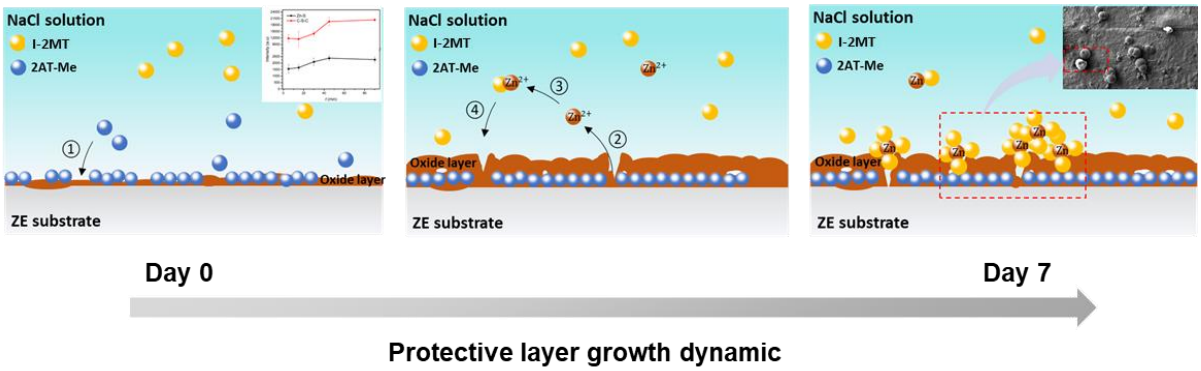

Figure 1 Evolution of surface protective layer upon ZE by inhibitor mixture in relation to corrosion resistance in 0.1 M NaCl.

Corrosion inhibition of copper by 2-mercaptobenzothiazole: The effects of native oxide reduction on improving interfacial properties in a neutral chloride environment

Vishant Garg, Sandrine Zanna, Antoine Seyeux,
Frédéric Wiame, Vincent Maurice, Philippe Marcus.

PSL University, CNRS-Chimie ParisTech, Institut de Recherche de Chimie Paris,
Research Group of Physical Chemistry of Surfaces, Paris, France.

2-Mercaptobenzothiazole (2-MBT) is well established as an effective organic corrosion inhibitor for the protection of copper and other metals. Despite numerous works discussing the inhibiting properties on copper, several questions remain, notably regarding the role played by the surface native oxide on the bonding mechanisms, the stability, and the inhibition efficiency of the organic film formed in various environments.

In the present work, electrochemistry was combined with advanced surface analysis techniques (XPS and ToF-SIMS) to investigate the effects of reducing the surface native oxide film on the formation and bonding mechanisms of 2-MBT organic layers on pure copper in a near neutral chloride medium (3.5% NaCl aqueous solution). Additionally, the influence of 2-MBT organic layers, pre-adsorbed in various electrochemically controlled conditions of formation of the interface, on the subsequent oxidation and protection against corrosion of the surface was studied.

The results show that the presence of 2-MBT poisons the formation of the passive oxide layer on the copper surface and inhibits corrosive attack up until the pitting potential. Reduction of the native oxide film in absence of 2-MBT prior to anodic polarization promotes surface protection compared to reduction in presence of the inhibitor. The effect of increased exposure time to the inhibitor is to further decrease the current density values during polarization indicating the formation of a more protective barrier layer. Surface analysis shows that the molecules bonded to both the metallic Cu surface and local oxidized regions via their 2 (exocyclic and endocyclic) S atoms. Additionally, the formation of organic multi-layers is confirmed with either pre-treatment method. This bonding of the molecules

prevents the formation of surface $CuCl^-$ or $CuCl_2$ species and protects the surface in the anodic potential range preceding breakdown.

This project has received funding from the European Research Council (ERC) under the European Union's Horizon 2020 research and innovation program (Advanced grant agreement No. 741123, CIMNAS).

Corrosion inhibition of pure zinc in 0.1 M NaCl by picolinoyl N4-phenylthiosemicarbazide

Thu Thuy Pham, University of Mons, Belgium and Institute for Tropical Technology, Vietnam; Chien Thang Pham, VNU University of Science, Vietnam; Thuy Duong Nguyen, Institute for Tropical Technology, Vietnam; Anh Son Nguyen, Institute for Tropical Technology, Vietnam; Thi Xuan Hang To, Institute for Tropical Technology, Vietnam; Marie-Georges Olivier, University of Mons, Belgium

The use of organic compounds as inhibitors of zinc alloys has shown great promise because they were able to either be adsorbed on the surface or chemically react with the metallic surface to form a barrier coating between the metallic surface and aggressive media [1]. The corrosion inhibition mechanisms of organic inhibitors were related to sharing the outer orbital electrons of heteroatoms and π-orbitals to unoccupied d-orbital spaces within corroded metals, which formed new coordination bonds and subsequently, a protective coating [2, 3]. The impact of picolinoyl N4-phenylthiosemicarbazide (HL) concentrations on the corrosion resistance of pure zinc substrate were investigated in this study. The inhibitory action of 10^{-5}, 10^{-4}, and 10^{-3} M HL on pure zinc substrate in 0.1 M NaCl was studied by electrochemical methods such as electrochemical impedance spectroscopy and potentiodynamic polarization, whereas the surface morphology and chemical compositions of all the surface substrates after exposure to 0.1 M NaCl with and without HL were observed via X-ray photoelectron spectroscopy (XPS), and electron microscopy/energy dispersive X-ray spectroscopy (SEM/EDS). The results indicated that the HL inhibitor can be considered as a mixed-type inhibitor with a predominant effect on the anodic zinc dissolution. The HL exhibited excellent corrosion inhibition of 99.26 % at 10^{-3} M. Based on our results, the adsorption of HL molecules formed coordination complexes with zinc cations at the metal/solution interface, which blocked the penetration of aggressive media, therefore the corrosion protection of pure zinc substrate was enhanced significantly.

[1] J. Wang, J. Zhao, M. Tabish, F. Shi, Q. Cheng, L. Peng, J. Mol. Liq., 361 (2022).

[2] N. El Hamdani, R. Fdil, M. Tourabi, C. Jama, F. Bentiss, Appl. Surf. Sci., 357 (2015) 1294-1305.

[3] U. Eduok, O. Faye, J. Szpunar, M. Khaled, J. Mol. Liq., 324 (2021).

Study of the inhibitory effectiveness of clay-based corrosion inhibitors on mild steel in the chemical pickling in a HCl medium

Salim Ayoub[a*],

[a]*Laboratory of Chemistry and Physics of Materials, Faculty of sciences Ben M'sik, Hassan II University of Casablanca, Morocco*

Said El Harrari[a],

[a]*Laboratory of Chemistry and Physics of Materials, Faculty of sciences Ben M'sik, Hassan II University of Casablanca, Morocco*

Siham El mazouzi[a,]

[a]*Laboratory of Chemistry and Physics of Materials, Faculty of sciences Ben M'sik, Hassan II University of Casablanca, Morocco*

Youssef Naimi[a]

[a]*Laboratory of Chemistry and Physics of Materials, Faculty of sciences Ben M'sik, Hassan II University of Casablanca, Morocco*

Résumé

The study of the inhibitory effectiveness of clay-based corrosion inhibitors on mild steel to combat corrosion in hydrochloric acid medium concentrated at temperature 60 °C (chemical steel stripping conditions) was studied using electrochemical and gravimetric methods for different concentrations. The morphological structure was examined by scanning electron microscopy and characterization of the elements of each inhibitor by EDS. The inhibitory efficiencies obtained by these methods are consistent.

From the electrochemical results of the polarization curves, we have shown that the mecha- nisms of action of these inhibitors differ according to the type of inhibitor but in most cases; they act as anodic inhibitors. However a remarkable effect is observed Zn Al Cl and Ni Fe Cl since the inhibitory efficacy reaches respectively 83.65% and 83.33% for the concentration of 1.2 g/l.

It follows from all this work that the fight against corrosion of steel in

hydrochloric acid medium is possible by using a new generation of natural inhibitors which have the advantage of being less toxic than conventional inhibitors, and they're easy to get. The results obtained are remarkable and encourage their deepening.

Mots-Clés: corrosion inhibitor, hydrochloric acid, chemical pickling, carbon steel.

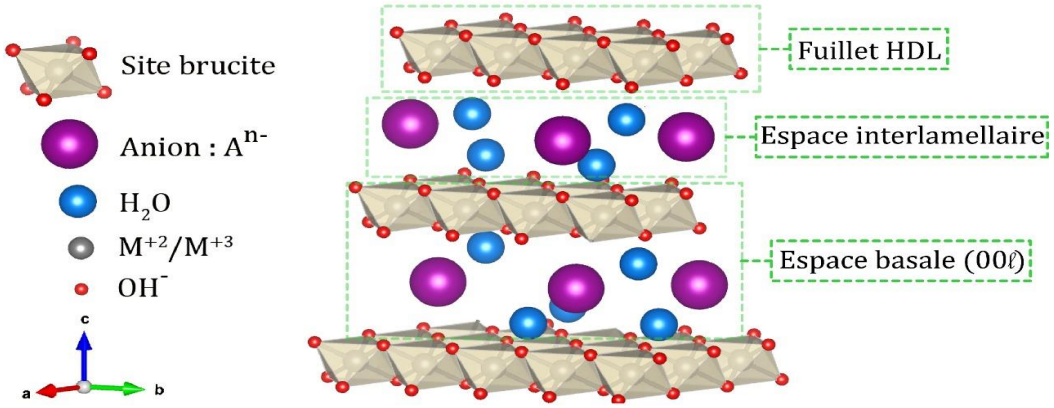

Figure 1: *Structure des Hydroxydes Doubles Lamellaires.*

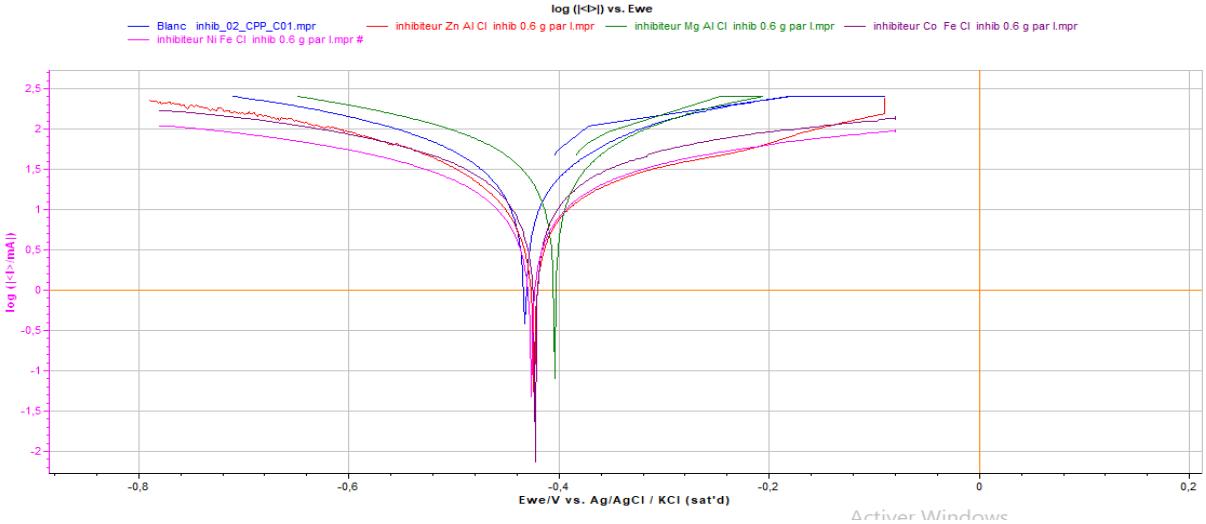

Figure 2. *Courbes de polarisation de l'acier en milieu HCl sans et avec prop-2-yn-1-ol, methyloxirane.*

Extension of continuum-scale corrosion simulations from grain-scale to part-scale

Milan J. Patel, School of Engineering, RMIT University, 124 La Trobe St, Melbourne, VIC 3000, Australia

Patrick Keil, BASF Coatings GmbH, Glasuritstr. 1, 48165 Muenster, Germany

Ivan S. Cole, School of Engineering, RMIT University, 124 La Trobe St, Melbourne, VIC 3000, Australia

Corrosion is a major contributing factor to degradation of fixed & mobile structures, with annual remediation costs reaching USD billions per industry sector. Corrosion inspection & prediction lie at the core of mitigation. However, corrosion of assets experiencing highly variable environmental conditions, e.g. automobiles & aircraft, are particularly difficult to prognosticate from inspection data alone. Thus, computational simulations of corrosion are increasingly used to improve prediction accuracy.

The material parameters underlying continuum-scale corrosion simulations are typically measured by forming an electrode from the metal of interest and employing controlled potential & current sweeps to determine its macroscale corrosion behaviour. However, this assumes that the electrode undergoes uniform corrosion & that the influence of microstructural inhomogeneities is similar for the electrode & manufactured asset. This is problematic as even pure metals feature a range of grain orientations & grain boundaries, resulting in a heterogenous distribution of corrosion parameters at the microscale.

Recent research demonstrates continuum-scale simulations of corrosion at the grain scale using enhanced finite element methods, phase-field modelling, and peridynamics. These focus on predicting the shape of the corrosion front, the distribution of corrosion products, and concentration distributions across the corrosion front. However, they do not address the relationship between microstructure & the apparent macroscale corrosion rate.

The current research presents 3D continuum-scale finite element corrosion simulations at the scale of individual grains of a pure metal (zinc). Continuum-scale corrosion parameters are assumed for grain faces at specific orientations. Grain boundaries are represented as planar discontinuities with unique corrosion

parameters. At different E_{corr}, the apparent corrosion rate (i_{corr}) is determined for several simplified microstructures by upscaling the microscale distribution of corrosion rate. The continuum-scale corrosion parameters for the different microstructural features are then varied to determine their contribution to i_{corr} for each microstructure. This establishes the critical features & corrosion parameters. The relationships between these critical parameters that deliver the originally predicted i_{corr} for each microstructure are extracted. Thus, a workflow is presented for estimating corrosion parameters for microstructural features from these relationships using results from a ‘small’ body of corrosion experiments on samples with known microstructures, and a large body of pre-run simulations.

05. Corrosion Mechanisms, Methods and Modelling (3M) (WP6 & WP8)

Understanding atomic-scale structures of copper/water interfaces by *ab initio* calculations

Zhongheng Fu, Xin Guo, Xinzheng Zhang, Dawei Zhang

National Materials Corrosion and Protection Data Center, Institute for Advanced Materials and Technology, University of Science and Technology Beijing, Beijing, 100083, China

An atomic-scale understanding of copper/water interface structures is of great significance for aqueous corrosion and electrocatalysis. Great success has been achieved in probing copper/water interface structures through advanced experimental characterization techniques. Ab initio quantum mechanics calculations provide an alternative approach to exploring the copper/water interfaces with the rapid development of computational methods and computer techniques. In this report, atomic-scale copper/water interface structures are built and simulated through *ab initio* molecular dynamics. Interfacial atomic fluctuation, interaction, and charge transfer are carefully detected. The effects of vacancies and heteroatoms at Cu surfaces on the interfacial structures are further understood. These results provide a fundamental understanding of copper/water interface structures, which are considered to be important for understanding aqueous copper corrosion.

Ab initio Monte Carlo simulations of the acidic dissolution of stainless steels : Effect of prior plastic deformation

B. Malki[1], I. Guillotte[2] and B. Baroux[3]

[1] Simorg Computing, 46 rue Yves Farge, 38600 Fontaine, France.

[2]Aperam Isbergues - Research Center, 62330 Isbergues, France.

[3]Formerly with Laboratoire Science et Ingénierie des Matériaux et Procédés (SIMAP), Grenoble INP, CNRS, 38402 Saint Martin d'Hères, France.

We used Ab initio based Monte Carlo simulation (AbMC) to study the dissolution kinetics of stainless steels in acidic media, focusing on the effect of prior plastic deformation. We employed relaxation techniques to measure the bonding energies as a function of interatomic distance, and then used an "On-the-fly" Monte Carlo scheme to evaluate the dissolution probabilities on pre-deformed austenitic microstructures. We found that the dissolution rate of a given atomic surface is strongly dependent on the strain field among the surface atoms, with compressed zones dissolving more quickly than extended ones due to increased electronic interactions when atoms are brought closer. Additionally, different mechanically induced defects such as twins, edges, screws, and loop dislocations were investigated and found to significantly affect the dissolution rate, with dislocation lines becoming preferential dissolution paths.

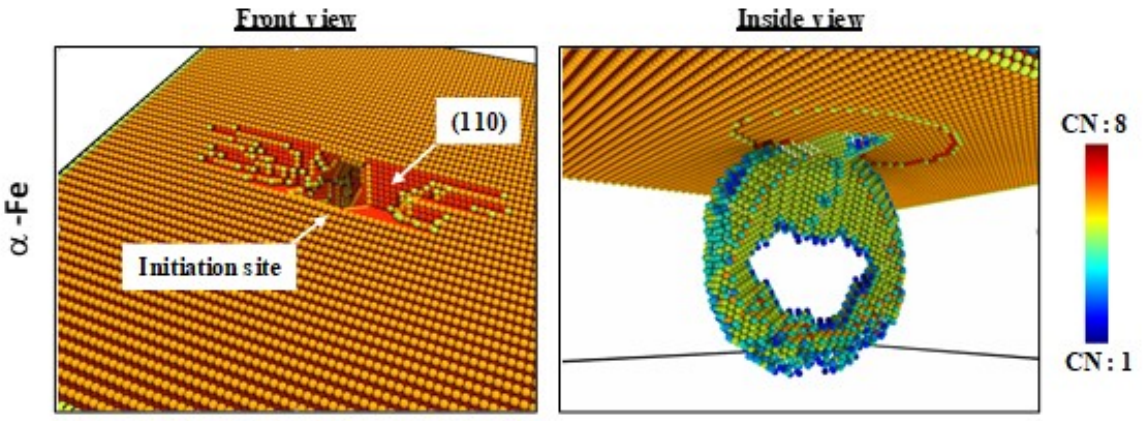

Dissolution of Pure α-Fe Monocrystalline Structure with a Dislocation Loop from Different Perspectives.

Space and time resolved modeling of accelerated atmospheric corrosion tests for automotive applications

Impact of film dynamics, flow field and material properties on evolution of film thickness and corrosion rate

Dr. S. Seifritz, Corporate Research Robert Bosch GmbH, Renningen/Germany
Dr. T. Troßmann, Corporate Research Robert Bosch GmbH, Renningen/Germany
Prof. Dr. U. Janoske, University Wuppertal, Wuppertal/Germany

Abstract:

Models for atmospheric corrosion, like the Dynamic Electrolyte Film Corrosion (DEFC) model of van den Steen et al. (1) or Saberi et al. (2), consider condensation, evaporation and hygroscopic effects of dissolved salts on mass transfer and corrosion rate during accelerated corrosion tests in climate chambers under defined T and rH conditions. The Lewis number, as the major coefficient for heat and mass transfer, needs to be defined to calculate evolution of the 1D film thickness and respective corrosion rate. It is set to correspond to free, moderate or forced convection for a given orientation of the surface of interest. Meanwhile 0D- and 1D-models allow fast assessment of complex load cycles, further left aside or generalized influences are worth to be analyzed. Such influences may result from the test setup (spray deposition, air flow in chambers), 3D geometry (film flow and retention depending on shape and orientation), surface conditions (wetting, formation and solvation of deposits) and material mix (homogenous vs. heterogenous composition and heat capacity and conductivity). Consideration of such influences for a complex 3D geometry and a transient environmental load cycle of an accelerated corrosion test suggest using multiphysics modelling. However, simplifications and optimizations must be introduced to limit calculation time and computational effort. The aim of the presentation is to rate the impact and effort for consideration of the additional influences during virtual testing.

A model is presented that considers the geometry and material mix of a sample, the flow around the sample as well as formation (spray, condensation), run-off and evaporation of fluid and surface films during a cyclic corrosion test. The model is implemented in the OpenFOAM® CFD framework (3) based on the solution of the 3D Navier-Stokes equations for the gas flow, a 2D wall film model on the surface as well as the energy equation in the part. All the phases are coupled regarding heat, mass and momentum exchange. The spray is described by a Lagrangian particle tracking method.

Depending on the geometry of a part, this approach offers the opportunity to determine the dynamics of the film in space and time by run-off, evaporation and condensation

considering material specific parameters (heat capacity and thermal conductivity).

Fig. 2.1-3 shows exemplary the dynamics of a film, the corrosion rate (based on film thickness and media composition) and the corrosive damage of a 70° inclined steel plate where a 5% NaCl solution is partly sprayed (35°) on top of the plate for 480s (a), followed by a 20s media run-off (b) and evaporation (60°C/30%rH) over 500, 1000 and 2000s (c-e). The corrosive damage was validated with different sodium chloride concentrations (0-5%) on steel plates (CR4) accord. ISO 9227 with a deviation from the experiment of +10 / -20%.

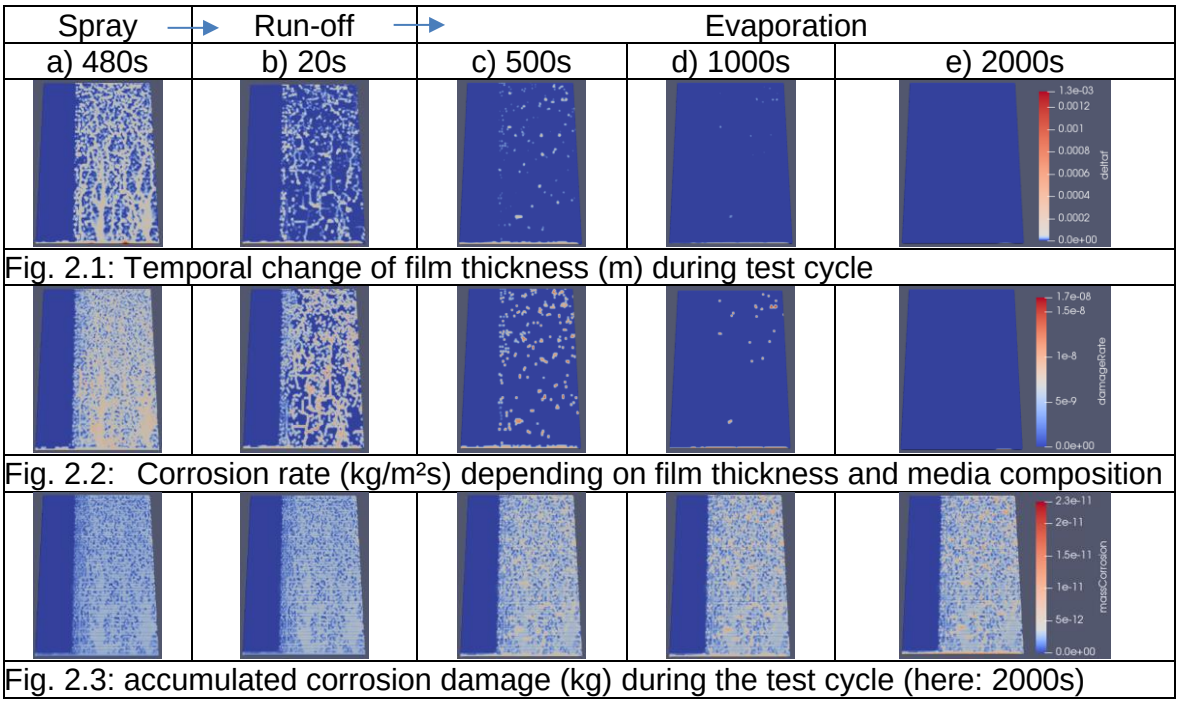

Fig. 2.1: Temporal change of film thickness (m) during test cycle

Fig. 2.2: Corrosion rate (kg/m²s) depending on film thickness and media composition

Fig. 2.3: accumulated corrosion damage (kg) during the test cycle (here: 2000s)

By using the local corrosive load and damage model, the first part of the presentation will show the consequence of the inclination of a plate and different test cycle on the film dynamics and corrosive damage. The second part of the presentation will show the application of the model on a 3D geometry of an automotive component in case of a cyclic corrosion test.

References

1. Van den Steen N, Simillion H, Dolgikh O, Terryn H, Deconinck J. An integrated modeling approach for atmospheric corrosion in presence of a varying electrolyte film. Electrochim. Acta 2016; 187, p. 714–23
2. Saberi L, Amiri M., Modelling atmospheric corrosion under dynamic thin film electroltye. J. Electrochem. Soc. 2021, 168 :081506
3. Seifritz S, Troßmann T, Janoske U. Modellbildung und Simulation von Klimawechsel-prüfungen. BHM Berg- und Hüttenmännische Monatshefte 2018; 163(7), p. 258–69

Modeling Passive Film Breakdown

Ingmar Bösing, Jorg Thöming, Fabio La Mantia, University of Bremen, Bremen/Germany

Metal oxides play a crucial role in many applications of our technological world. From oxide nano particles in daily products like room paint, over catalysts for (electro-) chemical reactions as in electrolyzers and as part of electronic components as in Metal Oxide Field Effect Transistors (MOSFET) up to corrosion protection by passive films.

Our metal-based civilization would not be possible without the formation of nano meters thin oxide films, called passive films, on the surfaces of many corrosion-resistant metals and alloys. Passive films can slow down corrosion rates about 3 orders of magnitude and thus enable long lasting metal constructions and metal-based devices.

Despite the importance of metal oxides, especially passive films, the mechanism of oxide film growth and breakdown are still not fully understood. A far developed model for passive film growth is the Point Defect Model, developed by Macdonald and co-workers in the 1980s and further extended since then. Even though, the PDM has been proven to describe many experimentally observed phenomena it is not uncriticized and it is based on some unproven assumptions, as the potential and space independence of the electric field.

On the basis of the PDM we developed a comprehensive model for the simulation of passive film growth, which replaces unproven assumptions by physical mechanism which are included to the model to test these assumptions (e.g. Band-to-Band tunneling of electrons). Furthermore, we extended the model to a time depending model, which includes initial stages of film growth and film breakdown.

Film breakdown is modeled by two different mechanism, anodic dissolution of the oxide film due to a high overpotential for iron electrodes, which shows very good agreement with experiments (Fig. 1). Second, film breakdown by halide ions for stainless steel electrodes due to a breakdown mechanism suggested by the PDM.

Especially, local corrosion, like pitting can lead to dramatic damage of steel constructions, since local corrosion is hard to detect and affects stainless steels. The possibility to model these effects brings us one step further to the prediction of corrosion processes and thus, safe and sustainable steel technologies.

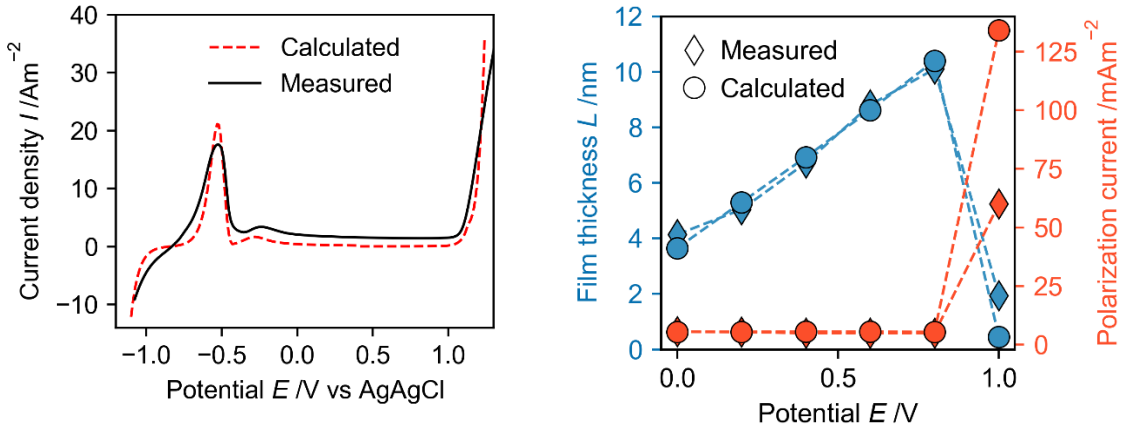

Figure 1: Measured and calculated polarization behaviour of iron electrode in borate buffer; left: dynamic polarization curve; right: static polarization.

Phase field modelling of localized corrosion damage: pitting, pit-to-crack transition, and stress corrosion cracking

E. Martínez-Pañeda, C. Cui, S. Kovacevic, M. Makuch, M. Wenman

Imperial College London, London, UK

Phase field models have had a significant impact on many interfacial problems, including the modelling of microstructural evolution and fracture mechanics. In this work, we show how phase field modelling can also open new horizons in a scientifically-challenging phenomenon of notable technological importance: corrosion damage [1]. The phase field paradigm can be exploited to enable tracking the aqueous electrolyte-solid metal interface. This enables predicting explicitly, as a natural by-product of the simulation, the evolution of pits, the pit-to-crack transition and stress corrosion cracking (see Fig. 1). The work constitutes the first formulation capable of capturing the film rupture–dissolution–repassivation mechanism and the role of mechanical fields in enhancing corrosion kinetics. Several 2D and 3D boundary value problems of particular interest have been addressed to showcase the predictive capabilities of the model, revealing an excellent agreement with analytical solutions and experimental measurements. The results that will be presented show how the model can naturally capture: (i) the transition from activation-controlled corrosion to diffusion-controlled corrosion, (ii) the sensitivity of interface kinetics to mechanical stresses and strains, (iii) the role of film passivation in reducing corrosion rates, and (iv) the dependence of the stability of the passive film to local strain rates.

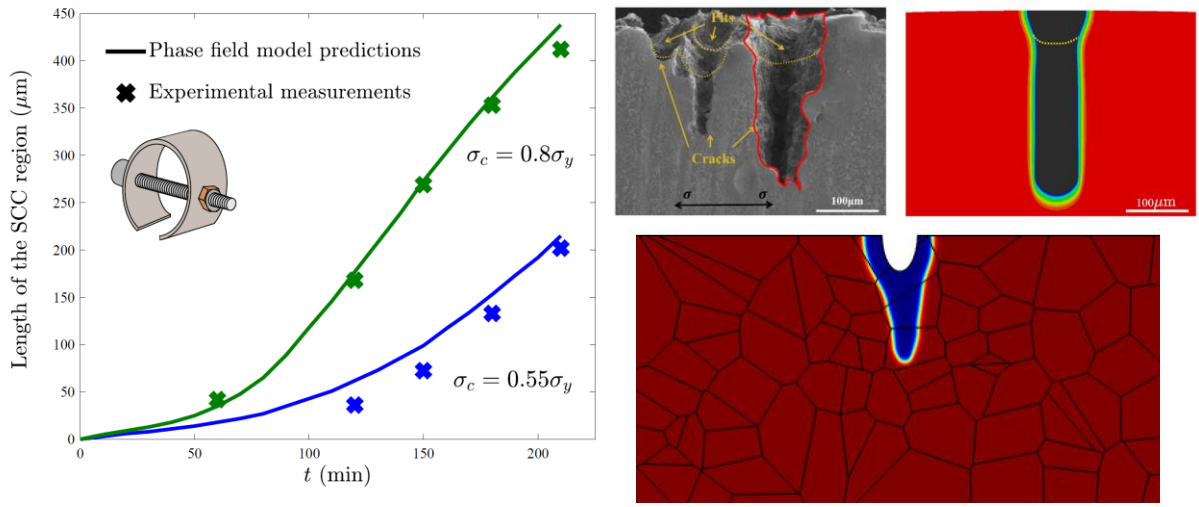

Fig. 1. Phase field modelling can enable Virtual Testing in corrosive environments, capturing the role of the applied load (left), pitting and cracking morphologies (top, right) and the influence of the microstructure (top, bottom).

Finally, the conference contribution will describe ongoing efforts aiming at generalising the model to capture: (i) microstructural effects, (ii) the electrochemical behaviour of the electrolyte, (iii) both anodic-driven and hydrogen-driven cracking mechanisms [2], and (iv) the corrosion of bio-degradable materials.

References

[1] C. Cui, R. Ma, E. Martínez-Pañeda (2021). A phase field formulation for dissolution-driven stress corrosion cracking. Journal of the Mechanics and Physics of Solids 147, 104254

[2] C. Cui, R. Ma, E. Martínez-Pañeda (2022). A generalised, multi-phase-field theory for dissolution-driven stress corrosion cracking and hydrogen embrittlement. Journal of the Mechanics and Physics of Solids 166, 104951

Estimation of damage parameters for ductile fracture of Zn-Ni coated ultra-high strength 300M steel using a finite element model

A. Ravikumar[1], D. Höche[1], C. Feiler[1], M. Zheludkevich[1], M. Prabhakar[2], M. Rohwerder[2], A. Salicio-Paz[3], M. Lekka[3], G. Artola[4], E. Mardaras[4].

[1]*Helmholtz Zentrum Hereon, Geesthacht Germany.*

[2]Max-Planck-Institut, Düsseldorf, Germany.

[3]*CIDETEC, Basque Research and Technology Alliance (BRTA), Po. Miramón 196, 20014 Donostia-San Sebastián, Spain*

[4]*AZTERLAN, Basque Research and Technology Alliance (BRTA), Aliendalde Etxetaldea, 6, 48200 Durango, Bizkaia, Spain*

Zinc-Nickel alloy coatings are being researched as a possible replacement for cadmium based coatings because of the health and environmental concerns associated with cadmium coatings. The Zn-Ni coating process is accompanied by the production of hydrogen. The hydrogen produced is primarily stored at the metal-coating interface and during the application of the part, this hydrogen may diffuse inwards into the metal and cause hydrogen embrittlement. Hydrogen embrittlement in ultra-high strength steels (UHSS) is detrimental to their application, as it leads to degeneration of properties and delayed cracking. Although outgassing steps are employed to remove the hydrogen from the steel, residual hydrogen might still be present in the steel and over the lifetime of the part, ingress of hydrogen in the part can be expected, which can lead to hydrogen embrittlement as well.

In this work, a numerical model is proposed to investigate the development of stresses and hydrogen concentration in a Zn-Ni coated UHSS part. The proposed model, which includes the transport of hydrogen in the coating and metal substrate, couples the hydrogen distribution with a continuum damage mechanics model. The geometry of the simulation domains for the coating were directly developed from micrographs of the coating, and this facilitated the study of the effects of the morphology of the coating on the behavior of the metal-coating structure. The metal-coating interface aspects are explored as well. Different coating conditions lead to contrasting morphologies, and the amount of hydrogen generated is varied as well. The model will compensate by implementing distinct initial conditions. The simulation

results are compared against experimental results from tensile test and small punch test, and the parameters of the damage model are calibrated.

The electrochemical impedance of organic coating defects: validation of a finite element model

Callum Ayres, The University of Manchester, Manchester, United Kingdom.

Professor Stuart Lyon, The University of Manchester, Manchester, United Kingdom.

Dr. Peter Visser, AkzoNobel, Sassenheim, The Netherlands

This project aims to carry out the development and validation of a predictive model for the electrochemical characteristics of an organic coating containing through-thickness defects. We report on a finite element model using the COMSOL multiphysics package with a view to electrochemical response model (DC voltammetry and AC impedance) delivering the forward problem (predicting the measured response from an arbitrary defect) as well as the reverse problem (predicting the nature of the defect from a measurement).

The model is verified against experimental data collected from the real equivalent to the modelled system using electrochemical impedance spectroscopy (EIS), localised EIS (LEIS) and the scanning vibrating electrode technique (SVET). The impedance response is of interest due to the effectiveness of detecting defective sites within the coating via the emerging faradaic processes contrasted with the capacitive response of an intact coating. Experimental validation will be crucial to ensure validity of model outputs.

Comparison of the corrosion of tungsten carbide hardmetal composites with the corrosion of their metallic binders

A.M. Ferro Rocha (University of Aveiro, Portugal), P. Pereira (INEGI and DURIT, Portugal), A. Santos (University of Aveiro, Portugal), J. Sacramento (DURIT, Portugal), A.M.R. Senos (University of Aveiro, Portugal), A.C. Bastos (University of Aveiro, Portugal), M.G.S. Ferreira (University of Aveiro, Portugal).

Abstract

Hardmetals are composite materials consisting of hard micron or sub-micron carbide grains (typically WC) held together in a matrix of a tough metallic binder, usually cobalt (Co). These composites possess superior hardness, fracture toughness and transverse rupture strength, and are used in applications requiring high wear and abrasion resistances. Examples are valves for pumping systems, drawing and extrusion dies, saw blades, metal forming tools, drill bits for rock, bearing tools, flux-cored wire tools, and more, used in the mining, chemical, oil and gas industries, among others. Despite the outstanding properties, the WC-Co system raises health concerns and faces supply uncertainties related to ore extraction. Moreover, its corrosion resistance is low in several service environments. Therefore, a quest for alternative binders is on the way. In this search, an important question arises: “is it possible to predict the corrosion behaviour of hardmetals based solely on the response of the binder?”. To help answer the question, this work compares que corrosion of a series of WC hardmetal composites with the corrosion behaviour of the respective binders. Pure metals and alloys of Co, Ni and Cr were produced by powder metallurgy. Hardmetal composites were produced with the same metals and alloys, keeping constant the amount of WC. Their corrosion was characterised by electrochemical techniques, such as open circuit potential monitoring, polarization curves and electrochemical impedance spectroscopy, complemented by optical and electron microscopies.

How will Corrosion and Integrity support a more Sustainable future?

Monica Hernandez, Infinity Growth, Canada/UAE

The Accidents and incidents due to Integrity Management continue to make the headlines of the newspapers, like the storage tank that fell-of the crane into a ship in the port city of Aqaba, Jordan; killing 13 people, injured at least 250, while releasing a huge cloud of toxic chlorine gas, during the summer of 2022.

In addition to that, it is no surprise that the cost of corrosion continues to raise eyebrows globally. See as example the Cost of Corrosion Report recently published in Canada, in which an outstanding $52 billion USD, almost 3% of the countries GDP is estimated to be spent in Corrosion Annually.

We live in a period of humanity that has generally developed high-quality code and standards, educated and qualified brilliant people, and developed breakthrough technologies. Unfortunately, it is the same era that has not yet managed to reduce the indicators of environmental protection, sustainability, and stability in its main industries.

The big question is: Why? -And what could we do?

The 3 main challenges we face in managing corrosion, integrity and sustainability are: efficiency, externality, and circularity (or circular economy).

This papers presents the practical interplay of integrity, corrosion, and sustainability, and how they relate to viable solutions that ultimately support long-term efficiency in organizations.

Merging concepts like designing for purpose, maintaining with integrity, and decommissioning with a second life in mind are some of the ideas that, if used in conjunction with the adequate management tools, can help industries go in the right

path of applying an effective Corrosion/Integrity and Sustainability management systems.

In short, ensuring a better corrosion/integrity management system, one that integrates sustainability at its core, not only helps minimize failures, environmental and health incidents, and saves money, but it also helps ensure each of the actions that can be taken, from design to decommissioning of an asset, focusing resources (materials, people, and money) on avoiding waste is another way to contribute to the circular economy and sustainability criterion. The final balance sheet shows that there are some points of the new economic and development models that need to be considered from the point of view of materials integrity.

A call to organisations, governments, universities, and society in general is needed to strengthen corrosion and integrity professions, including deeper research, fostering related curricula, more regulatory mandates, and a greater awareness by industrial leaders and managers. Collective actions are required that are directly related to a simultaneously positive effect on productivity and sustainability.

We are talking about implementing processes and being able to follow through with actions, this is a cultural change that should cascade from the top down of any organization, any institution, and any Country. However, it’s also an opportunity to be part of the turning point and change that we want to have as professionals, and, human beings. We are privileged to have a say in this transitioning point, as engineers, designers, project managers, we have the ability to influence how the projects in which we will participate will shape the future of this planet and how it will serve humanity in some years.

Keywords: Corrosion, Circular Economy, Sustainable, Costs, Integrity, Management, Design, Maintain, Operate, End of life.

The experience of an academic laboratory course on corrosion and protection of metals at Politecnico di Milano (Italy)

Andrea Brenna[1]

[1]*Politecnico di Milano, Department of Chemistry, Materials and Chemical Engineering "Giulio Natta", Milano, Italy, andrea.brenna@polimi.it*

Abstract

The course "Laboratory of Corrosion and Protection of Metals" described in this work is held for the students of the Master's degree program in Materials Engineering and Nanotechnology at Politecnico di Milano, Italy. The course consists of 50 hours, divided in laboratory experiences (30 hours, 60%) and ex-cathedra lessons for the remaining part (introduction to the practical experiences and final remarks). Due to logistic limitations, the course is currently held for a maximum of 25 students.

Practical experiences cover all the main aspects related to corrosion of metals and its protection: corrosion mechanism, electrochemical techniques, accelerated and field testing, selected corrosion forms in different environments, protection techniques, corrosion monitoring and failure analysis. Laboratory activities are anticipated by a brief theoretical introduction by the teacher. Moreover, seminars on specific topics are offered to students by corrosion experts from industry. An introductory seminar on philosophy of science is also proposed during the course to improve sensibleness of students on epistemology, semantics, and ontology.

Among the positive aspects of the course, there are the strengthening and improvement of the knowledge with an engineering (and experimental) approach, not always easy to transfer with numerical exercises in classroom, the interaction teacher-students and among students which helps the self-evaluation of the knowledge and the social interaction.

Keywords

Laboratory course; Education; Testing; Monitoring; Corrosion science and engineering.

Background

In this work, the experience of a laboratory course on corrosion and protection of metals is described. The "Laboratory of Corrosion and Protection of Metals" (LCPM) course is held for the students of the Master's degree program in Materials Engineering and Nanotechnology at Politecnico di Milano, Italy.

Although laboratory classes are often included in corrosion training courses offered by institutions, corrosion experts and professionals to companies and private operators, the presence of laboratory activities is often taugh at academic level, where students are mainly involved with the theory of a subject rather than its practical application; moreover, the number of attending students of an academic course is generally high and this introduces logistical complications related to the accessibility of laboratories and suitable equipment.

In 2019, the "School of Industrial and Information Engineering" of Politecnico di Milano [1] proposed the activation of "laboratory courses" to be included in the master of science programs. Three categories of laboratory course have been defined: a) *informatic lab*: didactic activity based on the use of software engineering tools which takes place in an equipped computerized classroom; b) *experimental lab*: didactic activity based on the use of laboratory instruments which takes place in equipped spaces of the university in which students are involved in carrying out guided procedures and measurements; c) *project lab*: didactic activity based on a project assigned by the teacher to individual students or groups on specific topics.

In the MS course of Materials Engineering and Nanotechnology, a group of ten laboratory courses was activated [2]: eight of them were existing courses converted to laboratory ones, while two new experimental courses, including LCPM, have been introduced. The selection of one laboratory course is mandatory for students of the MS in Material Engineering and Nanotechnology.

The LCPM course was proposed thanks to the experience gained in the PoliLaPP research group [3] (PoliLaPP – Laboratory of Corrosion and Protection of Materials "Pietro Pedeferri") of Politecnico di Milano in the organization of training courses in the field of corrosion and protection of metallic materials. Examples are the training course delivered for APCE (Association for the Protection of Electrolytic Corrosions) in the field of cathodic protection of metallic materials, ECU (Eni Corporate University) or Centro Inox (Italian association for the development of stainless steels). These courses include an experimental section (generally 20-25%) of laboratory and field tests in addition to the theoretical part. However, the main "driving force" was represented by the will to propose a new course with an original approach to teach corrosion.

Structure of the course

The aim of the course is to provide an experimental-laboratory approach to the study of metal corrosion and its prevention, supporting and consolidating the theoretical and phenomenological knowledge already possessed by the students.

LCPM consists of 50 hours, divided in laboratory experiences (30 hours, 60%) and ex-cathedra lessons for the remaining part (20 hours, introduction to the practical experiences and final remarks). The course is organized in 13 weeks (4 hours/week), from September to December.

The first edition of the course is dated 2021. Due to the laboratory nature of the course, the presence of at least 75% of students at the laboratory activities is recommended. The language of the course is Italian.

The academic context

LCPM offers students practical laboratory lessons on selected topics related to the corrosion and protection of metals. The course is strongly rooted on laboratory classes that allow the

students to put into practice their knowledge and skills, acquired in a propaedeutic and mandatory course in the Bachelor's in Materials Engineering and Nanotechnology (course of "Corrosion and Material Protection").
This educational assortment of courses in the field of corrosion and material protection is completed by a mandatory and specialistic course of "Corrosion Engineering" in the MS of Materials Engineering and Nanotechnology of Politecnico di Milano.
The coordination with the teachers of the two other courses has been essential for the proper definition of the program of the course, in order to ensure a thematic continuity, avoiding repetitions. In this context, the experimental laboratory (< 5 hours) originally planned in the course "Corrosion and Material Protection" has been converted by the teacher in a "corrosion homework", which consists of a corrosion case study identified by the student from everyday life with a detailed corrosion assessment. On the other hand, in the "Corrosion Engineering" course a project laboratory is proposed to the students during the semester. This harmonization improves the quality of the didactic offer to the students during their academic track.

Expected learning outcomes
Lessons and experimental activities allow the student to:
- understand the mechanism of wet corrosion of metals, the thermodynamic and kinetic aspects with the help of experimental measurements;
- know and use the fundamental instrumentation to investigate the corrosion behaviour of metals in aqueous solution (potential and current measurements);
- be able to determine the corrosion rate and the kinetic parameters obtained from electrochemical tests;
- master the key aspects of the different corrosion forms expected in natural and industrial environments (e.g., soil, waters, atmosphere, concrete);
- understand cathodic protection monitoring techniques in soil and seawater;
- learn the principles of the main corrosion protection techniques (cathodic protection, coatings, corrosion inhibitors) and their monitoring.

Topics. It's not just a matter of "corrosion"

Corrosion topics
The teaching is organized in lectures and experimental-laboratory activities. Frontal lessons aim to recall the basic concepts of corrosion of metals and to introduce the experimental activity. Experimental activities allow the students in-depth observation, participation, experimentation and practice ("hands-on") on specific themes in the field of corrosion of metals and protection techniques. Lab activities are carried out by students in small groups (max. 5 students per group) or, rarely, individually, always with the assistance of the teachers. Frontal lesson is carried out in a classroom in close proximity to the "Didactic laboratory" of the Department of Chemistry, Materials and Chemical Engineering "Giulio Natta" of Politecnico di Milano.
Table 1 reports, for each topic, the laboratory activities performed by the students. Practical experiences cover all the main aspects related to corrosion of metals and its protection; any practical experience is anticipated by a brief theoretical introduction by the teacher on specific topics.
For topics 6,9 and 15, specific seminars are included. About 45 hours are dedicated to classroom and laboratory activities. The remaining 5 hours of the course are dedicated to an educational and technical visit in an Italian company and to a seminar on philosophy of science (see next paragraph).

Table 1 – Corrosion topics, experimental activities and their duration

	Topic	Experimental activity	Duration Lesson + Lab (hours)
1	Electrochemical mechanism of corrosion	Evans "drop" experiment: corrosion under a drop of electrolyte, the role of oxygen in a corrosion process	2
2	Potential and current measurement, reference electrodes	The use of the voltmeter and the ammeter, potential and current measurements, conventions, types of reference electrodes and measurements	4
3	Corrosion potential and corrosion current density. Evans diagrams	Measurement of free corrosion potential of metals in different environments (pH, salinity) and interpretation by means of Evans diagrams	4
4	The experimental approach to corrosion. From accelerated to field tests: an overview		2
5	Corrosion rate by mass loss	Exposure tests in different electrolytes (acidic, neutral and alkaline solutions) simulating natural and industrial environments. Mass loss rate calculation of carbon steel, copper, aluminium, zinc, stainless steel after 1 month testing and corrosion analysis (**see 10**)	4
6	Corrosion kinetics: anodic and cathodic characteristic curves, Tafel's law, electrochemical impedance spectroscopy	The potentiostat: main components and function modes, the three-electrode corrosion cell; electrochemical test methods for obtaining corrosion kinetic parameters: linear polarization resistance, polarization curves on active and passive metals, Tafel extrapolation method and corrosion rate calculation, electrochemical impedance spectroscopy (**seminar and case study**)	4
7	Forms of corrosion: galvanic coupling	The effect of driving voltage, the effect of resistivity of the environment, cathodic-to-anodic surface ratio, measurement of ohmic drops	2
8	Forms of corrosion: pitting and crevice corrosion	Overview about standard tests to evaluate pitting corrosion resistance, ferric chloride standard test	2
9	Forms of corrosion: stress corrosion cracking	Standard tests for evaluating stress corrosion cracking resistance (**seminar**)	2
10	Microstructural and corrosion failure analysis	Evaluation and analysis of corrosion by means of optical and electronic microscopic investigation techniques, analysis of corrosion products (SEM-EDS, XRD, optical analysis)	4
11	Corrosion and cathodic protection in soil	Measurement of soil resistivity, corrosion by differential aeration, monitoring of anodic and cathodic areas due to electrical d.c. interference. Impressed current cathodic protection system: the d.c. feeder, IR-free potential, ON and OFF potential, potential probes, coating efficiency, verification of an insulating joint.	4
12	Corrosion and cathodic protection in sea water	Galvanic anode system: current and potential measurements; impress current CP system: anodic reaction and feeding voltage	2
13	Corrosion in atmosphere	Long-term exposure test on corrosion coupons exposed on a rack in urban and simulated-marine atmosphere: corrosion analysis and use of ISO equations to predict the corrosion rate	2
14	Corrosion of reinforced concrete	Potential mapping and identification of corroded areas, corrosion by carbonation, phenolphthalein test	2
15	Coatings and anodizing	Overview about test methods to evaluate coating efficiency (**seminar**). Cathodic disbonding test. Anodizing	2
16	Other corrosion protection methods (only one of the listed topics)	Anodic protection of stainless steel in acidic environments, the effect of corrosion inhibitors on corrosion potential and corrosion rate	2

Gallery

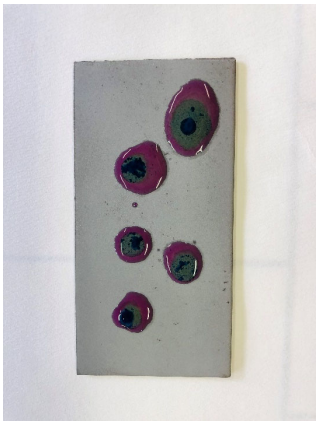

Electrochemical mechanism of corrosion (Topic #1)

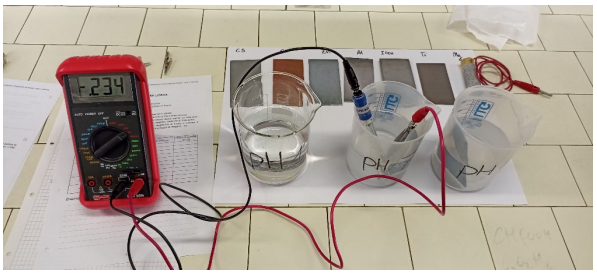
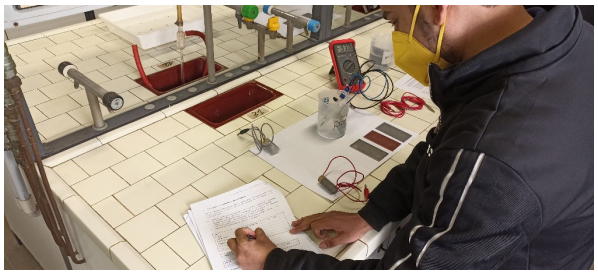

Potential and current measurement, reference electrodes (Topic #2 and #3)

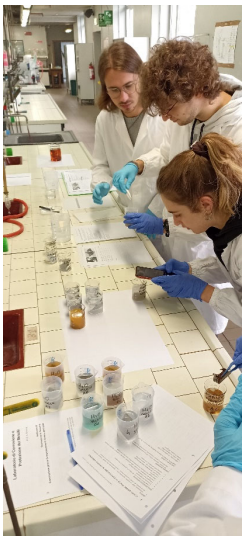

Corrosion rate by mass loss (Topic #5)

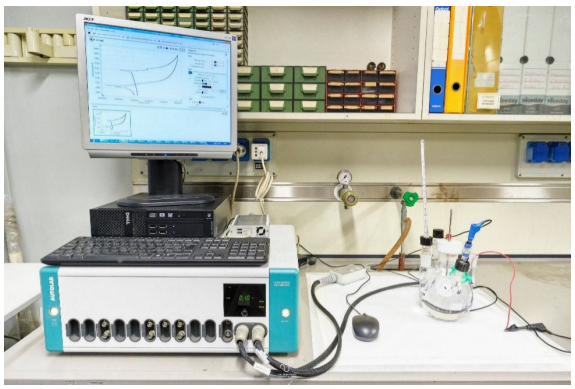
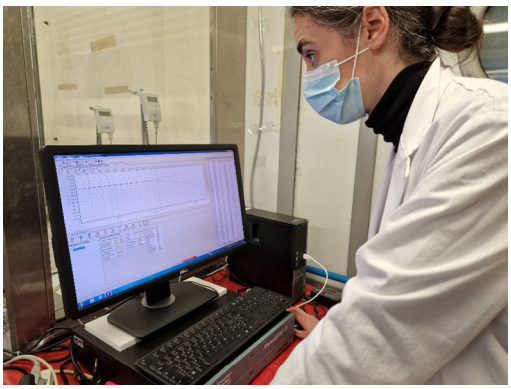

Corrosion kinetics: electrochemical tests (Topic #6). Copyright © 2021 PoliLaPP. All Rights Reserved [3].

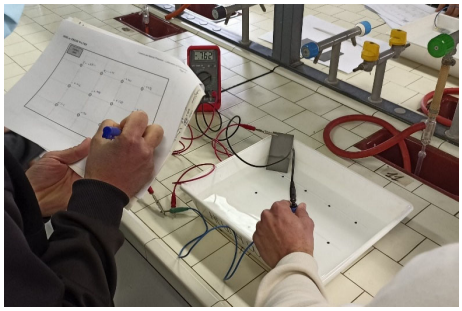

Galvanic coupling (Topic #7)

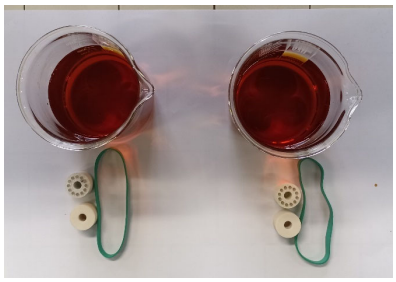
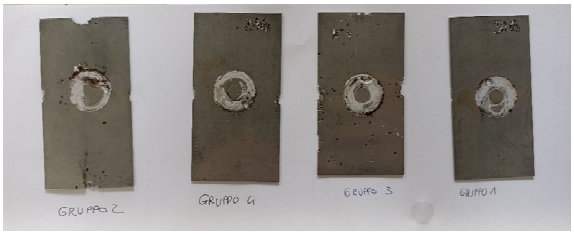

Pitting and crevice corrosion (Topic #8)

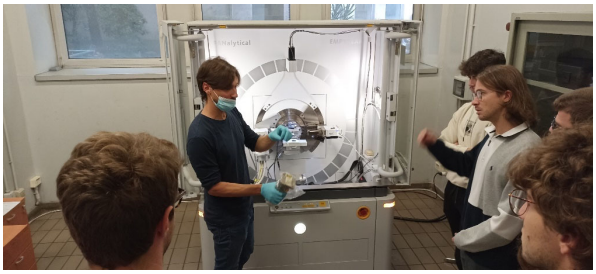
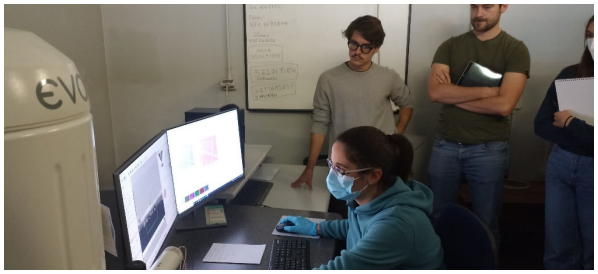

Microstructural and corrosion failure analysis (Topic #10)

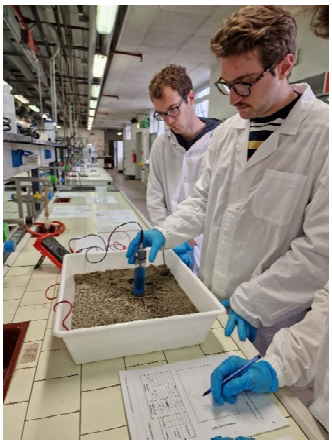
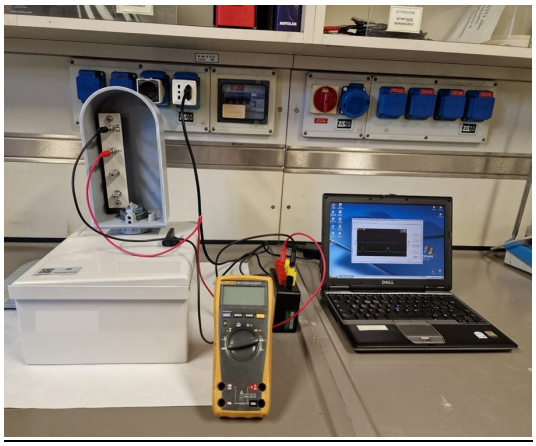

Corrosion and cathodic protection in soil (Topic #11)

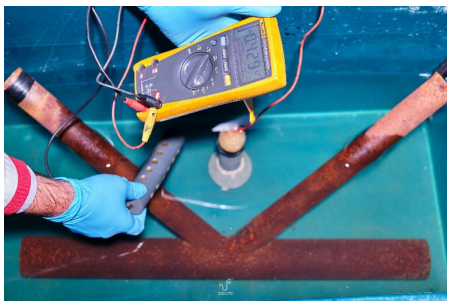

Corrosion and cathodic protection in sea water (Topic #12). Copyright © 2021 PoliLaPP. All Rights Reserved [3].

Corrosion in atmosphere (Topic #13)

Corrosion of reinforced concrete (Topic #14)

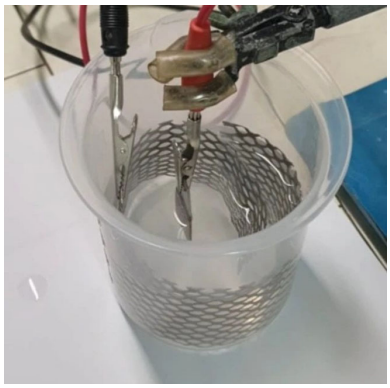
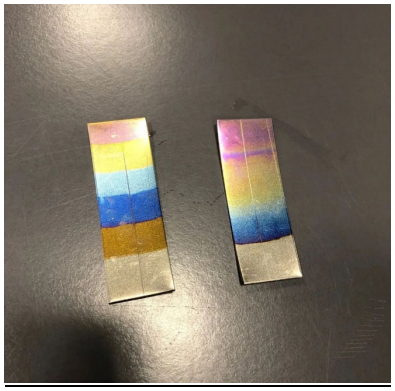

Anodizing of titanium (Topic #15)

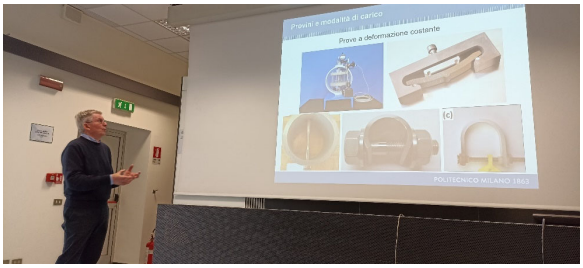

Seminar on stress corrosion cracking

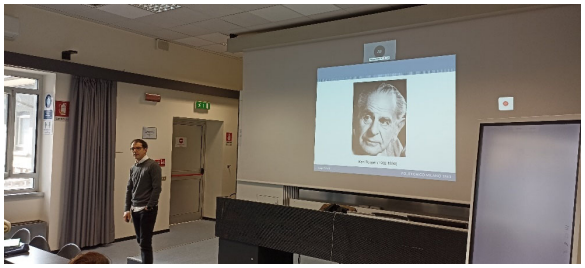

Seminar on philosophy of science

Philosophy of science and the course "mantra"

An introductory seminar on "philosophy of science" is also proposed at the beginning of the course to improve sensibleness of students on epistemology, semantics and ontology. High importance is given not only to the direct execution of the experiential activities but in particular to the rational interpretation of the measurements made and to the ability to re-elaborate the experience. The paradigm of the course is based on a scientific deductive approach, starting from the consolidated theories of corrosion, followed by tailored testing, data collection, analysis and interpretation according to the formulated theory. This approach allows a virtuous connection between theory and measurements, according to the "mantra" of the course repeated by the teacher to his students: *"knowing how to make a measurement does not mean understanding it"*.

Visit to an Italian company: a contact with the industrial approach

During the course, students have the opportunity to be hosted by the virtuous Italian company Snam S.p.A. in San Donato Milanese (Milan), whose main core business is related to the transportation of natural gas in all the country. The technical anti-corrosion group of the company illustrates the approach of the company in the management of corrosion prevention systems, namely cathodic protection of buried carbon steel pipes and insulating coatings. The discussion of the main aspects related to the design of anti-corrosion systems, their inspections and monitoring (from technical to economic considerations) stimulate a positive Q&A session which generates curiosity in students. The connection between theory, experimental activity from one side and management and monitoring of real structures/infrastructures on the other side generates a virtuous learning outcome in students.

Other activities

In parallel to the described activities, in the first edition of the course a "corrosion photo-contest" has been proposed to students. The only rule of the photo-contest is to take a "semi-amateur – semi-artistic" picture of a corrosion case from everyday life accompanied by a title and a short description, indicating the possible corrosion form and prevention method.

The last day of course, students describe in a few minutes their work to the class. The final ranking is defined by a vote of the students to each snapshot, considering the quality, originality and the visual impact of the work, while the teacher assesses the technical description of each picture. Although this ranking does not provide any additional score to the final evaluation of the written exam, almost 90% students participated to the photo-contest.

In the following year, the Instagram account of the course has been created. The name is "rusting" [4], which is the union of two words: "rust" and "ing", which stays for the Italian "ingegneria" ("engineering"). Each week a new post is published, consisting of some pictures from the laboratory activity performed by the students, accompanied by a simple and straight-to-the-point explanation of it. Some examples are reported in the section "Gallery".

Didactic material

Due to the particular structure and organization of the course, a list of corrosion books is provided to students. Moreover, before any experimental activities, a pre-filled "worksheet" is provided with a detailed description of the activity and the possibility to insert the experimental measurements and graphs.

Evaluation of student's preparation

The preparation achieved by the student is evaluated at the end of the course through a written exam. Oral test is optional. The written test is organized in three sections: theoretical questions with closed answers, open question and numerical exercises, aimed at verifying the student

theoretical and experimental knowledge, in particular the ability to understand and interpret experimental measurements of corrosion and protection.

"Noble" collaborators

Apart from the presence of the teacher, a group of 25 students requires minimum two permanent high-level collaborators for the design and preparation of the experimental activity (metallic materials, electrolytic solution, electrical instrumentation, etc.) and for the assistance of students during the activity in laboratory. The preparation of the material for the laboratory workshop is particularly time-consuming. A ratio 1:1 between "duration of the lab activity" and "time of preparation of the lab activity" could be defined as a rule of thumb.
In addition to the permanent staff, the temporary collaboration of two technicians of the SAMM laboratory [5] (Laboratory of Microstructural Analysis of Materials) of the Department of Chemistry, Materials and Chemical Engineering "Giulio Natta" of Politecnico di Milano is required (Topic #10 of Table 1).

Financial aspects

About financial aspects, the initial economic expense (equipment and materials) amounts to about 5 k€ the first year (200 € per student) and 1 k€/year of maintenance expenses for the following years. Expenses relating to the didactic support by technical collaborators amount to about 3 k€/year. Excluding the first year ("activation" of the course), the average financial cost is about 150-200 € per student each year. The seminars proposed in the course, as well as the visit in the company, are free of charge. All the expenses, including those related to the use of laboratory and classroom, have been covered by Politecnico di Milano.

Student opinion about the course

At the end of the academic semester, Politecnico di Milano provides to all students a satisfaction survey about each course they attended during the semester. The survey consists of 20 questions divided in three main categories: a) general satisfaction about the course; b) satisfaction about the teacher, c) quality of numerical and laboratory exercises proposed during the course, d) adequacy of infrastructures for didactic activity. The score ranges between 1 (poor) and 4 (very high). Table 2 reports the average response related to five selected questions of interest for this article. For the two editions of the course, the LCPM students' responses are compared with the average score of all the courses of the "School of Industrial and Information Engineering" (School I.I.E.) of Politecnico di Milano.

Table 2 – Responses to selected questions of the student's satisfaction survey. The responses of LCPM course are compared with the average of all the courses of the "School of Industrial and Information Engineering" (School I.I.E.) of Politecnico di Milano.

Selected question of the student's satisfaction survey	**Average responses**	
	2021 edition	**2022 edition**
1. Were your prerequisites good enough for an adequate understanding of the subject?	LCPM = 3.48 School I.I.E. = 3.05	LCPM = 3.63 School I.I.E. = 3.07
2. Is the required workload in this course proportioned to the awarded number of hours?	LCPM = 3.43 School I.I.E. = 2.99	LCPM = 3.66 School I.I.E. = 3.05
3. Are the supplementary activities (numerical and laboratory exercises) coordinated with classes?	LCPM = 3.91 School I.I.E. = 3.36	LCPM = 3.89 School I.I.E. = 3.33
4. Is the attending of non-class activities beneficial to the learning process?	LCPM = 3.91 School I.I.E. = 3.48	LCPM = 3.89 School I.I.E. = 3.43
5. On the whole, are you satisfied with the course?	LCPM = 3.78 School I.I.E. = 3.14	LCPM = 3.84 School I.I.E. = 3.15

Although the general satisfaction about the course depends on several factors, it is possible to state that laboratory activities were particularly appreciated by students and they were considered beneficial to the learning process (question 4). At the same time, the learning achievement of a laboratory course is also strongly related to its harmonization with the programs of propaedeutic courses in the MS program (question 1) in order to avoid an over-workload (question 2) for students.

Conclusions and new perspectives

Students' appreciation about the course reflects the extent to which their expectations are met by the teacher's didactic proposal. It is the outcome of a course that meets the basic requirements and delivers specialistic and laboratorial formation, as promised. However, students delight goes beyond mere satisfaction. Delight occurs when the didactic experience surpasses students' expectations, evoking positive emotions and a sense of surprise.
Among the positive aspects of the course, the strengthening and improvement of the knowledge with an experimental approach, not always easy to transfer with numerical exercises in classroom, the interaction teacher-students and among students which helps the self-evaluation of the knowledge and social interaction.
From teacher point of view, an experimental course introduces inevitably an "hazardous" component in the didactic activity compared to more traditional lessons and numerical exercises.
Nevertheless, when an experimental measurement apparently does not match with the theory previously explained to the students, it is always possible to cite the Nobel Prize Richard Feynman: - Even if the measurement agrees with the theory, "*we are never right, we can only be sure we are wrong*" - [6].
As new perspectives, is it possible to introduce arts, literature, philosophy and dialectics in an experimental course of corrosion? I think so, following the belief of the "universality of university". Actually, brilliant authors in the literature already proposed a universal approach, as recently Groysman in [7, 8].

Acknowledgment

A special thanks to the collaborators of the first two editions of the course, in particular Silvia Beretta, Marco Ormellese, Elena Messinese, Mattia Ronchi, Cinzia Ferrario, for accepting this didactic challenge.

References

1. https://www.ingindinf.polimi.it/en/
2. Materials Engineering and Nanotechnology program at Politecnico di Milano
3. https://polilapp.chem.polimi.it/
4. https://www.instagram.com/rusting_polimi/
5. https://samm.chem.polimi.it/
6. R. Feynman, Speech on "The Character of Physical Law", Cornell University, 1964
7. A. Groysman, Chapter 6 in Corrosion for Everybody: Humanitarian Aspects of Corrosion Science and Technology, Springer, 2010
8. A. Groysman, Humor in Corrosion Science and Engineering Education, European Corrosion Congress, EUROCORR 2016, Montpellier, France, 2016

The Role of Corrosion in the Premature Failure of Springs and the Means to Prevent Those Failures

By: Robert O'Shea Jr. P.E. Principal Engineer
&
Ryan O'Shea Staff Engineer
Applied Materials Technologies Inc.

The two most common causations of spring failures are the progressive failure or fatigue and the overloading failure of relaxation. Fatigue failure refers to failures which occur due to defects developing over an extended period, while relaxation failures generally take place once as a result of an excess load being placed on the spring causing it to fracture or rupture. On occasion relaxation spring failure can happen due to cyclic progressive failure, but this only occurs when the spring is dealing with creep at an elevated temperature.

When a spring is placed under repeating stresses below the strength necessary to deform the material, the spring may begin to experience signs of fatigue failure. Fatigue develops as the material becomes less resistant to stress as the number of times it experiences the load increases. Thus, as the cycles of loading increase, the stress limit decreases. There are three distinct stages of fatigue which occur as further cyclic loading follows and eventually, they may lead to the failure of a spring. The first step is crack initiation, which occurs at a microscopic level and usually takes place at areas where excessive amounts of localized stress concentrations are present. The second step is crack propagation, which develops as the cracks increase in size. These cracks often grow across grain boundaries and may develop visible indicators such as striations. If the fatigue development goes unnoticed, the spring may reach the final stage of fatigue which is the fracture failure of the material. This will happen when the material can no longer withstand the load being placed upon the spring and a fracture will occur in order to release the energy being stored.

The failure of a spring due to fatigue ensues when a defect which had been growing over time reaches a critical size and a sudden failure of the spring occurs. While this is one of the most common forms of progressive failure in spring, it is not the only progressive mode of failure that they may experience. Depending on the environment that the springs are in, they may experience different corrosion mechanisms. Corrosion of the spring appears when electrochemical reactions occurring on the metal composition of the spring causing it to experience progressive embrittlement, deterioration, and possible destruction. This electrochemical reaction typically develops because of the metal's interaction with the environment, such as being exposed to atmospheric or aqueous conditions. When the metal is gathered from the earth it is taken in the form of ores and then fabricated into the desired metal. This fabrication process requires substantial amounts of energy to create the desired material, which then leads to the metal having excess amounts of energy stored inside it. Thus, when the metal is placed into a natural environment, the metal wants to return to its original state of a metal ore and begins to react with its surroundings to release the energy it accumulated. The two most prevalent types of corrosion in springs are

aqueous corrosion and atmospheric corrosion. Aqueous corrosion occurs when the spring is being utilized and exposed in an aquatic environment. On the other hand, atmospheric corrosion occurs when the spring is being used in a dry or gaseous environment. Examples of this include pressure relief valve springs and automotive leaf and coil springs.

When analyzing a spring experiencing corrosion, it is advantageous to analyze the mechanisms assisting in the process. There are three common spring corrosive mechanisms that experience the initial stages of fatigue, they are: uniform corrosion, galvanic corrosion, and erosion corrosion. Uniform corrosion occurs when a corrosive attack takes place evenly throughout the entire surface area causing the material to thin until there is no longer enough present to function properly. When two dissimilar metals are placed in a corrosive electrolyte such as water, galvanic corrosion may develop. When the metals are placed into the electrolyte solution then electrons will begin moving from one metal (anode) to the other (cathode). This results in the anode experiencing a reduction in surface area and thus a decrease in energy. Erosion corrosion occurs when the surface of a metal is continuously impacted by a water stream causing the material to dissipate as a result of the abrasion and corrosion it experiences.

Although many spring failures due to fatigue do experience all three phases leading to failure, that is not always the case. Sometimes, the spring will develop crack-like defects rapidly and thus the crack initiation phase will be skipped, and the spring will begin the crack propagation phase. For example, intergranular corrosion occurs along the boundaries of the materials grains, but does not emerge within the grains themselves. This is common in materials such as austenitic stainless steel during weld decay. Another example of a corrosion mechanism that skips the crack initiation phase is crevice corrosion. Crevice corrosion occurs at the gap or space where two surfaces come together. This type of corrosion is often seen along seams, bolts, screws, nuts, couplings, and joints. Typically, this involves the electrons moving from the contact point to another area of the steel which is experiencing oxidation. As a result, the steel begins to be worn away at this contact point resulting in corrosion.

Finally, some springs experience both rapid development of crack-like defects and progressive development crack defects over time. These are the most dangerous forms of corrosive mechanisms as they drastically decrease the lifetime of the springs and can lead to premature spontaneous failures. Pitting corrosion is a common form of progressive corrosion which is difficult to predict and prevent. Typically, this mechanism occurs in aqueous environments when a coating or protective layer is cracked or damaged. Once this happens the metal is directly exposed to the aqueous solution and it becomes anodic, with the protective layer acting as the cathode. Pitting can appear in many shapes and is commonly seen in metals such as stainless steel, copper, and aluminum. Selective leaching is another prevalent progressive corrosive mechanism that springs may experience. This type of corrosion occurs when an element is removed from an alloy due to their different chemical potentials. Common examples of this corrosion mechanism include decarburization, dezincification, and decobaltification of various steel-alloys. The best way to combat this from happening is to use metals and alloys which are resistant to the dealloying present during leaching, such as ductile iron and inhibited brass. Additionally, protection systems such as sacrificial anodes or impressed cathodic currents also aid in limiting the possibilities of selective leaching.

When a crack formation develops because of a stress, while in a corrosive environment, another progressive corrosion mechanism, stress corrosion cracking, may transpire within the material. This type of corrosion is often sudden in nature and typically strikes in metals such as ductile iron and low alloy steels. Another example of a sudden and dangerous progressive corrosion mechanism is hydrogen damage. This takes place when a metal experiences damage due to interactions with hydrogen. Hydrogen molecules penetrate the metal creating pockets of excess hydrogen which then cause the material to expand or bubble, which can eventually lead to the metal rupturing.

When a spring experiences high cycle fatigue it is in the crack initiation phase for between 50% - 90% of the overall fatigue era, with the crack propagation stage occurring for 10%-50% of the materials fatigue life. However, when specific progressive corrosion mechanisms outlined previously are present, they can drastically reduce or completely eliminate the crack initiation stage. Therefore, the fatigue cycle can be reduced by as much as 90%, resulting in the springs failure in an accelerated period. In rare cases this fatigue endurance limit can result in the number of cycles necessary for failure to occur by over 100 times the original value. For example, a sudden rupture incident of a spring which was supposed to be in a stable condition for 25 years may hit within 3 months' time.

Due to the nature of springs, it is not feasible to create a spring that is completely immune to the resistance that develops over the exposure to numerous cyclic loading stresses when placed in a corrosive environment. However, it is possible to limit the effects of corrosion fatigue by decreasing the intensity of the cyclic loads the spring experiences or by utilizing measures which help control and limit the ramifications of corrosion. The first measure relates to the design and materials section of the spring. When creating a spring that will be used in a corrosive setting it is necessary to look at factors such as the environment, stress, compatibility, movement, and temperature it will interact with. It is advantageous to design the spring around the stresses it will experience and the environments in order to produce an adequate device capable of proper functionality for an extended period. It is also necessary to develop the spring to be compatible with other materials present in the systems as well as ensuring the spring material can manage the temperature and surrounding flowing exposures.

To ensure a spring will be able to manage these factors, it is wise to design some ways to manipulate the interaction they have with the spring. Adding cathodic protection or inhibitors may aid in increasing the springs resistance to corrosion. Additionally, periodic surface cleaning or an inspection and maintenance plan may also assist in extending the springs life span. Finally, when designing the spring, it may be advantageous to add coatings to the portion of the spring exposed to the corrosive environment. For example, Dip-Spin coatings are often used over zinc electroplating in the automotive industry as it allows for adequate corrosion resistance while also eliminating the opportunity for hydrogen embrittlement to occur.

Another key corrosion control measure takes place during the fabrication and processing of a spring. As mentioned above, coating the spring can reduce the impact corrosion has on the integrity

of the spring. During fabrication corrosion resistance measures will be enhanced by doing the following:

1. Providing basic corrosion protection which is usually performed for identification purposes. This also ensures that the springs are not cleaned in harsh acids before painting or Hydrogen embrittlement, or attack may arise.
2. Providing some basic corrosion protection, usually oiled afterwards.
3. Coatings electro-statically applied may lead to arcing but will provide good corrosion protection until the coating chips off. Springs must be baked immediately after plating to remove hydrogen. Common bake out practice is 400°F for 4 hours. Refer to ISO-9588-1999.
4. Keep processing steps to a minimum. Make sure there is no exposure to hydrogen after the stress relief.
5. Carbon residue can be formed on the wire surface if the springs are not cleaned before the stress relief or age. The presence of carbon on 302 or 17-7 degrades the corrosion resistance of the alloy.

One example of determining the causation of the failure of a spring used in a corrosive environment involved a zinc plated spring. This spring was being used in a salt water marine environment (see Photograph 1) and there were multiple complete fractures which indicated there was extensive pitting/corrosion present. There is red rust (iron oxide) corrosion, white zinc oxide and a corrosion pit shown in the SEM image (Photograph 2) at the fracture origin. The presence of the white zinc oxides indicates that there is still some zinc left in the spring material (Photograph 3).

Photograph 1 – Zinc plated spring that failed in salt water.

Photograph 2 – SEM image showing iron oxide, white zinc oxide and corrosion pit.

This area of the oxides iron indicated that most or all of the zinc has been dissolved due to its use as a sacrificial anode. Zinc plating of springs are used to protect the base metal of the spring which leads to it useful life being extended. The root cause of this failure was not corrosion, but the improper selection of material.

Photograph 3 - Presence of the white zinc oxides indicates that zinc was left in the spring material.

A second case study involved two 17-7 PH compression springs that controlled relief valves on a propane truck and failed. The springs were found to have failed due to hydrogen sulfide (H_2S) embrittlement (Photograph 4). The H_2S was formed as a result of contaminated propane being present in the system. The white deposit located on the film was found to be sulfur and with moisture also present, the sulfur and water reacted to create an acidic corrosive environment for the spring. This resulted in the formation of Sulfuric Acid and led to a Stress Corrosion Cracking

(SCC) in the spring. A microscopic image from the Scanning Electron Microscopy (SEM) analysis performed on the spring can be seen in Photograph 5. From this analysis it was determined that the spring had a brittle fracture origin located at the inner diameter where the stresses are normally located.

Photograph 4 - Failed Propane Truck's compression springs.

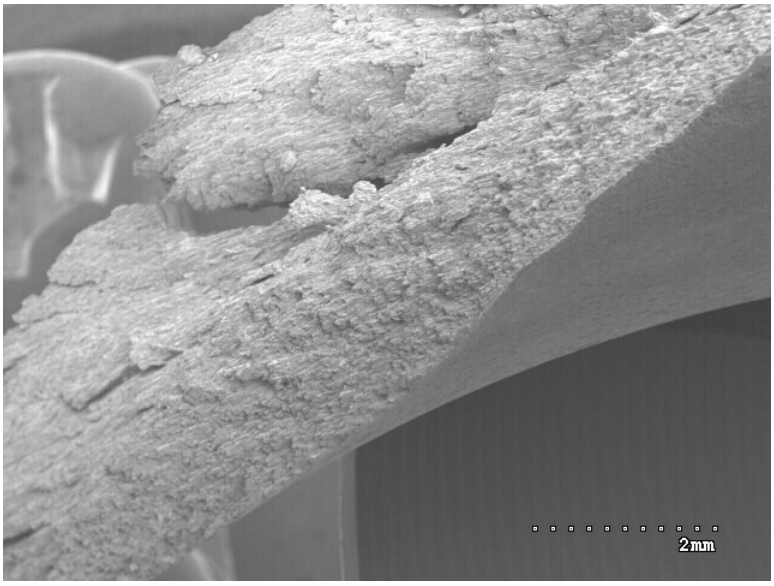

Photograph 5 – SEM image shows brittle fracture.

Energy Dispersive Spectroscopy (EDS) was also performed on the spring and the results are seen in Photograph 6 below. The spectroscopy test of the surface deposit confirmed that the Steel was 17-7 and that a significant amount of sulfur was present, which in turn led the spring to fail in a brittle, intergranular manner.

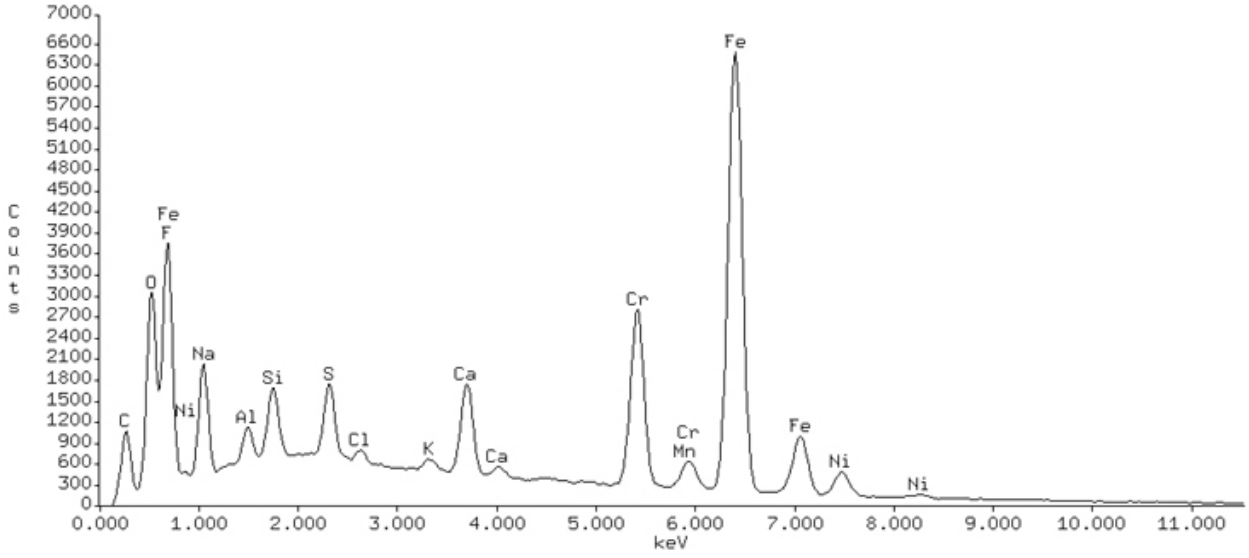

Photograph 6 – EDS of failed propane truck's compression springs.

----End----

Robert O'Shea, Jr., P.E.
Principal Engineer

Mr. O'Shea's career has focused on project management, OSHA compliance inspections, design evaluation, materials selection, engineering, fabrication, inspection & examination, and testing of plant equipment related to the energy industries (electric, gas and steam), marine industry and petrochemical industries. He has also focused on the application of materials, the manufacture of components and products, and the response of materials components and systems to the operational environments. He has extensive experience in industrial and vehicular accident reconstruction.

Mr. O'Shea has over 34 years' experience in comprehensive engineering and project management including failure analysis investigations. These investigations include field project management, utility gas electric and steam investigations, petroleum refineries accident investigation, code compliance (industrial and marine), maintenance, marine failure analysis and engineering, materials engineering, welding technologies, accident reconstruction, fire cause and origin determination and corrosion. Mr. O'Shea has been the lead engineer (Project Manager) on over 350 projects and assisted on over 500 projects. Mr. O'Shea has conducted projects ranging from simple failure investigations to complex engineering studies. He has also performed detailed quantitative risk assessment analyses for a variety of different clients for risk mitigation situations.

Mr. O'Shea is an approved Third-Party Examiner for the State of Illinois' hull inspection program (OSHA 29 CFR 1910 compliance). He was engaged to help implement the State of Illinois program for Permanently Moored Vessels since its inception in 1999. He has been the Project

Manager on numerous OSHA condition assessments throughout the Midwest. Mr. O'Shea has also been the Project Manager on over fifty inspections of floating casinos throughout the State of Illinois. He has developed and directed numerous construction quality assurance audits on multi-million-dollar projects throughout the United States.

Mr. O'Shea has been responsible for mechanical design and manufacturing of airborne electronic systems including management of cost for testing, process development, plant layout and implementation of state-of-the-art manufacturing, processing techniques, and systems. As a part of the many comprehensive failure analyses, Mr. O'Shea has developed numerous protocols for the examination and testing of evidence both on-site as well as in testing laboratories. He has directed and coordinated the execution of these protocols to obtain the necessary test results. These test protocols have contributed to investigations involving fires, gas explosions, dust explosions, incidents in a variety of process plant operations, boiler explosions, utility explosions (gas and electric) and the investigation of incidents in other industrial systems. Specific protocols have involved functional tests of systems that include heat exchangers, control valves, block valves, check valves, filtration systems and pump motors. Mr. O'Shea has developed metallurgical testing protocols which entails a complete examination (visual and microscopic) and documentation of the evidence, metallurgical sampling, fracture surface examination, hardness testing, mechanical testing, and destructive testing.

Mr. O'Shea has made numerous presentations at technical meetings and conferences in the areas of code compliance, material characteristics, vehicle fires, utility and industrial plant fires and investigative tools and technology techniques. He has taught laboratory courses at the University of Notre Dame and Georgia Tech and is a Hazwoper Site Supervisor and Confined Space Attendant, Entrant Supervisor.

Education: M.S. Material Science and Engineering, University of Notre Dame, 1986.
B.S. Metallurgical and Material Engineering, Illinois Institute of Technology, 1984.

Professional Chronology: Anixter Mark, 1982-1983; L. J. Broutman and Associates, Ltd., 1983-1984; University of Notre Dame, 1984-1986; Northrop Corporation, 1986-1988; Georgia Institute of Technology, 1988-1989; Engineering Systems Inc., 1989-2009; Applied Materials Technologies, Inc., 2001 – present.

Professional Registrations/Certifications: Registered Professional Engineer (Arkansas, Illinois, and Wisconsin)

Professional Memberships: ASM International (ASM); American Institute of Chemical Engineers (AIChE); National Fire Protection Association (NFPA), National/Illinois Society of Professional Engineers (NSPE, ISPE)

Ryan O'Shea
Staff Engineer

Ryan O'Shea is a Staff Engineer for Applied Materials Technologies Inc. (AMTI) whose areas of expertise include OSHA compliance inspections, materials engineering, project management, engineering testing and 2D AutoCAD. He has firsthand experience in photography, forensic evidence collection and report writing. In addition, Mr. O'Shea assists the senior staff in forensic investigations and marine inspections of permanently moored structures per the Illinois State Fire Marshal regulations. These inspections pertain to factors such as safety compliance and structural integrity.

Prior to joining AMTI, Mr. O'Shea had three internships while attending Michigan State University. These internships were with the following companies: J.F. Brennan Company Inc., ESI Consultants LTD, and Applied Materials Technologies Inc. During his time with J.F. Brennan, Mr. O'Shea created multiple reports detailing the dive division's findings during underwater inspections. Additionally, Mr. O'Shea also created 2-Dimensional models of the investigated structures and highlighted areas of interest such as repairs and deficiencies. For ESI Consultants LTD, Mr. O'Shea aided in the supervision of a road construction site in Evanston, Illinois. His responsibilities included keeping a detailed log of the equipment, workers, shipments, and issues observed daily. For Applied Materials Technologies Inc., Mr. O'Shea assisted in the project management and supervision of the resurfacing of two barges located at the Hollywood Casino in Joliet, Illinois. He also assisted the senior staff in the corrosive analysis of sacrificial anodes on a stainless-steel sludge barge for the NYC-EPA.

Education: B.S. Materials Science and Engineering, Michigan State University, 2020

Professional Chronology: Applied Materials Technologies Inc., Naperville, Illinois Staff Engineer, 2020 – Present, J.F. Brennan Company Inc., La Crosse, Wisconsin, Dive Division Engineering Intern, Summer 2019, Applied Materials Technologies Inc., Naperville, Illinois, Engineering Intern, Summer 2017 and Summer 2018, ESI Consultants LTD, Naperville, Illinois, Engineering Intern, Summer 2016

Professional Memberships: ASM International, Failure Analysis Society (ASM)

Applied Materials Technologies Inc.

Applied Materials Technologies Inc. (AMTI) is a multi-disciplined, engineering, design and consulting firm who has been in business since 2001. AMTI staff includes engineers with a wide range of expertise in design, electrical, mechanical, manufacturing, fabrication, inspection, quality

control, and construction regulations. The expertise of the firm encompasses all types of materials, components, systems, products, and engineered structures.

AMTI'S Senior Professional Team has demonstrated, with considerable experience and knowledge, expertise in the following areas: project management, design and engineering evaluations; OSHA compliance inspections (29CFR 1910 & 29CFR 1926), marine compliance, electrical engineering design; electrical installation; resolution of industrial problems; root cause failure analysis; corrosion and wear; welding/joining; nondestructive evaluation; electrical and mechanical testing; finite element analysis; utility and industrial steam/power generation; petroleum and chemical processing; natural and LPG gas production and distribution; rotating equipment; and safety issues. In addition, AMTI has been certified by The Illinois State Fire Marshall to conduct third party inspections of permanently moored facilities for structural integrity, electrical compliance, regulatory compliance, and safety.

Investigation of influences on the mechanical resistance of organic coatings in the offshore sector as a result of impact loads

Daniel Kelm, Dr.-Ing. Michael Irmer, Fraunhofer IGP, Rostock/Germany

The requirement of a service life of often more than 30 years for offshore wind turbines (OWT)[1], taking into account the mechanical and the corrosive stress, demands high-performance coating materials and corrosion protection concepts.

Structurally critical corrosion damages are due to inadequate quality of the corrosion protection and to damage in the coating. Coating damage frequently occurs as a result of transport and assembly processes. According to an evaluation of inspection activities, 30% of the damage to offshore wind platforms and 46% of the damage to the towers of OWT [2] [3] can be attributed to mechanical loads. In these cases, impact damage is typical for coating systems of OWTs. Damage in the coating often leads to significant corrosion phenomena under maritime environmental conditions, high humidity and high salinity[4].

For the approval of coating systems in the offshore sector, the passing of various tests is a prerequisite. These tests are summarized in numerous regulations and standards[5] [6]. Among other things, these regulations specify test methods and evaluation criteria for resistance to impact loads. According to NACE, impact energies of 3.4 J or 5.6 J are applied, and according to the VGB/BAW standard 5.9 J. In the subsequent assessment, no cracks must be visible in the coating system. Further evaluations or higher intensities are not provided in the standardized state of the art. The research on mechanical requirements for coatings only shows testing to a minimum standard, but no further differentiation beyond this. As a result, necessary information on the application limits of the coating and the possible reduction of corrosion resistance due to impact damage cannot be reliably estimated.

---

[1] H.-J. S. Artur Goldschmidt, BASF Handbuch Lackiertechnik, Hannover: Vincentz Verlag

[2] A. Momber, „Quantitative performance assessment of corrosion protection systems for offshore wind power transmission platforms," *Renewable Energy Vol. 94 ,* pp. 314-327, 2016

[3] H. Müller, „Ursache und Sanierung von Beschichtungsschäden an Offshore Windkraftanlagen. Korrosions-schutz in der maritimen Technik," in *DNVGL*, Hamburg, 2012

[4] DIN EN ISO 12944-9; 2018-06. Beschichtungsstoffe - Korrosionsschutz von Stahlbauten durch Beschichtungssysteme - Teil 9: Beschichtungssysteme und Leistungsprüfverfahren im Labor für Bauwerke im Offshorebereich.

[5] Bundesanstalt für Wasserbau , *VGB/BAW-Standard - Korrosionsschutz vonOffshore-Windenergie-anlagen und Windparkkomponenten,* Essen: VGB PowerTech Service GmbH, 2016

[6] VGB/BAW-Standard VGB-S-021-01-2016-03-DE, 2016

In order to determine more precise relationships between the influences on the mechanical impact resistance of organic coatings, as well as the relationship between the level of damage and the reduction of the corrosion protection effect, investigations were carried out at Fraunhofer IGP.

Commercially available single layer coatings and coating systems approved for offshore use were investigated. The application took place on steel sheets (S355+AR) of the size 150 x 100 x 5 mm. The surfaces were pressure-blasted (ISO 8504-2) [7]and achieved a surface cleanliness of Sa 2 ½ (ISO 8501-1)[8] with a minimum roughness Rz between 50-75 µm. The binders of the organic coatings were based on epoxy resin (EP) or polyurethane (PU). The nominal dry film thicknesses (NDFT) were based on the specifications of ISO 12944-9[9] with ≥ 60 µm for single layers and ≥ 350 µm for layered systems. The experimental investigations were carried out using the drop tower CEAST 9040 from Instron and a spherical test probe (Ø 20 mm). The investigation was specifically related to various influences of the impact resistance. These include the layer thickness dependence of single layers and total layer thicknesses, the load dependence of the impact energy and the composition of the binder.

To determine the layer thickness dependence, individual EP- or PU-based layers with varying layer thicknesses were applied to separate steel sheets and tested under the same loading conditions.

The load dependence was also investigated on separate EP- or PU-based single layers with increasing loads of 5-20 J but constant layer thickness.

To evaluate the mechanical resistance, optical damage was determined and measured on the basis of crack formations and material displacement, which could be detected on the specimen surface or in microsections.

Subsequently, the investigations were partially repeated on entire coating systems and evaluated. Conclusions could be made on the mechanical resistance of organic coatings and the influences of coating thickness, load and binder dependence.

---

[7] Paints and Varnishes, „ ISO 8504-2: Preparation of steel substrates before application of paints and related products - Surface preparation methods - Part 2: Abrasive blast-cleaning,“ March 2020

[8] Paints and Varnishes, “ISO 8501-1:2005: Preparation of steel substrates before application of paints and related products - Visual assessment of surface cleanliness - Part 1: Rust grades and preparation grades of uncoated steel substrates and of steel substrates after overall removal of previou,“ December 2007

[9] Paints and varnishes, „ISO 12944-9: Corrosion protection of steel structures by protective paint systems – Part 9: Protective paint systems and laboratory performance test methods for offshore and related structures“, 2018

Application methods for underwater coating as a repair process for coating damages on offshore structures

M.Sc. Valeska Cherewko, Fraunhofer Institute for Large Structures in Production Engineering, Rostock/Germany

Organic coatings can effectively protect maritime structures from corrosion. However, coating damages can occur during transport and installation as well as over the course of long operating periods. Corrosion protection concepts, for example for offshore wind turbines and their foundation structures, are based on an intact coating depending on the type of the offshore wind turbine. Consequently, there is an immense need for repair solutions of coating damages, especially in the area below the waterline and in the area between the lowest and the highest waterlevel, which is currently covered by the use of divers.

Fraunhofer IGP is working on the development of a process for the mechanized application of a corrosion protection coating by an underwater vehicle. The mechanized underwater application of coatings is subject to many influences. The quality of the coating is determined by numerous parameters, such as the application speed, the application tool and the coating material and its viscosity. As a result, an application process was developed and parameters were defined to achieve a good coating quality. The tests showed a big impact on coating quality, coating tool and viscosity of the coating material during application. To be able to use a wider range of different coating systems, further coating materials with different viscosities based on epoxy resins were tested in laboratory tests and special application processes were developed for them. The application with a rotating spatula is suitable for high viscosity coatings, whereas low viscosity coatings are better applied with a brush or roller. The aim of the tests is to develop special processes (application tools, parameters) for each coating.

The project will contribute to the diver-free coating repair of offshore structures in the underwater environment. Overall, the project will develop a process that combines underwater surface preparation and coating repair to provide an efficient and safe process for maintenance.

Corrosion behaviour of multilayer Cr/GLC coatings in 3.5 wt.% NaCl solution under different hydrostatic pressures

Hongyu Ma[a], Yu Cui[b,], Rui Liu[a], Li Liu[a,]*, Fuhui Wang[a]*

[a] Shenyang National Laboratory for Materials Science, Northeastern University, Shenyang 110819, China.

[b] Shi-changxu Innovation Center for Advanced Materials, Institute of Metal Research, Chinese Academy of Sciences, Wenhua Road 72, Shenyang 110016, China.

Amorphous carbon-based thin film coating has attracted a lot of attention because of its high stability, high hardness, good corrosion resistance and wear resistance, etc. and has become a new material that can be expected to be used for metal protection in deep-sea environments. Previous research has focused on the corrosion behaviour of coatings in atmospheric environments and the design of coating structures, however, there are few literature reports on the study of coating corrosion failure behaviour in deep-sea environments. Thus, there is an urgent need to elucidate the corrosion kinetics laws and failure mechanism of multilayer Cr/GLC coatings under different hydrostatic pressure, and to provide theoretical guidance for the design and application of coatings.

In this work, the corrosion behaviour of multilayer Cr/GLC coatings in 3.5 wt.% NaCl solution under different hydrostatic pressures was investigated by in-situ electrochemical measurements, and transmission electron microscopy (TEM). The results indicated that hydrostatic pressure exponentially reduces the corrosion resistance of multilayer Cr/GLC coating (Fig. 2(b)), which is attributed to hydrostatic pressure decreasing the thickness of the stern layer within the electric double layer (EDL) at the solution/coating interfaces (Fig. 2(c)) and hydrostatic pressure linearly promotes Cl^- adsorption on the coating surface (Fig. 2(d)), which together promotes the dissolution of the metal transition Cr layer and the metal substrate, leading to coating collapse and peeling (Fig. 1), reducing the protective properties of the coating.

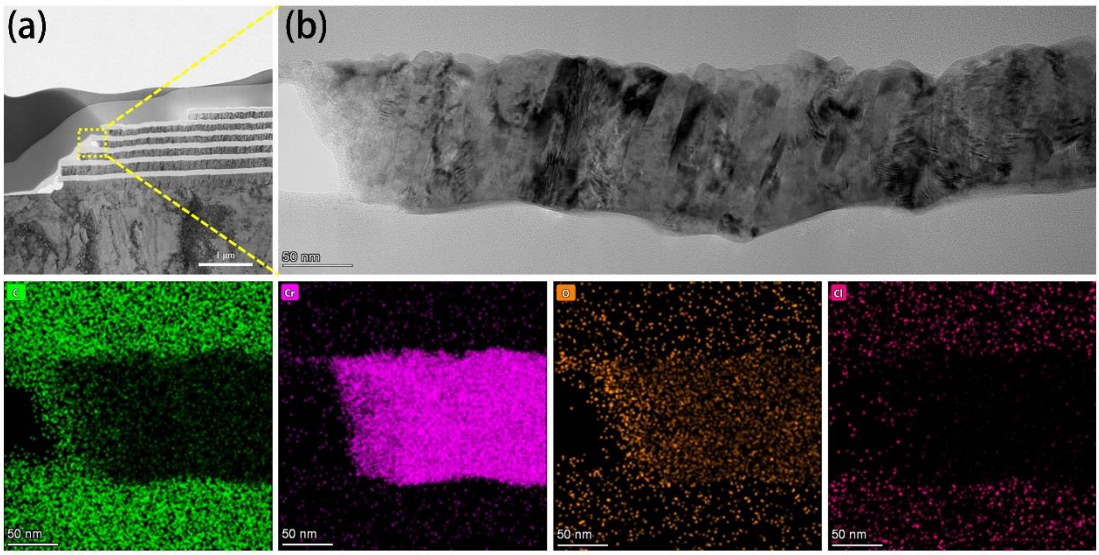

Fig. 1 Cross-sectional morphology and mapping results of multilayer Cr/GLC coatings after 720 h in 3.5 wt.% NaCl solution at 15 MPa

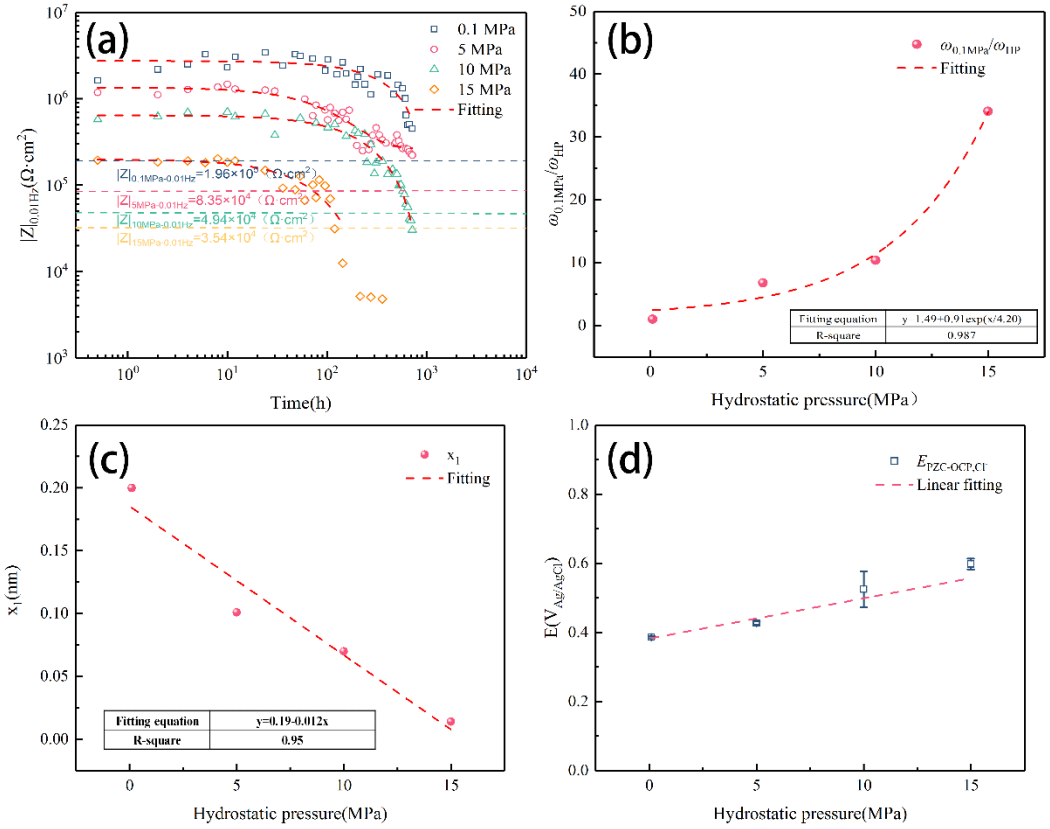

Fig. 2 The variation trend of multilayer Cr/GLC coatings performance under different hydrostatic pressures. (a) low-frequency impedance $|Z|_{0.01Hz}$; (b) low-frequency impedance decay coefficient fitting; (c) thickness of water molecule dipole layer, x_1; (d) Cl^- adsorption capacity of the coating surface

New insights into the influence of tensile stress and hydrostatic pressure on corrosion of high strength steel in deep sea environments

Rui Liu[a], Yushan Song[a], Yu Cui[b], Li Liu[a], Fuhui Wang[a]*

a Shenyang National Laboratory for Materials Science, Northeastern University, Shenyang 110819, China.

b Shi-changxu Innovation Center for Advanced Materials, Institute of Metal Research, Chinese Academy of Sciences, Wenhua Road 72, Shenyang 110016, China.

High strength martensitic steels show promising mechanical properties, and Ni-Cr-Mo-V steel is a type of high strength low alloy steel (HSLAS) that has been extensively applied in the deep-sea structure. In fact, the degradation of alloys in extreme deep-sea condition results from the multiple physicochemical factors, which is more complicated than the compared to the offshore environment. So far, accelerated corrosion under hydrostatic pressure and applied stress still lack basic theoretical studies, and the synergistic mechanism is uncertain in the deep sea.

In this work, Ni-Cr-Mo-V steel was used to study the synergistic actions of hydrostatic pressure and tensile stress on the early corrosion. We try to extend the compression effect of hydrostatic pressure on the electric double layer to tensile stress and pressure-stress action on the double layer so as to study the acceleration of electrochemical rate or corrosion rate in the coupled environment. It shows that pressure and deformation facilitate metal dissolution in the anodic process by the following aspects. Our results show that hydrostatic pressure and tensile stress synergistically facilitate metal dissolution: Tensile stress thins the electric double layer, similar to the effect of hydrostatic pressure, resulting in the promotion of anodic reactions of the steel;

The anodic current density calculated by the change of double-layer capacitance under tensile stress is approximate to that calculated by Gutman's theory.

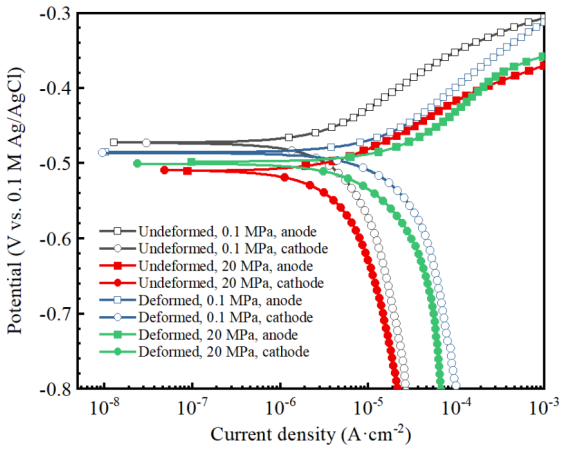

Fig.1 Polarization curves of the Ni-Cr-Mo-V steel under 0.1 MPa without U-bend, 20 MPa without U-bend deformation, 0.1 MPa with U-bend deformation, and 20 MPa with U-bend deformation, respectively.

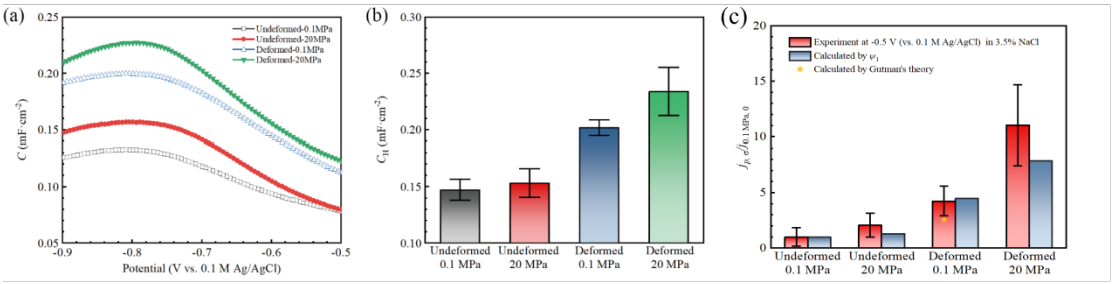

Fig.2 Differential capacitance and the calculated current density of Ni-Cr-Mo-V alloy. a) differential capacitance, b) the Helmholtz layer capacity under different conditions, and c) comparison of $j_{p,\sigma}/j_{0.1MPa,0}$ calculated by ψ1 effect modification, $j_{p,\sigma}/j_{0.1MPa,0}$ calculated by Gutman's theory, and the experimental results under different conditions.

Controlling Corrosion on Seawater Plant, Success Story

Abstract

Osamah M. Al-Ghamdi

The seawater plant and its associated piping networks suffers from the multiple causes of corrosion, and one of the most causes, is the Microbial Influenced Corrosion. As the control of corrosion requires deep study of the process/system, through a formal corrosion management program. Sitting robust program requires monitoring the process, collecting and analyzing data, develop action plan and then establish roles and responsibility to each involved individual and/or organization. The journey took long time to finally prove the effectiveness of the program. This paper summarizes a success journey in enhancing the plant reliability and availability through effective corrosion control. The corrosion control program is summarized under 5 pillars:

1- Stakeholder Engagement.
2- Data Analysis.
3- Corrosion Management Program.
4- Processes and Procedures Enhancement.
5- Capital Investments.

Stakeholder Engagement:

Engaging all stakeholder, and in particular the organization's leadership, was a key factor behind this success journey. The higher-level management were involved in most of the technical challenges and as a result all support was obtained in a smoother way, since they are well aware about consequences of the corrosion related failures. Also, the other organizations that are involved with us in the process of the sea water were closely involved with us, through the corrosion management program that was formally concurred by them.

Data Analysis

Starting the real work of developing corrosion management program requires massive work in analyzing all data available, such as process design and actual parameters, design and actual specification of the sea water, costumer input and concerns, lab data, failure analysis, leaks history… etc. After spending enough time in analyzing the available data, the team agreed to enhance the analysis through:

- Installing Additional instruments (analyzers, monitors, transmitters, … etc.).
- Introduce additional sampling location.

Saudi Aramco: Company General Use

- Change the frequency of the sampling.
- Review and adjust the sampling procedures.

Afterward, the team developed a road map to enhance the data analysis. Data were analyzed and corrosion management program was adjusted accordingly as needed.

Corrosion Management Program

Developing the corrosion management is an important step in order to have governance in all efforts being done toward controlling the corrosion. It also insures sustaining the high performance and serves as a good reference for the organization. The corrosion management program was developed by our corrosion engineers, and then reviewed and concurred by the central engineering entity in the corporate.

Processes and Procedure Enhancement

As majority of the corrosion management program items are assigned to operation and maintenance, and in order to ensure they are formally assigned, the corrosion engineers reviewed the current manuals and the formal reference documents in the organization and added items assigned to each unit in the department. These efforts resulted in a better alignment between the corrosion management program and the other operation documents and manuals.

Capital Investment

The corrosion management program, and based on the analysis done by the corrosion engineers, involves short term and long-term action plans to enhance the corrosion control. Action plan were basically considered as multiple projects with different size. The organization built valid and solid convincing case to the corporate Finance team were approval was obtained based on both technical and financial analysis.

Outcomes

As a result of implementing the corrosion management program, the organization successfully achieved the below outcomes:

- Number of water leaks was dropped by more than 70%.
- Enhanced specifications of the processed sea water.
- Enhanced the lab analysis in terms of sample locations, frequency, procedures, etc
- Higher equipment availability % for the corrosion related plant equipment such as hypochlorite generators/pumps.
- Clear road map on the corrosion control presented to the department head, attended by all stake holder, to track the progress of the road map.

Saudi Aramco: Company General Use

The oxalate green rust, a corrosion product of steel in marine sediments

Ph. Refait, K. Aggoun, M. Jeannin

Laboratoire des Sciences de l'Ingénieur pour l'Environnement (LaSIE),

UMR 7356 CNRS - La Rochelle Université, France.

A previous study dealing with the corrosion behavior of carbon steel in marine sediments demonstrated that various GR compounds could form as corrosion products in these specific conditions [1]. Four GR compounds were identified, among which GR(Cl^-), GR(CO_3^{2-}) and GR(SO_4^{2-}), that were already identified in the corrosion product layers of carbon steel immersed in seawater [2]. In the sediments, a fourth GR compound was identified and assumed to correspond to the oxalate GR, i.e., GR($C_2O_4^{2-}$), on the basis of XRD data [3].

A new laboratory study was devoted to GR($C_2O_4^{2-}$); i.e., the Fe(II-III) hydroxy-oxalate. First, the respective stability of GR($C_2O_4^{2-}$) and GR(SO_4^{2-}), the main GR forming on steel surfaces immersed in seawater, was studied. In experimental conditions where sulfate and oxalate concentrations were equal, the formation of GR($C_2O_4^{2-}$) was favored, indicating that the GR structure had a greater affinity for oxalate ions than for sulfate ions. Secondly, the oxalate GR was synthesized by coprecipitation from Fe(II) and Fe(III) salts at two Fe(III):Fe(II) concentration ratios in conditions where only oxalate ions were present. For Fe(III):Fe(II) = 1:3, the oxalate GR previously reported [1,3] was the main compound obtained, as demonstrated by XRD and µ-Raman spectroscopy analysis. In this GR compound, the oxalate ions present in the interlayers of the GR crystal structure are planar and parallel to the hydroxide sheets. For Fe(III):Fe(II) = 1:2, another oxalate GR was obtained. In this second variety of GR($C_2O_4^{2-}$), the oxalate ions are perpendicular to the hydroxide sheets. With this structural modification, a larger amount of oxalate ions can accumulate inside the interlayers and accommodate the larger Fe(III):Fe(II) ratio.

References:

[1] Ph. Refait, A.-M. Grolleau, M. Jeannin, E. François, R. Sabot, Corros. Sci., 130 (2018) 76-84.

[2] Ph. Refait, A.-M. Grolleau, M. Jeannin, C. Rémazeilles, R. Sabot, Corros. Mater. Degradation, 1 (2020) 198-218.

[3] J.A. Bourdoiseau, R. Sabot, M. Jeannin, F. Termemil, Ph. Refait, Colloids Surf., A: Physicochem. Eng. Aspects 410 (2012) 72-80.

Corrosion behavior of simulated monopile foundation by S355J2 steel in artificial seawater and sediment

Khalid Zekhnini[1], Gino Ebell

[1] Bundesanstalt für Materialforschung und -prüfung (BAM)

Division 7.6 Corrosion and Corrosion Protection

Unter den Eichen 87, 12205 Berlin, Germany

The development of offshore wind turbines (WTGs) presents many challenges in terms of safe operation over extended periods of time. One of these is the corrosive environment towards metallic materials, which can lead to a loss of material thickness and thus to a deterioration of mechanical performances, especially the strength of infrastructures. This can be counteracted by painting and cathodic protection (CP). Much research has already been done in this area about inhibiting the corrosion process. However, gaps exist regarding free corrosion. This plays a greater role especially for time intervals during the installation of the systems and their maintenance, during which often no CP can be operated. This is especially true for areas where painting surfaces is impossible e.g., sediment areas. This problem is exacerbated by the different corrosion rates caused by the different zones (water and sediment), with their different amounts of dissolved oxygen.

This presentation deals with experiments in artificial seawater and sediment. Classical S355J2 steel samples in the form of coupons were fitted with welding wires that carried out the electrical contact to the outer side of the basin. Inside the basins, the specimens are stored in different zones like water and sediment which should simulate the foundation situation of monopiles. The mass loss was determined gravimetrically, elemental currents between specimens in water and sediment were measured and electrochemical investigations were carried out. The influences of the zones, based on different solved oxygen contents, and the rolling skin towards the corrosion behavior of the mild steel samples were determined in this work. Especially the influence of the sediment showed unexpected behavior, determined by electrochemical investigations. These results allow better conclusions to be drawn about the corrosion behavior of low alloy steels in offshore environments used in sediment and seawater, which cannot always be protected.

Internal Corrosion of Near Stagnant Steel Marine Tidal Infrastructure

Igor A CHAVES[1], Robert E MELCHERS[1], Robert B PETERSEN[1]

[1]Centre for Infrastructure Performance and Reliability
The University of Newcastle, Newcastle, Australia
igor.chaves@newcastle.edu.au

Paper-ID: 244553 TOPIC: Marine Corrosion (WP9)

Abstract

Both short and long-term marine corrosion performance of steels have been measured extensively for open sea exposed surfaces. However, for enclosed, near-stagnant, sea water conditions information is only anecdotal. This paper reports empirical data from an ongoing multi-year study in near stagnant seawater immersion corrosion conditions for 3 to 5m long mild carbon steel strips. The data are particularly relevant to the offshore renewable energy industry which often is unable to ascertain the extent of corrosion within windmill support piles. The results show that, although the strips are subject to atmospheric immersion tidal and splash zone corrosion, no evidence was found of the classical corrosion profile for vertical steel structures (e.g. piles) or of accelerated low water corrosion. In the vertical direction, regardless of exposure site, the pattern of general corrosion through the various zones remained similar throughout the different exposure periods. For each exposure zone the magnitude of that corrosion displays bi-modal behaviour as a function of exposure time, consistent with much other data. As expected, the exposure site with elevated concentration of dissolved inorganic nitrogen showed greater corrosion losses. It is proposed that the observed corrosion behaviour primarily is the result of the shielded quiescent environment. A reliability case study analysis was performed to highlight how the data obtained so far can be translated into risk estimates for practical decision making. Internal corrosion, although negligible by itself in terms of generating risk of failure, when taken in combination with external corrosion losses highlight that internal corrosion should not be dismissed, at least not for when 50 year design life is targeted.

Keywords: Mild Steel, Corrosion, Stagnant, Seawater, Offshore

Introduction

Unforeseen complexities normally arise when moving from concept and design into operation. This is the case also for offshore infrastructure and can become a significant part of the project budget, even with extensive expertise to inform good decision making [1]. An example is the complexities created by marine fauna and flora and their localised ecosystems as a result of installation and continued presence offshore windmill monopiles [2,3]. Vertical zonation of biofouling communities is commonly observed, with clear differences in marine growth along the surface of the monopile and between monopiles and as a function of depth. The vertical effect is of interest because it tends to align with published studies for the vertical profile of corrosion of mild steel strips in open seawaters [4]. Such corrosion is known to be a function of dissolved oxygen for short-term exposures (e.g. < one year) but more importantly a function of available dissolved inorganic nitrogen (DIN) that has been shown to directly influence microbiological activity for long-term exposures [5]. Such corrosion effect with depth and

correlation with corrosion inferred to be from microbiologically influenced corrosion (MIC) has been shown for external corrosion of sheet piling and monopiles [5,6,7].

For monopiles an aspect of much interes for older monopiles not cathodically protected is the variation of the microsystems within the piles themselves and the related corrosion effects, in contrast to the established extensive experience with external monopiles monitoring and coating maintenance [2,3]. For internal corrosion some investigations have been carried out recently and results published for corrosion losses within a simulated internal corrosion environment with near stagnant seawater conditions [7]. The present paper reviews those results and follows those with an applied case study using reliability theory [8]. This is relevant because it provides a numerical assessment of the likely risk associated with prolonged deferral or neglect of of action for any observed (or unobserved) section losses within monopiles or any other hollow offshore infrastructure. Prediction and associated risk estimation is a useful tool since, as known, monopiles inherently are costly to inspect internally.

The following section summarises the field work methodology for collecting the empirical data that was used for the reliability study. Full details of the empirical data are given in the references [5,7,9]. A discussion is given focusing on the corrosion loss results obtained to date along with a brief case study.

Experimental Field Exposure and Data Collection

Several research questions were targeted for the present project. These include how structural mild steel, which is still the material of choice for offshore projects corrodes in a near-stagnant seawater environment when shielded from the atmosphere and when it extends through the immersion, tidal and potentially the splash zone [7]. The latter relates to whether there are any distinct zones in terms of corrosion morphology within a near-stagnant environment, as well as whether any of the corrosion, rust and biofouling phenomena typically observed for external surfaces still occur within the near stagnant environment, including the possibility of accelerated low water corrosion (ALWC) [10].
The study was conducted using multiple 3~6m long commercial mild steel strips (Infrabuild 1120X: 0.2 C, 0.012 P, 0.74 Mn, 0.21 Si, 0.022 S, 0.056 Ni, 0.15 Cr, 0.012 Mo, 0.21 Cu % wt). The trips were 50mm wide. One or two strip samples were recovered every 3 months for the first year of exposure, and every 12 months thereafter. The program is on-going. Strips were placed within 150 mm diam. open ended PVC tubes (test pods) (Fig. 1). They were held in place with non-conductive nylon spacers to avoid contact between them along their whole length and thereby obviate any potential galvanic corrosion concerns. Upon recovery, strips were carefully visually inspected and transported to the University of Newcastle Civil Engineering Laboratories for further examination and analysis.

As noted above, one of the research questions was to ascertain the likely effect of microbiological activity on the corrosion losses over time. To investigate this the project used exactly the same sample arrangements in two quite separate exposure sites with all water chemistry parameters essentiallly similar except for dissolved inorganic nitrogen (DIN), the sum of the concentrations of ammonia, nitrate and nitrite (Table 1). Several of the other parameters in Table 1 may be influential in different corrosion processes with time [5,11]. However in this paper discussion is focused on the effect of DIN on longer term corrosion loss, noting the considerable magnitude difference in DIN between the sites.

Figure 1. (a) Schematic view of one test pod containing steel strip samples, (b) uPVC tubes at Taylors Beach at mid-tide and (c) uPVC tubes at Port of Newcastle at low tide.

Table 1. Water chemistry extracted from water samples taken at the test sites immediately adjacent to test pods.*

Parameter Exposure Site	**Taylors Beach (TB)**	**Port of Newcastle (PoN)**
Water Temperature (Annual Ave.)	~19-23 ºC	~19-23 ºC
Salinity	31.3 g/kg	29.4.-31.8 g/kg
Sulphates	2470 mg/l	2400 mg/l
Sulphides	< 0.1 mg/l	< 0.1 mg/l
pH	7.9	7.8
Total Dissolved Inorganic Nitrogen (DIN): Ammonia (NH_3) Nitrate (NO_3) Nitrite (NO_2)	~0.037 mgN/l 0.037 mgN/l <0.05 mgN/l <0.05 mgN/l	~0.290 mgN/l 0.20 mgN/l 0.09 mgN/l <0.05 mgN/l
Dissolved Oxygen DO)	8.07 mg/l **	8.01 mg/l **
Calcium (Ca)	399 mg/l	491 mg/l
Total Phosphorous (P)	0.28 mg/l	0.08 mg/l

< X denotes limit of discrimination.
* Water quality assessment was performed by an independent laboratory.
** DO content determined approx. 3 h after being transported to independent laboratory.

The next section elaborates on the likely DIN influence based on comparing corrosion loss trends over time, which in turn have been zoned, based on clear differences in sample corrosion morphology [7]. These are also presented and discussed in the next section.

Corrosion Observations and General Loss Results

The pattern of corrosion morphology for all the strips along their length was very similar, irrespective of exposure period (ranging from 12 months to 48 months). Representative views of the surface topography are shown in Figure 2. These are for approx. 100mm off-cuts that were numbered sequentially for identification prior to being guillotined from the strip, starting from the very top of each recovered strip. For each of the offcuts the corrosion products were removed using established standard chemical cleaning procedures [12].

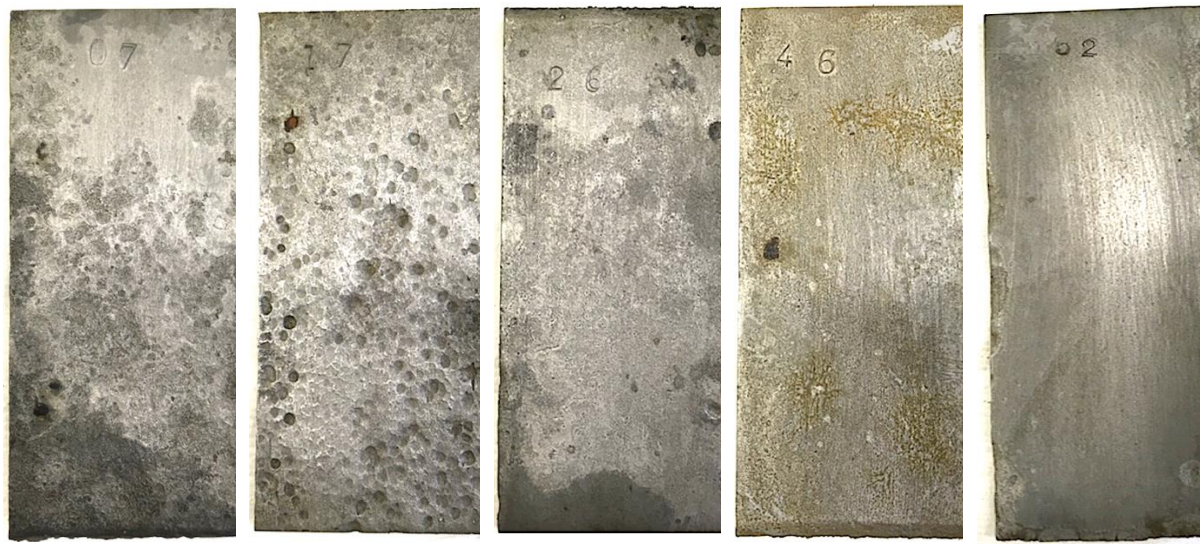

(a) Atmospheric (b) Tidal (c) Upper Immersion (d) Immersion (e) Buried / Soil

Figure 2. Representative views of the surfaces of cleaned segments after 12 months exposure in each of the exposure zones at the Port of Newcastle. Note the differences in surface morphology and the density of pitting, with the most severe pitting in the Tidal zone. Scale: Segment width: 50 mm. Upper immersion refers to the location one metre below mean-tide.

It has been postulated many times, by several authors, that the phenome of accelerated low water corrosion (ALWC) occurs in open sea waters, and for strips and other vertical steel surfaces within the first metre or two just below the low tide water level [5,10,11] with. ALWC usually evident as a band of noticeably increased corrosion losses. In Figures 3 and 4 a similar phenomenon is not evident for either of the test sites, regardless of exposure duration. For Figure 4 that shows corrosion losses for the site with increased DIN concentrations, there is an increase in corrosion losses after 24 months. This occurs for all exposure zones (i.e. immersion, tidal and atmospheric, shown in dark/light green, red and blue respectively). This behaviour in corrosion loss with time reflects the bi-modal corrosion behaviour observed in many longer term corrosion experiments and in practice [5]. It reflects a fundamental change in corrosion kinetics from aerobic to anaerobic [13] and also can relate to microbiological activity [5]. A similar behaviour for corrosion loss can be seen for the Taylors Beach site that has low DIN concentrations, even though comparatively it shows higher losses in the atmospheric band of the strips (Figure 3).

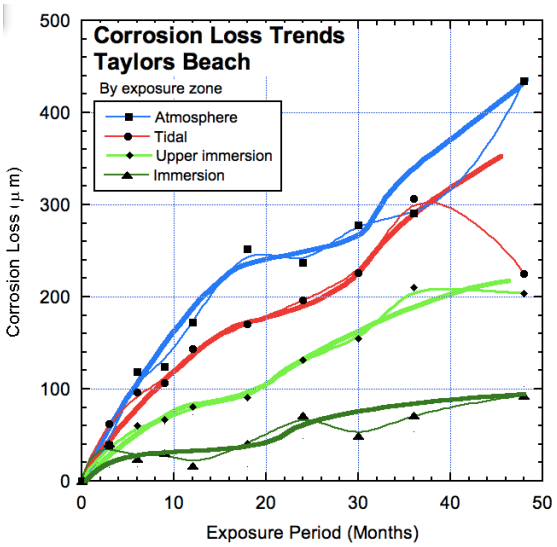

Figure 3. Development of corrosion loss with increased exposure period for strips at the Taylors Beach site (Chaves et.al 2022)

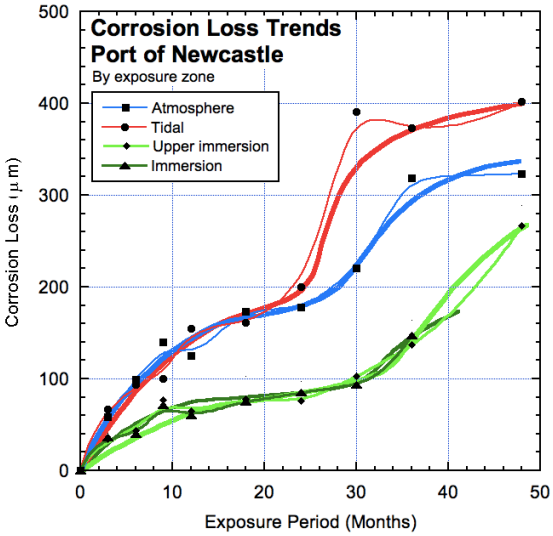

Figure 4. Development of corrosion loss with increased exposure period for strips at the Port of Newcastle site (Chaves et.al 2022)

Practical Implications for Design

The corrosion science likely involved in a near-stagnant environment has been considered elsewhere [7]. For practical situations, however, the matter of most importance is what the results in Figs. 3 and 4 and from the study overall are likely to mean for practical monopiles. This is considered by way of an example in the following.

Consider, as an example, a newly installed steel monopile with 80 mm wall thickness and expected to be serviceable for 25 years [14], although extended service life of 50 or even 100 years for offshore structures is often requested [1]. Let it be assumed, as is reasonable in practice, that the monopile remains unprotected, having no protective paint coatings or cathodic protection. Let it be assumed that failure of the monopile may be defined as visually observed excessive deformation of the monopile or through multiple ultrasonic thickness measurements with a 1/3 wall thickness corrosion cross-sectional loss. Assuming that long-term corrosion loss trends (i.e. >5 years) follow a relatively linear uniform behaviour, corrosion loss $c(t)$ over time t can be estimated from:

$$c(t) = cs + (rs * t) \quad (1)$$

where *cs* is the 'y-axis intercept' at time $t = 0$ and *rs* is the slope of the long-term trend [5]. The uncertainty of both cs and rs may bre modelled as Gaussian (Normal) with descriptive statistics shown in Figure 5. The random variables and their descriptive statistics for this exercise are shown in Table 2. It is important to note, however, that caution should be taken when decades long corrosion losses are estimated based on relatively short-term data. Water temperature, pollution levels, and other environmental changes such as deliberate perforation and or opening of the monopiles is likely to influence corrosion processes [5,9]. This indicates that to refine the approach used herein further research is required to obtain relevant long-term corrosion data (cf. [15]).

For determining the probability of failure the Monte Carlo technique [8] was used. It is sometimes considered a 'brute-force' but powerful method. In summary, corrosion loss for each year was each sampled one thousand times, and the number of times these estimates were higher than 1/3 of the original monopile wall thickness cross-section 'failure' was counted. The probability of failure is then estimated as the total number of 'failures' for any given year, divided by the number of cases sampled (i.e. 1000). Figure 6 plots such probability of failure, when considering external corrosion, and internal corrosion as well as with both losses combined. Considering that in structural limit state design, including for offshore infrastructure, the aim usually is to ensure a success rate (no-failure rate) of at least a 95% (or a maximum of 5% probability failure), the present results show that, although relatively small, there remains some influence of internal corrosion loss on overall probability of failure. Evidently, these results suggest that internal corrosion losses on their own do not make a significant contribution to structural risk (Figure 5). While this is based only on the results for 4 years exposure it is almost certain to apply for longer term exposures given that the corrosion rate is, for longer term exposures, linear. Evidently, internal corrosion should not be discounted. This may be particularly so if the internal environmental conditions are likely to change.

Table 2. Random variables, and their descriptive statistics, used for quantifying probability of a certain amount of corrosion being achieved at any given year.

Data Set	**Corrosion Loss Estimation Parameters (Gaussian Normal)**	
	***cs* (Normal)**	***rs* (slope)**
Internal Corrosion Losses (Based on Tidal zone pit depths) (Chaves et.al 2022)	Avg. 167.1 µm COV 7%	Avg. 15.8 µm COV 33%
External Corrosion Losses (Base on ALWC zone Pit depths) (Chaves et.al. 2016)	Avg. 502.1 µm COV 7%	Avg. 269.1 µm COV 58%
Combined Internal & External Corrosion Losses	Avg. 669.2 µm COV 7%	Avg. 284.9 µm COV 7%

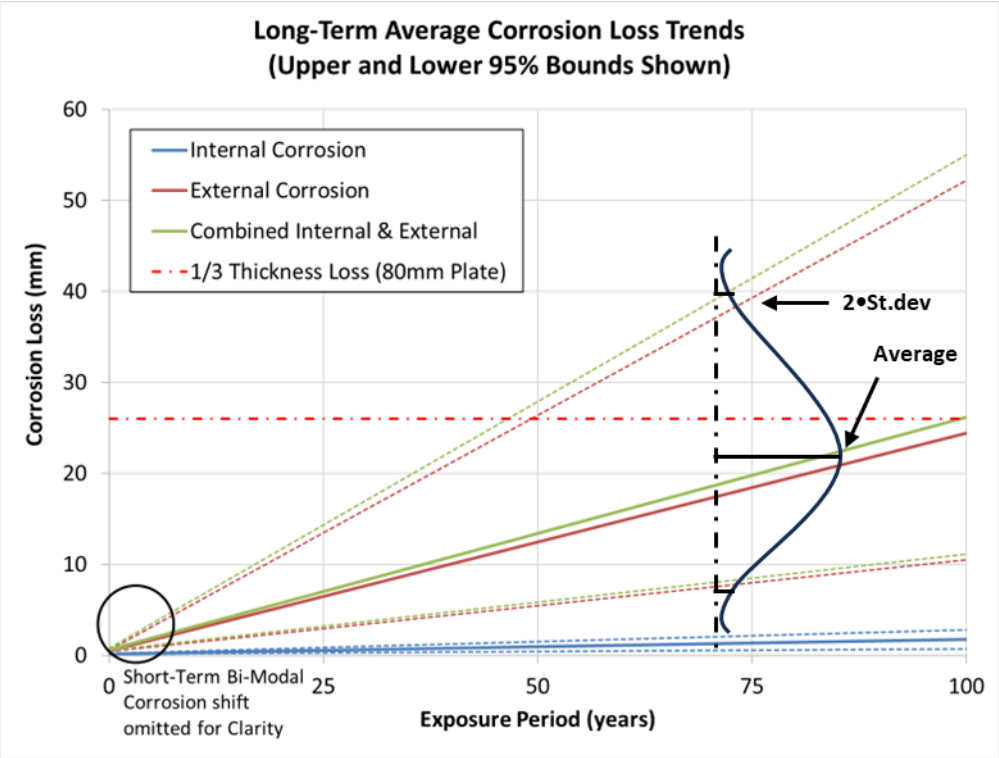

Figure 5. Internal (blue), External (red), and combined (green) long-term average corrosion loss estimated trends. Upper and lower 95% confidence bounds (i.e. 2 • St.Dev.) shown.

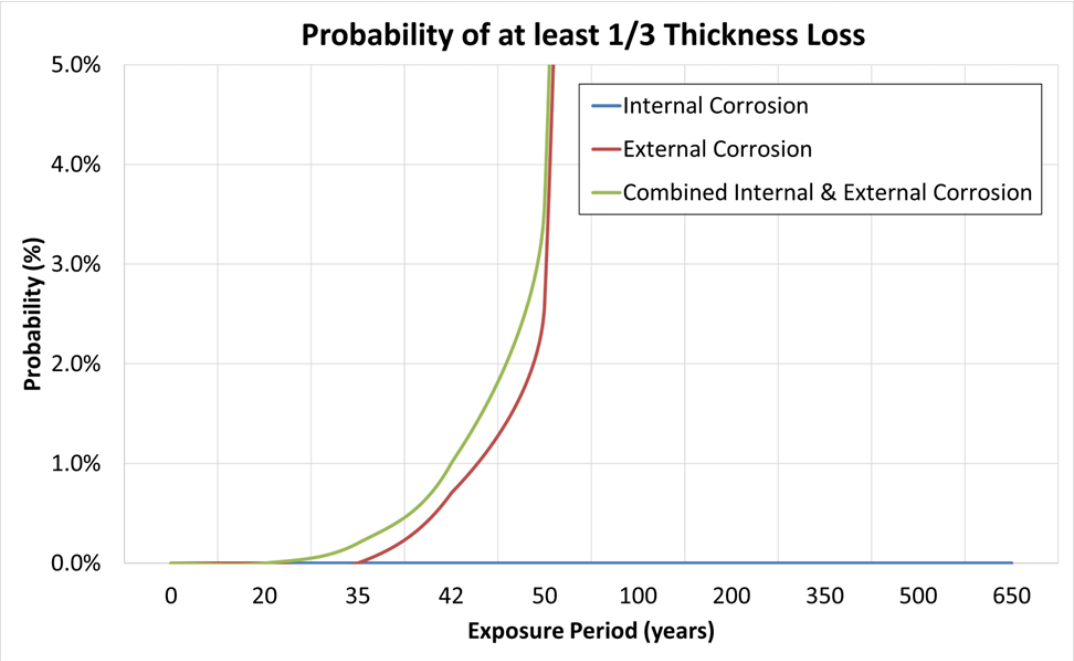

Figure 6. Estimated probability of failure based on internal corrosion data (blue), external corrosion data (red) and combined external and internal corrosion (green).

Further to the above comments, Figures 5 and 6 show that when considering internal corrosion losses alone (blue lines), there is very little risk of 'failure' being reached, even after a century of exposure. This is the case even when considering the worst-case scenario of considering extreme pit depth data collated from the internal tidal zone data set. If external corrosion data is considered then further from Figure 5, when extreme cases are considered with an approx. 5% chance (i.e 95% upper boundary) of occurring, it would still be about 30 years until 'failure' is reached. In this context it is important to note that future environmental conditions are also uncertain, particularly if openings and or other maintenance works lead to a change in microenvironment within the interior. If changes were to occur, it would affect the data, thus the statistics, and thus the probability estimations.

Although not quantified in this example, the possibility remains that internal corrosion and external corrosion zoning align vertically for a given hollow offshore structure. Considering that often water levers between the inside and outside of a hollow offshore pile are slightly offset in time, it is plausible that the two worst corrosion zones align. This is why the combined scenario was considered in the present example. Figure 5 suggests that little effect can be seen for the alignment of corrosion zones. In Figure 6, however, when the combined data losses are considered for the overall corrosion estimation, the probability of failure starts to increase about 15 years earlier than if it was omitted from the calculations. Nevertheless, the increase in probability of failure is not particularly significant to warrant intervention. Irrespective of these observations, it would be prudent for asset owners to perform periodic monitoring of the internal conditions to ensure no major changes have occurred, particularly as might influence microbiological activities as these can lead, in combination with external ALWC conditions, to a considerable increase in overall corrosion losses.

Conclusions

The main conclusions are:

1. Unlike the marine corrosion of conventional vertical steel infrastructure such as sheet piling exposed to open water conditions, the corrosion of vertical steels in enclosed tidal exposure conditions shows that the most severe corrosion occurs near the top of the tidal zone.

2. The more severe corrosion near the top of the tidal zone was observed already for quite early exposures and became relatively more severe with increased exposure period.

3. Corrosion losses over the whole corrosion loss profile as a function of elevation increase with the increased concentration of dissolved inorganic nitrogen (DIN) in the seawater, consistent with DIN being a critical nutrient for MIC.

4. Internal corrosion losses should not be ignored given the possibility that the most severe external and most severe internal corrosion zones could align, thereby noticeably increasing the probability of prematurely reaching unsafe levels of remaining cross-sectional strength.

Acknowledgements

The Australian Research Council is acknowledged for the financial support provided for this project (grant G1500081). The valuable continuous support of the Fisheries Research Station at Taylors Beach (Department of Primary Industries, NSW) and the Port of Newcastle is much appreciated.

References

[1] J.K. Paik and R.E. Melchers, "Condition assessment of aged structures", Cambridge: Woodhead Publishing Ltd (2008).

[2] S. Degraer, A. D.A. Carey, J.W.P. Coolen, Z.L. Hutchison, Offshore Wind Farm Artificial Reefs Affect Ecosystem Structure and Functioning, A synthesis, Special Issue on Understanding the effects of offshore wind energy development on fisheries, 33:4 (2020) 48-58.

[3] A. Durakovic, Offshore Wind Projects in Celtic Sea, Offshore Wind business (2022), www.offshorewind.biz, accessed in May 2022.

[4] R. Jeffrey and R.E. Melchers, Corrosion of Vertical mild steel strips in seawater, Corrosion Science, 51 (2009) 2291-2297.

[5] R.E. Melchers, Long-term immersion corrosion of steels in seawaters with elevated nutrient concentration, Corrosion Science, 81:1 (2014) 110-116.

[6] R.E. Melchers, A review of trends for corrosion loss and pit depth in longer-term exposures, Journal of Corrosion Materials and Degradation, 1:4 (2018).

[7] I.A. Chaves, R. Petersen, R.E. Melchers and R. Jeffrey, Corrosion of the interior steel surfaces of offshore monopiles, Journal of Ships and Offshore Infrastructure, (2022) 1-10.

[8] R.E. Melchers and A.T. Beck, "Structural Reliability Analysis and Prediction", Wiley 3rd Edition (2017) 502.

[9] I.A. Chaves, R.E. Melchers, L. Peng and M.G. Stewart, Probabilistic remaining life estimation for deteriorating steel marine infrastrucgure under global warming and nutrient pollution, Journal of Ocean Engineering 126 (2016) 129-137.

[10] R.E. Melchers and R. Jeffrey, Corrosion of long vertical steel strips in the marine tidal zone and implications for ALWC, Journal of Corrosion Science, 65:1 (2012) 26-36.

[11] R.E. Melchers, Modelling of marine immersion corrosion for mild steel and low-alloy steels Part 1: phenomenological model, Corrosion Science, 59 (2003) 319-334.

[12] ASTM G1-03, (2011) Standard practice for preparing, cleaning and evaluating corrosion test specimens. West Conshohocken (PA): American Society for Testing and Materials

[13] R.E. Melchers and R. Jeffrey, The transition from short- to long-term marine corrosion of carbon steels, Corrosion, 78 (2022) (5) 415-436.

[14] S. Anandavijayan, A. Mehmanparast and F. Brennan, A numerical analysis of the effects of manufacturing processes on material pre-strain in offshore wind monopiles, Journal of Structural Integrity, 13 (2018) 953-958.

[15] R.E. Melchers Corrosion of steels and irons immersed in natural seawater for up to 600 Y, Corrosion 78 (2022) (1) 87-95.

Marine corrosion of low alloy steel in natural seawater: role of Cr, Al, Cu and Ni

C. Rémazeilles, M. Serjaouan, Ph. Refait

Laboratoire des Sciences de l'Ingénieur pour l'Environnement (LaSIE),

UMR 7356 CNRS- La Rochelle Université, France.

Carbon steel and low alloy steel coupons were immersed for 3-6 months in natural marine medium (Les Minimes harbor – Atlantic Ocean, La Rochelle, France). The low alloy steels considered here contained 1 wt.% Cr and 0.5 wt.% Al (AMLC) or 0.6 wt.% Cu and 0.4 wt.% Ni (A690). The corrosion processes were studied by open circuit potential measurements, electrochemical impedance spectroscopy (EIS) and polarization resistance (R_p) measurements. At the end of the experiments, the corrosion product layers were characterized by µ-Raman spectroscopy and X-ray diffraction.

R_p measurements showed that the resistance to corrosion of A690 low alloy steel was similar to that of carbon steel, i.e., the addition of small amounts of Cu and Ni has no effect (neither beneficial, nor detrimental). In contrast, the AMLC low alloy steel showed improved resistance to corrosion, with R_p values increased by 40-100% with respect to carbon steel. The analysis of the corrosion product layers after 3 and 6 months of immersion illustrates the influence of fouling. After 3 months, the layer covering the steel surface was made of a mixture of corrosion products and minerals coming from the environment (quartz, clay and calcite coming from shells). After 6 months, the XRD analysis only revealed the fouling, which covered the corrosion product layer and had to be removed for further analysis. The underlying corrosion product layer then proved in any case mainly composed of magnetite (Fe_3O_4), green rust compounds and FeS; Fe(III)-oxyhydroxides were hardly seen. The predominance of Fe(II) and Fe(II-III) phases is typical of de-aerated conditions. This shows that the outer layer of fouling, enriched with aerobe micro-organisms, prevented dissolved O_2 to reach the underlying corrosion product layer as soon as 6 months of immersion. FeOOH phases were only detected in significant amounts for the AMLC low alloy steel, confirming that the combined influence of Cr and Al increases the stability/adhesion of an outer protective layer of Fe(III)-oxyhydroxides [1].

Reference:

[1] Ph. Refait, T. Urios, M. Jeannin, A. Fagot, R. Sabot, Mater. Corros. 70 (2019) 985-995.

Marine corrosion of low alloy steel at 25°C and 45°C: role of Al, Cr and Mo

M. Serjaouan, C. Rémazeilles, Ph. Refait

Laboratoire des Sciences de l'Ingénieur pour l'Environnement (LaSIE),

UMR 7356 CNRS- La Rochelle Université, France.

Many technical systems involve seawater at various temperatures, for instance heat exchangers. Marine corrosion of steel has been extensively studied but mostly in the range of average temperatures of the sea surface, i.e., between 0°C and 30°C. In the present study, the corrosion processes of various carbon and low alloy steels in seawater at controlled temperatures of 25°C and 45°C were investigated. During the two-month immersion in gently stirred natural seawater (sampled from the Atlantic Ocean), linear polarization resistance measurements and EIS were used to monitor the evolution of the corrosion system with time. At the end of the experiment, the corrosion product layers covering the steel surfaces were characterized by XRD and μ-Raman spectroscopy.

For both temperatures, the considered low alloy steels, containing 1 wt.% Cr plus 0.5 wt.% Al or 0.2 wt.% Mo proved to have a better resistance to corrosion than carbon steel; the R_p values were doubled with the addition of the alloying elements. In any case, the increase of temperature from 25°C to 45°C favored the formation of magnetite (Fe_3O_4) at the detriment of Fe(III)-oxyhydroxides. For carbon steel, the corrosion product layer formed at 45°C was then composed of magnetite, with γ-FeOOH (lepidocrocite) and carbonate green rust present as minor components. The corrosion product layers of the Cr and Al containing low alloy steel proved enriched in γ-FeOOH, which formed a protective outer layer on top of an inner layer composed of magnetite, with traces of green rusts. This result is consistent with a previous study performed in stagnant artificial seawater at room temperature (12°C to 25°C) [1]. For the Cr and Mo containing low alloy steel, the corrosion product layer was heterogeneous at both temperatures, which can be attributed to the presence of persistent cathodic and anodic areas on the steel surface.

Reference:

[1] Ph. Refait, T. Urios, M. Jeannin, A. Fagot, R. Sabot, Mater. Corros. 70 (2019) 985-995.

Corrosivity model for marine atmospheric corrosion

Bahman Daneshian,Helmholtz-Zentrum Hereon, Max-Planck-Straße 1, 21502 Geesthacht, Germany

Daniel Höche,Helmholtz-Zentrum Hereon, Max-Planck-Straße 1, 21502 Geesthacht, Germany

Ole Øystein Knudsen, SINTEF Industry, Richard Birkelandsvei 2B, N-7465 Trondheim, Norway

Anders Werner Bredvei Skilbred, Jotun Performance Coatings, Hystadveien 167, 3202 Sandefjord, Norway

Background

A reasonable estimate of corrosivity is essential for coatings selection and its durability assessments in marine atmospheric environments. A dose-response model for calculating the corrosivity of steel is given in ISO 9223, based on the annual average temperature, relative humidity, chloride deposition, and sulphur oxide deposition. However, the model is not easily applicable due to the limited data for chloride and sulphur oxide deposition rates. The Arrhenius equation has been used to predict the rate of chemical reactions as a function of temperature. However, in the Arrhenius equation, influences of relative humidity and atmospheric contaminations are not considered. The Eyring equation however, allows us to include these parameters.

Objectives

The objective with this study was to develop a corrosivity model based on the Eyring equation from a sensor-based dataset, including air temperature, relative humidity, wind and precipitation.

Results

The data were measured along with the corrosion current from a sensor developed by Luna Innovations. The sensor was exposed very close to the sea, so the high corrosivity is expected to be governed by chloride deposition. Chloride deposition data at this site was not available. Instead, wind speed and direction were used, which improve the accuracy of the corrosivity model. Deposition of sulfur dioxide at this site is about 200 mg/m²/year (Norwegian Environment Agency), which was assumed to be

negligible with respect to corrosion. The effects of air temperature, relative humidity, wind speed, and precipitation were added step vice and their influences on the accuracy of the model were investigated. Applying suitable boundary conditions for each accelerating parameter is key to the Eyring approach. These boundary conditions were determined by plotting the measured corrosion rate versus each parameter. For example, sensor measurements showed that the corrosion rate decreased both at low and high temperatures, due to freezing and evaporation. The applied boundary condition for each parameter must take such phenomena into account.

Conclusions

The resulting corrosivity model showed very good correlation with the measured corrosion rate on the sensor. Fig. 1 shows a comparison between the model and the accumulated corrosion from the sensor. The coefficient of determination (R^2) was 0.98, which is a very good fit.

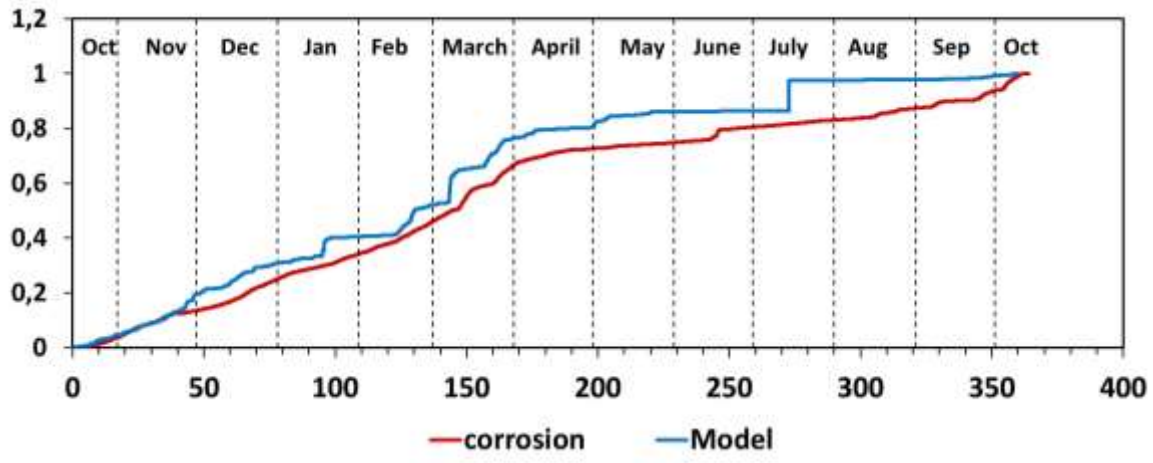

Fig. 1 correlation between the developed corrosivity model and the actual corrosion data over the time from 10.14.2020 until 10.14.2021. The applied parameters are (i) air temperature, (ii) relative humidity, (iii) wind speed and (vi) precipitation.

Marine atmospheric corrosion

Keywords; corrosivity, marine atmosphere, sensors, data analysis

Assessment of Damaged Thermal Spray Aluminium Coating in Synthetic Seawater by Using Complementary Techniques

Adriana Castro-Vargas, University of Leicester, Leicester/UK; NSIRC, TWI Ltd, Cambridge/UK; Universidad Tecnológica de Bolívar, Cartagena/Colombia
Shiladitya Paul, University of Leicester, Leicester/UK; TWI Ltd, Cambridge/UK

This work presents the results of a new method that uses complementary techniques such as in situ imaging and an analytical rotator combined with monitoring of Open Circuit Potential (OCP) to understand the performance of thermally sprayed aluminum (TSA) coating in simulated marine immersion service. The experimental work involves the evaluation of damaged TSA in quiescent and flowing synthetic seawater at room temperature. The coating (300 µm thick) was obtained by twin-wire arc spraying of 1050 aluminium alloy on a S355 carbon steel substrate.

In quiescent condition, TSA-coated steel samples were evaluated by the optical analysis of sequential images captured in-situ: (i) with defects machined before immersion (5% of exposed steel surface); and (ii) with a defect machined after 35 days of immersion (10% of exposed steel surface). The changes in the coating and defect were correlated with the evolution of the OCP during the 35-day immersion period. When the defect is machined before the immersion, initial dissolution of iron occurs until the air-formed oxide layer degrades, the electrolyte penetrates the coating, and the aluminium surface is activated. Conversely, when the defect is created after immersion, the aluminium activates rapidly, and the system reaches the range of protective potentials (according to DNV-RP-B401) providing immediate protection to the exposed steel.

In flowing synthetic seawater, rotating cylinder electrodes made of carbon steel were coated, and a scratch defect was created on the coated surface, exposing the substrate. TSA-coated steel samples were tested at a rotation speed of 50 RPM (3 cm/s) in parallel with the evolution of OCP. The flow velocity delayed the formation of the calcareous deposits on the exposed steel, but TSA was able to provide effective cathodic protection. The penetration time of the electrolyte in the porous coating and the activation of the surface are key to the protection mechanism and the kinetics of corrosion.

Development of a mobile instrumented test bench for in-situ assessment of biocidal treatments of seawater

Julie Flambard, Julie Rosec, Kada Boukerma, Jean-Luc Simon,
Anne-Marie Grolleau, Françoise Dubois
Naval Group Cherbourg, IFREMER Brest

Biocidal treatments are widely used in industry to prevent the development of biofouling which has a detrimental effect on thermal efficiency of seawater heat exchangers. Levels of biocidal substances must be lowered to limit environment impact and potential corrosion issues due to the use of high oxidizing treatments on metallic materials.

A mobile test bench equipped with a dozen of heat exchanger models and a wide range of instrumentation has been designed and built in order to assess the biofouling development and its effect on heat transfer resistance. The instrumentation consists in flowmeters, temperature probes, biofouling sensors and automatic chlorine analysers. The seawater feeding heat exchanger models can be treated either by chlorination or ozonation.

The test bench has been located in IFREMER site at La Martinique (French Antilles) for several test campaigns, as part of the SIMBIOSE project, with the support of the European Maritime and Fisheries Fund. Some alternatives to lower the amount of biocidal substances while ensuring an efficient heat transfer have been identified. Besides helping industries to reduce their environmental impact, these solutions also will help to minimize corrosion issues on metallic materials.

Hyperspectral Imaging as a Technique to Detect and Monitor The Corrosion of 2101 Lean Duplex Stainless Steel

A. Kablan[1], A. Keane[2], J. Jabalza[2], P. Murray[2], D. L. Engelberg[1,3]

1. Materials Performance Centre – The University of Manchester

2. Electronic and Electrical Engineering - The University of Strathclyde

3. Corrosion and Protection Centre – The University of Manchester

Department of Materials, The University of Manchester, United Kingdom

Abdulaziz.kablan@postgrad.manchester.ac.uk

Abstract

Since the early development of hyperspectral imaging (HSI) in 1970's, the main use and application has been intended for environmental monitoring, agricultural, military, and food quality control. However, in recent years HSI has extended its application to biology and art, though with very little research into corrosion detection and monitoring. This paper intends to demonstrate the use of hyperspectral imaging in the UV-VIS-SWIR spectral range to detect and differentiate between different types of corrosion products, more specifically the different forms of iron oxy-hydroxides, namely haematite, maghemite, magnetite, lepidocrocite and goethite, due to the atmospheric corrosion of 2101 lean duplex stainless steel in marine environment. Moreover, Raman spectroscopy analysis together with powder x-ray diffraction phase ID of the pure phases has been used to verify and confirm the presence of the aforementioned iron oxy-hydroxides.

Keywords: Hyperspectral Imaging, Corrosion Performance, Atmospheric Corrosion, Raman Spectroscopy, Powder X-Ray Diffraction, 2101 Lean Duplex Stainless Steel, Iron Oxide-Hydroxide.

Corrosion monitoring and modelling in three industrial settings: ports, port industry and on board.

Wikke Witteveen[1,2], Joeri Horvath[1], Katrijn Verhasselt[1,2], Raf Meskens[1,2], Kris De Baere[1], Silvia Lenaerts[2], Marjolein Vanoppen[3], Geert Potters[1,2]

[1]Antwerp Maritime Academy, Antwerp, Belgium

[2]University of Antwerp, Antwerp, Belgium

[3]UGent, Ghent, Belgium

Corrosion of structural steels and stainless steels in an aquatic environment is a complex phenomenon, driven by a non-linear interplay of various physicochemical causes, such as temperature, pH, salinity and oxygen concentration. This interaction is further modulated by the activity of different bacterial consortia. The SOCORRO project (www.socorro.eu), therefore seeks to assess the environment rather than focusing on corrosion itself - using physicochemical and microbial parameters that determine the risk of corrosion as markers instead of causal factors. The accumulated corrosion risk can then be determined by measuring environmental markers over time, thereby allowing for planned inspections and maintenance or to provide data in relation to lifetime expansion.

To explore the relation between the environment and corrosion, machine learning and a correlation analysis are conducted by measuring environmental markers and corrosion in several industrial settings to generate an extensive dataset. More specifically, three relevant industrial demonstrations are discussed in this presentation: process water in the petrochemical industry in Antwerp, port infrastructure in Ostend (Belgium) and Flushing (The Netherlands) and the engine room of a merchant vessel in the Persian Gulf.

Sensor units were placed in these settings to generate abovementioned dataset, over the course of six to nine months. Corrosion rates were obtained from frequent mass loss measurements (using steel coupons of Grade A S235 carbon steel, S355 carbon steel and 316L stainless steel) and as well as half hourly corrosion rate determination by linear polarization measurement. Environmental markers (dissolved oxygen,

temperature, conductivity, pH, chloride content, redox potential and chlorophyll) were measured half hourly as well with a commercially available multiprobe (Scuba90).

Insights into the most prominent corrosion markers, the main difficulties of performing long term linear polarization measurements (and potential differences between measuring methods) and the main difficulties of measuring environmental parameters in these industrial environments are presented.

Effects of Microstructural Features on Microbiologically Influenced Corrosion (MIC) of Copper 101 caused by *Oleidesulfovibrio alaskensis* G20

Amit Acharjee, Iwona Beech, Roberta Amendola

Montana State University, Bozeman, MT, USA.

Abstract:

Despite having a long record of research work, there are still a lot of unknowns in the study of Microbiologically Influenced Corrosion (MIC). Sulfate reducing bacteria (SRB), found in a broad range of anaerobic environmental conditions like deep subsurface, soil, shallow marine and freshwater sediments, were found to be responsible for almost half of all MIC related cases. Copper is widely used in infrastructures. However, despite its use as antimicrobial agent, copper is susceptible to MIC which shows that the fundamental interactions between microorganisms and metals are still not fully understood. The predominant trend of MIC research is to focus largely on the effects of microorganisms on the metal, resulting in a lack of studies where intrinsic properties of the substrate material (e.g., microstructure) are considered. This work evaluates the effects of microstructural features such as grain boundary distribution and residual stresses on copper MIC severity caused by exposure to the SRB species *Oleidesulfovibrio alaskensis* G20. Surface characterization was conducted before and after exposure in both biotic and abiotic environments. Field Emission Scanning Electron Microscopy (FE-SEM), Energy Dispersive X-Ray (EDX) and X-ray Diffraction Analysis (XRD) were used to investigate corrosion morphology and product development. Electron Back Scattered Diffraction (EBSD) combined with scanning Auger Electron Nanoprobe was used to investigate the grain boundary structures, strain distribution and surface potential in the copper surface before exposure to MIC environment, to then assess the damage after exposure. By including and investigating substrate dependent factors, results from this work aid in elucidating the underlying mechanism of copper MIC and may represent an inexpensive and novel approach to mitigate MIC.

The effect of alloying on microbially influenced corrosion and biofouling of stainless steels in Baltic Sea brackish water

Vilma Ratia-Hanby, Andressa Trentin, Maija Nuppunen-Puputti, Quynh Nguyen, Malin Bomberg, Elina Huttunen-Saarivirta, Pauliina Rajala

VTT Technical Research Centre of Finland Ltd., Espoo, Finland

Biofouling, unwanted biofilm growth on surfaces, can cause severe problems in a wide range of systems. For example, in industrial cooling circuits utilising natural water, biofouling can cause pipe blockages and lowered heat exchange capability of the system. Another example of a loss of efficiency due to biofilms is the increase in fuel consumption of ships through grown ship hull drag. Biofouling can also contribute to the initiation of microbially influenced corrosion (MIC), which can cause usability and safety issues due to the loss of material integrity.

The objective of this study was to define the behaviour of various stainless steel grades exposed to Baltic Sea water to determine the effect of alloying on biofouling and MIC in brackish water. Grades EN 1.4016 (main alloying element Cr 16-18 wt%), EN 1.4162 (main alloying elements Cr 21-22 wt%, Mn 4-6 wt%, Ni 1.35-1.70 wt%) and EN 1.4462 (main alloying elements Cr 21-23 wt%, Ni 4.5-6.5 wt%, Mo 2.5-3.5 wt%, Mn <2 wt%) were selected as materials. The samples were placed in natural Baltic Sea brackish water in a pilot scale water cycle, which allowed their monitoring through electrochemical techniques during the four-month exposure. Open circuit potential (OCP) and electrochemical impedance spectroscopy (EIS) measurements were conducted across the duration of the exposure, and cyclic polarisation curves were obtained at the start and finish of the experiment. After the exposure, the samples were examined with microscopy (optical and scanning electron microscopy) and molecular microbiological methods (qPCR and amplicon sequencing).

The OCP curves revealed that eventually all studied materials underwent ennoblement, but that the rate of this varied. In turn, the EIS results indicated that all the alloys had similar outcomes with short cycles of repassivation after pitting corrosion. Differences in corrosion behaviour were indicated by the cyclic polarisation curves, which showed differences in pitting susceptibility both between the materials

and their response to exposure. In this work, these results will be discussed with findings obtained with the microbiological methods and microscopy.

Influence of intermetallic particles for the natural formation of a protective layer on aluminum alloy 5083 in marine environment

J. Jaume[a], MJF Marques[a,b], M.L. Délia[a], B. Fori[c], R Basséguy[a]

a. Laboratoire de Génie Chimique, Université de Toulouse, CNRS, INPT, UPS, Toulouse, France

b. LMR – Laboratório de Materiais e Revestimentos, LNEG – Laboratório Nacional de Energia e Geologia, Lisboa/Portugal

c. Mecaprotec Industries, Muret /France ;

The new REACH regulations require to search new solutions to protect efficiently aluminum alloys without using hexavalent chromium. The MICOATEC project aims to meet this expectation by studying the natural biomineralization that can occur in the marine environment. The study of this phenomenon has already allowed to highlight the development of a protective layer on the surface of the 5083 aluminum alloy[1,2]. Observations performed during the formation of this layer show, however, that this layer does not develop homogeneously over the whole surface. The created layer can therefore present defects, decreasing the protection it provides. Thus, it is crucial to control all the parameters to allow the development of a more homogeneous layer. The grinding preparation, carried out before the formation of the layer, reduces the influence of surface irregularities. Nevertheless, in the same time, it removes the natural passive layer, which exposes reactive intermetallic particles to the aqueous medium. These particles have a potential significantly different from that of the alloy matrix and can therefore act on the electrochemical reactions in their vicinity. The aim of this work is to study the influence of intermetallic particles during the development of the protective layer in the presence of marine microorganisms.

The experiments consist in forming the layer by immersing a 5083 aluminum alloy electrode for 21 days in an aerated mixture of seawater and salt marsh sediment. In order to observe the role of intermetallics, three different surface treatments were performed on the electrode, prior to the immersion: 1) a 240 grit grinding, 2) a 240 grit grinding followed by an etching procedure and 3) a 240 grit grinding followed by an anodization. The etching procedure removes intermetallic particles and the anodizing process is one of the industrial reference treatments for aluminum alloy.

Several electrochemical analyses (OCP, EIS, polarization resistance) were performed during and after immersion to study the surface modification that led to the formation of the protective layer. Additionally, the electrodes were characterized by SEM observations and surface analysis (EDX, DRX ...).

The major result indicates that the layer is more homogeneous when the grinding is followed by an etching procedure, compared to a simple grinding. No layer has been developed on the ground & anodized electrode. The further analysis has allowed a better understanding of the formation mechanisms of the protective layer and the influence of intermetallic particles.

This work was financially supported by the ANR, in the framework of the MICOATEC project (ANR-19-CE08-0018).

(1) Jaume, J.; Marques, M. J. F.; Délia, M. L.; Basséguy, R. Surface Modification of 5083 Aluminum-Magnesium Induced by Marine Microorganisms. *Corrosion Science* **2021**, 109934. https://doi.org/10.1016/j.corsci.2021.109934.
(2) Marques, M. J. F.; Mercier, D.; Seyeux, A.; Zanna, S.; Marcus, P.; Basséguy, R. Effect of Marine Microbial Activity in Corrosion Inhibition of 5083 Aluminium Alloy. In *Oral presentation at EUROCORR 2022*; Berlin, 2022.

Surface faceting evolution and effect of grain size on microbially influenced corrosion behaviors of low-carbon steel AH36 by *Desulfopila corrodens* in artificial seawater

Ruiliang Liu[a,b], Nicolò Ivanovich[a,c], Xiaogang Wang[b], Yee Phan Yeo[a], Yang Chen[b], Matteo Seita[b,d], Federico M. Lauro[a,c,e]

a. Singapore Centre for Environmental Life Sciences Engineering, Nanyang Technological University, 60 Nanyang Drive, 637751, Singapore

b. School of Mechanical and Aerospace Engineering, Nanyang Technological University, 50 Nanyang Avenue, 639798, Singapore

c. Asian School of the Environment, Nanyang Technological University, 62 Nanyang Drive, 637459, Singapore

d. Department of Engineering, University of Cambridge, Trumpington Street, Cambridge CB2 1PZ, UK

e. Nanyang Environment & Water Research Institute (NEWRI), Nanyang Technological University, Cleantech ONE, 1 Cleantech Loop, 637141, Singapore

The influence of metallurgical features on microbially influenced corrosion (MIC) in low-carbon steel exposed to sulfate-reducing bacteria (SRB) in artificial seawater (ASW) is largely unexplored. In this study, we analysed the onset and rate of MIC on AH36 steel coupons with a wide range of grain sizes in ASW with *Desulfopila corrodens* strain IS4. Our research activities include analysing the microstructure of coupons, the extent and morphology of MIC upon coupons as a function of time using a number of novel imaging modalities and electrochemical testing techniques. The preliminary results indicate that the resistance to MIC of AH36 steel decreased with the increase in grain size. In addition, we observed a crystallographic orientation-controlled MIC dissolution process for the AH36 under the testing condition, and we identified the (100) type facet evolution during the MIC. The findings herein outline the relationship between the microstructural and MIC behaviours features of low carbon steel AH36 by *Desulfopila corrodens* in ASW. The findings also have significant implications on designing low carbon steel materials with enhanced resistance to MIC for marine application-fully understanding and hence better designing of materials.

Electrochemical Behavior and Microbiologically Influenced Corrosion Susceptibility of AISI 304 Stainless Steel Exposed in a Fresh Industrial Water

Yasuyuki MIYANO, Kotaro TAI, Akita Univ. Akita/Japan,
Shun TOKITA, Tohoku Univ. Sendai/Japan,
Toshiyuki SUNABA, Hirotaka MIZUKAMI, INPEX, Tokyo/Japan,
Satoshi WAKAI, JAMSTEC, Yokosuka/Japan

In our previous study, we analyzed the microbiome formed on the material surfaces of some structural materials exposed in a freshwater environment where MIC (microbiologically influenced corrosion) risk was suspected, then confirmed a tendency for high abundances of electrochemically active bacteria on some corrosion resistant materials.

As for the cause of ennoblement of stainless steel in fresh water, it has been reported that metabolites of microorganisms accelerate the consumption of electrons at the cathode. However, the actual state of the microbiome that leads to the ennoblement and the dynamics of the microbiome associated with the formation of anodes and cathodes have not yet been clarified.

In this study, an electrochemical cell with stainless steel as the sample electrode and counter electrode was placed in a lab-scale continuous culture system capable of maintaining microbial activity. The electrochemical cell was composed of a three-electrode system with a saturated Ag/AgCl electrode as the reference electrode (R.E.), an as-received AISI 304 stainless steel (304 SS) as the counter electrode (C.E.), and a sensitized 304 SS, electrochemical potentiokinetic reactivation ratio: 39%, as the working electrode (W.E.). The test solution was prepared by adding NB (nutrient broth) medium to the sampled fresh industrial water and adjusting the concentration to 0.1 v/v %. In addition, we prepared the system using sterilized water as abiotic control. In those experimental system, the potentials of both the W.E. and C.E. and the current density between them were measured during polarization. After the electrochemical test, NGS (Next generation sequence) analysis of the microbiome on the surfaces of both the W.E. and C.E. and test solution was also performed.

From the start of exposure test, the open circuit potentials of the sensitized material and the as-received material were measured separately, and the period until

the potential of the sensitized material exceeded that of the as-received material was used as the precursor duration to the start of polarization. Anodic polarization at 0.1 mV/min and constant potential polarization were then arbitrarily performed.

The potential of the sensitized material was lower than that of the as-received material at the initial. However, it ennobled quickly, and exceeded the potential of the as-received material at approximately 80 hours after the start of the exposure. After 120 hours-incubation, anodic polarization test was conducted. In the anodic polarization test, a rapid increase in the current density was observed when the potential of the C.E. reached -250 mV vs. Ag/AgCl. Because this behavior was not observed at all in the abiotic control, the involvement of microbial activity was suspected.

After that, biofilm formed on the surfaces of C.E. and W.E. were swabbed and the planktonic microbial cells in the test solution were collected using a membrane filter. From the cotton swab and membrane filter, DNAs were recovered using a commercial DNA extraction kit, and then partial 16S rRNA gene fragments were successfully amplified by PCR. Microbiome analysis by amplicon sequencing using these gene fragment is currently under investigation.

The study of microbially-influenced corrosion of carbon steel in North Sea oilfields installations: investigating metabolomes, microbiome and material microstructure

Iwona B Beech[1], *Jan A. Sunner*[1], *Turid Liengen*[2], *Matthew Fields*[1], *Solfrid Molid*[2], *Vincent Gregoire*[2]

[1] *Center for Biofilm Engineering, Montana State University, Bozeman, USA*

[2] *Equinor ASA, Norway*

Laboratory experiments using stagnant anaerobic batch reactors were carried out to determine whether corrosion of X--60 and X-65 grade carbon steels varied when the alloys were exposed to metabolically and genomically diverse pigging debris collected from two carbon steel production pipelines that differed in corrosion (low corrosion-LC and high corrosion-HC). Both pipelines are in the Norwegian Sector of North Sea.

Coupons manufactured from the X-65 and X-60 grade pipe material were inoculated with aqueous suspensions of debris representing outermost and innermost pigging material recovered from each pipeline system. Coupons exposed in debris-free, sterile reactors served as controls. Pigging material was analyzed using metabolic profiling with advanced mass spectrometry techniques. The debris harbored complex bacterial and archaeal microbiomes. Sulfidogenic microbiome was dominant in the HC system, while nitrate reduction and balanced sulfur cycling characterized microbiome from the LC pipeline.

The results of light and electron microscopy analysis demonstrated marked differences in steels microstructure and corrosion morphology and its severity between test coupons exposed to LC- and HC-debris, as well as between the innermost- and outermost- pigging material from the same system. In both the LC and the HC systems, more pronounced corrosion was noted when using the innermost pigging material as reactors inocula, irrespective of the steel grade.

The study revealed that (i) metabolomic profiling discriminated between the severity of corrosion, thus can serve as a tool in corrosion management of oilfield installations, (ii) the choice of field samples is of paramount importance when conducting laboratory investigations aimed to confirm whether and to what extent MIC is a threat, (iii) the analysis of material microstructure is of paramount importance for MIC prediction and its mitigation.

The effect of the hydrogenotrophic methanogens on the phosphate production of copper alloys: a structural and electrochemical study

Giorgia Ghiara, Università degli Studi di Milano, SEPA Milano (Italy)
Elena Cazzulani, Università degli Studi di Milano, Department of Chemistry, Milano (Italy)
Alessia Aiello, Università degli studi Milano Bicocca, DISAT, Milano (Italy)
Andrea Franzetti, Università degli studi Milano Bicocca, DISAT, Milano (Italy)
Gian Luca Chiarello, Università degli Studi di Milano, Department of Chemistry, Milano (Italy)
Pierangela Cristiani, Ricerca sul Sistema Energetico – RSE, Milano (Italy)

The interaction between microorganisms and metallic materials is one of the primaries focuses of the corrosion sector [1]. Over the past few years, there has been a shift in focus regarding MIC towards the Archaea domain, specifically targeting methanogens. These microorganisms have a detrimental effect on the pipelines within the natural gas network, resulting in damage to both the supply and distribution systems. In environments lacking oxygen, as copper gas piping systems, these microorganisms are one of the most common species detected, but rarely considered as possible promoters of MIC via methanogenesis. In CO_2-rich conditions and with H_2 available they use the metallic substrate (i.e. copper or its alloys) as a source of electrons to produce methane. Phosphates can thus precipitate as a byproduct of the methanogenesis as sometimes reported in literature studies on carbon steel alloys: they create a barrier that protects the metal from further corrosion. However, this inhibition mechanism (MICI) is still not well understood and never reported for copper alloys so far.

The purpose of this study is therefore to characterize, at a laboratory level, the role of a distinct group of hydrogenotrophic methanogens of the *Archea* domain on the corrosion behavior of two copper alloys (electrolytic Cu and duplex 60:40 brass), specifically related to the precipitation of phosphates. Through replicated two-week tests, we documented the corrosion caused by methanogens-enriched media compared to sterilized media. To conduct our investigations, we utilized a three-electrode cell comprising a working electrode (representing the test alloy), a reference electrode (3M Ag/AgCl electrode), and a counter electrode (titanium mesh). Our

research involved monitoring the open circuit potential (OCP) and performing electrochemical impedance spectroscopy (EIS) to distinguish the effect of microorganisms on the single time constants of the corrosion process. To detect the nature of corrosion products and possibly distinguish the composition of the phosphates produced, SEM and micro-Raman spectroscopy (μRS) were utilized. To identify target microorganisms as *Metanobacter* present in the microbial communities for each case, molecular analysis using next-generation sequencing (NGS) of 16S RNA was performed. Results not only evidenced a different electrochemical behavior according to the considered alloy (Mic of copper and MICI for duplex 60:40 brass), but also the presence of different phosphates according to the alloy composition and evolution of the pH at the interface metal/solution.

Subtopic: Microbial corrosion – Microorganisms and mechanisms

Microbiological Analyses in the Assessment of Microbiologically Influenced Corrosion

Rob Elzinga, Reinoud Homan and Elsemiek Croese

Microbial Analysis, Rozenburglaan 13, 9727 DL, Groningen, The Netherlands

Corrosion is ubiquitous and poses a threat for all sorts of systems. Many different corrosion mechanisms exist. One of the more complex corrosion mechanisms is corrosion where microorganisms are involved. This so called Microbiologically Influenced Corrosion (MIC) can be complex and unpredictable due to the diversity of underlying microbial and (electro)chemical processes.

To be able to get a grip on microbial processes, it is important to measure and monitor these microorganisms. Several techniques are available to quantify or identify microbial species and microbial traits, such as Adenosine triphosphate (ATP) measurements, culturing methods such as the Most Probable Number (MPN) method, and Molecular Microbiological Methods (MMM). MMM have been recognised as robust and reliable techniques specifically for environments where culturing methods are unable to represent the environmental conditions well, such as anaerobic or subsurface conditions.

Due to recent advancements in MMM, microbial species and traits active in a system can be determined by using Next Generation Sequencing (NGS) technology, based on genetic information present as DNA and RNA. This technique gives insight in possible threats and risks related to the microorganisms involved in MIC, and the effectivity of mitigating measures.

Based on a case study, we examined the microbiological analyses techniques and address the added value of those techniques in a produced water reinjection system showing the importance of those measurements for safe operations.

Modelling microbiologically influenced corrosion (MIC) in long term nuclear waste repositories

Marc Tamisier, Helmholtz Centre for Environmental Reseach, Leipzig/Germany
Vanessa Montoya, Belgian Nuclear Research Centre (SCK CEN), Mol/Belgium
Carsten Vogt, Helmholtz Centre for Environmental Reseach, Leipzig/Germany
Matthias Schmidt, Helmholtz Centre for Environmental Reseach, Leipzig/Germany

Nuclear energy production has generated radioactive waste that needs to be stored safely in a long term repository until decayed to a non-threatening degree of radioactivity, potentially for hundred thousands of years. Such repositories can be placed in deeper geological strata with candidate environments such as opalinus clay or crystalline rock. Among potential risks for the integrity of the repository is the degradation of the canisters containing highly radioactive waste by corrosion. Corrosion of the canisters will occur abiotically on one hand, but also, the presence of corroding microbes can significantly accelerate the process. It is known that microbiologically influenced corrosion (MIC) is carried out by microbes such as sulfate reducing bacteria which have been detected in the repository candidate environments. In order to estimate the risk associated with MIC over time scales covering thousands of years, it is important to incorporate microbially-driven processes into models of nuclear waste repositories to understand their impact on them.

In this light, we set out to develop a model of microbes as chemically (re-)active particles with mathematically well-described physico-chemical properties that can in a second step be incorporated into a geochemical model. The properties of these microbe-particles comprise shape, size, mass and chemical composition, to name a few. The interrelated processes considered in the model are microbial growth, cell death and metabolic activity which in turn directly relates to chemical reactivity. For sulphate-reducing corrosive microbial strains in the vicinity of the canisters the latter describes the microbial corrosion of the canisters in the complex environment of a repository. The suggested model of the microbe is called mibisim and is implemented in Python where it can be used to solve (artificial) homogeneous planktonic systems and biofilm system. Owing to the provided interface it can then be combined with the geochemical solver opengeosys by running mibisim in every cell of the model.

Here, the modelling concept with illustrative examples is presented to discuss how the different environmental factors such as temperature, pH, oxygen concentration, pore size etc. affect MIC in the repository environment with a presentation of their mathematical description. Also, a discussion about the input parameters needed for such model, how to get them and if available, what needs to be done experimentally to obtain them is presented. In summary, this work demonstrates a strategy to integrate knowledge on MIC processes into a geochemical model and forecast their impact on nuclear waste repository integrity.

Mathematical modelling of biofilm acidification by extracellular DNA and its potential effects on microbially influenced corrosion

Javiera Anguita[(1,2)], *Gonzalo Pizarro*[(1,2)], *and Ignacio Vargas*[(1,2)]

(1) Pontificia Universidad Católica de Chile, Chile.

(2) Marine Energy Research and Innovation Center (MERIC), Chile.

Localized acidification plays an important role in structural damage due to microbially influenced corrosion (MIC). Previous research has established that organic acid production is the main mechanism of microbiological acidification. However, experimental evidence indicated that the extracellular DNA (eDNA) presented in *Pseudomonas* biofilm could create an acid microenvironment inside the biofilm. Surprisingly, biofilm acidification by eDNA has still not yet been mathematically studied. Consequently, its potential effect on MIC has not been evaluated using mathematical simulations. The purpose of this research was (i) to evaluate the role of eDNA as a strong acid, (ii) to represent pH gradients inside biofilms due to eDNA, and (iii) to simulate and compare MIC due to biofilm acidification by eDNA and organic acids production. First, the potential effect of eDNA to act as a strong acid was evaluated using a mathematical model to describe the homogenous system under stationary conditions. Second, the generation of pH gradient was represented using a hybrid differential-discrete model to represent heterogeneous systems in transient conditions. Third, the MIC was simulated by adding a carbon steel surface to the biofilm representation and the interaction between biofilm and surface. Through these models, the capacity of eDNA to decrease pH was mathematically corroborated, and the stoichiometry of eDNA and nucleotide was close to one. Additionally, the pH gradients achieved were similar to the previously reported by biofilm-forming bacteria, depending on the conditions, which could be from 6.8 to 6.4 and, in another condition, from 8 to around 5. Finally, the MIC simulations described pits due to the pH gradients created by biofilms. Overall, our results provide strong evidence of the effect of eDNA in biofilm acidification and its potential effect on MIC.

The Vicious Circle of Microbial Corrosion:

How the Surface Selects the Microbial Biofilm that Changes it

Ignacio T. Vargas, P. Universidad Católica de Chile/ MERIC, Santiago/Chile
Leslie K. Daille, P. Universidad Católica de Chile/ MERIC, Santiago/Chile
Javiera Aguirre, P. Universidad Católica de Chile/ MERIC, Santiago/Chile
Javiera Anguita, P. Universidad Católica de Chile/ MERIC, Santiago/Chile
Carlos Galarce, P. Universidad Católica de Chile/ MERIC, Santiago/Chile
Luis Caro-Lara, P. Universidad Católica de Chile/ MERIC, Santiago/Chile
Francisco Armijo, P. Universidad Católica de Chile/ MERIC, Santiago/Chile
Gonzalo Pizarro, P. Universidad Católica de Chile/ MERIC, Santiago/Chile
Magdalena Walczak, P. Universidad Católica de Chile/ MERIC, Santiago/Chile
Rodrigo De la Iglesia, P. Universidad Católica de Chile/ MERIC, Santiago/Chile

The nature of the formed oxide film that passivates corrosion is determined by the alloy's composition and the exposure conditions (i.e., environmental factors). At the same time, the composition of this solid-liquid interface affects the selection of microorganisms that colonize the surface and, in terms, will determine the structure of the formed microbial biofilm. In complex and rich environments such as marine and coastal sites, this selection pressure could end in the formation (or not) of corrosive biofilms that accelerate material degradation.

This work aimed to understand how the oxide layer composition of different stainless steels (SS) could affect the selection and variability of bacterial communities. We studied the microbial corrosion of SS exposed to natural seawater. A total of 24 coupons of austenitic and superferritic SS grades were exposed for 30 weeks to natural seawater on the central coast of Chile. Surfaces characterization (i.e., SEM, GDOES), weight loss analysis, and 16 S rRNA gene sequencing through the Illumina platform were combined to reveal that the iron content of the oxide layer imposes a selective force on microorganisms and favors establishing a less variable microbial community. Finally, the corrosion rate results correlated with the similarity of the biofilm composition from each material and its corrosion-inferred capacity.

Thus, the findings of this research demonstrated that the iron content in the oxide layer of corroded SS surfaces represents an essential feature for selecting potentially corrosive microorganisms in marine environments.

Reference

Leslie K. Daille, Javiera Aguirre, Javiera Anguita, Carlos Galarce, Luis Caro-Lara, Francisco Armijo, Ignacio T. Vargas, Gonzalo Pizarro, Magdalena Walczak, Rodrigo De la Iglesia. *When material science meets microbial ecology: Bacterial community selection on stainless steels in natural seawater*. Colloids and Surfaces B: Biointerfaces, Volume 221, 2023,112955.
https://doi.org/10.1016/j.colsurfb.2022.112955.

Corrosion enhanced by hydrogenotrophic methanogens differently enriched on steel alloys

Elena Cazzulani, Università degli Studi di Milano, Department of Chemistry, Milano (Italy)

Giorgia Ghiara, Università degli Studi di Milano, SEPA, Milano (Italy)

Alessia Aiello, Università degli Studi di Milano Bicocca (Italy)

Pierangela Cristiani, Ricerca sul Sistema Energetico – RSE, Milano (Italy)

Andrea Franzetti, Università degli Studi di Milano Bicocca, DISAT, Milano (Italy)

Gian Luca Chiarello, Università degli Studi di Milano, Department of Chemistry, Milano (Italy)

The microbiological corrosion induced by methanogens is mainly studied on steel alloys, these being widely used in the Oil&Gas sector, where the most significant phenomena have been found. Most studies show that the effect of CO_2-rich environments, pH and flow conditions could modify the interaction of methanogens with the substrate as for the use of hydrogenase and the catalyzation of protective corrosion products, such as Siderite or Vivianite. In this work, the enrichment of a different pool of hydrogenotrophic methanogens and bacteria on the surface of different steel alloys, a pure Fe (ARMCO©, 0.02 wt.% of C), a duplex stainless steel (2205, with 22 wt. % of Cr) and a carbon steel (S355, 0.14 wt.% of C) was documented, starting from the same microbial pool. The corrosion induced by methanogens enriched media, in comparison with sterilized media, were documented during replicated two-week tests. Electrochemical investigations were performed using a three-electrode cell consisting of a working electrode (test alloy), a reference electrode (saturated Ag/AgCl electrode) and a counter electrode (titanium mesh). Investigations included open circuit potential (OCP) monitoring and electrochemical impedance spectroscopy (EIS). Chemical characterizations of the corrosion products and post-experiment observations were performed by SEM and micro-Raman spectroscopy (μRS). Molecular analysis by next generation sequencing (NGS) of 16S RNA was performed by swabbing the surface of the material and identifying the microorganisms constituting the microbial communities for each case. Results evidenced a different enrichment of microorganisms and corrosion products depending on the material.

Subtopic: Microbial corrosion – Microorganisms and mechanisms

Study on microbiological corrosion and toxic failure mechanism of copper

Wenwen Dou, Shiqiang Chen, Guangzhou Liu**

Institute of Oceanology, Shandong University, Qingdao, China 266237

Copper and its alloys are widely used in all aspects of industry, including heat exchange systems, fire protection systems, seawater pipelines, etc. Copper has excellent resistance to sea water and oxygen corrosion. However, in many practical cases, we found that microbial corrosion of copper, such as sulfate reducing bacteria (SRB) and nitrate reducing bacteria (NRB) caused corrosion, is very serious. As we all know, copper has excellent bactericidal effect, why in the presence of SRB or NRB, copper not only did not play a bactericidal effect, but also occurred serious microbial corrosion. When copper encounters the above two kinds of bacteria, what is the mechanism of microbial corrosion of copper? What is the mechanism of toxic failure? In order to solve the above two problems, we designed a series of experiments to study, including the regulation of organic carbon source (electron donor), bacterial living space and nutrient source content. Through the regulation of the above three aspects, the number and state of bacteria were observed, and the corrosion products and morphology were analyzed. Finally, through thermodynamic calculation, it was concluded that the microbial corrosion mechanism of copper was different by the action of different bacteria. The main reason for copper corrosion caused by SRB is the effect of its metabolite hydrogen sulfide (Fig. 1), while the main reason for copper corrosion caused by NRB is extracellular electron transportation (Fig. 2). The reason for the failure of toxicity of copper to bacteria is that cuprous sulfide and copper ammonia complex are formed respectively under the action of two kinds of bacteria, which leads to the low concentration of copper ion in the solution, thus losing toxicity.

Keywords: Copper corrosion, Microbial corrosion, Toxicity failure, Sulfate-reducing Bacteria, Nitrate reducing bacteria

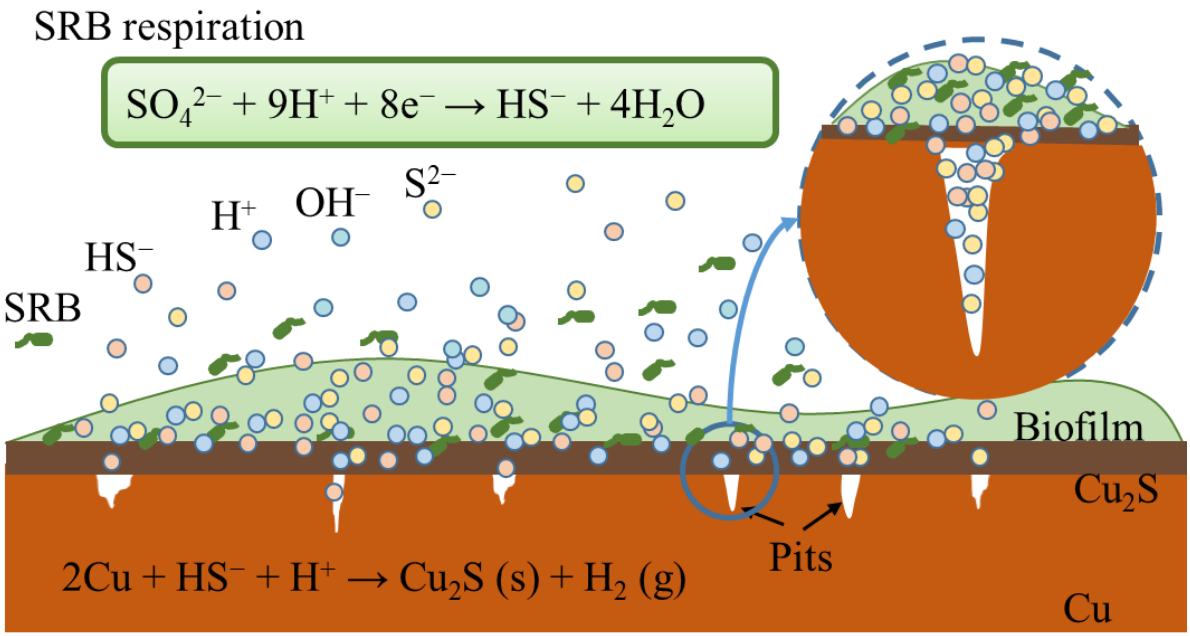

Fig.1. Copper corrosion mechanism caused by SRB

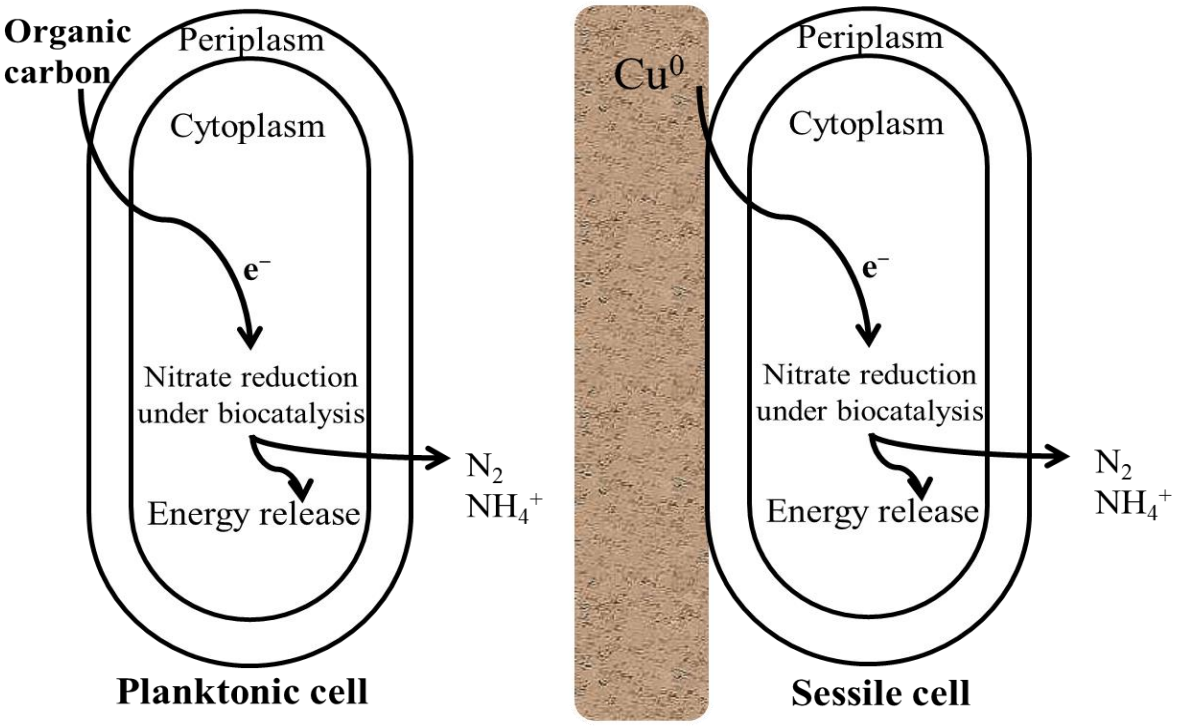

Fig.2. Copper corrosion mechanism caused by NRB

Corresponding author: Wenwen Dou, douwenwen2015@sdu,edu,cn; Guangzhou Liu, liuguangzhou@sdu.edu.cn

Corrosion Inhibition of Marine *Streptomyces* on Sulfate-reducing Bacteria

*Jian Wang, Min Du**

The Key Laboratory of Marine Chemistry Theory and Technology, Ministry of Education, College of Chemistry and Chemical Engineering, Ocean University of China, Qingdao 266100, P. R. China

Corresponding author: DU Min (1969-), Professor, Research focus: Marine corrosion and protection, Email: ssdm99@ouc.edu.cn

Abstract: The development of environmentally friendly and sustainable corrosion protection technologies is a longstanding yet difficult problem, especially for the Microbiological Influenced Corrosion (MIC) caused by sulfate-reducing bacteria (SRB). It is an effective strategy to control MIC with beneficial microorganisms. In this study, X65 steel was selected as the research object, and a marine *Streptomyces* stain with inhibition effect on SRB was selected to explore the effect of *Streptomyces* on corrosion of X65 steel, evaluated the inhibition effect on SRB corrosion, and discussed the inhibition mechanism. The growth of *Streptomyces* and SRB alone and mixed was evaluated by growth curve. The average corrosion rate of X65 steel was measured by weight loss method. The surface films and pitting corrosion of the samples were analyzed by scanning electron microscope (SEM), Raman spectroscopy and confocal laser scanning microscope (CLSM). The electrochemical process of the steel surface was studied by electrochemical impedance spectroscopy (EIS). The results showed that *Streptomyces* formed uniform "honeycomb" tissue on the surface of X65 steel at the initial stage, which was conducive to the diffusion and adsorption of cell tissue and various metabolites to the surface of the material. With the extension of time, the film became denser and had a certain protective effect on the matrix, but in the early stage of bacterial growth, the consumption and metabolism of organic matter lead to the decrease of solution pH, which accelerated the corrosion of X65 steel. Compared with sterile system, *Streptomyces* inhibited pitting to a certain extent. The addition of *Streptomyces* inhibited the growth of SRB. Compared with SRB system, the film layer on the sample surface was denser and more continuous, which played a good protective role. The coexistence of the two bacteria may play a synergistic role in mineralization, thus reducing the corrosion rate

of X65 steel. At the same time, the local corrosion caused by SRB was also significantly inhibited.
Key words: microbiological influenced corrosion; environmentally friendly; marine *streptomyces*; sulfate-reducing bacteria; corrosion inhibition

Peek-A-Boo, MIC. Where Are You?

AL MAZROUAI, BADAR
OQ Refineries and Petrochemical Industries
Sohar Industrial Port
Sohar, North Al Batinah, 00322
Sultanate of Oman

AL ABRI, NAIF
OQ Refineries and Petrochemical Industries
Sohar Industrial Port
Sohar, North Al Batinah, 00322
Sultanate of Oman

ABSTRACT

The Ethane steam cracking unit's product run down lines to the storage area experienced multiple pinhole leaks within a year of commencing operations. Despite the cryogenic process fluid handling liquid Ethylene and cold insulation using foam-glass with a vapor barrier coating, the threat of Stress Corrosion Cracking (SCC) was deemed unlikely.

The stainless-steel grade (SS304) lines with 9mm thickness underwent 100% Radiographic Testing (RT) during project construction and hydrotesting as part of mechanical completion before the pre-commissioning phase, with no significant defects reported. However, subsequent leaks were detected at the 6 O'clock position on the horizontal section, accompanied by a brownish slimy layer between 5 to 7 O'clock, suggesting the possibility of Microbiologically Influenced Corrosion (MIC).

Key words: Microbiological influence corrosion, Sulfate reducing bacteria, Microorganism.

INTRODUCTION

This paper highlights the challenges associated with screening and detection of tiny little pinholes which are subsequently identified to be caused by Microbial activity that set in between the post construction phase and the pre/commissioning phase. A section of the piping had a low point in the pipe rack, potentially leaving the traces of hydro test water to remain inside, creating a perfect place for microbes to expand the colonies.

Despite several advanced NDE techniques available in the market, detection of tiny pinholes in the order of 1.0 to 1.5 mm diameter in the 120-meter-long piping, posed a challenge; that too with cold insulation cladding on. With the limitations of the detectability of pin hole like defects, even the advanced NDE's such as profile RT, LRUT are proved to be uneconomical. OQ, did a holistic assessment and developed the failure mitigation strategy to manage the MIC by selective replacement of the sections and performing hydrostatic test with biocide injection to reduce the bacterial growth.

Process description

The LIWA Plastic project transitioned to the commissioning phase in early 2020. This newly established petrochemical complex is specifically designed for the cracking of ethane and mixed feed (naphtha, LPG) with the objective of producing polymer grade ethylene and polymer grade propylene, as well as various other by-products. A general overview of the steam cracking process is presented in Figure 1.

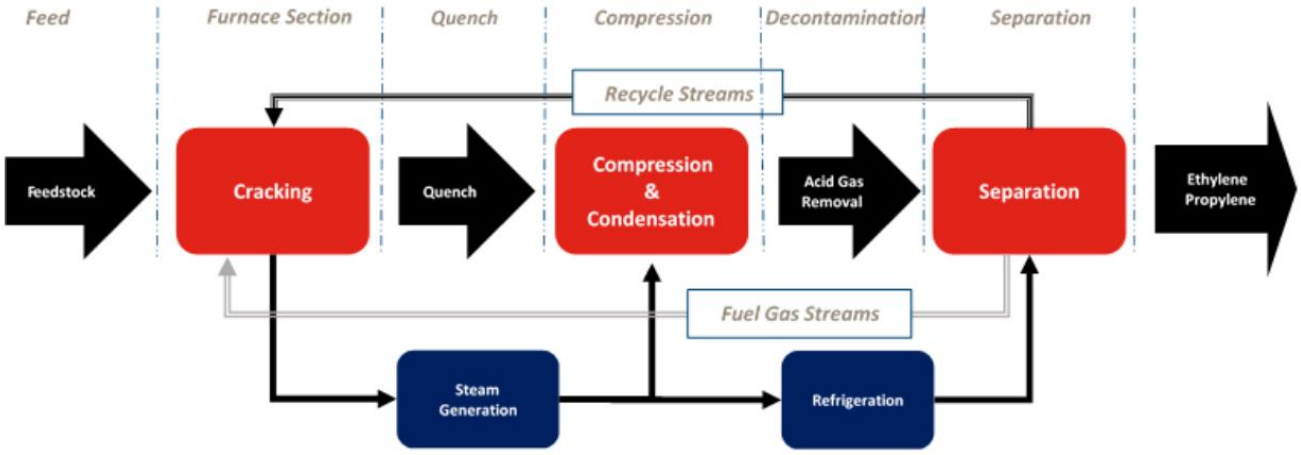

Figure 1 Ethylene Steam Cracker Process (Ref.1)

Polymer Grade Ethylene Storage Unit (Area of Concern)

PG Ethylene Cryogenic Storage has been designed for the following modes of operation:

- Standalone case
- Feeding Polyethylene Plant
- Rundown of Steam Cracking Unit
- Ship Loading
- Ship Unloading

PG Ethylene at (-)101°C is routed from Cold box located at steam cracking unit to PG Ethylene Cryogenic Storage Tank, where a vapor-liquid separator is installed in to separate the liquid from the vapor. Liquid Ethylene is stored at (-)103°C and atmospheric conditions in a double containment tank. Ethylene is transferred to the Polymer Plant by Cryogenic Ethylene Product Pump.

Incident Description

On 10th April 2021, and during commissioning phase activities, plant operators observed the formation of icing on the insulated ethylene line, precisely at the outlet of the polymer grade ethylene storage tank. Subsequently, after a month, additional leaks were reported in another ethylene line that was routed to the battery limit. A brief description of the incidents is provided in Table 1.

Table 1 Incident Summary

Line details	What happened?	Visual Inspection findings	Common findings
Ethylene line Line size: 3 inches Metallurgy: SS304	Icing was reported on 3" Ethylene line from Cryogenic Transfer Pump to Steam cracking Unit on 10th April 2021.	Close visual inspection revealed 2 pinholes (approx. 0.5 mm dia) were seen at 6 o'clock position, located about 0.5 m apart in parent metal	1. Both leaks at horizontal portion and away from low point drain.
Ethylene line Line size: 10 inches Metallurgy: SS304	Pressure drop reported from 10" Ethylene line. Insulation opened & visual inspection was carried out on 05th May 2021	Close visual inspection three (3) pinholes (approx. 0.5 to 1.5 mm dia) at 6 o'clock position. 1st leak approx. 530mm, 2nd leak approx. 1600 mm & 3rd leak approx. 3600 from the support	2. Both leaks found with debris, rusty deposit & water marks.

Figure 3 and Figure 4 shows the findings of visual inspection. At this stage, both lines have been commissioned recently. Plant operators confirmed that these lines were idle since hydrotest and mechanical completion activities. Leaks were observed at start of commissioning activities.

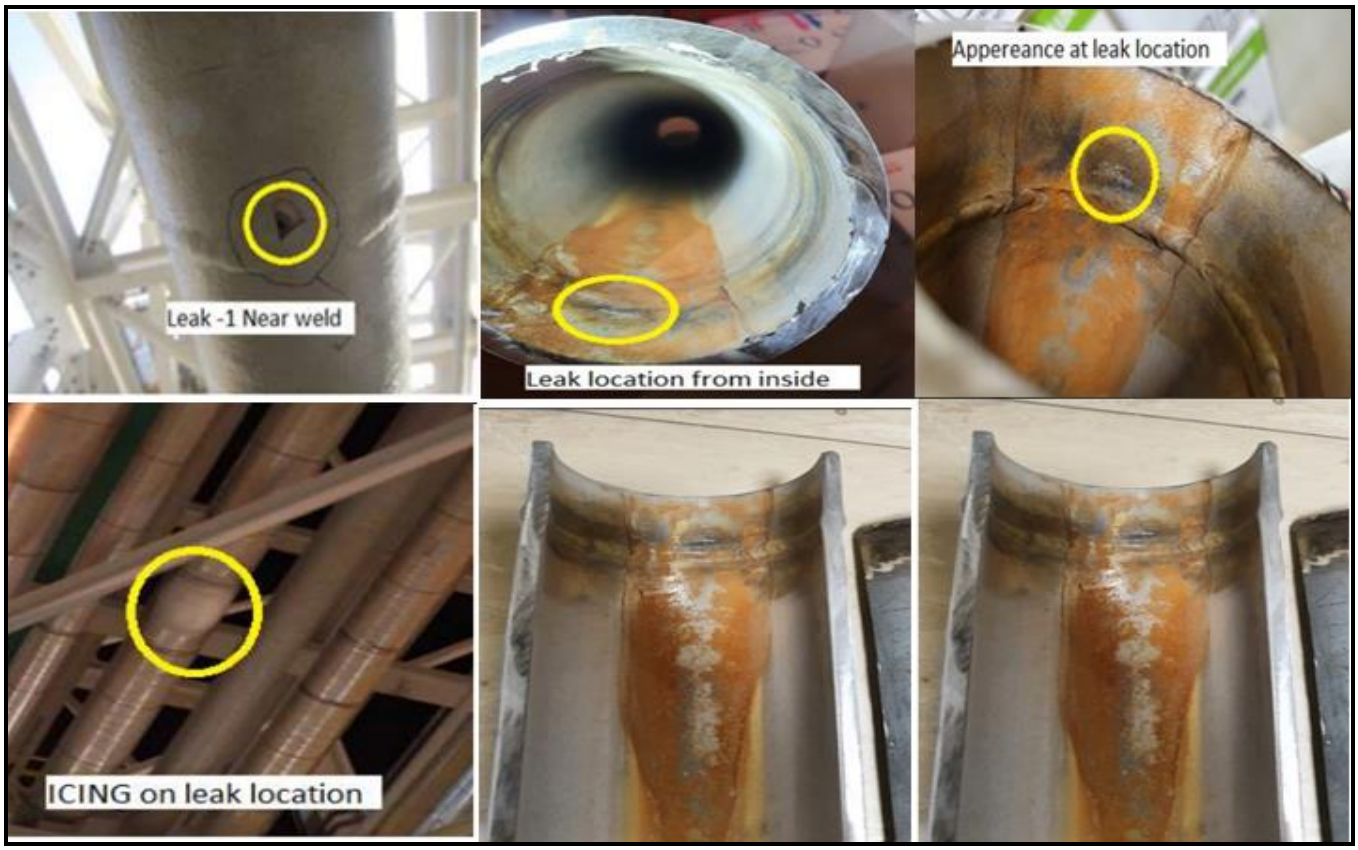

Figure 2 Visual inspection of 3-inches line

Figure 3 Visual Inspection Findings of 10 inches line

Sequence of events till failure occurred are explained in figure 4.

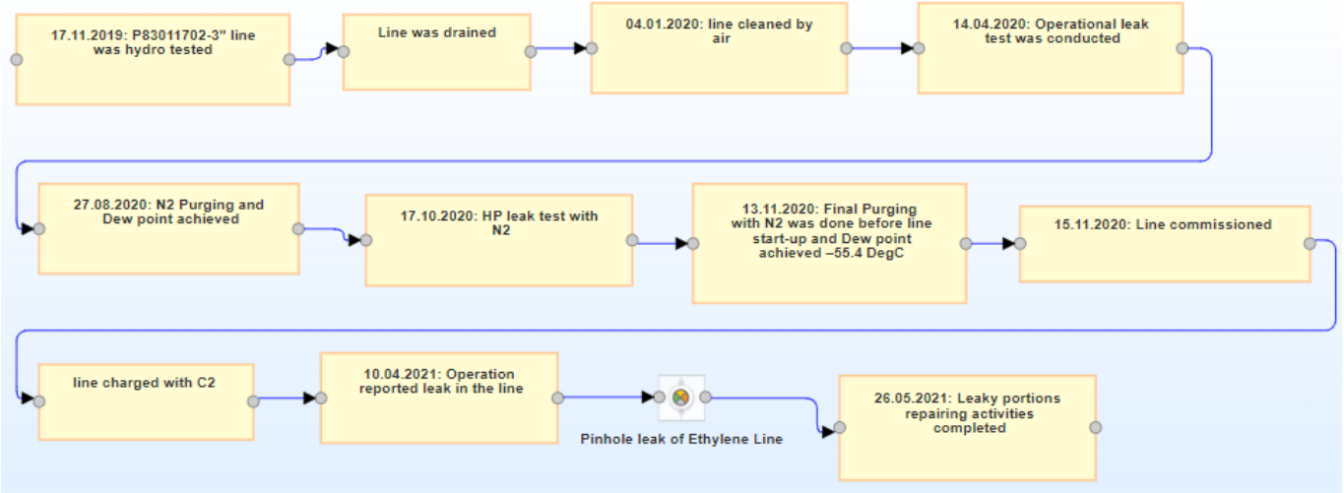

Figure 4 Sequence of events (screenshot from RCA report)

Root Cause Analysis

A thorough analysis conducted on the observed damage led to the identification of its cause. The morphology of the damage, characterized by a rough surface around the leak, clearly indicates that it should be classified as microbially induced corrosion (MIC). The presence of deposits and water stains can be attributed to improper cleaning of the pipe after hydrotesting during the commissioning phase. The delay in cleaning and drying the pipe after the hydrotest allowed for the initiation of microbiologically induced corrosion (MIC).

Shortage of Workforce during the COVID 19 Pandemic

he Covid-19 pandemic had a significant impact on commissioning activities of the project, particularly due to the construction industry's heavy reliance on on-site and in-person work. Lockdowns and social distancing measures imposed during the pandemic placed a substantial strain on employees working within the project.

As a consequence of these challenging circumstances, poor preservation management occurred in certain sections of the project, with the ethylene storage unit being particularly affected. The restrictions and disruptions caused by the pandemic hindered the proper preservation efforts for critical components.

Furthermore, it was noted that there were no records of proper preservation practices being followed, which further exacerbated the issue. The lack of documented preservation measures and protocols made it difficult to track and ensure that essential preservation activities were carried out as required.

Overall, the Covid-19 pandemic posed unique and unprecedented challenges to the commissioning process, impacting preservation practices and leaving some sections of the project vulnerable to potential issues related to inadequate preservation measures.

Strategies to Manage the risk of MIC

Assessing the overall integrity of the affected piping posed challenges due to its limited accessibility and insulation. The primary objective was to identify the leak before any recurrence. OQ investigation team evaluated two options for further action, which are illustrated in the subsequent flowchart.

Integrity Assessment by NDT trials

In order to investigate the most suitable nondestructive techniques for evaluating the integrity of the ethylene line, a nondestructive testing experiment was conducted on the 3-inch ethylene line. The trials facilitated the assessment of the effectiveness of various nondestructive testing (NDT) methods, and the advantages and disadvantages of each technique are presented in Table 2.

Table 2 Technical Comparesion of proposed NDT Techniques

NDT Method	Advantage	Disadvantage
Profile RT	1. Highly sensitive NDT technique. 2. Defect Diameter can be measured. 3. No insulation removal required.	1.Full length of piping scaffolding needs to be erected. 2. Each shot can cover up to 300 mm length only. For coverage of circumference, 3 nos shot required at every location. Very Slow NDT method. 3. Depth of the defect cannot be measured. 4. It cannot be done for 10'' line.
LRUT	1. Fast inspection method, considering sensitivity maximum coverage range cane be 20 meter from one test location. For higher size coverage range will be reduced. 2. 100% pipe length can be checked except fittings. 3. Test can be performed with insulation (only one-meter insulation removal required for each test location). 4. Through wall thickness integrity can be checked.	1. Probability of detection will be around 60% as per the LRUT trail. 2. Defect pit depth greater than 4 mm diameter can only be detected. 3. Defect identified locations by LRUT need to be cross checked with Profile RT for confirmation as technique is just screening tool. 4. Integrity of fittings not covered by LRUT. It should be check with Profile RT. 5. Exact defect location cannot be identified. Defect location can be identified within 200 mm range (+ or – 100 mm). For identification of location insulation removal required for nearby weld area to measure the defect location.
Borescope	1. Average 50 meter can cover from each testing spot for size more than 6" where the crawler camera can be inserted. 2. Wherever crawler camera insertion not possible, average 10 meter can cover from each testing spot. 3. Higher test coverage & Fast NDT method compared to other. 4. No insulation removal required	1. Proper internal cleaning of line is required. Debris, rusting & any particle available in line than inspection is not effective. 2. Possibility of minor pits can be missed out during inspection. Defect sizing not possible. 3. Scaffolding required at every test location. 4. Full line decontamination required as line cutting required to access the internal surface of pipe at test locations. All cut location rewelding & RT required.

Based on the technical comparison presented earlier, a comprehensive assessment of the lines' condition was not feasible using any of the NDT methods due to their associated time constraints and limitations. Consequently, the NDT specialist at OQ made the decision to forgo the use of these techniques.

Considering the complete replacement of the two lines was not justifiable from a management standpoint, OQ investigation team reached a consensus to pursue with the following:

i. Clean the entire 3" and 10" line at the earliest available opportunity (with suitable method like rotomal / pigging, etc) to remove debris, rust and the microbes at the active pits in piping.
ii. Carry out hydro-test of both the lines (3" and 10") using DEMIN water with biocide dosing.
iii. Developing special method statement for cleaning and hydrotesting with biocide.

Reducing The Risk by Cleaning and Hydrostatic Test

OQ team worked on develop hydrostatic procedure considering the use of biocides. In addition, technical discussions were held with local vendors to find the best type of biocide that would mitigate microbial growth while being compatible with 304 stainless steels. The following flowchart explains the additional measure taken to test the ethylene lines, including holding time with biocide and the pressure. Table 3 illustrates Holding and Hydrostatic Pressure for 3 and 10 -inches Ethylene lines.

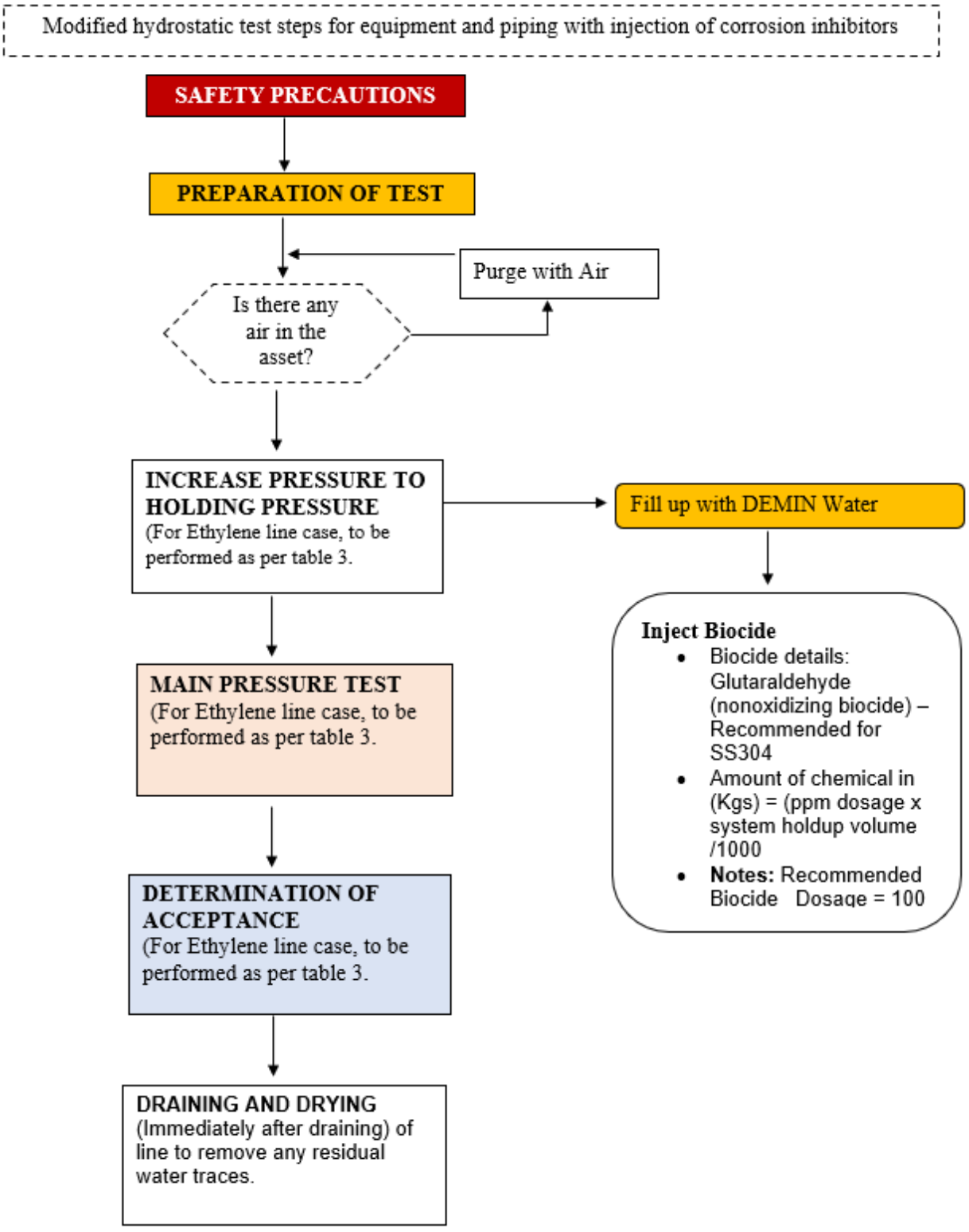

Table 3 Holding and Hydrostatic Pressure for 3 and 10 -inches Ethylene lines

Sr No	Line Details	Approximate pressure for holding 24 hrs, bar g	Hydrotest Pressure, bar g
1	3” Line – SS304	50-54	82.5
2	10” Line – SS304	17-19	29.4

CONCLUSIONS

The root cause analysis conducted on the failure revealed that microbiologically induced corrosion was the underlying reason. Poor preservation management in certain sections of the project, particularly in the ethylene storage unit, contributed to the occurrence of the issue, with the ethylene storage unit being the most affected area.

The examination and detection of tiny pinholes posed significant challenges, primarily due to the length of the line and its insulation cladding. As a result, the NDT specialist at OQ opted against using any of the NDT methods due to their time-consuming nature and associated limitations. Moreover, a complete replacement of the two lines was deemed unjustifiable from a management perspective.

As an alternative approach, OQ integrity team decided to implement a water with biocide injection process, holding it in the system for 24 hours to mitigate bacterial growth. Subsequently, a hydrostatic test was performed to ensure the line's integrity and leak-proof performance.

After 2 years of operation with no further observed leaks, the cleaning of the line and biocide injection proved to be an effective and economically viable solution to address the microbiologically induced corrosion issue.

ACKNOWLEDGEMENTS

A very sincere appreciation to Hani Ramadan, Singaravelu Sundaravel, Sanjay Chaudhari, and Ibrahim Al Hashmi, who have played a key role in this investigation, including conducting NDT trials and developing the method statement for cleaning and hydrotesting the affected lines. Also, the appreciation is extended to the company downstream teams who participated in root cause analysis task force.

REFERENCES

1. FLOWSERVE, *Application Solution Guide*, ETHYLENE, p9.

Quaternary carboxylates for mitigating MIC

Anthony E. Somers[1], Jhonatan Soto Puelles[1], Mahdi Ghorbani[1], Benjamin Tuck[2], Laura L. Machuca[2], M. Leigh Ackland[4], Fangfang Chen[1,3,] Maria Forsyth[1,3]*

[1]Institute for Frontier Materials, [3]ARC Centre of Excellence for Electromaterials Science (ACES) and [4]School of Life and Environmental Sciences, Deakin University, Burwood, VIC, 3125, Australia.

[2]Curtin Corrosion Centre, WA School of Mines: Minerals, Energy and Chemical Engineering, Curtin University, Kent Street, Bentley, WA, 6102, Australia.

**asomers@deakin.edu.auAutor,*

Abstract

Mild steel is one of the most used construction materials in the world, however, is vulnerable to corrosion, costing trillions of dollars worldwide to protect, maintain and replace. Much of this corrosion, up to 30% by some estimates, is exacerbated by the presence of bacteria. Inhibitors are a cheap and effective method of reducing both corrosion and the influence of bacteria, either by adding in to paint coatings or to process streams, though historically the most effective of these have been harmful to the environment and toxic.

Here we detail investigations into novel quaternary ammonium carboxylate compounds that can limit the effects of Microbiologically Influenced Corrosion (MIC) by both protecting the surface and reducing bacteria populations. This new system takes advantage of the surface activity of a known antimicrobial surfactant molecule, the cetrimonium cation and combines it with a known organic corrosion inhibitor, the trans-4-hydroxy-cinnamate anion.

Initial electrochemical studies on cetrimonium 4-OHcinnamate (CTA-4OHcinn) found the compound to be effective at reducing abiotic corrosion[1]. Diffusion NMR and Cryo-TEM experiments, along with results in the literature for similar structures, indicated micellar formation that was concentration and pH-dependent[2]. Electrochemical results were also found to correlate well with changes in micelle structure, with a likely transition from spherical to worm-like micelles resulting in improved performance.

Classic molecular dynamics simulations were then used to determine how the inhibitor compounds behaved in solution at different concentrations and how this affected the subsequent surface protection[3]. Following construction of an appropriate

model simulations showed the encapsulation of 4-OH-cinnamate into cetrimonium micelles, consistent with experiments. The newly formed micelles adsorb onto a hydrated iron oxide surface by forming hydrogen bonds between their carboxylate outer-shell and the surface hydroxyls. As the inhibitor concentrations increase, there is a morphological transition from spherical to wormlike micelles. The wormlike structure on the surface can more effectively block chloride ions, demonstrating a synergistic inhibitory mechanism between both cetrimonium and 4-OH-cinnamate.

In addition to abiotic corrosion studies, investigations into the performance of the inhibitors in limiting MIC were also conducted. Initially, basic studies were conducted, with the compound demonstrating biocidal effects against three marine isolates during the early stages of biofilm formation[4]. In natural aqueous environments, however, populations of microorganisms rapidly colonise surfaces forming biofilms. Species heterogeneity in natural systems confers higher tolerance to biocide treatment compared with single species laboratory simulations. This protection is due to the structure of the mature biofilm that often limits anti-microbial penetration. The biocidal capacity of CTA-4OHcinn against multi-species biofilms developed from oilfield samples was evaluated[5]. Results demonstrated that CTA-4OHcinn significantly reduced the viability of mature biofilms, supporting previous demonstrations on the secondary function of CTA-4OHcinn as a biocide. Analysis indicated that CTA-4OHcinn targets the cell membrane resulting in lysis.

Molecular dynamics simulations were used to determine how the CTA-4OHcinn micelles were able to both penetrate the mature biofilm and disrupt cell membranes. The main driving force for micellar attack on the cell membranes was found to be electrostatic interactions. The micelles were also shown to interact with extracellular DNA (e-DNA), which is one of the main components of biofilms. and hinder their ability to pack.

References

1. J Soto Puelles, et al., ACS omega 6 (3), 1941-1952, 2021.
2. M Ghorbani, et al., The Journal of Physical Chemistry Letters, 11 (22), 9886-9892, 2020.
3. J Soto Puelles, et al.,Journal of Colloid and Interface Science 610, 785-795, 2022.
4. R Catubig et al., Australian Journal of Chemistry 75 (9), 619-630, 2022.
5. B Tuck et al., Microorganisms 10 (6), 1227, 2022.

Microbiologically influenced corrosion inhibition of carbon steel via biomineralization induced by *Shewanella putrefaciens*

Yuntian Lou, Weiwei Chang, Tianyu Cui, Dawei Zhang

Microbiologically influenced corrosion inhibition (MICI) of Q235 carbon steel by biomineralization was investigated via a combination of surface analysis, electrochemistry, and scanning electrochemical microscopy (SECM). The results showed that *Shewanella putrefaciens* used the cell walls as the nucleation sites to induce the formation of a protective biomineralized layers which contained calcite and extracellular polymeric substances on the steel surface. The potentiodynamic polarization results demonstrated that the corrosion current density (i_{corr} value) of the biomineralized steel surface was 0.38 μA cm^{-2}, which was less than one-tenth that of the blank steel in a sterile medium (4.86 μA cm^{-2}) after 14 days. The biomineralized layers presented wear resistance and could self-repair after undergoing mechanical damage under microbial conditions as verified by morphological and SECM observations. Meanwhile, the effect of extracellular polymeric substance (EPS) expression on microbial-mineralization induced MICI was investigated using gene knockout technology. This work reveals that microbial-induced carbonate biomineralization, as a MICI approach, may be considered as a reliable, low-cost, environmentally friendly corrosion inhibition strategy.

Influence of calcareous deposition on MIC in seawater: Field observations

Robert E Melchers

The University of Newcastle, Callaghan, NSW 2308, Australia,
rob.melchers@newcastle.edu.au

Abstract

Calcareous deposits on and within corrosion products have long been known to inhibit the (abiotic) corrosion of steels immersed long-term in seawater. This paper investigates whether such inhibition applies also to microbiologically influenced corrosion (MIC) in seawaters, fostered by elevated concentrations of dissolved inorganic nitrogen (DIN), noting that in seawater DIN is, with P, the critical nutrient for microbiological metabolism in the presence of ferrous corrosion. A summary is given of the long-term corrosion rates r_s for more than 40 cases of shipwrecks and other steel and cast iron objects immersed at various depths in seawater and for periods of time (from 35 years to 140 years, mean 60 years) and at various depths. The results indicate that calcareous deposition in seawater inhibits abiotic corrosion as well as MIC. The likely reasons for these findings are discussed. Controlled laboratory testing is in progress and to date indicate similar findings.

Keywords: steel; mass-loss; calcareous deposition; MIC; inhibition.

Introduction

It has been known for a long time that calcareous materials such as calcium carbonate and magnesium carbonate deposited within or on marine rust products can inhibit the rate of marine immersion corrosion of steels and irons [1, 2]. Carbonate deposition can occur only when the solubility limit of the carbonate in seawater is exceeded, noting that most seawaters have carbonates at (near-)saturation concentrations [3]. Exceeding the saturation limit can come about by the inflow of hard fresh waters, such as within and near river mouths, or by the submarine inflow of hard coastal waters [4]. Calcareous deposition also is associated with impressed current 'cathodic protection' of steel piles [5, 6] and steel surfaces [7]. The deposits were noted to inhibit marine corrosion while the current remained turned on, and also for several weeks after the current was turned of when the calcareous deposits gradually deteriorated under wave action [5]. While most attention has focussed on corrosion 'protection', there is some evidence, from exposures up to about 200 hours, that biofilm formation also may be inhibited [8], suggesting that the carbonates also may inhibit microbiologically influenced corrosion (MIC). Supporting evidence for such an inhibiting effect over long-term exposures (up to 100 year) came as a result of observations of the corrosion of shipwrecks off the Belgian coast [9]. These showed less marine immersion corrosion than expected for the average seawater temperature10] despite the waters there having elevated nutrient concentrations [11]. Importantly, examinations of the rusts showed much presence of calcareous material but negligible presence of microorganisms typical of MIC. The latter suggested that MIC is less likely to occur in the presence of elevated presence of calcareous material in the rusts.

For marine immersion corrosion of ferrous alloys such as steels and cast iron over several centuries, data and trends are now available for the amount of corrosion, measured by mass loss, for exposures up to some 600 years [12]. The trends show a gradual reduction of instantaneous corrosions rate, roughly describable by a modified power law. A different set of data, all for locations where calcareous deposition could be considered highly likely given the geographic locations, showed less corrosion for corresponding time periods and also that the data extended over a much longer period [13]. In both cases most of the data were for sites unlikely to have been under the influence of elevated concentrations of nutrients critical for MIC, particularly Dissolved Inorganic Nitrogen (DIN) encompassing nitrites, nitrates and ammonium and also lower requirements for phosphorous (P). In the corrosion of steel alloys and alloys containing Fe is an alloy, the Fe ions required for bacterial metabolism usually are available as part of the alloy composition while organic carbon is available from the organic components of seawater. The required energy is supplied by the electron flows associated with the corrosion process.

The following section summarizes a number of field observations. In each case the data cover corrosion rates or corrosion loss estimates, period of immersion, depth of immersion, average seawater temperature at depth, DIN concentration and any observations about water currents or other factors that potentially may be relevant. Only limited information was available for nutrient concentrations, possibly because collecting such information has not been a core issue for previous observations of the corrosion of submerged objects such as shipwrecks, mooring chain and sheet piling. Also, the correlation between long-term corrosion rates (r_s) (Fig. 1) and elevated DIN has only recently become evident [10, 14]. Fortunately, for some regions there is wide-scale information about nutrient conditions in published environmental studies, for example for the North Sea [11] and for the Gulf of Mexico [15].

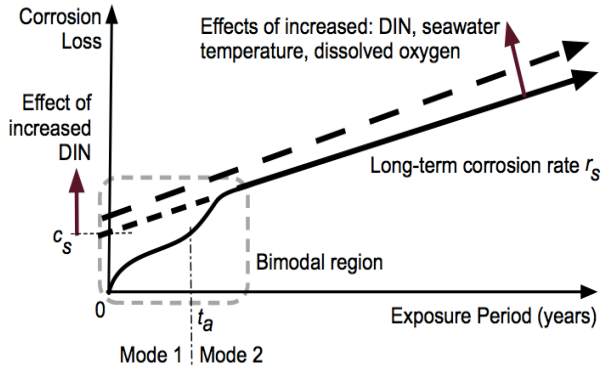

Figure 1: Schematic diagram showing the long-term corrosion rate r_s and intercept parameter c_s that define the longer-term corrosion trend. Also shown are the effects of increased DIN, increased mean seawater temperature and increased dissolved oxygen [16]. The linearity for extended exposures is sufficiently accurate for the present purposes.

The section that then follows takes the observations for corrosion losses to derive long-term corrosion rates and compares these for four different exposure conditions: natural seawater, natural seawater with elevated DIN, natural seawater with calcareous deposition on and within the rusts and the same but with elevated DIN concentrations. Despite relatively limited numbers of data in each category, a distinct difference in the long-term corrosion rates can be discerned. This is also despite the data having been derived from field observations with their invariably high degree of uncertainty as a result of the field conditions being uncontrolled and uncontrollable and thus being somewhat variable with time and climatic influences. The findings are the discussed in terms of the mechanisms likely responsible for the observations.

Data

The data used in the present study are summarized in Table 1. It includes only those cases for which information about DIN concentrations and about observations for, or information about, the likelihood of calcareous deposition was available. Many other cases were examined bur for these the data or information for DIN and calcareous deposition was considered unreliable or not quantifiable and thus are not shown here.

As shown, the data were divided into two groups - those in which there was no evidence of calcareous deposition and those for which there was such evidence. The presence of calcareous deposition was evident from several unbiased observations of the photos and videos of the underwater wrecks and other artifacts. A lack of calcareous material showed bright red-brown rusts under the illumination of diving lights as compared to dull reflections and ‘woolly’ surface topography when there was either a calcareous layer over the rusts or embodied within the rusts. Each of the two groups was then further subdivided into cases with no evidence of elevated concentrations of DIN at the observation site and those for which there was such evidence or for which it can be inferred from the location. In each case only the long-term corrosion rate r_s is reported. For such exposures the intercept c_s (Fig. 1) becomes negligible for extended period of exposure (Fig. 1) [16].

Table 1. Exposure, environmental and long-term corrosion loss data for steels and cast irons.

Case	Vessel or structure, location, comments [references]	D (m)	t_{eff} (y)	Av. DIN mgN/l	T ˚C	r_{sT} mm/y	$r_{12.5}$ mm/y
	Natural seawaters						
1	British gunboat (Meyer wreck) St George's boatyard. [17]	3.5	104		28.5	0.048-0.076	0.042 (ave)
M	Chain links, 76mm diam. More than 40 measured. Catherine Hill Bay, Pacific Ocean, Aus. [18]	0-10	100		20	0.06	0.05
3	Titanic, N Atlantic. r_s estimated from results of a 6 year field trial. [19, 20, 21]	3800	34		4	0.04	0.05
	Seawaters with elevated DIN						
4	Various WW2 wrecks, Chuuk Lagoon. 'Flash' fishing destroys calcareous layers and rusts. [22]	5-40	60		30	0.11-0.14	0.073-0.093
5	Steel piling / Boston, MA. [10]	1-3	18	0.2	10	0.064	0.068
6	Ditto / Norfolk, VA. [10]	1-3	16	0.4	16	0.070	0.065
7	Ditto / Key West, FL. [10]	1-3	22	0.03-0.04	21	0.075	0.060
8	Ditto / Coco Solo PCZ. [10]	1-3	24	0.03	27	0.12	0.083
9	Ditto / San Diego, CA. [10]	1-3	18	0.2	17	0.10	0.086
10	Ditto / Alameda, CA. [10]	1-3	21	0.07	16	0.075	0.068
	Calcareous seawater						
11	USS Monitor, Atlantic, 23 km off Cape Hatteras, NC. Chalky deposits [23, 24, 25]	67-80	130		~15	0.017	~0.016
12	Cast Iron cannon balls, Akko, Israel. Corrosion estimated from depth of graphitized layers. [26]	?	160		~20	0.021-0.022	0.017 - 0.018
13	Cast Iron cannons (HMS Swan), Isle of Mull, Scotland. r_s from graphitized layer [13, 27, 28]	?	337		~10	0.13	0.014
	Calcareous seawater with elevated DIN						
14	Belgian Wrecks (10 in total), North Sea coast. Various depths [9]	0-20		Elevated	12.5		0.016 (ave.).
15	USS Arizona, Pearl Harbour. Corrosion losses from coupons cut from hull [29, 30, 31]	4-10	61	Elevated	25	0.03-0.041	0.021-0.03

Notes for Table 1:
D = depth (metres), t_{eff} = effective exposure time period (years) (allows for paint coating deterioration), T = seawater mean temperature (˚C) at location, r_{sT} = estimated average long-term corrosion rate at mean seawater temperature T (mm/y), $r_{s12.5}$ = estimated average long-term corrosion rate at mean seawater temperature T= 12.5˚C (mm/y)

Data analysis

To allow comparison of the data in Table 1, the corrosion rates were all covered to the nominal rate at 12.5˚C to permit direct comparison with those reported for the Belgian North Sea [9]. The corrections were based on the information for seawater in ref. [10]. Grouping of the data in each set then provides the summary shown in Table 2 and more clearly seen in Fig. 2. The corrosion rates for the seawaters subject to calcareous deposition and those with no (or negligible) calcareous deposition are about 30% of those in natural seawater. This is the case irrespective of the presence of DIN.

Fig. 2 indicates that the presence of DIN increases the rate of longer-term corrosion by some 50-100%. This is not inconsistent with field observations for the localized corrosion (pitting) of steel mooring chains exposed in natural seawaters and in waters with high DIN [32].

Table 2. Quantitative estimates of long-term corrosion rates r_s, categorized by occurrence of calcareous deposition and evidence for elevated DIN concentration.

Calcareous deposition	No	No	Yes	Yes
Seawater nutrient quality	Natural	Elevated DIN	Natural	Elevated DIN
Number of individual measurements for r_s.	> 42	> 8	> 3	> 11
Approx. rate r_s (mm/y) @ 12.5˚C	0.042-0.05	0.06-0.14	0.016-0.02	0.016-0.03

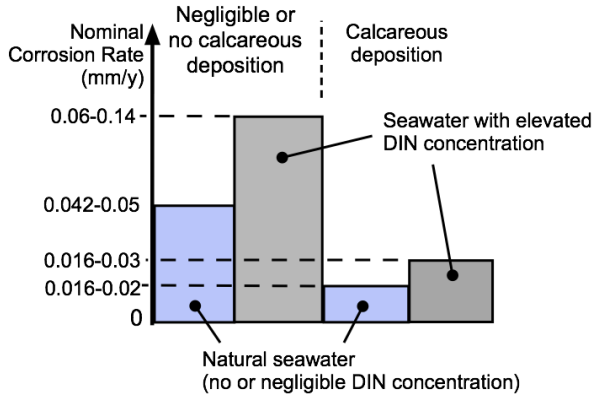

Figure 2. Comparison of estimated nominal longer-term marine immersion corrosion rates r_s and the effect of (a) calcareous deposition and of (b) the presence of dissolved inorganic nitrogen (DIN).

Discussion

The number of items of individual measurements that comprise the data summarized in Table 2 and as shown in Fig 2 varies considerably between the four exposure situations. The nominal corrosion rate estimated from the least number of data is for natural seawater subject to calcareous deposition. It is well-known that corrosion in such conditions is inhibited [1, 2, 3] and therefore the comparison shown can be considered reasonable even if subject to a degree of uncertainty. A considerably larger number of data are available for the other exposure conditions, so that, overall, they are sufficient to show that the rates of long-term corrosion differ considerably between them.

The most important observation in Fig. 2 is that for marine corrosion of steel in the presence of elevated nutrient (i.e. DIN) conditions the longer-term corrosion rate r_s also is inhibited by deposited calcareous material. Since the concentration of DIN has been positively correlated with MIC, it follows that MIC also is inhibited by deposited calcareous material. Fig. 2 shows that the effect of calcareous deposition lowers the rate r_s to about 1/3, irrespective of whether MIC is involved or not.

As is evident from earlier field observations for nutrient concentration measurements [10, 32], DIN concentrations need to be obtained at or as near as possible to the corroding steel. This is necessary because, unlike laboratory conditions, local water currents may dilute nutrient concentrations or may carry nutrient-charged waters away from the location of interest. Most observations suggest that the concentration of DIN generally is negligible in open seawaters away from anthropogenic pollution [33]. There is also the potential for depth to affect nutrient

concentration, with some uncertainty about the effect of depth on nutrient profiles, such as for DIN. Where surface DIN occurs, its concentration tends to decrease rapidly with depth [34] with other observations [35] indicating quite low DIN concentrations at depth, of the order of 10-20 μM, likely negligible in terms of the effect of any resulting MIC [10].

The data in Table 1 could be interpreted as showing that there is little evidence of calcareous deposition at depth. Observations regarding the decrease in concentration of $CaCO_3$ with depth have been reported [36]. Typically, this is measured by the so-called 'compensation depth', the depth at which the concentration of carbonates falls below 10% of the surface concentration. This depth appears to be highly variable between oceans, likely governed by factors such as rate of local carbonate supply, dilution and dissolution rates and variability in changes in pH with depth.

The presence of carbonates in rusts and on rusts is known to decrease the rate of corrosion of steels [2] and can be attributed to the carbonates decreasing the permeability of those rusts and thereby slowing the rate of oxygen diffusion to the corroding interface in Mode 1 of Fig. 1 when oxygen reduction is the dominant cathodic reaction [37]. A similar inhibition of diffusion will apply in Mode 2, but now of the gaseous hydrogen generated by the acidic hydrogen evolution cathodic reaction that then dominates the rate of the corrosion process [37]. In both Modes it is likely that the reduced diffusivity of the rust layers also will have the effect of reducing the rate of diffusion of nutrients from the external environment to the corrosion interface, thereby suppressing the rate of MIC particularly for Mode 2. Although plausible, this remains a matter for further investigation and confirmation. There are also other possibilities through which the presence of carbonates in and on rusts could influence the rate of MIC, since they also increase local pH conditions. For example, this may cause deviation from the optimal pH for bacterial metabolism [38]. Again, there is room for further detailed examination.

Overall, despite the admittedly limited data, the present results show that the net effect of calcareous deposition is positive in the sense that corrosion is depressed and that this is irrespective of whether corrosion occurs under abiotic conditions or involves some degree of microbiological influence. It is clear that observed influence of calcareous material could have practical implications, particularly for so-called impressed current cathodic 'protection', noting that this is actually cathodic inhibition caused by the lowering of surface pH by the calcareous deposits and also through inhibiting oxygen diffusion. The precise implications are currently being considered. Finally, laboratory testing presently in progress indicates similar findings to those given above.

Conclusion

1. Calcareous deposition on or within corroding steel surfaces tends to inhibit abiotic electrochemical corrosion in natural seawaters and also microbiologically influenced corrosion.
2. This effect appears to occur be irrespective depth of immersion, dissolved oxygen concentration and average seawater temperature,
3. The results appear to have implications for impressed current corrosion 'protection' as this tends to set up calcareous deposits on the metal surface.

References

1. LaQue, F.J. (1975) Marine Corrosion, Wiley, New York.
2. Hartt W.H., Culberson C.H. and Smith S.W. (1984) Calcareous deposits on metal surfaces in seawater: A review, Corrosion, **40**(11) 609-618.
3. Eilbeik S., Tseung A.C.C. and Mackay A.L. (1986) The formation of calcareous deposits during the corrosion of mild steel in sea water, Corros. Sci. **26**(9) 669-680.
4. Tanuguchi M., Dulai H., Burnett K.M., Santos I.R., Sugimoto R., Stieglitz T., Kim G., Moosdorf N., Burnett W.C. (2019) Submarine groundwater discharge: Updates on its measurement techniques, geophysical drivers, magnitudes, and effects, Front. Environ. Sci. **7**, 141 (pp. 1-26).
5. Humble R.A. (1949) The cathodic protection of steel piling in sea water, Corrosion **5**(9) 292-302.
6. Ackland B.G. and Dylejko K.P. (2019) Critical questions and answers about cathodic protection, Corr. Eng. Sci. Techn. **54**(8) 688-697.
7. Schwerdtfeger W.J. and Manuele, R.J. (1963) Coatings formed on steel by cathodic protection and their evaluation by polarization measurements, Corrosion, 19(2) 59t-68t.
8. Guezennec, J.G. (1994) Cathodic protection and microbially induced corrosion, Int. Biodeter. Biodegrad. **34** (3-4) 275-288.
9. De Baere K., van Haelst S., Chaves I.A., Luyckx D., Van Den Bergh K., Verbeken K., De Meyer E., Verhasselt K., Meskens R., Potters G. and Melchers R.E. (2021) The influence of concretion on the long-term corrosion rate of steel shipwrecks in the Belgian North Sea, Corros. Engi. Sci. Techn., **56** (1) 71-80.
10. Melchers R.E. (2014) Long-term immersion corrosion of steels in seawaters with elevated nutrient concentration, Corros. Sci. **81**, 110-116.
11. OSPAR (2017) Third OSPAR Integrated Report on the Eutrophication Status of the OSPAR Maritime Area, 2006-2014. OSPAR. see also Regional Quality Status Report II for the Greater North Sea, OSPAR Commission for the Protection of the Marine Environment of the North-East Atlantic, 2000. [http://www.ospar.org/eng/html/qsr2000, posted 29 June 2004].
12. Melchers R.E. Corrosion of steels and irons immersed in natural seawater for up to 600 Y, Corrosion **78**(1) 87-95.
13. Melchers R.E. (2021) Long-term immersion corrosion of irons and steel in seawaters with calcareous deposition, Corrosion **77**(5) 526-539.
14. Pillay, C. and Lin, J. (2014) The impact of additional nitrates in mild steel corrosion in a seawater/sediment system, Corr. Sci. **80** (3) 416-426.
15. Mason O.U., Canter E.J., Gillies L.E., Paisie T.K., Roberts B.J. (2016) Mississippi River plume enriches microbial diversity in the Northern Gulf of Mexico, Front. Microbiol. **7**, 1048.
16. Melchers, R.E. (2018) A review of trends for corrosion loss and pit depth in longer-term exposures, Corros. Mater. Degrad., 2018, **1**, 4.
17. Moore III, J.D. (2015) Long-term corrosion processes of iron and steel shipwrecks in the marine environment: A review of current knowledge, J. Maritime Arch. **10**(3) 191-204.
18. Watt M.A., Melchers R.E. & Jeffrey E. (2018) Long-term corrosion of steel chains on pacific ocean beach sand, Corrosion & Prevention, 11-14 Nov., Adelaide, Australasian Corrosion Association, Melbourne, paper 22.
19. https://www.bbc.com/news/science-environment-49420935 [Last accessed 16 March 2021]
20. Ballard R.D. (1987) The discovery of the Titanic, Warner Books, New York.
21. Anonymous (2012) Unseen Titanic, National Geographic **229**(3) 76-109.

22. MacLeod I.D. (2016) In-situ corrosion measurements of WWII shipwrecks in Chuuk Lagoon, quantification of decay mechanisms and rates of deterioration, Frontiers of Marine Science, **3**, Article 38.
23. Cook, C.D. & Peterson, C.E. (2005) Corrosion of submerged artifacts and the conservation of the USS Monitor, (in) Industrial applications of the Mossbauer effect, (Eds.) M. Gracia, J.F. Marco and F. Plazaola, American Institute of Physics, pp. 91- 96.
24. https://www.youtube.com/watch?v=-N6j6dGFoPo [Last accessed 8 April 2021].
25. https://www.youtube.com/watch?v=P7257ozFHkI [Last accessed 8 April 2021]
26. Cvikel D., Mentovich E.D., Ashenazi D., Kahanov Y., (2013) Casting techniques of cannonballs from the Akko 1 shipwreck: archaeometallurgical investigation, J. Min. Metall. Sect. B, Metall. **49**, 1, 107-119.
27. Martin J.M. (2004) An iron bastard minion drake extraordinary by John Browne from the pinnacle Swan (1641-53), The Int. J. Nautical Archaeology, **33**(1) 79-95.
28. http://www.historyscotland.com/features/resurrectingtheswan.html [8 April 2021]
29. M.A. Russell, D.L. Conlin, L.E. Murphy and J.D. Carr, "A minimum impact method for measuring corrosion rate of steel-hulled shipwrecks in seawater," The Inter. J. of Naval Archaeology, **35**(2) (2006), pp. 310-318.
30. D.L. Johnson, D.J. Medlin, L.E. Murphy, J.D. Carr, and D.L. Conlin, "Corrosion Rate Trajectories of Concreted Iron and Steel Shipwrecks and Structures in Seawater - The Weins Number," *Corrosion*, 67(12) (2011) pp. 125005-1-125005-9.
31. https://en.wijipedia.org/wiki/USS_Arizona_(BB-39) [Last accessed 13 April 2021]
32. Melchers R.E. & Lee T. (2021) Analysis of field observations of severe MIC of FPSO mooring chains (In) Failure Analysis of Microbiologically Influenced Corrosion, (Eds.) T.L. Skovhus & R.B. Eckert, CRC Press, Boca Raton.
33. Sverdrup H.U., Johnson M.W., and Fleming R.H. (1942) The Oceans: Their Physics, Chemistry, and General Biology, Prentice-Hall, New York.
34. Bristow L.A., Mohr W., Ahmerkamp S., Kuypers M.M.M., (2017) Nutrients that limit growth in the ocean, Current Biology, **27**, R474-R478.
35. Little B.J., Lee J.S., Briggs B.R., Ray R., Sylvester A. (2019) Examination of archived rusticles from World War II shipwrecks, Int. Biodeterior. Biodegrad., **143**, 104173.
36. Rezak R. (1974) Deep Sea Carbonates, (in) A. L. Inderbitzen (Ed.) Deep Sea Sediments: Physical and Mechanical Properties, Plenum Press, New York, pp. 453-461.
37. Melchers R.E. and Jeffrey R. (2022) The transition from short- to long-term marine corrosion of carbon steels: 2. Parameterization and modeling, Corrosion, B(5) 427-436.
38. Jin Q. and Kirk M.F. (2018) pH as a primary control in environmental microbiology: 1. Thermodynamic perspective, Front. Environ. Sci, B:21.

Passivation behavior of steel embedded in calcium sulfoaluminate cement mortar measured by impedance spectroscopy

R. Achenbach; M. Raupach;

Institute of Building Materials Research (ibac), RWTH Aachen University, Germany

Against the background of reducing CO_2 emissions in cement production, calcium sulfoaluminate (CSA) cement is an alternative to OPC because it can be burned at lower temperatures and therefore consumes less energy in production. Limestone, bauxite, and gypsum are required as raw materials and the binder type was invented in China and used there for a few decades. The pore solutions of concretes and mortars produced with CSA cement have a lower pH value than OPC. Literature values reported for the pH of CSA pore solution vary between 11.3 and 12.9. Since pH plays a decisive role in the passivation of embedded steel, the investigation of the passivation process is a fundamental component for the use of CSA cement in reinforced components. Nevertheless, few systematic studies on this are known to date.

In the investigations presented here, the passivation process of S235 steel in mortar made of CSA cement was investigated with various electrochemical measurements in comparison with a CEM I mortar. The focus was on electrochemical impedance spectroscopy (EIS) and its results in relation to other measurement methods such as open circuit potential (OCP), linear polarization resistance (LPR), and anodic polarization curves. In addition, two different storage conditions were investigated to depict the influence of oxygen availability on the passivation process in the CSA mortar.

Electrochemical study of steel reinforcement in the synthetic pore solution of alkali-activated binders

Ali Nikoonasab[1,2], Marina Licht[2], Thoralf Müller[1], Rebecca Achenbach[2], Michael Raupach[2], Gregor J.G. Gluth[1]

[1] Bundesanstalt für Materialforschung und -prüfung (BAM), Berlin/Germany, [2]RWTH Aachen University, Aachen/Germany

It is well known that cement manufacture, including CaCO3 calcination and clinker formation, is associated with substantial energy consumption and significant greenhouse gas emissions. Alkali-activated binders (AAB) and concretes made from them can significantly contribute to reducing CO2 emissions caused by the construction industry. However, to what extent and for how long concretes made from AAB can protect the steel in reinforced concrete components from corrosion is still unclear. Unlike PC-based binders, AABs are made by reacting alkaline solutions with solid precursors such as fly ash and ground granulated blast furnace slag (GGBFS). Therefore, steel reinforcement corrosion mechanisms in AAMs differ from PC-based binders. The present study aims to evaluate the corrosion behavior of steel rebar in alkali-activated materials (AAMs) synthetic pore solution with different chemical concentrations representing different GGBFS and Flay Ash based binders by performing electrochemical tests to measure the corrosion rate and corrosion potential of steel rebar. This information can be used to improve the design of AAMs in order to ensure a longer service life for these materials.

.

Passivation behavior of carbon steel in alkali-activated slag

Marina Licht, Institute of Building Materials Research – Conservation and Polymer Composites, RWTH Aachen University, Aachen, Germany; email: licht@ibac.rwth-aachen.de

Ali Nikoonasab, Federal Institute for Materials Research and Testing (BAM), Berlin, Germany; email: ali.nikoonasab@bam.de

Gregor J. G. Gluth, Federal Institute for Materials Research and Testing (BAM), Berlin, Germany; email: gregor.gluth@bam.de

Rebecca Achenbach, Institute of Building Materials Research – Conservation and Polymer Composites, RWTH Aachen University, Aachen, Germany; email: achenbach@ibac.rwth-aachen.de

Michael Raupach, Institute of Building Materials Research – Conservation and Polymer Composites, RWTH Aachen University, Aachen, Germany; email: raupach@ibac.rwth-aachen.de

Abstract:

By replacing Portland cement in specific applications, alkali-activated binders can make a significant contribution to reducing the CO_2 emissions caused by cement production and use. However, currently there is a lack of fundamental knowledge regarding the protection provided by alkali-activated binders to embedded steel reinforcement in concrete. For the use of alkali-activated binders in reinforced concrete structures exposed to chlorides or carbonation, the ability of the steel to reach and maintain the passive state is highly important. However, the processes of surface layer formation of steel in alkali-activated materials differ in some cases fundamentally from those in Portland cements. The present contribution describes first results of a DFG research project, in which the passivation behavior of carbon steel in alkali-activated slag concretes as well as CEM III/B concretes is being investigated.

The passivation behavior was characterized via various electrochemical techniques. Besides the measurement of the open circuit potential, electrochemical impedance spectroscopy was used to describe the developing passive layer. Along with the electrochemical measurements, the concrete pore solution was analyzed at relevant

stages. The examination of the pore solution is an effective method of classifying the environment surrounding the steel. In addition to the alkalinity, also the chemical composition of the solution is observed, which in turn provides information about the processes taking place on the steel surface and can be used for further evaluation.

Influence of polysulfide radicals on the mechanisms and intensity of corrosion of a carbon steel API 5L X65 in contact with cement grout in future nuclear waste disposal program

Yendoube Charles SANO MOYEME[1 2], Stéphanie BETELU[1], Johan BERTRAND[3], Stéphane GABOREAU[1], Karine GRONEN-SERRANO[2], Ioannis IGNATIADIS[1], [1]BRGM (French Geological Survey), Orléans, France, [2]LGC (University Paul Sabatier, UT3), Toulouse, France, [3]ANDRA, (French national radioactive waste management agency), Châtelet-Malabry, France

Cigeo is the future French deep Nuclear Waste Disposal (NWD) project for long-lived highly radioactive wastes. The clayey Callovo-Oxfordian formation (COx) was chosen as natural barrier to isolate the waste from people and environment. The waste will be placed in API 5L X65 steel linings, separated from the COx by a cemento-bentonic material (FS10B at the time), whose formulation may still evolve, and which will, among other things, keep the steel in a passive state thanks to its basic pH (>12). For safety reasons and reversibility of storage, continuous monitoring of the Corrosion Current Densities (CCD) or corrosion rate of the carbon steel in contact with this cementitious material is therefore necessary. That is the framework of this work.

A specific electrochemical methodology, consisting of i) stationary techniques (measurement of polarization resistance by Linear Polarization Resistance (LRP) and by Chrono-Amperometry (CA), Voltammetry around Open Circuit (VaOCP) by fitting the kinetic parameters), and ii) transitory techniques (measurement of impedance by Electrochemical Impedance Spectroscopy (EIS)), was carried out at regular intervals, for more than eight months, into a metric corrosion pilot, in which the steel was immersed into the cementitious FS10B material (water/solid ratio of 3). The system used a solid AgCl/Ag reference electrode that showed its robustness over the period and a Platinum counter-electrode. In complement, potentiometric measurements (pH, temperature, conductivity, redox potential, permittivity, dissolved O_2), and continuous analyzes of the level of sulfides were simultaneously made. Particular attention was given to the visual analysis of the evolution of the grout color, which acquired a green tint in the first days of the experiment, due to the anoxic conditions prevailing into the hydrated FS10B material and the presence of polysulfide radical anions ($S_n^{\cdot-}$) coming from the blast furnace slag used for CEM III/A cement production.

Indeed, the loss of the green tint was observed after five months of experiment. It suggested $S_n^{\cdot -}$ oxidation in agreement with FS10B partial dehydration and oxygen diffusion into the cement material. In addition to EIS, this specific behavior helped to understand, in particular, the reduction reaction involved during the API 5L X65 steel corrosion process and to choose the best kinetic model to apply during the first five month of experiment and beyong.

During the first five months of immersion into the cementitious FS10B material, the API 5L X65 steel was in an active state (2-5 µA/cm²) in the presence of $S_n^{\cdot -}$, despite the formation of a layer of corrosion products highlighted by EIS (Fig. 1A), and the corrosion current density was limited by the diffusion of $S_n^{\cdot -}$. Beyond five months, in the absence of $S_n^{\cdot}$, the steel become passive and the corrosion was limited by charge transfer of water molecules. These changes occurred in a few days and the corrosion current dropped down to about 0.02-0.07 µA/cm² (Fig. 1B).

Whatever the experimental conditions, the corrosion kinetics of API 5L X65 immersed in FS10B is dominated by the cathodic reduction reaction of water molecules. The latter is catalyzed by the presence of $S_n^{\cdot -}$. The use of the specific electrochemical methodology developed for corrosion sensing of API 5L X65 immersed in FS10B provides redundant information: it clearly identifies the changes at the API 5L X65 steel/FS10B interface as well as both the corrosion mechanisms and the kinetics.

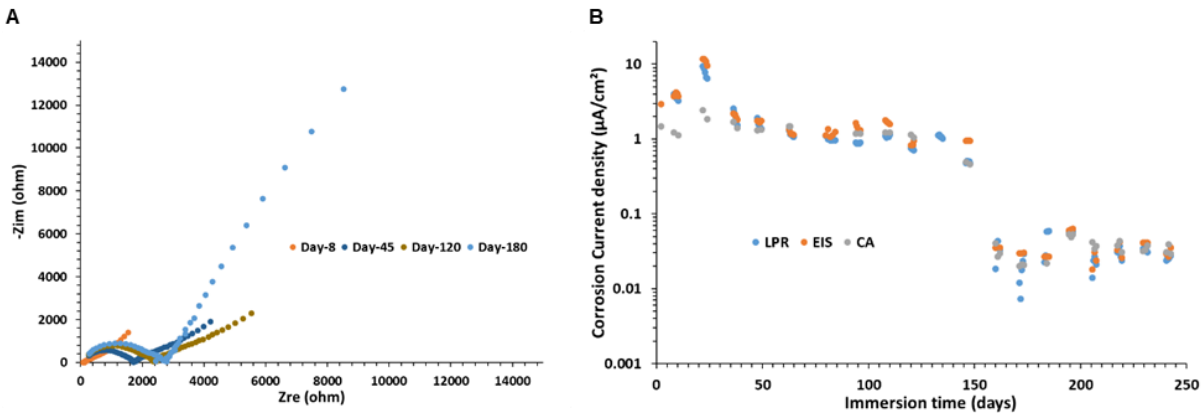

Figure 1. A) Evolution of impedance measurements in Nyquist mode derived from EIS measurements on API 5L X65 electrode immersed in a cement grout as a function of time. Evolution of API 5L X65-grout interface with time. B) Evolution of corrosion current densities (CCD) of an API 5L X65 carbon steel immersed in a cement grout as a function of time. LPR: CCD determined by Linear Polarization Resistance, EIS: CCD determined by EIS, CA: CCD determined by Chrono-Amperometry.

Impedance and Admittance Analysis on Corrosion Environment for Steel Rebar in Concrete

M. ITAGAKI, K. INOHIRA, H. WATANABE, and I. SHITANDA

[a] Department of Pure and Applied Chemistry, Faculty of Science and Technology, Tokyo University of Science
2641, Yamazaki, Noda, Chiba 278-8510, Japan
E-mail address: itagaki@rs.tus.ac.jp (M. Itagaki)

The degradation of concrete and the corrosion of steel rebar are serious problem in various infrastructures all over the world. The electrochemical measurements are useful to evaluate the stability of passive film formed on steel rebar in concrete [1]. An electrochemical impedance spectroscopy (EIS) has been used to investagate the rebar corrosion in concrete because the time constant of charge transfer at rebar/concrete interface can be determined [2, 3]. Due to the strong alkalinity of the healthy concrete environment, a protective passive film is formed on the surface of rebar and corrosion of the rebar is suppressed. However, the breakdown of passive film occurs by neutralization and enrichment of chloride ions in the water layer with the degradation of concrete. The authors investigated the critical values of pH and chloride concentration to maintain the passive film on steel rebar and discuss the depassivation mechanisms by the measurements of electrochemical impedance with the developed sensor probe [4]. When the passive film is formed on steel rebar, the impedance describes only part of semicircle with large diameter on the Nyquist plane, and it may be difficult to determine the passive film resistance from the convergent point in low frequency range. In this study, the corrosive environment of rebars in concrete was evaluated from admittance analysis with probe electrodes which were embedded in concrete. When the passive film was formed, a clear semicircle was observed in the admittance spectrum transformed from the impedance measurement results, and the film resistance could be obtained from the low frequency limit. In addition, probe electrodes were embedded in the concrete structure of viaduct of the superexpress trains in Japan, and the time variation of

corrosive state in concrete was investigated by combination of impedance and admittance analyses.

References:

[1] ASTM C 876-91 (Reapproved 1999): Standard Test Method for Half-Cell Potentials of Uncoated Reinforcing Steel in Concrete, Annual Book of ASTM standards, Vol. 03.02, pp. 457-462, 1999.
[2] J. L. Dawson, L. M. Callow, K. Hladky and J. A. Richardson, Corrosion/78, No-125 (1978).
[3] Y. Hoshi, T. Koike, H. Tokieda, I. Shitanda, M. Itagaki, and Y. Kato, J. Electrochem. Soc., vol. 166, p. C3316-C3319 (2019).
[4] Y. Hoshi, S. Watanabe, H. Tokieda, I. Shitanda, M. Itagaki, Zairyo to Kankyo, vol. 68, p. 303-308 (2019).

Further work on the use of electrochemical noise measurements to assess the corrosion of reinforcing bar in concrete

Paul Lambert[a] , Douglas Mills[b], Reuben Osahon[b] and Tayo Adeyinka[b]

a - Mott MacDonald, Spring Bank House, Stamford Street, Altrincham, WA14 1ES, UK

b - University of Northampton, Waterside Campus, Northampton, NN1 5PH, UK

Abstract

The assessment of corrosion rate by electrochemical noise has been made easier to carry out by the availability of a purpose-built proprietary device (ProCoMeter) designed to make electrochemical noise measurements (ENM) in the field and offering various electrode arrangements. In previous studies at the University of Northampton, mortar samples containing varying levels of chloride and with embedded steel bars were evaluated using three different ENM arrangements (Bridge , SSS, and NOCS) and these have been reported [1]. Comparisons were then made between the expected metal thickness loss obtained from the three ENM arrangements, and the actual metal thickness lost. It was found that the Standard Single Substrate arrangement (SSS) was the most accurate based on direct metal loss measurements. In the current study the work has been extended to assess whether ENM gave comparable results to the more established Linear Polarisation Resistance (LPR) method. This again employed mortar samples with embedded steel bars and varying levels of chloride and the results which are presented here showed a good correlation. In addition, the ENM method was employed to check the effectiveness of a cathodic protection (CP) system using zinc (galvanic) and MMO titanium (impressed) anodes. Whilst this study is on-going, the results to-date are presented here. It is intended that electrochemical noise measurements will shortly be made on reinforced concrete infrastructure, with and without applied CP.

Keywords

Electrochemical Noise; Reinforced Concrete; Chloride Pitting; Linear Polarisation; Cathodic Protection.

Introduction

Electrochemical methods are effective at non-destructively assessing the corrosion of steel in reinforced concrete. Angst et al. [2] reviewed the methods employed to identify reinforcement corrosion in published work and found the three most popular methods employed were, in order of popularity, half-cell potential, linear polarisation resistance (LPR), and visual assessment, the latter being destructive and requiring subsequent remediation of the test area.

The electrochemical noise method (ENM) as applied to reinforced concrete was assessed by Hardon et al. [3], comparing the results to the more widely used half-cell potential and LPR techniques. Due to limitations in the equipment available at the time (1988) it was concluded ENM would probably not be suitable for the site investigation of reinforced concrete corrosion. Subsequent studies [4-8] confirmed ENM had the capability to be an effective method to monitor the rate of corrosion of steel reinforcement in concrete whether in the laboratory or on site. A review of electrochemical noise carried out by Da-Hai Xia et al. [9] identified the various experimental arrangements and models that have been employed to achieve near-quantitative evaluation of corrosion rates for a range of environments, including steel in concrete.

The work reported here forms the most recent phase of a continuing study into the suitability and effectiveness of ENM, as provided by the purpose built ProCoMeter, for the measurement and monitoring of steel reinforcement corrosion rates in the field on actual structures suffering from corrosion resulting from carbonation or chloride induced pitting.

Experimental

The various phases of the study have employed moderately sized mortar samples with embedded steel bars and a range of chloride ion additions as admixed sodium chloride, dissolved into the mixing water. In the latest phase of the study a single steel cover depth of 30mm was employed. Each sample had three reinforcing bars, each nominally 7mm in diameter. A layer of clean (chloride free) adherent rust was left on the bars to encourage early bond development with the mortar. The centre bar which only protruded at one end was intended to be used primarily as a counter electrode for LPR. Figure 1 shows the dimensions and general arrangement of the steel bars employed in each specimen.

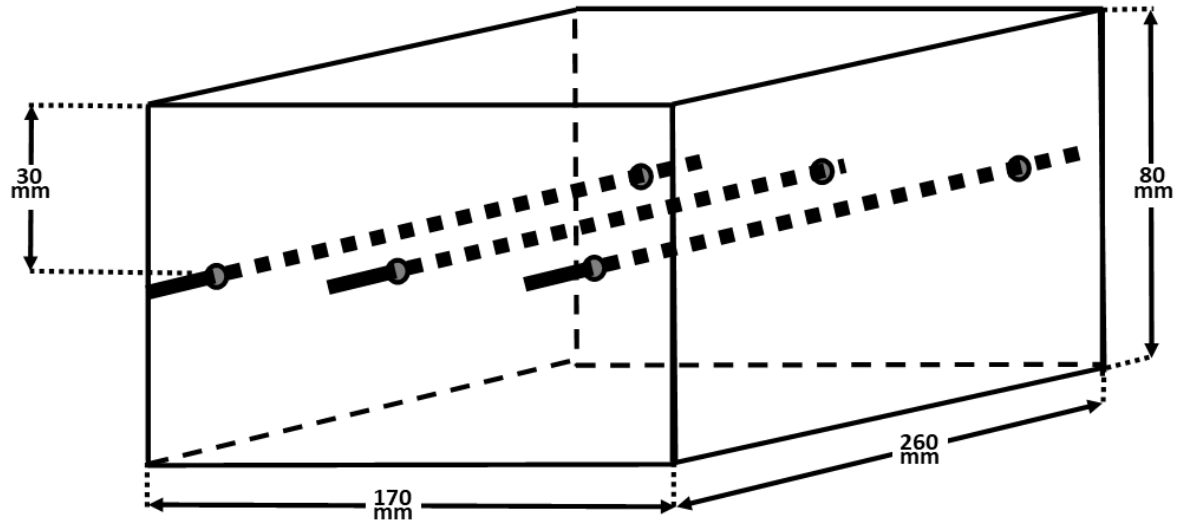

Figure 1: Schematic of mortar sample showing dimensions and position of bars (not to scale).

The bars were masked with a duplex coating system to limit crevice attack at the ends. This consisted of a first coat of a cement slurry coating (OPC/fine sand/SBR solution), and a second coat of bituminous coating. The first coating ensures the steel beneath the masking remains passivated with the bituminous coating preventing water (and chlorides) from accessing the steel. The second coating is applied in such a way as to ensure it does not touch the steel directly as this could itself result in crevice corrosion. This approach has proved effective in similar electrochemical studies [10].

The mortar mix consisted of 1-part OPC, 4-parts fine sand and 0.7-part water (all parts by weight). The water-cement ratio was therefore 0.7. The components were hand blended and mixed for several minutes prior to casting in layers and tamped to remove excessive air. They were then covered (using the close-fitting lids) and cured at room temperature for 96 hours. The sample with 4% chloride (by weight of cement) had the addition made to the mixing water as sodium chloride. A mortar with a high water-cement ratio was employed to facilitate easier breakout of the bars at the end of the test period and avoid aggregate bridging of the steel in the relatively small samples.

An example of the cast and cured samples is shown in Figure 2 and has the close-fitting lid removed to allow monitoring for half-cell potential, LPR and ENM to be carried out from the exposed surface of the mortar, directly above the steel bars. Upon completion of a set of readings, the lid is replaced to prevent the mortar from drying out excessively in the laboratory air.

Figure 2: Example of cast and cured specimen with lid removed to allow monitoring.

The embedded steel specimens were monitored by means of half-cell potential and ENM using the Bridge, SSS (simple single substrate) and NOCS (no connection to substrate) arrangements as shown in Figure 3.

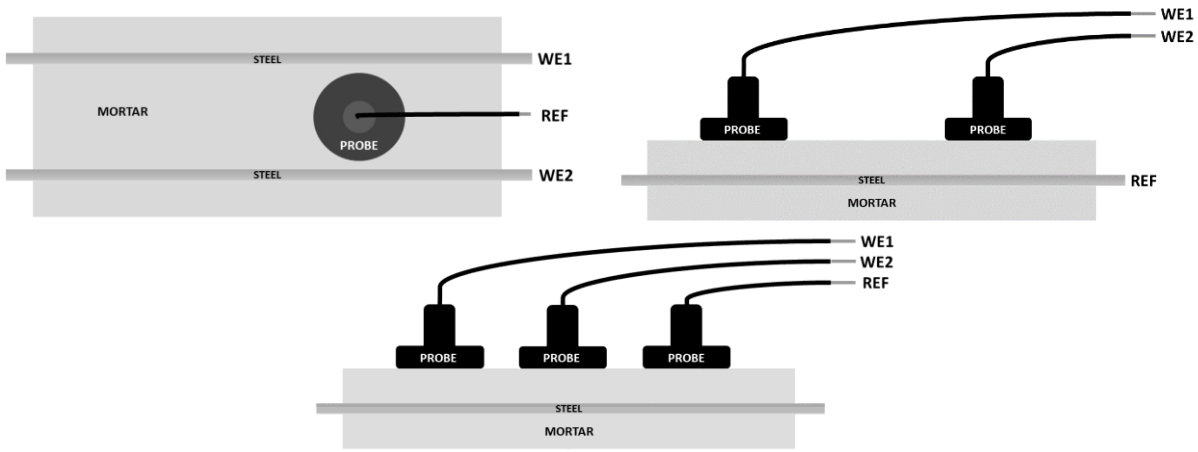

Figure 3: Bridge (upper left) and SSS (upper right) and NOCS (lower central) arrangements for ENM [1]

Readings were obtained by means of a proprietary ENM instrument (ProCoMeter) utilising solid state silver/silver chloride reference electrodes, both supplied by the DCVG Company, Wigan, UK.

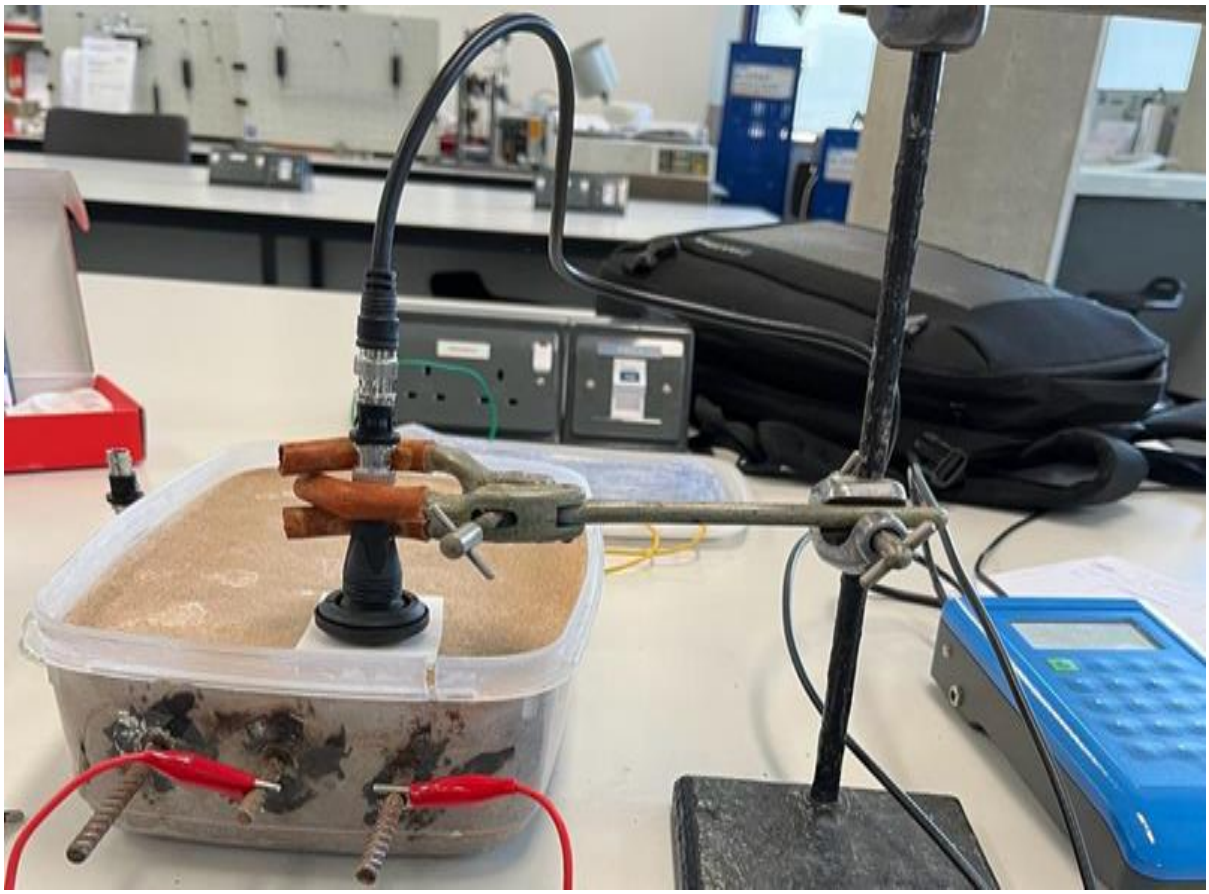

Figure 4: Arrangement for carrying out ENM by the bridge arrangement (ProCoMeter on right).

The data collected was used to calculate values of Rn (the SD of voltage noise divided by the SD of current noise) which in turn could be used to determine the corrosion current by means of the Stern–Geary equation. It has been confirmed by others that Rn can be considered equivalent to Rp [11]. The equipment used and general arrangement for the ENM tests arrangement are shown in Figure 4.

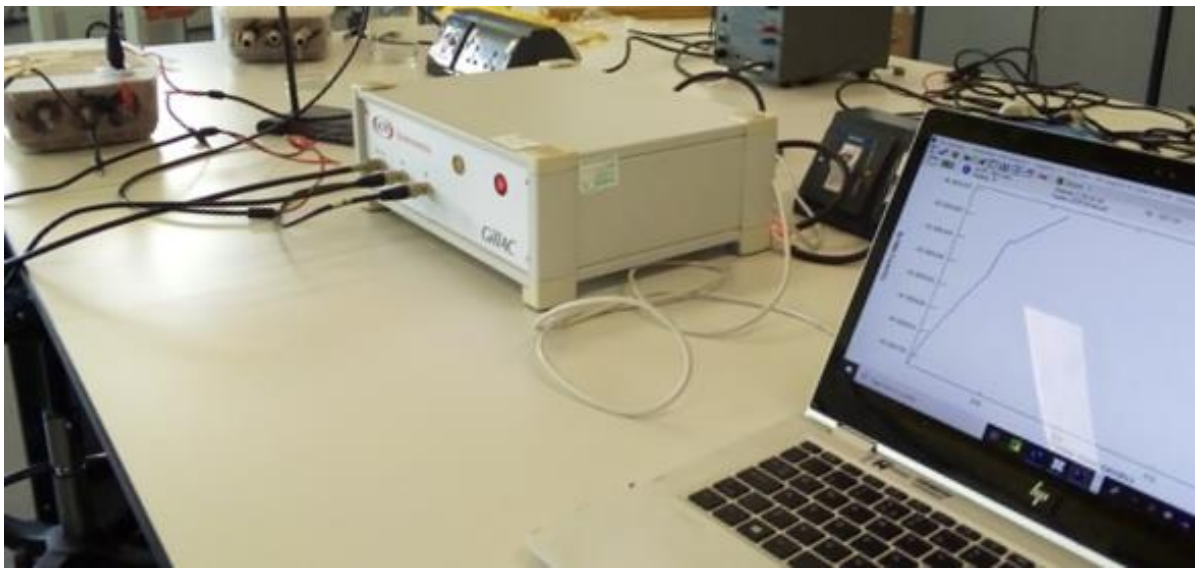

Figure 5: Arrangement for carrying out LPR measurements with the ACM GillAC automated potentiostat connected to laptop running dedicated software.

In addition to ENM, measurements of the corrosion behaviour of the embedded bars in the two specimens was assessed using the more widely applied linear polarization technique (LPR) [12]. A small DC voltage perturbation disturbance (-30mV to +30 mV with respect to the rest potential) by means of an ACM Instruments GillAC automated potentiostat, operating in LPR mode. The embedded steel bars acted as the working electrode (WE), a solid-state silver/silver chloride electrode was used as the reference (REF) and a stainless steel plate acted as the auxiliary electrode (AE). A pad moistened with 0.1 M chloride solution was placed between both the reference and auxiliary electrodes to maintain electrolytic contact with the mortar surface. The data generated was transferred to a computer where an ACM software package was employed to determine the polarisation resistance, Rp, see Figure 5.

The two specimens were then provided with cycles of cathodic protection by two methods; galvanic anode cathodic protection (GACP) utilising a hydrogel-backed pure zinc sheet; and impressed current cathodic protection (ICCP) by means of a mixed metal oxide titanium (MMOTi) mesh enclosed in a non-woven cloth wrap moistened with demineralised water and powered by a low-voltage DC power supply. For each CP type, the specimens were polarised for a total of 14 days and ENM employed to assess the influence on the steel of short-term cathodic protection.

Results

As the present study is ongoing the following results should be considered as preliminary, with the intention of developing the procedures examined, number and size of specimens and length of exposure time in future studies. While not definitive, they provide an indication of the potential value of the ENM technique in the evaluation of the corrosion of steel reinforcement and the most promising methods of application.

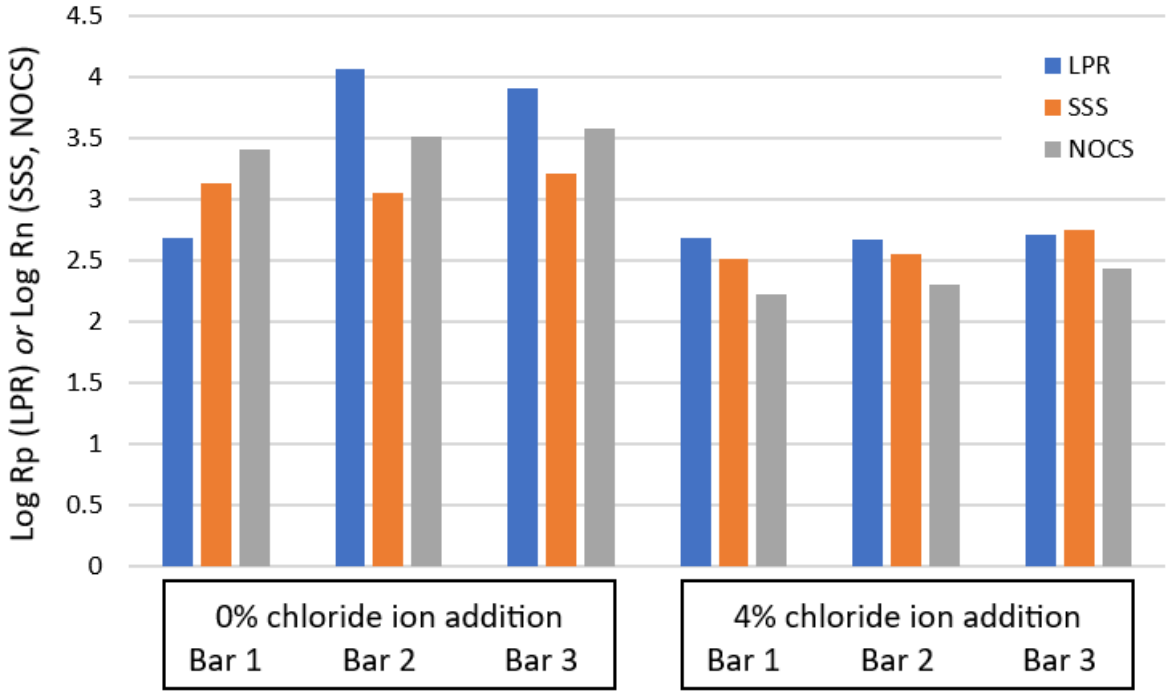

Figure 6: Comparisons of Rp and Rn values obtained by LPR or ENR (SSS ad NOCS arrangements).

Comparison of LPR and ENR

The values of Rp (from LPR) and Rn (from ENM using SSS or NOCS) were found to be comparable for the two specimens with 0% and 4% chloride ion addition. Average values from multiple readings taken from the three bars in each specimen are shown plotted against Log Rp (for LPR) or Log Rn (for ENM by either the SSS or NOCS arrangement) in Figure 6.

The relationship between the values of Rp obtained by LPR and Rn obtained by ENM using either the SSS (previous found to be the most accurate as a predictor of corrosion rate) and NOCS (favoured for site applications as no connection is required to the steel), is consistent. The measurements obtained by all methods showed the values of Rp or Rn to be higher for the 0% chloride specimens than the 4% chloride specimens, consistent with a lower corrosion rate in the former.

When comparing the two arrangements employed to obtain the ENM values it is noted that for the specimens tested the NOCS values were higher than the SSS values for the lower corrosion rate (0% Cl) specimen, with the trend reversed for the higher corrosion rate specimen (4% Cl). This has the effect of increasing the difference in value between the two conditions and if it can be shown to be a consistent effect could prove useful when employing the NOCS arrangement in the field by accentuating the difference between areas of low and high steel reinforcement corrosion rate.

Effect of CP on ENR

Values of Rn obtained by ENM using the Bridge and SSS arrangements were obtained from the steel bars in the two mortar specimens (0% and 4% chloride ion addition) by either GACP (zinc hydrogel sheet) or ICCP (MMO Ti) to assess whether a measurable change in the value of Rn (and therefore corrosion rate) could be determined after a relatively short initial polarisation of 14 days. The average results obtained from the sets of three bars in each specimen are shown in Table 1. For both specimens, the application of CP, either by GACP or ICCP, resulted in an increase in Rn, consistent with a reduction in corrosion rate.

Specimen	0% Cl ion addition	4% Cl ion addition
Average Rn before CP	407	13
Average Rn after GACP	1518	503
Average Rn after ICCP	868	4078

Table 1: Rn values (Ω) for 0% and 4% Cl samples before and after GACP and ICCP

The reasons for the 0% Cl specimen showing a greater increase with the galvanic rather than impressed current system are not immediately apparent but, based on observations made in the laboratory at the time of the testing, may be the result of the GACP treated specimen taking longer to depolarise following the disconnection of the anode, aggravated by a higher moisture content at the time of the measurements, which could have introduced a drift in the potential that could not be automatically accommodated by the monitoring equipment.

Discussion & Conclusions

The assessment of the corrosion rate of steel reinforcement in concrete by means of electrochemical noise measurement (ENM) offers potential benefits over existing methods commonly employed. LPR has proven to be highly effective in the laboratory and can be applied in the field but requires connections to the steel reinforcement and the area of steel being polarised to be determined.

Correlation has been shown, in this and other studies, between LPR, ENM using the SSS arrangement and direct measurement of extracted bars. The eventual aim of this extended study is to show that ENM can be used effectively on site by employing the NOCS arrangement where no connection to the steel is required. This would allow ENM to be routinely employed for the monitoring of existing structures, including those consisting of multiple pre-cast elements with no electrical continuity between units and therefore requiring multiple breakouts to the steel which subsequently require reinstatement.

In the work reported here it has been shown that measurements using LPR can be comparable to those obtained by ENM using various arrangements, specifically SSS which has previously been found to be the most accurate, and NOCS the preferred method for site use. Further studies are required to confirm the repeatability of such measurements, but the intention is to carry out a proportion of these on site in order to develop the methods and equipment best suited for the field application of the ENM technique.

With many vulnerable reinforced concrete structures now incorporating some level of cathodic protection, usually installed as part of a remediation programme, it is essential to identify any interactions between such systems and the methods of monitoring employed. The preliminary study reported above shows the ENM method to be capable of operating on embedded steel that has been subjected to both galvanic and impressed current CP. In both cases, measurements were taken when the operating CP system was disconnected, a standard procedure in all but the most basic of galvanic systems, in order to demonstrate the required polarisation of the steel. The preliminary results indicate that the benefits of CP in the reduction of corrosion rate can be identified at an early stage through the use of ENM on depolarised systems in the laboratory but requires further confirmation in the field.

References

1. D. Mills, P. Lambert and S. Yang, Materials, **14 (**2021) 5392.
2. U. Angst, B. Elsener, C.K Larsen, and Ø. Vennesland, Cem. Concr. Res., **39** (2009) 1122.
3. R.G. Hardon, P. Lambert and C.L. Page, Br. Corros. J., **23** (1988) 225.
4. K. Videm, Proc. 19th Int. Corrosion Congress, Granada, Spain, (2002) 22.
5. D.J. Mills and N.R Short, Proc. 19th Int. Corrosion Congress, Granada, Spain, (2002) 104.
6. D.J Mills, S.J. Mabbutt and N.R. Short, Proc. EUROCORR (2003) 55.
7. A. Legat, M. Leban and Ž Bajt, Electrochem. Acta, **49** (2004) 2741.
8. L. Mariaca, A. Bautista, P. Rodriguez and J.A. Gonzalez, Mater. Struct. **30** (1997) 613.
9. D. H. Xia, S. Song, Y. Behnamian, W. Hu, Y.F. Cheng, J.L. Luo and F. Huet, J. Electrochem. Soc., **167** (2020) 081507.
10. P. Lambert, C.L. Page and P.R.W. Vassie, Mater. Struct. **24** (1991) 351.
11. I.B. Obot, L.B. Onyeachu, A. Zeino and S.A. Umoren, J. Adhes. Sci. Technol. **33** (2019) 1453.
12. C. Andrade and C. Alonso, Mater. Struct. **37** (2004) 623.

Non-invasive corrosion diagnosis of reinforced concrete structures: A sensitivity analysis using a multi-channel resistivity approach

Benjarese ONIANGUE-ONGANIA[1,2], Julia HOLZHAUER[1], Romain RODRIGUES[3], Stéphanie BETELU[3], Stéphane GABOREAU[3], Rachid CHERIF[2], Ioannis IGNATIADIS[3], Karim AIT-MOKHTAR[2], Julien GANCE[1]

[1] IRIS Instruments, 1 avenue Buffon, 45100 Orléans, France.

[2] LaSIE, UMR CNRS 7356, La Rochelle University, avenue Michel Crépeau, 17042, La Rochelle Cedex 1, France.

[3] BRGM, 3 avenue Claude Guillemin, 45060 Orléans Cedex 2, France.

Abstract

Non-Destructive Electrical Methods (NDEM) using a four-electrode configuration are being developed for the corrosion monitoring of reinforced structures without altering their integrity [1]. Indeed, unlike conventional techniques based on a three-electrode configuration that requires a connection to the rebar, the measurement is performed directly on the concrete surface: two probes A and B inject a direct current while two other probes M_n and N_n measure an induced potential difference. However, despite the practical relevance of NDEM, their use is still at the margin. To promote such techniques, whose measured apparent resistivity ρ_{app} depends on both concrete resistivity and corrosion rate, a better definition of their sensitivity domain is required, along with a detailed sensitivity analysis to concrete and rebar properties.

This work reports a methodology designed to characterize the sensitivity domain for resolute corrosion rate determination from ρ_{app} measurements using five Wenner-Schlumberger-Reciprocal (WSR) configuration (Figure 1). Specifically, in this work, models were computed to establish the sensitivity domain of the novel CorImager®-device developed by IRIS Instruments.

The extensive modeling of synthetic data – considering several corrosion current densities j_{corr}, concrete resistivity ρ_c, effective depth c_{eff} and rebar diameter Φ – provided abacus showing three distinct regions: two regions for extreme j_{corr} values in which ρ_{app} is almost constant, and one region for intermediate j_{corr} values in which ρ_{app} significantly decreases with increasing j_{corr} (Figure 2a). The latter region, defined as the sensitivity domain, depends on ρ_c, c_{eff}, Φ, and the geometry of the chosen observation channel (Figure 2b). Within this domain, the amplitude of the sensitivity

increases with the decrease in c_{eff} or the increase in Φ, while increasing ρ_C by one order of magnitude shifts the domain of j_{corr} by one order of magnitude to lower values. The use of abacus allows quantifying the expected uncertainty on j_{corr}, according to the electronic noise of the monitoring device and to measurement uncertainties on c_{eff} or Φ. The interpretation of overall results allows providing good practices to limit the impact of potential errors for corrosion diagnosis in field application.

While developed specifically for the CorImager®-device in WSR configuration, the methodology can easily be adapted to any four-point configuration with apparent resistivity measurements. As a perspective, the data acquired with a multi-channel configuration open the way to inversion processes to determine the distribution of concrete resistivity and corrosion current density within the investigated volume.

References

[1] R. Rodrigues, S. Gaboreau, J. Gance, I. Ignatiadis, S. Betelu, Reinforced concrete structures: A review of corrosion mechanisms and advances in electrical methods for corrosion monitoring, Construction and Building Materials. 269 (2021) 121240. https://doi.org/10.1016/j.conbuildmat.2020.121240.

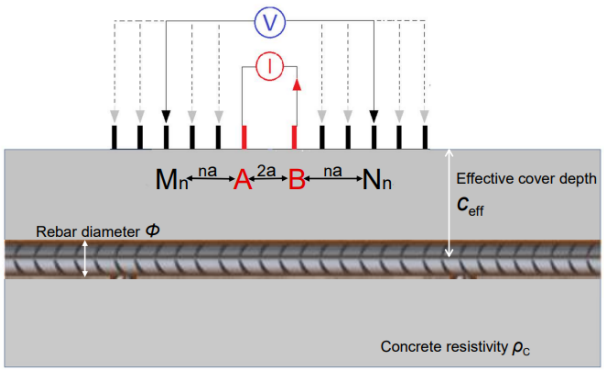

Figure 1. Schematic representation of WSR configuration and the different parameters of the model.

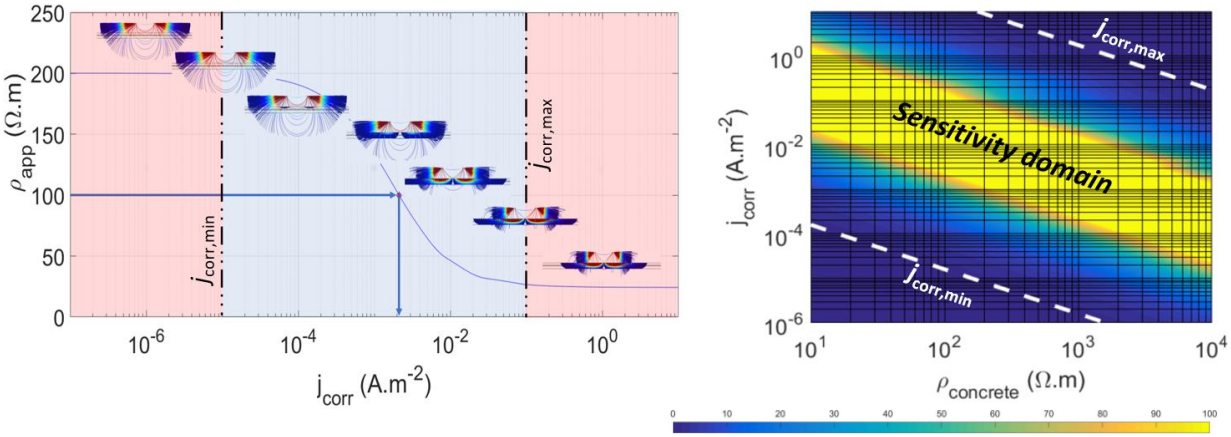

Figure 2. (a) Example of an abacus showing the evolution of ρ_{app} as a function of j_{corr}, with the three regions, (b) Example of a sensitivity diagram showing the evolution of j_{corr} as a function of ρ_c, with the color bar indicating the variation in sensibility. The limits $j_{corr,min}$ and $j_{corr,max}$ are defined relatively to a resolution of 1 %.

Inversion of non-invasive resistivity measurements in four-electrodes configuration for corrosion characterization in reinforced concrete samples.

Julia HOLZHAUER, Iris Instruments, Orléans / France
Julien GANCE, Iris Instruments, Orléans / France
Yannick FARGIER, Université Gustave Eiffel, Bron / France
Christophe CHIABERGE, BRGM, Orléans / France
Romain RODRIGUES, BRGM, Orléans / France
Stéphanie BETELU, BRGM, Orléans / France

In the context of corrosion diagnosis in reinforced concrete (RC), non-invasive four-point electrical measurements represent, by many aspects, an interesting alternative to classical three-point characterization with rebar connection. As a matter of fact, the four-point surface measurement without connection to the rebar, is known to be sensitive to the rebar corrosion. Yet, this rebar effect was first seen as a drawback to the method, initially meant to provide a reliable estimation of the structure durability by assessing the concrete resistivity.

The first advantage of this method, namely its absence of rebar connection, comes with a complexification of the current paths within the RC structure. Part of the current diffuses only in the concrete while a residual part will penetrate in the rebar depending on its corrosion current density j_{corr}. The determination of the rebar corrosion through that kind of measurement is therefore less straightforward than for three-point measurements. However, by multiplying the acquisition points and running an Electrical Resistivity Tomography (ERT), it becomes conceivable to spatially image the RC structure. The four-point resistivity data may be inverted in order to recover both the instantaneous corrosion rate of the rebar as well as the matrix electrical properties and heterogeneities.

We developed a laboratory ERT experiment (CorImager®-device from IRIS Instruments) designed to sequentially run multiple four-point measurements on prismatic reinforced mortar specimens of dimensions 10 x 10 x 40 cm^3. The device, composed on the one hand of 96 electrodes distributed over the 4 faces of a corset-like antenna (see Fig.1), and on the other hand of an acquisition central enabling multi-

channel measurement and switching, provides us with a 3D investigation of our probe. Our samples collection gathers about thirty specimens, most of them armed, differing in the mix or in the rebar preparation. Some have been specifically designed to test the widely reckoned ability of this method for heterogeneous matrix characterization, on our unusually small sample dimension.

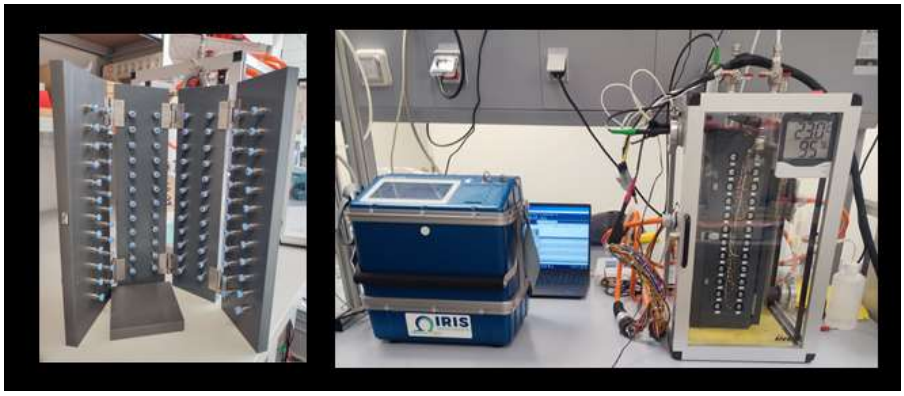

Figure 1 : On the left view of the open antenna counting 96 electrodes, on the right view of the acquisition central together with the closed antenna disposed within a confining unit

Preliminary results on such a heterogeneous sample, bearing two polystyrene resistive inclusions of dimension 4 x 4 x 3 cm^3 in a regular CEMI mortar matrix such as w/c = 0.5 and s/c=3, have already shown that this method can concomitantly provide, by data inversion, an image of the matrix heterogeneity (see Fig.2) together with an estimation of a uniform corrosion value. This j_{corr}-value of 16mA/m² obtained through inversion of ERT data, was comparable to the values of 8 ± 2 mA/m² determined by classical three-points measurements.

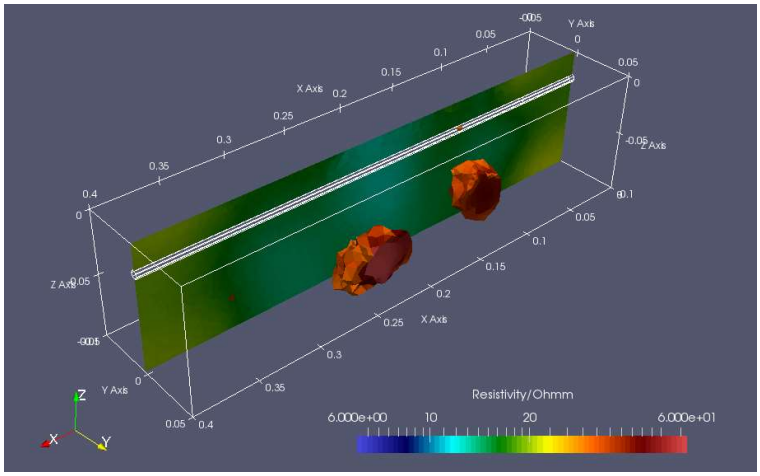

Figure 2: Results of ERT data inversion on a reinforced mortar sample having two resistive inclusions.

Corrosion mechanisms in macro-defects of reinforced and prestressed concrete structures

Sergio Lorenzi, University of Bergamo, Italy;
Marina Cabrini, University of Bergamo, Italy;
Denny Coffetti, University of Bergamo, Italy;
Tommaso Pastore, University of Bergamo, Italy;

For a long time the construction world considered reinforced concrete as an almost eternal material thanks to the protective capacity of the concrete made with Portland cement against rebars corrosion. In the last 50 years, however, the service experiences and the research conducted in the field of concrete durability have made it possible to clarify how the corrosion of reinforced concrete structures is strictly related to the ability of concrete to protect the reinforcements from the penetration of aggressive agents, such as carbon dioxide and chlorides. These substances can cause the breakdown of the passive film which naturally forms on carbon steel when the concrete is properly poured and compacted. In the presence of small defects- such as micro-cracks or fissures- hydration products of Portland cement act as self-healing agents able to counteract the penetration of aggressive substances from the outside, due to well-known and documented mechanisms. These phenomena can be considered "exogenous", as they come from the outside and they can cause corrosion initiation after a certain period of time, followed by a phase in which the attack propagates up to the expulsion of the concrete cover, according to the well-known Tuutti model. The cement matrix therefore behaves like a "smart protective coating", capable of protecting and sustaining over time the alkalinity contained within the pores in direct contact with the reinforcing bar, thus decreasing the corrosion rate at negligible values. The presence of defects of significant size within the cement matrix – i.e. lack of compaction, pouring in restricted zones or simply due to contingencies, represent a completely different problem. Corrosion can occur, in this case, for endogenous causes, regardless of the presence or absence of aggressive substances such as chlorides or carbon dioxide. In this context it is inappropriate to even consider the Tuutti diagram to describe the corrosion degradation process as it initiates and propagates inside the concrete starting from its placing. The evolution of the corrosion phenomena inside pre-existing defects is then strictly related to thermo-hygrometric equilibria inside

the concrete and the environment, as well as to transport phenomena in the cement matrix considered as a porous medium. The work deals with corrosion issues in macro-defects of reinforced concrete structures and aims to determine the environmental conditions that occur within the macro-defects in order to adequately identify and describe the corrosion mechanism which occurs in conditions in which there is no intimate steel-concrete contact, necessary for corrosion protection.

Development of cement with increased corrosion protection capacity through introduction of powder inhibitor

Serdar, M., Carević, I., Flegar, M., Ram, K./University of Zagreb, Faculty of Civil Engineering, Croatia, Miksic, B./Cortec Corporation, USA, Rogan, I./CorteCros Ltd, Croatia

Concrete structures are located in a wide variety of environments, in contact with various aggressive media, and simultaneously exposed to various mechanical and environmental stresses. Chloride-rich environments are considered the most aggressive for reinforced concrete structures, with the main cause of reduced serviceability being corrosion of reinforcement. In engineering practice, there is a constant need for new technologies and materials that allow better corrosion protection of reinforced concrete structures without complicating the application or prolonging the construction process. The objective of the study was to develop a hybrid cement containing corrosion inhibitor in powder form that can be used like a classical cement but with significantly improved corrosion protection for reinforcing steel. The relevant properties of cement and concrete required for the application of such a cement in the construction industry were systematically investigated.

Corrosion inhibitor used in the study, MCI-2006 NS, is a powder additive to concrete, which acts as a corrosion inhibitor to protect reinforcement in concrete structures. In order to identify the effect of the additive, it was added as 0.5% of different types of cements available on the market: normal strength gain cement with limestone (CEM II/B-LL 42,5 N), rapid strength gain cement with limestone (CEM II/A-LL 42,5 R), normal strength gain cement with slag and silica fume (CEM II/A-M (S-V) 42,5 N) and normal strength gain low heat cement with slag (CEM III/A 42,5 N LH). Chemical analysis of developed hybrid cements, fineness, density, heat of hydration, consistency, setting time, volume stability, and compressive strength were tested. Concrete was designed with a targeted compressive strength class C30/37, which is a minimum requirement for marine environment according to standard EN 206. Following properties were tested on concrete level: temperature, consistency, density, air content, compressive strength, water permeability, chloride migration, carbonation, gas permeability and freezing and thawing. Corrosion was analysed by impressing external current in NaCl environment. Samples for long-term monitoring of corrosion process according to ASTM G109 were also prepared within the study.

Hybrid cements with the addition of corrosion inhibitor satisfied all criteria for cements according to EN 197-1. The main effect of the inhibitor was observed on the consistency of cement. Mainly, with the addition of 0.5% cement wt. of corrosion inhibitor MCI-2006 NS, all cements required 5 – 15 % less water to reach the standard consistency. The addition of corrosion inhibitor also prolonged the initial and final setting, less pronounced for cements with limestone and more pronounced for slag and fly ash cements. Such retardation could be beneficial for the application of such cement in warm climates. Additionally, 2-day and 28-day compressive strength was slightly increased for cements with limestone and slightly decreased for cement with fly ash and slag.

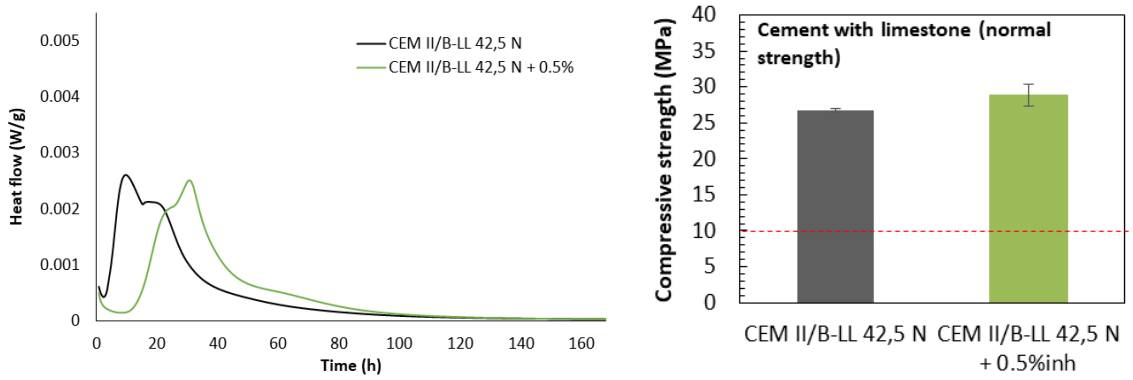

Figure 1. Heat of hydration and 2-day compressive strength of cement without and with 0.5% cement wt. inhibitor MCI-2006 NS

The same effect on workability was obtained on concrete level, with improvement in workability of concrete prepared with cement with corrosion inhibitor. The introduction of corrosion inhibitor MCI-2006 NS did not introduce any other significant changes on concrete behaviour; concrete remained in the same quality class across different degradation mechanisms (freezing and thawing, water and gas permeability, chloride migration, carbonation), with an improvement of corrosion protection capacity.

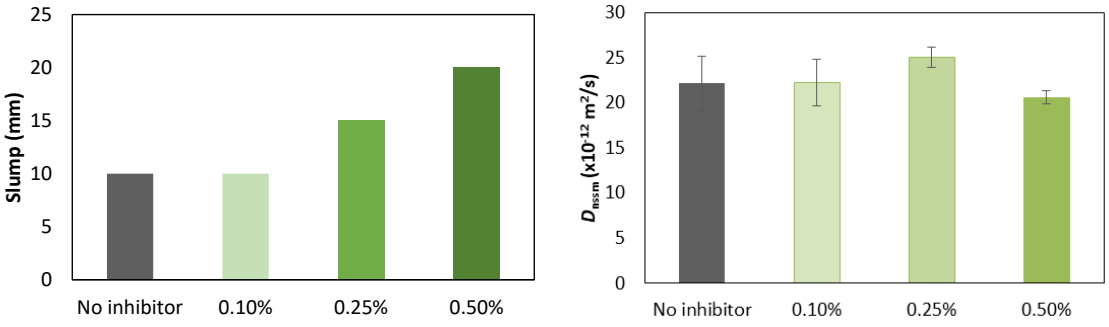

Figure 2. Workability and 28-day chloride migration of concrete with different amount of inhibitor added as % wt. of cement

Method for measuring corrosion-related properties of reinforced concrete

B. Díaz[1], X.R. Nóvoa[1], C. Pérez[1], A. Pintos[1], V. Vivier[2]

[1]CINTECX, Universidade de Vigo, EEI, ENCOMAT Group, 36310 Vigo, Spain.

[2]Sorbonne Université, CNRS, Laboratoire de Réactivité de Surface, Paris, France.

The present communication explores the possibilities of a Wenner-type probe for monitoring the rebar's polarization resistance and the cover's resistivity. The resistivity, determined in the local area under test, serves for normalization of the resistance measured so that the actual polarization resistance can be retrieved.

The experimental arrangement takes advantage of the concepts of the floating electrode[1,2] (electronic conductor embedded in an ionic conductor, the whole system under an electric field) and resistance for the flow of current to a disk[3,4].

The results presented, including numerical simulations, will demonstrate that the measurement is feasible, although upscaling the 4x4x16 cm^3 experiment made is needed before developing field applications.

References

[1] M. Keddam, X.R. Nóvoa, V. Vivier, The concept of floating electrode for contact-less electrochemical measurements: Application to reinforcing steel-bar corrosion in concrete, Corros. Sci. 51 (2009) 1795–1801.

[2] M. Keddam, X.R. Nóvoa, B. Puga, V. Vivier, Impedance based method for non-contact determination of the corrosion rate in buried metallic structures, Eur. J. Environ. Civ. Eng. 15 (2011) 1097–1103.

[3] J. Newman, N.P. Balsara, Electrochemical Systems, 4th Editio, J Wiley, 2021.

[4] J. Newman, Resistance for Flow of Current to a Disk, J. Electrochem. Soc. 113 (1966) 501.

Monitoring chloride induced corrosion in reinforced concrete: Non Destructive Testing and embedded sensors

V. Bouteiller, A. Bonnet, V. Da-Silva, Y. Jiang and G. Villain, University Gustave Eiffel, Marne - la- Vallée and Nantes, France,

E. Marie-Victoire, M. Bouichou, Laboratoire de Recherche des Monuments Historiques (LRMH), Champs-sur-Marne, France

B. Thauvin, R. Queguiner, Cerema DTer Ouest, Saint-Brieuc, France

M. Raupach, R. Achenbach and J. Biller, ibac, Institute of Building Materials Research, Aachen, Germany

Reinforced concrete is the most widely used building material but its durability in terms of concrete and corrosion of rebar is still a key issue. In order to address this topic, a long-term project with successive names "APOS" (Auscultation pour des ouvrages sûrs, 2013-2016), "Dur&Corr" (Durability and Corrosion of reinforced concrete structures, 2016-2020) and "SCOR2BA" (Surveillance de la corrosion des armatures dans les bétons armés à l'aide d'Essais Non Desctructifs et de capteurs, 2020-2022) aims to evaluate the rebar corrosion over time. Measurements have been performed using, on one hand, instant Non Destructive Testing (NDT) and, on the other hand, continuous monitoring with embedded sensors.

Two series of seven reinforced concrete specimens (with dimensions 70x90x13 cm and a network rebar) were cast with two concrete mixes (with Portland cement CEM I or Slag cement CEM III/A) and two types of rebar (carbon steel or duplex stainless steel 1.4062). For each concrete mix, two specimens were cast with embedded sensors such as ERE20©, Multi-Ring Electrode© (MRE), Anode Ladder© (AL) and HMP110© probe located in a concrete hole (Fig. 1). These specimens were exposed to a diffusion chloride ingress in a salted solution during five years in Saint-Brieuc. Since 2019, the reinforced concrete specimens are exposed to outdoor conditions at the University Gustave Eiffel in Marne-la-Vallée (Fig. 1).

Fig. 1 Location of sensors in the reinforced concrete specimens (left); reinforced concrete specimens exposed outdoor in University Gustave Eiffel in Marne-la-Vallée, France (right).

The objectives of this work are:

1) to evaluate the durability of concrete cover and rebar corrosion with time,
2) to study the corrosion of large reinforced concrete specimens exposed outdoor based on Non Destructive Testing- and on monitoring with embedded sensors and
3) to compare the durability of reinforced concrete specimens depending on the concrete mix or the nature of the rebar.

The results from NDT show the following corrosion ranking (in ascending order): RC with Duplex steel with cloride contamination < RC with carbon steel in Water < RC with carbon steel with chloride contamination. It also appears that carbon steel rebar in RC made with CEM I are corroding which is not the case with CEM III/B.

The results from monitoring allow to determine the time of corrosion initiation of the anode ladders depending on the concrete depth and therefore the AL sensor is a good candidate as a warning sensor for rebar corrosion determination.

Monitoring corrosion on prestressed concrete bridges using RFID corrosion sensors

Stéphane Rioual[1], Benoit Lescop[1], Karim Bouzzafour[1], Yannick Falaise[2], Cheikh Sarr[2], Sylvain Chataignier[2] and Laurent Gaillet[2]

[1]Univ Brest, Lab-STICC, CNRS, UMR 6285, F-29200 Brest, France

[2]MAST-SMC, Univ Gustave Eiffel, F-44344 Bouguenais, France

Steel corrosion in reinforced and prestressed concrete structures is recognized as a global issue that causes widespread damages ranging from cracks formation to ultimate structure collapse. It is often associated with carbonation and/or chloride ingress since these two actions lead to the degradation of the initial passive protective layer on steel. Within this context, there is a real interest in monitoring the corrosion of steel in concrete and the related parameters such as pH and chloride ingress using embedded wireless autonomous sensors in the infrastructures. Among the possible solutions, RFID (Radio Frequency Identification) based sensors are particularly attractive since it is possible to develop wireless battery-less sensors with low dimensions which are sensitive to steel corrosion. The absence of battery and cable facilitates their integration in concrete during construction or maintenance / repair operations and allows a long service lifetime. The first application of such sensors were made for atmospheric corrosion monitoring [1]. The principle of the method is based on an RFID tag which electromagnetically interacts with a thin conductive metallic sensitive layer. The variation of the electrical resistance of this sensitive layer, here steel, induced by corrosion, modifies this interaction leading to some information on its corrosion. It was subsequently proved that such sensors can be embedded in concrete to get some information on corrosion at different depths [2]. In particular, embedding a corrosion sensor at 3 cm depth which serves as an alert for corrosion of rebars located at larger depth was realized.

Several failures of prestressing strands due to penetration of water / chloride into HDPE (High Density Polyethylene) ducts were reported on Bridges in France since 2014 [3]. The present study therefore focuses on the application of RFID sensors for the monitoring of prestressing steel corrosion in such ducts. Applications to existing structures and new constructions are in the scope of the project. As it will be presented at the conference, RFID corrosion sensors were successfully placed

during inspection operations in HDPE ducts and interrogated from outside, demonstrating thereby the interest of the method. Corrosion tests were also performed in laboratory to get some insight on the sensitivity of the method. These pioneering investigations also highlighted the specificity of this application concerning the geometrical arrangement of strands in the ducts. Indeed, instead of a uniform distribution, they are eccentrically located resulting to strands in direct contact with the HDPE duct. This influences the corrosion process since strands are not protected from grout at the HDPE surface and hence the operating conditions and locations of sensors. Further developments are therefore in progress. They will be presented at the conference.

Authors would like to thank the French Ministère de la Transition Ecologique and CEREMA for its financial support within the call “ponts connectés”

References

1. Rioual S, Lescop B, Pellé J, De Alkmim Radicchi G, Chaumat G, Bruni MD, Becker J, Thierry D. Development of low-cost RFID sensors dedicated to air pollution monitoring for preventive conservation. Heritage Science 2022; 10; 124.

2. Bouzaffour K, Lescop B, Gallée F, Talbot P, Rioual S. Development of an embedded UHF-RFID corrosion sensor for monitoring corrosion of steel in concrete. IEEE Sensors Journal 2021; 21; 12306-12312.

3. Godart B, Gaillet L, Van Schoors L, Labourie L, Germain D, Vaurigaud B. Recent failures of external prestressing grouted tendons: the paramount role of the HDPE duct. Proceedings of IABSE Congress Christchurch, pp. 775-782, 2020 Resilient Technologies for Sustainable Infrastructures, Anthony Abu Ed., IABSE Publisher, Zurich Switzerland

Life Cycle Assessment of RC Structures via Web Application - Module of a Holistic Life Cycle Management for Traffic Infrastructures

Marc Zintel[1], Christian Linden[1], Ueli Angst[2],

[1]Steeltec AG, Emmenbrücke, Switzerland
[2]Institute for Building Materials (IfB), ETH Zurich, Zurich, Switzerland,
ueli.angst@ifb.baug.ethz.ch

Abstract:
A significant proportion of damage to transport infrastructure is caused by chloride-induced corrosion. Damage to highly exposed bridge elements in splash zones (XD3: e.g. caps and pillars) often occurs before the planned service life, resulting in enormous repair costs. Although recognised models for probabilistic life assessment exist and are integrated into regulations, their application and verification is currently limited to experts due to complicated and costly statistical software.
Using the newly developed and freely available web application "OCIMA" (Online Corrosion Initiation Modelling App), target service lives can be evaluated at the component level during the design phase. If the target life is not achieved, the effect of concrete technological optimisations can be estimated in real time.

Keywords
Durability; probabilistic service life design; chloride-induced corrosion; web application; life cycle management

Introduction

A large part of the bridge infrastructure in Germany consists of reinforced and prestressed concrete structures. The design of these structures is prioritised based on construction costs. The cost of future maintenance and repair (life cycle cost approach) is rarely considered as a decision criterion in tendering and awarding procedures.

In the recent past [1], it has been pointed out that the durability aspect, especially regarding chloride-induced reinforcement corrosion, has been neglected in the design and construction of tunnels and bridges. A recent analysis [2] shows that this neglect has an impact on the damage investigated in transport structures, where the proportion of damage due to chloride-induced reinforcement corrosion in the German motorway network is approximately 77%, see Figure 1.

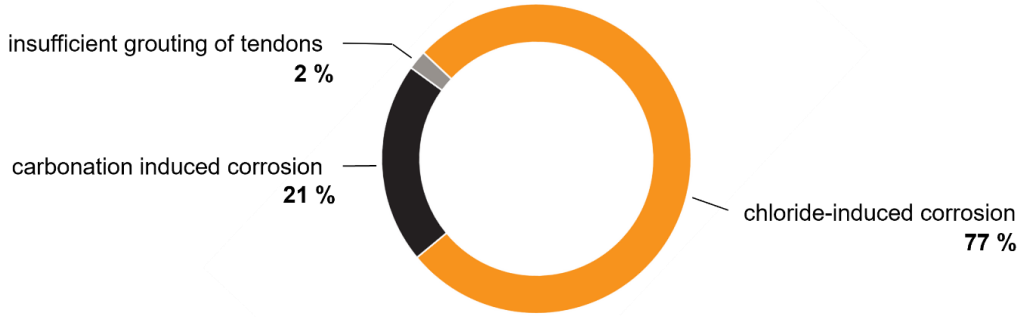

Figure 1: Distribution of damage to bridges in the German highway network [2].

According to [3], the direct cost of corrosion on engineering structures in the road network of Switzerland and the USA is approximately 0.1% of GDP. Applying this approach to the average

GDP of the last 5 years in Germany (2018 to 2022), the annual direct cost of corrosion to engineering structures in the German road network can be estimated at €3.6 billion.

If the targeted service life is not achieved and repairs are necessary, this results in high costs as well as restrictions on availability during ongoing measures (e.g. traffic jams). For this reason, the German Federal Ministry for Digital Affairs and Transport (BMDV) has recently initiated several pilot projects in which the durability of various traffic structures (e.g. tunnel Eching/Etterschlag [4]) is to be optimised through design and material measures.

Recent evidence for reinforced concrete bridges [5] shows that, depending on the impact category, external environmental impacts (e.g. traffic jams due to repairs) can significantly exceed the environmental impacts of production. In the case of CO_2 emissions (GWP), the external environmental impact exceeds the environmental impact of bridge construction by a factor of about 4! It is clear from this that sustainable bridge construction can only be achieved through 100% availability over the entire service life without repair. Therefore, focusing solely on production-related CO_2 emissions in the selection of construction variants is too limited and can lead to significant misinterpretations when considering the entire life cycle.

Regulation of the durability of reinforced concrete structures: Status quo and outlook

The durability of reinforced concrete structures is currently determined by compliance with descriptive rules (e.g. concrete cover, concrete strength, w/c ratio). The descriptive requirements specified in DIN 1045 and DIN EN 206-1 are intended to ensure a service life of at least 50 years for each exposure class. A performance-based assessment according to the performance concept of DIN EN 1990 and analogous to structural design is still the exception (e.g. for a service life of 100 years).

Practical experience shows that, even with the descriptive approach, the targeted service life (50 years) with respect to chloride-induced corrosion of the reinforcement is not always achieved with sufficient probability and is sometimes even significantly missed [6]. This means that for very high XD3 chloride loads in the infrastructure sector, the target service life of 50 years cannot be guaranteed in some cases with the current rules. It should also be noted that a target service life of 100 years is not currently covered by the descriptive approach, but is often required for infrastructure structures.

Existing design approaches based on tested performance properties (performance, e.g. chloride penetration resistance according to BAW) tend to be more complex and also require specialist knowledge and software. A breakthrough in simplification has been achieved with the development of a semi-probabilistic design approach for durability assessment using design nomograms [7].

European standardization (pr EN 1992-1-1, EC2 for short) is currently working on the introduction of a performance-based durability concept for reinforced concrete structures. This concept is based on prediction models (analogous to [8]) for the durability of concrete structures. In this context, a new classification of concretes into so-called Exposure Resistance Classes (XRDS) is planned. It is expected that the minimum concrete cover for XD will be variable in the future, depending on the chloride penetration resistance of the concrete via XRDS. Further reductions in concrete cover are expected to be possible, for example for higher alloyed reinforcing steel.
The transition from the descriptive to the performance approach is also an important building block for sustainable bridge construction under the aspect of new clinker-reduced cements and

resource conservation (targeted material use). Requirements for a performance approach can be derived from this:

1) Design with new binders:
   Does the current descriptive approach still apply to the new generation of binders? Long term behavior?
2) Efficient use of new binders:
   A good balance between exposure (S) and resistance (R) is required.
3) Durable construction with new binders:
   Compensate for possible disadvantages in durability (carbonation rate, chloride penetration resistance), e.g. by selective use of stainless reinforcement.
4) Take advantage of the life cycle approach:
   Life cycle cost comparisons in the design phase are only possible with reliable forecasting models for up to 100 years!

Considering the bridge modernization program launched by the BMDV, a significant increase in the number of bridge modernizations is expected in Germany in the next few years, see Figure 2.

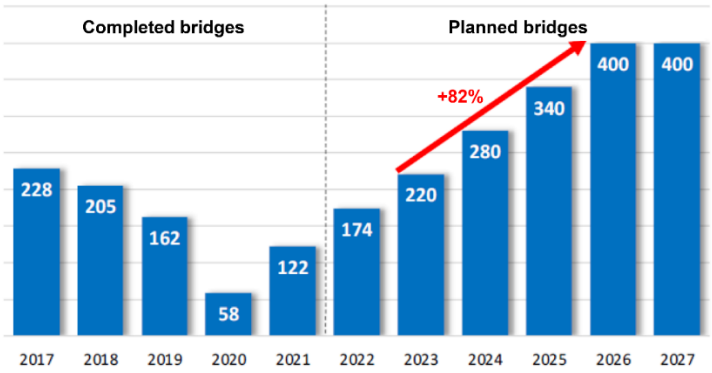

Figure 2: Increase in the modernization of bridges on highways [9].

The aim of Autobahn GmbH is to gradually increase the number of completed rehabilitated bridges from the current 220 in 2023 to 400 in 2026. This represents an increase of 82%. The general objective is to strengthen or renew all of the approximately 4,000 bridges in the bridge modernization network within 10 years.
For the large number of new replacements alone, simple (web-based) control of the target lifetimes of critical components such as caps or central pillars could reduce life cycle costs many times over in the next 50 or 100 years [10]. In addition, high CO_2 emissions are avoided directly and indirectly (external environmental effects, e.g. due to traffic jam) by eliminating repair work.

Probabilistic Service Life Design

General

The durability of reinforced concrete under chloride exposure is in many cases determined by chloride-induced reinforcement corrosion, as shown for bridges in Chapter 1. Chloride induced corrosion is usually a localized form of corrosion, often characterized by high corrosion rates (up to 1 mm/year depending on conditions). For this reason, service life is often conservatively equated with the onset of reinforcement corrosion.

According to the international state of the art [8, 11, 12, 13, 14], the initiation of rebar corrosion in concrete can be described conceptually by the following approach: Chloride transport through the concrete cover is described by a modified diffusion law, and thus the chloride concentration at the steel surface in the concrete is predicted over time. Once this chloride concentration exceeds a critical limit, called the critical chloride content (C_{crit}), reinforcement corrosion is assumed to start. The concept of corrosion initiation modelling is shown schematically in Figure 3 and implemented in the present web application OCIMA (Online Corrosion Initiation Modelling App).

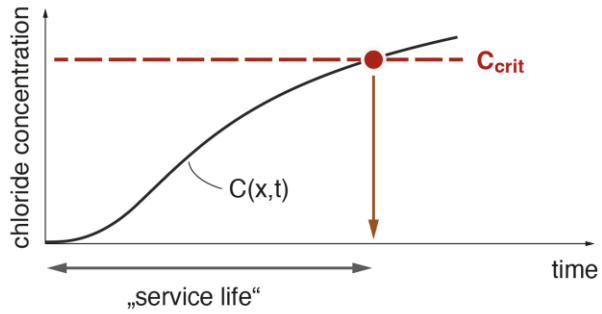

Figure 3: Concept of modeling the initiation of corrosion.

As it is known that many model parameters exhibit statistical variations, such as concrete cover or concrete diffusion properties, it is common to calculate this model probabilistically. Specifically, this means that all model parameters are described by a statistical distribution. Common statistical distributions include the normal distribution and the log-normal distribution.
Due to the statistical variability of the influencing factors, both resistance (C_{crit}) and exposure (C(x,t)) are not deterministic quantities but can be represented as random variables. This relationship is shown in Figure 4.

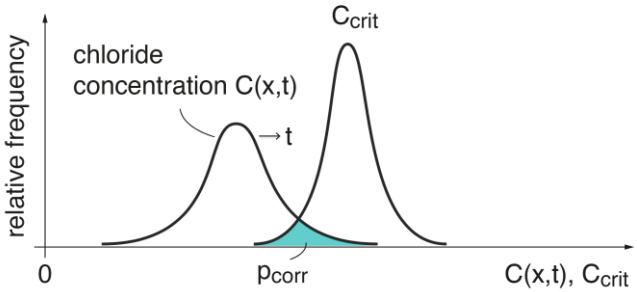

Figure 4: Probabilistic model with distributed variables «exposure» (chloride concentration at reinforcement depth x at time t) and «resistance» (critical chloride content Ccrit).

In general, it is not possible to solve this problem analytically. Therefore, to calculate the corrosion probability p_{corr}, OCIMA relies on Monte Carlo simulations using an algorithm developed at the ETH Zurich (30,000 iterations per run with a computing time of 2-3 s). This allows the comparison of the distributions of "resistance" and "exposure" over time and the calculation of p_{corr} at each time point. In durability modelling it is common to use its conversion to the so-called "reliability index β" instead of p_{corr}. The relationship between p_{corr} and β is given by the following equation.

$$\beta = -\Phi^{-1}(p_{corr}) \quad (1)$$

The reliability index β for reinforcement corrosion is typically assumed to be in the range of 1.5 to 0.5, corresponding to a corrosion probability range of 7% to 31% [15].

In OCIMA, the corrosion probability p_{corr} is presented as a function of time, as this value is more intuitive than the conversion into the reliability index.

Chloride transport model

The following equation is used to model chloride transport through the uncracked concrete, in accordance with the Fib Model Code for Service Life Design [8]:

$$C(x,t) = C_s \times \left(1 - erf\left(\frac{x-0.01}{2\times\sqrt{D_{app,0}\times\left(\frac{t_0}{t}\right)^n \times t}}\right)\right) \quad (2)$$

With the following parameters:

$C(x,t)$	Chloride concentration in concrete at level of reinforcement at time t	[M.-%/b]
C_s	Chloride concentration in concrete at depth of 10 mm (μ, σ)	[M.-%/b]
erf	Gaussian error function	
x	Concrete cover (μ, σ)	[mm]
$D_{app,0}$	Reference apparent diffusion coefficient measured at time t_0 (μ, σ)	[m^2/s]
t	Time	[s]
n	Aging exponent	[-]
$C_{crit,B500B}$	Critical chloride content for conventional B500B (μ, σ)	[M.-%/b]
$C_{crit,Top12}$	Critical chloride content for Top12 (μ, σ) as stainless rebar [16]	[M.-%/b]

Equation (2) has been derived from Fick's diffusion law, specifically for the case of one-dimensional diffusion under the assumption of certain boundary conditions that are generally considered to be representative of the conditions present in the structure. Based on extensive data collection and analysis of the critical chloride content (C_{crit}), it was found that C_{crit} can be well represented by a lognormal distribution [17].

OCIMA - Online Corrosion Initiation Modeling App

The approach described above has been implemented in the freely available web application OCIMA. This makes it possible to check the desired service life already in the design phase and, if necessary, to quickly estimate the effect of countermeasures such as optimized concrete technology, adapted concrete cover, etc.

Within OCIMA, the user is guided through the program based on the project location, the selection of the structure type (bridge, tunnel, car park) and the corresponding component selection (e.g. bridge → pillar). The program provides recommendations for all necessary input parameters, such as the applied chloride exposure C_s or the tolerable corrosion probability p_{corr} for the limit state calculation. To run the service life calculation, the user only needs to define the binder type, including the w/c ratio, and the concrete cover.

The result of the calculation is an estimate of durability in the form of an achievable service life in years. The result can be optimized by adjusting the parameters, e.g. by selecting a different binder or by adjusting the concrete cover. The display of the results includes both the achievable service life with conventional reinforcement (B500B) and the extended service life achievable

with Top12 as a stainless reinforcement. Figure 5 shows a screenshot of the application with an example calculation for a highway bridge pillar. To the left of the results display (graph and achieved service life) the input parameters used for the calculation are listed, which can also be subsequently modified.

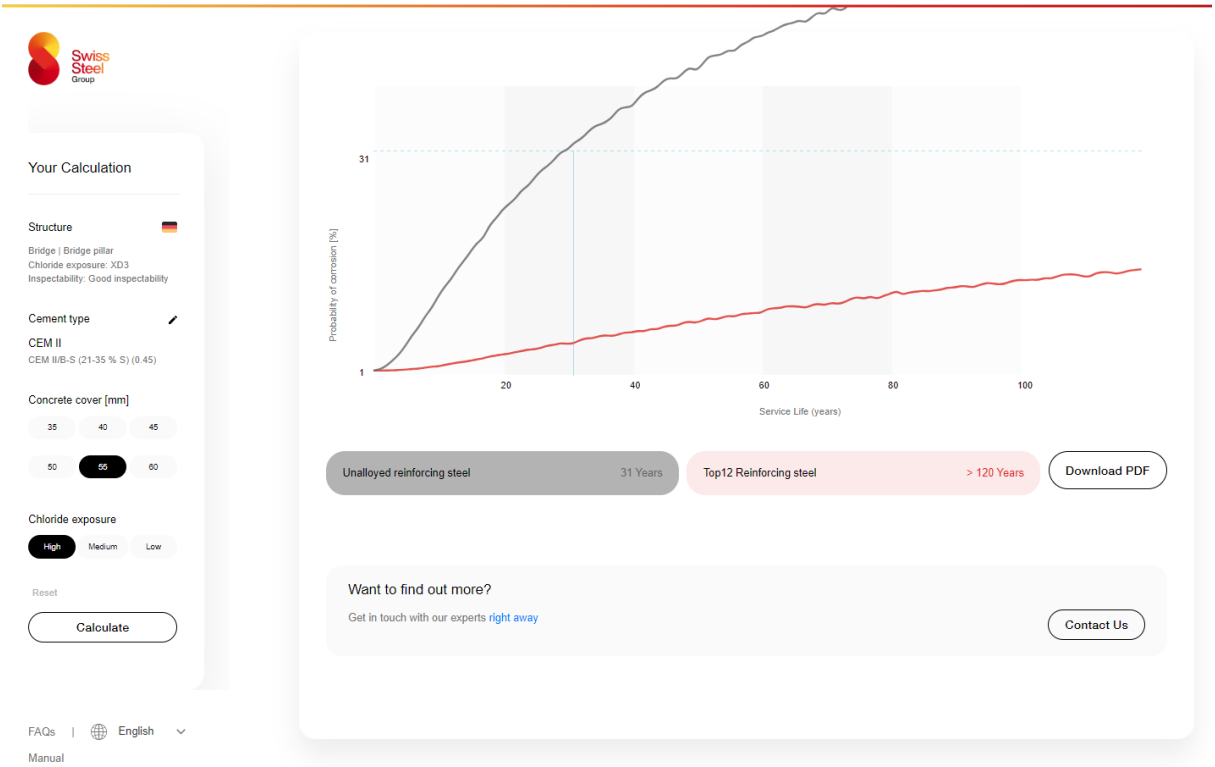

Figure 5: Screenshot of the freely accessible web application OCIMA in standard mode (Online Corrosion Initiation Modeling App).

The web application OCIMA basically consists of two modes: For the first, the so-called "standard mode", no previous knowledge is required; here the user is guided through the program by means of questions and supplementary instructions. Corresponding answers or selections (e.g. cement type with w/b value) are partly directly translated into relevant model parameters in the background. All model input parameters used in the standard mode and thus linked in the backend are based on recognized literature data, e.g. [18].
The calculation result with the selected parameters can be downloaded as a PDF document for archiving. To compare previous calculations with the current results, a drop-down menu for recalling previous calculations is available.
In the second so-called "expert mode" (available in English only), all model input parameters can be freely entered numerically as statistical parameters with mean (μ) and standard deviation (σ). This mode also allows the results to be exported as a CSV file for further external processing.

The goal of the OCIMA is to make service life estimation as simple and intuitive as possible for designers, owners or operators who do not have access to specialized statistical software. The intention is to raise awareness of durability and to provide professionals with a tool that allows them to quickly estimate and understand the impact of various input parameters.

In terms of holistic life cycle management, OCIMA is an essential building block for calculating component-related life cycle costs (= sum of construction costs (CC) and operating costs). In

addition to the monetary life cycle costs, the same calculation model can also be used in the planning phase to carry out sustainability comparisons (LCA) in various impact categories (e.g. CO_2) over the entire life cycle with the aid of so-called EPDs (Environmental Product Declarations). The basic relationship is shown in Figure 6.

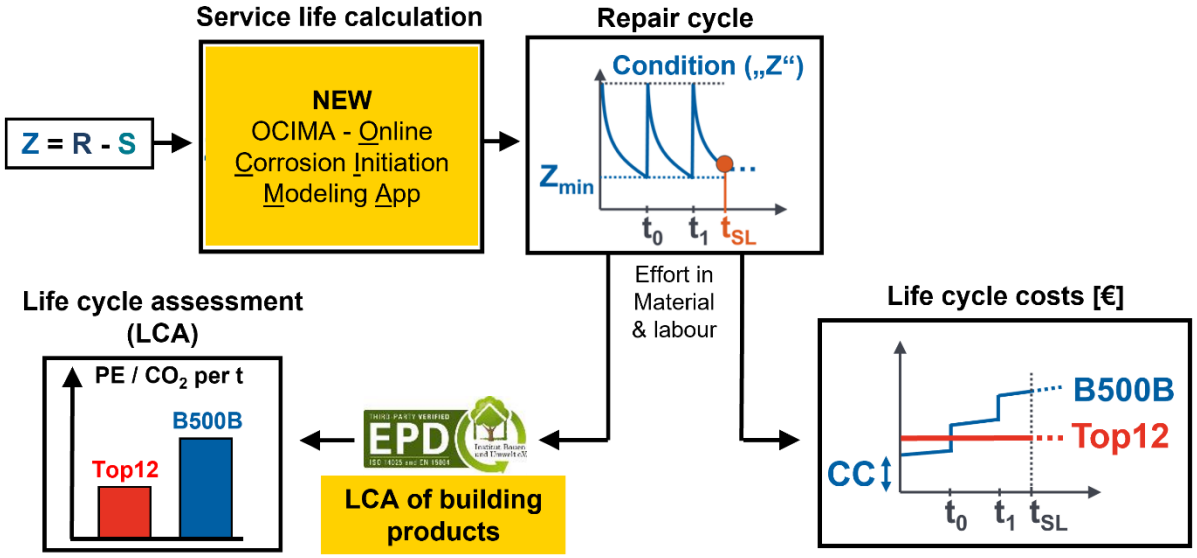

Figure 6: Schematic approach of a hollistic life management system for concrete components of transport infrastructure structures

Although the service life model implemented is internationally recognized as state-of-the-art, we would like to emphasize that simulations are highly dependent on the assumptions made and therefore cannot provide absolute service life predictions. Instead, the results provide probabilities of corrosion initiation that can be used as valuable decision support when considering different design options. An example is the comparison of different steel grades, such as the use of Top12 as a stainless reinforcement with higher corrosion resistance [16] compared to conventional B500B reinforcement.
Such model-based decision making in the design phase is an important step to avoid unwanted premature repairs and their negative economic and environmental consequences.

The web application "OCIMA" is freely accessible in standard mode at www.ocima-swisssteel-group.com. Access to the expert mode is generally available on individual request.

This contribution is similar to a previous conference contribution in German language [19].

Literature

[1] Schießl-Pecka, A.; Willberg, U.; Rausch, A.; Bäumler, W.: 100 Jahre Dauerhaftigkeit für Brücken- und Tunnelbauwerke. Beton- und Stahlbetonbau, 113 (2018), pp. 746-755 – DOI: 10.1002/best.201800032.

[2] Breit, W.: Kritischer korrosionsauslösender Chloridgehalt – Grenzwerte, Empfehlungen. In: Proceedings of the 4th Munich Building Symposium, 26.09.2019 in Munich, Munich University of Applied Sciences.

[3] Yilmaz, D.; Angst, U.: Korrosionsbedingte Kosten an Ingenieurbauwerken im Schweizer Straßennetz. Beton- und Stahlbetonbau 115 (2020), pp.448-458 – DOI: 10.1002/best.202000004.

[4] Willberg, U.; Schneck, U.; Schießl-Pecka, A.: A 96 Tunnel Eching und Etterschlag - Alternative Betoninstandsetzung. In: Conference Proceedings Colloquium Road Construction in Practice, 29./30.01.2019 in Esslingen, Techn. Akademie Esslingen.

[5] Zinke, T.: Nachhaltigkeit von Infrastrukturbauwerken - Ganzheitliche Bewertung von Autobahnbrücken unter besonderer Berücksichtigung externer Effekte. Karlsruhe: KIT Scientific Publishing, Dissertation, 2016, DOI: 10.5445/KSP/1000053695.

[6] Rahimi, A.; Gehlen, C.: Semiprobabilistische Dauerhaftigkeitsbemessung von Stahlbetonbauten unter Chlorideinwirkung. Beton- und Stahlbetonbau, 113 (2018), pp. 13-21 - DOI: 10.1002/best.201700062.

[7] Rahimi, A.: Semiprobabilistisches Nachweiskonzept zur Dauerhaftigkeitsbemessung und -bewertung von Stahlbetonbauteilen unter Chlorideinwirkung. DAfStb-Heft 626, Beuth, Berlin, 2016.

[8] Federation internationale du beton (fib): Bulletin 34 - Model Code for Service Life Design. Lausanne, Switzerland, 2006, DOI: 10.35789/fib.BULL.0034.

[9] Gunreben, Y.-C.: Brückenbilanz und Zukunftspaket leistungsfähige Autobahnbrücken. Vortrag auf VDI-Fachtagung „Zukunftsprogramm Brückenmodernisierung“ am 23./24. 11.2022 in Bonn.

[10] Schießl-Pecka, A.; Rausch, A.; Zintel, M.; Linden, C.: Lebenszykluskostenbetrachtungen für chloridexponierte Bauteile von Brücken- und Tunnelbauwerken. Beton- und Stahlbetonbau 114 (2019), pp.767-775 – DOI: 10.1002/best.201900038.

[11] Tang, L.; Nilsson, L.O.; Basheer, P.A.M.: Resistance of Concrete to Chloride Ingress: Testing and modelling, Spon Press, Abingdon, 2012.

[12] BAW Merkblatt „Dauerhaftigkeitsbemessung und -bewertung von Stahlbetonbauwerken bei Carbonatisierung und Chlorideinwirkung (MDCC)“, Federal Waterways Engineering and Research Institute (BAW), Karlsruhe, 2019.

[13] Gehlen, C.; Mayer, T.F.; von Greve-Dierfeld, S.: Lebensdauerbemessung. In: Beton-Kalender 2011: Kraftwerke, Faserbeton, Ernst & Sohn, Berlin, 2011, pp. 229-278.

[14] Gehlen, C.: Probabilistische Lebensdauerbemessung von Stahlbetonbauwerken - Zuverlässigkeitsbetrachtungen zur wirksamen Vermeidung von Bewehrungskorrosion, DAfStb-Heft 510, Beuth, Berlin, 2000.

[15] Positionspapier des DAfStb zur Umsetzung des Konzepts von leistungsbezogenen Entwurfsverfahren unter Berücksichtigung von DIN EN 206-1, Anhang J. Beton- und Stahlbetonbau, 103 (2008), pp. 837-839 – DOI: 10.1002/best.200808229.

[16] Käthler, C. B.; Ebell, G.; Keßler, S.; Schiegg, Y.; Dauberschmidt, C.; Angst, U.M.: A comparison of methods to assess the resistance of reinforcing steel against chloride-induced corrosion in concrete: Particular consideration of 12% chromium steel. Mater. Corros. 73 (2022), pp. 1-20 – DOI: 10.1002/maco.202112826.

[17] Boschmann Käthler, C.; Angst, U.M.; Aguilar, A.M.; Elsener, B.: A systematic data collection on chloride-induced steel corrosion in concrete to improve service life modelling and towards understanding corrosion initiation. Corrosion Science 157 (2019), pp. 331-336 – DOI: 10.1016/j.corsci.2019.06.008.

[18] Federation internationale du beton (fib): Bulletin 76 - Benchmarking of deemed-to-satisfy provisions in standards: Durability of reinforced concrete structures exposed to chlorides. Lausanne, Switzerland, 2015, ISBN: 978-2-88394-116-8.

[19] Zintel, M.; Linden, C.; Angst, U.: Probabilistische Lebensdauerbemessung von Stahlbetonbrücken über kostenlose Webanwendung. In: Conference Proceedings 32. Dresdner Brückenbausymposium, 31.05.2023 in Dresden, Technische Universität Dresden, ISBN: 978-3-86780-739-5.

Taking a closer look at reinforcement corrosion: creating digital twins of the steel-concrete interface from FIB-SEM nano-tomography

Thilo Schmid (schmithi@ethz.ch)[a]; Zhidong Zhang[a]; Michele Griffa[b]; O. Burkan Isgor[c]; Ueli Angst[a]

[a] Institute for Building Materials, ETH Zürich, Switzerland

[b] Swiss Federal Laboratories for Materials Science and Technology (Empa), ETH Domain, Switzerland

[c] Oregon State University, Corvallis, OR, USA

Corrosion in reinforced concrete occurs at the steel-concrete interface (SCI), at a rate dictated by a complex set of factors, including the moisture state, the chemical composition of the pore solution, and ion transport. Most transport models commonly employ homogenization techniques, which treat the material as a continuous medium with effective values for certain parameters, such as an effective diffusion coefficient, which are dictated by actual pore space geometry. However, estimating the effective values of distinct parameters involves averaging quantities over a representative volume element (RVE), which is usually significantly larger in scale than the SCI and mainly intended to represent bulk concrete. This calls into question whether homogenization approaches are adequate for the description of the transport processes relevant for corrosion as well as the distribution of corrosion products within the SCI. .

In this study, a new approach for analyzing the SCI is presented with the ultimate goal of enabling more realistic modeling of reactive-transport processes associated with steel corrosion. The presented approach uses three-dimensional data at the SCI, acquired by a dual-beam microscope (a focused ion beam, FIB, coupled with the electron beam of a scanning electron microscope, SEM) with a resolution of 30 nm.

While FIB-SEM has already found some applications in studying concrete at various scales, its application to the SCI's pore space characterization is a key novelty of the work presented here. It offers advantages for investigating the SCI's pore space and, more in general, its microstructure, compared to other more established three-dimensional imaging techniques such as micro X-ray computed tomography (μXRCT).

Different tomograms have been collected for both steel-mortar and steel-concrete interfaces. Each tomogram underwent an image-processing workflow, to produce a digital twin of the imaged region. This includes various steps, namely noise filtering, image stack alignment, background correction, and stripe filtering. Finally, the resulting tomogram was segmented into pore space and solid matrix.

The digital twins were used to quantify the pore structure of the interfacial zone in a number of ways. In addition to the porosity, which is obtained from the segmentation, the continuous pore size distribution was computed. The tortuosity of the pore space was estimated based on a random walk algorithm. These properties were then compared between the digital twins. In particular, an investigation of the representative character of the acquired tomograms provided insight into the size scale that a RVE in the SCI should have. The results show that the SCI is an anisotropic region, whose microstructure changes with the distance to the steel.

Ultimately, this study aims to improve reactive transport models by considering realistic pore structures, thereby providing conceptual insight into corrosion and related transport phenomena at the capillary pore scale.

Experimental and Numerical Investigation of the Pitting Corrosion on Steel Reinforcing Bars

Mohaddeseh Abdolhosseini[1], *Nicolas Maamary*[1], *Seyiwa Kope*[1] , *Masoud Zakeri*[1], *Ibrahim Ogunsanya*[1]

[1]*Civil and Mineral Engineering, University of Toronto, Toronto, Canada*

Abstract

Corrosion of the steel embedded reinforcing bars (rebars) is one of the main deterioration modes of reinforced concrete structures. Corrosion of rebar could be due to the exposure of the reinforced concrete structures to chlorides from marine or de-icing salt environments. Pitting corrosion is the most prevalent type and is a significant concern because it occurs locally and can drastically affect the structural load-bearing capacity and safety. Several models have been proposed to predict pit depth as a measure of the pitting corrosion propagation over time. Despite the efforts made in this field, due to the complex and stochastic nature of pitting corrosion, there remains a gap in our understanding of the corrosion process of steel rebar embedded in concrete structures, which poses significant challenges to an accurate prediction of corrosion durability.

To address this challenge, the main objective of this study is to investigate and gain insights into the pitting corrosion time-dependent process using experimented laboratory data and modelling analysis. The long-term goal is to use the existing Markov model, initially developed for corroded underground steel gas pipelines, as the basis for developing a new model applicable to study pitting corrosion process in the context of reinforced concrete structures. This new model will be used to describe the transition probabilities between different corrosion states in reinforced concrete structures, allowing us to account for the stochastic nature of the pitting corrosion process. The prediction made by this model will provide valuable information on the rebar's long-term pitting corrosion behavior based on the current state of the reinforced concrete structure they are embedded in.

To generate input parameters for this model, an experimental laboratory program was designed to cover a range of different chloride type and concentrations, as well as various types of steel rebars with varying compositions and microstructures. The data

collected from the tests will not only be used to calibrate the Markov model, but will also be used to validate it. The study will also include a sensitivity analysis to evaluate the effect of different parameters on the predictions of the Markov model.

The significance of this study lies in its potential to provide a better understanding of the factors that influence the corrosion rate and morphology of pits in steel rebar and to introduce a new and more accurate method for predicting the propagation of pitting corrosion in reinforced concrete structures. The results of this study have the potential to be widely adopted by the engineers and researchers working in the field of corrosion and concrete structures to predict the corrosion of rebars and improve the durability and safety of concrete structures and create a safer and more sustainable built environment.

Insights into the corrosion mechanism of steel liner in concrete

Elina Huttunen-Saarivirta, Edgar Bohner, Andressa Trentin, Miguel Ferreira

VTT Technical Research Centre of Finland Ltd, Espoo/Finland

Containment structure is the outermost building of nuclear reactors, serving as a safety barrier between the reactor and the surroundings in the case of an accident. It typically includes a steel liner, i.e., a gas-tight barrier, embedded in concrete. Leak tightness of the containment liner is an essential part of the safety of the nuclear power plant (NPP) structure. Unfortunately, corrosion of the embedded nuclear containment liner has been reported in several NPPs globally, even to such extent that the structures have not passed the leakage tests included in liner inspection practices. In many cases, the liner degradation has occurred in the presence of a foreign matter, such as the piece of wood retained from construction phase, and/or delaminated or porous concrete. Due to the large continuous surface area of the steel liner, these corrosion cases are unique to NPPs. Macrocell effect, also detected in reinforced concrete besides the microcell formation, may further contribute the steel liner degradation process. However, excluding the reports of failure cases of containment steel liners in NPPs, the topic has not received much research effort. We aim to shed light on the mechanism of steel liner corrosion based on experiments that were built on the scenarios of the presence of a 1) foreign matter and 2) delamination gap between steel and concrete.

The specimens were prepared using the inlays that defined the anodic area in the steel liner and contained the reference electrode. The experiments were performed in plastic containers which acted as moulds, in which a layer of concrete was first cast. Steel liner with the inlay and the counter electrode were then placed on the first layer of concrete, and another concrete layer was added to provide a concrete cover of 50 mm. After drying, the experiments were accelerated by selecting suitable environmental conditions and the use of chlorides and/or impressed current. In-situ electrochemical measurements were performed intermittently for the duration of the exposure, up to 2 years. Afterwards, specimens were removed from the moulds, the concrete cover was peeled away, and the liner specimens were subjected to surface characterization. The results from the experiments will be presented and discussed from the perspective of the prevailing corrosion mechanism.

Observations of carbonation for 60-year-old concretes and relevance to steel reinforcement corrosion

Robert E Melchers[1], **Peter J Richardson**[2]

[1]*The University of Newcastle, Callaghan, Australia 2308, rob.melchers@newcastle.edu.au*
[2]*The University of Newcastle, Callaghan, Australia 2308, peter.richardson@newcastle.edu.au*

Abstract
This paper considers recent observations of the depth of carbonation for exposed high-quality reinforced concrete columns demolished from a 3 storey building after some 60 years in a moderately humid environment. Random sampling was used to select the individual columns for analysis. These were from all four elevations and from the interior of the building. Samples cut from these columns showed no evidence of reinforcement corrosion, depths of 'carbonation' only up to some 15 mm into the concrete and concrete pH values still around 12 at the locations of the steel reinforcement, declining gently towards pH about 7 at the exposed concrete surface. XRD measurements showed the presence of calcium carbonates at and near the exterior surfaces of the columns but no detectable calcium hydroxide. There was no detectable sodium chloride. The region near the external surfaces showed evidence of calcium hydroxide leaching outwards. Based on the experimental evidence and observations in the corrosion literature for actual reinforced concrete structures rather than artificial laboratory testing it is proposed that for high quality, well-compacted the probability of loss of concrete alkali at the level of the reinforcement is very low to negligible, rendering the probability of reinforcement corrosion caused by what is known conventionally as 'carbonation', very low. Overall, it is argued that the critical mechanism for initiation of reinforcement corrosion is long-term leaching outwards of concrete alkalis. On this basis and with other observations a new model for initiation has been proposed.

Keywords: Carbonation;, reinforcement; corrosion; long-term; greenhouse.

Introduction

The cement industry and by implication the reinforced concrete industry has been accused of generating some 8% of all global greenhouse gas emissions and thereby being the 'biggest single emitter of CO_2' [1]. These are from (a) the crushing of rocks for use in concrete and the limestone in cement making, (b) the fuel burnt to clinker the limestone and clay and (c) grinding of the clinker to cement powder. Recent estimates, however, are that half of that total is recovered through the process of carbonation of exposed concrete in buildings and infrastructure [2]. It seems that until recently this role of concrete as a carbon sink largely had been overlooked [3], although how much of this occurs for different concretes, surface conditions, exposure areas and under what atmospheric and other conditions and, importantly, the rate and time period over which it occurs all remain unclear. In the UK there is controversy between environmentalists and the cement industry about the measurement of these effects and with the assessment processes and by whom they are carried out [3, 4]. Nevertheless, carbonation has other positive effects. It is well-known to cause the outer layers of the concrete so affected to become denser and have reduced permeability, as well as providing somewhat greater strength both in compression and in tension. These are both beneficial effects. However, it is also claimed that the major negative effect of concrete carbonation is that it causes reinforcement corrosion and that this offsets its beneficial effects [1].

Much recent research has focussed on attempts to replace Portland cement clinker content in concretes with supplementary cementitious materials (SCMs) with one underlying aim to reduce the greenhouse gas (CO_2) emissions attributed to cement production. However, it is now recognized that replacing some of the Portland cement clinker content in concretes reduces the availability of alkalis in the concrete and that this allows a faster rate of neutralisation by CO_2 of those alkalis in the concrete pore solution. In turn this implies an 'increased risk of reinforcement corrosion' [5]. The important role of alkali materials in the concrete and its relation to reinforcement corrosion is considered further below.

Since reinforcement corrosion attributed to carbonation depends on the uptake of CO_2 by concretes, considerable research also has focussed on the rates of such uptake [6]. Again, the rate of CO_2 uptake by itself is not the primary aim of this paper. It is concerned with the likelihood of reinforcement corrosion when carbonation occurs. Doubts about the importance of carbonation in causing reinforcement corrosion and about the logic of the mechanisms usual to apply are not new, based on practical observations and basic principles [7]. Most recently, in 2020, this was echoed by RILEM Technical Committee 281-CCC [8] that noted 'The circumstance that a reduced pH alone is not sufficient to lead to significant steel corrosion in concrete seriously challenges the established approach of assessing the durability performance based on carbonation testing and modeling.' and also 'the focus in research and engineering should shift from studying carbonation to studying corrosion of steel in carbonated concrete.' That is the focus of the technical side of the present paper.

Technical Investigation

Rather fortuitously for the present investigation, in 2020 the management of the University of Newcastle, Australia decided to demolish one of the earliest buildings on its main campus at Shortland in the northern part of Newcastle in a suburb now known as Callaghan. The three-story reinforced concrete framed building, constructed in 1965, comprised some 54 external exposed concrete aggregate columns 700 x 420 mm in size, with 25 mm diameter steel reinforcement with 60 mm (nom.) cover. During demolition one column at second story level was recovered from each of the elevations of the building together with one interior free-

standing exposed concrete column similar in size with similar reinforcement and concrete cover. Thus, each of the recovered columns can be considered essentially randomly selected from the available columns. All other columns and concrete was pulverized for recycling as road base.

Samples 150 x 150 mm were (saw-)cut from the columns at randomly selected locations along the columns (Fig. 1). The freshly cut concrete surfaces were immediately tested for pH from the external surface inwards, towards the reinforcement bar, at intervals of 10 mm. For this MColorpHast™ 7.5-14 pH indicator strips were used after lightly wetting the concrete with neutral pH fresh water for 10 seconds. This is an accepted, fast and accurate approach for measuring concrete pH and generally more reliable than pH meters owing to better contact with the pH reactant [9]. Such measurements were repeated, including by different persons, to obtain average, unbiased results. Typically, readings to within 0.5 pH unit were obtained. Three example pH profiles through the concrete are shown in Fig. 2. It shows, like all the other pH profiles obtained [10], pH around neutral at the exterior concrete surface and extending some 15-20 mm inwards, followed by a gradual increase in pH with distance in from the exterior surface, peaking at around pH 11-12. The latter pH values correspond with the expected maximum pH inside older reinforced concretes from which all alkali-forming materials (mainly NaOH, KOH) other than calcium hydroxide ($Ca(OH)_2$) have been leached [11]. Importantly, in all cases the pH at the depth where the reinforcement was located was around 12, well above any pH for which general corrosion of steel in water is thermodynamically possible [12].

(a) (b)

Figure 1. (a) Samples being cut from 60-year old (nom.) reinforced concrete column taken from a demolished building and (b) close-up of typical location of concrete sampling showing location of longitudinal column reinforcement bar (arrow).

To ensure that the samples cut from the columns were not some isolated examples, the concrete columns also were cut open along their 2-3 m length, along the line of one of the reinforcement bars. This revealed the complete absence of reinforcement corrosion (Fig. 3), consistent also with the visual observation of a complete lack of longitudinal cracking along the length of any of the columns, including those inspected for the building prior to demolition. There is also clear evidence of the excellent steel-concrete interface.

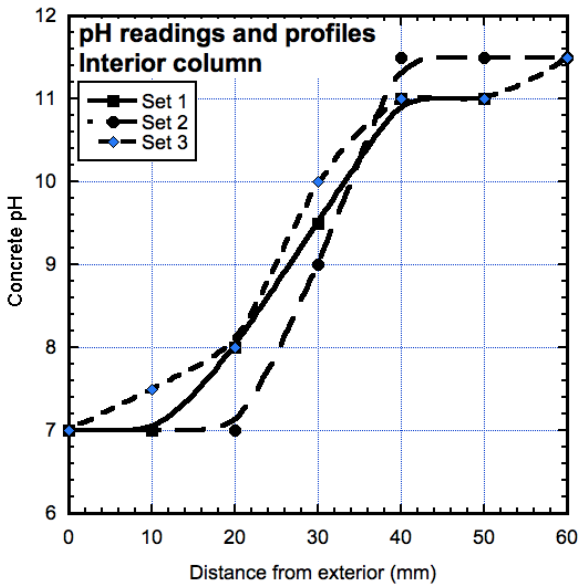

Figure 2. Example pH readings along lines perpendicular to exterior surface, towards the reinforcement bars (at about 60 mm inwards) and best fit pH profiles.

(a) *(b)*

Figure 3. (a) Longitudinal view of one of the exposed reinforcement bars in one of the exterior exposed concrete columns after 60 years exposure. Cover at top, about 60 mm, (b) close-up of steel bar and surrounding concrete showing excellent steel-concrete contact and no evidence of corrosion.

Material Investigations

Apart from pH measurements, the project investigations comprised chemical and microstructural analyses using scanning electron microscopy (SEM), energy dispersive spectroscopy (EDS) and X-ray diffraction (XRD). The details have been reported [10]. In brief, the SEM images showed that compared with further into the concrete matrix, the outer few millimetres showed a somewhat more open and less dense concrete matrix, together with what could be interpreted as micro-channels along the edges of sand or other particles in the concrete matrix. These channels were orientated generally toward the exterior (i.e. atmosphere exposed) concrete surface. Generally similar observations have been reported earlier for the outer zones of concretes ostensibly influenced by chloride effects [13]. Together with the observed loss of concrete alkali material, these micro-channels could be considered as pathways for the leaching-out and loss of concrete alkalis. Note that the presence of these pathways is despite

the fact that the outer zones are carbonated (see also below) and are known to be of somewhat higher concrete strength and lower overall permeability, both the result of the deposition of $CaCO_3$ within the concrete matrix.

In terms of components in the concrete, the EDS analysis identified O, C, Ca, Si, Al, Mg, S, and Na but there was no detectable Cl. The carbon component was interpreted as approximately uniform at greater distances into the concrete but was somewhat higher in the regions near the outer surfaces. This was attributed to the effect of atmospheric CO_2. On the other hand, Ca was found to be low near the exterior concrete surfaces but roughly uniform further inward. This is consistent with $Ca(OH)_2$ reacting with CO_2 near the exterior surfaces to produce $CaCO_3$ and also with $Ca(OH)_2$ having been leached out at the surface of the concrete.

The XRD analyses of the concrete at various locations showed the presence of $CaCO_3$ near and at the external surface (where $Ca(OH)_2$ was not detected) but that it became absent further into the concrete. This scenario is consistent with 'carbonation' of the concrete occurring at and near the exterior surfaces where CO_2 can penetrate into the concrete but has difficulty, owing to the presence of moisture (pore waters), penetrating further inwards. The depth of $CaCO_3$ presence (i.e. the depth of carbonation) was slight - only some 5 - 15 mm in from the exterior surface. It was found to be less for the boldly exposed exterior concrete and deepest for the interior concrete. This reflects the conventional wisdom that the depth of carbonation typically is greatest for mild to low relative humidity conditions compared to wetter, higher humidity conditions [14]. In all cases the depth of carbonation was much less than the depth at which the reinforcement was situated, even after 60 y of continuous exposure.

Interpretations

The observations for the 'interior' column (Fig. 2), as well as other measurements [10] made for the interior column are collected together in the average pH profile shown in Fig. 4. Also shown are the average profiles for exposed and sheltered exterior column surfaces [10]. Apart from the off-set between the profiles, they are remarkably similar. They all show close to neutral pH near the column exterior surfaces (i.e. at left in Fig. 4), and then a gradual increase in pH in a trend in each case that asymptotes to about pH =12. This value of pH can be associated with the pH of $Ca(OH)_2$ in solution [11]. Fig. 4 reminds that these profiles all are for pH values after some 60 years continuous exposure.

For each of the profiles in Fig. 4 the pH at the (nominal) location of the steel reinforcement bar(s) at about 60 mm depth is well above the pH for which corrosion is feasible according to standard thermodynamic conditions (e.g. as given for corrosion in the classic Pourbaix diagram) [12]. These thermodynamic conditions indicate that the (general) corrosion of steel is not feasible for pH values greater than about 9. This is indicated in Fig. 4. The reasons for this are based on the observation that for well-made, high-quality, well-compacted concretes (Fig. 3b), there are essentially no air-voids present at the steel-concrete interface and thus the pore water conditions inside the concrete are essentially stagnant. Under these conditions corrosion initiation is not feasible. This is the case even in the presence of chlorides [13] that could otherwise permit initiation of pitting corrosion [12)]. Unfortunately, these essential conditions for corrosion initiation have not always been recognized while the crucial quality conditions for the concrete appear seldom to have been applied in laboratory tests. With poor compaction and the presence of air-voids at the concrete-steel interface pitting corrosion is feasible even for elevated pH values but only in the presence of an aggressive species such as chlorides [12]. This likely is the reason for some investigations having concluded that corrosion was possible for pH less than about 11 [14]. However, without aggressive species such as chlorides, as

usually is the case for concretes exposed in inland conditions, corrosion, including pitting, is feasible only for porewater pH less than about 9. This is the limit shown on Fig. 4.

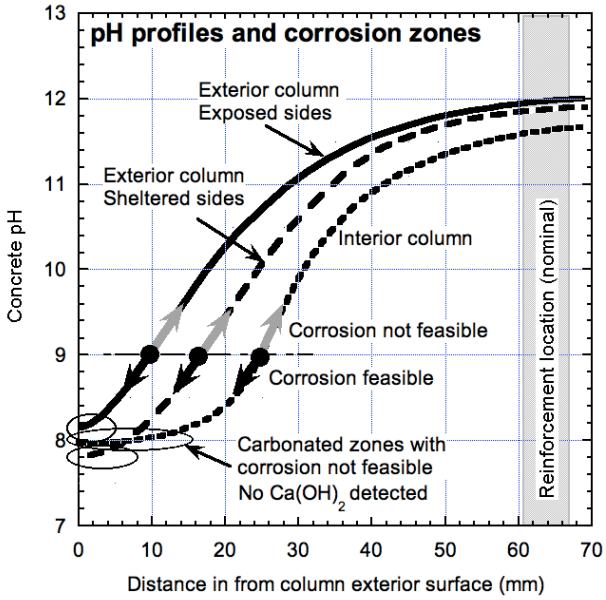

Figure 4. Averaged profiles for the observed pH values measured at 10 mm intervals from the concrete exterior surfaces inwards for 3 different exposure conditions, together with schematic representation of the depths of carbonation and the regions in which reinforcement corrosion is feasible according to thermodynamic criteria (see text). These results are all for nominally 60-year-old concrete.

Turning now to the situations with pH below about 9, Fig. 4 shows that corrosion of steel is feasible. Importantly, this is *provided* there is the presence of water and, in the early stages of exposure, also of oxygen. The development of reinforcement corrosion from initially under the cathodic oxygen reduction reaction to later being governed by the cathodic hydrogen evolution reaction has been described in detail elsewhere [15] but is not a central issue for the present paper - it is concerned essentially only with the conditions under which reinforcement corrosion can initiate. For reinforced concrete structures the availability and the rate of availability of water and oxygen depend on the depth of concrete cover and also on its water and oxygen permeabilities. Both permeabilities are likely low for well-made, well-compacted, dense concretes.

At pH levels approaching neutral at and near the exterior surface(s) the concrete (see lower left of Fig. 4) conditions are different again. There is now the presence of zones 'carbonation' that according to conventional wisdom have high concentrations of $CaCO_3$ as indeed confirmed for the present columns by XRD analyses. For these zones the XRD analyses also revealed that the concentration of $Ca(OH)_2$ was zero or negligible. Two mechanisms are likely at play to produce the conditions that give these observations. One is the reaction of $Ca(OH)_2$ with atmospheric CO_2 in the conventional (multi-step) process for which the reaction of $Ca(OH)_2$ with atmospheric CO_2 produces $CaCO_3$ and thus carbonation [10]. The second arises from the observation of the presence of micro-channels in the outer regions of the concrete, since this leaves the possibility of direct leaching (i.e. in water) of $Ca(OH)_2$ to the atmosphere and, in the case of the exterior columns, being washed away by rainwater rather than, or as well as, settling on and within the exterior concrete surface zone (see the circled zones in Fig. 4). Importantly, within these zones the presence of $CaCO_3$ in the concrete matrix and on any steel bars that

might be located within it render corrosion severely if not entirely inhibited [16, 17]. Such inhibition is in accord with, for example, observations that steel piles under impressed current corrosion protection (ICCP), show no corrosion under the build-up of calcareous material on the outside of the piles (18). This is possible in seawater because of its high (supersaturated) concentration of carbonates, and has been attributed as the primary reason for the success of ICCP [19]. These zones where corrosion is not feasible ('inhibited') are shown in Fig. 4.

These various observations highlight the difficulty of reconciling the conventional view of 'carbonation' as causing reinforcement corrosion with actual relevant field observations. They also hark back to quite early observations that distinguished between 'carbonation' and 'neutralization' [20] and that there was a gap or distance between the zones with which these two situations can be associated. Distinguishing between these two characteristic zones also is likely to explain the various inconsistencies noted in the literature [5, 10, 14, 20] about 'carbonation and its relationship to reinforcement corrosion.

Overall, it should be clear from the above that the critical mechanism for initiation of reinforcement corrosion is long-term outwards diffusion/transport of concrete alkalis, specifically that associated with $Ca(OH)_2$ in solution. This is responsible for the pH profiles and their dependence of relative humidity and concrete quality, the two main factors influencing concrete permeability [11]. The latter also has an effect on the inward diffusion of atmospheric carbon dioxide.

As already recognized, the formation of calcium carbonates in the outer concrete regions somewhat increases concrete strength [21] and, importantly, reduces the permeability of the concrete in those regions [22]. It follows that carbonation has the beneficial effect of (a) tending to inhibit the loss of concrete alkali and (b) tending to inhibit the inward diffusion of further CO_2. It can be visualized as providing a diffusion barrier for both. In turn, this tends to delay the overall loss of pH and hence the location of the pH profile in Fig. 4. Thus, the interior columns, with a higher degree of carbonation, have a pH profile further to the right in Fig. 4 and thus are likely to have earlier initiation of reinforcement corrosion for steel bars located closer to the exterior surface than for the other two exposure conditions. It follows that while increased carbonation is deleterious for initiation of reinforcement corrosion, as is also the conventional wisdom, it is not, by itself, indicative of when initiation of reinforcement corrosion will occur. That requires satisfaction of the pH conditions and knowledge of the concrete-steel interface.

For high-quality, well compacted concretes the above considerations can be used to propose a model for the depth $d(t)$ at which reinforcement corrosion initiation can be expected [11]. It is based on the depth of carbonation d_{carb} (E, t) that is a function of time t and the local environment E, and the added allowance for alkali loss $d_{pH}(t)$ which is the depth corresponding to a pH increase (ΔpH) from the carbonation region (at pH = 8 say) to the Pourbaix criterion (at pH = 9) (see Fig. 4). The carbonation depth d_{carb} (E, t) can be estimated by any of the known techniques [11].

For $d_{pH}(t)$ let it be assumed that it is a linear function of exposure time $d_{pH}(t) = \alpha\, t$. In the case of the present concrete columns, using a linearized trend that commences at the end of the carbonation depth, the increase in the depth $d_{pH}(t)$ owing to loss of alkali material can be estimated as about 10-12 mm. Since this has occurred over an exposure period of 60 years it follows that $\alpha = (\Delta \text{ distance})/(\Delta \text{ time}) = 12 \text{ mm} / 60 \text{ y} = 0.2 \text{ mm/y}$. As shown in Fig. 4, initiation of reinforcement corrosion can occur only in a relatively narrow band of depth into the concrete,

namely only in the depth range d_{carb} to $d_{carb} + d_{pH}$. Thus, for a given time period 0-t_1 that range (x) is $d_{carb}(t_1) < x < d_{carb}(t_1) + 0.2t_1$, Below this range carbonation renders corrosion infeasible due to the presence of carbonates and above this range the solution pH is too high to allow for initiation of corrosion (Fig. 4). Evidently, further investigation is required to determine the influence of environmental factors E and whether the assumptions of linearity used herein are sufficiently accurate. However, the principles and the requisite framework have now been established.

A question that sometimes arises is the effect of marine exposures or mixed carbonation and marine corrosion. The first point to note is that concretes in marine environments are likely to be subject to an enhanced relative humidity (RH) or extended periods of wetness. This renders the inward diffusion of atmospheric CO_2 more difficult. This means that the lower part of the 'exposed exterior' curve in Fig. 4 is the most relevant but also likely too far to the right for strong marine conditions since carbonation will not occur as readily. Related to this is what effect chlorides might have on the pH profiles in Fig. 4 and specifically what the effect might by on their slopes at around pH = 9, i.e. on α. As noted above, the important point here is that the slope of those curves represents the rate at which the concrete alkali material (mainly $Ca(OH)_2$) leaches out of the concrete matrix.

Under marine conditions in extended exposures there typically will be high concentrations of chlorides in concretes, including well into the concrete matrix. According to the conventional wisdom, this should cause more severe reinforcement corrosion - so-called 'chloride-induced' corrosion [11]. However, detailed experimental work [13], fundamental criteria [15] and also many detailed investigations of actual reinforced concrete structures subject to decades of marine exposure conditions have shown that chlorides cannot have, and do not have, a significant impact on reinforcement corrosion, *provided* the concrete is of high quality, well-made and *very well compacted to ensure negligible air-voids around the steel reinforcement* bars [23].

The most important effect of chlorides is to increase the rate of dissolution of $Ca(OH)_2$ in water. This permits the possibility of a faster rate of alkali leaching from the concrete matrix, i.e. the slope of the trends in Fig. 4 might increase, but whether this occurs in practice also depends on the diffusion/leaching barrier provided by the carbonated zone near and at the exterior concrete surface. Clearly, there is room for further investigation of these interactive effects. However, taking into the account the mechanisms and factors just outlined, it would seem likely, on balance, that carbonation is not a mechanism that will increase the risk of reinforcement corrosion in marine environments.

Further to the above, as a passing comment about electrochemical testing not necessarily representing actual conditions, it might be noted that often those studies use non-stagnant conditions and impose polarization potentials not reflecting the open circuit conditions that apply in practice. Further, despite the wealth of laboratory testing devoted to 'carbonation using concretes or mortars [5, 8] these tests also tend be made under artificial conditions, and under short-term exposures unlikely to represent the long-term effects such as those revealed herein. Extrapolation in time from such results also is problematic for proper consideration of the thermodynamic conditions that govern the initiation of corrosion of steels in essentially stagnant conditions. These and other reasons add to the recommendation [5] that the research community give less attention to 'carbonation' as a mechanism and more to initiation and progression of reinforcement corrosion and that this be done in conditions that are consistent with real structures and their environmental conditions. The examples given herein meet that

criterion. While the observations and modelling provided depart from much of the current literature on carbonation as a cause of reinforcement corrosion, they are, broadly, consistent with some of the earliest observations for real structures [14, 20] and with the concept that 'neutralization' of concrete alkali materials was a critical condition. These earlier works did not appear to have anticipated the role of carbonation as providing a barrier to species transport, but this might be attributed to the fact that they did not have at their disposal the modern material analysis techniques such as SEM, EDS and XRD. This would have made it more difficult to identify the various zones noted herein (Fig. 4) and also the corresponding changes in material properties as the neutralization process develops into the concrete.

Finally, it should be clear from the above analysis and reference to experiences with actual reinforced concrete columns that (a) carbonation is not a significant problem for well-compacted, well-made, high quality concretes with high degree of interfacial contact with the steel bars, (b) that this applies also for extended exposures (decades) and (c) that as a result carbonation of exposed concretes should be considered a positive factor for carbon dioxide absorption by reinforced concrete structures rather than a threat for reinforcement corrosion. Nevertheless, more investigation should be carried out to determine the extent and the rate of CO_2 absorption that occurs for exposed concretes in different atmospheres and climatic conditions as well as how this is affected by concrete surface quality.

Conclusion

The well-compacted, high quality reinforced concrete columns reported herein showed no evidence of reinforcement corrosion due to 'carbonation' even after 60 years exterior and interior inland temperate climate exposures. In all cases examination of the concretes showed the existence of carbonation in the outer surface zone. They also showed depletion of calcium hydroxide in that zone with pH around 7.5-8, increasing further into the concrete and peaking at around pH 12 some 50-60 mm into the concrete at the location of the reinforcement bars. The results are interpreted as showing that the carbonated zone act as a diffusion barrier for the loss, by the slow leaching-out, of the calcium hydroxide alkali material. Reference back to corrosion science fundamentals indicates that the carbonated zone also inhibits the corrosion process whilst further into the concrete the condition of pH greater than about 9 steel makes steel corrosion thermodynamically not feasible. Based on these observations a new model is presented for the zone in which reinforcement corrosion is feasible. It is concluded that 'carbonation' as a cause for reinforcement corrosion is misnamed and that the beneficial effects including higher concrete strength, lower concrete permeability and absorption of greenhouse-causing atmospheric carbon dioxide are not, as commonly believed, necessarily overshadowed by an increased risk of reinforcement corrosion.

Acknowledgements

The pH readings in Fig. 2 were taken in 2022 by 4th year University of Newcastle Civil Engineering Project student Beau Pihlak under the supervision of the first author. The assistance of the Electron Microscope and X-ray (EMX) Centre at the University of Newcastle is appreciated.

References.

1 Lehne, J., Preston, F. (2018) Making concrete change: Innovation in low-carbon cement and concrete, Chatham House Report 13, June, ISBN: 978 1 78413 272 9.

2 Intergovernmental Panel on Climate Change (2023) 6th assessment report, https://www.ipcc.ch/report/ar6/wg1/downloads/report/IPCC_AR6_WGI_Full_Report.pdf (last accessed 3 March 2023).
3 MPA (2020) UK Concrete and cement industry roadmap to beyond net zero, Mineral Products Association, London, 2020.
4 Fairs, M. (2022) UK appoints cement trade body the Mineral Products Association to calculate concrete's potential as a carbon sink, Dezeen, 12 Jan 2022.
5 RILEM (2020) Understanding the carbonation of concrete with supplementary cementitious materials: a critical review by RILEM TC 282-CCC, Materials and Structures, **53**: 136.
6 Possan, E., Felix, E.F., Thomaz, W.A. (2016) CO2 uptake by carbonation of concrete during life cycle of building structures, J. Build. Rehabil. **1**: 79.
7 Melchers, R.E. (2010) Carbonates, carbonation and the durability of reinforced concrete marine structures, Aust. J. of Struct. Eng., **10** (3) 215-226.
8 Angst, U., Moro F. and 9 others, (2020) Corrosion of steel in carbonated concrete: mechanisms, practical experience, and research priorities - a critical review by RILEM TC 281-CCC, RILEM Technical Letters (2020) **5**, 85-100.
9 Grubb, J.A., Limaye H.S., Kakade, A.M. (2007) Testing pH of concrete, Concrete Intl. **29** (4) 78-83.
10 Melchers R.E., Richardson, P.J. (2023) Carbonation, neutralization and reinforcement corrosion for concrete in long-term atmospheric exposures, Corrosion, **79** (4) 395-404.
11 Richardson, M.G. (2002) Fundamentals of durable reinforced concrete, SponPress, London.
12 Pourbaix, M. (1970) Significance of protection potential in pitting and intergranular corrosion, Corrosion, **26**, 431–438.
13 Melchers R.E., Chaves I.A. (2019) Reinforcement corrosion in marine concretes - 1: Initiation, ACI Materials J., **116** (5) 57-66.
14 Parrott, L.J. (1987) A review of carbonation in reinforced concrete, Building Research Establishment, Department of the Environment, Garston, Watford, UK.
15 Melchers R.E. (2023) Mechanisms in long-term marine corrosion of steel reinforcement in concretes, Corrosion, **79** (4) 380-387.
16 Mao, X., Liu, X. and Revie R.W. (1994) Pitting corrosion of pipeline steel in dilute bicarbonate solution with chloride ions, Corrosion, **50** (9) 651-657.
17 Davies D.H., Burstein G.T. (1980). The effects of bicarbonate on the corrosion and passivation of iron, Corrosion, **36** (8) 416-422.
18 Humble, R.A (1949) The cathodic protection of steel piling in sea water, Corrosion, **5** (9) 292-302.
19 Ackland, B.G., Dylejko, K.P. (2019) Critical questions and answers about cathodic protection, Corros. Eng. Sci. Technol. **54** (8) 688-697.
20 Hamada, M. (1968) Neutralisation of concrete and corrosion of reinforcing steel (in) Proc. Fifth Intl. Symp. Chemistry of Cement, Tokyo, Oct 7-11, part III, Properties of cement paste and concrete. Proc. pp. 343-369.
21 Cui H, Tang W., Liu W., Dong Z., Xing F. (2015), Experimental study on effects of CO2 concentrations on concrete carbonation and diffusion mechanisms, Const. Building Mat, **93**, 522–527.
22 Kim J-K, Kim C-Y, Yi S-T, Lee Y. (2009) Effect of carbonation on the rebound number and compressive strength of concrete, Cement Conc. Comp., **31** (2) 139–144.
23 Melchers, R.E., Chaves, I.A. (2020) Reinforcement corrosion in marine concretes - 2. Long-term effects, ACI Materials J., **117** (2) 217-228.

Green rust prediction and detection in reinforced concrete structures in marine environment

Dr Hamid Fatemi, School of Civil Engineering, Faculty of Engineering, The University of Sydney, NSW 2006, Australia

Dr Ali Hadigheh, School of Civil Engineering, Faculty of Engineering, The University of Sydney, NSW 2006, Australia

Abstract

Corrosion of concrete reinforcement in marine environment through aerobic red rust formation is very well documented in literature; however, very limited information is reported about the anaerobic green rust formation. More importantly, green rust does not manifest the usual concrete durability distress signs of cracking and spalling which is associated with normal red rust. Therefore, while green rust is as detrimental to structures as a normal rust, it is harder to detect.

This study explains the observed mechanism of green rust formation and the signs for prediction of such corrosion in reinforced concrete (RC) culverts and bridges in marine environment. The study also intends to alert the infrastructure asset owners and corrosion engineering community the danger of significant steel section loss without visible signs of the concrete deterioration.

The results of concrete durability condition assessment of two culverts and three bridges in New South Wales (NSW), Australia revealed very high levels of corrosion activity within the culvert and bridge elements. Two active corrosion mechanisms were found at these sites. One is the conventional red rust formation process and the other one is green rust, mostly at around high-water-level (HWL) areas resulting in severe corrosion of reinforcement bars (rebars) without any significant concrete spalling, cracking or delamination.

Investigation was carried out to elucidate what conditions are conducive to the formation of green rust; and thereby, facilitate the prediction and detection of green rust. Also, the study has highlighted the extent of damage due to green rust or anaerobic corrosion.

Introduction

Steel corrosion is an electrochemical process that has essential condition and elements collectively referred to as the corrosion cell including anode, cathode, metallic pathway and electrolyte. When steel in concrete corrodes it dissolves in the pore water and gives up electrons (the anodic reaction):

$Fe = Fe^{2+} + 2e^-$ (1)

The two electrons ($2e^-$) created in the anodic reaction must be consumed elsewhere on the steel surface to preserve electrical neutrality. This is a reaction that consumes water and oxygen (the cathodic reaction):

$2e^- + H_2O + ½ O_2 = 2OH^-$ (2)

Several more stages must occur for 'rust' to form. This can be expressed in several ways; one is shown below, where ferrous hydroxide ($Fe(OH)_2$) becomes ferric hydroxide ($Fe(OH)_3$) and then hydrated ferric oxide ($Fe_2O_3.H_2O$) that is normal red rust.

There is an alternative to the formation of above mentioned 'normal' red rust in anaerobic condition which can result in formation of green rust (Fe_3O_4). If the anode and cathode are well separated (by several hundred millimeters) and the anode is starved of oxygen the iron as Fe^{2+} will stay in solution. This type of corrosion is found under damaged waterproof membranes and in some underwater or water saturated conditions.

Another complication comes from bacterial corrosion. Bacteria in the soil (thiobacilli) converts sulphur and sulphides to sulphuric acid. This acid will attack steel causing corrosion. There are other species (ferrobacilli) that attack the sulphides in steel (FeS). This is often associated with a smell of hydrogen sulphide (rotten eggs) and smooth pitting, with a black corrosion product when rebars are exposed having been in water saturated conditions. Anaerobic conditions such as bacteria can contribute to the pitting corrosion discussed above [1-7].

The available literature on anaerobic corrosion for green rust formation is either focused on bacterial corrosion or is limited to the submerged structures. There is a very limited information available on the green rust formation in the structures above the ground water level. This paper is an attempt to raise awareness for predicting green rust formation in all areas of the RC structures and provides guidance on detection of this corrosion mechanism. It also highlighted the extent of damage due to green rust formation and particularly without usual RC durability distress telltales.

Experimental procedures

In this research, visual inspection and concrete cover meter survey were undertaken on suspected structures. Also, scanning electron microscope (SEM), energy dispersive spectrometry (EDS) analysis and X-ray diffraction (XRD) were performed on corrosion products.

SEM and EDS were undertaken using a JEOL JSM-6510LV SEM equipped with an Amptek silicon drift detector (SDD). Spectra were collected in a low vacuum at an accelerating voltage of 25 keV and analysed using Moran Scientific EDS microanalysis software. XRD diffractograms measurement was conducted using Bruker D8 Advance Diffractometer with CuKα radiation (λ = 1.5406 Å), LYNXEYE detector, and Bragg-Brentano geometry. The samples were examined in the 2θ ranges of 5° to 90° with a time/step of 3 s. The phases were identified using the Bruker EVA software and XRD data from the International Centre for Diffraction Data (ICDD) PDF database.

Condition assessment results and discussion

Durability investigation of two culverts, called culvert No.1 and culvert No.2 for the purpose of this paper, revealed very high levels of corrosion activity within the culvert walls. Preliminary investigation including visual survey, cove rmeter survey, carbonation testing, chloride content analysis, concrete resistivity testing and half-cell potential mapping revealed that the primary corrosion mechanism is chloride attack and carbonation poses a secondary corrosion risk. On the other hand, the extent of corrosion observed on the exposed reinforcement was considerably more severe than would normally be expected, considering the level of concrete deterioration; hence, further investigation was carried out to observe the presence of anaerobic corrosion.

Culvert No.1

Appendix A shows the photos for breakout 1 (photos A1 to A4). As shown in photos A3 and A4, green rust was observed at the location of breakout 1 which suggests the occurrence of anaerobic corrosion. Generally, such green rust is found on reinforcing steel in concrete under water or other water saturated conditions. Since corrosion of steel to form green rust does not produce a crystalline material, it will occupy voids in concrete or other available spaces in concrete without exerting

expansive pressures on the surrounding material; and therefore, has the ability to dissolve substantial amounts of reinforcing steel without the concrete cracking and spalling. This can result in a gross underestimation of the severity of corrosion and the weakening of reinforced concrete structures [8-10]. The mechanism of anaerobic corrosion can be explained as follows:

1. Within the zone of partially saturated concrete, around the culvert cell wall's mid-height plenty of oxygen exists at the reinforcement and also it is wet enough to provide sufficient water for the cathodic reaction. This reaction consumes oxygen and water as well as the electron created in the anodic reaction to preserve electrical neutrality.
2. The concrete at mid-height section of the cell walls within the partially saturated zone provides a low resistance electrolyte for effectively transferring hydroxyl ions produced at the cathode to be consumed at the site of rust formation. This condition supports a high corrosion rate.
3. The rebars at the bottom section of the cell walls act as an anode as this area is water saturated and starved of oxygen. Therefore the 'normal' formation of hydrated ferric oxide (red rust), which is very expansive, does not occur. Instead, the iron ions stay in solution and there are no expansive forces to crack the concrete. This is potentially serious since severe corrosion, and associated steel section loss, may occur undetected.
4. The existing green rust rapidly turns to the more conventional red/brown rust when it leaches out to the cell walls surface, as a result of being exposed to oxygen during the low tide (refer photo A2).

Appendix B shows the photos for breakout 2 (photos B1 - B4). Rebars were severely corroded. It is worthwhile to mention that the rebar at the bottom left-hand side of the photos B3 and B4 that is already corroded away. The extent of corrosion observed on the exposed reinforcement was considerably more severe than would 'normally' be expected, given the level of concrete deterioration. This further supports the above observations of 'green rust' and the likelihood of anaerobic corrosion. It would appear however that the extent of anaerobic corrosion occurring at breakout 2 is less than breakout 1, since insufficient 'green rust' has leached-out to form a rust stain on the surface (refer point 4 above).

Three more cores were drilled to further investigate the presence of 'green rust'. Appendix C shows the coring locations and the cores photos (photos C1 – C6). The

apparent observation of ‘more-severe’ anaerobic corrosion occurring at a consistent ~HWL, noted above, would appear to be further supported from these cores (cores 1-3, refer to photos C1, C3 and C5). Photos C2, C4 and C6 show that no rebar is left. Since the corrosion products were greenish at the time of coring it seems that the rebars were corroded due to anaerobic corrosion.

Culvert No.2

Photos of the coring locations and core holes are shown in Appendixes D-F. Corrosion products were observed in all of the core holes. Some red rusts were observed even within those cores that were not drilled at the rust stain locations. Furthermore, green rust was observed at core holes 2 (Appendix E) and 3 (Appendix F) which is an indication of anaerobic corrosion. The rust stains were not observed on the cell walls before the soffit repair works, in which the cell walls left dry for two weeks, otherwise it was unlikely that green rusts get to the concrete surface to form rust stains on the cell walls to be observed visually. However, the existing green rust rapidly turned to the more conventional red/brown rust as a result of being exposed to oxygen during the repair work that encountered a more oxygen rich environment.

Cover meter survey at core holes 2 and 3 showed loss of reinforcement signal or inconclusive signal which would be a sign of extensive section loss due to green rust formation which was proven by coring and visual inspection of the rebars’ corrosion state.

Bridge No.1

Appendix G presents green rust which was observed in two of the bridge No.1 columns. The section loss of reinforcement was calculated to be 67% and 75% on the exposed reinforcements of vertical main bar and horizontal stirrup, respectively. SED, EDS and XRD of the rust products confirmed formation of green rust (Fe_3O_4) along with different iron hydroxides showing gradual change of green to red rust where oxygen is available (Appendix H).

The sealing dome on the sample holder is polymer based and this gives a contribute to background signal. As such two amorphous humps can be seen at the start of the spectrum. As the samples were sensitive to air, Bruker airtight sample holders were utilised to prevent further oxidation. The sample holder was purged with argon gas and sealed.

Bridge No.2

Appendix I shows full section loss of the vertical stirrups as a result of anaerobic corrosion at around HWL. It is noted that the I1 images are taken at a low tide level.

Bridge No.3

Contrary to the previous examples where green rust had formed where rebar was fully or partially submerged, the breakout areas in bridge No.3 column had never been submerged even partially (Appendix J). However, the concrete in the breakout areas was found to be very porous and honeycombed which suggests possibility of oxygen deficiency due to water ponding in hollow areas of the concrete.

Conclusions

Observation of the green rust suggests the possibility of anaerobic corrosion, in the investigated culverts/bridges at all areas including, submerged, tidal and atmospheric zones where the situation is conducive to oxygen deficiency. The low oxygen areas (anodic sites) are usually close to oxygenated areas (cathodic sites) for an effective oxygen corrosion cell. Since corrosion of steel to form green rust does not produce a crystalline material, it will occupy voids or other available spaces in concrete without exerting expansive pressures on the surrounding material; and therefore, has the ability to dissolve substantial amounts of reinforcing steel without the concrete cracking and spalling. This can result in a gross underestimation of the severity of corrosion and the weakening of reinforced concrete structures.

This paper was an attempt to explain the mechanism of anaerobic corrosion in such culverts/bridges as a sample and alert the infrastructure asset owners the danger of significant steel section loss without visible signs of the concrete deterioration. It is recommended to inspect the assets of similar construction and in a similar environment looking for possible anaerobic corrosion. The areas of full loss of reinforcement are to be non-destructively tested (NDT) using ground penetrating radar (GPR) mapping followed by cover meter survey of the identified critical areas. The loss of cover meter signal or un-clear signal should be taken as full reinforcement section loss, pending concrete breakout and visual examination.

References

[1] Bromfield J P (1997) Corrosion of steel in concrete, understanding, investigation and repair. E & FN Spon London and New York

[2] Melchers R E and Li C Q (2009) Reinforcement corrosion in concrete exposed to the north sea for more than 60 years. 65 8 ProQuest Central p. 554

[3] West J S, Larosche C J, Koester B D, Breen J E and Kreger M E (1999) State of the art report about durability of post tensioned bridge substructures. Report number 1405-1, Center for transportation research, Bureau of Engineering Research, The University of Texas at Austin

[4] Wheeler M C (2003) Parameters influencing the corrosion protection service life of epoxy coated reinforcing steel in Virginia bridge decks. Thesis submitted to the faculty of Virginia Polytechnic Institute and State University in partial fulfillment of the requirements for the degree of Master of Science in Civil & Environmental Engineering

[5] Kahrs J T, Darwin D and Locke C E (2001) Evaluation of corrosion resistance of type 304 stainless steel clad reinforcing bars. The University of Kansas, Center for Research, Report No. 65

[6] Zemajtis J (1998) Modeling the time to corrosion initiation for concretes with mineral admixtures and/or corrosion inhibitors in Chloride-Laden Environments. Dissertation submitted to the Faculty of the Virginia Polytechnic Institute and State University in partial fulfillment of the requirements for the degree of PhD in Civil Engineering, Blacksburg Virginia

[7] persson M (2000) Investigation of the impact of load induced cracking on the initiation time on steel corrosion in concrete. Institution of Civil Engineering, Department of Structural Engineering, Lule a University of Technology, Master Thesis 348

[8] Claisse P A (2009) Construction materials notes. Coventry University, Faculty of Engineering and Computing, Civil Engineering Group

[9] Lindvall A (2003) Environmental actions on concrete exposed in marine and road environments and its response. Department of building Technology, Building Materials, Chalmers University of Technology, Publication P-03:2 Goteborg

[10] McLeish A (1994) Underwater concreting and repair. Halsted Press, An imprint of John Wiley & Sons Inc. New York Toronto.

Appendix A

Breakout 1 at culvert No.1.

<table>
<tr><td> 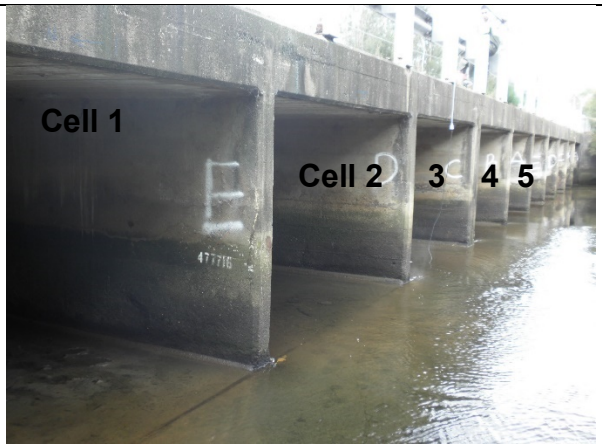
</td><td> </td></tr>
<tr><td>A1. Culvert walls North faces at downstream side.</td><td>A2. Cell 2 South face at downstream end prior to breakout 1.</td></tr>
<tr><td> </td><td> </td></tr>
<tr><td>A3. Exposed vertical rebar at breakout 1, showing green rust. Note the greenish-black corrosion products that form when iron or steel corrodes under conditions of limited oxygen availability.</td><td>A4. Same as A3, closer view.</td></tr>
</table>

Appendix B

Breakout 2 at culvert No.1.

<table>
<tr><td> </td><td> </td></tr>
<tr><td>B1. Culvert cell 5 North face at downstream end.</td><td>B2. Cell 5 North face prior to breakout 2.</td></tr>
<tr><td> </td><td> </td></tr>
<tr><td>B3. Exposed rebars at breakout 2, showing red rust.</td><td>B4. Same as B3, closer view.</td></tr>
</table>

Appendix C

Core holes and samples at culvert No.1.

<table>
<tr><td> 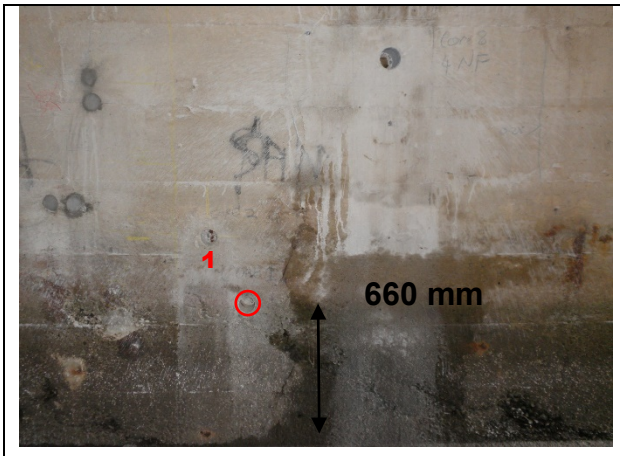
</td><td> </td></tr>
<tr><td>C1. Core hole 1 at Cell 4.</td><td>C2. Sample from core hole 1.</td></tr>
<tr><td> 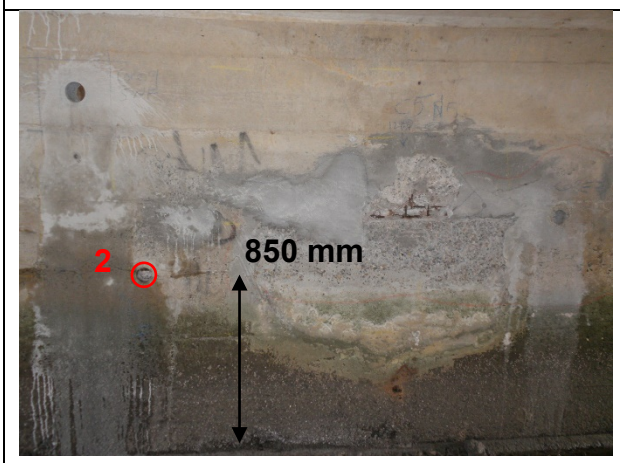
</td><td> </td></tr>
<tr><td>C3. Core holes 2.</td><td>C4. Samples from core hole 2.</td></tr>
<tr><td> 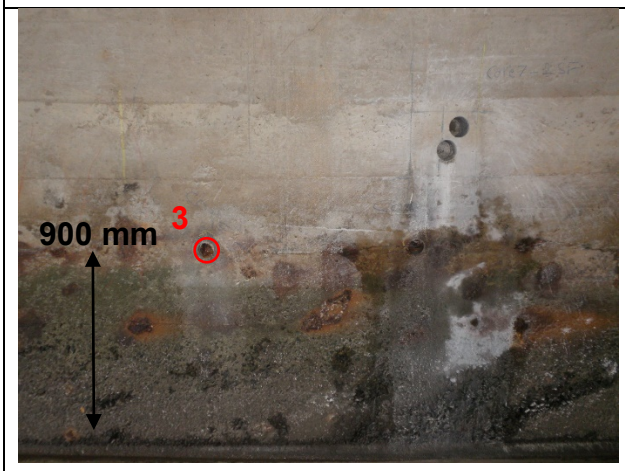
</td><td> </td></tr>
<tr><td>C5. Core hole 3 at Cell 5.</td><td>C6. Sample from core hole 3. Rebar is already corroded away.</td></tr>
</table>

Appendix D

Core hole 1 at culvert No.2.

<table>
<tr><td> </td><td> </td></tr>
<tr><td>D1. Cell 3 prior to coring hole 1.</td><td>D2. Core hole 1, at the rust stain on horizontal rebar.</td></tr>
<tr><td> </td><td> </td></tr>
<tr><td>D3. Sample from core hole 1, shows the corrosion products path from the horizontal rebar (right) to the wall surface (left).</td><td>D4. Core hole 1. Rebar is corroded away.</td></tr>
</table>

Appendix E

Core hole 2 at culvert No.2.

E1. Location of core hole 2 at the rust stain.

E2. Sample from core hole 2.

E3. Sample from core hole 2 shows the remaining corroded rebar. Green rust has already turned to the more conventional red/brown rust after encountered to a more oxygen rich environment at the time of taking photo.

E4. Core hole 2.

Steel bar is corroded. Note the greenish corrosion products that form when iron or steel corrodes under conditions of limited oxygen availability (anaerobic corrosion)

Appendix F

Core hole 3 at culvert No.2.

<table>
<tr><td> </td><td> </td></tr>
<tr><td>F1. Location of core hole 3 at the rust stain.</td><td>F2. Sample from core hole 3.</td></tr>
<tr><td> </td><td> </td></tr>
<tr><td>F3. Sample from core hole 3. Green rust was observed at the location that used to be the vertical rebar.</td><td>F3. Core hole 3.</td></tr>
</table>

Appendix G

Breakouts at bridge No.1.

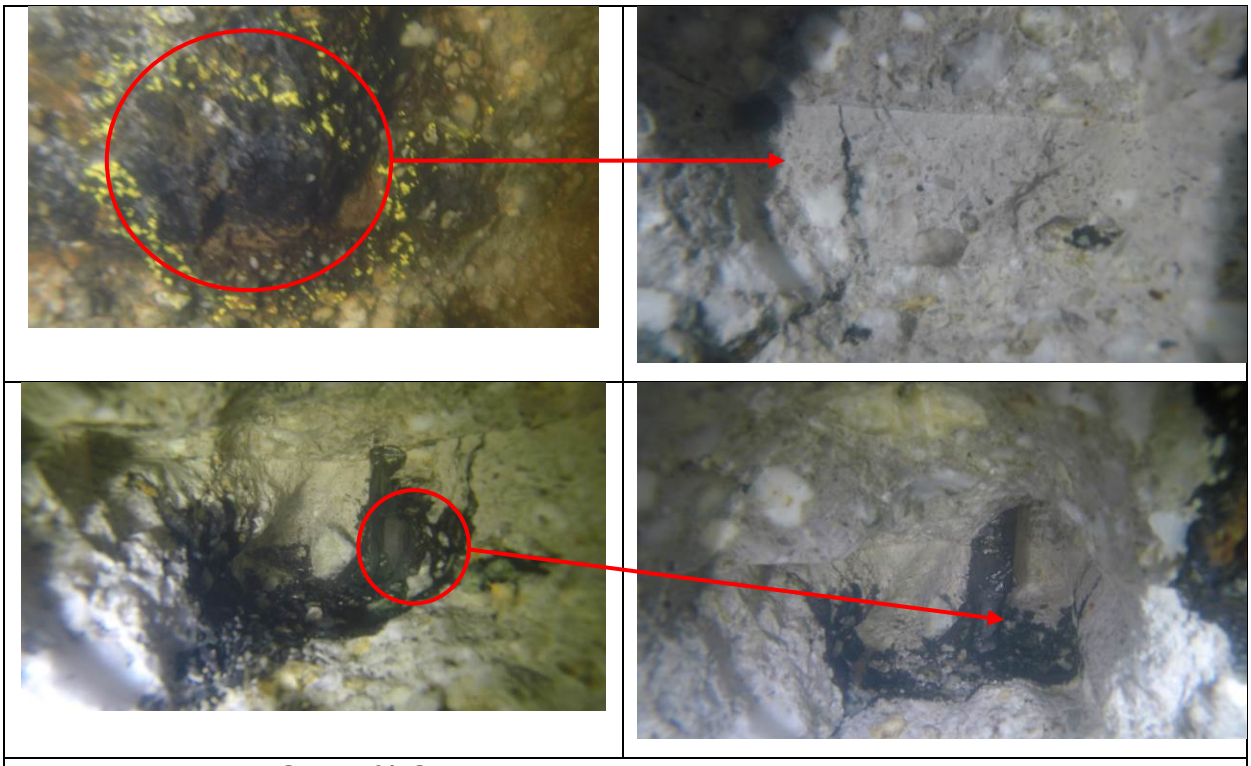

G1. 67% Section loss on the vertical main bar.

G2. 75% Section loss on the horizontal stirrup.

Appendix H – SEM/EDS

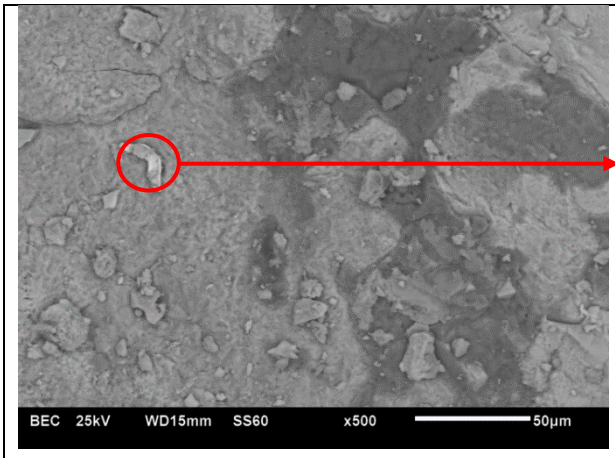

H1. SEM back scatter image the sample from G1.

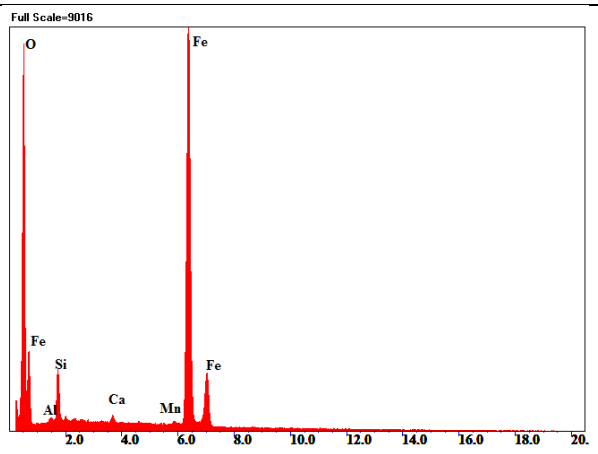

H1. EDS point elenmental analysis of the sample from G1.

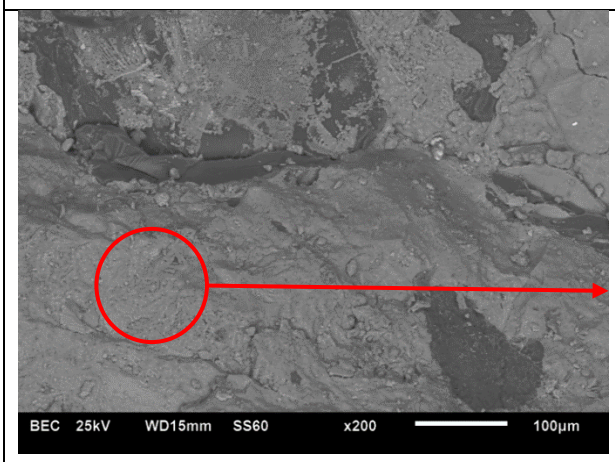

H3. SEM back scatter image the sample from G2.

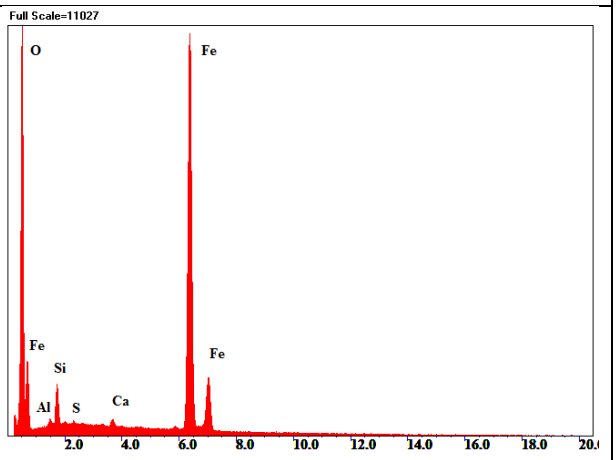

H4. EDS point elenmental analysis of the sample from G2.

Appendix H - XRD

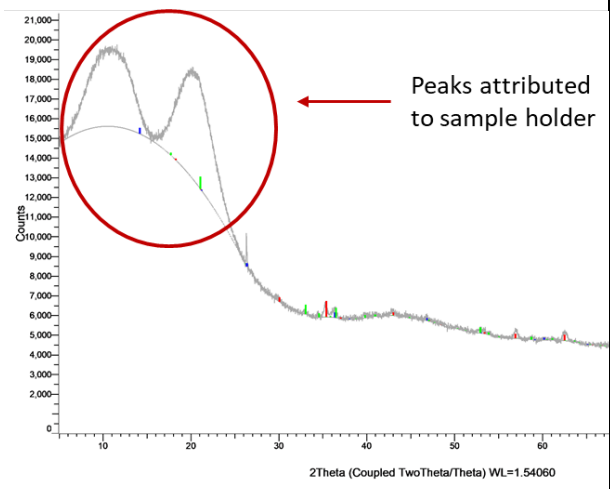

H5. Sample holder peaks.

H6. Burker airtight sample holder.

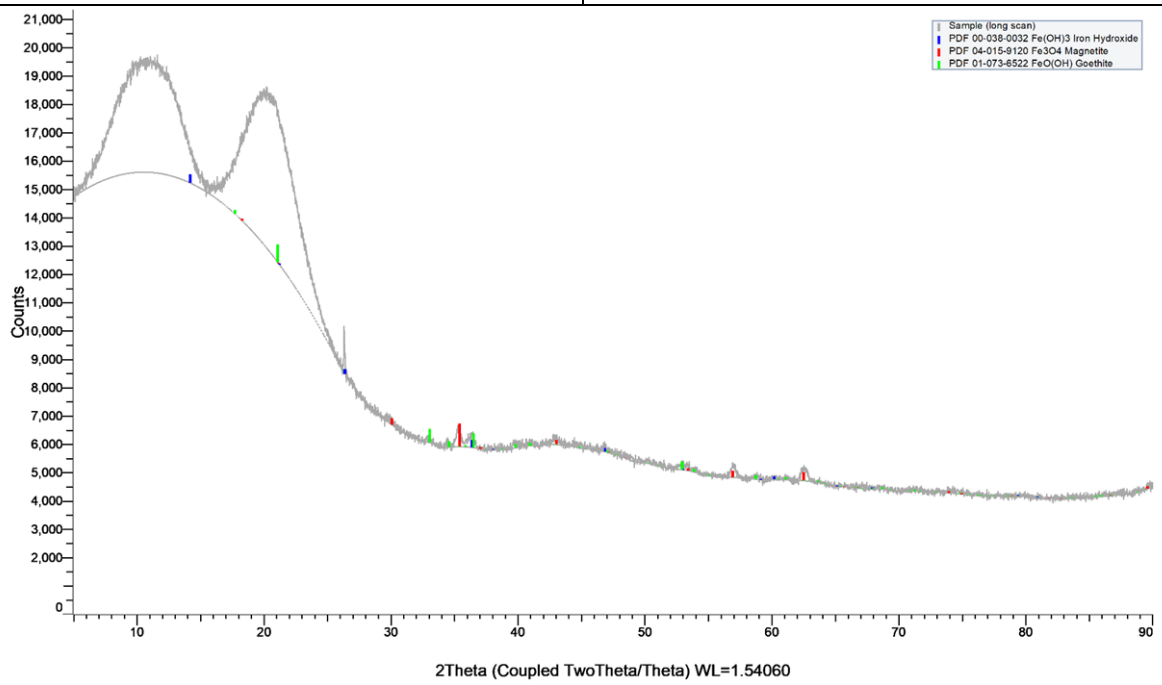

H7. Potential phases observed in raw data of sample G1

PDF 00-038-0032 – ($Fe(OH)_3$), Iron Hydroxide

PDF 04-015-9120 – (Fe_3O_4), Magnetite

PDF 01-073-6522 – ($FeO(OH)$), Goethite

Appendix H – XRD - continued

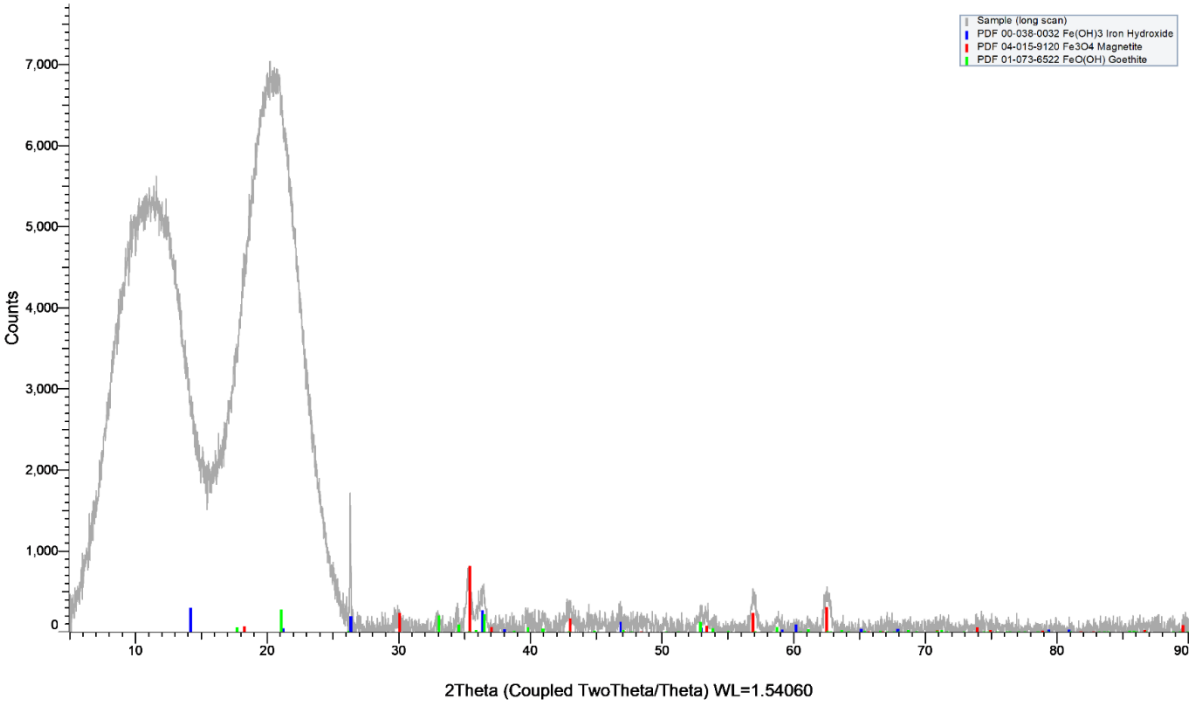

H8. Baseline flattened with peak matching of sample G1

PDF 00-038-0032 – $(Fe(OH)_3)$, Iron Hydroxide

PDF 04-015-9120 – (Fe_3O_4), Magnetite

PDF 01-073-6522 – (FeO(OH)), Goethite

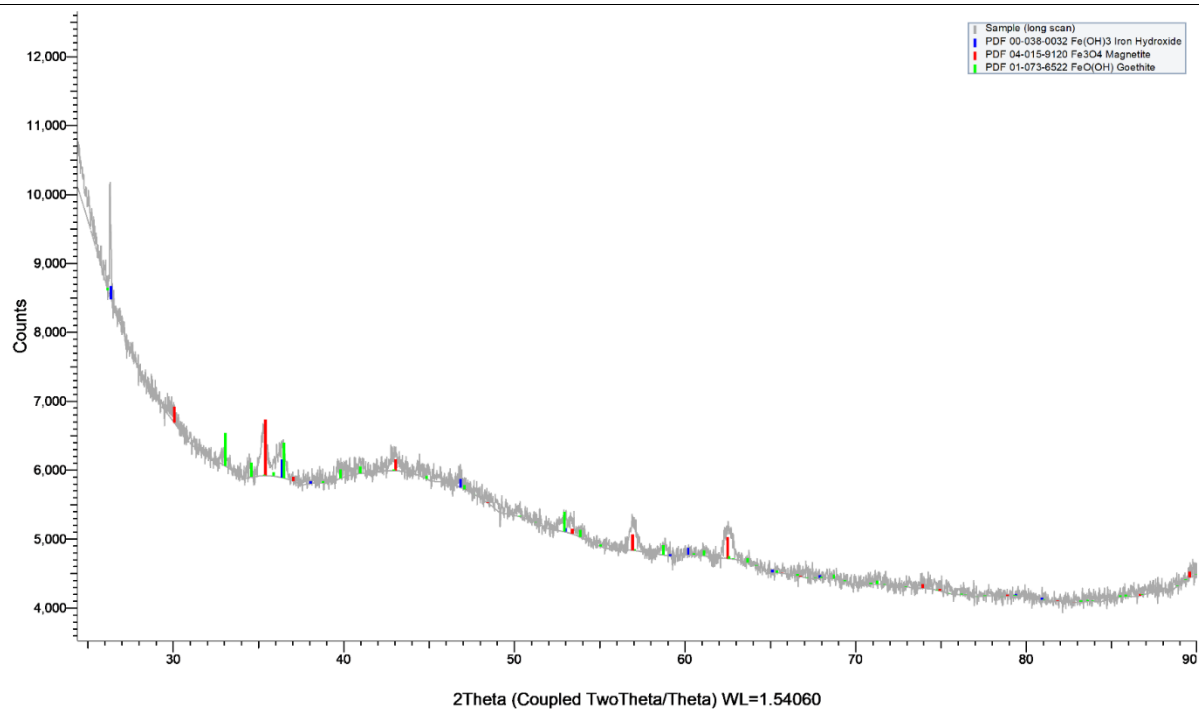

H9. Raw data of sample G2.

Appendix H – XRD - continued

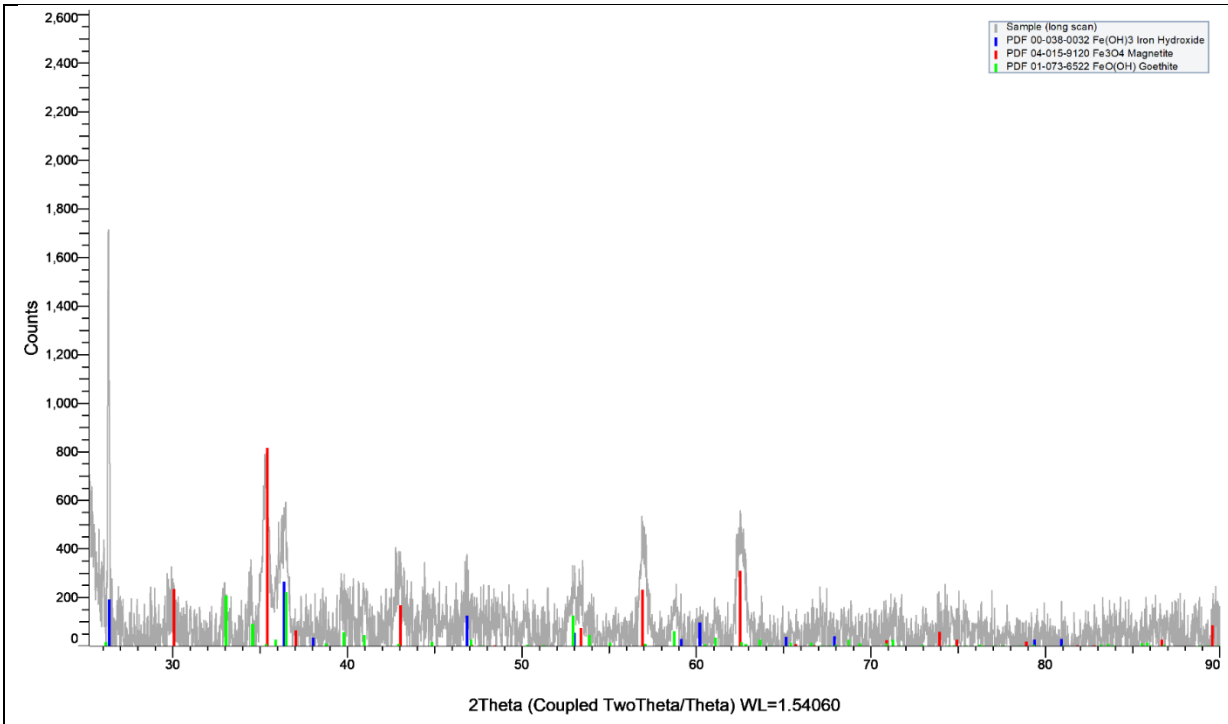

H10. Baseline flattened with peak matching of sample G2.

PDF 00-038-0032 – ($Fe(OH)_3$), Iron Hydroxide

PDF 04-015-9120 – (Fe_3O_4), Magnetite

PDF 01-073-6522 – ($FeO(OH)$), Goethite

Appendix I

I1. Total section loss of vertical stirrups due to anaerobic corrosion in bridge N0.2.

Appendix J

J1. Breakouts at atmospheric zone of bridge No.3

Experimental study on corrosion characteristics of steel bars in concrete located in tidal zone.

Masayuki Hara, Port and Airport Research Institute, Japan;
Nagate Hashimoto, Port and Airport Research Institute, Japan;
Kentaro Koike, Port and Airport Research Institute, Japan;
Toru Yamaji, Port and Airport Research Institute, Japan;
Hiroyuki Kobayashi, Nakabohtec Corrosion Protecting Co., Ltd., Japan;
Yukihiro Sone, Nakabohtec Corrosion Protecting Co., Ltd., Japan;
Hidenori Hamada, Graduate School of Kyushu University, Japan

Introduction

In port and harbor structures such as caissons and piers, concrete members span multiple environmental zones in the vertical direction. Therefore, corrosion of steel bars in concrete located in the splash/tidal zone is a concern due to the repeated exposure to seawater and oxygen. In this study, the effect of tidal fluctuations on the corrosion characteristics of steel bars in concrete was evaluated by electrochemical measurements.

Outline of the test

An overview of the test specimen is shown in Fig. 1. The rebars were connected to each other via a measuring wire and a switch. Reference electrodes were placed near the rebars and the rebar potential was measured. A shunt resistor (1 Ω) was connected to the measuring line of each rebar, and the measured terminal voltage was divided by the shunt resistor and converted to a current value. The concrete (ordinary portland cement, blast furnace slag cement type B) contained 10 kg/m^3 of chloride ions and was allowed to cure for 28 days after casting before testing.

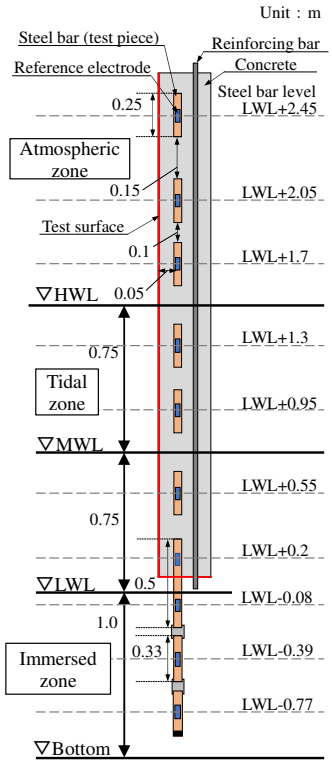

Fig.1 Test specimen overview

The specimens were exposed to a water tank in which seawater ebbs and flows twice a day. The ebb and flow cycle of the tank is shown in Fig. 2. In the figure, HWL is the highest tide level in the tank, LWL is the lowest tide level, and MWL is the tide level between HWL and LWL. All depths at which rebar was installed were based on LWL.

Results and Summary

The rebar potential and rebar current density of the specimens with blast furnace slag cement type B measured 6 months after the start of the exposure test are shown in Fig. 3 and Fig. 4, respectively. The rebar potential showed a potential gradient in the area above the LWL, and the potential tended to become more noble as the distance from the underwater area increased. The rebar current density showed anodic and cathodic currents depending on the depth of installation, indicating the formation of macrocells. At high tide, the rebar in the submerged area was the anodic part and the rebar in the tidal area was the cathodic part, but at low tide, the rebar in the tidal area was also the anodic part. The rebar potential in the tidal zone tended to be lowered at high tide and raised at low tide, corresponding to the behavior of the macrocell current.

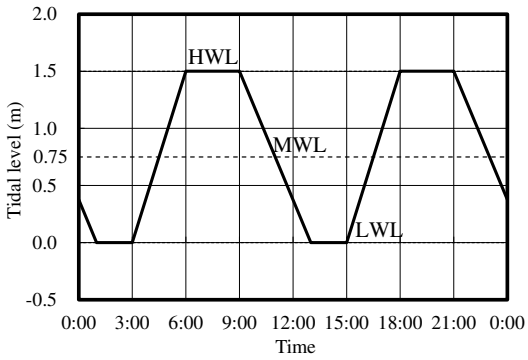

Fig.2 Tidal cycle

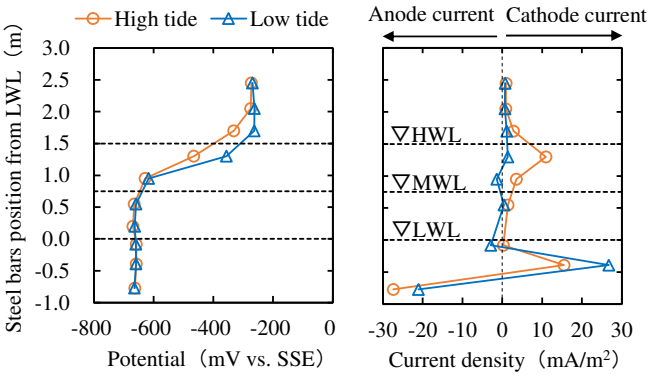

Fig.3 Rebar potential distribution

Fig.4 Rebar current density distribution

These results confirm that the rebar potential and current density in concrete change in synchronization with tidal fluctuations. It was also confirmed that under such environmental conditions, macrocell corrosion occurs between steel and concrete members.

Impedance spectroscopy study of aluminium alloy 1100 encapsulated in ordinary Portland cement pastes

X. Li[1,2]*, S. Caes[1], T. Pardoen[2], G. De Schutter[3], Tom Hauffman[4], B. Kursten[1]

1. Belgian Nuclear Research Center, SCK CEN, Boeretang 200, Mol, Belgium
2. Institute of Mechanics, Materials and Civil Engineering (IMMC), Université catholique de Louvain, B-1348 Louvain-la-Neuve, Belgium
3. Magnel-Vandepitte Laboratory, Department of Structural Engineering and Building Materials, Technologiepark-Zwijnaarde 60, B-9052 Ghent (Zwijnaarde), Ghent University, Belgium
4. Department of Materials and Chemistry, Research Group Electrochemical and Surface Engineering (SURF), Vrije Universiteit Brussel, Pleinlaan 2, 1050 Brussels, Belgium

**xiang.li@sckcen.be*

One possible route for the geological disposal of the Belgian reactor 1 (BR1) fuel, which will eventually become nuclear waste, could be the direct encapsulation of the whole fuel capsule in a cementitious matrix. Because the cladding of the BR1 fuel is made of aluminium alloy 1100 (AA1100), this alloy would be in direct contact with the cementitious matrix. Due to its amphoteric property, aluminium cannot form a passive corrosion product film in Ordinary Portland Cement (OPC) paste, which possesses a highly alkaline condition. Hence, the corrosion process can proceed rapidly and threaten the encapsulation safety. One potential solution for this problem is the addition of a corrosion inhibitor in the OPC paste, such as $LiNO_3$ or Li_2CO_3, to form a layered double hydroxide ($[LiAl_2(OH)_6]_n^{1+} \cdot X^{n-} \cdot yH_2O$, where X^{n-} is an anion ion) film [1]-[5].

A combined approach of electrochemical measurements, scanning electron microscopy and gas chromatography was used to study the corrosion rate of AA1100 in OPC pastes. The corrosion rate of the aluminium alloy is effectively inhibited owing to the formation of a protective corrosion product film in cement pastes containing $LiNO_3$ or Li_2CO_3. Without any inhibitor, the fast corrosion rate with an uncontrolled growth of the corrosion product film, leads to visible cracking of the cement paste matrix as early as after eight days. Both the hydration evolution and the curing environment of cement pastes are found to play important roles in the corrosion process.

Meanwhile, by the innovative combination of the equivalent circuit model and the General Effective Media theory, EIS is capable of providing the porosity information of cement pastes. Mercury Intrusion Porosimetry (MIP) confirmed the reliability of the porosity results obtained from EIS.

The following conclusions can be obtained from this research: (1) Both $LiNO_3$ and Li_2CO_3 are effective corrosion inhibitors for AA1100 in OPC paste. However, $LiNO_3$ seems to be more suitable. While using a water to cement ration equals to 0.36 and the addition of 3 wt.% of $LiNO_3$, the lowest corrosion rates were observed without any cement curing problems. The low and predictable level of hydrogen production of OPC+$LiNO_3$ samples is also beneficial for the long-term encapsulation; (2) The immersion of samples in saturated $Ca(OH)_2$ solution, mimicking the water resaturation of the cement paste after many years in the geological disposal, increases the corrosion rate; (3) Both the corrosion rate of AA1100 and the porosity variation of the cement paste can be simultaneously determined by EIS. These results were confirmed by other methods, such as SEM, GC and MIP.

[1] Buchheit et al., Corrosion, 50(3), 205-214.
[2] Delpech et al., Journal of The Electrochemical Society, 164(13), C717.
[3] Matsuo et al., Journal of Nuclear Science and Technology, 34 (1997), 823-828.
[4] Matsuo et al., Journal of nuclear science and technology, 32 (1995), 912-920.
[5] Williams et al., The Journal of Physical Chemistry B, 110 (2006), 10619-10629.

Global and Local Characterization of Chrome alloying for reinforced concrete steels via electrochemical testing

Reece Goldsberry[1], Deeparekha Narayanan[1], Ayush Raj[1], Homero Castaneda[1]

[1]Department of Materials Science and Engineering
National Corrosion and Materials Reliability Laboratory
Texas A&M University
College Station, TX 77843, USA

Abstract

This study focuses on the effect of chrome content as an alloying element on the corrosion resistance of reinforcing steel. Three systems were designed and tested with time to characterize and quantify the corrosion performance of the rebar. One system included a simulated pore solution to imitate the chemistry of the environment. The second system covered reinforced mortar samples subjected to continuous exposure with a NaCl solution. The third system comprises reinforced concrete samples exposed to NaCl solution. The steel was monitored for the occurrence of corrosion through the use of electrochemical testing. To further test the effect of chrome content on the corrosion of the reinforcing steels, different chrome content was used for the rebars, and real-time monitoring was performed for general corrosion. Localized electrochemical techniques were used to correlate the effect of chrome additions on corrosion resistance. Both scanning and frequency sweep modes of localized electrochemical impedance spectroscopy (LEIS) were used to compare the passive film formed on the various rebar in alkaline environments. Passive layers were formed on the surface after exposure to a simulated pore solution to allow a passive layer to form similar composition to what would form in a concrete/mortar system. LEIS testing was performed in an alkaline environment with and without chloride addition for passive layer characterization.

Keywords: Chrome rebar, pore solution simulation, corrosion monitoring, LEIS.

Introduction

Corrosion of the reinforcing steel in reinforced concrete (RC) structures can lead to severe reductions in load-bearing capabilities and overall safety. The corrosion process occurs once the concentration of aggressive species has reached a critical value at the rebar interface [1] or there is a change in the local pH due to the carbonation front [2]. Both conditions would cause the passive layer to break down, favoring the kinetics of the corrosion process. The initiation time of the corrosion process is influenced by the surrounding environment and concrete properties. Once the corrosion process starts, the buildup of corrosion products can lead to large expansive forces that can cause cracking of the concrete cover [3]. Once the concrete cover has cracked, it opens a direct path from the surrounding environment to the reinforcing steel, increasing the corrosion rate as well as severely damaging the mechanical properties of the concrete structure. The corrosion of RC structures is a critical topic due to the importance of maintaining the safety and sustainability of current and future infrastructure. Some of the most common methods to increase the life of reinforced structure are proper building practices, admixed or surface applied corrosion inhibitors, cathodic protection systems, coating technologies used to the concrete surface or rebar, and corrosion-resistant reinforcing material.

A standard method or action for long-term protection of new RC structures is to change the reinforcing metal from a low alloy steel to a more corrosion-resistant alloy (CRA). There are several number of materials and alloys that can be used as a RC rebar, such as galvanized steel, stainless steel, and chromium containing low alloy steel [3-6]. The use of a CRA rather than the typical low carbon steel is hindered by the higher initial costs, which is normally 4 – 8 times higher [7-9]. Even with the higher initial cost the use of CRA as reinforcing materials can lead to a decrease in the overall lifetime cost by reducing the need for corrosion inhibitors, surface coatings, and costly repairs. To lower the initial cost the use of steels with lower amount of certain alloy elements but still proving higher corrosion resistance compared to low alloy steels can be used. It has been shown that the addition of chromium even at lower concentrations has a beneficial impact on the corrosion resistance of low alloy steel [10, 11].

This work compares the corrosion resistance of two chrome containing steels to a commonly used reinforcing low alloy steel (ASTM A615). The overall performance of the chrome containing rebar tested with time to in three systems to characterize and quantify the corrosion performance of the rebar. The corrosion response of the bars was characterized via global electrochemical methods such as circuit potential and electrochemical impedance spectroscopy. The local conditions were also characterized LEIS.

Experimental Procedure

Materials

For this study three alloys were chosen: control rebar was common ASTM A615 [12] and a steel alloy with a minimum of ASTM1035 (9% Crome). The chemical composition of the used rebars is shown in Table 1. Rebar used in this study were #4 rebar with a nominal diameter of 0.5” and 6” in length.

Table 1: Rebar Chemical Composition

Rebar	C	Cr	Ni	Mo	Mn	P	S	Si	Cu	V	Sn	Al	N	Fe
ASTM A615	0.42	0.23	0.12	0.033	1.00	0.012	0.025	0.19	0.34	-	0.01	0.002	0.0045	Ba
ASTM1035 (9% Cr)	0.11	9.46	0.09	0.02	0.63	0.010	0.005	0.37	0.16	0.019	0.008	-	-	Ba

Electrochemical Test Methods

The tested rebar was subjected to continuous immersion for 35 weeks with real time electrochemical monitoring. For mortar and reinforced concrete samples, the used solution was a 3.5 wt% NaCl solution, which has been used to simulate marine conditions. Open circuit potential (OCP), linear polarization resistance (LPR), and electrochemical impedance spectroscopy (EIS) tests were selected to monitor the samples. All electrochemical testing were performed with a three-electrode set up with an Ag/AgCl electrode as the reference electrode, Pt/Nb mesh as the counter electrode, and the rebar material as the working electrode. The OCP was measured until stable values were reached before EIS measurements. EIS measurements were performed at OCP, with a 10 mV_{PP} sinusoidal signal and frequency range of 100kHz to 0.01Hz. The LPR was measured by varying the applied potential from -20 mV vs OCP to +20 mV vs OCP with a scan rate 0.1667 mV/s.

Simulated Pore Solution Testing

A simulated pore solution (SPS) was used to create a simplified testing environment for the reinforcing steel. Chemical composition of the SPS was as follows: 0.08M KOH, 0.02M NaOH, and 0.001 M $Ca(OH)_2$ with a measured pH around 13. Testing configuration is shown in Figure 1. To prepare the rebar samples for testing in the SPS solution the rebar was cut to a length of 7.5 cm. After cutting a wire was attached to one end of the sample to allow for electrical connection during testing. Epoxy was applied up to 1.25 cm from each end giving am exposed length of 5cm giving a total exposed area of 19.95 cm^2. Before testing the surface of the ASTM A615 and 9% Cr rebar were precleaned to avoid any corrosion products from the surface.

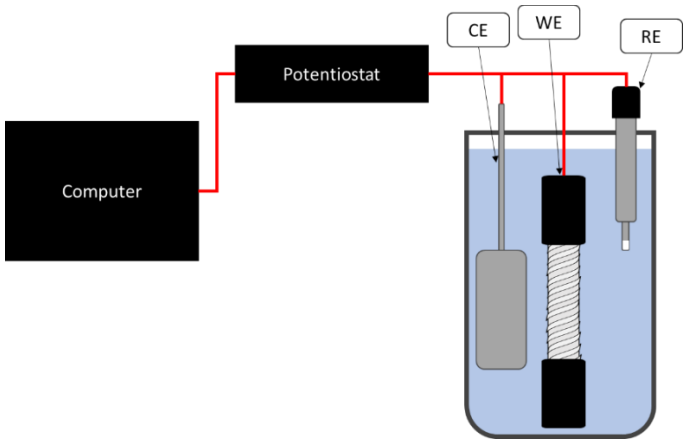

Figure 1: SPS testing set up

Reinforced Mortar and Concrete Testing

Rebar samples used for reinforced mortar and concrete testing were used in the as-received length of 15.24 cm. A wire was attached to one end of the sample to allow for electrical connection during testing. Epoxy was applied up to 5 cm from each end to isolate the rebar

from the testing environment. The exposed length of 5 cm giving a total exposed area of 19.95 cm^2. Before making the reinforced samples the rebars were sand blasted to clean any initial corrosion products from the surface. Reinforced mortar samples were composed of ordinary Portland cement (OPC), ASTM silicate sand, and tap water. The ratios for the mixture were as follows: water to cement ratio of 0.53 and cement to sand ratio of 0.33. The dimensions of the molds used for reinforced mortar samples were 10.16 cm x 10.16 cm x 5.59 cm with a cover depth of 1.52 cm. The reinforced mortar samples are shown in Figure 2. The reinforced concrete samples were made with OPC, ASTM silicate sand, and pea gravel aggregate. Concrete samples with a cement to sand ration of 1:1.5 were used with a water to cement ratio of 0.53 and cement to aggregate ratio of 1:2. The aggregates used were equal mixtures of 1.59 cm and 0.95 cm pea gravel. The samples were molded in self-manufactured molds with dimension of 20.32 cm x 10.16 cm x 5.08 cm with a rebar depth of 2.54 cm. Figure 3 shows the reinforced concrete samples. A higher water to cement ratio was selected to allow a quicker ingress of aggressive species to the rebar surface. The samples were cured for 7 days in a sealed bag. After curing the sample were demolded and a ponding dam was attached to the top surface of the sample as illustrated in Figure 3. All surfaces of the reinforced mortar samples were covered in epoxy to limit the oxygen intrusion in a confined area.

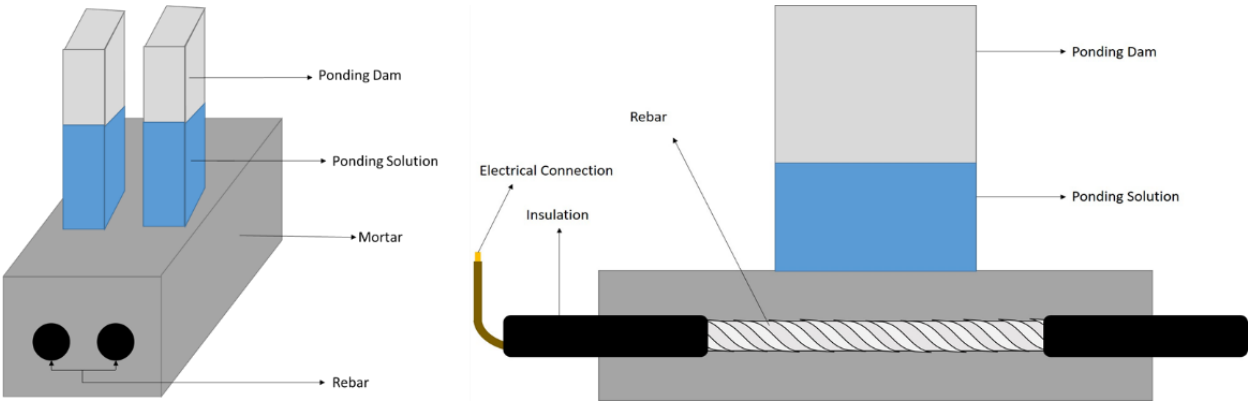

Figure 2: Reinforced mortar testing set up

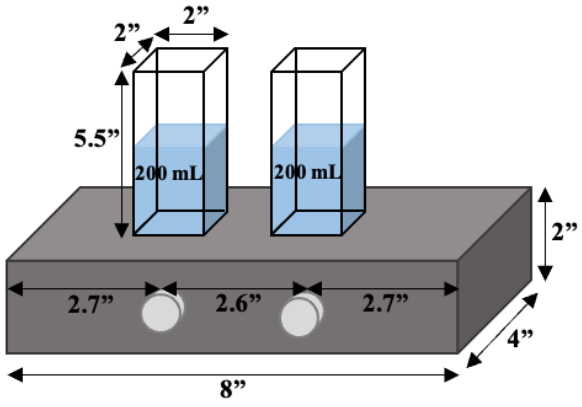

Figure 3: Reinforced Concrete Testing samples

Localized Electrochemical Impedance Spectroscopy (LEIS)

The corrosion resistance of the 9% chrome rebar was further studied using LEIS techniques to monitor the surface of the rebar during exposure to a chloride containing solution. LEIS measurements were taken on the cross section of the rebar. To prepare LEIS test samples

thin slices of the rebar were mounted in epoxy and then ground and polished to a 1µm finish. After the surface was masked to limit the total testing area to 3 mm by 3 mm area. LEIS was measured under open circuit conditions with a saturated calomel electrode as the reference electrode, graphite rod as the counter electrode, and mounted steel samples as the working electrode. Figure 4 shows the overview of the LEIS testing set up.

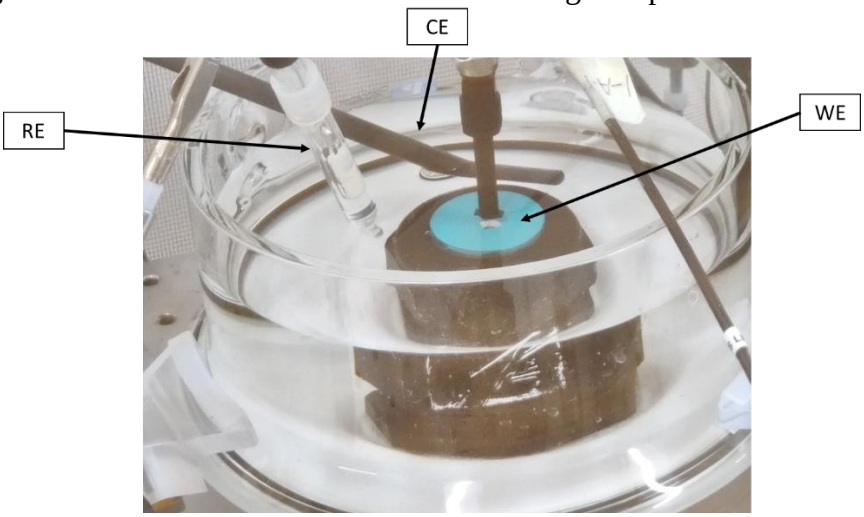

Figure 4: Overview of LEIS Testing

Before testing the tip of the probe was moved to roughly 100 µm above the exposed rebar. LEIS measurements were taken at a single frequency of 10 Hz with a scan area was 0.75 mm by 1 mm with a step size of 25 µm. Samples were monitored for 24 hours with measurements at the 0-, 4-, 8-, and 24-hour immersion times. Testing was performed under two conditions with and without passivation. LEIS testing performed in 0.01M NaCl with neutral pH. Testing with out passivation was to directly measure the effect of chrome on the corrosion resistance on the steels. For the passivated samples, they were immersed in SPS solution for 2 weeks to allow a stable passive layer to form on the samples. After two weeks the samples were rinsed with DI water and dried with nitrogen and then immersed in the LEIS testing solution. This was done to mimic the initiation of the corrosion process that occurs in RC structure once the local pH drops to lower values and a buildup of chlorides at the surface of the rebar.

Results and Discussion

SPS

Figure 5 shows the Nyquist, bode, and phase angle measurements from the SPS testing for ASTM A615 and 9Cr% samples. During immersion the 9Cr% chrome samples displayed more of a passive response compared to ASTM A615 samples. The Nyquist plots shown 9% chrome samples had higher impedance magnitudes with capacitor like behaviour. For ASTM A615 samples there is quick activation at the surface showing the chloride concentration being beyond the threshold magnitude for passivation breakdown. The 9% samples did show activation around 3 weeks of immersion but around week 15 it showed an increase in corrosion resistance that continued to increase until week 33. The measured OCP values were around -500 mV vs SCE and -600 mV vs SCE for 9% chrome and ASTM A615 rebar respectively.

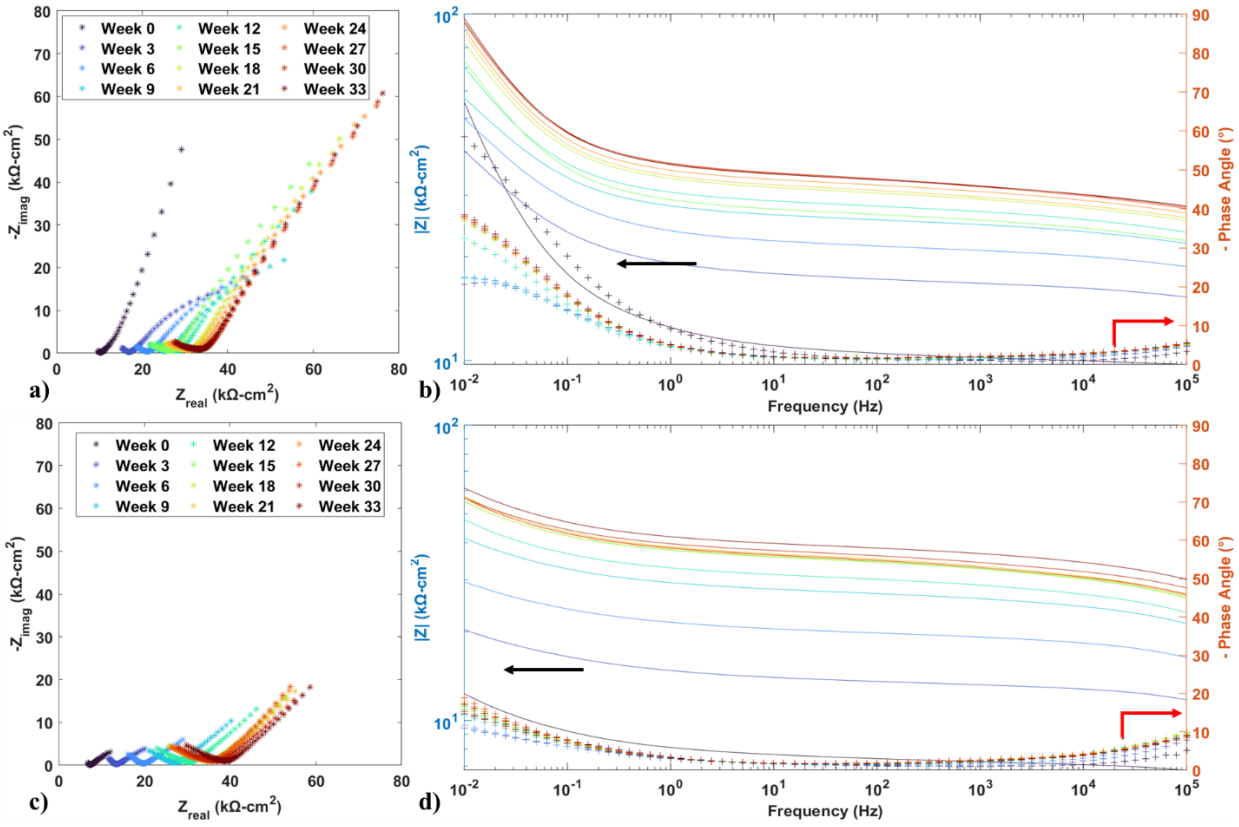

Figure 5: a) Nyquist and b) Bode-phase angle plots for 9% chrome samples and c) Nyquist and d) Bode-phase angle plots for ASTM A615 samples in SPS

Mortar

Comparison of the EIS results for the ASTM A615 and 9% chrome reinforced mortar samples is shown in Figure 6. It can be seen that the 9% samples shown a mass control process in the Nyquist diagram during the immersion time. This latter can be attributed to passive layer interface in which the mass transfer is the dominant mechanism. ASTM A615 samples displayed much lower corrosion resistance compared to 9% since they showed active corrosion behaviour through out the testing duration. The open circuit potential values of the of the 9% rebar was around -150 mV vs SCE while the control samples were around -250 mV vs SCE.

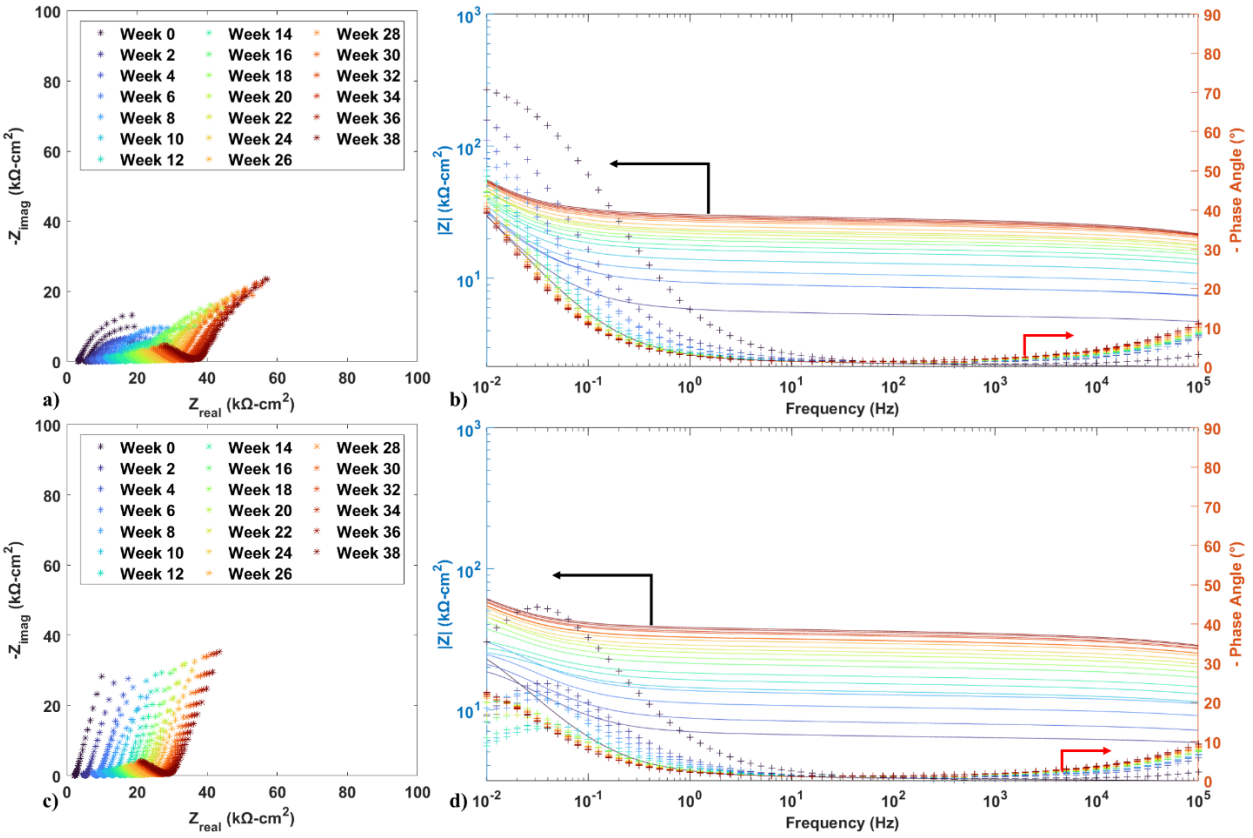

Figure 6: a) Nyquist and b) bode-phase angle plots for 9% chrome samples and c) Nyquist and d) bode-phase angle plots for ASTM A615 samples in 3.5%NaCl

RC

Figure 7 shows the measured Nyquist and bode-phase angle plots from reinforced concrete testing. 9% rebar showed a large amount of variability during exposed solution. The total impedance increases during 15 weeks of exposure and then decreased with time. ASTM A615 samples showed smaller impedance values for the duration of testing compared to 9 Cr% samples. The measured impedance dropped after the initial data point but held relatively constant for the rest of the testing period. In RC systems the probability of the occurrence of corrosion occurring based off of corrosion potential measurements can be estimated using ASTM C876: Standard Test Method for Corrosion Potentials of Uncoated Reinforcing Steel in Concrete [13]. Potentials over -124 mV vs SCE are >90% probability that no corrosion is occurring, potentials between -124 mV and -274 mV vs SCE corrosion activity is uncertain, and below -274 mV vs SCE there is a >90% probability that corrosion is occurring [13]. The OCP values of the 9% samples started around -425 mV vs SCE but became more positive during immersion to around -125 mV vs SCE after 18 weeks of immersion. ASTM A615 rebar followed a similar trend with a starting OCP around -475 mV vs SCE and rising to -160 mV vs SCE after around 18 weeks. From the potential measurements both the ASMT A615 and 9% Cr rebar started initially very low potential measurements meaning there was a high probability that corrosion on the reinforcing steel initially but the steel became less active over time as the passive layer was formed due to the surrounding environment.

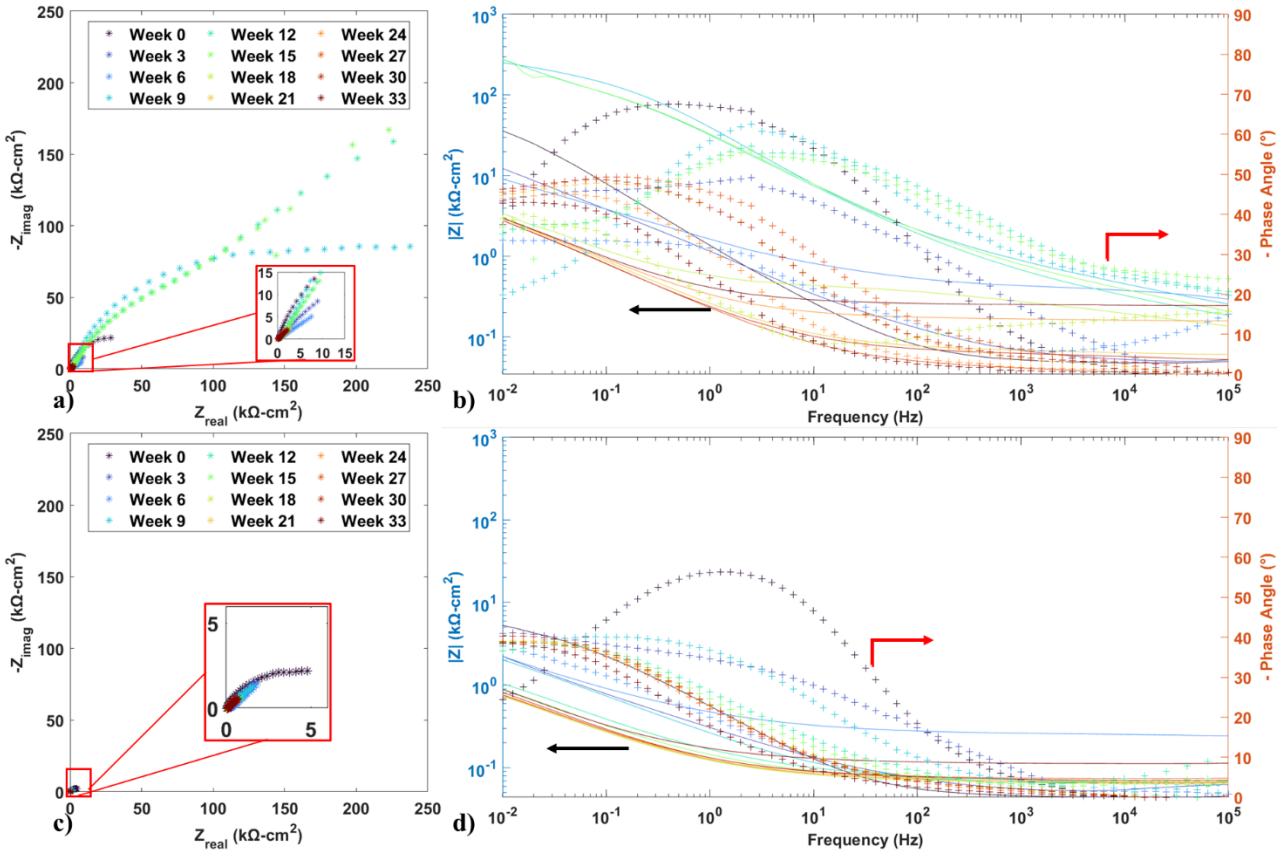

Figure 7: a) Nyquist and b) bode-phase angle plots for 9% chrome samples and c) Nyquist and d) bode-phase angle plots for control samples in 3.5wt % NaCl.

LEIS

Figure 8 displays the LEIS measurements of the non-passivated 9% rebar at various immersion times. There was no major change in the measured impedance values during immersion.

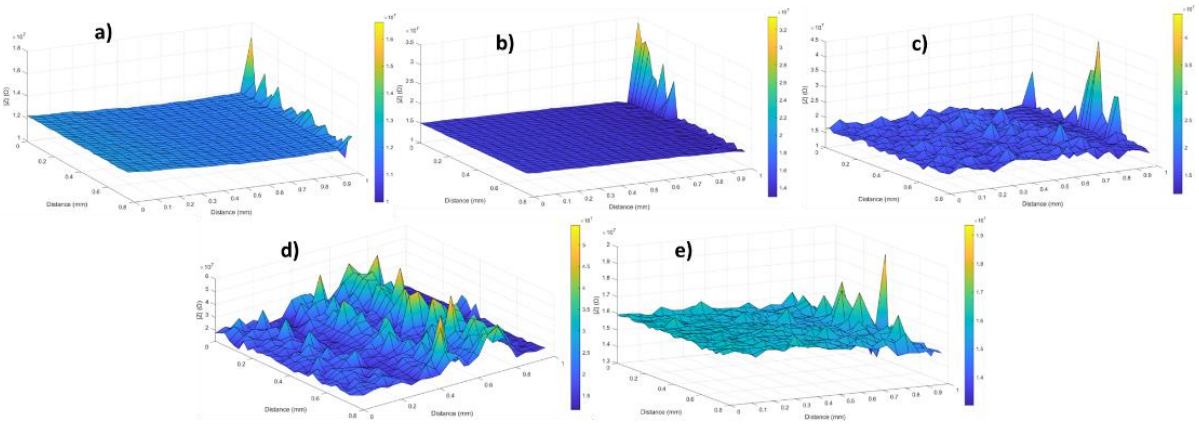

Figure 8: LEIS of 9% Cr samples without passivation at a) initial, b) 4 hours, c) 8 hours, d)12 hours, and e) 24 hours of immersion

LEIS measurements with time of the passivated 9% rebar are shown in Figure 9. Similar to the non-passivated samples there were no major changes in the measured impedance. After 24 hours of testing in the 0.01 M NaCl solution there were no visible signs of corrosion for either

9% samples. Showing that the formed passive film on the 9% rebar can provide protection when the surface is exposed to aggressive species possibly extending the time to initiation of corrosion of the reinforcing steel.

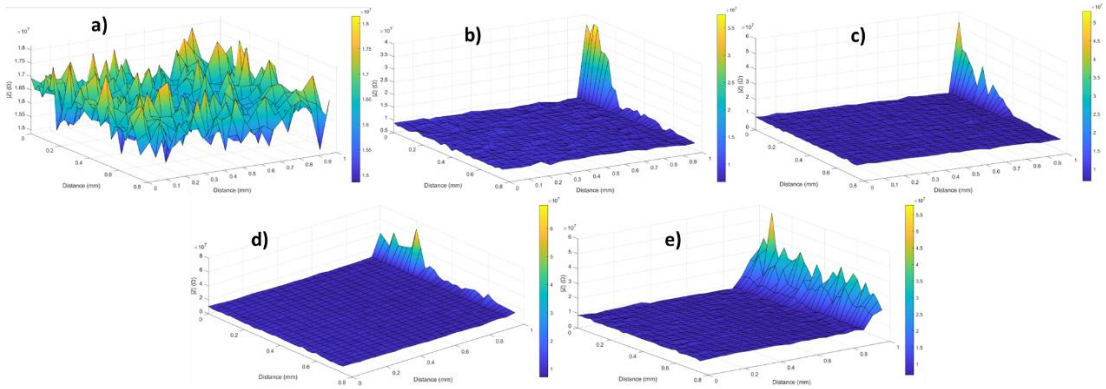

Figure 9: LEIS of 9% Cr samples with passivation at a) initial, b) 4 hours, c) 8 hours, d)12 hours, and e) 24 hours of immersion

Figure 10 shows the LEIS measurements of the ASTM A615 samples with out passivation. Corrosion products quickly formed on the surface of the material during testing after 8 hours of immersion as compared to 9% Cr samples which did not have any corrosion products on the surface after 24 hours of immersion.

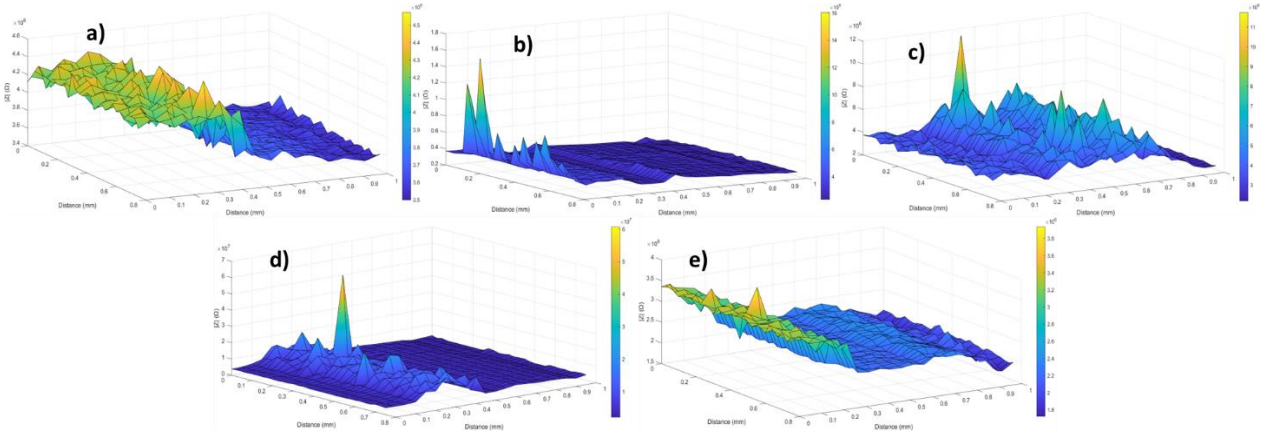

Figure 10: LEIS of ASTM A615 Samples with out passivation at a) initial, b) 4hours, c) 8 hours, d)12 hours, and e) 24 hours of immersion

From the LEIS testing it shows that the 9%Cr rebar showed an increase in the general corrosion resistance compared to ASTM A615 rebar. From the testing of the 9%Cr both with and without passivation it showed that the even in the event that aggressive species reached the surface of the rebar during use the increase corrosion of the 9%Cr rebar would still provide some protection possibly delaying the initiation time of the corrosion process.

Conclusion

From testing in all 3 systems the 9% chrome rebar showed a better corrosion performance compared to the control rebar. In SPS testing the 9% chrome samples varying degrees of active/passive response based on the impedance data while ASTM A615 samples were active for the duration of testing. 9% rebar samples stayed mostly passive for the duration of testing while control samples showed a depression in the higher frequency loops

of the Nyquist plots. Reinforced concrete samples showed higher amount of variability compared to the other two systems. Even with the higher variability it showed that the addition of chrome in the reinforcing provides better protection compared to the ASTM A615 rebar. 9% rebar in concrete displayed active-passive in the beginning of immersion but eventually showed activation with increasing immersion time, while control samples showed activation quickly and did not change during immersion. From the LEIS testing of the 9% rebar it showed that the alloy displayed corrosion resistance in both passivated/non-passivated cases. Interestingly the immersion of the 9% rebar in the neutral chloride containing environment did not induce corrosion as would be expected for the control rebar.

Acknowledgments

The authors would like to acknowledge CMC company for the samples provided.

References

1. Angst, U., et al., *Critical chloride content in reinforced concrete—A review.* Cement and concrete research, 2009. **39**(12): p. 1122-1138.
2. Steffens, A., D. Dinkler, and H. Ahrens, *Modeling carbonation for corrosion risk prediction of concrete structures.* Cement and Concrete Research, 2002. **32**(6): p. 935-941.
3. Böhni, H., *Corrosion in reinforced concrete structures*. 2005: Elsevier.
4. Kahl, S., *Corrosion resistant alloy steel (MMFX) reinforcing bar in bridge decks*. 2007, Michigan. Dept. of Transportation.
5. Shi, J., et al., *Influence of chloride concentration and pre-passivation on the pitting corrosion resistance of low-alloy reinforcing steel in simulated concrete pore solution.* Construction and building materials, 2016. **111**: p. 805-813.
6. Yeomans, S., *Performance of black, galvanized, and epoxy-coated reinforcing steels in chloride-contaminated concrete.* Corrosion, 1994. **50**(01).
7. Castro, H., et al., *Mechanical properties and corrosion behaviour of stainless steel reinforcing bars.* Journal of materials processing technology, 2003. **143**: p. 134-137.
8. Magee, J.H. and R.E. Schnell, *Stainless steel rebar.* Advanced materials & processes, 2002. **160**(10): p. 43-46.
9. McGurn, J. *Stainless steel reinforcing bars in concrete*. in *Proceedings of the International Conference of Corrosion and Rehabilitation of Reinforced Concrete Structures, Orlando, FL, FHWA*. 1998. Citeseer.
10. Carvalho, D., C. Joia, and O. Mattos, *Corrosion rate of iron and iron–chromium alloys in CO2 medium.* Corrosion Science, 2005. **47**(12): p. 2974-2986.
11. Dobbelaar, J., E. Herman, and J. De Wit, *The corrosion behaviour of iron-chromium alloys in 0.5 M sulphuric acid.* Corrosion science, 1992. **33**(5): p. 765-778.
12. International, A., *A615/A615M-20 Standard Specification for Deformed and Plain Carbon-Steel Bars for Concrete Reinforcement*. 2020, ASTM International.
13. International, A., *Standard Test Method for Corrosion Potentials of Uncoated Reinforcing Steel in Concrete*. 2015, ASTM International: 100 Barr Harbor Drive, PO Box C700, West Conshohocken, PA 19428.

Formation and Growth of Calcium Hydroxy Zincate on Zinc in Saturated $Ca(OH)_2$ Solution

Kotaro Doi and Sachiko Hiromoto

Research Center for Structural Materials, National Institute for Materials Science
1-2-1 Sengen, Tsukuba, Ibaraki, 305-0047 Japan

Introduction

The galvanized reinforcing steel shows high corrosion resistance in concrete because the calcium hydroxy zincate ($Ca(Zn(OH)_3)_2 \cdot 2H_2O$, CHZ) forms on the zinc plating. It is difficult to demonstrate the CHZ formation and growth in the laboratory because CHZ formation in concrete takes a long time. Recently, we developed an accelerated formation method for CHZ by increasing the dissolved oxygen (DO) concentration in the solution and enhancing the oxygen reduction reaction on zinc[1]. This study discussed the relationship between the density of the CHZ layer and the corrosion resistance of zinc using this method.

Materials and Methods

The samples were pure zinc plates (99.2%) of 15 mm×50 mm×1 mm. After polishing, the samples were immersed in the saturated $Ca(OH)_2$ solution, and the DO concentration of the solution was controlled by supplying the 0.02 (ambient air), 0.1, and 0.5 MPa oxygen gas to the solution to enhance the formation and growth of CHZ on the sample. The test period was 1, 3, and 7 days. After the CHZ formation, cyclic corrosion tests (CCT) were performed to investigate the corrosion resistance of zinc samples covered with CHZ.

Results and Discussion

The formation and growth of CHZ on the sample were accelerated by increasing the DO concentration of the saturated $Ca(OH)_2$ solution. This is because the oxygen reduction reaction, the rate-determined step of the CHZ formation, was enhanced with increasing in the DO concentration of the solution. The shape of CHZ changed from point-like to low dense layer and dense layer with increasing in the DO concentration of the solution and the immersion period. The denser the CHZ layer covering the samples, the higher the corrosion resistance the samples showed.

1) K. Doi and S. Hiromoto, *Zairyo-to-Kankyo*, 71(1), 21-29 (2022).

A Study on the performance of surface coating materials on concrete based on exposure tests under marine atmosphere environment for 30 years

Toru Yamaji[1], Jun Tomiyama[2], Satohiko Ishigaki [3]

[1] Port and Airport Research Institute, Japan, yamaji-t@p.mpat.go.jp
[2] University of the Ryukyus, Japan, jun-t@tec.u-ryukyu.ac.jp
[3] Naha Port and Airport Construction Office, Japan, satohiko.ishigaki.v5y@ogb.cao.go.jp

Abstract

In concrete structures located in marine environments, surface coatings are sometimes applied to the concrete surface to prevent the intrusion of chloride ions, which can cause corrosion of steel bars. The expected service life of these surface coatings is relatively short, around 10 to 20 years in the case of concrete. On the other hand, there are cases where the performance is maintained for longer than 20 years. Accumulation of such long-term application cases will increase the reliability of surface coating materials and make them easier to apply.
In this paper, five concrete specimens with surface coatings were exposed to the marine atmosphere environment for 30 years, and the performance of the coatings and the deterioration of the concrete were investigated in order to evaluate the performance of the coatings after a long period of time in the marine environment.

A concrete test specimen (15×15×80 cm) was placed on a trestle installed on the side of the bridge pier under the girder of the Naminoue Bridge in Naha Harbor. The trestle is located about 6 to 7 m above the sea surface and is subjected to a large amount of salt airborne.
The concrete mix was 37% water-cement ratio, and five types of surface coating materials were applied after the concrete was placed and demolded. Table 1 lists the coating specifications. Uncoated specimens were also prepared for comparison. After 30 years, the adhesion strength, salt barrier properties of the coating (measured using a coating cut from the specimen), and chloride ion content in the concrete were measured.

After 30 years of exposure of concrete specimens with five different surface coatings to the marine atmosphere environment, the performance of the coatings and the deterioration of the concrete were investigated and the following findings were obtained.
i) The deterioration status of the surface coating materials differed according to their specifications. Some showed almost no deterioration, while others had deteriorated top coatings .
ii) All of the surface coatings prevented chloride ions from entering the concrete for 30 years , and high protection performance had been ensured. In addition, the salt barrier performance of the coatings remained high even after 30 years.

In conclusion, it was confirmed that appropriate surface coating of concrete in the initial stage, when chloride ions have not penetrated, is very effective as a countermeasure against chloride attack. It was also confirmed that, under the conditions (coating material specifications, construction conditions, exposure environment, etc.) in this study, the performance was maintained for a long period of 30 years.

Keywords

Marine environment, concrete, surface coating, chloride ion, salt barrier property

Introduction

In concrete structures located in marine environments, surface coatings are sometimes applied to the concrete surface to prevent the intrusion of chloride ions, which can cause corrosion of steel bars. The expected service life of these surface coatings is relatively short, around 10 to 20 years in the case of concrete. On the other hand, there are cases where the performance is maintained for longer than 20 years. Accumulation of such long-term application cases will increase the reliability of surface coating materials and make them easier to apply.

The Tomari Bridge and the Naminoue Bridge, PC bridges constructed on the Naha Port Harbor Road between 1980 and 1982, were located in a severe salt-affected environment at sea, where they were constantly affected by wave spray and sea breezes. Despite these conditions, these bridges were designed with a very small concrete cover of 35 mm because they were designed before the revision of the "Standard and Commentaries for Protecting Highway Bridge from Chloride Attack [1]". Under these conditions, it was difficult to ensure long-term durability even if the concrete was of high quality, so it was decided to apply a surface coating to the concrete as a measure against salt damage. However, at the time, there were no clear criteria for selecting the surface coating, so exposure tests were started on specimens with five different surface coatings on the concrete surface in order to collect basic data for the selection [2].

In this paper, five concrete specimens with surface coating were exposed to marine atmospheric environment for 30 years and the various performances (adhesion strength, salt barrier property, etc.) were evaluated.

Outline of this test

Specimen

The concrete mix is shown in **Table 1**. This is the same value as that of the concrete used for the Naminoue bridge mentioned above. The cement used was ordinary Portland cement, fine aggregate was river sand from Taiwan

Table 1 Mixture proportion of concrete

W/C	s/a (%)	Unit weight (kg/m^3)			
		W	C	S	G
0.37	36.4	178	481	609	1080

Table 2 Specification of surface coating materials

No.	Process	Coating materials	Standard coverage (kg/m^2)	Note
1	Primer	Silane	0.30	Now available. Top coating was changed for enhancing in weathering resistance.
	Intermediate	Acryl polymer cement	2.00	
	Top	Chlorinated poly-olefine resin	0.20	
	〃	Silicon emulsion	1.00	
	〃	Silicon resin	0.15	
2	Primer	Epoxy resin	0.10	Now available. Putty was changed for enhancing in workability.
	Putty	〃	0.60	
	Intermediate	Elastic epoxy resin	0.35	
	Top	Elastic poly-urethane resin	0.12	
3	Putty	Polymer cement	1.50	Now available. Top coating was changed for enhancing in adhesion.
	Primer	Epoxy resin	0.30	
	Intermediate	Acryl rubber	2.00	
	Top	Acryl Urethane resin	0.34	
4	Putty	Rubber latex resin modified cement paste	3.75	Now available.
	Intermediate	Denatured epoxy resin	0.12	
	Intermediate	Chloroprene rubber	0.75	
	Top	Chlorosulfonie polyethylene	0.50	
5	Primer	Epoxy resin	0.10	Now not available.
	Putty	〃	0.30	
	Intermediate	Vinyl ester resin with glassflake	1.10	
	Top	Acryl Urethane resin	0.12	
0	-	Without coating	-	For comparison

(density: 2.66 g/cm^3, water absorption: 1.17%), coarse aggregate was crushed stone from the Sako River (density: 2.76 g/cm3, water absorption: 1.06%), and tap water was used. After casting, the specimens were demolded in 1 day, wet cured until 3 days, and then cured in the air in a room until 28 days. The outside dimensions were 150 x 150 x 800 mm, and two steel bars (φ13 mm round steel) were embedded inside the specimen, each with a cover of 20 mm (see **Figure 2**).

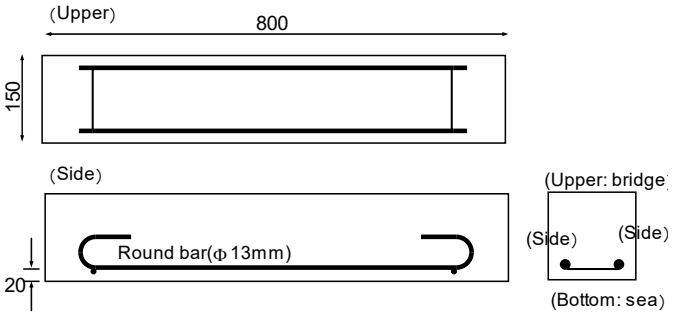

Figure 2 Scheme of specimen (unit :mm)

After the above curing, the surface coating was applied to the surface. The list of coating materials is shown in **Table 2** [2]. Uncoated specimens were also prepared as a comparison. The coating was applied at a humidity of less than 70% and a temperature of 15 to 25°C.

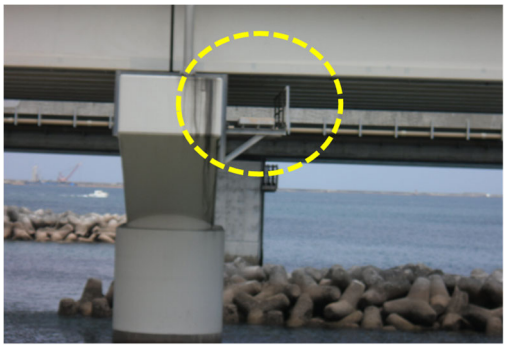

Photo 1 Exposure test site (Naminoue brige, Okinawa, Japan)

Exposure environment

The test specimen was placed on a trestle built on the side of the P4 pier, which is located under the girder of the Naminoue bridge. The general situation of the specimen exposure position is shown in **Photo 1**. The abutment is located about 6 to 7 m above the sea level and is subjected to a severe salt-affected environment where airborne salt adheres to the abutment. On the other hand, the bridge girders are located on the top, so they are not directly exposed to ultraviolet rays, which can degrade the cladding material.

Test methods

1) Visual observation

Deformities such as peeling, delamination, and cracking of the coating material were visually observed. For delamination, the percentage of the specimen's surface area was determined.

2) Adhesion strength

The adhesion strength was measured on the top surface of the specimen in accordance with JIS A 6920.

3) Elongation performance

As shown in **Figure 2**, a 120 x 40 x 10 mm specimen was cut from the top surface of the concrete specimen and pulled in the longitudinal direction to measure the elongation of the coating material.

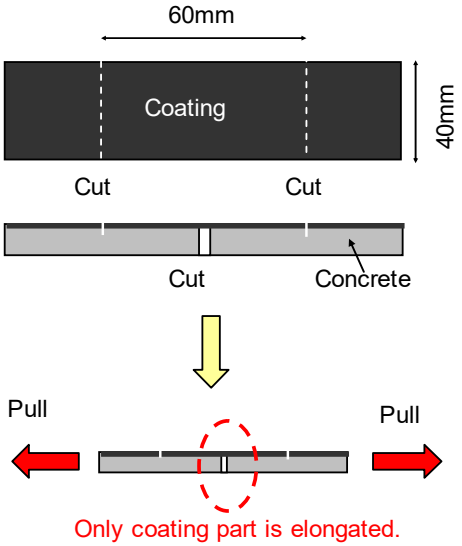

Figure 2 Test method for elongation performance

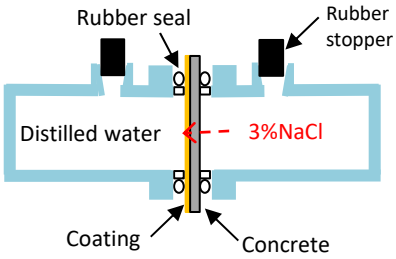

Figure 3 Test method for salt barrier performance [1][3]

4) Chloride ion content in the concrete
Samples were taken from three locations 0-10, 15-25, and 30-40 mm from the bottom of the concrete specimen, and the total chloride ion content was measured in accordance with JCI-SC4.
5) Salt barrier property of the coating material
The salt barrier property of the surface coating was evaluated in accordance with the method specified in the "Standard and Commentaries for Protecting Highway Bridge from Chloride Attack [1]". Concrete specimens (about 10 mm thick) with coating were cut out and placed with the concrete side of the specimen toward the 3% NaCl solution and the coating material side toward the distilled water, as shown in **Figure 3** [3]. After 30 days of installation, the amount of chloride ions that permeated through the specimens was measured. The initial values (see **Figure 8**) were obtained using only the coating.
6) Corrosion of steel bar
After the steel bar was removed, the corroded area was measured by tracing it onto a transparent film.

Test Results

Observation of appearance

The external appearance of the specimens is shown in **Photo 2**, and the change over time of the peeling area (area ratio) is shown in **Figure 4**. Specimen 1 was completely chalked. Specimens 2 and 3 showed only some peeling (slightly extended from 15 years). Specimen 4 showed some

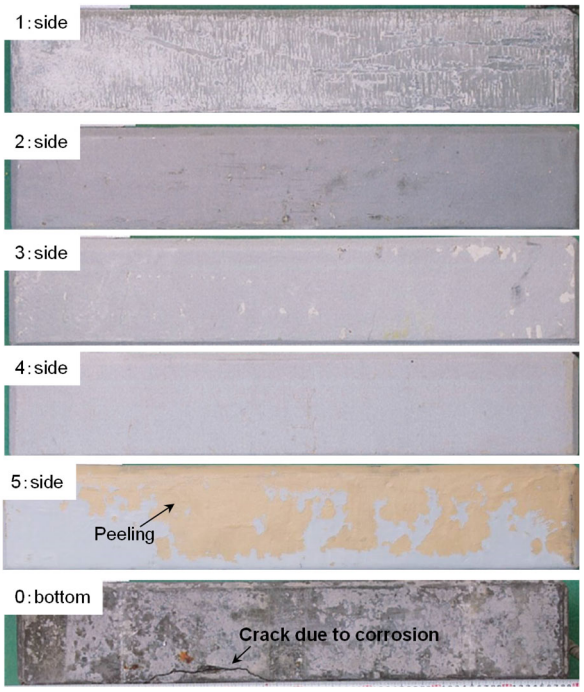

Photo 2 Appearance of specimens

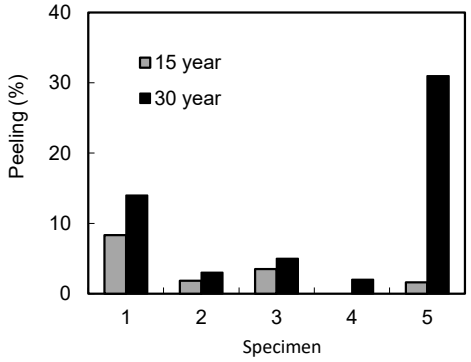

Figure 4 Change in peeling area over exposure period

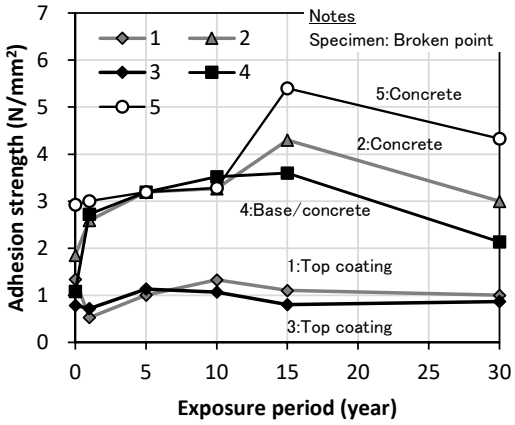

Figure 5 Change in adhesion strength over exposure period (Note : broken point)

peeling at the edges. Specimen 5 showed significant peeling. Specimen 0 showed cracking due to corrosion.

Adhesion strength

Figure 5 shows the relationship between exposure period and adhesion strength. The main broken points are shown in the figure. Although the values varied, they remained at least as high as the initial values. The correlation between the deterioration of the top coating and the adhesion strength was not clear.

Elongation performance

Figure 6 shows the elongation at break values for the elongation performance test. Specimen 3 had high elongation performance at 30 years. On the other hand, the elongation performance of specimen 4 decreased with exposure period.

Chloride ion content in the concrete

Figure 7 shows the profile of chloride ions in concrete. In the case of specimen 0, a large amount of chloride ions penetrated at the steel bar location (20 mm), indicating a highly corrosive environment for the steel bar. The surface chloride ion concentration C_0 and the apparent diffusion coefficient D_{ap} were calculated to be 11.2 kg/m^3 and 0.15 cm^2/year, respectively, by approximating the distribution in **Figure 7** with the solution of Fick's diffusion equation.

On the other hand, in the case of the concrete with surface coating, chloride ions have not penetrated into the concrete even after 30 years, indicating that the coating material has suppressed the penetration of chloride ion. It can be said that the chloride penetration was suppressed for 30 years in this environment (C_0 = 11.2 kg/m^3) of the present study.

Salt Barrier Property of Coating Material

Figure 8 shows the results of the salt barrier test. All of them satisfied the quality standard value (10^{-2} mg/cm^2/day) of the "Standard and Commentaries for Protecting

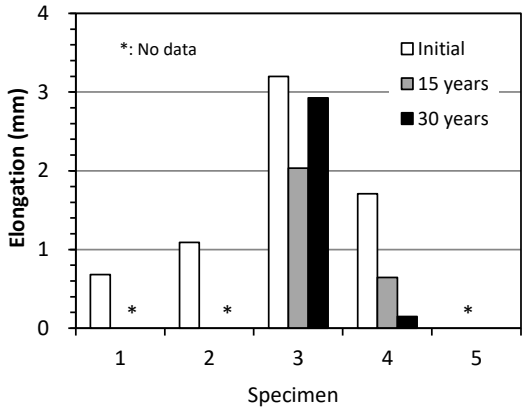

Figure 6 Elongation performance test results

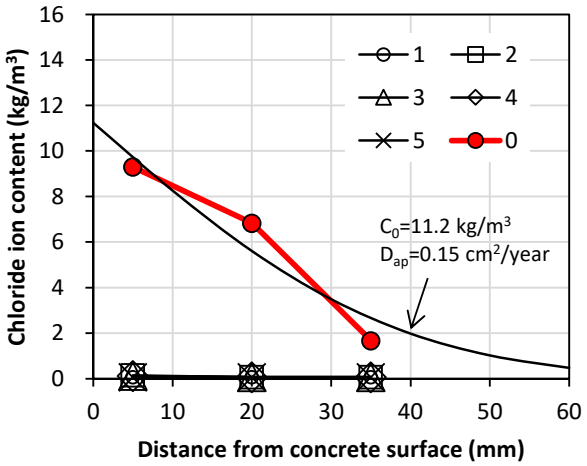

Figure 7 Chloride ion profiles in concrete after 30 years

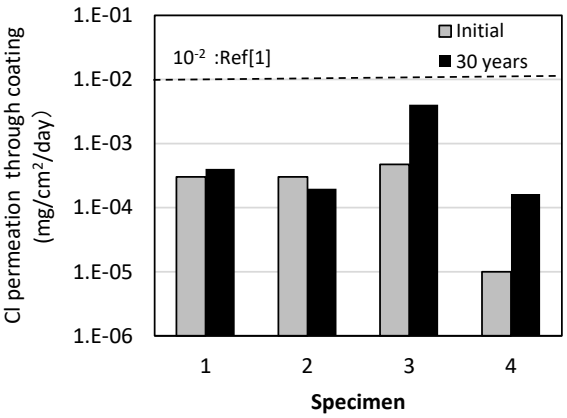

Figure 8 Salt barrier performance test results

Table 3 Corroded area of steel bars

(Unit : %)

	1	2	3	4	5	0
15year	0	0	0	0	0	14.9
30year	0	0	0	0	0	*

*crack due to corrosion

Highway Bridge from Chloride Attack [1]", indicating that high salt barrier performance was maintained even after 30 years.

Corrosion of steel bars

Table 3 shows the corrosion area percentages. All results are averages of two bars. Specimens 1 through 5 were not corroded at all due to the absence of chloride ion penetration. On the other hand, specimen 0 was corroded at 15 years due to the penetration of about 2.0 kg/m^3 of chloride ions at the steel bar locations. Here, 2.0 kg/m^3 is a chloride ion threshold value for corrosion in concrete used in standards related to the design and maintenance of Japan port facilities[4][5]. At 30 years later, the corrosion progressed further and cracks due to corrosion were observed.

Summary

After 30 years of exposure of concrete specimens with five different surface coatings to the marine atmosphere environment, the performance of the coatings and the deterioration of the concrete were investigated and the following findings were obtained.

i) The deterioration status of the surface coating materials differed according to their specifications. Some showed almost no deterioration, while others had deteriorated top coatings.

ii) All of the surface coatings prevented chloride ions from entering the concrete for 30 years , and high protection performance had been ensured. In addition, the salt barrier performance of the coatings remained high even after 30 years.

In conclusion, it was confirmed that appropriate surface coating of concrete in the initial stage, when chloride ions have not penetrated, is very effective as a countermeasure against chloride attack. It was also confirmed that, under the conditions (coating material specifications, construction conditions, exposure environment, etc.) in this study, the performance was maintained for a long period of 30 years.

Acknowledgments

This study was initiated by the Naha Port and Airport Development Office, Okinawa General Bureau, in cooperation with the University of the Ryukyus and the Port and Airport Research Institute, and summarizes the results of exposure tests conducted continuously. We would like to express our sincere appreciation to all parties involved.

References

1. Japan Road Association, Standard and Commentaries for Protecting Highway Bridge from Chloride Attack, 1984.2 (in Japanese).
2. T.Yamaji, K.Komure and H.Hamada: Durability of 15-year old concrete specimens with surface coating under marine environment, Report of the Port and Airport Research Institute, Vol.43, No.2, pp.73-109, 2004 (in Japanese).
3. I. Sasaki, I. Nishizaki, S. Moriya: Long-term durability of concrete surface coating materials in salt-affected environment, Proceedings of the Concrete Structures Scenarios, JSMS, Vol.10, pp.57-64, 2010 (in Japanese).
4. Port and Harbour Association of Japan, Technical Standards and Commentaries for Port and Harbour Facilities in Japan (English version), 2020.
5. Coastal Development Institute of Technology, Technical Manual for Maintenance and Repair of Port and Harbour Facilities (English version), 2022.

Lean duplex stainless steel: a solution to prevent corrosion for reinforced concrete exposed to severe chloride environments

Véronique Bouteiller [1)], Eric Chauveau [3)] Thierry Chaussadent [2)], L. Adelaïde [1)], Amandine Bonnet [1)], Philippe Mauger [3)] and Renaud-Pierre Martin [1)]

1) MAST-EMGCU, Univ Gustave Eiffel, IFSTTAR, F-77447 Marne-la-Vallée, France
2) MAST-CPDM, Univ Gustave Eiffel, IFSTTAR, F-77447 Marne-la-Vallée, France
3) Ugitech, CRU, avenue Paul Girod 73403 Ugine, France

The main objective of this work is to demonstrate that for severe chloride environments, lean duplex stainless steel can be an alternative to carbon steel as reinforcement in civil engineering structures. Although the initial cost of stainless steel is higher than carbon steel, the benefit will stand in a longer lifetime without degradation of the structure and therefore less or no maintenance.

In this eight years study, corrosion of reinforced concrete was investigated depending on rebar composition (carbon steel (Fe E235) and different stainless steel grades), and corrosive conditions: in the laboratory with accelerated tests, and on site in a tidal zone with realistic corrosion evolution.

In the first laboratory work, reinforced concrete prisms were cast with chloride ions in the mix (8%$_{weight}$ of cement) and were exposed to an aggressive environment (45°C and 92% relative humidity). The stainless steel grades considered were 1.4021, 1.4062, 1.4362 and 1.4462. The first one is a martensitic grade whereas the other three have a duplex microstructure containing both austenitic and ferritic phases in equivalent proportions.

In the second on site work, concrete beams reinforced with carbon steel or a 1.4362 lean duplex stainless steel were cast and exposed to a marine environment in a tidal zone in La Rochelle, France.

Visual inspections and electrochemical measurements such as half-cell potential, linear polarization resistance and impedance were used to investigate the corrosion behavior of the different reinforced samples (prisms and beams) versus time.

Results from the laboratory study based on measurements performed every 3 months showed that the first visual signs of corrosion degradation were observed on prisms with a carbon steel rebar after 6 months (rust and cracks) and on prisms with 1.4021 stainless steel after 33 months (rust). On the other hand, for duplex stainless steel no visual degradation appeared even after 90 months. These results were consistent with the corrosion rate values of 10, 1 and below 0.005 µA/cm² respectively for rebars of carbon steel, 1.4021 stainless steel and duplex stainless steels.

From the investigations conducted on the reinforced concrete beams on site, no visual sign of corrosion degradation was detected after 8,5 years. The electrochemical characterizations versus time showed different behavior based on potential values (-350 to -550mV/SCE for carbon steel and -100 to -200 mV/SCE for 1.4362 stainless steel) and on corrosion rates (corrosion current densities for duplex 1.4362 are one to two decades lower than for carbon steel).

Corrosion of different types of stainless steels after long-term exposure in real marine environment

Serdar, M., Zimprich, E., Bjegović, D./University of Zagreb, Faculty of Civil Engineering, Croatia

The use of certain types of stainless steel as a substitute for reinforcement in concrete is one of the methods that can significantly delay corrosion in reinforced concrete structures, even when high chloride concentrations are present in the environment. The use of high-alloy steels as reinforcement in concrete structures can hardly be justified economically, due to the high content of valuable alloying elements. For this reason, research is directed toward finding low-alloy steel grades that have higher corrosion resistance and satisfactory mechanical properties compared to carbon steel, and at a price that does not significantly increase initial construction costs.

The objective of this work was to analyze the corrosion behavior of different types of corrosion-resistant reinforcing steels in concrete subjected to long-term exposure in simulated and real marine environments. The behavior of a total of 6 types of reinforcing steel was analyzed in: 1) concrete exposed to a simulated marine environment for two years using a salt chamber, and 2) in concrete exposed to a real marine environment for 10 years as part of the test zone established under the Krk Bridge. The effect of alloy type on the long-term behaviour of steel in the marine environment was analysed. In addition, the effect of stainless steel reinforcement on the corrosion rate of carbon steel reinforcement when exposed to the marine environment in the same concrete element was studied.

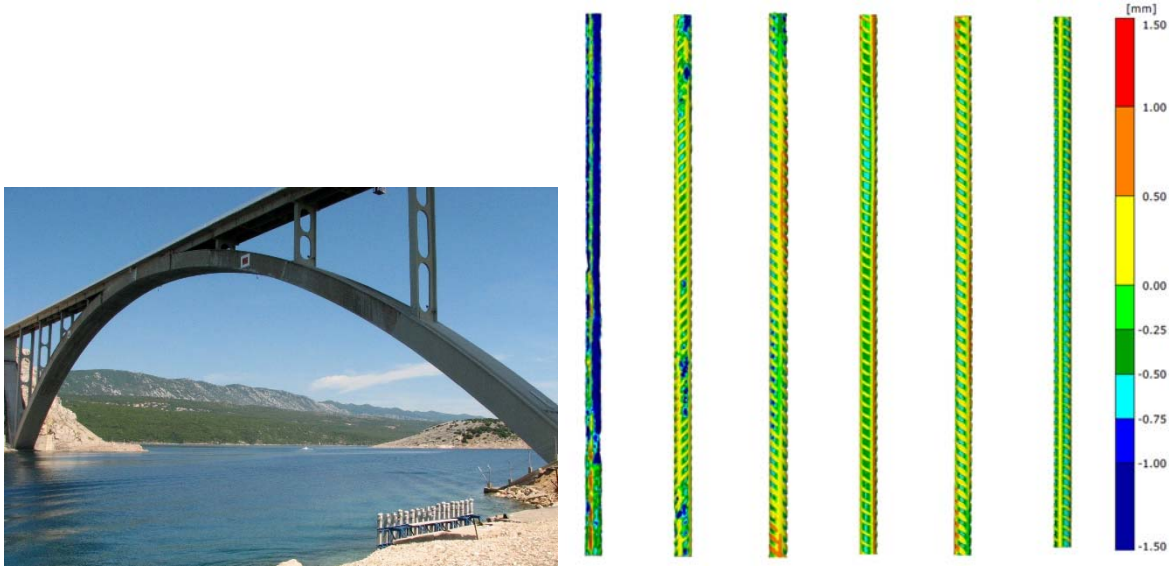

Figure 1 a) Exposure site under Krk Bridge, b) corrosion attack on different steel types

Long term performance of corrosion inhibitors in concrete

F. Bolzoni, A. Brenna, S. Beretta, M.V. Diamanti, M. Ormellese, MP. Pedeferri

Dipartimento di Chimica Materiali e Ingegneria Chimica "G. Natta", Politecnico di Milano, Via Mancinelli 7, 20131 Milano, Italia

Corrosion inhibitors may be used in case of aggressive environments, as a preventative technique (Admixed Corrosion Inhibitors), as well as a repair system (Migrating Corrosion Inhibitors). The performance of commercial inhibitors as well as the investigation on new organic and inorganic compounds have been studied in our research group for more than 20 years.

The results concerning different substances or mixtures or commercial inhibitors are briefly reviewed. Nitrite-based commercial inhibitors confirmed the literature: if properly dosed they delay the initiation of chlorides induced corrosion by increasing critical chloride threshold. Recently, nitrate-based inhibitors have been proposed: they are able to delay concrete carbonation but they have no effect on corrosion rate after initiation.

Organic commercial inhibitors, based on mixture of amines, alkanol-amines and carboxylates are able to delay chloride-induced corrosion, but only a small increase in the critical chloride threshold was detected. Among the organic substances, in concrete tests, only one amine and one amino acid were able to increase the critical chlorides threshold with respect to the reference condition.

Concerning migrating inhibitors (MCI), the results got in our experiments are not satisfactory: only a limited delay of corrosion initiation was noticed, mainly related to the reduction of chloride diffusion coefficient. After corrosion initiation, only in carbonated concrete corrosion rate was reduced, but the residual value of corrosion rate was not negligible.

The effect on service life was estimated in the case of admixed corrosion inhibitors used to prevent chloride induced corrosion. The evaluation was carried out by means of deterministic and simplified probabilistic methods, comparing the performance of corrosion inhibitors, with different effectiveness (i.e. critical chloride threshold) with other preventative methods.

Evaluation of corrosion protection of cementitious coating containing crystalline admixture

Suelen da Rocha Gomes[1]; Luis Sánchez[1], and Mercedes Sánchez Moreno[1]

[1] Department of Inorganic Chemistry and Chemical Engineering; Chemical Institute for Energy and Environment, IQUEMA. University of Córdoba (UCO), Córdoba, Spain

Abstract

Reinforcement corrosion is a well-known damage taking place in reinforced concrete structures and once started, if no treatment and recovery interventions are carried out, corrosion progresses causing significant performance losses. Corrosion can be chemically minimized by adding corrosion inhibitors during concrete casting, however, some types of inhibitors cannot be added directly into the mixture due to the possibility of unwanted reactions occurring during cement hydration. Another way of preventing corrosion is by using hydrophobic materials (such as oligomeric siloxanes) or protecting rebars with organic coatings. In this sense, this study proposes a physical protection for rebars based on a cementitious grout coating with and without a crystalline admixture (CA). The use of grout is advantageous, as it is expected to improve the low adhesion between the coated rebar and the concrete registered by usual organic coatings (as epoxy or polyurethane). In addition, the CA could provide extra protection, as it can form a less porous layer. In addition, different grout layer thicknesses were evaluated (from 1.0 mm to 4.9 mm). The rebars were first immersed in a supersaturated $Ca(OH)_2$ solution for 31 days to promote the passive layer formation and then, in a 0.5 mol/L NaCl solution for 10 more days to initiate corrosion. The corrosion current density (I_{corr}) was calculated from linear polarization resistance (LRP) measurements. The results showed that the grout without CA presented during passivation a I_{corr} slightly lower than grout with 3% of CA, but the difference between them were not so great and no significant improvement in the passive layer formation can be deduced to the presence of the CA. During corrosion, both grouts presented practically the same corrosion current. Regarding the thickness, the rebar coated with a layer of 4.9 mm presented better protection results as I_{corr} was practically the same during corrosion and passivation. The bars coated with 1.0 mm and 1.45 mm presented similar corrosion current density during corrosion, and corrosion spots were observed in both thicknesses due to uneven grout coverage.

Keywords: cementitious grouts, crystalline admixtures

Introduction

Despite the high alkalinity and the physical barrier provided by the concrete matrix, reinforcement corrosion can occur due to chemical, physical and electrochemical processes (combined or isolated). Electrochemical corrosion starts mainly due to potential differences between the anodic and cathodic areas at the surface of the metal rebar, due to an electrolyte with high ionic conductivity and by presence of oxidizing species such as oxygen. In cementitious materials, the corrosion resistance is, to a certain extent, ensured by the metal passivation. Observing an iron Pourbaix diagram [1], it is possible to identify areas where passivation is favored and what are the conditions in which the metal is more susceptible to corrosion as well. Although the passive layer is a thin layer, the oxide/hydroxide formed in this process is a very protective material. However, when aggressive ions (Cl^-, CO_2) are present, the corrosion rate increases considerably, even if the physical barrier provided by the cementitious matrix is very thick and highly alkaline.

Different electrochemical techniques have been employed to assess the corrosion evolution of reinforcements inside concrete. Among them, LPR is widely used in order to obtain kinetic data and correlate it with the corrosion rate of the metal [2,3]. Nowadays, there are numerous ways to delay the corrosion from the pre-treatment of the reinforced rebars (e.g., electrodeposition method; use of organic coatings) to selecting additives for cementitious matrix (e.g., additions of corrosion inhibitors and other additives to change fresh- and hardened-properties such as porosity).

Although the application of organic coating (as epoxy or polyurethane) has been reported as a good corrosion protection method, its application is limited by the decrease in the bond strength between the film and the cement matrix and by possible damages during transportation and handling that may favor future localized corrosion [4,5]. Thus, this work suggests an alternative physical barrier protection: a cementitious grout to be used as coating [5,6]. As grout is a very fluid material with long initial setting-time, its application as coating is not limited by design reasons. Furthermore, it is expected that the grout coating could overcome the losses in bond strength.

Therefore, the study aims to evaluate the corrosion protection of the grout containing a CA and to assess the corrosion evolution for various cover thicknesses. The CA selected was Penetron Admix provided by Penetron Italia. This CA is considered a permeability-reducing admixture that can react with moisture to form crystals reducing the permeability of the material [7].

Experimental

Materials and sample preparations

For this study, two group of grouts were designed differently, fixing the flow time: one without CA (G1) and another with 3 wt% CA (G2). The water/binder (w/b) ratio and superplasticizer additions varied between each group. G1 and G2 were produced replacing 20% of CEM I 42.5R by fly ash and with sand/binder = 1.0 (fine aggregates 0/2 mm). The amount of superplasticizer (MasterCast 228) was adjusted so that both grouts had the same flow time of 80 s. The dry materials were mixed in a rotary mixer with a flat beater for 40 s and then, after water addition, the grout was mixed for 2 more minutes. Table 1~~Table 1~~~~Table 1~~ gives the conditions for the grouts evaluated in this work.

Table 1. Grout conditions of experimental investigation.

Grout group	w/b	Penetron Admix (wt%)	Grout layer thickness (mm)	Specimen designation
G1	0.39	0	0.95 ± 0.07	G1
G2	0.46	3	0.99 ± 0.08	G2

G2	0.46	3	0.99 ± 0.08	G2_1.0
G2	0.46	3	1.45 ± 0.63	G2_1.45
G2	0.46	3	4.90 ± 0.74	G2_4.9

The ends of the rebars were manually painted with a water-based epoxy coating to fix the exposed area in 5.652 cm^2.After this, the rebars were coated with the cement-based grout using a dip-coater. To obtain a uniform layer, the speed range was set to have a layer around 1 mm. Bars with thickness greater than 1 mm had other layers applied between 15 and 30 minutes after applying the first layer. The final grout thickness varied between 0.95 and 4.9 mm. The test specimens were cured in laboratory environment (25 ± 1 °C) for 7 days. After that, the ends of cement coated rebars were coated again with the water-based epoxy coating as shown in Figure 1~~Figure 1~~~~Figure 1~~. After 3 days of complete curing of the epoxy coating, the electrochemical measurements began.

Experimental setup

Figure 1~~Figure 1~~~~Figure 1~~ shows the scheme of the electrochemical cell used in this study. The electrochemical tests were performed in a three-electrode electrochemical cell, being a steel rebar (ø = 8 mm, A = 5.652 cm^2) the working electrode (WE), Ag|AgC|/KCl(sat) the reference electrode (RE) and a stainless-steel mesh the counter electrode (CE). Before being covered with the grout, all rebars surfaces were chemically cleaned according to ASTM G1 [8]. The electrochemical technique employed for measuring corrosion current density was the linear polarization resistance. The polarization resistance (R_p) and open circuit potential (OCP) were measured at room temperature. After measuring OCP, the WE was polarized from -10 mV to 20 mV versus OCP at a scan rate of 0.167 mV. s^{-1} for R_P determination.

R_p and OCP were measured both during steel passivation exposing the samples to an alkaline solution and during the steel corrosion in a chloride solution. The rebars were first immersed in supersaturated calcium hydroxide solution. After the 31-day passivation period, the electrolyte was replaced with a 0.5 M sodium chloride solution. The LPR measurements were then conducted for 10 more days. The data were obtained by using an AUTOLAB PGSTAT204 Potentiostat.

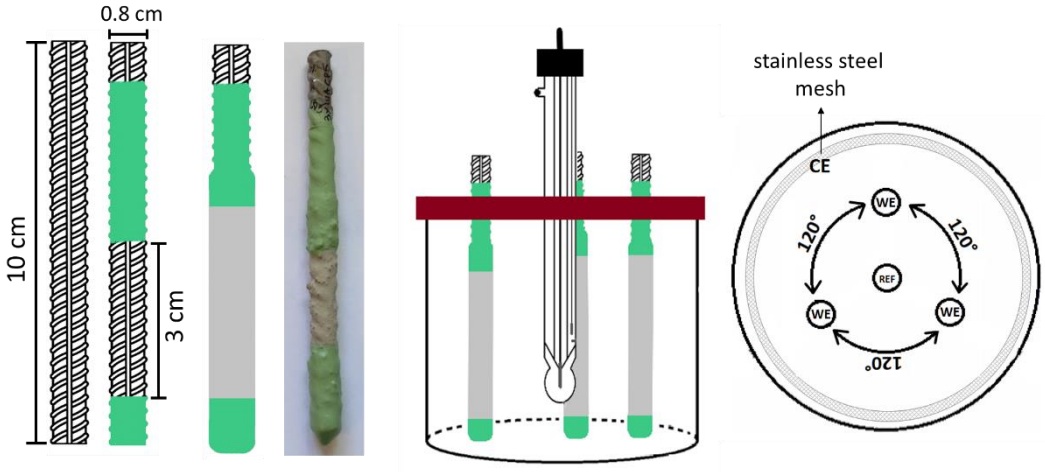

Figure 1- On the left, aspect of the grout lollipop and, on the middle and right, the schematic of three-electrode cell used to measure OCP and R_P.

Results and discussion

Usually, electrochemical tests in cementitious materials require protecting first certain regions of the metal (with tapes or coatings) before covering the rebars with the cementitious

material. This practice is normally done to prevent interfacial corrosion. As the smallest thickness evaluated in this study is not so thick (around 1 mm), the lack of adhesion at these interfaces would corrode more easily, hindering the conclusions. In order to avoid misinterpretation, two different ways of preparing the grout lollipops were assessed. As mentioned before, the ends of the rebars were first coated with a water-based epoxy coating. Then, the rebars were coated with cement-based grout layer. After that, the ends of some grouted rebars were coated again with the water-based epoxy coating as shown in Figure 2~~Figure 2~~~~Figure 2~~.

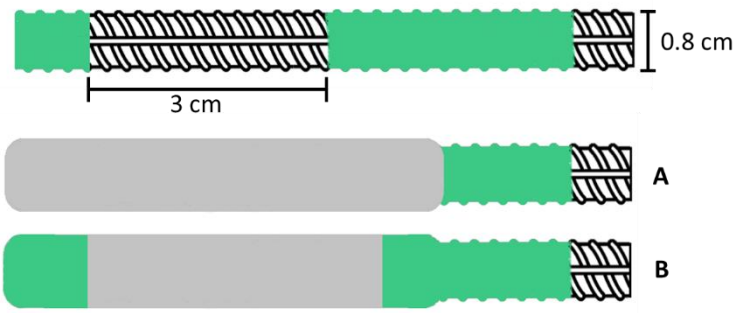

Figure 2. Aspect of the lollipops tested before starting the assessment of grout protection.

The specimens not coated twice with epoxy coating were named A, while the others coated again with epoxy were named B. The grout thickness was 0.90 ± 0.19 mm for rebar A and 0.87 ± 0.07 mm for rebar B. The grout used were the one without CA (G1). Figure 3~~Figure 3~~~~Figure 3~~ presents the evolution of the OCP and the I_{corr} during the passivation and corrosion. In passivation, the potential values were similar until day 20, after that each type of rebar showed opposite current flow. The potential of rebar B remained practically constant over time and dropped slightly to more negative values, while rebar A showed more anodic values over time. After immersion in chloride solution, both grouts presented a sharp drop in potential indicating the beginning of the corrosive process.

The fast destruction of the passive layer is confirmed by LPR results. The rebar A has a more active surface and the integrity of the passive layer seemed to be more preserved for rebar B. This fact was confirmed by visual inspection (Figure 4~~Figure 4~~~~Figure 4~~) of the rebars after each immersion period (calcium solution and chloride solution). Part of the grout on the rebar A fell off during the first days of immersion in the calcium solution. In some rebars, corrosion spots were seen on grout layer even in passivation (probably caused by the pH drop of the solution; pH was 9.5 by the end of passivation period). As a result, a more active interface appeared (on the edge between the epoxy and grouted metal) and, consequently, in the presence of chlorides, the corrosion rate was much higher, justifying the sudden drop in potential shown by the rebar A. The grout did not come off the rebar B, but corrosion spots appeared during passivation. This may have favoured the increase of the corrosion rate in the presence of chlorides. Therefore, the results indicated that the “mode B” preparation was more adequate to proceed with the tests.

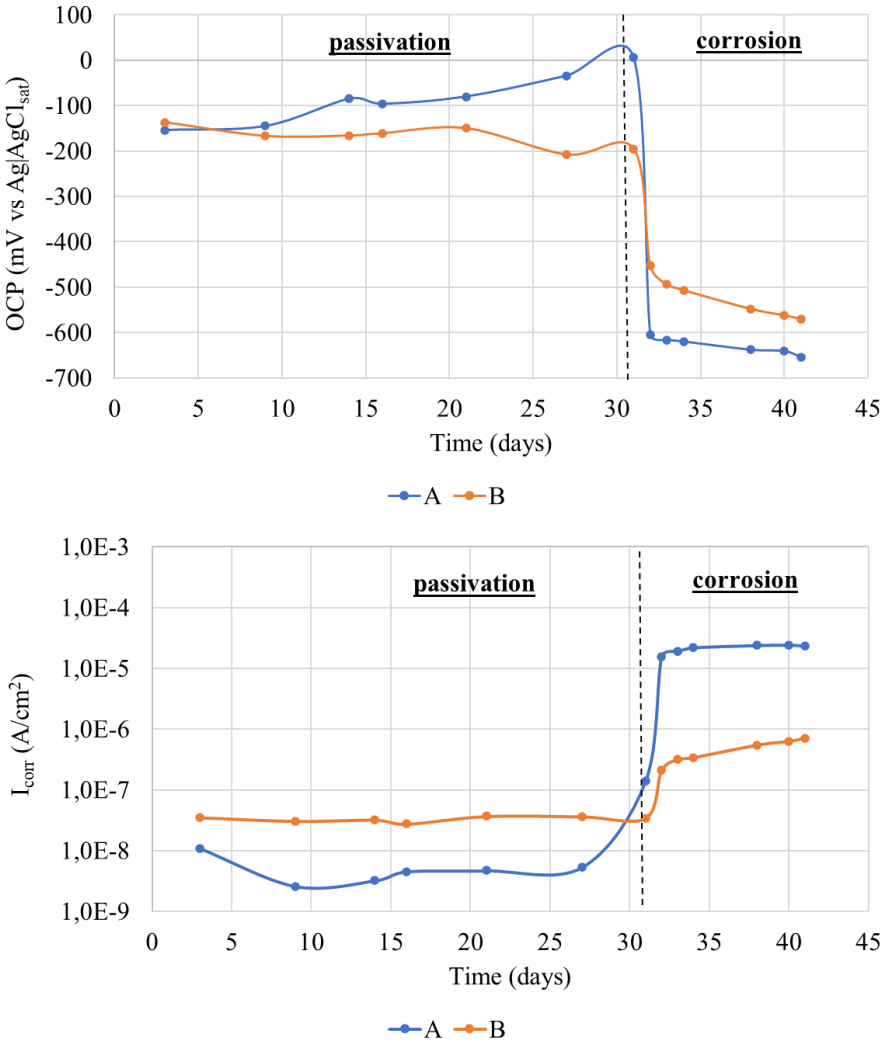

Figure 3. OCP and I_{corr} evolution of grout-coated specimens on exposure to calcium and chloride solutions.

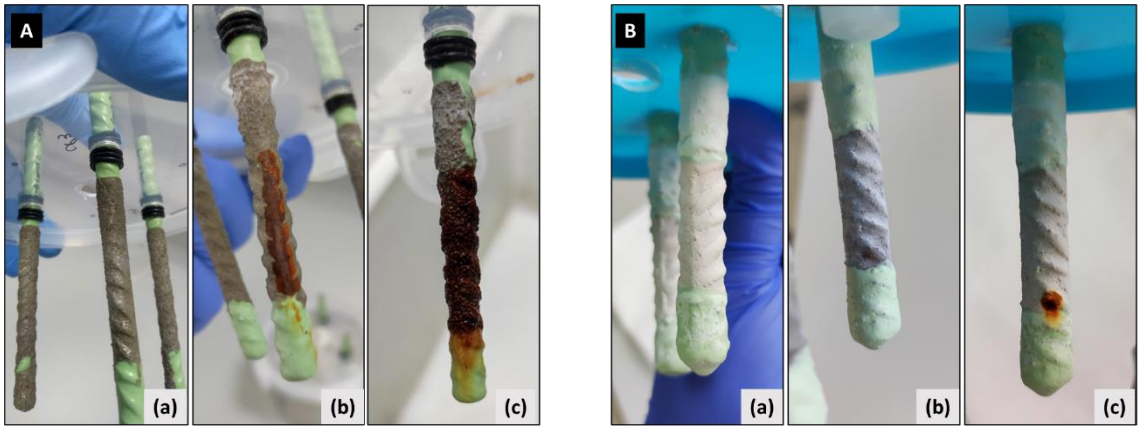

Figure 4. Photos of the rebars after electrochemical tests. Rebar A (on the left) and rebar B (on the right) after 3d (a) and 31d (b) of exposure to calcium solution and (c) after corrosion test completion.

After these tests, the effect of the crystalline admixture and the thickness of the grout coating were measured. Table 2 presents the results of OCP and I_{corr} values during passivation

(3rd and 31st day) and corrosion stage (1st and 10th day). The evolution of OCP and I_{corr} measurements are presented in Figures 5 and 7.

Table 2. Values of OCP and I_{corr} obtained for steel rebars coated with cementitious grouts after exposure to supersatured $Ca(OH)_2$ solution and NaCl 0.5 mol L^{-1} solution

	PASSIVATION OCP (mV)		CORROSION OCP (mV)		PASSIVATION I_{corr}(A.cm^{-2})		CORROSION I_{corr}(A.cm$^{2-2}$)	
Specimen /day	3	31	1	10	3	31	1	10
G1	-145	-264	-486	-544	3.52E-8	3.46E-8	2.10E-7	7.08E-7
G2	-225	-239	-450	-556	7.89E-8	5.36E-8	2.75E-7	1.69E-6
G2_1.0	-225	-239	-450	-556	7.93E-8	5.38E-8	2.77E-7	1.70E-6
G2_1.45	-287	-281	-558	-586	3.07E-7	5.35E-8	2.87E-7	1.29E-6
G2_4.9	-477	-277	-369	-491	2.35E-7	7.02E-8	2.12E-7	4.66E-7

Influence of CA on corrosion resistance for the same coating thickness

Figure 5~~Figure 5~~~~Figure 5~~ shows the influence of CA on OCP and I_{corr} during passivation and corrosion period. By OCP measurements, no significant effect during passivation is observed when CA is added to the grout. After 24 hours of exposure to NaCl solution, a significant potential drop is registered for both grouts and the potential continues decreasing until the end of the test (final values of -544 mV and -556 mV were registered for 0% of CA and 3% of CA respectively).

Regarding corrosion currents, although the grout without CA has I_{corr} values in the passivation slightly lower than grout with 3% of CA, both grouts registered the same magnitude order and the difference between them is not so great, therefore no significant improvement in the passive layer formation can be deduced or associated with the presence of the CA.

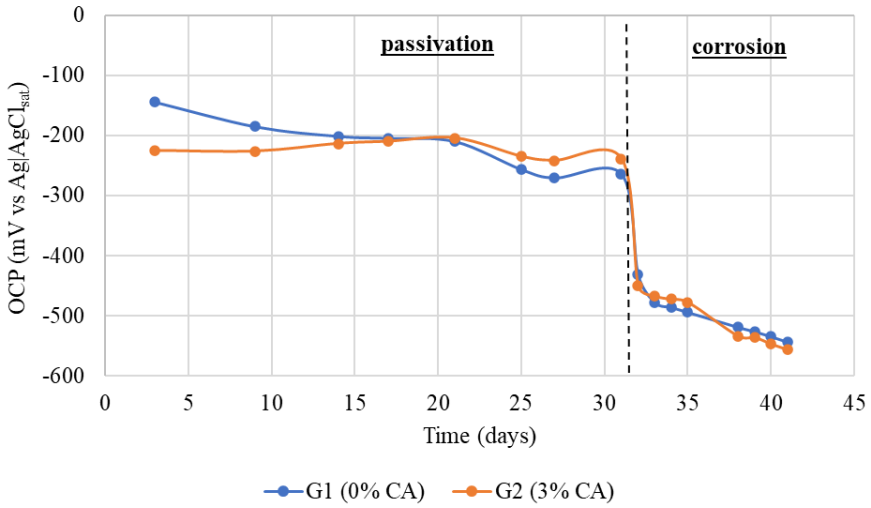

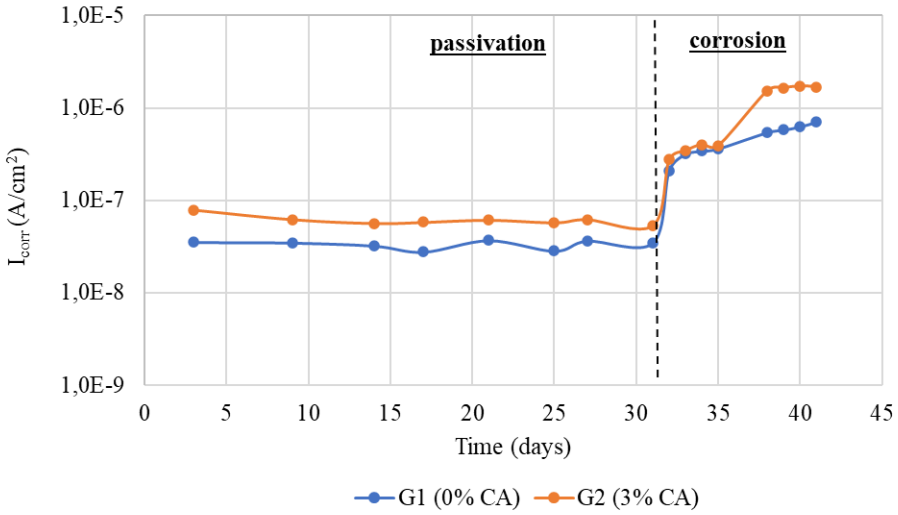

Figure 5. Electrochemical response of grouts without (G1) and with (G2) crystalline admixtures to $Ca(OH)_2$ and NaCl solutions.

At the end of the passivation and the corrosion periods, the visual analysis of the rebars was carried out. Observing Figure 6~~Figure 6~~Figure 6, after immersion in $Ca(OH)_2$ solution, it was noted that some rebars had corrosion spots and the corrosion stains in G2 were more intense than in G1. Most likely, crevice corrosion has governed the localized depassivation in both grouts and, consequently, the corrosion rate changed due to the nonuniformity of the grout layer.

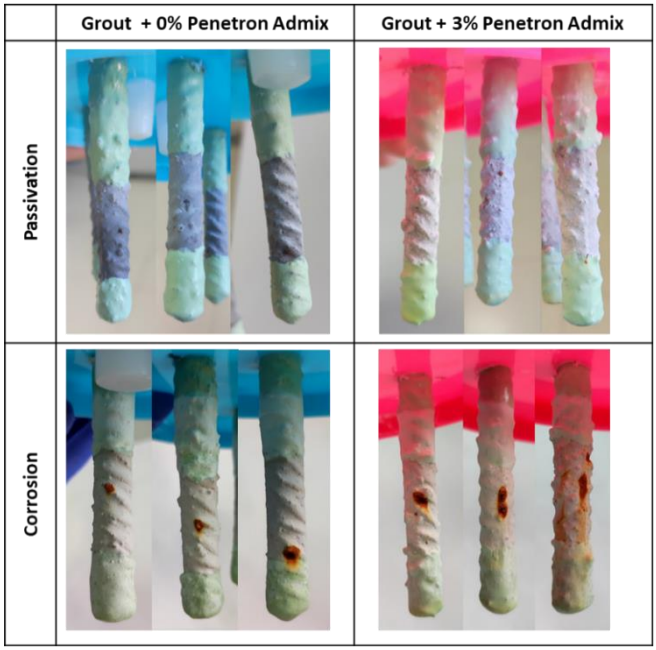

Figure 6. Visual observation of specimens after completion of corrosion testing

Influence of cover thickness on corrosion resistance

As mentioned previously, one of the objectives is to verify the corrosion protection of G2 grout for different thicknesses: 1.0, 1.45 and 4.9 mm. Figure 7~~Figure 7~~Figure 7 shows the growth and destruction of the passive layer by the potential evolution and corrosion rate. Despite the oscillation, it can be observed that the layer of 1.0 mm did not present an increase of the potential over time, maintaining the same range of potential around -230 mV. The layers

of 1.45 mm and 4.9 mm, in the first 10 days of immersion, registered potentials lower than -300 mV but, over time, evolved to more anodic potentials.

Although the OCP of all the grouts dropped in the first immersion days in chloride solution, the 4.9 mm-grout did not present a sharp fall, on the contrary, it was a gradual slope. Analysing the corrosion current density in the corrosion stage in Table 2~~Table 2~~Table 2, the integrity of the passive layer appears to be more preserved for the layer of 4.9 mm. The I_{corr} practically remained constant during passivation and slightly increased during the corrosion periods. The corrosion current for 4.9 mm and 1.45 mm layers were quite similar during the beginning of passivation and it decreased over time, showing the same corrosion current of 1.0 mm layer after 25 days of immersion in calcium solution. The effect of thickness is better observed during chloride solution exposure. The depassivation is faster for G2_1.45 and G2_1.0 rebars. The greater resistance of the layer of 4.9 mm (compared to the others) may be related to the greater and higher resistive barrier. Although a greater corrosion protection was expected for 1.45 mm-grout (compared to 1.0 mm-grout), no significant difference in I_{corr} was observed.

Figure 8~~Figure 8~~Figure 8 presents photos of the rebars after the end of corrosion period. The 4.9 mm-grout is well preserved, with no corrosion spots, which indicates that a good protection was achieved with this thickness. According to the I_{corr} results presented in Figure 7~~Figure 7~~Figure 7, the 1.45 mm-grout rebar was expected to be as corroded as the 1.0mm-grout rebar. However, its appearance after 10 days of immersion in chloride solution was not so damaged compared to the layer of 1.0 mm (Figure 8~~Figure 8~~Figure 8Figure 8~~Figure 8~~), but some corrosion spots are observed in both rebars. The localized corrosion in both rebars may have been caused by heterogeneities in the grout or due to the non-uniformity of the thickness.

Analysing these results with the results discussed in the previous section, we can assume that is not adequate to coat the rebars with a layer smaller than 1.5 mm mainly because the grout has aggregates grains with maximum size of 2 mm and clearly layers smaller than this size are not adequate. The uneven coating can generate flaws that facilitate the appearance of zones with different oxygen concentrations, which promotes localized corrosion.

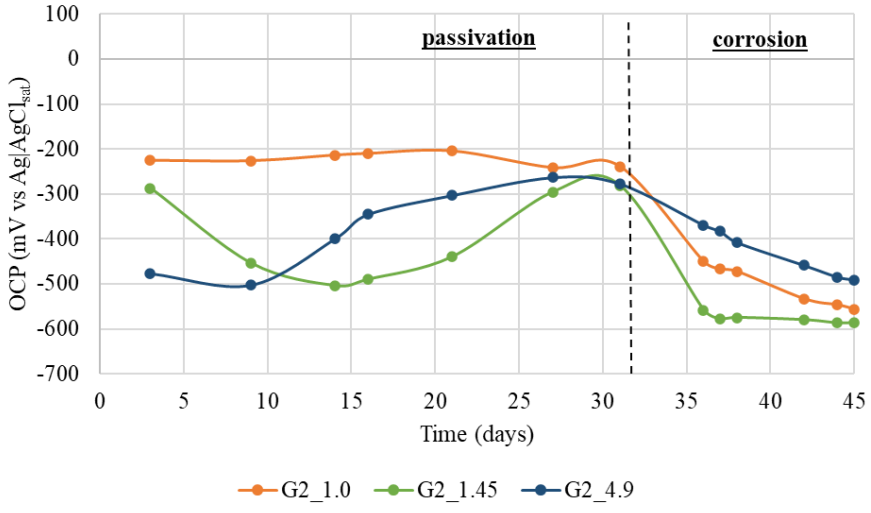

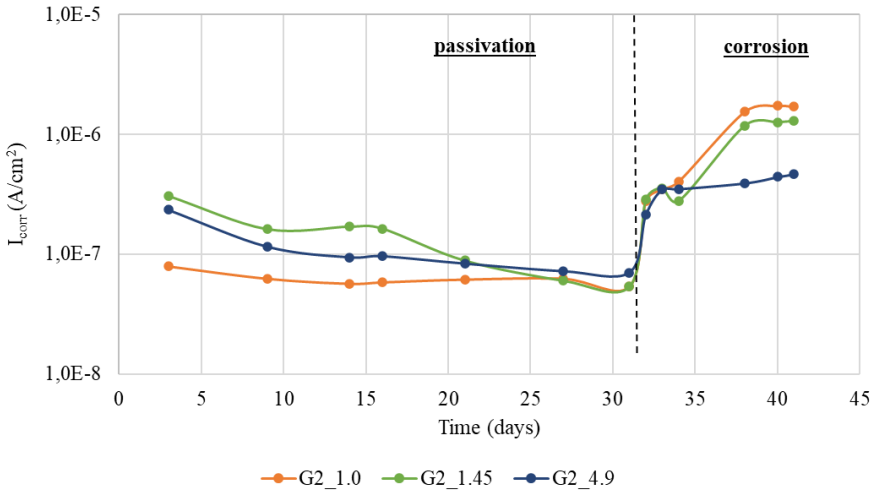

Figure 7. Variation of OCP and I_{corr} as function of grout thickness.

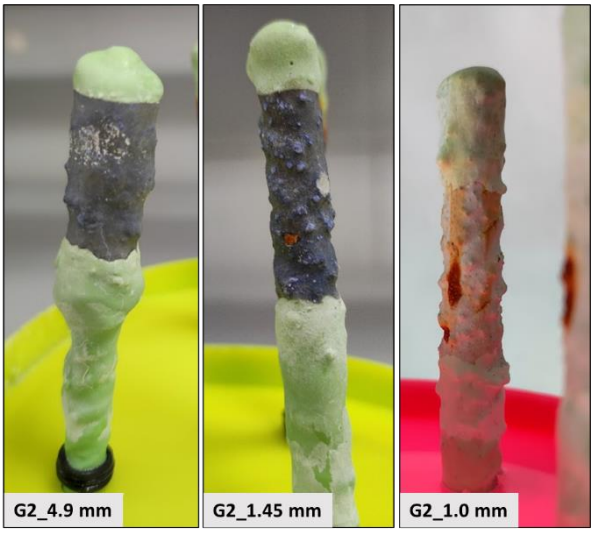

Figure 8.Visual examination of grout coating at the end of measurements.

Conclusions

Based on all experiments, the following conclusions were drawn:

- CA apparently did not present a significative effect on corrosion protection. After immersion in $Ca(OH)_2$ solution, it was noted that some G1 and G2 rebars presented localized depassivation and, consequently, high values of corrosion rate. The results were negatively influenced by this localized corrosion as it was not possible to identify the influence on corrosion promoted by the crystalline admixture.
- The passive layer of 4.9 mm-grout was the most preserved throughout the test, as its I_{corr} remained constant during passivation and increased slightly during the corrosion. During passivation, I_{corr} for the layers of 4.9 mm and 1.45 mm were similar and decreased over time presenting the same corrosion current of 1.0 mm layer after 25 days of immersion in calcium solution. During chloride solution exposure, the G2_1.45 and G2_1.0 rebars were depassivated faster than G2_4.9mm. The greater resistance of 4.9 mm layer compared to the others could be related to the bigger and high resistive physical barrier.
- Analysing the response of the rebars coated with less than 1.5 mm of thickness, could be observed that localized corrosion was more likely to occur. It could be associated to uneven coating due to the maximum grain size of the aggregates. As the grouts were

made with 0-2 mm aggregates, the sand grains between 1.5 and 2.0 mm could promote flaws that facilitate the appearance of zones with different oxygen concentrations, favouring., crevice corrosion.

This project has received funding from the European Union's Horizon 2020 research and innovation programme under the Marie Skłodowska-Curie grant agreement No 860006. The authors also thank Enrico Gastaldo, from *Penetron Italia Srl*, for providing the Penetron Admix, *Master Builders Solutions* (Sandro Moro and Pere Borralleras) for supplying the MasterCast 228 and *Cemento Cosmos S.A.* for supplying the cement.

References

[1] M. Pourbaix, Atlas d'equilibres életrochimiques, Gauthier-Villars Ed, 1963.

[2] A.R. Pacheco, A.J. Schokker, J.S. Volz, H.R. Hamilton, Linear polarization resistance tests on corrosion protection degree of post-tensioning grouts, ACI Mater J. 108 (2011) 365–370. https://doi.org/10.14359/51683107.

[3] S. Rengaraju, L. Neelakantan, R.G. Pillai, Investigation on the polarization resistance of steel embedded in highly resistive cementitious systems – An attempt and challenges, Electrochim Acta. 308 (2019) 131–141. https://doi.org/10.1016/j.electacta.2019.03.200.

[4] K. Kobayashi, K. Takewaka, Experimental studies on epoxy coated reinforcing steel for corrosion protection, International Journal of Cement Composites and Lightweight Concrete. 6 (1984) 99–116. https://doi.org/10.1016/0262-5075(84)90039-3.

[5] X. Pei, M. Noël, A. Fam, M. Green, Development length of steel reinforcement with corrosion protection cementitious coatings, Cem Concr Compos. 60 (2015) 34–43. https://doi.org/10.1016/j.cemconcomp.2015.04.003.

[6] X. Pei, M. Noël, M. Green, A. Fam, G. Shier, Cementitious coatings for improved corrosion resistance of steel reinforcement, Surf Coat Technol. 315 (2017) 188–195. https://doi.org/10.1016/j.surfcoat.2017.02.036.

[7] A. de S. Oliveira, J. Dweck, E. de M.R. Fairbain, O.R.D.T. Filho, Crystalline admixture effects on crystal formation phenomena during cement pastes' hydration, J Therm Anal Calorim. 139 (2020) 3361–3375. https://doi.org/10.1007/s10973-019-08745-0.

[8] ASTM G1, Standard Practice for Preparing, Cleaning, and Evaluating Corrosion Test Specimens., ASTM Special Technical Publication. (2017). https://doi.org/10.1520/G0001-03R17E01.2.

Performance of a New Nickel-Based Alloy, ATI 642®, for Severe Oil & Gas Environments and CPI Applications

Sabrina Nacéra Meck, David Bergstrom and John Dunn
ATI Specialty Rolled Products
Natrona Heights Operations
1300 Pacific Avenue
Natrona Heights, PA, 15065, USA

ABSTRACT

ATI 642® alloy (UNS N08642) is a corrosion-resistant alloy (CRA) that has recently been developed for Oil & Gas (O&G) and Chemical Process Industry (CPI) environments. This new Ni-Cr-Mo alloy fills a gap in corrosion resistance between two well-known Ni base alloys, 625 and 825. Alloy 625 is one of the most widely used materials for O&G and CPI applications, due to a combination of high corrosion resistance in both sour service and high chloride environments, while maintaining phase stability from process heat treatment exposures such as welding. However, it is relatively expensive because its chemical composition was developed for both aqueous corrosion-resistant and high-temperature applications. Alloy 825 is a less expensive option to 625, with less corrosion resistance. However, 825 cannot be used in aqueous environments with high chloride contents at elevated temperatures because of its susceptibility to pitting, crevice corrosion and stress corrosion cracking (SCC). New alloy ATI 642® has been designed with optimized phase stability, corrosion resistance, sour service performance, toughness, and weldability to perform better than 825, while its leaner alloy content makes ATI 642 alloy an attractive, lower-cost alternative to 625.

One example of an important application for CRA's in the O&G industry is their use in subsea bimetallic flowlines. These are pipes made with a carbon steel substrate material that are lined either by a hot-roll bonding process (HRBP) or through a mechanical lining process (MLP) with a corrosion-resistant liner. Less expensive alloys currently used as liner material include 825 and 316L stainless steel, but they are less corrosion resistant than 625 alloy and therefore have limited use. Other alloys have been considered to fill the gap in performance between 825 and 625, such as 904L, 6% Mo alloys, and duplex and super duplex stainless steels. However, these alloys have several disadvantages compared to 625, such as susceptibility to environmentally-assisted cracking and the formation of intermetallic phases adjacent to welds, which ATI 642 alloy has been designed to minimize.

This paper will present the results of chloride-stress corrosion cracking (SCC), intergranular attack (IGA), critical pitting temperature (CPT), SCC/SSC/GHSC sour tests, and natural seawater exposure tests on ATI 642 alloy as compared to other CRA's. Mechanical test comparisons for tensile and Charpy impact energy will also be presented.

Keywords: Alloy 642®, UNS N08642, stress corrosion cracking (SCC), sulfide stress cracking (SSC), galvanic hydrogen stress cracking (GHSC) intergranular attack (IGA), pitting corrosion, crevice corrosion in natural seawater, phase stability, weldability, flowline pipes

Effect of annealing temperature on the microstructure and corrosion resistance of Ti-6Al-4V-0.5Ni-0.5Nb titanium alloy plates

Yang Yu[1], Jinpeng Ge[2], Changheng Li[3], Songxiao Hui[4], Lei Wang[5]

1.GRINM (Guangdong) Institute for Advanced Materials and Technology, Foshan, 528051, China, yuyang@grinm.com
2.GRIMAT Engineering Institute Co., Ltd., Beijing 101407, China, 1303220179@qq.com
3.GRIMAT Engineering Institute Co., Ltd., Beijing 101407, China, l584211929@163.com
4.GRINM (Guangdong) Institute for Advanced Materials and Technology, Foshan, 528051, China, huisx@grinm.com
5.GRINM (Guangdong) Institute for Advanced Materials and Technology, Foshan, 528051, China, wangl@grinm.com

Abstract
The corrosion and passivation behavior of the TC4-0.5Ni-0.5Nb alloys at different annealing temperatures were investigated through electrochemical testing in both NaCl and HCl solutions. The corrosion resistance showed an improvement with the increase of annealing temperature. Microstructure analysis of the annealed alloy revealed that the grain size, volume fraction of β phase, and distribution of alloy elements in α and β phase were the primary factors that influenced the corrosion resistance of the alloys annealed at different temperatures.

Key Words: TC4-0.5Ni-0.5Nb alloys, electrochemical testing, corrosion resistance

Introduction

With the rapid progression of the economy and the prevailing global energy deficit, unconventional oil and gas resources, distinguished by high temperature, high pressure, and severe corrosion have become the pivotal focus of oil and gas development. The harsh operating conditions urgently require cutting-edge, high-performance oil well drill pipes [1]. Consequently, with the emphasis on future economic advancement and the fulfillment of the requirements for high-end oil and gas exploitation, it is increasingly crucial to investigate materials that possess high-strength, low-density, and corrosion-resistant properties for petroleum pipes[2][3]. Titanium alloy, with its high specific strength, low elastic modulus, ease of cold forming processing, excellent corrosion resistance in oxidizing and partially reducing acids, as well as good stress corrosion resistance, emerges as an ideal material for high-end oil well tubing[4][5].

Compared to pure titanium, Ti-6Al-4V(TC4) titanium alloy has superior strength, toughness, and corrosion resistance, making it highly suitable for hot pressing forging. Its comprehensive mechanical properties also make it the preferred material for developing new materials for oil well pipes[6]. In underground environments containing $Cl^-/H_2S/CO_2$, TC4 alloy also exhibits good resistance to both uniform corrosion and pitting corrosion [7]. In order to further enhance the applicability of TC4 alloy in the field of oil and gas development, researchers have conducted research on the TC4-0.5Ni-0.5Nb alloy obtained by adding alloy elements nickel (Ni) and niobium (Nb) to TC4 alloy. The research revealed that the strength and impact toughness of the alloy were significantly improved through various heat treatment processes, basically meeting the mechanical performance requirements for structural materials in deep oil and gas well development[8]. Generally speaking, heat treatment is a common means of structural control in industrial production. The mechanical properties of titanium alloys are highly correlated with the microstructure, and different heat treatment processes have a significant impact on the microstructure and mechanical properties of the alloy[9][10][11]. However, there remains a lack of corresponding studies on the impact of different heat treatment systems on the corrosion resistance of the alloy. Research has shown that the microstructure resulting from different heat treatment systems will significantly affect the corrosion resistance of the titanium alloy[12][13]. In addition, the addition of alloying elements and the distribution of alloying elements under different temperature heat treatments will also significantly affect the corrosion resistance of the alloy [14][15][16].

Therefore, this chapter focuses on investigating the TC4-0.5Ni-0.5Nb alloy subjected to various annealing treatment systems. Electrochemical tests was conducted in 3.5wt.% NaCl solution and 1 mol/L HCl solution respectively to study the microstructural variation of the alloy resulting from different heat treatment systems and their corrosion behavior in Cl- containing solutions. By analyzing the corrosion differences of the alloys from a microstructure perspective, new and useful data will be gained for the design of oil and gas extraction processes in marine and hydrochloric acid environments, ultimately avoiding the substantial harm caused by alloy corrosion.

Materials and methods

The experimental alloy was obtained by using two rounds of vacuum consumable melting and single-phase zone rolling. The nominal composition of the experimental alloy is TC4-0.5Ni-0.5Nb (the chemical composition is shown in Table 1, and the phase transition point of the alloy is 950±5°C). To investigate the microstructure and corrosion behavior of the alloy, annealing was performed at temperatures of 700°C, 750°C, 800°C, 850°C, 900°C, and 920°C for 1 hour, followed by air cooling (AC). These specific parameters were selected for the study.

Metallographic specimens measuring 10 mm×10 mm×10 mm were prepared from alloy plates by wire cutting and polished with SiO_2 suspension. The surface roughness was grinded to be less than 1.6μm by silicon carbide sandpaper. The specimens were then

etched with Kroll reagent in the volume ratio of HF:HNO_3:H_2O=1:3:7. Subsequently, the surface was thoroughly cleaned with deionized water and alcohol, followed by blow-drying. Optical microscopy (OM, Zeiss Axiovert 200), scanning electron microscopy (SEM, JSM-F100) with energy-dispersive spectroscopy (EDS) were used to analyze the microstructure.

Table 1. Chemical composition of Ti-6Al-4V-0.5Ni-0.5Nb alloy (wt.%).

Ti	Al	V	Ni	Nb	C	O
Bal.	5.96	3.95	0.58	0.64	0.0082	0.09

Electrochemical experiments were performed using a conventional three-electrode electrochemical cell system. The counter electrode was a platinum electrode, the reference electrode was Saturated calomel electrode (SCE), and the working electrode was the sample to be tested. The working electrode was sealed with epoxy resin to ensure a working area of 1 cm^2, and was ground to an 800 grit SiC before electrochemical tests. All electrochemical measurements were conducted at a constant temperature of 25±1℃. The electrolytes were 3.5wt.% NaCl and 1mol/L HCl solutions. Open circuit potential(OCP) measurements were conducted over a sufficient period(3000 s) to attain a stable value. Potentiodynamic polarization (PDP) curves were performed from −1000 mV to 1000 mV vs. SCE after OCP test at a potential sweep rate of 1 mV s^{-1}. To ensure experimental accuracy, three samples were tested for each heat treatment state.

Results and Discussion

Microstructure

Optical micrographs of Ti-6Al-4V-0.5Ni-0.5Nb alloy annealed at different temperatures are shown in Fig.1. The microstructure of annealing temperature 700 ℃ is characterized by an equiaxed α microstructure with approximately 80 vol% primary α phase, as shown in Fig.1(a). The grain size of the α phase is about 7 μm. At this temperature, the primary α phase is connected with each other(interconnected), while the βT is mainly located at the α grain boundary. The volume fraction and grain size of the primary α phase at different annealing temperatures were statistically analyzed as shown in Figure 2. It can be observed that within the temperature range of 700-850 ℃, with the increase of annealing temperature, the content of primary α phase slightly decreases, while the grain size remains basically unchanged.

With further increase in annealing temperature to 900°C, the primary α phase content of Ti-6Al-4V-0.5Ni-0.5Nb alloy decreases significantly, forming a typical duplex structure, as shown in Fig.1(e). The volume fraction of the primary α reduces to 45%, with β phase becoming the dominant component in the alloy microstructure evolution. With the increase of temperature, some primary α transformed to β, and then transformed to the secondary α phase during the subsequent cooling process. At this stage, the primary α phase is mainly connected with the β_T. The content of the primary α phase continues to decrease, indicating that further increase in annealing temperature induces α to β transformation, and part of the α phase converts to β phase. As cooling proceeds, the secondary α phase precipitates from the β phase, leading to another β to

α transformation. Consequently, the β transformation structure consists of a staggered arrangement of residual β phase and lamellar secondary α phase.

When the annealing temperature reached 920℃, the atomic diffusion rate becomes faster as the temperature increases. Therefore, the content of the β transformation structure further increases, and the content and size of the primary α phase further decrease. At this temperature, with a low volume fraction of the primary α phase, the strong solute partitioning and large diffusion lengths inhibited the coarsening of the primary α grains[17].

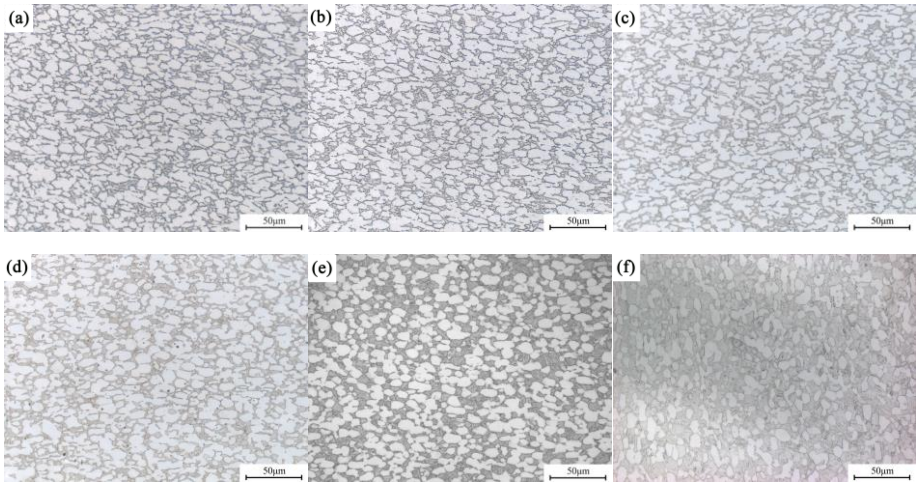

Figure 1. Microstructure of specimens annealed at various temperatures: (a)700°C/1 h/AC; (b) 750°C/1 h/AC; (c) 800°C/1 h/AC; (d) 850°C/1 h/AC; (e) 900°C/1 h/AC; (f) 920°C/1 h/AC

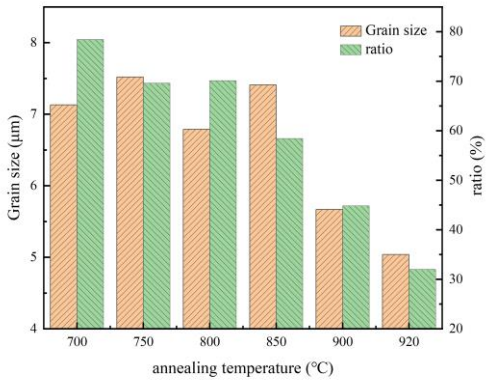

Figure 2. The volume fraction and the grain size of the primary α phase

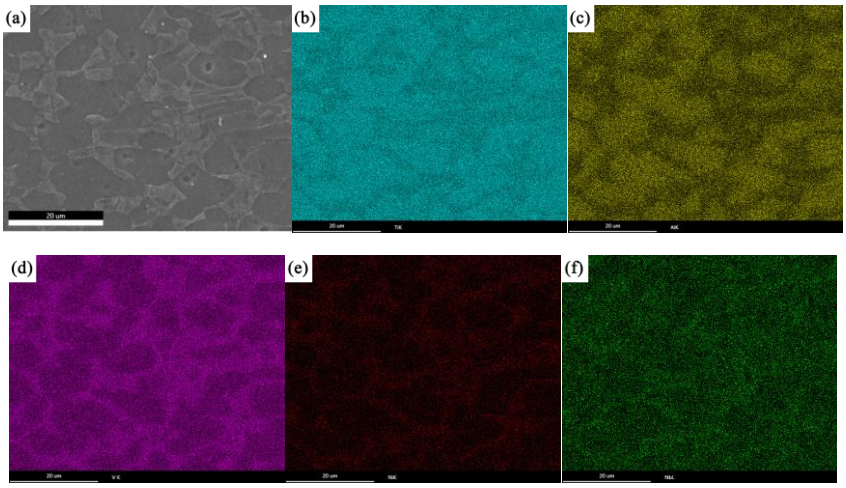

Figure 3. (a) SEM images of TC4-0.5Ni-0.5Nb alloy; (b-f) SEM-EDS different elemental maps of alloy

In addition, the SEM element surface scanning atlas shows distinct distribution characteristics of different alloy elements in α and β phases. The microstructure and element distribution of TC4-0.5Ni-0.5Nb alloy after annealing at 850 ℃ are shown in Fig.3. The SEM elemental maps (Fig.3(b–f)) demonstrate that Al (α stabilizer) partitions to the α phase (Fig.3(c)), while V, Ni and Nb (β stabilizer) tend to segregate to the β phase (Fig.3(d, e,f)). The EDS results of the relative concentrations of α and β phase after different heat treatment systems are presented in Table 2. The diverse elements distribution at the α and β phase will also affect the corrosion resistance of the alloy, which will be further discussed in subsequent chapters.

Table 2. EDS results for relative concentration of the α and β phases.

Sample	Relative concentration(wt.%)					
	Phase	Ti	Al	V	Ni	Nb
700℃	α	90.40	6.98	2.14	0.26	0.22
	β	83.96	4.87	8.70	1.61	0.87
750℃	α	89.83	7.04	2.51	0.35	0.27
	β	85.28	6.50	6.28	1.13	0.82
800℃	α	89.60	7.05	2.48	0.52	0.35
	β	85.49	5.90	6.23	1.26	1.12
850℃	α	91.07	6.79	1.78	0.32	0.35
	β	85.58	4.71	7.93	1.16	0.62
900℃	α	90.05	7.46	2.00	0.22	0.28
	β	86.69	5.70	6.06	0.96	0.58
920℃	α	89.43	7.82	2.17	0.24	0.34
	β	87.37	5.66	5.38	0.97	0.63

Corrosion behavior

The OCP can preliminarily reflect the electrochemical behavior of the surface of the sample to be tested, and the dissolution and formation of the alloy passivation film in solution can be learned through the OCP curves. The variation of the open circuit potential (E_{OCP}) for the annealed TC4-0.5Ni-0.5Nb alloys as a function of time in 3.5% NaCl solution is shown in Fig. 4. The results show that the E_{OCP} of the alloy fluctuates significantly during the initial period of immersion, with the immersion time prolongs, the E_{OCP} gradually stabilizes. During the initial period of immersion, the potentials all increase rapidly, indicating the formation and growth of the oxide film on the surface of the alloys, and ultimately in a stable passivation zone. This indicates that all annealed alloys exhibit spontaneous passivation during OCP measurements in a 3.5wt.% NaCl solution. Furthermore, as the annealing temperature increases, the final E_{OCP} stability value of the alloy gradually increases, indicating a corresponding improvement in the stability of the alloy's passivation film.

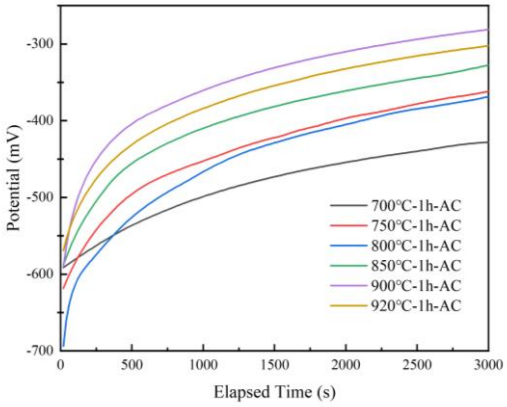

Figure 4. Variation of OCP with time for TC4-0.5Ni-0.5Nb alloys in 3.5wt.% NaCl solution

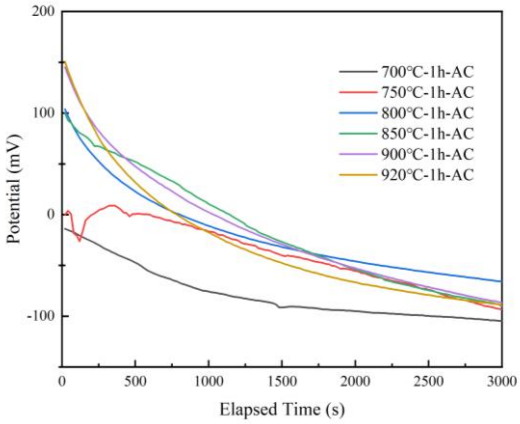

Figure 5. Variation of OCP with time for TC4-0.5Ni-0.5Nb alloys in 1mol/L HCl solution

However, in 1mol/L HCl solution, the corrosion behavior of the TC4-0.5Ni-0.5Nb alloy under different annealing states is completely different from the performance shown in 3.5wt.% NaCl solution. As shown in the Fig.5, the E_{OCP} shows a rapid decreasing trend with time during the initial immersion period, similar to the E_{OCP} of other titanium alloys in HCl solution[18][19]. This indicates that the native oxide film of the alloy is continuously dissolved or broken down, leading to the reduction of Ti^{4+} to TiOOH, which then dissolved as Ti^{3+} or directly as Ti^{3+}. As the immersion time prolongs, the new passivation films gradually form, and the E_{OCP} tends to stabilize, ultimately reaching an equilibrium state of dissolution formation of the passivation film. It is worth noting that the initial E_{OCP} and final E_{OCP} value of all samples under different annealing states are different, this difference can most likely be attributed to the differences in compositions of the α and β phases and microstructural morphology resulting from the annealing process, which will be discussed in subsequent chapters.

Fig.6 and Fig.7 show the potentiodynamic polarization curves of the annealed TC4-0.5Ni-0.5Nb alloys in 3.5wt.% NaCl and 1 mol/L HCl solutions. It can be seen that the

dynamic potential polarization curve characteristics of the alloy in both solutions are similar, showing cathodic polarization region, anodic polarization region, active-passive transition region, and stable passivation region, which indicates that the alloy undergoes an active to passive transition. In order to clearly compare the electrochemical corrosion performance of alloys under different heat treatment states, Table 3 and Table 4 list the corrosion potentials (E_o) and corrosion current densities (I_o) of alloys in 3.5wt.% NaCl and 1 mol/L HCl solutions, respectively. The corrosion parameters were obtained from the polarization curves using the Tafel method.

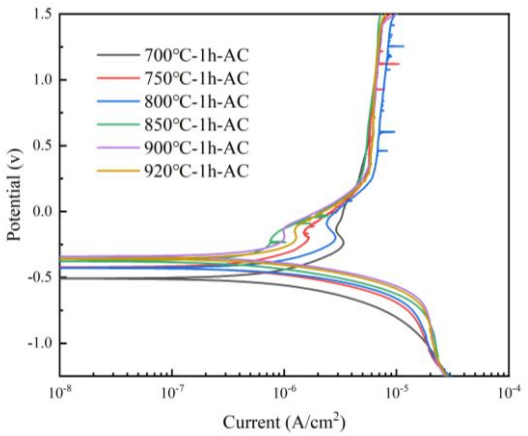

Figure 6. Potentiodynamic polarization curves of TC4-0.5Ni-0.5Nb alloys in 3.5wt.% NaCl solution

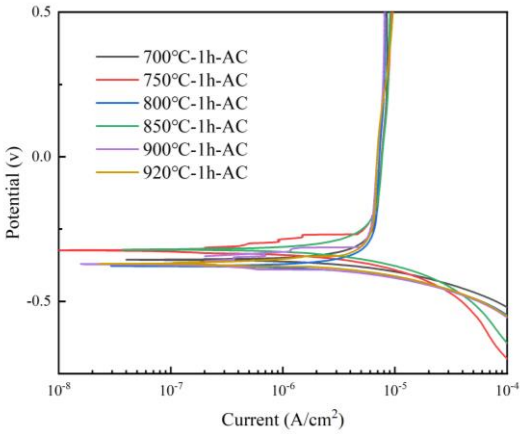

Figure 7. Potentiodynamic polarization curves of TC4-0.5Ni-0.5Nb alloys in 1mol/L HCl solution

From Table 3, it is evident that as the annealing temperature increases, the corrosion potentials of the alloy in NaCl solution gradually increase. Generally speaking, the corrosion potential refers to the potential at which the material begins to corrode in a corrosive environment. The lower the corrosion potential, the more susceptible the material is to corrosion. Corrosion current density refers to the current density at which a material dissolves in a corrosive environment. A higher corrosion current density corresponds to a faster corrosion dissolution rate of the material. Notably, the alloy exhibits the highest corrosion current density when annealed at 700℃, indicating that the TC4-0.5Ni-0.5Nb alloy has the highest corrosion dissolution rate and the worst corrosion resistance after annealing at 700℃. Conversely, the lowest corrosion dissolution rate is observed after annealing at 900℃, indicating the best corrosion resistance for the alloy under this condition. From Table 4, it can be seen that the corrosion potential of alloys under different heat treatment systems fluctuates less in HCl solution, but there is still a significant difference in corrosion current density. Similar to NaCl solution, the alloy has the highest corrosion current density and the worst corrosion resistance when annealed at 700℃, while the lowest corrosion current density is observed for samples annealed at 900℃ and 920 ℃. As a result, the alloy annealed at 900℃ and 920℃ exhibits the best corrosion resistance. Furthermore, it is worth noting that referring to the electrochemical performance of other TC4 alloys in NaCl and HCL solutions, it can be found that with the addition of Ni and Nb elements, the TC4-0.5Ni-0.5Nb alloy exhibits lower corrosion current density and higher

corrosion potential, indicating that the alloy has lower corrosion tendency and higher corrosion resistance

Table 3. Corrosion potentials, corrosion current densities and Tafel slopes(Ba and Bc) the TC4-0.5Ni-0.5Nb alloys in 3.5wt.% NaCl solution

	B_a(mV) (V SCE)	B_c(mV) (V SCE)	I_o(A/cm^2) $\times10^{-7}$	E_o(mV) (V SCE)
700	178.6	117.6	5.05	-508.5
750	192.7	96.3	3.94	-423.1
800	146.9	98.1	4.85	-428.5
850	296.1	91.4	4.10	-377.3
900	187.2	89.6	3.66	-341.2
920	164.5	92.9	3.91	-358.3

Table 4. Corrosion potentials, corrosion current densities and Tafel slopes(B_a and B_c) the TC4-0.5Ni-0.5Nb alloys in 1 mol/L HCl solution

	B_a(mV) (V SCE)	B_c(mV) (V SCE)	I_o(A/cm^2) $\times10^{-7}$	E_o(mV) (V SCE)
700	291.3	72.8	37.33	-356.1
750	112.7	74.9	14.78	-323.1
800	106.0	53.0	23.43	-377.8
850	220.4	86.3	27.54	-320.5
900	271.3	42.3	5.13	-371.4
920	56.6	21.9	4.53	-371.1

In these two solutions, the alloy annealed at 700℃ consistently exhibited poor corrosion resistance. However, when annealed above 900℃, the corrosion resistance of the alloy significantly improved. The difference in corrosion behavior can be explained by considering changes in grain size, volume fraction of β phase, and distribution of alloy elements in α and β phase. These factors play a crucial role in influencing the alloy's overall corrosion performance. From the experimental results, it can be found that as the annealing temperature increases, the grain size of the alloy gradually decreases. Consequently, the density of grain boundaries gradually increases. As surface lattice defects, grain boundaries will greatly increase the nucleation sites of the passivation film. When annealed above 900℃, the precipitation of secondary α phase will also provide more nucleation sites, thereby increasing the thickness of the passivation film and reducing the corrosion rate. In addition to the influence of grain size on corrosion resistance, the micro-galvanic couple effects formed between α and β phase are also significant factors for alloy corrosion. These effects originate from the potential difference between the two phases caused by different element segregation. According to Table 1, when annealed at 700 ℃, the element segregation between the two phases of the alloy is the largest. With the increase of temperature, the solute atoms disperse more widely, leading to a reduction in the degree of alloy element segregation,

and the role of micro area primary battery is weakened, thus improving the corrosion resistance of the alloy. Moreover, the change in the volume fraction of β phase can also affect the corrosion resistance of the alloy. From Fig.2, it can be seen that the volume fraction of β phase increases with the increase of annealing temperature. At this time, the enrichment of high corrosion resistant elements Ni and Nb in the β phase will also improve the corrosion resistance of the β phase. When the annealing temperature reaches 900 and 920 ℃, the β phase becomes the predominant component of the microstructure. At this point, the microstructure of the alloy is mainly composed of highly corrosion-resistant of β phase, which has high corrosion resistance.

Conclusions

The corrosion and passivation of TC4-0.5Ni-0.5Nb alloys in NaCl and HCl solutions at different annealing temperatures (700, 750, 800, 850, 900 and 920°C) were investigated. The following conclusions can be drawn from the study:

The alloys annealed at different temperatures exhibit spontaneous passivation behavior in NaCl solution, and exhibit active passive behavior of incomplete passivation in HCl solution.

The open circuit potential and potentiodynamic polarization curves revealed that the corrosion resistance of the alloy increases with the increase of annealing temperature. The alloy annealed at 700°C exhibited inferior corrosion behavior, while alloys annealed at 900°C and 920°C exhibit excellent corrosion resistance.

The grain size, the volume fraction of β phase and distribution of alloy elements in α and β phase are the main factors that influenced the corrosion resistances of the alloys annealed at different temperatures.

References

1. Shadravan A, Amani M. HPHT 101-what petroleum engineers and geoscientists should know about high pressure high temperature wells environment[J]. Energy Science and Technology, 2012, 4(2): 36-60.
2. Schutz R W, Baxter C F, Boster P L, et al. Applying titanium alloys in drilling and offshore production systems[J]. Jom, 2001, 53(4): 33-35.
3. Thomas R. Titanium in the geothermal industry[J]. Geothermics, 2003, 32(4-6): 679-687.
4. Kane R D, Srinivasan S, Craig B, et al. A comprehensive study of titanium alloys for high pressure high temperature (HPHT) wells[C]. Corrosion 2015 Conference Expo. NACE International, 2015: 5512-5527.
5. Pye D S, Holligan D, Cron C J, et al. The use of beta-c titanium for downhole production casing in geothermal wells[J]. Geothermics, 1989, 18(1-2): 259-267.
6. Schutz R W, Watkins H B. Recent developments in titanium alloy application in the energy industry[J]. Materials Science and Engineering: A, 1998, 243(1-2): 305-315.
7. Ueda M, Kudo T, Kitayama S, et al. Corrosion Behavior of Titanium Alloys in a

Sulfur-Containing HS CO Cl Environment[J]. Corrosion, 1992, 48(01): 79-86.
8. Ge J P, Guo J N, Yu Y, et al. Effect of annealing temperature on the microstructures and impact toughness of Ti-6Al-4V-0.5 Ni-0.5 Nb titanium alloy plates[C]. Journal of Physics: Conference Series. IOP Publishing, 2023, 2454(1): 012014.
9. Yuan L, Wang W, Li Y, et al. Effect of annealing temperature on texture and residual stress of Ti-6Al-4V alloy seamless tubing processed by cold rotary swaging[J]. Vacuum, 2020, 177: 109399.
10. Debta M K, Bishoyi B D, Sabat R K, et al. Microstructure and texture evolution during annealing of Ti–6Al–4V alloy[J]. Materials Science and Technology, 2020, 36(4): 1-8.
11. Dong E, Yu W, Cai Q, et al. Effects of β grain-growth behaviors on lamellar structural evolution and mechanical properties of TC4–DT alloy[J]. Materials Research Express, 2020,7(6): 66514.
12. Yang X W, Dong X R, Li W Y, et al. Effect of solution and aging treatments on corrosion performance of laser solid formed Ti-6Al-4V alloy in a 3.5 wt.% NaCl solution[J]. Journal of Materials Research and Technology, 2020, 9(2): 1559-1568.
13. Li J Q, Lin X, Wang J, et al. Effect of stress-relief annealing on anodic dissolution behaviour of additive manufactured Ti-6Al-4V via laser solid forming[J]. Corrosion Science, 2019, 153: 314-326.
14. Yang Y , Xia C , Feng Z ,et al.Corrosion and passivation of annealed Ti-20Zr-6.5Al-4V alloy[J].Corrosion Science, 2015, 101:56-65.
15. Liu Q, Liu H, Xie J, et al. Influence of Ru on structure and corrosion behavior of passive film on Ti-6Al-4V alloy in oil and gas exploration conditions[J]. Scientific Reports. 2022, 12(1): 16586-16614.
16. Schutz R W, Lower-cost ruthenium-enhanced titanium alloys for severe chemical service[J]. Platinum Metals Review, 1996, 40(2): 54-61.
17. Atapour M , Pilchak A , Frankel G S ,et al. Corrosion Behavior of Ti-6Al-4V with Different Thermomechanical Treatments and Microstructures[J].Corrosion -Houston Tx-, 2010, 66(6):065004.
18. Yu S Y, Brodrick C W, Ryan M P, et al. Effects of Nb and Zr alloying additions on the activation behavior of Ti in hydrochloric acid[J]. Journal of the Electrochemical Society, 1999, 146(12): 4429-4438.
19. Metikos-Huković M, Kwokal A, Piljac J. The influence of niobium and vanadium on passivity of titanium-based implants in physiological solution[J]. Biomaterials, 2003, 24(21): 3765-3775.

Corrosion Fatigue Testing of a Titanium Alloy for Sub-Sea Riser Systems

William D. MacDonald, Titanium Metals Corp., Henderson, USA

Mike Hogan Mikel Hogan, Oil States Industries, Arlington, TX

Fassett Hickey, Southwest Research Institute, San Antonio, TX

TIMETAL® 475 has been under development for use a as a capable but lower cost alternative to ASTM Grade 29 (R56404), an alloy that had been used for sub-sea stress risers many years. Following successful initial corrosion testing in NACE TM-0177 Level VII at elevated temperatures (1), further experiments were performed to determine the corrosion fatigue behavior. Results of fatigue testing in air as compared to results in NACE A + CP environment show that the alloy has sufficient capability to meet demanding sub-sea requirements. In addition, corrosion fatigue and slow stress rate tests in environment will presented and compared to existing data sets for Grade 29.

(1) *"Corrosion Behavior of a New Titanium Alloy for Geothermal Casing", W.D MacDonald EuroCORR 2022 Berlin*

Reeled pipelines: a methodology to qualify cold deformed pipelines according to NACE MR0175/ISO 15156.

Riccardo Rizzo, DNV AS, Thormølensgate 49a Bergen, 5006 Norway; presenting Author.

Bjarte Lillebø, DNV AS, Thormølensgate 49a Bergen,5006 Norway.

Stefan Marion, DNV AS, Veritasveien 1Høvik, 1363 Norway.

Karl Gunnar Solheim Subsea 7 Norway AS, Kanalsletta 9 Stavanger, 4033 Norway

Pipelines installed by reeling are subjected to a small amount of plastic deformation during installation because they are fabricated onshore, reeled on to a large reel on the installation vessel and subsequently reeled off on the installation site offshore. This plastic deformation can affect the resistance to SSC and/or SCC of the pipeline. This paper presents a technique to simulate the effect of the reeling during the sour service qualification of pipeline material. The specific work focuses on UNS 31603 lined and clad pipes. The methodology can be generalized to other materials. This approach is in line with DNV ST-F101 and DNV RP-F108. The methodology is described, and the learnings are discussed.

Pitting corrosion of stainless in brines – use of statistical analysis to evaluate the influence of viscosifying polymer

Clément BOISSY, MECM, Solaize/France ;
Vincent MARTIN, MECM, Solaize/France ;
Julien BONNIER, SNF, Andrézieux/France ;
Christophe RIVAS, SNF, Andrézieux/France ;

Enhance Oil Recovery permits to improve the efficiency of crude oil extraction. This technique consists of addition of viscosifying polymer to the brine injected into the reservoir. Different kind of polymers are industrially used and may be composed of acrylate and polyacrylamide. This anionic polymer may have an impact on the corrosion which has been proven on carbon steel. Stainless steel being more and more used, especially for injection skids, influence of such addition on pitting corrosion needs to be enlighten. Pitting corrosion being a stochastic phenomenon, statistical analysis is required and several theories have been proposed in the past in terms of discrimination between initiation sites. Based on these, the normal distribution of each family of initiation site is determined. This complete statistical analysis is compared to the corrosion potential in order to evaluate the risk of pitting corrosion. The basic analysis in terms of average and standard deviation may not be sufficient to explain the behavior of 316L in saline solution.

Objective

In terms of methodology, the comparison between the classic statistical analysis and the complete one permits to demonstrate that complete evaluation is more accurate to understand the pitting corrosion of 316L. The analysis has been done in different brines (from 0.056 mol/L to 4.09 mol/L of NaCl), in deaerated solutions, at 46 °C. Conditions has been chosen in order to be representative of some specific industrial fields. The influence of polymer additions is also investigated.

New results

The comparison between basic and complete statistical analysis permit to demonstrate that using only average and standard deviation may lead to misinterpretation of electrochemical data if several families of initiation site are coexisting at the surface of 316L. This phenomenon can be explained by the necessary limited size of the

samples. The influence of chloride concentration is determined for each initiation site. Linear evolution according to logarithm of chloride concentration is found but the slope depends on the family considered. A criterion in order to compare pitting potential statistic and open circuit potential is discussed in order to determine the criticality of each configuration. The influence of a commercial product composed of acrylate and polyacrylamide is discussed for each family over chloride concentration. At low chloride concentration, the viscosifying polymer may slightly decrease pitting potential, however, at such low concentration, the risk of spontaneous pitting corrosion can be considered as approaching zero (even with polymer). At higher concentration, when the risk of pitting corrosion increases, viscosifying polymer leads to a decrease of pitting potential but evolution of average and standard deviation of corrosion potential permits to demonstrate that the risk of pitting remains very low.

Conclusion

Present work permits to demonstrate the necessity to consider complete statistical analysis in order to accurately elucidate the influence of chloride concentration on pitting corrosion of 316L in deaerated solution. Two different initiation sites have been observed, each of them follows a different behavior according to chloride concentration. Viscosifying polymer does not modify the risk of pitting at lower concentration but, at higher chloride concentration, it helps to limit or avoid pitting corrosion on stainless steel. Viscosifying polymer permits to improve oil recovery which is its primary function but also limits pitting corrosion of 316L stainless steel when conditions are the most severe.

Evaluation of long-term corrosion behavior of CRA in CCS well environments

T. SUNABA, H. MIZKAMI, INPEX TRC, Tokyo/Japan,
H. MATSUI, J. GLIMOUR, V. HOSSEINI, INPEX Australia, Perth/Australia

Carbon capture and storage (CCS) is an attempt to reduce CO_2 emission after burning oil, gas, coal and associated CO_2 from oil & gas reservoir before it enters the atmosphere, and to store CO_2 underground. Typical storage of the CO_2 is in deep geological formations, depleted gas fields and aquifers. In addition, it is necessary to store CO_2 for an extremely long time, say 1000 years. Corrosion of well construction materials is one of the risks that some CO_2 might leak the ground. From viewpoint of material side, severe CO_2 corrosion should be considered for carbon steel and, stainless steel is necessary to consider two types of corrosion: general corrosion and localized corrosion.

In this study, immersion tests were performed to evaluate the long-term corrosion behavior of CRA OCTG materials.

Immersion tests

Immersion tests were performed in simulated CCS reservoir conditions by an autoclave equipped rotating cage. Test materials were 25Cr Duplex Stainless steels (DSS), 22Cr DSS, DP25U DSS and Super 13Cr SS. Test specimen (50mm x 10mm x 2 mm^t) was machined from actual OCTG tubing pipe and polished up to #600 by SiC paper. Test conditions, test temperature: 96ºC, Test solution: 55,000/80,000 ppm Cl^- + 0.4 wt.% CH_3COONa modified NACE solution, partial pressure of CO_2: 3.0 MPa, pH: 3.70, Flow rate: 0.1m/s, Test duration: 7, 30, 90 days. In addition, effect of small amount of H_2S was evaluated by four point bend beam test.

From test results, the calculated corrosion rate of S13Cr SS was approximately 0.001mm/y and DSSs were 0.0001mm/y by 90 days long term immersion. However, pitting corrosion was observed on S13Cr SS surface tested 90 days CO_2 and 30 days CO_2 + H_2S condition. It is considered that presence of H_2S causes pitting corrosion due to the effect of breaking the passive film. In contrast, DSS materials were stable in these conditions.

Elastic and Plastic Testing of Heavily Cold Formed 22Cr Duplex Stainless Steel Exposed to Liquid Mercury to Assess Liquid Metal Embrittlement Susceptibility

William Kovacs III, DNV, Dublin USA; Bjørn-Andreas Hugaas, AkerBP, Oslo Norway; Kristian Eriksen, AkerBP, Stavanger Norway; Stian Hauger, Aker Solutions, Trondheim Norway

AkerBP is planning to drill four wells (two in the Farsund and two in the Ula reservoir) during the first phase of the Valhall PWP – Fenris project, see Figure 1 and Figure 2. Early wireline chamber measurements indicate a maximum mercury content of 27.9µg/Sm^3. By applying conservatism on these measurements, results from modelling work indicates that some mercury will condense as a separate liquid phase during operation.

The project plans to install cold formed 22Cr duplex stainless steel bends topside. Existing literature suggests that while 22Cr may not be generally susceptible to Liquid Metal Embrittlement (LME) when exposed to mercury[1,2,3], heavily cold formed 22Cr materials may be susceptible[4]. Note that there have only been a few literature publications related to mercury exposure of typical Corrosion Resistant Alloys (CRAs) like 22Cr. A significant fraction of these publications is also reliant on slow strain rate test results only. This test method is useful for screening for susceptibility but may impart stresses that are unrealistic for engineering applications.

Due to the uncertainty with regard to the behavior of 22Cr in mercury, it was decided to run an experimental program assessing how cold formed 22Cr performs when exposed to liquid mercury. As part of this test program, four-point bend, slow strain rate testing, and interrupted slow strain rate testing were undertaken. The methods were chosen to simulate a range of strains from primarily elastic deformation of as-produced / as-welded pipe to high plastic deformation of cold formed pipe. The

[1] Drake, D.E., Sutanto, H., Colwell, J.A., Stiegelmeyer, W.N., Corrosion 90, 1990, (Paper # 57).
[2] Colwell, J.A., Stiegelmeyer, W.N., Drake, D.E., Sutanto, H., Corrosion 90, 1990, (Paper # 58).
[3] Wasson, A., Russ, P.R., Asher, S., Mercury Liquid Metal Embrittlement Testing of Various Alloys for Oil and Gas Production. CORROSION 2013, March 17-21, 2013, (Paper # 2519).
[4] Case, R., McIntyre, D.R., Mercury Liquid Metal Embrittlement of Alloys for Oil and Gas Production and Processing. CORROSION 2010, March 14-18, 2010, (Paper # 10294).

material of interest was prepared from welded pipe. Specimens were selected from the base metal, the weld metal / heat affected zone (HAZ), and from pre-strained material simulating cold forming. The testing was conducted in the presence of mercury (only) at both ambient temperature and 40 °C. The passive film was intentionally disrupted by scratching at the initiation of the tests. The results of this testing did not indicate evidence of LME for any of the material / environment conditions tested.

The results will be discussed further with regard to how they relate to other published literature on CRAs exposed to mercury at engineering/qualification strains.

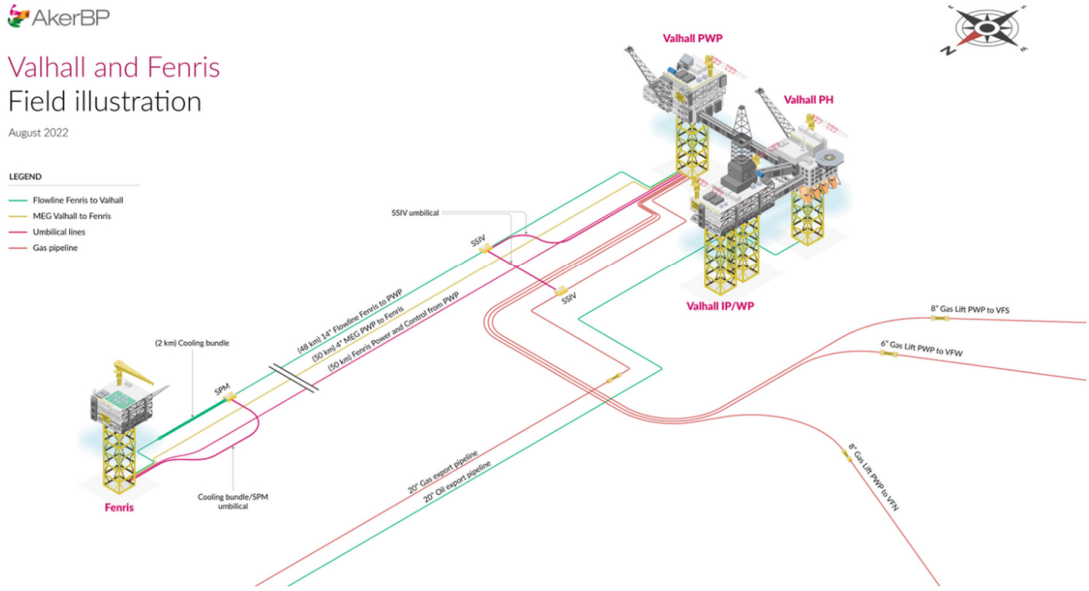

Figure 1: Valhall and Fenris Field Illustration

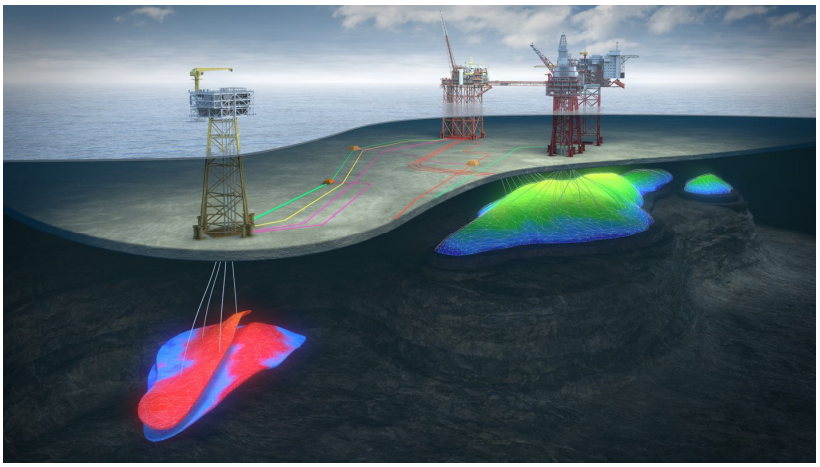

Figure 2: Fenris and Valhall Platform Illustration

Corrosion Behaviour of Martensite-Based Stainless Steels in Simulated Downhole CCS Environments

Kenichiro Eguchi, JFE Steel, Handa/Japan, Yuichi Kamo, JFE Steel, Handa/Japan, Hiroyuki Takai, JFE Steel, Handa/Japan, Tsuyoshi Yoneyama, JFE Steel, Dubai/UAE

Carbon Capture and Storage (CCS) is considered to be an effective countermeasure for global climate change, leading to a sharp growth in the number of CCS projects under planned and development. Stainless steels, especially 13Cr to 17Cr martensitic stainless steels have been applied for downhole tubing in high temperature and high CO_2 pressure conditions since they have high corrosion resistance in that environment. In CCS application, impurities such as O_2, SO_x and NO_x are expected to be included in the CO_2 gas stream, increasing the severity of the corrosive environment, yet published literature concerning corrosion behaviour in CCS application is very limited. The objective of this paper is to investigate the corrosion behaviour of martensite-based stainless steels in simulated downhole CCS environments.

Martensite-based stainless steels ranging from 13Cr to 17Cr were subjected to corrosion tests at various levels of temperature, chloride (Cl-) ion concentration and CO_2 partial pressure. In order to investigate the effect of impurities on the corrosion behaviour, O_2, SO_2 and NO_2 were added in some conditions. Crevice corrosion test specimens, simulating the tubing connection interfaces, were also prepared and evaluated.

Test results showed that oxygen contamination in a pure CO_2 environment caused an increase in corrosion severity. Under the conditions of 100 degrees C and 121,200 ppm Cl-, no pitting corrosion was observed with Modified 13Cr in pure CO_2 (19 MPa), but pits were observed when 53 ppm of oxygen was added. Under the same conditions, 15Cr steel and 17Cr steel did not show any pitting and the corrosion rate was as low as 0.002 millimetres per year (mm/y). In some environments containing SO_2 and NO_2, pitting occurred with Modified 13 Cr. Additionally, the influence of bicarbonate (HCO_3^-) ions and test duration on corrosion behaviour will be also presented and discussed.

Electrochemical and Rotating Cage: development of test protocol to evaluate corrosion under erosion condition replicating shale oil and gas production environment

Merlin C. E. Bandeira, Rogaciano M. Moreira, Felipe R. Assunção, Isabel M. Mattos, Oscar R. Mattos

LNDC – UFRJ, Rio de janeiro - Brazil

Lelio A. da Silva

YPF – Buenos Aires - Argentina

Luciana Lima

Vallourec, Aulnoye-Aymeries – France

Lívia Mangualde, Pedro Filgueiras

Vallourec, Belo Horizonte – Brasil

Kevin Schleiss

Vallourec, Houston - USA

Introduction

Argentina Vaca Muerta holds the second-largest shale gas and fourth-largest oil deposits in the world, with a daily production of around 90 million m^3 of gas and 300 thousand barrels of oil. The exploitation from shale formations requires as prior process the hydraulic fracking, in which the bedrock is fractured to allow the flow of fluids into the well. This process involves the injection of high-pressure fluids, composed by water, sand – tons per drilled foot, and other proppants. As a part of this sand returns through the well during production phase, mixed with the production fluid, the tubing string might be subjected to erosion. In several wells, where pipes in corrosion-resistant alloys are installed due to high contents of CO_2 and temperatures reaching 140°C and above, this erosion becomes a concern due to the risk of breaking the material passive layer and undermines corrosion resistance.

Goal

To develop laboratory test methodology that mimics, as far as possible, field condition on shale gas production, to evaluate the influence of erosion on corrosion resistance performance of tubular goods.

Methodology and Results

More than only estimate corrosion rates in each condition, it is important to understand the material corrosion susceptibility and its ability to repassivate. Therefore, the test protocol development reported here, designed an experimental setup able to perform simultaneously Rotating Cage (RC) test and electrochemical measurements such as: Open Circuit Potential (Eocp), Linear Polarization Resistance (LPR), Electrochemical Impedancy Spectroscopy (EIS) and Cyclic Potentiodynamic Polarization (CPDP). It was possible to compare the impact of erosion on material corrosion susceptibility by evaluating changes on LPR, EIS, Pit potential and Repassivation Potential. From RC tests, where the studied material was in dynamic condition (1,000 RPM), the flat coupon geometry gives good condition to evaluate both general and localized corrosion.

The critical points of this methodology development were:

1st Keep particles in suspension: task was to find the RC appropriate geometry to avoid trap sand over the cage or in the bottom of autoclave.

2nd Guarantee the homogeneity of particles (sand) distribution. To optimize laboratory test erosional regime, several visual pre-tests were performed, and a video will be presented to illustrate the harsh environment of such tests.

3rd Acquire stable electrochemical measurements even with such high particles' concentration.

The tests were carried out in an autoclave at 300 bar of total pressure with 10 bar of CO_2 and 1.2 mbar of H_2S partial pressure and balance of nitrogen; particles concentration of 50g/L, salinity around 260,000 ppm, stir velocity of 1,000 RPM and temperature of 115^{o}C.

The experimental setup allows to test simultaneously in autoclave: static electrochemical coupon and RC test in multiphase, HPHT conditions After optimization of test protocol, two set of tests were performed: reference test without sand, and erosion test with sand, both at condition described above. Based on electrochemical results, it was possible to evaluate the erosion influence on corrosion performance of S13CR, mainly the ability of oxide layer to repassivate on erosion environment No intense erosion attack, nor localized corrosion was observed through RC test with sand.

Investigation of Acetic Acid Transport in Top-of-the-Line Corrosion

Sondre Borg Gjertsen,
Institute for Energy Technology (IFE),
Kjeller/Norway

Marc Singer, Maryam Eslami* & Mengqiu Pan
Institute for Corrosion and Multiphase Technology,
Department of Chemical & Biomolecular Engineering, Ohio University
Athens/Ohio/USA

Tor Hemmingsen,
University of Stavanger (UiS),
Stavanger/Norway

Abstract

Acetic acid is a volatile species that can often increase corrosion in carbon steel pipelines transporting natural gas. Mitigating corrosion caused by a corrosive aqueous liquid dewing on the carbon steel wall, termed top-of-the-line corrosion (TLC), is a difficult problem. Therefore, it is important to develop a solid understanding and corrosion prediction models that accurately account for the presence of acetic acid during condensation.

The presented work focuses on the transportation of acetic acid from a bulk solution to a top-of-the-line condensing liquid in a glass cell setup. The transport of acetic acid to the condensing liquid was studied by varying the total acetic acid concentration and pH in the bulk solution. Experiments carried out with 1018 carbon steel specimens gave insights into how acetic acid increased the TLC rate and the acetic acid concentration in a condensing liquid. Experiments with stainless steel specimens showed that the corrosion reaction influences the transport of acetic acid to the top-of-the-line condensed liquid and that the transport seems fast enough to establish equilibrium.

* Now: University of Illinois at Urbana-Champaign

Introduction

Top-of-the-line corrosion (TLC) is a problem in operating unprocessed natural gas transport pipelines. Unprocessed natural gas is usually hot (90-120 °C) when it enters a pipeline from the wellhead. Water vapor and corrosive species, specifically CO_2, H_2S, and organic acids are also commonly carried in the gas fluid stream from the well. When the gas cools down due to the heat exchange with pipeline surroundings, it gives rise to an aqueous corrosive phase condensing on the steel walls. TLC problems have been documented since the 1960s, and over recent decades interest in investigating the phenomena involved has significantly risen [1].

TLC occurs in multiphase pipelines operated with a stratified flow regime. Under stratified flow, a condensed phase forms and hangs on the top-of-line (TOL) pipe wall as droplets or a liquid film [2]. The TOL condensation rate and the chemistry of the condensed phase are critical to the TLC rate[2, 3]. As mentioned above, CO_2 and H_2S are corrosive species that strongly influence the corrosion rate. However, this paper focuses on the effect of acetic acid on TLC. Among the organic acids, acetic acid (HAc) is especially known to increase TLC because of its low dissociation degree and high volatility. It is also the most commonly encountered organic acid in oil and gas production. In multiphase pipelines, the speciation and pH of the bottom-of-line (BOL) liquid phase are essential for determining the HAc content in the gas and condensed phase. This is because only the undissociated acid evaporates to the gas phase and condenses or dissolves into the top-of-line condensed liquid. Hence, smaller amounts of acetic acid will reach the TOL condensed phase with higher pH in the bottom-of-line solution stream due to its pH-related dissociation into acetate ions (Ac^-), following *equation (1)*:

$$CH_3COOH_{(aq)} \rightleftharpoons CH_3COO^-_{(aq)} + H^+_{(aq)} \qquad \frac{a_{H^+} \times a_{Ac^-}}{a_{HAc}} = K_{HAc} \qquad (1)$$

Here, K_{HAc} is the dissociation constant for HAc and a_i is the activity of a given species. Acetic acid is a weaker acid than, for example, formic acid. Hence, a larger amount of acetic acid species will remain undissociated (HAc_{free}) and be able to evaporate at the same pH. HAc is known to enhance the corrosion of carbon steel by mainly enhancing the limiting current of the cathodic part of overall electrochemical reactions [4, 5]. This is the same contribution as the other mentioned

corrosive species, CO_2 and H_2S [6]. An effect caused by HAc to retard the anodic part has been reported [4]. Acetic acid is also known to increase localized attacks and decrease the solubility of iron carbonate, diminishing surface layer formation and protectiveness of iron carbonate [7, 8]. There are papers discussing and investigating how the acetic acid concentration develops in the condensed phase ($[HAc_{free}]_{cond}$) during condensation [9, 10]. However, there are still limitations and issues with models predicting TLC when acidic acid is present in the pipeline system [11]. This paper looks at how the $[HAc_{free}]_{cond}$ and total HAc in the condensed phase ($HAc_{free} + Ac^-$, referred to as $[HAc_{total}]_{cond}$) change with changing the acetic species concentrations in a bulk solution ($[HAc_{free}]_{bulk}$ and $[HAc_{total}]_{bulk}$).

Experimental

A 4 L glass cell setup for TLC experiments, allowing steel specimens to be mounted in the lid over a bulk solution, was used in these experiments [12]. A plastic cup was aligned directly under the steel specimens to collect the condensed liquid dripping from its surface. A tap on the outside of the glass cell allowed the extraction of the collected drops. The collected condensed phase was extracted twice daily and used for spectrophotometric ferrous ion [Fe^{2+}] measurements and titration for evaluating the HAc concentration. The specimen materials were 1018 (UNS G10180) carbon steel and 304-stainless steel (AISI 304). The specimens had diameters of 3.14 cm and thickness (height) of 1.15 cm, the area exposed to the gas phase was 7.8 cm^2.

The specimens were cylindrical and mounted to the lid by a specially designed sample holder. The sample holder was connected to a thermostatic bath controlling the specimen temperature to 60 °C. A thermocouple was used to measure the specimen's backside temperature. Measurements varied from 57 °C to 62 °C throughout the experiments. A hot plate connected to a thermocouple heated and kept the bulk solution at a reasonably stable temperature of 75 °C. A reflective insulation foil was used to reduce the temperature gradient between the glass wall and the gas phase. This measure helps with temperature control and reduces unwanted condensation on the glass. A thermocouple intruding from the lid to the middle of the gas phase (halfway between the solution and the lid) measured the gas temperature at that location, varying from 64 °C to 68 °C throughout all the experiments. Each experiment lasted about two days (45 - 50 hours). A pH-electrode was used to monitor the bulk solution pH during the experiments and to ensure the

solution had the target pH before starting the experiments. The pH value typically increased by 0.1 - 0.2 units during the experiment periods.

After the initial assembly of the TLC glass cell apparatus, electrolyte solutions (the bulk solutions) were prepared using technical-grade chemicals dissolved in deionized (DI) water, according to the experimental matrix in *Table 1*. The bulk solution was sparged with nitrogen (N_2) gas for at least 1 hour and had a stable pH and temperature before a specimen was installed, representing the experiment's start. The specimen's surface exposed to the gas phase was prepared using these steps: 1. Polish using progressively finer silicon abrasive paper up to #600 grit. 2. Wash with DI water and isopropanol 3. Rinse in an ultrasonic bath with isopropanol for 5 minutes. 4. Dry using an air blower.

Five experiments were carried out to examine 1018 carbon steel specimens (referred to as corroding systems) and two experiments using 304 stainless steel specimens (non-corroding system); at least two repeated parallels of each experiment were done. The total bulk solution HAc concentration ($[HAc_{total}]_{bulk}$) varied exponentially from 5 mM to 500 mM for the corroding system (1018 steel). For the two non-corroding experiments (304 stainless steel), $[HAc_{total}]_{bulk}$ was set at 5 mM, with similar chemistry to the two corroding experiments. The bulk solution composition had acetic acid (HAc) and sodium acetate trihydrate ($NaAc*3H_2O$) added in ratios to yield pH values of about 4.4 or 6.2 in the bulk solution. These experiments were designed to investigate how varying $[HAc_{free}]_{bulk}$ affects the HAc transport through the gas phase and TLC. The $[HAc_{free}]_{bulk}$ was varied by varying the $[HAc_{total}]_{bulk}$ or the bulk solution pH.

Table 1. *Experimental matrix with added sodium acetate salt and acetic acid concentrations in the bulk test solutions, sparging gas, and calculated solution pH.*

Experi-ment code.	Steel type	$NaCH_3COO$/ mg/kg	CH_3COOH/ mg/kg	$[HAc_{total}]_{bulk}$/ mM	Sparge gas	pH @75 °C
H-1	carbon steel	13577	20088	500	N_2	4.4
H-2	carbon steel	1358	2009	50	N_2	4.4
H-3	carbon steel	3946	114	50	N_2	6.2
H-4	carbon steel	136	201	5	N_2	4.4
H-5	carbon steel	395	11	5	N_2	6.2

H-4-s	stainless steel	136	201	5	N_2	4.4
H-5-s	stainless steel	395	11	5	N_2	6.2

Specimens were weighed before and after the experiments to determine average corrosion over the experiment duration. Specimens were thoroughly rinsed with isopropanol immediately after extraction from the glass cell, and corrosion products and iron carbide leftovers at the surface were removed using the Clarke solution procedure according to ASTM Standard G1-03. The average corrosion rate in the period between two extractions of condensed liquid samples was determined by the amount of Fe^{2+} released by the corrosion. Each extracted sample of the condensed liquid was weighed to determine the average condensation rate (WCR) for that respective period. In addition to the spectrophotometry, most of the extracted liquid sample was used to perform titration using a potentiometric titrator (Hanna Instruments #HI931) with stirring, automatic burette, and pH electrode. Titration rate and range were selected based on previous studies [13]. The titrant was 0.1 M NaOH, and the extracted sample was diluted with DI water into a 100 ml titrant solution. The pH response data from the titrations were used to determine $[HAc_{free}]$, $[HAc_{total}]$, and $[Ac^-]$ in the condensed liquid sample.

Results

As stated above, experiments were carried out to analyse the relationship between the condensation rate (WCR), corrosion rate (CR), and chemical composition of condensed liquid samples on steel specimens in a glass cell setup. The $[HAc_{free}]_{bulk}$ and $[HAc_{total}]_{bulk}$ varied over the experiments. The $[HAc_{free}]_{bulk}$ is pH dependent and will therefore impact the $[HAc_{free}]_{cond}$ [3]. This effect can be seen in the corrosion rate and $[HAc_{free}]_{cond}$ measurements. In the reported results, the $[HAc_{free}]$ was a more determining parameter than solution pH. Hence, most of the reported findings are shown relative to $[HAc_{free}]_{bulk}$.

The measured corrosion rate increased with higher amounts of $[HAc_{free}]_{bulk}$ (*Figure 1 (a)*). This was expected and in line with earlier studies [8]. In order to isolate the effect of acetic acid concentration, the experimental conditions were kept constant during the testing; the bulk solution and specimen temperature were not changed over the campaign. *Figure 1 (b)* shows that the measured WCR increased with $[HAc_{free}]_{bulk}$. With an increase in $[HAc_{free}]_{bulk}$ from 0.18 to 334.3

mM, the WCR increased by approximately 50% on average (from 0.3 to 0.46 mL/m^{2}s). The WCR strongly impacts the TLC rate [2, 3, 14]. However, the heat flux between the gas phase and the steel is expected to govern the WCR. Due to the consistent temperature setup, the observed variation in WCR was unexpected for these experiments. The WCR was generally higher in the corroding experiments than in the non-corroding experiments.

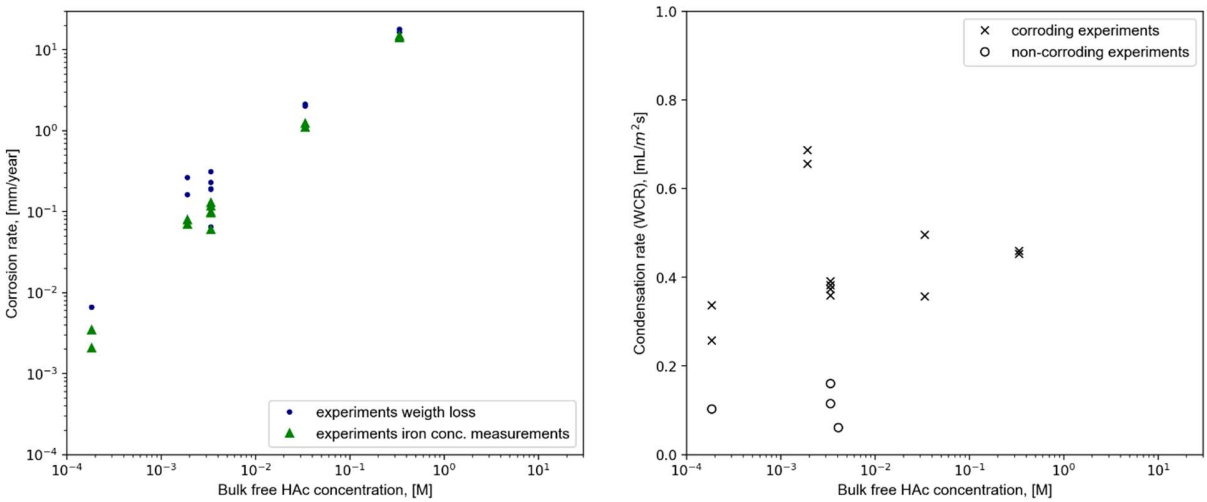

Figure 1: (a) Measured corrosion rate plotted against the $[HAc_{free}]_{bulk}$. (b) Condensation rate plotted against the $[HAc_{free}]_{bulk}$ for the corroding and non-corroding experiments.

Several reasons for the WCR-$[HAc_{free}]_{bulk}$ correlation can be proposed: experimental variability and increased condensation surface area. The surface area increases more drastically with higher corrosion rates due to more rapid changes in surface topography. The precipitation of corrosion products might also influence the surface area for condensation. Despite the mentioned trend of WCR with $[HAc_{free}]_{bulk}$, oddly high condensation rates were observed for the experiment with the second least $[HAc_{free}]_{bulk}$ of 1.897 mM (experiment H-4). As shown in *Figure 1 (b)*, the measured WCR was higher in both of the two repetitions of this experiment than those measured in other experiments. Both of the specimens had a porous black surface layer quite adhering to the specimen surface through washing with DI water and isopropanol (*Figure 3 (b)*). It should be mentioned that a porous black surface layer was always observed on the surface of specimens and even in the condensed liquid samples for all experiments (*Figure 2*). However, typically it was easily washed off.

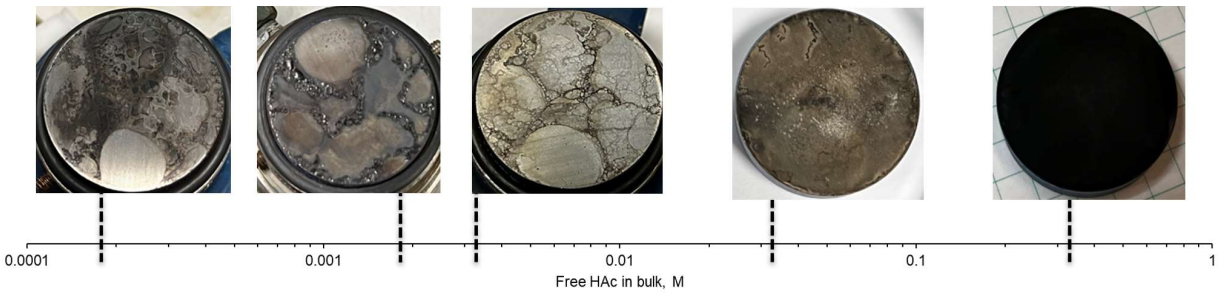

Figure 2: Images of the specimen surfaces after extracting at the conclusion of each experiment.

The condensation rates increased over the experiment durations for the corroding carbon steel experiments. This increase in condensation rate was more prominent when the corrosion rate was higher. The observed trends in this study substantiate that the changing surface topography and precipitation of corrosion products affect the condensation rate. Surface analysis by Raman spectroscopy of the H-4 specimens (*Figure 3 (a)*) indicated that the porous layer forming and sticking to the surface was magnetite (Fe_3O_4), a peak at 670 cm^{-1} is diagnostic for Fe_3O_4 [15]. The formation of Fe_3O_4 has been reported to form at higher temperatures in the iron-water system [16].

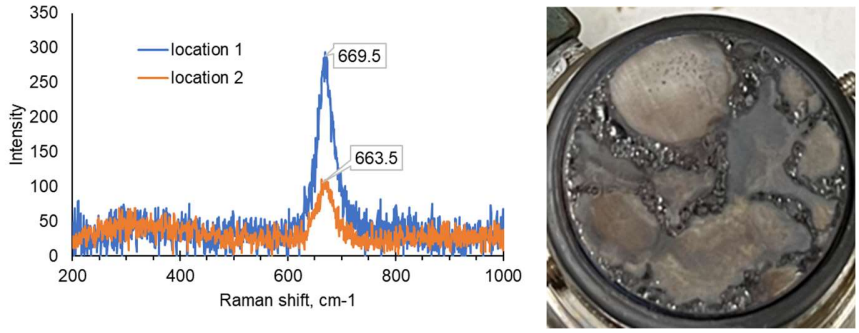

Figure 3: (a) The results from Raman spectroscopy analysis of the corroded specimen surface in experiment H-4. (b) Image of the corroded specimen after experiment H-4

Condensed phase chemistry

The chemistry of the condensed phase liquid was determined by titration and spectrophotometric measurements for ferrous ion concentration. The measured [Fe^{2+}] in the condensed liquid samples increased with increasing $[HAc_{free}]_{bulk}$ because of the increased corrosion rate. The correlation between more $[HAc_{free}]_{bulk}$ and increasing corrosion rate is clear and known for TLC [7, 8] and corrosion of steel samples immersed in a similar solution [4]. However, the corrosion reaction

increases the pH due to the release of ferrous ions into the solution. One could expect the opposite, i.e., that a higher $[HAc_{free}]_{bulk}$ could lead to a lower pH in the condensed phase (pH_{cond}) due to the higher $[HAc_{free}]_{cond}$. As shown in *Figure 4 (a)*, the assumption of decreasing pH_{cond} for the non-corroding experiments matched with the experiments (plotted as circles). When the $[HAc_{free}]_{bulk}$ was increased from 0.18 to 3.34 mM, the pH in the non-corroding system decreased from 4.1 to 3.6, which agrees with other studies [7, 10]. In the corroding experiments, the opposite trend was observed due to corrosion. The only exception was for the experiment H-1 with the highest $[HAc_{free}]_{bulk}$ (3.34 mM) and highest corrosion rates, where there was not a noticeable pH increase, possibly due to the formation of ferrous acetate ions (red dotted line in *Figure 4 (a)*). From the ratio between $[Ac^-]$ and $[Fe^{2+}]$ (*Figure 4 (b)*), it seems likely that the corrosion reaction is slower than the accumulation of Ac^- from the dissociation of acetic acid species (*equation (1)*) in the condensed phase at lower $[HAc_{free}]_{bulk}$. At higher $[HAc_{free}]_{bulk}$, it seems like the ratio converges at 2, which is the same ratio of $[Ac^-]$ and $[Fe^{2+}]$ products in reaction *equation (2)*. One may speculate if there is an equilibrium mechanism behind the converging $[Ac^-]/[Fe^{2+}]$ ratio, which could govern further corrosion rate increase at even higher content of HAc.

$$2CH_3COOH_{(aq)} + Fe_{(s)} \rightleftharpoons 2CH_3COO^-{}_{(aq)} + Fe^{2+}{}_{(aq)} + H_{2(g)} \qquad (2)$$

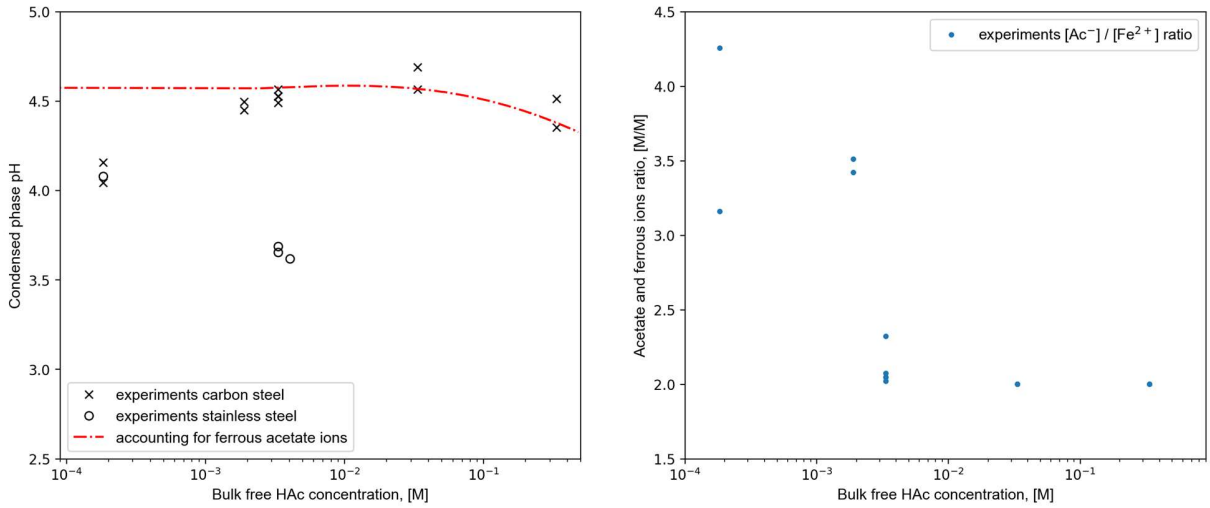

Figure 4: (a) pH in the condensed phase. The red dotted line is calculated pH accounting for the presence of complex ferrous acetate ions. (b) The ratio between Ac^- and Fe^{2+} ions in the condensed phase

The $[HAc_{free}]_{cond}$ was also higher than the $[HAc_{free}]_{bulk}$ (*Figure 5 (a)*), which indicates that the HAc transport is fast enough to support equilibrium concentrations in the condensed phase. The higher $[HAc_{total}]_{cond}$ for the corroding system than for the non-corroding system supports the observations of fast HAc transport mechanisms (*Figure 5 (b)*).

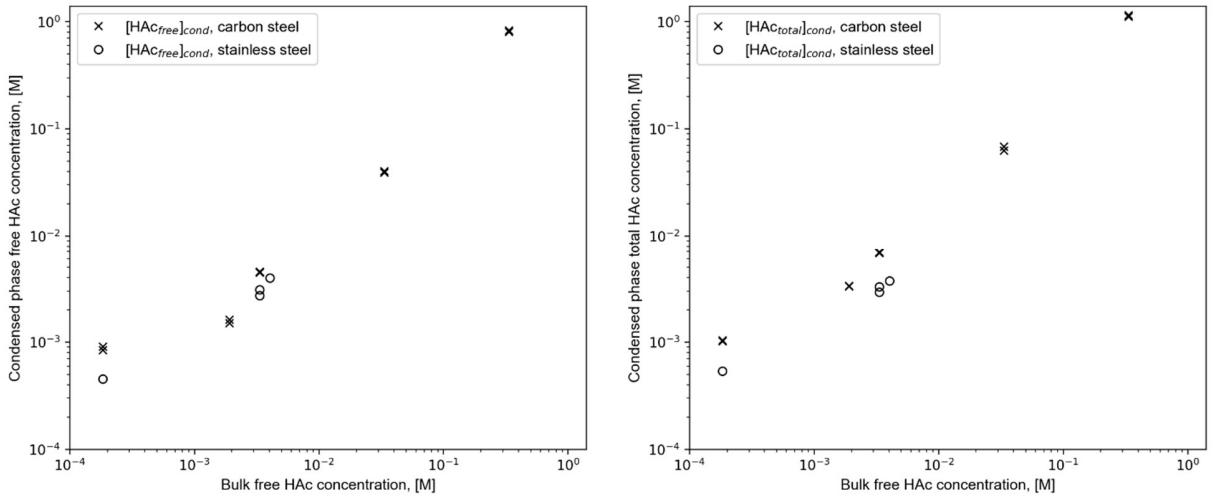

Figure 5: (a) $[HAc_{free}]_{cond}$ vs. $[HAc_{free}]_{bulk}$. (b) $[HAc_{total}]_{cond}$ vs. $[HAc_{free}]_{bulk}$

Conclusions

This study investigated how increasing amounts of acetic acid in a bulk solution can find its way and acidify a condensing liquid at a steel surface over the bulk solution. Increasing the undissociated acidic acid concentration in the bulk solution increases the transport of acidic acid to the condensed phase and its acetic acid concentration. The transport of acetic acid was fast enough to achieve what resembles equilibrium concentrations of acetic acid between the gas and the condensed phase. The corrosion rate increased with the condensed phase's increasing acidic acid content. The condensation rate was interestingly observed to relate to an increasing amount of acetic acid and corrosion rate.

Acknowledgments

This work was carried out while the author was on a stay as a Visiting Scholar at Ohio University as part of an ongoing Ph.D. study within the Joint Industry Project ModTLC at IFE with UiS as an academic partner. The author would like to acknowledge the support Dr. David Young provided

to arrange the stay and the financial support from Equinor ASA, A/S Norske Shell, and Chevron, as well as The Research Council of Norway (project nr 308774).

References

1. Al-Moubaraki, A. H. and Obot, I. B., *Top of the line corrosion: causes, mechanisms, and mitigation using corrosion inhibitors.* Arabian Journal of Chemistry, 2021. **14**(5): p. 103116.
2. Zhang, Z., Hinkson, D., Singer, M., Wang, H., and Nešic, S., *A mechanistic model of top-of-the-line corrosion.* Corrosion, 2007. **63**(11): p. 1051-1062.
3. Singer, M., *29 - Top-of-the-line corrosion*, in *Trends in Oil and Gas Corrosion Research and Technologies*, A.M. El-Sherik, Editor. 2017, Woodhead Publishing: Boston. p. 689-706.
4. Kahyarian, A., Schumaker, A., Brown, B., and Nesic, S., *Acidic corrosion of mild steel in the presence of acetic acid: Mechanism and prediction.* Electrochimica Acta, 2017. **258**: p. 639-652.
5. Kahyarian, A. and Nesic, S., *On the mechanism of carbon dioxide corrosion of mild steel: Experimental investigation and mathematical modeling at elevated pressures and non-ideal solutions.* Corrosion science, 2020. **173**: p. 108719.
6. Kahyarian, A., Brown, B., and Nesic, S. *Fundamental Mechanisms of Mild Steel Corrosion in H2S Containing Environments*. in *CORROSION 2019*. NACE, No. 12875.
7. Amri, J., Gulbrandsen, E., and Nogueira, R. P. *Role Of Acetic Acid In CO2 Top Of The Line Corrosion Of Carbon Steel*. in *CORROSION 2011*. NACE, No. 11329.
8. Singer, M., Camacho, A., Brown, B., and Nešić, S., *Sour top-of-the-line corrosion in the presence of acetic acid.* Corrosion, 2011. **67**(8): p. 085003-1-085003-16.
9. Andersen, T. R., Halvorsen, A. M. K., Valle, A., and Dugstad, A. *The Influence Of Condensation Rate And Acetic Acid Concentration On Tol-Corrosion In Multiphase Pipelines*. in *CORROSION 2007*. NACE, No. 07312.
10. Hinkson, D., Zhang, Z., Singer, M., and Nesic, S., *Chemical Composition and Corrosiveness of the Condensate in Top-of-the-Line Corrosion.* Corrosion, 2010. **66**(4): p. 045002-045002-8.
11. Svenningsen, G. and Nyborg, R. *Modeling of top of line corrosion with organic acid and glycol*. in *CORROSION 2014*. NACE, No. 2591.
12. Singer, M., Farelas, F., Belarbi, Z., Punpruk, S., and Jenkins, A. *Review of volatile corrosion inhibitors evaluation methods and development of testing protocols*. in *CORROSION 2019*. NACE, No. 13303.
13. Dreher, J. W., *Developing Methods for Proper Determination of Alkalinity in Oil and Gas Field Brines*. 2022, Ohio University.
14. Olsen, S. and Dugstad, A. *Corrosion under dewing conditions*. in *CORROSION 91*. Houston, TX: NACE, No. 472.
15. Hanesch, M., *Raman spectroscopy of iron oxides and (oxy) hydroxides at low laser power and possible applications in environmental magnetic studies.* Geophysical Journal International, 2009. **177**(3): p. 941-948.
16. Gao, S., Brown, B., Young, D., and Singer, M., *Formation of iron oxide and iron sulfide at high temperature and their effects on corrosion.* Corrosion Science, 2018. **135**: p. 167-176.

Chemical and structural information under corrosion films in undersaturated CO2 environments

Adriana Matamoros-Veloza[a,b], *Tomasz M. Stawski*[c], *Silvia Vargas*[d], *Anne Neville*[b]

[a] *Faculty of Engineering and Physical Sciences, University of Leeds, LS2 9JT, UK*

[b] *Institute of Functional Surfaces, School of Mechanical Engineering, University of Leeds, Leeds, LS2 9JT, UK*

[c] *Federal Institute for Materials Research and Testing (BAM), Richard-Willstatter-Straße 11, 12489 Berlin, Germany*

[d] *BP America, Inc., Houston, Texas 77079, United States*

For decades, we have accepted that corrosion in sweet environments involves the formation of a protective $FeCO_3$ as corrosion scale that dissolves if undersaturation conditions prevail; however, in this work we demonstrate that the effects on the integrity of steel is far more significant than the damage observed on the surface of the corrosion scale. We studied the dissolution of $FeCO_3$ of corrosion scales in sweet environments, under acidic and undersaturated conditions. Our results proved that dissolution of $FeCO_3$ involves the presence of an amorphous phase, the intermediate formation of $FeCl_2$ or $FeCl^+$, and the transient presence of a $Fe_2(OH)_2CO_3$-like phase.

The nature of the amorphous phase was identified as a mixture of retained γ-Fe and Fe_3C. Conditions that induce to dissolution affect not only $FeCO_3$ but α-Fe, and Fe_3C. We show that the lattice [10$\bar{2}$] from the $FeCO_3$ crystalline structure is the most affected, and the fastest to dissolve. Overall, partially broken α-Fe and Fe_3C structures prove the damage of material at the interface zone without evident damage on the corrosion scale. This evident damage of steel at the molecular scale was also manifested at the macro scale with pit depths of up to 250 μm. The impact of undersaturated conditions on the integrity of steel are more drastic than frequently reported in industrial operations of CO_2 transport industries that use cleaning procedures (e.g., acid treatment, pigging) as part of their operational activities.

Evolution of Corrosion Composite Layer for CO_2 corrosion Mitigation

Dilshad Shaikhah[ac], Wassim Taleb[a], Maalek Mohamed-Said[b], Bruce Cowe[b] and Richard Barker[a]*

[a]Institute of Functional Surfaces, School of Mechanical Engineering, University of Leeds, Leeds, LS2 9JT, United Kingdom

[b]TOTALEnergies, OneTech CSTJF, Avenue Larribau, F-64018 Pau, France

[c]School of Chemical Engineering, Soran University, 44008 Kurdistan Region, Iraq

**Correspondence: D.M.Shaikhah@leeds.ac.uk*

Abstract

The evolution of corrosion composite layer is investigated when microspheres of polystyrene applied in-situ during crystallisation of an iron carbonate ($FeCO_3$) corrosion product on X65 carbon steel surfaces in an aqueous CO_2 corrosion environment. We show the feasibility of microsphere intercalation into $FeCO_3$ crystal layer, which produces a composite structure with corrosion behaviour analogous to pure $FeCO_3$. The concentration optimisation, surface analysis, thickness and mechanical properties of newly formed composite $FeCO_3$ layers are characterised. The composite $FeCO_3$ layers are shown to offer unique physico-mechanical properties compared with naturally formed $FeCO_3$ layer.

CO_2 corrosion: Effect of carbonic species on the carbon steel dissolution mechanism – a discussion

Jéssica N. Cunha[1], Tatiana C. Almeida[2,3], Eliane D'Elia[1], Oscar R. Mattos[2]

1 IQ/UFRJ, Rio de Janeiro-RJ / Brazil.
2 LNDC/COPPE/UFRJ, Rio de Janeiro-RJ / Brazil.
3 UFF, Volta Redonda-RJ / Brazil.

CO_2 corrosion remains a problem in the oil and gas industry. In the pre-salt field in Brazil, CO_2 is present in high contents, and with it, the species formed in the H_2O-CO_2 system. Understanding the effect of the CO_2 and the ions generated by the interaction of this gas with water on carbon steel corrosion mechanism is important to improve the models that provide estimations of uniform corrosion rate.

The doubts about the action of CO_2 or HCO_3^- on steel surface can only be answered by using appropriate techniques for the study of reaction mechanisms. From electrochemical impedance measurements and based on calculations of faradaic impedance, Almeida *et al.*[1] demonstrated in a H_2O-CO_2 system that, if CO_2 was able to act on the free iron surface, producing $(FeCO_2)_{ads}$ as reported in the literature[2] its relaxations would appear as a capacitive loop. Thus, two consecutive capacitive loops should be seen. This diagram has never been observed, which means that the CO2 is not able to act on free iron surface. Nonetheless, if CO_2 or HCO_3^- are able to play any role in the anodic branch, it will be coupled with other anions role, such as chloride, since the anions have only influence in the capacitive faradaic loop, seen in the impedance diagram at lower frequency range.[3]

Considering the above, electrochemical impedance was used to investigate the effect of CO2 and bicarbonate anion on X65 carbon steel corrosion. An experimental methodology was performed to polarize anodically the system, with small and fixed quantities of chloride, in the presence and absence of CO_2 and in the presence and absence of bicarbonate, separating the chloride effect from any other that can be played by CO_2 or HCO_3^-. The pH was maintained constant at 4 throughout the duration of the experiment.

The preliminary results show that in general, the impedance has two faradaic loops: An inductive followed by a capacitive in a smaller frequency range. The inductive loop is associated with relaxation of FeOHads, relaxation of a specie from water, as shown by EPELBOIN and KEDDAM[4] for the first time. Therefore, for the studied corrosion media, with and without CO2, the impedance diagrams clearly showed that CO2 does not act directly on the free iron surface, even on the iron-water species. For the results with bicarbonate anion, the qualitative analysis of the electrochemical impedance diagrams also confirm that the inductive loop is not affected by the presence of bicarbonate, not competing for the free iron surface. Furthermore, this anion also did not influence the capacitive loop at lower frequencies, then, it did not act on the iron-water species in the corrosion potential. In order to guarantee such statements, measurements of electrochemical impedance at more anodic potential are carrying out in order to eliminate any influence of cathodic processes in this analysis. The first results, showed the same three loops already verified in the impedance at the open-circuit potential: a capacitive loop at higher frequencies and an inductive and capacitive loop at lower frequencies. The profile of the impedance diagrams, under different experimental conditions, remains the same, showing similarity of the corrosive process. An analysis of the literature shows that the impedance diagram for the saline medium deaerated with N_2 presented the same behavior for the iron immersed in a Na2SO4 solution at pH 4 seen in the study performed by Keddam *et al.*[4]. In more anodic potentials, in a region that precedes the pre-passivation characterized by the appearance of a shoulder in the anodic branch, two-time constants besides the capacitive loop at high frequencies attributed to the electrical double layer were observed, one of an inductive nature and the other capacitive in more low frequencies, which corroborate some of ours results.

The impedance results suggest that neither CO_2 nor HCO_3^- play additional role on carbon steel dissolution mechanism.

1. T.C. ALMEIDA, M.C.E. BANDEIRA, R.M. MOREIRA, O.R. MATTOS, “New Insights on the role of CO_2 in the mechanism of carbon steel corrosion”, *Corrosion Science*,120 (2017): p. 239.
2. NESIC, S., THEVENOT, N., CROLET, J.L., DRAZIC, D. M., “Electrochemical properties of iron dissolution in CO_2 solutions - basics revisited”, CORROSION/96, paper no. 3, (Houston, TX: NACE International, 1996b).
3. O.E. Barcia, O.R. Mattos, “The role of chloride and sulphate anions in the iron dissolution mechanism studied by impedance measurements”, ElectrochimicaActa 41 (1990) 1003–1009
4. EPELBOIN, I., KEDDAM , M., “Faradaic Impedances: Diffusion Impedance and Reaction Impedance”, Journal Electrochemical Society, v. 117, pp. 1052-1056, 1970.

Sweet corrosion in the Oil and Gas production: performance assessment of the Tafel-Piontelli model

Elena Messinese[1], Marco Ormellese[2], Andrea Brenna[3]

[1]Politecnico di Milano, Milan, Italy, elena.messinese@polimi.it
[2]Politecnico di Milano, Milan, Italy, marco.ormellese@polimi.it
[3]Politecnico di Milano, Milan, Italy, andrea.brenna@polimi.it

Abstract

Sweet corrosion is one of the main threats affecting the Oil&Gas production plants and is caused by carbonic acid in the transported fluid. The implementation of functional tools for the prediction of the corrosion rate of metals in acidic environments represents a powerful instrument in the design of a successful management strategy at the beginning and throughout the service life of every structure. The Tafel-Piontelli model is a mechanistic model developed with this purpose. Its theoretical foundations derive from one of the fundamental laws characterizing the kinetics of the corrosion process: the Tafel law. The environment in contact with the metallic surface is modelled as an acidic electrolyte with controlled water chemistry, in which hydrogen evolution is the dominant cathodic process. The two parameters describing the kinetics of the electrochemical processes, that are the cathodic Tafel slope and the cathodic exchange current density, are theoretically estimated and validated by comparison with the experimental results obtained via potentiodynamic polarization tests, conducted in weakly acidic solutions containing formic and acetic acid at different pH and temperature. The performance of the model in the assessment of the corrosion rate is tested by comparison with the experimental data derived from mass loss tests. The results are promising: the model is able to forecast with good approximation the corrosion rate in weak acids and its exponential trend with temperature and pH. Moreover, a comparison with industry-consolidated corrosion models is performed to test the predictive abilities of the model in the case of sweet corrosion attacks in Oil&Gas infrastructure at nominal operating conditions, resulting in a good fitting.

Keywords

Sweet corrosion; predictive model, oil and gas, weak acid, corrosion rate.

Introduction

The oil and gas industry is mainly affected by two severe corrosion problems: sweet corrosion and sour corrosion. Sweet corrosion refers to the deterioration of a metal when it comes into contact with carbonic acid, provided that the partial pressure of hydrogen sulfide remains below 3.5 mbar. When this value is exceeded, conversely, sour corrosion takes place [1]. The widespread failures deriving from corrosion losses in the field have urged the industry to adopt proper prediction and management tools, that play a crucial role in reducing costs and ensuring adherence to safety, health, and environmental regulations [2,3]. Many efforts are currently being put in place to better understand and predict sweet corrosion, the most prevalent form of corrosion in the field. Its mechanism, that involves hydrogen evolution as dominant cathodic process, is here presented in the common case of iron:

$$Fe + CO_2 + H_2O \leftrightharpoons FeCO_3 + H_2. \quad (1)$$

$FeCO_3$ is the scale that generally forms at high temperatures on the iron surface, which can be more or less protective and influences the corrosion rate of the process, together with a variety of other parameters, namely: pH, temperature, fluid chemistry and flow rate, CO_2 partial pressure, steel metallurgy, condensation, non-ideal behaviors, localized attacks, presence of organic acids, corrosion inhibitors and glycol [4].
The mathematical models employed to predict the corrosion behavior of metals can be empirical, semi-empirical and mechanistic. Empirical models rely primarily on experimental data, and the same principle applies to semiempirical models, but with the added benefit that the latter's fundamental functions stem from approximations of the underlying physicochemical processes governing the corrosion mechanism. On the other hand, mechanistic models are characterized by theoretical foundations, enabling them to make predictions beyond the range of experimental conditions used for their validation.
The Tafel-Piontelli model is a mechanistic model, here validated in the case of two weak acids (acetic acid and formic acid) and then applied to sweet corrosion by comparison with three consolidated models in the industry: De Waard-Lotz model (1993), De Waard-Lotz-Dugstad model (1995), and Cassandra model (1998).

Tafel-Piontelli Model

The Tafel-Piontelli model has mechanistic bases rooted in the kinetics of the corrosion process. It was first proposed in its base version by Lazzari in [5], and then developed over the years. The model is applied to the case of a stagnant acidic solution in which two semi-reactions take place simultaneously: iron dissolution ($Fe \rightarrow Fe^{2+} + 2e^{-}$) as anodic process, and hydrogen evolution ($2H^{+} + 2e^{-} \rightarrow H_2$) as cathodic process. The two reactions follow the Tafel law [6,7] and intersect in the Evans diagram at the free corrosion potential:

$$E_{corr} = E_{q,H_2} - b_{H_2} \cdot log\left(\frac{i_{corr}}{i_{0,H_2}}\right) = E_{q,Fe} + b_{Fe} \cdot log\left(\frac{i_{corr}}{i_{0,Fe}}\right) \quad (2)$$

where E_{corr} and i_{corr} are the free corrosion potential and corrosion current density, E_{q,H_2} and $E_{q,Fe}$ are the equilibrium potentials of the cathodic and anodic semi-reactions, calculated via Nernst equation, and i_{0,H_2} and $i_{0,Fe}$ are the exchange current densities.
From equation (2), i_{corr} is derived and applied in the Faraday law, thus obtaining the corrosion rate formula, here reported in the case of iron:

$$CR(T,pH) = \frac{M_{Fe}}{z_{Fe^{2+}} F \rho_{Fe}} i_{corr} = 1.17 \cdot i_{0,H_2}^{\frac{b_{H_2}}{b_{H_2}+b_{Fe}}} \cdot i_{0,Fe}^{\frac{b_{Fe}}{b_{H_2}+b_{Fe}}} \cdot 10^{\frac{E_{q,H_2}-E_{q,Fe}([Fe^{2+}])}{b_{H_2}+b_{Fe}}}, \quad (3)$$

where b_{H_2} and b_{Fe} are the Tafel slopes of the reactions, and $E_{q,Fe}$ depends on the activity of iron ions in solution $[Fe^{2+}]$. The cathodic exchange current density i_{0,H_2} is calculated as its value in standard conditions of temperature and neutral pH (i°_{0,H_2}), modulated by two functions: an exponential function of pH and an Arrhenius-type function of temperature [8]:

$$i_{0,H_2}(T,pH) = i^{\circ}_{0,H_2} \cdot \phi^{*}(pH) \cdot \psi^{*}(T) = i^{\circ}_{0,H_2} \cdot e^{\alpha \cdot (pH-7)} \cdot e^{-\frac{\Delta H_{act}}{R}\left(\frac{1}{T}-\frac{1}{T_0}\right)}. \quad (4)$$

The activity of iron ions in solution $[Fe^{2+}]$ is estimated for the general case of an n-protic acid by imposing chemical equilibrium and charge balance between acid, metallic iron and iron salts, as extensively discussed in [8], thus resulting in (5) for unsaturated solutions, and (6) for saturated solutions:

$$[Fe^{2+}] = \frac{\left(\sum_{i=1}^{n} [H^{+}]^{n-i} \cdot i \cdot \prod_{j=1}^{i} K_{a,j}\right)[H_nA] + K_w[H^{+}]^{n-1} - [H^{+}]^{n+1}}{2[H^{+}]^{n}}; \quad (5)$$

$$[Fe^{2+}] = \left(\frac{K_{sp}}{[A^{n-}]^2}\right)^{\frac{1}{n}} = K_{sp}^{\frac{3+(-1)^n}{2n}} \left(\frac{[H^{+}]^{2n}}{\prod_{i=1}^{n} K_{a,i}^{2} \cdot [H_nA]^2}\right)^{\frac{1}{n}}. \quad (6)$$

$[H^{+}]$ is the concentration of hydrogen ions estimated from the initial pH, and $[H_nA]$ is the initial concentration of an n-protic acid. Moreover, $K_{a,j}$, K_w and K_{sp} are the acid j-th dissociation equilibrium constant, the water self-dissociation equilibrium constant, and the solubility product constant.
The cathodic Tafel slope, b_{H_2}, is assumed independent from temperature and pH, and equal to its theoretical value of 0,120 mV/decade. Instead, the anodic Tafel slope b_{Fe} is defined as:

$$b_{Fe}(T) = \frac{1}{\delta} ln\left(e^{\delta\lambda(T-T_{scale})} + 1\right) \quad (7)$$

where the temperature dependence is controlled by the parameter δ, as graphically illustrated in Figure 1: for $T \ll T_{scale}$, $\lim_{\delta \to \infty} b_{Fe} = 0$, while for $T \geq T_{scale}$, $\lim_{\delta \to \infty} b_{Fe} = \lambda(T - T_{scale})$, meaning that b_{Fe} approaches a linear dependence of slope λ on temperature.

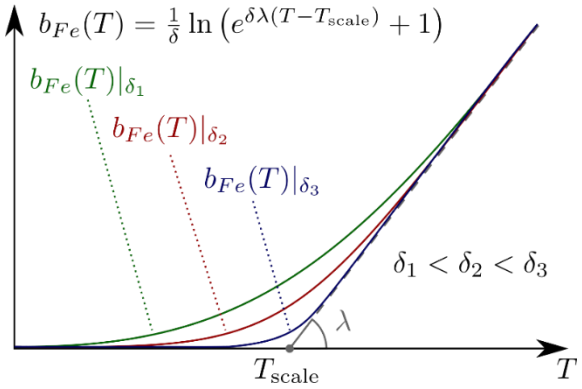

Figure 1: Dependence of the anodic Tafel slope on temperature.

Thanks to this description of the anodic Tafel slope, the Tafel-Piontelli model is able to account for the protective effects of scale deposits on the metal surface, that hinder the evolution of the corrosion process. The resulting Evans diagram is reported in Figure 2.

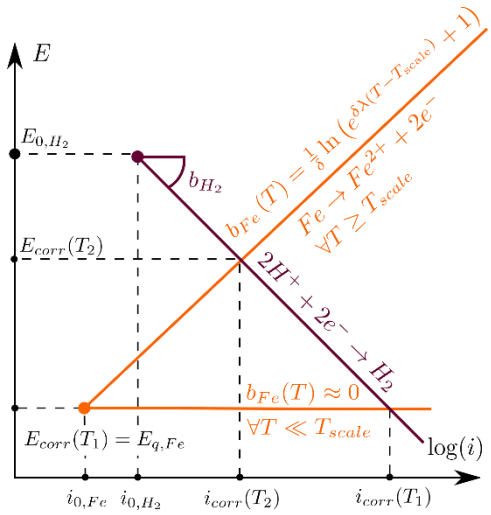

Figure 2: Evans diagram of iron dissolution and hydrogen evolution in the Tafel-Piontelli model.

Application in weak acids

Materials and methods

1 cm^2 surfaces of cylindrical carbon steel samples grinded with 320 grit SiC abrasive paper were exposed to weakly acidic solutions, prepared with acetic and formic acid at 20 and 60 °C, and pH 3 and 4. The kinetic parameters of the process (cathodic Tafel slope and cathodic exchange current density) were estimated with a theoretical approach and validated by comparison with the experimental results of potentiodynamic polarization tests. The performance of the model in the assessment of the corrosion rate was evaluated via mass loss tests, carried out by immersion of the samples in the acidic solutions for 3 to 5 days.

For each test, the cell used was placed on a heating system with vertex control (± 1 °C). pH measurements were performed at the beginning and at the end of the test with a digital pH-meter with a ± 0.1 accuracy. Nitrogen was constantly insufflated in the cell to make the oxygen presence negligible. Corrosion products were removed from the surface of the sample at the end of the test, via immersion in a water-based solution with 50% HCl and 3.5 g/L of hexamethylene tetraamine, followed by 4 sonication cycles each 2 minute-long. The sample was washed with water and then acetone, dried and weighted with a balance with 10^{-2} g resolution at the end of each cycle. The mass loss was obtained in compliance with ASTM G1-03 standard [9] and converted into a penetration rate value in [mm/y], following ASTM G-31 [10], resulting in:

$$CR = \Delta M / S \cdot t \cdot \rho \quad (8)$$

where ΔM [g] is the mass loss, S [m^2] is the surface of the sample exposed to the solution, t [s] is the immersion time, and ρ [g/ m^2] is the metal density.

Experimental validation

The model was broadly validated in strong acids in [8]. This work evaluates the model in the case of weak acids, by comparison with the experimental results obtained in formic acid and acetic acid solutions at pH 3 and 4 at 20 and 60 °C, as shown in Figure 3 and Figure 4.

The model succeeds in predicting a corrosion rate of the same order of magnitude of the experimental results in all test cases, while adapting the predictions to the different temperatures. Moreover, the experimental results show an exponential dependence of the corrosion rate with respect to the solution's pH. This exponential behavior is illustrated by the approximated regression lines between $\log CR$ and pH. The lines representing the estimated values using the Tafel-Piontelli models are also reported and well reproduce the exponential trend of the laboratory data.

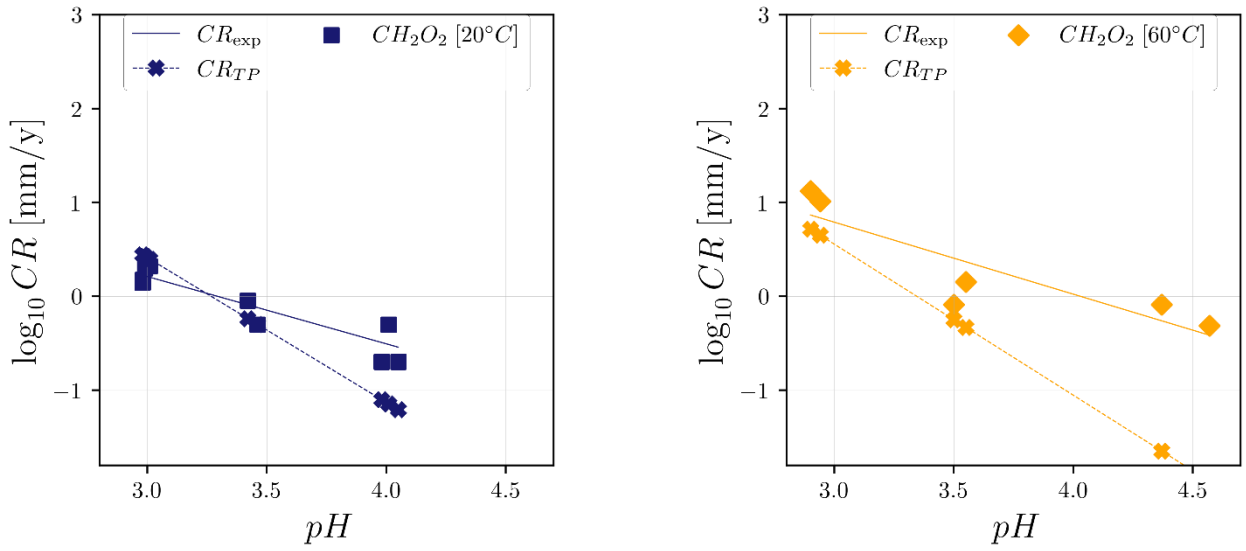

Figure 3: Comparison between experimental and predicted corrosion rate trends in formic acid solutions w.r.t. pH at a) 20°C and b) 60°C.

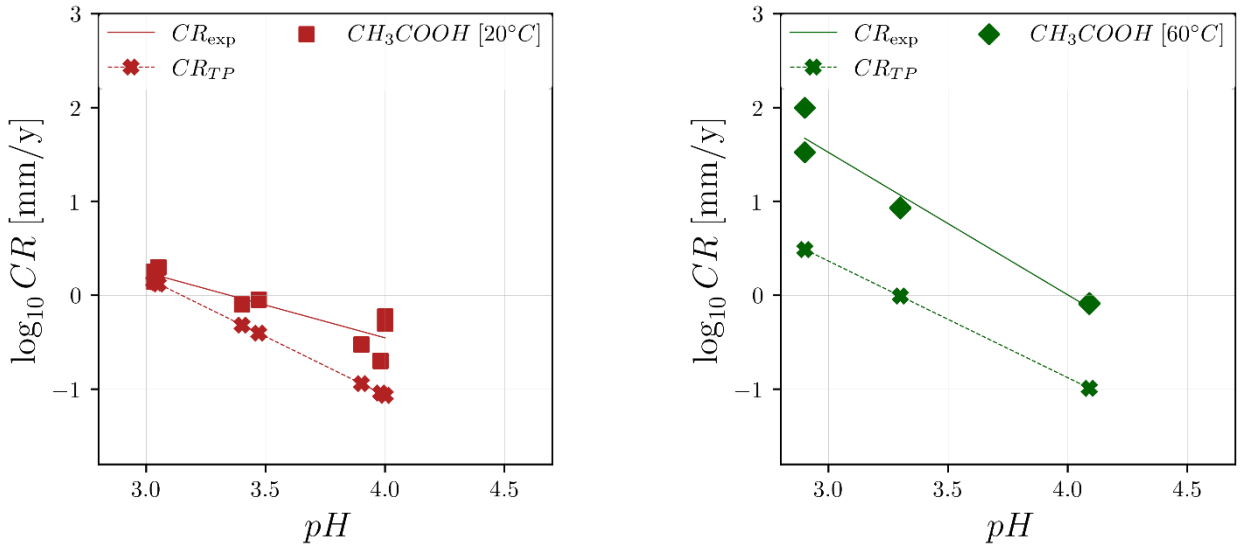

Figure 4: Comparison between experimental and predicted corrosion rate trends in acetic acid solutions w.r.t. pH at a) 20°C and b) 60°C.

Application to sweet corrosion

Parameters estimation

In CO_2 corrosion, the acid source is the pipeline internal production fluid, typically rich in carbon dioxide. To perform a comparative analysis using the Tafel-Piontelli model, it is necessary to estimate the pH of the solution from the total pipeline pressure and partial mass fraction of carbon dioxide. Considering a system at constant volume, the solution pH is estimated following the empirical model presented in [14]:

$$pH\left(f_{CO_2}(T,P,X_{CO_2}),T\right) = 3.71 + 0.00417 \cdot T - \frac{1}{2} log\, f_{CO_2}(T,P,X_{CO_2}) \quad (9)$$

where T is the pipeline temperature, P is the internal pressure of the system, X_{CO_2} is the mass fraction of CO_2 in the gas phase and f_{CO_2} is the carbon dioxide fugacity, calculated as:

$$f_{CO_2}(T,P,X_{CO_2}) = a_{CO_2}(T,P)\, X_{CO_2} P. \quad (10)$$

The fugacity coefficient a_{CO_2} is estimated according to the results presented in [18], such that, for $P \leq 250$ bar, $a_{CO_2}(T,P) = 10^{P\left(0.0031 - \frac{1.4}{T+273.15}\right)}$ and, for P > 250 bar, $a_{CO_2}(T,P) = 10^{250\left(0.0031 - \frac{1.4}{T+273.15}\right)}$.
The concentration of carbonic acid in solution can be estimated from the carbon dioxide partial pressure by exploiting the Henry law and the chemical equilibria in solution, extensively studied in [19–21]. Moreover, the reaction kinetics relating to these equilibria, particularly at the interface between the bulk fluid and the metal surface, have been investigated in [22–25]. In this work, the main chemical reactions considered in the CO_2 aqueous solution are carbon dioxide dissolution, carbon dioxide hydration, carbonic acid dissociation, bicarbonate anion dissociation, and water dissociation, reported in Table 1 with their kinetic constants, depending on the system temperature and salinity.

Table 1 – Chemical reactions in water/CO_2 environment and their equilibrium constants.

Chemical Reaction	Equilibrium Equation	Equilibrium Constant	Ref.	
$CO_{2_{(g)}} \leftrightharpoons CO_{2_{(aq)}}$	$H_{CO_2} = \frac{[CO_2]}{p_{CO_2}}$	$H_{CO_2} = \frac{1}{1.00258} e^{93.4517\left(\frac{100}{T}\right) - 60.240 + 23.3585\, ln\left(\frac{T}{100}\right)} \cdot e^{\left(0.023517 - 0.023656\left(\frac{T}{100}\right) + 0.0047036\left(\frac{T}{100}\right)^2\right) S\%}$	[21,26,27]	(11)
$CO_{2_{(aq)}} + H_2O_{(l)} \leftrightharpoons H_2CO_{3_{(aq)}}$	$K_{hyd} = \frac{[H_2CO_3]}{[CO_2]}$	$K_{hyd} = 2.85 \times 10^{-3}$	[28]	(12)
$H_2CO_{3_{(aq)}} \leftrightharpoons HCO_{3_{(aq)}}^- + H_{(aq)}^+$	$K_{a,1} = \frac{[HCO_3^-][H^+]}{[H_2CO_3]}$	$K_{\mathrm{a,1}}^{\mathrm{H_2CO_3}} = 378.6\, e^{\frac{-2307.1266}{T} + 2.83655 - 1.5529413\, ln(T)} \cdot e^{\left(\frac{-4.0484}{T} - 0.20760841\right) S\%^{0.5} + 0.08468345\, S\%} \cdot e^{-0.00654208\, S\%^{1.5} + ln(1 - 0.001005\, S\%)}$	[21,26,29]	(13)
$HCO_{3_{(aq)}}^- \leftrightharpoons CO_{3_{(aq)}}^{2-} + H_{(aq)}^+$	$K_{a,2} = \frac{[CO_3^{2-}][H^+]}{[HCO_3^-]}$	$K_{\mathrm{a,2}}^{\mathrm{H_2CO_3}} = e^{\frac{-3351.6106}{T} - 9.226508 - 0.2005743 ln(T) + \left(\frac{-23.9722}{T} - 0.106901773\right) S\%^{0.5}} \cdot e^{0.1130822\, S\% - 0.00846934\, S\%^{1.5} + ln(1 - 0.001005\, S\%)}$	[21,26,29]	(14)
$H_2O_{(l)} \leftrightharpoons OH_{(aq)}^- + H_{(aq)}^+$	$K_w = [OH^-][H^+]$	$K_w = e^{\frac{-13847.26}{T} + 148.9652 - 23.6521\, ln(T)} \cdot e^{\left(\frac{118.67}{T} - 5.977 + 1.0495 lnT\right) S\%^{0.5} + 0.01615\, S\%}$	[21,26,30]	(15)
$FeCO_{3_{(s)}} \leftrightharpoons Fe_{(aq)}^{2+} + CO_{3_{(aq)}}^{2-}$	$K_{sp} = [Fe^{2+}][CO_3^{2-}]$	$K_{\mathrm{sp}}^{\mathrm{FeCO_3}} = 10^{-59.3498 - 0.041377(T+273) - \frac{2.1963}{T+273} + 24.5724\, log(T+273) + 2.518 I^{0.5} - 0.657 I}$	[31]	(16)

The simultaneous solution of the equilibrium equations for all species and the electroneutrality constraint give a complete description of the bulk solution's water speciation [32]. From this assumption, the concentration of carbonic acid can be estimated as:

$$[H_2CO_3] = K_{hyd}(T, \%S) H_{CO_2}(T, \%S) a_{CO_2}(T,P)\, X_{CO_2} P, \quad (17)$$

where K_{hyd} is the hydration equilibrium constant, H_{CO_2} is the Henry's constant for carbon dioxide, T is the temperature of the oil brine, P is the system pressure, X_{CO_2} is the atmospheric mass fraction of carbon dioxide, I is the ionic strength of the solution, and %S is the salinity, here considered null.
The results presented in [12] are then employed to estimate the scaling temperature, T_{scale}:

$$T_{scale}(T,P,X_{CO_2}) = \frac{2400}{6.7 + 0.6\, log\, f_{CO_2}(T,P,X_{CO_2})} = \frac{2400}{6.7 + 0.6\, log\left(a_{CO_2} X_{CO_2} P\right)}. \quad (18)$$

Pre-existing models

Among the existing models for the prediction of sweet corrosion, three models will be used today for a comparison with the Tafel-Piontelli model.

The De Waard-Lotz model (1993) [14] is a semiempirical tool deriving from several implementations of the original De Waard-Milliams model (1975) [11]. Its formulation considers the corrosion reaction as consisting of two consecutive steps: the transport of corrosive species through the concentration boundary layer to the metal (CR_{mass}), characterized by the reaction rate constant k_{mass} ; and the reaction at the metal's phase boundary (CR_{react}), characterized by the reaction rate constant k_{react}, thus resulting in:

$$CR_{dWL} = \frac{[H_2CO_3]}{\frac{1}{k_{react}} + \frac{1}{\lambda k_{mass}}} = \frac{1}{\frac{1}{CR_{react}} + \frac{1}{\lambda CR_{mass}}}, \tag{19}$$

where $\lambda = 2.62 \cdot 10^6$ is an adjusting constant required to obtain unit consistency between the two corrosion rates in [mm/year].

The De Waard-Lotz-Dugstad model (1995) [15] is an updated version of the previous one, that adjusts the equation constants thanks to the best fitting with the Dugstad 1994 experiments' data [16]. Its most significant contribution is the inclusion of steel metallurgy conditions into the estimation of the corrosion rate, thanks to two correction factors accounting for chromium and carbon content: F_{Cr} and F_{C}. In particular, the steels were separated into two main categories, i.e., normalized steels and quenched and tempered steels.

The Cassandra model (1998) [17] is a semiempirical tool developed by British Petroleoum (BP), and validated in real oil field. It is based on the De Waard models, and implemented according to experimental results and data provided by the Institute for Energy Technology. This model differentiates itself from the De Waard mostly above the scaling temperature T_{scale}. Indeed, while the De Waard model predicts a decrease in the corrosion rate over T_{scale}, due to the formation of protective films, the Cassandra model follows the trend of its field results and assumes that the corrosion rate reaches a peak at T_{scale} and remains on a plateau at the same value for higher temperatures. Below T_{scale}, the corrosion rate estimated is the average between the De Waard-Lotz model and the De Waard-Lotz-Dugstad model.

Models comparison

The first comparison of the Tafel-Piontelli model is performed by analyzing the estimated corrosion rate for different fixed values of carbon dioxide partial pressure (p_{CO_2}) and temperature varying in the range $T \in [20, 120]°C$.

For low system pressure (i.e. $p_{CO_2} = 1$ [bar], illustrated in Figure 5a) below T_{scale}, the corrosion rate estimated by the De Waard-Lotz model is low and stable; the one estimated by De Waard-Lotz-Dugstad model is higher and characterized by a plateau, while the one predicted by the Cassandra model is an average of the two. Above T_{scale}, the De Waard models show a sudden decrease in corrosion rate to account for the protective effects of thick scales, while the Cassandra model keeps a more conservative approach and fixes the corrosion rate as the maximum value obtained in the range $T \in [20, T_{\mathrm{scale}}]°C$. For low to mid-range p_{CO_2} ($p_{CO_2} \in [1,4]$ bar), the Tafel-Piontelli model provides a moderate to low corrosion rate with respect to the other three models, with a more intense increase with respect to temperature, starting close to the De Waard-Lotz value for $T \in [0,25]°C$ and reaching the peak at T_{scale} close to the Cassandra value. Over T_{scale}, the sharp decrease in the corrosion rate, due to the corrosion inhibition effects of the deposited scale, brings the results of the Tafel-Piontelli model close to the predictions of the De Waard-Lotz model, as shown in Figure 5. This description of the corrosion process allows good estimates, that simultaneously avoid too conservative overestimations and dangerous underestimations.

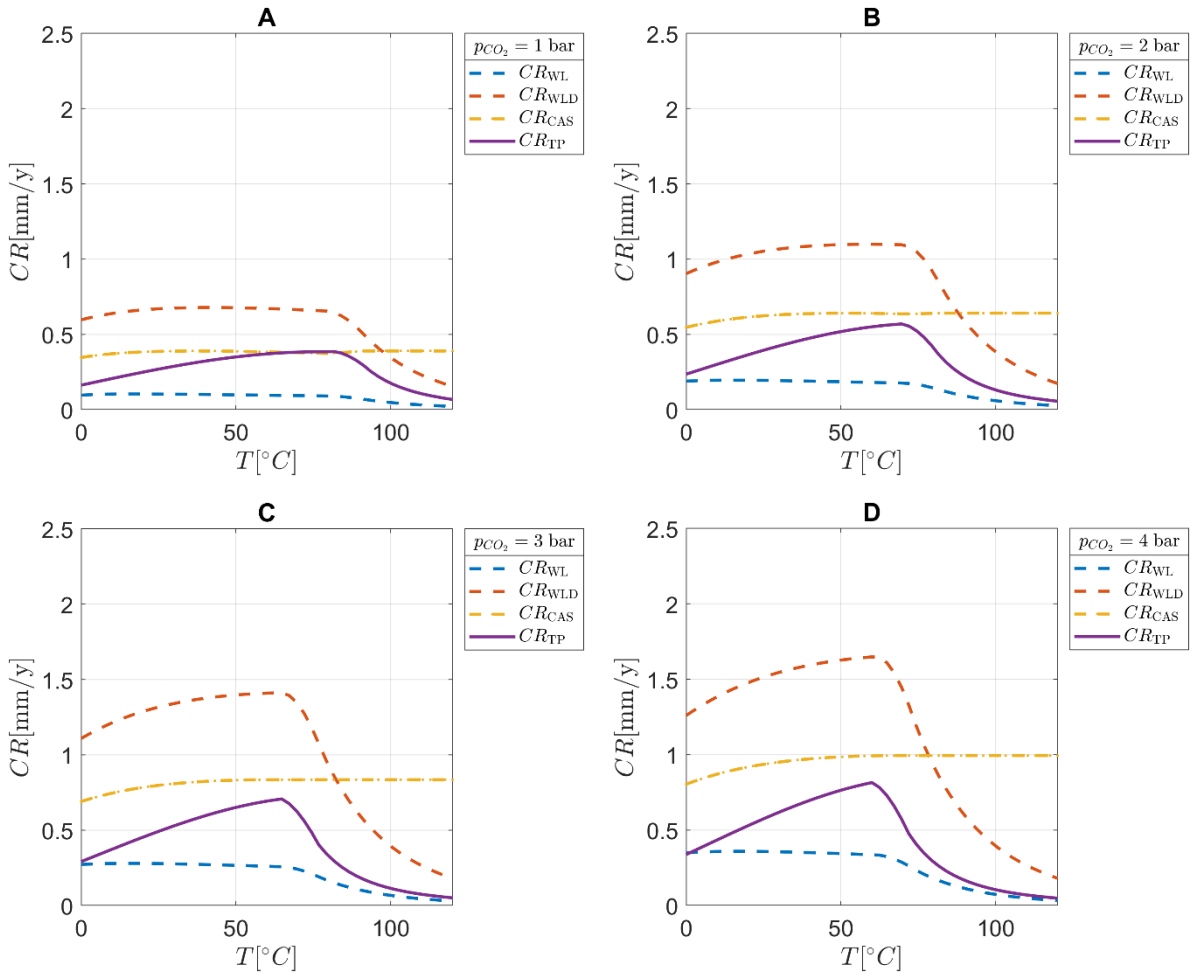

Figure 5 – Estimated corrosion rate w.r.t. temperature in sweet corrosion with a) $p_{CO_2} = 1\ [bar]$; b) $p_{CO_2} = 2\ [bar]$; c) $p_{CO_2} = 3\ [bar]$; d) $p_{CO_2} = 4\ [bar]$.

Figure 6 shows the comparison for high p_{CO_2} ($p_{CO_2} \in [7,10]$ bar): at mid-range temperatures ($T \in [25, T_{scale}]°C$) the predictions of the Tafel-Piontelli model are always between those of the De Waard-Lotz-Dugstad and the Cassandra, while at low temperatures ($T \in [0,25]°C$) they are slightly lower. Over T_{scale}, the corrosion rate follows the same trend obtained with the De Waard models and, in particular, approaches the estimates of the De Waard-Lotz. Therefore, also in high range temperatures ($T \in [T_{scale}, 100]°C$), the Tafel-Piontelli model returns low-to-moderate corrosion rates, circumventing the conservative approach used in the Cassandra model.

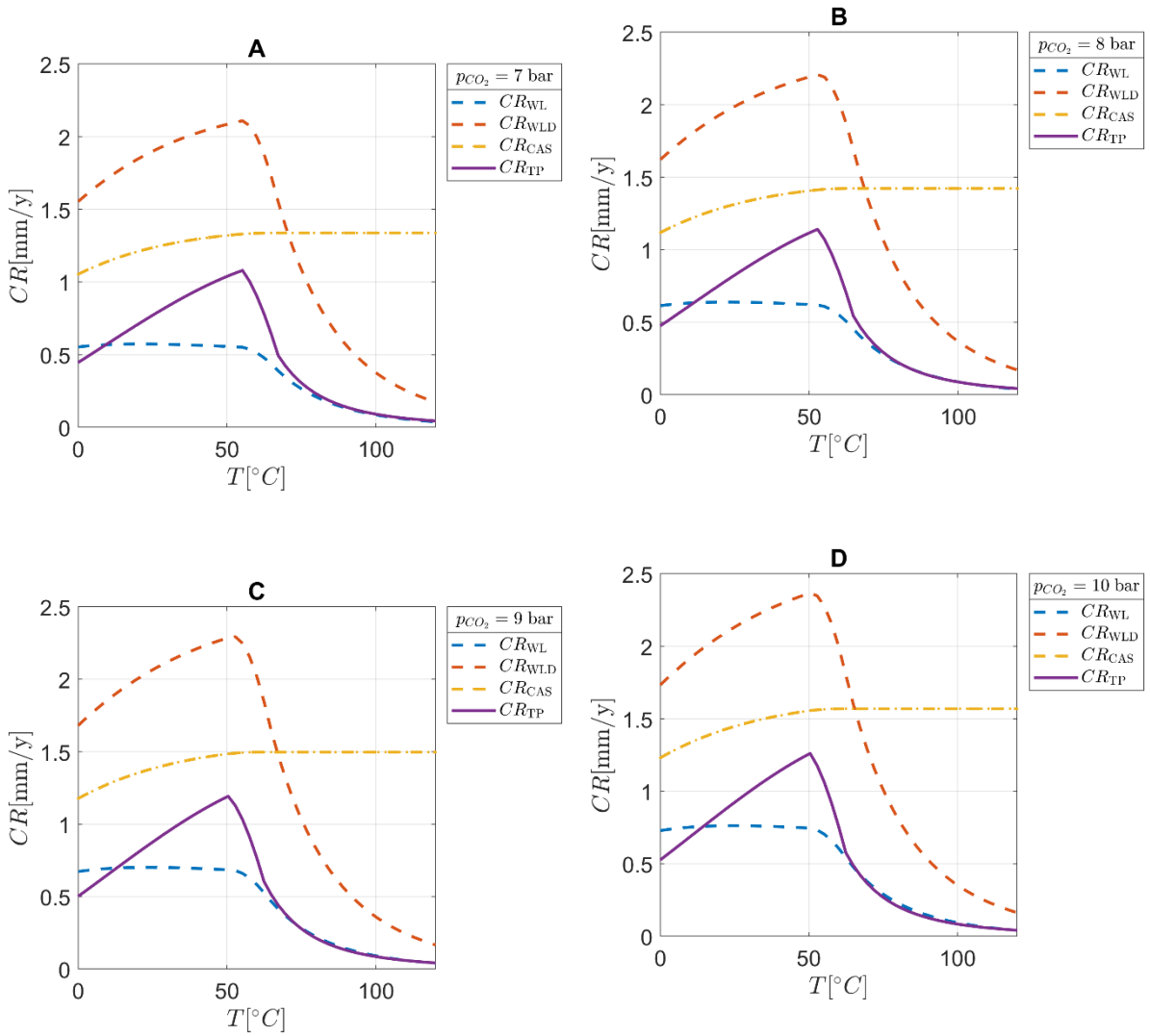

Figure 6 – Estimated corrosion rate w.r.t. temperature in sweet corrosion with a) $p_{CO_2} = 7\ [bar]$; b) $p_{CO_2} = 8\ [bar]$; c) $p_{CO_2} = 9\ [bar]$; d) $p_{CO_2} = 10\ [bar]$.

The second model comparison is performed by analyzing the estimated corrosion rate for fixed values of temperature and varying the p_{CO_2} in the range of $p_{CO_2} \in [1,10]$ bar, to obtain different values of pH.

The three semi-empirical models show similar exponential increase of the corrosion rate when the solution pH is reduced, as illustrated by their linear trends in Figure 7. The De Waard-Lotz-Dugstad and the De Waard-Lotz models give an upper and lower limit for the corrosion rate, while the Cassandra model gives the average between the two. In this scenario, the corrosion rate estimated by the Tafel-Piontelli model has two important characteristics. First, the dependence of the corrosion rate on pH is very close to the one obtained with the Cassandra model, highlighted by their parallel trends. Second, also in this case the predictions of the revised model may indicate an undervaluation of the corrosion rate for low range temperatures ($T \in [0,25]°C$) and very low pH ($pH \leq 3$), but a good agreement with the other models for moderate to high temperatures and high pH (pH > 3).

Overall, the Tafel-Piontelli model predicts a low to moderate corrosion rate in the range of analysis and is in good agreement with the consolidated models used in the Oil&Gas industry.

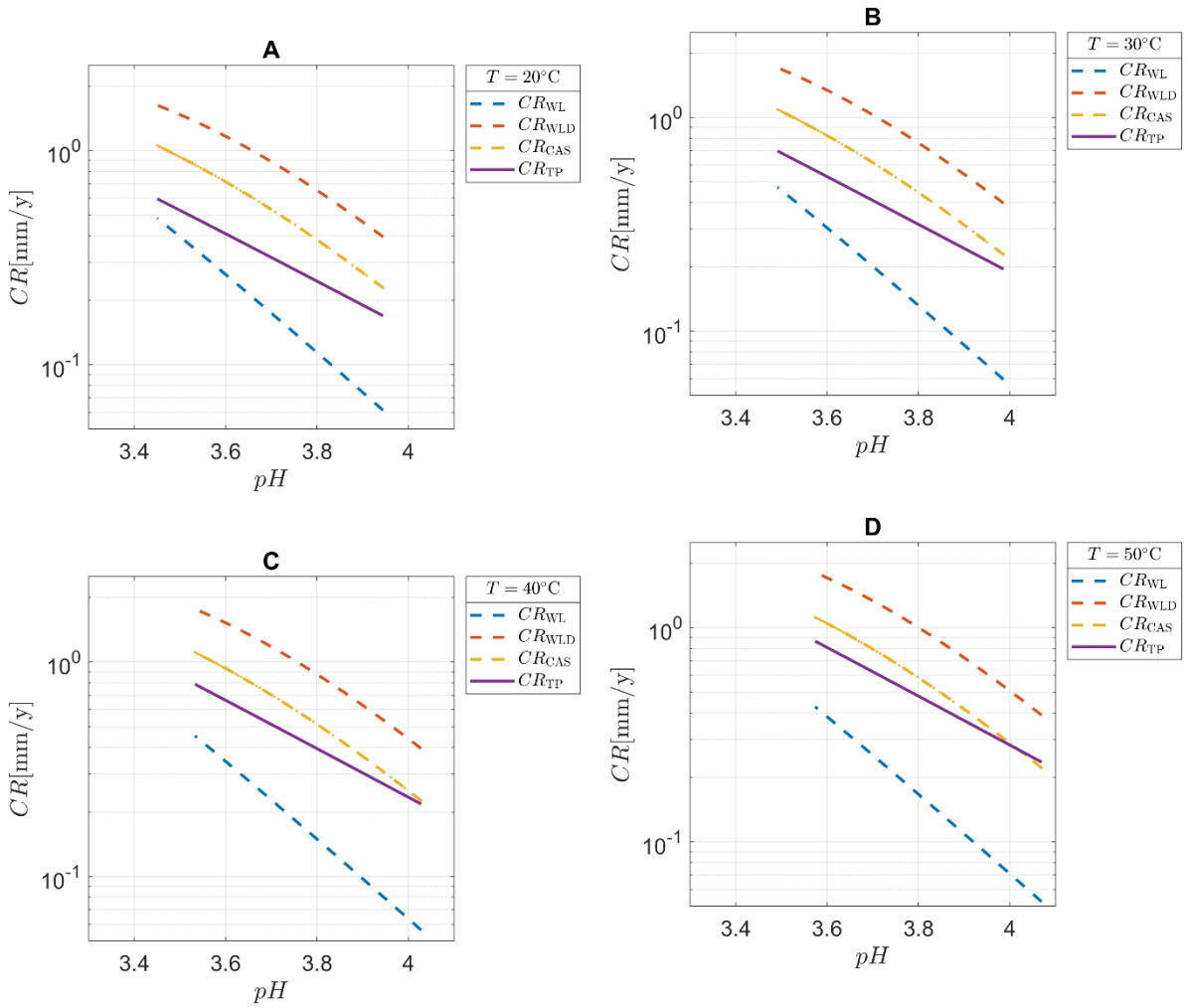

Figure 7 – Estimated corrosion rate w.r.t. pH in sweet corrosion with a) $T = 20.0°C$; b) $T = 30.0°C$; c) $T = 40.0°C$; d) $T = 50.0°C$.

Conclusions

The Tafel-Piontelli model was introduced and its effectiveness in predicting the acidic corrosion process was examined using experimental data obtained from weakly acidic solutions at various pH levels and temperatures. The evaluation revealed a strong correlation between the estimated and experimental corrosion rate values, affirming the model's ability to adequately represent the electrochemical behavior expected in the corroding system.
Furthermore, the model's applicability was tested in the case of sweet corrosion, very common in the oil and gas industry. A comparative analysis was conducted against established corrosion models (De Waard-Lotz, De Waard-Lotz-Dugstad, Cassandra). While some variations were observed in growth and decline rates within specific temperature and pH ranges, the overall comparison with other semiempirical methods indicated a favorable agreement in the order of magnitude for the predictions across the entire range of analysis.

Aknowledgements

The Tafel-Piontelli model was proposed by Prof. Luciano Lazzari in his book “Engineering Tools for Corrosion”, Woodhead Publishing, 2017. From September 2018 to September 2020 this research was funded by NACE International – Milano Italia Section.

References

1. Pedeferri, P. *Corrosion Science and Engineering*; Engineering Materials; 1st ed. 2018.; Springer International Publishing : Imprint: Springer: Cham, 2018; ISBN 978-3-319-97625-9. 10.1007/978-3-319-97625-9.
2. Fayomi, O.S.I.; Akande, I.G.; Odigie, S. Economic Impact of Corrosion in Oil Sectors and Prevention: An Overview. *J. Phys.: Conf. Ser.* **2019**, *1378*, 022037. 10.1088/1742-6596/1378/2/022037.

3. Popoola, L.; Grema, A.; Latinwo, G.; Gutti, B.; Balogun, A. Corrosion problems during oil and gas production and its mitigation. *Int J Ind Chem* **2013**, *4*, 35. 10.1186/2228-5547-4-35.
4. Nešić, S. Key issues related to modelling of internal corrosion of oil and gas pipelines – A review. *Corrosion Science* **2007**, *49*, 4308–4338. 10.1016/j.corsci.2007.06.006.
5. Lazzari, L. *Engineering Tools for Corrosion: Design and Diagnosis*; European Federation of Corrosion Publications; WP, Woodhead Publishing, an imprint of Elsevier: Duxford, 2017; ISBN 978-0-08-102425-6.
6. Tafel, J. Über die Polarisation bei kathodischer Wasserstoffentwicklung. *Zeitschrift für Physikalische Chemie* **1905**, *50U*, 641–712. 10.1515/zpch-1905-5043.
7. Burstein, G.T. A hundred years of Tafel's Equation: 1905–2005. *Corrosion Science* **2005**, *47*, 2858–2870. 10.1016/j.corsci.2005.07.002.
8. Messinese, E.; Ormellese, M.; Brenna, A. Tafel-Piontelli model for the prediction of uniform corrosion rate of active metals in strongly acidic environments. *Electrochimica Acta* **2022**, *426*, 140804. 10.1016/j.electacta.2022.140804.
9. G01 Committee *Practice for Preparing, Cleaning, and Evaluating Corrosion Test Specimens*; ASTM International; 10.1520/G0001-03.
10. J01 Committee *Guide for Laboratory Immersion Corrosion Testing of Metals*; ASTM International; 10.1520/G0031-72R04.
11. De Waard, C.; Milliams, D.E. Carbonic Acid Corrosion of Steel. *CORROSION* **1975**, *31*, 177–181. 10.5006/0010-9312-31.5.177.
12. De Waard, C.; Lotz, U.; Milliams, D.E. Predictive Model for CO_2 Corrosion Engineering in Wet Natural Gas Pipelines. *CORROSION* **1991**, *47*, 976–985. 10.5006/1.3585212.
13. Eriksrud, E.; Sontvedt, T. Effect of Flow on CO_2 Corrosion Rates in Real and Synthetic Formation Waters.; NACE: Houston, Tex, USA, 1983; p. 44. 1-44. 40.
14. De Waard, C.; Lotz, U. Prediction of CO_2 Corrosion of Carbon Steel.; NACE International, Houston, TX (United States): United States, 1993.
15. De Waard, C.; Lotz, U.; Dugstad, A. *Influence of liquid flow velocity on CO_2 corrosion: A semi-empirical model*; NACE International, Houston, TX (United States): United States, 1995;
16. Dugstad, A.; Lunde, L. [Inst. for E., Kjeller (Norway)]; Videm, K. [Univ. of O. (Norway)] *Parametric study of CO_2 corrosion of carbon steel*; NACE International, Houston, TX (United States): United States, 1994;
17. Hedges, B.; Sun, Y.; Chapman, R.; Harrop, D.; Mohammed, I. A Prophetic CO_2 Corrosion Tool - But When is it to be Believed? In Proceedings of the NACE-05552; NACE International, Houston, TX (United States): United States, 2005; p. 16.
18. Olsen, S. CO_2 Corrosion Prediction by Use of the NORSOK M-506 Model - Guidelines and Limitations. In Proceedings of the NACE-03623; NACE International: NACE, 2003; p. 12.
19. Butler, J.N. *Carbon dioxide equilibria and their applications*; Lewis Publ: Chelsea, Mich, 1991; ISBN 978-0-87371-624-6.
20. Stumm, W.; Morgan, J.J. *Aquatic chemistry: chemical equilibria and rates in natural waters*; Environmental science and technology; 3rd ed.; Wiley: New York, 1996; ISBN 978-0-471-51184-7.
21. Zeebe, R.E.; Wolf-Gladrow, D.A. *CO_2 in seawater: equilibrium, kinetics, isotopes*; Elsevier oceanography series; Elsevier: Amsterdam ; New York, 2001; ISBN 978-0-444-50579-8.
22. Nordsveen, M.; Nešić, S.; Nyborg, R.; Stangeland, A. A Mechanistic Model for Carbon Dioxide Corrosion of Mild Steel in the Presence of Protective Iron Carbonate Films—Part 1: Theory and Verification. *Corrosion* **2003**, *59*, 443–456. 10.5006/1.3277576.
23. Pots, B.F.M. Mechanistic models for the prediction of CO_2 corrosion rates under multi-phase flow conditions.; NACE International, Houston, TX (United States): United States, 1995.
24. Remita, E.; Tribollet, B.; Sutter, E.; Vivier, V.; Ropital, F.; Kittel, J. Hydrogen evolution in aqueous solutions containing dissolved CO_2: Quantitative contribution of the buffering effect. *Corrosion Science* **2008**, *50*, 1433–1440. 10.1016/j.corsci.2007.12.007.
25. Turgoose, S.; Cottis, R.; Lawson, K. Modeling of Electrode Processes and Surface Chemistry in Carbon Dioxide Containing Solutions. In *Computer Modeling in Corrosion*; Munn, R., Ed.; ASTM International: West Conshohocken, PA, 1992; pp. 67–81 ISBN 978-0-8031-5210-6. 10.1520/STP24687S.
26. Dickson, A.G.; Goyet, C. *Handbook of methods for the analysis of the various parameters of the carbon dioxide system in sea water. Version 2*; 1994; p. ORNL/CDIAC--74, 10107773; 10.2172/10107773.
27. Weiss, R.F. Carbon dioxide in water and seawater: the solubility of a non-ideal gas. *Marine Chemistry* **1974**, *2*, 203–215. 10.1016/0304-4203(74)90015-2.
28. Palmer, D.A.; Van Eldik, R. The chemistry of metal carbonato and carbon dioxide complexes. *Chem. Rev.* **1983**, *83*, 651–731. 10.1021/cr00058a004.
29. Roy, R.N.; Roy, L.N.; Vogel, K.M.; Porter-Moore, C.; Pearson, T.; Good, C.E.; Millero, F.J.; Campbell, D.M. The dissociation constants of carbonic acid in seawater at salinities 5 to 45 and temperatures 0 to 45°C. *Marine Chemistry* **1993**, *44*, 249–267. 10.1016/0304-4203(93)90207-5.
30. Millero, F.J. Thermodynamics of the carbon dioxide system in the oceans. *Geochimica et Cosmochimica Acta* **1995**, *59*, 661–677. 10.1016/0016-7037(94)00354-O.
31. Sun, W.; Nešić, S.; Woollam, R.C. The effect of temperature and ionic strength on iron carbonate (FeCO3) solubility limit. *Corrosion Science* **2009**, *51*, 1273–1276. 10.1016/j.corsci.2009.03.009.
32. Nešić, S.; Sun, W. Corrosion in Acid Gas Solutions. In *Shreir's Corrosion*; Elsevier, 2010; pp. 1270–1298 ISBN 978-0-444-52787-5. 10.1016/B978-044452787-5.00055-X.

Corrosion Inhibitor Efficiency _Case study for onsite monitoring using 'bubble test' method

Mioara STROE, TotalEnergies SE, Pau/France
Yann-Joel ASSASSA, TotalEnergies SE, Pau/France
Alvaro Mpaka SOUSA, TEEPA, Luanda/Angola
Jacira DOMBE, TEEPA, Luanda/Angola

Corrosion Inhibitor (CI) is commonly used to mitigate internal corrosion for carbon steel pipelines use on the oil and gas production. The injection dosage used to protect the lines is strongly dependent on the corrosivity of the produced fluid and of the corrosion inhibitor itself. In addition, for mature fields, where the BSW is increasing, the total quantity of corrosion inhibitor that is necessary to be injected is increasing in time. Our strategy is to treat the produced fluid with the required quantity of CI to reach the protection criterion, meaning decreasing the corrosion rate below 0.1 mm/y. The reliability and the accuracy of the associated corrosion monitoring is of outmost importance especially when the monitoring data are used to adjust and to optimize the chemical treatment.

The document presents how the corrosion monitoring is performed on our offshore facilities, for which corrosion inhibitor is injected subsea in continuous mode. The techniques used for the monitoring and their impact on our overall strategy to mitigate corrosion are presented.

The focus is on 'Bubble test' monitoring method which is more and more deployed on our assets. The method consists in measuring the corrosion rate of the sample under CO2 bubbling. The corrosion rates are measured using a LPR (Linear Polarisation Resistance) probe (Graph1). The corrosion rates are complemented by CI residual measurements in the water phase. The method is simple, requiring a compact equipment (Figure 1) that can be easily integrated in a laboratory on site. The method is very reactive and a decision of the adjustment of the CI treatment can be taken rapidly. Although the method is giving the corrosiveness of the fluid at the moment of the sampling, the cross-check with the CI injection monitoring data provides a valuable monitoring way to assess the robustness for the anticorrosion treatments. For the long-term monitoring, these results are compared with the other corrosion monitoring results

like corrosion coupons (CC), corrosion probes (ER probes) and ultimately with the results of internal inspection. The method was proved to be useful in field test or change of the anticorrosion treatment.

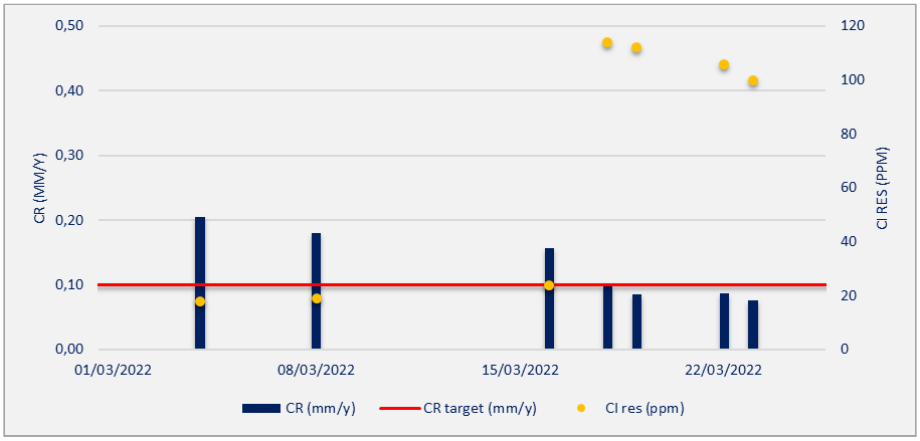

Graph 1. Bubble test results (CR and CI residual): tests performed to adjust the CI injection

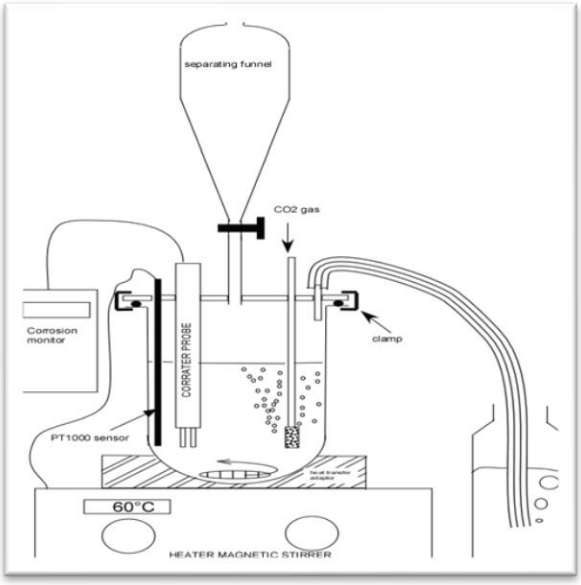

Figure 1. Schematic of bubble test equipment

Keywords: ‘bubble test’, LPR, corrosion management

CO_2 SCC testing of flexible pipe carbon steel tensile wires - Effect of temperature, precorrosion and accumulated plastic strain

P. Netto da Silva, Institute for Energy Technology, Norway
R. Nyborg, Institute for Energy Technology, Norway
H. Fordsmand, NOV Subsea Production Systems, Denmark
S. Landgraf, NOV Subsea Production Systems, Denmark
V. Chakravarthy Gudla, NOV Subsea Production Systems, Denmark
J. Gudme, NOV Subsea Production Systems, Denmark

Abstract

Flexible pipes used in offshore oil and gas production systems consist of polymer and metallic layers alternately wrapped around each other. The tensile armour typically consists of double layers of high strength carbon steel wires helically wound around the pressure armour and confined in the annulus of the pipe by the outer sheath layer. The main purpose of the tensile armour is to provide axial strength to the pipe, therefore these wires are usually stressed to a certain degree. During service, gas species may permeate from the bore and seawater might be present in the annulus of these pipes, in the area between layers or between the steel wires, generating a confined environment which is potentially corrosive to carbon steels. The combination of tensile stresses and a corrosive environment might result in stress corrosion cracking (SCC) of the carbon steel wires if unfavourable conditions are achieved. In 2017, CO_2 stress corrosion cracking (CO_2 SCC) was identified by the Brazilian National Agency for Petroleum, Natural Gas and Biofuels (ANP) as the potential cause of failure of carbon steel wires used in the tensile armours of gas-injection flexible pipes. The CO_2 SCC mechanism observed in these materials is not yet fully understood.

As part of a research effort to broaden the knowledge of this failure mechanism, a thorough testing program was launched to investigate how different parameters can affect the susceptibility to CO_2 SCC of tensile armour wires in simulated annulus environments. Small-scale tests have been carried out with wire specimens containing different levels of accumulated plastic strain and stressed by four-point bending to 90% ultimate tensile strength (UTS). The specimens were exposed at different temperatures and CO_2 partial pressures to synthetic seawater supersaturated with iron carbonate ($FeCO_3$). The high content of dissolved $FeCO_3$ was artificially achieved prior

to the exposure, and it compensated for the relatively large water volume to steel surface area (V/S) in the experiments in comparison to the V/S in the annulus of the pipe, which is typically very low. Prior to immersion in the $FeCO_3$-saturated seawater, some of the specimens, while already stressed in the four-point bending jigs, were precorroded in aerated seawater in order to simulate conditions following damage of the outer polymer layer. The duration of the experiments varied between 45 and 90 days.

The results have shown that temperature plays an important role on the formation of protective iron carbonate scales on the steel surface, which in turn has significant impact on the cracking susceptibility. The corrosion history of the steel surface also affects the properties of the iron carbonate scales, which can influence the cracking susceptibility as well.

Keywords: accumulated plastic strain, carbon steel, CO_2 stress corrosion cracking, flexible pipes, iron carbonate, temperature

Flexible pipes-corrosion when CO_2 is consumed

Arne Dugstad, Simona Palencsár

Institute for Energy Technology, Kjeller/Norway

Flexible pipes used in oil and gas production are composed of densely packed steel armour wires enclosed in an annulus confined by inner and outer thermoplastic sheaths. Hydrocarbons, water, CO_2 and H_2S from the bore permeate through the thermoplastic sheaths and oxygen/air might enter via the annulus venting system or through damages in the outer thermoplastic sheath. When the steel corrodes, CO_2 will be consumed, and the corrosion rate will decrease to a rate that is balanced by the permeation rate of CO_2 into the annulus. The balance and the corrosion rate will be affected by ingress of small amount of O_2. O_2 reacts with Fe^{2+} in the solution and prevents therefore $FeCO_3$ precipitation and CO_2 consumption.

$$4\,Fe^{2+}(aq) + 4\,H^{+}(aq) + O_2(aq) \rightarrow 4\,Fe^{3+}(aq) + 2\,H_2O(l) \quad (1)$$

$$Fe^{3+}(aq) + 3\,OH^{-}(aq) \rightarrow Fe(OH)_3(s) \quad (2)$$

Armor wires were exposed to water, various CO_2 partial pressures (0.001, 0.01 and 0.1 bar), various temperatures (25, 40 and 60 °C) and various amounts of O_2 in the gas phase (0-0.4 mol%). The experiments showed that protective corrosion product films ($FeCO_3$) formed fast in experiments without O_2 giving corrosion rates < 0.01 mm/y (the maximum corrosion rate regarded as acceptable for armour wires in flexible pipes). When the concentration of dissolved $FeCO_3$ was kept low due to the presence of O_2, protective $FeCO_3$ film did not form, and corrosion rates much higher than 0.01 mm/y were observed. The experiment demonstrated that the combination of CO_2 and O_2 can have serious consequences on the corrosion of armour wires even at very low concentrations of the gases.

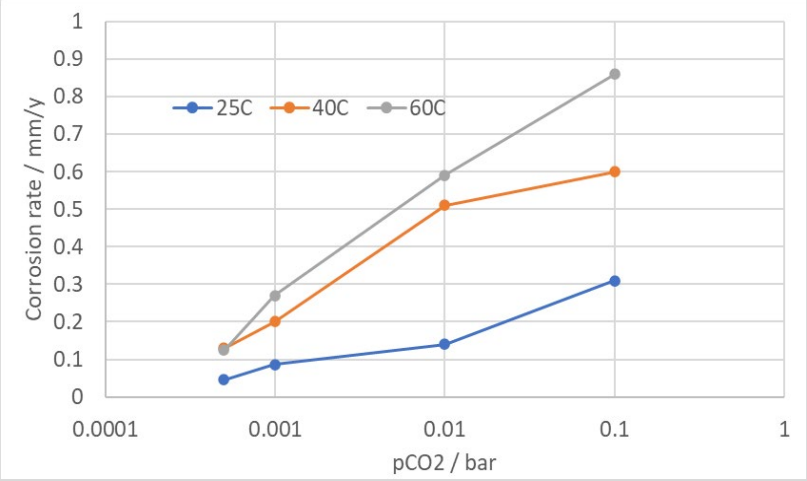

Development of a model system to investigate the effects of surface roughness and media on marine biofilm formation and microbiologically influenced corrosion

Liam Jones[1], Maria Salta[2,3], Torben Lund Skovhus[4], Kathryn Thomas[5], Timothy Illson[5], Julian Wharton[6], Jeremy Webb[1,7]

[1]School of Biological Sciences, University of Southampton, Southampton, United Kingdom; [2]School of Biological Sciences, University of Portsmouth, Portsmouth, United Kingdom; [3]Endures, MIC and Biofilm Department, Bevesierweg 1 DC002, 1781 AT Den Helder, The Netherlands, [4]Research Centre for Built Environment, Energy, Water and Climate, VIA University College, Horsens, Denmark; [5]DNV, Holywell Park, Ashby Road, Loughborough, United Kingdom; [6]School of Engineering, University of Southampton, Southampton, United Kingdom; [7]National Biofilms Innovation Centre, United Kingdom

Abstract

The energy sector continues to face corrosion challenges, with significant pipeline failures due to microbiologically influenced corrosion (MIC). This study aims to develop a representative model system in which inoculae relevant to operating pipelines can be cultured to investigate biofilms and MIC on carbon steels. Two identical anaerobic CDC reactors ran simultaneously for 28 days; one inoculated with a multi-species marine consortium and the other uninoculated. Carbon steel (UNS G10180) discs were used with two surface roughness profiles, R_a of 1.33±0.71 µm and 0.44±0.03 µm, as received and polished, respectively. Test media were either artificial seawater supplemented with yeast extract (1 g/L) or ATCC 1249 growth media. Molecular microbiological assessment, plus optical analysis and electrochemical tests were performed (see Figure 1). As expected, biofilms have a marked impact on the corrosion mechanism and reactor environment. Sulfide concentrations initially increased in the inoculated reactors (523±118 µmol/L). Additionally, there was a negative shift in corrosion potential, attributed to microbe attachment and biofilm formation/growth. Localised and shallow pits (see Figure 2) were clearly discernible in the biotic media, whereas only uniform corrosion was evident for the abiotic media. Electrochemical impedance was used to characterize the interfacial properties. This study provides insight into the role of biofilm formation on MIC and the importance of using multiple lines of evidence (MLOE), incorporating a multidisciplinary approach to develop understanding of the mechanistic relationship between the biofilm and metallic degradation. These insights will support a move towards evidence-based biocide dosing and influence recommendations for new industry standards.

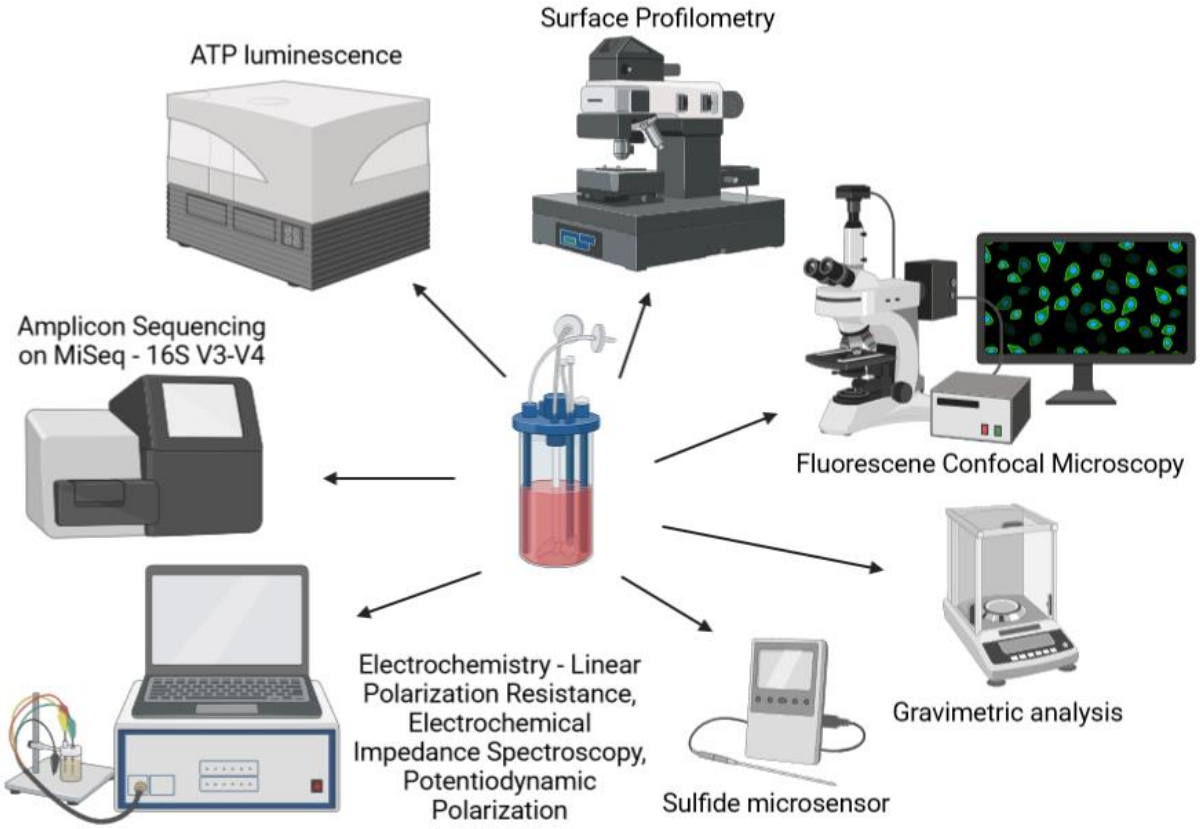

Figure 1. Illustration of the methods employed for this study, using multiple lines of evidence (MLOE) and incorporating a multidisciplinary approach, created using BioRender.com (2023).

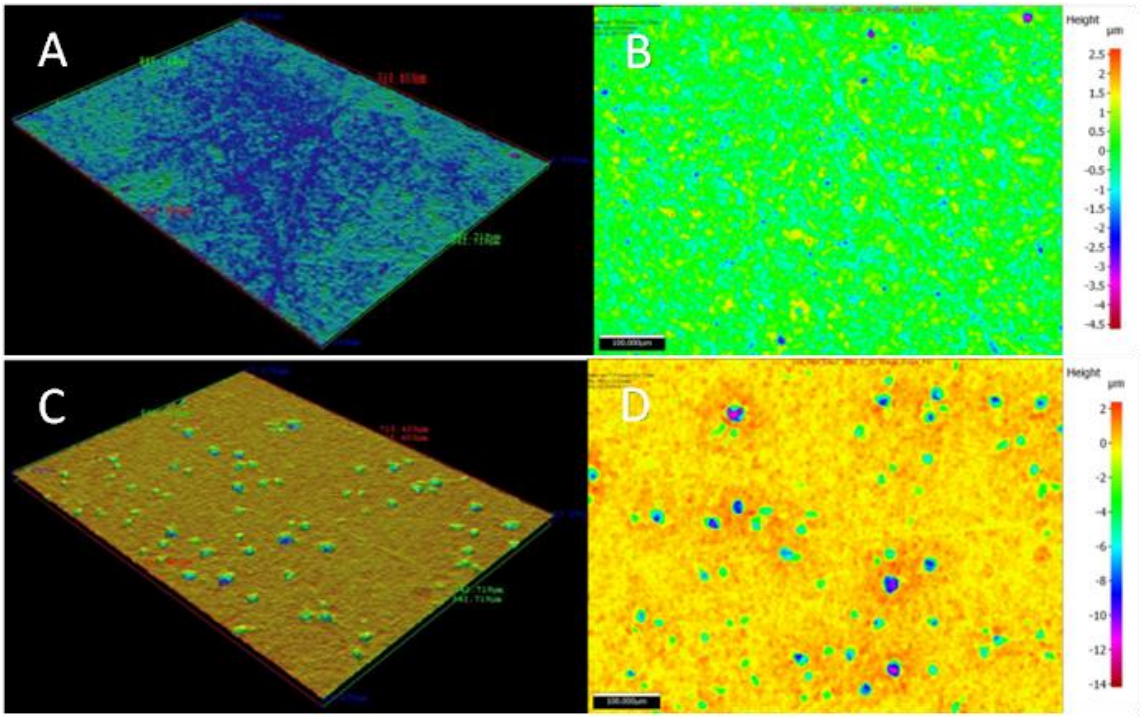

Figure 2. Optical surface profilometry (2D and 3D profiles: scan area of 142 µm × 715 µm) of the UNS G10180 carbon steel surfaces after 7 days (corrosion products and biofilm removed). **A** and **B** polished surface (abiotic media); **C** and **D** polished surface (biotic media).

TMCP Carbon Steel Pipes in Sour Service: performances in high H2S environments

L. Torri, ENI, San Donato Milanese, Italy

M.E. Gennaro, A. Pontarollo, F. Todesco, ENI VELAB, Venice, Italy

Pipe manufactured from the plate rolled by the Thermo-Mechanical Controlled Processing (TMCP) has given benefit for obtaining higher strength and superior toughness for a very long time.

TMCP pipes with Accelerated Cooling (AcC) has shifted high strength line pipe manufacturing away from the use of Quenched and Tempered (QT) grades for seam welded line pipes. This led to considerable economic advantages such as reduced alloying element content and faster rolling and heat treatment process with respect to phase transformation points as well as enhanced weldability.
In the early years of TMCP use in sour service, a primary concern was hydrogen induced cracking (HIC), a problem resulting from centerline segregation, the presence of non-metallic inclusions, and hard second phase products like pearlite and martensite-austenite constituent (MA). With steel making and processing improvements, HIC resistance has improved, particularly with the advent of low carbon, granular bainitic microstructures that are enabled by TMCP.

Despite notable improvements, hydrogen degradation, and particularly SSC, remains a concern for sour applications.

The test campaign was focused on carbon steels for pipeline, namely API 5L grades X52, X60. Specimens were machined from pipes retrieved by service, or from new pipes.

The types of test protocols considered for the investigation of the phenomenon are:

- Hardness test according to ASTM E384;
- Four Point Bent Beam testing (FPBB) according to NACE TM0177 method B;
- Double Cantilever Beam (DCB) test according to NACE TM0177 method D.

The results highlight that the behavior in H2S environment of X52 and X60 TMCP pipes is equivalent, as among all the investigated parameters hardness is confirmed as a discriminating criterion for the quality control to prevent SSC phenomena. For all the other investigated parameters: mechanical properties, microstructure, inclusion levels (HIC), chemical composition the requirements in the API5L and IOGP 616 standards are considered sufficient, and no additional requirements are to be considered. Additional requirements are instead requested for hardness values to guarantee the material compatibility with H2S mainly at intermediate and high ppH2S.

pH_2S from 8 bara up to 10 bara: Results suggest that material hardness must be controlled to avoid values above 220HV10; possibly is requested to perform HV0.5 close the surface with acceptance criteria below 230HV0.5.

pH_2S beyond 10 bara: any grade of TMCP pipes appears not to be suitable at hydrogen sulfide partial pressures beyond 10 bara due to the incumbent presence of small cracks and a significative reduction in the K_{ISCC} value.

Natural Buffered Iron Chloride Containing Solutions for Sulfide Stress Cracking Tests of Low Alloy Steels

Florian Thébault, Vallourec Research Center France, Aulnoye-Aymeries/France;

Hervé Marchebois, TotalEnergies, Pau/France;

Sulfide Stress Cracking (SSC) is a major risk of failure with Oil Country Tubular Goods (OCTG) used in Oil & Gas applications. SSC is mainly driven by pH values of the aqueous phase, partial pressures of H_2S (P_{H2S}) and stresses applied to the material (external and/or residual). Consequently, NACE TM0177 Method A test to assess SSC resistance of low alloyed steels (LAS) requires a tight control of those three parameters among others. However, the in-situ pH value is difficult to maintain constant along the test duration. pH drift is driven by several factors: initial pH value, H_2S concentration and the presence of chemical buffers. In general, pH drift is regulated using a large amount of acetic acid as defined in NACE TM0177 Solution B or an almost daily pH adjustment of the test solution with hydrochloric acid as per EFC (European Federation of Corrosion) 16. A third innovative strategy consists in the addition of a controlled quantity of $FeCl_2$ salt in the test solution. The motivation is to form iron sulfide corrosion products very early during the corrosion test, able to strongly buffer the solution at the target pH. This procedure uses a natural buffering process and does not require regular interventions along the test duration. The present work demonstrates that the use of $FeCl_2$ does not affect the environmental severity, still driven by the final pH value, compared to standardized test solutions. Consequently, $FeCl_2$ test solutions appear as relevant for evaluating SSC resistance of low alloyed steels without any additional chemical compound that may modify the hydrogen absorption while keeping a tight control on pH.

Effect of Strain on Metallurgical Factor and Hydrogen Absorption

Taishi Fujishiro[1], Yusaku Tomio[1], Taro Muraki[1], and Takuya Hara[2]

[1]Nippon Steel Corporation, Japan

[2]Tohoku University, Japan

In oil and gas industry, pipelines for oil and natural gas transportation are exposed to wet H_2S environments (sour environments) in some cases. It is well known that hydrogen embrittlement, such as sulfide stress cracking (SSC) and hydrogen induced cracking (HIC) occur in low-alloy carbon steels under the sour environment. When strain is introduced, various mechanical properties of the steel could change, for example, an increase in the strength (work hardening) or a decrease in the ductility and toughness. It is also known that an absorbed hydrogen in a low-alloy carbon steel increases with increasing the plastic strain introduced. Therefore, the susceptibility of hydrogen embrittlement increases with the plastic strain introduction. However, even though various kinds of strain are introduced through pipe manufacturing processes, the effect of strain path on a hydrogen entry behavior from the corrosive environment during an operation has not been fully understood yet. Furthermore, the metallurgical factors that increase hydrogen absorption with strain introduction have not been investigated well.

This paper describes the relationship between strain paths, metallurgical factors, and the amount of absorbed hydrogen in the low-alloy carbon steel. The effect of strain paths on dislocation density and absorbed hydrogen concentration were evaluated. The effective strain of various strain paths for dislocation that acts as a hydrogen trapping site and hydrogen absorption behavior were revealed. Various strain paths consisting of tensile, compressive, and cyclic strains were applied to the steel specimens. The dislocation density of the pre-strained specimen was measured by X-ray diffraction analysis. Hydrogen concentration in the pre-strained specimens were compared after hydrogen was charged by immersion test. The dislocation density and the hydrogen concentration of the pre-strained steel did not correspond to the integrated amount of each applied strain but to the maximum strain. The maximum strain was correlated with maximum stress during pre-strain introduction. The maximum stress corresponding to the yield stress strengthen by dislocation after pre-

straining. This result suggests that the strain affecting hydrogen absorption of the low-alloy carbon steel is the maximum strain related to dislocation density that acts as a hydrogen trapping site.

Corrosion integrity of natural gas pipelines in energy transition reflecting on decarbonisation strategies in Europe

[1]M. Halama, [2]L. Falat, [1]M. Petrik, [1]P. Slovensky, [1]J. Legemza

[1]Technical University of Kosice, Slovakia

[2] Slovak Academy of Science, Institute of Materials Research

In the context of decarbonisation of energy sector across Europe, esp. in one of key technology with enormous potential in transformation period is high-capacity and relatively cheap transit of hydrogen or mix with natural gas on long distances as more ecological energy media. The potential of retrofit of existing natural gas pipelines for future hydrogen backbone is of interest to many operators of large-scale high-pressure gas transmission system in EU territory with aim to safe, reliable and effective way to fulfilling energy security hand in hand with climatic ambitions. On the other hand, the issue of safety and sustainability of production, distribution and storage of hydrogen becomes an actual challenge [1]. From the point of view of interaction of hydrogen in gas infrastructures during transit we have developed series of tests including thermodynamic calculations of models of H_2 interaction with materials and contaminants, measurements of sensitivity for hydrogen embrittlement, detection of hydrogen diffusion via different grades of steels from X52 to X80, including welds made from dissimilar alloys and data analysis from continual monitoring in terrain. We have observed a decrease in ductility of X60 steel after being electrolytically hydrogenated which was proved by SEM analysis of fracture surfaces after tensile testing. All information gained from this research will serve as an internal database for later early warning “alarm” system for potential risk including assessment of corrosion risk.

Acknowledgements:

This work was carried out within the frame of the project VEGA 2/0072/22 and APVV-21-0142.

Corrosion of Piping in a Crude Oil Storage Facility

Václav Šefl[1], Jan Švadlena[1], Pavel Taraba[2], Tomáš Prošek[1]

[1]Technopark Kralupy of the University of Chemistry and Technology Prague, Kralupy nad Vltavou, Czech Republic

[2]MERO s. p., Kralupy nad Vltavou, Czech Republic

The paper focusses on mitigation of corrosion in the piping network in a crude oil reserve storage facility in Central Europe. The study takes a holistic approach, considering a number of typical suspects such as water content, presence of aggressive species, water-oil separation, dissolved oxygen, storage crude quality, level of stagnancy, steel grade, MIC and presence of deposits. As proved by chemical analysis, the crude oil is a corrosive environment; however, the corrosion rates of typical steel grades in simple immersion laboratory experiments were several orders of magnitude lower than the corrosion rates calculated based on results of on-site non-destructive measurements. Tests in model separated water showed about 20-fold increase in the corrosion rate, and up to 50-fold increase when comparing rates in predominantly stagnant and periodically stirred settings. Finally, a 10-fold increase in the corrosion rate was achieved using a model pit, enclosed by the formation of deposits. On the basis of these data, the overall corrosion mechanism is proposed. It explains the operator experience of the facility in question, where predominantly localized corrosion is observed with corrosion rates that reach up to 1 mm / year. In conclusion, the study presents several approaches to prevent this type of attack, paying close attention to the difficulties of design changes and costs.

Failure due to Corrosion at chemical injection points: Operational Feedback and Lessons Learnt

Yann Joel ASSASSA[1], Herve MARCHEBOIS[1]

[1] TotalEnergies, France

Various chemicals are injected through small bore connections, referred as chemical injection points, into production systems in order to maintain reliability and optimal performance of production operations.

Corrosion at such injection points may occur as some of these chemicals are acidic and lead to weight loss corrosion while highly concentrated.

This paper highlights four field cases where failure occurred in Oil and Gas upstream production facilities. Those specific failures resulted in the design misconception of the injection system and/or mis-used of the chemical product.

Some of these failures also helped to update the international standards associated to the injection systems in Oil and Gas Industry, as well as the evolution of the author's Company specifications.

In addition, the internal qualification procedure defined for chemicals (especially for corrosion inhibitors) was improved to consider this particular aspect.

Keywords: chemical, biocide, corrosion inhibitor, injection point, inspection

Effect of Conversion Coating on Corrosion Mechanism of Pipeline Steel Under Supercritical CO_2 Environment

Jie Pan[1,2], Yixuan Gao[1,2], Yan Li[2], Jian Zhang[1]

1 Sinopec CCUS Key Lab, Sinopec Petroleum Engineering Corporation, Dongying, China

2 School of Materials Science and Engineering, China University of Petroleum (East China), Qingdao, China

CCUS-EOR is one of the best choices to achieve carbon peak and carbon neutralization in the field of petroleum and petrochemical industry. It can effectively store the carbon dioxide generated by chemical plants or coal-fired power plants and increase oil and gas recovery at the same time. At present, North America, China and Europe have formalized several long CO_2 transmission pipelines with 100 km level to transport carbon collected at the upstream capture end.

Supercritical CO_2 is the main carbon transport medium in CCUS-EOR process. However, due to the limitation of cost control and capture technology, the purity of carbon dioxide produced at the upstream capture end is up to 99%. In the presence of multi-impurities such as H_2O, supercritical CO_2 will cause serious corrosion to pipeline steels, including weld region and matrix region. This problem has become one of the pain points of CCUS pipeline safety, especially for long-distance CO_2 transmission pipeline. This research explored the macro/micro corrosion behavior and mechanism of pipeline steel used in the Chinese first 100 km CCUS pipeline under supercritical conditions with impurities through classic and micro-area electrochemical methods. The critical water content index and corrosion behavior prediction model are also explored.

In addition, the construction of novel chrome-free chemical conversion coating regulated by biological extraction macromolecules such as chitosan has greatly improved the corrosion resistance of pipeline steel with different corrosion periods, especially for the supercritical CO_2 media. The surface and depth composition distribution of the conversion coating were characterized by means of SEM, TEM, XPS, FTIR and 3D-CT. The durability and how the conversion coating effect the corrosion behavior of the pipeline steel under normal and supercritical CO_2 conditions were also verified by electrochemical measurements. The research results provide a

corrosion control guidance for practical engineering problems with respect to long distance CO_2 transmission pipelines.

Corrosion Prediction Model Using Statistical and Machine Learning Approaches

Mohammed Attia, Meshary A. Al-Bahli, and Rakan Janbi, Saudi Aramco, Dhahran/Saudi Arabia

Recently the chemical, petrochemical and refinery sectors have been facing tougher safety, environmental and mechanical integrity challenges including the management of Corrosion growth that might lead to leaks and failures causing serious consequences. To overcome this concern, the use of statistical methods jointly with reliability methods offer a potential for a better use of inspection results to predicate of the probability of future leaks and equipment remaining life. The aim of this paper is to develop a methodology that estimates the time-dependent reliability, models the stochastic behavior of corrosion and demonstrate how different factors influence the corrosion growth of a selected piping and vessels of an operating facility. The study carried out an extreme value analysis using three different statistical models, these are, Linear Regression model, Triple Exponential smoothing model and the Machine Learning model. The study covered 922 Corrosion Monitoring Locations disturbed over 12 Corrosion loops. The study revealed different corrosion behavior prediction spectrums for different models and corrosion loops.

Abstract – “Light-weight” tomographic monitoring of pipe wall thickness

Geir Instanes, Vice President, ClampOn, Bergen/Norway

Whilst corroding subsea pipes remains a significant concern, detailed corrosion mapping of these pipes has required computer imaging capability which, until now, subsea permanent monitoring systems have been unable to handle, due to the computing capability and energy required in performing such mapping. This paper addresses the challenges and possibilities of online permanent tomography imaging/mapping of pipes, adopting new technologies and algorithms using low power instruments and providing real time processing.

In the mid-2000s, ClampOn developed its Corrosion-Erosion Monitor (CEM), utilising guided ultrasonic waves (GUW) to monitor wall thickness along a section of pipe. Transducers are permanently installed in two circumferential rings.

Later, the provision of a tomographic wall mapping algorithm operating on the data available from a permanent subsea thickness monitor has been asked for. Knowing the transducer positions and pipe geometry, the mean wall thickness losses measured by multiple partially overlapping acoustic paths are combined to improve the measurement of depth and location of the maximum wall thickness loss. The short calculation times makes it suitable for interactive post-processing of monitoring data, offering results in near real time.

Standard tomographic wall thickness mapping became an option mid-2010s, with the integration of the software package CorrPRINT. Systems with full coverage of a pipe section provide three-dimensional maps of wall thickness loss, with key results like minimum wall thickness and defect positions transmitted to the control system. Many wall thickness monitors are equipped with fewer transducers than what is required for standard tomographic wall thickness mapping. The intention and challenge of the “Tomography Light” system is use these simpler and more cost-effective systems and still be able to achieve tomography mapping of a local area where corrosion or erosion is expected to be most severe.

Preliminary numerical and experimental tests yield good results, even with the constraints of the physical measurement principle between CorrPrint and Tomography Light.

Author: Geir Instanes

Mechanical and corrosion properties of $CoCrFeNiMo_{0.85}$ high-entropy alloy coatings prepared by high velocity oxygen-fuel spraying technology

Ming Jing[1], Feifei Zhang[2] and Mengyan Nie[*,1]*

[1] Institute for Materials discovery, University College London, London, United Kingdom;

[2] TWI Ltd, Cambridge, United Kingdom

** Correspondence email: mengyan.nie@ucl.ac.uk*

Due to unique mechanical properties, high entropy alloys (HEAs) have attracted great interest. Compared with mechanical properties, corrosion behavior of HEAs have not been fully understood. Especially, corrosion properties of HEAs in alkaline environment are seldom reported by far to the best of our knowledge. In this paper, $CoCrFeNiMo_{0.85}$ HEA coatings were prepared on mild steel surfaces using high velocity oxygen-fuel (HVOF) spraying technology to investigate the feasibility of HEA coatings for downhole drilling applications. The as-prepared HEA coatings were characterized by scanning electron microscopy (SEM) and X-ray diffraction (XRD). It was observed that the phase composition of the $CoCrFeNiMo_{0.85}$ HEA coating is predominated by face-central cubic (FCC0 phase with a small amount of secondary phase, which is caused by the presence of large atomic radius element Mo. The surface of the as-prepared HEA coatings by HVOF is generally rougher with hierarchical micro-nano structures, which causes the coating surface superhydrophobic with water contact angles measured in the range of 120-150^{O}. The microhardness of the HVOF-prepared HEA coatings is significantly higher than that of the mild steel substrate. It is also observed that high oxygen and kerosene flow rates help to inhibit the generation of secondary phases, and that the presence of secondary phases brings about a more pronounced precipitation strengthening effect.

The corrosion properties of the as-prepared CoCrFeNiMo0.85 HEA coatings with HVOF technology were studied in an alkaline testing solution of 0.1 mol/L NaOH using electrochemical corrosion testing techniques including open-circuit potential (OCP), electrochemical impedance spectroscopy (EIS) and polarization curves. Electrochemical testing results showed that the HVOF prepared HEA coatings exhibited an unexpectedly poor corrosion resistance in the alkaline testing solution

compared to the mild steel substrate, with corrosion current densities two orders of magnitude higher than that of the mild steel substrate. The corrosion mechanisms of the HEA coatings in the alkaline solution was further investigated using SEM and energy dispersive spectroscopy (EDS) on corroded coating samples.

Corrosion properties of HVOF manufactured NiCrFeSiB self-fluxing alloy coatings in alkaline solution

Haowei Zhao[1], Feifei Zhang[2] and Mengyan Nie[*,1]*

[1] Institute for Materials discovery, University College London, London, United Kingdom;

[2] TWI Ltd, Cambridge, United Kingdom

** Correspondence email: mengyan.nie@ucl.ac.uk*

In this paper, Ni-base self-fluxing alloy (NiCrFeSiB) coatings were prepared on the carbon steel substrates using high velocity oxygen fuel (HVOF) technology under different oxygen flow rates to investigate the feasibility of applying them for down-hole drilling. The microstructure, morphology and elemental distribution of the as-prepared coatings were characterized by X-ray diffraction (XRD), scanning electron microscopy (SEM), and energy dispersive X-ray (EDX) analysis techniques. The corrosion properties of the as-prepared coatings were assessed in an alkaline solution of 0.1 mol L^{-1} sodium hydroxide using electrochemical corrosion techniques, including open-circuit potential (OCP), electrochemical impedance spectroscopy (EIS), and polarization curves. All corrosion testing results demonstrated that the as-prepared coatings exhibit enhanced corrosion resistance in the alkaline testing solution compared with the carbon steel substrates, in addition to significantly enhanced hardness. The corroded coatings samples were further analyzed using SEM, EDX and contact angle to understand the corrosion mechanisms of the self-fluxing alloy NiCrFeSiB coatings in the alkaline environment. Combined with optimized HVOF technology, NiCrFeSiB self-fluxing alloy demonstrated great potential as drill bit coatings for down-hole drilling.

The Study of the Anti-Corrosion Effect of NiCrAl Addition to Protective Coatings Applied to Carbon Steel Pipelines Used in Oil & Gas Industries

Mutairi S.A, ***Saudi Aramco, Dhahran/Saudi Arabia; sultan.mutairi.1@aramco.com***

Rasheedi N.A Saudi Aramco, Dhahran/Saudi Arabia; ***nayif.rasheedi@aramco.com***

Keywords: NiCrAl, Pipelines, Oil & Gas, Corrosion, Accelerated.

This paper investigates the anti-corrosion effect of NiCrAl addition to protective coatings applied to carbon steel pipelines used in oil & gas industries. An accelerated corrosion test used to study the corrosion resistance of NiCrAl applied to metallic carbon steel substrates. HVOF (high velocity oxygen fuel was used to develop four sprayed coatings, using WC-Co powders of various size micro and nano structured mixed with NiCrAl at ratio of 3 to 2 respectively in the top layer coat of 160 micron. The test was performed in a controlled corrosive environment designed to represent marine type atmospheric conditions in the Arabian Gulf area. All of coatings were exposed to a moist environment which was composed of 5% sodium chloride. The results revealed that the satisfactory properties of WC-Co-NiCrAl powder were strongly enhanced by the corrosion resistance of the multilayered coating in comparison to WC-Co coatings that used in this study.

Imaging and In Situ Force Probing of Electrodeposited Zinc Moderated by Polycationic Polymers

L. L. E. Mears, Vienna University of Technology, Vienna/AT, G. F. Tiétcha, Dörken Coatings GmbH & Co. KG, Herdecke/DE, M. Hahn, Vienna University of Technology, Vienna/AT, M. Roth, Dörken Coatings GmbH & Co. KG, Herdecke/DE, I. Klüppel, Dörken Coatings GmbH & Co. KG, Herdecke/DE, M. Valtiner, Vienna University of Technology, Vienna/AT

Electrodeposition of metals is relevant to much of materials research with the deposition of zinc particularly important for anticorrosion coatings. The sacrificial characteristics of zinc used as a protection for ferrous substrates is a central corrosion protection strategy used in automotive, aviation, and DIY industries. Although zinc layers are often applied to a base metal in a hot dip galvanizing step; there is a significant interest in less energy and material intense electroplating strategies for zinc. At present, large-scale electroplating is mostly done from acidic zinc solutions, which contain potentially toxic and harmful additives. Alkaline electroplating of zinc offers a route to using environment-friendly green additives. Further to our previous elucidation of the mechanism by which the polyquarternium polymer aids deposition of the negatively charged zincate,[1] within the scope of this study we probe the nature of the coating deposited.

Zinc was deposited from an electrolyte containing soluble zinc hydroxide compound and a polyquarternium polymer, as additive, on gold model surfaces. Atomic force microscopy and surface forces apparatus measurements have allowed us to image the deposited zinc layer to see why the addition of the polymer improves the quality of the coating. Importantly it also provides additional insight into the exact mechanism of layer formation in the first seconds of electrochemical polarisation.

[1] G. F. Tiétcha et al. ACS Applied Materials & Interfaces 2020, 12 (26), 29928-29936

Complex study of mild and strong alkaline cleaning of Zn-Al-Mg hot-dip galvanized steel

Maria Ponomareva,

CEST Centre for Electrochemistry and Surface Technology, Linz/Austria

Jiri Duchoslav, David Stifter,

ZONA Centre for Surface and Nanoanalytics, JKU Linz/Austria

Gerald Luckeneder, Roland Steger, Sandra Grienberger,

voestalpine Stahl GmbH, Linz/Austria

Matthias Kogler, Markus Valtiner, Vienna University of Technology, Vienna/Austria

Surface cleaning is one of the standard procedures in galvanized steel production. Mild and strong alkaline cleaners, that are utilized to remove oils and contaminants appeared during the steel processing, still how they affect the surface while pretreating is unclear to date. However, this can determine the corrosion behavior and corrosion kinetics of the surface after treatment and furthermore can influence the ability to apply organic and inorganic coatings.

In detail, although the Zn–Al–Mg (ZM) coatings show enhanced corrosion protection properties, they cannot withstand the attack of the mild and strong alkaline medium during cleaning. The surface chemistry of cleaned ZM coatings is decisive for the final corrosion resistance resulting in the material lifetime.

In this work, two perspectives were considered to investigate cleaning processes, with mild and strong alkaline cleaners. First, analysis of elements dissolved during the cleaning using inductively coupled plasma optical emission spectrometry (ICP-OES) was applied. Second, to evaluate the surface and its changes after the alkaline cleaning a range of complementary analytical techniques were used. Infrared reflection absorption spectroscopy (IRRAS) was used to evaluate the cleaning efficiency of mild and strong alkaline cleaners. Auger electron spectroscopy (AES) was applied to enable the analysis of resulting changes of surface chemistry, while Scanning Kelvin probe (SKP) registered a contact potential difference change. Surface analysis using X-ray photoelectron spectroscopy (XPS) was further used to determine the chemical composition of surface oxide layers, and Low energy ion scattering (LEIS) depth profiling, revealed novel insight of surface oxides relations before and after cleaning.

Our data suggest a very profound influence of the cleaning pH on the resulting oxide structure and surface chemistry, which in turn has a strong influence corrosion and the ability to apply organic and inorganic coatings.

Comparison on Corrosion Properties of Zn-Coated Steels under Accelerated Corrosion Tests Used in EU and Asian Industries

Frank Beier, Christian Vree, Salzgitter Mannesmann Forschung GmbH, Germany

Yun Ha Yoo, Su Jik Hong, POSCO Technical Research Lab., Korea

The anti-corrosion performance of steels is evaluated using accelerated corrosion tests standardized in various industries, and the corrosion behavior of the steels is influenced by accelerating conditions such as temperature, condensation, wet-dry transition and salt load. This also varies greatly depending on the materials (uncoated or Zn-coated) and types of corrosion, such as bare or painted surface, crevice, and bimetallic joints. In a recent study, the corrosion ratio of uncoated to Zn-coated steel is used as an index of relevance of field corrosion, and it is generally known that this ratio has a value of 4~10 under atmospheric corrosion for painted steels. However, this index sometimes shows significantly lower value under certain corrosion tests. That means the corrosion resistance of Zn-coated steel may be under-estimated, and lead to inappropriate steel selection in the industrial fields. Therefore, it is important to understand the effect of accelerating factors on the corrosion of steels.

A German steelmaker, Salzgitter and a Korean steelmaker, POSCO have conducted a co-research to understand the corrosion behavior of automotive and constructional steels under corrosion test standards mainly applied in each region of EU and Asia.

Representatively, VDA 233-102 (ISO 11997-3) is used for automotive corrosion test in EU and consisted with relatively lower salt load and dry condition. Meanwhile the tests with higher salt load and wet condition (5% salt, longer spray and condensation stages) such as ISO 9227 and ISO 14993 are prevailing in Asia. In this study, it is discussed on the corrosion characteristics in bare, painted surface of uncoated, Zn-coated and ZnMgAl alloy-coated steels, and bimetallic joint with aluminum under the different accelerated corrosion tests. From the results of this study, the importance of standardized corrosion test with high field-relevance and widely was suggested in steel suppliers' perspective.

INTERN

New methodology for microstructure evaluation of multiphase coatings to better understand corrosion mechanisms

Guilherme ADINOLFI COLPAERT SARTORI, Chimie ParisTech/ArcelorMittal, Maizières-lès-Metz, France, guilherme.adinolficolpaertsartori2@arcelormittal.com; Tiago MACHADO AMORIM, ArcelorMittal, Maizières-lès-Metz, France; Polina VOLOVITCH, Institut Photovoltaïque d'Île-de-France (IPVF), UMR 9006, CNRS, Ecole Polytechnique, IP Paris, Chimie Paristech, PSL, Palaiseau, 91120, France, France, polina.volovitch@chimieparistech.psl.eu

The classical solution to improve the corrosion protection of steel is hot-dip galvanizing (GI). In the last decades, the steel industry has worked on new solutions to improve the performance of coatings, either by alloying the Zn with other elements (Al, Mg) or completely replacing Zn galvanizing with other elements, as Al.

As a result, new coatings with complex microstructures are developed and need to be investigated. Moreover, these coatings present different phases with specific chemistry and electrochemical activities which can lead to different corrosion behavior. Knowledge of the nature of the phases, their amount and their distribution is, therefore, an important step for understanding corrosion mechanisms of new coatings which can guide the research for more performing compositions.

The main objective of the present work is to propose a quantitative tool for the description of the multiphase coating microstructure, which could anticipate the electrochemical behavior of multiphase metallic coatings. The approach is demonstrated on the example of ZnAlMg alloys using macros in the software specialized in image processing Aphelion™ SDK. It allows to obtain information regarding the phases that are present (and in which amount) as well as their size, distribution, and the different couplings situations.

To analyze the coating, the software analyses the cross-section backscattered electron images of the coating obtained by Scanning Electron Microscopy and elemental distribution maps obtained by X-rays. Based on the expected chemical composition of the phases, a specific one can be assigned to each pixel or a specific region. This can be useful for multi-constituent phases, as the eutectic binary and ternary phases, with lamellar microstructure, typical for ZnAlMg alloys. In addition,

phases that are easily identified by the BSE image can be attributed by greyscale thresholding.

Furthermore, some post-identification analyses are possible, such as quantification of the interfaces between specific phases in the coating, the distribution of the elements inside a selected phase, or if there is a non-homogenous in-depth distribution of different phases (for example if some phases are preferentially located close to the coating/substrate interface).

AluZinc and Magnelis galvanized steels were used to illustrate how the software can be used for corrosion prediction. For example, Figure 1 shows the SEM-BSE images and the images after the Aphelion™ SDK treatment procedure. Table 1 presents the values of the corrosion potential of different identified phases in NaCl and Na_2SO_4 solutions at pH 7, as well as their percentage in each coating. AluZinc contains mainly dendrites of Al and free Si, the first being little less noble than Fe and the second being nobler. Specially in Na_2SO_4, Al presents a potential close to iron, not corroding preferentially and generates preferential corrosion paths in the interdendritic zone. Magnelis, however, consists mainly of ternary ZnAlMg, binary ZnMg and Zn phases, that are considerably less noble than iron and will corrode homogeneously. Thus, is it expected that Magnelis will offer more sacrificial protection to the steel substrate than AluZinc. The better behavior of Magnelis was confirmed by cross-section corrosion tests.

This methodology allowed to successfully predict the corrosion behavior of different coatings by understanding the microstructure. This analysis is fundamental to comprehend the corrosion mechanisms. The predictions were validated by accelerated corrosion tests, confirming the interest of this approach.

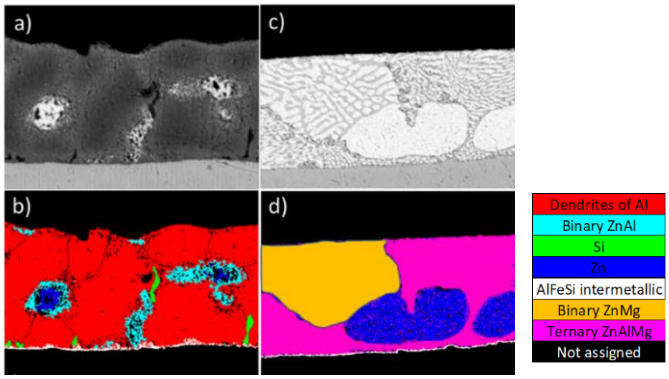

Figure 1 SEM-BSE images of the coatings AluZinc (a) and Magnelis (b) and theirs corresponding Aphelion™ results in (c) and (d) respectively. It can be noticed that AluZinc in mainly constituted by dendritic grains of Al while Magnelis in mainly constituted off the ternary ZnAlMg.

Table 1 Potential of different phases in NaCl pH 7 medium as well as the composition of the coatings AluZinc and Magnelis.

Phase	Potential in Na2SO4 pH7 (V/SCE)	Potential in NaCl pH7 (V/SCE)	Aluzinc composition (%)	Magnelis composition (%)
AlFeSi intermetallic	-0.4	-0.40	2	1
Si	-0.5	-0.5	1	0
Fe	-0.6	-0.6		
AlZn dendrite	-0.65	-0.94	76	0
Zn	-1.02	-1.02	1	14
ZnAl binary	-1.04	-1.04	12	0
Ternary Zn/Zn2Mg/Al	-1.06	-1.06	0	71
Binary ZnMg	-1.06	-1.06	0	11

Electrochemical Real-Time Monitoring of Cr(III)-based Passivation Processes of ZnNi Coatings

Eva Tarfeld, Tim Gommlich, Günter Schmitt*

Abstract

Within the ZIM** international cooperation project MONACO-PLATE*** it was found that the Cr(III)-based passivation process of galvanic ZnNi coatings can be monitored and controlled in real time by in-situ measurement of time-related open circuit potentials (OCP) at the ZnNi-plated surface.

After immersion of a ZnNi-coated probe into the passivation bath the OCP increases from potentials around -550 mV_H within 30 to 60 s to a potential plateau between -120 mV_H and -90 mV_H. The passivation step is finished when the slope of the OCP transient reaches the plateau at dU/dt close to zero. This time is approx. 30 seconds for a fresh bath and increases with the age of the bath characterized by a process-related increase of foreign ion concentrations (Zn, Fe). Using the slope of the OCP transient at characteristic immersion times the time to reach complete passivation and the age/integrity of the bath can be determined in real time. Correlating process parameters with the protectiveness of the produced passivation layers, the optimum service life of passivation baths can be determined. This methodology was already applied in a Cr(III)-based passivation bath of a ZnNi deposition pilot plant line. With appropriate electrical contacting the OCP transient can even be measured on the surface of bulk material in electroplating barrels. This is a first step in digitalization of process steps in commercial electroplating lines to assure product quality, save resources, reduce waste water, and improve economy. Work is under way to electrochemically monitor also other process steps like degreasing and pickling.

* Correspondence author for the MONACO-PLATE authors collective:
Eva Tarfeld, Tim Gommlich, Günter Schmitt (IFINKOR – Institute for Maintenance and Corrosion Protection Technologies gGmbH, Iserlohn, Germany);Thomas Nitzsche, Jacqueline Hatton (Hillebrand Chemicals GmbH, Wickede/Ruhr, Germany);
Peter Schrems (IPS Elektroniklabor GmbH & CO KG, Münster/Hessen, Germany;
Andre Berse, Marc Camminady (DOK Chemie GmbH, Kierspe, Germany);
Mai Thanh Tung (Hanoi University of Science and Technology, School of Chemical Engineering, Hanoi, Vietnam).
**Zentrales Innovationsprogramm Mittelstand (ZIM) des Bundesministeriums für Wirtschaft und Klimaschutz (BMWK); Central Innovation Program for Smaller and Medium Enterprise (SME) of German Federal Ministry for Economy and Climate Protection.
*** Förderkennzeichen KK5277101KO1

Electrodeposition of Zinc in Ionic Liquids- A Comparative Study

Kranthi Kumar Maniam, *Materials Innovation Centre, School of Engineering, University of Leicester, Leicester/United Kingdom;*
Shiladitya Paul, Materials and Structural and Integrity Technology Group, TWI, Cambridge/United Kingdom

Electrodeposition of zinc (Zn) from non-aqueous systems such as ionic liquids (ILs) are identified as one of the beneficial approaches in addressing the challenges associated with the conventional aqueous systems (such as hydrogen evolution). These coating systems are used for applications such as marine, automotive etc. While the choline chloride IL system has gained significant attention, research attempts has been shifting towards the development of halide-free ILs owing to their advantages in minimizing the environmental toxicity associated the formation of chlorinated compounds, that result during the Zn deposition from choline-based ILs. The objective of this work is to provide a detailed analysis of the electrodeposition of Zn on mild steel substrates performed using the newly developed halide-free IL electrolytes and compare them against halide based ILs and conventional aqueous electrolytes. The influence of deposition conditions (current, potential, time, pH, temperature, mode of deposition) studied in relation to the Zn nucleation and growth mechanism on mild steel substrates from both the electrolytes using electrochemical characterization techniques (cyclic voltammetry, linear sweep voltammetry), physical characterization techniques (scanning electron microscopy, X-ray diffraction) will be compared.

Preliminary Results

Initial hull cell study on the Zn deposition from acetate based IL yielded a good deposit at lower current densities with comparable cathodic current efficiencies. X-ray diffractograms of the Zn deposits from acetate based IL displayed the typical crystallographic characteristics in line with the conventional aqueous electrolytes.

Significance of Work

This work is intended to study the electrodeposition of zinc using a novel approach (halide free ionic liquids), which would overcome the existing environmental challenges associated with conventional aqueous and developed non-aqueous systems (halide based).

Tribocorrosion and tribological behavior innovative chrome coating produced by plasma transferred arc

Muslum YUNACTI[1], Ophélie RIOU[2], Alex MONTAGNE[3], Véronique VITRY[1]

1*Université de Mons, Faculté Polytechnique, Service de Métallurgie, Rue de l'Epargne, 56, Mons, BELGIUM*

2*CRITT Matériaux Innovation, 9 Rue Claude Chrétien, Campus Sup Ardenne, Bâtiment D, Charleville-Mézières, France*

3Université Polytechnique Hauts-de-France, LamiH UMR 8201 CNRS, Campus Mont Houy, Valenciennes, France

veronique.vitry@umons.ac.be , o.riou@critt-mi.com , alex.montagne@uphf.fr

muslum.yunacti@umons.ac.be

Plasma Transferred Arc (PTA) is a thermal spray surfacing technique derived from welding processes. It allows refurbishing of a worn piece, or local enhancement of the wear and corrosion resistance of a new part, without modification of the bulk properties. Depending on the applications and the desired properties, the existing materials deposited by PTA are an alternative to hard chrome plating. Indeed, stellite (cobalt-based alloys) deposits by PTA exhibit exceptional hardness and toughness and are very resistant to corrosion. They are used in particular to coat steel automotive engine valves.

Replacing electrolytic chromium with a deposit of pure chromium appeared as an innovative solution, combining the PTA process and the chromium materials. That type of coating presents interesting mechanical properties which are higher than stellite. In addition to mechanical properties, it is also necessary to investigate the tribological and tribocorrosion properties of the coating.

In the present study, stellite and chrome coatings produced by PTA were characterized in dry sliding and tribocorrosion tests. Reciprocal (pin on bloc) tests were used in this study. During the tests, the friction coefficient of the coatings was recorded and the results are shown in Figure 1. They present similar COF; however, the fluctuations for stellite coating are observed, which can result from debris formation due to the low hardness of the coating (see Table 1).

After tests, worn samples were analyzed to investigate the wear mechanism and wear volume using optical confocal microscopy, Scanning Electron Microscopy (SEM), and optic profilometer.

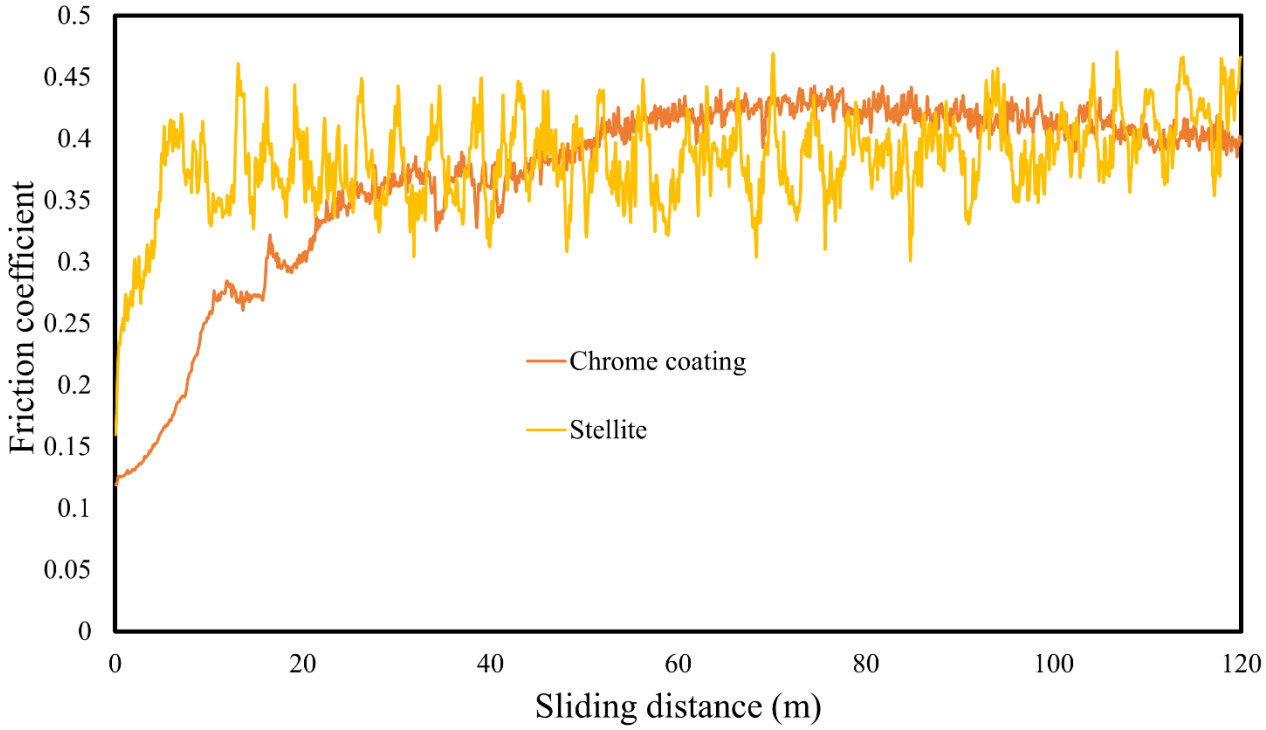

Figure 1: COF of the chrome and stellite coatings produced by PTA

Table 1: Coating hardness

Coating	Hardness (HV)
Stellite	300
Chrome	392

Keywords: PTA, chrome coating, tribocorrosion, tribology , COF

Using electrochemical noise technique to understand the pitting corrosion behavior of Ni-B-ND composite coatings

Sepehr Yazdani,[1], Loic Prince[2], Veronique Vitry[1]

1 Metallurgy Lab, UMONS, 20 place du Parc, 7000 Mons, Belgium

2 Materials Science Department, Faculty of Engineering, University of Mons, 20, Place du Parc, Mons, Belgium

Abstract

Electroless nickel boron (Ni-B) coatings can be used in various industries such as space, petroleum, automotive and plastic because of their desirable mechanical properties. However, due to the inherent porosity of the nickel boron coating, pitting and localized corrosion attack leads to coating degradation when it is exposed to corrosive environments. The progressive penetration of the corrosive media into the defects and grain boundaries results in high speed of the coating degradation. One of the main methods to improve the pitting corrosion behavior of Ni-B coatings is adding nanoparticle to fill the defects. Nanodiamonds (ND), as electrochemically inert particles, can be useful for filling the porosity of the coating. Therefore, in this study the effect of adding ND into electroless Ni-B to improve pitting corrosion resistance was examined using electrochemical noise technique. The lowest fluctuations of potential and current noise were observed when nanodiamonds are added to the Ni-B electroless plating bath which indicates a reduction of the formation of metastable pits or degradation of the passive layer. Using the stochastic theory, it was revealed that by introducing ND into the coatings, the pit initiation rate can be reduced. Further potentiodynamic polarization test also verified the stability of passive layer in Ni-B-ND, however, unstable passive layer formed for the Ni-B sample due to the severe pitting corrosion and localized attack. Results of this study shows the possibility of using nanodiamonds in Ni-B to prevent pitting corrosion.

Performance Study of HVOF Thermal Sprayed Nanostructured WC-12Co Mixed with Inconel-625 Coatings

Mutairi S. A., Saudi Oil Company, Dhahran; sultan.mutairi.1@aramco.com
Rasheedi N. A., Saudi Oil Company, Dhahran; nayif.rasheedi@aramco.com

Keywords: HVOF, Inconel-625, WC-12Co, Nanostructure, Erosion-corrosion.

Many components and machinery parts in the oil and gas industries suffer from erosion-corrosion degradations due to the impact of small solid particles entrained a liquid stream during transportations. To overcome such tribological problem, the demand for WC-12Co and Inconel-625 HVOF thermal spray coatings is becoming more and more stringent. To date the development of nanostructured WC-12Co feedstock materials have significantly improved the mechanical property performance of such coatings over conventional micro-structured coatings. This paper identifies the recent developments of WC-12Co nanostructured coatings and how they have performed when deposited using different thermal spray techniques, such as some of the successful spray techniques such as high velocity oxy fuel (HVOF) and cold gas dynamic spray. The research focuses also on the modification of WC-12Co by addition of Inconel-625 against erosion-corrosion. The results demonstrate that the significant improvement in nanostructured WC-12Co coating performance can be achieved by utilizing proper controlling parameters for HVOF technique and great improvement in erosion-corrosion resistance due to Inconel-625 addition.

The influence of the HVOF parameters on the corrosion behavior of coatings manufactured on aluminum parts obtained by Additive Manufacturing

S. García-Rodríguez, N. Abu-warda, J. Bedmar B. Torres, J. Rams

Área de Ciencia e Ingeniería de Materiales, ESCET, Universidad Rey Juan Carlos, C/ Tulipán s/n, Móstoles 28933 Madrid (Spain)

Additive Manufacturing processes (AM) have many advantages over conventional manufacturing techniques, such as the possibility of manufacturing highly complex geometric parts. However, the expansion of the field of application of AM parts is currently limited by its main drawbacks. These disadvantages are mainly related to the porosity, the surface irregularities, and the anisotropy of the manufactured parts. In order to improve the additive manufacturing surface parts, the manufacturing of coatings is one of the main solutions.

The aim of this study is to combine the advantages of additive manufacturing techniques with those offered by coating manufacturing techniques in order to obtain parts with improved surface properties, obtaining likewise an improvement in the corrosion behavior. Thus, 316L stainless steel coatings have been applied on aluminum additive manufacturing parts using the High Velocity Oxy-Fuel thermal spraying technique (HVOF). The optimal spraying conditions have been stablished varying the flame conditions and using the Accuraspray equipment to monitor the changes that these produce in the sprayed particles. The coating characteristics (thickness, continuity, homogeneity, and porosity) have been correlated with the spraying parameters used.

The protection against corrosion provided by these coatings has been tested in chloride solution, for different immersion times, by lineal polarization test, anodic-cathodic polarization test and by Electrochemical Impedance Spectroscopy (EIS). After testing, the morphology and optimum thickness of the coating to act as an effective barrier against corrosion for at least 7 days has been determined.

Subtopic – Coatings (WP14)

Corrosive Behavior Investigation of Decorative Physical Vapor Deposited Mild Steel in Different Media

Aleyna Bayatlı[1], Arif Akıllılar[2], Mustafa Kocabaş[1],*

[1] Konya Technical University, Metallurgical and Materials Eng., Konya, 42250, Turkey

[2]Tosunogulları Furniture Industry (Burotime), Konya, 42100, Turkey

Metallic parts use commonly in furniture and home design industries due to their shiny bright, decorative, and aesthetic appearance like chair arms, door handles, clothes-hanger, armature, etc. However, these parts generally expose to different corrosive media by hand-contacting or cleaning because these materials are designed as an office or home furniture. For design and decorative purposes, the metallic parts are colored with the physical vapor deposition (PVD) method to obtain attractive colors such as gold, dark black, and gray. This process fulfills attractive, uniform, and desired color to the metallic part demanded by customers. However, it is known that PVD coated metallic part cannot act as a fully protective layer because it has some imperfections like columnar structures, pinholes, pores, void zones around nodular defects or droplets (crevices), microcracks, grain boundaries, and other discontinuities. In order to equalize the detrimental outcomes from the PVD process, electroless coatings are commonly used as an interlayer coating to protect surfaces from corrosion. In this respect, some mild steel samples firstly were coated with electroless nickel (EN) with approximately 5 µm before PVD with dark (gun) black color. The corrosive behavior characteristic was compared with three characterization method which were i) electrochemical analysis, ii) dipping corrosion experiment with 14 days, and iii) salt spray test (ASTM B117) as follow samples: i) mild steel, ii) mild steel + EN, iii) mild steel + PVD, and iv) mild steel + EN + PVD. In order to investigate the pre-treatment effect (sandblasted and non-sandblasted surfaces) coatings were also compared. The corrosive environments were selected from popular cleaning solutions with different pH values. These are 10% commercial white vinegar (pH=2-3), tap water (pH=6-7), and 10% laundry bleach solutions (pH=12-13). In addition, the coated surfaces were characterized by using OCP (open circuit potential), EIS electrochemical impedance spectroscopy), and PDP (potentiodynamic polarization) analysis in the same three corrosive environments. After the dipping

corrosion test, the dipped surface was exposed to the same electrochemical analyses, again. The morphologies of coatings were examined with SEM (scanning electron microscopy) and optical microscopy from surface and cross-section. Finally, reciprocating wear tests were applied to observe the adherence behavior of PVD coatings on the EN layer. It was concluded that;

- PVD coating method is suitable for furniture design application which showed excellent dark color.
- PVD coatings have good adherence with EN interlayer and substrate material.
- The coating which have s interlayers has more corrosive resistance in all type of corrosion test.

Microstructure and corrosion resistance of Hf-coated Mg alloy by magnetron sputtering with thermal oxidation treatment

Zhoucheng Wang

College of Chemistry and Chemical Engineering, Xiamen University, Xiamen/China

Magnesium and its alloys are attracting tremendous attentions to aerospace and electronic industries owing to their low density, excellent electrical conductivity and good electromagnetic shielding characteristics. Nevertheless, the high sensitivity to wear and corrosion produces a sever challenge for their widespread practical application. As for magnesium alloy used in electronics and aerospace, the protective coatings are confronted with new requirements: high corrosion resistance and to be conductive to maintain the fine electrical and magnetic properties of magnesium alloy matrix. With the above in mind, metallic coatings have been fabricated on magnesium alloys. Metallic hafnium (Hf) coating fabricated by physical vapor deposition (PVD) with the merits of low potential difference to magnesium alloy reveals a satisfactory protection to magnesium alloy both in short and long-term tests.

Hf coatings are fabricated on Mg alloy by PVD magnetron sputtering and further submit to thermal oxidation treatment at temperature of 200℃, 300℃ and 400℃, respectively. The surface analysis indicates that new shallow grain boundaries are appeared on the coating surface when the treatment temperature is over 300℃. These changes in microstructure inhibit the permeation of corrosion media into the substrate and decrease the diffusion rates of corrosion products. As a result, surface densification and oxidation of the coating induced by the post treatment significantly decreased its susceptibility to corrosion. In addition, the release of the residual stress produced by the post treatment suppresses the delaminating of the coating as Mg is corroded. Consequently, the Hf coating post-treated with 400℃ exhibits more positive corrosion potential, lower corrosion current density and higher polarization resistance than that of the other coating in electrochemical test. However, salt spray test reveals that the Hf coating post-treated with 300℃ provides the most efficient long-term protection for Mg alloy. Scratch test reveals that it was mainly due to the poor adhesion strength resulted from the big difference in thermal expansion coefficients between coating and substrate during the high treatment temperature.

Functionalization of PEO/sol-gel systems with inorganic inhibitors for corrosion protection of AZ31 Mg alloy.

Esther López, Universidad Complutense de Madrid, Spain
Borja Pillado, Universidad Complutense de Madrid, Spain
Marta Mohedano, Universidad Complutense de Madrid, Spain
Enzdhe Matykina, Universidad Complutense de Madrid, Spain
Raúl Arrabal, Universidad Complutense de Madrid, Spain

Abstract: Plasma electrolytic oxidation (PEO) coatings offer many advantages such as improved corrosion and wear resistance. However, PEO requires a sealing post-treatment for long-term corrosion protection. In the present work, hybrid PEO/sol-gel systems loaded with inorganic corrosion inhibitors (Ca, Li, Zn and Ce) are used with the aim to provide self-healing properties to the AZ31 alloy. This is an alloy commonly used in transport and consumer applications.
The PEO coating was produced under DC conditions in an aluminate-phosphate based electrolyte for a short period of time (~100 s, i.e. Flash-PEO). Characterization of the coatings was carried out by means of X-ray diffraction (XRD), scanning electron microscopy (SEM) and Fourier transform infrared spectroscopy (FTIR). The water contact angle and the surface roughness were also evaluated. The corrosion behavior was studied in 0.5 wt. % NaCl aqueous solution using electrochemical impedance spectroscopy (EIS). The self-healing ability of the systems was also assessed by using scratched specimens. Findings revealed incorporation of the inhibitors into the sol-gel layer and improved corrosion performance.

Corrosion resistance enhancement of AZ31 Mg alloy by the formation of layered double hydroxide on a TiO_2-incorporated plasma electrolytic oxidation coating

Roya Malekkhouyan, University of Mons, Mons/Belgium

Marie-Georges Olivier, University of Mons, Mons/Belgium

Plasma electrolytic oxidation (PEO) has attracted attention as an environmentally friendly and inexpensive protection method for magnesium alloy substrates. The chemical composition of the PEO layer is influenced by the electrolyte. The concentration of a new electrolyte containing KOH, $NaAlO_2$, and $Na_6(PO_3)_6$ along with TiO_2 nanoparticles was optimized from an anti-corrosion resistance point of view. Layered double hydroxide (LDH) was then formed on the PEO layer via in-situ hydrothermal treatment to seal the pores and cracks, without the addition of metal cations to the LDH preparing solution. TiO_2 nanoparticles were incorporated into the PEO layer directly by adding them to the electrolyte and their effect on LDH structure as well as the corrosion resistance of the substrate was assessed.

Scanning electronic microscopy (SEM), energy-dispersive spectrum (EDS), X-ray photoelectron spectroscopy (XPS), and X-ray diffractometer (XRD), were performed for investigating the morphology, chemical composition, and crystalline structure. In addition, electrochemical impedance spectroscopy (EIS), and Time-of-Flight Ion Mass Spectroscopy (ToF-SIMS) were used for corrosion characterizations. The results revealed the better anticorrosion performance of the substrate after the addition of TiO_2 nanoparticles to the PEO layer and the formation of LDH nanosheets due to their synergic effect. The prepared conversion coating can be further used as a surface pretreatment for applying organic coatings.

Keyword

Magnesium, corrosion, conversion coating, plasma electrolytic oxidation, layered double hydroxide

Ultraceramic® protection for conventional and 3D-printed Mg-alloys

A. *Buling*, *J. Zerrer; ELB Eloxalwerk Ludwigsburg Helmut Zerrer GmbH, Ludwigsburg, Germany*

Magnesium and its alloys are the structural lightweight metals with the highest strength-to-density ratio, leading to extreme weight reduction up to 40 % in comparison to Aluminium alloys. However, high corrosion tendency of Mg and its alloys extremely limits the application range. Galvanic corrosion occurs easily at this metal since its electrochemical potential is lower compared to other metals. An appropriate environmentally friendly surface technique to prevent corrosion on lightweight metals is the PEO process (plasma-electrolytical oxidation), which converts the lightweight surface to ceramic-like oxides, leading to high corrosion and wear protection.

In this study we present the corrosion performance of state-of-the-art PEO surfaces on wrought Mg alloys and compare them with the adaptable Ultraceramic® PEO technique. Furthermore, the Ultraceramic® surfaces are adopted to powder bed fusion-Laser beam (PBF-LB) 3D-printed Mg WE43 alloy, increasing the lightweight potential, since material saving in production can be combined with outcoming components leading to an overall energy reduction due to reduced weight.

The corrosion protection will be demonstrated with help of electrochemical testing methods. Resulting surfaces and their cross sections are examined by SEM and EDS technologies to analyze the corrosion occurrences, comparing both, the unprotected and the PEO protected surfaces.

Plasma electrolytic oxidation on magnesium AZ31 with sepiolite as inhibitor carrier for improved corrosion protection

Robert Sottor[1], Stephan Lederer[1], Michael Schneider[2], Kerstin Kremmer[2], and Wolfram Fuerbeth[1]

[1] DECHEMA Research Institute, Frankfurt am Main, Germany

[2] Fraunhofer Institute for Ceramic Technologies and Systems IKTS, Dresden, Germany

Magnesium is the most lightweight metallic construction material. However, its use is limited due to its poor corrosion behavior. Typically, the corrosion properties can be improved by the generation of a thickened passive layer using plasma electrolytic oxidation (PEO). However, process inherent structures such as discharge channels, cracks or pores can be considered as “weak spots” for continuing corrosion attack. A cheap and easy way to optimize the vulnerable PEO coating structure is the use of corrosion inhibitor loaded sepiolite mineral striving an *in-situ* incorporation during the PEO process.

The present work deals with the investigation of different inhibitors loaded into nanosized ceramic fibres (sepiolite) and their incorporation into a PEO layer formed on magnesium alloy AZ31.

After the PEO process the sepiolite can be detected on the surface and especially inside the aforementioned “weak spots” of the PEO layer by scanning electron microscopy. It can be shown that the fixation of the particles is caused by sintering due to the heat development during PEO treatment. Investigations using electrochemical impedance spectroscopy and linear sweep voltammetry in 0.5% NaCl solution confirm an improvement in the corrosion protection. The use of the inhibitors not only lead to a decrease in the corrosion current densities but also to a shift of the critical pitting potential towards anodic direction. By means of efficiency, cerium loaded sepiolite showed the best behavior.

Effects of Post-treatments for plasma electrolytic oxidation coatings on Aluminium and magnesium alloy substrates

M. Wala[1], A. Olesiński[1], D. Szymura[1], J. Grzonka[1], M. Stec[1], M. Bik[2], P. Jeleń[2], P. Chulkin[1], W. Simka[1], M. Sowa[1]

[1]Faculty of Chemistry, Silesian University of Technology, Gliwice, Poland

[2]Faculty of Materials Science and Ceramics, AGH University of Technology, Kraków, Poland

Plasma electrolytic oxidation (PEO), as the younger sister of classic anodic oxidation is gaining more and more attention in the field of corrosion protection. This technique allows easy preparation of thick and dense layers that are capable of separating of protected elements from the corrosive environment. However, because of the nature of the PEO process, the obtained layers are porous, which can cause local corrosive attacks due to the trapping of the corrosive ions inside those pores.

Luckily, this feature of the PEO-modified structure can be used to our advantage – trapping of the different chemical compounds, i.e. corrosion inhibitors or colorants could not only increase the anticorrosive properties of the layer but also increase its aesthetics which may make it more attractive to be considered as a commercial product.

PEO layers on aluminium AW6061 and magnesium AZ91 alloys have been prepared using the asymmetric AC PEO regime in alkaline electrolytes containing silicates & phosphates or their mixture. After the process, the white-grey layers were dried and then immersed in the dye solution for 2-5 minutes. After dripping off the excess of the colorant and drying, the introduced chemicals (corrosion inhibitors, e.g. 8-hydroxyquinoline, acrylic acid; solvent dyes, e.g. nigrosine) have been sealed inside the PEO layer by an additional, short PEO process that lasted up to several minutes.

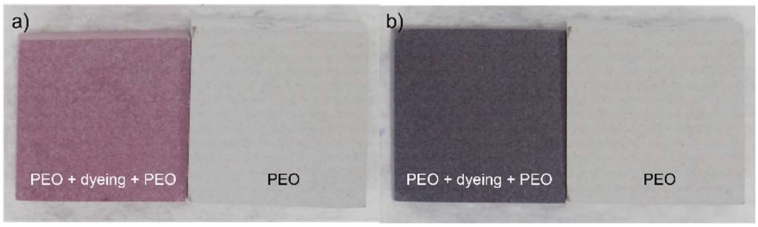

Fig. 1. Comparison of AZ 91 samples macro-images after PEO process and 3 repetitions of sequential dyeing with **a)** Solvent red 122 and **b)** Solvent black 7 (nigrosine).

As presented in **Fig. 1**, the proposed methodology has given good results in terms of the PEO layer dyeing. The final colour is not only homogenous but also durable thanks to the sealing of the colourant. The corrosion resistivity of the samples has also been improved during the sequential post-treatment. As presented in **Fig. 2,** sealing nigrosine in the PEO layer has increased the polarisation resistance of the sample, compared to the PEO process. Such results indicate that the proposed post-treatment sequence is effective in terms of increasing both the aesthetic values of the prepared samples and their corrosion resistivity.

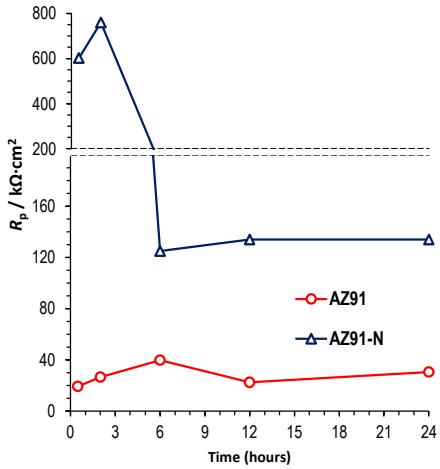

Fig. 2. Polarization resistance variation deduced from EIS experiments conducted on a dye-free AZ91 magnesium alloy sample with a PEO coating (AZ91 sample) and another sample triply-loaded with nigrosine (AZ91-N sample) over 24 h of contact with 0.1 M Na_2SO_4 + 500 ppm NaCl at 30°C.

Properties of the modified layers have been examined in terms of their morphology (SEM, R_a), composition (SEM/EDX, XRD, Raman spectroscopy), and corrosion protection (EIS, PDP, Salt spray). Additionally in situ UV + optical emission spectroscopy have been used to analyse the plasma activity during the second PEO process, that was sealing the colorants inside the layer.

This work was financially supported by National Centre for Research and Development of Poland (project no. LIDER/30/0116/L-11/19/NCBR/2020)

Tailoring the process of plasma electrolytic oxidation coatings formation on aluminum and magnesium alloys substrates for improved corrosion resistance

M. Sowa[1], A. Olesiński[1], M. Wala[1], M. Stec[1], M. Bik[2], P. Jeleń[2], P. Chulkin[1], W. Simka[1]

In recent decades, plasma electrolytic oxidation (PEO) has become to emerge as an environmentally friendly option for protecting the surface of some valve metals (most notably aluminum, magnesium, titanium or zirconium and their alloys) against mechanical wear and corrosion. It is an anodic treatment whereby the workpiece is oxidized in a dilute alkaline electrolyte at voltages exceeding the dielectric breakdown potential for the growing films. Because of the high electric fields generated during the process, plasma appears on the surface in the form of micro-discharges the presence of which modifies the classical anodizing process. The properties of the obtained oxide coatings are tightly dependent on the plasma conditions, i.e. population of discharges, their overall intensity, the type of ions present in the plasma as well as heat transfer situation. Deep understanding of the link between plasma state in the process and the properties of the grown films is a Holy Grail for the conscious design of the protection system with the use of PEO.

In this study we show how some PEO process parameters (current density, frequency, relative duration of positive and negative voltage pulses, the use of double-frequency composite waveforms or electrolyte composition) affect the plasma state on the treated surface and hence, the oxide properties. The experiments were performed on AW-6061-T6, AW-2024-T351 aluminum alloys and AZ91D, AZ31 magnesium alloys. The treatments were conducted with the use of various formulation of electrolytes composed of the base salts: sodium metasilicate (SM), sodium hexametaphosphate (SHMP) or the mixture of the two with the addition of modifiers (sodium aluminate or other phosphate salts, ethylene glycol, EDTA). During PEO (run by Kikusui PCR-1000LE or PCR-2000WEA high-voltage AC+DC power supplies, Japan), the electrical parameters of the process were monitored using digital oscilloscope (OWON XDS 2102A, China) while the surface plasma emissions were captured using a fast camera (Phantom T3610, Vision Research, Ametek, USA) and a four-channel UV-optical emission spectrometer (AvaSpec-ULS4096CL-EVO-

RM-USB3, Avantes, the Netherlands). The formed coatings were then analyzed with the use of SEM/EDX, XRD, Raman, FTIR, XPS. Some other surface properties of the oxide were also checked: microhardness, roughness and microroughness, tribological behavior, wetting angle. The corrosion performance of the formed coatings was at last assessed using electrochemical techniques (EIS, PDP), long-term exposure combined with mass gain/loss and salt spray tests.

It was found that the behavior of the surface sparks during the PEO of aluminum is strongly affected by the electrolyte composition, especially when the treatment is run under “soft-sparking” regime. The uniformity of soft-sparking (that lower the power demand of the process as well as increase the oxide formation rate) was higher for the higher SHMP contents as compared to SM. At high SM concentration, the process developed localized etching of the samples as opposed to uniform growth of the oxide. SHMP made the process less violent and more repeatable. However, it was at the expense of lower alpha-alumina/gamma-alumina content. However, the denser microstructure of the coatings obtained in the SHMP-rich electrolytes was much denser. The frequency of 100 Hz was found to be optimal for the treatment, however, superimposing an additional pulsation in the positive half-cycle of the waveform at 1000 Hz (a composite waveform) resulted in the more compact coatings. The amount of alpha-alumina in the coatings was higher for higher SM concentrations. The coating process for magnesium was different. Severe surface cracking was observed if low duty cycles (lower than 33%) were not used. The best quality coatings were obtained in the solutions where the main component was the SHMP. Ethylene glycol was found to be the best out of the tested organic additives. It stabilized the plasma and improved the uniformity of the oxide films. However, the bath composition was not stable and resulted in poor reproducibility of the results. The improved quality of the coatings was followed with increased corrosion resistance.

This work was financially supported by National Centre for Research and Development of Poland (project no. LIDER/30/0116/L-11/19/NCBR/2020).

Study of the incorporation of microparticles in titanium and aluminum coatings produced by plasma electrolytic oxidation (PEO)

F. Ceriani[1], L. Casanova[1], M.V. Diamanti[1], M. Ormellese[1], M. Pedeferri[1]

[1] Dept. of Chemistry, Materials and Chemical Engineering "G. Natta", Politecnico di Milano, Via Mancinelli 7, 20131 Milano, Italy

Abstract: The effects of incorporation of two types of TiO_2, rutile and anatase, microparticles (d < 5 µm), in PEO coatings produced in alkaline solutions on titanium and aluminum are studied.
PEO coatings are characterized by scanning electron microscope (SEM), energy dispersive spectroscopy (EDS) analysis and X-ray diffraction (XRD) testing. It is observed that anatase particles are successfully incorporated in the coatings, while rutile retention in coatings produced on the Al alloy is quite limited. The electrochemical behaviour of the oxides is evaluated by electrochemical impedance spectroscopy analysis (EIS) performed in a NaCl 3.5 wt% solution. It is found that all the PEO-coatings enhanced the corrosion resistance of the treated metals, especially when anatase is present in the oxide structure.

Keywords: PEO, titanium, aluminum, microparticles, EIS

Introduction

Titanium and aluminum alloys are largely employed in several applicational fields, as aerospace, aeronautical, automotive, constructions, and food industries thanks to their great combination of properties as improved corrosion resistance, mechanical stability, low density, and high strength-to-weight ratio. [1], [2]

To further enhance the corrosion resistance of these two metals in particularly aggressive conditions, as strongly acidic environments, where the natural passive layer present on the metal surface does not provide a sufficient protection, plasma electrolytic oxidation (PEO) could be performed. PEO consists in a high-voltage anodic oxidation of metals or alloys in aqueous solutions under the condition of plasma discharge. The discharge promotes local high temperature and pressure causing complex plasma-chemical reactions to occur and contributing to the stabilization of ceramic like structures. The treatment leads to the formation of a thick and hard oxide layer on the metal surface. [3], [4] Unfortunately, the structure of PEO coatings is affected by the presence of microdefects and pores, produced by plasma discharges, that may reduce the corrosion resistance, since aggressive species can easily penetrate through the oxide and reach the metallic substrate where corrosion may occur. A possible strategy to reduce defects is to add solid particles to the electrolytic bath, which can be incorporated during plasma events, with the aim of filling the porosity left by PEO treatment. [5]

This research is focused on the evaluation of the influence of two types of microparticles (MPs), namely rutile (TiO_2) and anatase (TiO_2) microparticles (diameter < 5 µm), on the resulting morphology, structure, and anticorrosive properties of PEO oxides applied on titanium and aluminum (AA2024).

Materials and methods

PEO treatment is performed on square samples (10 x 10 mm^2), 1.2 mm thick, of commercially pure titanium grade 2 (UNS R50400) cut by metal shearing and on AA2024 cylindrical disks (3.8-4.9 Cu; 1.2-1.8 Mg; 0.3-0.9 Mn; Si ≤ 0.5; Fe ≤ 0.5; Zn ≤ 0.25; Cr ≤ 0.1; Al balance) 5 mm thick with diameter 10 mm. The samples are polished with silicon carbide paper (120, 320 and 600 mesh) and rinsed with distilled water. The PEO treatment is performed in alkaline solutions whose composition is reported in Table 1. Rutile microparticles (average diameter ≤ 5 µm) and anatase microparticles (average diameter ≤ 5 µm), are added to the base solutions in concentration 5 $g \cdot L^{-1}$.

Table 1 - Chemical composition of the PEO electrolytic solutions (R = rutile, A = anatase).

Samples	Base solution	Type of microparticles	Microparticles concentration
Ti_R	1 M NaOH +4 g·L^{-1} Na_2SiO_3	Rutile	5 g·L^{-1}
Ti_A		Anatase	5 g·L^{-1}
Al_R	4 g·L^{-1} NaOH +1 g·L^{-1} KOH +6 g·L^{-1} Na_2SiO_3	Rutile	6 g·L^{-1}
Al_A		Anatase	6 g·L^{-1}

The PEO process is carried out in alternate electrical regime (AC) applying a duty cycle 60 % anodic, 40 % cathodic, with a cathodic peak equal to the 7 % of the anodic one. [6] All the electrical parameters used for the PEO treatment are listed in Table 2.

Table 2 - PEO electrical parameters (A = anodic, C = cathodic, CP = cathodic peak)

Samples	Current regime	Waveform	Frequency (Hz)	Time (s)	Voltage (V)
Ti	AC	60A%-40C%-7CP%	1000	320	90
Al					400

PEO coatings are analyzed by scanning electron microscopy (SEM), energy dispersive spectroscopy (EDS) analysis and X-ray diffraction (XRD) testing. In addition, the samples are electrochemically characterized by electrochemical impedance spectroscopy (EIS) in a NaCl 3.5 wt.% solution at room temperature after 1 h of immersion working in a frequency range between 10^{-2} and 10^{6} Hz.

Results and discussion

Morphology and structure

The surface images of the oxide are reported in Figure 1 a) for Ti and in Figure 1 b) for AA2024 (only samples treated with anatase are shown since there are no relevant differences with respect to those prepared using rutile). The morphology of the oxides appears significantly different depending on the metallic substrate. Observing Ti oxide, the presence of protuberances crossed by pores and cracks is noticed all over the surface, while in case of the Al alloy substrate a quite flat and porous oxide is observed. The formation of protuberances may be the consequence of the high pressure applied by the gas bubbles developed during the PEO process which remains entrapped within the molten material, while cracks formation is due to the release of thermal

stresses developed because of the rapid cooling of the oxide in contact with the electrolyte. [7], [8] The less textured surface of the aluminum oxide layer, instead, may be partially associated to the presence of KOH in the electrolytic solution. Potassium hydroxide, in fact, seems to decrease gas evolution at the electrode surface leading to a reduction of porosity, favored also by the presence of silicates, and to the formation of a quite flat surface. [9]–[11] Another characteristic of Al_R and Al_A is the presence of fine particulates on the oxide surface (some of them are indicated by red arrows in the enlargement of Figure 1 b)), which is not observed on Ti oxide surface.

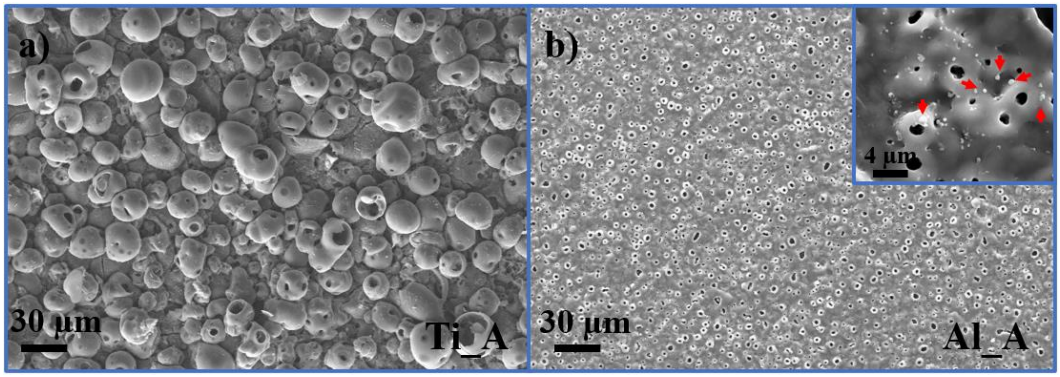

Figure 1 - SEM images of the surface of a) Ti_A and b) Al_A

The structures of the oxides are shown in Figure 2 and 3 for Ti and AA2024, respectively. Also in this case, substantial differences are observed. Firstly, the oxide thickness, the PEO-coatings produced on Ti have a thickness around 50 µm, while the maximum thickness reached in case of AA2024 is of about 5 µm.

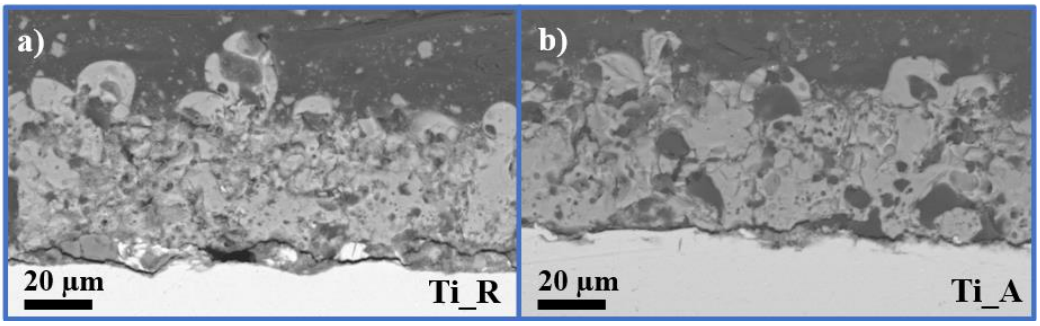

Figure 2 - SEM images of the cross-sections of Ti_R and Ti_A.

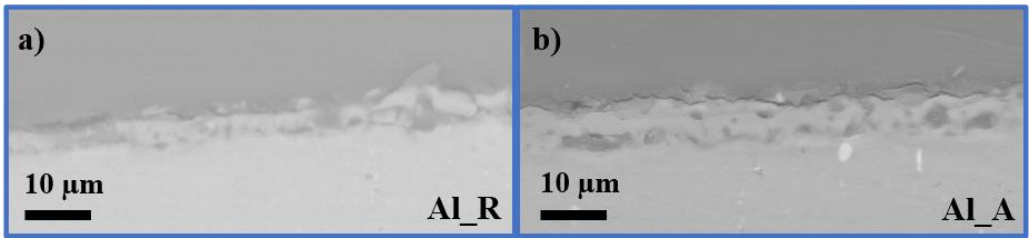

Figure 3 - SEM images of the cross-sections of Al_R and Al_A.

The achievement of large thicknesses is partially due to the action of sodium metasilicates able to promote the coating growth limiting its dissolution. Their effect is probably larger on titanium specimens, according to the SiO_3^{2-} retention mechanism. The anions enter the oxide through the discharge channels under the action of the strong electric field. Since Ti_R and Ti_A show pores across their entire thickness it is reasonable to assume that a larger quantity of SiO_3^{2-} is withdrawn to the bottom of discharge channels favouring the oxide growth. [12] Additionally, a large silicates retention favours the formation of silica in the final coating contributing to the thickness increase. This is confirmed by XRD analyses, Figure 4, in which a broad peak centred at about 32° and associated to amorphous silica is observed only for Ti PEO-oxides.

Comparing the oxides formed with different types of TiO_2 microparticles, it is possible to notice that in case of Ti the addition of rutile leads to the formation of a fine porosity interesting the entire oxide thickness, while when anatase is added larger pores are produced. In case of AA2024 the two structures appear similar, a uniform oxide layers affected by the presence of quite large pores at the interface with the metallic substrate is observed.

The presence of all the electrolytic elements (as Na and Si) is confirmed by EDS maps (not reported in this paper) of the sample surface, which allow to verify even the incorporation of titanium dioxide microparticles in the coatings grown on the Al alloy. Ti on the Al_R and Al_A surface is mainly concentrated in correspondence of the particulates described above and shown in the enlargement in Figure 1 b). This could mean that MPs with a small size (< 1 µm) are preferentially involved in the plasma events and remain sticked on the coating surface undergoing to an inert incorporation. However, analyzing the EDS maps of the cross-sections of the coatings, Ti results to be present in all the specimens apart from the one produced on AA2024 working with rutile. Then the incorporation of MPs in the latter case occurs only at the surface of the forming oxide. This is confirmed also by XRD analyses (Figure 4).

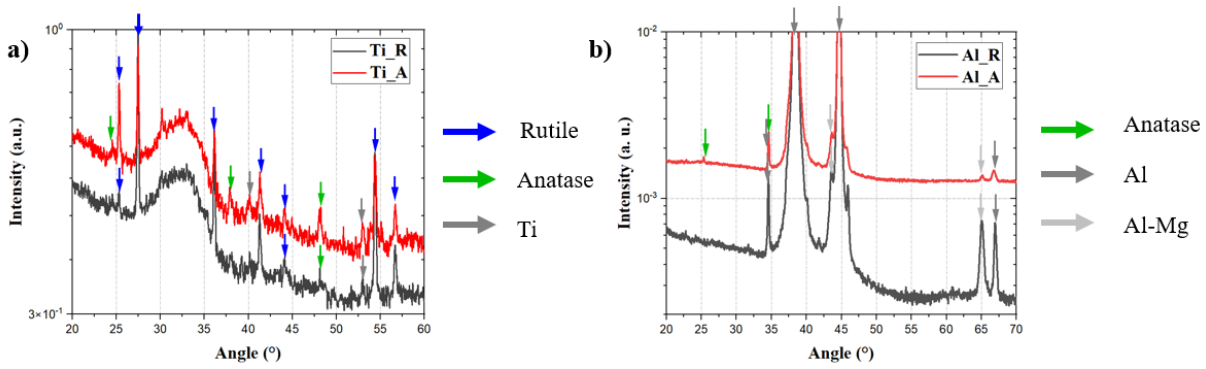

Figure 4 - XRD diffractogram of a) Ti and b) AA2024 PEO-samples.

The diffractogram of Al_R does not exhibit rutile signals, while the oxide prepared working with anatase microparticles produces reflections associated to such TiO_2 polymorph. Concerning Ti PEO-samples, they obviously show lines associated to both rutile and anatase, the latter appearing more numerous and intense for sample Ti_A.

The larger incorporation of anatase rather than rutile into the alumina coatings could be explained according with their different isoelectric points (IEP). Anatase, in fact, has a IEP (3.8 - 5.9) lower than rutile (6.0 - 6.5); consequently, when TiO_2 particles are immersed in the alkaline electrolyte (pH >> IEPs) anatase MPs acquire a negative charge larger than rutile. [13] As a result, the attraction towards the metallic substrate experienced by anatase particles under the action of the electric field, established during the anodic half cycle, is more intense than that experienced by rutile particles, leading to a larger anatase incorporation in the growing oxide.

Electrochemical behavior

The result of EIS analyses, performed in a NaCl 3.5 wt.% solution after 1 h of immersion, are reported in the Nyquist diagrams in Figure 5.

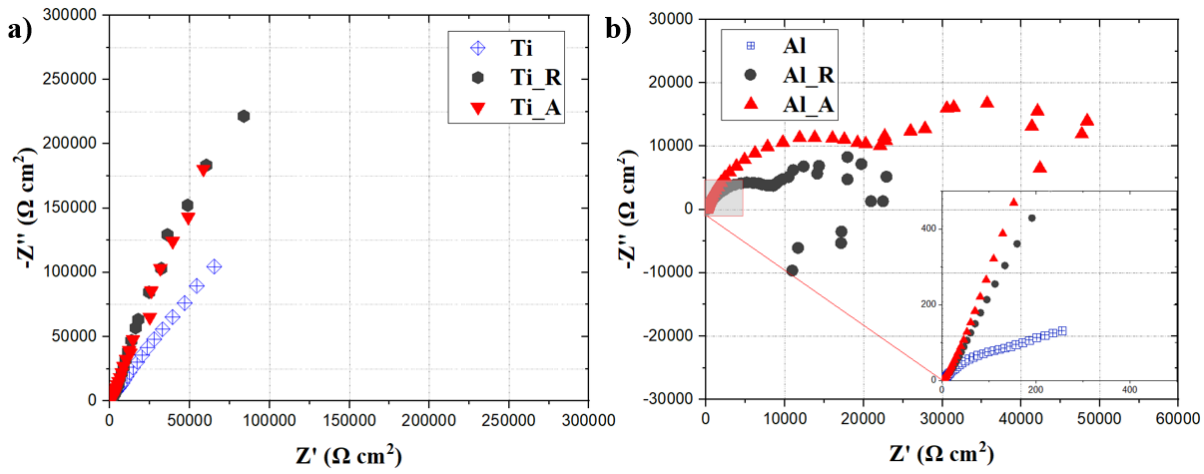

Figure 5 - Nyquist diagrams of bare metals and PEO-oxides for a) Ti and b) AA2024.

Comparing the impedance values of the coated samples with those of the bare metals it is evident how the PEO treatment successfully enhances the corrosion resistance of both Ti and Al alloy. This improvement is particularly significant for AA2024, for which Z' increases of two orders of magnitude. Considering Ti, the bare metal already exhibits a great corrosion resistance which is further promoted by the oxide coatings. No significant differences are observed between Ti_R and Ti_A, both the curves are characterized by a single capacitive loop and provides polarization resistance values around $4 \cdot 10^6\ \Omega \cdot cm^2$. On the other hand, the Nyquist

curves of Al_R and Al_A appear quite different. Even if in both the cases two capacitive semicircles and an inductive loop are present, the impedance values provided by Al_A is almost twice the value recorded for Al_R. This phenomenon is probably related to the greater incorporation of anatase microparticles in the forming oxide rather than rutile. In fact, according to SEM, EDS and XRD analyses the incorporation of rutile MPs in the coating is reduced and limited to the surface of the oxide. On the contrary, when anatase MPs are used, Ti is found through the entire thickness of the oxide and its crystalline structure is detected by XRD. Thus, the presence of anatase in the PEO-oxide promotes its corrosion resistance leading to the better electrochemical behavior of Al_A.

Conclusion

The incorporation of TiO_2 (rutile and anatase) microparticles in PEO oxides on Ti and AA2024 is investigated. Working with Ti a reactive incorporation occurs, while in the case of Al alloys the incorporation is partially inert, resulting in the presence of particulates whit high Ti content on the oxide surface.

The incorporation of anatase microparticles is favoured with respect rutile particles due to the lower anatase IEP, the latter promoting its attraction toward the metallic substrate during anodic periods of the duty cycle. The larger incorporation of anatase leads to a higher improvement of the corrosion resistance of AA2024 samples treated with such TiO_2 polymorph, for which impedance values two orders of magnitude greater than those of the bare metal are measured. In general, all the PEO-coatings on both Ti and Al alloys display an enhanced corrosion resistance proving the beneficial effect of incorporation of TiO_2 microparticles into the growing oxides.

References

[1] M. J. Donachie, "Titanium: A Technical Guide, 2nd Edition," *ASM Int.*, p. 128, 2000.

[2] G. M. Scamans and N. Birbilis, "3 . 08 Corrosion of Aluminum and its Alloys," 2010.

[3] S. Sikdar, P. V. Menezes, R. Maccione, T. Jacob, and P. L. Menezes, "Plasma electrolytic oxidation (Peo) process—processing, properties, and applications," *Nanomaterials*, vol. 11, no. 6, 2021, doi: 10.3390/nano11061375.

[4] R. O. and D. O., "Production of Anti-Corrosion Coatings on Light Alloys (Al, Mg, Ti) by Plasma-Electrolytic Oxidation (PEO)," *Dev. Corros. Prot.*, 2014, doi: 10.5772/57171.

[5] X. Lu, C. Blawert, M. L. Zheludkevich, and K. U. Kainer, "Insights into plasma electrolytic oxidation treatment with particle addition," *Corros. Sci.*, vol. 101, pp. 201–207, 2015, doi: 10.1016/j.corsci.2015.09.016.

[6] L. Casanova, M. La Padula, M. P. Pedeferri, M. V. Diamanti, and M. Ormellese, "An insight into the evolution of corrosion resistant coatings on titanium during bipolar plasma electrolytic oxidation in sulfuric acid," *Electrochim. Acta*, vol. 379, p. 138190, 2021, doi: 10.1016/j.electacta.2021.138190.

[7] X. Zhang *et al.*, "X-ray Computed Tomographic Investigation of the Porosity and Morphology of Plasma Electrolytic Oxidation Coatings," *ACS Appl. Mater. Interfaces*, vol. 8, no. 13, pp. 8801–8810, 2016, doi: 10.1021/acsami.6b00274.

[8] L. Casanova, F. Ceriani, M. Pedeferri, and M. Ormellese, "Addition of Organic Acids during PEO of Titanium in Alkaline Solution," *Coatings*, vol. 12, no. 2, 2022, doi: 10.3390/coatings12020143.

[9] L. O. Snizhko *et al.*, "Anodic processes in plasma electrolytic oxidation of aluminium in alkaline solutions," *Electrochim. Acta*, vol. 49, no. 13, pp. 2085–2095, 2004, doi: 10.1016/j.electacta.2003.11.027.

[10] M. Aliofkhazraei *et al.*, "Review of plasma electrolytic oxidation of titanium substrates: Mechanism, properties, applications and limitations," *Appl. Surf. Sci. Adv.*, vol. 5, no. January, p. 100121, 2021, doi: 10.1016/j.apsadv.2021.100121.

[11] J. H. Lee and S. J. Kim, "Effects of silicate ion concentration on the formation of ceramic oxide layers produced by plasma electrolytic oxidation on Al alloy," *Jpn. J. Appl. Phys.*, vol. 56, no. 1, 2017, doi: 10.7567/JJAP.56.01AB01.

[12] S. Moon and Y. Jeong, "Generation mechanism of microdischarges during plasma electrolytic oxidation of Al in aqueous solutions," *Corros. Sci.*, vol. 51, no. 7, pp. 1506–1512, 2009, doi: 10.1016/j.corsci.2008.10.039.

[13] G. L. Hyoung and J. M. Zuo, "Growth and Phase Transformation of Nanometer-Sized Titanium Oxide Powders Produced by the Precipitation Method," *J. Am. Ceram. Soc.*, vol. 87, no. 3, pp. 473–479, 2004, doi: 10.1111/j.1551-2916.2004.00473.x.

BLACK PEO COATINGS ON TITANIUM ALLOYS PRODUCED AT LOW CURRENT DENSITY

Lorena Kostelac[1], Luca Pezzato[1], Elena Colusso[1], Katya Brunelli[1], Manuele Dabalà[1]

[1] Department of Industrial Engineering, University of Padova, Via Marzolo 9, 31531 Padova, Italy

Titanium and its alloys are widely used metals in aeronautics and astronautics due to their high strength-to-weight ratio. It is light, however, strong metal with low density. The increased use of titanium in aerospace and other fields has been attributed to its ability to withstand reasonably high temperatures; however, its tendency to gall and seize and severe sensitivity to atmospheric oxygen at high temperatures prevent it from being fully utilized in aerospace. Surface treatment of titanium is crucial to overcome these limitations and meet some functional requirements. A titanium surface coated with black is used primarily for radar visibility reduction, as well as for temperature control coatings of equipment in space. Such coatings are coatings with high absorption and high emissivity. Black coatings on titanium are also used as decorative coatings, enhancing the final product's appearance.

Plasma electrolytic oxidation (PEO), developed from traditional anodic oxidation, is one method of preparing black coatings. PEO is an environmentally friendly alternative to conventional anodizing since its electrolyte is generally less toxic. This method provides thicker coatings with unique features such as excellent corrosion resistance and good thermal and tribological properties. PEO works under higher voltages, which causes the dielectric breakdown of the oxide films, manifested by moving plasma discharges at the surface of the treated workpieces. Different compounds, mainly oxides, can be found in the obtained coatings. The microstructure of the PEO coating is usually multi-layer and porous structures. Several parameters can influence the microstructure of PEO coatings, such as the electric regime, the electrolyte composition, the process's length, and the substrate's chemical composition. Among these factors, the electrolyte plays the most crucial role in the coating properties, especially in the colours of the PEO coatings. Representative components of electrolytes for the preparation of the PEO black coatings could be generally divided

into two types: anions such as VO^{3-}, WO_4^{2-}, MoO_4^{2-} and transition metal cations such as Fe^{2+}, Cu^{2+}, Co^{2+}, $Ni^{2+}$and Zr^{4+}.

Currently, there are only a few papers that demonstrate the preparation of black coatings on titanium using the PEO method, and most of them use carcinogenic compounds based on nickel and cobalt as electrolytes. Therefore, we examined the possibility of preparing black coatings on titanium alloys using non-toxic compounds at low current density.

In the present study, black PEO coatings were produced on Grade 2 and Grade 5 titanium alloys using a combination of two types of colourants $(NH_4)_6Mo_7O_{24}$ and $FeSO_4$ in the phosphate-based electrolytes. PEO worked in direct current (DC) mode at a very low current density of 0.05 A/cm^2. A comparison of coatings prepared with thirty-minute and sixty-minute PEO processes was conducted. In addition, the surface morphology was analyzed using scanning electron microscopy (SEM), and the phase composition was evaluated using X-ray diffraction (XRD). Black intensities were determined using ultraviolet–visible (UV-VIS) spectrometry, and electrochemical corrosion properties of the coatings were assessed by potentiodynamic polarization and electrochemical impedance spectroscopy (EIS) tests.

The results of UV-VIS analysis confirm the successful preparation of the black coatings on both titanium alloys. All black coatings improve the corrosion resistance of pure titanium alloys. Coated titanium alloys exhibit better corrosion resistance after one hour of preparation compared to those after thirty minutes. This can be explained by the morphology of the coatings. One-hour coatings have a more homogeneous and compact structure. All PEO coatings have a characteristic porous structure.

EFFECT OF GLASS POWDERS ON THE CORROSION AND WEAR RESISTANCE OF PEO COATINGS PRODUCED ON 6061 ALUMINUM ALLOY

Luca Pezzato[1], Lorena Kostelac[1], Lavinia Tonelli[2], Hamada Said Abdelwahab Elsayed[1], Daniel Kajánek[3], Manuele Dabalà[1], Enrico Bernardo[1], Carla Martini[2], Katya Brunelli[1]

[1] Department of Industrial Engineering, University of Padova, Via Marzolo 9, 31531 Padova, Italy

[2] Department of Industrial Engineering, University of Bologna, Viale del Risorgimento 4, 40136 Bologna, Italy

[3] Research Centre, University of Žilina, Univerzitná 8215/1, 010 26 Žilina, Slovak Republic

In the past decades the use of lightweight metals, e.g. aluminum (Al), magnesium (Mg) and their alloys has been of great importance for applications in various machinery and transportation system, especially in aerospace and automobile products. In order to increase their wear and corrosion performance and to modify their surface characteristics, several types of coatings have been developed and deposited on the substrate. Plasma Electrolytic Oxidation (PEO) is a very promising process that can enhance the corrosion and wear resistance by producing a relatively thick, dense and hard ceramic layer on light alloys. The corrosion and wear behavior of the treated samples strongly depends on process parameters: current density, voltage, treatment time and electrolyte composition. In particular, the use of additives in the electrolyte produces significant changes in the resistance of the coatings. In fact, one of the characteristics of PEO layers is the possibility to incorporate in the coatings particles that are suspended in the electrolyte. Particles can be inserted in the coating as inert incorporation or by partial melting and re-solidification process depending mainly by the melting point of the additive. In previous work of the authors was verified the possibility to incorporate borosilicate glass into the coating, and was found that this type of glass seals the pores of the PEO layer producing an improvement both in corrosion and wear properties.

However, no systematic studies on the effect of the addition of different types of glass in PEO coatings can be found in literature. In this work the addition of borosilicate, soda-lime and NEG glass into PEO coatings produced on 6061 aluminum alloy was studied. Also, the effect of different current modes (Direct Current or Pulsed Current) on the incorporation of the glass and on the morphology of the coatings was studied. The microstructure and thickness of the produced coatings were studied through SEM-EDS analysis and XRD. The wear resistance was evaluated by dry sliding tests vs. AISI 52100 bearing steel (block on ring contact geometry). The corrosion behavior was analyzed by potentiodynamic polarization (PDP), electrochemical impedance spectroscopy (EIS) and Localized Electrochemical Impedance (LEIS) tests.

The results evidenced that the addition of glass improved the corrosion resistance of the samples, due to the sealing effect on the pores that characterize the PEO layer. The effect on wear resistance is instead strictly related to the type of glass as, if compared to the base PEO layer, it improved only by selected additives.

Sealing effect of TiO_2 films deposited by atomic layer deposition on AA6xxx alloys

L. Fedrizzi[1], F. Andreatta[1], S. Porro[2], A. Lanzutti[1]

[1] University of Udine, Polytechnic department of engineering and architecture, Via del Cotonificio 108, 33100 Udine, Italy
[2] Politecnico di Torino, Department of Applied Science and Technology, Corso Duca degli Abruzzi 24, 10129 Torino, Italy

In this work, the sealing effect of nanometric coatings of titanium dioxide (TiO_2), deposited by means of atomic layer deposition (ALD) technique, was evaluated for an anodized Al 6XXX alloy. ALD coatings with controlled thickness (varying the number of cycles and the deposition temperature) were deposited on anodized substrates. In particular, three different thicknesses of the anodic oxide were considered (7, 14 and 26 µm). The corrosion resistance of the ALD coated specimens was compared to that of the current industrial state of the art, i.e. anodized Al specimens sealed by immersion in boiling water. The structure of the ALD deposits was characterized by field emission scanning electron microscope (FE-SEM) and their chemical composition was investigated by glow-discharge optical emission spectroscopy (GDOES). Corrosion resistance was assessed by means of potentiodynamic polarization measurements in a 3.5% NaCl solution.

The quality of the ALD coatings is dependent on the temperature at which the ALD process is performed. A deposition process at 130°C leads to crack-free TiO_2films for all investigated substrates. In contrast, deposition at higher temperature (200°C) leads to the formation of defective films. In particular, crack-free ALD films were obtained for anodized Al specimens with thickness of the oxide film of 7 µm, while sealing of thicker anodized layers was more difficult to achieve. A complete sealing of the anodized layer was obtained with 280 ALD deposition cycles, with thickness of the ALD film in the order of 30 nm. Potentiodynamic polarization curves show that TiO_2 films obtained with 280 deposition cycles significantly decrease the corrosion current density as compared to specimens sealed in boiling water.

Stable graphene dispersions: new anticorrosion additives

Thomas Bottein, Carbon Waters, France

With few exceptions, all metals are subject to corrosion due to interaction with the environment. Therefore, corrosion is an extremely expensive but also dangerous problem, leading to equipment malfunction and premature failure in a wide range of industries.

In the recent years, graphene has gain interest as an alternative solution for anticorrosion owing to its remarkable properties: not only it is the thinnest material, but it is also the strongest, most impermeable and thermal conductive material known. Only composed of carbon, it is fully degradable and does not impact the environment[1]. It can replace and supplant existing solutions such as organic additives and metals (e.g. zinc) but also work in synergy with those solutions to improve further anticorrosion performances.

However, graphene industrial production still faces major challenges that hinder the development of large-scale industrial applications. Carbon Waters produces pioneering stable high-quality graphene dispersions. Thanks to this technology, Carbon Waters' graphene is compatible with many matrices; aqueous and organic-based. This polyfunctional material presents anticorrosion effects even at very low concentration (<0.1%). This presentation aims at presenting the results of anticorrosion investigations conducted on graphene-enriched paints and the resulting applications.

1. Kurapati, R. *et al.* Degradation of Single-Layer and Few-Layer Graphene by Neutrophil Myeloperoxidase. *Angew. Chemie - Int. Ed.* 1–7 (2018). doi:10.1002/anie.201806906

Recycled zinc powders with low carbon footprint for formulation to primer paints for steel protection

Tomáš Prošek, Mehrdad Zia Hoseinpoor, Petr Antoš, Václav Šefl,
Zuzana Heřmánková, Technopark Kralupy of the University of Chemistry and Technology Prague, Kralupy nad Vltavou, Czech Republic
Tomáš Dáňa, COREZINC s.r.o., České Budějovice, Czech Republic

Recycled zinc powders were produced from zinc galvanization waste using a unique technology that allowed for the reduction of the oxidic fraction and the separation of regular particles with a mean size of 10 or 15 µm. The powders are almost free of soluble chloride and sulphate and have a metal fraction content of 88 %. Life cycle analysis (LCA) proved that the products have a significantly lower carbon footprint and environmental impact compared to zinc powders produced from primary zinc.

The mechanical properties, stability, and galvanic protection ability of epoxy and epoxyester primer paints filled with two types of recycled zinc powders were compared with those of reference paints filled with zinc powder produced from primary zinc. The durability of several paint systems with the recycled zinc powders was assessed in tests defined in the EN ISO 12944 standards, i.e., the neutral salt spray test and the constant humidity test. Comparable or even better mechanical and corrosion protection properties were observed for the experimental paint systems with recycled zinc and they were approved as highly durable in atmospheres with the corrosivity category C3 (C3-h according to EN ISO 12944-6). Electrochemical impedance spectroscopy (EIS) measurements and galvanic potential monitoring under immersion in a model rainwater solution proved the ability of the primers filled with recycled zinc to provide cathodic protection of steel for up to 60 days.

Application of a pretreatment in an organic coil coating line: differences and resemblance between laboratory and industrial practice

B. Boelen, Tata Steel Netherlands, IJmuiden/The Netherlands; K. Lammers, Tata Steel Netherlands, IJmuiden/The Netherlands; L.I. Fockaert, Delft University of Technology, Delft/The Netherlands; H. Terryn, Vrije Universiteit Brussel, Brussels/Belgium, J.M.C. Mol, Delft University of Technology, Delft/The Netherlands

Painted steels are produced in organic coil coating lines. The painting process is a sequence of different processing steps. It starts with cleaning of the metallic coated steel strip and followed by applying a pretreatment layer to improve adhesion properties of the metallic coated substrate before paint can be applied. In this work we describe the influence of the outer surface of zinc-magnesium-aluminum (ZM) coated steels on the formation of the pretreatment layer in laboratory experiments and in industrial practice. For the pretreatments hexavalent-chromium-free systems based on titanium/zirconium chemistries are chosen. These chemical treatment systems are water-based, chemically reacting to the metal surface. A layer of TiO_2 and ZrO_2 is formed on the metal surface.

In previous work[1,2,3,4] studies were focused on laboratory scale to understand the formation mechanisms and kinetics as well as the post-formation properties of these layers. We studied the outer surface of the separate metals, zinc, magnesium and aluminum. With ATR-FTIR and XPS we analyzed the oxide structure before and after pretreatment with titanium/zirconium based chemicals. It showed that the pretreatment layer build-up is different for all three metals. Mg was the most reactive metal and formed the thickest pretreatment layer, ten times thicker than the layer formed on aluminum.

In a coil coating line the outer surface layer of ZM coated steel consists of oxides of all three metals. The pretreatment layer build-up is depending on the reactivity of the metal but also on industrial line settings. In industrial lines the pretreatment layers are applied through a no-rinse process. This means that the pretreatment layer consists of the applied titanium/zirconium chemicals combined with the dissolved oxide layer. This can result in a different composition depending on the effectiveness of removing the oxide layer in the cleaning steps. Furthermore, based on the process parameters the pretreatment can change in morphology depending on the strip temperature during application. On a microscale, this can result in either a heterogeneous or a homogeneous pretreatment layer. With XPS and SEM element mappings we studied the morphology and composition of the outer surface of industrial line samples before and after cleaning and before and after applying a pretreatment layer.

1. Effect of organic additives in fluoacid-based Ti and Zr-treatments for galvanized steel on the stability of a polymer coated interface, L.I. Fockaert, M.V.E. Ankora, J.P.B. Van Dam, S. Pletincx, A. Yilmaz, B. Boelen, T. Hauffman, Y. Garcia-Gonzalez, H. Terryn, J.M.C. Mol, Progress in Organic Coatings 146 (2020) 105738
2. Effect of zirconium-based conversion treatments of zinc, aluminium and magnesium on the chemisorption of ester-functionalized molecules, L.I. Fockaert, S. Pletincx, B. Boelen, T. Hauffman, H. Terryn, J.M.C. Mol, Applied Surface Science 508 (2020) 145199
3. Zirconium-based conversion film formation on zinc, aluminium and magnesium oxides and their interactions with functionalized molecules, L.I. Fockaert, P. Taheri, S.T. Abrahami, B. Boelen, H. Terryn, J.M.C. Mol, Applied Surface Science 423 (2017) 817–828
4. Chemisorption of polyester coatings on zirconium-based conversion coated multi-metal substrates and their stability in aqueous environment, L.I. Fockaert, S. Pletincx, D. Ganzinga-Jurg, B. Boelen, T. Hauffman, H. Terryn, J.M.C. Mol, Applied Surface Science 508 (2020) 144771

BioPolyurethane Coatings – A Green Alternative for corrosion protection of steel

Tiago A.R. Silva[1], Ana C. Marques[2], Rui G. dos Santos[2], R.A. Shakoor[3], Maryna Taryba[1] and M. Fátima Montemor[1]

1 Centro de Química Estrutural (CQE), Institute of Molecular Sciences (IMS), Departamento de Engenharia Química (DEQ), Instituto Superior Técnico (IST), Universidade de Lisboa, Av. Rovisco Pais 1, 1049-001 Lis-boa, Portugal.

2 Centro de Recursos Naturais e Ambiente (CERENA), Departamento de Engenharia Química (DEQ), Institu-to Superior Técnico, Universidade de Lisboa, Av. Rovisco Pais 1, 1049-001 Lisboa, Portugal.

3 Centre for Advanced Materials (CAM), Qatar University, 9FHQ+JMF, Doha, Qatar

Abstract

Commercial polyurethanes synthesis often uses petroleum-based raw materials, not complying with the trendy "green chemistry" sustainability requirements and raising health and environmental concerns. However, these materials can be formulated from biobased sources such as vegetable oils obtained from various plant feedstocks (e.g. cotton, rapeseed, palm, soybean) as well as from lignin and lignin derivatives. Thus, nowadays the synthesis of biobased polyurethanes coatings for corrosion protection of steel, where petroleum-derived polyols and diisocyanates are fully replaced by bio-based feedstock raw materials is a major step towards more sustainable, functional and tailored solutions for corrosion protection.

In this work, bio-based polyols, namely alkylphenol polyols were obtained from the thermochemical liquefaction of biomass feedstocks, namely pinewood and Stipa tenacissima. These polyols were used as a green raw material for the production of bio-based polyurethanes (BioPU) coatings, using a commercial biobased polyisocyanate, The BioPU coating formulations were applied on steel plates using a bar coater. Electrochemical Impedance Spectroscopy (EIS) measurements were carried out on the coated panels for 60 days in 0.05 M NaCl solution. Good corrosion protection properties were achieved for the coatings tested that attained low frequency impedance above 100 MOhm.cm2 after the 60 days of testing. Localized

electrochemical measurements, namely localized electrochemical impedance spectroscopy and the Scanning Vibrating Electrode technique were used to study the corrosion inhibition ability of the modified coatings.

The results evidenced that the bio-based polyurethane coatings can be formulated from biomass wastes, using a green chemistry route and applied on steel for corrosion protection purposes. The modification of these coatings with silica-based particles impregnated with corrosion inhibitors further enhances the corrosion protection ability of the new developed coatings.

Acknowledgments:

This publication was made possible by NPRP13S-0120-200116 from Qatar National Research Fund (a member of the Qatar Foundation). Authors from Centro de Química Estrutural acknowledge the financial support of Fundação para a Ciência e Tecnologia, through grants UIDB/00100/2020, UIDP/00100/2020; and CERENA (Strategic Project FCT-UIDB/04028/2020)

Functionalized olive pit powder as hydrophobic bio-based pigment for waterborne paint

Massimo Calovi, Stefano Rossi, University of Trento, Trento/Italy;

Nowadays, natural wastes represent important resources for the production of fillers which give new life to the recycled material, add value to the composite product and reduce its production costs. Among all food refined by-products, the olive is perhaps the most interesting bio-filler resource. The olive stone is the most abundant residue of the olive oil manufacturing process and it is made of a complex structure of lignocellulose microfibrils. Despite the interesting mechanical features of the olive pit, this bio-based material has never been considered as a filler in organic coatings and paints. Nevertheless, a recent study has revealed the outcomes of applying different concentrations of olive pit powder in a waterborne paint. The work suggested that the bio-based filler could be employed as multifunctional pigment, as it provides particular aesthetic features, but it is also able to improve the mechanical features of the polymeric matrix. Otherwise, accelerated degradation tests evidenced the water absorption tendency of the lignocellulose-based filler and its severe chemical-physical degradation. Thus, the purpose of this work is to evaluate the effect of two different surface conversion treatments of the olive pit powders, in order to increase their hydrophobicity and maintain, or improve, the barrier properties of the waterborne paint. The coatings were spray-deposited and characterized, comparing the behavior of the functionalized powders with that of the untreated granules. The morphology and the aesthetic features of the samples were investigated by means of scanning electron microscope (SEM) and colorimetric analysis, respectively, to study the influence of the surface conversion treatment of the olive pit additives. Finally, several accelerated degradation tests and electrochemical analyses ware employed to assess the effect of the functionalization of the bio-based fillers on coatings durability, highlighting the hydrophilic/hydrophobic role of the olive pit powders. The functionalization process of the powder with silane has proved to be particularly effective in reducing the hydrophilicity of the olive-pit granules, consequently increasing the durability of the paint.

Electrochemical Impedance Spectroscopy for quantitative performance assessment of coatings

N. Surendran, A. Sabhapondit* T. Bos**

**Shell India Markets Private Limited, India*

Abstract

Corrosion, erosion, abrasion and chemical attack of process equipment is a challenge that costs industries billions of dollars every year. The energy industry, like many other industries, relies heavily on robust coating systems for the protection of assets. Protective coatings provide the substrate with good corrosion resistance by physically isolating the base substrate from its external environment.

Many researchers have attempted to speed up the natural coating degradation process by increasing the physical and chemical stresses (e.g. by altering temperature, humidity, pH, salt concentrations and the intensity of UV radiation) in so-called accelerated tests. Ideally, the degradation mechanisms in these tests stay the same as those under non-accelerated conditions. However, even the more complex cyclic salt fog/UV tests do not give accurate predictions of how many years a material will last in actual service. In addition, the standardized visual evaluation techniques are subjective. The results heavily depend on the ability of the operator to translate a visual observation into a performance rating. In case of high-performance coatings that almost show no visual signs of deterioration after weathering, discrimination between systems is even impossible.

Electrochemical Impedance Spectroscopy (EIS) is an electrochemical technique which is used to study the real-time impact of coating degradation on each component in a coating system. EIS not only provides more precise results in a short time but the obtained data can give indications on the actual corrosion mechanisms. Consequently, the sensitivity of this technique allows the total test time to be shortened.

This work assesses the use of EIS as a technique for quantitative coating assessment. A standard EIS test setup based on ISO 16773 was used to understand the long-term degradation effect of a polyurethane coating system with an activated zinc epoxy primer applied to a carbon steel substrate. The electrochemical data obtained from these tests were fitted to equivalent circuits to interpret the behaviour of each component over time. In long-term exposure studies, the modelled data showed

various trends indicating coating degradation phenomena. As an example, Figure 1 shows the trends of the coating capacitance and the charge transfer resistance. The increase of the coating capacitance is often associated by the permeation of water into the coating. A decrease of the charge transfer resistance indicates that the metallic surface area that is electrochemically active is increasing.

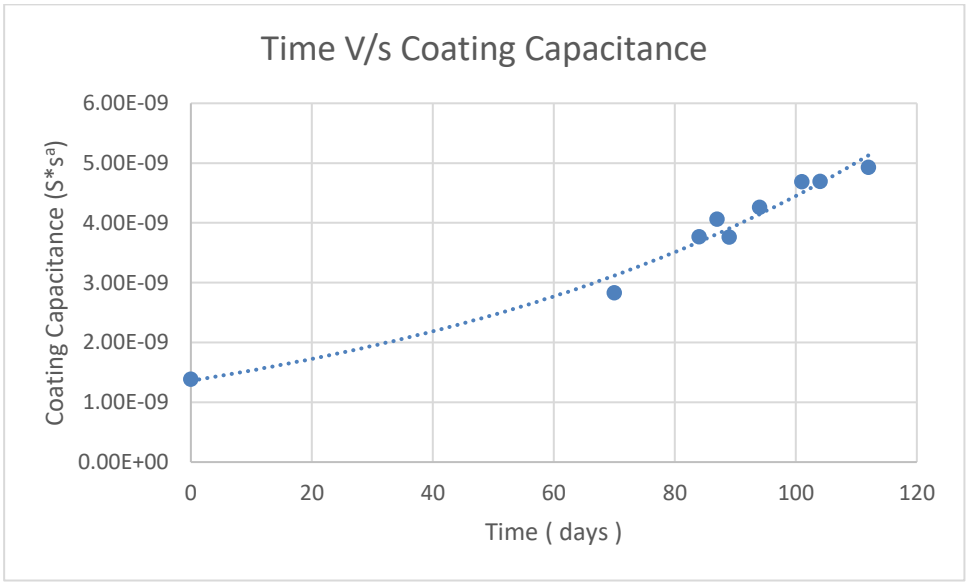

(a)

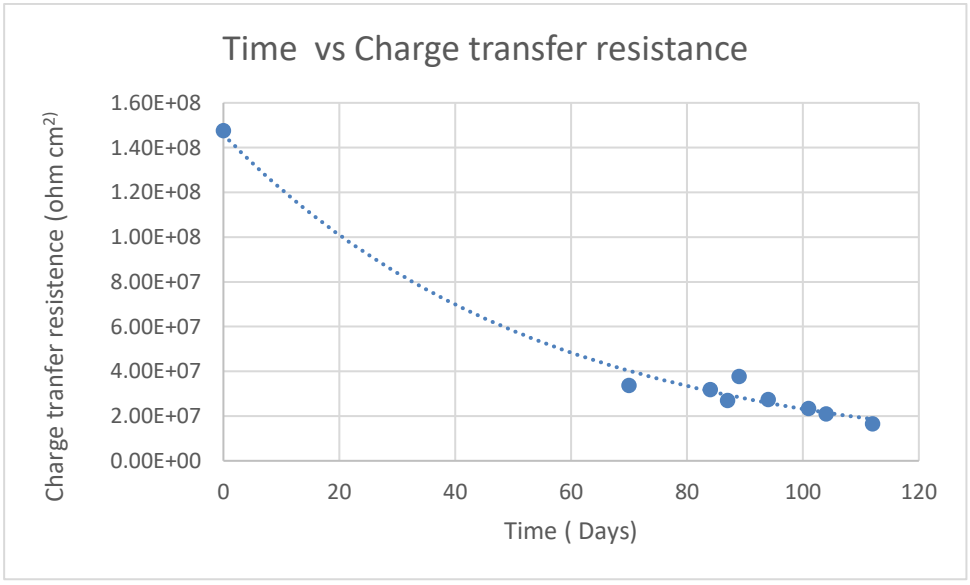

(b)

Figure 1: EIS data for a Polyurethane coating system coating with SP3 surface finish corelating (a) The change in coating capacitance with time (b) The charge transfer resistance with time.

How to test anticorrosive coatings performance? From accelerated testing to field exposure both in traditional field station and simulated service conditions

Krystel Pélissier[1], Nathalie Le Bozec[1], Dominique Thierry[2] and Nicolas Larché[1]

1 – French Corrosion Institute, Brest, France

2 – Research Institutes of Sweden, Kista, Sweden

Corrosion of metals is still and will always be a problem when designing any structures which will sustain the effect of the environment and one of the most popular ways to protect metals against corrosion is the application of anticorrosive coatings. The choice of an adequate anticorrosive coating as a function of the final application is crucial as it will determine the cost of the initial structure and its maintenance costs throughout its life. Two typical ways exist for the selection of an appropriate anticorrosive coating; by performing field testing or by performing accelerated corrosion testing at the laboratory.

An ideal accelerated test is designed to reproduce the degradation obtained during field exposures and to accelerate it correctly and homogeneously whatever the material considered. The major concern in field exposures is not necessarily its lack of representativity towards service conditions but rather its time consuming and costly nature as, generally, many years of field exposures are needed to properly characterize coating performance. Thus, it is better to connect the two approaches as accelerating testing will allow a quick identification of the coatings with poorer performance whereas field exposures will give information on the global performance of the coating (including all modes of degradation and environmental stresses).

It is well-known that some accelerated corrosion tests are not fully representative of field exposure results. However, it exists a lack of study in the literature correlating accelerated tests to field exposure especially when long term durations are considered. In this study, 11 different organic coatings have been investigated in terms of coating resistance to corrosion creep in two types of field exposure sites namely a stationary site and an operating ship and their performance was compared to two accelerated tests (ISO 12944-9 and modified ASTM D5894 standard). The results showed differences in the sites corrosivity and the coating systems performance as a function of the exposure sites. A lack of correlation between ISO

12944-9 standard with stationary site due to the high corrosivity of the standard and on contrary, a satisfying correlation for the operating ship were demonstrated whereas modified ASTM D5894 standard showed a satisfying correlation for both types of sites.

Adhesion and Anticorrosive performance enhancement in coil coatings using organophosphate additives

Kathleen Brook, University of Manchester, Manchester, England, Xiaorong Zhou, University of Manchester, Manchester, England, Mercedes Castro Cabado, AkzoNobel, Hilden, Germany, Niek Hijnen, AkzoNobel, Gateshead, England, Shima Khazraee Sheidaee Mehr, AkzoNobel, Hilden, Germany

Accelerated weathering techniques have shown a demonstrable improvement in adhesive and anticorrosive performance in coil coatings following the inclusion of an organophosphate additive. This effect is particularly pronounced when used in conjunction with a substrate pre-treatment. The precise mechanism of action is under investigation. X-ray and electron-based imaging, electrochemical, and spectroscopic analysis has been used for characterisation of the coating with particular focus on the coating microstructure, the coating-substrate interface, and the interactions of the additive with the binder and other coating constituents. These outputs have been correlated to the coating degradation mechanisms and kinetics following accelerated weathering conditions. The findings of this work will aid in the development of sustainable commercial coil coating products.

Combining Machine Learning and Electrochemical Impedance Spectroscopy to assess organic coatings performance.

V.Bongiorno [1], E.Michailidou [2], M.Curioni [1]

[1] Corrosion and Protection Centre, Department of Materials, The University of Manchester, Oxford Road, Manchester, M13 9PL, UK.

[2] AkzoNobel, 31 Rijksstraatweg, Sassenheim, 2171 AJ, Netherlands.

Protective organic coatings are used to extend the service life of metal components and structures. Technological tests allow estimating qualitatively the performance of organic coatings, but Electrochemical Impedance Spectroscopy (EIS) can provide numerical values, often correlated to the properties of the coating or its conditions. EIS interpretation, however, is a non-trivial task involving equivalent circuit fitting, which requires human input, specific knowledge, and it is not easy to automate in an industrial context. Machine Learning (ML) algorithms can perform a task after having been trained with previously interpreted data. Therefore they could be potentially used to automate the EIS interpretation. In this work, the corrosion behaviour of a wide set of organic coatings applied on cold rolled mild steel and AA2023-T3, with varying protective performance, was assessed by EIS in selected aggressive environments to obtain a large dataset for ML studies. The ML was then trained to discriminate between intact and failing coatings, identify a suitable equivalent circuit and provide estimation of the equivalent circuit component values. The results obtained show that ML has the potential to be employed to automate corrosion testing.

Inhibition of Filiform Corrosion on Acrylic coated steel by CaAL-LDHs anion exchange pigments

Andrea Cristoforetti*, Michele Fedel, Flavio Deflorian, Stefano Rossi, Federico Parola

Department of Industrial Engineering, University of Trento, via Sommarive n. 9, 38123 Trento, Italy;

* corresponding author: andrea.cristoforetti@unitn.it

The corrosion protection of steel often involves the use of organic coatings applied on the metallic surface. Their use combines the decrease in the diffusion ability of the aggressive species towards the metallic surface, and the possibility to add inhibitors able to delay or slow down the corrosive process. However, the addition needs to be completed wisely, as high quantities of additives may result in the formation of a zone prone to the formation of a defect or the formation of a preferential pathway for the electrolytes to diffuse. Still, the combination of paint and pigments can be tuned effectively. In the present work, the evaluated combination involves the calcium-aluminum Layered Double Hydroxide and the disodium sebacate inside an organic coating in the particular case of the mitigation of filiform corrosion. The inhibitors compounds and their performances are assessed both singularly and in combination with each other. The characterization involves spectroscopic techniques and a wide electrochemical characterization of the pigments synthesized and the acrylic-coated steel samples produced loading the primer layer with them. The capability of sodium sebacate to absorb on lamellar CaAl-LDH is highlighted by means of FTIR-ATR and XRD. The investigation involves also an evaluation of the effectiveness of the anion-exchange feature possessed by LDH compound and its potential regarding the corrosion inhibition field.

Fundamental Aspects of Corrosion Driven Coating Delamination: Old Beliefs and Novel Insights

Michael Rohwerder,

Max-Planck-Institut für Eisenforschung GmbH, Düsseldorf, Germany

Corrosion driven delamination of organic coatings is usually considered to occur either as cathodic delamination or anodic delamination. Cathodic delamination is the faster of these two and hence is considered the more dangerous one. Although a significant progress towards the fundamentals of delamination was achieved in the recent decades, the underlying key parameters are not fully understood. It is believed that in cathodic delamination either cation migration along the delaminated interface or oxygen reduction at the interface are rate determining [1, 2]. However, as was recently shown this is not the case [3]. Rather cation insertion into the yet unaffected, intact interface place a role. Nevertheless, delamination is usually observed to be slower on metals where the passive layer is less conductive, which at the first look would indicate that oxygen reduction is rate determining [4]. However, it is also observed that migration of cation in inert atmosphere is also slower on these surfaces [5]. This will be discussed in detail. Furthermore, the importance of higher resolution studies of delamination (see e.g. [6]) and the role of cathodic migration/delamination for anodic delamination will be discussed (see e.g. [7]).

References:

1. A. Leng, H. Streckel, M. Stratmann, The delamination of polymeric coatings from steel. Part 1: calibration of the Kelvinprobe and basic delamination mechanism, Corros. Sci. 41 (1998) 547–578
2. A. Leng, H. Streckel, M. Stratmann, The delamination of polymeric coatings from steel. Part 2: first stage of delamination, effect of type and concentration of cations on delamination, chemical analysis of the interface, Corros. Sci. 41 (1998) 579–597
3. N. Khayatan, M. Rohwerder, A new insight into the rate determining step of cathodic delamination, Corrosion Science 202 (2022) 110311

4. J. M. Prabhakar, R.S. Varanasi, C. Correa da Silva , Saba, A. de Vooys, A. Erbe, M.Rohwerder, Chromium coatings from trivalent chromium plating baths: Characterization and cathodic delamination behavior, Corrosion Science 187 (2021) 109525
5. J. M. Prabhakar, P. Kerger, A. de Vooys, Michael Rohwerder, Migration of ions on oxygen-deficient chromium oxide electrodeposited from trivalent chromium electrolyte, Corrosion Science 199 (2022) 110185
6. J.M. Prabhakar, A. de Vooys, M. Rohwerder, In situ microscopic investigation of ion migration on the surface of chromium coated steels, Npj Materials Degradation 6(1) (2022) 76
7. C. Senoz, S. Borodin, M. Stratmann, M. Rohwerder, In situ detection of differences in the electrochemical activity of Al2Cu IMPs and investigation of their effect on FFC by scanning Kelvin probe force microscopy, Corros. Sci. 58 (2012) 307-314

The inhibition of smart release organic anion pigments on the cathodic disbondment of organically coated galvanised steel

Gareth Jones[1], Patrick Keil[2] and Geraint Williams[1]

[1] Materials Research Centre, College of Engineering, Swansea University Bay Campus, Crymlyn Burrows, Swansea, SA1 8EN, U.K.

[2] BASF Coatings GmbH, Glasuritstrasse 1, 48165 Münster, Germany

Layered double hydroxide pigments containing exchangeable organic anions have been studied as an alternative to sparingly soluble salts due to their ability to store and release corrosion inhibitors when needed within an organic coating [1]. A group of organic compounds have been investigated as potential corrosion inhibitors for corrosion – driven cathodic delamination when dispersed in a polyvinyl butyl (PVB) coating. Due to the superior corrosion protection observed (see figure 1), 2-MBT was chosen and exchanged into an anionic ion-exchange clay, hydrotalcite (HT), and dispersed in a polyvinyl butyl (PVB) coating adherent to the zinc surface of hot-dip galvanised steel (HDG) at different pigment volume fractions. The inhibited coatings were evaluated in terms of their ability to halt corrosion-driven cathodic delamination using an in-situ scanning Kelvin probe (SKP) to study the influence of in coating 2-MBT loading on the delamination kinetics. Delamination rates decreased significantly with direct additions of 2-MBT and increasing HT–2-MBT pigment volume fraction (ϕ), with $\phi > 0.05$ having a significant effect. Further experiments were carried out using potentiodynamic techniques and in-situ scanning vibrating electrode analysis to study the influence of dissolved 2-MBT on the corrosion behaviour of a bare HDG defect immersed in 0.86M sodium chloride electrolyte. Initial results showed an increase in free corrosion potential and a reduction in corrosion current density with increasing 2-MBT concentration compared with the uninhibited solution. The mechanisms of inhibition in both the defect and underfilm regions will be discussed.

References:

*[1] H.N. McMurray, G. Williams, Corrosion **60** (2004) 219–228*

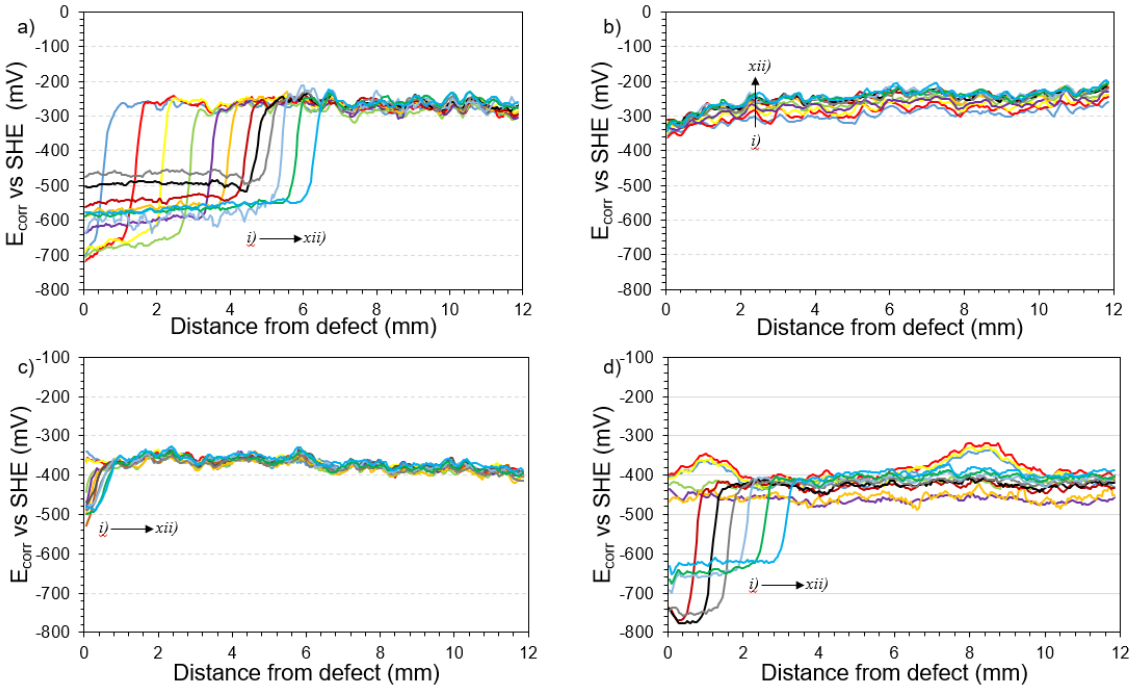

Figure 1: Plots of time-dependent E_{corr} versus distance (x) profiles for pigmented PVB coatings on HDG steel containing 1 wt% a) amino acid 1, b) 2-MBT, c) 8-HQ and d) nucleic acid 1, and initiated with 0.86M NaCl. Time key: curve i = 4 h, ii, iii… at 4h intervals thereafter

On the influence of the buried hybrid interface on the electrochemical behavior of coated metals: an ORP EIS approach

N. Madelat, B. Wouters, A. Hubin, H. Terryn, T. Hauffman

Research group Electrochemical and Surface Engineering, Dept. Materials and Chemistry, Vrije Universiteit Brussel, Brussels, Belgium

The application of organic coatings is among the top solutions to improve the corrosion resistance and durability of metallic structures in a broad range of industries such as automotive, aerospace, offshore platforms, and packaging. Dealing with protective organic coatings, the coating/metal oxide buried interface has significant impacts on the failure of the coated system [1]. Therefore, various methodologies are developed to engineer these hybrid interfaces and enhance their performance quality. As such different surface pre-treatments of the metal are carried out prior to the application of the barrier layer. Amongst other, anodizing is submitted as one of the most effective surface pre-treatments for aluminium, the primary material of choice in aerospace [2]. Understanding the response of the hidden, nanometer scaled interface/interface when exposed to a corrosive environment, is of uttermost importance in designing durable systems.

Corrosion resistance of the coated metals and their hybrid interfaces has been extensively studied using electrochemical impedance spectroscopy (EIS). However, the fast dynamics of these systems when exposed to a corrosive environment with respect to the measurement time in conventional EIS imposes non-stationarities. As a consequence, the condition required for a valid data treatment/modelling lays on the line.

In this work, we present an odd random phase electrochemical impedance spectroscopy (ORP-EIS) approach to investigate the interfacial influences on the general electrochemical behaviour of the coating/metal oxide system, where the short measurement time decreases the influence of the time-varying response, thanks to the multisine nature of the technique. Moreover, unique information on the non-stationarities and non-linearities are provided to generate valid experimental data [3,4]. To elaborate on the power of this approach in unravelling the contribution of the complex hybrid interfaces, aluminium 2024 test panels received different surface pre-treatments (acidic pickled versus tartaric sulfuric acid (TSA) anodizing) and were

evaluated prior and after application of industrial organic coatings. The complex hidden interface between the anodized aluminium and the barrier organic layer introduces many challenges to the evaluation of its contribution to the general behaviour of the coated system. In this work, the formation of the anodized layer has been confirmed using ORP-EIS and field emission scanning electron microscopy (FE-SEM). The ORP-EIS data of the coated test-panels were fitted using a two-layer model electrochemical equivalent circuit (EEC). This model enables us in following the diffusion of water and ions separate from each other through the organic coating towards the buried interface [5].

Despite the complex structure of the interface and the coating itself, this approach was proven to be successful in probing the interfacial influences. It was shown that initially after exposure of the coated panels to the electrolyte, although water is present at the buried interface, the influence of the interface is masked by the high barrier properties of the coating. With further diffusion of ions, the resistivity of the coating continuously decreases and eventually with the arrival of ions at the interface, the contribution of the acidic pickling and TSA anodizing is unravelled. The coated TSA panels remark higher corrosion resistance. This higher performance of TSA panels originated from the more resistant interface since the barrier properties of the coating stay similar regardless of the surface pre-treatment.

This approach is proven to be a promising candidate in generating key mechanistic insights about the tuning and failure of complex buried interfaces.

[1] Pletincx S. et al., An in situ spectro-electrochemical monitoring of aqueous effects on polymer/metal oxide interfaces, J. Electroanal. Chem. 848 (2019).

[2] Martínez-Viademonte M.P. et al., A review on anodizing of aerospace aluminum alloys for corrosion protection, Coatings. 10 (2020).

[3] Van Ingelgem Y. et al., Advantages of odd random phase multisine electrochemical impedance measurements, Electroanalysis. 21 (2009).

[4] Wouters B. et al., Monitoring initial contact of UV-cured organic coatings with aqueous solutions using odd random phase multisine electrochemical impedance spectroscopy, Corros. Sci. 190 (2021).

[5] Madelat N. et al., Differentiating between the diffusion of water and ions from aqueous electrolytes in organic coatings using an integrated spectro-electrochemical technique, Corros. Sci. 212 (2023).

Elucidation of Coating Heterogeneity and Charge-Transfer Mechanisms under Paint Films

Woraphan Intaphan; Stuart B. Lyon; Michele Curioni; University of Manchester, United Kingdom

Organic coatings have been widely used to provide surface protection against corrosive environments[1]. Over time, the coating degrades and allows water and ions to ingress into the bulk of the paint film, eventually, leading to the coating failure due to diffusion. However, the diffusion process does not occur at the same time and develops differently throughout every area of the paint film. Hence, the concept of coating heterogeneity Direct conduction (D-type) and Inverse conduction (I-type) was established by Mayne[2], Mills[3] [4], and Kinsella[5].

In order to investigate the D and I behaviours, electrochemical impedance spectroscopy (EIS) and localised electrochemical techniques (i.e. LEIS) were deployed to elucidate the charge-transfer mechanisms as well as the diffusion process. The epoxy amine coating consisting of Bisphenol A diglycidyl ether (DER332) and m-xylenediamine (MXDA) samples were exposed to various salt solutions with different water activities. It has been found that solvent-based DER332-MXDA curing at 60 ^{o}C provided much lower coating resistance around 60-200 MΩ/cm^2 and the diffusion occurred faster than the system that was cured at 160 ^{o}C as the resistance went up to 1-13 GΩ/cm^2. The solvent-free system also provided higher resistance than solvent-based film compared to the same curing temperature. Although the majority of the tested films exhibited D-type behaviour, there is a higher chance to find the I-type film at high curing temperature but this behaviour stayed for a while until the diffusion process occurred resulting decreasing in coating resistance and more importantly, switching from I to D type when the diffusion is fully developed without the appearance of rusts underneath the films.

In all coating systems, the resistance did not stay at the same value but reduced over time when the electrolyte concentrations along with water activities were changed. Not only the resistance can be used to categorise the D and I type behaviours, but coating capacitance can also be used because the behaviours are difficult to differentiate in

high resistance coating systems (~10 GΩ/cm^2 to TΩ/cm^2). The results suggest that D and I type conductions are highly related to continuous pathway 'hole' rather than the structure of the polymer itself. The I type can be switched into D type when the diffusion is fully developed and in some systems, both behaviours co-exist together which is rare to find.

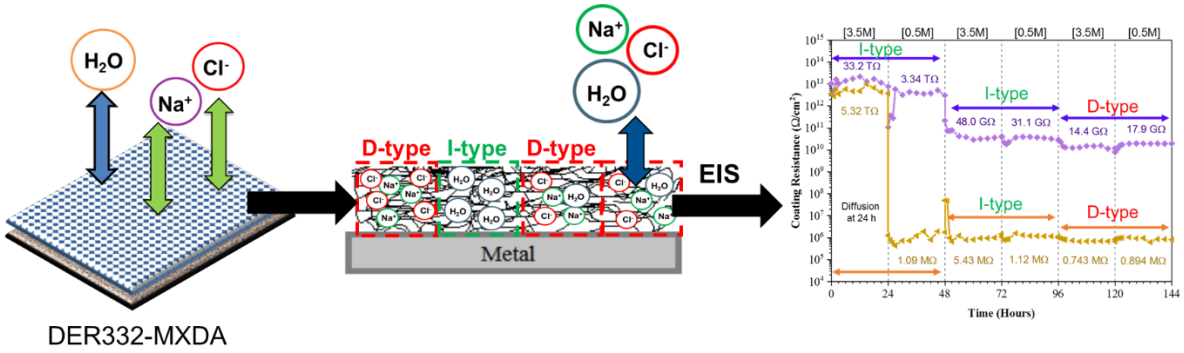

References

1 R. G. Buchheit, in *Handbook of Environmental Degradation of Materials (Third Edition)*, ed. M. B. T.-H. of E. D. of M. (Third E. Kutz, William Andrew Publishing, 2018, pp. 449–468.

2 J. E. O. Mayne, *Anti Corros. Methods Mater.*, 1952, **1**, 286–290.

3 J. E. O. Mayne and D. J. Mills, *J. Oil Colour Chem. Assoc.*, 1975, **58**, 155–159.

4 S. S. Jamali and D. J. Mills, *Corros. Eng. Sci. Technol.*, 2013, **48**, 489–495.

5 E. M. Kinsella and J. E. O. Mayne, *Br. Polym. J.*, 1969, **1**, 173–176.

Under-Film Corrosion of Transmission Tower Paint System in High Humid Environment

Teruhisa Tatsuoka [1], Hiromitsu Ijichi [1], Keiichi Yoshino [1], Nobuhiro Kishigaki [1]

Yuuki Yamato [2], Toshiyuki Saito [2], Motoyuki Yamazaki [2], Tomonori Shiraishi [2]

[1] TEPCO Research Institute, Tokyo Electric Power Company Holdings, Inc., Yokohama/ Japan

[2] Transmission Department, TEPCO Power Grid, Inc., Tokyo/ Japan

Steel structures such as transmission towers, bridges, plants, etc. are galvanized and/or painted to prevent corrosion. Steel structures paint system used to have several paint layers. The top coat has been degraded by ultraviolet radiation and the bottom layer has peeled off by water penetration. Increasing of peeled area of paint system caused by under-film corrosion are the main reason of re-painting. The sea salt deposition and time of wetness are the main factors of atmospheric corrosion and under-film corrosion.

It is very tough work to evaluate paint life accurately because environment of interface between bottom undercoat and metal is uncertain. Moreover, the paint system life is also influenced by the surface preparation before painting. The remaining corrosion products and sea salt depositions strongly depend on the quality of the surface preparation.

There are many researches about top coat degradation and under-film corrosion. However, a few studies have focused on quantitative evaluations of under film corrosion. Therefore, accelerated degradation tests of paint system and quantitative evaluation of under-film corrosion have been conducted to expect the paint system life.

KEYWORDS

transmission tower, under-film corrosion, surface preparation, time of wetness, deposition, sea salt

Characterization of molecular interactions at the (buried) metal oxide – silane interface

Kristof Marcoen [a], Beatriz de la Fuente [a], Herman Terryn [a, b] and Tom Hauffman [a]

[a] Vrije Universiteit Brussel, Department of Materials and Chemistry, Research Group Electrochemical and Surface Engineering, Pleinlaan 2, 1050, Brussels, Belgium
[b] Delft University of Technology, Department of Materials Science and Engineering, Mekelweg 2, 2628CD, Delft, The Netherlands

The use of organosilanes as adhesion promoters for the coupling of polymeric coatings to steel and aluminium surfaces, as well as for the corrosion protection of these surfaces, provides a less toxic and more environmentally favourable alternative to Cr(VI) treatments. Adhesion performance of such a coating system is largely determined by the chemistry at the hybrid interface. Quantification of adhesion (e.g. by peel or pull-off tests) is often used in industry to relate process parameters and resin compositions to coating performance, but unfortunately, such methods do not provide a thorough understanding of the underlying chemical mechanisms. A detailed molecular characterisation of interfacial chemistry is required for this purpose, but is quite challenging, especially when dealing with buried interfaces.

In this work, argon gas cluster ions were applied to sputter through thick coatings to access the buried metal oxide – silane interface for a molecular characterization by ToF-SIMS and XPS. Crucial prerequisite for this approach is the optimization of depth profiling parameters in order to reach the interface without severe degradation of its molecular structure. In regard of avoiding ion-induced sputter damage, hard X-ray photoelectron spectroscopy (HAXPES) could offer an additional asset in the study of buried interfaces. Owing to the application of hard X-rays, a larger probing depth is achieved for HAXPES as compared to conventional XPS. In this work, ToF-SIMS, XPS and HAXPES have been applied to characterize the organic – inorganic interface formed by application of 1,2-bis(triethoxysilyl)-ethane (BTSE) coatings to aluminium and steel oxides. New insights will be provided on the characterization of metal oxide-silane interactions with ToF-SIMS and XPS. Different approaches to characterize buried hybrid interfaces have been evaluated.

Interfacial processes in epoxy-coated galvanized steel surfaces under corrosive load

T. D. Singewald[1], T. Bruckner[1], R. Gruber[1], L. Hader-Kregl[1], G. Schimo-Aichhorn[1], S. Andronescu[2], M. Klotz[2], M. Müller[2], C. Kern[3], M. Rosner[3], G. Luckeneder[3], K.-H. Stellnberger[3], B. Strauß[3], M. Hafner[4] and M. Valtiner[5]

[1] CEST Competence Center for Electrochemical Surface Technology GmbH, Viktor-Kaplan Str. 2, 2700 Wiener Neustadt, and Stahlstr. 2-4, 4020 Linz, Austria

[2] Henkel AG & Co. KGaA, Henkelstraße 67, 40589 Düsseldorf, Germany

[3] voestalpine Stahl GmbH, voestalpine-Str. 3, 4020 Linz, Austria

[4] AMAG rolling GmbH, Lamprechtshausener Straße 61, 5282 Braunau-Ranshofen, Austria

[5] Vienna University of Technology, Institute of Applied Physics, Wiedner Hauptstraße 8-10/E134, 1040 Vienna, Austria

Abstract:

Adhesive bonding has become an accepted joining method in the automotive industry due to its cost effectiveness, the increasing importance of lightweight construction and the use of multi-material design. However, water absorption can cause electrochemical reactions at the adhesive-metal interface, which can lead to degradation or even failure of the adhesive bond.

In our study, several model formulations (MF) are investigated to simulate a commercially available epoxy coating. The present work addresses a comprehensive approach using electrochemical techniques to investigate the water absorption and delamination of the interface of galvanized steel/epoxy coating systems in NaCl solutions. Electrochemical impedance spectroscopy (EIS) was used to determine water absorption via a linear relationship between the dielectric constant of the wet coating and the dielectric constant of the dry coating and allowed to determine differences between several adhesives. Admixing different concentrations of commonly used additives to a model formulation allowed to understand the significant different delamination behavior of the used epoxy coatings. Additional scanning Kelvin probe (SKP) measurements allowed to observe the favored delamination process of different epoxy-coated galvanized steel surfaces, while cataplasma tests in oxygen-depleted and oxygen-rich atmospheres allowed to identify interfacial delamination processes. Our results showed that CaO additives can cause osmotic blistering and accelerates the diffusion of water into the adhesive due to a local increase in pH near the hydrated CaO particles, while $CaCO_3$ fillers reduce water diffusion.

Corrosion protection of HDG steel by epoxy-amine coatings: Influence of different amine linkers on transport properties and interfacial bonding

V. Cristaudo[1], B. Wouters[1], N. Madelat[1], B. Kannan[2], L. Steely[2], D. Clingerman[2], E. Brown-Tseng[2], T. Hauffman[1], H. Terryn[1]

[1] Department of Materials and Chemistry, Research Group Electrochemical and Surface Engineering (SURF), Vrije Universiteit Brussel, Pleinlaan 2, 1050 Brussels, Belgium
[2] Coatings Innovation Center, PPG, Allison Park, PA 15101, Unites States

The corrosion protection of hot dip galvanized (HDG) steel is of pivotal importance in the automotive industry. To this purpose, Zr-based conversion of the metal substrate for passivation and improved adhesion [1], in combination with the application of a polymeric primer coating often based on epoxy-amine resins offering good adhesive properties, is performed. The amine curing agent of the epoxy resin often consists of a diamine, although it can also be a more complicated polyamine or a polyamido-amine [2], and it influences both the water and ion transport properties of the organic coating (related to changes in the hydrophobicity/hydrophilicity of the network) as well as the interfacial interactions [3]. Indeed, preferential adsorption of the amine curing agent onto the oxidized metal surface has often been observed [2].

In this work, we want to elucidate the impact that three different amine linkers have on the water/ion uptake behavior and on the interfacial bonding at the initial state and under environmental exposure of an epoxy coating deposited on unconverted and converted pure zinc (i.e., model substrate). To this purpose, a spectro-electrochemical setup of in-situ ATR-FTIR in Kretschmann configuration and Odd Random Phase (multisine) Electrochemical Impedance Spectroscopy (ORP-EIS) on (100-nm) thin and (15-µm) thick coatings has been proposed by our group. This approach permits to monitor the formed bonds *at the metal oxide/polymer interface* as well as the water and ion arrivals under electrolyte exposure and to correlate with the electrochemical behavior of the system. Previous research conducted in our lab demonstrated the possibility with this combined setup to discriminate water and ion uptakes, and to correlate the latter with the onset of corrosion of the metal substrate [4]. Finally, the different mechanisms of chemisorption established by the amine linkers present in the resin with the metal substrate are elucidated by a combined ex-situ XPS/ToF-SIMS approach on ultrathin (nm range) organic films already validated in a previous investigation [3].

[1] V. Cristaudo *et al.*, A combined XPS/ToF-SIMS approach for the 3D compositional characterization of Zr-based conversion of galvanized steel. Applied Surface Science (2021) 562, 150166.
[2] M.-G. Barthés-Labrousse, Mechanisms of formation of the interphase in epoxy-amine/aluminium joints. The Journal of Adhesion (2012) 88, 699.
[3] V. Cristaudo *et al.*, Unravelling the chemisorption mechanism of epoxy-amine coatings on Zr-based converted galvanized steel by combined static XPS/ToF-SIMS approach. Applied Surface Science (2022) 153798.
[4] N. Madelat *et al.*, Differentiating between the diffusion of water and ions from aqueous electrolytes in organic coatings using an integrated spectro-electrochemical technique. Corrosion Science (2022) 110919.

Thin film pre-treatment on hot dip galvanized and ZnAlMg steel, differences in composition, morphology, and e-coat adhesion

Karin Beaussant Törne, RISE, Sweden; Dan Persson, RISE Sweden; Ville Saarimaa, TopAnalytica, Finland

In recent years TiZr thin films have received growing att ention as environmentally friendly alternatives to phosphating as pre-treatments in the automotive industry. However, several questions remain to be answered prior to large scale implementation. One such question is how the function of the TiZr pre-treatment is affected using Zn-alloys other than hot dip galvanized (HDG).

In this project HDG and ZnAlMg alloys were investigated. Samples were cleaned and pre-treated with a commercial automotive system. Surface characterization was done after cleaning and after pre-treatment using scanning electron microscopy (SEM), x-ray photoemission spectroscopy (XPS), Infrared reflection spectroscopy (IRRAS), Time of flight – secondary ion mass spectroscopy TOF-SIMS.

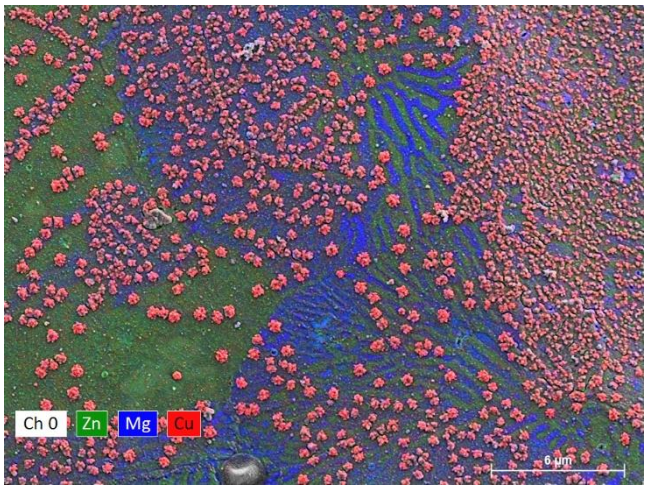

Figure 1 SEM/EDS image of pre-treated ZnAlMg alloy

To evaluate the effect of the pre-treatment on the adhesion properties, samples with and without pre-treatment were coated and exposed to a cataplasm test cycle. The adhesion was evaluated before and after exposure.

The surface characterization of HDG samples after alkalic cleaning showed relatively high amounts of Al. The surface after pre-treatment was covered with a homogeneous film.

The ZnAlMg alloy, on the other hand showed an inhomogeneous surface related to the phase separation in the microstructure. After pre-treatment selective precipitation was found on Zn rich areas and areas rich in Mg and Al, Figure 1.

The adhesion was evaluated by two methods, cross-cut and N-Methyl-Pyrrolidone (NMP) retention time. No difference in adhesion between HDG and ZnAlMg was found

with the cross-cut method. However, the NMP retention time was lower for the ZnAlMg alloy compared to HDG both before and after exposure.

Acknowledgement

Volvo cars AB are acknowledged for supplying samples

In-depth investigation of the formation mechanism of hybrid Zr-Cu-aminosilane conversion coating on Cold Rolled Steel (CRS)

Mohaddese Nabizadeh[1], Kristof Marcoen[1], Thomas Kolberg[2], Daniel Schatz[2], Herman Terryn[1], Tom Hauffman[1]

[1] Research Group Electrochemical and Surface Engineering, Department of Materials and Chemistry, Vrije Universiteit Brussel, Brussels, Belgium

[2]Chemetall GmbH, Frankfurt, Germany

Keywords: conversion coating, Tof-SIMS, XPS, Aminosilane, CRS

Abstract:

The automotive industry takes advantage of a multi-layer coating in order to have optimal properties of the final product. As such, conversion coatings are chemically applied to metal parts before painting to improve corrosion protection and paint adhesion.

After the restriction of chromate and phosphate conversion usage, Zr-based conversion coating has been introduced as a promising alternative for the automotive industry. However, the conversion system based on only Zr could not show satisfactory properties to substitute the aforementioned systems. In this regard, there have been quite a few attempts to finetune this system with the addition of organic and inorganic substances. For instance, Cu has been used frequently as an accelerator to enhance the deposition rate of the conversion coating on the surface [1].

In this research, the formation mechanism of a novel hybrid conversion treatment was studied on the surface of Cold Rolled Steel (CRS) as one of the common automotive materials. This hybrid coating is a combination of the well-known Zr-based conversion coating with a silane-based organic additive and $CuNO_3$ as an inorganic additive. In this study, four different samples have been prepared to clarify the role of each additive; Zr treatment, Zr-Cu treatment, Zr-aminosilane treatment, and Zr-Cu-aminosilane treatment. In this way, the effect of Cu and aminosilane addition in the Zr-based conversion system was comprehensively studied.

The results showed that Cu-containing treatment leads to the deposition of some Cu-rich particles on the top surface which indicate a higher concentration of Zr compared to the rest of the surface. However, Cu addition has not significantly enhanced the total amount of Zr deposition compared to the system without Cu. In addition, it was demonstrated that the simultaneous presence of Cu with aminosilane leads to the deposition of finer particles compared to the Zr-Cu system where the amount of deposited Cu has been shown to be less. The results exhibited that the simultaneous addition of Cu and aminosilane can lead to some interaction between them. It is previously reported that the amine groups present in the aminosilane tend to form a complex with Cu [2,3].

References:

[1] T. Lostak, S. Krebs, A. Maljusch, T. Gothe, M. Giza, M. Kimpel, J. Flock, S. Schulz, Formation and characterization of Fe3+-/Cu2+-modified zirconium oxide conversion layers on zinc alloy coated steel sheets, Electrochim Acta. 112 (2013) 14–23. https://doi.org/10.1016/j.electacta.2013.08.161.

[2] X. Liu, D. Vonk, K. Kisslinger, X. Tong, G. Halada, S. Petrash, K. Foster, Y.C.K. Chen-Wiegart, Unraveling the Formation Mechanism of a Hybrid Zr-Based Chemical Conversion Coating with Organic and Copper Compounds for Corrosion Inhibition, ACS Appl Mater Interfaces. 13 (2021) 5518–5528. https://doi.org/10.1021/acsami.0c19203.

[3] M. Nabizadeh, K. Marcoen, E.A.M. Cherigui, T. Kolberg, D. Schatz, H. Terryn, T. Hauffman, Unraveling the formation mechanism of hybrid Zr conversion coating on advanced high strength stainless steels, Surf Coat Technol. 441 (2022) 128567. https://doi.org/10.1016/J.SURFCOAT.2022.128567.

Zirconium conversion treatment of extruded Al-Mg-Si alloys with increased recycle content

Wouter Vereycken, Alexander Lutz and Iris De Graeve, Vrije Universiteit Brussel, Belgium

At the moment the maximum amount of scrap material that can be used in the production of recycled extruded Al-Mg-Si profiles is limited. This is due to strict rules on the alloy composition and difficult purification processes. Higher levels of certain alloying elements are feared to have a negative influence on, among other things, the corrosion resistance of final products. Electrochemical conversion treatments based on zirconium and/or titanium oxides are used to give an initial protection against corrosion and provide good adhesion with overlying paint coatings. The formation mechanism of conversion layers depends on the reactivity of the aluminium surface, determined by the alloy composition and nature and distribution of intermetallic alloying precipitates. In the context of recycled alloys, it is thus essential to investigate how the formation of these conversion layers and their protective properties are influenced by the presence of higher levels of alloying elements and precipitates. In the present study, zirconium based conversion of AA6060 aluminium alloys with increased recycle content Is investigated. Using open circuit potential measurements, the conversion layer formation process is studied and compared for recycled alloys versus classical alloys. The layers are morphologically and chemically characterised with SEM-EDX. Very similar formation mechanisms and layer characteristics are observed on recycled and classical alloys. Based on Volta potential maps recorded with SKPFM, it is seen that the conversion coatings decrease the potential difference between the cathodic precipitates and the aluminium matrix for high and low recycle alloys in a similar way, confirming that the layers passivate the aluminium surface. Additionally, with ORP-EIS their corrosion protection properties in NaCl are compared on the various alloys. Finally, to evaluate their real-life performance, the recycled and classical alloys are industrially pre-treated and powder-coated and exposed to accelerated corrosion tests. Due to the advanced fine tuning of the recycled alloy content, all alloys - recycled and classical - perform in a similar way, meeting the industrial test requirements.

Monitoring of ongoing corrosion protection surface treatment processes by the operando ORP-EIS

Meisam Dabiri Havigh[1], Mohaddese Nabizadeh[1], Benny Wouters[1], Noël Hallemans[2,3], Tom Hauffman[1], John Lataire[2], Herman Terryn[1], Annick Hubin[1]

1-Vrije Universiteit Brussel, Research Group Electrochemical and Surface Engineering, Pleinlaan 2, 1050 Brussels, Belgium

2-Vrije Universiteit Brussel, Research Group Fundamental Electricity and Instrumentation, Pleinlaan 2, 1050 Brussels, Belgium

3- University of Warwick, WMG, Coventry, 7AL CV4, UK

The application of conventional EIS, due to the linearity and stationarity requirements, is limited for the in situ monitoring of the oxide film formation during the conversion or anodizing processes [1]. The development of Odd Random Phase Electrochemical Impedance spectroscopy (ORP-EIS) to calculate the time-varying impedance of a nonstationary process [2] and an algorithm to quantify nonlinear distortions and obtain Best Linear Time Varying Approximation (BLTVA) of nonlinear time-varying processes like the corrosion process [3] mitigated the linearity and stationarity requirements. In this research, the operando ORP-EIS technique is used for in situ monitoring of corrosion protection surface treatments such as anodizing of aluminum (Al) [1] and the conversion treatment of zinc. For the anodizing process, the technique enables us to follow the growth of the barrier oxide layer and the impact of the anodizing parameters. As an example, the bode plot during the anodizing of Al is presented in figure1. Moreover, this technique makes it possible to monitor the conversion treatment and the role of organic and inorganic additives on the barrier properties of the conversion layer in situ in the bath. Therefore, the operando ORP-EIS can monitor surface finishing processes and pave the path to develop environmentally friendly surface finishing and modification technology such as chromium/phosphate free anodizing and conversion processes.

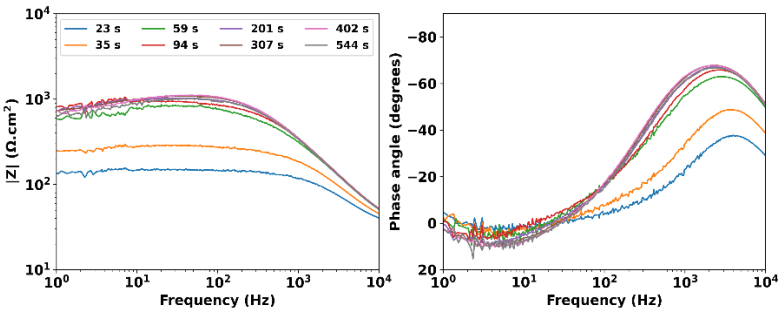

Figure1: Bode plot during the anodizing of AA2024 in the 0.5 M H_3PO_4 solution at room temperature. The anodizing DC potential 20 V (1 min sweep at a rate of 20 V/min and 9 min plateau at 20 V).

[1] M. Dabiri Havigh, B. Wouters , N. Hallemans, R. Claessens , J. Lataire, H. Terryn , A. Hubin, Electrochemistry Communications 137 (2022).

[2] T. Breugelmans, J. Lataire. T. Muselle, E.Tourwé, R. Pintelon, A. Hubin, Electrochemica Acta, 76 (2012).

[3] N. Hallemans, R. Pintelon, X. Zhu, T. Collet, M.D. Havigh, B. Wouters, R.I. Revilla, R. Claessens, K. Ramharter, A. Hubin, J. Lataire, IEEE Transactions on Instrumentation and Measurement, 71 (2022).

Increasing adhesion of polyurethane painting on aluminum by atmospheric pressure plasma jet treatment

J. Berckmans[a], C. Tubier[a], R. Revilla Castillo[b], C. Poleunis[c], H. Terryn[b], A. Delcorte[c], F. Reniers[a]

[a] Chemistry of Surfaces, Interfaces and Nanomaterials (ChemSIN), Faculty of Sciences, Université Libre de Bruxelles, Brussels, Belgium

[b] Research Group Electrochemical and Surface Engineering (SURF), Department of Materials and Chemistry, Vrije Universiteit Brussel, Brussels, Belgium

[c] Unité Physico-Chimie et de Physique des Matèriaux (PCPM), Université Catholique de Louvain, Louvain-la-Neuve, Belgium

Nowadays, industries are looking for replacement of chromium VI in aluminum pretreatment. In this quest, plasma treatments represent an interesting approach. Indeed, plasmas enable a wide range of possible modifications of materials (etching, grafting, surface functionalization) but also allow an easy industrial upscale.[1,2]

In this work, an atmospheric pressure plasma jet (APPJ) was used to modify aluminum 99,99% surfaces and study the effect on polyurethane paint adhesion. The difference induced by plasma treatments in wettability, chemistry, interface, and roughness were investigated by water contact angle, X-ray photoelectron spectroscopy, secondary ion mass spectrometry and atomic force microscopy respectively. In parallel, optical emission spectroscopy (OES) was used to characterize the plasma phase. The correlation between certain plasma species such as OH*, identified by OES and the resulting surface modification was investigated. Then, the adhesion of the polyurethane coatings on the plasma-modified surfaces was studied by a tape test according to ASTM D3359.

As a result, an increase of the adhesion of polyurethane coatings on plasma treated aluminum was shown (Fig. 1) and associated with surface modification of the aluminum.

Al 99,99% untreated Al 99,99% + Plasma treatment

Fig. 1 Effect of plasma treatment (Atomflo 600 300W, 30L/min Ar, 10 mm, 10 mm/s) on adhesion of polyurethane coating

References

[1] H. Butt, K. Graf, M. Kappl, Phys. Chem. Interfaces 2013, 28,1379.

[2] K. G. Kostov, T. M. C. Nishime, A. H. R. Castro, A. Toth,L. R. O. Hein, Appl. Surf. Sci. 2014, 314, 367.

Effects of measurement methodologies on the determination of fractal dimensions of blast-cleaned steel substrates

Tom Marquardt, Muehlhan Holding GmbH, Hamburg, Germany
Andreas W. Momber, Muehlhan Holding GmbH, Hamburg, Germany
Daniel Kelm, Fraunhofer IGP, Rostock, Germany

Surface preparation is a vital part of any corrosion protection process by means of coatings. The profile of blast-cleaned steel substrates affects the adhesion of the protective coatings, but also of linings, adhesives, and other materials applied onto them. Fractal dimensions, a measure of the complexity of a surface, are frequently used to quantify and characterize the profile of a surface. Understanding the fractal dimension of a blast-cleaned steel substrate will provide insight into the adhesion properties of the surface and helps to optimize blast-cleaning processes to achieve better adhesion and improved corrosion protection performance of coatings.

This study compares the fractal parameters of blast-cleaned steel substrates acquired with two methods, namely cross-sectional images, and tactile measurements. Samples of mild steel S355 were profiled with different blasting media (aluminium oxide, steel grit and steel shot). Cross-section images as well profiles of a total of 12 surface configurations were taken. Using an image processing software "ImageJ", 2D profiles of the steel surfaces were derived from the cross-sections (see Fig. 1). The fractal dimensions of these profiles were determined using the box-counting method, and they were compared with the fractal values obtained from the tactile measurements. A full factorial experimental design was employed to analyze the statistical relationships between the factors, including abrasive type, surface preparation grade, surface roughness, and measurement methodology.

Regardless of the measurement methodology, identical relative trends were found for the fractal dimensions from cross-sectional images and from tactile measurements. In terms of absolute numbers, the normalized values for the cross-section profiles were approximately twice as high as the values obtained from tactile measurements. Therefore, both methods are suitable for a relative comparison of blast-cleaned surfaces, but cross-section profiles seem to provide more accurate absolute values (see Fig. 2).

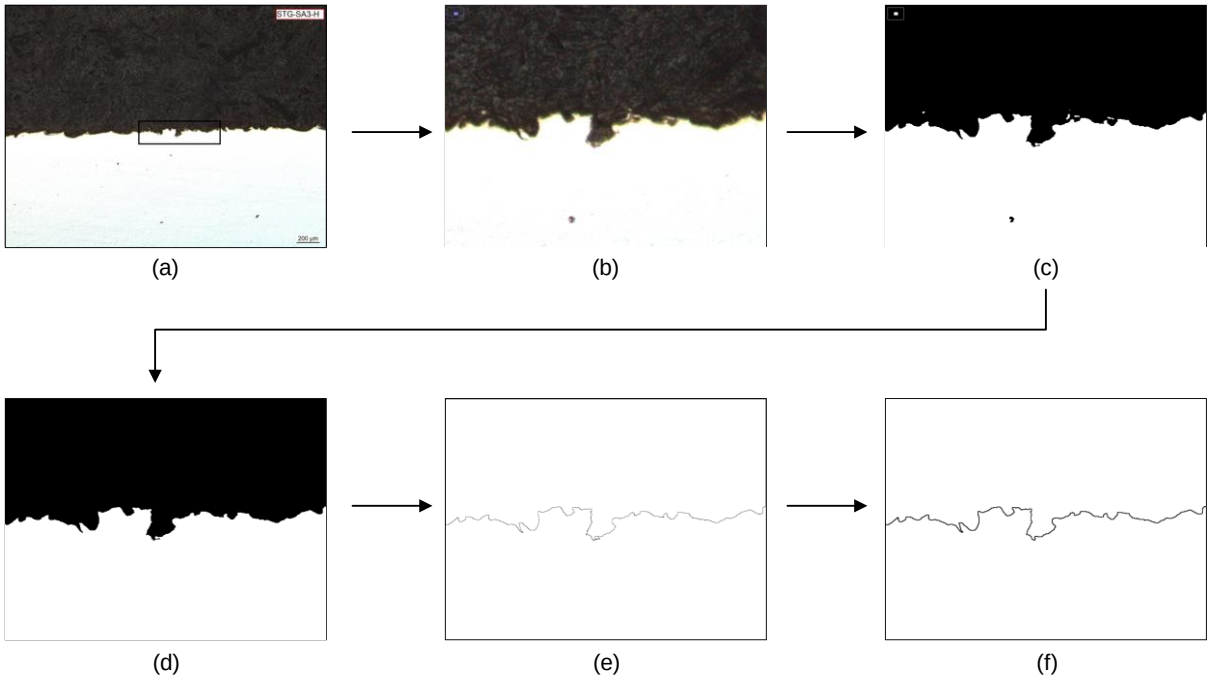

Figure 1 Detailed derivation of a sample 2D profile from a cross section image (factor levels: steel grit, Sa 3, 75 m). Initial image (a); Exemplary section (b); Binary (c); Fill holes (d); Outline (e); Dilate (f).

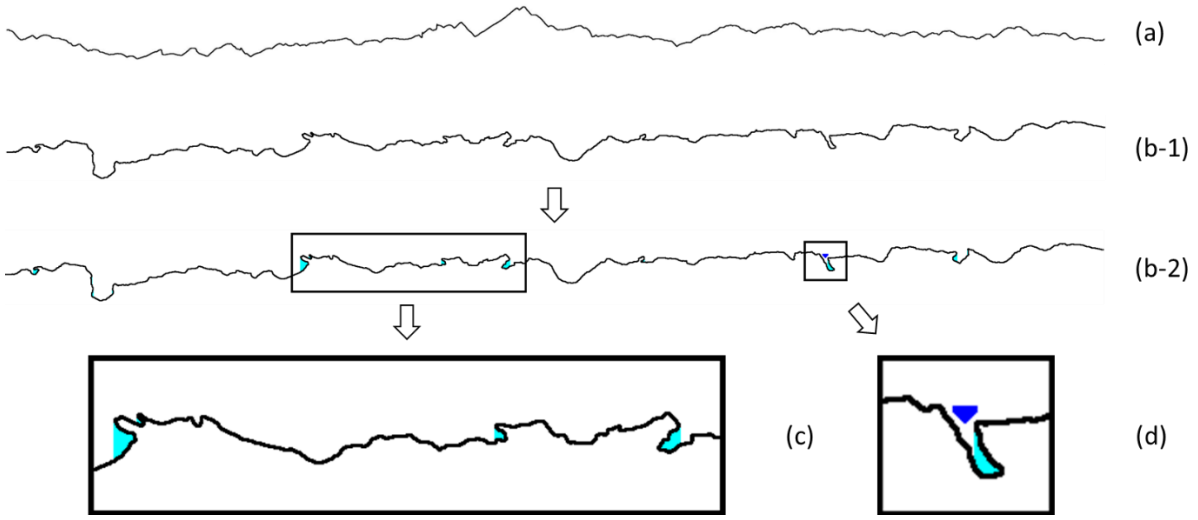

Figure 2 Comparison of tactile measurement (a) and cross section (b-1/b-2) in a 2D profile curve, together with a detailed image of the undercuts (c), and a detailed picture of the form of the stylus tip (d)

This investigation is funded in the frame of the '7. Energieforschungsprogramm' of the Federal Ministry of Economic Affairs and Energy (BMWi), Berlin, Germany, via the project 'FoKO-Wind' [03EE2006].

Use of chelating agents for in situ LDH formation on PEO treated active metals

Maria Serdechnova, Tatsiana Shulha, Anissa C. Bouali, Sviatlana V. Lamaka, Carsten Blawert, Mikhail L. Zheludkevich

Helmholtz-Zentrum Hereon, Geesthacht/Germany

In the past, the corrosion protection of Mg and Al alloys was dominated by chromate based coating solutions. Nowadays, the use of chromates is strictly limited in industrial applications due to their high toxicity. Thus, new alternative coating approaches for aluminum and magnesium need to be developed:

1. Plasma electrolytic oxidation (PEO) treatments, which is an environmentally friendly high voltage based anodizing process in non-toxic electrolytes. This process leads to the formation of hard well adherent ceramic-like layers on the surface of the metals due to short-living high-voltage electrical discharges. However, the inherent porosity and cracks, as a result of the discharges, strongly compromise the effectiveness of PEO coatings against corrosion.

2. LDH-based “smart” conversion treatment, in which the metal surface can be converted directly into nanocontainers. Being loaded with corrosion inhibitors, LDH can provide "smart" active corrosion protection. The release of a corrosion inhibitor and the formation of a protective layer occurs only when defects occur and corrosion starts.

In frame of the current work, we decided to combine these two approaches and create smart protective hybrid coatings, based on a subsequent LDH sealing treatment of PEO coatings. The hybrid coating provide both barrier and “smart” protection to the active substrate (AZ91 magnesium alloy and AA2024 aluminum alloy as well as their galvanic couple were selected). However, the direct replication of treatments, leading to LDH formation on bare substrate, is not possible due to the different reactivity of the surfaces and availability of cations from the substrates. Additionally, the traditional way of solubility control is using autoclave conditions. However, due to cost and time limitations such an approach is not suitable if the expected hybrid coatings are intended for automotive and aerospace applications.

Thus, a new approach of LDH formation on the surface and in the pores of PEO treated aluminum and magnesium alloys via additions of suitable chelating agents was developed. These compounds change the solubility of involved compounds (both from PEO layer and from substrate underneath) making the LDH formation possible at room or slightly elevated temperature. The mechanism of such a formation as well as characterization of formed hybrid PEO-LDH coatings is presented in the current work.

Acknowledgment: research project FUNCOAT, European Commission (Horizon2020, grant agreement No. 823942).

Combination of a layered hydroxide salt with molybdate and a layered double hydroxide with gluconate for active corrosion protection of carbon steel

Débora Abrantes Leal[a], Isabel Sousa[b], Fernando Wypych[c], Cláudia Eliana Bruno Marino[a], João Tedim[b]

a. *Department of Mechanical Engineering, Federal University of Paraná, 81531-980, Curitiba-PR, Brazil.*
b. *CICECO – Aveiro Institute of Materials, Department of Materials and Ceramic Engineering, University of Aveiro, 3810-193, Aveiro, Portugal.*
c. *Department of Chemistry, Federal University of Paraná, 81531-980, Curitiba-PR, Brazil.*

In this work, layered hydroxide salt loaded with molybdate (LHS-M) and layered double hydroxide with gluconate (LDH-G) were combined to provide corrosion protection to AISI 1020 carbon steel. Release studies performed showed that the release of inhibitors from LHS-M and LDH-G occurred in the presence of chlorides within different timescales. In addition, electrochemical studies performed for corrosion inhibitors directly in solution, as well as combined nanocontainers, showed that the inhibition of corrosion of carbon steel can be tuned using the right proportion of corrosion inhibitors. Consequently, epoxy coatings loaded with a mixture of LHS-M and LDH-G were found to render improved anticorrosion performance when compared to the neat coating. Overall, this study demonstrates that the combination of LHS-M and LDH-G can be a promising solution for corrosion protection of carbon steel for both early and long-term exposure under aggressive conditions.

Acknowledgements:

This work was financed by Coordenação de Aperfeiçoamento de Pessoal de Nível Superior – Brazil (CAPES) – (Finance Code 001 and CAPES/PrInt n° 88887.468259/2019-00), Conselho Nacional de Desenvolvimento Científico e Tecnológico (CNPq)- (C.E.B.M.: 303126/2019-1; F.W.: 300988/2019-2)., and by the project CICECO-Aveiro Institute of Materials, UIDB/50011/2020, UIDP/50011/2020 and LA/P/0006/2020, financed by national funds through the FCT/MEC (PIDDAC). Smallmatek Lda. for providing the LDH-G nanocontainer.

Self-healing coatings based on microcapsules containing novel drying oil applied to maintenance anticorrosive paintings

Felipe Garcia Nunes, University of São Paulo, São Paulo and Cepel, Rio de Janeiro/Brazil

Elber Vidigal Bendinelli, Cepel, Rio de Janeiro/Brazil

Idalina Vieira Aoki, University of São Paulo, São Paulo/Brazil

Self-healing coatings have attracted attention as they provide anticorrosive protection even when the painting is damaged. The encapsulation of drying oils, especially linseed oil, is an established strategy to promote self-healing for carbon steel paintings. However, the literature usually considers an efficient surface preparation of steel prior to coating application, such as dry abrasive blasting to the Sa 3 degree of cleaning. When it comes to maintenance painting of metallic structures and equipment during their operation in the field, due to complicated logistics, it is not always viable to carry out a thorough surface treatment, having to appeal to inferior surface preparation based on manual tools to the St 3 degree of cleaning. In this context, the main goal of this work is to access the performance of self-healing coatings in different surface treatments, including the Sa 3 and St 3 degrees of cleaning, simulation the case for maintenance painting as well. A novel drying oil in the smart coating field was encapsulated by in situ emulsion polymerization in poly(urea-formaldehyde-melamine) microcapsules. Additives were incorporated in an epoxy mastic primer with established performance in industrial maintenance painting. Coating systems were applied with a polyurethane topcoat, containing or not microcapsules in the primer, in Sa3 and St3 degrees of cleaning. Self-healing and barrier properties were assessed by electrochemical impedance spectroscopy with scratched and undamaged samples, respectively. Adhesion of the painting systems was analyzed by the pull-off test. Corrosion performance of the coatings was evaluated by long-term accelerated corrosion tests, namely: condensation chamber (4600 h), cyclic corrosion test (4200 h) and outdoor exposure in a CX atmosphere (2 years). The results obtained herein show that self-healing coatings can be applied to maintenance painting to improve its lifetime; however the self-healing and anticorrosive performance are greatly affected by the quality of the surface preparation.

Synthesis of zirconia nanocontainers and use in epoxy coatings to develop self-healing abilities

Brunela Pereira da Silva, University of São Paulo, São Paulo, Brazil

Idalina Vieira Aoki,University of São Paulo, São Paulo, Brazil

The development of smart coatings is a new and valuable technology been applied to avoid corrosion in metallic materials. Based on this fact, nanomaterials such as zirconia are an interesting type of carriers used to encapsulate inhibitors to further be applied in coating systems, developing self-healing properties. The aim of this work is the synthesis of zirconia nanocontainers containing corrosion inhibitor dodecylamine and the evaluation of self-healing abilities of epoxy coatings loaded with encapsulated inhibitor in such containers. Zirconia containers with dodecylamine as corrosion inhibitor were synthesized in a one step process using $Zr(BuO)_4$ as Zr precursor. The characterization techniques used were scanning electron microscopy (SEM), thermogravimetric analysis, infrared spectroscopy (FTIR), size distribution by DLS and pore diameter and specific surface area by N_2 adsorption-desorption technique. Electrochemical impedance spectroscopy (EIS) was applied as electrochemical technique to evaluate indirectly inhibitor release kinetics, as well as UV-vis spectroscopy, as analytical method. EIS, scanning vibrating electrode technique (SVET) and salt spray chamber test were used to evaluate self-healing and barrier properties. As result, SEM images and size analysis showed that zirconia containers presented a spherical morphology and nanometer scale size. FTIR spectra proved that inhibitor was encapsulated because of the presence of a band around 1600 cm^{-1} , been attributed to dodecylamine inhibitor. For inhibitor release kinetics, EIS and UV-vis results proved that dodecylamine is more easily released in acidic than in neutral or alkaline medium. The EIS technique results showed that loaded coated sample presented higher impedance modulus at low frequencies compared to the unloaded coated sample, and the addition of zirconia nanocontainers in the coated system did not reduce its barrier properties. SVET ionic current density maps of the loaded coated sample with a defect presented lower ionic current density values compared to the unloaded coated sample, and significant lower amount of corrosion products in the defect site; as well as salt spray chamber test results suggested lower corrosion products amount in the scratched area in inhibitor loaded coated sample. As

conclusion, zirconia nanocontainers were successfully synthesized and can be used as corrosion inhibitor carriers to develop self-healing coatings.

Acknowledgments: CNPq- Brazil (grant #140187/2017-0 and grant # 310504/2020-1).

Development of smart coatings with multi-responsive micro/nano capsules and the corrosion protection mechanism

*Lingwei Ma, Jinke Wang, Dawei Zhang**

University of Science and Technology Beijing, Beijing 100083, China

Metal corrosion is an electrochemical reaction in which metallic surfaces degrade seriously when reacting with the corrosive solutions in the presence of acid, alkali, and salt, resulting in severe safety issue and economic loss. It is highly necessary to develop advanced technologies to protect metals and alloys against corrosion degradation. Herein, multi-responsive micro/nano capsules are developed, illustrating pH-responsive, photothermal responsive, metal ion responsive properties to achieve the controllable release of corrosion inhibitors and corrosion indicators from capsules. Smart coatings loaded with these multi-responsive micro/nano capsules can achieve the self-healing and self-reporting performances, hence significantly prolonging the service life of coatings.

Corrosion inhibition performance of developed epoxy coatings containing carbon nanocapsules loaded with diethylenetriamine

Norhan Ashraf Ismail [1,2], R.A. Shakoor [1,*] , Ramazan Kahraman [2,*]

[1] Center for Advanced Materials, Qatar University, Doha 2713, Qatar

[2] Department of Chemical Engineering, College of Engineering, Qatar University, Doha 2713, Qatar

[*]Corresponding author:

R. A. Shakoor

E-mail: shakoor@qu.edu.qa

Tel:+974-4403-6867

Abstract

Because of their large surface area, loading capacity, and variable shape and structure, hollow structured nanomaterials have received a lot of interest in recent years. To that end, mesoporous hollow carbon nanospheres (MPHS) with an average diameter of 280 nm were manufactured utilizing the self-assembly process using silica particles as a hard template. The silica cores were etched using alkaline etching with NaOH, which efficiently removed the cores as validated by EDX. In the MPHS@ DETA, the DETA works as a corrosion inhibitor, surface modification, and hardener when loaded into MPHS. As an anti-corrosion pigment, 3 wt. % of the MPHS@ DETA was blended with an epoxy coating (MPHS@ DETA-EP), and the qualities of the produced epoxy coatings were systematically characterized.

[*] Corresponding author. Tel: +974-4403-6867. Email: shakoor@qu.edu.qa (R. A. Shakoor)

[*]Corresponding author. Tel: +974-4403-4130. Email: ramazank@qu.edu.qa (Ramazan Kahraman)

Slow and Sustained Release of Corrosion Inhibitors to Prolong the Corrosion Protection of Mild Steel

Aarti Gautam[1,2,#], *K.V. Gobi*[2], *R. Subasri*[1]

[1] *Centre for Sol-Gel Coatings, International Advanced Research Centre for Powder Metallurgy and New Materials (ARCI), Balapur, Hyderabad - 500005, Telangana State, India.*

[2] *Department of Chemistry, National Institute of Technology Warangal, Warangal 506004, Telangana State, India*

#- Presenting author, Email id: aartigautam1993@gmail.com

Abstract

The present investigation focuses on the use of different organic and inorganic corrosion inhibitors for corrosion protection of mild steel. Halloysite nanotubes (HNT) have been used as nanocontainers for loading three different corrosion inhibitors i.e., Benzotriazole, Zr^{4+} and Ce^{3+}. To confirm the loading of corrosion inhibitors into HNT various characterization techniques such as scanning electron microscopy equipped with energy dispersive X-ray spectroscopy, transmission electron microscopy, Brunauer-Emmett-Teller, Fourier Transform Infrared spectroscopy and X-ray diffraction analyses were used. The release rate kinetics of inhibitor loaded HNTs at different pH conditions and varying time intervals were investigated using UV-visible spectroscopy. Different mathematical models were proposed to explain the release rate kinetics of corrosion inhibitors from HNT. To evaluate the corrosion performance of the inhibitor loaded HNTs, 2 wt% of loaded HNTs were added into the sol-gel matrix. The prepared sols were deposited on mild steel substrates using dip-coating technique, followed by curing at 130° C for 1 h. Improved barrier performance and self-healing behaviour of the coatings were tested in 3.5 wt% NaCl solution using electrochemical impedance spectroscopy and potentiodynamic polarization studies. Electrochemical studies revealed that the organic corrosion inhibitor when loaded into HNT exhibited better corrosion performance with current density of the order 10^{-10} A/cm^2 when compared to inorganic corrosion inhibitors showing current density of 10^{-6} A/cm^2. To confirm the inhibition mechanism of corrosion inhibitors, coated mild steel substrates were exposed to salt spray for different time intervals as per ASTM

standard B3117 which results were found to be in agreement with those from electrochemical tests.

Keywords: Halloysite nanotubes; Sustained release; Corrosion inhibitors; Silica Coatings; Mild steel

The effect of depositing a cerium-acetate sol on active corrosion behavior on PEO coated AZ31B Mg alloy

E. Merino[1], A. Durán[1], Y. Castro[1]

[1]Instituto de Cerámica y Vidrio, CSIC, Campus de Cantoblanco, 28049 Madrid, Spain.

The use of magnesium alloys in structural parts of airplanes or cars would be a viable method to reduce the overall weight of vehicle bodies, the fuel consumption and thus the greenhouse gas emissions (GHE). Nevertheless, their high susceptibility to corrosion, strongly limits its widely applications. In order to improve the corrosion resistance, the surface of the Mg alloy can be modified combining plasma electrolytic oxidation (PEO) and sol-gel technique. PEO is an advanced electrochemical surface treatment which is used to develop ceramic and porous coating with good tribological properties. However, this porous coating cannot provide a long-term corrosion protection because corrosive agents can quickly diffuse through the pores and reach the substrate. To provide a smart and longer-term corrosion protection, the deposition of a cerium sol to seal the pores and provide a self-healing effect has been explored. Due to the ability of cerium species to dissolve and re-precipitate as cerium oxides or hydroxides over cathodic sites on the metal surface, cerium sol-gel coatings can provide self-healing corrosion protection.

For this reason, the aim of this work is focused on the development of a cerium sol-gel using cerium (III) acetate hydrate, diethylenetriamine, and acetic acid as transition metal salt, stabilizing agent and pH modifier, respectively. To achieve an active coating system, the cerium sol was deposited by dipping onto the PEO-coated AZ31B alloy and subsequently cured at 120ºC. The sol and the coating system were mainly characterized using infrared (IR) spectroscopy, x-ray diffraction (XRD), Field Emission Microscopy (FESEM) equipped with energy dispersive X-ray spectroscopy (EDS) detector, and Electrochemical Impedance Spectroscopy (EIS).

Preliminary results showed, a self-healing behavior produced by the cerium sol-gel coating. After maintaining the active coating system in immersion in a 3.5% NaCl solution, cerium oxide/hydroxide precipitates were identified, blocking the

corrosion and protecting the surface of the light alloy for prolonged immersion times.

Graphical abstract

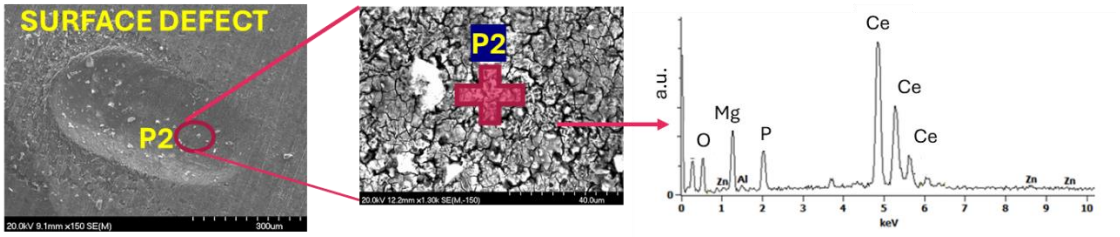

Keywords: AZ31B Mg alloy, PEO, Ce-based sol-gel coating, corrosion performance

Hybrid organic–inorganic coatings for corrosion protection of friction stir welded magnesium–titanium joints

S. Aliasghari[a], *T. Hashimoto*[a], *B. Mingo*[a]

[a] *Henry Royce Institute, Department of Materials, The University of Manchester, Manchester, M13 9PL, UK*

Abstract

Joining of dissimilar light metals by friction stir welding (FSW) is of interest to reduce weight and fuel consumption in the transport industry. The joints, if unprotected, are prone to severe galvanic corrosion in chloride-containing environments. Plasma Electrolytic Oxidation (PEO) is an environmentally friendly electrolytic technique that has been used widely to treat separately Mg and Ti. PEO capable of producing ceramic coatings with improved hardness, adhesion, corrosion and wear resistance. PEO coatings present a layered morphology formed by a nanometric and dense inner barrier layer and a thick outer layer with variable porosity. While the morphology of the inner layer cannot be modified, the porosity of the outer layer can be tailored as required during the coating synthesis. This porosity can serve as reservoirs for active species capable of providing smart functionalities to the coating.

In the previous work by the authors, was shown potential of this technique to use protect dissimilar materials from corrosion degradation with the formation of plasma electrolytic oxidation (PEO) coatings in a silicate electrolyte for corrosion protection of FSW AZ31B magnesium alloy-titanium joints. The severe corrosion of the unprotected AZ31B alloy led to precipitation of a large amount of $Mg(OH)_2$ from the sodium chloride solution by the end of the test. The weight of precipitate was reduced by a factor of ≈8 by the application of the PEO coating.

The aim of this study is to develop a multifunctional PEO coatings to improve the long term corrosion performance of Mg-Ti joints. The functionalisation is based on the combination of a two shell structure PS@CeO2 nanocontainer loaded with an organic inhibitor 8- hydroxyquinoline (8-HQ) for corrosion protection of composite coating of epoxy coated PEO on friction stir welded (FSW) AZ31B magnesium alloy-titanium joints. The two-shell nanocontainer were formed to release organic and inorganic encapsulated inhibitors on demand when the coating is damaged. Each shell has different responsive to corroded surface. Top layer synthesised with inorganic reservoir cerium ions as an inhibitor for Magnesium alloys. Polystyrene (PS) inner

layer loaded with 8-HQ is designed to release in water based solutions. Therefore, at the same time an inorganic and organic inhibitor release and protect the joint surface properly. The synthesized protective nanostructures were characterized with transmission (TEM) and scanning electron microscopy (SEM) and fourier transform infrared (FT.IR) spectroscopy. The corrosion behaviour of the uncoated and epoxy coated PEO joint without and with inhibitors is evaluated with polarization measurements in 3.5% NaCl electrolyte.

Thermal resistance and self-healing properties of a shape-memory epoxy coating with polycaprolactone microspheres

Fernando Cozim Melges, University of São Paulo, São Paulo, Brazil
Brunela Pereira da Silva, University of São Paulo, São Paulo, Brazil
Idalina Vieira Aoki, University of São Paulo, São Paulo, Brazil

Self-healing coatings have been amply studied as a way to reduce maintenance costs, prolong service life and improve upon the anticorrosive performance of coatings. A recent approach that has been proposed is the use of a shape-memory epoxy coating with thermoplastic agents, that can heal upon heating of the coating in a two-step process, in which there is first a reduction of the damaged area by the reversible plasticity mechanism, followed by the sealing of the damage by the flow of the thermoplastic agent. The self-healing properties of coatings prepared with this or similar approaches have been studied and showed promising results, however, despite the fact that heating is necessary for the healing mechanism to be activated, the resistance to thermal cycling has been scarcely evaluated. In this context, in the present work a shape-memory epoxy coating with polycaprolactone microspheres (SMEP-PCL) was prepared and its resistance to thermal cycles and self-healing properties were studied. The thermal cycles were conducted and evaluated according to the ASTM standard D6944-15, method B – Freeze/Thaw, and the self-healing properties of two different types of damage were evaluated by scanning electron microscopy (SEM), electrochemical impedance spectroscopy (EIS) and scanning vibrating electrode technique (SVET). The prepared coating was able to completely seal the defect when the damage was made with a thin blade, but no significant recovery of the coating was observed when it was damaged with a 0,2 mm drill, showing that the efficiency of healing of this approach is highly connected with the type and extension of damage. The thermal cycled samples did not present any degree of checking or cracking and the EIS measurements showed only a slight diminishment of the barrier properties of the coating, after the thermal cycles. Overall, the results seem to corroborate the great potential of this approach towards making self-healing coatings, as seen on other works, and also signal towards some possible limitations, which should be further studied.

Acknowledgments: Coordenação de Aperfeiçoamento de Pessoal de Nível Superior – Brasil (CAPES) – Finance Code 001. CNPq- Brazil (grant #140187/2017-0 and grant # 310504/2020-1).

Self-healing effect of damaged coatings via biomineralization by *Shewanella putrefaciens*

Xiangping Hao, Yun Bai, Hongchang Qian, Yuntian Lou, Dawei Zhang**

Beijing Advanced Innovation Center for Materials Genome Engineering, Institute for Advanced Materials and Technology, University of Science and Technology Beijing, Beijing 100083, China

Organic coatings are widely applied to mitigate corrosion thanks to the barrier effect against corrosive media, the adhesion to the metal substrate and the inhibition effect on corrosion reactions. The severe marine corrosive environments cause a prominent problem of coating damage, which promotes the development of self-healing anticorrosive coatings. Compared with abiotic mechanisms such as intrinsic or extrinsic mechanisms, self-healing mechanisms based on biological or microbiological activities are rarely reported in the development of smart protective coatings. This study reported the self-healing effect of damaged epoxy coatings on carbon steels via biomineralization by *Shewanella putrefaciens* (*S. putrefaciens*) in artificial seawater. The mineralization products accumulated in the coating scratch were composed of inorganic-organic hybrid matters. The EIS results demonstrated that the biomineralization could repair the corrosion resistance of the scratched coatings, with the $|Z|_{0.01\ Hz}$ value recovered to ~10^{11} $\Omega \cdot cm^2$ after 14 days of inoculation. The results proved that the co-existence of *S. putrefaciens* and Ca^{2+} was a necessary condition for the mineralization repair of damaged coatings. Interestingly, the bacteria preferred to colonize in the coating scratch instead of the coating surface, which may be attributed to the fact that *S. putrefaciens* can harvest energy from the steel substrate to support their growth. This work will provide a new idea for the development of marine self-healing anticorrosive coatings based on biological or microbiological activities.

Keywords: Corrosion protection, Microbiologically induced corrosion inhibition, Self-healing coatings, Biomineralization

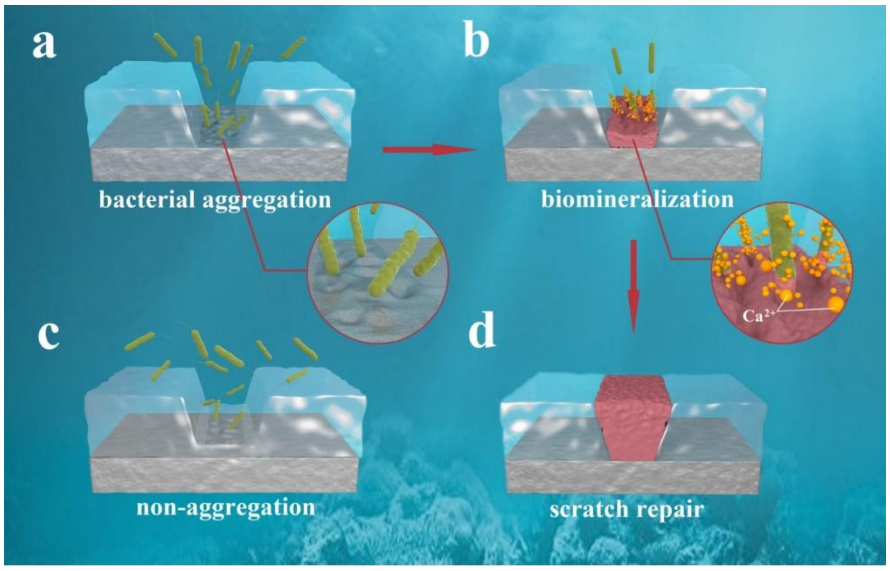

Figure 1 The self-healing mechanism based on biomineralization induced by S. putrefaciens in artificial seawater

Corresponding author: Xiangping Hao, xphao@ustb.edu.cn; Dawei Zhang, dzhang@ustb.edu.cn

Preparation and physicochemical characterization of graphene-enriched tung oil-urea formaldehyde microcapsules

*Abdullah Naseer Mustapha**, Maitha Almheiri, Nujood AlShehhi, Nitul Rajput, Zineb Matouk, Natasa Tomic*

Advanced Materials Research Centre, Masdar City, Abu Dhabi, United Arab Emirates

Abstract

A series of tung oil (TO) microcapsules (MCs) were synthesized via one-step in situ polymerization, with the addition of graphene nanoplatelets (GNPs) (1-5 wt. %). These MCs were then immersed in an epoxy coating to create a self-healing and corrosion resistant coating to be applied on a steel substrate. The addition of GNPs conveyed a series of advantageous properties to the MCs, including the enhanced curing behaviour of the TO, reduction in size distribution, reduced foaming during the formulation process and a reduction in the contact angle with the addition of GNPs. Furthermore, there was significant corrosion mitigation with the addition of the MC on the metallic substrate after 1 week immersed in 3.5 wt. % NaCl solution. XRD analysis show that the GNP had excellent dispersion in the TO. Furthermore, the XPS results expresses the confirmation of TO adsorption on the surface of the GNP. Moreover, the Raman spectra shows the reduction in intensity of the Raman intensity peaks over a duration of 4 days, associated with the degradation of the C=C double bonds. Synergistic effects of emulsifiers between gelatin and Tween 80 were observed, with gelatin chosen to formulate the MCs due to droplet stability. SEM images then displayed enhanced shell roughness for the TO-GNP MCs in comparison to the pure TO MCs. High resolution TEM images confirm the presence of GNPs on the outer layer of the MCs, with the graphene layers composed of 5-7 layers with interlayer distance of ~ 0.37 nm.

A review on the characteristics and current results of VDM® Alloy 699 XA: an alloy designed for applications in the petrochemical industry

Daniela Kremer, Dr. Benedikt Nowak, Dr. Bodo Gehrmann, Dr. Helena Alves,
VDM Metals International GmbH, Altena/Germany

VDM® Alloy 699 XA (UNS N06699) is a nickel-chromium-aluminium alloy, which has been primarily designed for metal dusting bearing environments. Based on the combination of its alloying constitutes, Alloy 699 XA shows a significant better resistance against metal dusting compared to VDM® Alloy 602 CA which has been proven in laboratory scale as well as in field tests.

Plates, bars, seamless tubes, wire as well as powder have been successfully produced, underlining the good workability of Alloy 699 XA. Another crucial property, which is important for materials to be used in applications in the petrochemical industry, is that the material shows a good weldability and a matching filler metal is available, as it is the case for Alloy 699 XA.

The aim of this contribution is to outline the characteristics and advantages of Alloy 699 XA by presenting the results not only on laboratory scale (for example on welded samples as well as printed samples), but also by presenting examples of successful use of Alloy 699 XA in demanding high temperature corrosion applications in field tests in the petrochemical industry.

Developing 3D Models of Liquid Water and Vapor Transport and Condensation in Insulated Systems to Understand Corrosion Under Insulation

Åsmund Ervik, SINTEF Energy Research; Ole Meyer, SINTEF Energy Research; Øivind Wilhelmsen, SINTEF Energy Research; Magnus Aa. Gjennestad, SINTEF Energy Research; Niels Aakvaag, SINTEF Digital; Vincent Gregoire, Equinor; Andres Rivero, Equinor; Sieger Terpstra, Shell; Ikesh Patel, Shell; Kristin Huseland, Gassco; Roe Tverrå, Gasso

Corrosion Under Insulation (CUI) is a major threat to process plant integrity and could be responsible for around half of all costs related to insulated process component maintenance [1]. CUI has been the focus of significant attention and R&D for half a century, with development of advanced coatings, insulation materials, non-destructive testing and risk-based inspection strategies. An excellent overview of CUI R&D as well as practical guidelines is found in EFC publication no. 55 "Corrosion Under Insulation Guidelines" [2]. Yet the challenge remains serious and the resulting damage seemingly stochastic, as is observed in the study by C. Watt et al. [3].

Surprisingly, given the scale of the CUI problem, little research has been focused on the fundamental root cause – how does liquid water and vapor enter insulated systems and propagate to those locations where corrosion happens and which conditions are necessary for corrosion to occur at the metal surface? While systematic efforts have been made to collect observations and findings from inspection and maintenance [3], [4], the answers to these questions are still not clear.

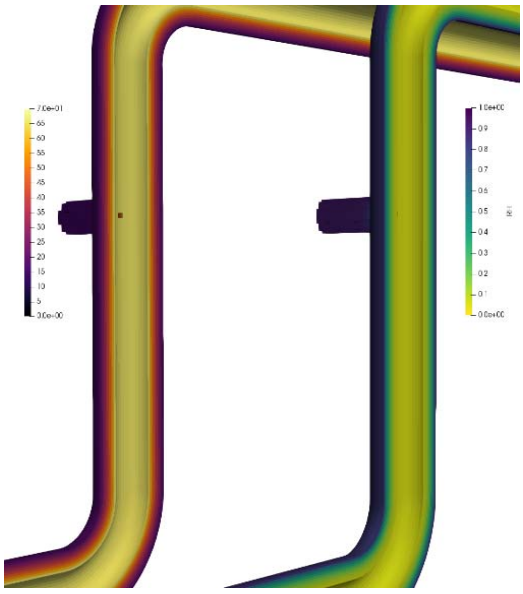

Figure 1: Numerical simulation of temperature (left) and moisture distribution (right) in insulated piping with dead leg protruding.

Inspired by the broad success of numerical models for heat and mass transfer in other engineering disciplines, including insulation design and moisture control in buildings, we have developed a three-dimensional computational thermo-fluid-dynamics solver tailored for the CUI problem, which is able to answer such questions.

Here we give an overview of the approach and provide some example cases that can be addressed, as illustrated in Figure 1.

We then proceed to give an overview of our research into combining distributed humidity sensors deployed throughout the process plant, with intelligent physics-based data analysis to determine the present and historic state of humidity in the insulation and water wetting, giving input to models for coating degradation and corrosion. A time history of temperature and relative humidity obtained from spot sensors installed on insulating piping is shown in Figure 2. When combined with the capability of performing detailed numerical modelling of liquid water and vapor transport in the insulation system in a digital twin, this approach can provide process plant operators and fabric maintenance companies with a toolbox that allows genuinely predictive CUI maintenance and prevention.

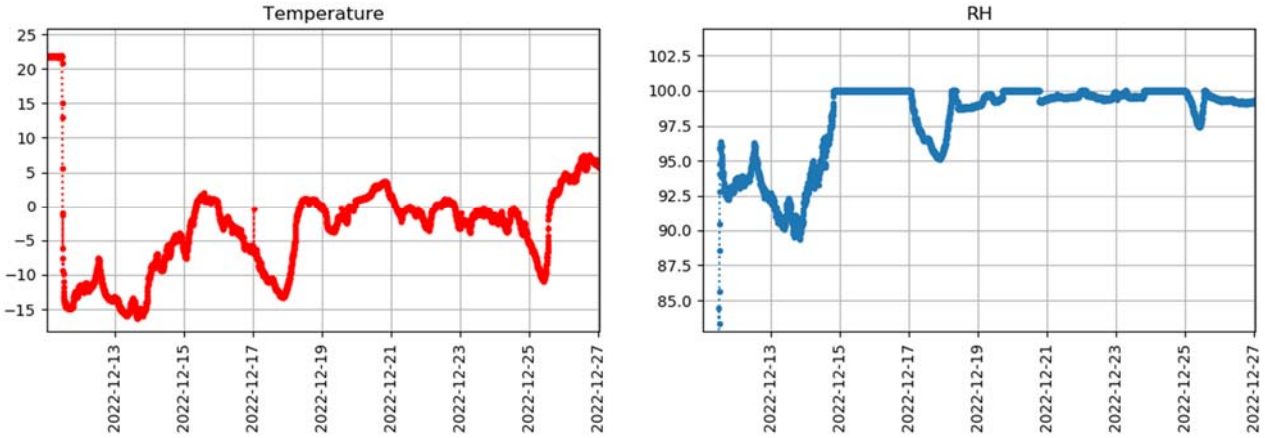

Figure 2: Example of temperature and relative humidity time history from spot sensors installed on insulated piping.

[1] B. J. Fitzgerald and S. Winnik, 'A Strategy for Preventing Corrosion Under Insulation on Pipeline in the Petrochemical Industry', Journal of Protective Coatings & Linings, vol. 22, no. 4, May 2005

[2] Gino de Landtsheer and Stefan Winnik, Corrosion Under Insulation (CUI) Guidelines - Technical Guide for Managing CUI, 3rd ed. Elsevier, 2020.

[3] C. Watt, S. Paterson, C. White, and T.-P. Wilk, 'Using Industry Data to Develop Improved Methods to Manage Corrosion Under Insulation', presented at the SPE International Oilfield Corrosion Conference and Exhibition, Jun. 2021.

[4] A. Marquez, J. Singh, and C. Maharaj, 'Corrosion Under Insulation Examination to Prevent Failures in Equipment at a Petrochemical Plant', Journal of Failure Analysis and Prevention, vol. 21, no. 3, pp. 723–732, Jun. 2021

InnovateCUI – A Joint Industrial Initiative investigating Sensors and Coatings for improved management of Corrosion Under Insulation

Jeroen Tacq, Sirris, Zwijnaarde/Belgium; Sebastiaan van der Vaart, Scalda, Terneuzen/The Netherlands

Corrosion Under Insulation (CUI), is one of the major corrosion phenomena affecting assets in the process industry. It is notoriously difficult to predict when and where CUI will occur, and what the rate of CUI will be under specific circumstances. While CUI is not new, our quantitative understanding of CUI is limited. To cost-effectively manage CUI, a combination of improved understanding, innovative preventive measures (e.g. insulation system design, coatings) and improved detection methods are required (CUI sensors and NII methods to identify CUI areas).

Sensors and the impact of operating conditions on CUI

To study CUI in a controlled, yet realistic environment, a unique CUI test-rig has been developed within the framework of an Interreg Flanders-The Netherlands project, replicating realistic water delivery and operating conditions. Results from an 8 month long experiment will be presented. Carbon steel pipes have been subjected to various amounts of wetting of the insulation, as well as internal pipe temperatures (room temperature; 82°C; cyclic conditions). Significant differences in dry-out, location of water retention and corrosion have been observed as a function of pipe temperature and amount of water infiltration. Significant CUI was observed on an uncoated pipe, already after 2 weeks at 82°C. The impact of cyclic operating conditions on the corrosion rate will be presented. In addition, the test-rig has been used to evaluate two innovative CUI moisture sensors (Fluves, isenspro). The obtained sensor data show good correlation with amount of water ingress and provides insights in insulation wetting and dry-out.

Following the first results obtained in the Interreg project, an industrial initiative led to the expansion of the test-rig towards a more realistic, industrial design. A number of CUI sensor technologies are currently being evaluated in this test facility. An overview will be given of the design of the test-rig, and of the sensor technologies being evaluated.

CUI Coatings

An important tool to help control CUI is the application of coatings. To evaluate the performance of CUI Coatings, a number of coating test standards have been

developed (ASTM G189, ISO 19277, AMPP TG516). Other test methods have also been developed by individual companies. However, the question of how representative these test methods are for real field-performance remains unanswered. In an effort to answer this question, coating degradation curves will be determined by means of an Electrochemical Impedance Spectroscopy (EIS) based field inspection tool. EIS measurements will be performed at regular intervals during (1) an accelerated test and (2) a slow ageing test. The ageing test comprises a 1.5 year test in which coatings are tested on the developed realistic CUI test-rig. The established experimental design will be presented, as well as the developed methodology to correlate accelerated testing to real field performance of coatings.

Acknowledgement: The infrastructure is developed with funding of The European Regional Development Fund (ERDF), under the Interreg Flanders-The Netherlands program.

Advanced Sprayed Nanostructure Coatings Against Corrosion for Refinery Applications

S.A. Mutairi, Saudi Oil Company, Dhahran; sultan.mutairi.1@aramco.com
N. A. Rasheedi, Saudi Oil Company, Dhahran; nayif.rasheedi@aramco.com

Keywords: Nanostructure, corrosion, thermal, pipelines.

Effective coatings of pipelines in refineries are vital in ensuring safety availability, increased production, reduced repair cost, and minimize the none productive time. Due to the high cost of coating used in refineries sectors, there is a need to enhance the coatings performance through choosing a strong and hard feedstock material by reducing the particle size to nanostructure size. The paper explores existing problems in pipeline due to corrosion and shows the different mechanisms occur. This paper also identifies the recent developments of WC-12Co nanostructured coatings and how they have performed when deposited using different thermal spray techniques, such as some of the successful spray techniques such as high velocity oxy fuel (HVOF) and cold gas dynamic spray. The research focuses on assessing such deposits (HVOF WC-12%Co nanostructured and HVOF WC-12%Co microstructured) against mechanical performance and corrosion performance. These results demonstrate that the significant improvement in nanostructured WC-12Co coating performance can be achieved by utilizing proper controlling parameters for each technique.

Matching Welding Filler and similar welded joint for UNS S34752

Shinnosuke Kurihara, Yuhei Suzuki, Masaki Ueyama and Takahiro Osuki
NIPPON STEEL CORPORATION, Japan

Background

It has been known that application of distinctive version UNS S34751 with extra low Carbon and Higher Nb/C ratio was effective to prevent both Polythionic Acid Stress Corrosion Cracking (PTA-SCC) and stress relaxation cracking without Post Welding Heat Treatment (PWHT) in several plants of petroleum refineries. However, it is difficult to apply UNS S34751 to high temperature facilities due to lower creep rupture strength compared to UNS S34709 over 675 deg. C (1,250 deg. F).

UNS S34752 was developed by adding some elements like Copper to UNS S34751 to achieve higher maximum allowable stress compared with UNS S34709 and S34751. UNS S34752 also shows both excellent resistance to PTA-SCC and stress relaxation cracking without PWHT as well. Therefore, UNS S34752 can be applied to high temperature facilities such as Delayed coker & Hydrogen reformer operated below 816 deg. C (1,500 deg. F) and was adopted as first order for actual plant in 2022.

Development of Matching welding filler and properties of similar welded joint

On the other hand, the similar properties of welded joint to base metal using matching welding filler of UNS S34752 are also required for actual application in such plant. In this study, this matching welding filler for Gas Tungsten Arc Welding (GTAW) was developed by optimizing chemical composition based on base metal and the properties of similar welded joint of UNS S34752 were evaluated regarding PTA-SCC resistance, weldability, aging toughness and creep rupture strength without PWHT.

Key words: Polythionic acid stress corrosion cracking, Stress relaxation cracking, Sensitization, PWHT, Creep rupture strength, Austenitic stainless steel, UNS S34752, UNS S34751, UNS S34709, GTAW, Matching welding filler, Similar welded joint, Weldability, Aging toughness

Structure and Related Effectiveness of Naphthenic Acid Corrosion Inhibitors

Oussama Zenasni, Nalco Water, USA, oussama.zenasni@ecolab.com
Maria Marquez, Nalco Water, USA, maria.marquez@ecolab.com
Chris Claesen, Nalco Water, Belgium, cclaesen@ecolab.com
Josep Marca, Nalco Water, Spain, jmarca@ecolab.com
Martin Vosecky, Nalco Water, Czech Republic, mvosecky@ecolab.com

Petroleum refineries often encounter naphthenic acid corrosion when processing opportunity crudes with a high total acid number (TAN). The formation of oil soluble iron carboxylates in refinery units that operate at high temperature regimes (200 °C to 400 °C), with corresponding high fluid velocities, can potentially lead to high rates of corrosion in the affected zones. Among the means for mitigating such corrosion is the application of chemical additives (i.e., corrosion inhibitors). These inhibitors are largely composed of phosphorus-based compounds, which have come under scrutiny due to possibly phosphorous related fouling events at multiple refineries and their potential impact on downstream processes. Consequently, Nalco Water has developed a new high temperature corrosion inhibition technology, that achieves the industry most effective passivation of mild steel. Industry accepted corrosion testing, shown in **Figure 1**, substantiates this new technology to provide effective metal surface passivation while simultaneously utilizing the 70% less phosphorous content. Additionally, the new technology mitigates the impact of phosphorus on downstream assets through the low phosphorus content and the extremely low volatility of the passivator.

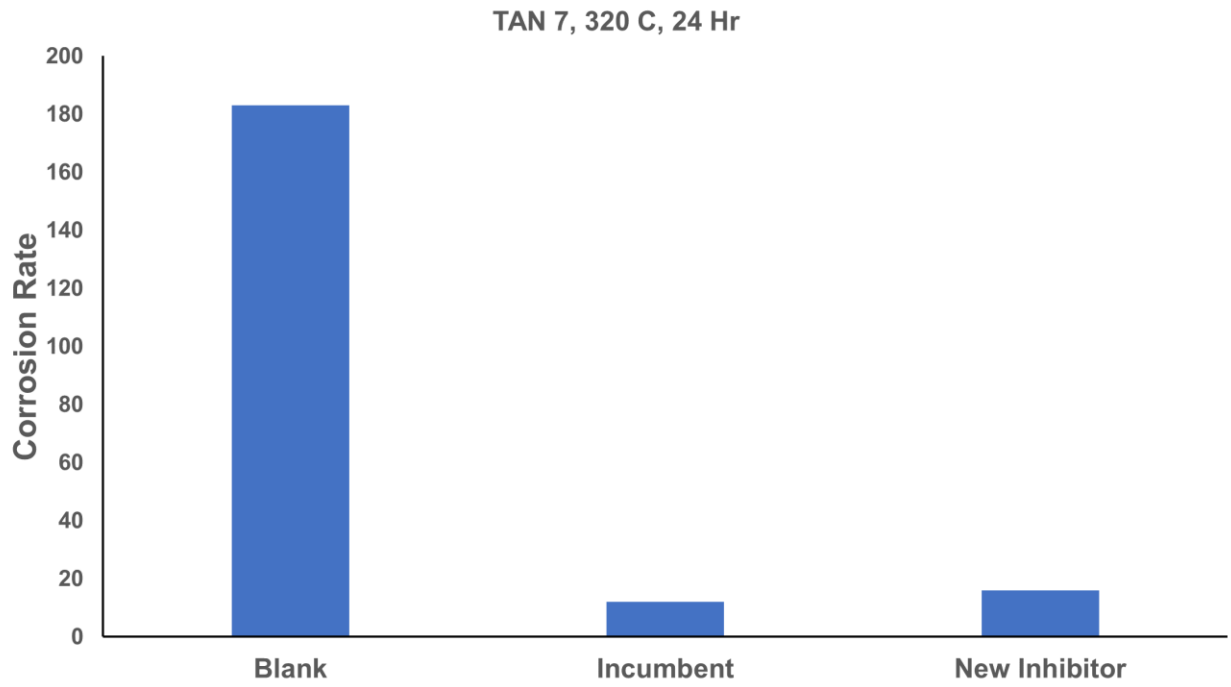

Figure 1. High temperature autoclave corrosion results on C1018 coupons for the new technology vs the incumbent.

In summary, this new technology represents an opportunity to mitigate naphthenic acid corrosion in crude units processing high TAN crudes, while facilitating increased unit run lengths with the associated reduction in maintenance costs and lost operating margins.

Defect-Free Commissioning:
Challenges & Opportunities Amidst the COVID-19 Pandemic

Zakaria Al-Hadhrami & Faisel Amin, OQ Refineries & Petroleum Industries, Sohar, North Al-Batinah/Sultanate of Oman

Background

Commissioning a new plant requires support from process licensors, critical plant asset subject matter experts (SMEs), and engineering consultants on site. OQ commissioned its first Steam Cracking Unit (SCU) in Oman amidst the COVID-19 pandemic. With partial commissioning in progress, the COVID-19 pandemic peaked, impacting the mobility and availability of critical resources and challenging the project team to move forward.

This paper intends to discuss critical mechanical integrity issues associated with materials and corrosion during the commissioning stage of a major petrochemical project; from the context of challenges in managing the matters despite the scarcity of resources due to the COVID-19 pandemic. The lessons learned could be beneficial in developing a business continuity plan from a project standpoint.

Introduction

Despite the numerous challenges amidst the COVID-19 pandemic, OQ pivoted and redirected the existing resources at the project site to successfully commission the SCU plant with remote support from the process licensors, critical plant asset subject matter experts (SMEs), and engineering consultants. This paper discusses the challenges that the project Asset Integrity Team (Inspection, Materials, and Corrosion) experienced during the project commissioning and the strategies implemented to overcome the obstacles.

Critical mechanical integrity issues associated with materials and corrosion during the commissioning stage of a major petrochemical project are highlighted. Lessons learned from the project commissioning are reflected in the selected petrochemical plant case studies.

Case Study 1: A review of flow-induced vibration defect of small-bore connections (SBC) in a steam piping system due to a mismatch between design and actual process parameters.

Case Study 2: An inspection and corrosion analysis of Microbiologically Influenced Corrosion (MIC) in a cryogenic hydrocarbon piping system (SS304L) due to poor hydrotest waste-water management.

Case Study 3: An assessment and welding repair of a thermal shock failure on radiant tubes due to rapid and uncontrolled furnace firebox temperature drop.

Significance

This paper intends to discuss critical mechanical integrity issues associated with materials and corrosion during the commissioning stage of a major petrochemical project; from the context of challenges in managing the matters despite the scarcity of resources due to the COVID-19 pandemic. The lessons learned could be beneficial in developing a business continuity plan from a project standpoint.

The paper also covers the asset integrity management strategies typically used for an in-service plant; the adopted risk-based approach coupled with a practical root-cause analysis tremendously helped the team to manage all of the impending challenges, even though the plant has not been contractually handed over to the client team.

Life Extension of Ageing Critical Process Assets

Colin Bateman, IGS Europe sro, Newark, UK

Process critical equipment, including process vessels, towers and columns play a major part in maintaining the success, profitability, and levels of production for the downstream refining industry. Over time, corrosion ultimately leads to metal wastage and shell thickness loss in ageing assets. Plant and process shutdowns caused by issues with these critical assets can quickly run up losses of millions of dollars. If the vessel wall thickness wastage has exceeded its minimum corrosion allowance, options available for the operators become significantly narrowed down to major mechanical repairs or replacement of the equipment. Taking timely action to address the corrosion is key.

Addressing Corrosion

When faced with metal wastage, asset owners and operators have viable options available to them in addressing the corrosion mechanisms with the internal application of a robust corrosion resistant alloy (CRA) barrier which is inert to the operating environment and will protect the asset for the long term.

With years of laboratory testing, field applications, post project inspections and a thoroughly vetted and proven quality control system in place; IGS high velocity thermal spray (HVTS) alloy cladding is a proven alternative to welding CRA barrier solutions to mitigate corrosion in mission critical assets and pressure vessel equipment.

Critical Process Asset Life Extension

The paper will present an overview of the IGS HVTS technology and its development but focus on an in-depth case study at a UK refinery where IGS HVTS was used to extend the life of a key processing asset (amine column) which was suffering from serious integrity challenges from accelerated internal corrosion and metal wastage, picked up through external wall thickness checks prior to the turnaround.

After initial inspection and application in 2019 of IGS HVTS to the highest risk areas where the vessel wall thickness was critical, with continuous monitoring of integrity the client was able to run the vessel through to their 2023 scheduled outage before

the planned application of the HVTS cladding to protect the entire internal surface area of the column for long term life extension.

Depolarisation phenomena in soils: residual protection after interruption of cathodic polarisation

Clemence Rogier, RICE GRTgaz, France; Ahmed Fakhry, RICE GRTgaz, France; David Sellam, GRTgaz, France; Laurent Henry, GRDF, France; François Castillon, Teréga, France; Yves Zannier, Storengy, France

Cathodic protection conveys an active protection against corrosion to pipeline steel surface in case of coating defect. Operators can be confronted to cathodic protection interruptions leaving the steel surface exposed to corrosion and without active protection during a certain amount of time. This work studies depolarisation phenomena that occurs after cathodic protection interruption. The term “depolarisation” refers to the pipes returning to its free potential value after cessation of cathodic protection. Here we present a laboratory study in soils which shows that shortly after cathodic protection interruption the free potential value of the metallic steel coupon doesn’t return to initial free potential value. A higher free potential value than before cathodic protection is measured for a long period of time, up to 60 days depending on test condition. This effect can be attributed to the formation of a passive layer at the metallic surface due to pH increase during cathodic protection application. This passive layer confers a residual protection against corrosion of the metallic surface after cessation of cathodic protection. After a certain amount of time a sudden drop of free potential value is observed. This phenomenon can be attributed to the damage of the passivation layer explaining the end of the remanence of protection and localized corrosion initiation.

This study focuses on understanding this depolarisation behaviour depending on various parameters: level of cathodic protection, time duration of uninterrupted cathodic protection, composition of the soil media and successive cathodic protection interruptions. The objective is to give insight to pipeline operators as to the safety of cathodic protection interruptions on the network depending on environmental conditions.

Keywords: cathodic protection, depolarisation, pipelines, corrosion

Classification GRTgaz : Public [ ] Interne [X] Restreint [ ] Secret [ ]

Test protocol to qualify potential probes for cathodic protection monitoring

M. Ormellese, S. Beretta, A. Brenna
Dipartimento di Chimica, Materiali e Ingegneria Chimica “Giulio Natta”
Politecnico di Milano, Milano, Italia

In recent years, the use of potential probes for monitoring the efficiency of a cathodic protection plant has spread. At least in Italy, in the last five years, the new international standards, as ISO 15589-1 and ISO 22426, forced the companies to install such probes in order to guarantee an efficient cathodic protection level. A potential probe is a device consisting of an internal reference electrode, usually copper/copper sulphate (CSE) immersed in a liquid, solid or gel electrolyte, and one or more metal coupons, simulating a defect in the pipe coating with a surface area between 1 to 10 cm^2. Once installed and connected to the structures, the probe allows monitoring the effectiveness of the protection by measuring the IR-free potential, i.e., the protection potential purified by the ohmic drop contribution in soil. In 2019, the Italian standard UNI 11094 introduced a more detailed definition of potential probe, in which a maximum distance of 5 cm between the reference electrode and the coupon is considered acceptable..

A huge variety of probes are available on the market, which differ in size, number of metal coupons, type of electrolyte, size of the porous septum.

To evaluate the quality of these devices, a test protocol is here proposed, based on two important checks: 1) determination of the accuracy and stability of the internal reference electrode potential with a statistical approach; 2) evaluation of the probe's ability to minimize the ohmic drop in the potential measurement, at different polarization levels. The experimental campaign, performed on a large number of commercial probes, revealed different stability and accuracy of the probes in minimizing the ohmic drop contribution. As expected, the most accurate probes are characterized by a minimum distance between the reference electrode and the coupon. However, even in the presence of an excellent potential stability, some probes have not been able to adequately filter the ohmic drop contribution.

Some typical design and construction mistakes are discussed.

Development of a new method for assessing the importance of coating defect found by DCVG on buried pipelines

Christophe BARTHE[ab], TRAPIL, FRANCE, Elie SASSINE[c], CORROHM, FRANCE, David GARCIA[c], CORROHM, FRANCE

[a]TRAPIL, Immeuble PALATIN 2, 3-5 Cours du Triangle 92 800 Puteaux,
[b]SURVEY, 30 chemin d'Enrobert, 32200 Gimont, France, e-mail : c.barthe@survey-groupe.fr
[c]CORROHM, 815 la Pyrénéenne - 31670 Labège, France, e-mail : elie.sassine@corrohm.com

Abstract :

The Direct Current Voltage Gradient (DCVG) method is a technique for detecting areas where the external passive protection of buried pipelines is absent. Therefore, corrosion phenomenon could occur if the level of cathodic protection is not sufficient.

DCVG technique is an efficient method for locating coating defects and even pinholes. However, the operating modes currently used for estimating the area tend to minimize the real surfaces of the defects. The gap between the estimated and the real surface could be very large and may lead to an underestimation of the importance of the defect.

The surface assessment of coating defects is based on a direct comparison between the actual defect gradient measured at the pipe surface and the gradient measured at the nearest potential test point on a calibrated metal control surface buried.

Typically, operators measure the gradient of the test piece by placing a first DCVG electrode in the immediate vicinity of the controlling piece. By doing that, the voltage gradient is overestimated and is different than the voltage gradient of the defect.

This study, has been conducted on-site with several coupons, buried at different depth. The coupons were connected to a cathodic protection system. The voltage gradient for each buried coupon was compared to the voltage gradient on calibrated coupon buried on the ground surface

In conjunction, a numerical simulation under COMSOL Multiphysics® has been conducted. The results have shown that the voltage gradient must be measured by moving the first electrode away from the surface of the coupon by a characteristic distance. In this condition, the voltage gradient of the calibrated coupon perfectly matches with the voltage gradient of the coating defect and therefore the estimated area is very representative to the surface of the defect.

Key-words **:** cathodic protection, DCVG, coating defects sizing, numerical simulation

Introduction

The buried pipeline's integrity is ensured both by an efficient cathodic protection and a good coating. Even on a new modern coated polyethylene pipeline, coating damage may occur by external work (mechanical diver, …).
The DCVG (Direct Current Voltage Gradient) method is widely used in the pipeline industry to assess the quality of the coating and repair (or not) the surface where the coating is damaged or absent
DCVG is a very efficient method for locating coating defects but is less precise in estimating the defect size. Many factors can greatly affect the calculation : soil resistivity, pipeline burial depth, shape of the defect, girth position, or also maybe the method used to measure the gradient
There are 2 methods to assess the significance of the defect :

- By calculating the % IR drop (which is the ratio between the voltage gradient created by the defect and the voltage gradient due to the CP system)
- By calculating the size of the defect according to a temporary probe with a known area

Context of this study

DCVG Surveys implemented on onshore pipelines have highlighted that in the great majority of cases errors were made very often in the characterization and sizing of coating defects.
This study was conducted to try to understand where errors come from and to improve the method of coating defects sizing.
2 cases from DCVG Survey undertaken on field are listed in this study.
The first situation come from a DCVG Survey implemented on a 400 km steel pipeline with 3 layers polyethylene coating. The DCVG was carried out 6 months after installation and filling. The survey has highlighted 200 areas where the coating was absent or damaged ranging from pinhole to few hundred of square milimiters. The total area of defects calculated with the method describe before was about 630 square centimeter (about a A4 sheet size).
One of the defects with the most important voltage gradient was chosen to be investigated. An excavation was undertaken to confirm the surface of the bare steel and a non coated girth weld was found with an area about 4000 square centimeters (see figure 1).

Figure 1 : photography of the girth weld found as the coating defect

A second case was met on a pipeline with an asphalt coating.
The defect has been estimated to 50 square centimeters and in reality the area was about 900 square centimeters so with a factor to 20 with the estimated surface. In this case also the significance of defect was underestimated.

Both examples confirm that the current method used to estimate the size of defects is not suitable and must be improve.

Experimental protocol

An experimental protocol has been implemented to simulate in the laboratory a DCVG Survey. Coating defects was simulated with steel plate. The piece of steel has been sticked on a piece of wood. Each piece has a known area. A wire is connected on each sample to be connected to a DC power supply.
The wooden ruler was buried in a hole and the depth of each piece of steel can be known and noted "h".
In the first step of this experimentation, each sample are connected to the CP system and for each piece, voltage gradient measurement were conducted near the soil surface is the same way as doing to detect coating defect on a pipeline (referred as ΔVi). With this experiment it's also possible to test the influence of depth, CP current and surface of defect. The test was carried on 3 samples of 5, 25 and 37 cm² area. Measurements were realized for h=45 and 85 cm (see figure 2).

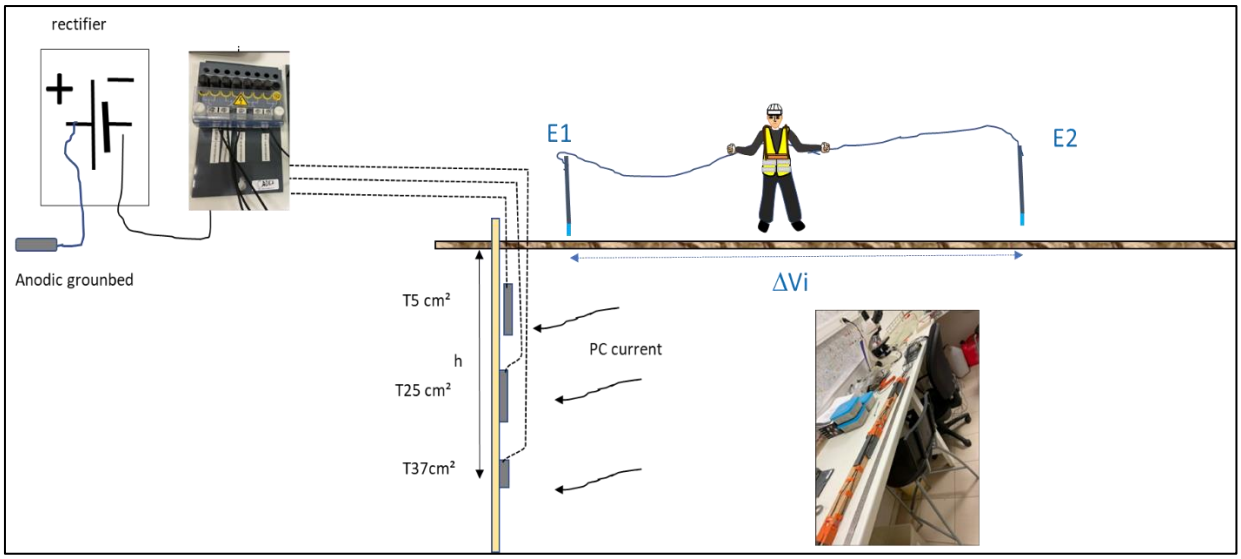

Figure 2 : experimental protocol part 1

In the step 2, the gradient voltage is measured through a calibrated coupon installed near the soil surface with a known area (see figure 3). In the same way, the coupons (one for each surface) are under cathodic protection by connection to the rectifier. The voltage gradient, referred as ΔVtm, is measured by DCVG method. In the test, the surface of the coupon is equal to the surface of the sample used as a defect.

The purpose of the test is for each "defects" to measure the distance "d" for which the gradient on the defect is equal to the voltage gradient measured on the calibrated coupon of the same surface by moving the first electrode. The electrode E2 being located at the remote earth.

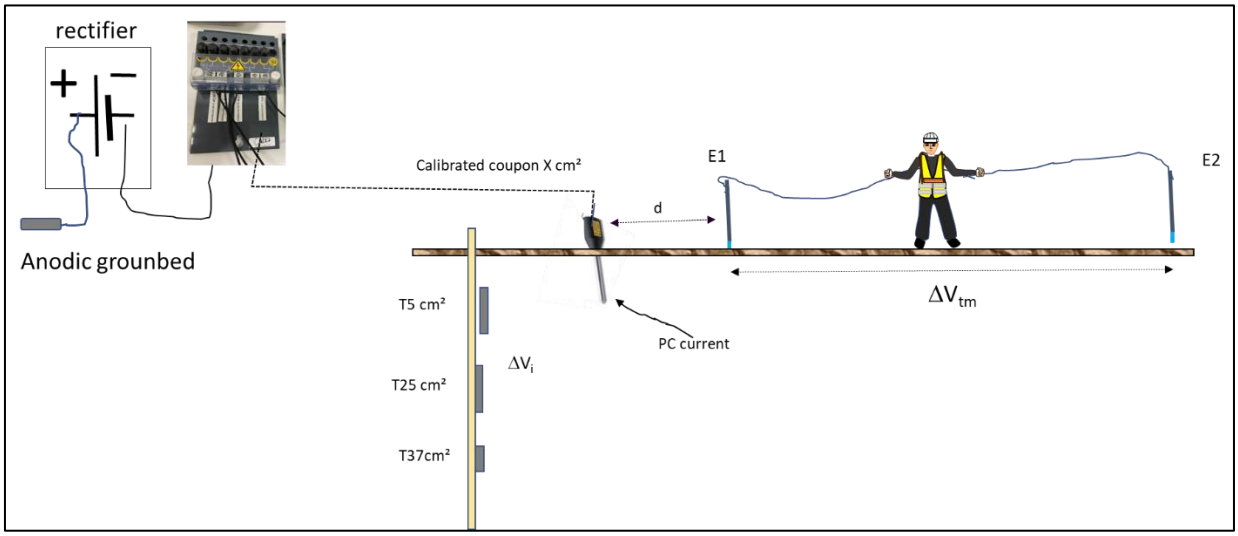

Figure 3 : experimental protocol- part 2

In parallel to the experiment, numerical simulation was carried out (see figure 4) by CORROHM using Comsol© software.
Two models were used to calculate the voltage gradient $V_C - V_{Ai\ (i=1,2)}$ due to a defect buried at a certain depth and the voltage gradient on a calibrated coupon both connected to the CP system. V_C corresponding to the potential at the remote earth, V_{A1} the ground potential close to the defect on the pipeline and V_{A2} the ground potential of the calibrated coupon. In other words, measured ΔVi and ΔVtm corresponds (in principle) to calculated $(V_C - V_{A1})$ and $(V_C - V_{A2})$, respectively.
The purpose of the simulation is to calculate the distance "d" such that the voltage gradient measured on the calibrated coupon is equal to the voltage gradient due to the defect.
The distance d can be extrapolated from the point of intersection of the 2 curves: the blue curve corresponding to the default voltage and the green curve corresponding to the evolution of the gradient on a calibrated sample.
The point of intersection is the point where the voltage on the defect is equal to the gradient on the coupon and the offset distance "d" is read on the x-axis.

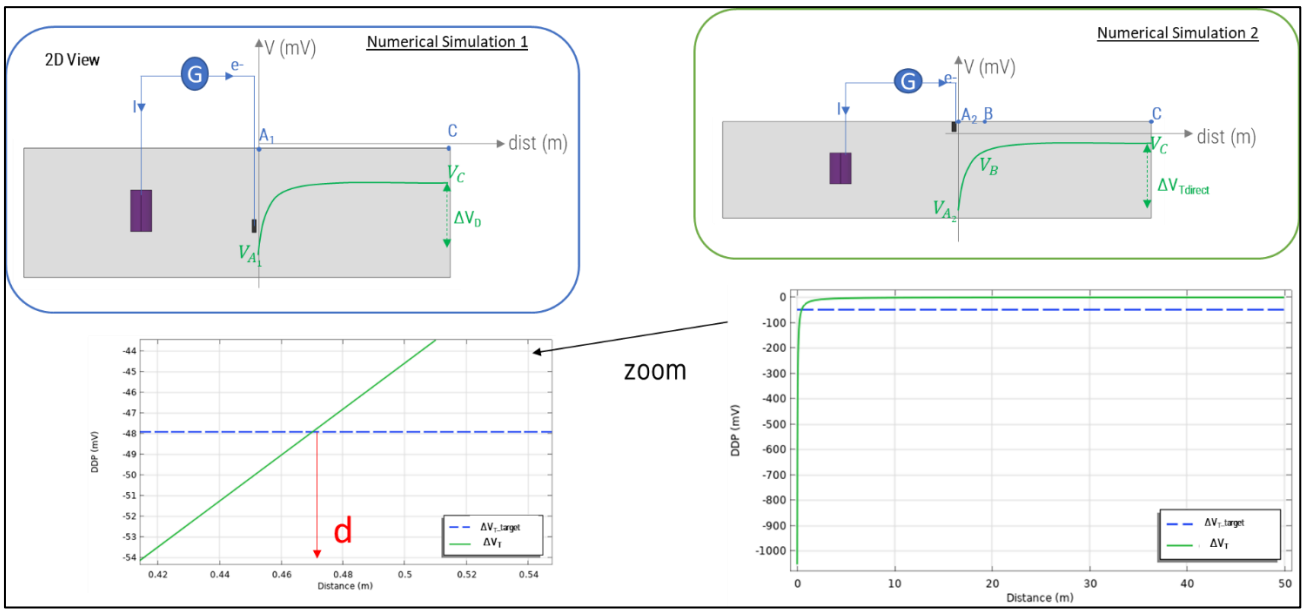

Figure 4 : Numerical simulation

Results

A comparison between experimental measurements (Exp) and numerical calculations (Simulations) is presented in figure 5. This comparison shows that:

- except the differences in resistivity between the numerical model and the reality of the field, there is a good match between the measures made (column "Exp") and the results of the numerical simulation ("simulation"). It means that the numerical simulation is valid and in good accordance with the reality
- By removing the 1st electrode from the coupon by a distance equal to the depth of the pipeline, the surface of the real coating defect will be equal to the surface of the calibrated coupon that gives the same gradient.

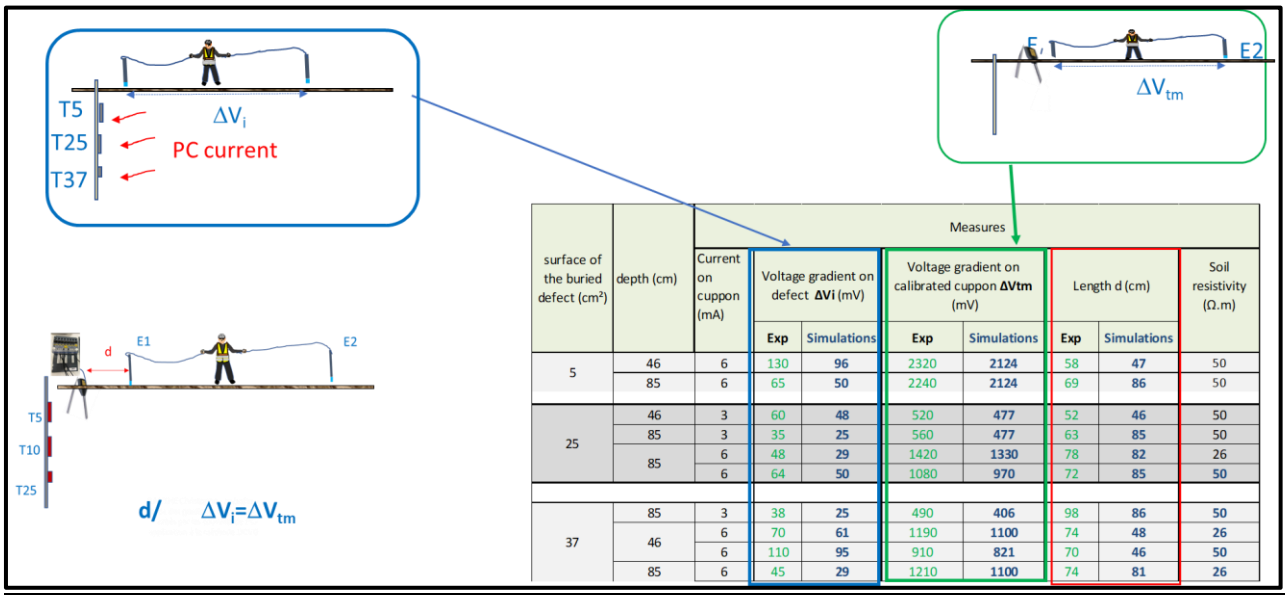

surface of the buried defect (cm²)	depth (cm)	Measures: Current on cuppon (mA)	Voltage gradient on defect ΔVi (mV) Exp	Voltage gradient on defect ΔVi (mV) Simulations	Voltage gradient on calibrated cuppon ΔVtm (mV) Exp	Voltage gradient on calibrated cuppon ΔVtm (mV) Simulations	Length d (cm) Exp	Length d (cm) Simulations	Soil resistivity (Ω.m)
5	46	6	130	96	2320	2124	58	47	50
	85	6	65	50	2240	2124	69	86	50
25	46	3	60	48	520	477	52	46	50
	85	3	35	25	560	477	63	85	50
	85	6	48	29	1420	1330	78	82	26
		6	64	50	1080	970	72	85	50
37	85	3	38	25	490	406	98	86	50
	46	6	70	61	1190	1100	74	48	26
		6	110	95	910	821	70	46	50
	85	6	45	29	1210	1100	74	81	26

Figure 5 : summary of the results

Conclusions

DCVG is both a good and precise method for locating the coating defects on buried pipelines. But the feedback shows that the real surface of defects can be underestimated by the measures currently made on field and the error could be great.

Thus, such an error on the defect area may lead to an incorrect interpretation on the defect for companies who based their maintenance plan on a Risk Assessment method.

The errors come from resistivity, pipeline depth but mainly because of the method of measuring the voltage gradient on a calibrated coupon.

This study based on experimental measurements and numerical simulations made it possible to improve the method of measuring the voltage gradient on the surface coupon during coating defect estimation operations. The voltage gradient measurement of the surface calibrated coupon must be taken by shifting the first measuring electrode to a distance corresponding to the depth of the pipe.

The calibrated coupon must be buried progressively until his gradient is equal to the gradient of the default found on the buried pipeline. And then the surface of the coupon should be equal to the surface of the coating defect on the pipeline.

Numerical simulation and optimal design of cathodic protection systems using accelerated BEM

Dimitrios T. Kalovelonis, Department of Mechanical Engineering and Aeronautics, University of Patras, GR-26504, Patras, Greece.

Demosthenes Polyzos, Department of Mechanical Engineering and Aeronautics, University of Patras, GR-26504, Patras, Greece.

Corresponding author: d.kalovelonis@upnet.gr

Abstract

Cathodic protection (CP) is a widely used practice to mitigate the corrosion of metals. The boundary element method (BEM) is ideal for solving CP problems. The present work is twofold.

First, accelerated BEM formulations are presented to efficiently solve large-scale CP and stray current-induced corrosion problems of ships, offshore structures, periodic concrete reinforcement structures, and underground tank bottoms. With the aid of the proposed formulations, a problem of millions of degrees of freedom is solved in a standard workstation. Compared to non-accelerated BEM, at least 3 times acceleration in computing time and at least 25 times less memory demand is achieved. The presented numerical results are verified by comparing them with ones obtained by commercial software packages.

Second, a methodology for the optimal design of CP systems, combining machine learning and optimization methods, is proposed. Various objective functions are presented, and their efficiency is evaluated. The optimization methods evaluated are genetic algorithms (GA), the non-dominated sorting genetic algorithm II (NSGA-II), the strength pareto evolutionary algorithm 2 (SPEA2), the particle swarm optimization (PSO), the mesh adaptive direct search (MADS) and the mesh adaptive direct multisearch (DMulti-MADS).

Influence of overprotection on AC corrosion. Analysis of a real case.

I.MAGNIFICO
Automa S.r.l. – Via Casine di Paterno, 122/A – 60131 Ancona - Italia
ivano.magnifico@byautoma.com

ABSTRACT:

The risk of AC corrosion has always been linked in particular to the parallelisms of underground pipelines with HVAC lines, especially in those geographical areas where the morphology of the territory creates obligatory so-called "technological corridors", and therefore forces the coexistence of different services over long distances.

More recently, the greater diffusion of AC-powered railway networks has further increased the AC interfering sources, while the use of more performing coatings on underground pipelines has on the one hand increased their insulation from the surrounding soil, and on the other has increased the risk of overprotection compared to old, less performing, or more degraded coatings.

This paper, starting from a real case found in a gas distribution network in a European capital, will present the normative criteria to be used to keep the AC corrosion risk under control, and will highlight how precisely the simultaneous presence of cathodic overprotection may result in an autocatalytic cycle leading to accelerated AC corrosion, in which monitoring becomes essential in order to be able to carry out on time the appropriate corrective actions.

In-situ photometric reflectance measurements of carbon steel surfaces upon cathodic protection

Federico Martinelli-Orlando and Ueli Angst,

Institute for Building Materials, ETH Zurich, Zurich, Switzerland

Cathodic protection (CP) is an electrochemical technique used to reduce corrosion rate of carbon steel to negligible values. CP has been used since almost 100 years to protect underground structures, e.g., soil buried pipelines. Despite the worldwide use of the technique, the working mechanism of CP is still under debate. On the one side, researchers suggest that the modification of the electrolyte in the vicinity of the steel surface (i.e., increase in pH and oxygen consumption) might promote the formation of a passive film that contributes to the protection mechanism by reducing the corrosion rate of steel to negligible values. On the other side, other researchers suggest that the protection mechanism achieved by the CP system can be explained based on corrosion kinetic considerations, with the iron dissolution reaction being reduced to negligible values.

On both sides, experts based their reasoning on theoretical approaches or indirect measurements. Up to now, investigation regarding the modifications of the steel surface upon the application of cathodic protection is still missing. To fill this gap of knowledge, the aim of the work is to analyze the changes of the carbon steel surface with in-situ photometric reflectance measurements upon the application of CP.

Carbon steel samples were immersed in a soil simulated solution and CP was applied for 30 minutes at different potentiostatic conditions. During the experiments, the increase in the absorbance in the UV region of the light upon the application of CP suggested the formation and growth of an oxide film at the carbon steel surface in presence of a cathodic current. The results obtained in this study are of main importance concerning the advancing in understanding cathodic protection mechanisms.

CP upgrade with new cost-effective approach

Metallic Buried tanks are major assets for all oil and gas facilities. Tanks are used for storage and contain the gas and refined products as part of daily operation requirements. In addition, the metallic buried tanks are critical structures that need to be well inspected and maintained for reliability assurance. Saudi Armco has a quite large number of buried tanks and part of which are now due for Cathodic Protection upgradation. The original Cathodic Protection design was considering anodes installation at the bottom level of tanks. This design philosophy is very efficient during the construction of the tanks where the surrounding area around the tank is open. However, it's very expensive to replace these anodes due to excessive excavation to find the old anodes. On the other hand, the excavation around buried tank under operation is associated with high risk due to coating damage and tank settlement issue.

Therefore, a new approach is developed to install vertical anodes around the tanks to cover the external surfaces and provide full protection. The approached optimization helps to reduce the implementation cost and execution period.

After Commissioning, buried tanks are receiving required protection level in compliance with company internal protection criteria. Finally, same system will be applied for all other buried tanks.

Saudi Aramco: Company General Use

Study on new TiO_2 - Al photocatalytic composite anode for marine environment

Li Liu[a], Xiayu Lu[b], Xuan Xie[a], Fuhui Wang[a]*

a Shenyang National Laboratory for Materials Science, Northeastern University, Shenyang 110819, China.

b Shi-changxu Innovation Center for Advanced Materials, Institute of Metal Research, Chinese Academy of Sciences, Wenhua Road 72, Shenyang 110016, China.

As a cheap and industrialized cathodic protection technology, sacrificial anode protection can provide effective protection for most metals used in the marine environment. Photocathodic protection technology has attracted extensive attention as an environmentally friendly cathodic protection technology. However, due to the poor stability of the photocatalytic materials and the formation of a large number of corrosion products at the interface, the stability of the new composite photoanode material needs to be improved.

In this work, an improved new photocatalytic composite anode was designed: $Co(OH)_2$/GR/TiO_2 photocatalytic material was combined with Al-Zn-In-Mg-Ti sacrificial anode to obtained the photocatalytic composite anode material (Al-TGC photocatalytic composite anode), which effectively realized the long-term cathodic protection of Q235 carbon steel (Q235CS) in 3.5% NaCl solution. Based on the characterization of morphology, composition and electrochemical protection performance of improved new Al-TGC photocatalytic composite anode during long-term immersion, a dual cathodic protection mechanism of improved new Al-TGC photocatalytic composite anode for Q235CS in the simulated marine environment was proposed. The improving of magnetron anode deposition layer structure (double-layer structure) can effectively reduce the formation of oxidation products in the improved new Al-TGC photocatalytic composite anode after long-term

immersion; The addition of graphene can significantly improve the photoelectric conversion efficiency of photocatalytic materials. The synergistic effect of the two promoted the long-term and stability of the new photocatalytic composite anode for Q235CS cathodic protection.

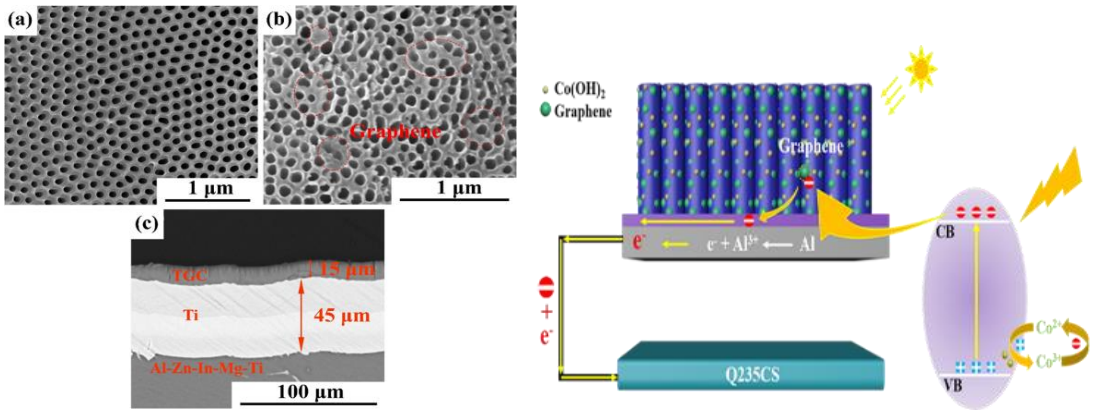

Fig. 1. SEM morphology images: (a) top-view image of $Co(OH)_2/TiO_2$-Al photocatalytic composite anode, (b) top-view and (c) cross-section images of Al-TGC photocatalytic composite anode. Proposed mechanism on the dual cathodic protection of the Al-TGC photocatalytic composite anode for Q235CS.

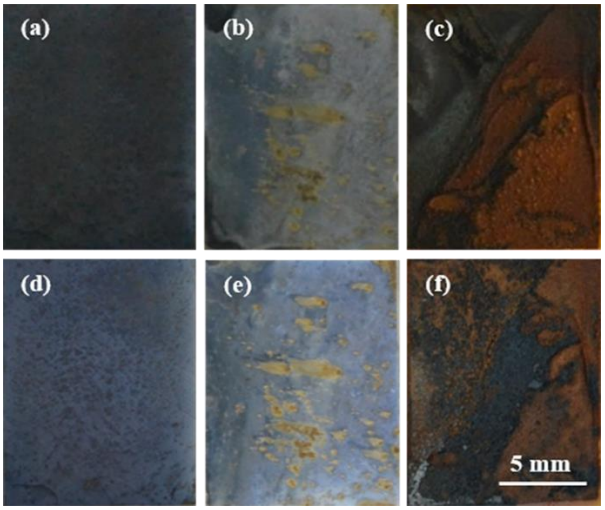

Fig. 2. Macro corrosion surface morphologies: (a) Q235CS protected by the Al-TGC photocatalytic composite anode (18 d), (b) Q235CS protected by the Al anode (18 d), (c) unprotected Q235CS (18 d), (d) Q235CS protected by the Al-TGC photocatalytic composite anode (30 d), (e) Q235CS protected by the Al anode (30 d), (f) unprotected Q235CS (30 d).

Surface pretreatment of Al – die cast to increase corrosion resistance of adhesive joints

B. Leitner, Robert Bosch Fahrzeugelektrik Eisenach GmbH, Eisenach/Germany
L. Reyes Tello, Robert Bosch GmbH, Hildesheim/Germany

Introduction

As a result of the transformation away from the combustion engine to electrification, aluminum die-cast components are increasingly being used. Housings for the electric motor, the electric axle drive or a battery are made of it. An adhesive is often used to join two aluminum components. Adhesives offer the advantage to fulfill several requirements on the joint, such as mechanical fixation, sealing and/or corrosion resistance. The correct selection of the adhesive system in terms of media resistance, cohesion but also sufficient adhesion of the adhesive to the surface of the part to be joined is crucial. For sufficient wetting/adhesion of the adhesive to the surface, a surface pretreatment is usually necessary.

Experimental

To produce a bonded composite, a 2-component epoxy resin adhesive was used and as a pretreatment method a laser from Trumpf respectively the PlasmaPlus technology from Plasmatreat were used. For application-related investigations, battery housings made of aluminum die-cast with a tongue-and-groove geometry were taken from production and treated according to the pretreatment methods and then built up. These were tested initially and after aging. The aging of the battery packs was carried out according to internal specifications. For the analysis of the mechanical strength and fracture pattern as well as the corrosion resistance, tensile specimens were cut from the assembled battery packs.

Results and Discussion

The tensile specimens destructively tested were evaluated regarding strength, fracture pattern and corrosion behavior.

The strength for both types of specimens showed significant differences. The laser-pretreated specimens exhibited high tensile strength as well as a cohesive fracture pattern both before and after aging. Similarly, no corrosive infiltration was observed in the bond after aging. This is because the pretreatment significantly increased the surface area and changed the surface chemistry. Both lead to the epoxy resin adhesive being able to wet the surface better and interact chemically with it (hydrogen bonding).

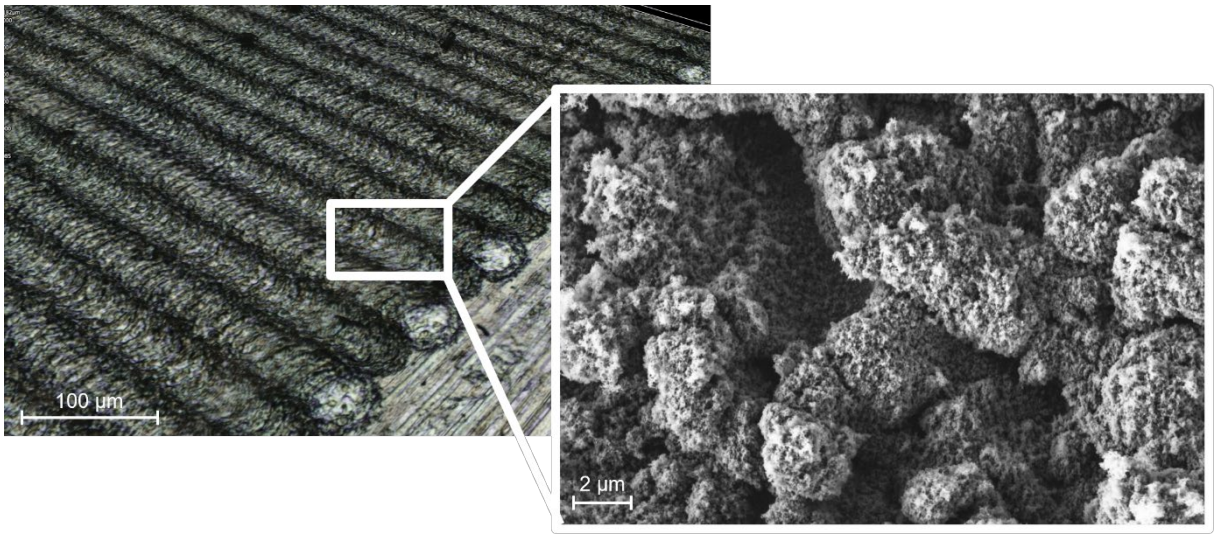

Fig. 1: Laser scanning microscopy (left) and raster electron spectroscopy (right) image of a laser-structured aluminum die-cast surface

In contrast, the specimens coated using PlasmaPlus technology showed low strength and adhesive fracture behavior. Corrosive infiltration of the adhesive-coating respectively coating-metal interface was also not observed. A possible reason for this behavior could be the thickness of the applied corrosion protection layer. This influences the hydrophilic/hydrophobic behavior of the corrosion protection layer. Accordingly, further investigations are necessary to increase the adhesion of the adhesive to the coating while maintaining good corrosion properties.

Influence of Dry-Film Lubricants on Bond Strength and Corrosion Behaviour of 6xxx Aluminium Alloy Adhesive Joints for Automotive Industry

R. Gruber[1,2], T. Bruckner[1], T. D. Singewald[1], L. Hader-Kregl[1], M. Hafner[2], T. Greunz[2], M. Müller[3], C. Kern[4], M. Rosner[4] and D. Stifter[5]

[1] CEST Competence Center for Electrochemical Surface Technology GmbH, Viktor-Kaplan Str. 2, 2700 Wiener Neustadt, and Stahlstr. 2-4, 4020 Linz, Austria

[2] AMAG rolling GmbH, Lamprechtshausener Straße 61, 5282 Braunau-Ranshofen, Austria

[3] Henkel AG & Co. KGaA, Henkelstraße 67, 40589 Düsseldorf, Germany

[4] voestalpine Stahl GmbH, voestalpine-Str. 3, 4020 Linz, Austria

[5] ZONA Center for Surface and Nanoanalytics, Johannes Kepler University Linz, Altenbergerstraße 69, 4040 Linz, Austria

Abstract:

The application of dry lubricant on aluminium for automotive industry is indispensable for a high-quality forming behaviour. To provide a short production time those forming aids will not be removed during the joining step. The aim of this study was the characterization of the influence of dry lubricants on the bond strength and the corrosion resistance of an 6xxx aluminium alloy for automotive applications. For this purpose, samples with a well-defined surface were lubricated with 1 g/m² dry lubricant and joined with a commercial thermosetting 1K-epoxy structural adhesive. The bond strength was characterized by means of lap shear test. To evaluate the corrosion resistance of the adhered aluminium samples an immersion test in 5 w% NaCl-solution was used. Based on fracture pattern analysis, the corrosion behaviour could be described. Dissolved corrosion products were examined using ICP-MS and NMR. By means of SEM/EDX the elementary composition of precipitated solids was determined. The results showed a dry lubricant independent bond strength for standard testing conditions. However, a significant effect of the forming aid, regarding the corrosion resistance of adhered aluminium samples against corrosive infiltration of the metal-adhesive-interface, was observed.

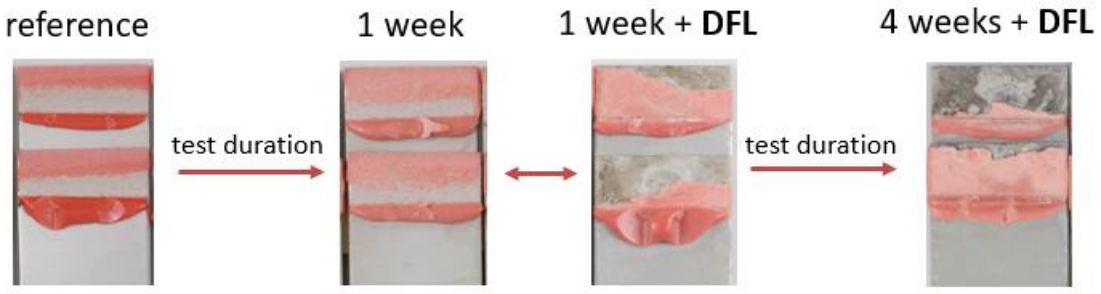

Effect of friction material degradation on stiction in automotive braking systems

F. Andreatta[1], M. Motta[1], A. Rondinella[1], V. Iodice[2], A. Sin[2], L. Fedrizzi[1]

[1] University of Udine, Polytechnic Department of Engineering and Architecture, Via del Cotonificio 108, Udine, Italy
[2] ITT Italia S.r.l., Via San Martino 87, 12032 San Martino (CN), Italy

ABSTRACT

Corrosion attack of grey cast iron in rotors of automotive braking systems might cause stiction phenomena leading to adhesion of the pad material on the rotor. This might result in damage of the pad, reduced braking performance and even impossibility to drive the vehicle in most severe cases. The degradation of the friction material during service might further affect its stiction behavior.
This work investigates the effect of thermal degradation of different friction materials employed for the production of brake pads on their stiction behavior. The friction material samples were heat treated at 250°C and 300°C to induce thermal degradation, in order to simulate thermal effects due to braking. A dedicated testing method was developed for the investigation of the stiction between a brake pad sample and a disc sample (gray cast iron) by electrochemical methods. A dedicated cell was employed to promote stiction by polarization experiments between a brake pad sample and a disc sample (gray cast iron). The adhesion force between disc and pad was measured by means of a test bench providing information about stiction susceptibility of the friction material.
Thermal degradation of the friction material strongly increases the susceptibility to stiction. Moreover, prolonged thermal treatments (up to 5 h) can significantly reduce the mechanical properties of the friction material impairing their performance.

Metallic Wire Resistance Method combined with Scanning Electron Microscopy and Energy-dispersive X-ray Spectroscopy, a multi-technique approach for Corrosivity Assessment of Automotive Lubricants and Fluids.

Dr. Fabio Cova Caiazzo, Petronas Lubricants International, Santena (Turin) Italy
Ilaria Travi, Petronas Lubricants International, Santena (Turin) Italy
Andrea Elia, Petronas Lubricants International, Santena (Turin) Italy
Vanessa Bordignon, Petronas Lubricants International, Santena (Turin) Italy
Emanuele Verda, Petronas Lubricants International, Santena (Turin) Italy
Dr. Alejandra De Los Rios Gonzalez, Petronas Lubricants International, Santena (Turin) Italy

Active Sulfur compounds remaining in the petroleum products after refining process or added to formulated lubricants for enhancing extreme pressure performances (e.g. driveline fluids) affects detrimentally the corrosion resistance of copper and yellow alloys in contact with these fluids. For traditional systems, yellow metal corrosion issue affects bushing supports, sintered bronze friction material, synchro rings, bronze cage bearings, heat exchangers etc. The progress and evolution towards e-mobility amplified the importance to introduce lubricants with low corrosiveness. Second generation electrified driveline systems require lubricants able to deliver excellent wear protection to the gears wheels/hypoids, remove the heat generated by the electric motor and low corrosiveness towards metals, in particular copper and magnetic steels.

To develop lubricants able to meet and exceed the requirement of these new hardware, it is crucial to get over a qualitative evaluation of the corrosiveness of lubricants by introducing more accurate methods allowing to study the mechanisms of the corrosion process and the impact of each single component of a formulation.

The Global Research & Technology Center of Petronas Lubricants International (GR&T-PLI) since the 2019 is anticipating the requests of the market by introducing and developing cutting-edge methodologies to study the corrosion of lubricants.

One of the main reasons of this need is the misleading interpretation of results of the main industries standards (e.g. ASTM D130 and ASTM D665) which might happen

in presence of surface-active molecules (e.g. corrosion inhibitors). Based on traditional industry standard ASTM D130, higher is the level of tarnishing of copper surface, higher is the corrosivity of a lubricant. In contrast, the use of Scanning electrochemical microscopy (SCEM) clearly demonstrated that the increase in tarnishing of a copper surface in presence of benzotriazole is associated to decrease to the corrosion current.

Considering this situation, beside industries standards method, GR&T-PLI decided to implement and further improve the wire resistance method.

The key expects improved by GR&T-PLI refers on the data analysis and interpretation and the execution of a failure analysis of the wires after each test.

GR&T-PLI decided to use a Scanning Electron Microscope equipped with Energy-dispersive X-ray Spectroscopy to investigate the morphology of the corrosion attack and the chemical composition of the surface after the test.

By combining these two techniques it was possible for example identify additives which preferentially, by dissolving copper, generates conductive copper sulfides (main root-cause of failure of electronic components in contact with lubricants).

Considering the multiple application of these combined techniques, the aim of this memory will be to present to the approach adopted at GR&T-PLI for the study of corrosion phenomena and its direct implication on the formulation of automotive fluids.

Controlled RH Corrosion Tests: Understanding Electrolyte Solution Application Methods and Correlating Delivered Volume with Corrosivity

Sean Fowler, William Tobin, Dr. Andy Francis, David Duecker

Q-Lab Corporation, Westlake, Ohio, USA

Dr. Andreas Giehl

Q-Lab Deutschland, Saarbrucken, Germany

Kobe Qu, Sunny Sun

Q-Lab China, Shanghai, China

Types of salt spray in corrosion test chambers and confusing terms

Automotive corrosion test methods employ a variety of electrolytic solutions and application regimes. All or nearly all electrolytic solutions contain sodium chloride in concentrations ranging from 0.05% to 5% by weight or volume. Sometimes additional salts are added, and sometimes the solution is acidified, but the standards leave little ambiguity about the precise content of the prescribed electrolyte. The method of application is not as clear due to the use of the singular term “salt spray” for the different types. The presentation will discuss the types of salt spray in standards and propose terms and definitions that might reduce confusion.

Measuring the effect of salt spray volume on corrosion rates of steel panels

Additionally, some automotive standards prescribe spray volumes in a quantified range, while others avoid numerical requirements. Is one approach better than the other? This presentation will show data comparing corrosion rates of steel panels as a function of the quantity of salt spray in an attempt to answer this question.

Implementation of a methodology of Wet-Dry Cycling Conditions to Accelerate Corrosion Damage Using Snow-Depth/Climate Information

Victor Ponce[1], Shaik Merkatur Hakim Marjuban[1], Walter Tarr[2], Heather Eich[2], Allison Mahood[2] and Homero Castaneda[1]

[1]Department of Materials Science and Engineering
National Corrosion and Materials Reliability Laboratory
Texas A&M University
College Station, TX 77843, USA

[2]Toyota Motor North America
Ann Arbor MI 48105, USA

Abstract

This study presents the implementation of a wet-dry cycling protocol to accelerate corrosion damage. The protocol was determined using snow-depth data extracted from the Rust Belt states, obtained from the Global Historical Climatology Network Daily (GHCNd) database, spanning from 2015 to winter 2021. The wet condition was found to last four days (96 hours), followed by a dry condition lasting three days (73 hours), completing a whole week of a single cycle. Corrosion testing was conducted using a Cyclic Corrosion Test (CCT) chamber with a 5%wt NaCl solution at 30°C. Four distinct coating sample types with different corrosion control mechanism, intact and scratch depths were created in the samples, and electrochemical assessments were conducted in real time. The analysis of phase angle plot data over a 30-day period provided valuable insights into the corrosion behavior of different coatings and scratch depths, highlighting the significant influence of surface damage on the corrosion process. Samples with 0% scratch depth exhibited gradual corrosion onset similar to steady state, while those with partial scratching displayed delayed activation, emphasizing the protective capabilities of sacrificial coatings. Conversely, samples with complete scratch depth showed immediate activation, indicating a lack of a protective barrier against corrosion. These findings underscore the importance of accelerating protocol to simulate real operation conditions.

Keywords: Corrosion accelerating testing, Wet-dry cycle conditions, Cyclic Corrosion Test (CCT) chambers, Phase angle plots, Anti-icing programs, EIS.

Introduction

Corrosion, the progressive degradation of materials brought on by environmental factors, is a pervasive and costly issue that affects various industries, ranging from manufacturing and electronics to transportation and infrastructure.[1] For different components and structures to have prolonged durability and reliability, understanding and minimizing corrosion is essential.[2] Traditional methods based on steady state conditions often take years to observe noticeable corrosion resistance decline, making the demand for accelerated corrosion testing techniques increasingly significant.[3]

Accelerating the testing of corrosion has emerged as a crucial aspect of materials science and engineering, offering the ability to simulate and predict long-term corrosion behavior in significantly shorter time frames.[4] By subjecting materials to harsher and accelerated environmental conditions, researchers can expedite the corrosion process, enabling them to evaluate the performance of materials, coatings, and corrosion protection strategies more rapidly and efficiently.[5]

Corrosion accelerating testing (CAT) has emerged as a crucial tool in materials science and engineering to simulate and predict the long-term effects of corrosion in a compressed timeframe. One of the most effective and widely used techniques for conducting accelerated corrosion testing is through Cyclic Corrosion Test (CCT) chambers. These chambers provide controlled and accelerated corrosive environments, allowing researchers to subject materials to harsh conditions that promote fast corrosion reactions.[6, 7]

In a CCT chamber, various corrosive factors, such as temperature, humidity, and exposure to corrosive agents, can be precisely regulated and manipulated to simulate real-world environmental conditions.[8]

The primary objective of this paper is to develop a reliable accelerated corrosion testing methodology that can characterize real-world corrosive environments. In addition, this work explores the significance of real time monitoring in CCT chambers as a critical tool for evaluating material performance and building a database for modeling prediction. Finally, we present phase angle plots to discuss the corrosion mechanism based on the damage evolution that can quantify different coating/substrate samples.

Determining Wet-Dry Cycle Conditions

The formation of a strong and hazardous bond between snow or ice and the road surface during winter storms is effectively prevented through the application of chemical freezing-point depressant salts, including compounds like NaCl, $CaCl_2$, and $MgCl_2$.[9] These salts are crucial components of anti-icing programs widely implemented across North American territories, where harsh winter conditions pose significant challenges for safe road travel.

The process involves strategically spraying these chemical salts onto the pavement of highways By doing so, the salts effectively lower the freezing point of the accumulated snow and ice, preventing it from forming a stubborn, dangerous bond with the road. As a result, road maintenance

and safety teams can proactively combat treacherous ice formation, allowing for safer driving conditions during winter storms.

However, while the use of these chemical salts is undeniably advantageous for preventing ice formation, there is a trade-off to consider. The salts, when dispersed onto the roads, eventually form solutions that have the potential to accelerate the corrosion of the undercarriages of vehicles. These corrosion conditions pose challenges for car owners and fleet operators, as it can lead to increased maintenance costs and reduced vehicle longevity and reliability.[10]

We analyze diverse climatic data points in order to establish the most favorable wet-dry cycling conditions for the implementation of the anti-icing program. Representing upon a wealth of invaluable information, we focused on extracting snow-depth data from the Rust Belt states, a region renowned for its challenging winter conditions. To achieve this, we tapped into the Global Historical Climatology Network daily (GHCNd), [11-13] an integrated and authoritative database curated by the esteemed National Oceanic and Atmospheric Administration (NOAA).

The GHCNd provided us a daily climatic record from 2015 through the winter of 2021, affording us a detailed and extensive perspective on snow-depth patterns within the region. Using the data, we developed an algorithm.

Previous studies [14] consider “the amount of salt applied annually does not follow a consistent trend; rather it is dependent upon weather conditions and maintenance schedule” – The method included in this study covers one of many methods under development to simulate real de-icing conditions. Consequently, vehicles traveling on treated roads are exposed to this solution, which can have implications for corrosion on their undercarriages.

Our analysis reveals that Rust Belt wet conditions typically last between 3 to 6 days, as depicted in Figure 1. Moreover, a closer examination of the data presented in Table 1 indicates an average duration of approximately 4 days for these wet conditions and 3 days for the dry condition. These findings are important in enhancing our understanding of the temporal patterns of snow depth accumulation.

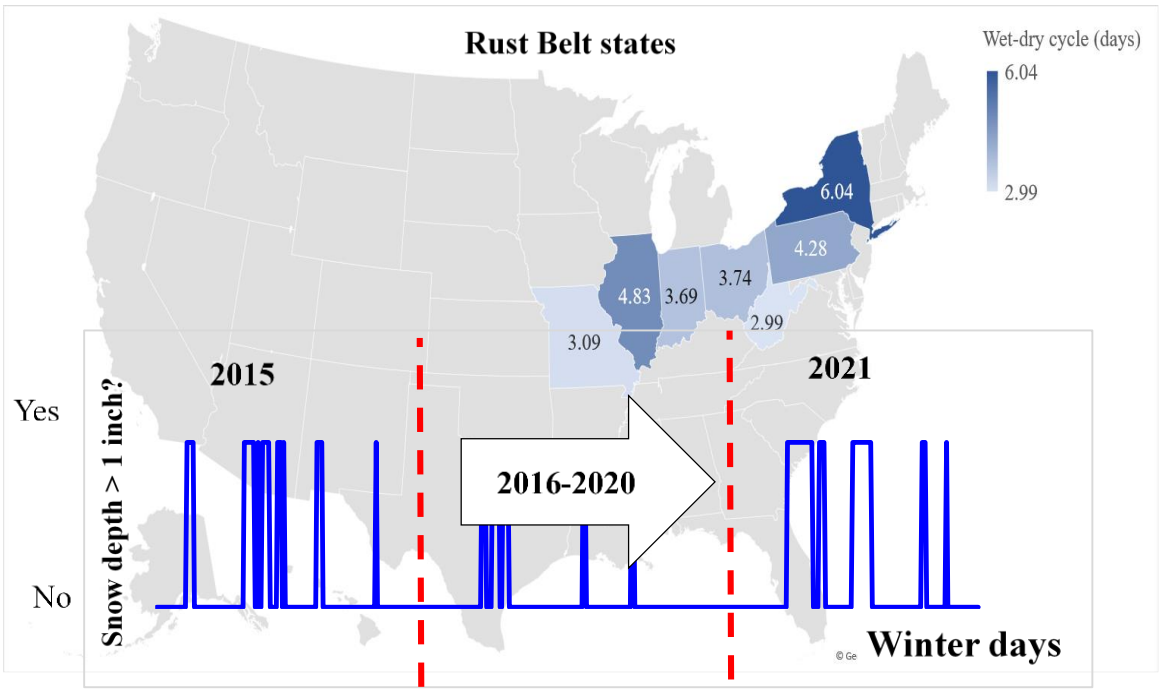

Figure 1. Schematic of the duration of wet condition at Rust Belt states from the winter 2015 to winter 2021.(from NOAA)

Table 1. Duration of wet condition along Rust Belt States [from NOAA]

States	Duration of wet condition (days)
Illinois	4.83
Indiana	3.69
Missouri	3.09
New York	6.04
Ohio	3.74
Pennsylvania	4.28
West Virginia	2.99

Test methodology

In our experimental setup, we subjected the CCT (Cyclic Corrosion Test) chamber to alternating wet and dry conditions for a comprehensive evaluation. The wet condition was maintained for 96 hours, while the dry condition was sustained for 72 hours, completing a full week of a single cycle. This cycle was repeated for a total duration of 30 days to compare different standard testing protocols.

Within the CCT chamber, we created an environment by filling it with a 5%wt NaCl solution, maintaining a temperature of 30°C.

We conducted our experimentation using four different coating corrosion control systems. The first system comprised a barrier coating (BC1) applied to a cold-rolled steel (CRS) substrate with a thickness of 10 µm. The second system involved the same barrier coating (BC2) with same CRS substrate, this latter with a 25 µm in thickness. For the third system, we employed a sacrificial coating consisting of Zn+Ni on a CRS substrate with a thickness of 14 µm. Lastly, the fourth system featured a hybrid coating combining both barrier and sacrificial properties, featuring Zn flakes disperse on a polymeric matrix applied on CRS substrate with a thickness of 30 µm. Each system underwent scratch testing at various percentages, specifically at 0%, 50%, and 100% scratch depths.

To monitor and measure the corrosion process accurately, we utilized a set up comprising a clamp fitted with a copper circle terminal acting as the electrodes. These electrodes were thoughtfully designed to establish contact with both the substrate and coating surfaces. This capacitor-like configuration allowed us to capture precise data on the coating status throughout the testing period.

To conduct our electrochemical assessments, we employed a Gamry 600+ potentiostat. We initiated an Open Circuit Potential (OCP) test for a duration of 300 seconds. Following OCP testing, we performed Electrochemical Impedance Spectroscopy (EIS) to explore the electrochemical response over a wide range of frequencies. The EIS analysis spanned from 100,000 Hz to 0.01 Hz, with an applied amplitude of 0.01V. To ensure comprehensive coverage and accurate characterization, we employed 10 frequencies for each decade.

Test Results

By utilizing the phase angle plot data presented in Figures 2, 3 4, and 5, we conducted a comprehensive analysis of the coating performance/degradation and corrosion mechanism and detected the various corrosion phases over a period of 30 days.

The results of the first sample system (barrier coating with 10 µm thickness) are represented by Figure 2. Where we noted that the sample with 0% scratch depth exhibited activation during the second cycle of wet-dry conditions. On the other hand, the sample with a 50% scratch depth showed activation during the third cycle. Interestingly, the sample with a full scratch depth of 100% immediately activated upon insertion into the chamber.

The results from the second sample system (barrier coating with 25 µm thickness) are graphically presented in Figure 3. We observed that the sample with 0% scratch depth showed activation on day 30, indicating a gradual onset of corrosion. Conversely, the sample with a 50% scratch depth exhibited activation on day 21, highlighting the reduced protection provided by the coating. The sample with a complete scratch depth of 100% immediately activated upon insertion into the chamber, indicating a lack of protective barrier against corrosion.

Figure 4 illustrates the outcomes derived from the third sample system featuring a sacrificial coating with a thickness of 14 µm. Notably, distinct activation times were observed for samples with varying scratch depths. The sample with 0% scratch depth displayed activation on day 11, signifying a gradual onset of corrosion. This observation suggests that, over time, the sacrificial coating observes interfacial reactions at the initial time. Conversely, the sample with a 50% scratch depth exhibited activation on day 30, demonstrating the protective passive capabilities of the sacrificial coating. The presence of partial scratching significantly delayed the onset of corrosion, underscoring the coating's efficacy in safeguarding against corrosion under such conditions. The sample with a complete scratch depth of 100% activated on day 7, indicating a lack of corrosion protection. This finding highlights the activation and interfacial reactions of the coating/substrate when subjected to full surface damage, leading to different corrosion initiation mechanisms.

Figure 5 presents the results obtained from the fourth sample system, featuring a mixed coating composed of both barrier and sacrificial coatings with a thickness of 30 µm. The sample with 0% scratch depth displayed activation on day 30, indicating a gradual onset of activation. This observation suggests that, even in the absence of scratches, the sacrificial component of the coating eventually will react with time before any polymeric damage. Conversely, the sample with a 50% scratch depth exhibited activation on day 28, showcasing the protective capabilities of the sacrificial coating. The presence of partial scratching significantly delayed the onset of corrosion, underscoring the coating's efficacy in protecting against corrosion under such conditions. The sample with a complete scratch depth of 100% activated on day 21, indicating a lack of protective barrier against corrosion. This finding highlights the susceptibility of both corrosion control coating concepts. The competition between the barrier and sacrificial is demonstrated in short time.

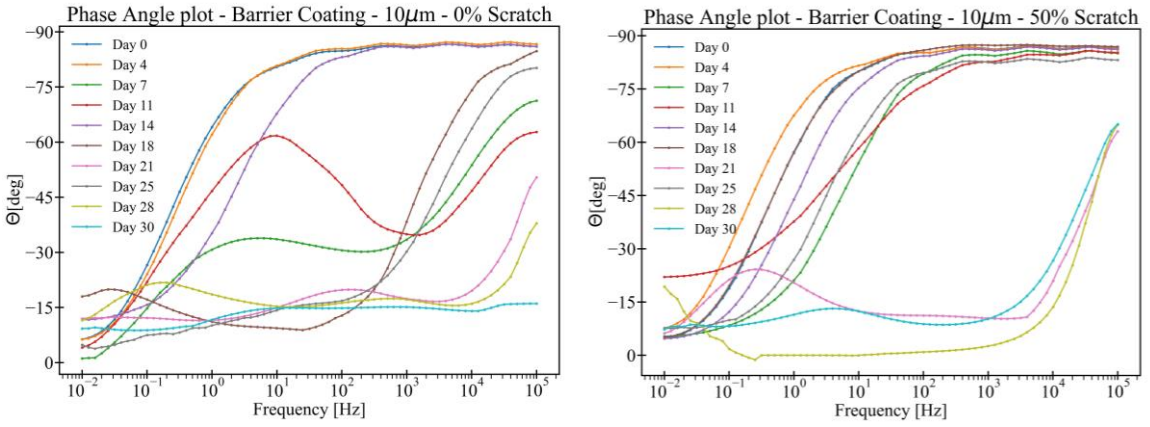

(a) (b)

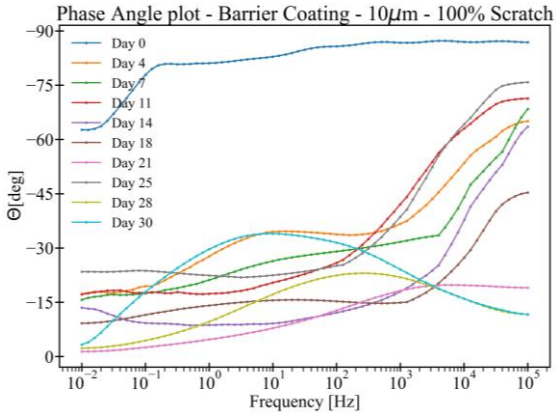

(c)

Figure 2. Barrier coating BC1 with CRS substrate of 10 µm thickness with a scratch of (a) 0%, (b) 50% and, (c) 100%.

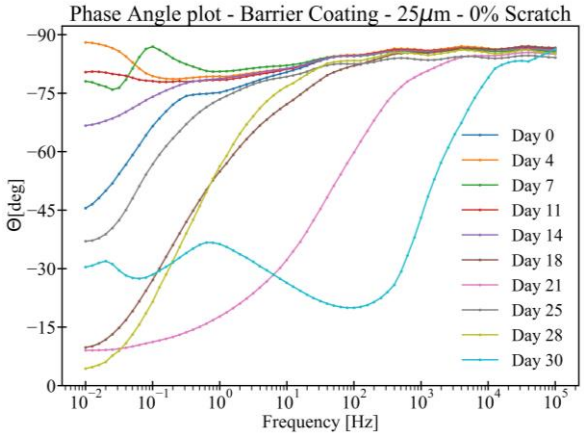

(a)

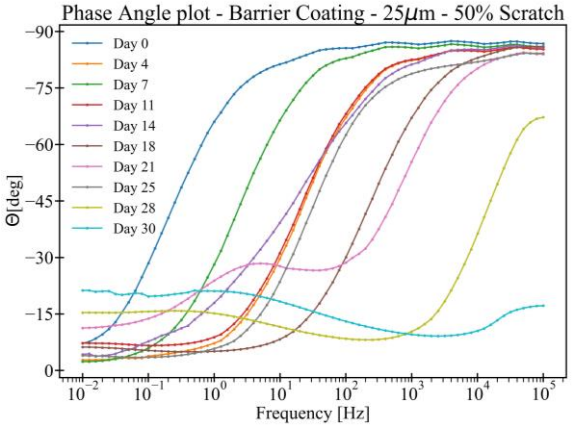

(b)

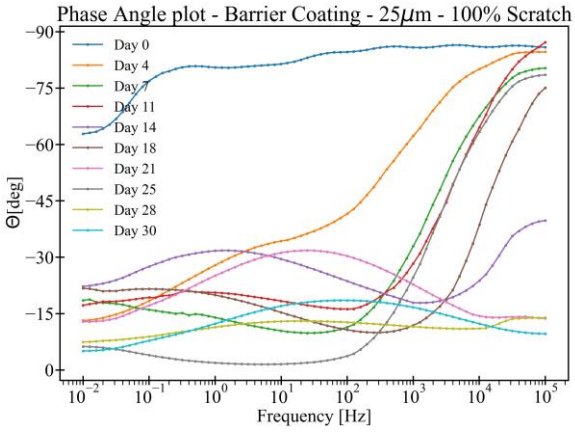

(c)

Figure 3. Barrier coating BC2 with CRS substrate of 25 µm thickness with a scratch of (a) 0%, (b) 50% and, (c) 100%.

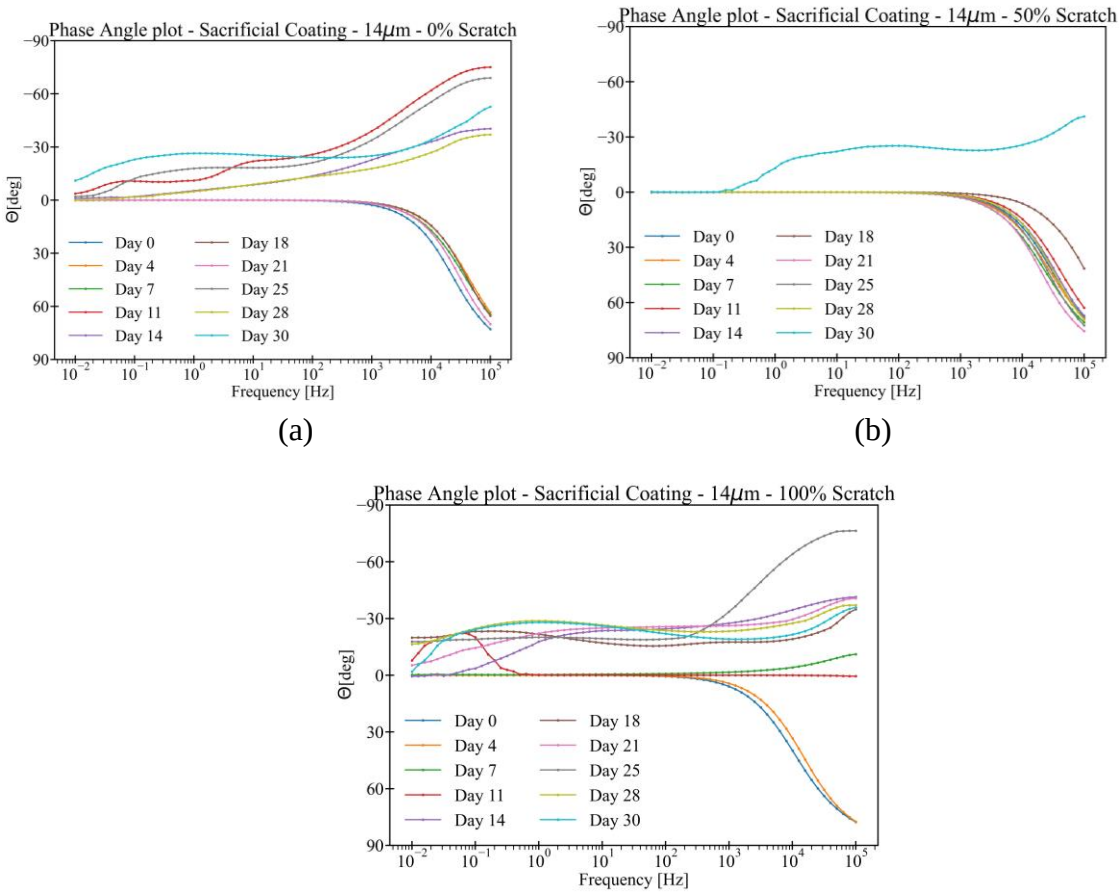

Figure 4. Sacrificial coating with Zn+Ni and CRS substrate of 14 µm thickness with a scratch of (a) 0%, (b) 50% and, (c) 100%.

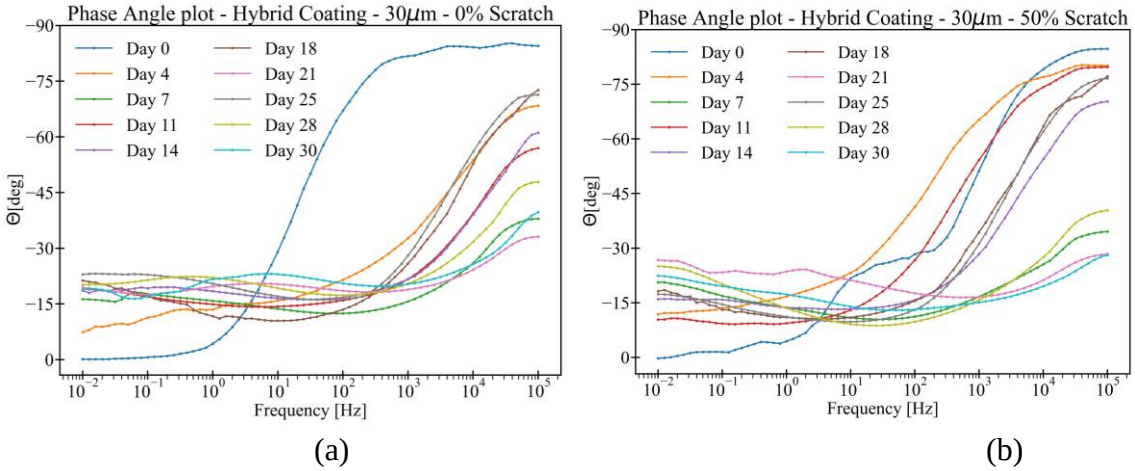

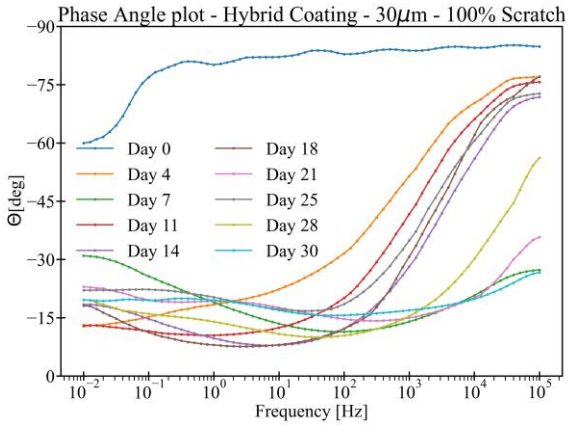

(c)

Figure 5. Barrier and sacrificial coating with Zn flake and CRS substrate with 30 µm thickness with a scratch of (a) 0%, (b) 50% and, (c) 100%.

Conclusion

In conclusion, our phase angle plot data has provided valuable insights into the coating performance and corrosion behavior of different coatings systems. The intact vs. scratch depths can characterize the corrosion control mechanism over a 30-day period. We observed distinct activation times for samples with varying scratch depths, indicating the significant influence of surface damage on the protection and corrosion process. Samples with 0% scratch depth generally exhibited gradual corrosion onset similar to those on steady state. The systems with partial scratching displayed delayed activation, characterizing the protective capabilities of sacrificial coatings. In contrast, samples with complete scratch depth showed immediate activation, signifying the competition between substrate passive/active conditions. By understanding these corrosion mechanisms, we can further optimize the testing methodology and protocol contributing to the development of more resilient and durable coatings.

References

1. B. Wei and J. Xu, Coatings, **12**, (2022) 1013.
2. A. F. A. Fuhaid and A. Niaz, Buildings, **12**, (2022) 586.
3. Q. Li, X. Xia, Z. Pei, X. Cheng, D. Zhang, K. Xiao, J. Wu and X. Li, npj Materials Degradation, **6**, (2022) 1.
4. L. A. Escobar and W. Q. Meeker, Statistical Science, **21**, (2006) 552.
5. Z. Yu, Z. Ren, J. Tao and X. Chen, Mathematical Problems in Engineering, **2014**, (2014) 839042.
6. B. Daneshian, D. Höche, O. Ø. Knudsen and A. W. B. Skilbred, npj Materials Degradation, **7**, (2023) 10.
7. P. Montoya, I. Díaz, N. Granizo, D. de la Fuente and M. Morcillo, Materials Chemistry and Physics, **142**, (2013) 220.

8. C. Perez, A. Collazo, M. Izquierdo, P. Merino and X. R. Novoa, CORROSION, **56**, (2000) 1220.
9. A. P. Mathews, Journal of Environmental Management, **293**, (2021) 112888.
10. F. C. Robles Hernández, G. Plascencia and K. Koch, Engineering Failure Analysis, **16**, (2009) 281.
11. M. J. Menne, I. Durre, R. S. Vose, B. E. Gleason and T. G. Houston, Journal of Atmospheric and Oceanic Technology, **29**, (2012) 897.
12. I. Durre, M. J. Menne, B. E. Gleason, T. G. Houston and R. S. Vose, Journal of Applied Meteorology and Climatology, **49**, (2010) 1615.
13. I. Durre, M. J. Menne and R. S. Vose, Journal of Applied Meteorology and Climatology, **47**, (2008) 1785.
14. Kittelson & Associates, inc., Salt Usage on Roadways in Canada and the United States (2017), Project No. 20510

Modifying cyclic corrosion tests to distinguish between different qualities of pretreatment

Konrad Tarka, RISE AB, Borås/Sweden
Dan Persson, RISE AB, Kista/Sweden
Charlotte Ireholm, RISE AB, Mölndal/Sweden

The environmental stability of organically coated metals is of utmost importance for materials used in automotive. Today, the most important pre-treatment technology used by the automotive industry is based on zinc phosphating (ZnPh) for which zinc phosphate crystals are deposited. It is often combined with an electrocoat and further coatings layers forming surface protection with adequate adhesion and corrosion protection properties. Due to the presence of heavy metals such as nickel in the process, as well as problems when pre-treating large amounts of aluminium due to sludge formation, negative impact on the working environment, increasing cost for waste etc more environmentally friendly alternatives must be considered.
During the last decades, commercial systems based on hydrofluoric acid salts of zirconium (Zr) and titanium (Ti) have been introduced by several chemical suppliers. The systems have a more environmentally friendly profile compared to ZnPh.

However, there were several gaps of knowledge identified which must be filled before this type of pre-treatments can be implemented on a larger scale in the automotive industry.
One example is the lack of process verification methods which provides quality assurance of the finalized coating as well as of the process baths. The relationship between the corrosion resistance of the coated materials and the coating weight of Zr, measured by XRF, is not fully understood, and further studies are needed to find such correlation or to find methods which provide a better correlation with the corrosion resistance
Another topic within verification methods is the accelerated corrosion methods currently used in the automotive industry. Although the accelerated corrosion methods currently used such as the ACT and ACTII are robust and work well as general quality control on a variety of painted substrates. These are not necessarily best suited for determining the long-term corrosion protection of thin film pre-

treatment systems. It has been shown that it is often difficult to distinguish the corrosion resistance on painted hot dipped galvanized steel (HDG) when it has been pre-treated with different pre-treatments (phosphating or thin film pre-treatments) or indeed without any pre-treatment at all when subjecting the samples to accelerated corrosion testing such as ACTII [1, 2 ,3].

In this study we have performed 3 modifications to an existing cyclic corrosion exposure regime (ACT). The modifications were 1 – simulation of a constant salt presence without rain; 2 – low temperature ACT (8-25C) and 3 – high humidity ACT. The results for two different substrates (HDG and ZM) with two Zr – based pretreatments (one which should be a better coating and one worse) as well as a traditional zinc phosphate pretreatment will be presented. The response in terms of underpaint creep and corrosion morphology in is significantly affected by the changes of the exposure regime. It was also evident that what was expected to be a “better” pretreatment on one substrate showed the inverse on the other substrate. There are also significant differences in the morphology of the corrosion front with the between the different modifications of the exposure regime.

[1] K. Tarka, Lic. thesis, Chalmers University of Technology (2015)
[2] G. Ström, “Volvo Laboratory Study of Zinc-Coated Steel Surface Treatment Properties and Outdoor Behavior,” SAE Tech. Pap. Ser., (1989)
[3] K. Tarka et al, Modified cyclic corrosion test for thin film pretreated and painted galvanized steel for the automotive industry, EUROCORR2016, Montpellier, France, 11 - 15 September 2016

Development of a sol-gel based layer with improved residual formability and active corrosion protection for the hot forming of galvanized medium manganese steels

A. Anthes, W. Fürbeth , DECHEMA-Forschungsinstitut, Frankfurt am Main, Germany.

Safety-relevant components in the automotive industry (e. g. B-pillars) are currently made of press-hardened manganese-boron steels like 22MnB5 or 20MnB8. This procedure allows high-strength components to be manufactured from inexpensive alloys, but there are still problems in manufacturing that have not yet been resolved. During the hot stamping process an oxide scale is formed on the steel surface, which increases the wear on the pressing tool. In addition, this oxide scale must be removed for further processing. Therefore, nowadays Al-Si-layers are mostly used to prevent steel oxidation. Unfortunately, these layers are not ideal either, as they adhere to the oven rollers and do not offer any active protection against corrosion. Alternatively, zinc coatings can be used to protect the substrate against corrosion, but the press-hardening process must be adapted to prevent liquid metal embrittlement or the formation of brittle Zn-Fe phases. There is currently only one company using galvanized strip material in a patented indirect press hardening process. As a result, galvanized press-hardened components only have a market share of around 5%.

This presentation will show the approach of the development of a sol-gel based layer with improved residual formability and active corrosion protection on medium manganese steels. Sol-gel chemistry and inorganic micro-/nanopowders are used for the formation of these SiO_2-based layers with low sintering temperatures (Fig. 1). The dispersions are characterized by determination of the solid content by means of re-drying, measurement of the particle size distribution with dynamic light scattering and determination of the viscosity. The coatings applied by dip-coating are characterized by light microscopy and SEM on the substrate surface and at cross-sections. Their performance in terms of corrosion and oxidation protection is determined.

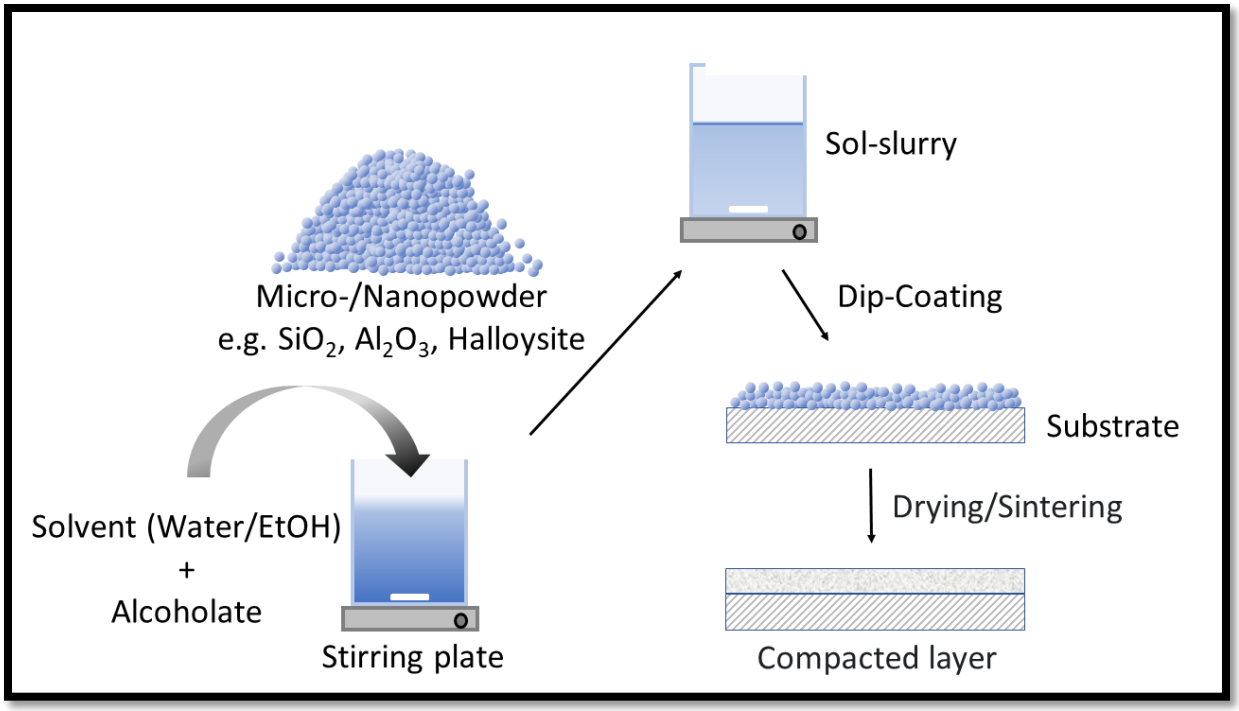

Fig.1: Schematic representation of the sol-slurry production and layer deposition.

Characterization of the Galvanic Protection of Zinc Flake Coating by Spectroelectrochemistry and Industrial Testing

Florian Feldmann, Vienna University of Technology, Institute of Applied Physics, Vienna, Austria / Dörken Coatings GmbH & Co.KG, Herdecke, Germany;
Laura Mears, Vienna University of Technology, Institute of Applied Physics, Vienna, Austria;
Marcel Roth, Dörken Coatings GmbH & Co.KG, Herdecke, Germany;
Markus Valtiner, Vienna University of Technology, Institute of Applied Physics, Vienna, Austria

The properties of hot-dip galvanised and electroplated zinc coatings on steel have been widely studied, but the corrosion mechanisms of zinc flake coatings have not yet been investigated in similar detail. Here, we present the protective effect of inorganic lamellar zinc coatings, comparing the metallic dissolution rates of different zinc, aluminium and alloyed flakes using an Inductively Coupled Plasma Mass Spectrometry (ICP-MS) flow cell. These experiments were carried out on both intact and pre-damaged coatings with different electrolytes. Data is also compared to accelerated laboratory corrosion tests and outdoor weathering results.
The chloride concentration, and its effect on the passive oxide film, appears to be a key aspect moderating the dissolution rate and hence sacrificial zinc dissolution under various conditions.
The complementary use of accelerated tests and ICP-MS flow cell analysis provides new insights into both the influence of the corrosive environment and the impact of the zinc flake (alloy) used. Based on this approach tailored coating solutions using zinc flake coatings can be developed.

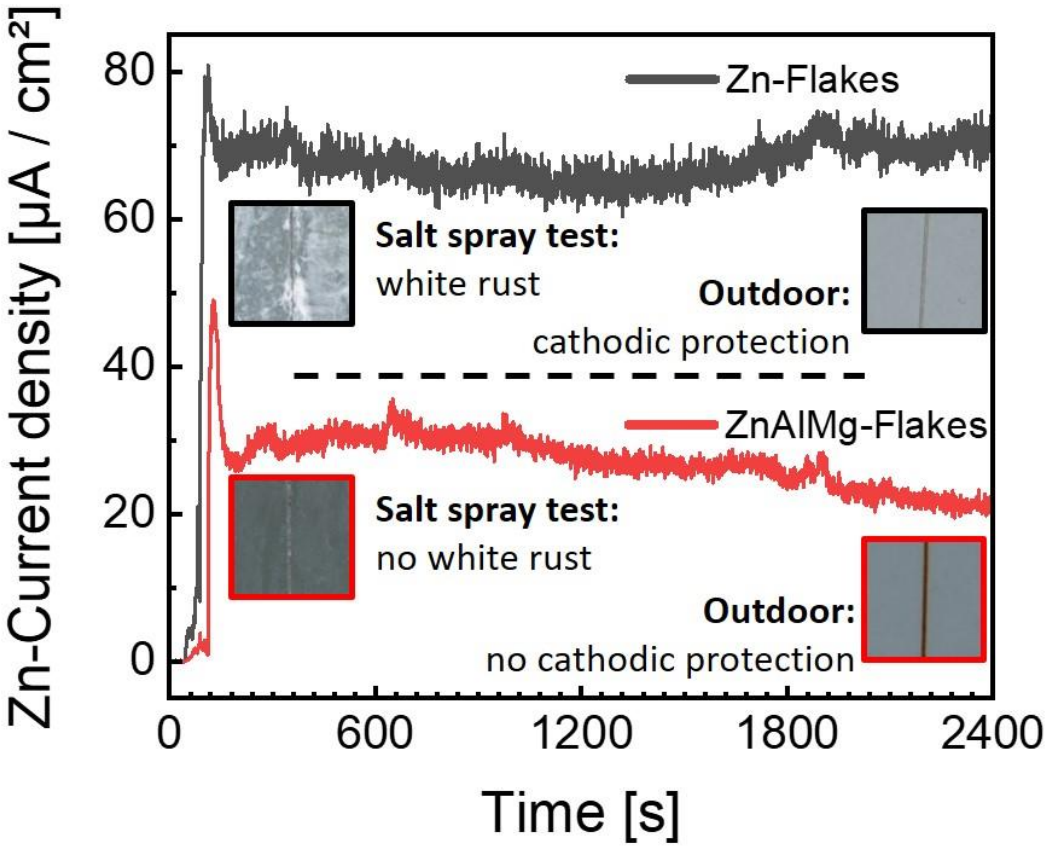

Figure 1: ICP-MS zinc dissolution rates of zinc flake systems with pure zinc flakes and ZnAlMg flakes compared with the corresponding salt spray test and outdoor weathering results

Effect of the magnesium rich surface phase on under-creep corrosion of painted ZMA coated automotive panels

The use of zinc-aluminium-magnesium (ZMA) based alloys as coatings for automotive bodies offers advantages in corrosion resistance, which in return allows for a reduction in zinc coating weight. Still, field experience offers some rare surprises in performance, suggesting a gap between accelerated tests and actual usage. Such a gap was discovered by Volvo Cars for the commonly used hot-dip galvanized coil coating, GI50, on fenders with a standard automotive paint system. Here the mode of paint under-cutting corrosion from edges in long-term field exposure was different from those observed in commonly accepted accelerated test methods.

By developing a scheme simulating temporary aggressive field conditions with high chloride loads, but under well aerated and cool exposure conditions (the maximum temperature is 15 °C), the corrosion mode found in field could be successfully replicated. The resulting, so-called *Corrosion from edge on Zn-coated parts (test)* was applied to evaluate the corrosion properties of thin film pre-treatments vs. traditional phosphating conversion coatings on GI50, then extending the same comparison to ZMA. The results confirmed the gap in outcome for the new test scheme vs. standardized cyclic tests, and especially so for the combination of thin film pre-treatments on ZMA-coatings.

For standard phosphate-based conversion coatings the results of the new test scheme are not contradicting those of the VDA621-415 cyclic test, with ZMA-type coil-coatings offering the usual advantage in corrosion performance. For thin film conversion coatings, however, the performance is dependent on the surface conditions prior to the application of the thin-film coating. If the concentration of especially magnesium in the outer layer of the ZMA surface is too high, preferential corrosion of the magnesium rich surface phase results in extensive blister formation.
The accumulation of magnesium corrosion products, possibly as soluble oxychloride intermediates, at the outer ZMA surface is demonstrated with SEM/EDX mappings of cross sections, and can be understood in terms of solubility and pH gradients, when the associated oxygen reduction reaction takes place at the cut edge.

The phenomenon of preferential dissolution of the magnesium rich surface phase is specific to the *Corrosion from edge on Zn-coated parts test* and is absent in the more general VDA cyclic test, where the anodic dissolution of the ZMA coating progresses more plug-like, as observed also for GI regardless of conversion coating type. Tuning the steps prior to the application of the thin film conversion coating to remove part of the ignoble surface phase would provide a way to eliminates the problem.

Sensitivity: general

Investigating the effect of rivet coating on SPR joint performance for dissimilar materials joints

Muhammad Haris[1,3], Sullivan Smith[2], Lorna Anguilano[1] Ben Robinson[2], Timothy Minton[1], Briony Holmes[2]

[1]College of Engineering, Design and Physical Sciences, Brunel University London, Uxbridge, UK

[2]TWI Ltd, Cambridge, UK

[3]NSIRC, TWI Ltd, Granta Park, Great Abington, Cambridge, CB21 6AL, UK

The combination of traditional materials like metal alloys together with Fibre Reinforced Polymer (FRP) materials have received growing attention recently. Increasing demand of lightweight structures in transport industry is growing stronger due to the need for a high strength to weight ratio, required for better performance, safety, and environmental concern. It has become an important challenge to incorporate these lightweight materials in a structure as they are beneficial for environment and consume less fuel. The overall weight of the cars, trucks, aircraft, or aerospace vehicles is reduced due to lightweight structural components, which subsequently decreases the fuel consumption of the vehicle, providing lower operational costs. With UK having set a net-zero target of at least 100% (previously 80%) emission reduction by 2050 which means the progress needs to be accelerated in coming year(s) and lightweight structures will be an integral part for the structural integrity and transportation industry. Traditionallly, automotive vehicles have mostly been made up of iron and steel, in recent decades the use of Aluminium (Al) in the automotive sector has increased. However, with the ongoing pursuit of even lighter materials, which may not provide equally good corrosion resistance, a greater understanding of the corrosion behaviour of these emerging automotive materials is required. Furthermore, the use of even lighter materials such as composites and plastics is growing, especially in the automotive industry. To be able to use lightweight materials in combination with more traditional materials such as aluminium, steel or alloys etc. current joining techniques must be adapted as it offers less production time, well-established, requires low capital investments and more independence in joining of materials. Industries that need to join dissimilar materials are looking for simple and faster techniques such as Self-piercing rivets (SPR) that is used to join Steel-Aluminium and Steel-Steel but not been utilized to join Carbon fibre reinforced polymer (CFRP) with Al. These dissimilar joining techniques offer unique challenges, one of which is the formation of a galvanic coupling between the two dissimilar materials in a joint causing corrosion and strength degradation of the structure overall. Several methods and technologies have been developed for joining metals and composites which includes adhesive, mechanical and metallurgical joining. The Self-Piercing Riveting (SPR) process attracts a lot of attention in industry due to its ability to

join a variety of similar and two or more dissimilar materials of different thicknesses. Moreover, SPR also offers flexibility for automation and high joining speed.

Therefore, this work investigated the effect of different coatings on joint performance for mechanical fastener in dissimilar materials joining applications by using salt spray exposure test and single lap shear test. This work focuses on understanding the interactions of the coatings on CFRP/rivet and CFRP/Al interfaces when joined and its corrosion properties. The joint performance of different coatings in dissimilar material joints were investigated by using single lap-shear test, and photomacrography including characterization techniques such as Scanning electron microscopy (SEM), profilometry, nanoindentation providing information supporting the understanding of the effect of these coatings on the strength behaviour.

This work highlights the critical factors governing the coating effect on the strengh and corrosion of carbon fibre reinforced polymers when joined to aluminium in car body constructions, and highlights new areas on the role of fastener coatings for dissimilar material joints.

This research/publication is made possible by the sponsorship and support of Brunel University London and TWI. This work was enabled through, and undertaken at, the National Structural Integrity Research Centre (NSIRC). This research is funded by TWI's Core Research Programme, a market-driven programme of research and development activities that underpin the creation and optimization of joining, materials, and engineering technologies.

Evaluation of Corrosion Properties of Aluminum/Steel SPR Joints for Automotive

Jin-Ho Rhee[1], Ji-Hyung Park[1], Jun-Mu Park[1], Seung-Pill Jung[1], Ji-Won Seo[2]

[1]R&D Center, Hyundai-Steel, 1480 Bukbusaneop-ro, Songak-eup, Dangjin-si, Chungcheongnam-do, 31719, Republic of Korea

[2]Accelerated Durability Test Team, Hyundai Motor R&D Center, 150 Hyundaeyeonguso-ro, Namyang-eup, Hwaseong-si, Gyeonggi-do, 18280, Republic of Korea

Key words: automotive steel, galvanic corrosion, SPR (Self-Piercing Riveting)

Abstract

The use of lightweight material such as aluminum and related application technologies in the automotive are needed to improve fuel efficiency and minimize carbon emissions. Both aluminum and ultra-high strength steel (UHSS) among materials are already widely used for weight-saving of the automotive body. The mechanical fastening technique is necessary for joining automotive bimetallic parts usually because conventional resistance spot welding is not suitable for hybrid joining due to the difference in properties between materials. SPR among mechanical joining techniques is applied for hybrid joints generally because of advantages such as high productivity and flexibility. However, galvanic corrosion has been reported in SPR joints exposed corrosive field environment because there was electrochemical potential difference between materials inducing the accelerated corrosion of aluminum as anode. [1, 2]

In this study, corrosion behavior of 6,000 series aluminum alloy used for car body was analyzed depending on hybrid combination with different 4 types of steel. Each hybrid SPR joint was evaluated after vehicle accelerated corrosion test and investigated by distinguishing detailed 3 areas from that to compare the corrosion level. As a result, both cold rolled steel and Al-Si coated hot stamping steel caused the corrosion of aluminum alloy at least 2 times faster than zinc alloy coated steels. Severe thinning and pits of aluminum alloy were detected at the outermost bonding interface among 3 areas of SPR joint especially. It was thought that crevice corrosion was occurred through the gap where oxygen concentration gradient and the permeation of salt water could be expected from the outside environment. On the other hand, Zn-Mg-Al coated

steel protected aluminum alloy from corrosion effectively resulting less pits and white corrosion products on the aluminum alloy interfacial surface. Corrosion life of aluminum alloy was dominated by which steel sheet was joined and the combination of 2 materials acted as major effect factor in SPR joints consequently. Coating types of SPR influenced the tensile shear load after corrosion in mechanical joining test. Zn-Ni coating indicated higher corrosion resistance than other coating types in hybrid area. Corroded sample applied with Zn-Ni coating SPR joints also showed the least change in load value, whereas Sn based coating couldn't protect the base metal of SPR from corrosion and corroded sample had the lowest load value.

[1] Kotadia, H. R., Rahnama, A., Sohn, I. R., Kim, J., & Sridhar, S., Performance of dissimilar metal Self-Piercing Riveting (SPR) joint and coating behaviour under corrosive environment, Journal of Manufacturing Processes, 39, 270 (2019)
[2] He, X., Pearson, I., & Young, K., Self-pierce riveting for sheet materials: state of the art, Journal of materials processing technology, 199, 29 (2008)

Ion selectivity of corrosion products formed in the crevice of CFRTP and high-strength steel/aluminum alloy

Kosaku Nomura[1], *Masatoshi Sakairi*[2], *Koji Fushimi*[2]

[1]*Graduate School of Chemical Sciences and Engineering, Hokkaido University, Sapporo/Japan*

[2]*Faculty of Engineering, Hokkaido University, Sapporo/Japan*

The use of multi-materials such as composites of carbon fiber reinforced thermoplastic (CFRTP) and high-strength steel or CFRTP and aluminum alloy is one of the main strategies for weight reduction in automotive body. However, multi-materials are subject to galvanic corrosion, which increases the risk of failure and shortens their service life. Therefore, wet-and-dry cycle test was conducted on a coated multi-material joint consisting of CFRTP and high-strength steel/aluminum alloy plates to simulate winter road conditions in Northern Europe, and corrosion products formed in the crevice of multi-materials joint were investigated using a membrane potential measurement as well as Raman spectroscopy and X-ray fluorescence microscopy.

The wet-and-dray cycle test, in which a sample was immersed in a mixture of NaCl and $CaCl_2$ solutions for 0.25 h and then repeatedly subjected to a wet atmosphere of 90%RH, 10°C, 3 h and a dry atmosphere of 35%RH, 25°C, 3 h more than a dozen times, was performed according to Kozaki [1]. After several weeks or more of exposure under the wet-and-dry cycle test conditions, corrosion products filled the crevice of the multi-material sample and did not to allow air leakage through the crevice gap. The membrane potential of the corrosion products in the crevice was measured using several NaCl solutions of different concentrations, and it was found that the products were anionic rather than cationic selective in all tests. The products formed in the test using dilute mixture solution were relatively porous hydroxides and oxides and showed larger fixed charge concentrations than those formed in the test using concentrated solution. This suggests that the density of corrosion products plays an important role in preventing galvanic corrosion in the gap between CFRTP and high-strength steel/aluminum alloy joints.

[1] T. Kozaki, M. Umeta, *J. Surf. Finish. Soc. Jpn.* 73 (2022) 384-389.

The corrosion behavior of plasma electrolytically oxidised MgAlZn and MgZnZr alloys for the use in car and motorcycle wheels

Daniel Bengtsson Blücher, Otto Lunder, John E. Lein, Dirk Nolte, (SINTEF Industry, Trondheim, Norway), Reinis Drunka (Riga Technical University, Riga, Latvia), Marks Lisnanskis, Nika Borisova (SMW, Riga, Latvia)

Automotive Corrosion (WP17)

Magnesium alloys can reduce the weight of the rotating mass on car and motorcycle wheels by about 20-50% compared to aluminium. This weight reduction will significantly reduce the energy consumption and the CO_2 emissions, when fossil fuels are used. However, since Mg-alloys are prone to corrode, plasma electrolytic oxidation (PEO) can be used to protect the surface[1]. This work aims at investigating the corrosion protective properties of forged MgAlZn and MgZnZr Magnesium-alloys coated with PEO. By optimising the process parameters of the PEO application and by integrating certain additions to the electrolyte, the corrosion protective properties of the coating can be enhanced.

The surface morphology and composition, chemical- and phase composition of the obtained protective coatings and the underlying substrate are analysed by means of Eddy current, metallographic cross section, FIB and SEM/EDS equipped with BSED. The electrochemical corrosion behaviour is studied in 3% NaCl solution with OCP, polarisation curves, LPR and EIS. Also, the corrosion performance is then analysed after exposing the samples in a salt spray chamber. The anodic delamination of the PEO is analysed in-situ in humid air with and without NaCl addition to the corroding surface with scanning kelvin probe.

The PEO application process was successful, and the process parameters were optimized to obtain a dense and adherent coating. The corrosion studies showed some interesting results which are used to further improve the PEO process.

Acknowledgement: This work is financed by the Norway Grants / Innovation Norway and the Investment and Development Agency of Latvia under the project ID. AK-IES/35.

[1] https://doi.org/10.1016/j.surfcoat.2013.09.021

Study to measure and extrapolate corrosion of exhaust components under real driving conditions

Daniel Hornauer, Dr. Muhammad Yasir
Faurecia Emissions Control Technologies, Augsburg, Germany

Modern automotive exhaust systems are getting more and more complex due to **stringent environmental** regulations and packaging constraints. Therefore, a variety of subcomponents are needed like valves, heat exchangers, emission reduction systems, direct insulations and many more. With this growing complexity and the increased **lifetime** requirements, the needs for improved corrosion prediction as well as for adapted corrosion tests arise.

To be able to extrapolate the corrosion behavior of **such complex systems** and to optimize specific corrosion lab tests, it is important to know about the exact corrosion conditions under real conditions in the field. There *are* variety of different influencing factors like the driving behavior (city cycle, highway cycle or idling) and the associated temperature profile, the use of de-icing salts, the fuel quality and many more.
For this purpose, a corrosion sensor with an on-board equipment for the data acquisition and an automated tool for data processing were developed. The linear polarization resistance (LPR) was measured and compared with on board diagnostics (OBD) signals and the temperature data.

The results from various driving profiles were analyzed and correlation was established among different influencing factors and measured corrosion rates.

Keywords: Automotive, Corrosion, Electrochemistry

Investigation of the Influence of Friction Stir Welding Parameters to the Microstructure, Local Hardness and Local Corrosion Behavior of EN AW-7075 T6

C. Chandra[1], J. Ellermeier[1], R. Reitz[1], M. Oechsner[1]

[1]*Center for Structural Materials (MPA-IfW), Technische Universität Darmstadt, Germany*
caroline_karina.chandra@tu-darmstadt.de
joerg.ellermeier@tu-darmstadt.de
ruediger.reitz@tu-darmstadt.de
matthias.oechsner@tu-darmstadt.de

Abstract
In recent years, the transportation industry focused on reducing CO_2 emission by cutting vehicle fuel consumption. The straightforward key is weight reduction, and high-strength aluminum alloy EN AW-7075 T6 is a popular choice. This alloy has shown great potential where high-temperature is not a concern. Its impressive mechanical properties, especially the strength-to-density ratio, can be derived from finely dispersed precipitates in the matrix.
Although beneficial for strengthening, precipitates impact corrosion behavior negatively. Some precipitates act anodic towards the bulk matrix (e.g., $MgZn_2$ and Mg_2Si), while some are cathodic (e.g., Al_7Cu_2Fe, Al_3Fe and Al_2CuMg). Corrosion in this alloy stems from the electrochemical potential difference between precipitates and bulk matrix. From sheets to real components, joining processes are inevitable. Limited research focuses on the influence of the welding process on corrosion behavior and mechanical properties. Welding introduce heat and alters the microstructure. In addition, friction stir welding involves high mechanical force, further contributing to microstructure and precipitates distribution. Once welded, the local hardness and the local corrosion behavior of the weld seam and its adjacent area deviate from its parent metal. These investigations aim to understand the correlation between microstructure and welding process, as the microstructural changes affect the local hardness and the local corrosion behavior.
Keywords
EN AW-7075, friction stir welding, heat input, microhardness, immersion test

Introduction

Heat input plays a significant role in the corrosion behavior of materials in joining technologies. Excessive heat input can lead to the formation of undesirable phases, grain growth, and altered microstructures, all of which can increase the material's susceptibility to corrosion and decrease or increase strength with decrease of toughness. However, in the context of welding processes, heat is unavoidable due to the nature of the joining mechanism. One effective approach to drastically reduce heat input during the welding process is by employing solid-state welding techniques instead of traditional melting arc or laser welding methods. Solid-state welding techniques, such as friction stir welding, rely on mechanical forces and severe plastic deformation rather than melting the materials [1]. These processes generate significantly lower heat input compared to traditional fusion welding methods, resulting in minimal thermal effects on the workpieces. By minimizing heat input through solid-state welding, the detrimental effects on the material's corrosion behavior can be mitigated, leading to improved corrosion resistance. This approach is particularly advantageous for joining materials that are sensitive to heat-induced corrosion or possess complex microstructures that may be prone to degradation during fusion welding, such as EN AW-7075. [2, 3]

In its un-welded state, EN AW-7075 in the peak-aged state (T6) displays localized corrosion tendencies. This behavior can be attributed to the coexistence of precipitates and intermetallic phases within the aluminum matrix. The presence of these phases introduces an imbalance in their electrochemical potentials, resulting in localized corrosion susceptibility. The coexisting phases in EN AW-7075, such as $MgZn_2$ and Mg_2Si, exhibit anodic behavior, while phases like Al_7Cu_2Fe, Al_3Fe, and Al_2CuMg behave cathodically towards the bulk aluminum matrix [4, 5]. This galvanic coupling between the anodic and cathodic phases creates localized electrochemical cells within the material. Consequently, areas that behave anodic are prone to corrosion attack, while adjacent cathodic areas act as protective sites. This phenomenon highlights the importance of carefully managing the composition and distribution of precipitates and intermetallic phases in the T6-condition of EN AW-7075 to achieve improved corrosion resistance. Precise control over the aging process, including temperature and duration, can help to optimize the precipitation and distribution of these phases, minimizing the galvanic coupling and reducing the susceptibility to localized corrosion.

An attempt to decrease the heat input during welding process was carried out in this study by means of lowering the tool rotation speed, while maintaining the traverse welding speed [6]. By decreasing the rotation speed, less heat is generated and transferred to the material, resulting in a narrower region that experiences thermal effects. This reduction in heat input is expected to be beneficial as it helps minimize the extent of microstructural changes, such as grain growth and phase transformations, that typically occur within the heat affected zone (HAZ). One of the novelties of this study lies in the application of a 2-pin welding tool, which allows rotation to traverse ratio of 0.6:1. A relatively fast traverse speed at 1000 mm/min with such a low rotation speed cannot be achieved using a conventional 1-pin welding tool. This unique configuration facilitates better control over the heat input, which in turn can influence the resulting microstructure and mechanical properties of the weld. [7]

This study aims to investigate the corrosion and mechanical behavior of friction stir welded EN AW-7075 T6 in dependance of the obtained microstructure due to reduction of tool rotation speed and the associated reduction of heat input. The investigation encompasses assessing the corrosion resistance of the weld through corrosion testing, analyzing the mechanical properties using hardness measurements and examining the microstructural features.

Materials and Experimental Procedure

Sheet Materials and Welding Procedure

High-strength EN AW-7075 sheet material in T6-condition, measuring 350 mm x 100 mm with a thickness of 2 mm, was utilized as sheet material. The butt-joint friction stir welding (FSW) process was carried out using a five-axis friction stir welding machine (PTG Heavy Industries) in a depth-controlled mode. The machine had a maximum load capacity of 60 kN in the z-direction. In contrast to the industrial standards single pin friction stir welding tool, a novel 2-pin friction stir welding tool was employed in this study,
Figure 1.

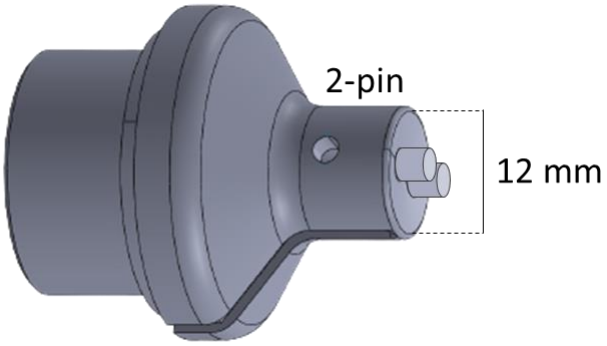

Figure 1. CAD model of 2-pin friction stir welding tool employed in this study. [6]

The tool tilt angle during welding was 2°. The shoulder diameter of the tool was set at 12 mm. It consisted of two cylindrical pins with a diameter of 3 mm each. The pins were positioned with a 2 mm gap between them. The plunge-depth of the tool was 1.76 mm and the length of the pin was 1.64 mm. To introduce variations in the degree of plastic deformation, alternating rotation speeds were utilized. A type K thermocouple was attached to the shoulder of the tool to record the temperature during welding process. A constant welding speed of 1000 mm/min was maintained, and the friction stir welding tool was rotated in a counter-clockwise direction for all weldments. Preliminary experiments were carried out to determine suitable parameters to achieve a rotational speed to traverse speed ratio of 1:1. From there on, an attempt to reduce the heat input was done by reducing the rotation speed. Sample A was welded with a rotation speed of 1000 min^{-1}, while sample B had a lower rotation speed of 600 min^{-1}.

Microstructural Characterization

The surface condition of the specimens and the topographic images in plane view were evaluated by microscopic analysis using a digital light microscope, specifically the Keyence VHX-6000. Cross sections of the samples were prepared for further metallographic analyses. These analyses were performed using a digital light microscope, in particular the Leica Aristomet.

To prepare the sample surface for documentation, both the metallographic cross-sections and the top surface underwent a grinding and polishing process. Following the polishing, an etchant was applied to reveal the microstructural features. The final polishing agent used was OP-S 0.25 µm. For the etching process, a modified Murakami etchant was employed, and it was applied at a temperature of 40 °C. To ensure the accuracy of the microhardness measurement, the etching of the sample surface was conducted subsequent to the hardness measurement process. This precautionary step was taken to prevent any form of surface alteration that could potentially influence the integrity of the measurement results.

Microhardness Test

The Vickers microhardness test is a widely used method for measuring the hardness of materials at a microscopic level. It involves pressing a diamond indenter into the material's surface and measuring the resulting indentation. By examining multiple zones within the material, insight is gained into the different hardness properties of the various regions. In addition, the microstructure of a material, i.e., the internal arrangement of grains or phases, plays a crucial role in determining its mechanical properties. Analysis of the microstructure in conjunction with the results of Vickers microhardness testing can provide a comprehensive understanding of the hardness distribution of the material and its correlation with microscopic features.

Within the scope of this study, Vickers hardness mapping with a force of 0.981 N (0.1 kgf, HV 0.1) and an indentation duration of 10 s was carried out in accordance to DIN EN ISO 6507-1:2018-07 over the weld seam at the surface (top-view, yellow rhombus) and on the cross-section (red rhombus), Figure 2. The measurements were performed on a micro-hardness testing instrument by DuraScan-70 Struers.

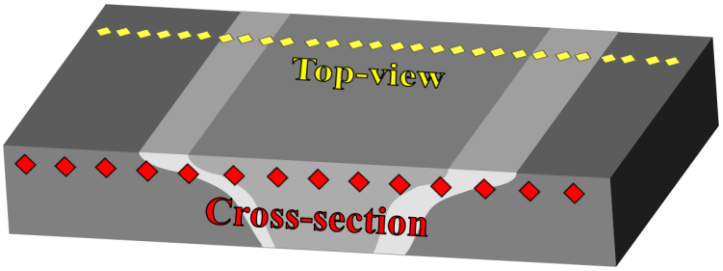

Figure 2. Schematic illustration of Vickers hardness mapping positioning.

The distance between the individual indentation point is 250 µm for the measurement on the top, fulfilling the required minimum distance of 3x the average diagonal length left by the indenter for aluminum alloys. On the other hand, a distance of 600 µm was chosen for the measurement on the cross-section in order to comply with the minimum distance recommended by DIN EN ISO 9015-2 for the hardness characterization of aluminum alloys at HV 0.1. The hardness measurement was performed on a sample surface that underwent a polishing process utilizing OP-S as the final polishing agent with a particle size of 0.25 µm. This polishing procedure was employed to ensure the attainment of a uniformly smooth and polished surface prior to the hardness measurement.

The decision to conduct hardness measurements on the top surface rather than on the cross-section was motivated by the need for a more direct comparison between the hardness values and the corrosion behavior observed during an accelerated immersion test in a harsh environment. This approach is expected to allow a better understanding of the increased susceptibility to corrosion of region adjacent to the weld seam (heat affected zone).

Immersion Test

The immersion test is conducted as outlined in DIN EN ISO 11846:2008-08 part B, employing 3 wt.% NaCl with an addition of 1 vol.% HCl as the immersion electrolyte. Due to its aggressiveness, this test heavily accelerates corrosion process of the anodic site within the welded joint. The duration and the temperature of the immersion was chosen according to the standard, which is 24-hour at room temperature.

The sample surface used for the experiment was in the “as-received” condition. Galvanic adhesive tape (ORACAL® High Performance Cast 751C) was applied to isolate the back and sides of the sample from direct contact with the electrolyte. The exposed area of the sample had dimensions of 25 mm x 50 mm, with the dimensions aligned parallel and perpendicular to the welding direction. The volume of the electrolyte used in the experiment was 200 ml. The ratio of the exposed area to the volume of the electrolyte complied with the DIN standard mentioned earlier. The evaluation includes the assessment of the corroded area as well as the extent of the width of the (from corrosion point-of-view) sensitized zone in the vicinity of the weld seam.

Results and Discussions

The **microstructural** investigation elucidates the pronounced disparities in the visual characteristics exhibited by individual zones. Etchant was applied with the objective of enhancing the discernibility of grain boundaries, as well as metallic and intermetallic phases present on the investigated surface, by accentuating their shape and size. The observable distinct visual appearance of each zone is expected to exhibit a notable influence on both the corrosion and mechanical behavior of materials, Figure 3.

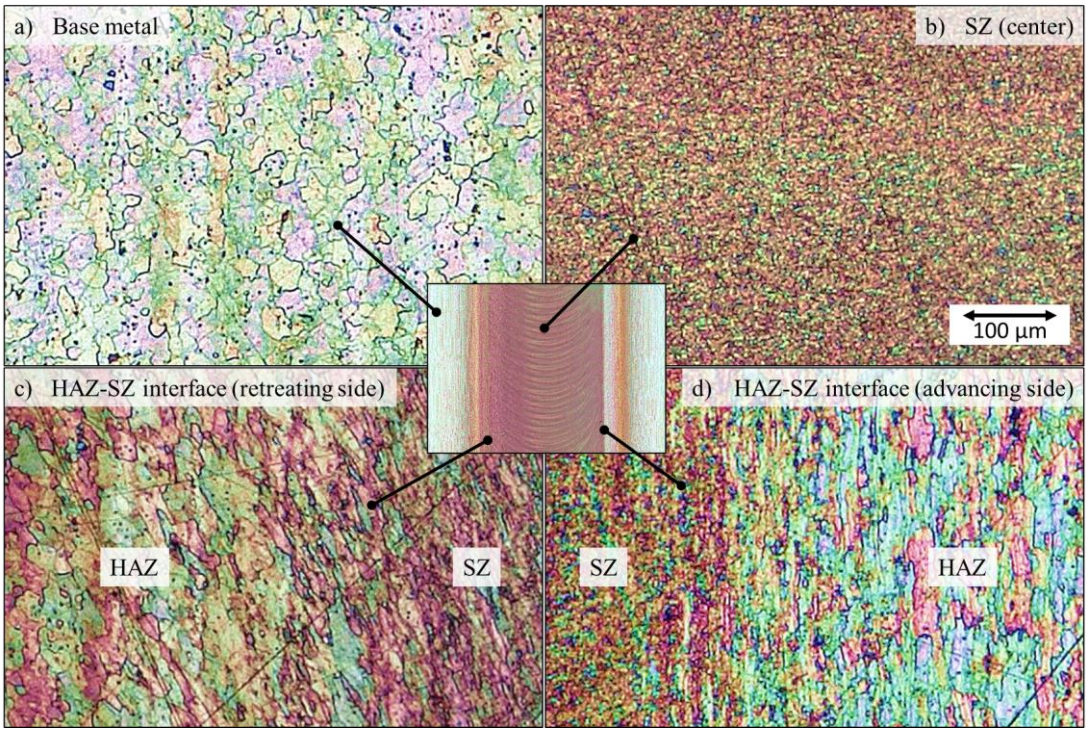

Figure 3. Top-view optical micrograph at various position of etched sample A (1000 min^{-1}). HAZ = heat affected zone, SZ = stir zone.

Base metal has a relatively uniform grain shape and size, Figure 3a. Similar observations regarding a uniform grain structure can be made for the central area of the stir zone, Figure 3b. However, it is worth noting that the grain size in this region is significantly smaller in comparison. The substantial disparity in grain size is to be expected and can be attributed to the mechanical stirring process involved in friction stir welding that disrupts the original grain structure. This process exerts sufficient force to induce the physical fragmentation of grains, leading to the formation of smaller grain sizes within the material. As a result of this phenomenon, the microstructure of the stir zone region exhibits very fine grain which cannot be resolved using light microscope due to insufficient resolution. The finer details and individual grain boundaries may not be adequately resolved, leading to the appearance of a blurred area rather than a clear representation of the microstructure. Scanning electron microscopy (SEM) was conducted in attempt to gain a more comprehensive understanding of the microstructure at the micrometer scale. However, the desired results were not achieved, indicating that the grain size in this particular case likely lies within the nanometer scale. It is worth noting that transmission electron microscopy (TEM) would be a suitable technique to explore such fine-scale details (outside the scope of this study). The microstructural appearance of the heat affected zone interface region on both sides of the weld displays significant differences when compared to the base metal and stir zone, Figure 3c: retreating side and Figure 3d: advancing side. These disparities are notable in terms of grain structure, grain size, and possibly the presence of distinct phases or alterations in the microconstituents. Obvious changes in both, grain sizes and shapes, are observable. Presumably, the dissimilarities in precipitation's phase and distribution also exist, albeit unverifiable within the confines of this study due to inherent instrumental constraints. These discrepancies are likely attributed to the thermal effects, as well as thermo-mechanical effects experienced during the welding process, which can lead to microstructural transformations and changes in the material properties within the heat affected zone.

A similar observation can be made on sample B (lower rotation speed: 600 min^{-1}), Figure 4a-d. This finding suggests that the grain structure in sample B exhibits a similar pattern to that observed in sample A.

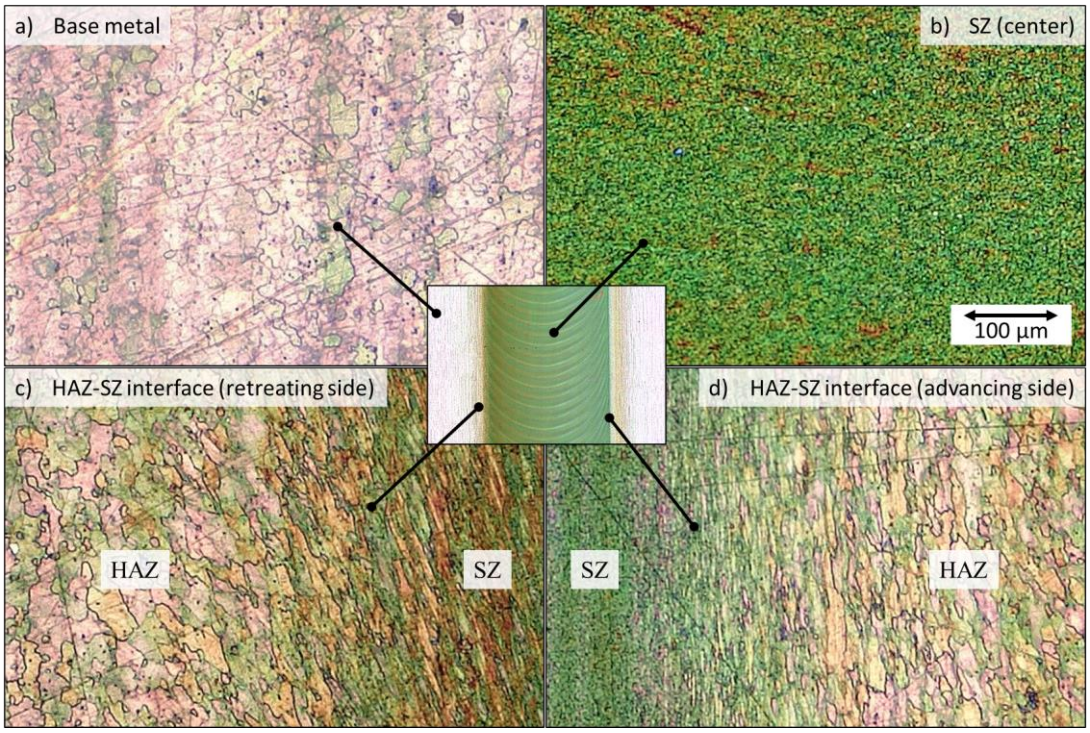

Figure 4. Top-view optical micrograph at various position of etched sample B (600 min^{-1}). HAZ = heat affected zone, SZ = stir zone.

The microstructure of a material is known to have a significant influence on its mechanical properties, including **hardness**. In some cases, materials with similar macroscopic appearances can exhibit different microstructures, leading to distinct hardness behaviors. This discrepancy in microstructure can result in a drastic drop in hardness between the materials, even though they may appear similar to the naked eye. Hence, it is crucial to consider the microstructural attributes when examining variations in hardness since they elucidate the observed distinctions in mechanical properties. In addition to conducting hardness analysis on the cross-section, hardness analysis was also carried out on the welded surfaces (top-view). This consideration is crucial because the surface of is the part that is most exposed to the environment, whether it is a corrosive environment or subjected to mechanical loads. By assessing the hardness on the welded surfaces, a more comprehensive understanding of the mechanical properties and potential vulnerability to both corrosion and mechanical stresses can be obtained. This approach takes into account the practical implications of the surface's exposure and ensures a thorough evaluation of the weld's performance in real-world conditions. Microhardness tests on the cross-section and on the top-view surface were conducted on sample A and sample B, Figure 5.

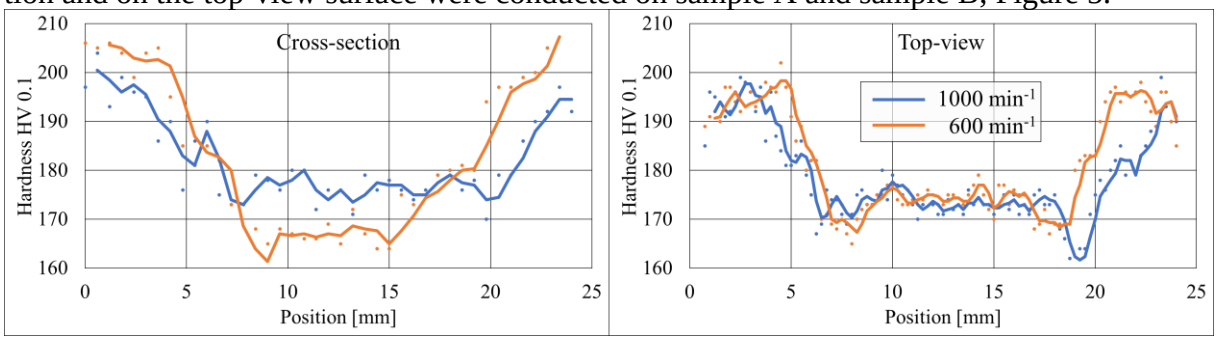

Figure 5. Comparison between microhardness profiling across the weld seam conducted on the cross-section (left) and on the top-view surface (right).

There are discrepancies between the hardness measured on the cross-section and on the top-view. The observed discrepancies in hardness measurements between the cross-section and top-view could potentially be attributed to a violation of the rule stated in DIN EN ISO 6507-

1:2022-08. According to this standard, the minimum thickness of the sample should be 1.5 times the average Vickers indentation diagonal. In this case, the lowest recorded hardness of 160 HV 0.1 corresponds to a diagonal of approx. 34 µm. Insufficient sample thickness can affect the deformation behavior of the material and compromise the reliability of hardness measurements. It is important to consider that even if the overall sample thickness exceeds the specified threshold (minimum thickness of approx. 50 µm), there could still be challenges in ensuring the homogeneity of the underlying layer of the "block" material. The homogeneity of the material in the vicinity of the indentation site is crucial for accurate hardness measurements. For this reason, hardness measurement of “thin” sample thickness is often carried out on the cross-section instead of on the top-view surface. Despite the observed discrepancies in the absolute values, the measurement results obtained from the top-view surface are consistent with the measurements conducted on the cross-section of the weld. While the hardness values may differ, the relative variations and trends in hardness across different regions or zones of the weld are similar between the two measurement orientations. This agreement in trends suggests that although the absolute hardness values may vary due to factors such as surface alterations or local variations, the overall comparison and assessment of hardness distribution within the weld can still be reliable and meaningful.

There are variations in the hardness values in each zone. Each color of the line represents a specific zone, along with their respective microstructure images, where the hardness value differs, Figure 6 and Figure 7. The highest measured hardness colored blue corresponds to the hardness of base metal, while the yellow line in the middle can be assigned to the hardness of the stir zone. The region of interface between heat affected zone and stir zone demonstrates the lowest observable hardness value (green), particularly heat affected zone of sample A, Figure 6. Here, the hardness is in its absolute lowest value. There is a significant drop in hardness in the region between the heat affected zone – stir zone interface and the base metal (orange) that cannot be attributed to any noticeable changes in the microstructure image. Moreover, by examining the role of hardening particles in EN AW-7075 T6, specifically in the form of $MgZn_2$, which is known to behave anodically towards the aluminum bulk matrix, the contrasting juxtaposition of cross-section images of the sample after an immersion test and the corresponding hardness profile can be explored [4, 8].

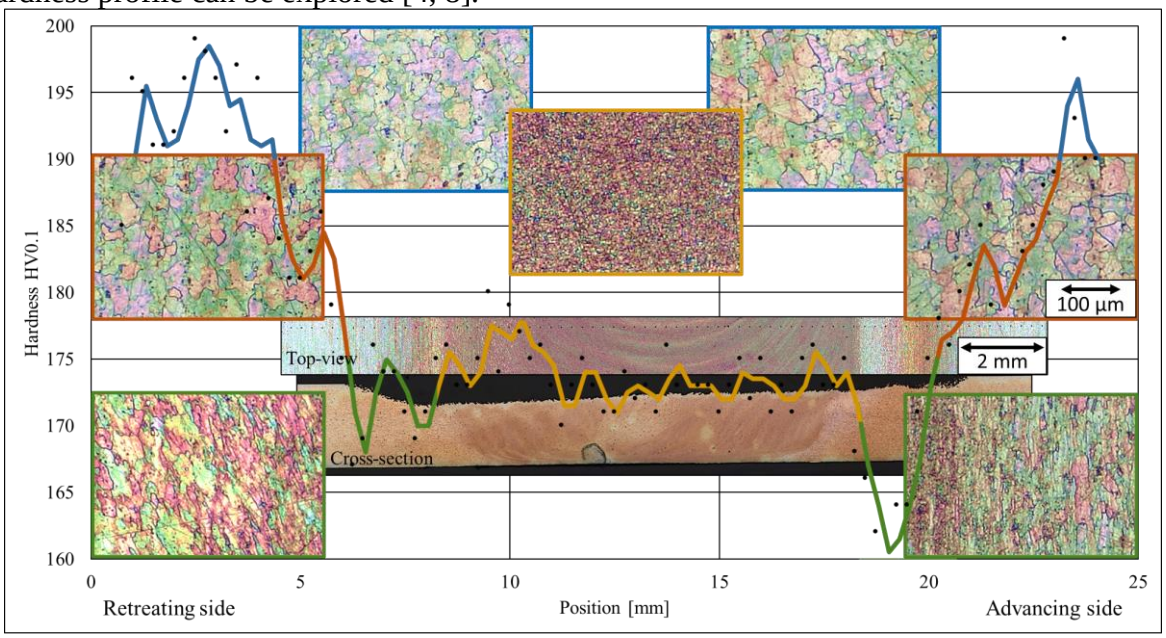

Figure 6. Microhardness profile across the weld conducted at the surface (top-view) of sample A (1000 min^{-1}), as well as the cross-section after 24-hour immersion test.

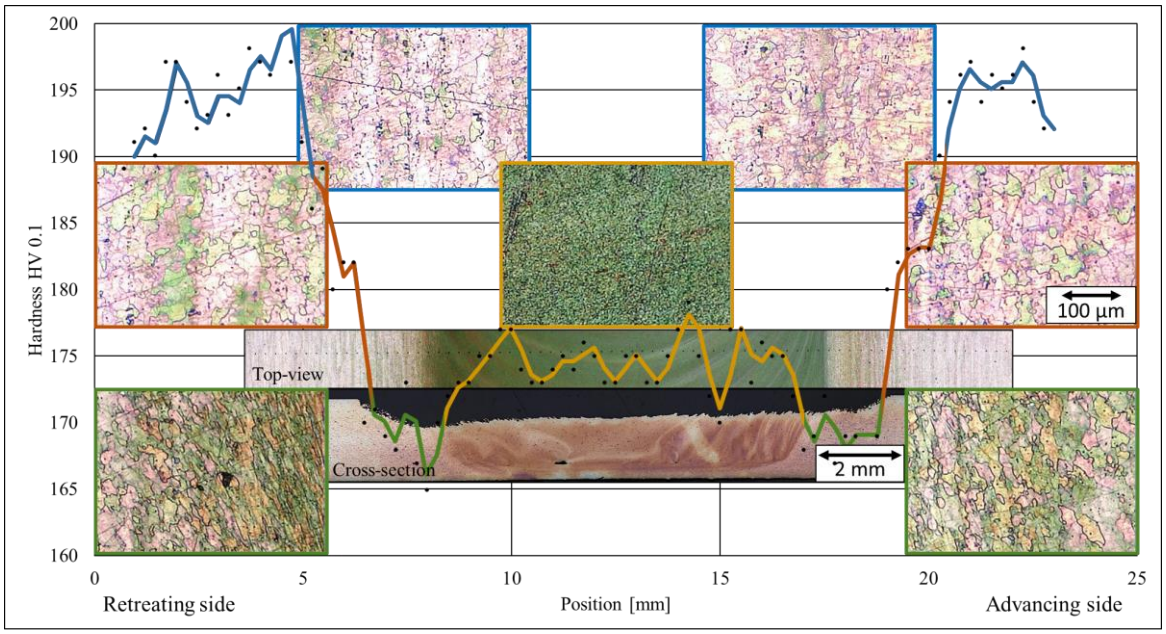

Figure 7. Microhardness profile across the weld conducted at the surface (top-view) of sample B (600 min^{-1}), as well as the cross-section after 24-hour immersion test.

This investigation aims to provide insight into the interdependency among these properties, namely microstructure, hardness and **corrosion**. The corrosion attack mostly the welded joint, followed by the area adjacent to it, the heat affected zone. Upon comparing the position of the cross-section image and the hardness profile, it becomes evident that the region where a noticeable decrease in hardness occurs (indicated by the color orange) is not significantly (if at all) affected by heightened susceptibility to corrosion. A straightforward explanation for this observation could lie in the high degree of similarity in microstructure between the area indicated by the color blue (representing the base metal) and the color orange. This similarity in microstructure contributes to the consistent corrosion behavior observed in both areas. This leads to a conclusion, that the distinct microstructure variations within different zones can serve as valuable indicators of corrosion susceptibility, aiding in the selection and optimization of materials. Another noteworthy aspect is that the corrosion behavior within the heat affected zone itself exhibits variations. Despite the heat affected zone being a distinct region influenced by thermal effects during welding, the corrosion response can differ across different subregions within the heat affected zone. According to the definition, the heat-affected zone encompasses all areas that have been influenced by heat, Figure 8. However, it is important to note that the intensity and duration of heat exposure varies. Therefore, the observed disparities in hardness decline can be hypothesized as a consequence of the diverse degrees and duration of heat encountered during the welding process.

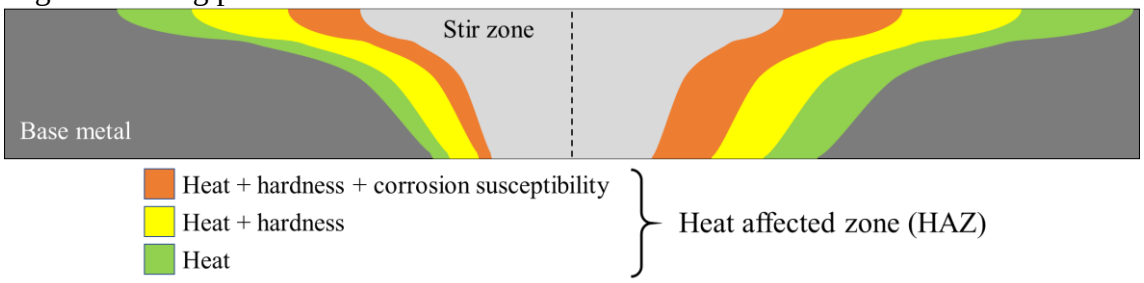

Figure 8. Schematic image of welded joint and its heat affected zone.

Notably, not all areas affected by the heat input are expected to undergo alterations in corrosion or mechanical properties. The region nearest to the heat source, the stir zone, experiences the highest temperature for an extended duration. Consequently, it is reasonable to anticipate that the most profound microstructural alterations, leading to potentially destructive effects,

transpire close to this zone. In the stir zone itself, the involvement of mechanical forces could be responsible for the slightly higher hardness value. The deliberate asymmetrical illustration serves the purpose of highlighting the contrasting levels of heat input between the advancing and retreating sides.

The main objective of reducing the rotation speed from 1000 min^{-1} (sample A) to 600 min^{-1} (sample B) was to minimize the width of heat affected zone by reducing the amount of heat input during the friction stir welding process. This reduction aimed to reduce the corrosion-promoting microstructural changes by employing overall lower temperature during the welding process. The underlying rationale behind this expectation is based on premise that by limiting the heat affected zone to a minimal extent, the magnitude of microstructural alterations can be kept in minimum as well. The correlation between the reduction in tool rotation speed, which leads to a lower heat input and a narrower heat affected zone underscores the corresponding mitigation of corrosion attack within that region, Figure 9.

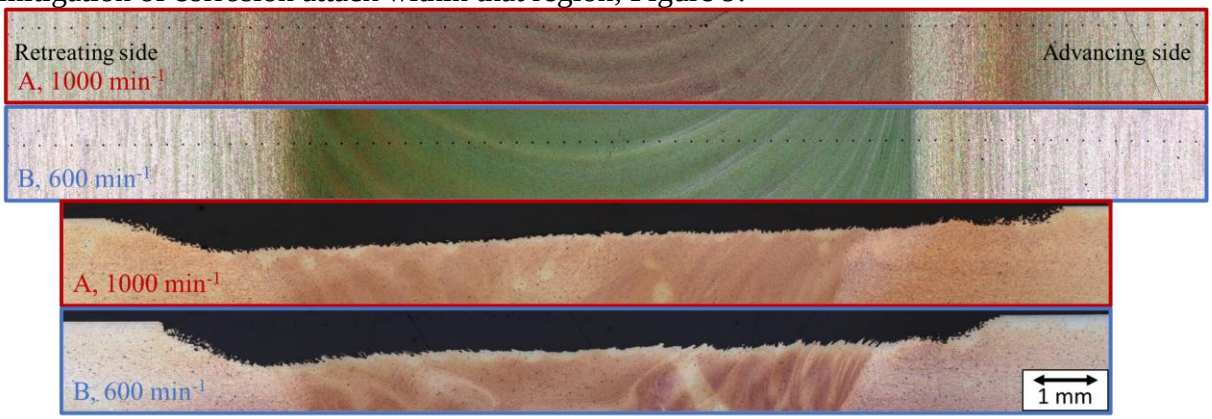

Figure 9. Comparison of sample A and sample B; top two images depict the etched top-view surface and bottom two images the cross-section of both samples after immersion test.

By reducing the rotation speed, the width of the heat affected zone is minimized, resulting in a narrower region susceptible to corrosion. This reduction in heat affected zone width can lead to a noticeable decrease in the depth of corrosion attack, indicating an improvement in the corrosion resistance of the material. It is important to note that the observed benefits in corrosion resistance resulting from the reduction of tool rotation speed is primarily pertain to the mitigation of corrosion attack only in the lateral direction. In other words, the reduction in rotation speed predominantly achieved a decrease in the width of the heat affected zone. However, this reduction did not correspond to a decrease in the occurrence of corrosion attack (depth). It is crucial to consider this directional dependency when evaluating the effectiveness of the reduced rotation speed approach in enhancing corrosion resistance. Contrary to the earlier assumption, the depth of the corrosion attack, which correlates with the corrosion intensity, is actually more pronounced in sample B. This unexpected result suggests that the reduction in tool rotation speed from 1000 min^{-1} (sample A) to 600 min^{-1} (sample B) has not yielded the anticipated improvement in corrosion resistance. Instead, sample B exhibits a higher degree of corrosion damage, indicated by a greater depth of corrosion attack. This finding indicates that factors other than the heat input during welding process may be influencing the corrosion behavior and intensity in this particular case. Further investigation is required to identify and understand these contributing factors. A preliminary hypothesis for this phenomenon is that the decreasing tool rotation speed is accompanied by a reduction in the stirring effect during the welding process. As the rotation speed decreases, the intensity of the stirring action, which promotes mixing and distribution of alloying elements, which are crucial for corrosion resistance, diminishes as well. As a result, localized areas with lower alloying element concentrations or inconsistent microstructural characteristics may form within the welded material, making them more susceptible to corrosion attack. Further investigation and analysis are necessary to validate this hypothesis

and gain a comprehensive understanding of the underlying mechanisms influencing the corrosion behavior in relation to the tool rotation speed.

Conclusion

Based on the aforementioned observations, the following can be concluded from the results:

1. The notable microstructural discrepancies observed among the different zones can serve as valuable indicators of corrosion susceptibility. These variations in visual appearance can be utilized to aid in the selection and optimization of materials.
2. On the contrary, it is apparent that the variation in hardness does not play a substantial role in distinguishing the susceptibility to corrosion in this particular context. One plausible explanation for this phenomenon is that even a minimal amount of heat input is sufficient to induce a change in hardness, despite the fact that this alteration may not be readily apparent in the microstructural analysis conducted using a light microscope.
3. The reduction in tool rotation speed proves effective in reducing the amount of heat input during the welding process, as evidenced by the narrower heat affected zone observed in sample B (600 min^{-1}) with a lower rotation speed compared to sample A (1000 min^{-1}).
4. The reduction in heat input does not always result in improved corrosion behavior, as evidenced by the increased corrosion intensity observed in sample B despite the lower heat input. The rationale behind this finding may be attributed to the reduced stirring effect that occurs when the rotation speed is decreased.

Further studies involving more comprehensive microstructural investigations and electrochemistry, such as potentiodynamic polarization, are planned for follow-up studies. These additional investigations will provide a more in-depth understanding of the microstructural features and the electrochemical behavior of the friction stir welded EN AW-7075. Incorporating electrochemical techniques, such as potentiodynamic polarization, will allow for a quantitative assessment of the corrosion resistance of the friction stir welded EN AW-7075. This technique measures the electrochemical response of the material to varying potentials, providing valuable information on the corrosion kinetics, corrosion potential, and corrosion current density.

Acknowledgment

The IGF project No. 21.433 N/ DVS No. 05.3296 (project RührKorro) of the Research Association for Welding and Allied Processes (Deutscher Verband für Schweißen und verwandte Verfahren e.V. – DVS) was funded by the Federal Ministry for Economic Affairs and Energy via the AiF within the framework of the program for the promotion of joint industrial research (IGF) on the basis of a resolution of the German Bundestag. The authors gratefully acknowledge the financial support from the research association and the AiF.

References

1. M. Lipińska, L. Olejnik, A. Pietras, A. Rosochowski, P. Bazarnik, J. Goliński, T. Brynk, M. Lewandowska, Materials & Design, **88** (2015) 22.
2. C.J. Dawes, W.M. Thomas, TWI Bulletin, **6** (1995) 124.
3. C.J. Dawes, W.M. Thomas, Welding Journal, (1996) 41.
4. B. Heider, E. Scharifi, T. Engler, M. Oechsner, K. Steinhoff, Materialwiss. Werkstofftech., **52** (2021) 145.
5. S.V. Sajadifar, T. Suckow, C.K. Chandra, B. Heider, A. Heidarzadeh, J. Zavašnik, R. Reitz, M. Oechsner, P. Groche, T. Niendorf, Journal of Manufacturing Processes, **86** (2023) 336.
6. C.K. Chandra, N. Sommer, B. Heider, M. Hatzky, R. Reitz, S. Böhm, M. Oechsner, Adv Eng Mater, (2023).
7. M. Hatzky, S. Böhm, Metals, **11** (2021) 1219.
8. W. Yang, S. Ji, M. Wang, Z. Li, Journal of Alloys and Compounds, **610** (2014) 623.

Factors affecting hydrogen embrittlement of 1.5GPa grade cold-rolled Gigasteel in automotive applications

A In Hwang, Yeon-Seung Jung, Young Hoon Jin, Yonggyun Jung

POSCO, Pohang, Republic of Korea

Recently, there has been a rise in the use of 1.5 GPa grade UHSS in the market, particularly in the electric vehicle industry, in order to address the need to reduce the weight of batteries [1,2]. However, the 1.5GPa grade UHSS can be severely deteriorated in terms of ductility and strength, even with only a few ppm of hydrogen content [3,4] as a result of hydrogen embrittlement (HE). This failure may occur during the production of Body-in-White parts, by cutting, bending, E-coating, and baking and also during the vehicle usage, including corrosion and various types of loads [5]. HE is a result of the interaction between the properties of material, hydrogen contents, and stress level [6-8]. Therefore, it is necessary to evaluate all factors that affects HE during the production and service time.

The purpose of our research is to investigate the main factors that influence HE of the 1.5GPa grade, cold-rolled Gigasteel, since HE is sensitive to residual stress that is generated during the manufacturing processes of cold-rolled steel. A series of experiments were carried out to assess Body-in-White production process and various stages of vehicle usage as mentioned previously. For example, the edges of the sample were trimmed by milling and shearing, then stress was applied via U-bending and 4-points bending, followed by E-coating and baking. The corrosive environment was simulated with 0.1N HCl and 5% NaCl solution. The level of hydrogen was measured by thermal desorption spectroscopy (TDS) analysis.

As a result, we can determine that bendability, hole expandability, and shear clearance were the main factors from the point of view of stress. In terms of hydrogen contents, it was found that the baking process not only releases hydrogen but also prevents the introduction of hydrogen in a corrosive environment. Reducing the amount of corrosion-vulnerable elements in the material also contributed to improving resistance to HE. This suggests the possibility of safe use from HE in the application of BIW parts of 1.5GPa grade cold-rolled Gigasteel.

[1] Chen, Hao, et al. "Progress and Perspective of Ultra-High-Strength Martensitic Steels for Automobile." Metals 12.12 (2022): 2184.
[2] Keeler, S., and M. Kirnchi. "Advanced High-Strength Steels Application Guidelines V6; WorldAutoSteel." World Steel Association: Brussels, Belgium (2017).
[3] Huh, Hoon, et al. "Dynamic tensile characteristics of TRIP-type and DP-type steel sheets for an auto-body." International Journal of Mechanical Sciences 50.5 (2008): 918-931.
[4] Moshtaghi, Masoud, Mahdieh Safyari, and Gregor Mori. "Hydrogen absorption rate and hydrogen diffusion in a ferritic steel coated with a micro-or nanostructured ZnNi coating." Electrochemistry Communications 134 (2022): 107169.
[5] Bergmann, C., et al. "Hydrogen embrittlement resistance evaluation of advanced high strength steel for automotive applications." Proceedings of the Steely Hydrogen, Ghent, Belgium (2018): 29-31.
[6] Takai, Kenichi, and Ryu Watanuki. "Hydrogen in trapping states innocuous to environmental degradation of high-strength steels." ISIJ international 43.4 (2003): 520-526.
[7] Liu, Qinglong, et al. "Hydrogen trapping in some advanced high strength steels." Corrosion Science 111 (2016): 770-785.
[8] Takai, K., et al. "Lattice defects dominating hydrogen-related failure of metals." Acta Materialia 56.18 (2008): 5158-5167.

Institut de la Corrosion
French Corrosion Institute

Hydrogen embrittlement of high strength press-hardened steels under simulated atmospheric corrosion conditions

Flavien Vucko[1], Varvara Helbert[1], Andrej Nazarov[1], Dominique Thierry[2]

[1] French Corrosion Institute, 220 rue Pierre Rivoalon, 29200 Brest, France

[2] RISE Research Institutes of Sweden, Isafjordsgatan 28A, 164 40 Kista, Sweden

Abstract

Advanced high strength steels (AHSS) are particularly interesting for the transport industry such as automotive to reduce the weight and consumption, as observed from their growing use in vehicles. However, the potentiality of these new steels is not being fully exploited due to their cracking sensitivity, particularly in the presence of hydrogen, through hydrogen embrittlement (HE). Indeed, ultra-high strength steels are known to be sensitive to HE and nowadays, from early steps, the fabrication processes are adapted to control the risks of delayed fracture for instance. However, atmospheric corrosion can be an additional source of hydrogen during service life, which was probably not so dangerous for low grades, but become critical for AHSS with ultimate tensile strength above 1000 MPa. Thus, the hydrogen assisted cracking (also called environmental assisted cracking) must be particularly considered due to the high tensile strength of such steels, which decreases drastically the critical level of hydrogen.

The phenomenon of HE is strongly linked to the activity of hydrogen at the surface of the corroded steel. In the case of AHSS with active metallic coating, the galvanic coupling at cut edges or at the location of defects in the coating can be an important source of hydrogen [1]. Red rust, consequence of strong local acidification, can also enhance hydrogen activity, particularly during wet/dry transients with increased corrosion rates, leading to hydrogen assisted cracking and failure.

The objective of this study was to correlate the risk of hydrogen embrittlement of high strength press-hardened steels to the activity of hydrogen under atmospheric corrosion conditions. The hydrogen uptake during wet/dry phases and accelerated corrosion tests was measured to evaluate the critical hydrogen activity. Then, 4-point bending specimens were tested under similar conditions at various steel levels to determine the stress/strain threshold leading to cracking. The results were discussed in terms of critical hydrogen uptake and stress related to the microstructure of the steel and metallic coatings.

This project has received funding from the Research Fund for Coal and Steel under grant agreement No 101034041.

References

[1] A. Nazarov, F. Vucko, D. Thierry, Scanning Kelvin Probe for detection of the hydrogen induced by atmospheric corrosion of ultra-high strength steel, Electrochim. Acta. 216 (2016) 130–139.

Feasibility study on the effect of cold sheet metal forming on corrosive hydrogen uptake

Andreas Drexler, Graz University of Technology, Research Group of Lightweight and Forming Technologies, Graz/Austria
Emir Hodzic, Graz University of Technology, Research Group of Lightweight and Forming Technologies, Graz/Austria
Besim Helic, Graz University of Technology, Research Group of Lightweight and Forming Technologies, Graz/Austria
Klemens Mraczek, voestalpine Stahl GmbH, Linz/Austria
Josef Domitner, Graz University of Technology, Research Group of Lightweight and Forming Technologies, Graz/Austria

Objectives

Hydrogen embrittlement (HE) of advanced high-strength steel (AHSS) sheets is a major problem in the automotive industry. The risk of HE rises with increasing hydrogen absorption during corrosion of galvanized sheets. Corrosion of zinc causes evolution of hydrogen on the reduction site of the bare metal. Hydrogen diffuses into and saturates inside the microstructure of AHSS. Beyond a critical hydrogen content, cracking may occur in the presence of stresses. It is well known that uniaxial plastic strain increases the hydrogen solubility, since additional trapping sites form in the microstructure. However, less is known on the effect of multiaxial strain on the corrosive hydrogen uptake, which is typical for deep-drawn parts. Therefore, this work investigates the difference of uniaxial and biaxial forming on the corrosive hydrogen uptake. Parts of a dual phase (DP) steel were deep-drawn at room temperature using a cross-shaped tool. The strains were measured using a GOM Argus system, and samples for corrosive hydrogen charging were wire-cut from selected positions. As reference, uniaxially strained samples were cut from the gauge section of bone-shaped samples. The samples were immersed into 3.5 vol% NaCl solution. After defined immersion times the hydrogen uptake of each sample was determined using a Bruker Galileo G8 thermal desorption analysis (TDA) system.

New results

Figure 1 (a) shows the measured plastic strain in the deep-drawn cross-shaped part. High biaxial strain of about 20 % occur in particular at the corners of the deep-drawn part. In Figure 1 (b), the effect of the equivalent plastic strain on the diffusible hydrogen content is shown for

both uniaxially and biaxially strained samples. Compared to uniaxial straining, it is evident that biaxial forming decreases the corrosive hydrogen solubility than uniaxial forming.

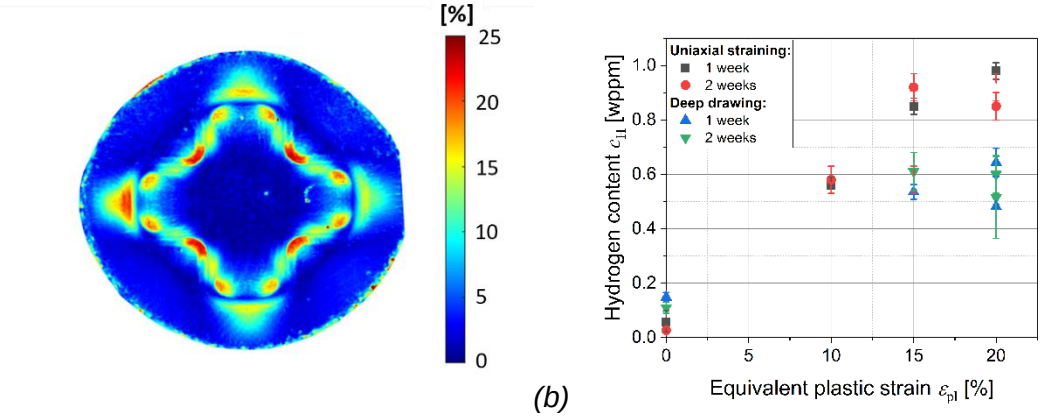

(a) *(b)*

Figure 1: (a) Measured von Mises equivalent plastic strain. (b) Difference between uniaxial and biaxial plastic straining on corrosive hydrogen uptake.

Figure 2 (a) correlates the hydrogen content caused by corrosive charging with the equivalent plastic strain of uniaxially strained samples of three different DP steels. The fitted curve illustrates the increase of the hydrogen content due to plastic deformation, which can be used for identifying critical areas of high corrosive hydrogen solubility in deep-drawn parts, as exemplarily shown in Figure 2 (b)

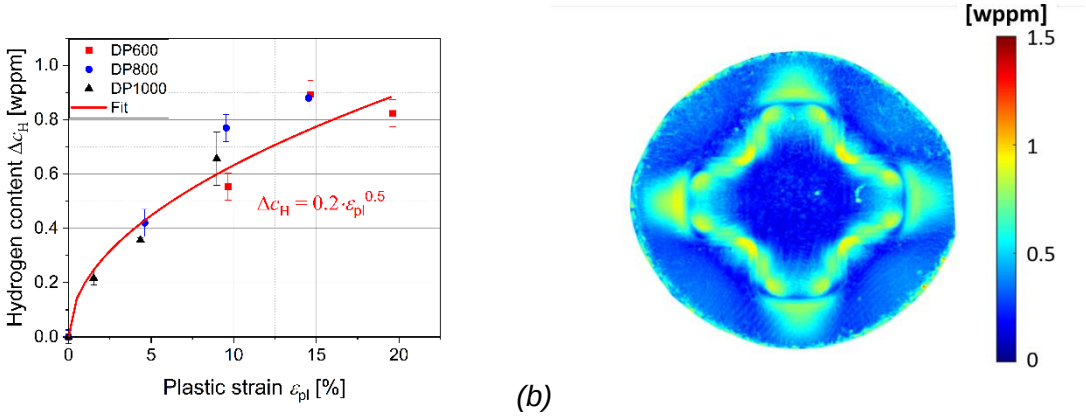

(a) *(b)*

Figure 2: (a) Mathematical correlation between hydrogen content and uniaxial plastic strain. (b) Mapping of the corrosive hydrogen solubility on the deep-drawn part.

Conclusions / significance of the work

The present work investigates the effect of multiaxial plastic straining on the corrosive hydrogen uptake of DP steels at room temperature. At large plastic strain differences in the hydrogen uptake were observed between uniaxial and biaxial straining. A fit function was proposed, which allows to map the corrosive hydrogen solubility on formed parts. This function can be used in the postprocessing of finite element (FE) simulations to minimize the corrosive hydrogen uptake in formed parts and, thus, to reduce the risk of HE.

Characterizing corrosion and passivation processes on steel samples after scratching the surface

L. Kalchgruber[1,2], M. Hahn[1], L. Mears[1], M. Valtiner[1,2]

[1] Institut für Allgemeine Physik, Technische Universität Wien, Austria
[2] Cest, Kompetenzzentrum für elektrochemische Oberflächentechnologie, Austria

Steel has many different applications in industry. In 2020, a total of 1877.5 Mt of crude steel was produced. [1] Due to corrosion, much of this important resource is lost. Thus, it is necessary to gain a fundamental knowledge of corrosion and passivation processes of steal samples.

To gain insight about the passivation and corrosion processes a coupling of ICP-MS with an electrochemical flow cell is utilized. Within this setup, the electrochemically dissolved material can be transported directly into the ICP-MS, where the ratios of dissolved elements can be analyzed. [2]

Within the EC flow cell different external potentials can be applied. The data of the ICP-MS then gives insight about the reduction and oxidation steps. To get a deeper insight, different electrolytes, potential steps and steel samples can be used.

One further aspect for studying corrosion is the behavior of the oxide layer. To retrieve information about the ability of the oxide layer to re-passivate the EC flow cell was upgraded. For this, the EC flow cell was adapted in a way that makes it possible to scratch the surface of the steel sample in situ. After scratching the surface, the dissolution first increases, but then decreases over time. The data can be fitted with exponential and linear functions, which allows to calculate the “half-live time”, which gives insight on the re-passivation speed of different samples after mechanically damaging the surface. The working theory to describe why there are different functions present during the re-passivation process is, that the exponential part shows the kinetic reaction of first order, which relates to a concentration dependent step. The linear part of the fit implies that a reaction of order zero takes place. A concentration independent process could be the transport of species from underneath the oxide layer to the surface along the defects of the oxide layer. Over time, the defects on the surface heal, which gives the species less pathways to dissolve through. Therefore, less dissolution over time is monitored in the ICP-MS.

[1] https://en.wikipedia.org/wiki/List_of_steel_producers, Retrieved 14.01.2022.
[2] D. Dworschak, C. Brunnhofer, and M. Valtiner, “Complementary electrochemical ICP-MS flow cell and in-situ AFM study of the anodic desorption of molecular adhesion promotors, ”Preprint submitted to Applied Surface Science, 2021

Erosion-corrosion properties of two novel Fe-based multicomponent alloys for marine applications

Weverson C Batalha[1], Virginie Roche[1], Alberto M. Jorge Jr[1,2], Yannick Champion[2], Marc Mantel[2], Nicolas Mary[3]

[1] LEPMI, Univ. Grenoble Alpes, Univ. Savoie Mont Blanc, CNRS, Grenoble INP, LEPMI, 38000 Grenoble, France

[2] SIMAP, Univ. Grenoble Alpes, CNRS, Grenoble INP, SIMaP, 38000 Grenoble, France

[3] INSA-Lyon, MATEIS UMR CNRS 5510, Université Lyon F-69621 Villeurbanne, France

The erosion-corrosion behavior in piping and drilling systems is a significant concern for their durability because of the presence of hard particles in fluids. Fe-based alloys are promising coatings materials for this kind of application, combining high corrosion and wear resistance and reducing costs [1–3]. This work aims at studying the erosion-corrosion behavior of two novel Fe-based multicomponent alloys containing a low amount of Cr (11%at.) fabricated by spray forming and correlate the effect of the compositional difference on the microstructure and consequent erosion-corrosion behavior. Samples of two compositions, $Fe_{61}Cr_{11}Mo_8Nb_4B_{16}$ and $Fe_{61}Cr_{11}Mo_8Ni_4B_{16}$, were processed by spray forming deposition on an AISI 1020 substrate under N_2 gas and temperature of 1750°C. The coating thicknesses were about 1-3mm. The microstructure was analyzed by scanning electron microscopy and X-Ray diffraction. Vickers microhardness was also evaluated, and values around 800 HV were found for both compositions. Polarization curves were carried out in a chloride-rich environment, E_{corr} of -311 mV and i_{corr} equal to 0.7 μA/cm^2 were obtained for the Nb-containing composition, with better values when comparing to the Ni-containing and similar compositions found in the literature [4]. Degradation tests were performed in a jet erosion-corrosion cell using commercial sand with a maximum flow rate of 5.5 m/s and jet angle of 45° and 90°. The potential fluctuated during the two hours of impingement, and a slight recovery was observed for both compositions. The measure of OCP after impingement indicates a better recovery capacity for the Nb-containing alloy, suggesting a better capacity of repassivation.

[1] G.Y. Koga, R.P. Nogueira, V. Roche, A.R. Yavari, A.K. Melle, J. Gallego, C. Bolfarini, C.S. Kiminami, W.J. Botta, Corrosion properties of Fe-Cr-Nb-B amorphous alloys and coatings, Surf. Coatings Technol. 254 (2014) 238–243. https://doi.org/10.1016/j.surfcoat.2014.06.022.

[2] C. Rasse, N. Mary, H. Abe, Y. Watanabe, B. Normand, Role of the jet angle, particle size, and particle concentration in the degradation behavior of carbon steel under slow slurry erosion-corrosion conditions, Metals (Basel). 11 (2021). https://doi.org/10.3390/met11081152.

[3] F. Huang, J. Jie Kang, W. Yue, X. bin Liu, Z. Qiang Fu, L. Na Zhu, D. shun She, G. Zheng Ma, H. Dou Wang, J. Liang, W. Weng, C. Biao Wang, Effect of heat treatment one erosion-corrosion of Fe-based amorphous alloy coating under slurry impingement, J. Alloys Compd. 820 (2020) 1–9. https://doi.org/10.1016/j.jallcom.2019.153132.

[4] G.Y. Koga, T. Ferreira, Y. Guo, A.M. Jorge, C.S. Kiminami, C. Bolfarini, W.J. Botta, Challenges in optimizing the resistance to corrosion and wear of amorphous Fe-Cr-Nb-B alloy containing crystalline phases, (n.d.).

Effect of strain degrees on the tribochemical properties of TWIP steels in oxidizing and reducing media

A. Bermúdez-Castañeda[1], S. Espinoza Rangel[2], E. Klyatskina[1], M. Vinogradova[1], V. Amigó[1], G. González[2]

(1) Instituto de Tecnología de Materiales (ITM), Universitat Politècnica de València, Valencia, Spain. (2) Instituto de Investigaciones en Materiales, Universidad Nacional Autónoma de México.

Key words

TWIP steels, pin on disc, strain degrees, corrosive media, tribocorrosion

Abstract

TWIP steels are an interesting group of steels, resulting in high ductility and formability compared to materials with similar strengths. These characteristics are attributed to twins formed during deformation. TWIP steels are used in different industries such as transport and structural applications. These materials are subjected to different deformation degrees where high strain hardening occurs in the bulk material, but some tribocorrosion phenomena can affect the surface during processing or even in service.

The corrosion and tribochemical properties of TWIP steels (Fe25Mn2,5Al0.5Cr) with 0%, 20%, 50% and 85% of deformation were studied in this work. To study the corrosion properties in oxidizing and reducing media, a typical three electrode cell was used to carried out polarization curves in 1N H_2SO_4, 1M Na_2SO_4 and 3.5% NaCl. The passivation of the material can be controlled from the electrochemical and chemical variables. To study the influence of the chemistry, electrochemistry and the deformation degree on the tribocorrosion performance of TWIP steels, Pin on Disc tests were done using a 6mm Al_2O_3 ball. A normal load of 1N was applied during 1 hour. The employed media and electrochemical conditions were chosen from the electrochemical tests mentioned before, as well

as the cathodic and anodic potentials applied. Corrosion products formed on the surface change the COF behavior, as well as the evolution of the mechanical and electrochemical answer. These differences were also observed in the wear mechanisms found in the wear track examined by profilometry and SEM. From pin on disc tests, the wear rate was influenced by localized corrosion found in the TWIP steel evaluated, which was in turn affected by the deformation degree and the potential applied.

Effect of the Cashew Nut Shell Liquid on the Tribocorrosion Behavior of Passive and Active Alloys

C. Pino[1], A. Bermúdez-Castañeda[2], E. Klyatskina[2], V. Amigó[2], J. Esguerra-Arce[3], J. Urbano[1], C. Ayala-Garcia[4], O. Alvarez[5], A. Maranon[6], A. Porras[5], C. Hernandez[1]

(1) Mechanical Engineering, Escuela Colombiana de Ingeniería Julio Garavito, Bogota, Colombia (2) Instituto de Tecnología de Materiales (ITM), Universitat Politècnica de València, Valencia, Spain (3) CIMSER. Industrial Engineering, Escuela Colombiana de Ingeniería Julio Garavito, Bogota, Colombia (4) Department of Desing, Universidad de los Andes, Bogota, Colombia (5). Department of Chemical and Food Engineering, Universidad de los Andes, Bogota, Colombia (6). Department of Mechanical Engineering, Universidad de los Andes, Bogota, Colombia.

Over the last decades, the consumption of Cashew nut (*Anacardium occidentale*) has increased drastically due to its nutritional benefits and great taste. Additionally, its increasing demand is potentiated by the harnessing of its byproducts such as the Cashew Nut Shell Liquid (CNSL), an oily liquid extracted from the cashew nutshell which contains components appreciated by the chemical industry. This increase in the demand of the cashew has brought new challenges to the cashew industry because to extract the nut and CNSL, materials from the equipment (blades, extruders, and structural parts) are subject to mechanical action, such as: cyclic stresses, impact, slide and oscillating contact. Additionally, materials are exposed to corrosion phenomena, which is attributed to the contact with CNLS and cleaning solutions. This combined situation leads to a tribocorrosion phenomenon. Although, there are studies where the tribochemical properties of the stainless steel, aluminum alloys and mild steel have been evaluated in electrolytes with chlorides and oils independently [1–3], there are some particularities which are worth to look into.

In this scenario, CNSL which is composed by anacardic acid, cardanol, cardol and other minor components, in contact with cleaning substances results in an oily mixture that remains in contact with equipment parts. Chlorides, changes of the initial pH, and changes in the conductivity of the system were found. Therefore, this especial

environment can lead to differential aeration and galvanic cells in passive and active materials, respectively.

In this work the tribochemical behavior of stainless steel AISI 420, low carbon steel AISI 1012 and aluminum alloy 6061 was evaluated on mixtures of CNSL, ethanol and NaCl solution. Polarization curves were done to identify the corrosion performance of the alloys in the solution mentioned before, as well as in 3.5% NaCl. Tribocorrosion experiments were carried out using a ball on flat configuration in a Pin on Disc tribometer. A 6mm alumina ball was used, while 1N of normal load, and a frequency of 1Hz for 1 hour were applied. Wear tracks were exanimated by profilometry and SEM.

From the tests, lower coefficients of friction were found in systems with CNSL compared to tests performed in NaCl solution. However, the effect of chlorides species, in the passivity of the passive alloys, was not completely mitigated by the low mass transferred as it was expected, according to results from the electrochemical tests. In spite of this, an interesting mechanical accommodation of the system was found which could suggest a potential use for the CNSL as lubricant if it is chemically modified.

Acknowledgements

The authors wish to express their gratitude to Sistema General de Regalías, OCAD Fondo de Ciencia, Tecnología e Innovación FCTeI and Ministerio de Ciencia, Tecnología e Innovación which funded this research through the Project "Aprovechamiento de los subproductos Agroindustriales en la producción del marañón en el departamento del Vichada - BPIN 2020000100571"

References

[1] G. Rozing, V. Alar, V. Marušić, y I. Samardžić, "Tribocorrosion wear of austenitic and martensitic steels", *Metalurgija*, vol. 55, núm. 3, pp. 441–444, jul. 2016.
[2] Y. Sun y V. Rana, "Tribocorrosion behaviour of AISI 304 stainless steel in 0.5M NaCl solution", *Mater. Chem. Phys.*, vol. 129, núm. 1, pp. 138–147, sep. 2011, doi: 10.1016/j.matchemphys.2011.03.063.
[3] T. Gupta, B. Bhattacharjee, S. Mohanty, A. Acharjee, y P. Chakraborti, "Experimental Investigation of Tribo-Corrosive Nature of Biodiesel and its Effect on Lubricating System", *J. Bio- Tribo-Corros.*, vol. 6, núm. 4, p. 119, ago. 2020, doi: 10.1007/s40735-020-00416-0.

STUDY OF THE TRIBO-CORROSION BEHAVIOUR OF NICKEL ALUMINIUM BRONZE (NAB) AND MANGANESE ALUMINIUM BRONZE (MAB) IN MARINE ENVIRONMENTS

C.Berlanga-Labari1, A. Claver1, M.V. Biezma-Moraleda2, José F. Palacio3

1 Engineering Department, Institute for Advanced Materials and Mathematics (INAMAT2),
Public University of Navarre, Campus Arrosadía s/n, 31006 Pamplona, Spain; carlos.berlanga@unavarra.es
2 Departamento de Ciencia e Ingeniería del Terreno y de los Materiales; , Universidad de Cantabria, 39004 Santander, Spain;
3 Centre of Advanced Surface Engineering, AIN, Cordovilla, 31191 Pamplona, Spain; jfpalacio@ain.es

* Correspondence: carlos.berlanga@unavarra.es;

Subtopic –Tribocorrosion

Aluminium bronzes are alloys widely used in the marine sector due to their good combination of mechanical properties and corrosion resistance. So far, several studies have been carried out on the resistance to localised corrosion of aluminium bronzes (NABs) in marine environments, but very few in situations where appears friction, erosion and/or cavitation supported by corrosive environments.

In this work, the tribo-corrosion resistance of a nickel aluminium bronze and an aluiminium manganese bronze has been investigated both in the as-cast state and with different heat treatments. Firstly, both alloys have been microstructurally characterised by optical and electron microscopy (SEM) and by nanoindentation to define the particular phases.

The samples have been polished to a P1200 finish and tribocorrosion tests have been carried out using the pin-on-disk method in a Teflon cell with three electrodes connected to a potentiostat (Figure 1).

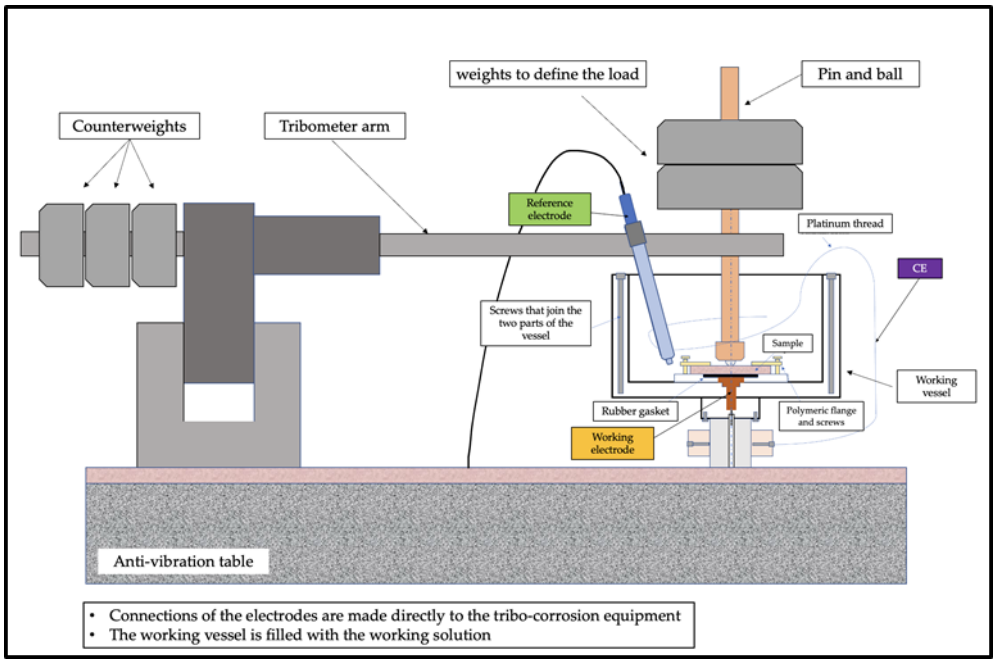

Figure 1. Diagram showing configuration of equipment for tribocorrosion tests.

Loads of 5 N and 10 N and three potentials: E=0V , E=-50V and E=-150V have been used in a simulated seawater. Under these conditions, open circuit potentials and coefficients of friction with time were recorded. Based on the ASTM G119 standard, the synergistic effect between friction and corrosion was examined. Finally, the wear rate was measured by measuring the wear track volume. Moroever, The corrosion erosion products were analysed using X-ray diffraction and XPS techniques.

Finally, all the results obtained have been analysed globally and related to the different microstructures of the NAB and MAB alloys and their effect on tribocorrosion behaviour pointing out the passive layer influence of both materials.

Effect of Wear on Corrosion Behavior of WC-based Cemented Carbide in Artificial Seawater

N. Ito[1], R. Yamamoto[1], K. Sugiyama[1],

H. Yakuwa[1], A. Ooi[2] and E. Tada[2]

1: Ebara Corporation, Japan

2: Tokyo Institute of Technology, Japan

Abstract

WC-based Cemented carbide is used as a wear-resistant material for slide bearings in pumps. When wear parts made of WC-based Cemented carbide are used in seawater containing silica sand, the WC-based Cemented carbide becomes thinner due to mechanical wear in addition to electrochemical corrosion. It is expected that the surface condition of WC-based Cemented carbide will change depending on wear conditions such as silica sand concentration and contact pressure, and the corrosion behavior of WC-based Cemented carbide will change. The purpose of this study is to clarify the corrosion behavior of WC-based Cemented carbide when silica sand concentration and contact pressure are varied.

A corrosion wear test was performed by pressing a WC-based Cemented carbide specimen against a SiC ring rotating at a sliding velocity of 2 m/s with a constant load while polarizing the specimen at 0.441 V vs. SSE in artificial seawater containing silica sand. The corrosion rate was evaluated from the current density flowing through the worn portion. As a result, the corrosion rate of the worn part was about 0.65 to 0.85 μm/h when the contact pressure was 5 MPa or higher in an environment with a silica sand concentration of 3000ppm. Under the environment of 100ppm silica sand concentration, the corrosion rate increased as the contact pressure increased in the range of 5 to 25 MPa. In environments with silica sand concentrations of 500 ppm and 1000 ppm, the corrosion rate increased with increasing contact pressure until the contact pressure reached 15 MPa. On the other hand, above 15 MPa, the corrosion rate reaches a constant value of 0.65 to 0.85 μm/h.

Under the conditions in which the corrosion rate increased with increasing contact pressure, flat spots and dents due to dissolution of WC were observed on the worn surface. On the other hand, under the condition where the current was constant regardless of the surface pressure, all the worn surfaces were flat. Under severe

wear conditions, the surface always became a new surface due to wear, and the corrosion rate due to electrochemical corrosion did not change depends on the location. On the other hand, in an environment with moderate wear, there were places where the new surface was not exposed. As the wear conditions became more severe, the new exposed surface area increased and the corrosion rate increased.

Phase Transformation and Tribocorrosion Characterization of Plasma Thermal Spray Coatings

Mutairi S. A Saudi Aramco, Dhahran/Saudi Arabia;sultan.mutairi.1@aramco.com

Rasheedi N. A Saudi Aramco, Dhahran/Saudi Arabia; nayif.rasheedi @aramco.com

Keywords: Tribocorrosion, Plasma, Thermal-spray, Micropowder, Nanopowder.

This research focuses on studying powder reactions and coating microstructure produced by spraying tungsten carbide cobalt powder at different particle sizes (micro and nano sizes). It presents the use of Plasma thermal spray method to perform a multi-layer coating on carbon steel specimens. Tribocorrosion, surface roughness measurement of the coating, its hardness assessment, and evaluation of coating porosity and adhesion were conducted to determine the coating characterization. The comparative metallographic results of the various test coatings are discussed. Results revealed that extent of phase transformation occurred more during the plasma thermal spray and more cobalt evaporation occurred during spraying the nano-sized powder. The use of nano-sized powders in the plasma spray system helped to lower the coating roughness while it increased the roughness when sprayed by HVOF system. The porosity was improved when the nano-sized powders were used, but the improvements were not significant. However, the higher percentage of nano-sized particles in the starting powder increased the hardness in the coatings

Influence of micro-arc oxidation on tribocorrosion behavior of Ti-5.5Al-4.5V-2Zr-1Mo alloy drill pipe under oil &gas drilling conditions

LIU Qiang[1], XIONG Mao-xian[2], ZHAO Mi-feng[2], YIN Hang[1], ZHANG Yi-ming[1], ZHU Guo-chuan[1], ZHANG Juan-tao[1]

[1]State Key Laboratory for Performance and Structural Safety of Petroleum Tubular Goods and Equipment Materials，CNPC Tubular Goods Research Institute，Xi'an，Shaanxi 710077

[2]Petroleum Engineering Institute，Tarim Oil field Company of CNPC，Kuerle 841000，Xinjiang，China

The tribo-electrochemical performance of a new Ti-5.5Al-4.5V-2Zr-1Mo alloy before and after micro-arc oxidation (MAO) treatment was accessed under reciprocating sliding conditions and controlled electrochemical conditions (-0.5 V, OCP and +0.5 V), the effect of different drilling fluid and electrode potential on the synergistic interaction between wear and corrosion of Ti-5.5Al-4.5V-2Zr-1Mo alloy after MAO treatment were deeply investigated and compared with the untreated samples. Results revealed that the fine porous, uneven, and multi-layer ceramic oxide layer with a thickness of 6μm were fabricated on the Ti-5.5Al-4.5V-2Zr-1Mo alloy after MAO treatment, which is mainly comprised of 34 % of anatase and 38.3 % of rutile. The MAO coating exhibited the higher hardness and adhesion strength than that of substrate, and significantly decreased the current densities of Ti-5.5Al-4.5V-2Zr-1Mo alloy both in the water–based drill fluid and oil–based drill fluid due to the higher passivation film resistance. Tribocorrosion experiments showed that MAO treatment can significantly reduce the coefficient of friction of Ti-5.5Al-4.5V-2Zr-1Mo alloy both in the water–based drill fluid and oil–based drill fluid, an obvious drop in potential values and large oscillations were observed when MAO coating slide in the water–based drill fluid, but that was not found in the oil-based drilling fluid. When sliding under different electrochemical conditions, depassivation-repassivation took place during sliding processes, the coefficient of friction and mass losses were both significantly decreased when tribocorrosion experiments performed at +0.5 VSCE anodic applied potential in water–based drill fluid, which was contributed to the lower friction coefficient, better stability and thicker thickness of repassivation oxide film on the surface of MAO treated alloy than that of substrate and at cathodic potential.

However, the tribo-electrochemical and wear behavior of MAO coating sliding in the oil–based drill fluid was independently of the electrochemical conditions applied, this is because there were not enough dissolution and oxidation environment in the oil-based drilling fluid to supplement the high-valence oxides lost during friction, the surface of the MAO layer was depassived and replaced by loose and porous metastable oxide, which are more likely to be worn out in tribocorrosion process, deeper and wider grooves, as well as a large number of delamination and debris, are generated by the synergistic interaction between wear and corrosion.

The work will provide profound insight and contribute detailed knowledge of the tribocorrosion behavior of Ti-5.5Al-4.5V-2Zr-1Mo alloy for prolonging the service life and reducing the failure accidents of titanium alloy drill pipe in ultra-deep well drilling conditions.

Subtopic –Tribocorrosion

Fretting Corrosion Investigation of Spinal Fixation System Materials

Philipp N. Keller[1], R.M. Hall[2], A.R. Beadling[1], M.G. Bryant[1]

[1]Institute of Functional Surfaces, School of Mechanical Engineering, University of Leeds, Leeds – UK

[2]Institute of Thermofluids, School of Mechanical Engineering, University of Leeds, Leeds – UK

Posterior spinal fixation systems, typically consisting of cobalt chromium and titanium alloy screw-rod assemblies, are modular metallic components widely used to treat spinal instability, traumatic spinal injuries, or spine deformity. However, evidence of fretting corrosion, often described as corrosion and wear, has been reported at the contact interfaces of modular components and linked to inflammation of surrounding spinal tissues, early surgical intervention and early unplanned implant removal[1]. This work aims to develop an in vitro model to assess the influence of simulated inflammatory (SI) conditions on the fretting corrosion behaviour as well as the associated tribomaterial and wear debris formation at the contact interface of clinically relevant materials.

In this study, a bespoke fretting tribometer with in situ corrosion measurement has been deployed to investigate fretting between low-carbon CoCrMo pins and Ti6Al4V discs, exploring the effects of SI environments. Tests included gross-slip fretting regimes over 6000 cycles. The addition of hydrogen peroxide (H_2O_2) assured representative SI conditions, imitating periprosthetic corrosive environments. An integrated 3-electrode cell enabled the corrosion performance assessment using a series of open circuit potential, linear polarisation resistance and potentiostatic polarisation measurements. The metallic volume loss from both pin and disc was assessed by employing Vertical Scanning Interferometry. The material transfer and the released wear debris were examined using Scanning Electron Microscopy and Energy Dispersive X-Ray analyses. Corrosion by-products were identified by Inductively Coupled Plasma-Mass Spectrometry.

The presence of H_2O_2 resulted in a decrease in the polarisation resistance along with an increase in the recorded corrosion current during fretting by approximately

sevenfold. Impaired passive layer recovery was observed in PBS+30 mM H_2O_2 solution. Furthermore, the total material loss due to wearing and corrosion tripled under SI conditions. However, similar tribological data in conjunction with the analysed wear scars indicated a greater contribution of corrosive degradation.

ACKNOWLEDGEMENTS: This project has received funding from the European Union's Horizon 2020 research and innovation programme under the Marie Skłodowska-Curie grant agreement No 812765.

REFERENCES

1. Keller, P.N., et al., *Tribology and Corrosion Engineering of Spinal Instrumentation Systems: A Systematic Literature Review*, in *5th International Conference on BioTribology*. 2021.

The influence of inflammation conditions on corrosion resistance and tribo-corrosion behavior of the new Ti-Nb-Sn alloys obtained by electrical resistance sintering

María Vinogradova, Universitat Politècnica de València, Valencia, Spain;
Elizaveta Klyatskina, Universitat Politècnica de València, Valencia, Spain;
Ángela Bermúdez Castañeda, Universitat Politècnica de València, Valencia, Spain;
Francisco Segovia, Universitat Politècnica de València, Valencia, Spain;
Vicente Amigó, Universitat Politècnica de València, Valencia, Spain.

Abstract

Nowadays, active research of new beta titanium alloy compositions is underway, as it has been found wide application in medicine including dental implantation. In this work the Ti-Nb-Sn powder metallurgical alloys were sintered by promising technique - electrical resistance sintering (ERS). The microstructure and mechanical properties of the alloys were obtained. The Ti-Nb-Sn alloys demonstrated their applicability as materials for dental implants. One of the main reasons for implant failure is a high risk of inflammation. It is known when inflammation and infection occur, the pH may decrease, or even peroxide formation may occur. In our research the influence of Sn in the corrosion and tribocorrosion properties in TiNb alloys was investigated. For electrochemical tests Hartmann-Ringer solution as well as H2SO4 3M were chosen as an electrolyte. The corrosion experiments showed a more active evolution of the TiNbSn over TiNb alloys, being clear in H2SO4 3M, as expected. Also, tribo-corrosion pin on disc tests were carried out to investigate the influence of the Sn presence in the tribochemical answer, materials were evaluated under OCP, and passive potential applied using a ball on flat configuration. Pin on disc experiments were performed using a 6mm Al2O3 ball, a normal load of 1N, a length movement of 68 m, during 60 minutes. Indeed, under the most acidic solution, the evaluated alloys showed differences in electrochemical behavior because of the strongest effect of the passivation and repassivation phenomena. Under the Hartman-Ringer solution, the material does not show big differences in the coefficient of friction for all the alloys, which showed that mainly electrochemistry governs the phenomenon and variation of wear rates. Wear tracks were characterized in order to identify the differences on the wear mechanisms produced by the composition of the alloys and the electrolytes.

Key words

Electrical resistance sintering, beta titanium alloys, Ti-Nb-Sn, electrochemical studies, corrosion behavior, tribo-corrosion, Hartmann-Ringer solution, biomedical application, dental implants

Subtopic

Corrosion, tribo-corrosion, and biomedical studies

Tribochemical behavior of beta and alpha+beta Titanium alloys in simulated saliva

E. S. Gouvêa [1], M. Vinogradova [1], A. Bermúdez-Castañeda [1], V. Amigó[1]

(1) Instituto de Tecnología de Materiales (ITM), Universitat Politècnica de València, Valencia, Spain.

Key words

Beta Titanium alloys, pin on disc, Ringer Hartmann solution, powder metallurgy, tribocorrosion, high entropy alloys

Abstract

Titanium (Ti) alloys have been widely used in biomedicine mainly for their high stiffness, corrosion resistance, and biocompatibility. Ti-6Al-4V is a Ti-α + β alloy, which is one of the most widely used metals as a biomaterial for the manufacture of orthopedic implants besides its elastic modulus which is very similar compared to bone (100 - 120GPa). [1,2] However, due to the cytotoxicity of Al and V, it is a material thatat very prolonged use can lead to diseases due to ions, metallic and oxidized particles release inside the human body. In consequence, stabilizer elements of β phase, such as: Nb and Mo have been used because their biocompatibility and low cytotoxicity. Moreover, Ti-β alloys provide a lower elastic modulus close to the bone (50 - 70GPa). [3]

In this work, the corrosion and tribocorrosion properties of a Ti-35Nb-6Mo alloy (Ti-β) were studied through electrochemical and tribochemical experiments. Samples materials were obtained from mechanically alloyed powders, sintered by ERS (Electrical Resistance Sintering) technique at a current intensity of 11 kA. Polarization curves were performed using a typical three electrode cell in Ringer's Hartmann solution. Likewise, pin on disc experiments were performed using a 6mm Al2O3 ball, a normal load of 1N, a

frequency of 60 Hz m, during 60 minutes under OCP and a passive potential. Results were compared with the Ti-6Al-4V alloy, Tiα + β, produced by forging and the same alloy, Ti-35Nb-6Mo, produced by casting. The microstructures were characterized by XRD, MEV and EBSD. Wear tracks were characterized by profilometry, optical microscopy and SEM. The results indicate that the coefficient of friction of the alloy produced by ERS has a slightly higher compared to the TiAl4V. However, the OCP values during the experiment show a more negative values, which means, a system with a faster passivation. By the other side, potential applied results, show similar coefficient of frictions even though current densities measured were higher for β alloys.

References

[1] Çaha, I., Alves, A. C., Chirico, C., Tsipas, S. A., Rodrigues, I. R., Pinto, A. M. P., Grandini, C. R., Rocha, L. A., Gordo, E., & Toptan, F. (2020). Interactions between wear and corrosion on cast and sintered Ti-12Nb alloy in comparison with the commercial Ti-6Al-4V alloy. Corrosion Science, 176. https://doi.org/10.1016/j.corsci.2020.108925

[2] Buciumeanu, M., Bagheri, A., Shamsaei, N., Thompson, S. M., Silva, F. S., & Henriques, B. (2018). Tribocorrosion behavior of additive manufactured Ti-6Al-4V biomedical alloy. Tribology International, 119, 381–388. https://doi.org/10.1016/j.triboint.2017.11.032

[3] Chen, L. Y., Cui, Y. W., & Zhang, L. C. (2020). Recent development in beta titanium alloys for biomedical applications. Metals, 10(9), 1–29. https://doi.org/10.3390/met10091139

Corrosion and tribocorrosion performance of additive manufactured CoCrMo produced by selective laser melting in simulated body fluids

M. Rodriguez Ripoll, AC2T research GmbH, Wiener Neustadt/Austria
R. M. Eder, AC2T research GmbH, Wiener Neustadt/Austria
T. Varadi, AC2T research GmbH, Wiener Neustadt/Austria
K. Koschatzky, AC2T research GmbH, Wiener Neustadt/Austria
C. Bauer, University for Continuing Education Krems, Krems/Austria
F. Franek, AC2T research GmbH, Wiener Neustadt/Austria
S. Nehrer, University for Continuing Education Krems, Krems/Austria

Additive Manufacturing (AM), also commonly known as 3D printing, is a group of processes used for building up components layer by layer, as opposed to conventional subtracting manufacturing technologies. AM allows the direct fabrication of functional parts with complex shapes from digital models and is particularly suitable for low production volumes and for geometrically complex components requiring high machining costs when conventionally produced. The AM concept perfectly suits to the needs of medical implants and prosthesis, which are unique from patient to patient, making AM a particularly suitable technique for producing custom-made personalized implants.

The additive manufactured CoCrMo specimens were manufactured using Laser Beam Melting. The microstructure of the as-printed samples is characterized using scanning electron microscopy accompanied by electron backscattered diffraction. Afterwards, the corrosion and tribocorrosion performance of the CoCrMo samples is investigated using a three-electrode electrochemical cell coupled to a nanotribometer. The experiments are performed under open circuit potential (OCP) and under potentiostatic conditions in phosphate buffered saline (PBS) with and without bovine serum albumin (BSA). Special emphasis is set in quantifying the synergistic effects between corrosion and wear and ion release during the tribocorrosion experiments. The tribocorrosion performance of additive manufactured CoCrMo is benchmarked against wrought CoCrMo in order to foresee the potential of additive manufactured CoCrMo as biomedical implants.

Prediction of tribocorrosion damage of CoCrMo biomedical implants from in-vivo electrochemical measurements

Y. Bao, A. Igual Munoz, B. M. Joles, S. Mischler

[1]Tribology and Interface Chemistry Group (TIC) École Polytechnique Fédérale de Lausanne. CH-1015 Lausanne, SWITZERLAND

[2]Swiss BioMotion Lab, Lausanne University Hospital and University of Lausanne (CHUV-UNIL), CH-1011 Lausanne, Switzerland

[3]Institute of Microengineering, Ecole Polytechnique Fédérale Lausanne (EPFL), CH-1015 Lausanne, Switzerland

*

Material degradation of CoCrMo alloys due to the combine action of wear and corrosion has been described by analytical models considering the main phenomena found in biomedical implants, mechanical wear, chemical wear or corrosion and lubrication. The established models allow not only for better understanding the involved mechanisms occurring in tribocorrosion but also for quantifying the overall material loss as a function of a certain mechanical (load, sliding velocity, geometry), material (hardness, young modulus, density), environmental (viscosity) and electrochemical (potential) parameters. In the present work, the prediction of chemical wear of implants will be quantified by using experimental data from in-vivo electrochemical measurements (in synovial fluid directly extracted from patients) and the analytical model describing the galvanic coupling between the worn and unworn areas. This combination of experiments carried out in-vivo and theoretical approach, has allowed to quantify and further understand the different degradation rates of the same biomedical alloy implanted in different patients.

Tribocorrosion

Correlation between corrosion, metal release and reliability for brass alloys in drinking water

Olivier Rod, RISE Research Institutes of Sweden
Charlotta Obitz, RISE Research Institutes of Sweden

The updated European directive on drinking water quality strengths the strict control of metal release into the water, with a large focus on lead release. This is an important issue for both traditional leaded alloys as well as newer low-lead or lead-free materials. At the same time, this directive solely considers the hygienic aspects of metal release, without considering the reliability and failure risks aspects. Both these aspects, metal release and failure risks, are closely related to corrosion mechanisms in different ways. There has been numerous testing and research works investigating in different ways the metal release from brass on one side, as well as on the failure mechanisms and on the corrosion mechanisms on another side. However, only few if any studies are presenting these different aspects together, to give a clear picture of how the different and failure modes. Increasing the understanding of these correlations and how they differ from each other would allow a more effective alloy further development.

Through this presentation, we explore the correlation between the corrosion mechanisms of different bras alloys in different conditions and on one side the metal release into drinking water and on the other side the failure modes. This evaluation is done both based on published results in the literature and investigations performed at RISE.

Assessment of the localized corrosion resistance of lean duplex stainless steel DX2202 in urban wastewater treatment plants

Audrey Allion, Aperam Research Center, Isbergues - France
Charles David, Aperam Stainless Europe, Isbergues – France
Benoit Emo, Véolia Water, Aubervilliers – France
Nicolas Larché, French Corrosion Institute, Brest - France

Subtopic –Corrosion & Corrosion Protection of Drinking Water Systems (WP20)

Austenitic stainless steel grades (e.g. EN 1.4307 / 304L and EN 1.4404 / 316L) are used as standard materials for the construction of urban wastewater treatment plants (WWTP) due to their good corrosion resistance and ease to shape and weld. Usually, environmental parameters such as chloride content does not present major issues for these austenitic grades. However, in certain conditions, facility location or season, corrosiveness of the environment may increase drastically requiring more corrosion resistant alloys such as duplex stainless steel grade DX2205 (EN 1.4462). Considering a lower alloying cost, a good corrosion resistance and higher mechanical properties, the more recently developed lean duplex stainless steel (EN 1.4062 / DX2202) can be a good alternative to the commonly used austenitic grade (316 L) but is still too rarely chosen probably due to limited case studies.

The present study deals with the pitting corrosion performances of lean duplex DX2202 through pitting potential in solution simulating pre-treatment water units. Pitting potential tests were adapted from standard electrochemical test methods ASTM G150 and ASTM G61 to assess critical pitting temperature (CPT) and pitting potential (PP) respectively. Chloride content, pH and temperature parameters were selected to be representative of the environments that can be encountered in wastewater pre-treatment units. Critical pitting temperature was determined in solutions with chloride contents from 200 to 3000ppm. Pitting potentials were assessed in electrolytes containing also chloride concentrations from 200 to 3000ppm, at 35°C and 50°C. All these tests were also performed on the austenitic 316L and the duplex DX2205 for comparison.

The results permit to have an overview of corrosion properties according to temperature and chloride content and to choose properly the most appropriate stainless steel grade for urban wastewater treatment units. This study permits also to have a clearer view of the behavior of duplex stainless steel grades versus austenitic grades in such environments. It confirms that lean duplex DX2202 can be used as alternative to the austenitic 316L.

"Grabenkorrosion": A historic scientific debate to the solution, still modern failures

J.W. Erning, BAM, Berlin

In the late 1980s, a new type of corrosion appeared in drinking water installations where galvanized steel pipes failed forming a deep groove with no corrosion at the other surfaces. The reason was discussed quite fiercely between failure analysts and material suppliers. In the end the discussion lead to the solution: inductive welded pipes of a certain sulphur content were prone to selective corrosion. The history of the arguments is discussed using old communications between Wilhelm Schwenk and Wolfgang Stichel, who later published the results in a paper unfortunately only I german.
Thus the knowledge got lost and new cases based on the same material problems are observed in application of so-called C-Steel piping systems. Failure cases are shown.

Monitoring air pollution at the Musée des Arts Décoratifs : an example of low-cost corrosion RFID sensor application

Stéphane Rioual[1], Benoit Lescop[1], Catherine Didelot[2], François Mirambet[3], Diane Baustert[3], Juliette Remy[3], Johan Becker[4] and Dominique Thierry[5]

[1]Univ Brest, Lab-STICC, CNRS, UMR 6285, F-29200 Brest, France

[2]Musée Des Arts Décoratifs, 107 rue de Rivoli, 75001 Paris, France

[3]Centre de Recherche et de Restauration des Musées de France (C2RMF), Paris, France; Chimie-ParisTech, PSL Research University, CNRS, Institut de Recherche de Chimie de Paris (IRCP), Paris, France

[4]French Corrosion Institute (RISE), Brest, France

[5]RISE, Isafjordgatan 28A, 16440 Kista, Sweden

Air pollution monitoring is of crucial interest for conservation and protection of historical artifacts in indoor environments. Indeed, gaseous pollutants in air are responsible of the degradation of many types of objects and materials. They are of diverse natures (organic acids, H_2S, NH_3, SO_2, NO_2 …) and are produced either internally in the building where are localized artifacts or externally due to outdoor pollution. Some devices dedicated to the monitoring of air quality exist and may be applied for cultural heritage conservation. These include the use of sampling techniques or gas sensors. An alternative to these methods is to consider the development of dosimeters based on the chemical reactivity of metallic surfaces with these pollutants. This cumulative monitoring method based on coupons has been applied in numerous cases to define air quality or corrosivity index [1,2]. More recently, the electrical resistance (ER) method was demonstrated to be an effective tool to monitor the air corrosivity. In this case, the sensitive part of the sensor is constituted by a thin copper or silver metal track produced by physical vapor deposition and sensitive to pollutants. From the change in geometry of this metallic element (i.e., thinning) induced by corrosion, it is possible to measure the corrosion rate in real time and hence the corrosivity class [3]. Despite the interest of the method, its cost limits the number of potential applications. Recently, the development of RFID (RadioFrequency IDentification) corrosion sensors was shown to be an innovative solution for the realization of similar sensors but with ultra-low

cost and low visual nuisance. The principle of the method is based on an RFID tag which electromagnetically interacts with a thin conductive metallic sensitive layer. Similarly to the ER method, the variation of the electrical resistance of this sensitive layer modifies this interaction leading to some information on its corrosion and on the air quality [4]. The principle of these sensors and recent achievements will be detailed through an application at the Musée des Arts Décoratifs (Paris). Moreover, as it will be shown, combining sensor's results with subsequent surface analysis of the sensitive part of the layer after exposure by X-Ray Photoelectron Spectroscopy unambiguously help to identify the origin of the pollution.

References

1. Sacchi E, Muller C. Air quality monitoring at historic sites. ASHRAE J. 2005;47:40–6.

2. ISO 11844-1. Corrosion of metals and alloys—classification of low corrosivity of indoor atmospheres—Part 1: determination and estimation of indoor corrosivity. Genève: International Organization of Standardization; 2006.

3. Prosek T, Taube M, Dubois F, Thierry D. Application of automated electrical resistance sensors for measurement of corrosion rate of copper, bronze and iron in model indoor atmospheres containing short-chain volatile carboxylic acids. Corros Sci. 2014;87:376–82.

4. Rioual S, Lescop B, Pellé J, De Alkmim Radicchi G, Chaumat G, Bruni MD, Becker J, Thierry D. Development of low-cost RFID sensors dedicated to air pollution monitoring for preventive conservation. Heritage Science 2022; 10; 124.

How microorganisms can preserve metal structures

R Basséguy[a], MJF Marques[a,b]

a. Laboratoire de Génie Chimique, Université de Toulouse, CNRS, INPT, UPS, Toulouse, France

b. LMR – Laboratório de Materiais e Revestimentos, LNEG – Laboratório Nacional de Energia e Geologia, Lisboa/Portugal

In the anticorrosion domain, Nature is a fruitful provider of new concepts for green solutions and in this context, the recognition that microorganisms do not only accelerate corrosion but also can inhibit or protect against corrosion [1] has led to suggest microbial-based solutions for metal corrosion inhibition. In particular, biomineralization process on the surface of materials such as stones, concrete and various metals (especially steel), was recently regarded as a potential new and environmentally friendly approach to produce protective layers [2-6]. The objective of this presentation, is to show through two case studies what are the techniques and methodologies that can be used to study the impact of micro-organisms and the synergistic effect between micro-organisms and other environmental parameters in the biomineralization process.

The first case study deals with the formation of vivianite (iron (II) phosphate) on carbon steel in presence of *Geobacter sulfurreducens*, an iron reducing bacteria [4]. A thermodynamic analysis showed the importance of physical-chemical parameters such as redox potential and chemicals' concentration on the vivianite precipitation. In solution containing phosphate species, the high availability of Fe(II) ions, produced by the bacteria that reduce Fe(III), promotes the formation of a vivianite layer. This phosphate layer is believed to be formed by the combination of decreasing the redox potential in the solution and the direct electron transfer between bacteria and corrosion products.

The second case concerns the formation of a protective layer on Al-Mg alloy surface during its immersion in marine environment [5,6]. Work, carried out at three different scales (field, semi-field and laboratory), concludes that marine microbial activity has a significant effect on the evolution of the Al-Mg surface from the early stages of

exposure. This leads to the development of a protective compact layer, which thickness and nature depend on immersion time and exposure zone. In the MICOATEC French project (ANR-19-CE08-0018), the natural protection phenomena developed during the interaction process between living organisms and the metal surface is envisaged as a novel vision to develop anticorrosion solutions. These two examples can also serve as a basis for discussing and evaluating biomineralization applied to conservation and restoration of heritage artefacts.

[1] N. Kip, J. A van Veen, *The dual role of microbes in corrosion*. The ISME Journal (2015) 9, 542–551 ; doi:10.1038/ismej.2014.169

[2] T. Liu, Z. Guo, Z. Zeng, N. Guo, Y. Lei, T. Liu, S. Sun, X. Chang, Y. Yin, X. Wang, *Marine bacteria provide lasting anticorrosion activity for steel via biofilm-induced mineralization.* ACS Appl. Mater. Interfaces 2018, 10, 40317−40327; doi: 10.1021/acsami.8b14991

[3] L. Comensoli, M. Albini, W. Kooli, J. Maillard, T. Lombardo, P. Junier, E. Joseph, *Investigation of Biogenic Passivating Layers on Corroded Iron*. Materials 2020, 13, 1176; doi:10.3390/ma13051176

[4] C. Cote, O. Rosas, R. Basseguy, *Geobacter sulfurreducens: An iron reducing bacterium that can protect carbon steel against corrosion?* Corrosion Science, 94 (2015) 104–113; dx.doi.org/10.1016/j.corsci.2015.01.044

[5] M.J.F. Marques, A. Benedetti, F. Castelli, M. Delucchi, M. Faimali, S. Delsante, F. Valenza, F. Garaventa, G. Pavanello, R. Basseguy, *Influence of natural seawater variables on the corrosion behaviour of aluminium-magnesium alloy.* Bioelectrochemistry 149 (2023) 108321, doi.org/10.1016/j.bioelechem.2022.108321

[6] J. Jaume, M.J.F. Marques, M.L. Délia, R. Basséguy, *Surface Modification of 5083 Aluminum-Magnesium Induced by Marine Microorganisms.* Corrosion Science 2021, 109934 ; doi.org/10.1016/j.corsci.2021.109934.

Stabilization treatment of very corroded ancient Al-Cu alloys: the wreck of Antoine de Saint Exupéry's aircraft

François MIRAMBET, C2RMF, Louvre, Paris/France
Agnès PARIS-MIRAMBET, Air and Space Museum, Le Bourget/France
Emmanuel ROCCA, Institut Jean Lamour – Université de Lorraine, Nancy/France

An increasing number of aluminums made materials are nowadays registered in museum collections especially in technical museums like Air and Space museums but also in modern art collections.

Their conservation is a challenge for the curators and conservators since the aluminum surface can undergo important corrosion processes, especially, the Al–Cu alloys used as structural materials in aircrafts, which are very sensitive to atmospheric corrosion.

Among the various materials preserved in the French Air and Space museum of Le Bourget, the remains of the Lockheed P38 lightning of Antoine de Saint-Exupéry, discovered in 2003, near the Ile of Riou, at the south of the Marseille town (France), are conserved in the storage rooms of the French Air and Space museum of Le Bourget: the left landing gear strut in aluminum alloys (Figure 1a) and some elements of fuselage, especially some aluminum riveted structures (Figure 1b).

The objective of this study is to stabilize the surface without changing the surface aspect and try to conserve the traces of the stay in seawater during about 60 years such as marine concretions.

Firstly, a microstructural analysis of of the Al-Cu alloys corroded parts in were carried out, especially the microstructure of the deep pitting phenomenon by electronic microscopy and X-ray diffraction. The goal is to evaluate the risk of corrosion resumption during future exhibitions scheduled in other Air and Space museums.

Then, a corrosion inhibiting treatment was set-up to stabilize the surface layers and the electrochemical activity of the different metals. In the case of aluminum parts, electrochemical tests were performed to evaluate the efficiency of the treatment on mock-ups and also on real corroded parts.

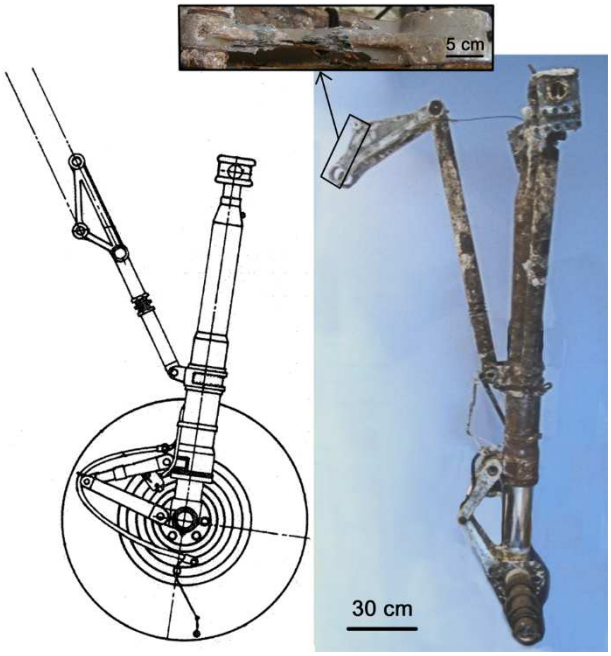

a)

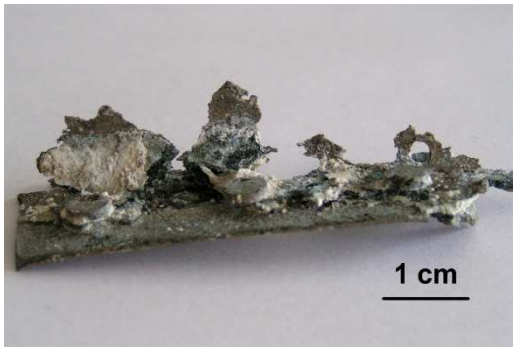

b)

Figure 1: Macroscopic photo of (a) the landing gear leg of Lockheed P38 Lightning of St Exupéry, corresponding to initial plan, and (b) part in corroded fuselage in 24S alloy

This simple chemical conversion treatment allowed both to inhibit the electrochemical activity of the different metals, especially the deep pits and the Cu-enriched surfaces, and to reduce the risk of water uptake of $Al(OH)_3$-enriched corrosion layer during possible cyclic conditions of exposition.

The phenomenon of “Arsenification”: the oldest intentional metal surface alteration

Giorgia Ghiara[1,2], Marianne Mödlinger[2,3], Elyse Canosa[4], Angelica Salanitro[1], Pietro Manfrinetti[4], Marei Hacke[4], Stefano Trasatti[1]

[1] Università degli Studi di Milano, Milan/Italy

[2] Universität Salzburg, Salzburg/Austria

[3] Università degli Studi di Genova, Genoa/Italy

[4] Swedish National Heritage Board, Visby/Sweden

Some of the Late Bronze Age daggers found in the cemeteries in Koban and Chmi and today held in the Natural History Museum of Vienna, Austria, show some very peculiar surface features: though made of tin-bronze (blade) and arsenical bronze (hilt), the hilts often have a silvery surface, which cannot be traced back to any form of silvering. Similar features were noted also on other arsenical bronzes, mainly daggers and swords, from the Iberian Peninsula and, rarely, from elsewhere in Europe. It was usually assumed that this phenomenon is related to the long deposition in the ground and/or to “inverse segregation”, i.e. arsenic sweat during casting. From a preliminary characterization of specimens from Bronze Age daggers it was possible to attribute the silvery surface to the formation of Cu_3As (γ-phase). The reason for the silvery color could lay in: i) intentional patination by prehistoric craftsmen as a specific treatment of the bronze after deformation and polishing; ii) the result of unintended later reactions after the deposition of the objects in the soil.

In this study we want to prove the feasibility of artificially induced formation of Cu_3As (γ-phase) on the surface of new arsenical copper by comparing the results to archaeological arsenical copper artifacts with silvery surfaces. To achieve this goal a specific Design of Experiment (DoE) was carried out, focusing on the most important parameters that could induce an intentional alteration of the surface. CuAs replicas of different composition (6, 8, 10 wt.%) and thermomechanical treatments (as-cast, cold rolled, recrystallized) were immersed to different aggressive environments for a total of 90 days to trigger the formation of Cu_3As. The sample's surface and matrix were investigated through spectroscopic analyses as SEM-EDXS, XRD, colorimetry measurements and classical metallographic techniques (LOM). Results show that the noted “arsenification” predates any other chemical surface alteration of one metal or

metalloid with another (such as tinning, silvering, or gilding) and can be considered the first intentional change of color of an alloy, leaving aside patination.

New insights in atmospheric corrosion monitoring of outdoor bronze artworks

L. Es Sebar, L. Iannucci, S. Grassini, E. Angelini

[1] Department of Applied Science and Technology, Politecnico di Torino, Corso Duca degli Abruzzi 24, Torino

The study of the degradation phenomena affecting bronze artworks exposed to atmospheric corrosion is fundamental in order to develop tailored preventive conservation strategies. Indeed, the characterization of the corrosion products grown on the metallic surface and the assessment of the atmospheric and microclimatic parameters affecting the material/environment interaction allows for obtaining important information on the conservation state of the artworks and on the strategies to be implemented to ensure their long-lasting safeguard.

This work presents, in particular, the results of the in-situ monitoring campaign carried out on several bronze artworks which are part of the Gori Art Collection, a private collection of environmental art exhibited outdoors at the Fattoria di Celle, Santomato (Pistoia, Italy). The campaign, which started in 2019 and is still in progress, is carried out by employing multiple portable analytical techniques. Electrochemical Impedance Spectroscopy (EIS) is employed to study the corrosion processes that are affecting the metallic artworks; X-rays fluorescence (XRF) and Raman Spectroscopy are employed for chemical and microstructural characterizations of the corrosion products layers. Finally, a 3D photogrammetry survey is carried out to create a complete documentation of the artworks.

At a first visual examination, the bronze artworks showed different corrosion morphologies correlated to the different exposure conditions to atmospheric agents; phenomena of galvanic corrosion resulting from the coupling between the bronze artworks and the steel grips used for their positioning have also been observed. EIS, XRF, and Raman spectroscopy made it possible to determine the composition of the metallic alloys and the corrosion products grown on the different decorative elements, as well as to assess the electrochemical behaviour and the protective effectiveness of the corrosion patinas. Moreover, it was possible to highlight the surfaces that were more exposed to the aggressive agents present in the atmosphere and to the washing action of the rain. In fact, these environmental factors induced the formation of reactive corrosion products and selective degradation of the protective coating previously applied on the metallic surface. The collected data were employed by conservators to tailor their actions, paying particular attention to the areas identified to be at risk.

The results of the in-situ monitoring campaign obtained till now will be presented and discussed, highlighting the advantages of the proposed approach, and discussing the challenges still open in the development of tailored safeguard methodologies for outdoor bronze artifacts.

Preliminary Results on Multimodal Imaging Analyses of Undisturbed Archaeological Iron Artefacts

Ocson Cocen[1], Elodie Granget[1], Mahdieh Shakoorioskooie[2], Qianru Zhan[2], David Mannes[2], Anders Kaestner[2], Laura Brambilla[1]

[1)] Haute École Arc Conservation-restauration, HES-SO University of Applied Sciences and Arts Western Switzerland, 2000 Neuchâtel, Switzerland

[2)] Laboratory for Neutron Scattering and Imaging, Paul Scherrer Institute, 5232 Villigen, Switzerland

CORINT is a Swiss National Science Fund (SNSF) sinergia project aiming at elucidating corrosion of iron in various porous media using new quantitative multimodal in-situ tomography (further information: link). Part of this study focuses on realizing a comprehensive investigation of undisturbed archaeological iron artefacts while still in their burial environment, i.e. soil. As of today, capturing an extensive profile of the corrosion condition of both the artefact and its burial environment is still a challenge. Many corrosion investigations are performed only after removal of the burial media. Accordingly, some key points to fully represent the corrosion state when the artefact was still buried might be unwittingly overlooked. The nature of the iron corrosion products is much influenced by the environment in which they formed, and can evolve when exposed to new environments post- excavation.

In- and ex-situ analyses are coupled in this study to depict the corrosion state of undisturbed archaeological iron artefacts found in the Roman archaeological site of Aventicum, Avenches, Switzerland. Using a cylindrical aluminum shell, the undisturbed artefacts together with the surrounding soil was extracted from a bigger soil bloc excavated from the archaeological site. In-situ investigations on the whole aluminum shell and object inside were performed by means of neutron and X-Ray multimodal imaging in NEUTRA radiography facility at SINQ of PSI. The multimodal imaging results were confirmed through multiple ex-situ analyses on the archaeological objects, such as optical microscope, SEM-EDX, XRF, and Raman spectroscopy.

Characteristic attenuation coefficients of commercially available and/or synthesized corrosion products of iron are used as reference to identify and localize various iron

compounds in the archaeological iron objects. A similar approach is used to characterize the attenuation coefficients of various soils of Aventicum sites. Neutron and X-Rays have different sensitivities to different elements, hence, are complementary. Tomography techniques take multiple 2D images while rotating the sample in angular range of 180°, therefore, enable 3D image reconstruction of the object also high-resolution spatial distinguishment of layered corrosion products and soil constituents. Based on the preliminary characterization, goethite and lepidocrocite were found in the nails.

This ongoing study is being performed until 2026 with the SNSF grant number 20588.

Corrosion of a Roman iron ring, or how to understand the corrosion history of an object from its conservation state.

Valentina Valbi[1], Delphine Neff[2], Philippe Dillmann[2], Fabio Furcas[3], Ueli Angst[3], Myriam Krieg[4], Anika Duvauchelle[4], Marion Berranger[1], Stefano Mischler[5], Laura Brambilla[6], Naima Gutknecht[6], Christian Degrigny[6]

[1] Laboratoire Métallurgies et Cultures (LMC-IRAMAT-UMR7065-CNRS), Université Technologique de Belfort-Montbéliard, Belfort, France

[2] Laboratoire Archéomatériaux et Prévision de l'Altération (LAPA-IRAMAT-UMR7065-CNRS), Université Paris-Saclay, CEA Paris-Saclay, Gif-sur-Yvette, France

[3] Durability of Engineering Materials, ETH Zurich, Switzerland

[4] Site et Musée romains d'Avenches (SMRA), Avenches, Switzerland

[5] Tribology and Interfacial Chemistry (TIC), EPFL, Lausanne, Switzerland

[6] Haute Ecole Arc Conservation-restauration / HES-SO, Neuchâtel, Switzerland

In the frame of the MetalPAT project, the conservation conditions of several ancient metallic objects were assessed. An iron signet-ring from the Roman site of Avenches (CH) presented a specific morphology with a curved surface attributable to a corrosion-driven deformation. A transdisciplinary collaboration was necessary to understand the corrosion mechanisms that lead to this deformation. First, a non-invasive characterization (X-Ray tomography, SEM-EDS, µ-Raman spectroscopy) was carried out. A silver metal leaf covered with iron oxides and oxyhydroxides was identified on top of the ring, and a cavity underneath the silver leaf was observed. A certain number of questions could thus be answered and a first hypothesis regarding the genesis of the deformation was elaborated. The object was then mounted in resin, cut in a half and polished. Optical microscopy, electronic microscopy (SEM-EDS) and µ-Raman spectroscopy were performed in cross-section in order to better observe the morphology of the corrosion products and determine their composition. Iron oxides, oxyhydroxides and carbonates were identified in the cavity underneath the silver leaf. A marbled corrosion composed of iron oxides and oxyhydroxides was also observed on the sides and bottom of the object. The morphology and nature of the corrosion products suggest that a phenomenon of crevice corrosion, favored by the occluded slit between the original iron surface and the silver leaf, together with an osmotic pressure, might explain the deformation of the surface of the object.

120 years submersed: marine corrosion of the steamer's wreck *Liban* (Marseille, France)

Justine Vernet[1], Marine Bayle[2], Clémentine Caubisens[2], Jean-Bernard Memet[2], Eddy Foy[1], Jean-Paul Gallien[1], Laurent Urios[3], Lila Reboul[4], Nathalie Huet[4], Philippe Dillmann[1], Florence Mercier[1].

[1]NIMBE-LAPA CEA Saclay-CNRS (UMR 3685), Gif-Sur-Yvette, France
[2]A-CORROS Expertise, Arles, France
[3]IPREM CNRS-UPPA (UMR 5254), Pau, France
[4]DRASSM Ministère de la Culture, Marseille, France

Despite being well known from recreational divers, historical shipwrecks from the end of the 18th to the 20th century has been given little attention by academics, leading to severe looting and degradation. Beyond the loss of our modern cultural heritage, the collapse of these structures also provokes the release of polluting compounds, e.g. oil, toxic compounds from chemical weapons, with drastic consequences for the marine environment.

These last decades, conservative strategies have been proposed to preserve metallic-hulled historical shipwrecks. In particular, the implementation of Cathodic Protection (CP) have been tested on aging structures but its application on bio-colonized and corroded structures remains a real scientific and technical challenge. In literature, only global in situ studies on wrecks have been carried out (measurements of electrochemical potentials, corrosion rates) and fine characterization of wrecks corrosion systems have not been performed yet. Thus, the project *Save Our Shipwrecks* (SOS) proposes a complementarity approach of global measures on two shipwrecks with a multiscale characterization of the system wreck-corrosion-environment in order to install CP on two test shipwrecks.

The *Liban* is a steamer wreck lying off the Marseille bay in France, built in 1882, that sunk in 1903 due to its collision with another transport ship. In spite of its high historical value in terms of naval construction and, no historical study, nor a description of its state of conservation.

This work aims to present the first conservation diagnostic carried out on the shipwreck *Liban*. A multi-scale methodology including both in-situ and laboratory characterization from the macroscopic to the nanometric scale, has been applied in order to draw up a complete state of conservation of the wreck:

1. Global on-site measurements of electrochemical corrosion potential and metal residual thickness with the prototype Triton©;
2. Determination of corrosion profiles from the metal core to the superficial concretion layers;
3. Biodiversity analysis on historic samples and surrounding environment;
4. Electrochemical tests on each corrosion layer (OCP, chronoamperometry);
5. Quantification of pollutants trapped by sediments located close to the shipwreck.

A comparative study with the *HMS Daffodil* (Dieppe, English Channel) is also proposed.

MODIFIED TANNATE COATINGS FOR IRON ARTEFACTS

Roman Košťúr and Matilda Zemanová, STU in Bratislava, Faculty of Chemical and Food Technology, Institute of Inorganic Technology and Materials, Bratislava/Slovakia

Conversion coatings based on tannic acid belong to basic procedures in a protection of iron artefacts against corrosion. The procedure consists in modification of iron corrosion layers forming protective barrier. It is usually connected with using of top protective layer (waxes, oils etc.) to ensure protection against humidity. The project deals with a modification of the tannate conversion coating to enhance corrosion protection. The modification of the coatings was realized by addition of hydrotalcite. Hydrotalcites are environmentally friendly, ionic clays, with anion-exchange ability, which is desirable for corrosion protection of metals.

Application of the modified coatings was performed by dipping technique on pre-treated iron samples with thin layer of corrosion products in 2 layers with curing time 24 hours. Influence of dipping time on the quality of the modified tannate coatings was studied as well. The specimens were characterized and tested against corrosion. Corrosion behaviour of the specimens was studied by electrochemical measurements in ASTM D1384-87 solution[1]. It was found that influence of dipping time is neglectable. On the other hand, growing addition of hydrotalcite in the tannate coatings increases the protective properties of the studied specimens.

Acknowledgements

This research has been supported by a grant from the Scientific Grant Agency of the Ministry of Education, Science, Research and Sport of the Slovak Republic and the Slovak Academy of Sciences (VEGA) under the contract number VEGA 1/0747/21 and STU Grant scheme for Support of Young Researchers

References

1. Rocca E., Faiz H., Dillmann P., Neff D., Mirambet F.: Electrochim. Acta *316*, 219 (2019).

Restoration of a demonstration model of a single-cylinder steam engine with Rider valve gear

Jan Růžička, National Technical Museum, Prague, Czech Republic

Objectives

The goal of the project was to restore a damaged, defunct steam engine model so that it can be used for its original purpose, i.e., as a manually driven demonstration model. The engine is part of the collections of the National Technical Museum in Prague, Czech Republic. An essential aspect of the intervention was to fully preserve the item's wear and tear and the surface finishes, so as to reflect the 150 years of its existence (Fig. 1).

This is why a thorough examination of the surface treatments was performed using FTIR spectroscopy (Fig. 2). XRF spectroscopy was employed to determine the composition of preserved parts made of non-iron metal alloys in order to select appropriate materials in manufacturing the missing parts.

New results

The cleaning procedure involved the removal of dust deposits, residual lubricants and degraded conservation layers. An innovative laser cleaning technology was used to remove iron corrosion products (Fig. 3). This method is highly precise and poses minimal risk of damaging the surface finish adjacent to the treated spot.

All missing parts were replaced by copies manufactured according to preserved models or spatial analogies being fully reversible. Besides traditional methods such as manual processing and machining (Fig. 4), water jet cutting was used in manufacturing the bronze eccentric strap and steel eccentric rod.

Conclusions

After the restoration, conservation treatment was applied and appropriate guidelines for storage and operation were determined. The item has since been used for live public demonstration at the University of Chemistry and Technology Prague Open day in 2019 at the Czech European Researchers' Night in 2021.

Significance of the work

Experimental varnish B-Impact with a fluoropolymer base was applied to the cast iron back cylinder cover, with the aim to compare its long-term properties with the commonly employed acrylic options.

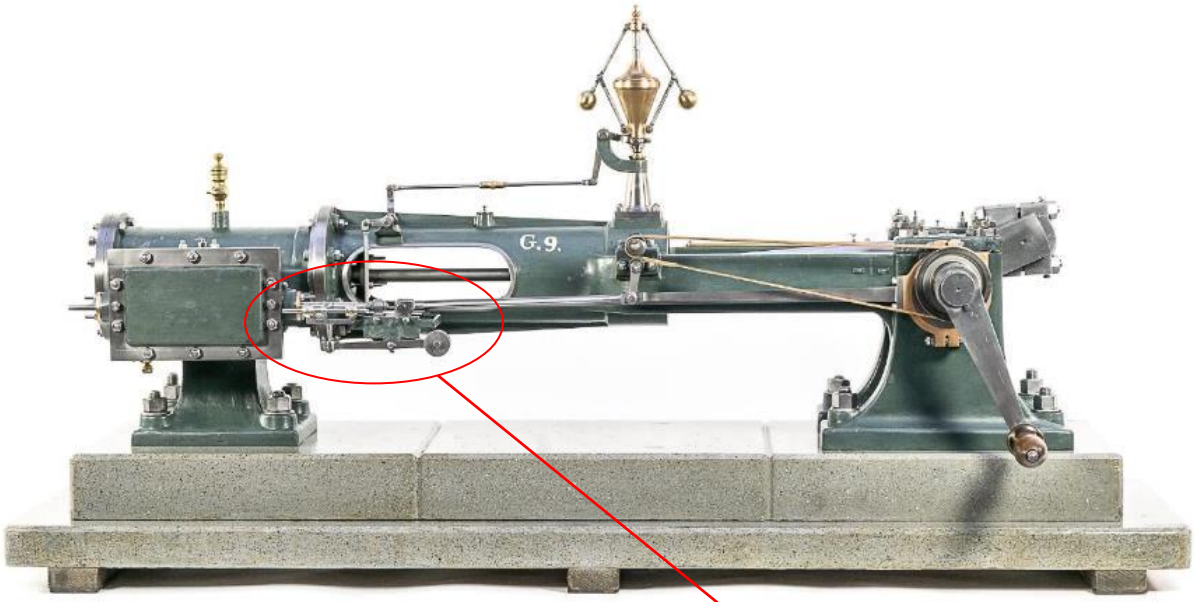

Fig. 1 Single-cylinder steam engine model with expansion Rider valve gear, Porter centrifugal governor and bored-out crosshead guide after restoration-conservation

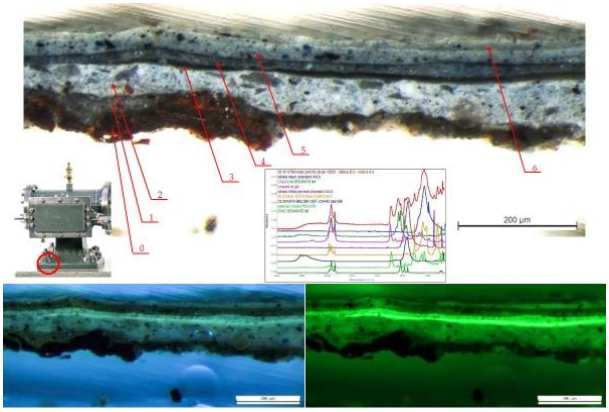

Fig. 2 Cross section of the surface finishes in visible and UV light

Fig. 3 Iron corrosion products removal using cleaning laser

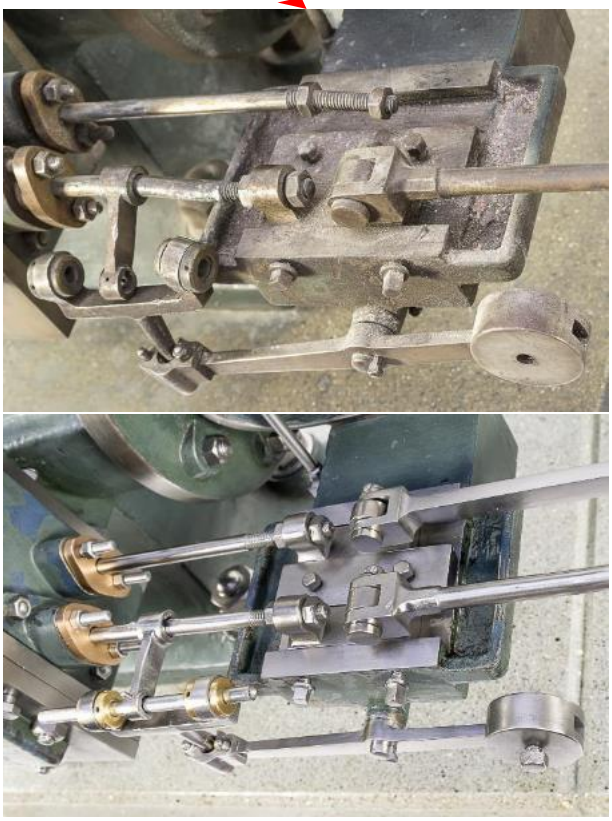

Fig. 4 Slide valve control before and after restoration-conservation: cleaning, corrosion products removal, missing parts supplementation, straightening, conservation, lubrication

Challenges for environmental corrosion protection systems in aerospace applications

Martin Beneke, Airbus Operations GmbH, Bremen/Germany

The European aerospace industry is about to make the biggest change in history for the entire anti-corrosion system when the REACH regulation for chromate replacement comes into force. The REACH (Registration, Evaluation, Authorization and Restriction of Chemicals) regulation is a European Union (EU) legislation that aims to improve the protection of human health and the environment from risks associated with chemicals.

This is a technical challenge for all involved companies, as not only one process or product is affected. Replacement is required for various treatment processes such as anodizing, conversion coatings and passivation's, but also for primers, sealants, greases and other products.

The lecture gives an overview of various technical topics for the replacement of affected processes and products for corrosion protection, but also an understanding of the necessary compatibilities of the new developments. In a second part, the presentation will deal with the simplified question to distinguish what is good or bad and what is sufficient?

The protection concepts developed over decades often go beyond the requirements and hidden properties and functions are not addressed or covered by specifications that were also implemented decades ago.

Research is needed to identify the features of the new replacement and compare the functionalities to the old systems.

A parallel task is to develop suitable test conditions and adapt the requirements to the needs of the application. As a simple example, the majority of corrosion tests used today are performed under static conditions in terms of temperature and humidity and do not cover the real operating and in in-service conditions.

Measurement of Environment and Corrosivity to Characterize Severity for Aerospace Applications

Fritz Friedersdorf, Liam Agnew, Brandi Clark, Rebecca Marshall, Kevin Farinholt,
Luna Labs USA, LLC, Charlottesville Virginia, USA

Reliability and maintainability are critical to the availability and operation of aircraft. One of the biggest threats to availability is corrosion of aircraft systems. The impact of corrosion is managed, in part, through routine schedule-based inspections and maintenance. Current classifications of environment severity that utilize location severity categories do not capture the influence of microclimate conditions within the airframe, operations, weather events, and climate change that are needed to improved individual aircraft and fleet corrosion management. Measurement and monitoring of base environments and microclimate severity within aircraft structures may improve preventative maintenance practices.

Testing has been conducted at multiple geographic locations and in conditions that simulate aircraft structures. The objectives of this investigation are to quantify environmental severity, compare corrosion rates of different materials, and determine relationships between ambient environment and conditions within a structure. Outdoor testing has been performed at four Continental US costal locations. The materials tested were aluminum alloy AA7075-T6 free corrosion and galvanic corrosion of AA7075-T6/A286 stainless steel, AA7075-T6/Ti-6Al-4V, 7075-T6/carbon fiber reinforced polymer (CFRP). Simulated aircraft structure (SAS) boxes were used to shelter sensing devices and coupons at one site (Figure-Left). The environment and corrosivity monitoring devices include measurements of temperature, humidity, conductance (a proxy for salt contaminant loading), and free and galvanic corrosion (Figure-Right). National Oceanic and Atmospheric Administration (NOAA) weather station data was also used for comparison to the other measurements. Wet candle measurements (ASTM G140) were collocated with the measurement systems and witness coupons at two test sites.

The environment and monitoring devices were effective for quantifying severity and measuring material corrosion performance. Self-consistent results were obtained for assessing site, test condition, and material performance using environment, conductance, and corrosion rate data from monitoring devices and witness coupons.

Assessing environment severity by wet, semiwet, and dry time may be more informative than the ISO 9223 time of wetness alone. Classifications relative to ISO 9223 that utilized aerospace materials and galvanic couples are suggested. These measurements clearly demonstrated that an open structure that allows salt contaminant ingress, but that has minimal rinsing by rain and condensation, can dramatically increase corrosion severity. The open structure in the least aggressive outdoor environment tested was approximately twice as severe as the most severe marine test site in the study. The results demonstrated that rain and condensation events may reduce corrosion severity relative to a drier site that has high salt deposition and less rinsing by rain and condensation. Severe weather events (wind and rain) were seen to increase environment ingress into simulated aircraft structures. The results indicate that monitoring can be used to assess microclimate conditions within airframes and that interior areas that allow environment ingress may have the highest severity due to operations and local environmental conditions.

Figure - Test racks at Florida intracoastal test site with witness coupons, monitoring devices, and simulated aircraft structure devices (left). Monitoring device with temperature, conductance, relative humidity, free corrosion, and galvanic corrosion sensors (right).

Effect of Ce post-treatment on the corrosion resistance of AA2024-T3 anodized in TSA and sealed with hybrid coatings

Oscar M. P. Ramirez[a], *Hercilio G. de Melo*[a]

[a]*Escola Politécnica da Universidade de São Paulo, Av. Prof. Mello de Moraes, 2463, São Paulo – SP – Brazil.*

Abstract

Chromium-based anodizing and post-treatment steps are the benchmark in the aircraft industry. Despite offering good corrosion resistance and self-healing properties, as chromate compounds are toxic for health and the environment, these surface treatments will be prohibited in the aerospace industry in a near future. Tartaric-sulfuric acid (TSA) anodizing is a promising environment compliant alternative, which is already being used at industrial level. However, the corrosion resistance of the anodized layer alone is not sufficient to guarantee the required safety levels for an aircraft and more complex systems should be employed.

In this investigation, AA2024 T3 specimens were anodized in TSA and subsequently post-treated in a Ce-H2O2 solution and sealed by a hybrid sol–gel coating (tetraethoxysilane (TEOS) and 3-glycidoxypropyltrimethoxysilane (GPTMS)), which hydrolysis solution was aged for different times. The morphology of the sealed anodic films, their thicknesses and the Ce distribution were evaluated by field emission scanning electron microscopy (FE-SEM) and Rutherford backscattering spectroscopy (RBS). Aging of the hydrolysis solution was followed by FTIR spectroscopy. The corrosion resistance of the samples anodized, with and without Ce post-treatment, and hybrid sol-gel coted was evaluated by electrochemical impedance spectroscopy (EIS) and salt-spray tests. FE-SEM characterization showed good coverage of the anodized surface by the hybrid layer (Figure 1). EIS experiments demonstrated improved corrosion resistance for the Ce post-treatment and for increased hydrolysis time and good responses were obtained for up to six months of ageing (Figure 2). The relatively long shelf life of the hydrolysis solution is a good prospect for future industrial use of hybrid coatings.

Keywords: anodizing, TSA, hybrid sol-gel aging, EIS

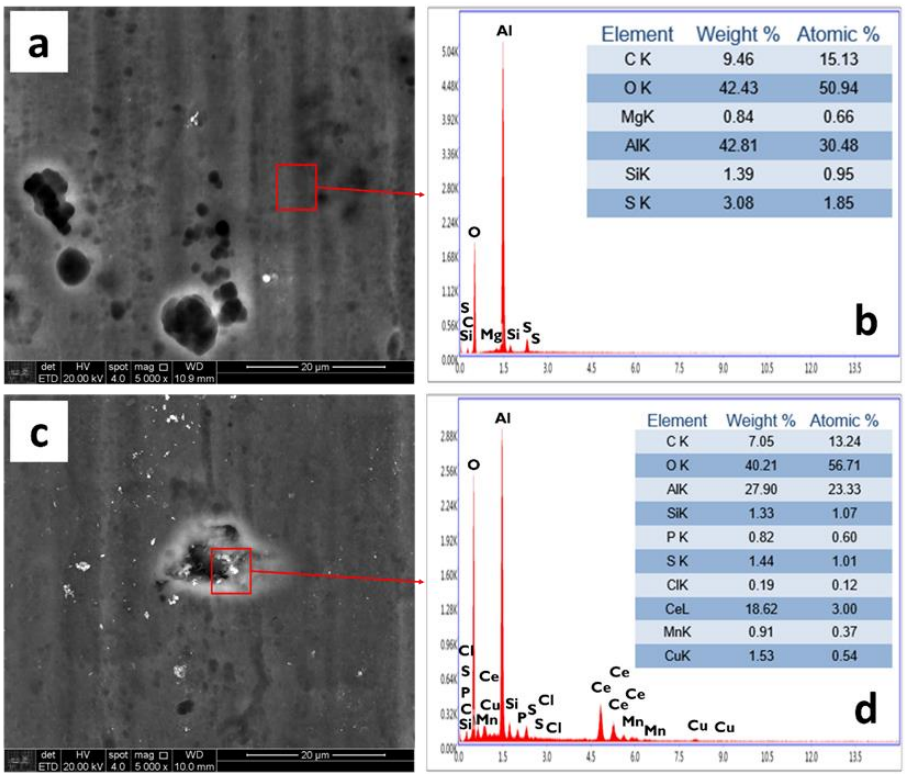

Figure 1. SEM micrographs and EDX characterization of as-prepared: (a,b) Hyb and (c,d) CeP Hyb sample.

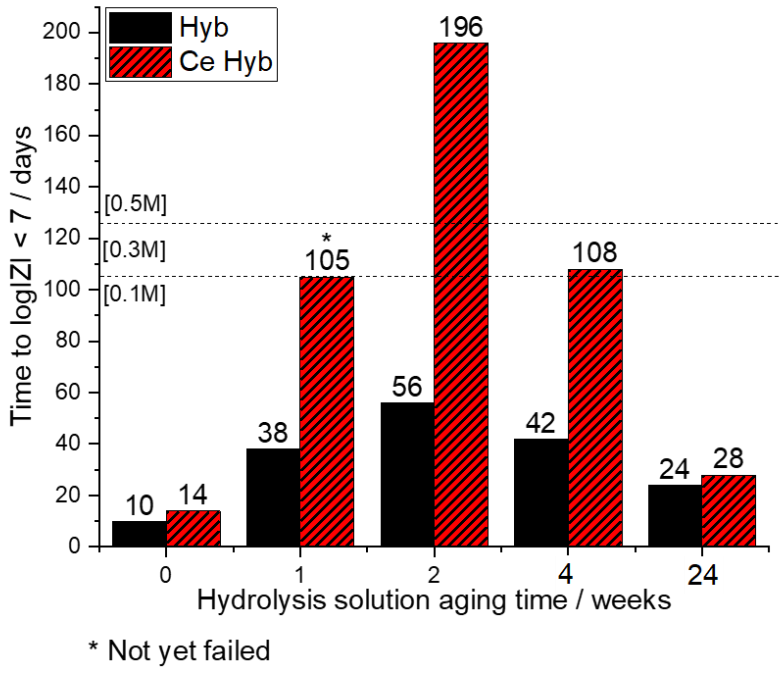

Figure 2. Time to log (IZI), at 0.01 Hz, be lower than 7.

Influence of the anodic layer on localized corrosion propagation in the AA7475-T761

João Victor de Sousa Araujo [1] *and Isolda Costa* [1]

[1] *Instituto de Pesquisas Energéticas e Nucleares, IPEN–CNEN/SP, Av. Prof. Lineu Prestes, 2242 – Cidade Universitária – CEP 05508-000 São Paulo – SP – Brasil*

Anodizing of the AA7475–T761 in tartaric sulfuric acid (TSA) produced an anodic aluminum oxide (AAO) film that was affected by the microstructure of the bare alloy and influenced corrosion propagation in the alloy comparatively to the bare alloy. The corrosion behavior of the bare and anodized alloy was investigated in sodium chloride solutions by cyclic potentiodynamic polarization. After corrosion tests, the morphology and extent of corrosion propagation was evaluated by optical microscopy, optical profilometry and scanning electron microscopy. It was observed that corrosion propagation varied depending on the surface condition, bare and anodized. Corrosion propagation in the bare alloy was shallower and more distributed along the exposed surface than for the anodized one. Besides, repassivation was easier for the bare alloy whereas for the anodized alloy repassivation was very difficult due to highly deep pits formed. Also, due to the heterogeneity of the AAO film formed, pitting potentials were not reproducible for the anodized alloy. The electrochemical results correlated well with the morphology of the AAO surface film and to the microstructure of the bare alloy.

ZnNi coating on UHSS for aeronautical applications: effect of base material and coating´s microstructure on the degassing process for preventing hydrogen embrittlement

A. Salicio-Paz[1], E. Mardarás[2], G. Artola[2], E. García-Lecina[1], M. Lekka[1]*

[1]CIDETEC, Basque Research and Technology Alliance (BRTA), Po. Miramón 196, 20014 Donostia-San Sebastián, Spain

[2]AZTERLAN, Basque Research and Technology Alliance (BRTA), Aliendalde Etxetaldea, 6, 48200 Durango, Bizkaia, Spain

*mlekka@cidetec.es

Ultra-high strength steels (UHSS) are currently used in applications where high mechanical loads are required as it is the case of landing gears in aeronautical applications. Among the wide range of UHSS available in the market, 300M is one of the preferred choices for aeronautical components manufacturing. However, despite the excellent mechanical properties exhibited by this UHSS components, their corrosion resistance is far from fulfilling the requirements of the aeronautic sector. Historically, UHSS have been plated with sacrificial coatings for enhancing the corrosion performance of the components, where cadmium coatings were applied on UHSS for providing corrosion protection. However, due to the increasingly stringent environmental regulations, cadmium coatings are being replaced by the more benign ZnNi alloy coatings. As ZnNi plating presents a lower efficiency with respect to Cd plating, a higher amount H is incorporated into the coating, and it is susceptible to migrate into the base material where it can contribute to hydrogen embrittlement. To prevent the risk of H embrittlement the plated components are subjected to H degassing which is affected both from the initial H content and the coating microstructure. Additionally, H diffusion into the base material and its effusion behaviour is also affected by the nature of the UHSS as well as the pre-treatment and plating process sequence, which might be different depending on the material nature of the substrate.

The aim of this work is to investigate the influence of the base material and the ZnNi coating´s microstructure on H content and degassing efficiency of electroplated ZnNi coatings on different UHSS. Thus, EZ2NKD18 and CUSTOM465 UHSS have been plated with different ZnNi coatings exhibiting different microstructures as those shown

in figure 1, namely closed, semi-open and open microstructure, correlating substrate´s nature, chemical composition, thickness, mechanical properties and microstructure with H content and degassing efficiency under different conditions. The coatings features and degassing performance have been compared to those obtained on 300M base materials. Microstructural characterization has been carried out by FESEM. GDOES has been used for determination of H content and its distribution on both the ZnNi and the base material. The effect of hydrogen embrittlement in the mechanical properties of the coated components has been evaluated according to the ASTM F519. These results will boost the understanding of the impact of the ZnNi coatings morphology on the H embrittlement susceptibility of plated components on different UHSS.

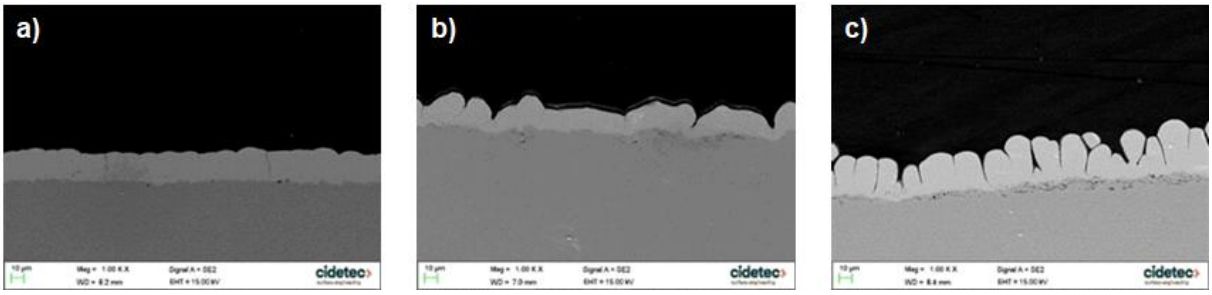

Figure 1. ZnNi microstructure as a result of plating conditions where a) closed, b) semi-open and c) open structure.

The corrosion protective behavior of differently aged lithium-based conversion layers

Ziyu Li[1], Axel Homborg[1,2], Yaiza Gonzalez-Garcia[1], Peter Visser[3], Arjan Mol[1]

[1]Delft University of Technology, Department of Materials Science and Engineering, Mekelweg 2, 2628CD Delft, The Netherlands, [2]Netherlands Defence Academy, Het Nieuwe Diep 8, 1781 AC Den Helder, The Netherlands, [3]AkzoNobel, Rijksstraatweg 31, 2171 AJ, Sassenheim, The Netherlands

Lithium salts are considered as a promising candidate within the range of environmentally friendly inhibitors for the corrosion protection of aerospace aluminium alloys[1]. Lithium ions play a critical role in the stabilization of surface (hydr)oxides, leading to the formation of a conversion layer with multiple distinct sublayers[2]. These prior studies have shown high barrier protection of lithium-based conversion layers as compared to other chromate-free conversion coatings. However, the influence of post-formation ageing on their corrosion protectiveness has yet remained unknown.

This work studies the influence of ageing under ambient conditions on the corrosion protective behavior of a lithium-based conversion layer using electrochemical noise (EN) measurements and top-view as well as cross-sectional micrographs. Conversion layers aged for a duration of 0 h and 4 h show an initially high degree of protection as well as large variations in the barrier resistance as determined by EN. These variations are similar to the resistance variations during the growth of the lithium-based conversion layer[3]. After termination of the inhibition stage, the protectiveness is notably lower. Conversion layers with ageing times of 24 h and 72 h show a more stable corrosion resistance which is higher than that of shorter-time aged samples. Further analysis reveals that the freshly-formed conversion layer has trapped a certain amount of lithium carbonate ions and water, leading to ongoing and heterogeneous growth of the conversion layer after extraction from the conversion bath.

1. P. Visser, H. Terryn, and J. M. C. Mol, *Surf. Interface Anal.*, **51**, 1276–1287 (2019).
2. A. Kosari et al., *Corros. Sci.*, **190**, 109651 (2021).
3. Z. Li et al., *Electrochimica Acta*, **426**, 140733 (2022).

A comparative study of different sol-gel coatings for sealing the plasma electrolytic oxidation (PEO) layer on AA2024

Sajjad Akbarzadeh[a,b], *Yoann Paint*[c], *Marie-Georges Olivier*[a,c]

[a] *Materials Science Department, Faculty of Engineering, University of Mons, 20, Place du Parc, Mons, Belgium*

[b] *Metallurgy Department, Faculty of Engineering, University of Mons, 20, Place du Parc, Mons, Belgium*

[c] *Materia Nova Research Centre, 1, Avenue N. Copernic, Parc Initialis, Mons, Belgium*

Abstract

Owing to the inherent porosity of the coatings produced through the PEO process, the application of sol-gel coatings as a post-treatment has drawn immense attention thanks to their eco-friendly and reliable protective characteristics. Various parameters affect their performance, and the type of sol-gel precursors plays a significant role. In this study, different combinations of sol-gel precursors including Tetraethyl orthosilicate (TEOS), Methyltriethoxysilane (MTES), (3-Glycidyloxypropyl)trimethoxysilane (GPTMS), (3-Aminopropyl)triethoxysilane (APTES), Zirconium(IV) propoxide (ZTP), and 3-(trimethoxysilyl)propyl methacrylate (MAPTMS) were employed to scrutinize the sealing ability and corrosion resistance properties of the duplex PEO/sol-gel coating system on AA2024 alloy. PEO layer on AA2024 was acquired at 5 A constant anodic current, 100 Hz frequency, and 30% duty cycle in an electrolyte containing sodium silicate and potassium hydroxide. Sol-gel solutions were applied by dip-coating method at a 100 mm/min withdrawal rate. The corrosion prevention performance of the coatings was studied by Electrochemical impedance spectroscopy (EIS) along with Scanning Vibrating Electrode Technique (SVET) analyses. Some chemical characterization tests, such as Fourier Transform Infrared Spectroscopy (FT-IR) and rheology measurement, affirmed the influence of the sol-gel chemical composition on its compactness and the network viscosity. The distinctive sealing ability

of different sol-gel coatings for the defects and pore filling of the PEO layer was visualized by Scanning Electron Microscope (SEM). To this end, different sol-gel formulations and various sol-gel network properties accordingly caused dissimilar sealing features for the PEO pores and, subsequently, the corrosion resistance of the duplex PEO/sol-gel coating is widely dependent on the used sol-gel precursors.

Keywords: *Plasma electrolytic oxidation; Sol-gel precursors; Sealing; AA2024; EIS.*

Why is it still corroding?
Local corrosion triggers of AA2024-T3 after inhibition with $Ce(NO_3)_3$

Marlon Mopon Jr.[1,2], Arjan Mol[3], and Santiago J. Garcia[1]

[1]Aerospace Structures and Materials Department, Delft University of Technology, Delft 2629HS, The Netherlands

[2]Department of Chemical Engineering, University of the Philippines, Diliman, Quezon City 1101, Philippines

[3]Department of Material Science and Engineering, Delft University of Technology, Delft 2628CD, The Netherlands

Recent studies have established the role of rapid intermetallic (IM) dealloying on degradation and the local deposition of Ce-rich protective oxides from Ce salts in solution. Despite long-term protection during immersion we recently showed that, for samples pre-exposed to a Ce-rich inhibiting solution, local degradation eventually re-initiates once the alloy is re-exposed to an inhibitor-free corrosive environment. So far elusive, a better understanding of the mechanisms that trigger this local corrosion re-initiation is important in developing more efficient inhibition strategies, especially since inhibitor supply is finite in real-life coated systems.

To this aim, we studied how IMs in AA2024-T3 initially exposed to 0.05 M NaCl and 0.001 M $Ce(NO_3)_3$ behave upon re-exposure to a solution containing NaCl only. To better understand the role of IM dealloying on Ce deposition and stability during re-exposure, we supplied the inhibitor salt ($Ce(NO_3)_3$) at different times based on our recent findings on IM dealloying kinetics, i.e. at t_{supply} = 0, 60, 180 s based on quantified IM composition-dependent dealloying onset (t_{onset}). A hyphenated optical-electrochemical technique that provides highly spatially-resolved optical and electrochemical information of local IM activity was used to quantify local changes during exposure and re-exposure. This was supported with ex-situ characterization such as SEM-EDX and Laser Confocal Microscopy.

We observed that most corrosion during re-exposure initiate at IMs with more than three elements (e.g., AlCuFeMnSi) as opposed to more commonly studied IMs like S-phase and θ-phase. Local corrosion at these IMs uncovers surrounding particles and leads to regional corrosion on the alloy surface. Besides this, partial breakdown of inhibitor deposits during re-exposure also lead to some local corrosion at longer immersion times. This susceptibility to breakdown appears to increase with the delay in inhibitor supply time.

Ultrasound supported nucleation and growth of LDH conversion layers on AA 2024 – Correlation of structure and corrosion resistance

Lukas Ruhm[1], Pascal Vieth[1], Ralf Peipmann[2], Wolfram Fürbeth[2], Guido Grundmeier[1]

[1] Paderborn University, Paderborn/Germany

[2] DECHEMA-Forschungsinstitut, Frankfurt am Main/Germany

Layered double hydroxides (LDH) are a promising material for advanced conversion coatings, as they consist of a layered system with intercalated anions.[1] LDHs can be used either as anticorrosive particles in coatings or as in-situ grown conversion layers. However, the in-situ growth of LDH on metal alloys is a slow process.[2] Based on the published promotion of conversion layer formation on magnesium alloys[3] the presented approach considers the US supported nucleation and growth of LDH layers with a focus on industrially relevant process times of less than 300 sec.

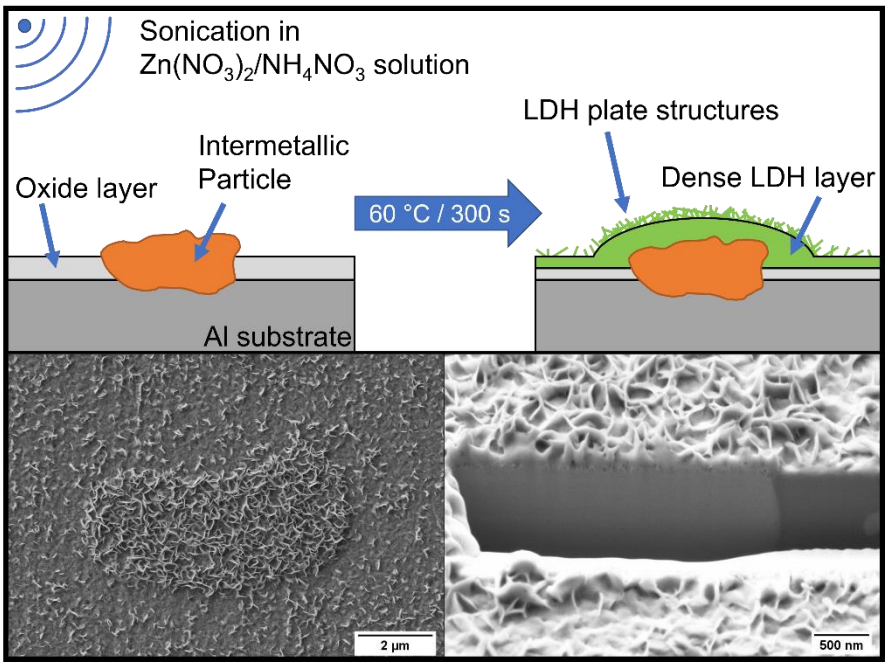

FE-SEM and FIB-FE-SEM analysis of the formed LDH layers on aluminum alloy 2024 under the influence of high-power ultrasound.

ZnAl-LDH-NO_3 conversion coatings were grown on AA 2024 in a time frame of 300 sec based on an US-supported process. Their morphology, surface chemical

composition and corrosion properties were investigated and consequently compared to samples fabricated in the same process without support of ultrasound. The formation of LDH layers was confirmed by means of X-ray diffraction (XRD) and their chemical composition was analyzed by X-ray photoelectron spectroscopy (XPS) and infrared reflection absorption spectroscopy (IRRAS). An influence of the ultrasound on the structure of the layers could be clearly revealed. The local morphology and thickness of the LDH layers was examined by scanning electron microscopy (FE-SEM). The sonication resulted in a lower number of larger LDH plate structures on top of the dense interfacial LDH layer. The chemical and morphological modifications also led to changes in the corrosion protection properties of the films. The corrosion resistance was investigated electrochemically by linear sweep voltammetry (LSV) and electrochemical impedance spectroscopy (EIS), whereby a positive influence of ultrasound on the corrosion protection could be shown. Additionally, a model adhesive was applied to investigate the resulting wet-adhesion and resistance to corrosive delamination of the polymer film. To achieve interfacial chemical bonds at the adhesive/LDH interface the LDH layer was modified with aminopropyl-phosphonic acid (APPA). The corrosion tests showed a significant improvement of the wet-adhesion and corrosion resistance assigned to the interfacial modified LDH layer.

References:

[1] A. C. Bouali, M. Serdechnova, C. Blawert, J. Tedim, M. Ferreira, M. L. Zheludkevich, *Applied Materials Today* **2020**, *21*, 100857.
[2] M. A. Iqbal, L. Sun, A. T. Barrett, M. Fedel, *Coatings* **2020**, *10*, 428.
[3] C.-N. Liu, M. Wiesener, I. Giner, G. Grundmeier, *Front. Mater.* **2015**, *2*, 68.

Use of gas-phase deposition to improve organic inhibitor/epoxy resin coating matrix compatibility and anticorrosion efficiency

Jingjing Zhao, J.R. (Ruud) van Ommen, Santiago J. Garcia
Delft University of Technology, Delft, The Netherlands

Organic corrosion inhibitors such as 2,5-Dimercapto-1,3,4-thiadiazole (DMTD) have shown remarkable corrosion inhibition efficiency in solutions for aluminum alloys such as AA2024. Despite the progress in strategies to load corrosion inhibitors in coatings through the use of nano and micro inorganic carriers, the loading of very efficient organic inhibitors in reactive matrices such as epoxy-amine primers has proven more complex than for inorganic salts. [1]

In this work, we studied gas-phase deposition applied earlier in the pharma field [2] to coat organic molecules to decrease their solubility as a method to decrease organic inhibitor-matrix interaction without negatively affecting release and inhibitor anticorrosion efficiency. To this aim, we used pulsed chemical vapor deposition (CVD) in a fluidized bed of DMTD corrosion inhibitor powder. The morphology and chemical composition of the DMTD particles were characterized by transmission electron microscopy (TEM) and X-ray photoelectron spectroscopy (XPS). The effect of the CVD layers on the dissolution kinetics of DMTD was studied by in-situ ultraviolet-visible spectroscopy (UV-vis). Finally, the DMTD powders surface modified by CVD were incorporated into an epoxy/amine coating, applied on an AA2024-T3 substrate and studied in detail. The effect of the CVD modification on the coating's barrier and active corrosion protection at damages was studied by in-situ optical-electrochemical measurement and a visual corrosion assessment. The results show an effect of the CVD cycles on dissolution and release kinetics as well as an increase of the anticorrosion behavior of coatings made using this strategy.

Reference

[1] Denissen, P. J., Shkirskiy, V., Volovitch, P., & Garcia, S. J. "Corrosion inhibition at scribed locations in coated AA2024-T3 by cerium-and DMTD-loaded natural silica microparticles under continuous immersion and wet/dry cyclic exposure." ACS applied materials & interfaces 12.20 (2020): 23417-23431.

[2] Zhang, D., La Zara, D., Quayle, M. J., Petersson, G., Van Ommen, J. R., & Folestad, S. "Nanoengineering of crystal and amorphous surfaces of pharmaceutical particles for biomedical applications. " ACS Applied Bio Materials, 2.4 (2019): 1518-1530.

Stress-facilitated corrosion behavior of GH4169 under the NaCl-contained humid intermediate environment

Wenquan Wang[a], Yu Cui[b], Rui Liu[a], Li Liu[a], Fuhui Wang[a]*

a Shenyang National Laboratory for Materials Science, Northeastern University, Shenyang 110819, China.

b Shi-changxu Innovation Center for Advanced Materials, Institute of Metal Research, Chinese Academy of Sciences, Wenhua Road 72, Shenyang 110016, China.

The complex coupled service conditions of elastic stress loading and the marine environment, which contained water vapor and solid NaCl, caused the shortened service life of aircraft engine blades at intermediate temperatures. Previous works have focused on the corrosion caused by the synergetic effect of deposited solid NaCl and water vapor. Yet, the facilitated corrosion induced by stress loading in the environment has seldom been considered. Accordingly, the widely used Ni-based superalloy, GH4169, was employed to study the influence of the coupled humid intermediate temperature environment with solid NaCl contained and elastic stress load on the corrosion behavior.

In this investigation, the NaCl-contained humid intermediate temperature environment was established with stress load inflected via the four-point bending method. Corrosion characteristics such as morphologies of surface and cross-section, corrosion products, and internal corrosion depth were observed and analysed. The results indicated that a stress-promoted "active oxidation" mechanism at the internal corrosion zone facilitates deeper internal corrosion in an exponential form with external stress and by the parabolic law with time. Stress and Cl synergistically change the single corrosion product of Cr_2O_3 to mixed Cr_2O_3 and Fe_2O_3 at internal corrosion tips due to the promoted inward diffusion of oxygen and the reduced activation energy of internal corrosion via the external stress-disrupted balance of oxygen vacancies.

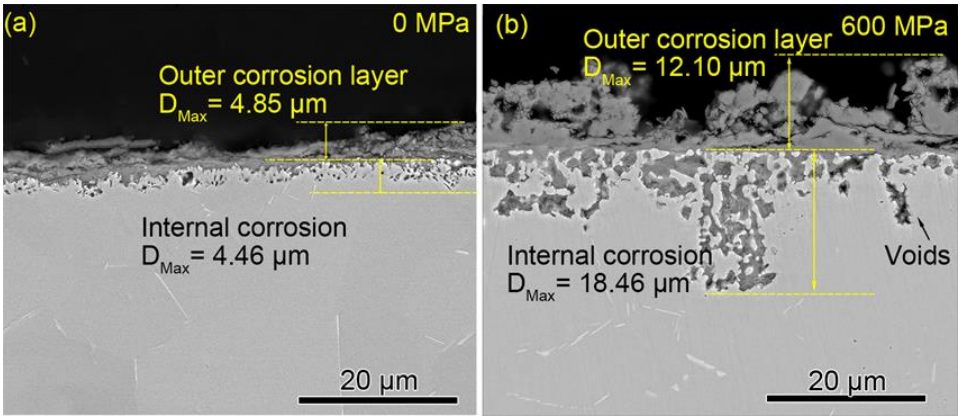

Fig.1 Morphology of stress-promoted internal corrosion penetration of GH4169 alloy with NaCl deposited exposed in water vapor and air for 20 h at 600°C under different stress loading conditions (a)0 MPa and (b) 600 MPa.

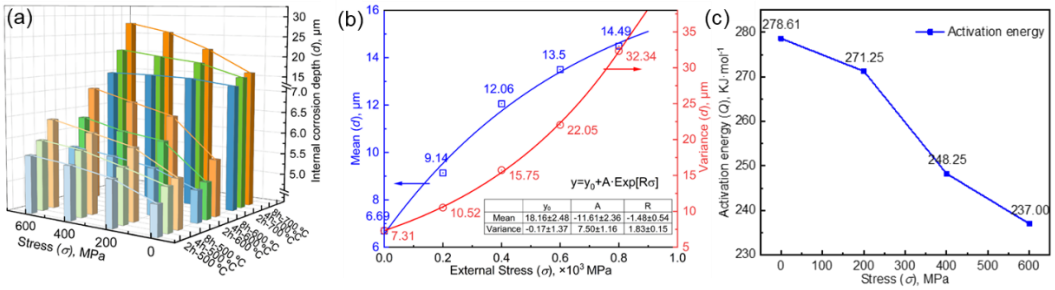

Fig.2 The variation trend of internal corrosion penetration depth with factors of temperature, stress level and exposure time. (a) internal corrosion depth statistics; and (b) dynamics (c) and active energy of internal corrosion depth growth with stress.

Corrosion investigations on SAC-1Bi-xMn lead-free solder alloys: an overview

Bálint Medgyes[1], Ali Gharaibeh[1], Gábor Harsányi[1], Béla Pécz[2] and Ilona Felhősi[3]

[1] Department of Electronics Technology, Faculty of Electrical Engineering and Informatics, Budapest University of Technology and Economics, Műegyetem rakpart 3, 1111 Budapest, Hungary

[2] Centre for Energy Research, Institute for Technical Physics and Materials Science, Konkoly-Thege M. út 29–33, 1121 Budapest, Hungary

[3] Institute of Materials and Environmental Chemistry, Research Centre for Natural Sciences, Magyar tudósok körútja 2, 1117 Budapest, Hungary

The effects of Ag and Mn content were investigated from the electrochemical corrosion (ECC) and electrochemical migration (ECM) point of view in the case of SAC0307-1Bi-xMn (x = 0.1, 0.4 and 0.7 wt%) and SAC305 lead-free solder alloys in NaCl solution. ECC was examined by potentiodynamic polarization and electrochemical impedance spectroscopy (EIS) tests. On the one hand, long-term results showed that lower silver content showed higher corrosion resistance. On the other hand, the microstructure and elemental composition of the dendrites formed after the ECM test were investigated by transmission electron microscopy (TEM) and energy disperse X-ray spectrometer (EDS) which demonstrated that micro-alloying elements (i.e. Mn) also contributed to the ECM processes. This study demonstrates and discusses the silver content effect on corrosion and the participation of Mn in the ECM process. Furthermore, the ECM model of Mn was established as well.

From the corrosion to short circuiting in electronics: Investigation of the detrimental dendrite development

Feng Li, Rajan Ambat

Centre for Electronic Corrosion, Department of Mechanical and Civil Engineering, Technical University of Denmark

Abstract

With the development of electrification and digitalization in different fields, materials in electronic function units are also expected to work under exposed climatic condition as conventional structural materials. The structural materials exposed outdoor usually face the challenge of corrosion, while the durability of materials could last for years before occurrence of destructive failure. However, corrosion in electronics cause functional issues for example on Printed Circuit Board Assembly (PCBA) surface due to water film acting as a bridge between closely spaced biased points, which ultimately lead to dendrite formation by electrochemical migration mechanism. Due to the accelerated hydrolysis of water under applied bias voltage exceeding 1.2V, the corrosion cell formed in electronic units are much more aggressive, where the local pH close to the anode and cathode can significantly change to acidic and alkaline conditions respectively. Under the driving force of the electric field, the dissolved metallic ions from the anode transport to the cathode for reduction reaction, and deposit at the edge of the cathode as dendrite growing towards anode finally for a short circuit. For electrochemical migration related failure, the whole process of ions migration and dendrite formation might take only few minutes if conducive conditions of ion stability exist in the electrolyte. For many years, the dendrite from the electrochemical migration was qualitatively investigated under the scope of mechanistic, structure, and elemental composition. However, none of the research could illustrate how much ions required to initiate the detrimental point for electrochemical migration and how much ions required to cause short circuiting by dendrite formation. This paper quantitatively demonstrates the whole process of the dendrite formation form initial dissolution of anodic material until the occurrence of short circuiting. The effect of the corrosion on electrode was analyzed using scanning electrochemical cell microscopy (SECCM). The corrosion product at electrodes was investigated using X-ray photoelectron spectroscopy (XPS) and Raman spectroscopy. The droplet induced dendrite formation was directly analyzed using Inductive Coupled Plasma Optical Emission Spectrometry (ICP-OES) with 30 sec interval of 5V/10V DC bias until failure occurred. To understand the chemical composition and structure of the dendrite formed under a variety of testing conditions, transmission electron microscopy (TEM) and scanning transmission electron microscopy (STEM) were conducted at the same position on the dendrite.

Key words: electrochemical migration, dendrite, electronic corrosion, short circuiting

Correlation between high current-driven dendrite formation and water layer thickness

Jyothsna Murli Rao[1] and Rajan Ambat[1]

[1] Materials and Surface Engineering, Department of Mechanical Engineering, Technical University of Denmark, 2800 Kongens Lyngby, Denmark

With the industry-wide shift towards electrification and miniaturization, use of higher voltage in various applications (for example, Electric vehicles) has been increasing rapidly, along with a requirement for reduced size and spacing of components to increase density of functions. These higher system operating voltages (>400V), when applied across shrinking pitch distances, induce a significantly higher electric field and thus higher leakage currents (than observed in regular lower voltage devices such as consumer electronics), which exponentially increases the risk of dendrite formation and device failure during exposure to humid environments.

In an attempt to study this mechanism of higher-current driven dendrite formation, PCB laminates have been placed in humid environments (90%RH) and cooled to different temperatures below dew point (where room temperature is maintained at 25^{o}C) to induce different levels of condensation on the surface. Formation of this water layer has been visually recorded with the help of an in-situ Digital microscope. A galvanostatic approach (with applied current levels of 0.5mA, 1mA, 5mA, 10mA, all above the current levels higher than those observed during failure of low-voltage range of 1-10V driven PCBs in previous studies) has been chosen to maintain a high reaction rate in the electrochemical cells formed when condensing water droplets bridge oppositely biased metallic conducting points. The electrochemical testing has been supplemented with image analysis of water layer formation and material characterization techniques such as XRD (to understand the level of crystallinity and structure of dendrites formed) and SEM-EDS (to observe any differences in appearance and elemental make-up of dendrites formed at different current levels).

The study provides a holistic understanding of the combined effects of higher currents and water layer formation observed in high-powered electronic devices, on dendrite morphology and growth characteristics.

Key Terms: Condensation, Dendrite Formation, Dendrite Morphology, High Current Levels, High Voltage, Humid Environment, Printed Circuit Board Assemblies (PCBA)

Influence of sodium and chloride ions on electrochemical failures of AlCu metallized test chip surfaces at very small distances

D. Nienhues, Robert Bosch GmbH, Reutlingen Germany

L. Müller, Robert Bosch GmbH, Reutlingen Germany

M. Nowottnick, Universität Rostock, Rostock Germany

Corrosion in microelectronics is a recurring problem, which has become even more critical with miniaturization and the demand for more and more durable devices. Ionic contamination, especially chloride, is one of the biggest issues when it comes to the cause of corrosion. Not only because of its ubiquity but also because of the critical role when it comes to pitting corrosion regarding aluminum and pH changes which accelerate the corrosion process. Therefore, it is crucial to investigate the concentration of impurities as well as the environmental factors which can cause problems, to prevent failures in safety-relevant devices like airbag systems. The requirements for microelectronics, with their small distances, are therefore much higher compared to larger scaled systems like printed circuit board assemblies. In some sensible devices an increase in leakage current of around 100 pA can already cause a falsified measurement signal. Such an increase, for example caused by chloride in combination with humidity, can be the initial step to electrical changes and corrosion. In addition, a relation between increased surface current and time to failure was already shown in previous works.

Firstly, this paper discusses the increase in leakage current using exact DC current measurements up to a few picoampere. Secondly the change in impedance and thirdly the formation of corrosion products, all three related to sodium chloride contamination. The test dies have aluminum copper (AlCu(0.05)) interdigital structures on the surface with small distances (<20 um), are mounted on PTFE-based PCBs (see Fig. 1) and were tested at high humidity and temperature. The results allow to suggest limits in the range of 10^11 to 10^15 ions per cm^2 for semiconductor surfaces with aluminum metallization. These limits depend on the combination of change in leakage current, impedance and distance. The authors assume that the limits are transferable to similar systems using AlCu to identify critical processes before they cause problems by comparison of the layout, environment, and contamination level. Transfer of this concept to other metallizations, ions and distances remains to be checked.

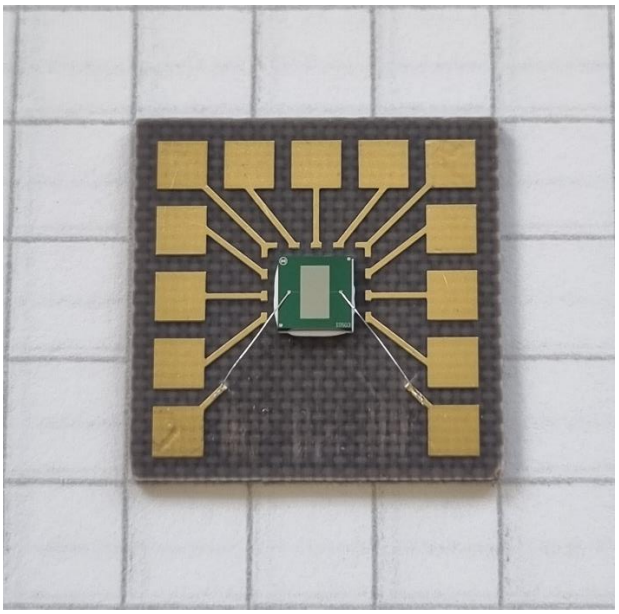

Figure 1: Si/SiO_2 test die with AlCu interdigital structures on the surface mounted on PTFE-based PCB with ENIG metallization

Characterization of the harmful gas degradation (iodine vapor test) of polymer-based protection systems for electronic assemblies using impedance measurement

Dr. Markus R. Meier, ZESTRON Europe, Ingolstadt

Dr. Helmut Schweigart, ZESTRON Europe, Ingolstadt

The quality test based on iodine vapor, which was presented for the first time at the GUS annual conference in 2019, now represents a quick alternative to characterizing coatings and molds on electronic assemblies or power electronics modules. The comparison of the iodine vapor test (IVT) with the Flower of Sulfur (FoS) and mixed gas damage tests (MFG) on different coatings have shown that comparable test results can be obtained with a simultaneous increase in the test time. In addition to these results, this article also presents studies on the development of iodine and water vapor in the test vessel depending on the selected test temperature and duration as well as the concentration of the test solution used.

In addition, it is shown how the previous problem with non-transparent protection systems of not having an optical evaluation option can be solved by means of LCR measurement of the test specimen to be examined before and after application of the IVT. The measurement of the AC resistance before the iodine vapor exposure acts as a reference value - a deviation from these initial properties of the sample then indicates corresponding interactions of the iodine vapor with the materials present. These interactions can be storage processes of iodine and water in existing polymer structures or pores, but also corrosion products on metallization in the course of delamination of the protective system on the assembly surface.

Evaluation of High Humid Air Respiration and Corrosion Environment in Electronic Control Cabinets

Teruhisa Tatsuoka, Hiromitsu Ijichi, Keiichi Yoshino

TEPCO Research Institute, Tokyo Electric Power Company Holdings, Inc., Yokohama/Japan

Electric power equipment, factories, etc. are monitored and controlled by electronic devices. These devices and electric equipment are installed in electronic control cabinets and boxes which have gaskets on their doors and sealant for crevices and cable access holes. Electronic control cabinets used to have the structure to prevent from water and dusts invasions according to the International Protection Code of IEC 60529, “Degrees of protection provided by enclosures”. However, the code does not refer the ingress protection capability of high humid air. The high humid air permeation from gaskets and sealants and dew condensation on the electronic devices in the electronic control cabinets and boxes deliver the corrosion of electric and electronic devices and decrease in insulating performance.

Invasion phenomenon of high humid air from gaskets and sealants of the electronic control cabinets and boxes has not been clear. Moreover, corrosivity of semi-hermetic structures such as electronic control cabinets and boxes are very complicated and interaction between humidity, temperature, ventilation, dew condensation, changes in inside and outside pressures are not known well.

In this research, Atmospheric Corrosion Monitor, ACM, sensors are applied as a wetness sensor to detect the thin water films caused by dew condensation on the electric and electronic devices and to evaluate corrosion environment. The barometer, hygrometer and thermometer are also installed inside and outside of electronic control cabinets and boxes to understand high humid air respiration and compare the corrosion environments.

KEYWORDS

Electronic control cabinets, Storage box, Corrosion, Moisture permeation, Gasket, Sealant

Correlating PCBA water layer build-up with Electro-Chemical Migration and subsequent dendrite formation- a Mechanistic viewpoint

A.R. Lakkaraju[1] and R. Ambat[1]

[1] Materials and Surface Engineering, Department of Mechanical Engineering, Technical University of Denmark, 2800 Kongens Lyngby, Denmark.

The electronics industry adopts an increased device miniaturization, and devices are expected to perform optimally in a multitude of climatic conditions worldwide, which adds to the list of possible failure modes. Changing temperature and humidity are a major driving force for condensation regime on the electronics surface, which can eventually lead to failure modes such as high leakage currents and Electro-Chemical Migration (ECM). ECM failures are becoming more important because of increased use of power electronics with higher voltages and power in applications such as electrified vehicles and renewable energy. The formation and coalescence of water droplets to form larger drops on the PCB surface determines the bridging pathway between two connector pads, and subsequent direction of growth of conductive dendrites, which form a short-circuit and seriously hamper device functionality.

Simulated condensation experiments on test PCB laminates have been performed. A test setup using a heat-exchanger allows the cooling of the specially-designed test PCB laminates (coated with different solder masks for experimental variation) while being exposed to high-humidity conditions at room temperature, resulting in water layer build up. This build-up has been monitored using visual (in-situ Digital Microscope), electrical (Impedance and leak current measurements) and gravimetric (weight gain due to condensed water, which is converted to average water layer thickness) methods, in order to create a correlation to Electro-Chemical Migration and subsequent dendrite formation.

The results utilize a combination of image analysis and gravimetric measurements to give an insight into the bridging of condensed water droplets on the solder mask surfaces and the subsequent coalesced droplet size, which along with changes in measured impedance and leakage current, and SEM analysis, present a unified picture of the effect of water droplet size on dendrite formation, dendrite morphology and functional electrical properties.

Key Terms: Coalescence, Dendrites, Electro-Chemical Migration, Gravimetry, Humidity, Image analysis, Impedance, Leakage current, Morphology, Printed circuit board laminate, Scanning Electron Microscopy, Temperature, Water droplet size, Water layer formation

Enhanced mechanical properties and barrier performance of nanosilica-filled silicone rubber coating for implantable electronic devices performance

Shiyao Du[1,2], Hui Yan[1,2], Ao Tang[1,], Ying Li[1*]*

[1]*Institute of Metal Research, Chinese Academy of Sciences, Shenyang, P.R.China*

[2]*School of Materials Science and Engineering, University of Science and Technology of China, Shenyang, P.R.China*

Implantable electronic devices (IEDs) are increasingly used in medical treatment and diagnose for physiological monitoring. However, encapsulation of IDEs still faces significant challenges as full prevention of body fluid penetration into the coating remains unsolved. To enable an extended lifecycle for IEDs, water transport impact on failure mechanism of silicone rubber coating was systematically investigated in this study. Water absorption and morphology characterization firstly indicate an increased water diffusion into the free coating due to crack development. Subsequent electrochemical characterizations further verify a three-step water penetration behavior in the coating/substrate system, and meanwhile quantify the crack growth and evolution. By further experimental and finite element studies, it is proved that crack propagation is responsible for coating failure in IEDs, while a comprehensive failure mechanism of medical silicone rubber coating in simulated body fluid is also uncovered in a detailed manner for the first time.Next, we develop a high-

performance composite coating for IED encapsulation by introducing SiO_2 nanoparticles into silicone rubber, which synergistically enhances mechanical properties and improves barrier performance. By fabricating composite coatings with different nanosilica contents, 3% nanosilica is proved to be an optimal additive content with an excellent combination of improved fracture strength (from 2.5 Mpa to 4.5 Mpa), increased coating resistance (from 10^4 $\Omega \cdot cm^2$ to 10^9 $\Omega \cdot cm^2$) and ideal coating uniformity. Mechanical and electrochemical characterizations subsequently confirm substantially enhanced mechanical properties and barrier performance of the composite coating, which effectively resist crack propagation and impede penetrations of water and chloride ions through the coating. Theoretical calculations further uncover that modified SiO_2 particles with enriched methyl groups endow a strong bridging effect to interact with silicone rubber monomer, which, together with anti-agglomeration property of methyl groups, contributes to a pronounced improvement in mechanical performance of nanosilica-filled silicone rubber. Benefitting from the enhanced mechanical and barrier properties, the as-fabricated nanosilica-filled silicone rubber demonstrates a superior protection for the encapsulated circuits with a significantly improved lifetime (709.1 h) compared to that of circuits coated by pure silicone rubber (472.8 h) and bare circuit boards (1 h), which offers great values for packaging material design in future IED encapsulation.

How to reduce humidity ingress in electronics by use of EquiLung

Jan Bjerre Christensen, FORCE Technology, Denmark

For electronic equipment, a high level of humidity can cause corrosion damage and shorten the functional lifetime. High humidity combined with temperature variations are problematic for most electronic equipment and can result in failures due to, for instance, creeping currents, delamination of Printed Circuit Board (PCB) and disconnection of electrical connections. At FORCE Technology, we are working on a mechanical principle to reduce the humidity ingress into enclosures of electronic equipment. We call it an "equipment lung" (EquiLung). This presentation will give a short introduction to EquiLung with examples of test results, implementation and verifications.

For electronic equipment used in humid environments, there is potentially a risk that humidity will penetrate the encapsulation and functional product failures will occur over time. The EquiLung is a mechanical device that can reduce the accumulating water in electronic equipment when it is located in an environment with high humidity and temperature changes. The EquiLung reduces the pumping effect of humidity in the air inside the electronic products. The pumping effect can be caused of changing temperature in the surrounding atmosphere or due to the rising temperature from the electronics during function. As the EquiLung is an integrated part of the enclosure, it must be "designed" in during the initial design of the enclosure. This presentation will give an overview of the:

- Project background
- The diversity of implementation
- Verification results
- Examples of EquiLung in real products

A systematic corrosion failure analysis of Li-ion powered hearing aids from various markets.

Markus Asikainen[*1], *Abhijeet Yadav*[*2], *Rajan Ambat*[*1]

[*1]*Department of Civil and Mechanical Engineering, Technical University of Denmark, DK 2800 Lyngby, Denmark*

[*2] *WS Audiology A/S, DK 3540 Lynge, Denmark*

Hearing aids (HA) are low-power electronic devices used worldwide and the ongoing trend in the hearing aid industry has been to move towards Li-ion battery technology replacing conventional zinc-air batteries. Li-ion powered devices have a few key differences compared to the conventional systems, namely: (1) a higher operating potential of 4.3V, (2) a power management unit to control the charging/discharging cycles and to ensure the safe use of the Li-ion cell and (3) implementation of charging method “induction” or “galvanic”. The corrosion reliability of HA devices is a critical issue, due to their exposure to harsh user environments including body fluid contact and external environments with high humidity, temperature, and atmospheric contaminants. The combined effect of higher voltage and miniature electronic design poses new risks for Li-ion devices to have corrosion-related issues caused by user environments. To understand the effect of increased operating voltage, charging/discharging cycles and overall performance of the Li-ion powered HA design on corrosion reliability, it is crucial to investigate the performance in the field and conduct a root cause failure analysis on the field returned failed devices.

In this study, three different Li-ion-powered HA models from various markets such as China, India, and USA were investigated. The analysis was conducted by using a scanning electron microscope (SEM), energy dispersive spectroscopy (EDS), and inductively coupled plasma optical emission spectroscopy (ICP-OES) to locate and understand failure modes, mechanisms, and effects. Based on the analysis, failure data was created and used for statistical analysis to compare the performance of the different hearing aid models in the different markets to show failure probability and failure percentage for different components. Passive components, battery soldering connection, RIC connector soldering, and galvanic charging contact showed the highest failure percentages and probability across all markets. The presence of high

levels of Cl ions from human sweat, high humidity, and insufficient conformal coating protection were the most common causes for corrosion failures in Li-ion-powered HAs.

Author list:

1. Markus Asikainen (mkaas@dtu.dk)
Department of Civil and Mechanical Engineering, Technical University of Denmark, DK 2800 Lyngby, Denmark (Presenting author)

2. Abhijeet Yadav (abhijeet.yadav@wsa.com)
WS Audiology A/S, DK 3540 Lynge, Denmark

3. Rajan Ambat (ram@dtu.dk)
Department of Civil and Mechanical Engineering, Technical University of Denmark, DK 2800 Lyngby, Denmark

Investigation of Electrochemical Migration on Chip Components under Electrolyte Condition with same Contamination and Conductivity Level

Sajjad Bahrebar, Rajan Ambat

Center for Electronic Corrosion, Section of Materials and Surface Engineering, Department of Mechanical Engineering, Technical University of Denmark, 2800 Lyngby, Denmark
Email: sajbahr@dtu.dk

Abstract: The soldering process, especially wave soldering because of the use of liquid flux by spraying process, introduces ionic residues on the printed circuit board assembly (PCBA) surface during the manufacturing process, which along with other factors, affects the corrosion failures related to humidity on the PCB surface. No-clean fluxes are used today for automated soldering processes, which contain many weak organic acids as activators. Residue arising from the soldering process and use of no-clean flux is one of the main factors contributing to humidity-assisted failures in electronics such as electrochemical migration (ECM). Adipic acid, glutaric acid, and succinic acid as contamination types and main solder flux residues on PCB surfaces at three low levels of contaminations, as well as in the same conductivity level in comparison with sodium chloride (NaCl) on time to failure (TTF) owing to ECM on the chip components were studied. The relation between TTF and leakage current (LC), conductivity, as well as the number of failures using applicable statistical analysis in various conditions combined with varied contamination types/levels and voltage were analyzed. Droplet test results investigation showed that in the same contamination level at whole contamination types, from the low level to the high level of voltage, TTF decreased, and the number of failures increased. Except for NaCl, at a similar voltage level, the lower contamination level has the lowest average of TTF. In the equal conductivity level, the average TTF with increasing voltage levels decreased from NaCl, Succinic, Glutaric, and Adipic, respectively.

Keywords: contamination, conductivity, Failure, ECM, LC, TTF, chip component.

Triethylene glycol solubility and corrosion in dense phase CO_2

Bjørn Helge Morland, Arne Dugstad, Gaute Svenningsen,
Institute for Energy Technology, Kjeller/Norway

TEG (Triethylene glycol) can be used for hydrate control and acid gas removal in CO_2 from Carbon Capture plants. The possibility for carryover to the compressed CO_2 side is present and this work focused on TEG in dense phase CO_2 both with and without water.

The solubility and dissolution time of TEG and TEG/H_2O was determined by visual observation at 25 °C (100 bar). Corrosion coupons was exposed to TEG (see Figure 1) and TEG/H_2O dissolved in CO_2. The carbon steel was only exposed to dissolved TEG and water. The behavior difference of TEG and MEG (Monoethylene glycol) in dense phase CO_2 will also be discussed.

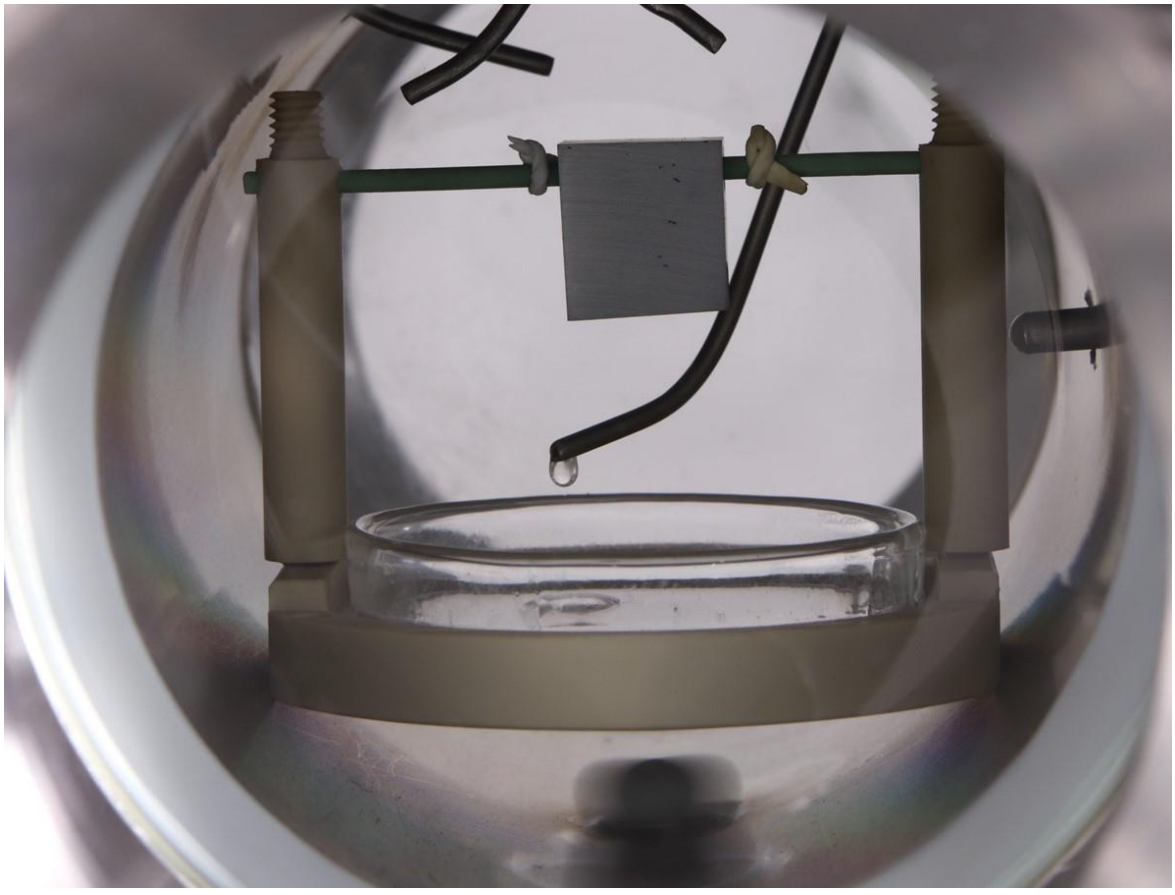

Figure 1. Carbon steel coupon exposed to TEG in dense phase CO_2.

CO_2 System Chemistry Evolution in Laboratory Experiments - Impact on $FeCO_3$ Formation

Rob Jacklin[1,2], Joshua Owen[1], Danny Burkle[2], Richard Woollam[1], Richard Barker[1]

[1] University of Leeds, Leeds, UK; [2] LBBC Baskerville, Leeds, UK

When carbon steel corrodes in a CO_2 environment H^+ ions are reduced in the cathodic reaction while Fe^{2+} ions are released in the anodic reaction. In laboratory experiments, despite a buffering capacity to replenish H^+, the proliferation of Fe^{2+} in a finite volume will shift the equilibrium speciation of the system. The magnitude of any transition in solution chemistry is relative to the concentration of metal ions that enter the system as well as the starting conditions such as pH, temperature, and ionic strength. The complexity is compounded by the fact that these starting conditions also determine the rate at which test specimens will corrode by influencing the kinetics of the corrosion reaction. The corrosion rate is in effect a measure of flux of metal ions into the system.

One parameter that is often overlooked when conducting CO_2 corrosion experiments is the size and number of carbon steel specimens that are immersed in a test solution. Increasing the surface area of specimens will increase the amount of iron ions entering the system. If the solution volume is not substantial this flux of iron ions will quickly give rise to high concentrations of bulk Fe^{2+} and higher pH leading to potentially premature precipitation of corrosion and/or scaling products. The relationship between the exposed surface area of the metallic specimen and the volume of solution it is exposed to is referred to as the area-to-volume (A/V) ratio. ASTM standards G111 and NACE G31 both give arbitrary recommendations for maximum A/V ratio when conducting corrosion experiments but do not offer a systematic approach to establishing sensible values for specific operating conditions.

In the present study the impact of system chemistry evolution rates on $FeCO_3$ formation is explored through the variation of A/V ratio. Experiments were conducted in autoclaves at 80°C, 5.5 bar pCO_2 and unbuffered pH. Corrosion layer performance was assessed through gravimetric analysis and Electrochemical Impedance Spectroscopy while the structure of the layer was assessed using Elctron Back Sacttered Diffraction. The results indicate that A/V ratio significantly affects $FeCO_3$ formation, changing the structure of the corrosion layer which impacts the mechanism for substrate protection.

Performance evaluation of copper catalysts for CCUS

Corentin Penot[1], Kranthi Maniam[1,2], Vikas Kumar[1], Shiladitya Paul[1,2]

[1]Materials Innovation Centre, School of Engineering, University of Leicester, Leicester, UK

[2]Surface, Corrosion and Interface Engineering, Materials Integrity and Performance Group, TWI, Cambridge, UK

The development of carbon capture and utilization (CCU) technology has gained significant attention as a means of mitigating the effects of climate change. One of the key element of CCU is CO_2 capture. Amine solutions have been effectively used in large-scale facilities for the treatment of CO_2-rich gas stream and have been shown to have a high efficiency in capturing CO_2. However, the energy-intensive process of releasing the absorbed CO_2 is one of the main issues with amine-based CO_2 capture technology. This problem may be overcome if the captured CO_2 was transformed into a useful chemical instead of releasing it for further processing. This may be accomplished by using electrochemical CO_2 reduction (ECR) to create high-value C_2 derived products like ethylene, increasing the process's economic feasibility. Copper (Cu) catalysts have been intensively studied as they possess the ability to achieve good selectivity towards C_2 products while allowing for industrially-relevant current densities. Research has focused on improving the faradaic efficiency, selectivity and current density, with operating time typically limited to a few hours. However, the sustainability of ECR depends on the ability to maintain efficient performance over extended periods of time. The degradation of Cu-catalysts during ECR has not been extensively studied and is an area in need of further investigation. The dissolution and reconstruction of the electrode surface, or refaceting, as a consequence of potential, is believed to play a role in the performance degradation of Cu-catalysts. Thus, there is a need to investigate the degradation mechanisms of Cu-catalysts to improve their design and/or devise electrolysis procedures that can stably produce C_2 products, making the ECR technology more economically competitive. The present study investigates the degradation mechanisms of different electrodeposited copper catalysts in amine solutions and ECR-like conditions and to examine the effect of crystallographic orientation on the performance of these catalysts using

electrochemical characterization methods. The work was carried out as part of the ACT3 Project “CoCaCO$_2$la” (UK ACT ERA-NET EC GA 691712).

Corrosion Resistance of Stainless Steels for CCS Usage in Supercritical CO_2 Environment containing O_2 as a contaminant

Kyohei Kanki, Daisuke Matsuo, Yuji Arai, Hisashi Amaya

Nippon Steel Corporation, Japan

In Carbon dioxide Capture and Storage (CCS), the CO_2 emitted from various industries containing impurities is captured and injected to underground in dense or supercritical phase through a tubing. In order to evaluate corrosion resistance of the tubing materials in supercritical CO_2 environment with O_2 as a contaminant, corrosion tests were performed in the conditions of CO_2, containing 5 wt.%NaCl with the variation of O_2 contaminant level at total pressure of 130 bar and 100 °C. Super Martensitic Stainless Steel (UNS S41426, 13CR SMSS), Duplex Stainless Steel (UNS S82551, 25CR DSS), and Super Duplex Stainless Steel (UNS S39274, 25CR SDSS) were evaluated. The corrosion rates of UNS S41426 were higher than 0.1 mm/year and pitting occurred even in 0.1%O_2 (0.13 bar O_2 partial pressure) condition. On the other hand, UNS S82551 and S39274 showed good corrosion resistance, 0.1 mm/year or less of corrosion rate and no pitting corrosion even in 2.0 %O_2 (2.6 barO_2 p.p.) condition. It is considered that UNS S82551 and S39274 would be a suitable material even when flow back of formation water occurred in the supercritical CO_2 environment contaminated with O_2.

CO_2 Transport and Injection, Effect of Impurities, chemical Reactions and Consequences

J. Sonke, Y. Zheng

Shell Global Solutions International B.V., Amsterdam, The Netherlands

hans.sonke@shell.com

Carbon Capture and Storage (CCS) involves capturing, treating, transporting and storage of CO_2 to ensure long-term isolation from the atmosphere. In recent years there has been a significant increase in CCS project proposed and initiated. A number of these proposed projects aim to capture CO_2 from multiple industrial emitters (sources) to reduce the carbon footprint for these companies.

Depending on the CO_2 composition and operating conditions, separate corrosive liquid phases may be formed. It has been identified that these phases can comprise of water or reaction products including strong acids and elemental sulphur. To ensure long term integrity of the facilities, a safe project CO_2 specification needs to be identified. Tight control of CO_2 stream composition and operating conditions together are essential to ensure the integrity for all operating scenarios.

This paper focuses on identification of impurity limits for a CCS project, which is captured in a project CO_2 specification. Special attention given to one specific group of impurities that can react with each other and form a strong acids and elemental sulphur, that can cause a separate phase that can drop out of the CO_2 stream. Sound understanding of the mechanisms behind these chemical reactions, thermodynamics, the role phase behaviour plays and potential consequences are needed to be able to identify or adjust impurity limits for a project CO_2 specification. This work aims to improve understanding provide guidance and to reveal knowledge gaps that require addressing in order to identify a safe CO_2 specification for a CCS project.

CO_2 specification, Impurity limits, Liquid drop-out corrosion

Development of High Entropy Alloys for CCUS Applications

Shiladitya Paul,[1,2] Catherine Leahy,[2] Krzysztof Wieczerzak,[3] Jihad Zraibi[4], Marzuk Kamal[4], Dibakor Boruah,[2] Amir Shamsa,[2] Sokkalingam Rathinavelu,[1] Alvise Bianchin[5]

[1]School of Engineering, University of Leicester, University Rd, Leicester LE1 7RH, UK

[2]TWI Ltd., Granta Park, Cambridge CB21 6AL, UK

[3]Empa, Swiss Federal Laboratories for Materials Science and Technology, Laboratory for Mechanics of Materials and Nanostructures, Feuerwerkerstrasse 39, CH-3602 Thun, Switzerland

[4]AeonX AI SAS., Paris, France

[5]MBN Nanomaterials S.P.A., Treviso, Italy

There is a global drive to reduce carbon emissions without impacting economic growth. The reduction in CO2 emissions is technically feasible in vast majority of cases, but it is not always possible. Energy-intensive processes such as cement production inherently generate CO2 due to the chemical reactions involved in the process. For such industries, carbon capture, utilisation and storage (CCUS) provide a technology for reducing CO2 emissions to the atmosphere. To ensure the economic viability of CCUS, cost-effective materials need to be developed for the industry. Cement is not the only energy-intensive industry where reducing the carbon footprint depends on materials that can withstand aggressive environments for extended periods. Industries such as steel, transport, power generation, construction, marine etc. rely on materials performance in harsh environments. In many cases, the currently used materials have reached their limits, and thus, new materials need to be developed from non-critical raw materials to provide adequate performance.

High entropy alloys (HEAs) and compositionally complex alloys (CCAs) are new sets of materials that offer a vast compositional field which provides a challenging opportunity for designing alloys with improved combinations of properties. These

materials can be applied in the form of coatings to have functional surfaces that reduce the overall cost compared to cast or forged components.

This paper presents work carried out in a Horizon2020 project 'FORGE' which is looking at the 'Development of novel and cost-effective coatings for high-energy processing applications. New alloys were developed and tested in simulated CCUS environments. The paper will present results from the corrosion studies on the newly developed alloys.

This project has received funding from the European Union's Horizon 2020 research and innovation programme under grant agreement No 958457

Cathodic reaction mechanisms in CO_2 corrosion of low-Cr steels

Jinyang ZHU[1]

[1] *University of Science & Technology Beijing, China PR*

The cathodic reaction mechanisms in CO_2 corrosion of low-Cr steels were investigated by potentiodynamic polarization and galvanostatic measurements. Distinct but different dominant cathodic reactions were observed at different pH levels. At the higher pH level (pH > ~5), H_2CO_3 reduction was the dominant cathodic reaction. The reaction was under activation control. At the lower pH level (pH < ~3.5), H^+ reduction became the dominant one and the reaction was under diffusion control. In the intermediate area, there was a transition region leading from one cathodic reaction to another. The measured electrochemical impedance spectrum corresponded to the proposed cathodic reaction mechanisms.

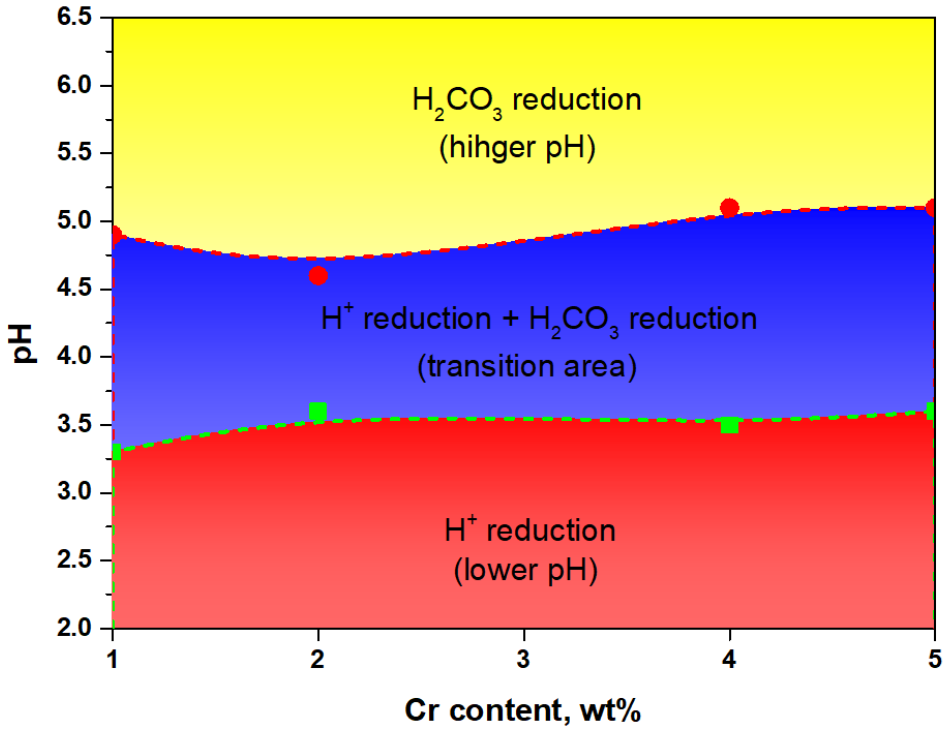

Improving predictions of $FeCO_3$ solubility and precipitation using a Pitzer activity coefficient-based method

Mustafa M. Alsalem[1], Mary, P. Ryan[2], Kyra Sedransk Campbell[3]

[1]Research and Development Centre, Saudi Aramco, Dhahran, 34466, Saudi Arabia
[2]Department of Materials, Imperial College, South Kensington Campus, London, SW7 2AZ, United Kingdom
[3]Department of Chemical and Biological Engineering, University of Sheffield, Sheffield, S1 3JD, United Kingdom

Carbon dioxide (CO_2) corrosion remains a long-standing challenge impacting processes in both the oil and gas industry and CO_2 capture and storage (CCS). Whilst the severity of CO_2 corrosion attacks (general and localised) has been widely investigated, some of its essential thermodynamic processes have not received much attention. In particular, the solubility product (K_{sp}) of its corrosion product, iron carbonate ($FeCO_3$), needs to be further investigated under non-ideal conditions, reflecting a broader range of challenging environments of industrial applications (*i.e*. high temperature and ionic strength). The development of this knowledge is critical for predicting $FeCO_3$ precipitation behaviours in CO_2 corrosion environments.

In order to predict $FeCO_3$ solubility product under non-ideal conditions, a CO_2 solubility and speciation model was developed and validated across a wide range of temperatures (20 – 100 °C) and ionic strengths (0 – 2.5 M NaCl). Herein, this model relies on Pitzer activity coefficients to reflect the effects of varying the ionic strength (0 – 2.5 M NaCl) and temperature (20 – 90 °C) on CO_2 dissociation reactions (ionisation of carbonic acid and bicarbonate). Utilising this model (with Pitzer), the activity coefficients of $FeCO_3$ constituents (Fe^{2+} and CO_3^{2-}) were estimated; these were employed to modify a well-established temperature-dependent K_{sp} to predict the effect of ionic strength variations under high temperatures. The development of this new model for CO_2 solubility and speciation under non-ideal conditions was implemented to update a broader model for $FeCO_3$ precipitation rate.

The revised $FeCO_3$ solubility model developed in this work showed that the new K_{sp} was significantly different from the widely employed prediction model, known as the unified model; this deviation is particularly evident as the strength exceeds 0.5 M

NaCl. This deviation represents an importance in how this new model addresses an inherent limitation of the unified model (constructed using two discrete limited models); the proposed new model is able to capture the evolution of the solubility product, where it initially increased as a function of ionic strength followed by a reduction with a further increase in ionic strength. The reduction point is influenced by temperature; the activity coefficients of Fe^{2+} and CO_3^{2-} cause this shift to occur at lower ionic strengths for higher temperatures (2.5 M at 25 °C *vs*. 1.5 M at 90 °C). Furthermore, it was shown that $FeCO_3$ precipitation rate deviated significantly when the effect of ionic strength and temperature were not adequately incorporated; considerably lower precipitation rates were observed. This suggests the need for a new model derived specifically for challenging environments of high ionic strengths and temperatures.

Corrosion in geothermal brine: the role of temperature and flow

Arne Simons[1], Willem Faes[2], Tom Depover[1], Steven Lecompte[2], Michel De Paepe[2], Kim Verbeken[1]

[1]Ghent University, Department of Materials, Textiles and Chemical Engineering, Research group Sustainable Materials Science, Ghent, Belgium, Arne.Simons@UGent.be; Tom.Depover@UGent.be; Kim.Verbeken@UGent.be
[2]Ghent University, Department of Electromechanical, Systems and Metal Engineering, Research group Sustainable Thermo-Fluid Energy Systems,Ghent, Belgium, Willem.Faes@UGent.be; Steven.Lecompte@UGent.be; Michel.DePaepe@UGent.be

Abstract: The uniform corrosion behavior of carbon steel in CO_2-saturated brine is studied for the possible application of carbon steel in heat exchangers. The corrosion rate was studied via weight loss experiments as a function of temperature, i.e. the entrance vs the exit of the heat exchanging section, and flow. Subsequently, the sample surface was studied with SEM and EDX. It was found that protective $FeCO_3$ is favored at higher temperature and lower flow rate (i.e. static conditions). The protective layer formation could explain the corrosion behavior as a function of time and temperature.

Keywords: Brine, Corrosion, Geothermal energy, Iron carbonates, Iron oxide, Sweet corrosion

Introduction

According to several sources [1]–[3], the total cost of corrosion for the electrical power industry was $15.4 billion in the U.S. in 1998. This amount is split into categories, where corrosion of heat exchangers takes up 5.55% or $855 million annually. Heat exchangers are often exposed to corrosive fluids, e.g. geothermal CO_2-saturated brine, possibly leading to material degradation characterized by uniform corrosion and/or localized corrosion. Stainless steels, titanium or other passivating metals usually show limited uniform corrosion. However, they are often more prone to local corrosion, e.g. pitting corrosion. Local corrosion is virtually impossible to monitor in-situ yet crucial for the heat exchanger's useful lifetime. Hence, metals showing uniform corrosion without localized corrosion are sometimes preferred over passivating metals. Even more, from an investigation in static brine [4], it was seen that carbon steel could form a protective iron carbonate layer, decreasing the corrosion rate with time. However, it is unknown whether uniform corrosion affects the thermohydraulic behavior of the heat exchanger, and vice versa, whether the thermohydraulic behavior influences the corrosion. However, within the current context of the energy transition, these are relevant topics. The goal of this work is to study the corrosion processes in geothermal CO_2-saturated brine.

Methodology

A set-up was build including a double-pipe heat exchanger. The inner tube of the heat exchanger is made of carbon steel (type E235+C, according to standard EN 10305-4 [5]) with an inner diameter of 8 mm and a wall thickness of 2 mm. Hot brine is flowing inside the inner tube, and a cooling liquid (a 50% water-ethylene glycol mixture) is flowing in the annulus between the inner tube and the outer tube. Due to the brine, the inside surface of the inner tube will corrode. Additionally, the tubes do not have a uniform temperature, since at either side of the tube wall, a different fluid at a different temperature is flowing. This could have an impact on the characteristics of the environmental degradation of the material. Moreover, the fluid movement could wear off possible corrosion products, impacting the formation of a protective layer.
Weight loss experiments and microscopic analysis (i.e. SEM and EDX) were performed on test samples that were periodically removed from the set-up. An experiment with static brine was used as a reference.

Results and discussion

From the periodical weight loss experiments, it was found that the corrosion rate decreased with increasing exposure time in static conditions, which is probably related to the formation of a protective layer. This behavior was not observed in dynamic conditions. On the other hand, with increasing temperature, the corrosion rate initially increased but later decreased in static conditions, while it continuously increased in dynamic conditions. Overall, the corrosion rate was higher in dynamic conditions than in static conditions.
To further study this behavior, the corrosion products were analyzed with EDX (see Figure 1). It was found that iron carbonates are formed on the carbon steel in the geothermal brine in static conditions. The $FeCO_3$ has a lower solubility at higher temperatures. Therefore, a more dense layer of corrosion products is formed, which is more protective to corrosion than the layer formed at lower temperature. Consequently, the corrosion rate is lower at 130 °C than at 80 °C. On the other hand, the EDX analysis on the samples in dynamic conditions showed that the corrosion products mainly consisted of iron oxides rather than iron carbonates. Iron oxides are insoluble in water, hence the temperature only affects the reaction kinetics via the Arrhenius relation. Consequently, the corrosion rate increases with increasing temperature.
In literature, it can be found that the formed corrosion products depend on the oxygen concentration [6]. The results in the current study indicate that the formed corrosion products also depend on the flow rate.

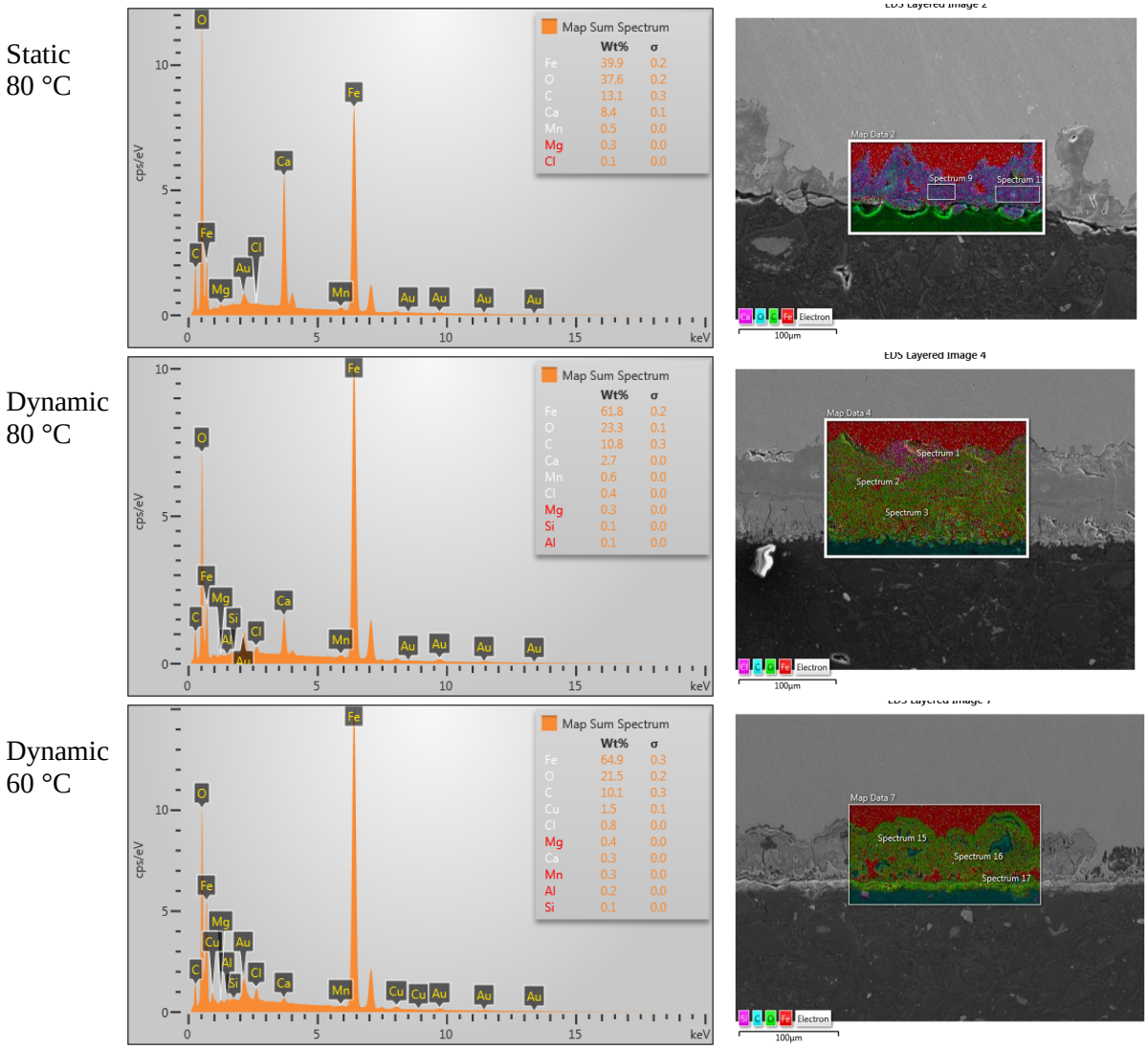

Figure 1: Results obtained after 4 weeks under static conditions at 80 °C, dynamic conditions at 80 °C and dynamic conditions at 60 °C via: (a) EDX; (b): SEM

Conclusion

It can be concluded that static conditions favor a protective carbonate layer, whereas dynamic conditions favor a less protective oxide layer. In static conditions, the formation of this carbonate layer results in a decreasing corrosion rate as a function of the exposure time. Moreover, the solubility of $FeCO_3$ decreases with increasing temperature. Therefore, the carbonate layer is more stable at higher temperature, resulting in a decreasing corrosion rate with increasing temperature.

In a dynamic experiment, an iron oxide layer is formed on the sample. As the protectiveness of this layer is limited, no clear effect as a function of the exposure time was observed. Moreover, iron oxide is insoluble in water, hence the stability does not vary significantly as a function of time. Therefore, the temperature only affects the reaction kinetics via the Arrhenius equation. Consequently, the corrosion rate in dynamic conditions increases with increasing temperature.

References

[1] P. R. Roberge, *Corrosion Engineering - Practices Vs Principles.*, vol. ChE9, no. 2. 2008.

[2] "Cost of corrosion in the electric power industry," 2001.

[3] B. C. Syrett and J. A. Gorman, "Cost of corrosion in the electric power industry: An update," *Mater. Perform.*, vol. 42, pp. 32–38, 2002.

[4] W. Faes *et al.*, "Corrosion behaviour of different steel types in artificial geothermal fluids," *Geothermics*, vol. 82, no. January, pp. 182–189, 2019, doi: 10.1016/j.geothermics.2019.05.018.

[5] Bureau for Standardisation, "NBN EN 10305-4: Steel tubes for precision applications - Technical delivery conditions - Part 4: Seamless cold drawn tubes for hydraulic and pneumatic power systems," 2016. [Online]. Available: https://www.nbn.be/shop/en/standard/nbn-en-10305-4-2016_19566/. [Accessed: 27-Jan-2023].

[6] P. N. Silva, G. Svenningsen, A. Dugstad, and J. A. C. P. Gomes, "The effect of oxygen on the CO2 corrosion of tensile wires in simulated annulus environments of flexible pipes," *Mater. Corros.*, vol. 73, no. 5, pp. 669–686, 2022, doi: 10.1002/maco.202112787.

Corrosion behavior of L80-1Cr steel as well tubing material for CO_2 storage applications

Avinash Ingle[1], Kapil Kumar Gupta[1], Sajjad Bahrebar[1], Benjamin Lorenzen[2], Andreas Christensen[2], Rajan Ambat[1]

Section of Materials and Surface Engineering, DTU Construct, Technical University of Denmark, 2800 Kgs. Lyngby, Denmark

[2]IKM Ocean Team A/S

Email: aviin@dtu.dk

Carbon capture and storage (CCS) is being extensively used to restrict climate change and environmental impacts caused by CO_2 emissions. Carbon steel (L80-1Cr) pipelines are most widely used in oil and gas as well tubing material. Corrosion occurs on the steel tubing during the injection and storage of CO_2, especially due to the impurities present in the CO_2 such as water, H_2S, SO_2, NH_3, O_2 etc. and is one of the key challenges in CCS applications. Therefore, it is critical to understand the corrosion behaviour of well tubing material and benchmark the corrosion levels to determine the allowable concentration of various impurities to estimate the integrity and service life of the wells for providing long-term safe storage. In this work, lab-scale parametric experiments were conducted on L80-1Cr specimens in an aqueous CO_2-saturated solution at ambient pressure with varying concentrations of different impurities at different temperatures in order to simulate CO_2 conditions after injection in CCS applications. The corrosion rate (CR) was determined using conventional electrochemical techniques such as polarization resistance, electrochemical impedance and weight loss measurements using ASTM standards. A flow loop test facility was also used to simulate the actual well conditions and calibrate the corrosion data determined from the lab-scale to actual well conditions. The results illustrated that the CR depends on the impurity levels and temperature, with a sharp increase observed at higher temperatures due to accelerated corrosion kinetics.

Electrochemical testing of Corrosion Resistant Alloys in aqueous media under high vs. dense phase partial pressures of CO_2

G. Sundararajan[1], and A. Sabnis[1]

[1]Shell India Markets Pvt. Ltd., Shell Technology Center, Bangalore/India

The objective of this work was to compare the effect of subcritical vs. super-critical partial pressures of CO_2 on the localized corrosion performance of corrosion resistant alloys (CRAs) that are used as tubulars for downhole/injection wells applications in the oil and gas industry. For Carbon Capture and Sequestration (CCS) applications, CRAs are required for resisting aggressive conditions of brine at acidic pH (due to high pressure CO_2) and elevated temperatures in CO_2 injection wells (that may also experience water-flow back scenarios). Cylindrical specimens of alloys UNS S41427 (Super 13-Cr), and UNS S32750 (25-Cr) Stainless Steels have been tested for determining localized corrosion performance based on measurement of corrosion potential (E_{corr}) and repassivation potential (E_{rp}) in aqueous solutions containing 150,000 ppm (mg/L) of NaCl at different partial pressures of CO_2. The alloys were tested in an autoclave at two levels of chlorides and pCO_2 independently to determine the effect of these variables on E_{corr} and E_{rp}. 25-Cr Super duplex stainless steel specimens were tested independently in aqueous NaCl in equilibrium with 30 bars and 85 bars pCO_2 at 75^{o}C. OLI Modeling tools enabled pH adjustment of brine at RT to attain the same in-situ pH at 30 bars as that for 85 bars at 75^{o}C. It was found that E_{corr} of 25-Cr alloy at both partial pressures were comparable within the range of experimental error. E_{rp} determined using Tsujikawa-Hisamatsu Electrochemical (THE) method at both levels of pCO_2 were comparable (within experimental error) for a given chloride and temperature condition. The effect of bi-carbonate concentration in the brine due to these 2 levels partial pressures of pCO_2 could not be clearly differentiated from the polarization scans of these alloys. Based on the comparable values of the magnitude of $E_{rp} – E_{corr}$ for 25-Cr alloy at 30 and 85 bars, it was concluded that the localized corrosion resistance of CRAs in chloride media in equilibrium with super-critical or dense phase CO_2 could be determined at sub-critical but high pressures (>30 bars) of pCO_2 at equivalent pH. This greatly reduced the complexity of aqueous electrochemical testing of CRAs under dense phase CO_2 for CCS applications.

Key words: Dense phase, Super-critical, pH, Super Duplex, CO_2, Repassivation, CCS

Corrosion Resistance of Stainless Steels in High CO_2-Brine phase with Hydrogen Sulfide or Oxygen Impurities for CCS applications

Karthik Krishnan, Halliburton, Carrollton, TX, USA

Cheng Chau Lum, Arpana Verma, Halliburton, Singapore

Understanding the corrosion behavior of various alloys in high CO_2-brine phase having impurities would be key for material selection in CCS (Carbon Capture Sequestration) wells where the wet CO_2 phase is likely to be more corrosive than the supercritical phase having little water content. Various stainless steel Corrosion-Resistant Alloys (CRAs) are used in typical oil and gas upstream wells for CO_2 corrosion resistance. Hence studying their corrosion performance in wet, saline high CO_2 conditions with some of the likely impurities that can be seen in CCS wells can help device strategy for material selection.

In this study, common stainless steel CRAs used for downhole well equipment has been evaluated for corrosion resistance in high CO_2 content having Hydrogen Sulfide (H_2S) or Oxygen (O_2) Impurities. The selected CRAs ranged from common martensitic stainless steels in 410SS, 13Cr (AISI 420mod); supermartensitic stainless steels having 13Cr-5Ni-2Mo (Super 13Cr) nominal composition, austenitic stainless steel in 316L, super duplex stainless steel (25Cr) with Pitting Resistance Equivalent Number (PREN) over 40. Autoclave testing was done in 200 bar (2900 psi) CO_2, 140000 mg/l Cl^- brine phase using NaCl solution at a temperature of 120°C (248°F) with (a) H_2S (100 ppm), (b) O_2 (20 ppm) impurities separately for total duration of 30 days each. Crevice coupon dimensions of 50mm x 25mm x 3mm with an 8mm hole in the center to allow for the attachment of crevice formers were used per ASTM G48 with duplicate samples of each material tested. The coupons were also used to evaluate pitting outside of the crevice regions and overall mass loss for general corrosion analysis post testing.

The test results showed that : (1) testing in the O_2 conditions above led to more severe localized and general corrosion than with H_2S in all the materials tested, (2) 410SS, 13Cr showed general corrosion and significant localized corrosion attack in both H_2S, O_2 test conditions with higher localized corrosion attack in O_2 conditions, (3) Super 13Cr, 316L, 25Cr saw little general corrosion or localized corrosion attack in H_2S conditions, (4) Super

13Cr, 316L showed little general corrosion but did show some pitting, crevice corrosion attack in O_2 conditions (5) 25Cr showed little general corrosion and no pitting corrosion but did show some crevice corrosion attack in O_2 conditions.

Details of both general and localized corrosion rates seen in the materials tested in the two environments will be presented. The study shows supermartensitic stainless steels and austenitic stainless steels do hold promise for use in CCS applications even in the highly corrosive wet CO_2 phase with high salinity having significant H_2S, O_2 impurities. Super duplex stainless steels as expected with their high pitting resistance also can be options for this environment.

Key words: Stainless Steel, CRA, CCS, Brine, H_2S, Oxygen, Pitting, Crevice Corrosion

Dense-Phase CO_2 Corrosion: Modeling the Chemistry of CO_2 – Rich Phases with Impurities using the MSE Thermodynamic Framework

Ronald D. Springer, OLI Systems, Inc, USA
Andre Anderko, OLI Systems, Inc., USA
Anthony J. Gerbino, OLI Systems, Inc., USA
Diana M. Miller, OLI Systems, Inc., USA

A web-based application has been developed to predict the behavior of oxidizing/reducing impurities that lead to corrosion damage in supercritical CO_2. This tool is based on experimental work completed at IFE coupled with a mathematical/thermodynamic Mixed Solvent Electrolyte (MSE) developed at OLI Systems, Inc. The application predicts the formation of a strong electrolyte phase when concentrations of impurities reach critical values. To make this calculation possible, we did an extensive revision of the algorithm for computing phase and chemical equilibria. This made it possible to simulate simultanelusly, redox reactions, and liquid-liquid-solid equilibrium reactions from a non-aqueous solvent (CO_2). The key impurities include N- and S- containing components an their ability to oxidize/reduce and subsequently form strong acids (HNO_3 and H_2SO_4) which are detrimental for metalurgies used in CO_2 transportation.

Introduction

The behavior of impurities in CO_2 transportation is very complex due to the coupling of phase and chemical (both acid-base and redox) equilibria. The phase and chemical equilibria are a sensitive function of temperature, pressure, and impurity concentrations. Therefore, in addition to the fundamental measurements in CO_2-rich phases, it is necessary to establish a thermodynamic model for predicting the equilibrium behavior of such systems. While such a model cannot predict the kinetics of reactions between impurities, it can predict the worst-case scenario when the reactions between the impurities lead to the formation of highly corrosive phases. The model needs to be inherently applicable to multicomponent mixtures and include the behavior of other impurities (such as NO_x, SO_x, H_2O, H_2S, and O_2). Furthermore, it needs to be capable of simulating reactions between the impurity species within both

the H_2O-rich and CO_2-rich phases. This results in requirements for unique thermodynamic modeling. The thermodynamic framework for such a model is provided by the Mixed-Solvent Electrolyte model of Wang et al. [1], [2], which has been designed for the simultaneous calculation of phase and chemical equilibria in systems containing strong and weak electrolytes in aqueous, non-aqueous and mixed solvents. The theoretical structure of the model has been described in previously published articles [1]–[5].

This thermodynamic model in the MSE framework is capable of reproducing the phase behavior of the following impurities in mixtures with CO_2 and H_2O:

a. Nitrogen oxides, i.e., N_2O, NO, N_2O_3, and NO_2
b. Sulfur dioxide

As well as being capable of reproducing the solubility of the key products that may result from the reactions between the impurities, i.e.,

a. Elemental sulfur
b. Sulfuric and nitric acids

Finally, an extension of the algorithm for phase and chemical equilibria was added to enable the computation of redox transformations within CO_2-rich phases and not only aqueous phases.

As a result of the research and development conducted thus fur, a web-based app (a.k.a. the CO_2 Transportation App) has been created for simulating the behavior of impurities in CO_2 phases. This was based on extensive thermodynamic modeling efforts that resulted in introducing various impurities into the Mixed-Solvent Electrolyte databank. Thermodynamic modeling was accompanied by an extensive revision of the algorithm for computing phase and chemical equilibria, which made it possible to simultaneously simulate redox and liquid-liquid-solid equilibria in primarily nonaqueous phases, and now it is easily accessed using a web based app without compromising the rigour of the thermodynamic preditctions. This app will then be able to orient users to determine which concentration of impurties will be detrimental for CO_2-tranport pipelines, and can take preventive measures before a corrosion failure happens.

Abstract

The casing system is one of the main structural systems in a vertical well which is made of a number of components like the casing in different sizes and the production tubing. Casings and tubing corrosion is one of the main causes of serious incidents and failures. Their failure is primarily due to internal corrosion which is a function of process conditions mainly temperature, flow rate, pressure and concentrations of corrosive substances that exists naturally in the produced fluid like carbon dioxide. In this work, a prediction model of CO_2 (sweet) corrosion of steel casing is developed using COMSOL Multiphysics. The effect of temperature and pH on the corrosive species concentrations from the bulk solution to the surface of the steel is studied. The concentration of iron ions is found to be increasing with temperature at a constant pH of 5 at the surface of the steel due to the dissociation of the steel surface. Also, due to absence of mixing effect, the variation in species concentrations at the boundary layer shows that there is a significant turbulent sublayer that is present near the surface of the steel influencing the kinetics of the corrosion process. It was also found that sweet corrosion rate of steel increased with increasing temperature and decreasing solution pH. Finally, for different partial pressures of carbon dioxide in the produced fluid, the corrosion rate variation with temperature and solution pH was reported.

Comparing experimental and modelled atmospheric corrosion rates under droplet distributions

N. Van den Steen, Vrije Universiteit Brussel, Belgium; E. Rahimi, Delft University of Technology, The Netherlands; K. Zhang, Delft University of Technology, The Netherlands; Y. Gonzalez-Garcia, Delft University of Technology, The Netherlands; J.M.C. Mol, Delft University of Technology, The Netherlands; H. Terryn, Vrije Universiteit Brussel, Belgium

The complex, convoluted and relatively slow nature of atmospheric corrosion makes the development of physics-based models very challenging. Before an accurate physics-based model can be implemented, a deep understanding of the phenomena is needed. The stepwise development of such models can however highlight the strengths and gaps in the current state-of-the-art.

The electrolyte properties: quantity, composition, geometry, etc. are known to play a crucial role in corrosion processes, but due to the complexity the electrolyte formation (nucleation and growth) is outside the scope of most corrosion research. Previously, a new approach in corrosion modelling [1] was presented to combine experimental (electrochemical kinetics and size distributions of droplets) and modelling approaches implementing the strengths and bypassing the limitations of both. For example, the modelling of droplet nucleation and growth is highly complex. Measuring the droplet size distribution instead of modelling reduces the complexity of the endeavor. On the other hand, experimentally, it is hard to assess the effect of different parameters or to control contact angles and droplet sizes, while in a model, this is relatively easy to do. For initial validation, the system was further simplified to reduce the complexity: the limiting current density was compared showing relatively good agreement.

With electrical resistance (ER) measurements, the complete system is considered: the effect of mass transport, droplet size distributions, electrochemical processes and kinetics. During the ER measurements, the droplet size distribution was monitored simultaneously. The time derivative of the ER values is directly related to the corrosion rate. The initial droplet distribution is established by spraying a known NaCl solution on the surface in a high humidity environment. After a fixed time, the humidifier is turned off and the droplets dry gradually. The measured droplet size distributions and initial concentrations are input for the model, while the

instantaneous corrosion rates based on the ER measurements are compared with the model. Different trends can be observed depending on the conditions. By comparing the output of the model with experimental results, new insights into the corrosion mechanisms and key parameters are obtained. These new insights enable the identification of the next incremental steps in order to get the most reliable and accurate model improvements.

This research was carried out under project T18016 in the framework of the Research Program of the Materials innovation institute (M2i) (www.m2i.nl) supported by the Dutch government.

[1] N. Van den Steen, Y. Gonzalez-Garcia, J. M. C. Mol, H. Terryn, and Y. Van Ingelgem, “Predicting the effect of droplet geometry and size distribution on atmospheric corrosion,” Corrosion Science, vol. 202, p. 110308, Jul. 2022, doi: 10.1016/j.corsci.2022.110308.

Design and construction of a rainfall simulator to test metal runoff at atmospheric conditions

Nasrin Haacke[b], Mario Sahre[a], Sven Schlau[c], Sven Gersdorf[c], Gino Ebell[b]

Bundesanstalt für Materialforschung und-prüfung (BAM)

[a]Division 6.1 Surface Analysis and Interfacial Chemistry

[b]Division 7.6 Corrosion and Corrosion Protection

[c]Division 9.2 Testing Devices and Equipment

Unter den Eichen 87, 12205 Berlin, Germany

A rainfall simulator was designed and constructed to test the influence of selected environmental and exposure parameters and corrosion product layer characteristics on the first flush and runoff rates of zinc, copper, and their alloys from roofing materials at laboratory conditions. A key feature of the simulator is the accurate representation of raindrops, often neglected in other laboratory setups but stated as a limiting and crucial factor. This setup simulates rainfall using medical grade capillary tubes, which, using an integrated pressure regulator to adjust rainfall intensity, can simulate light, moderate, and heavy rain. An adjustable sample holder also permits sample inclination angles of 15 – 65° and can be extended in height according to a modular system. The composition of artificial rain used in experiments mimics the composition of precipitation in the northeastern part of Germany, reflecting local environmental conditions. The effect of precipitation pH ranging between pH 4.5 and 6.5 on the runoff behavior is also part of the investigation and is based on the variation in precipitation pH from a rural and urban area in Germany.

The laboratory data will be used to explain variations in runoff rate at different locations, between different sampling periods observed in field data and to evaluate the degree of various environmental impact factors. It also introduces a possible laboratory testing device that can be used more generally to evaluate building materials under atmospheric conditions.

A new systematic approach in multi-electrochemical analyses of the corrosion behavior of iron under a single saline droplet

Ehsan Rahimi (Delft University of Technology, Delft, the Netherlands), Keer Zhang (Delft University of Technology, Delft, the Netherlands), Nils Van den Steen (Vrije Universiteit Brussel, Brussels, Belgium), Herman Terryn (Vrije Universiteit Brussel, Brussels, Belgium), Arjan Mol (Delft University of Technology, Delft, the Netherlands), Yaiza Gonzalez-Garcia (Delft University of Technology, Delft, the Netherlands)

Gradual corrosive degradation through exposure to an atmospheric environment may jeopardize the functional and mechanical integrity of a wide variety of metallic structures and applications during their service lifetime. Hence, a deep understanding of the atmospheric corrosion process of metallic materials under tiny single or multiple droplets and thin electrolyte films is of pivotal importance in the development of bespoke material and surface treatment processes as well as accurate service life prediction. In this research, utilizing a dedicated micro-sized three-electrode cell, we systematically monitor the electrochemical properties and corrosion behavior of commercially pure iron under single droplets. Different volumes (1.5 µL, 3 µL, and 5 µL) and Cl^- concentrations (0.01M, 0.1M, and 0.2M) were considered during the evaporation-driven shape and dimensional evolution of single droplets. Moreover, a combination of techniques, incuding potentiodynamic polarization and electrochemical impedance spectroscopy (EIS) was considered along with the monitoring of electrochemical current and potential noise (ECN and EPN) signals during the dynamic evolution of the droplets. These measurements showed that by reducing the droplet size from 5µL to 1.5µL at low Cl^- concentration (0.01M), the electrochemical activity of pure iron surface initially decreased which can be ascribed to the rate determining step being oxygen diffusion over the chloride ions. Additionally, an enhancement in noise resistance (R_n) and polarization resistance (R_p, recorded by EIS) was observed and a switch from concentration- to activation-controlled electrochemical reduction. However, at higher Cl^- concentrations (0.1M and 0.2M), by reducing the droplet size and using the same approach, the relatively high chloride ion concentration dominates over oxygen diffusion, triggering enhanced localized corrosion.

On the effect of relative humidity and formation of surface water film on atmospheric corrosion

Tomáš Prošek, Mehrdad Zia Hoseinpoor, Technopark Kralupy of the University of Chemistry and Technology Prague, Kralupy nad Vltavou, Czech Republic

Atmospheric corrosion cannot proceed without presence of a thin film of water electrolyte on the metal surface. It is believed that at least ≈5 monolayers of water need get adsorbed for water to behave as an electrolyte. This fundamental fact is behind the practically important threshold of 80% relative humidity (RH) above which the corrosion rate of non-polluted metals increases to technically relevant levels. This threshold defines the time of wetness criteria. However, atmospheric corrosion is a surface reaction and air temperature does not necessary correspond to surface temperature.

Field and laboratory measurements have been performed to show that the metal surface temperature often varies from the air temperature, affecting the actual surface relative humidity (SRH) and the actual time of wetness. A yearly monitoring programme showed that the real time of wetness was up to 40 % longer than the theoretical one calculated from the air RH. The importance of the SRH in corrosion is shown by galvanic current measurements on a sensor with independent control of surface temperature and air parameters.

Several implications of the SRH concept for atmospheric corrosion are suggested, including deeper drying, a longer actual time of wetness, and a lower temperature at which atmospheric corrosion processes proceed. Practical applications of the concept are demonstrated in understanding the corrosion degradation of sandwich panels, corrosion in overlaps, and development of better accelerated corrosion tests. Finally, a simplified procedure is proposed to estimate the actual time of wetness from available climatic data.

Corrosion of carbon steel under electrolyte droplet distributions

K. Zhang, Delft University of Technology, The Netherlands; E. Rahimi, Delft University of Technology, The Netherlands; N. Van den Steen, Vrije Universiteit Brussel, Belgium; H. Terryn, Vrije Universiteit Brussel, Belgium; J.M.C. Mol, Delft University of Technology, The Netherlands; Y. Gonzalez-Garcia, Delft University of Technology, The Netherlands

Field exposure testing (FET) and accelerated corrosion testing (ACT) are two typical approaches applied in industry to assess the atmospheric corrosion rate of a certain material, both relying on visual inspection and weight change of the specimen. FET takes place under natural atmospheric conditions but requires decades-long exposure time, while ACT shortens the exposure time to weeks but the link between the natural environment and ACT chamber conditions is still unresolved. Efforts have been made to correlate ACT results with those obtained in FET based on weight loss both qualitatively and quantitatively, mainly empirically and limited to small datasets [1]. Linking FET results with environmental conditions has been performed by introducing real-time corrosion rate monitoring technics, such as galvanic coupons and electrical resistance (ER) coupons during FET [2]. The latter usually involves big datasets and multi-variables, resulting in the need for using machine learning based data analysis.

In general, this work studies the link between modified FET and the environment from the electrolyte point of view, under controlled laboratory conditions. *In-situ* monitoring and analysis of corrosion rate, electrolyte condition and environment are shown to be feasible and the effect of NaCl concentration and droplet configuration on the atmospheric corrosion rate of carbon steel has been addressed [3].

While the corrosion rate assessment has shed some light on the atmospheric corrosion mechanism and its kinetics, still more detailed analysis is needed. A user-designed modifiable setup has made it possible to not only visualize electrolyte conditions, but also the initiation and growth of pits can be monitored. *Ex-situ* XRD analysis has been performed to analyze the formed corrosion product with a time interval of 1h for a group of parallel exposed carbon steel samples. Besides, OCP measurement has also been introduced onto an ER sensor for thermodynamic assessment of the corrosion process.

These investigations make it possible, from the electrolyte and corrosion product formation point of view, to explain the finding that carbon steel atmospheric corrosion rate is not very sensitive to environmental condition changes in an atmospheric exposure test chamber, as proposed by Prosek et al. in 2014 [4].

[1] Wu, H., Lei, H. and Chen, Y.F., 2022. Grey relational analysis of static tensile properties of structural steel subjected to urban industrial atmospheric corrosion and accelerated corrosion. *Construction and Building Materials*, 315, p.125706.

[2] Pei, Z., Zhang, D., Zhi, Y., Yang, T., Jin, L., Fu, D., Cheng, X., Terryn, H., Mol, J.M.C. and Li, X., 2020. Towards understanding and prediction of atmospheric corrosion of an Fe/Cu corrosion sensor via machine learning. *Corrosion Science*, 170, p.108697.

[3] Van den Steen, N., Gonzalez-Garcia, Y., Mol, J.M.C., Terryn, H. and Van Ingelgem, Y., 2022. Predicting the effect of droplet geometry and size distribution on atmospheric corrosion. *Corrosion Science*, 202, p.110308.

[4] Prosek, T., Le Bozec, N. and Thierry, D., 2014. Application of automated corrosion sensors for monitoring the rate of corrosion during accelerated corrosion tests. *Materials and Corrosion*, 65(5), pp.448-456.

Impact of *Sargassum* seaweed degradation on atmospheric corrosion of copper and zinc materials in the French West Indies

Mahado Said Ahmed[1], Stéphane Rioual[2], Mounim Lebrini[1], Christophe Roos[1] and Benoit Lescop[2]

[1]Univ Antilles, L3MA, EA7526, Campus de Schœlcher*, France*

[2] Univ Brest, Lab-STICC, CNRS, UMR 6285, F-29200 Brest, France

Since 2011, large amounts of floating species of *Sargassum* seaweed arrived periodically on the coasts of some Caribbean islands, the Gulf of Mexico and northern Brazil. The decomposition of these seaweeds in beaches cause major environmental and economic problems in the affected areas. Indeed, this phenomenon leads to the release of different toxic gases such as hydrogen sulfide (H_2S) and ammonia (NH_3). As recently reported [1], *Sargassum* stranding leads to deleterious consequences on human health in Martinique. Moreover, the presence of H_2S may cause corrosion problems due to its aggressive nature for different metals such as Cu, Zn … [2].

This work studies the effects of *sargassum* algae degradation on corrosion of Cu and Zn in Martinique (French West Indies). The climate of this island, located in the center of the Caribbean Sea, has a harsh tropical marine climate with high relative humidity (80 %) and constant temperature (30°C). Metallic coupons were exposed in three different localizations during 3, 6, 9 and 12 months in 2022. The first site (*Frégate est*) is close to a beach exposed to *sargassum* degradation, the second one (*Diamant*) is a beach without *sargassum* and the last one (*Vert pré*) is far from the sea (several kilometers). This choice enables to differentiate between the effect of the H_2S and those due to NaCl.

Initially, the corrosion rates were measured for Zn and Cu coupons by gravimetry. The corrosion rate was drastically higher in *Frégate est* compared to the other sites, confirming the impact of *Sargassum* degradation. The corrosion products were determined using Scanning Electron Microscopy (SEM), Energy Dispersive Spectrometry (EDS) and X-Ray Diffraction (XRD) techniques. The corrosion products observed in the sites of *Vert Pré* and *Diamant* are classical in atmospheric tropical marine environment: gordaite, simonkolleite for Zn and cuprite, $Cu_2Cl(OH)_3$ for Cu

[3]. The corrosion process is clearly dominated by the presence of oxygen and NaCl. Note that the corrosion rate is lower in *Vert Pré*, due to the higher distance to the sea.

On the coupons exposed in *Frégate est*, high percentages of sulfur is reported by EDS. The corrosion products are clearly dominated by CuS and ZnS. The absence of corrosion products including Cl even close to the seawater confirms the very strong efficiency of hydrogen sulphide in corrosion. No clear evolution of corrosion products is reported for different exposures.

References

1. Resiere D, Mehdaoui H, Florentin J, Gueye P, Lebrun T, Blateau A, Viguier J, Valentino R, Brouste Y, Kallel H, Megarbane B, Cabie A, Banydeen R and Neviere R, Sargassum seaweed health menace in the Caribbean: clinical characteristics of a population exposed to hydrogen sulfide during the 2018 massive stranding, Clinical Toxicology, 59 (2021) 215-223.

2. Becker J, Pellé J, Rioual S, Lescop B, Le Bozec N, Thierry D, Atmospheric corrosion of silver, copper and nickel exposed to hydrogen sulphide: a multi-analytical investigation approach, Corrosion Science, 209 (2022) 110726.

3. Morcillo M., Chico B., de la Fuente D. and J. Simancas J., Looking Back on Contributions in the Field of Atmospheric Corrosion Offered by the MICAT Ibero-American Testing Network (2012) 824365.

Comparative study of the atmospheric corrosion of carbon steel in cold and temperate marine environment

Zhongyu Cui[a, b], *Maoxin Yan*[a], *Xin Wang*[a], *Herman Terryn*[b], *Hongzhi Cui*[a]

a School of Materials Science and Engineering, Ocean University of China, Qingdao 266100, China

b Research Group Electrochemical and Surface Engineering, Vrije Universiteit Brussel, Brussels, 1050, Belgium

Atmospheric corrosion behavior of Q235 carbon steel exposed to Zhongshan station in Antarctica and the temperate Qingdao environment for 12 months was investigated. The results indicate that the corrosion rate of carbon steel exposed to Antarctica environment for 1 month is higher than that of the temperate Qingdao environment, while the corrosion rate of carbon steel after exposure for 12 months is lower than that exposed in the temperate Qingdao environment. The freeze-thawing of ice and snow causes the local long-period existence of thin electrolyte films to accelerate the corrosion of carbon steel. Pitting corrosion occurs when carbon steel is exposed to the Antarctic environment, and the skyward surface is more serious. The corrosion products of carbon steel are mainly composed of lepidocrocite, goethite, magnetite/maghemite, and akaganeite. There is no akaganeite in the corrosion products of carbon steel after atmospheric exposure in the temperate Qingdao environment. Electrochemical test results showed that the corrosion product layer formed after 12 months of exposure exhibit protection effect.

Atmospheric corrosion of carbon steel and galvanized steel: one-year exposure in Valle de Aburrá, Colombia

Ana C. Santa [a]; Libia M. Baena [a]; Jose A.Tamayo [a]; Maryory A. Gomez [b]; Diego A. Montoya [b]; Jose F. Aguirre [a]; Juan G. Castaño [a], a Grupo Calidad metrología y producción, Instituto Tecnológico Metropolitano –ITM-; b Centro de Investigación, Innovación y Desarrollo de Materiales – CIDEMAT, Facultad de Ingeniería, Universidad de Antioquia UdeA, Medellín Antioquia Colombia.

Atmospheric corrosion of carbon steel and galvanized steel was measured during one year exposure in urban and industrial test sites located in the Valle de Aburrá, Colombia. Tests have been performed to determine chlorides, sulfur dioxide, time of wetness (TOW), and corrosion rates, following ISO 9223 and 9225, and ASTM G1 and G50 standards, for station installation and chemical cleaning. Valle de Aburrá is a subregion that falls within the definition of a “Metropolitan Area” and is situated in the southernmost portion of the Colombian department of Antioquia, in the heart of the Central Andes mountains. It has geographical, meteorological, and urban growth characteristics that cause a very particular atmospheric contamination problem. The valley is surrounded by high mountain elevations that restrict air circulation at certain times of the year, difficulting the dispersion of air pollutants and particulate matter. Despite that, research about atmospheric corrosion in the valley has not yet been conducted until now.

The general objective of this work is to analyze the influence of air pollutants and climatological parameters on the atmospheric corrosion of carbon steel and galvanized steel after exposure to the atmosphere for one year at 5 test stations in the Valle de Aburrá. Weigh losses were determined to establish the corrosion kinetics in all sites. Scanning electron microscopy (SEM), X-ray energy dispersion (EDX), X-ray diffraction (XRD), and Raman spectroscopy (RS) were used to characterize corrosion products.

Correlations between atmospheric variables and corrosion rates are presented. Higher corrosion rates are observed in the south of the valley, where higher values in SO_2 deposition and TOW are measured. The influence of the particular regime of winds in the valley is analyzed. Lepidocrocite and goethite phases have been observed in

carbon steel in all of the test locations, with minor differences in their morphologies and amounts. For galvanized steel, low mass losses are obtained, as well as little amount of corrosion products, in which zincite is predominant.

Atmospheric Corrosion Resistance of Stainless Steel Welds after Heat tint removal by several cleaning techniques.

Jens Conderaerts, Belgian Welding Institute

The corrosion resistance of heat tinted areas of stainless steel weld faces is lower compared to the base and weld material. This has been shown in previous investigations in Belgium [1] and Germany [2] and in a recent European project [3]. This problem can be overcome by removal of the heat tint by cleaning the weld seam. Pickling with solutions containing fluoric acid (HF) and nitric acid (HNO_3) has been found as the best method to restore the corrosion resistance of the welded zone to the levels of the base material.

However, HF and HNO_3 are dangerous substances, with corrosive and toxic effects for skin and lungs. Consequently, safety precautions are taken to work with HF and HNO_3. Recently, safety measures tend to avoid the usage of HF and HNO_3 especially in the chemical industry. Alternative treatments are available on the market, but independent research lacks on the performance of these alternative techniques to restore the corrosion resistance.

This research presents results of corrosion testing on stainless steel welds in AISI type 304L after cleaning with

- Pickling paste
- Electrochemical cleaning with phosphoric acid
- Electrochemical cleaning with neutral solution
- Laser cleaning
- Brushing
- Wet blasting technique

These techniques are compared to the reference case without cleaning. The presentation will show results of 3 years atmospheric exposure testing in different corrosion categories (C3, C4 and C5) and exposure testing in the outdoor atmosphere of a chemical plant for 2 years. Samples are evaluated by visual examination, 3D microscopy, SEM and metallography.

The results show that the heat affected zones of welds may be more susceptible to corrosion, but that this does not come from the heat tint nor from the chosen cleaning technique.

Acknowlegdement

The research project is funded by SIM-VLAIO under project number HBC 2017.0683.

Reference

[1] Eindrapport collectief BIL-NIL project “Verwerking en Gebruik van Roestvast Staal”, Defrancq en Heerings, 1994.

[2] Köstermann H., Schweißbedingte Anlauffarben – müssen grundsätzlich blanke Nähte gefordert werden? Abschätzung des korrosiven Einflusses von gelben Anlauffarben auf geschweißte CrNi(Mo)-Stähle, AiF 11.381 N/1, DVS 1.017, Technische Universität Braunschweig, 2001

[3] JOINOX Final Report, Guidelines for use of welded stainless steel in corrosive environments, RFCS-project, 2018

Effect of blue light on oxidation and chloride-induced atmospheric corrosion of copper

Tingru Chang[a], Gunilla Herting[a], Inger Odnevall[a], Christofer Leygraf[a]
[a]KTH Royal Institute of Technology, Department of Chemistry, Division of Surface and Corrosion Science, Teknikringen 29, SE-100 44 Stockholm, Sweden

Copper is an important functional material that is widely used in many industrial and societal applications, such as electronics, façade and roof materials and heat exchangers due to its favorable electrical conductivity, corrosion resistance and heat transfer ability [1]. Depending on practical applications, the atmospheric corrosion of copper has been extensively studied in various indoor and outdoor conditions by introducing corrosion stimulators such as relative humidity (RH), corrosive gases, airborne salt particles and artificial sweat [2]. The role of photo-radiation, including visible light and ultraviolet (UV) light, on the corrosion process of different metals has gained attention in recent years due to the potential photovoltaic effect of the corrosion products formed [3]. The effect of blue light on the atmospheric corrosion of copper, nevertheless, has not been investigated. The effect is significant when copper is used as a high-touch surface in, e.g., healthcare or hospitals, where blue light can be used to disinfect the settings.

This study investigated the influence of blue light on the oxide formation and corrosion product evolution of copper in humid air with and without pre-deposited Cl with respect to surface appearance, corrosion product morphology and composition, and corrosion resistance by means of a multi-analytical approach including microscopic, spectroscopic, and electrochemical techniques. The results show that the formation of Cu_2O was accelerated by the exposure under blue light and humidified air, leading to a slightly increased corrosion resistance compared to no light exposure. With the pre-deposition of NaCl, the formation of CuCl/$Cu_2(OH)_3Cl$ was also enhanced upon blue light exposure, resulting in enhanced concomitant flaking of the corrosion products layer (induced by the phase transformation of CuCl to $Cu_2(OH)_3Cl$ [4]), thereby leading to a slightly inferior surface barrier property.

References

[1] J.R. Davis, Copper and copper alloys, ASM international, 2001.
[2] C. Leygraf, I. Odnevall Wallinder, J. Tidblad, T. Graedel, Atmospheric corrosion, 2nd ed., John Wiley & Sons, 2016.
[3] J. Wu, J. Wang, Y. Wu, Investigation of photo-induced corrosion of copper in aqueous solution based on point defect model, Mater. Chem. Phys., 255 (2020) 123648.
[4] X. Zhang, I. Odnevall Wallinder, C. Leygraf, Mechanistic studies of corrosion product flaking on copper and copper-based alloys in marine environments, Corros. Sci., 85 (2014) 15-25.

Corrosion inspection and corrosion characterization using hyperspectral imaging technology in Near Infrared range

Thomas De Kerf[1], *Zohreh Zahiri*[1], *Simon Verspeek*[1], *Steve Vanlanduit*[1], *Paul Scheunders*[1]
University of Antwerp, Belgium

Effective and efficient detection of corrosion is crucial for maintaining the integrity of metal structures and reducing the long-term cost of industrial infrastructure. A significant portion of the cost of maintaining these platforms and infrastructure is the time and effort spent identifying and repairing corrosion damage through major overhauls or replacements[1]. Early detection of corrosion can help to minimize these costs[2]. There are several methods for detecting atmospheric corrosion in carbon steel samples, which can be divided into two main categories: techniques that detect material changes caused by corrosion and techniques that characterize corrosion products. Physical measurement techniques, such as coupons, electrical resistance, ultrasonic testing, and acoustic emission, directly measure the damage caused by corrosion. Electrochemical measurement techniques, including linear polarisation resistance, electrical impedance spectroscopy, electrochemical noise, and the scanning vibrating electrode technique, measure changes in the electrochemical signal of a material caused by corrosion. These methods can be useful for determining the overall corrosion rate of a structure, but may not be suitable for identifying corrosion in specific locations on a larger structure.

An alternative approach to corrosion detection is to identify, locate, and quantify corrosion products. There is a correlation between the correct identification and quantification of corrosion minerals and corrosion rate. A protective ability index (PAI) can be used as a metric to evaluate the protective properties of a corrosion layer. There are two main categories of techniques for identifying minerals: chemical analysis and optical imaging. Chemical analysis methods, such as Fourier transform infrared spectroscopy, Raman spectroscopy, X-ray diffraction, scanning electron microscopy, and atomic force microscopy, can accurately identify different corrosion minerals, but are not practical for use outside of a laboratory on large samples. Optical measurement techniques, such as standard visual spectrum cameras, multispectral cameras, and hyperspectral cameras, can be used to image larger areas, but using RGB cameras to identify corrosion minerals is challenging due to the similar red-brown hue of many corrosion minerals.

Multispectral and hyperspectral imaging offer a balance between optical imaging and chemical detection. These cameras provide more spectral information (usually 3-10 wavelengths for multispectral and more than 10 wavelengths for hyperspectral) than an RGB camera and can operate in various spectra, from ultraviolet to long-wave infrared. Hyperspectral imaging has various applications, such as remote sensing, food analysis, biomedical research, waste separation, and agriculture. While there is limited research on the use of hyperspectral imaging for corrosion detection, some studies have used it to examine corrosion on bronze statues, steel samples, and copper oxide layers.

In recent years, low-weight, low-cost hyperspectral cameras have been developed that can be mounted on tripods, drones, or robots for easier, safer, and faster in-situ

inspection. The aim of this study is to evaluate the potential of hyperspectral imaging data in the shortwave Infrared range (SWIR) in characterization of corrosion and identifying corrosion minerals.

To investigate the potential of hyperspectral imaging in SWIR range for corrosion characterization, we performed hyperspectral imaging on several case studies from different applications. The samples were sent to us from different companies for different characterization. We scanned these samples in laboratory with an FX17 Specim camera (900-1700nm) and applied different image analysis algorithms (depending on the application) to detect the problems.

Several case studies were performed such as:

- The analysis and detection of corrosion on zinc electroplated steel
- The detection of aluminum oxidation on PU guns
- Analysis of the cleanliness of laser cleaned corrosion surfaces
- The detection and characterization of atmospherical corrosion products
- The detection of chloride presence on carbon steel after sandblasting.

The results of our experiments showed that hyperspectral imaging can be used as a non-contact non-destructive monitoring technique to detect corrosion, estimate the amount corrosion content left on a cleaned surface, identify the corrosion minerals and their abundance in every pixel, and detect where more material loss due to corrosion has occurred.

References

[1] NACE International, “NACE study estimates global cost of corrosion at $2.5 trillion annually,” Mar. 08, 2016. https://inspectioneering.com/news/2016-03-08/5202/nace-study-estimates-global-cost-of-corrosion-at-25-trillion-ann (accessed Nov. 13, 2022).

[2] G. Koch, J. Varney, N. Thompson, O. Moghissi, M. Gould, and J. Payer, “International Measures of Prevention, Application, and Economics of Corrosion Technologies Study,” Houston, 2016. Accessed: Nov. 09, 2022. [Online]. Available: http://impact.nace.org/documents/Nace-International-Report.pdf

[3] J. M. Amigo, H. Babamoradi, and S. Elcoroaristizabal, “Hyperspectral image analysis. A tutorial,” Analytica Chimica Acta, vol. 896. Elsevier B.V., pp. 34–51, Oct. 08, 2015. doi: 10.1016/j.aca.2015.09.030.

[4] M. Sai Bhargava Reddy, Deepalekshmi Ponnamma, Kishor Kumar Sadasivuni, Shampa Aich, Saraswathi Kailasa, Hemalatha Parangusan, Muna Ibrahim, Shady Eldeib, Omar Shehata, Mohammad Ismail, and Ranin Zarandah. Sensors in advancing the capabilities of corrosion detection: A review. Sensors and Actuators A: Physical, 332:113086, 2021. ISSN 0924-4247. doi: https://doi.org/10.1016/j.sna.2021.113086

Evaluating Coating Protection Against Environmentally Assisted Cracking

Liam Agnew, Nate Brown, Fritz Friedersdorf

Luna Labs USA, Charlottesville, Virginia, USA

Environmentally assisted cracking (EAC) of high strength aluminum alloys in corrosive atmospheres presents significant maintenance and safety issues for aircraft and other lightweight structures. Corrosion inhibiting coatings are the primary means of protecting lightweight structures from atmospheric corrosion in harsh environments. Generally, standard test methods for evaluating performance of corrosion inhibiting coatings do not incorporate a stressed substrate, and significant risk is assumed if these tests are used to infer protection provided against EAC. A test system and method have been developed to assess corrosion inhibiting coatings and their capacity to protect structures from EAC initiation in corrosive atmospheres. EAC initiation and propagation is influenced by the complex interactions of load, environment, and alloy microstructure (Figure).

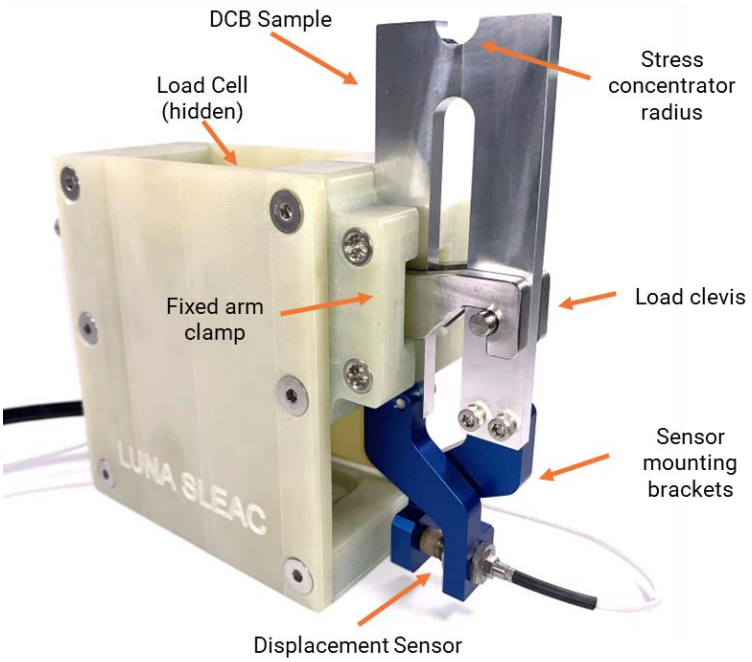

Figure – Annoted image of the EAC test system, including an instrumented load fixture and double cantilever beam (DCB) specimen

These factors were explored to produce a method that quantifies the resistance to crack initiation provided by protective coatings using a high strength aluminum alloy (AA7075-T651) substrate. This EAC system and test method enables coating performance comparisons. Accurate assessment of coating performance will reduce the risk associated with introducing new environmentally compliant coatings. A corrosive environment, smooth-notch double cantilever beam fracture sample, static loading condition, and continuous monitoring system are employed to measure onset and propagation of cracks in atmospheric corrosion tests. The EAC test system has been developed for use in laboratory corrosion test cycles or at outdoor corosion test sites for evaluation in service environments. Results demonstrate a strong dependence of the cracking resistance on inhibited primer type.

Insight into atmospheric corrosion mechanism of press hardened steel using local electrochemical techniques

Varvara Helbert[a], Andrei Nazarov[a], Maryna Taryba[b], Flavien Vucko[a], Fatima Montemor[b], Dominique Thierry[c]

[a] *French Corrosion Institute, 220 Rue Rivoalon, 29200 Brest, France*

[b] *Centro de Química Estrutural, Instituto Superior Técnico, Universidade de Lisboa, 1049-001 Lisboa, Portugal*

[c] *RISE Research Institutes of Sweden, Isafjordsgatan 28A, 164 40 Kista, Sweden*

Abstract

Good formability and high tensile strength are the key parameters for steels in the transport industry. For these reasons, press hardened steels (PHS) are of most interest to fulfil environmental issues and lightweight constructions in the automotive industry. Nevertheless, PHS shows a high sensitivity to hydrogen embrittlement (HE) and hydrogen assisted corrosion cracking (also called environmental assisted cracking). The phenomenon of HE is strongly related to a sub-surface hydrogen activity during the atmospheric corrosion process. Hydrogen can enter in steel during both fabrication and manufacturing, as well as it can be produced by atmospheric corrosion during the service-life of steel. In presence of protective coatings, such as zinc, the galvanic coupling at cut edges, or at the location of defects in the metallic coating, can be also an additional source of hydrogen.

In this work, Scanning Vibrated Electrode Technique (SVET) and Scanning Kelvin Probe (SKP) were used for better understanding of atmospheric corrosion mechanism of PHS. At first, Kelvin Probe was used as a reference electrode to obtain cathodic polarization curves on PHS surface which was covered by thin electrolyte films of 0.1 M NaOH and 3.5 %wt NaCl in the range of 60 to 2000 µm. The applied current densities were chosen in the range of -20 to -200 µA cm^{-2} based on the SVET results. For both electrolytes, a strong increase of the limiting current density (i_{lim}) with an electrolyte thickness decrease has been clearly demonstrated. Data correlated well with a theoretical plot determined by Nernst-Fick equation. In fact, the Oxygen Reduction Reaction (ORR) was strongly accelerated with the decrease of the electrolyte thickness due to an easier oxygen diffusion process through the thinner electrolyte layer.

As in case of outdoor exposure, PHS is initially covered by porous rust scales, which greatly influence the mechanism of the oxygen reduction. Therefore, the mechanism of the oxygen reduction on rust covered PHS surface was investigated in details. It was shown, that in case of rusted surface, the ORR moves from *PHS/electrolyte* to *rust/electrolyte* interface accompanied by iron rust reduction. The limited current density progressively increased as the corrosion products accumulated on the surface and the corrosion potential of the rusted PHS was shifted to noble values. Thus, ORR was accelerated with rust accumulation. Further investigation of corrosion products

using micro-Raman spectroscopy were done to correlate this increase of cathodic current to the identified iron oxide. Distribution of anodic and cathodic locations under/inside rust was investigated using SVET.

The experimental data of this work will be further used to feed a mechanistic model of atmospheric corrosion within the framework of the European project AtHyCor “Modelling of hydrogen activity from atmospheric corrosion in ultra-high strength steels for light structure application”.

Acknowledgments:
This project has received funding from the Research Fund for Coal and Steel under grant agreement No 101034041.

Corrosion of carbon and stainless steels in an artificial geothermal solution: effect of mineral scales

Gabriela Aristia, Sabrina Marcelin, Nicolas Mary, Bernard Normand, François Ropital

Univ. Lyon, INSA LYON, MATEIS UMR CNRS 5510, 69621 Villeurbanne cedex, France

Geothermal energy extraction requires reliable and safe infrastructures, which are often subjected to corrosive fluids. Pipelines transporting geothermal fluids are mostly made of steel, e.g., carbon steels and stainless steels that are susceptible to corrosion and scaling when exposed to geothermal fluids. To ensure an efficient and reliable energy production strategy for geothermal powerplants operation, the effect of scales deposits on the mechanisms of localized and uniform corrosion on steels should be further investigated. This study evaluated two types of carbon steels (K55 and P110) and stainless steel (Cr13).

Experiments were performed in an artificial geothermal solution to understand the kinetics of the corrosion processes on the different types of steel. This artificial geothermal solution represents Dogger geothermal well in France, mainly consisting of Na^+, Ca^{2+}, Mg^{2+}, Cl^-, and HCO_3^- ions and saturated with CO_2. Experiments were performed using a two-compartment cell to simulate the effect of temperature differences on the production pipelines. The first compartment (side 1) contained 0.05 M Na_2SO_3 at 80 °C to heat the specimen surface. The second one (side 2) was filled with a geothermal solution at 40 °C.

Electrochemical measurements were performed on the face of the sample in contact with the geothermal fluid. The measurement of the corrosion potential and the electrochemical impedance allowed to follow the evolution of the surface reactivity of the sample and to characterize the impact of scales on corrosion mechanisms. Compositional and structural analyses of the scales were obtained using a scanning electron microscope equipped with energy-dispersive X-ray and X-ray diffraction.

This work has been founded by the French Research Agency ANR, contract ANR 21 CE05-0024 (GeoSteelCor project)

Thermal and durability performance evaluation of coatings for condenser heat exchangers in ORC geothermal power plants

D. Martelo, N. Kale, G. Schneider, A. Wojdyla-Cieslak,
G. Mittal, D.I. Snorrason & S. Paul

Geothermal energy offers a reliable and sustainable source of power and heat, reducing dependence on fossil fuels and contributing to the transition to a greener energy mix. While geothermal resources are not as widely accessible as some other renewable energy sources, they provide a significant opportunity for countries and regions with suitable geological conditions to tap into a reliable and constant source of clean energy. Heat exchangers play a crucial role in geothermal power plants by facilitating the transfer of thermal energy from geothermal fluids to other working fluids within the power generation system. In organic rankine cycle (ORC) geothermal power plants, this component represent more than 50% of the capital cost. In this investigation, it has been studied the thermal and durability performance of superhydrophobic and superoleophobic surfaces which exposed to the ORC fluid with the intention to simulate a condenser heat exchanger. Polysilazane based coating, among other formulations were used on aluminium and stainless steel substrates for the tests. Statistical analysis were performed for the thermal evaluation of the coatings, the results has shown that in some cases thermal performance increased from 30kWm-2 to more than 100 kWm-2 in the presence of the coating. Some other durability performance indicators i.e. water contact angle, adhesion, among others has also been measured over periods of 200h, with some degradation in the properties observed. However, even with degraded performance the coating performs better than the substrate material in terms of heat transfer performance.

Corrosion in geothermal environments containing sulphuric acid

Joseph Thevakumar [1], Joshua Owen [1], Frederick Pessu [1], Trevor Hughes [2], Evgeny Barmatov [2], Richard Barker [1]

[1]Institute of Functional Surfaces, School of Mechanical Engineering, University of Leeds, Leeds, LS2 9JT, United Kingdom

[2]Schlumberger Cambridge Research, High Cross, Madingley Road, Cambridge, CB3 0EL, United Kingdom

Steel infrastructure (e.g., pipelines) applicable within renewable energy sources, such as geothermal energy systems, can encounter corrosion because of exposure to low pH fluids at elevated temperatures. Sulphuric acid (H_2SO_4)-containing environments presents a significant corrosion threat, with the high temperature resistance of carbon steel in the pH range 2-4 existing as a knowledge gap. This research is aimed at exploring the severity of steel corrosion in acidic geothermal environments, specifically those containing H_2SO_4. Through the implementation of a tantalum-lined autoclave, the corrosion behaviour of N80 carbon steel was investigated in acidic solutions (pH 2-4) and temperatures up to 150°C. *In-situ* electrochemical techniques, including linear polarisation resistance and electrochemical impedance spectroscopy, were used to monitor instantaneous corrosion rate, which would improve our understanding of corrosion mechanisms in real time. The techniques were complimented by evidence obtained from surface analytical techniques (scanning electron microscopy, X-ray diffraction) to characterise the nature of the steel surfaces before and after exposure to the corrosive environments. The results indicated a greater corrosion rate for carbon steel at lower pH and higher temperatures, and as we expected, the highest corrosion rate (>25 mm/year) was observed under the most extreme conditions (pH 2, 150°C). The corrosion performance of carbon steel is compared with alternative, more corrosion resistant high-alloy materials that may be selected as alternative durable materials for application in low pH geothermal environments.

Corrosion Testing of Titanium Alloy Ti-745 in Simulated Environment of Superhot Deep Geothermal Wells

Sigrun Nanna Karlsdottir, Gifty Oppong Boakye, Maria Y. Thrainsdottir, Erlend Straume

University of Iceland, Reykjavik, Iceland

Several challenges are encountered in the design and construction of deep superhot (>300°C) geothermal wells due to high temperatures, high pressure and increased corrosiveness of the geothermal fluid present in the system. The corrosiveness of the geothermal fluid is due to the chemical composition including corrosive gasses such as H_2S and CO_2. Additionally in vapor dominated geothermal system hydrogen chloride (HCl) can be present in wells with superheated geothermal steam. Examples where this has been encountered is at the Larderello geothermal area in Italy, in Krafla geothermal area in Iceland and Tiwi area in the Philippines. Commonly used high temperature geothermal well casing materials such as API K55 carbon steel will not withstand the aggressive environment of these wells and are susceptible to various corrosion form such as uniform corrosion, hydrogen embrittlement, sulfide stress corrosion cracking and micro-cracking due high temperature hydrogen attack. Additionally carbon steel casings in superhot wells such as in the first well of the Iceland Deep Drilling project have failed due to high plastic strains generated because of large temperature difference during heating and cooling of the well and strength reduction at temperatures above 200°C. Thus, materials that have higher corrosion resistance and better resistance against thermal cycling effects are needed to achieve structural integrity and increased lifetime of superhot wells. In this study a newly developed titanium alloy Ti-745 (Ti-0.4Ni-3.6Mo-0.75Zr) is tested in simulated superhot geothermal well environment at 350 and 400°C in H_2S an CO_2 containing steam for 168 hrs. in High Temperature and High Pressure (HTHP) autoclave laboratory. The results from microstructural and chemical composition analysis with SEM and EDS equipment as well corrosion rate measurements are reported, and the corrosion behaviour described and compared to results for carbon steel sample tested at the same conditions and exposure time.

Thermal storage by molten chlorides - Corrosion on alloys with a focus on their nickel content

Esraa Hamdy, Aida Nikbakht*, Christine Geers

Department of Chemistry and Chemical Engineering, Chalmers University of Technology, Gothenburg, SE-412 96 Sweden

Molten chlorides are considered an economical and very high-temperature stable alternative as a thermal storage medium. However, as soon impurities of water or oxygen are present in such a melt or the cover gas above, molten chlorides become highly corrosive. Metals in contact with chloride salts containing impurities undergo rapid oxidation and dissolution.

In the present study, we investigate the influence of different commercially available alloy compositions on elective element leaching mechanisms by molten chlorides, KCl/$MgCl_2$, at 800°C. Focus hereby is set on different nickel contents, 20-100 wt%.

Besides chromium as primary alloying element, certain Mn, Si and Cu variations must be considered.

Deliberately, aluminium has been avoided as an alloying element in this study since we observed already its facilitated leachability [1].

1. Hamdy, E., J. Nockert Olovsjö and C. Geers, *Perspectives on selected alloys in contact with eutectic melts for thermal storage: Nitrates, carbonates and chlorides.* Solar Energy, 2021. **224**: p. 1210-1221.

Corrosion Behaviour of Stainless-Steel Alloys in Molten Salts for Concentrated Solar Power Applications

Stefano Mori, Cranfield University, Cranfield, United Kingdom
Andrew Potter, Cranfield University, Cranfield, United Kingdom
Nigel Simms, Cranfield University, Cranfield, United Kingdom
Joy Sumner, Cranfield University, Cranfield, United Kingdom

The world is now facing the challenge of climate change, and many countries (including the United Kingdom and European countries) have agreed to reduce their carbon emissions, reaching net zero by 2050. To achieve this target the energy generation industry needs to decrease its emission of green-house gases. Over the years, several routes have been proposed to decrease the industry sector's carbon emissions, from the use of greener fuels to the use of so-called renewable energy. One of the most promising are concentrated solar power plants (CSP). Since such plants rely on the energy emitted by the sun, which is intermittent, a way of storing the thermal energy collected is needed. To do this, salts are usually used, which can release and store the energy when cycling between temperatures. The use of molten salts and high temperatures poses a risk for the metals in contact with them, which are then prone to high corrosion rates.

In this work two stainless steels (SS316 and SS304) have been tested as parent tube material, as well as welded material. The samples were produced from seamed tubes with dimension of about 15mmx15mmx3mm. These samples were buried in molten salt and then inserted into a laboratory furnace, at 600°C. The samples were measured prior to exposure, to allow the study of the surface regression via dimensional metrology. The corrosion microstructures formed on the different samples was studied via optical microscopy, scanning electron microscopy and energy dispersive x-ray spectroscopy.

It is anticipated that the welded area would be more prone to corrosion damage with respect to the bulk alloy. The impact of the alloys' chemical compositions on the degradation mechanism have been noted.

Impact of various salt ageing conditions on solar salt chemistry and instantaneous corrosion rate measurements

Frédéric Novello[1], Ridha Harzallah[2], Murilo Borges Masalskas[3]

[1]*CRM Centre for Research in Metallurgy, Liege, Belgium, frederic.novello@crmgroup.be*
[2]*John Cockerill Renewables, Liege, Belgium, ridha.harzallah@johncockerill.com*
[3]*CRM Centre for Research in Metallurgy, Liege, Belgium, murilo.borges@crmgroup.be*

Abstract

Concentrated solar power (CSP) systems have become a relevant renewable source for power generation with 114 worldwide operational plants and 10 under construction as of January 2023. CSP plants are designed to operate for at least 25 years. The high temperatures utilized on CSP systems cause the solar salt ($NaNO_3$-KNO_3 3:2) to degrade over time. Some of the degradation products, particularly alkali oxides, are known to increase the corrosive behavior of the Molten Solar Salt (MSS). Mastering the degradation mechanisms of the MSS can help increasing the lifetime of a CSP installation and monitoring the corrosion behavior over time can secure a reliable service during its operation. In this context, a corrosion cell was developed to study the ageing of the MSS and its impact on the corrosion of a nickel alloy (Haynes 230). Various electrochemical tests have been performed at 565°C under different ranges of alkali oxide initial concentrations (0% Na_2O / 1% Na_2O), various pressures, two cover gas compositions (air / O_2-N_2 1:1) and two cover gas flow rates (0 mL/min / 40 mL/min). The evolution of the instantaneous corrosion rate over a period of 48h of ageing was analyzed via polarization resistance.

Keywords: Molten salt corrosion cell (MSS), Concentrated Solar Power (CSP), Solar salt degradation, Polarization resistance

Introduction

Concentrated solar power (CSP) is a technology with great potential as it can produce utility-scale electricity, offering firm capacity and dispatchable power on demand. Its flexibility is a breakthrough in the field of renewable energies and made possible by integrating thermal energy storage using a high temperature fluid (HTF). The unit can quickly ramp up or down as required by the network and the energy demand. When ramping down, output is not wasted. Instead, it is stored as heat in molten salt tanks and deployed hours or even days later: stored heat can be converted into electricity at night or during cloudy periods of the day, providing green energy 24 hours a day.

CSP systems have become a relevant renewable source for power generation with 114 worldwide operational plants and 10 under construction as of January 2023. CSP plants are designed to operate for at least 25 years.

Currently, the molten salt used in most CSP plants as HTF is the binary nitrate molten salt (60% $NaNO3$ and 40% $KNO3$) called Solar Salt, which has a working range of 290˚C to 570 ˚C. Close to the maximum working temperature Solar Salt start decomposing producing corrosive species such as alkaline oxides. The first step of decomposition leads to the formation of nitrites [1]:

$$NaNO_3 \leftrightarrow NaNO_2 + ½\ O_2 \qquad (1)$$

In a second step, the nitrite ions decompose to form sodium oxide:

$$2\ NaNO_2 \leftrightarrow Na_2O + NO + NO_2 \qquad (2)$$

The same reactions occur with KNO_3 but generally at a slightly higher temperature.

Corrosion using the binary nitrate molten salt is observed on metallic materials used in solar plant components: solar receiver tubes, collector, piping…

The experiments described in this paper aim at mastering the degradation of the Solar Salt when it goes through a solar receiver of a solar tower. At this location the salt is heated to 565°C under pressure (5 to 10 bar) and flows in tubes made of Haynes 230 alloy.

Corrosion rates are mainly controlled by temperature as it accelerates oxidation reactions and the production of aggressive compounds due to the degradation of the Solar Salt. However, the overall impact of the atmosphere is not yet well known. In this context, a corrosion cell was developed to study the ageing of the MSS and its impact on the corrosion. Various electrochemical tests have been performed at 565°C under different ranges of alkali oxide initial concentrations (0% Na_2O / 1% Na_2O), various pressures, two cover gas compositions (air / O_2-N_2 1:1) and two cover gas flow rates (0 mL/min / 40 mL/min). The evolution of the instantaneous corrosion rate over a period of 48h of ageing was analyzed via polarization resistance.

Description of the corrosion cell

A sealed corrosion cell was designed in order to study the corrosion behavior of the Haynes 230 alloy in molten solar salt at high temperatures. The challenge lies on the fact that the salt tends to decompose and evaporate at temperatures above 550°C, which means the corrosion cell must be sealed. In addition, the sealing of the corrosion cell allows for gas composition control.

Figure 1 a) and b) show the schematics of the cell used in this work. The body (gray) is a stainless steel cylinder which contains two chambers: a larger one (top) and a smaller one (bottom). The bottom chamber acts like a crucible, containing the molten salt. In the bottom area, an electrically insulating crucible (purple) is placed to hold Haynes 230 coupons, impeding their contact with the cell wall. The top area is a chamber where an electrically insulating guide (red) is placed. The electrodes (black) are maintained by the guide at their correct position. Three electrodes were used in this study: a working electrode (Haynes 230H, rectangular section), a counter-electrode (Haynes 230H, rectangular section) and a reference electrode (platinum wire, 0.5mm diameter). Lateral tubes (dark gray) are used to guide the electrode wires to the outside of the cell so that they can be connected to the potentiostat. These tubes are electrically insulated on the inside. At the exit of the tubes, a polymeric cap is placed to ensure tightness and electrical insulation. Finally, the top lid (green) ensures tightness with a classic flange and a graphite gasket. A gas inlet (center) is connected to a tube that delivers the gas to the bottom chamber where the molten salt is contained, allowing for atmosphere control during the corrosion tests. The other holes are connected to gas outlets.
The cell is placed in a vertical tubular oven, as depicted on Figure 1 c) and d). This allows the bottom chamber to be heated at the desired temperature without overheating the graphite gasket or polymeric caps. Figure 2 shows some pictures of the corrosion cell.

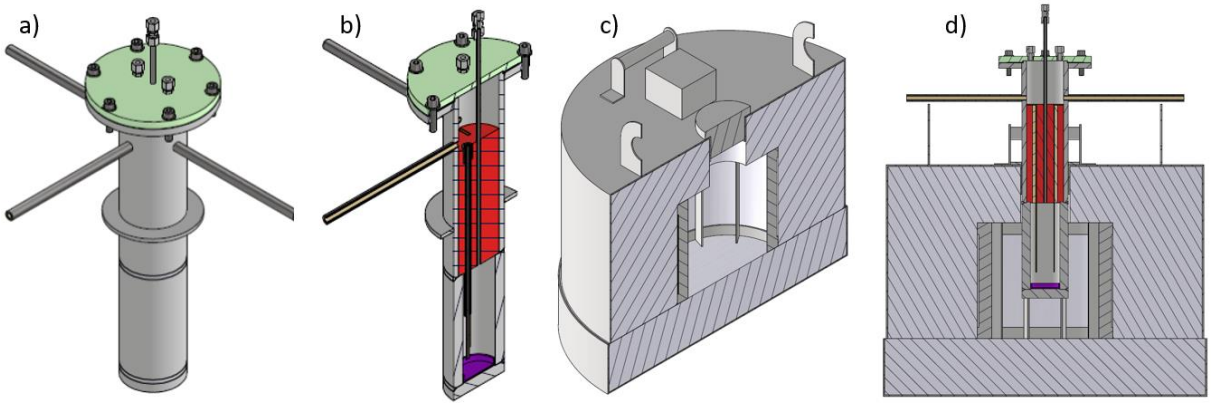

Figure 1 - Sealed corrosion cell design

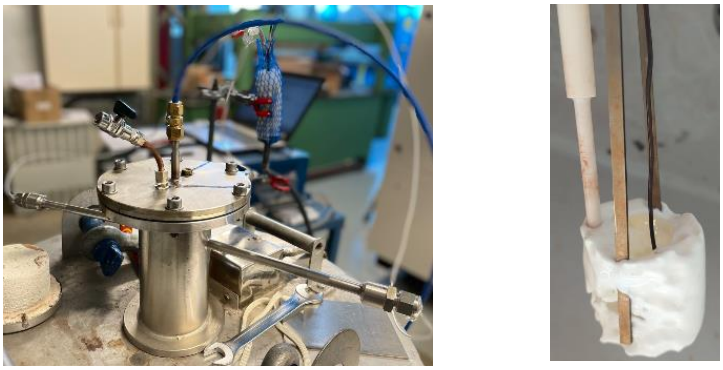

Figure 2 –Top of the cell (left) and electrode system (right)

Methodology

A series of electrochemical tests were carried out to understand the impact of various test parameters on the corrosion rate of the Haynes 230 in molten solar salt. Each electrochemical test was performed containing 220g of dried solar salt kept at 565°C for a total of 48 hours. The main electrochemical characterization was the corrosion rate estimation based on the polarization resistance method. It was well verified that the free potential of the cell is stable within 1mV variation over a period of 5 minutes, which is why the 5-minute period was chosen for each polarization resistance reading. In order to calibrate the electrochemical corrosion rate measurements, three coupons of Haynes 230 were placed at the ceramic crucible for mass loss measurements. After each test, a salt sample was collected and both Na_2O and NO_2^- were quantified to study the salt decomposition. Table 1 presents the condition of each test.

Table 1 - Conditions of the tests performed on this study

Test	Na2O (Wt%)	Pressure [bar]	Flow rate [mL/min]	Atmosphere
A	0%	0,25	0	Air
B	1%	0,25	0	Air
C	0%	5,0	0	Air
D	0%	0,25	0	O_2/N_2
E	0%	5,0	0	O_2/N_2
F	0%	0,25	40	Air
G	0%	5,0	40	Air

Table 2 presents the comparisons performed in this study in order to understand the various parameters affecting the decomposition of the salt and the impact on the corrosion rate of Haynes 230 in molten solar salt:

- Comparison 1 aimed to study the effect of initial concentration of Na_2O (0% and 1%) on the corrosion rate. Na_2O being one of the main corrosive products of the salt decomposition;
- Comparison 2 aimed to study the effect of the air flow rate (0 and 40mL/min) as well as the pressure (0.25 and 5 bar) on the corrosion rate. A flowing atmosphere is expected to accelerate salt decomposition by washing away the products from the decomposition reactions;
- Comparison 3 aimed to study the effect of the gas composition (air and a 1:1 mixture of $O_2 – N_2$) as well as the pressure (0.25 and 5 bar) on the corrosion rate. As the first equilibrium reaction of the equation the decomposition of the salt implies the production of oxygen, an atmosphere richer in oxygen should decrease the rate of decomposition of the salt.

Table 2 - Summary of comparisons made in this study

Comparison	Tests	Na_2O (Wt%)	Pressure [bar]	Flow rate [mL/min]	Cover gas
1	A-B	0% / 1%	0.25	0	Air
2	A-C / D-E	0%	0.25 / 5.0	0 / 40	Air
3	A-C / F-G	0%	0.25 / 5.0	0	Air / O_2-N_2

Results and discussion

The effect of initial concentration of Na_2O (0% and 1%) on the corrosion rate at 565°C is presented in Figure 3 (comparison 1). The results of the instantaneous corrosion rate estimation are normalized to correspond to the mass loss measurements. Each point represents a 5-minute measurement of polarization resistance. The average corrosion rate increased from 60 µm/year to 163µm/year with the addition of Na_2O, reinforcing its effect on the corrosivity of metals exposed to molten solar salt. As for the corrosion rate evolution, test A (0% initial Na_2O) presented an increasing corrosion rate over time, which indicates Na_2O is being created as the salt ages, while test B (1% initial Na_2O) presented a decreasing corrosion rate over time up to a constant level, which indicates Na_2O was consumed. It appears that the amount of Na_2O in the salt reaches an equilibrium over time whether the initial concentration is above or below said equilibrium concentration.

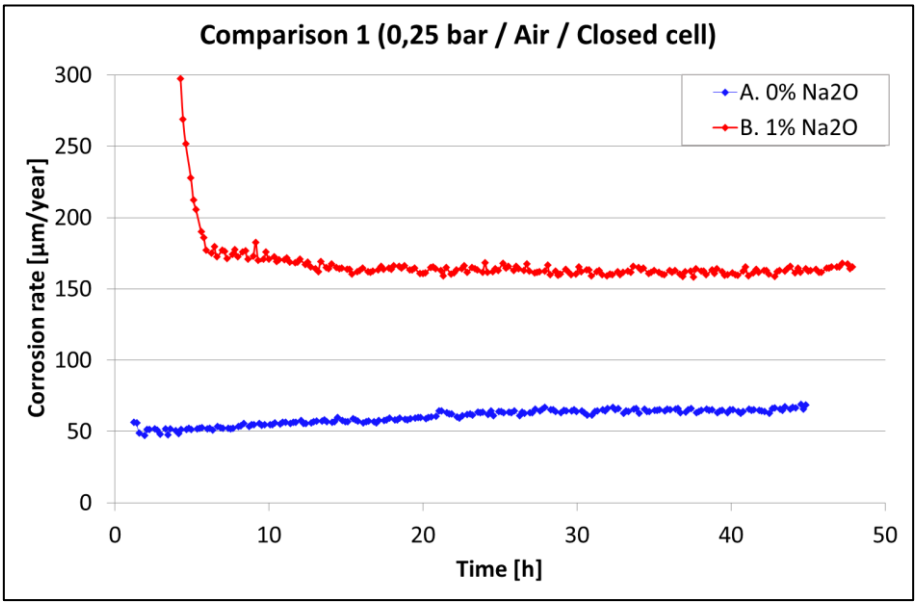

Figure 3 – Instantaneous corrosion rate estimation of comparison 1

Table 3 presents the results of the salt characterization for tests A and B (comparison 1) in terms of Na_2O and NO2- presence as well as the average corrosion rate obtained via mass loss. It can be observed that Na_2O was created in salt A (0% initial Na_2O), while it was "consumed" in salt B (1% initial Na_2O) suggesting that there is an equilibrium concentration to be reached. This equilibrium is likely dependent on the temperature and the atmosphere composition.

Table 3 – Salt analysis and average CR of cells in comparison 1

Initial Na_2O (wt.%)	Na_2O (wt.%)	NO_2^- (wt.%)	Average CR [µm/y]
0% (A)	0,21%	1,89%	60
1% (B)	0,34%	1,32%	167

As for the nitrite quantification, the results point in opposite directions: a larger fraction of initial Na_2O resulted in a lower fraction of nitrites. This result does not correlate directly with the chemical equilibrium reactions found in the literature:

$$NaNO_3 \leftrightarrow NaNO_2 + ½\ O_2 \qquad (1)$$

$$2\ NaNO_2 \leftrightarrow Na_2O + NO + NO_2 \qquad (2)$$

According to equation (2), the presence of a large fraction of Na_2O should inhibit the decomposition of nitrites, leading to an increase of its fraction. The fact a lower nitrite fraction was measured implies that a separated mechanism was inhibiting the decomposition of $NaNO_3$ into $NaNO_2$ in test B.

A possible explanation could come from the powder used to increase the initial Na_2O content of the salt as it also contains around 10 wt.% of sodium peroxide (Na_2O_2), an impurity present in Na_2O-rich powders. Its decomposition at high temperature is given by the reaction:

$$2\ Na_2O_2 \rightarrow 2\ Na_2O + O_2 \qquad (3)$$

The fact Na_2O_2 decomposition forms oxygen could be linked with a lower formation of nitrites as the increased dissolved oxygen concentration would dislocate the chemical equilibrium of reaction (1) towards the nitrate formation. It is thus likely that nitrites were not being formed at the same rate as in test A up until the point of total decomposition of Na_2O_2. In short, it is likely that formation of nitrites in test B was slowed down by the presence of sodium peroxide in the Na_2O powder, which might explain its smaller nitrite fraction.

During the first 7 hours, the solar salt was oversaturated with Na_2O due to its addition in powder form, which is indicated by the fact that the corrosion rate is strongly decreasing up until that point (see Figure 3). Since NO_x were not initially present at the cover gas, the "reverse route" of nitrite formation was not possible, and the consumption of Na_2O was linked exclusively to the corrosion of the metallic elements exposed to the salt (electrodes and the cell walls).
After the first 7 hours, equilibrium is reached, which is indicated by the fact that the corrosion rate is practically constant from that point on.

Figure 4 shows the effect of flow rates and pressure (comparison 2) at 565°C. The average corrosion rate obtained from mass loss varied from 40 µm/year to 60µm/year by varying the air flow rate between 0 (closed cell) and 40 ml/h (renewed atmosphere) and the pressure from 0.25 to 5 bar. For the same flow condition, a higher pressure caused a decrease in corrosion rate, which could be linked to the fact that the products of decomposition of the salt are gaseous, and a higher pressure could inhibit the decomposition. As for the effect of the flow rate, when comparing C-E (P = 5bar), the presence of a gas flow has led to an increase in corrosion rate,

as hypothesized. However, when comparing A-D (P = 0.25bar), the presence of a gas flow appears to have caused a decrease in the CR. It should be observed, however, that the curve D presents a change in behavior after around 20 hours: when the increasing corrosion rate was about to overtake the one of test A, it started decreasing. It is believed that a flow issue has happened during test D, and the gas flow might have stopped working. Thus, although the average corrosion rate was higher for test A in comparison to test D, it becomes clear that the corrosion rate decreases as the flow stopped, which once again validates the hypothesis of the gas flow washing away the salt decomposition products and thus accelerating it.

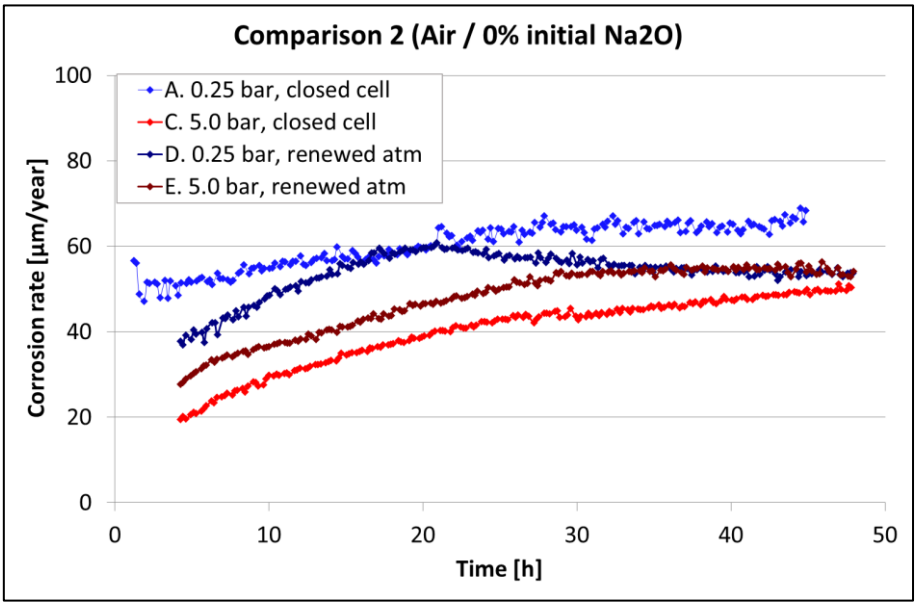

Figure 4 – Instantaneous corrosion rate estimation of comparison 2

Table 4 presents the results of the salt characterization for the comparison 2 in terms of Na_2O and NO_2^- presence as well as the average corrosion rate obtained via mass loss. When comparing tests C and E (P = 5 bar), the presence of a flow rate increased the fraction of alkali oxides and nitrites as well as the average corrosion rate. The opposite is observed when comparing tests A and D (P = 0.25 bar): the presence of a flow rate decreased the fraction of alkali oxides and nitrites as well as the average corrosion rate, which is likely linked with the flow issue during test D.

Table 4 - Salt analysis and average CR of cells in comparison 2

	Pressure [bar]	Na_2O (wt.%)	NO_2^- (wt.%)	Average CR [µm/y]
Closed cell	0,25 (A)	0,21%	1,89%	60
	5,0 (C)	0,07%	1,03%	40
Renewed atmosphere	0,25 (D)	0,04%	1,27%	54
	5,0 (E)	0,12%	1,16%	48

Figure 5 presents the effect of the gas composition (air and a 1:1 mixture of O_2 – N_2) as well as the pressure (0.25 and 5 bar) on the corrosion rate at 565°C (Comparison 3). The average corrosion rate value over the 48h test varied from 40 µm/year to 70 µm/year. Similarly to comparison 2, an increase in pressure caused a decrease in corrosion rate. This reduction,

however, was more significant under air (-50%) than under O_2/N_2 (-6%). In addition, for the same pressure, an increase of cover gas O_2 fraction caused an increase in CR. As O_2 is produced during the first step of the decomposition of nitrates, increasing the partial pressure of O_2 was expected to decrease the decomposition rate of the salt and thus also the corrosivity. Higher corrosion rate can be explained by a higher amount of dissolved oxygen induced by the higher O_2 partial pressure.

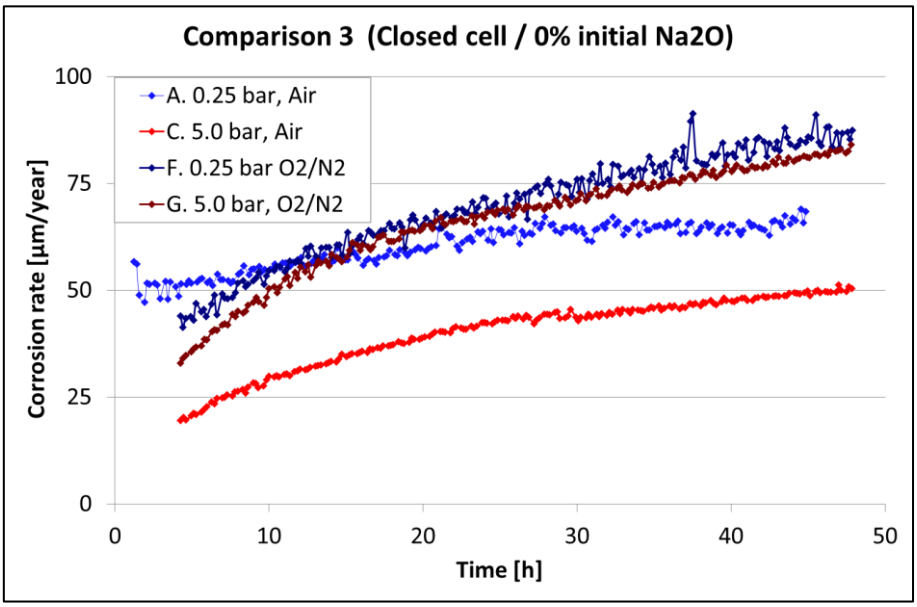

Figure 5 – Instantaneous corrosion rate estimation of comparison 3

Table 5 presents the results of the salt characterization for the comparison 3 in terms of Na_2O and NO_2- presence as well as the average corrosion rate obtained via mass loss. For a same pressure (A – F or C – G), an increase in O_2 fraction on the cover gas has decreased the formation of both alkali oxides and nitrites. The corrosion rate, however, increased for both pressures. This indicates that the increase in oxygen fraction can indeed reduce the decomposition of nitrates into nitrites and consequently the amount of alkali oxides (see equations (1) and (2)). On the other hand, oxygen can by itself accelerate the corrosion of metals at high temperatures. Thus, although the effect of preserving the salt was likely positive from a corrosion rate standpoint for reducing the formation of alkali oxides, the increase in O_2 solubility (caused by the increase of O_2 partial pressure) appears to be large enough to overcome the positive effect it caused.

Table 5 - Salt analysis and average CR of cells in comparison 3

	Pressure [bar]	Na_2O (wt.%)	NO_2^- (wt.%)	Average CR [µm/y]
Air	0,25 (A)	0,21%	1,89%	60
	5,0 (C)	0,07%	1,03%	40
O_2 / N_2 1:1	0,25 (F)	0,06%	1,11%	70
	5,0 (G)	0,03%	0,82%	66

Conclusions

The main trends observed on corrosion rate estimation results are summarized in Table 6.

- **Higher initial concentration of Na_2O** resulted in higher average corrosion rates. It appears that the excess of Na_2O was consumed quickly, and the equilibrium concentration of Na_2O was reached. This reduced the formation of nitrite in comparison with the pure salt.
- **The presence of a flow rate** appeared to result in higher average corrosion rates than in absence of flow, likely caused by the removal of salt degradation products as indicated by the increase in Na_2O and $NO2^-$. It should be noted that test D presented a flow issue and must be repeated for well confirming this trend.
- **A larger O_2 cover gas fraction** resulted in higher average corrosion rates. Although a larger oxygen content can have a positive impact on the corrosion rate by reducing the nitrite decomposition and thus the formation of alkali oxides, an excessively large fraction will increase the O_2 dissolution into the salt. Since oxygen is a strong oxidant, its negative impact on the corrosion rate can become large enough to overcome the effect of reducing the salt decomposition. This implies the existence of an optimum O_2 cover gas fraction for a given operation condition.
- **Higher pressures** resulted in lower average corrosion rates, as well as in a slower salt degradation as NO_2^- and Na_2O fractions were also smaller. The exception to this trend is the test that presented the flow issue (D).

Table 6 - Main trends on corrosion rate

	Na_2O (wt.%)	NO_2^- (wt.%)	Average CR [µm/y]
↑ Initial Na2O	↑	↓	↑
↑ Pressure	↓	↓	↓
↑ Flow rate*	↑*	↑*	↑*
↑ O_2 fraction	↓	↓	↑

* Exception: test D (flow issue)

References

1. Kurt H. Stern, High Temperature Properties and Decomposition of Inorganic Salts Part 3. Nitrates and Nitrites (1972).

Corrosion resistance of 3D printed Ni-Al bronze in molten carbonate: Effect of porosity design

C. Arcos[1], C. Guerra[1], C. Martínez[2], M. Walczak[1], and M. Sancy[3]

[1]*Department of Mechanical and Metallurgical Engineering, Faculty of Engineering, Pontifical Catholic University of Chile, Santiago, Chile.*

[2]*Faculty of Engineering, Uniersidad de la Frontera, Temuco, Chile*

[3]*School of Civil Construction, Santiago, Chile, Faculty of Engineering, Pontifical Catholic University of Chile, Santiago, Chile.*

Abstract

Fuel cell technology has been developing in response to the necessity of diminishing the dependence on fossil fuels and reducing the carbon footprint of energy production. This work focuses on anode material and its corrosion resistance for application in molten carbonate fuel cells. In particular, nickel-aluminum bronze (NAB) produced by additive manufacturing was studied to verify the effect of designed porosity on mechanical and chemical stability in exposure to molten carbonate. The apparent porosity of 84% was produced in differently shaped, ordered, and interconnected pores (different tortuosity) and exposure to molten carbonate eutectic (Li_2CO_3-K_2CO_3) that was conducted at 550 °C for 21 days. Microstructural and chemical characterization has revealed general degradation of mechanical resistance (compressive strength and microhardness) but an extension of the effect depends on the type of porosity. In addition, corrosion resistance can be further improved by heat treating the as-built materials. EDS, GD-OES, and XRD analysis have shown that this effect can be attributed to the formation of protective Al-rich oxide.

Offshore wind Structures internal corrosion protection failure: Case study of using sacrificial anodes

Jesper Lund Madsen, Vattenfall, Kolding, Denmark

Mehdi Attarchi, Vattenfall, Hamburg, Germany

Abstract: An internal cathodic protection system failure was observed after 3-5 years of operation. The system is an Al-based GACP system protecting the internal surface of monopile foundations of offshore wind turbines, that was designed a decade ago, with some degree of water replenishment.

The CP design was re-visited and analyzed with monitoring and inspection data of dissolved oxygen, pH, ER probes, and drop cell measurements beside seawater replenishment data to determine the root cause of the system failure and appropriate mitigation actions. Two main issues of the GACP design were identified.

- Al is not the ideal anode material for the internal protection of monopiles with low water replenishment.
- The steel wire, which serves as an anode cable and structural support, has a small cross-section that leads to high resistance and unbalanced current output from different anodes in the string.

Despite these obvious CP design issues, electrical resistance probes indicate full protection (zero corrosion) for several years, even with potentials far above the protection criteria. Then, at a certain point in time, the paradigm shifts, CP breaks down, and corrosion initiates. The transition from "no corrosion" to "corrosion" is abrupt.

A Zn-based anode retrofit design is proposed to restore the CP with individual electrical anode cables. As an interim solution, Al anodes with larger cable sizes were installed, as spare anodes were readily available in the warehouse. The new design returns the monopile's internal surface to the protection state and low corrosion rate.

An experimental study of magnetite growth on tubes of Heat Recovery Steam Generators

Pierangela Cristiani, Ricerca sul Sistema Energetico – RSE, Milano (Italy)
Gian Luca Chiarello, Università degli Studi di Milano, Milano (Italy)
Marco Carnelli, Università degli Studi di Milano, Milano (Italy)
Vincenzo Casamassima, Ricerca sul Sistema Energetico – RSE, Milano (Italy)

The increasing demand for electricity together with the related emissions and the actual concern of climate change are key factors that are leading industries worldwide to give up the use of coal and invest in cleaner and efficient technologies such as Combined Cycle Power Plants (CCPP). In CCPP, the hot gases leave the turbine at temperature above 500°C and an Heat Recovery Steam Generator (HRSG) made of carbon steel tubes is used to recover the superheated steam.

This work investigated, by in-field measures and modelling, the effect of magnetite growing on HRSG high-pressure evaporator tubes. The goal was to determine, in terms of deposit thickness, if a chemical cleaning of the HP-EVA module is mandatory or not in CCPP plant where the maximum of tube temperature is lower than in a coal fed plant.

Results documented a good state of preservation of tubes bundles. Moreover, this investigation has led to define *thickness*, *composition* and *porosity* of the deposits, fundamentals to develop a realistic simulation model of the plants.

Through a series of steady-state simulations, the distribution of the main process variables along high pressure modules has been determined. The most interesting result is the distribution of external wall temperature that tends to decrease along the rows and from the bottom upwards.

A series of steady-state simulations under design conditions, have allowed to determine 500 µm as limit of deposit thickness beyond which the tube wall can reach the creep temperature (371°C). Therefore, there is no actual risks of tubes overheating such as to lead to creep. However, other failure mechanisms can occur such as Under Deposit Corrosion, that is strongly influenced by excessive deposit growing.

Regarding stream production, at the current conservation status of the investigated plant, the loss due to tubes fouling (*ca.* 150 µm of deposit) is *ca.* 0.8%, corresponding to less than 0.6 Kg/s. With a thickness of 500 µm, the loss of steam production would be 2% or *ca.* 1.6 Kg/s in this case.

Influence of relative humidity and light over the ageing of $Cu(In_xGa_{1-x})Se_2$ with the benefit of photoemission

Anna Gagliardi[1], Solène Béchu[1], Amelle Rebai[2], Mathieu Frégnaux[1], Negar Naghavi[2], Arnaud Etcheberry[1], Jean-François Guillemoles[2], Muriel Bouttemy[1]

1. Institut Lavoisier de Versailles (ILV), Université de Versailles Saint-Quentin-en-Yvelines, Université Paris-Saclay, CNRS, UMR 8180, 45 avenue des Etats-Unis, 78035 Versailles, France

2. CNRS, Institut Photovoltaïque d'Île de France (IPVF), UMR 9006, 18 boulevard Thomas Gobert, 91120, Palaiseau, France

One of the flagship solar absorbers is the quaternary alloy $Cu(In_xGa_{1-x})Se_2$ (CIGS), with solar cells reaching up to 23.3% efficiencies.[1]. Attaining these performances has only been achieved thanks to breakthrough research over years. The new developments on CIGS are numerous, but in recent years, an important effort has been carried out on the ageing aspect.

Indeed, studies have been performed on the evolution of the performances of CIGS solar cells but also, conducted on the different constitutive layers of the solar CIGS.[2] However, very few papers deal with the evolution of the absorber itself, the CIGS.

In this work, with the help of photoemission, we evaluate the influence of two of the main parameters responsible for the degradation of CIGS, namely the relative humidity and the light. Photoemission provides the access to different probed thicknesses, accordingly to the photopeak or transition observed. This work will present the evolution of the elements III of CIGS (Ga and In) over air ageing, by exploring different thicknesses (≈ 5 nm, 9 nm and 12 nm), and the degradation processes associated with time. To do so, specific data treatments, especially of the X-AES (X-ray Auger electron spectroscopy) lines, were developed.[3]

We first explored the influence of relative humidity. To do so, CIGS absorbers were exposed to different relative humidities: 20 % RH and 60 % RH, in ambient light and at a constant temperature of 20 °C. At 60 % RH, ageing was characterized by the growth of In-O and Ga-O species, gradually from the top surface (≈5 nm) to the subsurface (≈12 nm). At 20 % RH, no modifications were noticed. This difference can be explained by the number of adsorbed monolayers on top of the CIGS absorber.

While at 20 % RH the number of adsorber layers is inferior to 2, at 60 % RH, this value can reach up to 5 monolayers, and thus, can be compared to bulk water.[4,5]
Secondly, the influence of light was investigated. To do so, the ageing at 60 % RH was repeated but this time, in dark. A slower kinetic was observed when the ageing was performed in the dark, thus, it is possible to consider that light is an indispensable stimulus to activate the oxidation of CIGS material. This stimulus necessity is in good correlation with the fact that CIGS is a p-type absorber, and the reactivity of p-type materials under light stimuli is well known, with the creation of photoelectrons.
In conclusion, we were able to understand the importance to control the relative humidity and the light that really concern the integrity of CIGS solar absorber.

References

[1] M. Nakamura, K. Yamaguchi, Y. Kimoto, Y. Yasaki, T. Kato, H. Sugimoto, *IEEE J. Photovoltaics* **2019**, *9*, 1863.

[2] M. Theelen, F. Daume, *Sol. Energy* **2016**, *133*, 586.

[3] S. Béchu, B. Humbert, V. Fernandez, N. Fairley, M. Richard-Plouet, *Appl. Surf. Sci.* **2018**, *447*, 528.

[4] C. Leygraf, I. O. Wallinder, J. Tidblad, T. Graedel, *Atmospheric Corrosion, 2nd Edition*, Wiley, **2016**.

[5] S. Béchu, M. Bouttemy, J. Guillemoles, A. Etcheberry, *Appl. Surf. Sci.* **2022**, *576*, 151898.

Degradation Mechanisms in Perovskite Materials and Devices

Vikas Kumar[1], Shiladitya Paul[2]

[1]Materials Innovation Centre, School of Engineering, University of Leicester, Leicester, UK

[2]Surface, Corrosion and Interface Engineering, Materials Performance and Integrity Group, TWI, Cambridge, UK

Email: vk115@leicester.ac.uk

Over the past decade, there have been significant improvements in the photovoltaic efficiencies of metal-halide perovskite solar cells (PSC), which are now on par with silicon (Si) solar cells. Perovskites may also be produced in big volumes utilising techniques including printing onto a variety of substrates and low-temperature solution-based procedures, unlike Si. Perovskite solar cells could therefore be cheaper than Si in volume production. However, in spite of these advantages the long-term stability of these perovskite materials is still a hurdle for their applications and commercialisation. The degradation of hybrid perovskite materials depends on several factors such as processing conditions, humidity, heat, trapped charge, local stoichiometry and UV light.

In the HORIZON EUROPE project 'SUNREY', we are working to develop an enhanced characterisation tool including the use of electrical impedance spectroscopy (EIS) coupled with modelling and high resolution electron microscopy to analyse the interaction between environment, materials and the fabricated photovoltaic (PV) structures to better understand the degradation pathways to predict the lifetime-limiting mechanisms. The present study investigates perovskite PV structures with or without any encapsulation under different operative conditions by optimizing the constituent active layer materials, charge collection layers and their interconnections by using EIS and high resolution electron microscopy. Our results reveal localised degradation in these metal-halide perovskite materials which is highly dependent on the operational conditions and local composition of the perovskite materials. These results, therefore, show that precise control over the materials stoichiometry and the novel encapsulation techniques can be the key factors to improve the stability of these highly efficient perovskite materials and thus the overall lifetime of the PSC devices.

This project has received funding from the European Union (Grant agreement 101084422). The University of Leicester received funding from UKRI through the UK Government's Horizon Europe Guarantee (UKRI: 10052189).

Atmospheric corrosion of CIGS-based solar cells

A. Debono [a,b], *A. Rebai* [b], *N. Schneider* [b], *J.-F. Guillemoles* [b], *P. Volovitch* [a,b]

[a] *Chimie ParisTech-CNRS, PSL Research University, Institut de Recherche de Chimie Paris (IRCP), 11 rue Pierre et Marie Curie, 75005 Paris, France*

[b] *Institut Photovoltaïque d'Île-de-France (IPVF), UMR 9006, CNRS, Ecole Polytechnique, IP Paris, Chimie Paristech, PSL, Palaiseau, 91120, France*

adele.debono@chimieparistech.psl.eu ; *polina.volovitch@chimieparistech.psl.eu*

Photovoltaic (PV) industry aims a 25 to 35 years warranty for its installations. To achieve it, numerous degradation tests are used [1]. However, the role of the service environment on degradation is considered only for the metallic components (frame, busbars, metallic contacts) but barely for the semi-conducting materials of the cell itself. This work focuses on the role of atmospheric chemistry in the reliability of photovoltaic cells on the example of thin layer Cu(In,Ga)Se_2 (CIGS) based-solar technology for flexible applications (see Figure 1).

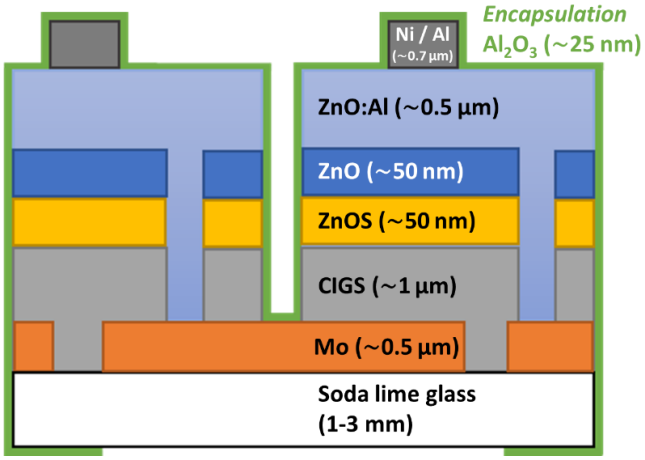

Figure 1 - Typical architecture of the studied CIGS cells

Methodology

The day/night variation was modeled by cycling temperature and humidity in a climatic chamber. A drop of solution containing selected salts were daily deposited during the test to simulate marine and coastal (NaCl), agricultural ($(NH_4)_2SO_4$) or low polluted rural (Na_2SO_4) environments. The chemical evolution of individual layers and complete cell was surveyed with the help of Raman spectroscopy, X-ray diffraction, Scanning Electron Microscopy and Electron Dispersive X-Ray Spectroscopy, Glow Discharge-OES. The cell performance loss was evaluated using IV Curves, External Quantum Efficiency, and resistivity measurements.

Results

The importance of the chemical environment has been demonstrated. $(NH_4)_2SO_4$ was found to be the most aggressive pollutant for most systems, followed by NaCl then Na_2SO_4 (see Figure 2). Molybdenum back contact and Aluminum-doped ZnO transparent conductive oxide layer seem to be the most sensitive to the environmental chemistry while CIGS absorber layer seems to be more stable in the tests of CIGS individual layers deposited on glass but degraded in the cell architecture when deposited on Molybdenum back contact. The study has also confirmed that thin layer of inorganic encapsulation protect the cells effectively against temperature and humidity but not against pollutants [2].

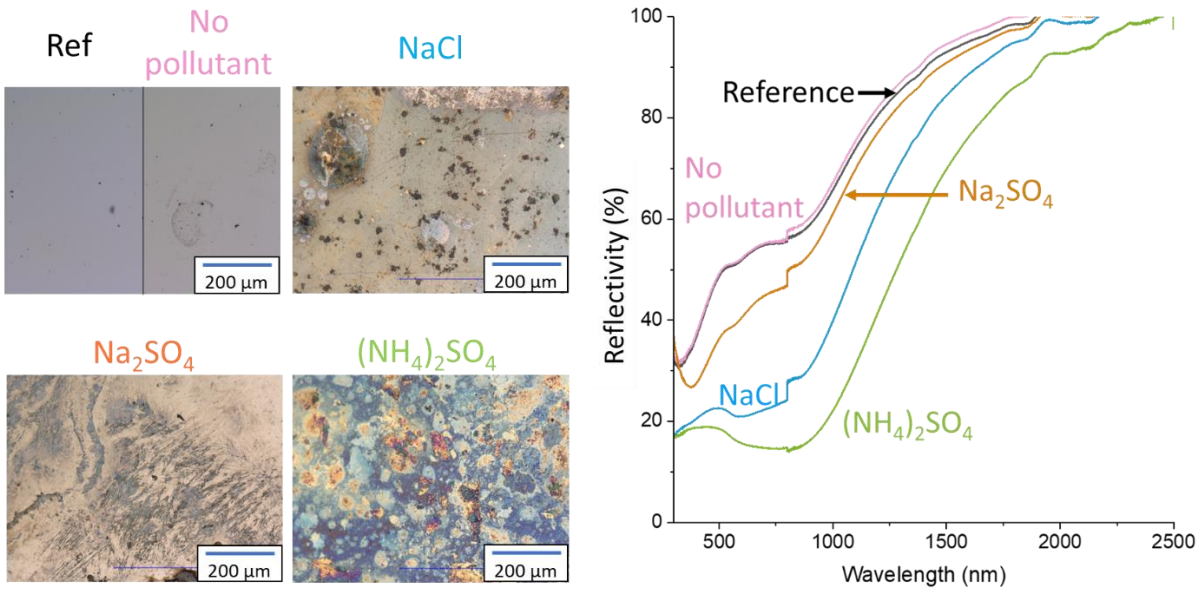

Figure 2 – Visual (microscopic image) and optical (reflectivity) impact of the pollutants on the degradation of encapsulated back contact Molybdenum after rinsing

Degradation mechanisms of different layers and interfaces and their interplays are discussed.

References

[1] J. H. Wohlgemuth et S. Kurtz, *2011 International Reliability Physics Symposium* (2011), doi: 10.1109/IRPS.2011.5784534.
[2] S. Zhang *et al.*, *Progress in Photovoltaics*, (2021) doi: 10.1002/pip.3527.

Anode design for rechargeable zinc-air battery

Kasım Erdem Erik[1] *and Çiğdem Toparlı*[1]

[1]*Middle East Technical University, Department of Metallurgical and Materials Engineering, Ankara/Turkey*

Climate change is a very urgent problem in today's world. The trouble is brewing due to the usage of fossil fuels, while the energy demand of the world is strictly increasing.[1] Renewable and sustainable energy could replace fossil fuels, however, energy storage is an important issue since renewable energy sources do not ensure consistent energy. Hence, new ways of energy storage are being studied hard.[2] Metal-air batteries are up-front among the energy storage strategies.[3] Zinc-air batteries are one of the most promising battery technologies thanks to their high specific energy, high volumetric energy density, low toxicity and high amount of earth abundance.[4] One of the main problems of zinc-air batteries is corrosion and hydrogen evolution at the anode part of the battery.[5] This study aims to solve this problem with a zinc anode design with novel additives. Anodes are produced in powder form to be pressed and pelletized further. Then, the anode performance of the zinc-air battery will be investigated in this study.

References

1.Omer, A. M. (2008). Energy, environment and sustainable development. *Renewable and Sustainable Energy Reviews*, *12*(9), 2265–2300. https://doi.org/10.1016/j.rser.2007.05.001

2.Longstaff, T. (2017, June 13). *Business models in Energy Storage*. Roland Berger. Retrieved January 15, 2023, from https://www.rolandberger.com/en/Insights/Publications/Business-Models-in-Energy-Storage.html

3.Gür, T. M. (2018). Review of Electrical Energy Storage Technologies, materials and systems: Challenges and prospects for large-scale grid storage. *Energy & Environmental Science, 11*(10), 2696–2767. https://doi.org/10.1039/c8ee01419a

4.Li, Y., & Dai, H. (2014). Recent advances in Zinc–Air Batteries. *Chem. Soc. Rev.*, *43*(15), 5257–5275. https://doi.org/10.1039/c4cs00015c

5.Chang, J., Wang, G., & Yang, Y. (2021). Recent advances in electrode design for rechargeable zinc–Air Batteries. *Small Science*, *1*(10), 2100044. https://doi.org/10.1002/smsc.202100044

Improvement of bioactivity of Ti-6Al-4V by electrochemical processes.

Davide Pupillo[a], L. Iannucci[a], Francesco Di Franco[b], Andrea Zaffora[b], Pasquale Picone[c], Domenico Nuzzo[c], S. Grassini[a] Monica Santamaria[b].

[a]Dipartimento di Scienza Applicata e Tecnologia, Politecnico di Torino, Torino
[b]Dipartimento di Ingegneria, Università degli Studi di Palermo, Palermo
[c]IRIB-CNR, Palermo

Currently, biomaterials are studied to be used as implants to replace damaged soft and hard tissues in the human body. In particular, biomedical materials used as implants for load-bearing applications must be durable and reliable, such as high corrosion resistance, biocompatibility, mechanical strength, absence of cytotoxicity and good osteointegration to avoid revision surgery

Ti and its alloys are good candidate for orthopaedic and traumatology implants because have elastic moduli close to those of bones and lower density with respect to that of Co-Cr alloys and stainless steels.

However, Ti and Ti alloys are considered bioinert materials, i.e. they do not react (chemically or biologically) with surrounding tissues in the human body. Moreover, corrosion phenomena of Ti alloy, namely Ti6Al4V alloy, can lead to the release of element, e. g. Al and V, that can be considered hazardous elements for human body. In addition, it is important to make antibacterial implant surface in order to reduce or even cancel bacterial adhesion and implant failure.

For these reasons several strategies have been investigated to improve the bioactivity and osteointegration of Ti alloys. The presence of hydroxyapatite (HA, $Ca_{10}(PO_4)_6(OH)_2$) can enhance the osteointegration of foreign biomaterials due to its high biocompatibility with soft and hard tissues. Therefore, inducing the incorporation or the growth of HA particles has been revealed as a good strategy to improve the materials bioactivity. Moreover, Ag is one of the most studied metals as antibacterial agent to avoid the proliferation of bacteria and other microorganisms to possible infection during the healing period.

In this work we want to design a multi-step process aimed to simultaneously enhance biocompatibility, corrosion resistance and antibacterial activity of TAV alloys for biomedical applications.

The success of this strategy is studied by evaluating the morphological/compositional changes after the surface treatment by using Scanning Electron Microscopy (SEM), Energy-Dispersive X-ray Spectroscopy (EDS), and Raman spectroscopy, by carrying out electrochemical tests (Electrochemical Impedance Spectroscopy measurements) in Simulated Body Fluid (SBF) at 37°C, as well as by in vitro tests to study cytocompatibility, antibacterial activity and hemocompatibility of the prepared TAV samples.

Subtopic: Ag, alginate, antibacterial activity, bioactivity, hydroxyapatite, Ti alloys

In vitro corrosion and stress corrosion cracking of Ti6Al4V alloy in H_2O_2-containing physiological solutions

Flavien Vucko[1], Lorenz Holzer[2], Maxime Dumouchel[3] and Michel Prestat[1]

[1] French Corrosion Institute, 220 rue Pierre Rivoalon, 29200 Brest, France

[2] Institute of Computational Physics, Zurich University of Applied Sciences, Wildbachstrasse 21, 8400 Winterthur, Switzerland

[3] Regional University Hospital (CHRU) Brest, Faculty of Odontology, avenue Foch, 29200 Brest, France

Abstract

Titanium and its alloys are among the most widely used non-biodegradable materials as implants in the human body. The corrosion resistance of titanium is mainly attributed to the presence of a thin passive layer on its surface that degrade in the presence of oxidizing species, such as oxygen peroxide (H_2O_2), leading to the device degradation and release of its constituents in the peri-implant tissues. H_2O_2 is produced by the immune system during inflammatory episodes and is also utilized by surgeons as antimicrobial treatment of peri-implant infection. Ti6Al4V alloy is a popular implant material because of its high mechanical properties, but it could be susceptible to stress corrosion cracking (SCC) under mechanical load due to its β phase dissolution in H_2O_2-containing physiological solutions [1]. However, no clear link has been established between the corrosive environment, the mechanical load and the microstructure of the Ti6Al4V alloy.

This contribution will report about the influence of H_2O_2 concentration on the corrosion of Ti6Al4V simulating in vitro inflammation conditions (low concentration) as well as disinfection procedures (high concentrations). Results on H_2O_2-driven degradation of the microstructure (mainly in the β phase) and the mechanical properties of the alloy will be discussed.

[1] M. Prestat, F. Vucko, L. Holzer, D. Thierry, Microstructural aspects of Ti6Al4V degradation in H2O2-containing phosphate buffered saline, Cor. Sci. 190 (2021)

Passive film formation on the new biocompatible Ti21Nb24Mo23Hf17Ta15 high entropy alloy

V. Roche[a], Y. Champion[b], I.A. Bataev[c], A. Moreira Jorge Jr[a,b,d]

a Univ. Grenoble Alpes, Univ. Savoie Mont Blanc, CNRS, Grenoble INP, LEPMI, 38000 Grenoble, France.

b Univ. Grenoble Alpes, CNRS, Grenoble INP, SIMaP, 38000 Grenoble, France

c Novosibirsk State Technical University, K. Marx Ave. 20, Novosibirsk 630073, Russia

d Department of Materials Engineering, Federal University of Sao Carlos, 13565-905 Sao Carlos, Brazil

This work presented a first exploratory analysis of the new Ti21Nb24Mo23Hf17Ta15 high entropy alloy intended to be used as a biomedical implant material [1]. The Ti21Nb24Mo23Hf17Ta15 biocompatible was analyzed for different air-exposure times before corrosion tests in simulated body fluid (SBF) in the dark, simulating implant air storage before implantation, presenting tremendous surface passivation capacity. Samples were polished and air-exposure times before immersion varied from 0 h to 360 h. Inbody passive film formation after implantation was simulated by resting the alloy for seven days in the SBF solution. A deep analysis of Electrochemical impedance spectroscopy data was performed using complementary Cole-Cole representation [2] and EEC fitting with Brug's equation. Electrochemical impedance spectroscopy indicates layers thickening during air exposure with a very capacitive behavior. Two-time constant relaxation confirmed the formation of a double layer and an oxide one. The equivalent Relectrolite+ (Coxide)+ (R//CPE) circuit model simulated the EIS behavior. Atoxic inert oxides were observed by X-ray photoelectron spectroscopy before and after SBF immersion for seven days, not impairing biocompatibility and producing a stable passive film

[1] Virginie Roche, Yannick Champion, Ivan A. Bataev, Alberto Moreira Jorge Junior
Corrosion Science 207 (2022) 110607

[2] B. Tribollet, V. Vivier, M.E. Orazem EIS Technique in Passivity Studies: Determination of the Dielectric Properties of Passive Films, Ed. Klaus Wandelt, Encyclopedia of Interfacial Chemistry, Elsevier, 2018, Pages 93–107, ISBN 9780128098943, https://doi.org/10.1016/B978–0-12–409547-2.13817-X

Self-expanding-biodegradable composite implants

Lisa Hanke, University of Kiel, Kiel/Germany; Duygu Dengiz, University of Kiel, Kiel/Germany; Felix Weisheit, University of Kiel, Kiel/Germany; Eckhard Quandt, University of Kiel, Kiel/Germany

Aneurysms are balloon-like formations on the arteries. This anomaly creates weak zones with increasing the risk of rupture. Due to the severity of the ruptures, several implants with different designs, varying from stents (tubular) to contour (hemispherical) intrasaccular designs, and from different materials have been developed for the treatment[1].

In this study, Mg-based hemispherical intrasaccular implants with auxetic designs and NiTi shape-memory backbones are developed. The auxetic structures exhibit a negative Poisson's ratio, which leads to improved crimpability and the ability of conformal bending of the implant. Moreover, NiTi is widely used for biocompatible self-expandable implants due to the shape memory effect. Combining NiTi (supporting layer) with Mg (main layer), self-expanding-(partially)biodegradable composite implants can be fabricated. Thus, reducing the amount of NiTi and replacing it with a biodegradable material gives advantages such as less material remaining in the body after healing and fewer long-term effects of the implant are expected.

The samples are prepared by UV-lithography, sacrificial layers, and magnetron sputtering, allowing complex 2D structures in sizes of 10-20 µm. In this case, NiTi also gives us another ability to shape set 2D structures to 3D implants with heat treatments.

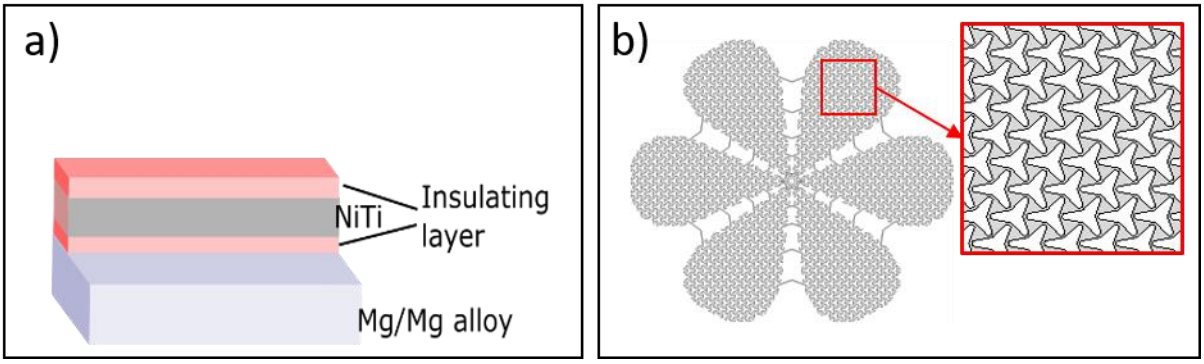

Figure: a) Schematic layer system of the structure. The ratio of layer thickness is not according to the actual design. b) Auxetic intrasaccular device design adapted from literature [2].

The structure, however, leads to challenges for the material regarding degradation control. Firstly, the degradation of Mg thin films needs to be lowered due to the small structure size to ensure the device's stability during the first months of treatment. Secondly, the combination of metals in one device leads to galvanic coupling and an increase in the degradation rate of the Mg structure. Therefore, additional insulation layers (e.g., SiO_2) are included in the layer stack to avoid direct or close-range contact of Mg and NiTi.

The corrosion rate of Mg and NiTi films and material combinations is analysed by potentiodynamic polarisation and weight-loss measurements in Hanks' balanced salt solution at a pH of 7.4 and a temperature of 37 °C to measure similar to biological conditions. Additionally, the stability of the structures in the solution is analysed optically. While the structures of Mg and Mg alloys are found not to degrade fast even though the surface area is increased, the galvanic coupling effect increases the corrosion by a factor of over 100. However, including insulating layers reduces the degradation rate to a range similar to the rate of pure Mg of approximately 0.1 mm/yr. Further possibilities to reduce corrosion rates by, e.g., surface treatment make the usage of the material stack feasible for the application of partially biodegradable implants.

[1] K. S. Lee *et al.*, “The evolution of intracranial aneurysm treatment techniques and future directions,” *Neurosurgical Review 2021 45:1*, vol. 45, no. 1, pp. 1–25, Apr. 2021, doi: 10.1007/S10143-021-01543-Z.

[2] J. N. Grima and K. E. Evans, “Auxetic behavior from rotating triangles,” *Journal of Materials Science 2006 41:10*, vol. 41, no. 10, pp. 3193–3196, Mar. 2006, doi: 10.1007/S10853-006-6339-8.

Metal release of CoCrMo manufactured by selective laser melting during sliding against articular cartilage

M. Rodriguez Ripoll, AC2T research GmbH, Wiener Neustadt/Austria

R. M. Eder, AC2T research GmbH, Wiener Neustadt/Austria

T. Varadi, AC2T research GmbH, Wiener Neustadt/Austria

C. Bauer, University for Continuing Education Krems, Krems/Austria

F. Franek, AC2T research GmbH, Wiener Neustadt/Austria

S. Nehrer, University for Continuing Education Krems, Krems/Austria

Hemiarthroplasty, a medical procedure consisting on the replacement of half of the affected joint, was introduced during the last decades as a less aggressive alternative to full replacement surgery. However, it has been widely observed that the remaining native cartilage left after hemiarthroplasty, total knee arthroplasty without patella resurfacing and other partial resurfacing procedures which create a metal-on-cartilage interface, experiences accelerated wear when in contact against metallic implants.

The aim of this work is to evaluate the potential of additive manufactured CoCrMo using selective laser melting as hemi implants. The CoCrMo additive manufactured specimens are investigated under reciprocating sliding motion against bovine osteochondral plugs in controlled electrochemical conditions using a floating cell with a three-electrode set up coupled to a nanotribometer. Phosphate buffer saline was used as an electrolyte. Throughout the experiment, the coefficient of friction and the open circuit potential is monitored. Afterwards, the electrolyte is analyzed using Inductively Coupled Plasma Atomic Emission Spectroscopy and mass spectrometry in order to measure the amount of released Co ions and correlate it with the frictional behavior. The molecules present on the cartilage surface after the experiment are unveiled using high resolution mass spectrometry. The results obtained are benchmarked against wrought CoCrMo currently used in hemi implants in terms of friction, tribocorrosion performance and metal release. Further, the impact of implant material on cartilage damage is assessed based on the metabolic activity of chondrocytes and the expression of catabolic genes.

Tough but weak: the role of carbides in the biocorrosion susceptibility of Co-Cr-Mo implants

M. Cihova[1], J. Gonzalez-Frutos[1], B. Weisse[2], P. Schmutz[1]

1 Laboratory for Joining Technologies and Corrosion, EMPA-Swiss Federal Laboratories for Materials Science and Technology, Ueberlandstrasse 129, 8600 Dübendorf, Switzerland.

2 Laboratory for Mechanical Systems Engineering, EMPA-Swiss Federal Laboratories for Materials Science and Technology, Ueberlandstrasse 129, 8600 Dübendorf, Switzerland.

Cobalt–chromium–molybdenum (CoCrMo) alloys are established passive metals routinely used in orthopedics and dentistry for their low wear and excellent mechanical properties, particularly high strength and extended service duration. While continuous materials development has pushed the optimization of the alloy's composition and microstructure towards maximized mechanical performance, the concomitant impact on the resistance towards biocorrosion was left behind [1]. This comes at a risk to the patient health and safety. In the clinical practice, two CoCrMo alloy types of different carbon content are specified by to ASTM, namely low (LC, < 0.14 wt.%) or high-carbon (HC, 0.15-0.35 wt.%) alloys [2]. In both types, carbides are present, the volume fraction of which is significantly greater for the HC alloy, and their distribution and size are a function of the materials' thermomechanical processing history [3]. While their role in enhancing the alloy's strength and hardness are undisputed, the specific role that metal carbides play in (*i*) the *local* biocorrosion susceptibility of HC-CoCrMo alloys and (*ii*) concomitant implications to the *macroscopic* material durability as an implant safe to the patient remains incomplete.

In this study, we scrutinize the biocorrosion behavior of a carbide-containing HC-CoCrMo alloy as used for commercial implants, ISO 5832-12. Its corrosion behavior is studied in correlations to the underlying microstructure, aiming at establishing a thorough understanding of the microstructure–corrosion susceptibility correlations in relevant physiological media. Particular focus is set on the distribution of carbides, and the elemental distribution with local variations of chromium content as the passivating element in this system. To this end, the macroscopic electrochemical response is assessed via electrochemical impedance spectroscopy (EIS) and potentiodynamic polarization, both conducted in HyClone™ solution used as a simulated joint fluid at physiological conditions (pH 7.0-7.4, 37 °C). The macroscopic electrochemical analysis is complemented by local analysis using scanning kelvin probe force microscopy (SKPFM). The electrochemical behavior is then correlated with the material microstructure, which is analyzed before as well

as after corrosive exposure across different length scales using light and analytical electron microscopy. The local bulk and surface oxide chemistry is analyzed by energy-dispersive X-ray spectroscopy (EDS) and Auger spectroscopy. LC-CoCrMo with <0.1 wt.% will serve as a control without carbides.

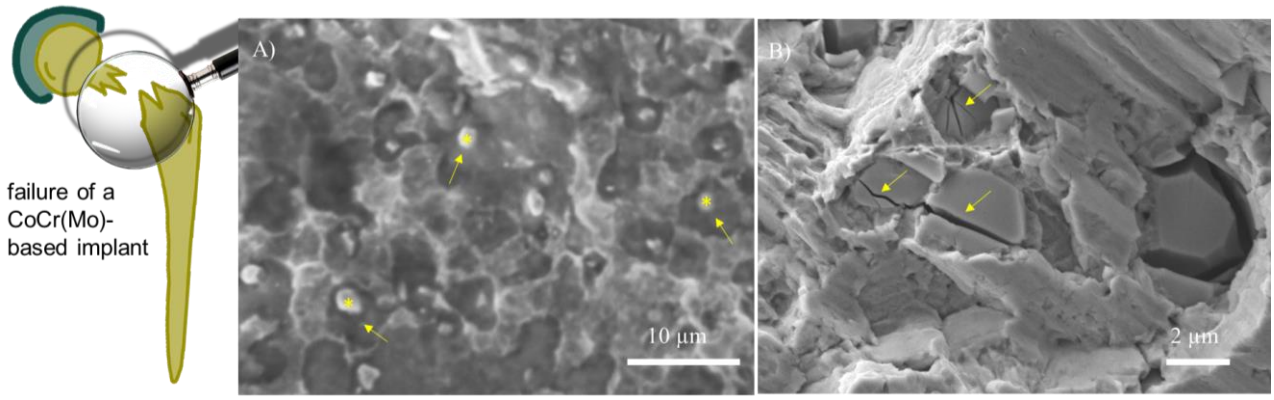

***Fig. 1**: Scanning electron microscopy images of an HC-CoCrMo implant fracture surface. (A) Corrosive attack around carbides. Asterisks mark carbides; arrows mark matrix dissolution in their direct vicinity; (B) Close-up of carbides, revealing their fracture. Arrows mark microcracks, indicating their brittle nature.*

The analysis confirmed a high density of lower micrometer-sized carbides in the material microstructure of the used HC-CoCrMo alloy. Localized matrix dissolution was observed around these carbides upon the material's exposure to HyClone™ solution (Fig. 1A), as expected for chromium-depleted zones according to literature reports. The created matrix voids are detrimental, because they might further accelerate the continuous rate of corrosion and create protruding asperities of hard material at the implant surface that can damage opposing softer materials, ultimately causing wear. Furthermore, evidence of brittle fracture of these carbides were recorded (Fig. 1B), indicative of considerable mechanical mismatch to the matrix. Both, dissolution-derived voids and mechanical mismatch are considered potential players to local crack formation under cyclic load, which can act as initiation sites for macroscopic fatigue cracks. In this contribution, we will discuss the derived microstructure–corrosion susceptibility correlations in light of a clinical implant failure case of a total hip arthroplasty prosthesis, for which the corrosion mechanisms at play – when acting synergistically – can lead to catastrophic failure, namely implant fracture.

[1] Lanzutti, A., Andreatta, F., Rossi, L., Di Benedetto, P., Causero, A., Magnan, M., & Fedrizzi, L. (2019). *Corrosion fatigue failure of a high carbon CoCrMo modular hip prosthesis: Failure analysis and electrochemical study*. Engineering Failure Analysis, 105, 856-868.

[2] ASTM F1537-11. (2011). Standard Specification for Wrought Cobalt-28Chromium-6Molybdenum Alloys for Surgical Implants (UNS R31537, UNS R31538, and UNS R31539).

[3] Cawley, J., Metcalf, J. E. P., Jones, A. H., Band, T. J., & Skupien, D. S. (2003). A tribological study of cobalt chromium molybdenum alloys used in metal-on-metal resurfacing hip arthroplasty. Wear, 255(7-12), 999-1006.

Interest of mineralogical analysis and questionnaire in a case of granulomatosis related to metallosis following total hip replacement

M. Catinon, Minapath Developpement 56 Bd Niels Bohr Insavalor CS : 52132 Villeurbanne 69603, France
M. Vincent, Minapath Developpement 56 Bd Niels Bohr Insavalor CS : 52132 Villeurbanne 69603, France
E. Roux Minapath Developpement 56 Bd Niels Bohr Insavalor CS : 52132 Villeurbanne 69603, France
V. Massardier, Univ Lyon, CNRS, INSA Lyon, LaMCoS, UMR5259, 69621 Villeurbanne, France
AM. Sfarghiu, Univ Lyon, CNRS, INSA Lyon, LaMCoS, UMR5259, 69621 Villeurbanne, France
F. Geistel, Department of Internal Medicine, Hôpital de la Croix Rousse, Hospices Civils de Lyon, Université Claude Bernard Lyon 1, F-69004 Lyon, France
F. Lifermann, Service de Médecine Interne Hématologie, Centre Hospitalier de Dax, Dax, France
Y. Dauzan, Service d'Anatomie et Cytologie Pathologique, Centre Hospitalier de Dax, Dax, France
P. Sève, Department of Internal Medicine, Hôpital de la Croix Rousse, Hospices Civils de Lyon, Université Claude Bernard Lyon 1, F-69004 Lyon, France

Introduction: Hip prostheses are medical devices used to replace damaged or defective hip joints. However, there can be complications with these prostheses, including wear and release of particles into the body. Wear is the process by which the materials of the prosthesis wear down over time, causing damage to the surrounding bone and joint. Release of particles occurs when pieces of prosthesis material break off and move within the body, causing damage to surrounding tissues and organs. These problems can cause pain, infections, and other complications, and may require additional surgeries to fix. We present here the case of a filthy-one year old woman presenting with bilateral granulomatous pan-uveitis associated with abnormal hilio-mediastinal and pelvi-abdominal diffuse nodes and pseudo-tumor around a right metal (chrome-cobalt) / ceramic total hip prosthesis. Patient had no hip pain. A diagnosis of sarcoidosis-like reaction was made following histological study of an inguinal adenopathy. Light microscopy of the slide showed the presence of refractive foreign bodies in polarized light within the granulomas. This observation led to mineralogical analysis by scanning electron microscopy (SEM) coupled with chemical analysis of the observed particles.

Materials and methods: A questionnaire on lifetime exposure to mineral particles was completed as well as a mineralogical analysis of the lymph node from the inguinal adenopathy excision. A 5µm thick histological section was analyzed by scanning electron microscopy (JEOL JSM-6010LV) coupled to an EDX spectrometer (EDS detector Oxford Aztec-DDI X MAXN 50). In order to compare the EDX spectra of the different particles, they were analyzed under the same experimental conditions (backscattered electrons; Intensity: 20.0kV; Working distance: WD = 12mm; spot size SS55; Pressure P = 20Pa; magnification x500).

Results: SEM analysis of the section (surface area 0.3cm^2) revealed the presence of 124 inorganic particles. The classification of these particles according to their elemental composition is as follows: titanium compound (53.2%), titanium + vanadium (25.8%), calcium phosphate (13.7%), calcium phosphate + iron (2.4%), steel (2.4%), calcium oxide (1.6%) and silica (0.8%).

Conclusions: Only two cases suspecting relationship between hip prosthesis wearing and granulomatosis have been reported [1, 2]. It's the first time that SEM-EDX analysis of granuloma biopsy has been used. More than half of the particles analyzed correspond to titanium compounds. The element titanium is mainly accompanied by tissue constituents and/or endogenous elements (phosphorus, sulphur and calcium) and small amounts of aluminum. The titanium + vanadium (TiV) particles have the same elemental composition profile as the titanium compounds with the addition of vanadium in small amounts. The manufacturer's product sheets indicate that the femoral stem is made, in part, of TA6V titanium alloy. This alloy contains aluminum (up to almost 7%) and vanadium (up to 4.5%). It is also made of stainless steel. We did not identify any cobalt chromium particles although the data sheets mention it in the femoral head and/or cup. It is possible that these particles are in nanometric form and therefore not detected during our analysis. This clinical case illustrates the interest of the questionnaire as well as of a mineral analysis by SEM-EDX for any granulomatosis and particularly suspected to be related to the release of particles by various prostheses.

[1] Peoc'h,M, Moulin C, Pasquier B Systemic granulomatous reaction to a foreign body after hip replacement N E J Med 1995; 335: 133-4

[2] Balbouzis T, Georgiadis T, Gregoris P A novel complication following metallosis from hip prosthesis Case report Hip pelvis 2016;28:249-53

Biocorrosion and Biodegradation of Iron Oxide-Based Nanostructures and Their Potential Biomedical Applications

Yuyun Yang[1], Juncen Zhou[2], Xiufang Cui[1], Guo Jin[1], Sannakaisa Virtanen[3], Aldo R. Boccaccini[4]*

[1] Institute of Surface/Interface Science and Technology, Department of Material Science and Chemical Engineering, Harbin Engineering University, Harbin, China

[2] Department of Biomedical Engineering, Stony Brook University, Stony Brook, NY, USA

[3] Institute for Surface Science and Corrosion, Department of Materials Science and Engineering, University of Erlangen-Nuremberg, Erlangen, Germany

[4] Institute of Biomaterials, Department of Materials Science and Engineering, University of Erlangen-Nuremberg, Erlangen, Germany

Abstract

Surface nanostructures like titanium oxide nanotubes and nanopores have revealed excellent functionalization performance and favorable corrosion resistance. In certain cases, corrosion and degradation are, however, an advantageous feature for biodegradable implant materials. Specifically, iron-based materials have been recently studied as promising degradable biomaterials in the biomedical application. Therefore, surface nanostructured arrays are considered as one feasible surface modification approach for iron-based implants. Anodization method is regarded as a suitable strategy to fabricate iron oxide nanostructures, including nanopores and nanotube arrays with tunable thicknesses, on the surface of iron-based metallic biomaterials. Biocorrosion and biodegradation behavior of the nanostructured arrays are investigated. In order to further functionalize the iron-based metallic biomaterials, a surface functionalization system combining two biodegradable components, iron oxide nanostructured arrays and polycaprolactone coatings has been developed. With the relatively stable PCL coatings, the stability and cytocompatibility of the iron oxide nanostructured arrays could be enhanced. As we know, the iron oxide nano materials have been studied and applied in the biomedical applications including diagnostic, therapeutic, and theranostic aspects, such as MRI, drug delivery, anticancer and antimicrobial activity, cell labelling, DNA purification, etc.. In consideration of the mass surface area of the nanostructures, the iron oxide nanostructured arrays are applied as ideal drug carriers, and PCL coatings serve as

physical stabilizer to the nanostructured arrays and as barrier to control the drug release behavior.

Iron oxide nanostructured arrays developed in this study are therefore promising for functionalizing iron-based biomaterials targeted for degradable bone scaffolds and bone fixation devices. The surface functionalization strategy is expected to be suitable for various iron-based materials and different clinical applications.

Keywords: Biocorrosion; Biodegradation; Iron Oxide Nanostructured Arrays; Biocompatibility; Biomedcial Application.

Cathodic reactions of biodegradable metals in different physiological solutions investigated with respirometric measurements

Mark Bruns, Michael Strebl, Ghina Schulze, Sannakaisa Virtanen, Friedrich-Alexander-Universität Erlangen-Nürnberg, Germany

Biodegradable metals as medical implants face complex application media, and there is a multitude of simulated body fluids for in-vitro studies aiming to simplify and understand the corrosion processes. While substantial research has already been conducted, new developed technologies enable further elucidation of mechanisms.

In this work, besides conventional electrochemical measurements and different surface analysis, biodegradation is also investigated with respirometric measurements, which enable non-destructive, real-time, and universal monitoring of the corrosion rate. The working principle is based on quantification of the cathodic reaction, which in aqueous solutions can consist of H2 evolution reaction (HER) and the O2 reduction reaction (ORR). Respirometric measurements are applicable for both, atmospheric [1] and immersion corrosion [2], and reliably show a good correlation with mass loss and electrochemical measurements [3].

Particularly for magnesium corrosion, this technique proves useful as a non-negligible amount of ORR can occur under certain conditions. On magnesium a wide screening on different electrolyte constituents has been conducted [4], however not in regard to other cathodic reactions than HER. In the presentation, the in-depth influence of the concentration of different amino acids on the corrosion behavior of Mg alloy AZ31 will be shown and compared to more complex solutions.

Zink is another emerging biodegradable material, whose cathodic reactions are still to be studied in detail. One ORR pathway can lead to production of hydrogen peroxide, which can be especially relevant in bioapplications. This pathway is investigated at both open circuit potential and utilizing electrochemical measurements, each coupled with the respirometric technique. Furthermore in contrast to literature findings Zn shows not only ORR but in certain conditions also some HER, which will further elaborated.

[1] Strebl, M.; Bruns, M.; Virtanen, S.; Editors' Choice—Respirometric in Situ Methods for Real-Time Monitoring of Corrosion Rates: Part I. Atmospheric Corrosion. In: J. Electrochem. Soc. 167 (2), S. 21510 (2020) DOI: 10.1149/1945-7111/ab6c61

[2] Strebl, M.; Bruns, M.; Schulze, G.; Virtanen, S.; Respirometric In Situ Methods for Real-Time Monitoring of Corrosion Rates: Part II. Immersion J. Electrochem. Soc. 168 011502 (2021) DOI: 10.1149/1945-7111/abdb4a

[3] Strebl, M.G.; Bruns M.P.; Virtanen S.; Coupling Respirometric HER and ORR Monitoring with Electrochemical Measurements, Electrochimica Acta 412 (2022) 140152. https://doi.org/10.1016/j.electacta.2022.140152.

[4] S. V. Lamaka; B. Vaghefinazari; Di Mei; R. P. Petrauskas; D. Höche; and M. L. Zheludkevich; Corrosion Comprehensive screening of Mg corrosion inhibitors; Corrosion Science 128 (2017) https://doi.org/10.1016/j.corsci.2017.07.011

Towards an accurate prediction of magnesium biocorrosion by closer mimicking the in-vivo environment

Mustafa Yalcinkaya, Arie Bruinink, Martina Cihova, Patrik Schmutz,

Laboratory for Joining Technologies and Corrosion, Empa - Swiss Federal Laboratories for Materials Science and Technology, Dübendorf CH-8600, Switzerland

The use of magnesium (Mg) as biodegradable metallic implants has attracted great interest in the medical sector due to its wide range of applications, from orthopedic surgeries to biodegradable sensors[1,2]. In the physiological environment, Mg dissolves upon the formation of a degradation layer containing multiple species, including various phosphates and carbonates. The chemical structure of the layer governs the overall implant dissolution and biocompatibility[3]. Yet, the detailed understanding of application-dependent Mg biocorrosion mechanisms is still incomplete.

A main concern in tackling this complex endeavor arises from the strong variations in results between preclinical animal studies (in-vivo) and standard laboratory experiments (in-vitro)[4]. In the body, the implant surface is exposed to the interstitial body fluid containing inorganic, organic, and metallic species. The flow rate of the fluid can vary depending on where the implant is placed. As a result, the implantation site determines the local chemistry, such as the concentration of physiological species and pH. In in-vitro experiments, Mg samples are typically immersed in simulated body fluids without any fluid flow. These fluids generally consist of inorganic salts with nonphysiological synthetic pH buffers. The use of these buffers might increase the corrosion rate through the complex formation and alter the chemical structure of the degradation layer. Hence, a reliable prediction of the corrosion rate and biocompatibility of the implant becomes impossible. Although many attempts have been made to bridge the gap between in-vitro and in-vivo conditions, it remains challenging to mimic the physiological environment in its full complexity.

In this study, we substantially revise the established protocols in the community to reflect the often overlooked in-vivo aspects. With the development of an integrated in-vitro setup, the flexibility to control the flow rate and the pH of test solutions was obtained. A newly formulated simulated interstitial body fluid (SIBF) containing inorganic, organic, and metallic species was used to simulate the in-vivo conditions.

The pH of SIBF was regulated with a "dynamic" CO_2 buffer. The solution was then sent to Mg samples at different flow rates. The electrochemical behavior was recorded by performing Electrochemical Impedance Spectroscopy (EIS). After the experiments, the samples were taken out for ex-situ characterization.

In this work, Mg samples with different purities and textures were tested. The initial crystallographic orientation of the samples was characterized by X-Ray diffraction. The morphology of the corrosion layer was analyzed across different length scales via light microscopy, optical profilometry, Scanning Electron Microscopy, and the chemical composition via Energy-Dispersive X-ray spectroscopy. It was found that the presence of organic components such as albumin accelerated the corrosion of Mg and induced the formation of an insulating organic film. Under this film, Mg-phosphates and –carbonates were found, whose local characteristics were governed by the flow rate, underlying grain orientation, and material purity. In static conditions, a homogenous spongy layer formed while increasing the flow rate led to a laterally heterogeneous surface with intergranular corrosion and preferential grain etching.

Specifically, the formation of Mg-phosphates appeared to be favored on samples with (100)/(110) initial orientation, for which the charge transfer resistance values obtained from EIS measurements were notably higher in comparison to the (002) initial texture. Interestingly, EIS measurements indicated that ultra-high (99.999%) and low-purity (99.9%) samples behave comparably in SIBF solution, where the formation of Mg-phosphates and -carbonates might retard the chloride-induced corrosion.

These findings support the view that small changes in the in-vitro environment and material properties may greatly affect the formation of the degradation layer and its characteristics. Therefore, a better understanding of their relationship is crucial for advances in mimicking the in-vivo situation with laboratory-based setups. It will also support the clinical safety and continuous material development of Mg-based implants.

[1] D. Zhao et al., Biomaterials, 112 (2017), DOI: 10.1016/j.biomaterials.2016.10.017

[2] N. Ashammakhi et al., Advanced Functional Materials, 31 (2021), DOI:10.1002/adfm.202104149

[3] E. Bonyadi Rad et al., Journal of Materials Science: Materials in Medicine, 28 (2017), DOI: 10.1007/s10856-017-5969-5

[4] J. Walker et al., Journal of biomedical materials research. Part B, Applied biomaterials, 100 (2012), DOI: 10.1002/jbm.b.32680

Effect of geopolymer-chitosan composite coatings on magnesium biocorrosion

A. Rondinella[1], M. Zanocco[1], E. Tubaro[1], F. Andreatta[1], S. Maschio[1], L. Fedrizzi[1]*

[1] University of Udine, Polytechnic Department of Engineering and Architecture, Via del Cotonificio 108, Udine, Italy

Abstract

Magnesium-based bioresorbable materials have become excellent candidates for bone regeneration applications in recent years. They possess a bone-like elastic modulus and antibacterial and osseointegrative properties. The magnesium bioresorption rate, however, is directly correlated to its corrosion processes which, if too high, can potentially exert detrimental effects on the biological tissues involved. The presence of chlorides (very common chemicals in bodily fluids) can cause extensive corrosion phenomena and, consequently, a rapid loss of mechanical properties long before the bone tissue has healed. In addition, the rapid dissolution of magnesium and its alloys can generate toxic products such as hydroxides and hydrogen bubbles that can accumulate in tissues.

In this work, composite coatings made of geopolymer and chitosan were produced to modulate the corrosion rate of magnesium in simulated biological environments. The composite coating microporous nature can regulate the rate at which the electrolyte reaches the substrate, thus avoiding a complete barrier effect but trying to ensure that the corrosion rate remains within suitable levels.

The coatings were produced by dip-coating deposition. SEM/EDXS measurements were carried out to study the coating morphology and chemical composition. The samples were then immersed in saline, phosphate buffered saline solution (PBS) and Hanks' Balanced Salt Solution (HBSS), respectively, to test their behavior in solutions progressively similar to the biological environment.

Initially, the amount of hydrogen evolved was monitored at different time steps. Then open circuit potential measurements, potentiodynamic polarization tests and electrochemical impedance spectroscopy (EIS) measurements were carried out to verify the behavior difference between coated and uncoated samples in the solutions used.

*Corresponding author Tel. +39 (0)432 558863
E-mail address: alfredo.rondinella@uniud.it

In vitro evaluation of the degradation and mechanical integrity of sol-gel coated AZ31 magnesium alloy for biomedical applications

J.P. Fernández-Hernán, Universidad Rey Juan Carlos, Móstoles (Spain)
F. Cuadrado, Universidad Rey Juan Carlos, Móstoles (Spain)
B. Torres, Universidad Rey Juan Carlos, Móstoles (Spain)
J. Rams, Universidad Rey Juan Carlos, Móstoles (Spain)

Due to their outstanding properties, magnesium and its alloys are very interesting materials for the manufacture of temporary biodegradable implants for osteosynthesis that could contribute to reducing the postoperative process time and to improving the quality of life of patients. However, magnesium is a very reactive material that will degrade rapidly when implanted in a physiological environment. Thus, implants made out of these materials will suffer a rapid loss of mechanical resistance that could end up in the failure of the implant. The application of coatings on these materials can retard and minimize their degradation rate, letting the fractured bone heal before the loss of mechanical integrity of the implants. In this research, two different sol-gel coatings, one of them doped with a low concentration of COOH-GNPs were used to protect AZ31 magnesium alloy substrates immersed in a bath of a simulated body fluid solution over a month. The presence of the coatings managed to retard and reduce the degradation of the coated samples compared with the bare AZ31 substrates for all the testing times. After one month of immersion, the mechanical resistance of the coated samples was up to 30% higher than the resistance of the bare substrates and the degradation process was retarded between two and three weeks. Thus, the application of these coatings is interesting for coating implants for small bone fracture treatments, letting the damaged bone heal before the loss of the mechanical resistance of the implants.

Medical Implants and Devices (TF)

Dr. Patrik Schmutz (Swiss Federal Laboratories for Materials Science and Technology (EMPA), Switzerland)

Effect of alcohols addition on the growth of PEO layer on AZ31 alloys and its corrosion performance for biomedical purposes

Isis Tournay-Dufrenne[a], *L. Dangreau*[b], *M-G Olivier*[a,b]

[a] *Materials Science Department, Faculty of Engineering, University of Mons, 20, Place du Parc, Mons, Belgium*

[b] *Materia Nova Research Centre, 3, Avenue N. Copernic, Parc Initialis, Mons, Belgium*

Abstract

Nowadays, many researchers are investigating different materials that could be used as resorbable implants to reduce the number of surgical procedures without weakening the bone. Magnesium alloys are of interest due to their good mechanical properties (e.g., modulus of elasticity close to that of bone), but their degradation rate due to corrosion is still considered too high, which could lead to the loss of mechanical integrity of the implant and its rapid failure. Therefore, a compromise between magnesium dissolution and sufficient lifetime is required. It is therefore interesting to develop layers with reinforced mechanical properties but also with porosity to promote osseointegration and to limit implant dissolution. This dual effect can be attained with plasma electrolytic oxidation (PEO) coatings which generally have a dense inner layer (to maintain strength) and a porous outer layer (to improve cell interaction).

A previous study showed that alcohols added in the electrolyte bath could improve the PEO layer performance.[1] Therefore, a study mixing fluorides and alcohols in the electrolyte bath is carried out to investigate their effect on the properties of the PEO layer on AZ31 alloys. The different alcohols studied are ethanol, ethylene glycol and glycerol. The samples are analyzed in sodium chloride solution as well as in physiological electrolytes using Electrochemical Impedance Spectroscopy (EIS). The cross-section of the samples is characterized by Scanning Electron Microscopy (SEM) and micro-hardness studies.

Keywords: Plasma electrolytic oxidation; biomedical applications; alcohols; EIS; SEM.

[1] Asoh H, Asakura K, Hashimoto H. Effect of alcohol addition on the structure and corrosion resistance of plasma electrolytic oxidation films formed on AZ31B magnesium alloy. *RSC Adv*. 2020;10(15):9026-9036. doi:10.1039/d0ra01154a

Corrosion and embrittlement research needs for the hydrogen sector – an overview of the EU R&D funding ecosystem and current research topics

Authors:

- Luigi Crema, Hydrogen Europe Research President, Fundazione Bruno Kessler (Italy): crema@fbk.eu
- Christian Sattler, Hydrogen Europe Research vice-President, Deutsches Zentrum für Luft- und Raumfahrt (Germany): Christian.sattler@dlr.de
- Louis Mazurkiewicz, Hydrogen Europe Research Innovation Manager: l.mazurkiewicz@hydrogeneuroperesearch.eu

Title: *Corrosion and embrittlement research needs for the hydrogen sector – an overview of the EU R&D funding ecosystem and current research topics*

Hydrogen embrittlement is a phenomenon in which hydrogen atoms diffuse into metals and weaken their mechanical properties, making them more susceptible to cracking and failure. This can be particularly problematic in hydrogen technologies such as electrolysers, fuel cells, hydrogen storage tanks and pipelines. In addition, hydrogen can also cause corrosion of certain metals, which can lead to leaks and other safety hazards. Careful selection of materials and design components that are resistant to hydrogen embrittlement and corrosion are therefore crucial for hydrogen technologies.

As such, there are several research needs related to hydrogen embrittlement and corrosion in hydrogen technologies:

- Material selection and testing: further research is needed to identify materials that can withstand prolonged exposure to liquid or gaseous hydrogen without experiencing embrittlement or corrosion. This involves developing new testing methods to evaluate the resistance of materials to hydrogen-related degradation, as well as understanding the underlying mechanisms that lead to embrittlement and corrosion.

- Hydrogen safety: further researcher is needed to investigate the failure mechanisms associated with hydrogen embrittlement and corrosion in order to design safer systems that can withstand the high pressures and corrosive effects of hydrogen.

- Computational modeling: computational modeling can be used to predict the behavior of materials under different conditions, including exposure to hydrogen. Researchers can use modeling to design materials with specific properties that are resistant to hydrogen embrittlement and corrosion, as well as to optimise the performance of existing materials.

- Standardisation and regulation: further research is needed to work with regulators and industry stakeholders to develop standards and regulations that address the risks associated with hydrogen embrittlement and corrosion. This will require collaboration between scientists, engineers, policymakers, and industry stakeholders.

At EU institutional-level, research on hydrogen is mainly undertaken via the Clean Hydrogen Partnership. This partnership will support research and innovation actions in the field of hydrogen with a total budget of 1 billion EUR from 2021 until 2027. The three participants of this partnership are the European Commission (DG RTD, DG ENER & DG MOVE – with the support of the Joint Research Centre), Hydrogen Europe and Hydrogen Europe Research.

Due to the cross-cutting nature of the sector, hydrogen technologies may be further supported in other European research and innovation programmes such as Processes for Planet, Zero-Emission Waterborne Transport, Clean Aviation, EU Rail…

In the Clean Hydrogen Partnership, the following Annual Work Plan 2022 and 2023 topics included elements on corrosion/embrittlement in their scope:

- HORIZON-JTI-CLEANH2-2022-01-03: Development of low temperature water electrolysers for highly pressurised hydrogen production
- HORIZON-JTI-CLEANH2-2022-02-01: Compatibility of Distribution non-steel metallic gas grid materials with hydrogen
- HORIZON-JTI-CLEANH2-2022-02-07: Increased hydrogen capacity of GH2 road trailers
- HORIZON-JTI-CLEANH2-2022-03-02: Innovative and optimised MEA components towards next generation of improved PEMFC stacks for heavy-duty vehicles
- HORIZON-JTI-CLEANH2-2022-03-05: Large scale demonstration of hydrogen fuel cell propelled inland waterway vessels
- HORIZON-JTI-CLEANH2-2023-01-02: Innovative Solid Oxide electrolysis cells for intermediate temperature hydrogen production
- HORIZON-JTI-CLEANH2-2023-01-04: Photoelectrochemical (PEC) and/or Photocatalytic (PC) production of hydrogen
- HORIZON-JTI-CLEANH2-2023-02-02: Pre-Normative Research about the compatibility of transmission gas grid steels with hydrogen and development of mitigation techniques
- HORIZON-JTI-CLEANH2-2023-07-01: Advanced materials for hydrogen storage tanks
- HORIZON-JTI-CLEANH2-2023-07-02: Increasing the lifetime of electrolyser stacks

In addition, potential future actions on corrosion/embrittlement are included in the Strategic Research and Innovation Agenda of the Clean Hydrogen Partnership:

- Grades of steel in pipes and their welded joints and induced phenomena (embrittlement, crack propagation, etc);
- Metallic materials existing in the distribution network (cast iron, copper, brass, lead, aluminium) and induced phenomena (embrittlement, propagation of cracks, fatigue, etc);

Involvement of the corrosion research community is therefore of vital importance to find solutions to the corrosion/embrittlement issues experienced by hydrogen technologies.

Effect of hydrogen partial pressure, humidity, oxygen and contaminants on the service behavior of a X100 seamless pipeline

L. Moli Sanchez[1], C. Mendibide[1], F. Vucko[1], M. Martinez[2]

[1]Institut de la Corrosion - RISE, Fraisses/France

[2]IFP Energies Nouvelles, Solaize/France

As expressed in the EU Hydrogen Strategy and adopted by many countries outside Europe, it is crucial that hydrogen (H) becomes a part of the energy system. Therefore, a large hydrogen logistical infrastructure needs to be developed in order to transport, store and expand the uses of hydrogen across countries. In this context, steel solutions are the most used for the hydrogen transport and storage. However, it is well known that hydrogen can be absorbed and diffused into steels causing, potentially, degradation of the mechanical properties (hydrogen embrittlement). Leading to material qualification questions.

In this work, the degradation of the fracture toughness in presence of high hydrogen pressure of a X100 seamless pipeline steels has been assessed. The critical stress intensity for crack initiation was estimated using incremental step loading on compact tension pre-cracked specimens with electric crack growth monitoring to estimate the minimum applied force necessary to initiate the propagation. The effect of humidity, contaminants (H_2S concentration representative of the possible residual contents in biogas) and oxygen was also studied at pressure of 100bar of H_2.

The results clearly showed the hydrogen susceptibility of this material to crack initiation and propagation. In addition, subcritical crack growth was observed leading to K_{IH} values <30MPa$\sqrt{m}$. Nevertheless, the final failure of the specimens occurred at K values close to the ones obtained in air.

Finally, the effect of H_2S and O_2 traces on the fracture toughness is discussed.

Qualification of Seamless Tubes for H2 Gas Applications

Florian Thébault, Vallourec Research Center France, Aulnoye-Aymeries/France;
Vincent Designolle, Vallourec NewEnergies, Meudon/France

With an increasing number of projects involving production and use of low-carbon hydrogen, the compatibility with hydrogen gas of assets for storage and transport shall be guaranteed. Indeed, hydrogen is a threat for steel equipment integrity as it promotes subcritical crack growth. In this work the fracture toughness resistance and corrosion fatigue behavior of a selection of seamless pipes for OCTG, pipeline and pressure vessel in pressurized H_2 is investigated. It covers a large variability of materials in terms of microstructures (ferrite-pearlite, bainite, martensite) and yield strengths (from 400 MPa to 950 MPa).

Fracture toughness evaluations were performed via fatigue pre-cracked bolt-load specimens exposed to 100 bar hydrogen gas during 1000 h at room temperature. All materials presented hydrogen stress intensity factor thresholds K_{IH} largely above 55 $MPa.m^{1/2}$, compliant with the ASME B31.12 option B requirement that defines materials requirements for hydrogen service. Nevertheless, severe limitations were observed when using constant displacement test method. The lack of cracking, even on high strength materials, makes this test method extremely conservative when estimating K_{IH} from ASME BPVC.VIII-3 KD-10 prescriptions. Consequently, an alternative test method has been evaluated, which consisted into a slow strain rate test on compact tensile specimens. It allows a better resolution of the fracture toughness.

Corrosion fatigue tests were performed on compact tensile specimens, also prior pre-cracked. Fatigue crack growth rate measurements were determined from 0.01 to 30 Hz and load ratios at 0.1 or 0.9 for covering applications susceptible to present very different internal pressure variations during service life. A focus is given on the influence of load ratios on threshold ΔK for initiating fatigue in presence of hydrogen. It has been observed that close to the threshold ΔK, air environment becomes more conservative than dry dihydrogen due to the presence of residual moisture.

Hydrogen uptake and embrittlement of A220 steel under gaseous hydrogen charging up to 1000 bar and 200°C

Matthias Eichinger[1], *Gregor Mori*[1]

[1]*Chair of General and Analytical Chemistry, Montanuniversität Leoben*

Franz Josef-Straße 18, 8700 Leoben, Austria

Abstract:

In hydrogen storage and transport applications steels come in contact with hydrogen at various pressures and temperatures. Under high pressures and temperatures, the hydrogen uptake of steel is increased, which can cause hydrogen embrittlement and lead to operation risks. To prevent hydrogen embrittlement, it is of crucial importance to investigate the used materials under the conditions encountered during their application. Therefore, a new autoclave test bench for constant load tests and charging experiments, with the operation range of up to 1000 bar hydrogen pressure and 200 °C was established.

Hydrogen uptake of A220 stainless steel has been investigated for solution annealed and 27 % cold deformed condition with and without a constant load of 90 % yield strength as function of hydrogen partial pressure and temperature. In addition, the effective diffusion coefficient has been determined by charging and permeation measurements to be able to simulate uptake in form of time dependent hydrogen profiles. Results from experiments and simulation are discussed.

Keywords: Hydrogen uptake, High pressure, Hydrogen embrittlement, austenitic stainless steel

Passivation of Thermally Sprayed Ti-coatings for Bipolar Plate Application in PEMWE

K. Bobzin[1], H. Heinemann[1], E. Burbaum[1], K. Radermacher[1], N. Bagcivan[2], M. Öte[2], N. C. Kruppe[2]

[1]Surface Engineering Institute, RWTH Aachen University, Aachen, Germany, info@iot.rwth-aachen.de
[2] Schaeffler Technologies AG & Co. KG, Herzogenaurach, Germany,

Abstract: In the field of research of the proton exchange membrane water electrolysis (PEMWE), Ti-coated stainless steel bipolar plates are investigated to substitute the anodic bipolar plates out of titanium bulk material. During cell operation, titanium forms a passivation layer. While the passivation layer is desirable for a long lifetime of the bipolar plate (BPP), the passivation layer reduces the electrical conductivity of the BPP. As a result, the overall cell performance is decreased. Thermal spraying is a thermo-kinetic and solvent-free coating technology, commonly applied for corrosion protection coatings. The advantages of thermal spraying for this application are an elevated degree of automation and high deposition rates for serial production. To function as corrosion protection coating, the Ti-coating must exhibit a high structural density. Two thermal spraying technologies, cold gas spraying (CGS) and high velocity air-fuel (HVAF) spraying, at atmospheric pressure, are employed to meet the desired criteria. The technologies are characterized by different particle temperatures and particle velocities. The coating development is conducted with regards to the requirements of high corrosion resistance and sufficient electrical conductivity. For coating development, titanium grade 4 is deposited on steel plates of X2CrNiMo17-12-2 of s = 5 mm thickness. The interfacial contact resistance (ICR) is determined of representative samples before and after electrochemical polarization. As the ICR-results show, the titanium grade 1 reference displays a higher ICR after the polarization than the tested coatings. In order to explain this result, chronoamperometry is conducted at the passivation potential of titanium grade 1 to observe the passivation in dependency of time. For this, the coatings are deposited onto a steel sheet, ten times thinner than of the initial coatings. The coatings are compared with the chronoamperometric properties of a titanium grade 1 titanium refrence, a typical BPP material of s = 200 µm thickness. The results of the chronoamperometry are correlated with examinations of the coating surface and the phase composition by confocal laser scanning microscopy (CLSM) and x-ray diffraction (XRD). According to the chronoamperometry, the passivation of the CGS-coating is more hindered than of the HVAF-coating and the bulk material. These results can be explained by the differences between the CGS- and the HVAF-coating in surface structure and phase composition.

Keywords: PEMWE, HVAF, CGS, bipolar plate, titanium

Introduction

Hydrogen is a versatile fuel for energy and transport applications enabling a carbon free combustion. Due to the increasing demand for hydrogen in the future, research activities have grown in the field of water electrolysis. To prepare hydrogen electrochemically from water, there are several electrolysis technologies available. The alkaline water electrolysis (AWE) is the most mature and has been investigated intensively since the 1980s[1]. However, the bottleneck of this water electrolysis is the high demand of space, the large amounts of chemical base necessary and the low efficiency in dynamic load changes[2]. For these reasons, many endeavors have been made to promote the proton exchange membrane water electrolysis (PEMWE).

The PEMWE is an acidic and compact water electrolysis technology achieving current densities up to $i = 2$ A/cm²[2]. Titanium is one suitable material for the structural cell components. The bipolar plate (BPP) and the porous transport layer are manufactured of grade 1 or grade 2 bulk titanium[3]. The reason for this choice of material is the high electrochemical stability under the high proton concentration and the elevated cell potential[4]. From an economic perspective, the structural cell components and the catalyst materials amount to the biggest contribution to the manufacturing costs[5]. In order to minimize the titanium material input, stainless steel BPPs of $s \leq 0.5$ mm thickness coated with a titanium coating of a few hundred microns are currently investigated.

One investigated coating technology for coated BPPs is thermal spraying. In thermal spraying, the feedstock material, such as powder, is heated and accelerated to the substrate by a hot gas stream, see Figure 1. The accelerated particles impact on the surface of a roughened substrate and are flattened into lamellae. The deposited particles and the roughened surface are mainly bonded by mechanical interlocking.

In the gas stream, the molten or semi-molten particles interact with the air in the environment and an outer shell of oxides is formed on the particle surface. The thickness of the oxidic shell is a function of the spraying distance, the gas stream temperature and the particle size. Finer particles share a higher surface area to volume ratio, promoting the oxidation reaction. At the impact on the substrate surface, the oxidic shell is cracking and the oxidic fractures are enclosed in the coating.[6]

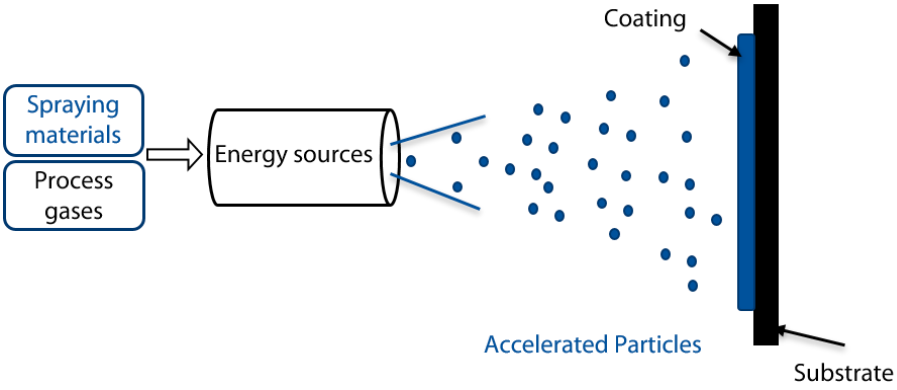

Figure 1. Schematic illustration of the thermal spraying process

Depending on the application, the partial oxidation of the coating can affect the coating properties negatively e. g. by weakening coating cohesion[6] and increasing the electrical resistivity. As titanium is the material of choice for the corrosion protection coating on the BPP, the formation of TiO_x during the spraying process on air can be expected.

By executing the titanium coating deposition in a vacuum chamber, the oxidation of the material is prevented. In previous PEMWE related studies, vacuum plasma spraying (VPS) was used to test thermally sprayed titanium coatings on stainless steel for the PEMWE application[7]. In the study, the corrosion protection by an oxygen-free titanium coating, $s = 60$ µm, was demonstrated. While the deposition related oxidation was controlled, the formation of electrochemical passivation layers was identified as a new challenge in coating development. In electrochemical processes, an oxidic insulating passivation layer is formed on the titanium surface which is mainly responsible for the good corrosion properties. However, the passivation layer leads to a diminishment of current transport. Regarding the PEMWE application, ohmic losses in the stack design, e. g. due to high interfacial contact resistances (ICR) between the cell components, should be avoided[8]. To prevent the negative effect of the passivating titanium for the PEMWE application, the VPS-coatings were refined by films of gold[7], platinum[8] or niobium[9].

Experimental

In this publication, for the first time, titanium coatings are deposited with commercially available thermal spraying processes in air on BPP-substrates of $s = 0.5$ mm thickness. By changing the coating technology from VPS to atmospheric processes, manufacturing costs are expected to be reduced. However, the electrochemical, electrical and mechanical performance of these coatings are still to be demonstrated.

This study is divided in two parts. In the first part, coating development on metal plates of $s = 5$ mm thickness is outlined. The ICR is examined for representative samples before and after a polarization test. In the ICR-measurement, the BPP is sandwiched between two electrodes and the contact resistance is determined in dependency of the applied pressure[10].

In the second part, coating structures with presumably the highest coating density and the lowest oxygen content are deposited onto metal sheets of $s = 0.5$ mm. The passivation behavior of newly-developed coatings under defined conditions should be investigated. In chronoamperometry, the current density in $A \cdot cm^2$ is determined over a period of time at a constant potential[11]. Thus, time dependent reactions, as the electrochemical passivation, can be examined. The results from the preliminary ICR-measurements are correlated with the results from the chronoamperometry and the suitability of the coatings for the PEMWE application should be estimated.

Choice of thermal spraying processes

In high velocity thermal spraying processes, the heated particles are accelerated beyond supersonic speed and because of the high kinetic impact on the substrate, the coatings are deposited with a high density. Furthermore, due to the short dwell time in the hot gas stream, low degrees of oxidation can be achieved.[6]

For the investigation of thermally sprayed corrosion protection coatings, the high velocity processes cold gas spraying (CGS) and high velocity air-fuel (HVAF) spraying are chosen. In HVAF, the particle temperatures typically vary between $1{,}200\ °C \leq T \leq 1{,}500\ °C$[12]. The processing of titanium with HVAF was published in Markocsan et al. for aerospace application[13] and Khamsepour for inner diameter coating application[14]. In contrast, the process temperature in the CGS process is below $T = 800$ °C in this study, see Table 3. While the process temperature of the CGS-process is the lowest of all thermal spraying processes, the particle velocity is the highest. At the impact of the particles on the substrate, the substrate and

the particle are locally sheared and bond in a cold working manner[15]. Cold gas spraying of titanium has been published firstly for light-weight applications by Segall et al.[16].

Preliminary results on metal plates, s = 5 mm thickness

Initially, coating development started on l = 60 mm and w = 40 mm grid blasted steel substrates, X2CrNiMo17-12-2, of s = 5 mm thickness. The chosen steel is typical for chemical application in contact with acids and has been established as potential BPP-material because of the electrochemical properties[3]. The initial testing matrix for both thermal spraying processes is illustrated in Figure 2. In total, over 27 different parameter variations have been tested for CGS- and HVAF-spraying.

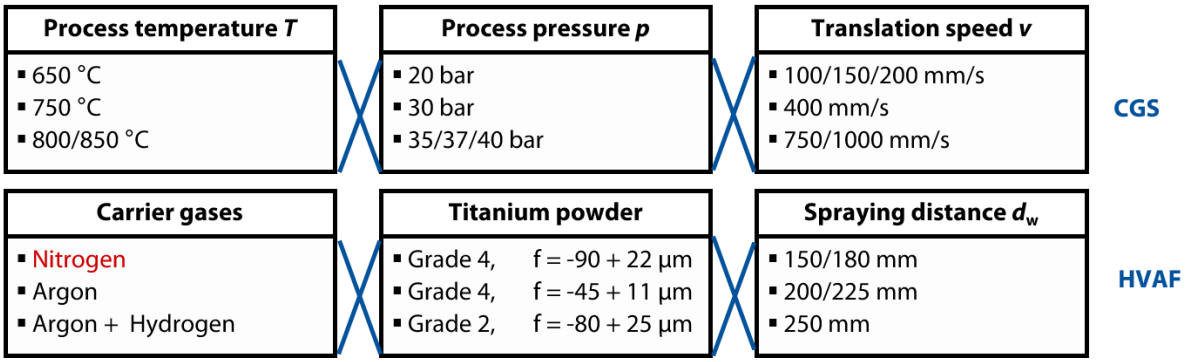

Figure 2. Schematic illustration of the initially tested parameter matrix on s = 5 mm substrate

For the HVAF process, a higher reactivity of the titanium powder was expected because of the higher process temperature. The use of nitrogen, which has been reported before by Khamsepour et al.[14], led to exothermic reactions forming possibly TiN in preliminary tests. In order to oppose these effects, a coarser powder was used than in the CGS-process and a mixture of argon and hydrogen was set up as a carrier gas. Nitrogen was no longer used afterwards.

To gain an overview about the electrical and electrochemical properties of these coatings, the ICR was measured before and after short-term polarization as a qualification criterium for further investigations. Out of the test matrix from Figure 2, six CGS-coating variations prepared with the highest possible process pressure for the highest densification and three HVAF-coating variations with different carrier gas compositions were chosen for an ICR-testing. Table 1 shows the deviation of the determined ICRs among the tested samples. Even though different parameters were measured, the samples of the same coating technology showed similar ICRs indicating similar coating structures among the same coating technology.

Table 1. Preliminary results from ICR-measurements at F = 100 N/cm² before and after electrochemical polarization, -0.4 V ≤ E vs. $Ag/AgCl_2$ ≤ 3 V in t = 5h, s = 5 mm

Sample	Average ICR, before polarization in mΩ · cm²	Average ICR, after t = 5 h polarization in mΩ cm²
CGS-coating, n = 6	21 ± 6	25 ± 7
HVAF-coating, n = 3	35 ± 2	38 ± 7
Grade 1 titanium bulk material	12	70

Comparing the average electrical properties of the tested CGS- and the HVAF-coating, the ICR of the CGS-coating was up to 40 % lower than the ICR of the HVAF-coating. The results also showed that the CGS-coating and the HVAF-coating can maintain its electrical properties even

after the polarization test. In contrast, the electrical properties of grade 1 titanium bulk material have worsened by the factor of six, possibly because of a long-lasting passivation layer. Based on this observation, the thermally sprayed coatings outperform the standard BPP-material in the short-time test in terms of the electrical properties after electrochemical loading.

Results of the passivation testing of coatings on metal sheets of *s* = 0.5 mm

In the next step, the coating structures of the substrates of s = 5 mm thickness are transferred to more realistic substrate thicknesses regarding the BPP-application. Because of the high kinetic impact in CGS and HVAF-spraying, bending of the thinner steel substrate was expected. In order to control the deformation during the thermal spraying process, a special steel fixture was constructed, see Figure 3.

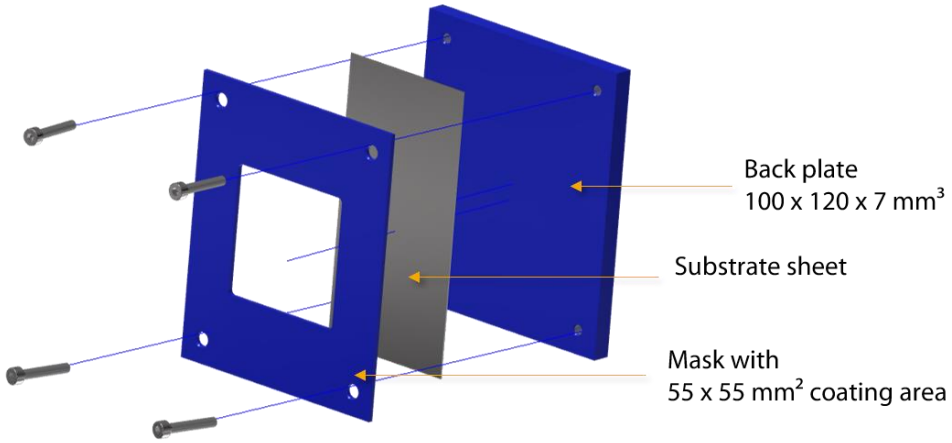

Figure 3. Steel fixture to enable coating application onto thin metal sheets with thermal spraying

All coatings are deposited on unstructured steel sheets, X2CrNiMo17-12-2, of s = 0.5 mm thickness. Before coating deposition, the steel sheets are grinded by hand horizontally and vertically with #P80 sandpaper to enhance the bonding. The coating parameters for the HVAF process are depicted in Table 1. By the chosen ratio of fuel to air, the adiabatic flame temperature of T_{ad} = 2.255 K is targeted[17]. The coating parameters for the CGS process are given in Table 3. For CGS, to achieve a high plasticization degree of the particles, a high process pressure and a relatively high process temperature were set.

Table 2. HVAF process parameters for AK-07 by Kermetico Inc., California, US, with 2L-nozzle and combustion chamber #3

Com-pressed air in MPa	Propane in MPa	Spray distance in mm	Trans-lation speed in m/s	Pass	Meander thickness in mm	Powder feeding rate in 1/min	Coating thickness in µm
0.62	0.55	200	1	4	5	3.3	62 ± 2

The HVAF-coatings are produced from a coarser grade 4 titanium feedstock, F = -90 + 22 µm, Höganäs AB, Sweden, than the CGS-coating, F = -45 +11 µm, Oerlikon Metco AG, Switzerland. Thus, reactivity of the titanium particles during the HVAF-process should be reduced. Grade 4 was used instead of grade 2 or lower for economic reasons in regards to the PEMWE application. The powders were manufactured by hydrid-dehydrid process and consist of α-titanium. The manufacturers of both powders declare an oxygen content of $\omega(O_2)$ = 0.4 %.

Table 3. CGS process parameters for Kinetiks 8000 by Oerlikon Metco AG, Pfäffikon Switzerland

Heating temperature in °C	Process pressure in MPa	Spray distance in mm	Trans-lation speed in m/s	Pass	Meander thickness in mm	Powder feeding rate in 1/min	Coating thickness in µm
800	3.5	30	0.15	1	5	2.7	182 ± 3

Structural characterization

To minimize material costs and stack weight, a thin coating thickness is desired for the PEMWE application. The coating thickness is determined by measuring at six different points with a micrometer screw. The surface properties are analyzed by confocal laser scanning microscopy (CLSM), VKX 200, Keyence Corporation, Japan, at 200x-magnification. In addition to the non-destructive methods, cross sections were metallographically prepared for structural analysis. In the investigation of detonation sprayed titanium coatings, variations of titanium oxides were observed with x-ray diffractometry (XRD) by Kovaleva et al[18]. Since particle temperatures and impact kinetics are different between CGS and HVAF, the deposition of different TiO_x and titanium phases is possible as well. The as-sprayed coatings are investigated for surface properties with the XRD 3000, GE Energy Germany GmbH, Ratingen, Germany, and a Cu-Kα x-ray tube source in a 2Θ-range of $24° \leq 2\Theta \leq 51°$ with a step size of 0.02°. The oxygen content is determined with the energy dispersive x-ray spectroscope (EDS) of the Zeiss Sigma scanning electron microscope (SEM) at Fraunhofer Center for Silicon Photovoltaics (CSP), Halle, Germany. The Zeiss Sigma SEM is operated with an acceleration voltage of $U = 20$ kV and at a vacuum pressure of $p = 10^{-4}$ Pa.

Chronoamperometric set-up

A sample coating area of $A = 10$ cm² each is exposed to a static fluid column of approx. $c = 0.5$ mmol H_2SO_4 at room temperature. Thus, convection is avoided and diffusion controlled processes can be examined. The coatings are tested as-sprayed since the economic interest is to avoid post-processing. A chronoamperometric measurement is conducted at the passivation potential of a bulk grade 1 titanium sheet for $t = 18$ h. To determine this value, a grade 1 titanium sheet of $s = 200$ µm thickness is grinded with SiC-paper of #400 and #800 and polarized afterwards from $-0.25\ V \leq SHE \leq 1.0\ V$. A resulting passivation potential is $E_p = 0.87$ V vs. SHE. By applying the passivation potential, the corrosion of the material is prevented.

Results and Discussion

Looking from the top-view on the three-dimensional structure of the surface topography in Figure 4, the HVAF-coating consists of larger homogeneous areas with isles of titanium particles. In contrast to that, the CGS-coating surface is characterized by statistically distributed roughness peaks.

By using a XRD line scan, the two phases in the surface region of the HVAF-coating can be distinguished. Next to α-titanium, a crystalline titanium (II) oxide, TiO, with a lattice parameter of $d = 4.2043$ Å is detected. The same oxide was identified in plasma sprayed porous transport layers in [19]. The results from the XRD are depicted in Figure 5.

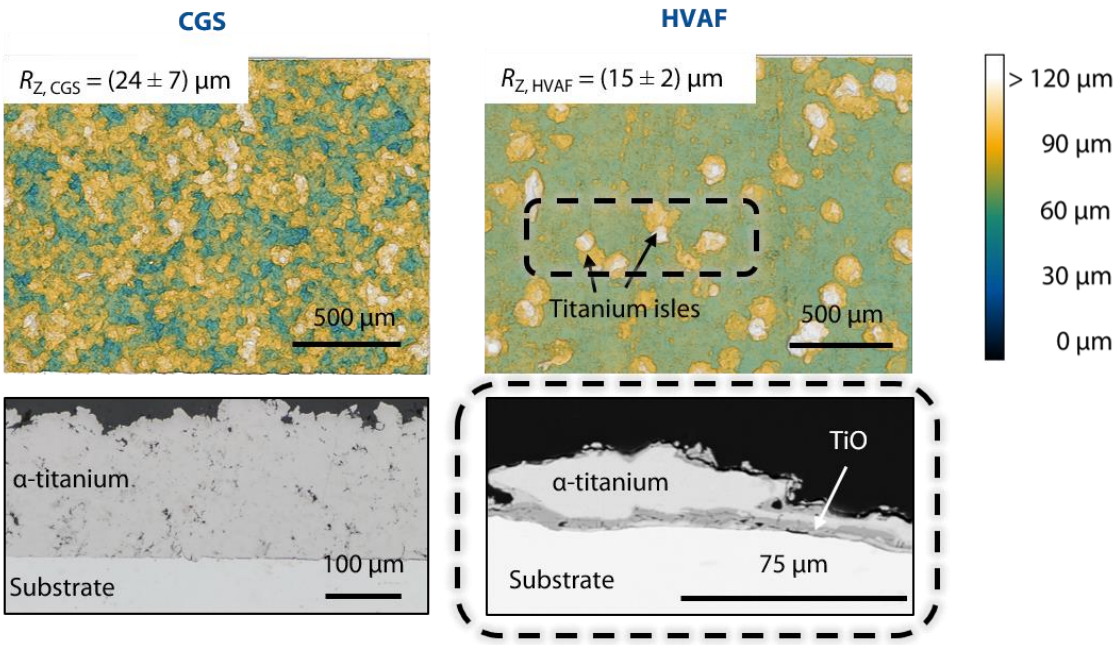

Figure 4. Topography measurement conducted with CLSM, cross section of deposited CGS-coating, left, and close-up of the cross sectioned HVAF-coating, right

The isles, as identified from the CLSM, consist mainly of unmolten α-titanium particles from the powder feedstock according to the XRD. The chosen powder fraction for the HVAF-process is constituted out of coarser particles and relatively finer particles. The coarser particles inherit a smaller surface area causing a slower oxidation reaction in the hot gas stream on the particle surface. Consequently, the coarser particle is only oxidized on the surface but not in the core of the particle. This outer shell is visible as dark layer in the close-up of a unmolten particle on the right hand side in Figure 4. Furthermore, the plasticization of the coarser particles in the hot gas stream is impeded in comparison to finer particles because of the bigger mass. As a result, the flattening of the coarser particle is hindered at the impact on the substrate. The coarser particles are deposited as a top layer from the final pass, pass 4. It is possible that previously deposited coarser particles in the passes 1 to 3 have been removed, similar as to a sandblasting process. The surrounding of the coarser particles consists of fully molten finer particles. Accordingly, the main material phase in this area of the coating is TiO which appears dark grey in the cross section of the HVAF-coating in Figure 4.

In contrast to that, unchanged α-titanium is deposited with the CGS-process, as demonstrated in the XRD in Figure 5. Since the process temperature is lower in the CGS-process than in the HVAF-process, titanium can be deposited without macroscale oxidation or phase transformation. According to the EDS-measurements from the Zeiss Sigma SEM at the Fraunhofer CSP, the oxygen content in the HVAF-coating is up to 10-times higher than the CGS-coating. The effect of this difference in oxygen content and phases composition will be studied in the chronoamperometry.

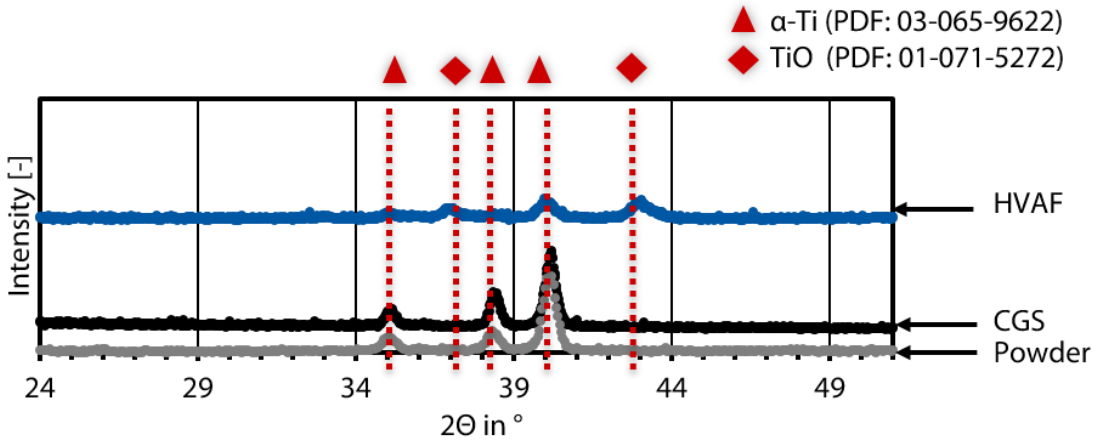

Figure 5. XRD-spectrum of the investigated coatings examined with XRD 3000, I = 40 mA, U = 40 kV

For the chronoamperometry, the coatings are exposed to the acidic electrolyte for t = 18 h as described in the experimental section. At the beginning of the chronoamperometry, see Figure 6, the grade 1 titanium reference and the CGS-coating exhibit the highest current output. Comparingly, the current density of the HVAF-coating is the lowest which can be deduced to the insulating TiO in the coating.

After t = 30 min, the grade 1 titanium reference has reached a lower current density than the HVAF-coating indicating a higher passivation velocity. In less than t = 1 h, the current density of the HVAF-coating has stabilized as well. At this point, the free α-titanium on the coating surface has completely reacted.

On the opposite, the current density from the CGS-coating is not constant until t = 7 h. In comparison to the grade 1 titanium reference and the HVAF-coating, the CGS-coating, overall, shows higher levels of current density for at least t = 10 h. Apparently, the transport of the oxygen molecules to the CGS-coating is rather delayed.

By the end of the testing time, t = 18 h, the current density of the CGS-coating is doubled as high as of the HVAF-coating. At the same time, the current density of the grade 1 titanium reference is ten times lower than of the coatings. Concluding the passivation behavior, the passivation affinity is the highest for the standard BPP-material and the lowest for the CGS-coating in this test. Although the CGS-coating consists mainly of α-titanium, just as the bulk material, the passivation behavior is completely different. This deviation may be explained by the different microstructure of the grade 1 titanium reference in comparison to the coating characteristics of the CGS-coating.

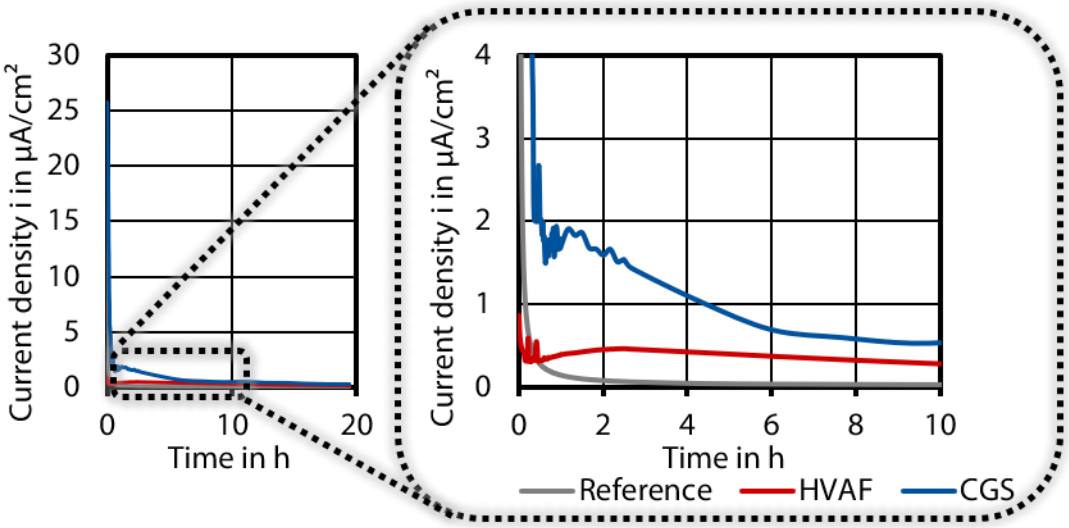

Figure 6. Results of chronoamperometric measurements at room temperature for t = 18 h at E = 0.87 V vs. OCP

Comparison of chronoamperometric results and ICR-measurements

Accounting the results from the ICR measurements, see Table 1, the similar phenomenon is observed. Comparing the coatings, the ICR of the CGS-coating is lower than of the HVAF-coating which can be explained by the delayed passivation behavior of the CGS-coating. The grade 1 titanium reference passivates with a higher velocity than the deposited coatings leading to the elevated ICR after the polarization test. The results show that electrical conductivity of the BPP can be maintained at a higher level if coated with titanium by thermal spraying.

Conclusion

In this publication, two commercially available thermal spraying processes are used to deposit corrosion protection coatings of titanium on steel BPPs. The coating development was described in the first part to underline the challenges.

- Process development for thermally sprayed titanium coatings in atmosphere necessary in terms of:
  - oxidation prevention
  - coating density
  - coating deposition efficiency
- Deformation and overheating of metal sheets, s = 0.5 mm, is prevented with fixture

In the second part, the passivation behavior was observed over time and correlated with ICR-measurements conducted previously. The results are as followed:

- passivation is not as promoted on surface of the thermally sprayed coatings as on the surface of the grade 1 titanium reference
- CGS-coating and HVAF-coating show a ten time higher current density after t = 18 h than the grade 1 titanium reference.

With regards to the PEMWE application, the thermally sprayed coatings outperform the electrical properties of the reference material as the coatings can maintain promising electrical properties in the short time testing. In order to further quantify the suitability of these coatings for the PEMWE, long-term investigations will be necessary.

Acknowledgements
The project StacIE (03HY103B) is funded by the German Federal Ministry of Education and Research. The authors like to thank Schaeffler Technologies AG & Co. KG, Herzogenaurach, Germany, and Fraunhofer CSP, Halle, Germany for conducting measurements on behalf of the project StacIE.

Literatur

[1] J. Divisek, H. Schmitz, DE3108255C2, **1982**.
[2] T. Smolinka, M. Günther, J. Garche, *Stand und Entwicklungspotenzial der Wasserstoffelektrolyse zur Herstellung von Wasserstoff aus regenerativen Energien. Kurzfassung des Abschlussberichts*. NOW-Studie, **2011**.
[3] N. Rojas, M. Sánchez-Molina, G. Sevilla, E. Amores, E. Almandoz, J. Esparza, M. R. Cruz Vivas, C. Colominas, *International Journal of Hydrogen Energy* **2021**, *46*, 25929.
[4] M. Pourbaix, *Atlas of Electrochemical Equilibria in Aqueous Solutions*, NACE International, **1974**.
[5] K. E. Ayers, E. B. Anderson, C. Capuano, B. Carter, L. Dalton, G. Hanlon, J. Manco, M. Niedzwiecki **2010**, *33*, 3.
[6] J. R. Davis (Ed.) *Handbook of thermal spray technology*, ASM International, Materials Park, Ohio, **2004**.
[7] A. S. Gago, A. S. Ansar, P. Gazdzicki, N. Wagner, J. Arnold, K. A. Friedrich, *Meet. Abstr.* **2014**, *MA2014-02*, 1236.
[8] A. S. Gago, S. A. Ansar, B. Saruhan, U. Schulz, P. Lettenmeier, N. A. Cañas, P. Gazdzicki, T. Morawietz, R. Hiesgen, J. Arnold et al., *Journal of Power Sources* **2016**, *307*, 815.
[9] P. Lettenmeier, R. Wang, R. Abouatallah, B. Saruhan, O. Freitag, P. Gazdzicki, T. Morawietz, R. Hiesgen, A. S. Gago, K. A. Friedrich, *Scientific reports* **2017**, *7*, 44035.
[10] D. P. Davies, P. L. Adcock, M. Turpin, S. J. Rowen, *Journal of Applied Electrochemistry* **2000**, *30*, 101.
[11] B. Speiser, *Chem. Unserer Zeit* **1981**, *15*, 21.
[12] X. Luo, R. Chidambaram-Seshadri, G.-J. Yang in *Advanced Nanomaterials and Coatings by Thermal Spray* (Eds.: G.-J. Yang, X. SuO), Elsevier, **2019**, pp. 61–117.
[13] N. Markocsan, L. Christophe, Östergren, L., G., M. Sieger, *Comparison between High-Velocity-Air-Fuel- (HVAF) and Cold-Gas-Spray (CGS) by evaluating mechanical properties of Ti-6-4- and INCONEL718-coatings*.
[14] P. Khamsepour, J. Oberste-Berghaus, M. Aghasibeig, F. B. Ettouil, A. Dolatabadi, C. Moreau, *J Therm Spray Tech* **2023**, *32*, 568.
[15] H. Assadi, F. Gärtner, T. Stoltenhoff, H. Kreye, *Acta Materialia* **2003**, *51*, 4379.
[16] A. E. Segall, A. N. Papyrin, J. C. Conway, D. Shapiro, *JOM* **1998**, *50*, 52.
[17] C. K. Law in *Combustion Physics* (Ed.: C. K. Law), Cambridge University Press, **2010**, pp. 14–50.
[18] M. Kovaleva, Y. Tyurin, N. Vasilik, O. Kolisnichenko, M. Prozorova, M. Arseenko, V. Sirota, I. Pavlenko, *Physics Research International* **2015**, *2015*, 1.
[19] K. Bobzin, L. Zhao, H. Heinemann, E. Burbaum, K. Radermacher, *Thermal Spray bulletin* **2023**, *16*, 42.

Techniques for In-Situ Characterisation of Hydrogen in Steel

T. Hillman, R.Kroll, D.L. Engelberg,
Department of Materials, School of Natural Sciences, Metallurgy & Corrosion,
The University of Manchester, Oxford Road, M13 9PL, UK

With a greater move towards hydrogen to supplement the world's energy consumption, electricity producers look towards using hydrogen in existing infrastructure, such as storage tanks and pipelines. However, the ability of hydrogen to transport readily through steel matrices, with phenomena such as microstructure embrittlement and leakage present structural and efficiency problems. To improve inspection routines and reduce potential shutdowns; in-situ and ideally non-destructive techniques for hydrogen monitoring and detection need to be developed.

During exposure to high pressure hydrogen gas, cathodic polarization in aqueous environment, or even under de-aerated/wet conditions, adsorbed monoatomic hydrogen can form at exposed surfaces and disperse into the steel matrix. Hydrogen then settles into reversible and non-reversible trapping sites, depending on chemical composition, microstructure condition, and surface state of the exposed component. In these sites, saturation of hydrogen can lead to localized stress on the surrounding matrix and grain boundaries, which in turn lowers the local tensile strength, potentially leading to embrittlement and cracking. As diffusible hydrogen from reversible sites leaves the metal, it can reform into molecular hydrogen and disperse into the environment. This paper aims to explore the suitability of characterisation techniques to detect the presence of hydrogen at the surfaces of Type 316L stainless steel and X52 carbon steel. Cathodic charging will be used to produce hydrogen containing steel and stainless steel matrices, with surface hydrogen content characterisation performed by laser-induced breakdown spectroscopy (LIBS). This technique provides an instantaneous measure of the hydrogen concentrations on sub-mm length-scale. The observed results are compared to melt extraction analysis and thermal desorption spectroscopy (TDS).

Critical parameters for metallic materials in contact with a mixture of natural gas and hydrogen

Klára Kuchťáková, Darya Rudomilova, Václav Šefl, Tomáš Prošek, University of chemistry and technology in Prague, Czech Republic

Nowadays, with an increasing use of hydrogen as an energy vector, gaseous hydrogen transport as well as high-capacity storage are becoming important issues. The possibility of repurposing and retrofitting existing natural gas infrastructure for gaseous hydrogen is connected with many technical challenges, including the hydrogen embrittlement phenomenon of steel components. To avoid the safety risks, it is necessary to determine conditions under which hydrogen can be added to the existing natural gas system.

Although the detrimental effect of atomic hydrogen on steel is already well-recognised, a full understanding of the underlying processes has not been achieved up to now. The crucial information to understand the behaviour of steels in the presence of hydrogen is the amount of hydrogen absorbed in the steel structure. In the gas network environment, two possible sources of hydrogen have to be considered in the future: corrosion-induced hydrogen entering the material due to the reduction of H^+ ions during steel corrosion and hydrogen entering the steel structure after dissociation of gaseous hydrogen.

In the present study, steel specimens were exposed to different environments at stable temperature and pressure to assess critical environmental factors that promote hydrogen entry into the steel most significantly. Factors such as the partial hydrogen pressure, temperature, type and composition of corrosive environment, presence of recombination poisons and exposure duration were studied. However, the main focus has been on the combination of hydrogen sources that leads to a synergic effect in the hydrogen entry process. The obtained results imply the possible critical sites in the gas network system and critical factors that should be considered when assessing the risk of hydrogen embrittlement in the gas network.

Hydrogen permeation and embrittlement of ferritic SOEC/SOFC interconnect materials

D. Kniep, S. Schewe, J. F. Drillet, M. Rudolphi, M. C. Galetz

DECHEMA Forschungsinstitut, Frankfurt/Germany;

Metallic interconnects are an essential component for the stack setup in SOEC/SOFC systems. Interconnect materials require not only high electronic conductivity and creep resistance, but also thermal conductivity and mechanical stability in the stack system. Within the SOEC/SOFC application, materials must withstand a high percentage of hydrogen and water steam on the fuel side of the cell at temperatures above 825°C. Thus, certain degradation mechanisms are being studied, which reduce the lifetime for the whole stack. Hydrogen is under investigation due to its diffusibility through ferritic stainless steel. The diffusibility can lead to more internal oxidation in working mode and hydrogen embrittlement when the stack is shutdown. Within this framework, the following experiments take a closer look at the hydrogen degradation mechanisms of SOEC/SOFC interconnects.

Six ferritic interconnect materials with decreasing amount of Chromium (AISI446, Crofer 22 APU, Crofer 22 H, AISI442, AISI410, P91), of which can be candidate materials for SOEC/SOFC stacks, are tested on their hydrogen susceptibility. Vickers hardness, metallographic analytic tests, and strain rate tests of the received samples have been studied. With a Devanathan and Stachursky cell, the diffusibility of hydrogen in the different materials is detected and the diffusion coefficients are calculated. To connect the time of Hydrogen Charging with the actual content, the samples were charged in a different setup followed by Thermal Desorption Analysis (TDA) to detect the absorbed hydrogen in ppm. Different ramps were administered to investigate the diffusible fraction and the trapping mechanisms of the steels. To measure the total amount of hydrogen within the steel, melt extraction was applied. The samples are also exposed over 700 hours at 900°C at a typical SOEC/SOFC hydrogen/water vapor atmosphere. Following the exposure, a TDA and melt extraction are applied and compared to the as-received measurements to investigate if hydrogen became trapped in the exposure process. To test and rank the materials, a slow strain rate test was performed after a certain time of charging to test the hydrogen susceptibility of the

materials. A scanning electron microscope investigated fracture surfaces to detect intergranular fracture. Finally, the ferritic stainless steels are ranked according to diffusibility, absorption and mechanical properties.

Review of Mitigation Methods for Embrittlement in Hydrogen Pipelines – Coatings, CP and Inhibitors

Daniel Sandana[1], Neil Gallon[2] and Jozef Soltis

[1]ROSEN UK, Newcastle Upon-Tyne, United Kingdom, dsandana@rosen-group.com, Presenting Author
[2] ROSEN UK, Newcastle Upon-Tyne, United Kingdom, ngallon@rosen-group.com
[3] ROSEN UK, Newcastle Upon-Tyne, United Kingdom, jsoltis@rosen-group.com

Abstract

The deployment of a hydrogen chain economy at an industrial scale requires transportation. The realisation of such infrastructure will likely revolve with the repurposing of the existing natural gas transmission pipelines owing to higher CAPEX, new installation permits and production challenges associated with new builds.

The introduction of gaseous hydrogen brings its own specific challenges to conversion, owing to the absorption and diffusion of atomic hydrogen within the steel microstructure. One key problem (and widely discussed) is the direct negative impact of hydrogen on pipeline integrity and its safe operational life, due to hydrogen embrittlement and time-dependant crack growth mechanisms. Various research is ongoing to slow down or inhibit the passage of hydrogen into the steel. One path of mitigation is the use of oxygen. While presenting available test data, the paper will review the mechanism of inhibition, and gaps and hurdles, hampering the deployment of such alternative, will be highlighted.

Other fundamental problematics are associated with the potential prejudice of hydrogen conveyance on the reliability of external coatings and cathodic protection, which could compromise long-term pipeline operational integrity. The paper discusses the likelihood of hydrogen leading to the physical degradation (and reduced functional performance) and decohesion of external coating materials from current research and literature. Mechanism(s) by which this could occur are discussed. Similarly, the paper will review whether, and how, hydrogen could impair the performance of CP – this will rise the interesting question whether the existing industry acceptance criteria remain fit in a hydrogen world, both from an underprotection and overprotection perspective. The paper will take the opportunity to highlight uncertainties, gaps and research opportunities.

Key words: hydrogen, cracking, pipeline repurposing, coating, cathodic protection

Introduction

Back in 2015, the COP 21 Paris Climate conference provided a strong incentive and purpose for global governments to tackle climate change and drive transition to a low-carbon economy. Any resulting shift will inevitably lead to decarbonisation of the world's energy models and associated infrastructure, in almost every respect from generation to distribution, with ambitious objectives preceding 2050. In this context and as part of the '*net-zero emission energy equation*', hydrogen has been championed as a vital player of the future energy alternatives [1]. More recently, this transition has been further accelerated by the energy security concerns, stemming from the Russian invasion of Ukraine.

The deployment of hydrogen requires transportation, and given the many economic and legal obstacles to construction of new pipelines, it appears inevitable that a large proportion of the future hydrogen pipeline network will consist of repurposed existing infrastructure [2]. This is exemplified by the 'European H_2 backbone' [3] that estimates the system at 53,000 km by 2040, of which 60% is planned to be from existing pipelines.

The introduction of gaseous hydrogen into the existing natural gas infrastructure brings its own specific challenges, including hydrogen-natural gas blending, impact on end-use systems, safety, material durability, integrity management and leakage.

In the current work we focus on key issues associated with hydrogen impacts on material durability that stems from its absorption and diffusion within steel [4][5][6], potential mitigation measures and its potential impact on conventional external corrosion control practices involving coatings and cathodic protection (CP).

Impact of Hydrogen on Material Durability

The introduction of gaseous hydrogen brings its own specific challenges, owing to the hydrogen interaction with pipeline steels. The topic of the interaction of hydrogen with pipeline steels has been largely discussed elsewhere [7,8]. Clearly, the fundamental feature is the absorption and diffusion of atomic hydrogen within the steel microstructure, which could lead to cracking induced by Hydrogen Embrittlement (HE) [9]. The particular mechanism of HE remains an area of great debate, but it is nevertheless interesting to note that cracking due to gaseous hydrogen service is believed to occur by a mechanism referred as Hydrogen-Environment Assisted Cracking (HEAC), which relays the direct dissociation and absorption of hydrogen at crack tips, and embrittlement of the crack front leading to growth under stress. As a note of caution, while it is not believed presently that gaseous hydrogen is able to induce cracking in bulk material away from existing crack; it is nevertheless reasonable to think that this may be possible in exceptional circumstances over time, especially in the presence of stress raisers, plastic deformation and / or susceptible microstructures (hard spots).

A direct and major result of HE is the degradation of steel mechanical properties, which manifests as a major decrease in ductility and fracture toughness. Table 1 summarises the effects of hydrogen on linepipe materials based on industry reviews [7,8].

Table 1. Effect of H_2 on linepipe material properties.

Material Property	Effect of H_2
Strength	↔ (?)
Ductility and Fracture Toughness	↓
Fatigue Growth Rate	↑

Ductility appears to decrease by 20-80% in H_2, with the extent of this drop varying due to the material and test method used. Similarly, most sources agree on a reduction of 35-70% in fracture toughness, while 1% H_2 in a blend has been reported as being sufficient to lead to more

than a 50% decrease in fracture toughness [7]. Another important observation is that, while fatigue is usually a negligible threat for NG pipelines, HE makes it a critical threat under hydrogen service. Aside of the mechanistic role of hydrogen, Fatigue is expected to be further amplified under hydrogen transportation as more severe cyclic loading may be expected especially in a "green hydrogen economy", where line packing storage could occur. It is noted that irrespectively of the influence of hydrogen on the realisation of time-dependant cracking mechanisms, the threat of cracking will be escalated in hydrogen service due to the reduction in fracture toughness.

The actual levels of variations in ductility properties and fatigue growth rates are dependent on the pipeline material (and hydrogen partial pressures and blend compositions); this puts emphasis in testing materials under hydrogen [10]. Quantifying such behaviour is an important input of addressing the impact of the pre-conversion pipeline integrity condition on the repurposing feasibility, and ultimately for the safe management of the pipeline integrity under a hydrogen service.

Internal Mitigation Measures

As HE depends on absorption of atomic hydrogen into the steel and its diffusion to microstructural locations, factors that change the ease of this absorption and its interaction with the steel have been the subject of much recent work. The key consensus [7] is that hydrogen absorption relies on the presence of a bare metal surface in contact with gaseous (molecular) hydrogen. There are two major candidate approaches to inhibit this absorption:

(i) Application of some form of barrier coating to the internal surface of the pipe to physically separate the metal from the gas.
(ii) Addition of some form of inhibitor molecule to the gaseous hydrogen to effectively outcompete the hydrogen at the metal surface and slow / stop the absorption reactions.

Internal Coatings

With respect to (i) above, there are theoretical benefits which may be achieved for polymeric coatings [11], while the use of metallic cladding is a widely accepted mitigation for severe internal environments (e.g. sour service). Despite the apparent attractiveness of this approach there are, however, various practical challenges associated with implementation of a barrier coating solution.

For new-build pipelines it is relatively easy to envisage the application of an internal barrier coating during manufacture, in the same way that existing flow coatings or external coatings are applied. The major issue is likely to arise during field construction, especially of girth welds. Manufacturer-applied coatings, both internal and external, normally have a deliberately introduced gap at the ends of each pipe joint to allow for field welding. Externally this gap (an intentional holiday) is normally addressed by field coating after welding, while internally the gap is normally left in-situ (not a significant issue if the primary purpose of the coating is for flow purposes). If the primary purpose of the coating is to protect against hydrogen absorption then 100% coverage becomes imperative, especially around girth welds which are more prone to high stresses (including residual welding stresses) and irregular internal profiles, stress raisers and defects. A robust mechanism to both apply and inspect any proposed internal girth weld barrier coating is therefore required.

If a pipeline is to be repurposed, application of a protective barrier coating becomes significantly more challenging. By its nature, any barrier coating relies for its effectiveness on having 100% coverage 100% of the time, any holidays or imperfections in the coating will act as weak spots and potential focal points for hydrogen embrittlement. The retrospective application and testing of a barrier coating to an existing pipeline, which can often be hundreds

of miles long, have an uneven internal surface profile including potential areas of corrosion, erosion, contamination and weld root protrusion, and have various ancillary components including valves and branches, is a major technical challenge. It is unfortunately true that any barrier coating is only ever as strong as its weakest part, those areas where application is likely to be most challenging (primarily associated with weld roots) are also likely to be those areas of highest criticality where the coating is most needed. For these reasons it appears unlikely that this retrospective application will be feasible for the ~32,000 km of repurposed pipelines envisaged by the European hydrogen backbone.

Even for new build pipelines, any internal barrier coating needs to be effective for the design life of the pipeline. The coating therefore should be robust enough to maintain its integrity under normal operational conditions. In this context the robustness of the coating to foreseeable non-standard events becomes important, examples of this include mechanical damage or deformation to the pipeline resulting from external loading including third party activities and ensuring that the coating can survive the passage of an internal inspection tool. As a result of the above, the current authors do not believe that internal coatings can be relied upon to mitigate against hydrogen embrittlement.

Inhibitor Gases

In addition to the potential use of barrier coatings, there is a lot of interest in the use of inhibitor gases to be deliberately added as impurities to the hydrogen. Laboratory studies indicate that various molecules can have a beneficial effect in terms of mitigating against hydrogen embrittlement (e.g. O_2 and CO) [12]. Staykov et al. [13] report that these potentially beneficial additives effectively compete with hydrogen for surface adsorption sites due to the greater attractive force acting on the impurity molecule compared to hydrogen, therefore small additions of oxygen can lead to large reductions in the amount of adsorbed hydrogen. Likewise, the effect of additives to hydrogen gas on fatigue crack growth rate has been comprehensively investigated by Fukuyama and discussed by Zhang [14]. The fatigue crack growth rates of 2.25Cr-1Mo steel in hydrogen with small amounts of different additives were determined at a constant ΔK of 758N/mm$^{3/2}$ and a hydrogen gas pressure of 1.1MPa (Figure 1).

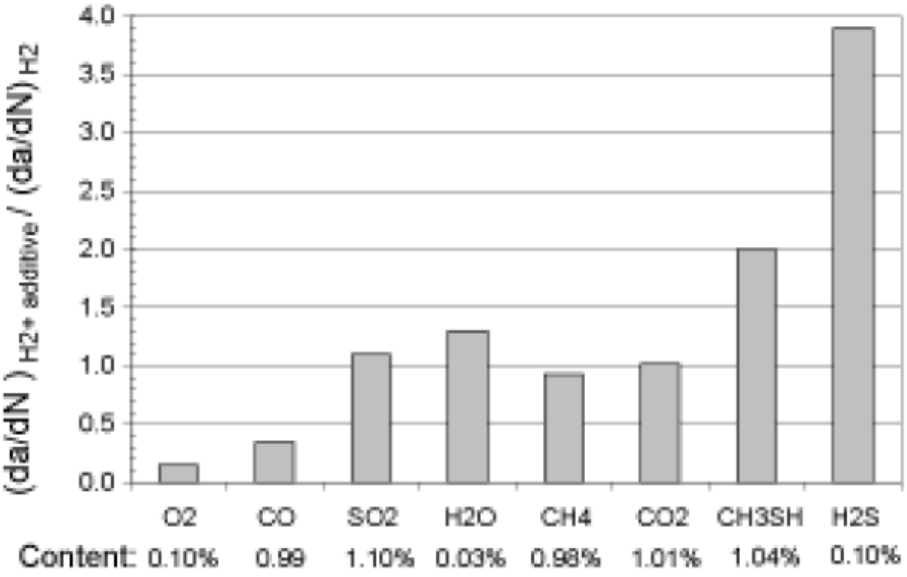

Figure 1. Effect of additives on FCGR. [14]

The effects of adding O_2 and CO to prevent HE thus appear to be beneficial in reducing the FCGR, while the additions of H_2S and CH_3SH (methanethiol) cause an acceleration in the FCGR. Similar effects, even for very small amounts of O_2, are reported by Adams et al. [15].

The mechanism of hydrogen-assisted fatigue crack growth (HA-FCG) and the effect of oxygen on this, is the topic of much current research. In pure hydrogen, data shows that hydrogen-assisted (accelerated) fatigue crack growth (HA-FCG) only becomes active when the maximum stress intensity factor over the cycle (K_{max}) exceeds a certain threshold value [16]. When HA-FCG is active, testing in both pure hydrogen and mixed hydrogen-oxygen gas has shown that the crack growth rate can be ten times higher, or more, than in air or inert gas. Below this threshold, the fatigue crack growth rate is equivalent to that in air or inert gas. This value of K_{max} is expected to be material dependent so the onset of HA-FCG may occur under different conditions and parameters for different materials. Additionally, since K_{max} is a function of ΔK (the stress intensity factor range) and the R-ratio (K_{max}/K_{min}, HA-FCG may be activated by increases in ΔK or R.

As also demonstrated by Somerday et al. [16], oxygen additions can delay the onset of HA-FCG to higher ΔK (or K_{max}) values, until a critical ΔK or critical growth rate is reached. Above this threshold, the crack growth rate deviates from the in-air rate and accelerates until it reaches the rate associated with pure hydrogen, i.e. the oxygen inhibition effect is nullified. Increasing the oxygen partial pressure can further suppress the onset of HA-FCG to higher crack growth rates. However, the transition to HA-FCG still occurs once a high enough ΔK or crack growth rate is reached.

The effect of time on oxygen inhibition is probably the major unknown with respect to the above. The ability of oxygen to passivate these new surfaces and thereby suppress HA-FCG relies on the rate of diffusion or transport along the advancing crack channel towards the crack tip, followed by passivation of the surfaces (by adsorption and dissociation). The onset of HA-FCG in the presence of oxygen therefore occurs when the new surfaces as the crack advances can no longer be fully passivated due to these time-dependent factors. The implication of this time dependence is that the critical da/dN value may be also dependent on test frequency. Although this frequency effect is not seen in the results reported, this may be more due to the limited range of frequencies tested. Some discussion if this effect is found in the work of Ronevich et al. [17].

It seems [18] that the mechanism of oxygen passivation is transient and dependent on a continued presence of oxygen at the required levels, i.e. the inhibiting effect is lost almost immediately if the oxygen is removed or its partial pressure is decreased below required levels. Also, in regard to potential effects of small additions of oxygen on hydrogen-affected fracture toughness, relevant examples [18,19] demonstrate that hydrogen-affected fracture toughness can be restored to virtually in-air performance with the addition of small amounts (~100-250 ppm) of oxygen, although again the effects of time on this restoration do not appear to have been fully investigated.

In summary it is difficult to visualise how these additive methods could be proven to be effective 100% of the time for the lifetime of the pipeline. It should also be noted that there are potentially other consequences, particularly with respect to safety, of adding either oxygen or carbon monoxide to a fuel.

Pipelines External Corrosion and its Control

External corrosion is one of the main contributing factors to gas transmission pipeline failures. For instance, in Europe, corrosion was associated with approximately a quarter of the incidents of onshore natural gas transmission pipelines, between 2010-2019 [20]; see Figure 2.

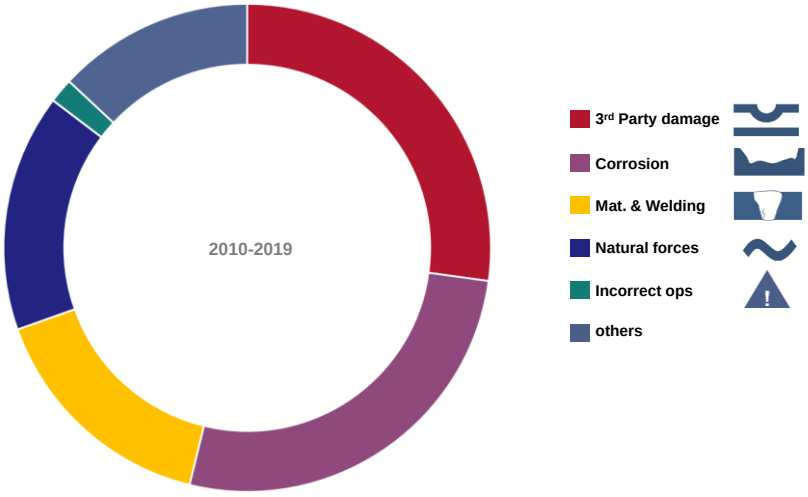

Figure 2. Failure causes in gas transmission pipelines in Europe, 2010-2019.

The primary methods of controlling external corrosion of pipelines include applications of protective coatings and adequate CP. The current international standards which codify application of external coatings and CP for on-shore pipelines are the ISO 21809 suite [21] and ISO 15589-part 1 [22].

External Coatings

ISO 21809 currently allows for the application of shop-applied continuous fusion bonded epoxy (FBE), multi-layer polyolefin (propylene (PP) and polyethylene (PE)) coatings. However, around 60% of the European network is more than 30 years old (and 45% is over 40 years old) [20][23], and would have been subject to historical coating practices, e.g. thermoplastic coatings (coal tar, bitumous (asphalt)), and field cold-applied backed tape (e.g. PE) systems [24]. These coatings have been used for the external protection of on-shore pipelines for many years, throughout the world, but are particularly susceptible to deformation under soil loads, and prone to loss of adhesion and corrosion beneath the loose coating due to CP shielding.

Figure 3 shows the distribution of external coating types applied at construction and coating age vs. covered length for the European NG transmission network in 2019 [20]. It shows that almost 50% of the infrastructure is coated with PE; although no distinction is made between tape wrap and factory-applied PE. Cold-applied tapes and two-layer PE coatings were both developed in the 1950s. Pipeline coating practices are likely to have differed between geographical regions; for example, western European operators may have historically favoured the use of factory-applied PE (over tape), whilst the use of tape wrap may have been more prominent on Eastern European pipelines. In recent times, there is a clear preference by operators to design pipelines with factory-applied PE. A significant proportion (up to 40%) of the system is also coated in coal tar and bitumen, which is symptomatic of the age of the system and earliest construction practices. Such coatings have generally been in place, in the majority, for more than 40 years.

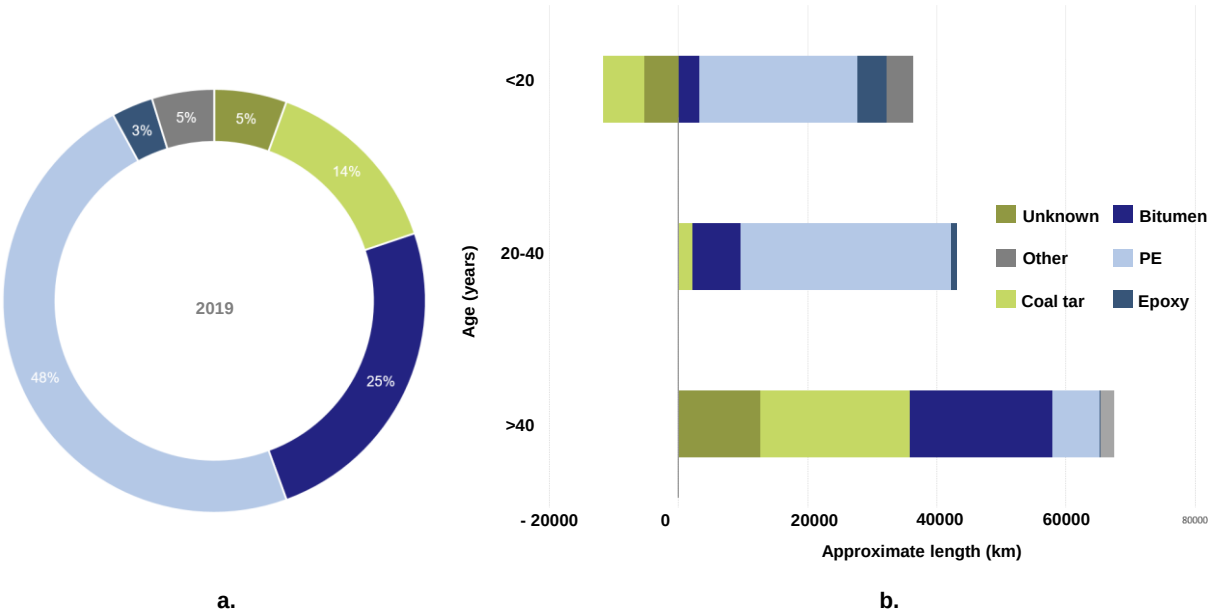

Figure 3. External coatings on natural gas transmission lines in Europe around 2019; showing (a) prevalence and (b) coating age vs. covered pipeline length.

Cathodic Protection

There is no need to introduce the importance of CP and CP criteria. The emphasis is on polarising all sections of a given buried pipeline to levels more electronegative than –850 mV vs. $Cu/CuSO_4$ reference electrode (CSE); although the criteria of –950 V_{CSE} has been adopted for anaerobic environments to manage Microbiologically Influenced Corrosion (MIC). The ISO 15589-Part 1 standard also recommends the pipeline-to soil potential to be more electropositive than –1200 mV_{CSE} to prevent coating disbondment due to excessive alkalization / production of hydrogen. Note that the latter restriction is not explicitly stipulated in the standard in order to minimise the risk of HE; however, for pipeline steels of yield strength exceeding 550 N mm^{-2} ($\geq$ X80), the standard requires the limiting critical potential (most negative) be documented or experimentally determined to prevent HE. There is therefore a window of applied potential which should be hit to ensure both adequate protection and reduced risk of HE.

Past Experience

In general, existing hydrogen pipelines show decades of incident-free operation. More than 4,500 km of hydrogen pipelines were purpose-built, with the most widely recognised international code being ASME B31.12 [25]. We note that the code does not provide guidelines for the application of coatings, whilst the CP criteria reflect on the best industry practice applicable for the oil and gas pipeline systems. Equally, other guidelines [26] refer to BS EN 12954 [27] for CP requirements.

Impact of hydrogen on pipeline external condition

For a steady state conditions, whilst neglecting hydrogen trapping, a permeation path between hydrogen adsorbed at a pipeline internal surface and hydrogen liberated at the external surface can be described by four main fluxes [28]:

- Changing flux at the internal surface, representing transfer of hydrogen from adsorbed to absorbed state.
- Degassing flux at the internal surface, representing transfer of hydrogen from absorbed to adsorbed state.
- Diffusion of hydrogen in the bulk metal from the internal surface to the external surface.

- Extraction flux at the external surface, representing a balance between surface-bulk and bulk-surface transfer at the external surface.

In terms of potential impacts that transported hydrogen may pose on a given pipeline external condition, e.g. coating, external corrosion etc., the extraction flux would provide information on the hydrogen volumes.

External Coatings

Any potential impact of permeated hydrogen on external coatings may include effects on: (i) coatings' intrinsic properties, (ii) coating-steel interface and (iii) existing coating defects.

Information on hydrogen-induced degradation of coating's intrinsic properties is relatively scarce. However, as coating systems can be considered a blend of polymeric materials, an educated projection can be made, based on the current understanding of the subject of hydrogen vs. polymeric materials. A good demonstration is captured in ISO 11114-2:2013 [29]. In general, hydrogen seems to have limited impact on polymeric integrity, their ductility, strength, or fatigue [30]. This is not surprising, given the more open structure of polymers, when compared to metals. No hydrogen-induced degradation or interaction between hydrogen and PEs was reported to date, and PE pipes in a hydrogen service have a life-time of at least 100 years [31,32]. However, there is a knowledge gap when it comes to atomic hydrogen and its potential impact on polymers / external coatings. One can argue that hydrogen represents a more reactive species than natural gas.

In terms of potential impacts that hydrogen may have on pipeline coating-steel interface, as it degasses from a coated surface, it seems that the risk of disbondment is relatively low [33,34]. If, however, areas of disbonded coating exist or develop, the interface environment will be complex and containing electrolytes of various composition and pH. Interfacial corrosion is more probable than hydrogen (gas) accumulation, given its high solubility / diffusion rates in polymers and low hydrogen permeation rates through the steel. However, limited number of studies and a wide range of coating systems available make this subject a knowledge gap, especially when it comes to non-epoxy coatings, coal tar / bituminous coating systems.

Lastly, coating defects in the form of holidays may be considered as the simplest situation, with a direct exposure of pipeline surface to the external environment, and thus a direct path for molecular hydrogen escape. However, the direct exposure of pipeline surface would ultimately lead to surface corrosion that would hinder hydrogen recombination reaction [35]. It is plausible to argue that this could divert permeation of hydrogen away from the defects / holidays and direct it to the rest of the coating.

Cathodic Protection

The question of the potential influence of permeated hydrogen on CP can be considered for the perspective of it impact (i) on CP performance and polarization protection criteria, and (ii) Hydrogen-Induced Stress Cracking (HISC), because of CP overprotection.

To date, there are no published reports on impacts of hydrogen on CP performance and polarization, and thus this clearly is an area worthy of applied research and laboratory testing. In our opinion, it is entirely possible that permeated hydrogen, i.e. atomic and surface adsorbed hydrogen, in the area of disbonded coating may be consumed though a series of hydrogen evolution reactions. These would lead to pipeline depolarization, i.e. loss of CP polarisation, and such pipelines should be subject to a more electronegative CP potential criteria.

As already noted, adsorbed hydrogen atoms may recombine and diffuse into the outer environment or diffuse into the grain of the steel. The latter case can result in HE that is caused by CP overprotection. The risk of hydrogen cracking of pipeline steels due to CP overprotection

has widely been commented upon in the industry [36]. Overprotection relates to the application of an CP_{OFF} potential typically more negative than the –1200 mV_{CSE}. Generally, standards recommend polarisation limitations for high yield strength (YS) typically > 550 N/mm^2. However, hydrogen-assisted cracking has actually been also observed in multiple instances in grades as low as X52 or X60, particularly in the presence of overprotection and high plastic strain (e.g. gouges) [23,37,38]. More recently (2018), a 22-inch onshore natural gas transmission pipeline (X52) failed by hydrogen cracking, driven by CP providing polarization near −1200 mV_{CSE} [39].

The steady state membrane permeation of hydrogen due to CP is proportional to root square of the cathodic current. As demonstrated in Figure 4, hydrogen permeation increases from –800 to –1200 mV, from which point a plateau is reached, due to the balancing increased influence of hydrogen desorption at large cathodic potentials [40]. Taking into account the additional source of permeation of atomic hydrogen from (continuous) internal charging, and the potential resulting susceptibility to hydrogen embrittlement, there is the genuine question, whether subcritical (external side) hydrogen concentrations could be reached at more positive potentials, and ultimately whether limitations on maximum cathodic polarisation (i.e. more positive than –1200 mV) may need to be introduced to limit the threat of external hydrogen-assisted cracking, particularly for higher operational utilisations (beyond current ASME B31.12-2019 limits). To date, there are no published reports to assess these potential impacts.

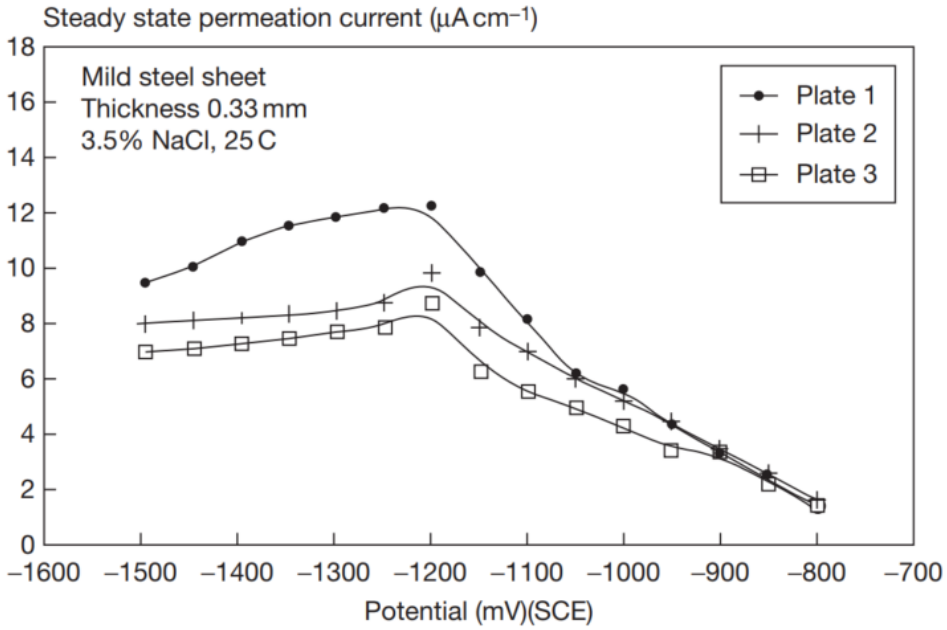

Figure 4. Steady state hydrogen permeation current in steel vs. CP potential in 3.5% NaCl. [40]

Remarks

The main objective of this work was to highlight key points specific to material durability and external corrosion of pipelines, as they pertains to hydrogen transportation in repurposed pipeline systems. We highlight that:

- Mitigation against hydrogen embrittlement by means of internal barrier coatings is superficially appealing, but it unlikely to be a practicable solution due to the difficulties in ensuring complete coating continuity, especially when retrofitted to existing pipelines.

- The use of inhibitor molecules (especially low amounts of oxygen) shows promise in terms of mitigation against HE in a laboratory environment. However there are still challenges with respect to practical implementation and uncertainty over long term efficiency.
- Many existing hydrogen pipelines – built to codes / standard applicable at the time of their construction – have shown decades of incident-free operation; although, they have been operating at lower pressures and hoop stresses than those experienced by natural gas pipeline systems.
- Impact of hydrogen on durability of metallic materials is now well established; the emphasis is on HE and other hydrogen-related cracking mechanisms.
- As information on hydrogen-induced degradation of coatings is scarce, their potential performance is largely estimated, based on the current understanding of the behaviour of hydrogen vs. polymeric materials. Consequently, these areas requires targeted research and validation, and should be inclusive of various types of external coatings which are in service today.
- It is surprising that there are no data or reports on potential impacts that permeated hydrogen may have on CP performance. It is possible that adsorbed atomic hydrogen may have a depolarising effect and thus an improved CP requirement may be necessary. Also, we contemplate whether limitations on maximum CP polarisation (i.e. more positive than –1200 mV_{CSE}) needs to be introduced to limit the threat of external hydrogen-assisted cracking. In our opinion, these identified gaps should also be confirmed or refuted through targeted testing.

References

1 Hydrogen Council, How hydrogen empowers the energy transition, 2017.

2 GRTGaz, « Technical and economic conditions for injecting hydrogen into NG networks », Report INIS-FR-20-0156, June 2019.

3 European Hydrogen Backbone, April 2022.

4 N. Gallon, S. Hopkin, T. Martin, EPRG Hydrogen Pipelines Repurposing Guideline White paper Energy fuels symposium -Attaining a low carbon future together", PRCI-EFS2023-053, Orlando, June 2023.

5 D. Sandana, N. Gallon, O. Burkinshaw and A. Bhatia, "Safe Repurposing of Vintage Pipelines for Hydrogen in North America," International Pipeline Conference, Calgary, 2022.

6 O. Burkinshaw, D. Sandana, N. Gallon, A. Bathia, "Susceptibility of a virtual pipeline network to fatigue and cracking threats in hydrogen service", International Pipeline Conference, Calgary, 2022.

7 Gallon, N., Guest, L., Andrews, R.M., for EPRG, "Design and Material Challenges and Mitigations", EPRG 221/2020, 2020.

8 Laureys, A. et al., "Gaseous Hydrogen Transport In Existing Pipelines: A Review Of Factors Affecting Material Degradation", Technology for Future and Ageing Pipelines, Ghent, 2022.

9 Sandana, D., Gallon, N., Andrews, R.M., Palmer-Jones, R., "Crack Management of Hydrogen Pipelines," International Conference on Hydrogen Safety, Edinburgh (Virtual), 2021.

10 Daniel Sandana, Neil Gallon, Ollie Burkinshaw, Arti Bhatia, Safe repurposing of vintage pipelines for hydrogen in North America, IPC 2022-87088, IPC 2022, 2022.

[11] Y.Lei, E.Hosseini, L.Liu, C.A.Scholes and S.E.Kentish, Internal Polymeric Coating Materials for Preventing Pipeline Hydrogen Embrittlement and Theoretical Model of Hydrogen Diffusion Through Coated Steel, International Journal of Hydrogen Energy, Vol.47, Iss. 73, pp31409-31419, 2022

12 Gallon, N., Guest, L., Andrews, R.M., for EPRG, “Design and Material Challenges and Mitigations”, EPRG 221/2020, 2020.

13 Effect of Hydrogen Gas Impurities on the Hydrogen Dissociation on Iron Surface. Staykov, A. Yamabe, J., Somerday, B.P. 2014, Vol. 114, pp. 626-635.

14 Review of the Effect of Hydrogen Gas on Fatigue Performance of Steels. Zhang, Y.H. Shanghai : s.n., 2010. Proceedings of the ASME 2010 29th International Conference on Ocean, Offshore and Arctic Engineering, OMAE2010.

15 Adams, T.M. Evaluation of Natural Gas Pipeline Materials for Hydrogen Service. Savannah : DOE Hydrogen Pipeline R&D Project Review Meeting, 2005.

16 B.Somerday et al., “Elucidating the variables affecting accelerated fatigue crack growth of steels in hydrogen gas with low oxygen concentrations”, Acta Materiala. 2013, vol .61, pp 6153-6170

17 Ronevich et al., Understanding the bounds of oxygen mitigated hydrogen embrittlement in ferritic steels, SAND2019-11638C

18 NATURALHY, “Durability of steels for transmission pipes with hydrogen,” 2009.

19 L. Briottet and H. Ez-Zaki, “Influence of hydrogen and oxygen impurity content in a natural gas / hydrogen blend on the toughness of an API X70 steel”, ASME 2018 pressure vessels and piping conference, Prague

20 Compiled from Data presented in « Gas pipeline incidents », 11th report of the European Gas Pipeline Incident Data Group (1970-2019), Doc No VA 20.0432, December 2020

21 ISO 21809 Petroleum and Natural Gas Industries – External Coatings for Buried or Submerged Pipelines used in Pipeline Transportation Systems

22 ISO 15589-1:12017 Petroleum, petrochemical and natural gas industries. Cathodic protection of pipeline systems – on-land pipelines

23 D. Sandana, N. Gallon, R.M. Andrews, R. Palmer-Jones, « Crack Management of hydrogen pipelines », International Conference on Hydrogen Safety (ICHS), HySAFE, Edinburgh, 21-24th September 2021

24 R. Varley and K. Leong, Polymer Coatings for Oilfield Pipelines. In: A. Hughes, J. Mol, M. Zheludkevich, R. Buchheit (Eds.), Active Protective Coatings. Springer Series in Materials Science, Vol. 233, Springer, Dordrecht (2016)

25 ASME, « ASME B31.12, Hydrogen Piping and Pipelines », New York, 2019

26 European Industrial Gases Association, « Hydrogen Pipeline Systems »,. EIGA, IGS 121/14, Brussels, 2014

27 BS EN 12954 :2019, « General principles of cathodic protection of buried or immersed onshore metallic structures”

28 J. Kittel, F. Ropital, J. Pellier. « Effect of membrane thickness on hydrogen permeation in steels during wet H2S exposure », Corrosion, National Association of Corrosion Engineers, 2008, 64 (10), pp.788-799.

29 ISO 11114-2:2013, Gas cylinders — Compatibility of cylinder and valve materials with gas contents — Part 2: Non-metallic materials.

30 O. Huising and A. Krom, « H2 in an existing natural gas pipeline », Paper No. IPC2020-9205, Proc. Of 13th Int. Pipeline Conference, Virtual-Online, September 28-30, 2020

31 A. Raju et al., « Hydrogen Blending Impacts Study », Report No. R.13-02-008, California Public Utilities Commission, 18 July 2022

32 D. Muckle, « Hydrogen Fuel Gas Distribution through polyethylene pipes », Radius Systems, April 2021

33 L. Lam-Thanh, Hydrogen Deep Dive Session – Integrity, Inspection & Maintenance, MEAS 15-02, PRCI 2021 Virtual Research Exchange, March 2-5, 2021.

34 Payer, Damage to FBE and Liquid Epoxy Coatings from Hydrogen Outgassing from Welds, PRCI Catalog No. L51903, Pipeline Research Council International Inc., May 26, 2004.

35 S. Ajito, E.Tada, A. Ooi & A. Nishikata, Effect of iron rust on hydrogen uptake during steel corrosion under an aqueous NaCl droplet, ISIJ Int., 61, 1186 (2021)

36 Schoeneich, H-G., Considerations on the risk of hydrogen embrittlement of pipeline steel

due to cathodic overprotection, Pipeline Technology Conference, Berlin, 2015

37 Private industry meeting report, HISC in a dent, case history and lab tests, 1995

38 Punter, A., Fikkers, A.T., Vanstaen, G., HISC on a pipeline, Materials performance, June1992

39 P. Cazenave, K. Jimenez, M. Gao, A. Moneta, Hydrogen assisted cracking driven by cathodic protection operated at near −1200 mV CSE – an onshore natural gas pipeline failure, Journal of Pipeline Science and Engineering, Volume 1, Issue 1, March 2021, Pages 100-121

40 Shreir's Corrosion, Vol. 1, 2.10, Hydrogen Embrittlement, Figure Reproduced from Obuzor, U. W. PhD Thesis , UMIST , Manchester 1989

Effect of hydrogen on nanoindentation behavior of heat treated selective laser melted 316L stainless steel

Ali Nabizada[1], Lisa Claeys[2], Kim Verbeken[3], Tom Depover[4]

[1,2,3,4] Ghent University, Department of Materials, Textiles and Chemical Engineering, Research group of Sustainable Materials Science, Ghent, Belgium
[1]ali.nabizada@ugent.be
[2]lisa.claeys@ugent.be
[3]kim.verbeken@ugent.be
[4]tom.depover@ugent.be

Abstract

Selective Laser Melting (SLM) is an increasingly advantageous Additive Manufacturing (AM) technique for fabricating intricate components with potential applications in hydrogen storage and transport. Austenitic stainless steels (ASS) produced via SLM exhibit enhanced mechanical properties when compared to their conventionally manufactured (CM) counterparts. Nevertheless, the response of ASS to hydrogen exposure remains uncertain and requires further investigation. The interaction of hydrogen with heat-treated SLM 316L ASS was examined through exposing the net-shaped specimens to cathodic electrochemical hydrogen charging and nanoindentation loading tests correlated with Electron BackScatter Diffraction (EBSD) analysis. Thermal Desorption Spectroscopy (TDS) and melt extraction are used to evaluate the diffusivity and solubility of hydrogen, respectively. The low diffusion coefficient of hydrogen arising from the crystallographic and microstructural properties of SLM parts led to a restricted depth of hydrogen penetration. Therefore, nanoindentation, being a surface-based methodology, offers an effective means to assess the impact of hydrogen. The charged samples exhibited an observed enhancement in nanohardness, which can be attributed to the hydrogen-increased lattice friction and pinning effect. An explicit correlation between nanohardness displacement and grain orientation was observed for grain orientations close to <001>, <101>, and <111> parallel to building direction. This correlation was explained by considering the role of the different deformation mechanisms, solidification structure and dislocation density affecting the nanoindentation behavior.

Keywords

Selective Laser Melting; Austenitic Stainless Steels; Hydrogen; Nanohardness; Electron Backscatter Diffraction

Introduction

Hydrogen is receiving great attention as an alternative energy carrier against escalating environmental problems of fossil fuels [1]. Among structural metals exposed to direct hydrogen, Austenitic Stainless Steels (ASSs) and particularly stable series such as type 316 L, are known to show limited degradation of mechanical performance via hydrogen embrittlement (HE). However, annealed ASSs, with a face center cubic structure, show a relatively low strength which is not favorable for use at elevated pressures in hydrogen environments [2]. A major research interest has been generated by additive manufacturing (AM) technologies, in which molten metals are deposited layer by layer to fabricate complex products. Parts manufactured using additive manufacturing have distinct mechanical properties due to their microstructure, texture, and surface properties, which differ from conventionally manufactured (CM) parts. It is generally accepted that AM ASSs have higher yield and tensile strengths compared with CM ASSs [3]. Research efforts have focused on the macroscopic mechanical properties of AM 316L when in contact with hydrogen [4]. However, it is still necessary to further explore the underlying deformation mechanisms and mechanical behavior at the nanoscale. A combination of Electron Backscattered Diffraction (EBSD) and nanoindentation is an efficient method to characterize nanoscale elastic-plastic properties and correlate them with local microstructures and crystallography. This in turn, provides new insights into deformation behavior of AM specimens leading to optimization of its microstructure and nano-mechanical properties [5]. Therefore, the present project aims to investigate the effect of hydrogen on the nanomechanical behaviour of a heat treated SLM 316L ASS.

Materials and Methods

A solution annealing heat treatment was performed to the printed specimens with the as-built surface in air at 1066 °C for 1h. A profound analysis was performed to compare both hydrogen charged and uncharged specimens. Hydrogen was introduced in the specimens via electrochemical charging at a constant current density of 5 mA/cm². An electrolyte of 1.3M borax in glycerol at 50°C for 24h was used. The hydrogen absorption behaviour was evaluated with Thermal Desorption Spectroscopy (TDS) and melt extraction. Electron Backscatter Diffraction (EBSD) measurements were performed in a FEI Quanta 450 SEM. The nanoindentation tests were carried out on the polished EBSD examined surfaces using an ASMEC nanoindenter device with a Berkovich indenter tip at room temperature. Three grain orientations close to {111}, {001} and {101} with their plane normal parallel to the building direction of the samples were selected for detailed characterization. The nanoindentation tests were conducted on a load-controlled mode with a maximum load of 10 mN at constant loading rates of 1 mN/s.

Results and discussion

The dissolved hydrogen content (C_t) and hydrogen diffusion coefficient at room temperature (D_{RT}) are given in Table 1.

Table 1: Averaged hydrogen content of specimen charged at 50°C for 24h and hydrogen diffusion coefficient at room temperature (RT)

	D_{RT}(m^2/s)	C_t (wppm)
Heat treated SLM 316L	4.20E-16	21

Figure 1 compares the load displacement curves of uncharged and hydrogen charged specimens tested with a loading rate of 1 mN/s. Each curve consists of three stages: initial elastoplastic loading, creep and final elastic unloading. The loading stage represents the nucleation, interaction and long range movement of dislocations while the creep stage mainly shows nucleation and thermally activated movement of dislocations. According to Figure 1, hydrogen has an influence on the loading and creep stage by its interaction with dislocations. Due to the pinning effect of hydrogen, movement of dislocations is hindered resulting in a decrease in the length of the loading stage. The different effects of hydrogen on the creep stage can be attributed to two reasons: (1) enhanced dislocation mobility by hydrogen's elastic shielding effect and (2) increased nucleation rate of dislocations during creep as hydrogen decreases the maximum shear stress [6]. Consequently, hydrogen increased the length of the creep stage.

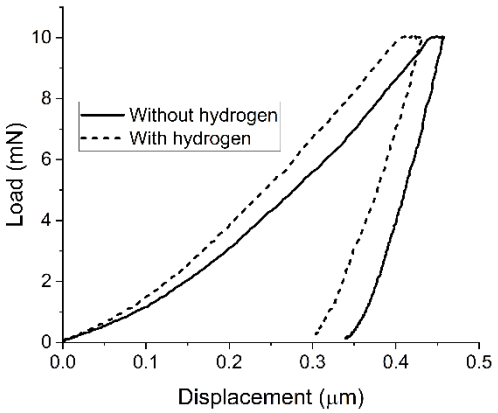

Figure 1: Representative Load-Displacement curves of uncharged and hydrogen charged heat treated SLM 316L under constant loading rate of 1 mN/s.

In Figure 2a, the EBSD inverse pole figure (IPF) map of the tested material is presented. The crystal axis is parallel to the building direction. Grains are elongated along the building direction and there is a solidification-driven orientation gradients within the grains. Figure 2b shows the Kernel Average Misorientation (KAM) map of Figure 2a, which qualitatively exhibits the local strain distribution and geometrically necessary dislocation (GND) density. The load-displacement curves were used to measure nanohardness according to the Oliver–Pharr method. The resulting hardness (H) values can be obtained from Equation 1.

$$H = \frac{F_{max}}{A_c} \qquad \textit{Equation 1}$$

where F_{max} is the maximum applied load and A_c is the projected area at a given contact depth h_c [7]. The nanohardness result of uncharged and hydrogen charged specimens are presented using a box plot in Figure 2c for better visualization. The statistics are categorised for grains with orientations close to <100>, <101>, and <111> parallel to the building direction. The hardness values for grains with <101> is the highest among the two other orientations in both uncharged and charged condition. According to Schmid's law, orientation-dependent hardness can be explained by an easy-slip model, which gives insight into how slip and twinning systems are activated. Hardness is inversely proportional to the maximum Schmid factor calculated from this model which depends on crystal slip system. According to previous studies maximum Schmid factors for fcc slip and twinning systems under compressions along with <111> are the lowest, indicating the highest hardness and <100> has the largest Schmid factor owning the lowest

hardness [8]. However, this is not consistent with this work where <101> is the hardest orientation, while slip is the dominating deformation mechanism because twinning was not observed. A study by Tekumalla et al. found that the nanohardness scales inversely to the cell spacing along slip direction (CSSD), which quantifies the linear density of solidification cell boundaries on activated slip systems [9]. Dislocation density may also affect the measured hardness in different orientations. As a result of the SLM method, dislocation density may change depending on the orientations, thereby contributing to the findings. As it is shown in Figure 2b, the KAM intensity is higher in grains with <101> orientation which indirectly indicates a higher dislocation density compared with <100> and <111> grain orientations. An increase in nanohardness was observed in the hydrogen charged samples. It can be proposed that the hardening effect of hydrogen is related to the hydrogen-impeded dislocation motion due to the increased lattice friction caused by the interstitially dissolved hydrogen. A Cottrell-like atmosphere of hydrogen can be formed around the dislocation core and hinder its motion. Also hydrogen distribution in the elastic field of dislocations can form narrow cylinders with random orientations along dislocations and hence hinder the dislocation motion [10].

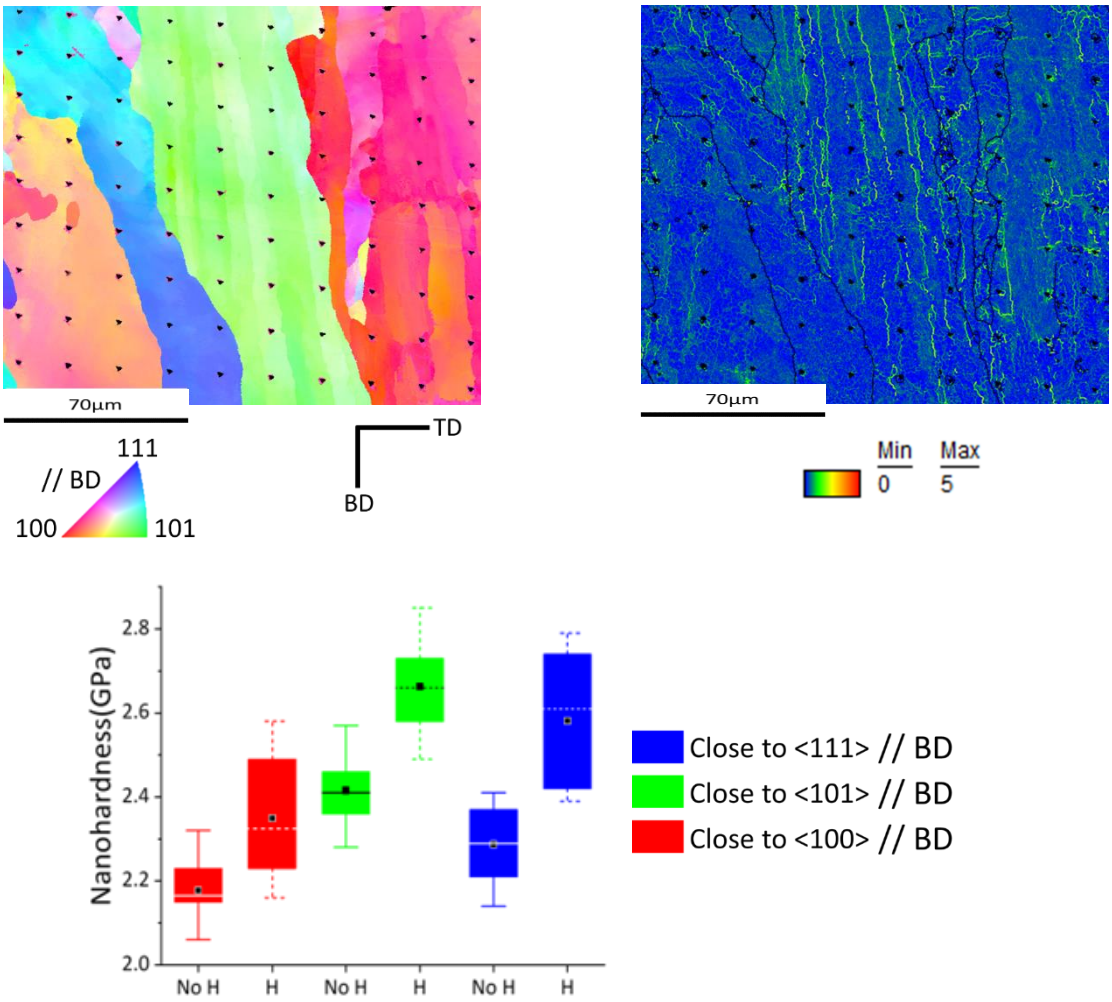

Figure 2: EBSD maps of SLM 316L showing the nanoindentation regions; a) IPF map; b) KAM map; c) comparison of the nanohardness results of uncharged and hydrogen charged SLM 316L for <100>, <101>, and <111> // BD grain orientations.

Conclusion

The nanomechanical behavior of a heat-treated SLM 316L ASS with and without dissolved hydrogen was investigated via load-displacement curves. The hydrogen-charged samples showed higher hardness values compared to their uncharged counterparts due to the effect of hydrogen on dislocation behavior. Dislocation movement was hindered by hydrogen leading to a decrease in the contact depth (h_c) while creep displacement was lengthened because hydrogen improved dislocation nucleation and movement. Due to a high dislocation density, grains with <101> orientation showed higher hardness than other orientations in both charged and uncharged conditions.

Acknowledgement

The authors would like to acknowledge the financial support of the Energy Transition Fund via the BE-HyFE project. The research was also supported by FWO (senior postdoctoral fellow project number 12ZO420N) and the special research fund (BOF) of Ghent University (grant BOF15/BAS/062 and BOF20/BAS/121) for the used equipment. Moreover, Engie Laborelec is acknowledged for the fabrication of the AM316L specimens.

References

[1] H. J. Undertaking, "Hydrogen roadmap Europe: a sustainable pathway for the European energy transition," 2019.

[2] T. Michler, C. San Marchi, J. Naumann, S. Weber, and M. Martin, "Hydrogen environment embrittlement of stable austenitic steels," *Int J Hydrogen Energy*, vol. 37, no. 21, pp. 16231–16246, 2012.

[3] W. E. Frazier, "Metal additive manufacturing: a review," *J Mater Eng Perform*, vol. 23, pp. 1917–1928, 2014.

[4] K. M. Bertsch, A. Nagao, B. Rankouhi, B. Kuehl, and D. J. Thoma, "Hydrogen embrittlement of additively manufactured austenitic stainless steel 316 L," *Corros Sci*, vol. 192, Nov. 2021.

[5] J. England *et al.*, "Nanoindentation Hardness and Corrosion Studies of Additively Manufactured 316L Stainless Steel," *J Mater Eng Perform*, vol. 31, no. 8, pp. 6795–6805, Aug. 2022.

[6] Y. Hong, C. Zhou, Y. Zheng, L. Zhang, J. Zheng, and X. Chen, "Effect of hydrogen and strain rate on nanoindentation creep of austenitic stainless steel," *Int J Hydrogen Energy*, vol. 44, no. 2, pp. 1253–1262, Jan. 2019.

[7] Z. M. Jiao, Z. H. Wang, R. F. Wu, and J. W. Qiao, "Strain rate sensitivity of nanoindentation creep in an AlCoCrFeNi high-entropy alloy," *Appl Phys A Mater Sci Process*, vol. 122, no. 9, pp. 1–5, Sep. 2016.

[8] T. Chen, L. Tan, Z. Lu, and H. Xu, "The effect of grain orientation on nanoindentation behavior of model austenitic alloy Fe-20Cr-25Ni," *Acta Mater*, vol. 138, pp. 83–91, Oct. 2017.

[9] S. Tekumalla, B. Selvarajou, S. Raman, S. Gao, and M. Seita, "The role of the solidification structure on orientation-dependent hardness in stainless steel 316L produced by laser powder bed fusion," *Materials Science and Engineering: A*, vol. 833, p. 142493, Jan. 2022.

[10] X. Lu, Y. Ma, D. Peng, R. Johnsen, and D. Wang, "In situ nanomechanical characterization of hydrogen effects on nickel-based alloy 725 under different metallurgical conditions," *J Mater Sci Technol*, Aug. 2022.

Catalytic performance and degradation of bifunctional $Ni_xMo_yFe_z$ materials synthetized by DC-sputtering for alkaline water electrolysis

D. Kurchavov[1], M. Mendez[1], M. Al-Katrib[1], N. Loones[1], V. Daniau[2], M. Bouttemy[3], F. Donsanti[2], P. Volovitch[4], N. Naghavi[4]

[1] Institut Photovoltaïque d'Ile-de-France (IPVF), 18 boulevard Thomas Gobert, 91120 Palaiseau, France

[2] Institut Photovoltaïque d'Ile-de-France (IPVF), EDF Energy Research and Development, 18 boulevard Thomas Gobert, 91120 Palaiseau, France

[3] Institut Lavoisier de Versailles (ILV), Université de Versailles Saint-Quentin-en-Yvelines, Université Paris-Saclay, 45 avenue des États-Unis, 78035, Versailles, France

[4] Institut Photovoltaïque d'Île-de-France (IPVF), UMR 9006, CNRS, Ecole Polytechnique, IP Paris, Chimie Paristech, PSL, 91120, Palaiseau, France

Alkaline Water Electrolysis (AWE) is considered as one of the most promising methods for hydrogen production due to no greenhouse gases emission and relatively high efficiency [1]. It consists of two parallel processes, named Oxygen Evolution Reaction (OER) and Hydrogen Evolution Reaction (HER) on anode and cathode, respectively. To industrialize the process, non-precious-metal catalysts should be employed. Bifunctional materials, based on Ni, demonstrate excellent electrocatalytic performance towards HER and EOR. It has been shown that the state of Ni-based electrode surface (oxidized or reduced) largely determines their electrocatalytic activity [2]. This work is dedicated to the analysis of the state of the electrode surface and their impact on the degradation mechanism of $Ni_xMo_yFe_z$ based materials towards HER and OER in long term polarization tests.

Methodology

Electrocatalytic properties and durability of binary and ternary based on $Ni_xMo_yFe_z$ materials synthetized by DC-sputtering technique on borosilicate glass and Ni-plate substrates were studied and compared in half-cell and full-cell configurations. Chemical and electrochemical stability of these catalysts were studied using a combination of in situ electrochemical analysis coupled with time lapse microscopy and ex situ surface evolution analysis such as X-ray Photoelectron Spectroscopy (XPS),

X-ray Diffraction (XRD), Scanning Electron Microscopy coupled with Energy Dispersive Spectroscopy (SEM-EDS), Raman spectroscopy, Atomic Force Microscopy (AFM) and contact angle measurements.

Results

Depending on the composition of catalysts different behavior of the studied materials have been observed. Preliminary results show that NiFe has the best initial electrocatalytic properties towards HER and OER in term of overpotential, η, at |10| mA/cm^2 (at 0h on the fig. 1). During polarization, however, its electrocatalytic properties towards HER rapidly degrade (fig. 1). No significant degradation occurs for NiMo and NiMoFe. Live images demonstrate NiFe and NiMoFe catalysts detachment from the borosilicate glass substrate during HER (fig. 1), but not during OER. NiMo demonstrated the best stability for both HER and OER. Based on surface analysis and chemical composition of electrodes it will be shown that the formation of oxides and hydroxides on the surface of these electrodes affect their electrocatalytic properties and stabilities. Mechanism of the surface evolution of catalysts and its impact on electrocatalytic properties are discussed.

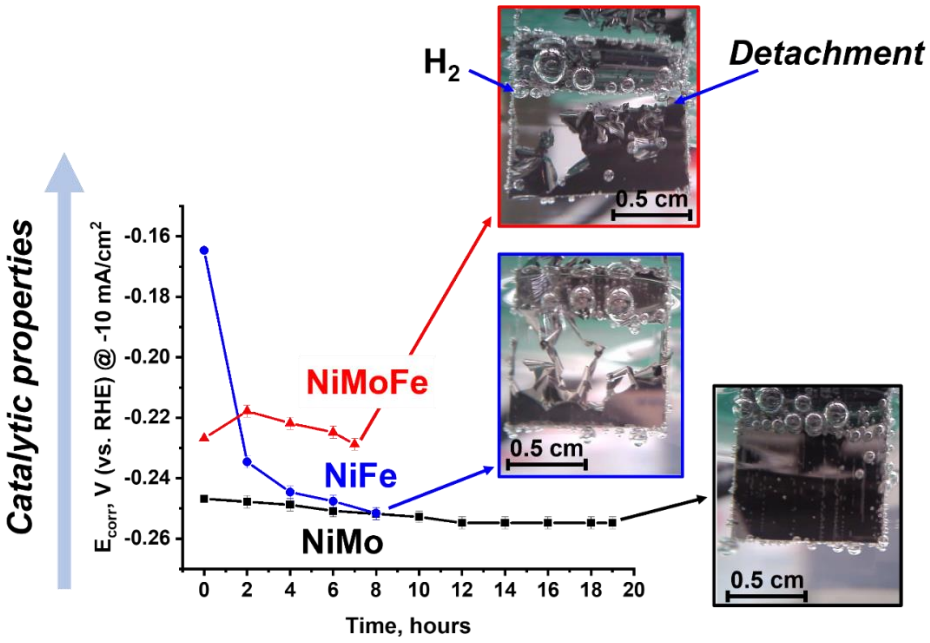

Figure 1 – Electrocatalytic performance of NiMo (black), NiFe (blue) and NiMoFe (red).

[1] J. Wang, et al., Chem. Soc. Rev. 49 (2020) 9154–9196.

DOI : https://doi.org/10.1039/d0cs00575d

[2] Oshchepkov A, et al., ACS Catalysis. 10(13) (2020) 7043-7068.

DOI : https://doi.org/10.1021/acscatal.0c00101

Parametrization of Sieverts' law using electrochemical hydrogen charging and thermal desorption analysis

Andreas Drexler, Graz University of Technology, Institute of Materials Science, Joining and Forming, Graz/Austria;

Wolfgang Siegl, HyCentA Research GmbH, Graz/Austria;

Thomas Hafner, HyCentA Research GmbH, Graz/Austria;

Alexander Trattner, HyCentA Research GmbH + Graz University of Technology, Institute of Thermodynamics and Sustainable Propulsion Systems, Graz/Austria.

Objectives

The aim of the present work is to parametrize Sieverts' law [1] of gaseous hydrogen solubility by performing electrochemical charging and subsequent thermal desorption spectroscopy (TDS). This contributes to a better understanding of gaseous and electrochemical hydrogen uptake and allows to extrapolate the gaseous hydrogen solubility to low temperatures and high gas pressures without performing tests in autoclave systems.

The material of interest is the pipe material L485 (X70). Samples are prepared from the pipeline wall. A metallographic characterization is performed to analyse the ferritic-pearlitic microstructure. To cover a broad range of hydrogen content, electrochemical charging is performed using different electrolytes: 3.5% NaCl, 3.5% NaCl + Thiourea and 0.5 M H2SO4 + Thiourea. The saturation time for each electrolyte is determined in advance by recording absorption curves. Fully saturated samples are used for recording TDS spectra at different heating rates. Trap density and trap energies are evaluated from the measured TDS spectra at different hydrogen contents by performing inverse parametrization of generalized diffusion models [2–4].

Based on Oriani's approach, a mathematical model is proposed, which describes the equilibrium hydrogen content in the material depending on temperature, hydrostatic stresses and hydrogen fugacity. Validation of the parametrized model is done by gaseous hydrogen charging at various pressures up to 500 bar and various temperatures up to 500 °C using an autoclave setup.

New results

The proposed mathematical model can be used to calculate the hydrogen solubility in steels after being exposed to pressurized hydrogen gas. Considering electrochemical charging in the parametrization of Sieverts' law allows to reduce the number of tests in autoclave systems to a minimum. Furthermore, the model is fully physical based, which allows to extrapolate the hydrogen solubility to very low temperatures and to very high pressures.

Significance of the work

As a result of the decarbonization of economies and energy systems, hydrogen is gaining increasing importance as an energy carrier. For the adaptation of natural gas grids to hydrogen, pipeline steels must be thoroughly investigated regarding their resistance and behavior in contact with hydrogen. The proposed model allows predictions of the hydrogen uptake at a given pressure and temperature and facilitates the assessment of the material's suitability for transporting hydrogen.

References

1. Drexler, A.; Konert, F.; Sobol, O.; Rhode, M.; Domitner, J.; Sommitsch, C.; Böllinghaus, T. Enhanced Gaseous Hydrogen Solubility in Ferritic and Martensitic Steels at Low Temperatures. *Int. J. Hydrogen Energy* **2022**, *47*, 39639–39653, doi:10.1016/j.ijhydene.2022.09.109.
2. Drexler, A.; Depover, T.; Verbeken, K.; Ecker, W. Model-Based Interpretation of Thermal Desorption Spectra of Fe-C-Ti Alloys. *J. Alloys Compd.* **2019**, *789*, 647–657, doi:10.1016/j.jallcom.2019.03.102.
3. Drexler, A.; Depover, T.; Leitner, S.; Verbeken, K.; Ecker, W. Microstructural Based Hydrogen Diffusion and Trapping Models Applied to Fe–C[Sbnd]X Alloys. *J. Alloys Compd.* **2020**, *826*, 154057, doi:10.1016/j.jallcom.2020.154057.
4. Drexler, A.; Helic, B.; Silvayeh, Z.; Mraczek, K.; Sommitsch, C.; Domitner, J. The Role of Hydrogen Diffusion, Trapping and Desorption in Dual Phase Steels. *J. Mater. Sci.* **2022**, *57*, 4789–4805, doi:10.1007/s10853-021-06830-0.

Investigation and prediction of hydrogen uptake kinetics of cathodic polarized metals in aqueous electrolytes

Livia Cupertino-Malheiros[a], *Alfredo Zafra*[a], *Tim Hageman*[a], *Emilio Martínez-Pañeda*[a]

[a]*Department of Civil and Environmental Engineering, Imperial College London, London SW7 2AZ, UK*

A wide range of commonly used metals and alloys are susceptible to hydrogen embrittlement (HE), which currently limits the design of structures in multiple industrial sectors. Since any hydrogen-assisted fracture phenomenon is strongly related to the local hydrogen concentration, HE predictive models require proper consideration of hydrogen uptake kinetics on metal surfaces. In aqueous electrolytes, hydrogen absorption into alloys is governed by hydrogen evolution reactions (HER), resulting in the production and desorption of the adsorbed hydrogen intermediate state. The recently developed modelling framework [1] with rate constants (k) for all competing reactions independent of pH and potential allowed for a better incorporation of HER kinetics than previous HE models. This framework being capable, for the first time, to fully resolve the physics of hydrogen uptake by explicitly linking the electrolyte with the hydrogen ingress into metals. However, the complexity of properly evaluating HER kinetics experimentally, seen by a large scatter between the values of reaction rate parameters in the current literature, may limit the reliability of the framework's predictions, and hence the application of the model in predicting hydrogen local concentration and assisted fracture.

This work investigates the kinetics of HER and hydrogen absorption, providing a first database of reaction rate input parameters for the developed model of hydrogen uptake into cathodically polarized metals. First, the surface activities of the studied metals, Fe and Ni, are studied using potentiodynamic cathodic polarization and electrochemical impedance spectroscopy (EIS) techniques in relatively-mild electrolytes from pH 1 to 13. Polarization reveals dependencies of the HER-associated cathodic current on the applied potential strongly linked to electrolyte pH, but very similar for both metals studied. EIS analyses provide the evolutions of dominant mechanism (Volmer-Tafel or Volmer-Heyrosvky) for both metals with applied cathodic potential and pH. These results are complemented by investigations

of hydrogen absorption and diffusion kinetics by analyzing electrochemical permeation transients. The full set of obtained reaction rate parameter values is incorporated into the model framework and a sensitivity analysis is performed to assess the impact of variations in the chosen parameter values, helping to identify the most significant ones for predicting local hydrogen concentration at various pH and potential regimes.

[1] T. Hageman, E. Martínez-Pañeda, An electro-chemo-mechanical framework for predicting hydrogen uptake in metals due to aqueous electrolytes, Corros Sci. (2022) 110681. https://doi.org/10.1016/j.corsci.2022.110681.

Impact of thermal oxide layers on the hydrogen transport through the surface of a Fe11Cr stainless steel

Tim Rubben[1], Kitty Baert[1], Tom Depover[2], Kim Verbeken[2], Reynier I. Revilla[1], Iris De Graeve[1,2]

1 Department of Chemistry and Materials, Vrije Universiteit Brussel (VUB), Research Group of Electrochemical and Surface Engineering (SURF), Pleinlaan 2, 1050 Brussels, Belgium
2 Department of Materials, Textiles and Chemical Engineering, Ghent University (UGent), Research Group of Sustainable Materials Science, Technologiepark 46, B-9052 Ghent, Belgium

Most research on hydrogen embrittlement is limited to the interaction between bulk microstructural features and hydrogen, whereas the surface is the first to come in contact with potentially hydrogen-containing environments. Steel (when un-polarized) is always covered with an oxide layer and depending on alloy type and environmental conditions, a wide variety of oxide layers can develop. The impact of these oxide layers on the hydrogen absorption/desorption needs to be investigated. This study focused on the effect of controlled pre-formed thermal oxide layers on the hydrogen release and uptake through the surface of a low chromium - low nickel stainless steel. Model thermal oxide layers were used to emphasize the importance of considering the surface characteristics in order to have a full description of the hydrogen transport through metallic components. Results demonstrated that thermal oxides can significantly limit the hydrogen release, which was mainly attributed to a lower diffusion coefficient in the oxide and not to a barrier effect of the oxide-steel interface for chromium enriched magnetite layer formed on this Fe11Cr alloy, where for a pure magnetite layer (as was formed on low carbon steel) the metal-oxide interface was seen to be the limiting barrier. From the analyses, the diffusion coefficient in the oxide was estimated. The presence of a thermal oxide resulted in a slower hydrogen uptake as well, demonstrating that oxide layers can also act as an important barrier for hydrogen entry into the material.

Antagonist effect of hydrogen on plasticity investigated by nano-indentation

Y. Ben Jedidia, A. Oudriss, S.P. Murugan, N. Iskounen,
M. Landeiro Dos Reis, X. Feaugas
LaSIE La Rochelle Université, UMR CNRS 7356, La Rochelle, France.

The influence of electrochemical hydrogen charging and subsequent room temperature hydrogen desorption on elastic modulus, incipient plasticity (or pop-in) and indentation hardness were investigated in nickel single crystals using a series of nanoindentation tests. Antagonist softening and hardening effects of hydrogen are related and commented on the base of TEM, HR EBSD observations and Molecular static simulations using embedded-atom method potential. The irreversible reduction of reduced modulus, i.e., softening in elastic regime, is a result of hydrogen induced vacancy clusters in the surface and subsurface zones due to the hydrogen charging. The analysis of incipient plasticity disclosed the hydrogen-vacancy clusters enhanced lattice friction against the formation dislocation, which resulted in an increase in the critical load and critical resolved shear stress for the first pop-in. Moreover, the activation volume for the pop-in and dislocation nucleation decreased by the hydrogen intake. From this, it is rational to conclude that the mechanism governing the pop-in in hydrogen charged condition is the hydrogen-vacancy clusters induced heterogeneous dislocation nucleation.

The role of zinc coating in the formation and entry of hydrogen in advanced high-strength steel

Nikola Macháčková, Darya Rudomilova, Tomáš Prošek, University of Chemistry and Technology Prague, Czech Republic

The phenomenon of hydrogen embrittlement of advanced high-strength steels is the subject of intense research in view of their safe application. Atmospheric corrosion has been shown to be a possible source of hydrogen that can enter the steel structure. The formation of corrosion products and pits leads to a decrease of pH on the steel surface, and the cathodic hydrogen evolution reaction (HER) then proceeds parallel to the oxygen reduction reaction (ORR). For galvanized steels, the presence of coating defects is considered as the main risk factor for intensification of hydrogen evolution and absorption due to galvanic coupling between steel and zinc.

The aim of this work was to describe the role of zinc coating in the process of hydrogen formation and absorption to press-hardened steel PHS1500 under atmospheric corrosion conditions. In addition to traditional techniques, such as thermal desorption analysis and electrochemical permeation, a method called respirometry was applied. This method allows in situ monitoring of corrosion processes and determination of a ratio between the cathodic reactions. The impact of this ratio, the total amount of formed hydrogen and the effect of individual intermetallic phases of the coating on hydrogen entry into steel was investigated.

It was shown that HER occurs during atmospheric corrosion even on zinc where this reaction is usually considered negligible. It was demonstrated that zinc acts as a hydrogen reservoir. However, despite high levels of formed hydrogen, only small quantities of diffusible hydrogen were detected in the steel specimens. These findings show that hydrogen recombination was a highly efficient process. The relationship between cathodic reactions and hydrogen entry was significantly influenced by the presence of CO_2 in the air and the composition of the corrosion products. For the investigated coating, the presence of artificial defects had no significant effect on the ORR/HER ratio, but it affected the hydrogen entry.

Corrosion morphology and hydrogen absorption of steel under salt deposits during atmospheric corrosion

Xiaole Han, Masatoshi Sakairi, Hokkaido University, Sapporo, Japan

Atmospheric corrosion of steel is often regarded as a cyclic wet-dry process attributed to hygroscopic particles such as sea salts that adhere to the steel surface. The salt particles can absorb moisture and form electrolyte layers on the steel, where corrosion and hydrogen evolution reactions occur. A considerable amount of atomic hydrogen is subsequently absorbed by the steel, presenting a cracking risk to the durability of steel components. In addition to the common sea salts such as NaCl and $MgCl_2$, the anodic dissolution of the protective coatings introduces Zn and Al ions in the electrolyte, resulting in the participation of new hygroscopic particles such as $ZnCl_2$ and $AlCl_3$ during atmospheric corrosion. The corrosion morphology and hydrogen absorption behaviour of steel under such salt deposits are the interest of the present research.

The steel samples were set in a cyclic wet-dry environment with an initial deposition of 10mM NaCl, 5mM $MgCl_2$, 5mM $ZnCl_2$, and 3.3 mM $AlCl_3$ solutions respectively on one side. An electrochemical cell was employed on the other side of the sample to detect the permeated hydrogen during the corrosion process. The corrosion morphology during the wet-dry cycles was observed and recorded using an optical microscope. After the corrosion tests of 72 h, the surface and cross-section analysis of the specimens was conducted using SEM-EDS and AES.

The results showed that the composition of the salt deposits has a significant influence on the corrosion morphology and hydrogen absorption behaviour of steel. Zn^{2+} and Al^{3+} exhibited an inhibition effect on the rust formation under droplets. The amount of permeated hydrogen through the steel under salt deposits increases in the order of NaCl, $MgCl_2$, $ZnCl_2$, and $AlCl_3$. The difference in the hydrogen absorption under salt deposits was related to the varied deliquescent values of different salts. The high deliquescent property of the deposited salt increases the wetness time of corrosion and hydrogen entry into steel.

Experimental characterization and numerical simulation of hydrides distribution in a Grade 2 titanium alloy after gaseous charging

F. Amendola, S. Chroeun, Y. Charles, M. Gaspérini

Université Sorbonne Paris Nord, Laboratoire des Sciences des Procédés et des Matériaux, LSPM, CNRS, UPR 3407, F-93430, Villetaneuse, France

The understanding and prevention of hydrogen embrittlement in titanium alloys is an important issue for the lightening of structural components. The formation of hydrides plays a key role in hydrogen embrittlement of titanium, and is highly dependent on the composition and microstructure of the material, as well as the mode of hydrogen loading [1-3].

In the present study, experimental investigations of gaseous hydrogen charging are conducted on a single phase α titanium alloy (Grade 2). Various conditions are considered [4]: pressure (from 3 to 300 bar), temperature (up to 500°C) and surface conditions (as-received and polished), to exhibit the main factors controlling the overall absorbed hydrogen concentration and the spatial distribution at the SEM scale of the formed hydrides throughout the samples.

At the same time, Finite Element simulations of the experimental hydrogen charging experiments with the device developed at LSPM are realized, using the numerical tools developed for coupling hydrogen diffusion and trapping with mechanical fields [5]. Phenomenological laws are introduced into the code to mimic hydride formation and to estimate the subsequent residual stresses induced by hydride expansion.

Comparison of simulation with experiment is made on available data, including overall hydride densities and the global deformation of the sample observed after hydrogen charging. Parametric studies are made to analyze the influence of hydrogen charging conditions and of material parameters on the macroscopic response, in order to optimize the experimental procedure. Extension of the modeling at a more local scale is discussed.

[1] E. Conforto, I. Guillot, et X. Feaugas, Phil. Trans. R. Soc. A 375 (2017) 20160417.

[2] C.L. Briant, Z.F. Wang, et N. Chollocoop, Corros. Sci., vol. 44, no 8, p.1875-1888.

[3] C.Q. Chen, S.X. Li, H. Zheng, L.B. Wang, et K. Lu, Acta Mater 52 (2004) 3697-3706.
[4] F. Amendola, N. Fagnon, W. Beucia, T. Chauveau, M. Redolfi, M. Gaspérini, Proc. of the Fourth International Conference on Metals & Hydrogen, ISBN 9789081794237, H01, 2022
[5] Y. Charles, M. Gaspérini, N. Fagnon, K. Ardon and A. Duhamel, Eng Frac Mech 218 (2019) 106580.

Hydrogen embrittlement of the multiphase stainless steel

Menghao Liu[1], *Cuiwei Du*[1], *Xiaogang Li*[1]

[1]Institute for Advanced Materials and Technology, University of Science and Technology Beijing, China

Abstract

Hydrogen embrittlement is one of the main concerns for high-strength steel. In this study, the hydrogen embrittlement behavior of a new-developed multiphase stainless steel (ferrite-austenite-martensite) was investigated.

The test was conducted with the assistance of Slow strain rate testing (SSRT) after hydrogen charging. Electron backscattered diffraction (EBSD) was adopted to study the crystallographic information of the material. Scanning Electron Microscopy (SEM) was adopted to analyze the fracture morphology after SSRT. Results shows that the multiphase stainless steel is sensitive to hydrogen embrittlement in the test condition. The fracture shows a combination of cleavage and quasi-cleavage morphologies. Secondary cracks initiate preferentially at the phase boundaries.

Keywords

Stainless steel; Hydrogen embrittlement

Imaging Hydrogen Interactions with Materials at the Nanoscale: SIMS-Based Correlative Microscopy

Santhana Eswara[*], *Dustin Andersen*[1] *and Tom Wirtz*[1]

[1.] *Advanced Instrumentation for Nano-Analytics (AINA), Materials Research and Technology Department, Luxembourg Institute of Science and Technology (LIST), Belvaux, Luxembourg.*

** Corresponding author: santhana.eswara@list.lu*

Hydrogen embrittlement degrades the mechanical properties of steel and other alloys impacting their durability and occasionally resulting in catastrophic consequences [1]. Clear understanding of the local hydrogen-metal interaction mechanisms will help to identify the most effective strategies to mitigate or eliminate the degradation of mechanical properties. While high-resolution electron microscopy is suitable for imaging materials even at the atomic scale, direct imaging of hydrogen in solid materials with nanoscale lateral resolution is a challenge for the typical analytical techniques available on an electron microscope. Secondary Ion Mass Spectrometry (SIMS) is capable of detecting all elements (and isotopes) of the periodic table including hydrogen, but the lateral resolution of SIMS imaging is fundamentally limited to ~ 10 nm by the ion-solid interaction volume. In practice, the lateral resolution of SIMS imaging is often poorer than the fundamental limit because of insufficient ionization efficiencies of the sputtered species and/or too low concentrations of the elements imaged for a given voxel size. In the context of combating hydrogen embrittlement, nanoscale precipitates may be dispersed within the matrix to act as hydrogen traps, making it essential to correlate nanoscale structures (e.g., precipitates) with hydrogen maps. To overcome this challenge, we use a correlative microscopy approach combining electron microscopy and SIMS imaging [2]. As the hydrogen in steels and other metallic alloys is highly mobile, advanced experimental protocols are needed to obtain accurate hydrogen maps in steels. Hence, we started with relatively easier cases where hydrogen is bound to the sample such as in passivating layers in solar cells [3] and hydrogen storage materials [4] in order to optimize the SIMS image acquisition protocols. We then proceeded to investigate the correlation between microstructure and hydrogen trap sites in a

TWinning Induced Plasticity (TWIP) steel in both the as-received and annealed states. With these case studies, we will present the challenges and opportunities in SIMS based correlative microscopy to directly visualize hydrogen-metal interactions with nanoscale lateral resolution.

References

[1] M. Koyama et al, Mater. Sci. Technol., 2017, 33, 1481–1496
[2] S. Eswara et al, Appl. Phys. Revs., 6, 021312, 2019
[3] S. Pal et al, Appl. Surf. Sci, 555, 149650, 2021
[4] D.Andersen, et al, Intl. J. Hydrogen Energy, DOI: 10.1016/j.ijhydene.2022.12.216, 2023
[5] The authors acknowledge funding from the Luxembourg National Research Fund (FNR) by the grants C18/MS/12661114 (MEMPHIS), INTER/MERA/20/13992061 (INTERBATT) and PRIDE21/16758661/HYMAT.

Evaluation of the interactions between the absorbed hydrogen and the microstructure in a pre-strained 316L

Victor Ortolland, Université Paris-Saclay, CEA, Service de recherche en Corrosion et Comportement des Matériaux dans leur environnement, 91191 Gif-sur-Yvette, France

Frantz Martin, Université Paris-Saclay, CEA, Service de recherche en Corrosion et Comportement des Matériaux dans leur environnement, 91191 Gif-sur-Yvette, France

Quentin Auzoux, Université Paris-Saclay, CEA, Service de recherche en Corrosion et Comportement des Matériaux dans leur environnement, 91191 Gif-sur-Yvette, France

Krzysztof Wolski, Mines Saint-Etienne, Université de Lyon, CNRS, UMR 5307 LGF, Centre SMS, F – 42023 Saint-Etienne, France

Austenitic stainless steels, such as 316L, are widely used in hydrogen-rich environments due to their resistance toward corrosion and hydrogen embrittlement. Several mechanisms have been proposed to explain the hydrogen embrittlement phenomenon based on microstructural interactions. Understanding the interactions between the hydrogen and the microstructural defects is of prime importance to identify the main factors that distinguish a H sensitive material to a lesser one (e.g. 316L), and subsequently to propose tracks to develop new materials less susceptible to HE. This study aims at clarifying the interactions between hydrogen and the microstructure of pre-strained 316L.

Large tensile specimens were cut out of a reference solution-annealed 316L sheet, then strained up to 1.5, 10, 20, and 30% or not. The associated dislocation densities were quantified by XRD characterizations and the microstructure was qualified by microscopic observations. Small coupons were extracted from the gauge part of these specimens, then deuterium was cathodically charged in a NaO^2H solution. Different aging treatments at 323 K were then performed to increase the trapped over interstitial ^2H ratio [1], [2]. The influence of the pre-strain level on the hydrogen distribution in volume and among the potential sites in the microstructure was finally evaluated by combining TDS and SIMS analyses.

It appears that the large increase of the dislocations density with the pre-strain level affects poorly the ^{2}H amount and distribution in the specimens: pre-strain causes only a slight increase of the hydrogen fraction that remains after aging and a slight decrease in the mean depth of the hydrogen distribution. With increasing aging duration, thermograms showed the appearance of an additional desorption peak whose increasing contribution suggests a strong trap site, indicated by the red arrow in Figure 1. These results will be discussed in light of the evolution of the microstructure with the pre-strain level.

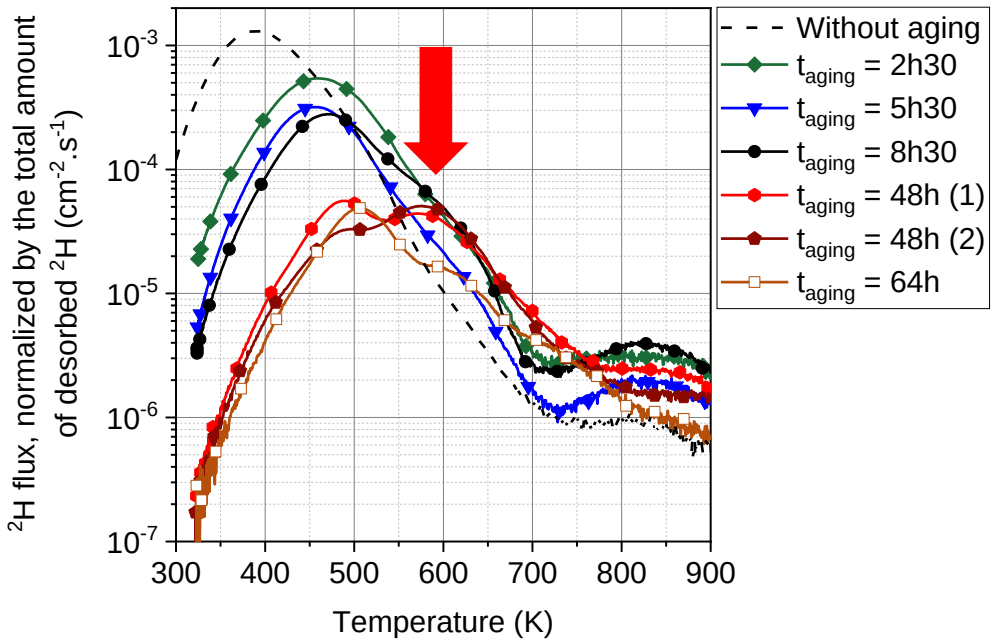

Figure 1 : ^{2}H normalized thermograms in logarithmic scale of the unstrained samples (with a temperature ramp of 10 $K.min^{-1}$) obtained after the aging treatment at 323 K

[1] C. Hurley, PhD, Université de Toulouse, 2015.

[2] A.-C. Bach, F. Martin, C. Duhamel, S. Perrin, F. Jomard, and J. Crepin, 'Hydrogen trapping by irradiation-induced defects in 316 L stainless steel: A combined experimental and modeling study', Journal of Nuclear Materials, vol. 562, p. 153603, Apr. 2022.

Multi-physics phase field modeling of hydrogen-assisted cracking

Emilio Martínez-Pañeda[1], Tim Hageman[1], Chuanjie Cui[1], Philip K. Kristensen[2]

[1]Imperial College London, London, UK

[2]Technical University of Denmark (DTU), Kongens Lyngby, Denmark

Phase field models have had a significant impact on many interfacial problems, including the modelling of microstructural evolution and fracture mechanics. In this wo Virtual Testing can be a game-changer in the deployment of a hydrogen energy infrastructure, enabling efficient and optimal component design, providing mechanistic predictions of material behaviour and fitness-for-service assessment, and preventing catastrophic failures. However, this highly-sought ambition has long remained elusive due to the challenges associated with the complex multi-scale and multi-physics nature of hydrogen embrittlement. This work shows how those challenges can be overcome by improving our understanding of the physical phenomena at play, and by developing robust computational electro-chemo-mechanical schemes that can resolve the underlying physical processes.

A comprehensive finite element framework has been developed that can: (i) quantify hydrogen uptake from both gaseous and aqueous electrolyte environments [1], (ii) simulate the diffusion and trapping of dissolved hydrogen [2], and (iii) predict the nucleation and growth of cracks, assisted by hydrogen [3,4]. This has been largely facilitated by the development of two computational technologies: coupled multi-physics models and phase field modelling. Predictions can be obtained for problems of arbitrary complexity (3D, multiple cracks, etc.), at both laboratory and component scale levels (see Fig. 1) [5,6]. Importantly, these predictions are obtained based purely on physical parameters that can be independently measured.

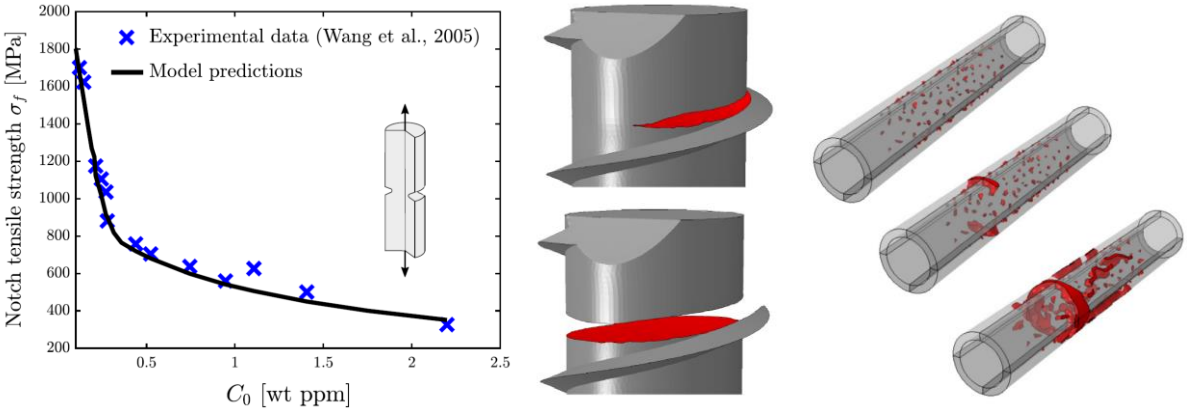

Figure 1. Multi-physics phase field models enable predicting laboratory experiments and component behaviour.

The potential of the proposed electro-chemo-mechanical phase field modelling framework is demonstrated by means of representative case studies. First, crack growth resistance curves are computed in a wide variety of scenarios, showing that the model appropriately captures the sensitivity to material strength, loading rate and hydrogen concentration. Secondly, model predictions are benchmarked against

experiments on Ni-based alloys and ferritic and martensitic steels. Results reveal a promising agreement. Insight is also gained into the suitability of standardised experiments; slow strain rate testing (SSRT) is revisited, showing that subcritical crack growth compromises its validity. Finally, the capabilities of the modelling framework in enabling Virtual Testing are showcased. Large-scale multi-physics predictions are obtained for technologically-relevant applications. The phase field method easily enables capturing damage evolution from an initial distribution of defects, as measured from in-line inspection or other non-destructive techniques. More recent extensions, such as the modelling of fatigue damage [7] or the consideration of the microstructure in both trapping and mechanical behaviour [8], will also be presented.

References

[1] Hageman, T., Martínez-Pañeda, E. (2022) An electro-chemo-mechanical framework for predicting hydrogen uptake in metals due to aqueous electrolytes. *Corrosion Science* 208, 110681

[2] Fernández-Sousa, R., Betegón, C., Martínez-Pañeda, E. (2020) Analysis of the influence of microstructural traps on hydrogen assisted fatigue. *Acta Materialia* 199, 253-263

[3] Martínez-Pañeda, E., Golahmar, A., Niordson, C.F. (2018) A phase field formulation for hydrogen assisted cracking. *Computer Methods in Applied Mechanics and Engineering* 342, pp. 742-761

[4] Martínez-Pañeda, E., Harris, Z., Fuentes-Alonso, S., Scully, J.R., Burns, J.T. (2020). On the suitability of slow strain rate tensile testing for assessing hydrogen embrittlement susceptibility. *Corrosion Science* 163, 108291

[5] Kristensen, P.K., Niordson, C.F., Martínez-Pañeda, E. (2020) A phase field model for elastic-gradient-plastic solids undergoing hydrogen embrittlement. *Journal of the Mechanics and Physics of Solids* 143, 104093

[6] Kristensen, P.K., Niordson, C.F., Martínez-Pañeda, E. (2020) Applications of phase field fracture in modelling hydrogen assisted failures. *Theoretical and Applied Fracture Mechanics* 110, 102837

[7] Golahmar, A., Kristensen, P.K., Niordson, C.F., Martínez-Pañeda, E. (2022) A phase field model for hydrogen-assisted fatigue. *International Journal of Fatigue* 154, 106521

[8] Valverde-González, A., Martínez-Pañeda, E., Quintanas-Corominas, A., Reinoso, J., Paggi, M. (2022) Computational modelling of hydrogen assisted fracture in polycrystalline materials. *International Journal of Hydrogen Energy* 47, 32235-32251

Hydrogen permeation properties of stainless steels for SOEC/SOFC stack interconnects

S. Schewe[1], D. Kniep[1], A. Pereira[1],J.-F. Drillet[1], M.C. Galetz[1], W. Fürbeth[1],

[1]DECHEMA Research Institute, Frankfurt am Main/Germany

In the future, SOEC/SOFC systems can play an important role in the supply and conversion of energy from renewable, climate-neutral sources. For a further improvement of efficiency and lifetime, the various components need to be optimized. Interconnect materials must not only provide high electrical conductivity and creep resistance, but also thermal conductivity and mechanical stability for the individual stacks and entire cells. An important subject of investigation here is the influence of hydrogen in terms of its diffusion behavior through and its interaction with the various components, as this can cause internal oxidation during operation as well as hydrogen embrittlement during shutdown processes.

For this purpose, the hydrogen permeation properties of six stainless steels with different chromium contents (AISI 446, Crofer 22 APU, Crofer 22 H, AISI 442, AISI 410, P91) are investigated. Microstructural analysis, hardness measurements and hydrogen permeation tests are used to evaluate the materials. A Devanathan-Stachursky cell is used to study the diffusibility of hydrogen through the different alloys during charging as well as the effusion behavior after charging. The diffusion coefficients for the different processes are determined and used as a basis for comparison of the hydrogen traps in the different stainless steels.

Impact of hydrogen embrittlement on mechanical behavior of martensitic and bainitic steel.

A. D'Orazio[1], A. Oudriss[1], J. Bouhattate[1], C. Berziou[1], G. Lotte[1], S. Cohendoz[1], L. Leclair[2], B. Resiak[2], B. Cofino[2], X. Feaugas[1], (1) La Rochelle University LaSIE UMR CNRS 7356, Avenue Michel Crépeau, 17042 La Rochelle, France, (2) ArcelorMittal Maizières Research, Voie Romaine, 57280 Maizières-lès-Metz, France

Abstract

The impact of hydrogen on the mechanical behavior of a high strength steel grade was investigated in the present study. Two conditions were compared: tempered martensitic obtained after a quenching and tempering treatment, and bainitic obtained after an austempering treatment. In this purpose, microstructural characterization (EBSD, XRD, TEM) of two steel structures (bainite and tempered martensite) with the same composition was performed to identify different defects that can affect hydrogen solubility and thus hydrogen embrittlement (HE) [Frappart11, Creus16, Cupertino23]. In the meantime, cathodic polarization in sulfuric acid solution has been used to evaluate hydrogen solubility which appears lower in bainite than in martensite. Tensile tests at four different strain rates (10^{-3} to 10^{-6} s^{-1}) were performed on uncharged and charged specimens to decorrelate the effect of strain rates and hydrogen on the mechanical properties. At high strain rates, both structures presented the same HE sensibility, but with opposite behavior at low rates. Indeed, tempered martensite shows brittle fracture due to hydrogen, whereas it remains a ductile fracture for bainite. The difference of behavior between both structures will be discussed.

[Frappart11] S. Frappart, A. Oudriss, X. Feaugas, 2011. *Hydrogen trapping in martensitic steel investigated using electrochemical permeation and thermal desorption spectroscopy*. Scripta Materialia, vol. 65, no 10, p. 859-862.

[Creus16] J. Creus, A. Oudriss, R. Milet, C. Berziou, P. Girault, C. Rebere, S. Cohendoz, X. Feaugas, J.M. Sobrino, H. Morillot, 2016. *Influence of baking time at different temperatures on the hydrogen embrittlement of quenched and tempered*

martensitic (QTM) steel. NACE - International Corrosion Conference Series, 3, pp. 2229-2240.

[Cupertino23] L. Cupertino Malheiros, A. Oudrissa, F. Thébault, M. Piette, X. Feaugas, 2023. *Hydrogen diffusion and trapping in low alloy tempered martensitic steels*. Metallurgical Transaction A. to be published.

Mechanistic understanding of hydrogen uptake and diffusion in novel alloys for hydrogen service

Arunima Bhuvanendran Nair Jayakumari, University of Leicester,UK;NSIRC,TWI Ltd,Cambridge/UK

Hongbiao Dong,University of Leicester,UK,

Shiladitya Paul ,TWI Ltd,Cambridge; University of Leicester, UK

Hydrogen is heralded as the key fuel for a 'net zero' future. The production, storage and transportation of hydrogen is crucial for achieving the potential it offers. All of the above operations require materials for containment of hydrogen, often at high pressures. Although many materials exhibit remarkable mechanical and corrosion-related properties, interactions with hydrogen have raised questions regarding their suitability to service in hydrogen-containing atmospheres. In these situations, where hydrogen is present and can have a negative impact on the materials, especially when hydrogen embrittlement (HE) is a possibility, it is extremely important to synthesise materials that exhibit both excellent mechanical properties and HE resistance. High entropy alloys (HEAs) are a class of potential contender materials that may be taken into account. The crystal structure of HEAs indicate that the diffusion of hydrogen in such materials would be significantly lower than carbon steels. Research on the HE phenomena thus far has focused heavily on the intimate relationship between HE and the rapid diffusion of hydrogen. This would indicate that study of hydrogen diffusion in new materials is key to identifying materials, at least initially, which could be used for hydrogen containment. Nonetheless, further work would be required to quantify the HE behaviour in such materials.

The work presented in this paper used Devanathan-Stachurski Cell (DS Cell) for hydrogen diffusion measurements of a newly synthesised high entropy alloy. This allowed continuous measurement of hydrogen uptake in-situ. The diffusion coefficients calculated from the oxidation current values would help in understanding the mechanism and kinetics associated with the transport process. The preliminary examination and calibration of the DS Cell was carried out using AISI 1010 steel and the thermal dependence of hydrogen diffusion at different temperature (295K, 310K, 318K) were characterized.

The synthesised alloy's sensitivity to HE and its suitability as a material for hydrogen service requires further work, but initial characterisation is usually carried out using SEM/XRD (microstructural information) and hydrogen permeation behaviour.

This publication was made possible by the sponsorship and support of Lloyd’s Register Foundation [LRF].The work was enabled through, and undertaken at, the National Structural Integrity Research Centre (NSIRC), a postgraduate engineering facility for industry-led research into structural integrity established and managed by TWI through a network of both national and international Universities. The authors gratefully acknowledge the sponsorship and support of University of Leicester.

Study the Effect of Cathodic Plasma Electrolytic Nitriding on Corrosion and Hydrogen permeation resistance of 2.25Cr-1Mo ferritic steel

Ramachandran Chellappandian [a*], *Lakshman Neelakantan* [b], *Ilaksh Adlakha* [a]

[a] *Department of Applied Mechanics, Indian Institute of Technology Madras, Chennai 600036, India*

[b] *Department of Metallurgical and Materials Engineering, Indian Institute of Technology Madras, Chennai 600036, India*

Abstract

2.25Cr-1Mo ferritic steel is widely used as a structural material for pressure vessels, hydrogenation reactors, steam generators, and boilers in nuclear power plants and the petrochemical industry. This steel possesses excellent mechanical properties with good machinability and weldability, however, is prone to hydrogen embrittlement.

Surface modification techniques are extensively utilized to reduce the entry of hydrogen in steels to mitigate the hydrogen embrittlement problem. The cathodic plasma electrolytic nitriding (c-PEN) is a promising surface modification technique that provides enhanced mechanical and electrochemical properties due to the highly efficient energy utilization and reduced processing time.

In this work, the c-PEN treatment was adopted to modify the 2.25Cr-1Mo ferritic steel surface and assess the effect of the c-PEN layer on the corrosion and hydrogen permeation behaviour. At the onset, the c-PEN treated surface was comprehensively analysed to understand the phase composition and morphological features of the c-PEN layer. The c-PEN treated surface was found to possess a globular network morphology of iron nitride and expanded ferrite. The potentiodynamic polarization and EIS test results found that the c-PEN treatment created an electrochemically noble surface and a higher modulus of impedance value than the untreated steel. The hydrogen permeation test clearly showed that the c-PEN treated surface noticeably decreased the hydrogen permeability and diffusivity, as compared to the untreated steel. Overall, these findings demonstrate the applicability of c-PEN treatment to create a better surface that can withstand harsh environmental conditions.

Application of Electrochemical Microscopy with Blue Laser for Detection of Locally Diffusing Hydrogen in Iron

T. Haruna, H. Ishida, R. Kadowaki, H. Tani and Y. Hirohata

Department of Chemistry and Materials Engineering,

Kansai University, Suita, Osaka, JAPAN.

Abstract

Hydrogen embrittlement (HE) has been big issue for employing high-strength steels in humid environments, so that a lot of researches have been conducted to understand its mechanism and to discover prevention methods from it. It is well known that some cracks initiate locally in a high-strength steel suffering HE, and that a concentration of diffusible hydrogen strongly affects a susceptibility of HE. Since the evidences suggest that hydrogen exists and/or diffuses at the site where the cracks initiate, the techniques for detecting the sites have been developed so far. Although most of techniques such as hydrogen microprint method and tritium auto-radiography were already developed and employed ex-situ to detect locally-accumulated hydrogen, there are few techniques to in-situ detect the sites of locally-diffusing hydrogen. Therefore, our group have tried to detect the locally-diffusing hydrogen in-situ using a new system of electrochemical microscopy with blue laser.

The new system consisted of an optical microscope, an irradiation system of semiconductor-type blue laser, micro double cells for electrochemical hydrogen permeation test, a dual-potentiostat and a data acquisition system. A Fe plate specimen was set between the cells. The cells for hydrogen detection was filled with 0.1 $kmol \cdot m^{-3}$ NaOH solution and one side of the specimen was subjected to 0 V_{Pt}. The cell for hydrogen absorption was filled with sulfuric acid of pH 2 and the other side of the specimen was subjected to a constant cathodic current in order to absorb hydrogen. Thereafter, an anodic current of hydrogen detection side was monitored as a hydrogen permeation current. Under the situation, a fine blue laser was irradiated to the hydrogen detection side of the specimen to enhance the detection current. By scanning the laser, distribution of locally-diffusing hydrogen was obtained.

When a cathodic current was constantly applied to the absorption side of the specimen, a hydrogen permeation current was stably monitored on the detection side.

As maintaining the condition, the blue laser was irradiated on the detection side, and then a hydrogen permeation current increased. The laser-enhanced current increment increased with an increase in a hydrogen permeation current. This means that the spot detecting a larger laser-enhanced current increment is the spot having a larger hydrogen permeation rate. When the laser was one-dimensionally scanned on the detection side under the stable hydrogen permeation condition, the larger values of laser-enhanced current increment were monitored at some sites around grain boundaries of the specimen.

The research was conducted by financial support from Grant-in-Aid for Scientific Research (C) (18K04784) of JSPS, the ISIJ study groups “Comprehensive Understanding of Hydrogen-Passive Surface on Steels for Prevention of Hydrogen Embrittlement” from 2013 to 2015 and “Corrosion-induced Hydrogen Absorption to Steels” since 2018.

Stability of electrochemical hydrogen charging into iron in an aqueous solution containing NH_4SCN

Saya Ajito, Tomohiko Hojo, Motomichi Koyama, Eiji Akiyama, Tohoku University, Sendai/Japan.

High strength steels are widely used in various industrial fields such as automobiles and constructions. However, there is concern about the high susceptibility to hydrogen embrittlement of high strength steel. To investigate the hydrogen embrittlement susceptibility of the high strength steels, specimens are often subjected to electrochemical hydrogen charging in an aqueous solution prior to mechanical testing. It takes a long time to introduce hydrogen in the specimen uniformly when the specimen is relatively thick and/or the diffusivity of hydrogen in the material is low. However, the hydrogen absorption rate may change due to changes in solution composition caused by electrochemical reactions during hydrogen charging, which prevents quantitative control of introduced hydrogen content. In this study, the time dependence of the hydrogen absorption behavior into iron during electrochemical hydrogen charging in an aqueous solution containing NH_4SCN, which is commonly used to enhance hydrogen absorption[1], was investigated.

The material used in this study was a pure iron sheet. Both sides of the iron sheet were mechanically and electrically polished. The hydrogen absorption behavior into the specimen was measured using the Devanathan-Stachurski (DS) method[2]. One side of the specimen was electroplated with Ni to use as a hydrogen detection side. A Pt wire and a Hg/HgO electrode were introduced into the DS cell for hydrogen detection as the counter and reference electrodes, respectively. The electrolyte solution for the hydrogen detection was a 1 mol/L NaOH aqueous solution. The Ni-plated iron was polarized at a constant potential of +0.1 V vs. Hg/HgO. In the DS cell for the hydrogen charging side, a Pt wire and an Ag/AgCl electrode (SSE) were introduced as the counter and reference electrodes, respectively. The hydrogen charging side of the specimen was polarized at −1.6 V vs. SSE in a 0.5 M $NaHCO_3$ aqueous solution containing 3 g/L NH_4SCN and the hydrogen permeation current was measured for 200 h.

During the hydrogen charging, the hydrogen permeation current gradually decreased with time, indicating instability of the hydrogen charging condition. Ion chromatography analysis of the composition of the hydrogen charging solution after hydrogen charging indicated that the concentration of SCN^- ion drastically decreased and correspondently SO_4^{2-} ion was formed. In conclusion, the gradual decrease in the hydrogen absorption rate is attributed to the decomposition of SCN^- ion during hydrogen charging, resulting in a decrease in the effect of SCN^- ion to enhance hydrogen absorption.

References

1. S. Ajito, T. Hojo, M. Koyama, and E. Akiyama, ISIJ Int., 61 (2021) 1209-1214. http://doi.org/10.2355/isijinternational.ISIJINT-2020-551.
2. M. A. V. Devanathan and Z. Stachurski, Proc. R. Soc. A, 270 (1962) 90-102. http://doi.org/10.1098/rspa.1962.0205.

Acknowledgement

The authors are indebted to Mr. Kabasawa and Mr. Sakamoto (Analytical Research Core for Advanced Materials, Institute for Materials Research, Tohoku University) for solution analysis.

Influence of hydrogen on the texture evolution in pure nickel during cold-rolling deformation

Alfredo Zafra, Imperial College London, London/UK
Zachary Harris, University of Pittsburgh, Pittsburgh/USA
Livia Cupertino Malheiros, Imperial College London, London/UK
Emilio Martínez-Pañeda, Imperial College London, London/UK

Hydrogen is known to degrade the mechanical properties of pure metals and alloys. However, the fundamental mechanisms responsible for hydrogen-induced degradation are still being debated. Two primary candidates are hydrogen enhanced localized plasticity (HELP) and hydrogen enhanced decohesion (HEDE). Understanding these mechanisms is the first step towards the prevention of hydrogen damage and the generalization of H_2 as an energy carrier. Therefore, novel approaches able to assess the interaction between hydrogen atoms and microstructural parameters (dislocations, grain orientation) during deformation processes are becoming a necessity. Although some authors have already explored this path, their results are inconclusive due to the limited number of grains examined [1] or the low levels of strain attained [2]. The aim of this work is to elucidate the influence of hydrogen in the texture evolution (EBSD-based texture measurements) of pure nickel deformed by means of cold-rolling up to an equivalent plastic strain of 1.5.

The study was conducted using a 20-mm thick plate of annealed pure nickel (>99.9% wt. Ni). 25x20x2.5 mm^3 samples were EDM machined, ground and polished until 1 μm to ensure good surface quality. Afterwards, a group of samples was electrochemically charged with hydrogen in deaerated 3.5 wt. % NaCl solution at 70ºC. To do so, a three-cell electrode system with a Pt counter electrode and a silver/silver chloride (Ag/AgCl) reference electrode was used. A constant potential of -1.2 $V_{Ag/AgCl}$ was applied to the specimens using a Gamry 1010B potentiostat. The samples were charged for 11 days to ensure a uniform hydrogen concentration of ~15 wppm across their thickness. After charging, the samples were stored in liquid nitrogen to minimize hydrogen egress prior to cold-rolling. Next, uncharged and hydrogen pre-charged samples were cold-rolled at room temperature in a laboratory rolling mill operated at a speed of 5 rpm. Several pass-reductions were employed until attaining equivalent plastic strains of 0.1, 0.25, 0.5, 0.75, 1.0, 1.25 and 1.5. For hydrogen pre-charged

samples, the whole rolling process took less than 30 minutes, being the hydrogen losses negligible, as confirmed by means of FEM simulations. FEM was also employed to verify the strain level attained in the samples after each thickness reduction in cold-rolling. Cracking or damage was not detected on the surface of the hydrogenated samples after cold rolling, which had been previously identified as one of the main challenges of this novel approach to assess textural evolution in presence of hydrogen due to the significant reduction in ductility for hydrogen-charged Ni [3]. Finally, orientation imaging microscopy (OIM) was conducted *via* EBSD using a ZEISS Sigma 500 VP FE-SEM equipped with a Symmetry detector (Oxford Instruments) operated at an accelerating voltage of 25 keV and probe current of 4.0 nA. All the samples were cut, mounted in epoxy resin, ground with SiC grinding papers and polished with diamond slurries, finishing with 0.25 μm colloidal silica suspension. For each deformed specimen, OIM maps were collected from 5 different regions along the width of the sample at a magnification of 40x using a step size of 5 μm. Approximately 500 grains were evaluated per map, yielding a total of ~2500 individual grains examined per condition. Texture analysis of all orientation mapping data was performed using the MTEX software package for MATLAB [4], supported by ABAQUS simulations of the texture evolution.

The results derived from this work provide a better understanding of the microscale processes responsible for hydrogen-induced degradation.

References

[1] K. M. Bertsch, S. Wang, A. Nagao, and I. M. Robertson, Hydrogen-induced compatibility constraints across grain boundaries drive intergranular failure of Ni, Mater. Sci. Eng. A 760,May (2019) 58–67.

[2] Z. D. Harris, M. A. Ritzo, J. M. Schulte, S. R. Agnew, and J. T. Burns, Assessing the influence of hydrogen on texture evolution in polycrystalline nickel deformed under uniaxial tension, Scr. Mater. 188(2020) 238–243.

[3] Z. D. Harris, S. K. Lawrence, D. L. Medlin, G. Guetard, J. T. Burns, and B. P. Somerday, Elucidating the contribution of mobile hydrogen-deformation interactions to hydrogen-induced intergranular cracking in polycrystalline nickel, Acta Mater. 158(2018) 180–192.

[4] F. Bachmann, R. Hielscher, and H. Schaeben, Texture analysis with MTEX - Free and Open Source Software Toolbox, Solid State Phenom. 160(2010) 63–68.

A mechanistic interpretation for the initiation and propagation of hydrogen induced and assisted cracks

Margot Pinson, Aurélie Laureys, Tom Depover, Kim Verbeken

Department of Materials, Textiles and Chemical Engineering, Research group of Sustainable Materials Science, Ghent University, Belgium

Abstract

The goal of this work is to propose a mechanism for hydrogen-induced crack initiation valid for a wide range of steel grades based on a microstructural evaluation. Therefore, different types of steels with considerable microstructural variations were studied, at first: an ultra-low carbon (ULC) steel, a transformation induced plasticity (TRIP) steel an industrial pressure vessel grade. For all types of materials, initiation is found by either debonding or fracture of inclusions or at hard secondary phases present in the steel. Interface debonding leads to hydrogen induced crack initiation at non-metallic inclusions such as Al_2O_3 or MnS, while the initiation occurs at the hardest constituent in TRIP steel, i.e. the martensitic islands. The role of the martensite type has further been evaluated for generic high strength-low ductility Fe-C steels (0.2 wt.%, 0.4 wt.% and 1.1 wt.% carbon). Due to the brittle nature of these materials, a novel in-situ 3-point bending technique is developed to evaluate the proneness to hydrogen. The mechanism of hydrogen assisted cracking and degradation is studied by post-mortem SEM-EBSD fractography. Hydrogen causes a transition from a microvoid (Fe-0.2C), intergranular (Fe-1.1C) or mixed (Fe-0.4C) fracture surface appearance, to a hydrogen induced brittle cleavage fracture presence, linked to the embrittlement of the martensitic packets/blocks and the hydrogen enhanced decohesion (HEDE) mechanism. To increase the ductility, some ferrite can be introduced at the grain boundaries by the addition of Al. As a results, an almost purely intergranular fracture is detected for these materials. In this case, the ferritic film at the grain boundaries suffers from an interplay of the HEDE and hydrogen enhanced localized plasticity (HELP) mechanism, often termed as the hydrogen-enhanced-plasticity mediated decohesion.

Used of KPFM analyses to evaluate the cathodic hydrogen charging of a low duplex stainless steel

***Ingrid PRORIOL SERRE*[1], *Jean-Marc OLIVE*[2], *Gilles PECASTAINGS*[3]**

[1]*Univ. Lille, CNRS, INRAE, Centrale Lille, UMR 8207—UMET—Unité Matériaux Et Transformations, 59 000 Lille, France*

[2] *CNRS, Institut de Mécanique et d'Ingénierie, Université de Bordeaux, 33400 Talence, France*

[3] *CNRS, Centre de recherche Paul Pascal, Université de Bordeaux, 33600 Pessac, France*

Hydrogen and metallic materials

Duplex Stainless Steels (DSS) are used in industrial sectors such as petrochemicals, nuclear and gas transport for their corrosion resistance and mechanical properties. Moreover, the presence of hydrogen could induce not only a modification in the fracture mechanisms (and so a ductile to brittle transition), but also changes in the plasticity mechanisms. However, the duplex microstructure (austenite and ferrite) of DSS constitutes a real difficulty in understanding their mechanical behavior in the presence of hydrogen. Indeed, it is at the scale of the microstructure that the effects must be investigated: accommodation of the plastic deformation by each of the two phases, interactions of the effects taking place in each phase. But one of the key points is the localization of hydrogen in the material and in particular at the level of the two phases. The hydrogen localization and quantification depend on the diffusion during the charging, and after on the solubility of hydrogen in each phase but also on the hydrogen trapping sites. The microstructure (grain size, phases distribution and orientation) is an influential factor. Moreover, the macroscopic techniques do not allow either to quantify the presence of hydrogen at the level of the microstructure of a duplex steel or to localize the hydrogen.

Thus, the object of the present study is to show how KPFM (Kelvin Probe Force Microscopy) analyzes allow a better knowing and understanding of the hydrogen localization after the cathodic charging of a low duplex stainless steel DSS2304.

For the studied steel, the austenitic phase which embeds in the ferritic matrix is in the form of elongated islands in the rolling direction. Hydrogen was introduced into the steel by using an electrochemical cell with a cathodic current density of 10 mA/cm^2 in a 0.5M H_2SO_4 electrolyte containing 0.2 g/L As_2O_3 for different durations: 5 hours, 24 hours, 7 days. The hydrogen was charged perpendicularly to the rolling direction.

MFM (Magnetic Force Microscopy) and KPFM have been carried out at the surface of the hydrogen charging samples but also for cross sections of these samples.

The KPFM analyzes show the evolution of the surface potential with the presence of hydrogen. This depends on each phase and is more important for the ferrite. The KPFM analyses of the cross sections allow to estimate the penetration of hydrogen thickness into the steel. The austenite islands appear as barriers to the penetration of hydrogen into the thickness of the steel. The influence of a plastic deformation of the hydrogen penetration is studied by the used method and the effect of the microstructure on the hydrogen penetration and localization is discussed.

Real-time hydrogen visualization system with high spatial and temporal resolutions: Imaging the preferential hydrogen permeation at grain boundaries of pure Ni

Hiroshi Kakinuma, Saya Ajito, Tomohiko Hojo, Motomichi Koyama, Eiji Akiyama,
Tohoku University, Sendai/Japan

For a hydrogen society to be realized, it is crucial to develop structural materials with superior resistance to hydrogen embrittlement. However, the mechanism of hydrogen embrittlement in metals remains unclear. The difficulty of detecting hydrogen atoms makes it challenging to investigate the hydrogen embrittlement. There have been a limited number of techniques to analyze the smallest atom. To elucidate the hydrogen embrittlement mechanism, hydrogen imaging techniques with high spatial and time resolutions are required.

Silver decoration and hydrogen microprint techniques are common approaches to visualizing hydrogen distribution. They can image the hydrogen distribution on a metal surface with high spatial resolution, but the time-dependent hydrogen distribution cannot be visualized. SKPFM (scanning Kelvin probe force microscopy) measures the work function of the specimen by scanning an electrode near the specimen surface, resulting in the visualization of hydrogen distribution and its time variation with a micro- to nano-scale spatial resolution. However, it is still challenging to visualize the microstructure-dependent hydrogen distribution of a large observation area in real-time, because the spatial and time resolutions are governed by the scan rate of the electrode. In this work, we developed a hydrogen observation system that can visualize the microstructure-dependent hydrogen distribution in real-time.

The hydrogen distribution in pure Ni film and its time variation were analyzed using the hydrogen imaging system. A mixed solution of perchloric acid and acetic acid was used to electrically polish the pure Ni film. The final thickness of Ni film was 110 μm. In order to polymerize a polyaniline (PANI) layer on one side of the specimen, the specimen was polarized at a constant voltage of 1 V in a sulfuric acid-aniline solution for 200 s. The bare Ni side was used for electrochemical hydrogen charging. In 0.1 M NaOH, hydrogen charging was conducted at a current density of -1 mA / cm^2. The color change of PANI was observed *in situ* using an inverted microscope to analyze the hydrogen distribution in pure Ni during hydrogen charging. After hydrogen

charging, the specimen was immersed in a NaOH aqueous solution to remove PANI, and electron back scattered diffraction (EBSD) pattern analysis was performed to analyze the microstructure of Ni film.

After 20 h of hydrogen charging, the color of PANI partially changed. The grain boundary map obtained by EBSD revealed that the color-changed area of PANI corresponded to the grain boundaries of pure Ni. The hydrogen flux in pure Ni was found to be larger at around the grain boundaries than in grains. Furthermore, the preferential diffusion of hydrogen mainly occurred at around random grain boundaries, and almost no preferential diffusion of hydrogen was confirmed at around the corresponding grain boundaries. The atmospheric-control-free and inexpensive hydrogen imaging system succeeded to visualize the microstructure-dependent hydrogen distribution in pure Ni with high spatial and time resolutions. The system is expected to become a versatile approach for hydrogen visualization in metals.

References

[1] H. Kakinuma, S. Ajito, T. Hojo, M. Koyama, E. Akiyama, Real-time visualization of hydrogen distribution in metals using polyaniline: an ultrasensitive hydrogenochromic sensor, Adv. Mater. Interfaces, 9 (2022), 2101984.

[2] H. Kakinuma, S. Ajito, T. Hojo, M. Koyama, S. Hiromoto, E. Akiyama, Simultaneous observations of the corrosion behavior of an Fe sheet and the associated hydrogen distribution therein employing a hydrogenochromic sensor, Corros. Sci., 206 (2022), 110534.

[3] H. Kakinuma, S. Ajito, T. Hojo, M. Koyama, S. Hiromoto, E. Akiyama, *In situ* 2D mapping of hydrogen entry into an Fe sheet under a droplet of NaCl solution using a hydrogenochromic sensor, Int. J. Hydrog. Energy, 47 (2022), 38468-38476.

Alloy chemistry influence on microstructure and hydrogen permeability in Al-Zn-Mg-Cu-Zr 7xxx Alloys: Insights on the role of minor Cr and Ag additions

Chijioke Kenneth Akuata and Daniela Zander

RWTH Aachen University, Aachen, Germany

Motivation and objective

For decades, high strength 7xxx alloys have been the material of choice for structural applications in the aerospace industry due to their superior strength and generally good corrosion resistance properties. However, susceptibility to hydrogen environmentally-assisted cracking (HEAC) in humid air has been reported in some new generation alloys in certain temper conditions [1]. Crack growth rate has been correlated with alloy chemistry, which affects the final grain structure and composition of grain boundary (GB) precipitates [1, 2]. Furthermore, suppression of HEAC by partitioning hydrogen at intermetallic particles with high trapping energy and reducing the width of the precipitate free zone (PFZ) have been proposed in recent investigations [3, 4]. Hydrogen-induced failure mechanisms in aluminum alloys, such as Hydrogen Enhanced Decohesion (HEDE) and Hydrogen Enhanced Localized Plasticity (HELP) [5] are related to the interaction of atomic hydrogen with the microstructure, of which absorption and transport within the material are important processes. Hence, the goal of this study is to investigate the influence of minor changes in the alloy chemistry of a high strength 7xxx alloy by Cr and Ag additions, on the microstructure and hydrogen permeability and provide new insights on their influence on the environmentally-assisted cracking behavior.

Experimental approach

The materials used in this study are Al-Zn-Mg-Cu-Zr alloys within the composition range of the commercial AA7449 alloy. Alloy chemistry modification was done by adding 0.1 wt. % Cr and 0.3 wt. % Ag to 7449 to achieve 7449+Cr and 7449+Ag, respectively. The alloys were cast and processed in a similar manner up to the T76 aging condition. Microstructure characterization was performed by Electron backscatter diffraction (EBSD) and Transmission electron microscopy (TEM), while investigation of hydrogen permeability was done with a modified Devanathan-Stachurski (DS) permeation cell [6].

Results

EBSD shows differences in grain size and recrystallized fraction with minor Cr and Ag additions. Relative to only Al_3Zr dispersoids in 7449 and 7449+Ag, additional E-$Al_{18}Mg_3Cr_2$ dispersoids are formed with Cr addition which enhanced recrystallization inhibition in 7449+Cr. On the other hand, a decrease in the stacking fault energy by Ag resulted in a higher recrystallized fraction in 7449+Ag [7]. TEM characterization of GB microstructure equally shows differences in the size of GB η $Mg(Zn,Cu,Al)_2$ phase, suggesting differences in GB coverage, which increased in the alloys as follows: 7449+Ag < 7449+Cr < 7449. Furthermore, an unreported Ag-rich AlAgZnMgCu phase was observed in 7449+Ag, which is believed to have an influence on the chemistry of GB η $Mg(Zn,Cu,Al)_2$ phase. Hydrogen permeation results indicate an increase in H diffusivity as follows: 7449+Cr < 7449 < 7449+Ag, which strongly correlates with the observed microstructural differences. A model for the role of Cr and Ag addition on microstructure and H diffusivity is proposed and shown in Fig. 1 [8]. These results provide new insights on the understanding of HEAC behavior of high strength Al-Zn-Mg-Cu-Zr 7xxx alloys.

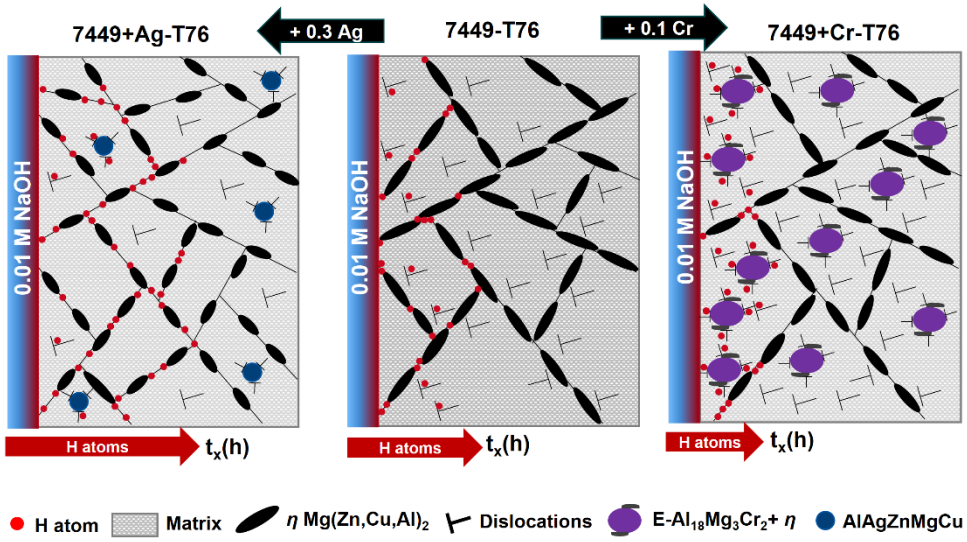

Fig. 1. Model of the role of Cr and Ag on microstructure and H diffusivity in 7449 [8]

References

[1] E. Schwarzenböck et al.: Corros. Sci., 171 (2020), 108701
[2] A. Garner et al.: Acta Mater., 202 (2021), 190 – 210
[3] Y. Xu et al.: Acta Mater. (2022), 118110
[3] H. Zhao et al.: Nature 602 (2022), 437 – 441
[5] S. Lynch: Corrosion Rev. 37 (2019), 377 – 395
[6] J. Ai and J. R. Scully: Corrosion, 69:8 (2013), 752 – 767
[7] H. Liu et al. J. alloys compd. 908 (2022), 164640
[8] C. K. Akuata and D. Zander, ICAA 18 (2022), Toyama Japan

Contribution of hydrogen to the embrittlement of Alloy 82 welds exposed to pressurized water reactor environment

A. Barou, Univ. Toulouse/CIRIMAT, Toulouse/France; E. Andrieu, Univ. Toulouse/CIRIMAT, Toulouse/France; P. Joly, FRAMATOME, Courbevoie/France; L. Laffont, Univ. Toulouse/CIRIMAT, Toulouse/France; C. Blanc, Univ. Toulouse/CIRIMAT, Toulouse/France

Literature data proposed that the decrease in mechanical properties (ductile tearing resistance) measured at low temperature (<100°C) for Alloy 82 welds after exposure to environmental conditions typical of pressurized water reactor (PWR) could be attributed to hydrogen. However, this has not been demonstrated and many unresolved issues remain. The objective of the present work is to evaluate the susceptibility to hydrogen embrittlement of Alloy 82 welds, and to contribute to a better understanding of the elementary mechanisms governing the interactions between hydrogen and Alloy 82 microstructure.

Experimental work was performed on deposited Alloy 82, representative of welds used in PWR plants, and obtained by GMAW process. Combination of different techniques of characterization at various scales (optical and transmission microscopes, electron probe microanalysis, microhardness measurements, electron backscattered diffraction) allowed the heterogeneous microstructure of the deposited alloy to be described and the representative elementary volume to be determined for further mechanical tensile tests. The susceptibility to hydrogen embrittlement of the alloy was studied by performing tensile tests on cathodically hydrogen-precharged samples, the results being compared to those obtained for non-precharged samples. Tensile tests were performed for both as-received samples and samples heat treated at 300 °C for 200h to consider the potential evolution in mechanical properties due to exposure to PWR conditions. Experiments were completed by an analysis of the fracture surfaces using scanning electron microscope. The evolutions in mechanical properties and fracture mode due to hydrogen precharging were compared to those observed for samples exposed to simulated PWR conditions in an autoclave (exposure to the simulated primary medium in autoclave at 300 °C for 200 h) and then submitted to a tensile test in the autoclave or in air. Measurements of the

hydrogen amount inside the cathodically precharged samples and those exposed to simulated PWR conditions were also performed using a melting method.

Results from tensile tests obtained for the cathodically hydrogen precharged samples allowed the influence of hydrogen on the mechanical properties of deposited Alloy 82 to be analyzed and quantified. Comparison with the results obtained for the samples pre-exposed to simulated PWR conditions allowed to demonstrate that such an exposure led to similar decrease in mechanical properties and evolution in fracture mode. Considering the results from hydrogen content measurements, this suggested a contribution of hydrogen to the embrittlement of Alloy 82 welds due to exposure to PWR conditions.

Understanding of the mechanisms of hydrogen embrittlement (HE) of nickel base alloys: A review of some recent advances on intergranular fracture

A. Oudriss, M. Landeiro Dos Reis, J. Bouhattate, X. Feaugas,
La Rochelle University, LaSIE CNRS UMR 7356, Avenue Michel Crépeau, 17000 La Rochelle, France

In order to provide elements of understanding to the mechanisms of hydrogen embrittlement (HE) of nickel base alloys, some implications of elasticity on hydrogen-defects interactions under tensile loading were questioned in relation with microstructural features (crystal orientation, grain-boundary, precipitation, etc.). Several investigations were conducted to evaluate the hydrogen-defects interactions and their consequences on the diffusion and trapping process, and on the mechanisms of fracture assisted by hydrogen. These investigations were based on several experimental and numerical approaches such as atomistic calculations, nano-indentation and electrochemistry pulse techniques and applied on nickel single crystals, nickel bicrystals, nickel polycrystals, IN718 AM and Waspaloy alloys. Based on Beremin's fracture model, the impact of hydrogen on intergranular mechanism is discussed in relation with the metallurgical state.

Fractographic study of quasi-static tensile tested, electrochemically hydrogen charged X70 pipeline steels

Jubica[1], Laura De Pue[2], Lisa Claeys[1], Wim De Waele[2], Stijn Hertelé[2], Tom Depover[1], Kim Verbeken[1]

[1]Ghent University, Department of Materials, Textiles and Chemical Engineering, Research group Sustainable Materials Science, Ghent, Belgium, jubica.jubica@ugent.be; lisa.claeys@ugent.be;tom.depover@ugent.be;kim.verbeken@ugent.be

[2]Ghent University, Department of Electromechanical, Systems and Metal Engineering, Soete Laboratory, Ghent, Belgium, laura.depue@ugent.be;wim.dewaele@ugent.be; stijn.hertele@ugent.be

Abstract: Fractography evaluates surface features of failed materials to understand causes of failure and subsequently enhance material performance. This work discusses different features identified on quasi-static tensile tested, electrochemically hydrogen charged X70 pipeline steel. Ex-situ quasi-static tensile testing is performed on smooth round bars at two conditions: in air as the reference condition and after electrochemical hydrogen charging in 0.5M H_2SO_4 electrolyte with 1g/l thiourea at a constant current density of 0.8 mA/cm^2. Scanning electron microscopy is used to characterize the fracture surfaces of the samples. A database quantifying hydrogen embrittlement indices is developed. This reveals trends in fracture behaviour with respect to microstructure and hydrogen condition applied. The macroscale features manifest as splits, delaminations, and fisheyes, whereas on the microscale dimples and quasi-cleavage areas are observed. The findings emphasize the correlation of microstructure to hydrogen-affected fractographic pattern recognition for the identification of possible failure mechanisms.

Keywords: Pipeline steels, Hydrogen embrittlement, Ex-situ quasi-static tensile test, Fractography

Introduction

The constant need for non-renewable energy resources, such as fossil fuels, is a consequence of our societal ever-increasing demand for energy. In recent years, this has had an impact on a global level, hindering smooth economic, social, technological, and environmental progress. The realization of a technologically sound solution for renewable resources is still under development. Consequently, there is a search for alternative energy carriers capable of efficiently complementing fossil fuels. Hydrogen falls into such a category as it possesses the potential to serve as an energy carrier. Most high-pressure gas and oil pipelines are, however, made of ferritic steels, which are known to be mechanically embrittled by atomic hydrogen [1], [2]. Replacing natural gas with hydrogen gas in current pipeline grid, which operate at high pressures, might inevitably accelerate the deterioration of mechanical properties [3]. It is crucial to also consider any structural variation in pipelines, including bends, cracks, or weld faults, as they can aggravate the interaction between hydrogen and materials. Besides, impressed current cathodic protection is frequently used to protect steels from corrosion. However, atomic hydrogen can as such also end up in the material's microstructure, equally resulting in a loss of structural mechanical integrity, especially when cathodic overprotection takes place [4]. Thus, during hydrogen transport, there are two potential hydrogen sources: the internal source, which refers to the hydrogen being transported and delivered, and the external source, due to cathodic (over-)protection. Both are expected to possibly contribute to the overall degradation of mechanical properties.

Consequently, it is crucial to investigate these pipeline steels to comprehend the reasons behind their failure, also when in contact with hydrogen. In this context, fractography analysis is crucial for examining and characterizing fractured pipeline steel surfaces. This work aims to study fracture patterns, traits, and characteristics of electrochemically hydrogen charged ex-situ quasi-static tensile tested X70 pipeline steel samples to understand the underlying causes and mechanisms of material failure due to hydrogen embrittlement. Scanning electron microscopy (SEM) technique is used to obtain detailed images of fracture surfaces.

Materials and Methods

L485MB ISO 3183 pipeline steel, referred as base material (BM) is investigated in this work. Table 1 gives the chemical composition obtained from optical emission spectroscopy(OES). Specimens were taken from the mid-thickness of a DN1000 pipe. Smooth round bars were machined in a longitudinal orientation. Figure 1 depicts the geometry of the specimens. Ex-situ quasi-static tensile testing was performed on specimens that were electrochemically charged with hydrogen at a constant current density of 0.8 mA/cm^2 in a 0.5M H_2SO_4 electrolyte containing 1g/l thiourea at a strain rate based on ISO 6892-1:2016 standards. Similar tests were done in air as a reference condition. After hydrogen charging, the specimens were preserved in a nitrogen bottle until tensile testing. The interval between the end of charging and putting in nitrogen was kept to a minimum and never exceeded 1 minute. Following the tensile test, the specimens were cleaned to analyse the fracture surface.

Table 1 Chemical composition of BM determined through OES

Wt%	C	N	Al	Si	P	S	Ca	Ti
BM	0.089	0.006	0.035	0.430	0.016	0.002	0.003	0.004
Wt%	**V**	**Cr**	**Mn**	**Ni**	**Cu**	**Nb**	**Mo**	**Fe**
BM	0.090	0.036	1.701	0.050	0.029	0.049	0.005	97.412

Figure 1 Tensile geometry of a smooth round bar (SRB)

Results and discussion

Figure 2a shows an SE image of fractured BM after hydrogen charging. Presence of delaminations is clearly seen in all conditions, indicating a widespread presence of cracks. A delamination is a separation within a material, resulting in fractures that spread throughout the sample. Splits are also seen which are often similar to delamination except that they are much smaller, thinner and are distributed on the fracture surface.

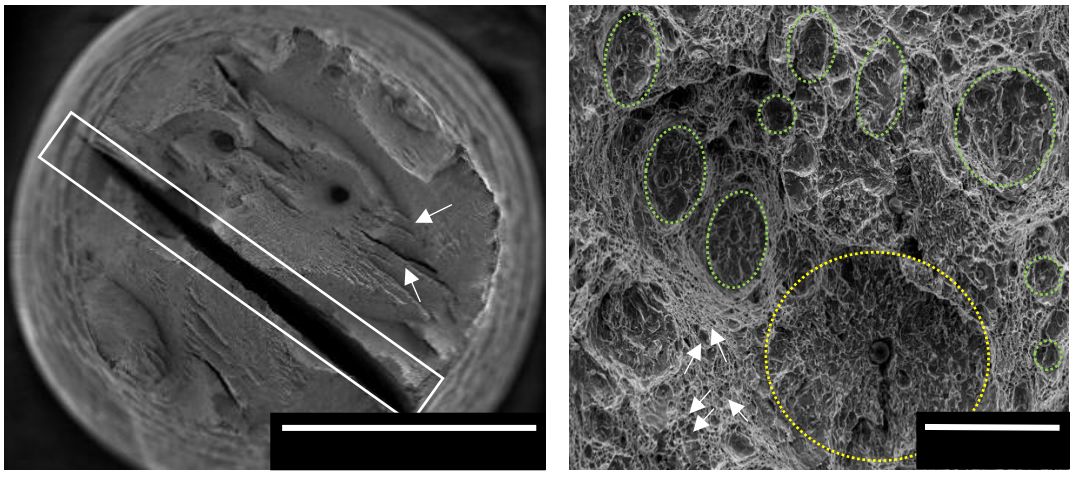

(a) (b)

Figure 2 SE image of BM SRB after hydrogen charging (a) fracture surface showing delamination (white box) and splits (white arrows) (b) fracture features like quasi cleavage areas (green ovals), fisheye (yellow circle), and dimples (white arrows)

Fracture features other than delaminations are also present such as fisheyes, quasi cleavage areas and dimples (Figure 2b). These features are accentuated by hydrogen embrittlement, a phenomenon that occurs when hydrogen atoms interact with the material microstructure and weaken it over time [5]. Fisheyes consist of elliptical or circular quasi cleavage areas centred around a defect such as an inclusion or an agglomeration of inclusions or microscopic splits [6]. Quasi-cleavage areas cover a larger portion of the fracture surface which is a characteristic feature of hydrogen embrittlement [7]. Apart from quasi-cleavage areas, microvoid coalescence

also takes place leading to the formation of dimples [6]. As more hydrogen interacts with the material, it becomes increasingly susceptible to fracture, resulting in more pronounced hydrogen-induced fracture features. To quantify the extent of hydrogen embrittlement experienced by these pipeline steels, a hydrogen embrittlement index is determined. The formula used for calculating the hydrogen embrittlement index (EI), as a percentage is given by:

$$EI = \left(1 - \frac{XHydrogen}{XAir}\right) \times 100\%$$

Where, X refers to the area reduction in air and hydrogen obtained from the ex-situ tensile tests.

The hydrogen embrittlement of BM SRB based on area reduction was calculated to be 21.43% using this formula.

Conclusions

Presence of hydrogen resulted in delaminations, and numerous fisheyes leading to embrittlement. Hydrogen amplified the formation and severity of delaminations and splits. Moreover, hydrogen presence introduced fisheyes, while dimples were still observed similarly as in reference tested specimens. The embrittlement index was measured to accurately quantify the level of hydrogen-assisted damage in this steel. A more in-depth study of several materials as well as welds is needed to understand the underlying mechanism for hydrogen embrittlement to occur in pipeline steels.

References

1. N. Nanninga, A. Slifka, and Y. Levy, Journal of Research of the National Institute of Standards and Technology, **115** (2010) 437.
2. C. San Marchi and B.P. Somerday, Sandia Report, 2012.
3. M. Kappes and T.Perez, Corrosion Reviews, **41** (2023) 319.
4. V. Olden, C. Thaulow, R. Johnsen, E. Østby and T. Berstad, Engineering Fracture Mechanics, **75** (2008) 2333.
5. H. Li, R. Niu, W. Li, H. Lu, J. Cairney, and Y.-S. Chen, Journal of Natural Gas Science and Engineering, **105** (2022) 104709.
6. E.D. Merson, P.N. Myagkikh, V.A. Poluyanov, D.L. Merson, and A. Vinogradov, Procedia Structural Integrity, **13** (2018) 1141.
7. May L. Martin, Jamey A. Fenske, Grace S. Liu, Petros Sofronis, and Ian M. Robertson, Acta Materialia, **59** (2011) 1601.

In situ Tensile Testing with Digital Image Correlation for Understanding and Predicting Maximum Susceptibility to Hydrogen Embrittlement of Super Duplex Stainless Steel

Cem Örnek[1], Bilgehan M Şeşen[1], Mustafa K Ürgen[1]*

[1]Istanbul Technical University, Department of Metallurgical and Materials Engineering, Istanbul, Türkiye

**Corresponding author: email: cornek@itu.edu.tr, tel.: +90 212 285 6864*

Super duplex stainless steel is a workhorse material in engineering applications where high strength, ductility and high corrosion resistance are required. Nevertheless, the harsh environments require cathodic protection, which has been shown to render duplex stainless steel with coarse austenite spacing (> 50 microns) brittle due to hydrogen-induced stress cracking. It has become understood that the austenite spacing matters and that the resistance to hydrogen embrittlement determines the material lifetime.

In this study, we used a novel approach to investigate hydrogen-induced microstructure degradation of grade 2507 super duplex stainless steel. By using in-situ and real-time microstructure imaging during electrochemical hydrogen charging while capturing mechanical stress and strain data, we were able to produce local strain maps of the microstructure and gain a unique insight into the mechanism of hydrogen embrittlement. First, we electrochemically charged with hydrogen miniature-sized flat tensile specimens (25 mm gauge length) and performed in situ tensile tests while imaging the microstructure using a digital microscope. Then, Digital Image Correlation was used to analyze the recorded micrographs to produce local strain maps.

The results have shown that the “diffusing” hydrogen atoms soften the microstructure, thereby reducing the tensile strength and toughness, causing

embrittlement. However, when the tensile test is done with pre-charged hydrogen for several days, mechanical softening occurs only in the austenite phase while the ferrite phase is hardened, also causing embrittlement. No matter how and how much hydrogen is charged, the super duplex stainless steel can plastically deform before fracture suggesting immunity to hydrogen embrittlement. Our findings provide important insights into the mechanisms of hydrogen-induced microstructure degradation and could potentially lead to developing new strategies to prevent hydrogen embrittlement.

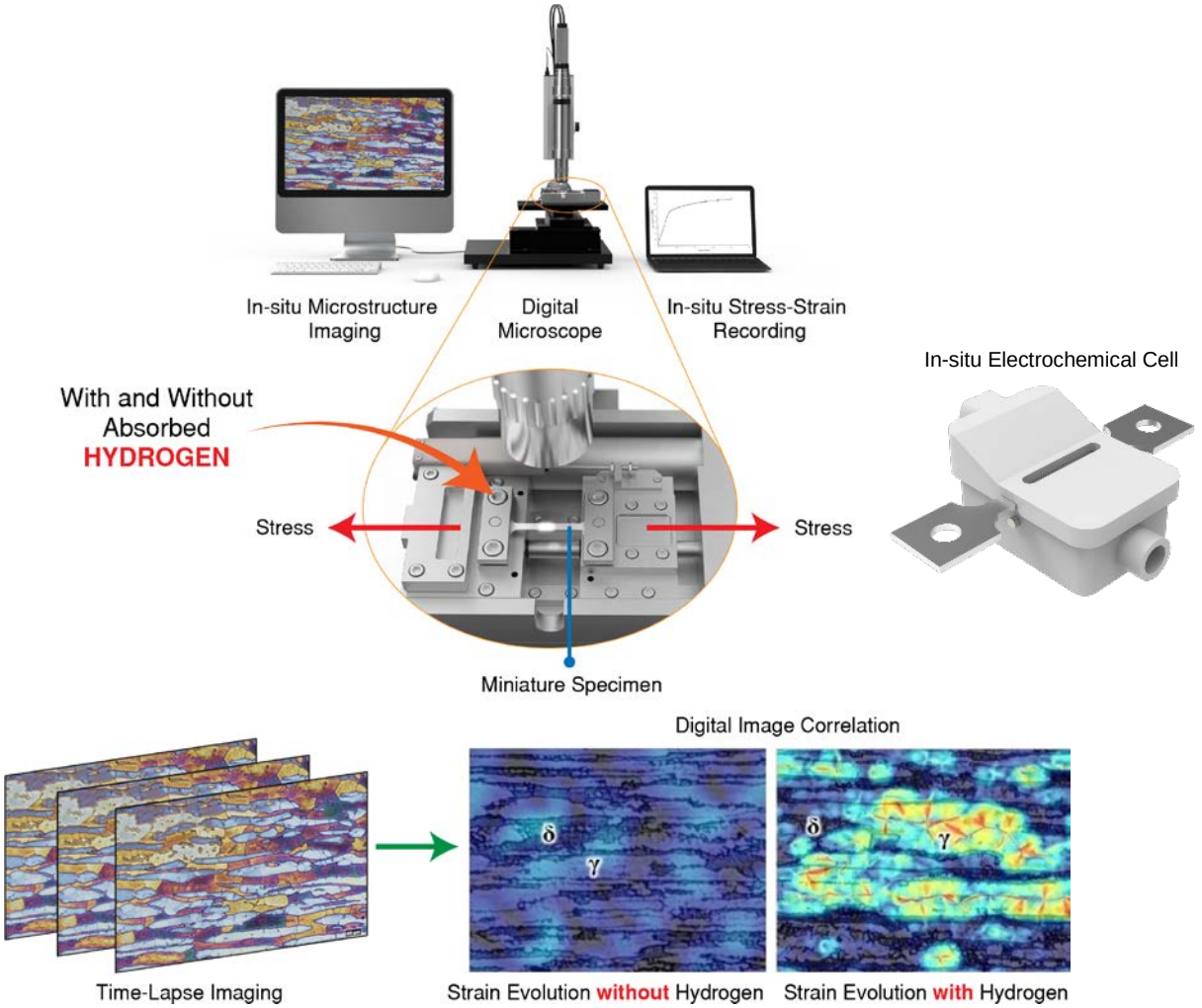

SSRT of austenitic grades for hydrogen gas service – influence of test methods on fracture appearance

Ulf Kivisäkk, Ulrika Borggren, Nian Zhou, Guocai Chai, Alleima EMEA AB, Sandviken/Sweden

Today hydrogen for use as fuel is widely discussed and stainless steels can be used for tubing and as fittings or for the boss in the gas tank as well as for tubing and fittings for filling stations. Earlier the susceptibility to hydrogen embrittlement of three austenitic stainless steels tested by different methods for use in high pressure hydrogen has been reported. Two versions of 316L stainless steel with high and low nickel content, Alleima 3R60 and Alleima 3R65 respectively as well the high strength Alleima HP 160 were tested, see Table 1. The tests included a variety of conditions, e.g., with and without hydrogen environment, in-situ charging and pre-charging, cathodic hydrogen charging, thermally charged hydrogen and high-pressure hydrogen gaseous charging. The high-pressure hydrogen gas SSRT was performed at -40°C with a hydrogen pressure of 850 to 875 bar. The results showed similar ranking for the three materials to hydrogen embrittlement. However, different metrics needs to be applied between the test methods. The 3R65 stainless steel with 11.5% Ni is prone to hydrogen embrittlement while 3R65 with 13% Ni and HP 160 showed good resistance. In this work a study regarding the difference in fracture mechanisms from the different testing methods has been made by investigating the fracture surfaces in SEM. The examination reveals that the overall fracture is similar but for 3R65 that is prone to hydrogen embrittlement, intergranular fracture was observed from testing in hydrogen gas, but intergranular and quasi-cleavage from testing with electrochemical charging, see Figure 2. The results indicates that even though different acceptance criterions need to be applied for the different test methods, the amount of hydrogen is enough for evaluating the resistance against hydrogen embrittlement for all methods.

Table 1. Chemical compositions of tested materials in weight-%.

Name	EN	C	Si	Mn	P	S	Cr	Ni	Mo	Cu	Nb	N	Ni_{eq}
3R65	1.4404	≤0.03	0.4	1.8	≤0.040	≤0.015	16.6	11.4	2.0	0.3		0.06	27.4
3R60	1.4435	≤0.03	0.4	1.5	≤0.040	≤0.015	17.2	13.0	2.6	0.3		0.05	29.6
HP 160	-	≤0.06	0.5	4.1	≤0.025	≤0.003	20.6	9.6	2.3	0.1	0.3	0.39	33.9

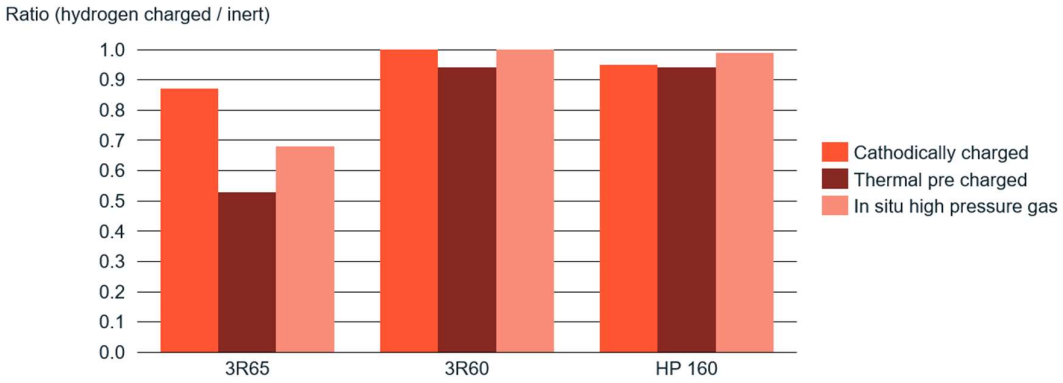

Figure 1. Results from SSRT testing as ratio reduction of areas between hydrogen charged and inert environment.

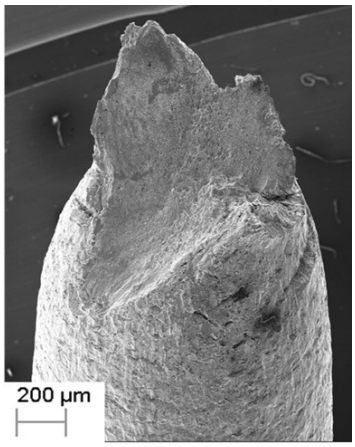

a) Electrochemical charging

b) 875 bar at -40°C

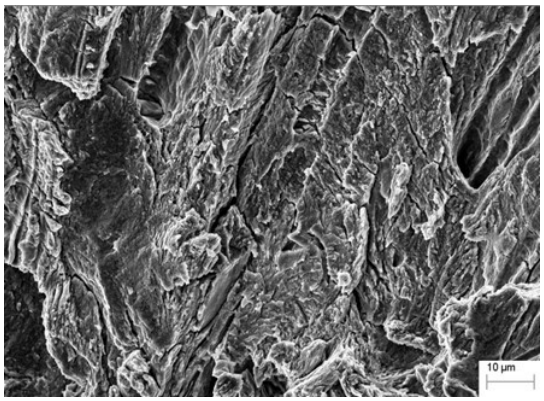

c) Intergranular and quasi-cleavage

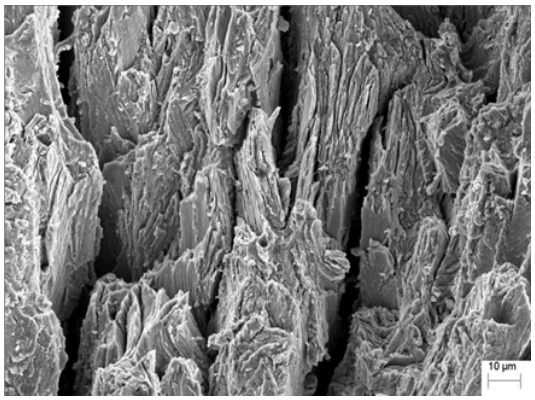

d) Intergranular

Figure 2. Fracture surface for 3R65, a) and c) from electrochemical charging and b) and d) from testing at 875 bar at -40°C.

Hydrogen and nitrogen contents effects on mechanical behavior of austenitic stainless steel

I. Hamdaoui, A. Oudriss, X. Feaugas

La Rochelle University, LaSIE UMR CNRS 7356, Av. Michel Crépeau, 17042 La Rochelle, France

Abstract

Hydrogen and nitrogen content effects on the mechanical behavior of the AISI 316L austenitic stainless steels were investigated. Several nitrogen alloyed austenitic stainless steel were uniformly hydrogen-pre-charged to around 80 wppm using cathodic polarization in deaerated NaOH + NH4SCN electrolyte. Specimens with different thicknesses (1, 0.5, and 0.2 mm) were used to perform the tensile test with a strain rate of 3 10-4 s-1. The stress-strain curve for hydrogen charged 0.2 mm specimen showed a decrease of ductility. However, a less remarkable effect was observed for thicker specimens due to the low hydrogen penetration far from the surface. Microstructural examination with the scanning electron microscope (SEM) revealed an intergranular cracking in hydrogenated specimens along with the formation of vacancy clusters. The non-charged specimen reports a decrease in the martensitic transformation induced by deformation by increasing nitrogen concentration. It is also observed that nitrogen increases yield strength and tensile strength. Furthermore, the triggering stress « σ(θ2) » increases with increasing nitrogen concentration due to the stabilization of the γ phase [1]. The nitrogen effect on charged specimens was also reviewed.

[1] C. Quitzke, C. Schroder, C. Ullrich, M. Mandel, L. Krüger, O. Volkova, M. Wendler, Evaluation of strain-induced martensite formation and mechanical properties in N-alloyed austenitic stainless steels by in situ tensile tests, Materials Science & Engineering A 808 (2021) 140930

Hydrogen in Steel for Bearing Applications

Claes Olsson, SKF, Göteborg - Sweden

Hydrogen is an element that has a strong impact on material properties. It is readily measurable in the laboratory, but more difficult to track in real applications. This is particularly true for bearing steel, which has a heat treatment optimized for hardness, and as a consequence is prone to brittle fracture already at low hydrogen contents (wt-ppm).

This talk will present a couple of applications where hydrogen has a significant influence on bearing performance. It will cover compressor operation in high hydrogen environments, how it is possible to monitor bearing performance, and some possible remedies to avoid hydrogen assisted fracture. The countermeasures may include microstructural stability, coatins as well as material selection.

Hydrogen embrittlement susceptibility of martensitic stainless steel AISI 431 with conventional and deep cryogenic treatment

Bojan Zajec [a], *Mirjam Bajt Leban* [a], *Patricia Jovičević-Klug* [b], *Bojan Podgornik* [c], *Andraž Legat* [a], *Tadeja Kosec* [a]

[a] Slovenian Building and Civil Engineering Institute, Ljubljana, Slovenia

[b] Max-Planck-Institute for Iron Research, Düsseldorf, Germany

[c] Institute of Metals and Technology, Ljubljana, Slovenia

Low carbon and high chromium martensitic stainless steel AISI 431 was prepared using two different heat treatment processes, conventional (CHT) and deep cryogenic treatment (DCT). To take eventual effect of austenitizing and tempering temperature into account, two different austenitizing (1050°C or 980°C) and tempering temperatures (480°C or 600°C) were selected in combination with or without DCT. Application of DCT for tested groups was performed after quenching and before tempering step by submersion of specimens into liquid nitrogen (holding temperature 77 K, cooling/warming rate 10 K/s and holding time 24 h).

Slow strain rate test (SSRT) with simultaneous cathodic hydrogen charging was selected as a method to assess the possible susceptibility to hydrogen embrittlement (HE). A relatively low-intensity hydrogen charging with constant current density of 0.1 mA/cm^2 in non-corrosive, slightly alkaline buffer solution exhibited clear reduction in the ultimate tensile stress. This reduction and therefore HE susceptibility was more pronounced for the tested group with 1050 °C / 480 °C austenitizing and tempering temperature. DCT treatment did not appear to have any impact on the mechanical properties, regardless of hydrogen presence. Fractographic analysis however showed clear evidence of HE in all hydrogen charged tensile specimens.

In the presentation, the overall results of SSRT and further results of fractography will be presented along with the proposed mechanism of hydrogen embrittlement. The possible impact of conventional and deep cryogenic treatment on HE sensitivity will be also discussed.

J-integral measurement following cathodic hydrogen charging as alternative approach to assess hydrogen gas susceptibility of steels

M. E. Gennaro, F. Todesco, A. Pontarollo, Eni VELAB, Venice, Italy

L. Torri, ENI MACO, M. Bianchi, V.S. Iorio, G. A. Nutricato, Eni, San Donato Milanese, Italy

Decarbonising is one of the goals that countries around the world have set for 2050, and all the Energy Companies have set an integrated strategy for a low-carbon future, where hydrogen represents one of the key decarbonization levers.

As energy vector hydrogen needs to be transported and stored. At atmospheric pressure, hydrogen has a lower volumetric energy density (~0.0108 MJ L^{-1}) than natural gas (0.0364 MJ L^{-1}): this means transmitting hydrogen at high pressures using large-size pipelines to be financially competitive.

On the other hand regarding hydrogen transport, high pressures and large sizes require high-strength steels for pipeline material. However, high-strength steels are more susceptible to hydrogen damage.

ASME B31.12 is the only existing code regarding pipelines for hydrogen service and poses strict limits to the maximum operating pressure and the design pressure depending on steel grade and material properties characterization, both for new and repurposed pipelines. ASME B31.12 code requires determining K_{IH} (the threshold fracture toughness in presence of Hydrogen) and to characterize material fatigue behavior, with long-term testing (1000h) in high-pressure gaseous environments. This is very time consuming, moreover, only few laboratories can perform such tests.

An alternative is proposed which envisions the use of electrochemical techniques. Hydrogen atmosphere is simulated by generating hydrogen molecules on the surface of the specimens in an electrochemical cell and diffusible H_2 average concentration in metal lattice is estimated by electrochemical oxidation to obtain hydrogen outgassing current. Fracture mechanics compact tension specimens are cathodically charged in an aqueous solution, providing hydrogen with a chemical activity comparable to the one in a pressurized gaseous atmosphere. Fracture

mechanics tests are then performed to determine J_c fracture toughness. This property is assessed in samples both in the as-is and in the electrochemical hydrogen-charged conditions.

The electrochemical charging allows a pre-characterization of materials so that the extensive and demanding tests required for their full qualification are applied only to the most promising ones with low probabilities of failure.

Tests were performed on six different steels API 5L X60 Q&T and TMCP, and API 5CT L80-1, J55, T95, and P110, with two charging levels. Results showed that low charging conditions cause measurable effects only on higher strength materials, while the high charging conditions can be critical for more materials.

Abstract

High temperature hydrogen attack is a damage mechanism that occurs in critical steel components in petrochemical plants and refineries when the hydrogen penetrates the steel and reacts with the carbides within to produce pores containing methane. With the motivation of understanding the role of carbide stability on the reaction with hydrogen, samples of a classic $2\frac{1}{4}$Cr-1Mo steel were subjected to a variety of heat treatments that generate a corresponding variety of precipitates, prior to exposure to high-pressure hydrogen in an autoclave. Using quantitative carbide, porosity and microstructural characterisation, it has been possible to demonstrate the roles of four variables: (a) the carbon residue present in the ferrite; (b) the non-equilibrium chemical composition of carbide; (c) the fraction of the carbide that is closest to the thermodynamic equilibrium state and (d) the initial microstructural state, i.e., whether it is martensitic or bainitic prior to heat treatment.

Keywords: hydrogen attack, carbides, synchrotron diffraction, tempering, non-equilibrium.

Hydrogen retention in fusion components submitted to thermal loadings

S. Bian, Y. Charles, J. Mougenot, Université Sorbonne Paris Nord, Laboratoire des Sciences des Procédés et des Matériaux, LSPM, CNRS, UPR 3407, F-93430, Villetaneuse, France

X. Bonnin, T. Wauters, R. Pitts, ITER Organization, Route de Vinon-sur-Verdon, CS 90046, 13067, St. Paul Lez Durance, France

Running a fusion reactor generates important heat and particles fluxes on its inner wall materials. The retention of the hydrogen isotope tritium, used as part of the fusion fuel, in the wall components is of particular concern as it may pose a safety risks. Firstly, the transport of hydrogen through the plasma-facing components, leading to an inventory build-up, may present a contamination risk of the surrounding infrastructure in case of an accidental release. Secondly, hydrogen may affect the mechanical behavior of the materials, and especially their resistance to failure (hydrogen embrittlement). To quantify these risks, it is necessary to develop an improved understanding of hydrogen transport in plasma facing materials through numerical simulation tools.

In this work, we focus on a key part of the ITER divertor, the multi-material and actively cooled monoblocks that will be subject to the most intense cyclic loadings (particle and heat fluxes). The hydrogen that diffuses through the component can be trapped on material defects. These vacancies can follow, on the one hand, from transient heat transfer processes resulting in an expansion mismatch at dislocations and plasticity. The intense particle loads at the surface, on the other hand, create vacancies also. Vacancies diffuse and react to create vacancy clusters, which are understood to be the precursors for the formation of dihydrogen bubbles.

A 3D modeling of this component is proposed, using the Abaqus Finite Element software extended with newly developed User Subroutines. Hydrogen transport and trapping is modelled based on the classical Fick law, modified to account for trapping in the presence of (transient) thermomechanical fields. The vacancy mobility and clustering are based on reaction diffusion equations. The computations estimate the time evolution of the diffusive and trapped hydrogen in the monoblock.

Workshop: Hydrogen and metallic materials

Hydrogen determination in welded metallic materials -necessity and challenges

Michael Rhode, Bundesanstalt für Materialforschung und -prüfung (BAM), Berlin, Germany

Thomas Kannengießer, Bundesanstalt für Materialforschung und -prüfung (BAM), Berlin, Germany

In the course of tomorrow's hydrogen-based energy transition, the construction of the corresponding infrastructure will play a central role. The majority of materials used to date are typically welded for component fabrication. In that context, steels are widely applied and can be prone to hydrogen embrittlement. For the evaluation of any hydrogen effect on, for example, the mechanical properties of a welded metallic material, the hydrogen content must be precisely determined. According to ISO 3690, carrier gas hot extraction (CGHE) can be used. In addition to the pure quantification of hydrogen, thermal desorption analysis (TDA) with varied heating rates can be used to determine and evaluate the bonding state at microstructural defects in the material. For both techniques, experimental and measurement influences have to be considered, which have a great effect on the result. For CGHE, for example, ISO 3690 suggests different sample geometries as well as minimum extraction times. The present study summarizes results and experiences of numerous investigations with different sample temperatures and geometries (ISO 3690 type B and cylindrical TDA samples) regarding: the influence of the sample surface (polished/welded), measurement accuracies depending on the sample volume. In particular, a deviating extraction temperature to the set temperature, can significantly falsify the measurement results. Based on the results, methods are shown to quickly reach the desired extraction temperature without having to physically interfere with the measurement equipment. This serves to substantially improve the reliability of hydrogen measurement through increased signal stability and accelerated hydrogen desorption. In general, an independent temperature measurement with dummy samples for the selected heating procedure is advisable to exclude possible unwanted temperature influences already before the measurement. In addition (and way more important), the methods described can be transferred directly to industrial applications.

On the aspect of time in testing strategy for hydrogen embrittlement in martensitic steel

Vatter, J.M.; Gosheva, O.; Reitz, R.; Oechsner, M., Center for Structural Materials TU Darmstadt, Darmstadt Germany

It is discussed in literature what influence different material properties may have on the susceptibility and risk of hydrogen embrittlement. However, test parameters, such as the source of hydrogen, in-situ vs. ex-situ charging, loading profiles or strain rate may itself influence the test outcome and therefore impede their comparability and interpretation. In this study, slow strain rate tests (SSRT) were performed on notched tensile samples from a martensitic high strength steel (> 1200 MPa) under in-situ cathodic polarization in a 0.1 M NaOH solution. To address the role of the time factor in the experiment, the cross-head speed is varied between 0.2 mm/s and 0.00002 mm/s in accordance with current regulations. Additionally, same test procedure was applied to the samples pre-charged with hydrogen prior to the test and samples with a delay in the cathodic polarization relative to the application of mechanical loading. Results are showing that time given for hydrogen absorbtion and diffusion in 100 h pre-charging is neglectable compared to the effect of strain rate.

A nano-sized NbC precipitation strengthened CoCrFeNi high entropy alloy with superior hydrogen embrittlement resistance

Heng Chen[1], Yunhua Huang[1], Hong Luo[1], Lin Lu[1], Xiaogang Li[1]

[1] Institute for Advanced Materials and Technology, University of Science and Technology Beijing, Beijing 100083, China

FCC high entropy alloys (HEAs) represented by CoCrFeNi HEA tend to be insufficiently strong and susceptible to hydrogen embrittlement (HE), which extremely restrict their pratical applications. In this study, an equiatomic CoCrFeNi HEA with high strength and excellent HE resistance was developed by the precipitation of nano-sized niobium carbide (NbC) during thermo-mechanical processing. A comprehensive microstructure characterization using various advanced microstructural characterization techniques such as scanning electron microscopy (SEM), electron backscattering diffraction (EBSD) and transmission electron microscopy (TEM) was performed. And the mechanical properties and HE susceptibility were evaluated using the slow strain rate tensile test. NbC precipitates make the CoCrFeNi HEA obtain extraordinary mechanical properties via pinning the movement of dislocation. With the precipitation strengthening also comes the grain refinement strengthening. Furthermore, the coherent/semi-coherent NbC interfaces are regarded as reversible hydrogen traps based on thermal desorption analysis, thereby increasing the tolerance of HEA to dissolved hydrogen. Despite owning higher strength than the unreinforced one, the precipitation strengthened HEA still manifests superior HE resistance due to NbC preventing hydrogen transport by dislocations effectively. Our findings suggest that dispersing intensive nano-sized NbC precipitates in the matrix is an appropriate strategy that allows for designing hydrogen-resistant HEAs with high strength.

Keywords

High entropy alloy; NbC precipitate; Precipitation strengthing; Hydrogen embrittlement

Hydrogen trapping and HIC susceptibility of X70 grade acid-resistant submarine pipeline steels via trace-Mg treatment

Feng Huang[1], Qiyun Wen, Hu Xiao, Yunfeng Xu, Qian Hu, Jing Liu

a The State Key Laboratory of Refractories and Metallurgy, Wuhan University of Science and Technology, Wuhan 430081, Hubei, China;

Abstract

Hydrogen induced cracking is one of the biggest service risks faced by high-strength acid-resistant submarine pipeline steel. In this work, we reported a low-carbon, low-cost and high-efficient method for remarkably improving HIC resistance of the high-strength acid-resistant submarine pipeline steels by trace-Mg treatment. The non-metallic inclusions steels were obviously refined, softened, spheroidized and dispersed by trace-Mg treatment, the modified core-shell or like core-shell structure inclusions had a larger critical size for HIC initiation and a higher saturated hydrogen concentration, and then effectively trapping more hydrogen, dispersing hydrogen pressure and reducing the diffused hydrogen content, thus effectively improving the HIC resistance. With the further increasing of Mg contents, the inclusion modification would be weakened, the hydrogen trapping efficiency decreased, and the HIC susceptibility of the tested steel increased again. In the research range, the tested steels treated with 4ppm Mg present the lowest HIC susceptibility.

Keywords: High strength submarine pipeline steel; Trace-Mg treatment; Non-metallic inclusions; HIC susceptibility; Hydrogen trapping efficiency

1 Introduction

In recent years, Mg treatment and other oxide metallurgy technologies have attracted the attention of researchers. Micro/nanoscale inclusions with deep hydrogen trap functions, sufficient quantities and dispersion distributions in steel can be obtained via Mg treatment, and the low temperature toughness of heat -sffected zone (HAZ) the hydrogen-induced cracking (HIC) susceptibility of high-strength steel has dramatically improved. In this study, a batch of X70 grade acid resistant submarine tested pipeline steels with Al-Ti deoxidation and different trace-Mg contents were smelted and rolled. The HIC susceptibility of tested steels were evaluated, and the diffusion and trapping

[1] This work was supported by the National Natural Science Foundation of China (No U21A20113) and Natural Science Foundation of Hubei Province of China (NO. 2021CFA023).

kinetics of hydrogen in steel were analyzed. The hydrogen trapping efficiency and HIC susceptibility of high strength submarine acid resistant pipeline steel via trace-Mg treatment was systemically discussed. It is anticipated to provide theoretical basis and data supporting for the application of trace-Mg treatment in industrial production.

2 Result and Discussion

Mg could promote the heterogeneous nucleation of ferrite, making the grain furtherly refinement and the “core($MgAl_2O_4$)-shell(MnS.TiN)” inclusions fromation. For the “core-shell” inclusions, not only the interface of core and shell, but also the interface of shell or core and the steel matrix can trap hydrogen atoms effectively, improving hydrogen trapping efficiency and increasing its critical hydrogen concentration, and then lower HIC susceptibility (Fig.1).

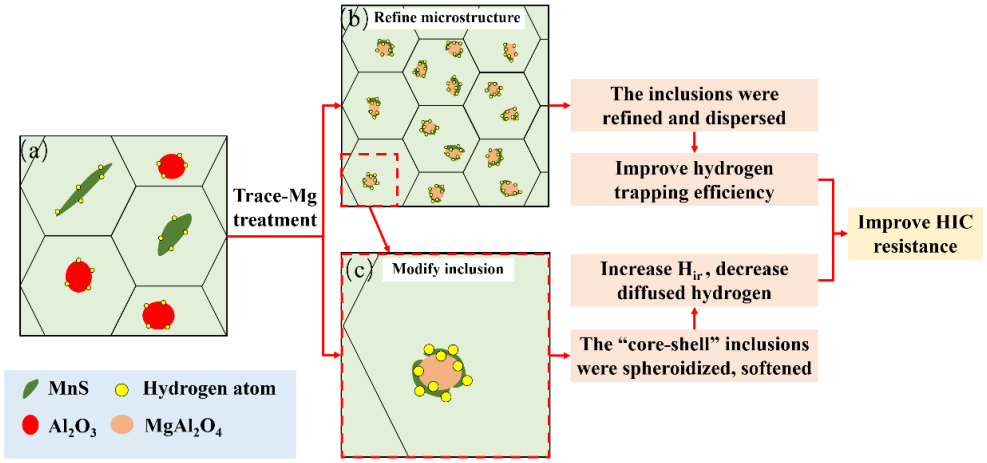

Fig. 1. Schematic view of the effect of “core-shell” inclusions on hydrogen trapping and HIC susceptibility of the steels treated with or without trace-Mg.

4. Inclusions

(1) With trace-Mg treatment, the microstructure of the tested steels was obviously refined; Most composite inclusions were of “core” of $MgO{\cdot}Al_2O_3$ and “shell” of MnS and/or TiN structure and appearing dispersed distributed.

(2) With the trace-Mg treatment, the tested steel with more refined, spheroidized and dispersed “core-shell” structure inclusions had the lowest $J_\infty L$ and D_{app} and highest C_o and N_T, the highest hydrogen trapping efficiency.

(3) With the trace-Mg treatment, the inclusions in the steel micro-nano and dispersed “core-shell” structure inclusions could provide more sites to trap hydrogen, increased hydrogen trapping efficiency and the saturated hydrogen concentration in the steel, and then improved HIC susceptibility remarkably. 4ppm should be a better appropriate Mg addition content for HIC improving.

The Origin of Hydrogen Embrittlement

John Campbell

School of Metallurgy and Materials
Faculty of Engineering
University of Birmingham, UK
jc@campbelltech.co.uk

Abstract

During casting of our engineering metals, including light alloys, steels and superalloys (but with a few interesting exceptions) it is not widely known that the turbulence of pouring in air (and 'vacuum') folds over the oxide on the surface of the melt, forming doubled-over films in suspension. The double films do not bond, therefore forming effective cracks. Turbulent pouring fills the liquid with cracks. The cracks, known as 'bifilms', are subsequently frozen into the solid. The bifilms remain as a population of pre-existing cracks, mainly located in grain boundaries. The precipitation of carbides in steels can force open the bifilms to form enlarged sinks. At low hydrogen concentrations the bifilms act as sinks to reduce the degradation by hydrogen, but at higher concentrations, act as cavities which hydrogen progressively pressurizes to first produce blisters, then eventual failure.

Key Words: hydrogen embrittlement; bifilms; cracks; blisters.

137 words abstract.

Repair welding of in-service hydrogen pipelines

Michael Rhode, Bundesanstalt für Materialforschung und -prüfung (BAM), Berlin, Germany

Thomas Kannengießer, Bundesanstalt für Materialforschung und -prüfung (BAM), Berlin, Germany

In the course of tomorrow's hydrogen-based energy transition, the construction of the corresponding infrastructure will play a central role. In that context, large diameter long-distance transmission pipelines for hydrogen will be the backbone in the European Union with service pressures from 70 to 90 bar (e.g., depending on national regulations). It is a major goal to re-dedicate the existing LNG infrastructure despite the necessity of new pipelines. From that point of view repairing of such transmissions pipelines via welding can be necessary. For the LNG infrastructure, it is state of the art that repair welding is conducted at pipelines under service, i.e., the LNG is still flowing as pressurized gas in the steel pipes, see Figure 1.

Figure 1: On-site repair welding of LNG pipeline under service conditions (© Ontras Leipzig, Germany)

The reason is that a shut-down of large diameter pipelines is not so easy or sometimes impossible. In fact, as long no oxygen enters the pipeline, there would be any

combustion or (in the worst case) explosion. At the moment, it is entirely open if current repair welding procedures for LNG pipelines can be transferred to pure hydrogen pipelines. In opposite to LNG, hydrogen can be way easier absorbed to the pipeline steels and diffuses through the material. If it accumulates in susceptible regions, i.e., in the welded joint, hydrogen assisted embrittlement could occur. The planned welding procedure requires a so-called preheating and maintenance of the weld joint of up to 300°C for several hours. This temperature is way higher compared to the typical service temperature of max. 40 to 50°C at operational pressures of 100 bar. In accordance to API 941, these low-alloyed pipeline steels are subjected to short-term service loads, which they are not designed for. For that reason, a collaborative project between BAM and DVGW (German Association for Gas and Water professions) was initiated in 2022 to answer the following questions by experiments and numerical simulation of:

- How many hydrogen is additionally absorbed during the heating of the material to max. 300°C under remaining operational pressures?
- Is the hydrogen concentration sufficient to reach a critical condition?
- Which material and weld microstructure is the most susceptible?
- Is there a significant difference in the repair welding behavior of LNG pipelines that had been already in use for long-term?
- Which welding parameters and joint dimensions must be ensured for safe repair welding repair of typical pipelines?

The final aim of this project is the publication of a recommended practice for repair welding of in-service hydrogen pipelines. For that reason, the present study gives an overview on:

- the current practice in repair welding of in-service pipelines,
- the industrial importance of this topic for the hydrogen-based energy transition and
- summarizes first results.

Pitting Corrosion Resistance and Passivity of Laser Powder Bed Fusion (LPBF) Produced Type 316L Stainless Steel Microstructure

Yiqi Zhou[*1], Dirk Lars Engelberg[2]

1. Beijing Advanced Innovation Center for Materials Genome Engineering, Institute for Advanced Materials and Technology, University of Science and Technology Beijing, Beijing 100083, China

2. Metallurgy and Corrosion, Department of Materials, The University of Manchester, Manchester, M13 9PL, Manchester, UK

Bipolar electrochemistry was used to assess the pitting corrosion susceptibility and resistance of LPBF manufactured type 316L stainless steel. Application of bipolar electrochemistry allows simultaneously to obtain the anodic and cathodic corrosion behaviour. The nucleation and growth of pitting corrosion can be measured along the oxidation edge in the Cl^- containing environment. LPBF 316L stainless steel has a cellular microstructure and small grain size, showing better pitting corrosion resistance than wrought type 316L stainless steel. The surface of the LPBF type 316L stsainless steel was further analysed to reveal passive film characxteristics with electrochemical impedance spectroscopy (EIS) and standard 3-electrode potentio-dynamic polarisation tests. Differences in the passivation and re-passivation characteristics of wrought vs. LPBF produced microstructure are discussed.

Effect of heat treatment on the microstructure and corrosion performance of additively manufactured 316L stainless steel prepared by different manufacturing methods (L-PBF & L-DED): A comparative study

Reynier I. Revilla, Iris De Graeve

Vrije Universiteit Brussel (VUB), Department of Materials and Chemistry, Electrochemical and Surface Engineering (SURF), Pleinlaan 2, 1050 Brussels, Belgium

Metal additive manufacturing (MAM), a process by which complex multifunctional metal parts are produced in a layer-by-layer fashion, is characterized by highly localized melting and rapid solidification, which promotes the formation of a very fine microstructure with unique directional growth features. Numerous studies have been dedicated to investigating the influence of the unique microstructure generated during MAM on the corrosion performance of these materials. Moreover, due to the build up of internal stresses during MAM and the formation of non-equilibrium microstructure, several heat treatments practices have been explored for additively manufactured (AM) metal parts. However, these heat treatments are known to greatly modify the microstructure of the alloy, and therefore their corrosion behavior and performance. Several studies have also been conducted analyzing the effect of heat treatment on the microstructure and corrosion behavior of AM materials, and various and contradictory results can be found in the literature. Furthermore, the majority of these studies have been dedicated to metal parts fabricated by laser powder bed fusion (L-PBF) technique, while a very limited number of investigations have been conducted on alloys prepared by directed energy deposition (DED). Besides differing in the process parameters (range) and manufacturing setup used, these techniques also differ in the intrinsic cooling/solidification rates induced during the manufacturing process, which prompts the formation of intrinsically different microstructures. This work presents a systematic characterization of 316L stainless steel specimens fabricated by different MAM techniques (L-PBF and L-DED). It explores the effect of heat treatment on the microstructure and corrosion behavior of these specimens, bringing insights on the role of the formed inclusions on their corrosion performance. The results showed that,

although DED specimens are characterized by a high density of Mn-silicate and some Mn-chromate inclusions, its corrosion resistance is higher than that of the wrought material. The corrosion resistance of the L-PBF samples is the highest of all the samples analyzed due to the higher degree of refinement in their microstructure. Heat treatments of up to 1000 degree Celsius did not influence much the microstructure of the samples and, therefore, maintained their corrosion resistance similar to that of the non-heat treated specimens. For heat treatments at temperatures higher than 1000 degree Celsius, a significant coarsening of the inclusions and an increase in the density of MnS containing inclusions was evidenced, which greatly affected the corrosion resistance of the specimens.

Study of the corrosion behaviour of 316L stainless steel lattices fabricated by Laser Powder Bed Fusion.

J. Bedmar, S. García-Rodríguez, N. Abu-warda, B. Torres, J. Rams

Área de Ciencia e Ingeniería de Materiales, ESCET, Universidad Rey Juan Carlos, C/ Tulipán, s/n, Móstoles, 28933, Madrid (Spain)

Lattice structures show a good combination of lightness and mechanical properties. Also, lattice structures stand out for their heat transfer properties, being very interesting in their application in, for example, solar systems. In the case of the 316L stainless steel (316L ss) lattices, in most applications, are used to reduce the weight while complying with high compression resistance and energy absorption. However, the corrosion behavior of the 316L ss lattice structure is different to those of bulk alloys and should be completely characterized. In this study, 316L ss lattices with diamond geometry have been fabricated by Laser Powder Bed Fusion (LPBF) using two types of lasers: fiber laser and CO_2 laser. Also, bulk parts were fabricated by LPBF to complete the corrosion tests. Austenitic columnar grains appeared in both types of lattices, like in the case of the bulks. However, these grains were bigger in the case of the structures fabricated by CO_2 laser. Open Circuit Potential and Polarization Resistance tests showed that the bulk samples have better behaviour than the lattices. These results were also confirmed by the Tafel tests. In addition, fabricating the parts with a fiber laser also improves the corrosion resistance of the lattice structures. The Nyquist and Bode plots were obtained for all the systems and the equivalent circuits were obtained. The same equivalent circuits could be used to fit all the materials, showing that there were similarities in the corrosion mechanisms of the different structures. Finally, the thickness of the passive layers of the parts was calculated by Brug's equation. In this case, despite the previous results, the passive layers on the lattice structures were thicker than on the bulk, and it did not depend on the type of laser used to fabricate them.

Subtopic: Corrosion and Corrosion Protection of Additive Manufactured Metals

Effect of heat treatment on the high-temperature oxidation of additively manufactured L-PBF 316L stainless steel

Najib Abu-warda, Javier Bedmar, Sonia García-Rodriguez, Belén Torres, Victoria Utrilla, Joaquín Rams

Universidad Rey Juan Carlos, Madrid/Spain.

One of the most common additive manufacturing of metals is the Laser Powder Bed Fusion (L-PBF), which fabricates near net shape parts from metallic powder. This method is based in the selective melting of the metallic powder after its deposition in a powder bed using a laser as the energy source.

One of the best advantages from L-PBF against conventional manufacturing methods is its ability to provide pieces with complex geometries, high customization, and near full density. Thus, L-PBF is seen as a good future option to fabricate parts for high-temperature applications in transport and energy sectors.

This work intends to shed light on the high-temperature oxidation behavior of 316L stainless steel focusing on (i) the effect of different heat treatments (0.5 h at 1100 ºC and water quenching; 2 h at 850 ºC and normalizing; and 4 h at 650 ºC and annealing), and on (ii) the effect of the manufacturing process, comparing L-PBF and wrought samples. For this porpoise, after heat treatments, 316L stainless steel samples were exposed at 800 ºC for a maximum of 360 h in a dry air atmosphere to perform high-temperature oxidation tests.

The oxidation behavior of each steel was quantified by gravimetric measurements and both the cross-section, and the surface of the samples were characterized by SEM and EDX techniques to analyze the morphology and composition of the grown oxides in function of the exposure time.

Gravimetric results show that the samples have a corrosion kinetic that can be adjusted to a parabolic law, where the corrosion rate diminishes with time due to the formation of a protective layer of oxides. Particularly, the as-built L-PBF 316L stainless steel has better oxidation resistance than its counterpart water quenched. In contrast, the L-PBF 316L stainless steels normalized and annealed had similar oxidation behavior

Corrosion and Corrosion Protection of Additive Manufactured Metals

Comparative investigation of the corrosion resistance of as-produced 17-4 PH stainless steel fabricated by two additive manufacturing technologies

Luiz Resende Coelho[1], Patrícia Hatsue Suegama[2], Dany Michell Andrade Centeno[1], Hélio Goldenstein[1], Hercílio Gomes de Melo[1]

Departamento de Eng. Metalúrgica e de Materiais, Escola Politécnica da Universidade de São Paulo, Av. Prof. Mello de Moraes, 2463, Cidade Universitária, 05508-030, São Paulo – SP – Brazil

Faculdade de Ciências Exatas e Tecnologia, Universidade Federal da Grande Dourados, Rodovia Dourados/Itahum, Km 12, Cidade Universitária, 79.804-970, Dourados – MS - Brazil

In this work the corrosion resistances of as-produced 17-4 PH stainless steel samples fabricated by additive manufacturing (AM) using Laser Power Bed Fusion (L-PBF) and Laser Directed Energy Deposition (L-DED) technologies were compared. In these two AM techniques pieces are produced layer-by-layer; however, whilst in L-PBF a high-energy laser beam scans the entire area covered by the powder, in L-DED the laser beam is focused on a specific area, and the powder is simultaneously injected into the same area through a nozzle, resulting in different microstructural patterns, as shown in Figure 1. The two producing technologies also differ by their cooling rates (1.0×10^5 to 1.0×10^6 $^oC/s$) for L-PBF and (1.0×10^3 to 1.0×10^4 $^oC/s$) for L-DED. L-PBF is characterized by high geometric tolerance (0.05-0.1 mm) and the possibility to produce parts with minimum dimensions between 40-200 μm; however, one of its main limitations is the low production speed [1]. L-DED produces pieces with almost final shapes, high density, good mechanical properties and minimal imperfections; however, the large number of variables involved in the production process makes it difficult to predict the properties of the manufactured parts [2]. The electrochemical characterization in NaCl 0.5M showed that L-PBF samples present higher open circuit potential and better corrosion resistance, characterized by lower passive current density and higher pitting potential (Figure 2) and higher impedance modulus (Figure 3). SEM characterization of corroded samples showed that preferential corrosion sites for localized corrosion initiation could not be correlated with microstructural defects generated by the AM procedure and powder composition. Instead, it could be better

correlated with thermal stress and cooling during the samples production, as revealed by EDS analysis.

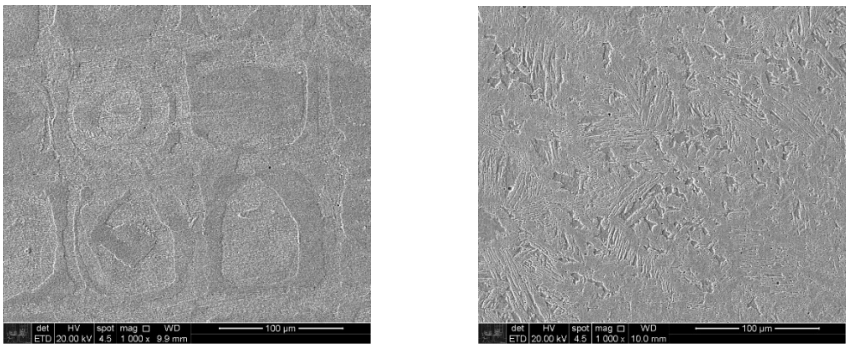

Figure 1: SEM images obtained to L-PBF (A) and L-DED samples (B).

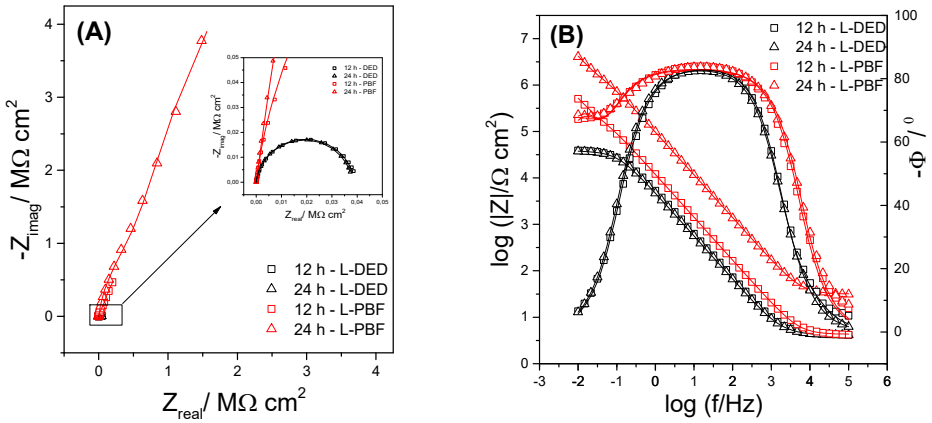

Figure 2: Experimental (symbols) and fitted (solid lines) EIS diagrams for the L-PBF and L-DED after 12 and 24 h of immersion in 0.5 M NaCl solution, (A) Nyquist and (B) Bode plots.

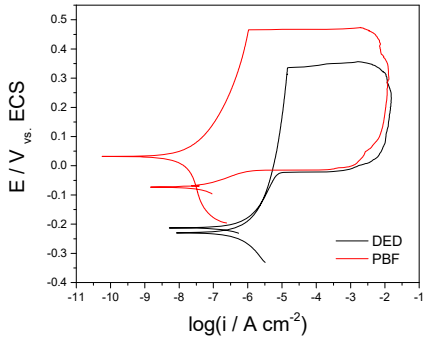

Figure 3: Polarization curves of L-PBF and L-DED samples obtained in in 0.5 M NaCl solution.

[1] A.B. Badiru, V.V. Valencia, D. Liu, Additive Manufacturing Handbook, CRC Press, 2017. https://doi.org/10.1201/9781315119106.

[2] N. Shamsaei, A. Yadollahi, L. Bian, S.M. Thompson, An overview of Direct Laser Deposition for additive manufacturing; Part II: Mechanical behavior, process parameter optimization and control, Addit Manuf. 8 (2015) 12–35. https://doi.org/10.1016/J.ADDMA.2015.07.002.

Pitting Corrosion of WAAM Type 2209 Duplex Stainless Steel

H. Z. Attar[a,b], J. W. Fellows[c], M. Roy[d,e], V. A. Hosseini[f], D. L. Engelberg[a]

a: Materials and Performance Centre & Corrosion and Protection Centre, Department of Materials, The University of Manchester, Sackville Street, Manchester M13 9PL, United Kingdom

b: Research & Development Centre, Saudi Aramco, Dhahran 31311, Kingdom of Saudi Arabia

c: Electron Microscopy Centre, The University of Manchester, Manchester M139PL, United Kingdom

d: Department of Mechanical, Aerospace and Civil Engineering, The University of Manchester, Manchester M139PL, United Kingdom

e: Henry Royce Institute, Department of Materials, University of Manchester, UK, M13 9PL

f: ESAB AB, SE-417 55 Göteborg, Sweden.

Duplex stainless steels have been used in different applications for the oil and gas industry, where they may be exposed to low-pH and high chloride-containing environments. The potential of producing fit-for-service DSS via the Wire and Arc Additive Manufacturing (WAAM) technique was evaluated in this study by correlating the evolved microstructure after wire deposition to the corrosion performance using a range of screening techniques. The WAAM DSS microstructure contains multiple austenite types with different corrosion susceptibilities, varying in phase fraction across the building direction. As a result of this phase fraction heterogeneity, differences in corrosion behaviour are observed. A novel bipolar electrochemistry screening technique was first applied, revealing deep corrosion pits associated with locations that contained a higher fraction of secondary acicular austenite. Their presence in a middle-hight location with respect to the building direction led to a deterioration in critical pitting potential and temperature. The acicular austenite contained lower contents of Cr, Mo and N. Results were compared to critical pitting temperature measurements using an Avesta cell. This study provides information about process parameters that can be applied to limit the formation of secondary austenite to improve pitting corrosion resistance in WAAM 2209.

Corrosion behaviour of additively manufactured Ti-6246 alloy

L. Iannucci, A. Arcieri, A. Martucci, M. Lombardi, S. Grassini

Department of Applied Science and Technology, Politecnico di Torino, Torino, Italy

The aerospace industry is constantly looking for innovative solutions to produce lightweight components in complex shapes. Additive manufacturing can surely address part of these needs thanks to the possibility to produce complex-shaped functional components with good surface quality, excellent dimensional tolerance and unprecedented mechanical properties. Among possible materials, titanium alloys are commonly used in aerospace gas turbine for components subjected to high loads in hot and potentially corrosive environments.

In this work, the corrosion behaviour of the Ti-6Al-2Sn-4Zr-6Mo (Ti-6246) alloy processed by Laser-based Powder Bed Fusion (PBF-LB/M) was assessed by means of electrochemical measurements and hot-corrosion tests. The samples were produced in the shape of cubes (1.5 cm x 1.5 cm x 1.5 cm) by using the PBF-LB/M processing parameters optimized in a previous study [1]. Then, the samples were cut along the printing direction and perpendicularly to it, to investigate possible anisotropic behaviour. Electrochemical Impedance Spectroscopy (EIS) and Potentiodynamic Polarization measurements were carried out at room temperature in electrolyte solutions with different aggressiveness (0.9 wt% NaCl and 0.9 wt% NaCl + 0.6 wt% NaF, respectively). Hot-corrosion tests were carried out at 450°C for 60 hours in air; a droplet of NaCl solution was applied at the centre of each sample and then allowed to dry before the beginning of the test. After each experiment, the samples surface were observed by Scanning Electron Microscopy (SEM) to investigate the corrosion morphology.

Results showed the good electrochemical stability of the Ti-6246 alloy in both environments. The presence of fluoride increased the corrosion kinetics, and some localized attacks were found after potentiodynamic polarization measurements. Despite this, no difference in the corrosion behaviour was observed as a function of the printing direction. Although the PBF-LB/M process can lead to anisotropy in the microstructure, the present work proved that this has no significant influence on the hot corrosion behaviour of Ti-6246 alloy.

Results revealed the good corrosion behaviour of the Ti-6246 alloy produced by SLM technology, making it a promising candidate for different components subjected to hot corrosion in aerospace applications.

[1] Carrozza, A., Aversa, A., Fino, P. & Lombardi, M. 2021, "A study on the microstructure and mechanical properties of the Ti-6Al-2Sn-4Zr-6Mo alloy produced via Laser Powder Bed Fusion", *Journal of Alloys and Compounds*, vol. 870.

Pitting resistant additively manufactured N-doped CoCrFeNi high-entropy alloy

Liang Wei, Max-Planck Institut für Eisenforschung, Düsseldorf Germany

Jingyao Chen, Shanghai University, Shanghai China

The combination of high-entropy alloy (HEA) concept and additive manufacturing (AM) technique is conducive to the design of new engineering structural or functional metal materials with better comprehensive properties. However, as a new type of corrosion-resistant alloys, the pitting behavior of the AM-HEAs as well as how to enhance their pitting resistance needs further study. In this work, a N-doped CoCrFeNi HEA with hierarchically heterogeneous structure and well mechanical property is fabricated using the powder-bed fusion technique, which performs superior pitting resistance compared to the other AM-HEAs or as-cast HEAs in Cl^--containing electrolyte. The outstanding pitting resistance is primarily attributed to the protectiveness of the dense Cr-rich amorphous passive film (~2 nm of thickness) and the enrichment of NH_4^+ within the surface layer of passive film that could combine with Cl^- to reduce the destroy of Cl^- to the passive film and alloy matrix.

Mechanism of Stress corrosion cracking initiation in additive manufactured Ni-Fe-Cr based alloy 718

Arshad Yazdanpanah[a*], Reynier I. Revilla[b], Iris De Graeve[b], Manuele Dabalà[a]

[a] Department of Industrial Engineering, University of Padova, Via Marzolo 9, 35131 Padova, Italy

[b] Department of Materials and Chemistry, Research Group Electrochemical and Surface Engineering, Vrije Universiteit Brussel (VUB), Pleinlaan 2, 1050 Brussels, Belgium

Corresponding author: arshad.yazdanpanah@phd.unipd.it

Stress corrosion cracking (SCC) is one of the major corrosion-assisted failures that could cause under even highly controlled water chemistries such as boiling and pressurized water reactors. The history of detecting SCC propagation rate by means of finding the correlation of crack growth rate with the measured electrochemical polarization responses is a long-lasting effort back to the 50s with gradual improvements during the past 70 years. However, the most time-intensive and critical stage of SCC formation is related to the incubation/initiation stage. Any possible enhancement of the materials for prolonging the incubation/initiation stage could lead to a substantial increase in the life cycle of critical components. Despite the importance of this stage, to the best of our knowledge, a limited effort had been made to fully understand the underlying mechanisms responsible for crack initiation in the case of conventional alloys.

Additive manufacturing is the most promising technology which has the potential for substituting conventional manufacturing techniques as a consequence of lower production time, cost, and material waste, and freedom in the design of complex geometries with a single computer-aided designed file. During the past decade, the laser powder bed fusion (L-PBF) technique proved to be the most precise method capable to manufacture parts with almost full density. Extensive research has been done on process parameters optimization for various alloys for further enhancement of mechanical properties, fatigue, and creep resistance.

Alloy 718 is a nickel-iron based superalloy with the combination of both great corrosion resistance and mechanical properties which is the material of choice for highly demanding applications in nuclear, oil, and gas industries. The substitution of end of life components in critical industries is a common practice in which additive manufacturing can reduce substantially the time and cost of production (for complex geometries) for the production of substitutive components. However, the comparability of the corrosion behaviour of additive manufactured components with the conventional counterparts must be thoroughly examined before further consideration of such methods. To the best of our knowledge, the SCC initiation behaviour of L-PBF and in general additive manufacturing techniques has not been investigated systematically.

In the current investigation, the SCC initiation behaviour of L-PBF 718 was assessed for the first time utilizing microcapillary electrochemical techniques and the results were compared with the conventional counterpart. The comparative study was performed in a solution with mild contamination of chloride ions, as the most common contamination in industries located in coastal regions. Obtained results revealed the formation of the cracks from the close vicinity of the subgrain boundaries highlighting the importance of submicron structure in SCC initiation susceptibility. The electrochemical response of the L-PBF specimens revealed significantly higher breakdown potential (from potentiodynamic polarization results), maximum potential, and duration (from galvanostatic polarization results), and lower current density (from potentiostatic polarization results) compared to conventional counterpart, revealing substantially enhanced localized corrosion resistance. The size of the observed cracks was also significantly bigger for the case of conventional specimens. SCC mechanism was elucidated hypothesizing based on observations as the synergistic effect of the formation of a coupled environment at submicron level combined with higher energy state of the zones adjacent to subgrain boundaries as a result of higher dislocation density.

Formation and failure mechanisms of the transpassive film of laser additive manufacturing nickel-based superalloy

Pengfei Guo, Qingdao University of Technology, Qingdao/China

(dr2019guopf@163.com)

Inger Odnevall, KTH Royal Institute of Technology, Stockholm/Sweden

(ingero@kth.se)

Abstract

Post-processing of the laser additive manufacturing (LAM) difficult-to-machine metallic materials using electrochemical machining (ECM) has attracted more and more attentions from both scientific and industrial aspects, especially for nickel-based superalloys. However, the surface quality after ECM is rough due to the transpassive film is susceptible to localized attack and thus induces selective dissolution and the occurrence of a non-uniform electrodissolution current density. Until now, it is puzzling that the albeit meager studies of transpassivity, over many decades, including investigation of the formation of transpassive films during ECM processing has not led to a precise understanding of transpassivity, particularly under flowing electrolyte conditions. In the present work, the non-homogeneous microstructure characterizations of the LAM-Inconel 718, and its anodic behavior including potentiodynamic polarization measurements and the atomic-scale observations of the transpassive film formed in $NaNO_3$ solution were conducted. The results show that the highly textured microstructure of LAM-Inconel 718 is mainly composed of γ phase, Nb-rich region, and Laves phase. With the increasing of current density during ECM, the transpassive film becomes more and more porous and finally ruptures. It is the secondary passivation induces the formation of a transpassive film. Further, the failure of the transpassive film is dominated by self-induced cracking of the film on niobium-segregated phases and the erosion-induced degradation via shear stress on the film coupled with cation vacancy condensation at the metal/barrier layer interface that results in decohesion of the barrier layer from the alloy substrate. Finally, A mechanism

is proposed that postulates that the Cr_2O_3 barrier layer (bl) of the primary passive film that forms at a potential at the end of the active dissolution region of the alloy breaks down via the simultaneous cation vacancy condensation at the metal/barrier layer interface and the electrodissolution of chromic oxide at the barrier layer/solution interface and is replaced by a secondary barrier layer film (such as NiO/Ni_2O_3, Fe_2O_3, Nb_2O_5) that induces secondary passivation. However, as the voltage is made more positive, this secondary barrier layer also undergoes breakdown, again via a potential-mediated generation of cation vacancies coupled with vacancy condensation of the bl/m interface and oxidative dissolution of the bl.

Graphic Abstract

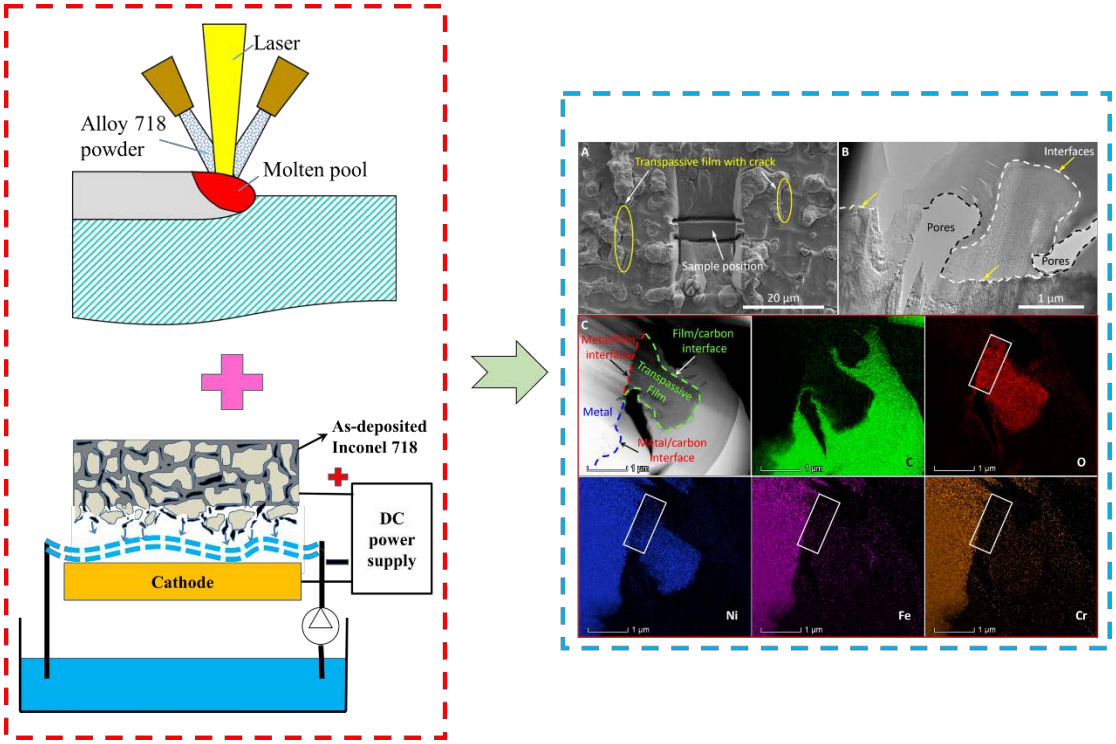

High temperature corrosion of compositionally graded materials fabricated by Laser Metal Deposition – powder

A. Curnis [1, 2], I. Popa[2], A. Prillieux[1], S. Chevalier[2]

[1] Institut de Recherche Technologique (IRT) Saint Exupéry, 3, rue Tarfaya, 31 400 Toulouse, France

[2] ICB, UMR 6303 CNRS Univ. Bourgogne Franche-Comté, 9 avenue Savary, 21 078 Dijon, France

Laser Metal Deposition – powder (LMD-p) is a layer-by-layer Additive Manufacturing (AM) process using powder injection technology, directly inspired from laser cladding [1]. This process makes possible the customization and fabrication of compositionally graded material systems. Progressive change of composition can be used to limit incompatibilities between two different materials. It also allow to redesign industrial parts by locally adjusting the material composition so that it is adapted to the service conditions (mechanical stress, corrosive environment, wear resistance).

Figure 1: Cross-section of the compositionally graded system after chimical etching

A compositionally graded material system starting from a low alloy steel substrate (ASTM A387) toward the nickel based superalloy Ni625 was successfully fabricated using LMD-p. The composition gradient is achieved by varying the ratio of pure iron to Ni625 alloy in a powder mixture. Micrograph of as-build cross-section after chemical etching highlights interfaces between the different selected compositions (*Figure 1*).

Higher magnification SEM observations revealed dendritic structure resulting from Nb and Mo segregation because of their low solubility in the γ matrix. According to the local composition variation, different types of secondary phases have been identified in the interdendritic regions.

The high-temperature oxidation behavior of compositionally graded system with and without NaCl solid deposit on Ni625 surface were investigated after being exposed in air atmosphere at 800°C for different dwell times up to 2500 hours.

In absence of NaCl deposit, LMD-p Ni625 oxidation in air obeys to a parabolic rate law and kinetics is similar to those measured on other conventionally or additively manufactured Ni625 alloys [3,5,6]. SEM and XRD characterization of Ni625 surface revealed that the oxide scale is mainly composed of Cr_2O_3 with a thin layer of $(Cr,Mn)_3O_4$ spinel located on top surface. At oxide/Ni625 interface, large precipitates of δ-Ni_3(Nb,Mo) phase are also observed due to the migration of Nb toward the oxide scale as result of Cr depletion [2–4] (*Figure 2-a*).

Reactivity of Ni625 in presence of NaCl solid deposit is drastically different, leading to a very thick oxide scale. SEM and XRD analyses show that the scale is made of NiO, $(Ni,Cr)_3O_4$ and Cr_2O_3. Thus, characterization of the thick layer of corrosion products indicates that NaCl presence results in a faster degradation of the material. Furthermore, the area beneath the oxide scale is strongly damaged by an interconnected voids network which has been characterized by X-ray tomography. These voids result from gas transport occurring in the active oxidation process. Large δ-Ni_3(Nb,Mo) phase precipitates were observed near the voids (*Figure 2-b*). The precipitation might be due to a similar diffusion mechanism to that observed beneath the oxide scale of samples exposed in air in absence NaCl.

(a) *(b)*

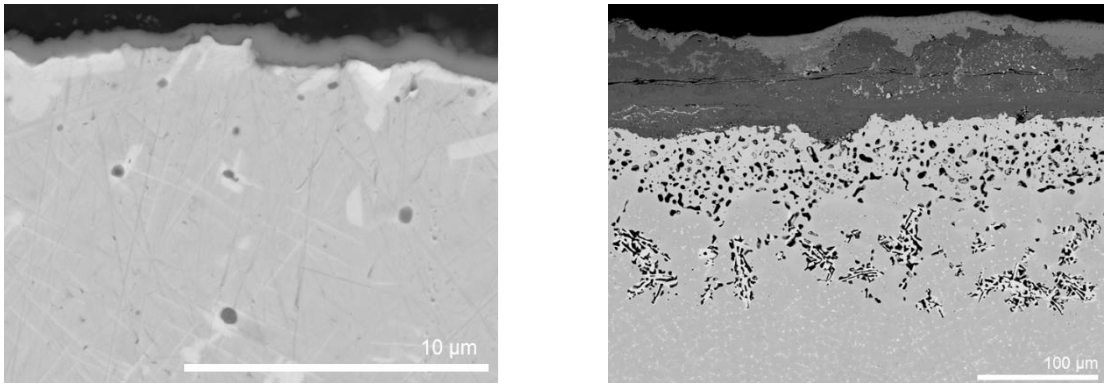

Figure 2: SEM Micrograph showing the cross-section of Ni625 oxidized in air atmosphere for 1000h at 800°C (a) without, (b) with NaCl solid deposit.

[1] *L. Thivillon, Ph. Bertrand, B. Laget, I. Smurov, Journal of Nuclear Materials. 385 (2009) 236–241. https://doi.org/10.1016/j.jnucmat.2008.11.023.*

[2] *A. Chyrkin, P. Huczkowski, V. Shemet, L. Singheiser, W.J. Quadakkers, Oxid Met. 75 (2011) 143–166. https://doi.org/10.1007/s11085-010-9225-3.*

[3] *N. Ramenatte, A. Vernouillet, S. Mathieu, A. Vande Put, M. Vilasi, D. Monceau, Corrosion Science. 164 (2020) 108347. https://doi.org/10.1016/j.corsci.2019.108347.*

[4] *M. Sharifitabar, S. Khorshahian, M. Shafiee Afarani, P. Kumar, N.K. Jain, Corrosion Science. 197 (2022) 110087. https://doi.org/10.1016/j.corsci.2022.110087.*

[5] *D.M. England, A.V. Virkar, J. Electrochem. Soc. 146 (1999) 3196. https://doi.org/10.1149/1.1392454.*

[6] *A. Chyrkin, K.O. Gunduz, I. Fedorova, M. Sattari, A. Visibile, M. Halvarsson, J. Froitzheim, K. Stiller, Corrosion Science. 205 (2022) 110382. https://doi.org/10.1016/j.corsci.2022.110382.*

The pathway to the Oil&Gas qualification of alloy 625 produced by different additive manufacturing technologies

Sergio Lorenzi, University of Bergamo, Italy;
Marina Cabrini, University of Bergamo, Italy;
Alessandro Carrozza, University of Bergamo, Italy;
Tommaso Pastore, University of Bergamo, Italy;

In last years, metal Additive Manufacturing (AM) technologies are redefining traditional design and manufacturing strategies, thus opening the possibility of obtaining materials and products with high added value and unique performances. These technologies grant the possibility to design the alloy microstructures with a layer-by-layer approach, thus producing brand new materials from traditional compositions. Lots of efforts have been made by researchers and industry to optimize process parameters and heat treatments to achieve optimal tensile properties. However, other properties – i.e. corrosion – are fundamental if the alloy has to be considered for severe service applications, typical of the oil and gas industry. In this field, nickel-based alloys are strategic, as they exhibit high tensile strength alongside with outstanding corrosion resistance. The Oil&Gas industry faces very challenging applications in harsh environments, that require materials with high resistance to corrosion, thus granting reliability and safety of the assets. This results in a reduction of the risk of leakage, preventing consequences on the environment and guaranteeing the safety of people. Among the corrosion resistant alloys, alloy 625 has a combination of strength and corrosion resistance in aggressive environments that make it suitable and convenient in demanding applications in several industrial fields. Alloy 625 is an age-hardenable alloy, where the formation of very fine phases strengthening the austenitic matrix occurs after heat treatments in the temperature range between 550 and 750 °C. The formation of such phases, or their decomposition, during high temperature operations significantly modifies the yield strength and ductility of the alloy. Consequently, the formation of carbides and secondary phases can affect the corrosion resistance and environmental assisted cracking susceptibility. Therefore, the alloy may become susceptible to intergranular corrosion if subjected to improper solution treatments.

Due to the very high solidification rates typical of powder-bed fusion technologies, and the low rates typical of the sintering processes of the most innovative polymer-metal

technologies (e.g, binder jetting and material extrusion), the microstructures that can be obtained via additive manufacturing are rather unique. The mechanical and corrosion performances are strictly related to the microstructure of the alloy itself, ranging from sub-micrometric cellular/columnar structures to coarse equiaxed grains. In addition, post-processing heat treatments, generally considered to reduce internal stresses and increase mechanical performances, further increase the complexity of such microstructures, highlighting the important topic of material qualifications for specific applications. The American Petroleum Institute just released the API20s standard for defining the supply chain requirements for AM materials qualification in the Oil&Gas field. Additionally, the Association of Materials Protection and Performance (AMPP TR21522) is active in the definition of corrosion testing protocols for corrosion assessment of additive manufactured alloys. In this panorama, a first step towards the qualification of AM-processed alloys was taken through the analysis of the corrosion behavior of several alloy 625 specimens. To achieve that, four different AM technologies were considered: laser powder bed fusion, directed energy deposition, material extrusion and binder jetting. By doing so, all the available forms of feedstock were analyzed: powder, metal wire and metal-polymer filament. An initial investigation aimed at understanding the correlation between the manufacturing technology and the micro-/macro-defects generated in the material was carried out. Advanced characterization techniques, such as micro computed tomography, were adopted in specific cases. Then, microstructural analyses and phase identifications were performed and linked with the manufacturing route. In the end, the susceptibility to intergranular corrosion tests (ASTM G28-A) were adopted to assess possible variations between the specimens. All the evaluations performed allowed to establish a connection between the different AM technologies adopted and the corrosion behavior of the material, which proved to be very different according to the considered additive manufacturing technology. This work lays the foundation for further studies in the future, aimed at establishing which AM technology might be more suitable for every specific applications.

Microstructure and corrosion evolution of Hastelloy X alloy fabricated by laser powder bed fusion

Xing He[1], Jiekun Dai[1], Ruixue Li[1], Chaofang Dong[1]*

[1] National Materials Corrosion and Protection Data Center, Beijing Advanced Innovation Center for Materials Genome Engineering, Institute for Advanced Materials and Technology, University of Science and Technology Beijing, Beijing 100083, China

ABSTRACT: In recent years, additive manufacturing has become popular in many fields due to its unique advantages. However, there is no effective method to completely eliminate the formation of pores and lack of fusion (LOF) defects during the laser powder bed fusion (LPBF) process. Defects in LPBF are characterized by a global distribution, diverse morphology, a large size span, and a complex formation mechanism. When exposed to aggressive environments, defects can become potential sites of corrosion initiation for LPBF materials. This effect becomes even more important when considering that suppressing defect formation remains a challenge in LPBF process, especially LOF pores, which may not be considered as simple pores because they are partially covered by oxide films formed during melting and solidification in LPBF process. Previous studies have shown that the reduced pitting resistance of LPBF Hastelloy X alloy occurs at pores with a diameter larger than 55 μm, while a passive state still occurs when the pore diameter is less than 10 μm. To this end, this paper investigates the relationship between defects and corrosion kinetics of Hastelloy X for LPBF in terms of static defect characterization and dynamic defect evolution, aiming to provide a reference for process selection, defect characterization, revealing the corrosion mechanism, and evaluating the service performance of LPBF parts.

Keywords： Laser powder bed fusion; Hastelloy X; Corrosion; Porosity; X-ray computed tomography

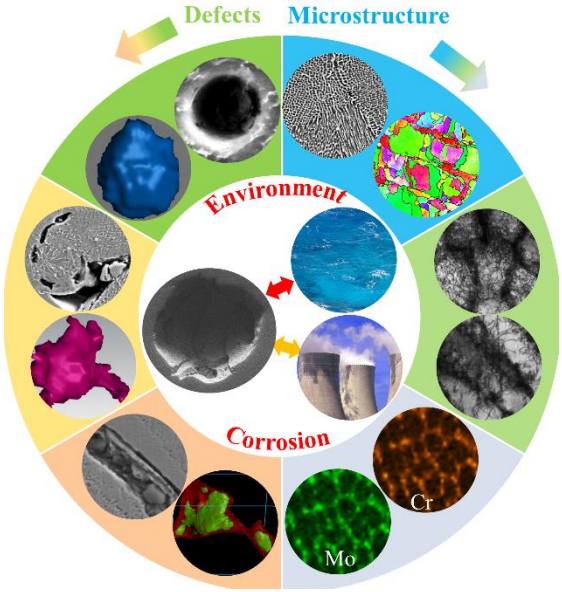

Figure 1. Schematic diagram of the interaction between Microstructure/defects and corrosion of additively manufactured Hastelloy X alloys.

HIGH TEMPERATURE OXIDATION BEHAVIOR OF ADDITIVELY MANUFACTURED INCONEL 939 AT 800, 900 AND 1000°C IN AIR

Batuhan Başbozkurt, Cevat Sarıoğlu,

Marmara University, Istanbul/Turkey

The aim of this research was to investigate and compare the high temperature oxidation behavior of Inconel 939 produced by selective laser melting (SLM) technique and conventional casting. Samples were subjected to following heat treatments: Heat treatment steps for 3D samples included solution heat treatment at 1160˚C± 14°C for 4 hours ± 15 minutes, then cooling with a rate faster than air cool, followed by aging at 845°C± 8˚C for 16 hours± 30 minutes and then air cooling. Heat treatment steps for as cast samples were solution heat treatment at 1160±14°C for 4 hours, then gas furnace quench (GFQ), followed by primary aging at 1080±14°C for 4 hours and GFQ followed by secondary aging 843±14°C for 20 hours, and then cooling to room temperature at any rate. Isothermal oxidation tests were carried out at 800, 900 and 1000°C in muffle furnace. Weight gain data were collected at different time intervals to reveal the oxidation kinetics. Weight gain results showed that at 800 and 900°C all samples obeyed parabolic rate law. There was no visible spallation at 800 and 900°C tests. Spallation started after 36 hours for heat treated as cast IN939 and 64 hours for heat treated SLM IN939 at 1000°C. SEM, EDS and XRD results showed that the oxide scale at 800, 900 and 1000°C was mainly Cr_2O_3. XRD measurements indicated that at 800°C Cr_2O_3 phase was very thin that Ni_3Al phase could be detected easily from substrate. At 900 and 1000°C surface oxidation products were mixed oxides of Cr_2O_3 and TiO_2. Microstructure of heat treated SLM and as cast IN939 was studied as well. Stereo microscope results showed that after heat treatment melt pools of SLM IN 939 disappeared. Results showed that there was no significant difference between heat treated SLM and casting IN 939 samples in terms of oxidation kinetics (parabolic rate laws), indicating that the heat treated SLM Inconel 939 alloys exhibited the same oxidation resistance as casting Inconel 939 alloys

Key Words: Selective Laser Melting (SLM), Oxidation, Inconel 939, Superalloys

Localized Corrosion induced by Precipitates in Laser Powder Bed Fusion Alloys

Bowei Zhang, Zequn Zhang, Pengcheng Zuo, Junsheng Wu, Xiaogang Li
University of Science and Technology Beijing, Beijing, China

Localized corrosion induced by precipitates is the key problem that must be solved before the large-scale application of additive manufactured alloys. In this paper, laser powder bed fusion (LPBF) Cu-15Ni-8Sn alloy and Al-Mn-Mg-Sc-Zr were used as the objects to systematically describe the characteristics of precipitates in typical multi-scale structures such as microscopic cell structure and mesoscopic molten pool boundary, including the influence of heat treatment on the evolution of precipitates. Based on the results, the impact of precipitates distribution on the electrochemical activity of the alloy surface was revealed, the correlation between the surface microstructures and the corrosion behavior was also established, followed by the mechanism of localized corrosion initiation and propagation induced by precipitates. In addition, the microstructure and composition distribution characteristics of the oxide film on LPBF alloys were also analyzed at nano-scale, where the internal relationship between the precipitates and the film formation mechanism was clarified.

Influence of heat treatment on the corrosion behaviour of additively manufactured aluminium-silicon-based alloys

Lisa Ott, Thomas Wegener, Thomas Niendorf

University of Kassel, Institute of Materials Engineering, Kassel/Germany

Besides the advantages of an excellent strength to weight ratio, good castability and high recycling potential, aluminium- silicon alloys are also characterized by a good corrosion resistance. Thus, they are widely used for automotive and aerospace components. Recently, numerous studies focused on additively manufactured (AM) Al-Si-based alloys. Compared to cast components, AM conditions were found to feature a finer microstructure and up to four times higher yield strength. [1] AM in general offers the unprecedented combination of producing complex geometries and unique functionalities. The microstructure of AlSi12 manufactured using powder bed fusion of metals (PBF-LB/M), formerly known as Selective Laser Melting (SLM), consists of a fine Al-rich cellular structure with a three-dimensional Si-network in the as-built condition. Previous studies reported a significant influence of different heat treatments on the microstructural appearance and will, therefore, most likely have a huge impact on the corrosion behaviour of Al-Si-based alloys.

The major objective of the present study was to investigate the influence of different heat treatments on Al-Si-based alloys with respect to the microstructure and, thereby, the corrosion behaviour. Two different heat treatment procedures with varying temperature and time parameters have been employed. The microstructural characterisation for as-built and heat-treated conditions revealed different morphologies of the Si-network. The electrochemical corrosion behaviour was examined by open circuit potential and potentiodynamic polarization measurements. Additionally, immersion tests using thin plates were carried out to determine the weight loss due to the corrosion process. A 3.5 wt.% NaCl solution was used for all corrosion tests at room temperature. After testing the damage induced by corrosion was analysed by means of optical microscopy and scanning electron microscopy.

[1] Prashanth et al., Mater. Sci. Eng. A 590 (2014), DOI: 10.1016/j.msea.2013.10.023

Analysis of the boundaries of surface treatments to protect AlSi10Mg additive manufacturing surfaces against corrosion

*M.B. García-Blanco, H. Mora-Sanchez, E. Espinosa, E. García-Lecina, M. Lekka**

[1]CIDETEC, Basque Research and Technology Alliance (BRTA), Po. Miramón 196, 20014 Donostia-San Sebastián, Spain

*mlekka@cidetec.es

Additive manufacturing (AM) technologies have the ability to produce complex geometry components at affordable costs in different materials such as Al alloys. The properties, and in particular the corrosion performance of AM products should meet those obtained by conventional technologies. Therefore, AM parts need to be protected using the same surface treatments applied to conventionally produced ones.

However, the high surface roughness, the different microstructure, the surface oxidation state and the porosity of metal parts obtained by AM affect not only the properties of the material (mechanical properties, corrosion resistance...), but also its response to chemical and electrochemical surface treatments.

In this context, it is necessary to adapt surface treatments, to treat and protect against corrosion this new type of surfaces. However, different boundaries have been detected when treating these AM surfaces and the aim of this research is to identify and understand them in order to improve their application. In particular, the effect of chemical polishing, anodising and anaphoretic e-coating on AlSi10Mg alloy obtained by Laser Powder Bed Fusion technology (L-PBF) has been analysed.

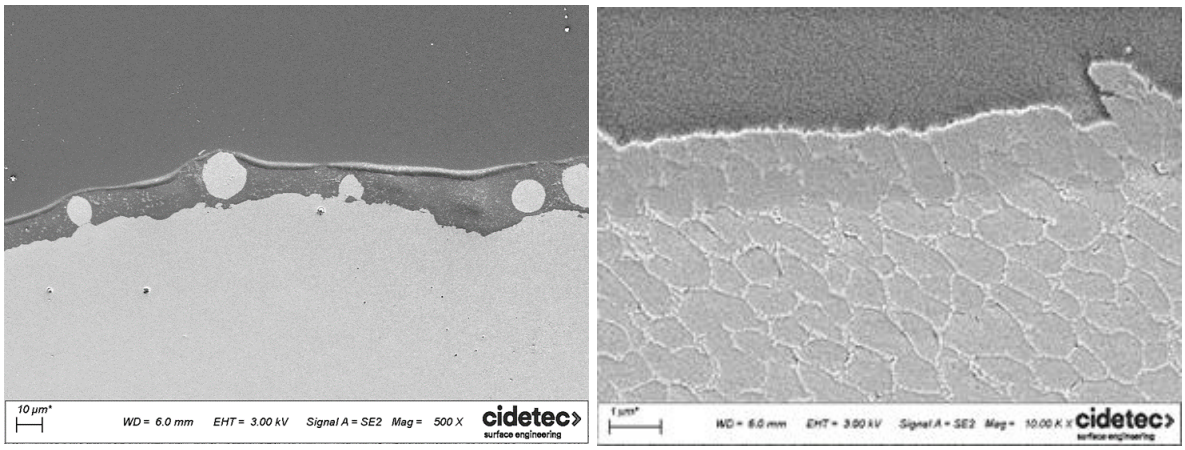

Figure 1. FESEM micrographs of anaphoretic e-coating on as-built AlSi10Mg surface (left) and anodising layer on polished AlSi10Mg surface (right)

For this purpose, microstructural and morphological characterization of as-built, chemically polished, anodised and e-coated surfaces have been carried out together with electrochemical corrosion studies. The obtained results will enhance the understanding of the behaviour of AM surfaces against commonly used surface treatments boosting the acceptance of AM components by the industry.

Assessing the corrosion performance of Al-based composites produced by selective laser melting

Noémie Ott[1], Adriaan B. Spierings[2], Cord Henrik Surberg[1]

[1] Institute for Microtechnology and Photonics, OST – Eastern Switzerland University of Applied Sciences, Buchs, Switzerland

[2] Inspire AG, Innovation Center for Additive Manufacturing, St Gallen, Switzerland

Aluminum matrix composites (AMCs) are attractive candidates for many lightweight applications in the automotive and aerospace industries, since they combine the specific properties of Al alloys with the unique properties of their reinforcement agents. In particular, carbon-based reinforcing particles, such as carbon nanotubes (CNTs) and graphene flakes (GPs), offer excellent mechanical properties, high specific surface area, and enhanced thermal properties.

Additive manufacturing, e.g. selective laser melting (SLM), offers new opportunities to produce such advanced materials. One of the main limitations however is the production of powders with homogeneous distribution of reinforcement agents. Typically, they tend to agglomerate during mechanical mixing, which drastically affects the composite mechanical properties and corrosion resistance.

In this study, we explore new strategies for carbon-based reinforced Al-Si powder production, aiming at a more uniform distribution of reinforcements in the obtained bulk materials. With this in mind, different allotropes of carbon, e.g. CNTs, graphene, graphite and polymers, were also evaluated as reinforcement agents.

A correlative approach, combining electrochemical characterization with scanning Kelvin probe force microscopy, nanoindentation and microstructural analysis, was used to determine the influence of added reinforcements on the mechanical properties as well as corrosion resistance of the SLM produced Al-Si composites. The effect of the SLM process variables, in particular the use of recycled powder in relation to the integrity of the carbon-based reinforcements, on the nature of the build, i.e. microstructure and defects, will also be discussed.

Health and corrosion aspects of alloy powders used in powder bed fusion additive manufacturing

Xuying Wang, KTH Royal Institute of Technology, Stockholm, Sweden
Inger Odnevall, KTH Royal Institute of Technology, Stockholm, Sweden
Hanna L. Karlsson, Karolinska Institutet, Stockholm, Sweden
N. V. Srikanth Vallabani, Karolinska Institutet, Stockholm, Sweden

Exposure to metal particles via the inhalation route unavoidably takes place at workplaces, e.g., upon handling, use, and powder disposal, upon additive manufacturing (AM) of metals and alloys. Possible adverse health effects caused by human contact with the metal powders deserve attention to ensure a safe working environment. This study aims to elucidate the importance of surface and corrosion properties of metal and alloy powders used in laser-based additive manufacturing, and assess possible acute toxic effects from a work safety perspective. The investigations, employing a physical, chemical, and toxicological perspective, include a large range of virgin and reused metallic powders as well as non-intentionally generated particles formed during various AM processes. This was achieved by characterizing the surface morphology and composition, microstructure, size distribution, and corrosion behavior of the powder particles, and assessing their bioaccessibility properties in artificial lysosomal fluid (ALF, simulating lung exposure to respirable particles). Their in-vitro toxicity towards cultured human lung cells was investigated from a cytotoxicity and oxidative stress perspective. Some powder materials showed the laser melting process to affect the chemical and physical properties of non-fused particles, whereas other materials were non-affected. Reuse of such particles was at certain conditions shown to influence the corrosion properties of the printed parts. The particles from AM showed in general no or small toxic effects on the cultured lung cells.

The corrosion resistance of Alloy 825 (UNS N08825) in function of nickel content and annealing temperature

Julia Botinha, Dr. Peter Maas, Dr. Helena Alves, VDM Metals International GmbH, Altena/Germany

The Alloy UNS N08825 is a fully austenitic nickel-iron-chromium alloy, stabilized by titanium and with additions of copper and molybdenum that was designed originally for applications in the chemical process industry, that later found usage in the Oil & Gas Industry. Within its UNS composition range, the nickel content of this alloy is allowed to vary from 38 to 46 %, a variation that can affect in some level its susceptibility to intergranular corrosion in both as-delivered as well as after PWHT (Post Weld Heat Treatment) conditions.

As well as the composition, corrosion resistance of UNS N08825 can be dependent of the thermal history of the material.

This work consists on the variation of the nickel content within the UNS analysis of UNS N08825 and the variation of the annealing temperature in order to better understand the influence of these both variables on the intergranular corrosion resistance of the material.

Heats from large-scale production of Alloy UNS N08825 with different Ni contents of 39 % and 42 % were annealed at different temperatures and tested according to the ASTM G28 method A to verify the intergranular corrosion resistance in the as-delivered condition and after heat treatments that lead to sensitization (PWHT). The results show that different material compositions require different optimized heat treatments that grant optimized properties. There is an advantage in adapting the heat treatment temperature to the material according to its level of nickel content.

A review of the B- and C- family nickel alloys and their applications in the CPI

Philipp Hübner (VDM Metals International GmbH); Dr. Helena Alves (VDM Metals International GmbH); Dr. Bodo Gehrmann (VDM Metals International GmbH)

In the chemical and petrochemical process industry, the use of different, highly corrosive media is common. Depending on the medium, different severe corrosion mechanisms can occur. For decades, the 300-series of stainless steel was and still is one of the most important materials used in the industry because of its good corrosion resistance and high mechanical strength. However, as the industry has evolved and requirements for product quality, environmental regulations and plant efficiency have increased, so have the demands for the used materials. In order to achieve maximum economic efficiency and to enable the implementation of new, more severe corrosion processes or product purity, the use of suitable materials is crucial, especially in critical components of the plants.

Nickel alloys from the so-called C- and B- families have proven to be the most essential materials used in the highly corrosive areas of the chemical process industry. The development began in the early 20th century and continues to this day. In this presentation, the development history and its close connection to the requirements of the chemical and petrochemical industry will be elaborated. Also, an overview of the challenges of each material family both in manufacturing as well as in application will be presented, leading to a closer look at some of the individual family members and their distinguished properties. Also, the differences between the two families as well as potential application gaps and the latest alloy developments will be presented. Finally, exemplary applications of materials from both families in the chemical and petrochemical industry will be shown.

Influence of Cashew Nut Shell Liquid in the Metallic Alloys Corrosion Behavior

C. Pino[1], A. Bermúdez-Castañeda[2], E. Klyatskina[2], V. Amigó[2], J. Esguerra-Arce[3], J. Urbano[1], C. Ayala-Garcia[4], O. Alvarez[5], A. Maranon[6], A. Porras[5], C. Hernandez[1]

(1) DSIM, Mechanical Engineering, Escuela Colombiana de Ingeniería Julio Garavito, Bogota, Colombia (2) Instituto de Tecnología de Materiales (ITM), Universitat Politècnica de València, Valencia, Spain (3) CIMSER. Industrial Engineering, Escuela Colombiana de Ingeniería Julio Garavito, Bogota, Colombia (4) Department of Desing, Universidad de los Andes, Bogota, Colombia (5). Department of Chemical and Food Engineering, Universidad de los Andes, Bogota, Colombia (6). Department of Mechanical Engineering, Universidad de los Andes, Bogota, Colombia.

In recent years, global demand of Cashew (*Anacardium occidentale*) kernel is rising due to its great flavor and its excellent nutritional properties. This increase in the demand has brought new challenges to the cashew industry as a consequence of the corrosion and wear shown in the processing equipment, associated to opening of the nut and extraction of one of its subproducts for its valorization: the Cashew Nut Shell Liquid (CNSL). This oily substance, that is present in the shell of the cashew nut is composed of anacardic acid, cardanol, cardol and other minor components, shows a corrosion behavior on the components of processing equipment that is not completely understood. However, chlorides present in cleaner agents, humidity and nut boiling temperature are important aspects to consider. Therefore, to a correct design of new cashew processing equipment is essential to understand the influence of CNSL in metallic alloys corrosion behavior in aggressive environments.

CNSL mechanically extracted from closed cashew nuts from Vichada, region in Colombia, was characterized using FTIR analysis. Significant differences with other vegetables oils were found. Absence of triglycerides and the existence of phenolic compounds due to benzene rings in the chains were observed. These characteristics of CNSL makes the corrosion influence on metallic alloys interesting to study.

Corrosion behavior of stainless steel AISI 420, low carbon steel AISI 1012 and aluminum alloy 6061 was evaluated on mixtures of CNSL, ethanol and NaCl solution by alternative immersion and electrochemical tests. Cyclic polarization and electrochemical impedance were made at different CNSL concentrations employing an electrochemical cell with Ag/AgCl as reference electrode and graphite as counter electrode. Weight loss was measured at a constant concentration of CNSL by alternative immersion condition. Surfaces of tested materials were characterized by SEM and corrosion products were assessed by EDS and XRD.

On the other hand, the influence on the corrosion behavior of residual CNSL film left on the surface of low carbon steel AISI 1012 was studied. Optimal polymerization temperatures of CNSL on the steel surface were found using DSC/TGA analysis. Residual CNSL film was developed by applying a heat treatment following those temperatures. Electrochemical properties of the AISI 1012 with the polymerized CNSL film on the surface were evaluated using the same procedure previously described. Additionally, properties of the film were evaluated using SEM and adhesion test.

Electrochemical and alternative immersion tests showed that due to the high presence of anacardic acid the CNSL effect on the passive metals could lead to the evolution of localized corrosion phenomena in presence of aggressive species. On the other hand, the evaluation of the CNSL residual film on the surface of low carbon steel showed an interesting electrochemical behavior, which could lead to potential industrial applications of CNSL in the corrosion protection field.

Acknowledgements

The authors wish to express their gratitude to Sistema General de Regalías, OCAD Fondo de Ciencia, Tecnología e Innovación FCTeI and Ministerio de Ciencia, Tecnología e Innovación which funded this research through the Project “Aprovechamiento de los subproductos Agroindustriales en la producción del marañón en el departamento del Vichada - BPIN 2020000100571”

Corrosion Behavior of Stainless Steels in Nitric Acid Environment

***Paweł Capała**, Lukasiewicz Research Network – New Chemical Syntheses Institute, Nitric Acid Technologies Department, Puławy, Poland, pawel.capala@ins.lukasiewicz.gov.pl, ORCID ID: 0000-0002-7574-9433*
Monika Ostapiuk, The Lublin University of Technology, Mechanical Engineering, Lublin, Poland, m.ostapiuk@pollub.pl*, ORCID ID:0000-0002-8209-4770*
Monika Ruszak, Lukasiewicz Research Network – New Chemical Syntheses Institute, Nitric Acid Technologies Department, Puławy, Poland, monika.ruszak@ins.lukasiewicz.gov.pl, ORCID ID: 0000-0002-7883-7439
Anna Rudawska The Lublin University of Technology, Mechanical Engineering Faculty, Lublin, Poland, a.rudawska@pollub.pl, ORCID ID: 0000-0003-3592-8047

Abstract

The aggressive environment in nitric acid plants means that the equipment design requires suitable construction materials. Difficult operating conditions for steel exist in the boiler system, absorption and bleaching column, condensers, and tail gas preheaters [1]. Awareness of corrosion under specific process conditions makes it possible to predict the life span of individual equipment components. The present work aims to determine the corrosivity of steels used in nitric acid plants. For testing, we selected materials used in a nitric acid plant. These are austenitic steels [2].

The electrochemical tests OCP and potentiodynamic polarization to check the corrosion tendency affect the corrosion activity on the passive surface and its interrupt (ASTM G3, G5, G59, G61) [3].The high value of the obtained oxidation-reduction potentials (E(ORP)) on the surface of austenitic steels indicates high solution oxidation strength and corrosion resistance.

SEM microscope observations show that nitric acid is the most aggressive medium in nitric acid plants. It poses a risk of intergranular corrosion. Concentrated acid is a strong oxidant and affects corrosives on many metals. Corrosion can occur in the boiler water. In the boiler system downstream of the ammonia oxidation reactor, chloride ions or dissolved oxygen is present [4]. The pitting corrosion depends on dissolved oxygen concentration, pH, and boiler water temperature. An increase in temperature contributes to an acceleration of the corrosion phenomenon. Therefore, a high risk of pitting corrosion occurs in heat exchangers.

A high chloride ions concentration in the process water can occur during the formation of nitric acid in an absorption column. Test results indicate that intergranular and pitting corrosion can occur under these conditions.

The corrosion tests are crucial for predicting damage to nitric acid plant equipment. Corrosion can cause material damage and economic losses. In addition, a breakdown of the plant or reducing production capacity can occur. Therefore, corrosion testing of the steel ensures the safety of plant operation.

References

1. M.M. Martín, Industrial Chemical Process Analysis and Design, Chapter 6 – Nitric Acid, 299-345 (2016)
2. Capała P., Ruszak M., Olszak A., Nieścioruk J., Inger M., Wilk M., *Construction materials used in nitric acid plants*, Przemysł Chemiczny 101/08 2021. DOI:10.15199/62.2021.8.1
3. Woodhouse, R. C., Boxall, C., & Wilbraham, R. J. Nitric acid reduction on 316L stainless steel under conditions representative of reprocessing. ECS Transactions, 53(21), 33, 2013. DOI:10.1149/05321.0033ecst
4. Parrott, R., H. Pitts, and H. Derbyshire Hill. "Chloride stress corrosion cracking in austenitic stainless steel." The Health and Safety Laboratory for the Health and Safety Executive: Buxton, UK, 2011.

Influence of nanoparticle additives in the molten carbonate corrosion resistance of structural materials at 700ºC

Pauline Audigié, Alina Agüero, National Institute for Aerospace Technology, INTA, Metallic Materials Area, Torrejón de Ardoz, Spain;

M. Teresa de Miguel, M. Isabel Lasanta, Francisco Javier Pérez Trujillo, Complutense University of Madrid, UCM, Surface Engineering and Nano-Materials Research Group, Madrid, Spain.

To be able to replace molten nitrates by molten carbonates and considering them as a new route for thermal energy storage in Concentrated Solar Power plants, new carbonate mixtures with a reduced melting point and optimized thermo-physical properties are required. To this end, 0.5% of α-Al_2O_3 nanoparticles were incorporated as additives into the 32% Li_2CO_3, 33% Na_2CO_3 and 35% K_2CO_3 mixture. Beneficial effect of the nanoparticle addition was obtained by reducing the melting point and increasing the decomposition temperature of the new formulation. Then, a comprehensive analysis of the corrosion performance of structural materials in contact with the new developed carbonate mixture at high temperature was imperative to evaluate their resistance and possibly identify new coated and/or uncoated material candidates for such salt. Thus, this work focused on the corrosion study of the 310H austenitic steel and IN617 nickel-based alloy, in their coated and uncoated versions, to be tested with the Li, Na and K carbonate mixture with α-Al_2O_3 additives for up to 1000 hours at 700ºC. Aluminide coated samples were obtained by slurry spraying onto each based substrate, leading to the formation of Ni-Al rich coatings. After 500 hours of exposure, the uncoated materials exhibited higher mass gains than the coated samples, demonstrating the benefit of using slurry coatings under those conditions. Interestingly, the uncoated austenitic steel performed better than the uncoated IN617 by developing a much thinner scale of corrosion products containing $LiFeO_2$ and NiO revealed by XRD. The slurry coatings evidenced a very high corrosion resistance and developed a thin oxide scale mainly formed by $LiAlO_2$. The morphology of the coating was maintained after exposure although the Al-rich external layer present on the coated 310H consumed due to both oxide formation and interdiffusion. Thin cracks were also observed but did not reach the underneath substrate.

Review of cyclic oxidation and hot corrosion life of the coatings (diffusion (aluminizing) and overlay (MCrAlY) coatings) used in power generation turbines and jet engines

Sercan Soyöz, Cevat Sarıoğlu,

Marmara University, İstanbul/Turkey

Ni, Fe and Co-based superalloys have been used in power generation turbines and jet engines due to their excellent mechanical and chemical properties in corrosive environment at high temperature for many decades. These materials exhibit high fatigue and creep life in high temperatures as well as cyclic oxidation and hot corrosion resistances. Coatings such as diffusion (aluminizing) or overlay (MCrAlY type) have been applied to superalloys to prolong their operation life. Regardless of the type of coating, the mechanical and high temperature corrosion performances of coating in the aggressive environment play important role in the failure of superalloys in power generation turbines and jet engines applications. Substrate, coating type, as well as the elements in diffusion and overlay coatings affect the life and performances of coatings. All these parameters have forced to engineers and scientists to select coating methods and chemistry of coatings to improve high temperature the performances (cyclic oxidation and hot corrosion performances) and life of the coatings in the extreme working environments.

In this work, cyclic oxidation and hot corrosion performances of the diffusion (NiAl and Pt-NiAl) and overlay (MCrAlY) coatings in the literature were reviewed and analyzed for selected widely used conditions. The conditions of the cyclic oxidation were selected as 1100 or 1150^{O}C oxidation temperature and 1-hour cycling time. Cyclic oxidation performance criteria for all coatings were determined from specimen's weight (mass) change (mg/cm^2) vs. time (total cycle time) plots. The cyclic oxidation performance of a coating was chosen as the cycle time when the mass change value of the coated sample drops to a negative (-) value.

Hot corrosion conditions were selected as either only Na_2SO_4 salt solution or Na_2SO_4 with alkali salt solutions (K_2SO_4, NaCl, etc.). The amount of salt solution was picked as maximum 3 mg/cm^2. The time of beginning of propagation stage in the specimen's weight gain vs. time plot were selected as a hot corrosion life. Beyond this, additional characterization methods such as SEM and EDS data in the literature were investigated to verify the propagation stage of the coating.

The results of cyclic oxidation and hot corrosion performances (life) of the coatings were represented in Figure 1a and 1b. Pt-aluminizing coating has the best cyclic oxidation performance with around 1700 hours. Among the overlay coatings, NiCrAlY and CoNiCrAlY – type coatings showed higher cyclic oxidation life.

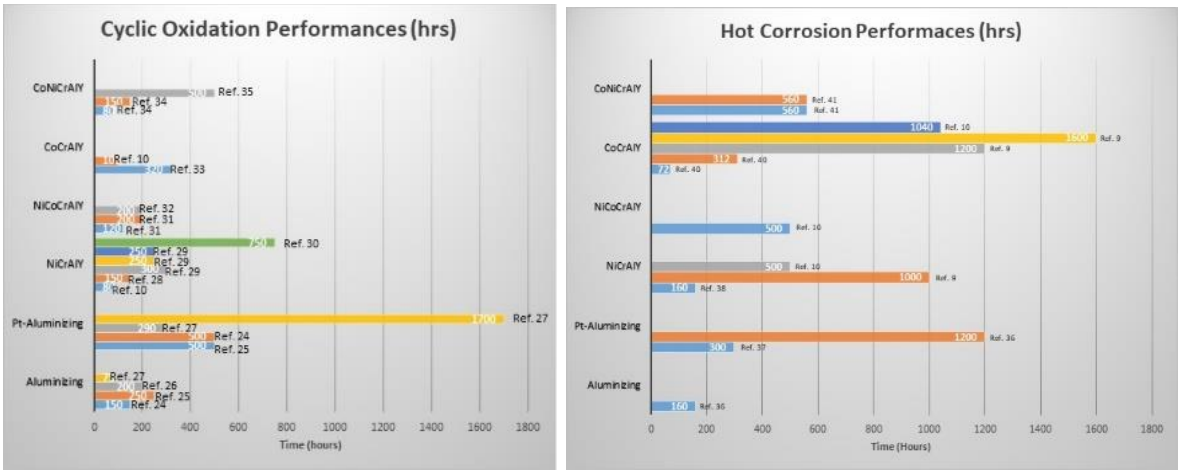

a b

Figure 1. a-Cyclic oxidation life of the coatings, b- Hot corrosion performances of coatings.

Figure 1b showed that, CoCrAlY has the best hot corrosion performance. Additionaly, Pt-Aluminizing showed great hot corrosion performance, second to CoCrAlY overlay coatings.

As a result of review of coatings, it has concluded that state of the art Pt-aluminizing has great resistance of oxidation and hot corrosion even though high cost of Pt increases its manufacturing cost. Understanding the effects of elements and phases on cyclic oxidation and hot corrosion can improve the overlay coating performance. The effect of composition, phases and coating techniques on cyclic oxidation and hot corrosion life were discussed with respect to reviewed literature to search the new overlay coatings for higher operational life.

Keywords: Diffusion coating, overlay coating, cyclic oxidation, hot corrosion, Na_2SO_4 salt solution

Vapor Phase Aluminizing of Inco 939 Alloy by Single Step High Temperature High Activity Process (HTHA)

Ece Canan Karabastık[a,b], *Cevat Sarıoğlu*[a]

[a]*Marmara University, Istanbul/Turkey*

[b]*TUSAS Engine Industries Inc. (TEI), Eskişehir/Turkey*

The alloys used for turbine sections of aero engines shall fulfill certain mechanical properties during operating conditions. The chemistry modifications to these alloys to improve mechanical properties reduce their intrinsic resistance to high temperature corrosion. Accordingly, diffusion coatings are applied to protect these alloys against environmental conditions. Aluminide coatings previously have been produced by pack cementation. During pack cementation, the substrate is directly in contact with source powder. Source powder contains pure aluminum or alloyed aluminum, halide salt activator and alumina filler. Depending on the aluminum activity of the powder and process temperature, the process is named as high temperature low activity (HTLA) or low temperature high activity (LTHA). Recently, pack cementation has been replaced by vapor phase aluminizing (VPA), which is also called out-of-pack aluminizing process, where the substrate is physically separated from source powder. In this study, a laboratory scale VPA set-up has been established. Inco 939 alloy specimens were coated via VPA by selecting different aluminum to activator ratio at 1100 °C. Effect of reactive element (RE) addition was also investigated. Coated specimens have been characterized via optical microscopy, SEM-EDS, XRD techniques to determine coating thickness, diffusion to additive layer ratio, %Al and formed phases within coating.

The resulting microstructures have shown that high temperature high activity (HTHA) condition during VPA ended different than the conventional two step high activity process. Results discussed with literature where limited number of articles found for discussing dominant diffusion mechanims based on processing temperature and Al activity.

Keywords: aluminizing, VPA, HTHA, Inco 939

COMPANY CONFIDENTIAL

Protection of γ-TiAl based alloys by TiAlSiN and CrAlSiN coatings at high temperature

Li Xin, Hao Chang, Kai Zhang, Institute of Metal Research, Chinese Academy of Sciences, Shenyang, China

γ-TiAl based alloys have been used in aero-engines due to their low density, reliable strength and good oxidation resistance. However, their application above 800°C is limited by their poor oxidation resistance. In the present investigation, TiAlSiN and CrAlSiN coatings with different aluminum and silicon contents were deposited on γ-TiAl based alloys to improve their high-temperature oxidation resistance.

The results showed that the TiAlSiN and CrAlSiN coatings with cubic NaCl type crystal structure exhibited excellent oxidation resistance when oxidized at 900°C for 1000 cycles (1000 hours at high temperature). The c-Cr(Al,Si)N coating also showed good oxidation resistance at 950°C after 1000 cycles oxidation. Si played an important role in the improvement of the oxidation resistance of the coatings.

For the $Ti_{0.50}Al_{0.40}Si_{0.10}N$ and $Ti_{0.50}Al_{0.45}Si_{0.05}N$ coatings, silicon in the coating promoted the selective oxidation of Al and the formation of an outer continuous α-Al_2O_3 layer. The aggregation of SiO_2 at the columnar grain boundaries of the inner a-TiO_2 layer in the oxide film inhibited the growth of a-TiO_2 grains and their transformation to r-TiO_2 and ensured long-term stability of the outer α-Al_2O_3 layer. The formation of SiO_2 layer at the oxide film/coating interface and the segregation of SiO_2 at the degraded coating and the a-TiO_2 layer inhibited the internal diffusion of oxygen and the external diffusion of titanium and reduced the oxidation rate of the coating. Furthermore, a continuous Ti_5Si_3 diffusion barrier layer formed at the coating/matrix interface at the initial stage of oxidation due to inner diffusion of silicon from the coating to the TiAl alloys, which was stable and effectively hindered the internal diffusion of N element in the coating and the external diffusion of the alloy

elements during the long-term oxidation process at 900 ^{o}C.

For the $Cr_{0.40}Al_{0.50}Si_{0.10}N$ coating with cubic structure, after oxidation at 900^{o}C and 950^{o}C for 1000 hours, a thin oxide scale consisted of an outer Cr_2O_3 layer and a continuous inner Al_2O_3 layer formed. After 1000 hours oxidation at 950^{o}C, although the $Cr_{0.40}Al_{0.50}Si_{0.10}N$ coating decomposed into c-CrN, c-Cr_2N, Cr and h-AlN, and h-AlN phases precipitated at the grain boundaries of Cr-rich phases, the crystal grains in the coating were still very fine. Therefore, it is considered silicon in CrAlSiN coating refined the crystal grains and inhibited the growth of the grains during oxidation, so the outer diffusion of aluminum and the formation of the continuous Al_2O_3 layer was promoted, which inhibited the internal diffusion of oxygen. For $Cr_{0.28}Al_{0.62}Si_{0.10}N$ coating with hexagonal ZnS type crystal structure, a large number of cracks formed in coatings during cyclic oxidation at 900^{o}C owing to the large difference in thermal expansion coefficient of the coating with the γ-TiAl based alloy. Many oxide ridges formed on the surface of the coatings due to the counter-diffusion of oxygen and the substrate elements along the cracks. During the oxidation processes both at 900^{o}C and 950^{o}C, serious inter-diffusion occurred between the CrAlSiN coatings and the TiAl-based alloy and a thick inter-diffusion zone(IDZ) containing a lot of voids formed. Contrary to the TiAlSiN coated alloys, due to the obvious inward diffusion of both Cr and Si in the CrAlSiN coatings, besides Ti_5Si_3 phase Cr-containing Laves phase also formed in the IDZ which destroyed the continuity of the Ti_5Si_3 layer.

Effect of the liquid metal on the plastic deformation and on the fracture of metallic alloys: copper and α-brasses in presence of In-Ga eutectic

***Ingrid PRORIOL SERRE*[1], *Marco EZEQUIEL*[1], *Marwa MOULA*[1], *Thierry AUGER*[2], *Eva HERIPRE*[2,4], *Zéhoua HADJEM-HAMOUCHE*[2], *Antoine CLEMENT*[2], *Eric LEROY*[3], *Julie BOURGEON*[3], *Loic PERRIERE*[3], *Maxime VALLET*[4]**

[1]*Univ. Lille, CNRS, INRAE, Centrale Lille, UMR 8207—UMET—Unité Matériaux Et Transformations, 59 000 Lille, France*

[2]*PIMM/Arts et Métiers Technology Institute, CNRS, CNAM, 151 Bd de l'hôpital 75013 Paris, France*

[3]*ICMPE - UMR 7182 2/8, rue Henri Dunant 94320 Thiais, France*

[4]*Université Paris-Saclay, CentraleSupélec, ENS Paris-Saclay, CNRS, LMPS - Laboratoire de Mécanique Paris-Saclay, 91190, Gif-sur-Yvette, France*

Environmentally-assisted crack initiation

In presence of liquid metal, a metal alloy, ductile in air, can be susceptible to liquid metal embrittlement (LME), which results in a loss of ductility that can cause brittle failure. LME sensitivity depends on different conditions (materials, liquid metal chemistry, strain rate, temperature, microstructure). Moreover, the mechanisms leading to LME are still poorly understood. Indeed, different models exist but their validity is only verified for very specific couples of liquid metal / metallic alloy without observations at microscopic and nanoscopic scales to explain them.

In order to advance on the understanding and the prediction of LME phenomena, we have studied in detail the LME sensitivity of the copper and α-brasses in the presence of the liquid In-Ga eutectic (EGaIn), not only the conditions of LME sensitivity, but also the study of mechanisms at macroscopic and microscopic scales through *in-situ* observations, as well as the modeling of phenomena. The interface between the copper and the α-brasses and the liquid metal has been studied because the interface is a key point in the LME occurrence.

When the EGaIn enters in contact with the copper or the α-brasses, there is the formation of the $CuGa_2$ intermetallic which forms rapidly to hundreds of nm in tens of seconds. The intermetallic forms via the dissolution of Cu into the EGaIn and then the reaction between the dissolved Cu and the Ga. Zn also dissolves into the EGaIn but does not participate in any reaction. Despite the presence of the intermetallic, the contact angle which represents the wetting of the solid material by the liquid metal is inferior to 50° for the copper and the studied brasses. It decreases with the increasing of the Zn content in the brass.

The LME susceptibility of copper and brasses containing 15, 20, 25 and 30% depends on the microstructure, the hardness, the zinc composition and the strain rate. The most important factor seems to be the composition of the copper alloy, and therefore through the plasticity mechanisms of the solid metallic material. In the cases leading to LME sensitivity, for macroscopic tests, the fracture is ductile and then brittle, which is explained by not only the formation of the intermetallic $CuGa_2$, but also a plastic deformation necessary to initiate LME. The brittle fracture is intergranular. Tests with *in situ* observations with SEM (Scanning Electron Microscopy) or TEM (Transmission Electron Microscopy) showed a brittle fracture localized at the interface of the microstructure after plastic deformation of the 30%Zn-brass. Correlation between bending micro-tests and simulation by finite elements made possible to evaluate a toughness in the presence of liquid metal for the 30%Zn-brass. The value appears consistent with that obtained from simulation at the atomic scale.

This work was funded by the ANR through the ANR GauguIn project (N° ANR-18-CE08-0009-01).

Investigations on the stress corrosion cracking initiation behavior of 316L stainless steel in high temperature water

Xiangyu Zhong[1], Tetsuo Shoji[2]

[1] *Tohoku University, Sendai, Japan, E-mail: zhong.xiangyu.d4@tohoku.ac.jp*
[2] *Tohoku University, Sendai, Japan, E-mail: tetsuo.shoji.c2@tohoku.ac.jp*

Abstract

Austenitic stainless steels have been widely used in the nuclear power plants because of their good corrosion resistance in the high temperature water. However, the stress corrosion cracking (SCC) during prolonged exposure to the high temperature water have been observed in the austenitic stainless steel components in the nuclear power plants. Several cases of SCC have been identified in the non-sensitized austenitic stainless steel components of several boiling water reactors (BWR) and pressurized water reactors (PWR) over the past years. The components actually spend most of their life in the initiation regime. Understanding the SCC initiation response has become an area of increased interest due to new efforts to extend the life of reactors with these materials.

The effects inner surface finish condition of the hollowed specimen on stress corrosion crack (SCC) initiation and small crack growth behaviors of 316LN stainless steel were investigated in a simulated pressure water reactor (PWR) primary water at 325 ^{o}C with DH levels of 15 cc (STP) H2/kg H2O by using slow strain rate tensile (SSRT) test. The SSRT tests were interrupted at different strain (at 7.5% strain and strain at the maximum load). The drilled specimen showed higher surface hardness and more enhanced SCC initiation and short crack growth behavior than honed specimen. There are many cracks were observed along the gauge length direction. Even though the tests were interrupt at a small strain (about 7.5%), many cracks were observed. It indicated that the crack initiated at the early stage of the specimen deformation. The crack depth and crack numbers are measured and collected. The depth, crack numbers and the average crack growth rate of the drilled specimen were larger than those of honed specimen. The statistical results show that the depth of most of the cracks less than 10 μm and 5μm for the specimen that was interrupt stopped at the maximum load and at the strain of 7.5%, respectively. Fractographic examinations showed mixed modes of transgranular and intergranular cracking. The influences of surface condition on SCC behaviors are discussed.

Keywords: stress corrosion cracking, stainless steel, pressure water reactor, crack initiation.

Introduction

Austenitic stainless steels have been widely used in the nuclear power plants because of their good corrosion resistance in the high temperature water [1]. However, the environmentally assisted degradation problems such as stress corrosion cracking (SCC) during prolonged exposure to the high temperature water have been observed in the austenitic stainless steels components in the nuclear power plants. Several cases of SCC have been identified in the non-sensitized austenitic stainless steel components of several boiling water reactors (BWR) and pressurized water reactors (PWR) over the past years [2, 3]. The effects of several variables, such as water chemistry, testing temperature, degree and paths of the pre-strain have focused on understanding the phenomenology of SCC of stainless steels in the nuclear power plant [4-6]. However, most of these studies have concentered on the crack propagation stage rather than initiation, the mechanistic understanding of the SCC initiation is still missing.

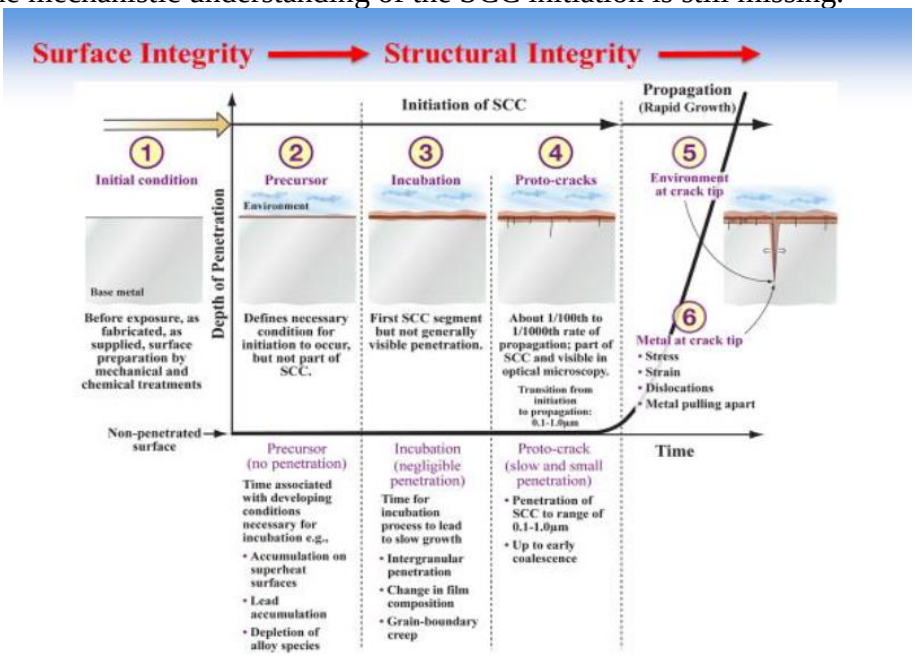

Fig. 1 The quantitative micro-nano (QMN) approach for understanding the SCC of alloys in nuclear power plants (final version from Staehle, QMN meeting) [7].

Initiation of SCC includes the precursor events, incubation and proto-cracks stage based on the quantitative micro-nano (QMN) approach proposed by Staehle (as shown in Fig. 1) [7]. Surface finish state plays an important role in SCC because all SCC cracks initiate at the surface that exposed to the high temperature water environment. The surface deformation induced by manufacturing can promote the initiation of SCC of stainless steel components in BWR. Laboratory studies suggested that localized oxidation is an important contribution factor for SCC initiation in stainless steels in BWR and PWR environment [8, 9]. Machining always introduces heavily deformed layer with residual tensile stress in the near surface region of materials. The exits of the deformed layer can accelerate SCC initiation [8, 9]. But Chang et al. [10] found that machining produced a deformation layer with an ultrafine-grained outer layer and a highly deformed inner layer on the surface of warm-forged 304L. The ultrafine-grained layer promoted the formation of protective oxide film and enhanced SCC initiation resistance compared to the polished deformation-free surfaces. Thus, in order to develop appropriate machining practices for components with extended service life, it is necessary to investigate the effect of surface machining on SCC initiation in materials used in nuclear power plants.

The slow strain rate tensile (SSRT) technique is a convenient method for the evaluation of SCC susceptibility; however, the results cannot be applied directly to the prediction of the lifespan. In order to obtain a substantial percentage of intergranular SCC (IGSCC) area on the fracture surface, Totsuka, et al., proposed the application of a V-shaped specimen with a cold-pressed hump in the middle of the gauge length, which can allow lower strain rates than flat samples and the localization of strain and damage as well as one of the important strain paths of the compression field followed by tension [11, 12]. Deleume, et al., showed that a particular V-shaped geometry of the SSRT specimen increases the crack-initiation sensitivity [13]. Although the V-shaped specimen is sensitive to IGSCC, it is difficult to calculate the local deformation in the sample as a function of the stretch of the V-shape. Especially, the strain path and the local strain rate in the apex of the V-shape are significantly more complex than that of the smooth specimen. In our previous work, we demonstrated that SSRT tests using a hollowed cylindrical specimen with a hardened machined inner surface is a useful test for the assessment of the SCC susceptibility on nonsensitized stainless steels with the relative short testing time compared with a constant load test [14, 15]. The crack depth distribution shows a feature of two peaks, related to the treated hardened layer on the inner surface. The specimens tested at a lower strain rate show a higher fraction of IGSCC, larger number of crack initiations, shorter elongation, and smaller crack opening displacement, suggesting the importance of a transitional behavior of the IGSCC initiation and short crack growth [14]. The effects of dissolved hydrogen (DH) and the condition of the inner surface finish of the hollowed specimen on the SCC initiation and small crack growth behaviors of Type 316 stainless steel (316 SS) were investigated in high-temperature water with various DH levels [15]. The drilled specimen exhibited higher surface hardness and more SCC initiations and short crack growth behavior compared with a honed specimen; however, both show a similar trend in water chemistry with different DH levels. The testing of the environment assisted fatigue (EAF) behavior of 316 SS was also conducted by using a hollowed smooth specimen in a simulated PWR primary water environment at 325°C with different strain rates and strain amplitudes [16, 17]. Crack initiation was promoted by the simulated PWR primary water environment at low strain rates under high strain amplitudes.

In the present paper, the SSRT tests have been performed on the 316LN stainless steel in a simulated PWR environment. The effects of surface condition on the SCC crack initiation behavior of 316LN in PWR primary water with various DH levels of 15 cm^3 (STP) H_2/kg H_2O at 325 ^oC were investigated.

Experimental

The material used for this study was a solution-annealed 316LN with the composition of (in wt.%): C: 0.01, Si: 0.48, P: 0.023, Cr: 17.5, Mn: 1.42, Ni. 11.64, Mo: 2.08, N: 0.116, O: 0.047, S < 0.003, the balance being Fe. Fig. 2a is the geometry and dimension of the hollowed cylindrical SSRT specimen. The preparation processing of the specimen was detailed described in our previous work [12, 13] and described briefly in the following texts. The surface finish of the inner surface of the specimens was formed by two different machining processes. One is by drilling (marked as 316LN-drilled) where a drill with 4 mm in diameter was used and machining was performed with the drill speed of ~460 rpm. The other surface finish was honed after drilling (marked as 316LN-honed) to remove the heavily machined surface and also to make the surface smoother.

The test was performed using an SSRT system with a circular high temperature water loop system (Fig. 2b). The test environment is simulated PWR primary water with 500 ppm B (as H_3BO_3), 2 ppm Li (as LiOH), dissolved oxygen (DO) < 10 ppb at 325 ^oC, 15.6 MPa. DH in the inlet water were controlled by bubbling either pure nitrogen gas, pure hydrogen gas or a mixture of nitrogen and hydrogen gases in the reservoir water tank until equilibration reached. The DH levels (15 cm^3 (STP) H_2/kg H_2O) was used in this study. Before heating the autoclave to high

temperature, the water tank was N_2 gas bubbled to deoxygenate the inlet water to <10 ppb DO. Then the autoclave was kept for one day with the H_2 gas bubbling with an over pressure at the reservoir tank to control DH of inlet water at the pre-determined level and which was continuously monitored during the test.

The strain rate of the SSRT test in the present study is about 2×10^{-7} s^{-1}. The tests were interrupted when the load reached the maximum on the Load-Displacement curves (marked as 316LN-drilled-max, 316LN-honed-max) and the strain of 7.5% (marked as 316LN-drilled-7.5%, 316LN-honed-7.5%). After a SSRT test, a longitudinal cross section was obtained by electrical discharge wire-cutting and metallographic polishing and the depth of the cracks on the cross section was measured by optical microscope (OM) and scanning electron microscope (SEM).

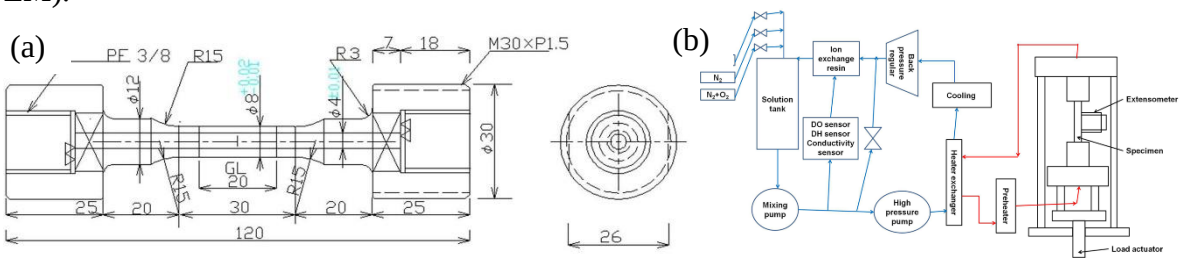

Fig. 2: (a). The schematics of SSRT tube specimen. (b) The schematics of SSRT testing system with high temperature and high pressure water loop.

Results and discussion

Fig. 3 is the stress-strain curves of 316LN different surface condition in PWR environment with DH level = 1515 cm^3 (STP) H_2/kg H_2O, which were calculated from Load-Displacement curves. The strain-stress curves show that the elongations of the specimens were affected by the surface condition significantly. The elongations of the honed specimens are larger than the drilled specimen. It means that the SCC susceptibility of honed specimen is lower than drilled specimen. Serrated stress - strain curves were also observed (Fig. 3b). They are features related to dynamic strain aging (DSA).

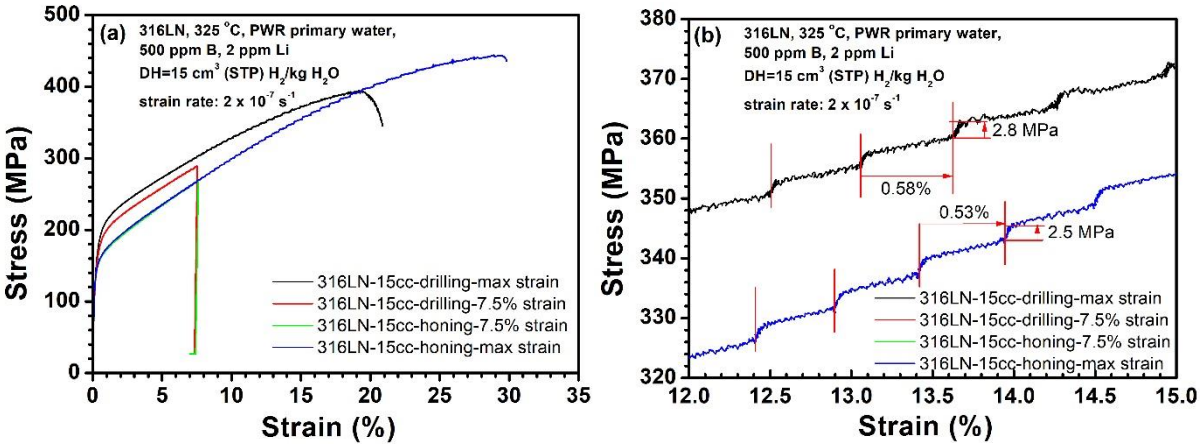

Fig. 3. The Stress-strain curves of 316LN in PWR environment with different surface condition.

Fig. 4 shows the optical morphologies of inner surface of 316LN-drilled and 316LN-honed in PWR environment with DH = 15 cm^3 (STP) H_2/kg H_2O. Many cracks were observed along the gauge length direction in all specimens irrespective of surface finish condition. Even though in the specimens interrupted at the strain of 7.5%, lots of tiny cracks were observed on the inner

surface along the gauge length direction. It indicates that the crack initiated at the early stage before the maximum load. The continued nucleation of new cracks may result in the reactivation of dormant cracks and coalescence between the dormant crack and a subsequently nucleated crack. The number and length of cracks for the drilled and honed specimen are statistically analyzed based on the optical images. The analyzed area is about 11.44 mm^2.The cracks in the 316LN-drilled specimen are longer than that of 316LN-honed specimen (as show in TABLE I). The histograms of crack traces distribution of 316LN after SSRT in PWR environment was shown in Fig. 5a. The statistical results show that the length of most cracks less than 0.2 mm for both drilled and honed specimen. The number of cracks in 316LN-drilled specimen is less than that of 316LN-honed specimen (as shown in Fig. 5b). The number of cracks for the specimen interrupt at the 7.5% strain is much larger than that of interrupt at the maximum strain for both drilled and honed specimen. The number of crack decreases may relate to the crack coalescence during the SSRT test. Fig. 5c shows the total crack length of the cracks in the analyzed area. It is clear that the total crack length for the honed specimen is longer than that of drilled specimen.

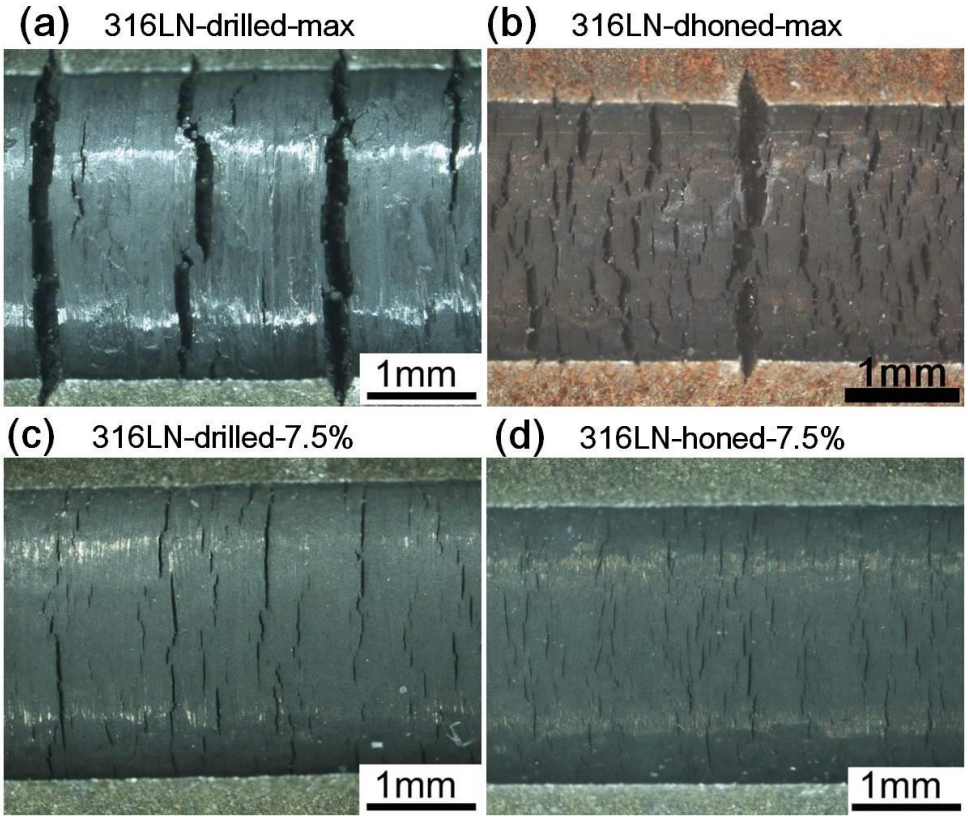

Fig. 4. The Optical morphologies of inner surface of 316LN in PWR environment with DH=15 cm^3 (STP) H_2/kg H_2O. (a, c) drilled specimen, (b, d) honed specimen.

Table 1. Crack length of drilled and honed specimen.

specimen	Length of the longest crack (mm)	Length of the shortest crack (mm)
316LN-dilled-max	2.854	0.09
316LN-dilled-7.5%	1.115	0.045
316LN-honed-max	1.725	0.074
316LN-honed-7.5%	0.551	0.037

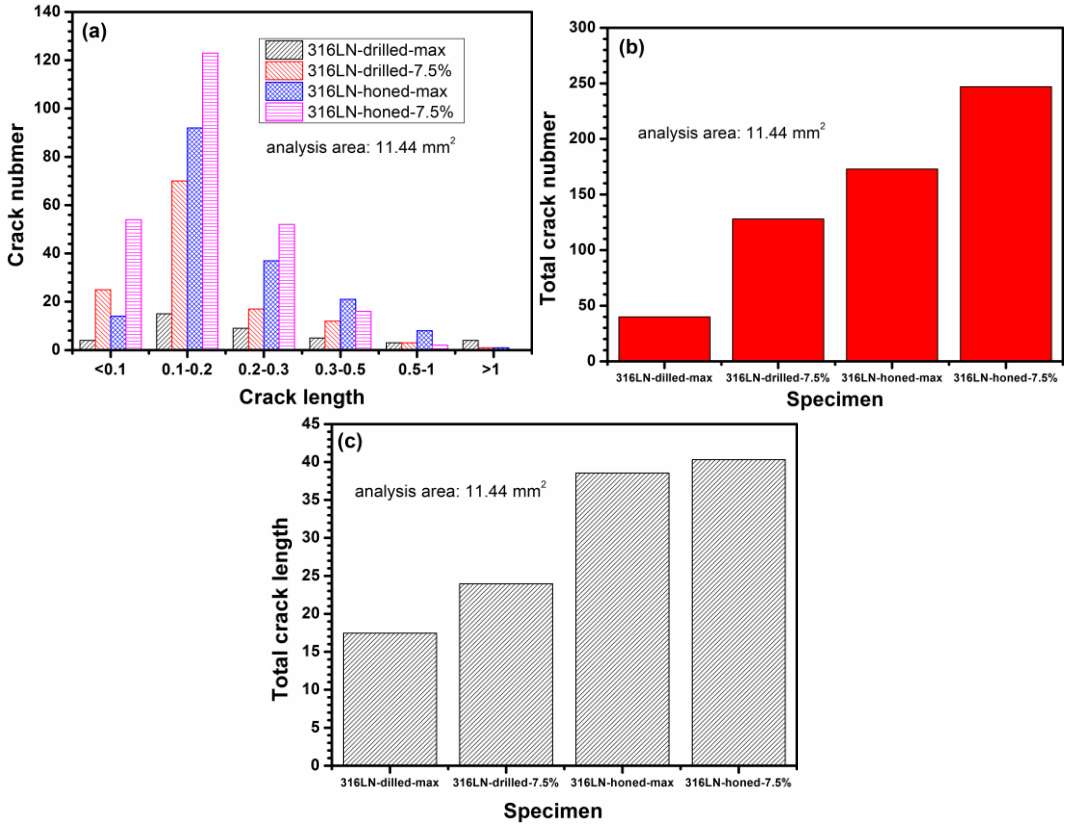

Fig. 5 (a) Histograms of crack traces distribution of 316LN after SSRT in PWR environment. (b) Total crack number for different specimens of 316LN after SSRT in PWR environment. (c) Total crack length for different specimens of 316LN after SSRT in PWR environment.

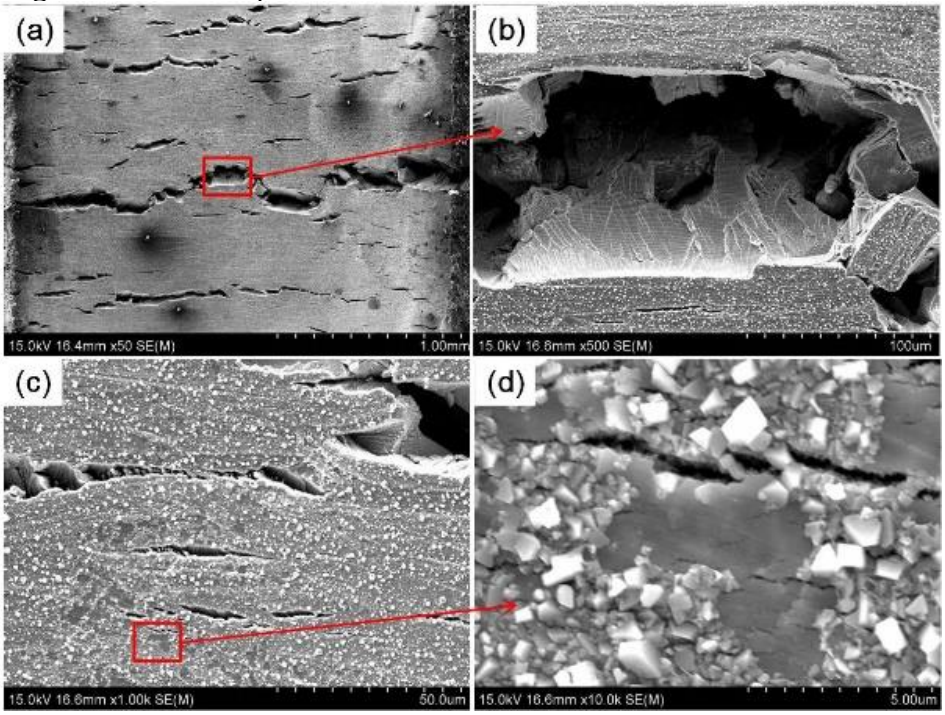

Fig. 6. The SEM secondary electron images showing the morphologies of inner surface of 316LN-honed-max in PWR environment with DH=15 cm^3 (STP) H_2/kg H_2O.

Fig, 6 and Fig. 7 show the SEM morphologies of cracks of 316LN-honed- max and 316LN-honed-7.5% specimen, separately. The crack open distance for the long cracks of 316LN-

honed-max is larger than that of 316LN-honed-7.5% specimen. The small cracks tend to achieve coalescence (Fig. 6d and Fig. 7d). Such coalescence may take place in the form of two slightly misaligned cracks on growing until their closest tips passed one another with a small distance.

Fig. 8 shows the SEM images of the cross-section of the typical long crack and short crack. The long crack opened, while the short crack closed and filled with oxide. According to the morphologies of short crack, as shown in Fig. 6d and Fig. 7d, the inner surface was covered by continuous oxide film, it is believed that the crack initiated from the damage of oxide film.

Fig. 9 shows the EBSD analysis results of the crack tip. Both transgranular crack (TG crack) and intergranular crack (IG crack) were observed. It is also found that the crack initiates as TG crack, and then transform to IG crack during the crack propagation.

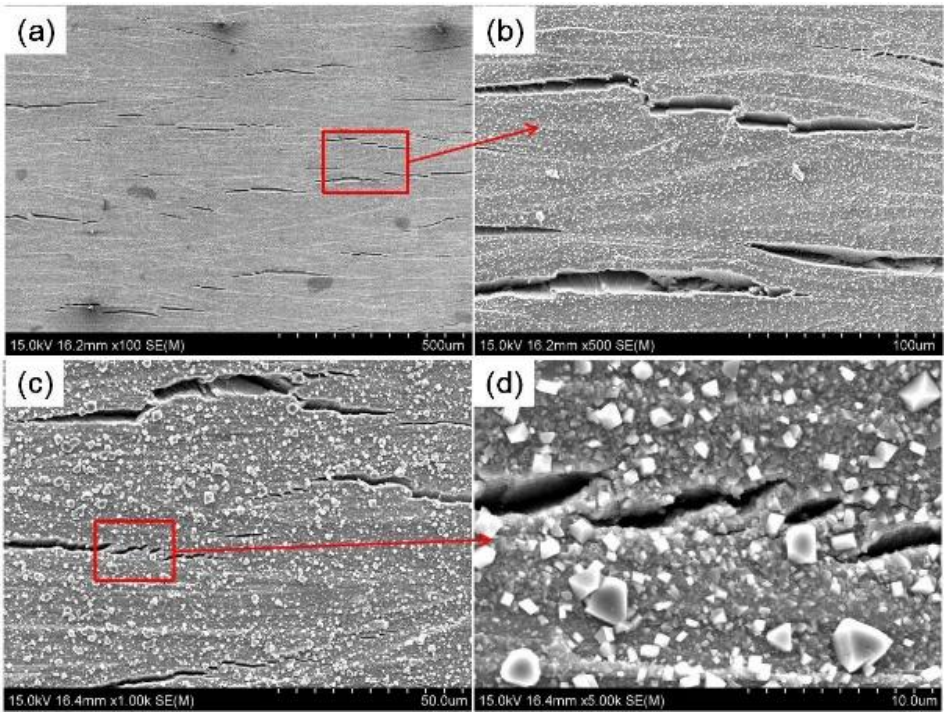

Fig. 7. The SEM secondary electron images showing the morphologies of inner surface of 316LN-honed-7.5% in PWR environment with DH=15 cm^3 (STP) H_2/kg H_2O.

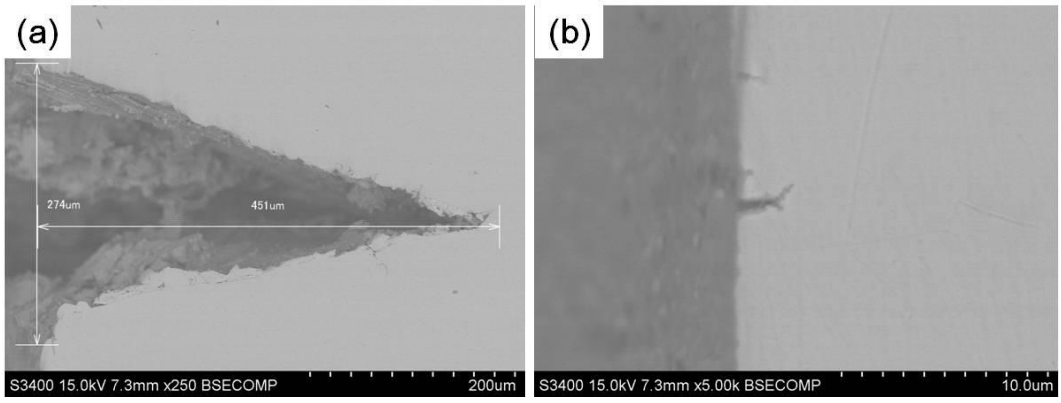

Fig. 8 SEM backscattered electron image of typical (a) long crack, (b) short crack observed in 316LN after SSRT in PWR environment.

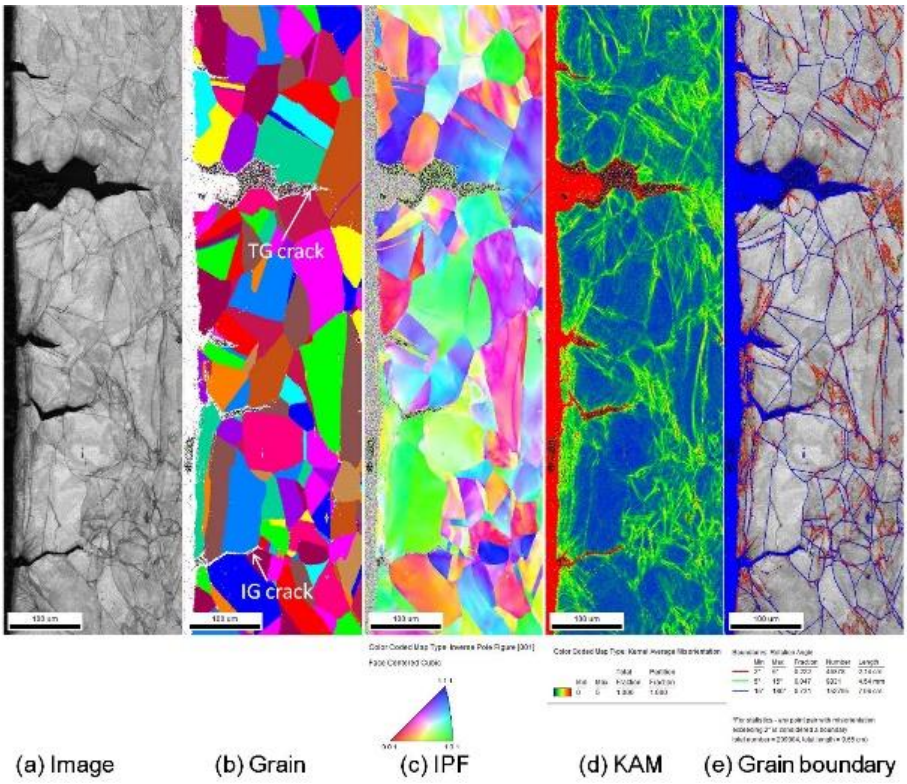

Fig. 9 EBSD results of typical crack tip of 316LN after SSRT in PWR environment.

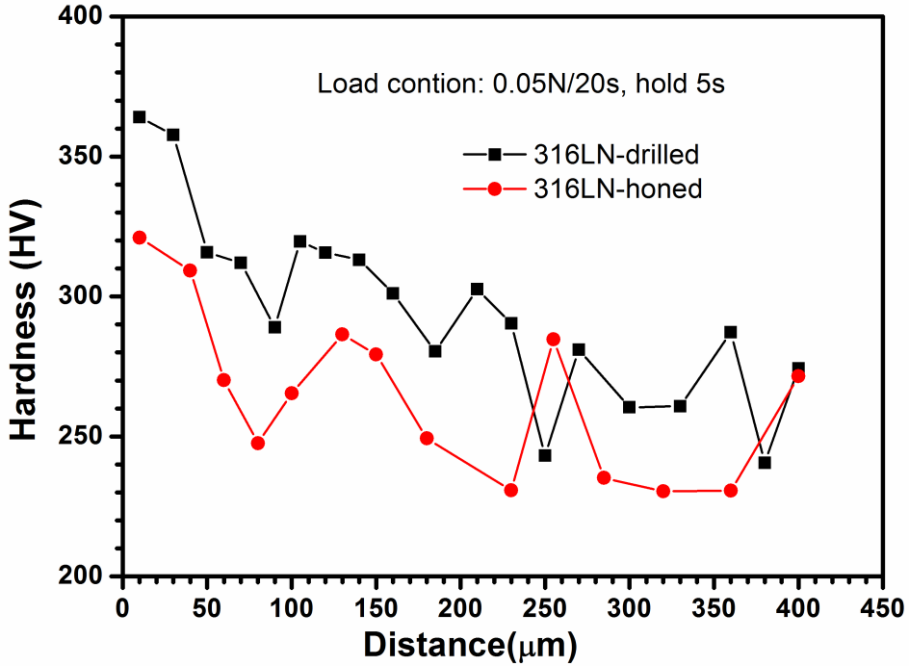

Fig. 10 Microhardness profile measured from the inner surface to the outer surface of the 316LN drilled and honed specimens

Fig. 10 shows the micro-hardness from the inner surface to the outer surface of drilled and honed specimens. It is clear that the inner surface hardness of drilled specimen is much higher than that of honed specimen, and the cold worked layer in drilled specimen is also deeper than

honed specimen. This difference of inner surface hardness could explain the difference of crack initiation behavior between 316LN-drilled and 316LN-honed specimens.

The elongation of the honed specimen is larger than that of drilled specimen (as shown in Fig. 3). Table 1 shows that the max crack length drilled specimen are larger than those of honed specimen. The typical cracks in the drilled specimen opened wider and penetrated much deeper than those of honed specimen (as shown in Fig. 4). All the above results indicate that SCC susceptibility of drilled specimen is higher than that of honed specimen. But according to Fig. 5, the crack number of 316LN-drilled specimen is less than that of 316LN-honed specimen. The honed specimen with lower surface hardness, even though under lower stress during SSRT test, exhibited more cracks than drilled specimen. This indicates that the SCC initiation susceptibility of the drilled specimen is lower than that of honed specimen. Chang et al. [10] also found that the SCC surface machined warm-forged 304L has lower SCC initiation susceptibility than that of highly-polished surface specimen due to the presence of a deformation layer with an outer ultrafine-grained layer on the machined surface. When the deformed surface was exposed to the high temperature water, it is easy to form a protective uniform oxide film than honed specimen. Due to the brittle nature of the oxide and the incompatible Young's modulus with the metal matrix, cracks initiate in the oxide layer during SSRT test, resulting in the metal matrix re-expose to the high temperature water. The fine-grain layer is easy to form uniform oxide film again. In this case the cracks terminate in the fine grain layer, leading to less crack initiation sites in the drilled surface. The cracks penetrated much deeper in the drilled specimen due to the higher crack propagation rate under higher stress during SSRT test.

Conclusions

The effects inner surface finish condition of the hollowed specimen on SCC initiation and small crack growth behaviors of 316LN stainless steel were investigated in simulated PWR primary water at 325 ^{o}C with DH levels of 15 cc (STP) H_2/kg H_2O by using SSRT test. The SSRT tests were interrupted at different strain (at 7.5% strain and strain at the maximum load). There are many cracks were observed along the gauge length direction. Even though the tests were interrupt at a small strain (about 7.5%), many cracks were observed. It indicated that the crack initiated at the early stage of the specimen deformation. The crack length and crack numbers are measured and collected. The maximum crack length of the drilled specimen was larger than those of honed specimen. The crack number of drilled specimen is less than that of honed specimen. The statistical results show that the length of most of the cracks less than 0.2 mm for the specimen that was interrupt at the maximum load and at the strain of 7.5%. Fractographic examinations showed mixed modes of transgranular and intergranular cracking. The drilled specimen showed higher surface hardness and more enhanced SCC initiation and short crack growth behavior than honed specimen.

Acknowledgments

This work has been performed as a part of the program which is jointly financially supported by the Tohoku Electric Power Co., Inc., Chubu Electric Power Co., and Tokyo Electric Power Co., Holdings, Inc..

References

[1] S.E. Ziemniak, M. Hanson, P.C. Sander, Electropolishing effects on corrosion behavior of 304 stainless steel in high temperature, hydrogenated water, Corros. Sci., 50 (2008) 2465-2477.

[2] S.J. Zinkle, G.S. Was, Materials challenges in nuclear energy, Acta Mater., 61 (2013) 735-

758.
[3] G.S. Was, P.L. Andresen, Stress Corrosion Cracking Behavior of Alloys in Aggressive Nuclear Reactor Core Environments, Corrosion, 63 (2007) 19-45.
[4] Z. Lu, T. Shoji, F. Meng, Y. Qiu, T. Dan, H. Xue, Effects of water chemistry and loading conditions on stress corrosion cracking of cold-rolled 316NG stainless steel in high temperature water, Corrosion Sci. 53 (2011) 247-262.
[5] F. Meng, J. Wang, E.-H. Han, W. Ke, Effects of scratching on corrosion and stress corrosion cracking of Alloy 690TT at 58 ◦C and 330 ◦C, Corros. Sci. 51(2009) 2761–2769.
[6] L. Zhang, J. Wang, Effect of temperature and loading mode on environmentally assisted crack growth of a forged 316L SS in oxygenated high-temperature water, Corrosion Sci. 87 (2014) 278.
[7] R. W. Staehle, Quantitative micro-nano approach to SCC mechanism and prediction. TMS Fifteenth International Conference on Environment Degradation in Nuclear Power System-Water Reactors, North Oaks;2011
[8] S. Wang, T. Shoji, N. Kawaguchi, Corrosion, Initiation of environmentally assisted cracking in high-Temperature water, 61 (2005) 137-144.
[9] S. Wang, Y. Takeda, K. Sakaguchi, T. Shoji, Role of work-hardened surface layer in initiation of environmentally assisted cracking in high-temperature water, Corrosion, 62 (2006) 651-656.
[10] L. Chang, L. Volpe, Y.L. Wang, M.G. Burke, A. Maurotto, D. Tice, S. Lozano-Perez, F. Scenini, Effect of machining on stress corrosion crack initiation in warm-forged type 304L stainless steel in high temperature water, Acta Mater., 165 (2019) 203-214.
[11] N. Totsuka, E. Lunarska, G. Cragnolino, Z. Szklarska-Smialowska, , A sensitive technique for evaluating susceptibility to IGSCC of alloy 600 in high temperature water, Scr. Metall. 20 (1986): p.1035-1040.
[12] N. Totsuka, Z. Szklarska-Smialowska, , Activation energy for IGSCC of alloy 600 in an aqueous solution containing dissolved H2 at 300 to 350 ◦C, Scr. Metall. 21 (1987):p.45-47.
[13] J. Deleume, D. Poquillon, V. Garat, J.-M. Cloué, E. Andrieu, Mechanical behaviour of SSRT specimens optimized for IGSCC concerns, Corros. Sci. 50 (2008):p.737-743.
[14] X. Zhong, S.C. Bali, T. Shoji, Accelerated test for evaluation of intergranular stress corrosion cracking initiation characteristics of non-sensitized 316 austenitic stainless steel in simulated pressure water reactor environment, Corros. Sci. 115 (2017):p.106-117.
[15] X. Zhong, S.C. Bali, T. Shoji, Effects of dissolved hydrogen and surface condition on the intergranular stress corrosion cracking initiation and short crack growth behavior of non-sensitized 316 stainless steel in simulated PWR primary water, Corros. Sci. 118 (2017):p.143-157.
[16] C. Shim, Y. Takeda, T. Shoji, Fatigue life prediction of 316 stainless steel in simulated PWR primary water by time domain analysis based on short fatigue crack growth behavior, Mech. Eng. J. 4 (2017):p.17-00035.
[17] C. Shim, Y. Takeda, T. Shoji, Continuity of Environmentally Assisted Fatigue and Stress Corrosion Cracking Based on Short Crack Growth Behavior of 316 Stainless Steel in Simulated PWR Primary Water, in: ASME 2017 Pressure Vessels and Piping Conference, ASME 2017 Pressure Vessels and Piping Conference, (2017) V03BT03A013.

Towards understanding the effect of residual stress on Atmospheric Chloride-Induced Stress Corrosion Cracking (AISCC) of austenitic stainless steels

C. Sanchez[1,2], A Bannister[1] & D. L. Engelberg[2]

[1]The Health and Safety Executive (HSE), Buxton, United Kingdom, carlos.sanchez-tobar@hse.gov.uk
[2]University of Manchester, Manchester, United Kingdom, dirk.engelberg@manchester.ac.uk

Abstract

The effect of residual stress on the propensity for Atmospheric Chloride Induced Stress Corrosion Cracking (AISCC) of austenitic Types 304L and 316L stainless steel was investigated. ASTM G58 welded plates with the surface residual stress characterised by X-ray diffraction measurements prior and after to sample AISCC exposure under controlled climatic conditions. The environmental conditions included the application of salt-laden $MgCl_2$ droplets with exposure at near-ambient temperatures and 30% relative humidity for up to 7 months. The magnitude of residual stress required to initiate AISCC cracks and the associated stress intensity factors with the propagation of SCC cracks were also evaluated.

The results showed that AISCC cracks initiated in areas with measured residual tensile stresses of 373 MPa and 483 MPa for the 304L and 316L samples. Stress intensity factors (SIF) for surface cracks ($K_{I_{sur}}$) and sub-surface cracks ($K_{I_{sub}}$) were 13 MPa$\sqrt{m}$ and 16 MPa$\sqrt{m}$ for the 304L plates, and 21 MPa$\sqrt{m}$ and 28 MPa$\sqrt{m}$ for the 316L plates. The developed cracks resulted in a stress relief of 268 MPa for 304L and 230 MPa for 316L. This work provides a better understanding of the critical exposure parameters leading to AISCC in welded test samples containing residual stress and explore a fracture mechanics approach for quantifying the relative stress conditions around a surface crack.

On the native oxide formation on 7xxx series Al alloy surfaces

Oliver Beyss, RWTH Aachen University, Aachen/Germany
Uwe Breuer, Research Center Jülich, Jülich/Germany
Daniela Zander, RWTH Aachen University, Aachen/Germany

Motivation

High strength 7xxx series aluminum alloys are widely used in the aeronautic industry, owing to their high specific strength and the generally good corrosion properties of Al base materials. These properties are enabled by the corrosion protection effect of Al oxide, which readily forms in the presence of oxygen e.g. in ambient air. While many authors described the nanometer thick amorphous oxide layer on top of pure Al and the effects of temperature and humidity [1-3], the investigation of the native oxides on Al alloys has become a more recent field of study with the increasing availability of surface analytical techniques. Studies on the surface chemistry of 7xxx alloys are limited and mostly focus on the effects of surface treatments and corrosion processes [4,5], while newer publications on Al-Cu alloys focus on the influence of alloying elements on the oxide formation and surface chemistry [6,7]. Cu enrichments at the metal/oxide interface were reported as well as oxide thickness and chemistry deviations at intermetallic Al_2Cu particles. These effects can play an important role in the initiation stages of environmentally assisted cracking phenomena and aqueous corrosion [8]. Hence, this work aims to improve the understanding of the surface chemistry of 7xxx series alloys and to elucidate the role of the additional alloying elements Zn and Mg.

Experimental Details

Samples were prepared from commercial AA7050 T7651 plate material by cutting, grinding and polishing with a water-free silica suspension in order to prevent the dissolution of alloying elements while preparing a pristine surface. Polished samples were exposed to ambient air with moderate humidity for >24 h to fully establish the native oxide. Subsequent analyses by XPS involved depth profiling by Ar sputtering with intermediate recording of survey and high-resolution spectra. ToF-SIMS depth profiling was performed both on the matrix and on Al_7Cu_2Fe particles.

Results

Both XPS and ToF-SIMS depth profiles consistently reveal the influence of the alloying elements on the resulting surface chemistry of the native oxide. An enrichment of Mg was found at the outer rim of the oxide, which is associated with its high tendency towards oxidation. Accordingly, Zn and Cu, which exhibit a lower oxygen affinity, remain primarily in metallic state and enrich at the metal/oxide interface. The native oxide on top of coarse intermetallic Al_7Cu_2Fe particles showed deviations from this general trend. Similar to Al_2Cu particles [6] the oxide on top of these particles is thinner than for the matrix and the Cu enrichment at the Al_7Cu_2Fe/oxide interface is increased. Additionally, indications for the onset of Cu oxidation were found at this interface.

A model for the native oxide on top of 7xxx series alloys is proposed (see Figure 1) considering both the matrix oxide as well as coarse Al_7Cu_2Fe particles at the surface. Both the enrichment of alloying elements near the surface and at microstructural inhomogeneities can lead to micro galvanic coupling and are hence believed to be an important factor in the initiation of (localized) corrosion processes for 7xxx series Al alloys.

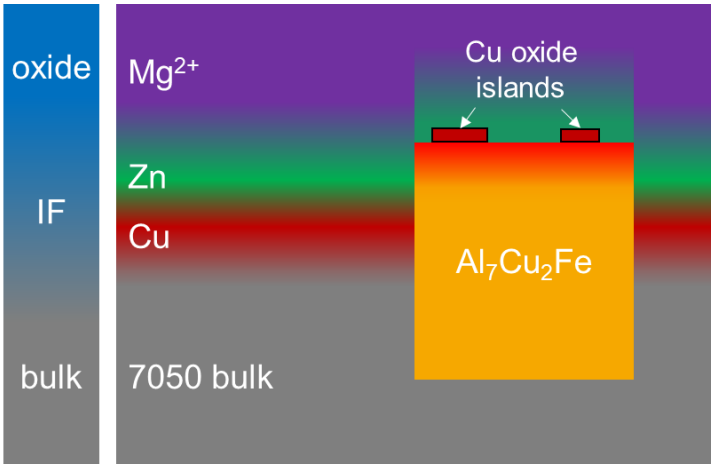

Figure 1: proposed model for native oxide on 7xxx series alloys [9]

References

[1] B. R. Strohmeier: Surf. Interface. Anal., **15** (1990) 52-56.
[2] A. Nylund and I. Olefjord: Surf. Interface. Anal., **21** (1994) 283-289.
[3] I. Olefjord and A. Nylund: Surf. Interface. Anal., **21** (1994) 290-297.
[4] C.E. Moffitt et al.: Surf. Coat. Technol., **137** (2001) 188-196.
[5] S.P. Knight et al.: Corros.Sci., **98** (2015) 50-62.
[6] P. Cornette et al.: Corros. Sci., **174** (2020) 108837.
[7] M. Li et al.: Appl. Surf. Sci., **534** (2020) 147633.
[8] M. Li et al.: Corros. Sci., **176** (2020) 109040.
[9] Beyss et al., ICAA 18, 2022, Toyama, Japan.

Environmentally-assisted Crack Initiation of 35Cr-45Ni Modified Microalloy in a Steam-Cracking Furnace

Zakaria Al-Hadhrami & Faisel Amin, OQ Refineries & Petroleum Industries, Sohar, North Al-Batinah/Sultanate of Oman

Background

Environmentally Assisted Cracking (EAC) is a phenomenon that embodies a wide range of degradation mechanisms that typically reduces the toughness value of a ductile metal that is subjected to mechanical stresses in the presence of a specific aggressive environment. The term environment applies to the chemistry of the process condition in contact with the component and other integrity operating window (IOW) parameters such as temperature and the redox potential.

This paper will discuss EAC on 35Cr-45Ni modified micro-alloy furnace tubes, which had been significantly affected by the precipitation of niobium carbide and chromium carbide along its grain boundaries.

Introduction

The paper will discuss and elaborate on actual case studies from a steam cracker unit designed to produce 867 KTA of polymer-grade ethylene and 300 KTA of polymer-grade propylene. The area of focus would be the steam-cracking furnaces commissioned in 2020, with ethane being the primary feed. A pyrolytic cracking process occurs inside the radiant coil tubes via a non-catalyzed process of high thermal decomposition of the ethane feed. The cracking process is categorized as a short residence time (SRT) cracking reaction within 0.15 – 0.20 seconds duration; the maximum tube metal temperature (TMT) is 1150°C at end of run (EOR) condition, with an expected internal coke formation.

Case Study 1: An inspection and corrosion analysis of thermal shock failure on 35Cr-45Ni modified micro-alloy furnace due to rapid and uncontrolled furnace firebox temperature drop.

Case Study 2: A review of localized crack on 35Cr-45Ni modified micro-alloy furnace tubes due to localized burning during decoking.

Significance

EAC requires three key factors to be present simultaneously before it can occur – mechanical stresses, a susceptible microstructure, and an aggressive environment. A sound understanding of the contributing factors in a specific process environment and an effective mechanical integrity management system to monitor/control these factors will reduce the likelihood of failure.

For example, avoiding excessive stresses on a modified micro-alloy furnace tube that had been significantly affected by carbide precipitation will eliminate the likelihood of catastrophic fracture due to EAC. On the other hand, mitigating the precipitation of niobium carbide and chromium carbide on modified micro-alloy furnace tubes – by effectively managing the IOW parameters – will avoid premature tube failures due to EAC.

Optimising the application of acoustic emission technique by advanced data processing for in-situ monitoring of filiform corrosion on coated aluminium alloys

C. Abarkane[a], A. M. Florez-Tapia[b], J. Odriozola[b], A. Artetxe[b], J. M. Vega[a,c], M. Lekka[a], E. García-Lecina[a]

[a] CIDETEC, Basque Research and Technology Alliance (BRTA), Donostia-San Sebastián, Spain

[b] VICOMTECH, Basque Research and Technology Alliance (BRTA), Donostia-San Sebastián, Spain

[c] Departamento de Ingeniería Química y de Materiales, Facultad de Ciencias Químicas, Universidad Complutense de Madrid, 28040, Spain

Abstract

Structural health monitoring (SHM) systems based on non-destructive techniques (NDT) have proven to enable the detection of damage in real structures. Among them, Acoustic Emission (AE) is one of the most powerful and promising techniques for in-service monitoring, due to its special features: passive and full-structure method for early detection of dynamic processes (real-time).

Filiform corrosion (FFC) on coated aluminium alloys has been successfully monitored by AE, using unsupervised clustering to analyse the AE data. In addition, the progress of the FCC filaments was visually followed as well as by Scanning Kelvin Probe (i.e. potential, filament´s head topography). Initially, the key descriptors were selected from the AE data by principal component analysis, and then the AE signals were classified by means two clustering algorithms: K-Means and DBSCAN. Results have revealed that DBSCAN algorithm is providing the most robust clustering according to the Bhattacharyya Coefficients´ evaluation: the most effective on detecting outliers and undesirable data (noise) coming from spurious sources.

Regarding the FFC mechanism itself, three different clusters were obtained, which could be related to the following phenomena: metal-coating interface delamination due to opening (tensile), sliding (shear) and mixed mode. Similar signals to the former were obtained from delamination tests that were conceived to subject the aluminium alloy-epoxy interface to opening (tensile) delamination.

Finally, the peak frequency, which evidenced a high correlation with the dominant frequencies (Power Spectrum Density), was found to be the most relevant AE

descriptor for clustering thanks to Random Forest classifier. In other words, the peak frequency provides a useful tool to detect and monitor FFC.

Corrosion detection using hyperspectral VNIR and SWIR imaging for drone-based inspection of electrical pylons.

Zakaria Bnoulkacem[*], Michiel Vlaminck[‡], Gonzalo Luzardo[‡], Hamed Zivariadab[†], Zohreh Zahiri[†], Bikram Koirala[*], Ljiljana Platisa[‡], Hiep Luong[‡], Paul Scheunders[*], Frédéric Mangialetto[◦], Irid Bufi[◦]

UAntwerp[*], imec[†], Ghent University/imec[‡], Elia[◦]

Background:

High-voltage power pylons are often located in remote or hard-to-reach areas, and inspecting them for corrosion can be dangerous for human workers. Therefore, drones can be used to safely inspect these towers from a distance. In this work, we aim for inspection using drones that are equipped with hyperspectral cameras as they provide more information on the spectral reflectance of the material enabling more accurate corrosion detection and classification of its severity. However, there are several challenges related to hyperspectral imaging in outdoor environments. First, the environment is subject to varying incident solar radiation (as opposed to lab environments where the light can be controlled). Second, the measurements depend on the sensor viewing angle and is a mixture of reflection and diffusion. Third, the shadows, both from other objects and self-shadowing influence the reflectance of the material. Fourth, spectral corrections are needed to deal with the inherent effects of the sensors, such as harmonics, cross-talks and leakage.

Objectives

The objective of this study is to develop a method for detecting outdoor corrosion using multispectral imaging in the visible and near-infrared (VNIR) and short-wave infrared (SWIR) wavelength regions, and to validate it on the problem of non-destructive corrosion detection on electricity pylons using drones.

Methodology:

A camera system, designed for use on drones is used to take ground measurements from corroded samples of decommissioned pylons. The system consists of 2 snapshot cameras from imec: a VNIR camera with 24 bands, and a SWIR camera with 9 bands. Three levels of corrosion (superficial, medium and severe) have been defined, related to the material loss after cleaning it. Before detecting and classifying corrosion, i.e. to differentiate between the various levels of corrosion, several pre-processing steps are carried out: dark noise correction, demosaicking, radiometric and non-uniformity correction and spectral normalization. Subsequently, spectral unmixing is applied as

follows. First, based on visual inspection, endmember spectra are selected from the image data that represent the 3 levels of corrosion. Then, the fully constrained least-squared unmixing algorithm is employed. To validate the classification results, they were compared with the material loss of the imaged samples after corrosion cleaning.

Results:

Fig. 1 and Fig. 2 show a sample VNIR and SWIR image, respectively, and the obtained classification result. After validation, the results indicate that both SWIR and VNIR data can effectively detect corrosion in outdoor conditions. The combined use of both types of imaging allows for a more comprehensive analysis of the samples, as the different wavelength regions provided complementary information about the state of the samples. One of the main challenges encountered was the presence of hard shadows that obstruct light from the samples, which make it difficult to accurately detect and classify corrosion.

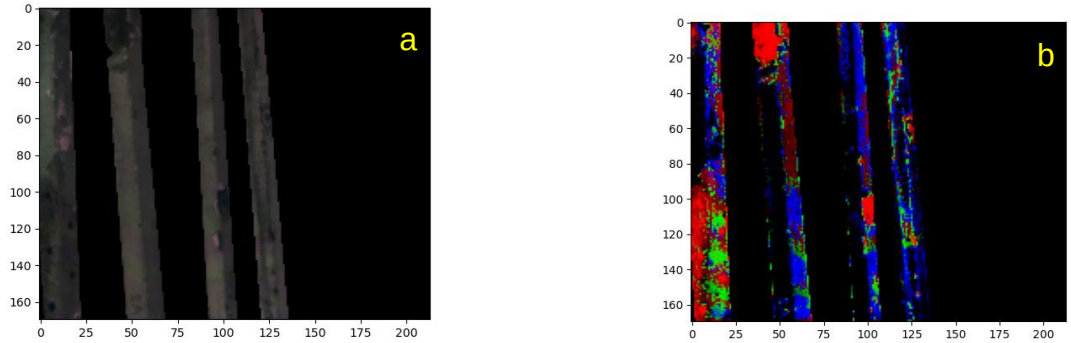

Fig. 1: a: False color composite of the original SWIR image b: Corrosion characterization maps of severe (red), medium (green), and superficial corrosions (blue) from SWIR Image.

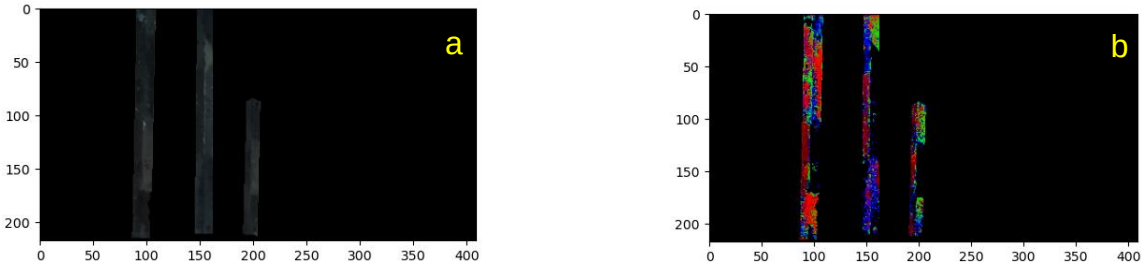

Fig. 2: a: False color composite of the original VNIR image b: Corrosion characterization maps of severe (red), medium (green), and superficial (bleu) corrosions from VNIR Image.

Conclusion

This study presented an efficient and non-destructive technique for detecting outdoor corrosion on electricity pylons using VNIR and SWIR imaging, with the purpose of reducing the manpower and risks associated with electricity pylon inspections.

Development of a new sensor-based method to investigate corrosion under insulation (CUI), supported by ORP-EIS data

Z.Jiryaeisharahi[1], D. De Keukeleere[2], Y. Desmet[2], B.Wouters[1], H.Terryn[1], A.Hubin[1]

1- Research Group Electrochemical and Surface Engineering, Department of Materials and Chemistry, Vrije Universiteit Brussel, Pleinlaan 2, 1050 Brussels, Belgium

2- IsensPro, Technologielaan 3, 3001 Leuven, Belgium

Corrosion under insulation (CUI) is a form of localized corrosion that occurs due to penetration through the insulation of moisture and ions which comes into contact with the underlying metal. Penetrated moisture and ions are trapped in the gap between insulation and metal surface, and due to their accumulation this type of corrosion is more aggressive than the external corrosion of uninsulated metals. CUI is a serious concern for petroleum and chemical process industries and it is the significant cause of sudden and hazardous failure of pipelines in gas and oil industry. It is reported that the cost of CUI detection and failure damage is around 40–60% of the total pipe maintenance costs [1-3].

Several on-line techniques have been used to investigate CUI such as Infrared (IR) imaging and neutron backscattering, radio frequency identification (RFID), transmission X-ray and conventional monitoring corrosion methods such as electrochemical impedance spectroscopy (EIS) and electrochemical Noise (EN) [4]. Monitoring CUI with aforementioned techniques is a complicated and time consuming process since some methods require the removal of insulation and cladding or cannot give a direct and reliable indication of the corrosion status of the materials.

In this research we are focusing on the development of a new sensor-based method to study corrosion under insulation. This technique, which is developed by IsensPro, is used as a non-destructive and in-situ method for detecting CUI. This new method works on the basis of changes in capacitance due to the water-uptake. To understand and validate the results of the sensor, experiments have been conducted by odd random phase electrochemical impedance spectroscopy (ORP-EIS) simultaneously. This method is a multi-sine technique and allows for fast measurements [5]. With these two methods, we investigate corrosion under insulation from the top surface of the pipes (cladding) without insulation removal. The main purpose of this research is

finding a correlation between ORP-EIS data (such as resistive and capacitive behavior, electrochemical reaction at interface and time of onset of corrosion) and sensor data to study the electrochemical reactions and monitor electrolyte-uptake under insulation.

[1]. Burhani, N. R. A., Muhammad, M. & Ismail, M. C. Corrosion under insulation rate prediction model for piping by two stages of artificial neural network. AIP Conf. Proc. 2035, 030004 (2018).

[2]. Fitzgerald, B. J. & Winnik, S. A strategy for preventing corrosion under insulation on pipeline in the petrochemical industry. J. Prot. Coat. Linings 22, 52–57 (2005).

[3]. Q. Cao, M. Esmaily, R. L. Liu, N. Birbilis and S. Thomas. Corrosion of mild steel under insulation – the effect of dissolved metal ions. Corrosion engineering, science and technology. 1743-2782 (2020).

[4]. Y.Hou, T.Pojtanabuntoeng and M.Iannuzzi. Use of electrochemical current noise method to monitor carbon steel corrosion under mineral wool insulation. Material degradation. 39 (2020).

[5]. T.Breugelmans, E.Tourwé, Y. Van Ingelgem. J.Wielant, T.Hauffman, R.Hausbrand, R.Pintelon, A.Hubin. Odd random phase multisine EIS as a detection method for the onset of corrosion of coated steel. Electrochemistry communications. 12 (2010).

Application of novel resistometric sensors for corrosion monitoring in atmosphere

Kateryna Popova; Tomáš Prošek; Václav Šefl; UCT Prague, Czech Republic

Corrosion monitoring is a powerful tool for evaluating the environmental corrosiveness and corrosion behaviour of metallic materials and, consequently, predicting their service lifetime, preventing rapid failures and understanding corrosion processes. The resistometric corrosion monitoring technique is based on the electrical resistance (ER) measurement of a thin metal track exposed to an aggressive environment. As the track corrodes, its thickness decreases, leading to an increase in ER, directly reflecting the material loss and the corrosion rate. Compared to other monitoring methods, the resistometric technique is rather simple in terms of sensor fabrication and data interpretation and is applicable from low-corrosive atmospheres to highly corrosive conditions.

The CorrSen monitoring system was developed based on the resistometric principle for corrosivity evaluation in various environments. The system includes resistometric sensors with three simultaneously exposed measuring tracks, small wireless loggers that record ER, temperature and relative humidity (RH), communication interface, and cloud software for data processing and presentation. Depending on the logger modification and ER sensor characteristics, corrosivity of clean indoor, polluted industrial, or aggressive outdoor atmospheres can be measured.

The paper gives examples of CorrSen applications. As monitoring using fresh sensors may not fully reflect corrosion behaviour of pre-exposed materials, sensors with pre-corroded surface were developed and their application e.g. in cultural heritage protection is documented. In another application, copper and iron sensors were applied to determine the reasons for rapid material degradation in a swimming pool hall. It is shown that a few short air conditioning failures accompanied by increases in RH were responsible for the principal part of material degradation. Another case study deals with a model experiment on the effect of vehicle parking conditions during winter and the role of natural crevices. Owing to the simple operational principle and user-friendly communication interface, the system provided direct real-time and easy to interpret environmental and corrosivity data.

Correlation between weather and corrosivity – analysis of time resolved sensor data on three different coastal locations

Ole Øystein Knudsen [1], Bahman Daneshian [2], Daniel Höche [2], Anders Werner Bredvei Skilbred [3], Yves van Ingelgem [4]

1. SINTEF Industry, Richard Birkelandsvei 2B, N-7465 Trondheim, Norway
2. Helmholtz-Zentrum Hereon, Max-Planck-Straße 1, 21502 Geesthacht, Germany
3. Jotun Performance Coatings, Hystadveien 167, 3202 Sandefjord, Norway
4. Zensor, Witte Patersstraat 4, 1040 Brussels, Belgium

Background

Corrosivity is a key parameter for selecting protective organic coatings and predicting coating lifetime, as described in ISO 12944-5 "Corrosion protection of steel structures by protective paint systems". Corrosivity is defined by the first-year corrosion, and the limits for the various corrosivity categories are given in ISO 9223 "Corrosivity of atmospheres - Classification, determination and estimation". Measuring corrosivity (ISO 9226) takes one year and will give the accurate corrosivity that year, but corrosivity will vary somewhat from year to year. The standard also describes some typical environments for the various categories of corrosivity, but this will be a rough estimate. ISO 9223 also provides a dose-response model for calculating corrosivity. However, this model includes deposition rate of chloride and sulfur dioxide. These two parameters are difficult to measure, and more difficult than to measure corrosivity directly.

Objectives

The objective with this work has been to improve our understanding of corrosivity and to predict corrosivity in coastal environments from investigate if readily available weather data, without using chloride and sulfur dioxide deposition rates.

Results

Sensors for measuring corrosion, temperature, relative humidity, and surface conductivity was deployed on four different locations in Norway (x2), Sweden and

South Korea. In addition, local estimates of wind and precipitation were collected from other sources. The data sets were collected with 1 hour resolution. From a previous data set, it was found that both time of condensation and wind speed increase corrosion, while precipitation seems to decrease corrosion [1].

Corrosivity on the various test sites vary from C2 to C5. Strong correlation between weather and corrosion is found for each specific site. Corrosion was discontinuous on all locations but occurred partly as discrete events with intervals of no corrosion between. Specific weather events must have both triggered and stopped corrosion. Chloride deposition affect corrosivity significantly, as documented by the ISO 9223 model, but this parameter is also highly dependent on distance to shore and elevation over the sea. Any model for predicting corrosion must take this into account. Formation of salt particles in the air over the sea depends on wind and waves.

References

1. B Daneshian, D Höche, OØ. Knudsen, AWB Skilbred, "Effect of climatic parameters on marine atmospheric corrosion: correlation analysis of on-site sensors data", npj Materials Degradation, in press.

A global corrosivity map constructed from open-source climatic data

Anders W. B. Skilbred, Jotun AS, Sandefjord/ Norway
Sergiu Paereli, Jotun AS, Sandefjord/ Norway
Andreas Krapp, Jotun AS, Sandefjord/ Norway

Abstract

Atmospheric corrosivity is one of the most important parameters in order to assess proper corrosion protection and maintenance intervals for steels constructions. However, although corrosion is estimated to cost society more than 3.4 % of the industrialized worlds GDP, corrosivity is not an easily accessible value that can be extracted for any given location. Various studies and research projects have over the last three decades gathered corrosivity data as well as climatic conditions and thereby provided the background for developing the ISO 9223 standard. The ISO 9223 provides guidance on how to calculate the corrosivity rate at a certain location based on input data such as temperature, humidity, pollution and chloride deposition. Weather- and climatic data is readily available in various open source meteorological databases. Over the last years databases collecting other climatic data have also been made available, including databases containing data on atmospheric sea salt and sulfur dioxide.

One of the challenges with the available data for e.g. sea salt distribution is the limited spatial resolution of the dataset. This means that one datapoint can cover widely different geographical locations e.g. offshore and inland environment.

In this paper a method for estimating first year corrosion rate for any given global longitude and latitude pair is presented. The method uses various techniques such as linear interpolation for estimation of sea salt distribution, humidity and temperature, and correction of the coastal areas. ISO 9223 has then been used to estimate first year corrosion rate and corrosivity category for any location. The estimated corrosivity rates

and categories have been verified and validated using literature data and collected data.

The solution provides the user with high resolution information describing the corrosion rate at any given location.

Deep transfer learning leveraging the prediction of atmospheric corrosion monitor sensors

V. Vangrunderbeek[1], L.B. Coelho[1], D. Zhang[2], Y.V. Ingelgem[1], H. Terryn[1]

[1]Department of Materials and Chemistry, Research Group Electrochemical and Surface Engineering, Vrije Universiteit Brussel, Brussels, Belgium

[2]Beijing Advanced Innovation Center for Materials Genome Engineering, Institute for Advanced Materials and Technology, Uni. of Science and Technology Beijing, China

Atmospheric corrosion sensors (ACM sensors), based on the principle of measuring galvanic corrosion between two electrodes with different electrochemical potentials, have proven to be an efficient way of assessing the corrosiveness of the environment from which the expected corrosion performance of a metal can be derived. Nonetheless, the data generated by ACM sensors is complex, and it is challenging to determine interpretable correlations between the different variables measured using only analytical corrosion expertise. Recently, studies[1,2] have shown that machine learning models are able to unravel unexplored patterns between the environment and the current output, thereby unlocking the potential to develop predictive atmospheric corrosion models. However, one limiting factor is the large amount of data from long testing times required to make proper predictions in the environment where the sensor was placed.

Our research argues that the specific subdomain of machine learning called transfer learning (TL) can solve this issue. In essence, TL attempts to transfer knowledge from a previously developed machine learning model (the source) to another similar task (the target). As such, it provides a way to improve the modeling performance in domains where data is scarce. When predicting the sensor's output for a year, fine-tuning of previously trained source model is required. This source model can be trained on data derived from a sensor installed in a controlled lab environment or a different geographical setting. The results obtained so far suggest that when only 1 to 3 weeks' worth of hourly ACM sensor data is available in a particular outdoor setting, a two-fold increase is expected in the target model accuracy of 1 year.

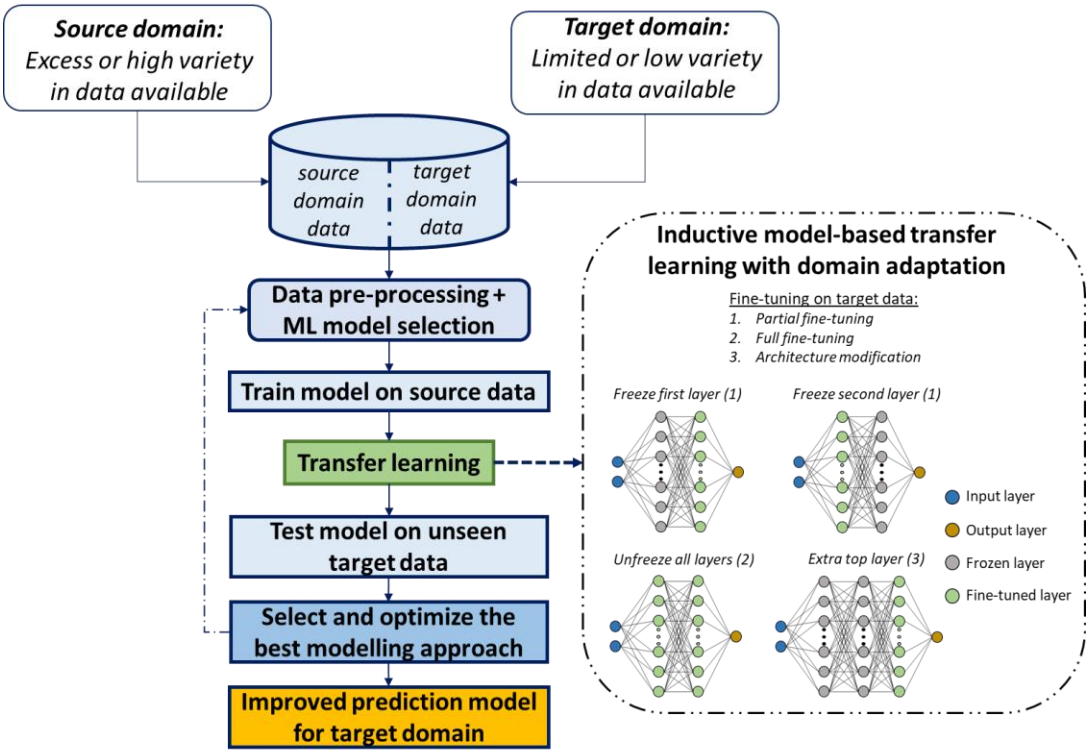

[1]Coelho, L.B. et al. Reviewing machine learning of corrosion prediction in a data-oriented perspective. npj Mater. Degrad. 6, 8(2022).doi:10.1038/s41529-022-00218-4

[2]Pei, Z. et al. Towards understanding and prediction of atmospheric corrosion of an Fe/Cu corrosion sensor via machine learning. Corrosion Science 170 (2020).doi: 10.1016/j.corsci.2020.108697

Major Challenges and Future Perspectives of Corrosion Science and Engineering

Mike Yongjun Tan

School of Engineering, Deakin University, Waurn Ponds, VIC 3216, Australia

* M. YJ Tan (mike.tan@deakin.edu.au)

Over the past century, substantial progresses in corrosion science and engineering have facilitated the development and application of a wide range of anti-corrosion materials and methods for the effective control of corrosion and materials degradation in various engineering structures. In this current 'age of change' in environmental and social policies, safety and industrial regulations, energy and resource sustainability standards, it would be appropriate to ask ourselves, 'what will corrosion science engineering look like in the future, say 50 to 100 years' time'? This paper presents some thoughts and discussion on current challenges and future prospects of corrosion science and engineering, with an aim to initiate new ideas and further thinking on the future of the field.

The ultimate goal of corrosion science and engineering should be to effectively prevent the pre-mature failure and to economically extend the safe operational life of engineering structures for the provision of the world's essential services and the maintenance of its economic activities. Unfortunately, currently there are knowledge and technological gaps that limit the ability of engineers to proactively, reliably, environmentally friendly and economically detect, predict and control localised forms of corrosion in complex environmental conditions. Based on literature review and analysis, several major challenges have been identified: (i) The effective detection, control and management of localised forms of corrosion in complex and variable industrial environments remain major challenges in corrosion engineering. (ii) The protection and life extension of future renewable energy infrastructures will probably be the biggest future need and challenge for corrosion engineering in order to sustain the world's future greener energy supply. (iii) More reliable and accurate corrosion forecast and prediction capabilities are needed in order to meet the society's increasingly higher safety standards. (iv) New eco-informed and environmentally

friendly anti-corrosion materials and methods are needed to meet progressively strict regulations for environmental protection.

Discussions on future perspectives of addressing these challenges are presented. It is considered that a prerequisite for addressing all these major challenges is the capability to effectively sense, locate, monitor and predict complex forms of localised corrosion, the prime threat to the integrity of metallic structures, and the timely and accurate application of environmentally friendly and economically sustainable corrosion control materials and measures. Considering the variable nature of corrosion environments and mechanisms in practical engineering structures, corrosion management and prevention actions may need to be adjusted smartly and dynamically based on the prevailing local corrosion conditions and mechanisms. For this reason, acquiring corrosion data more frequently and location-specifically would be necessary not only for early warning of unanticipated structural failure but also for evaluating the efficiency of corrosion control measures such as cathodic protection, corrosion inhibitors and protective coatings. An ‘ideal’ future corrosion prediction and control system would be one that not only provides in-situ and site-specific corrosion data required to visualise localised corrosion, but also to analyse and use such data to inform more effective corrosion prediction and control actions, for instance, to guide local coating repair and to regulate local cathodic protection potential and corrosion inhibitors injection. In this manner, the threat of localised corrosion to the integrity and safety of future engineering structures would be minimised and the safe operational life of infrastructure would be maximised in an economical, sustainable and environmentally friendly manner.

Corrosion rate prediction of zinc and steel in accelerated corrosion tests using machine learning and real-time corrosion sensors

Johan Becker[1], Erwan Diler[1], Franky Tanguy[1], Flavien Vucko[1]

[1]French Corrosion Institute (RISE), Brest, France

The ability of electrical resistance (ER) corrosion sensors to monitor corrosion and corrosion rates of zinc and steel has been shown in a wide range of laboratory and field conditions, including accelerated corrosion tests and natural weathering conditions. The possibility to acquire a large amount of real-time corrosion rates and *in situ* environmental information combined with machine learning appears of great interest to develop predictive model for atmospheric corrosion. Under accelerated test conditions, such method is relevant in terms of reactional mechanism understanding and lifetime prediction. Moreover, it allows obtaining a critical approach in terms of climate chamber abilities to follow cycle specifications, possibly explaining some corrosion deviation observed since decades in such tests. The deployment of this method to field conditions appears very promising for a more global corrosion prediction.

Hence, the development of a model able to predict corrosion rates of zinc and steel under several standards and modified accelerated tests was initiated. The model was trained using a wide range of parameters such as salt concentration, contamination frequency, temperature and relative humidity. Several machine learning approaches were considered and compared. The model was finally assessed with a specific corrosion test.

Using machine learning for the investigation of corrosion behavior in steel structures located in marine environment

Mohamed El Amine Ben Seghier, Institute of Surface Science, Helmholtz-Zentrum Hereon, Geesthacht 21502, Germany

Daniel Höche, Institute of Surface Science, Helmholtz-Zentrum Hereon, Geesthacht 21502, Germany

Bahman Daneshian, Institute of Surface Science, Helmholtz-Zentrum Hereon, Geesthacht 21502, Germany

Mikhail Zheludkevich, Institute of Surface Science, Helmholtz-Zentrum Hereon, Geesthacht 21502, Germany

Steel alloys are used to build the majority of offshore energy structures, including fossil and renewable energy (e.g. wind turbines and support jackets) sectors due to their mechanical properties, high strength, and resistance to the exterior environment. However, the marine environment is usually rich in many factors that can cause the initiation, development, and growth of corrosion on the surfaces of these structures. In this conference paper, machine learning technique are used to predict the behavior of corrosion in steel structures located in marine environment. To achieve this goal, a comprehensive database that includes real state of corrosion and the environmental factors surrounding the structure is used. The results are then compared to investigate the model's performance and the impact of corrosion on the safety of such structures. The study demonstrates the utility of using machine-learning models as a powerful alternative tool for predicting corrosion state in marine structures

Estimating the rate of corrosion under insulation (CUI) with a remote monitoring system

Aliakbar Oskuie[1], Joy Sumner[2], Sue Impey[3], Andy Pidcock[4], Hoi Yeung[5], Claudia Martinez Pinon[6]

[1]Cranfield University/CorrosionRADAR Ltd., UK, a.oskuie@corrosionradar.com
[2]Cranfield University, UK, j.sumner@cranfield.ac.uk
[3]Cranfield University, UK, s.a.impey@cranfield.ac.uk
[4]CorrosionRADAR Ltd., UK, a.pidcock@corrosionradar.com
[5]Cranfield University/CorrosionRADAR Ltd., UK, h.yeung@cranfield.ac.uk
[6]CorrosionRADAR Ltd., UK, c.martinez@corrosionradar.com

Abstract

Corrosion under insulation (CUI) is an insidious type of corrosion. The fact that CUI is not detectable until the failure of the asset causes extreme safety risks and substantial costs for plant operators. Due to its location, CUI can proceed unnoticed. To detect CUI at an early stage, various non-destructive testing (NDT) and monitoring techniques have been proposed and commercialized [1-3]. For certain applications, CUI monitoring is the preferred way of managing the CUI risk. This is because it provides more reliable real-time data on the state of the asset and can offer information over a larger coverage as compared to most non-destructive testing (NDT) techniques.

Across the sector, to date CUI monitoring systems rely on sensors that detect changes in certain physical properties of the insulated system. Available sensors either detect the water inside insulation materials or are sacrificial sensors that corrode. Validation and calibration of the sensor data with field conditions has been the main challenge. It is vital to ascertain that the alarms given by the systems are true and lead to suitable action.

In this study, a novel CUI monitoring system based on electromagnetic guided radar (EMGR) technology has been employed to observe moisture movement pattern in the insulation and to obtain corrosion rates, which could then be compared against those obtained for corrosion coupons. Different corrosive environments with various corrosivity potentials were compared using a bespoke CUI test rig. Post-exposure correlation of the sensors' data to coupons' weight loss measurements has been found. In addition, microscopic examination has been carried out to observe the morphology of corrosion on the samples. The study revealed pitting pattern in corrosion and emphasizing non-uniform moisture movement within the cladding. The implementation of this monitoring system holds great promise for proactive maintenance, cost reduction, and enhanced safety in CUI-related industries. The results of this study are essential for CUI monitoring field applications and will offer insight to others looking to estimate CUI rate using monitoring systems.

Keywords
Corrosion under Insulation; Monitoring; Sensor; EMGR

Introduction

Corrosion under insulation (CUI) is a costly and prevalent form of corrosion, accounting for a substantial portion of pipe maintenance budgets and leading to incidents and near misses [4,5]. To tackle this challenge, Asset Integrity teams have made significant efforts to comprehend CUI phenomena and develop effective mitigation strategies [5]. While carbon steel and stainless steel are both susceptible to CUI, their corrosion modes differ [6]. Laboratory tests have shown that corrosion rates under insulation conditions far exceed those in aerated environments due to the unique microenvironment formed beneath the insulation. This has led to improved design measures and the adoption of CUI monitoring methods [7].

To control CUI risks, a robust inspection and maintenance process is essential. Traditional inspection techniques may miss critical spots, prompting the need for continuous monitoring. CUI monitoring provides real-time data on the asset's condition, enabling timely corrective actions. Particularly in cases where insulation removal is impractical, CUI monitoring proves invaluable. As such, various monitoring technologies have been developed, including those detecting water or moisture inside the cladding and sacrificial sensors that corrode over time, offering valuable corrosion rate data [8].

This study introduces a novel CUI monitoring system utilizing both types of sensors and incorporating Electromagnetic Guided Radar Technology (EMGR) to estimate the CUI rate [9]. By detecting water presence, a necessary condition for corrosion propagation, this system estimates the corrosion rate. Electrochemical tests and weight loss measurements were conducted on a bespoke CUI rig to compare the monitoring system's results with coupons under simulated corrosive conditions. The significance of this study lies in its potential to aid integrity teams in understanding the value of CUI monitoring, enabling them to prevent conducive conditions for CUI and predict corrosion through corrosion rate estimations. This predictive capability can empower a proactive and efficient predictive maintenance approach, shifting from corrective to preventive measures.

Experimental Methodology

CUI rig tests

In this study, a custom-designed CUI test rig with a 100 mm diameter coated pipe and internal heating element for temperature control was used. An expansion chamber accommodated oil expansion. The rig allowed investigation of ring samples at 12 o'clock, 6 o'clock, 3 o'clock, and 9 o'clock positions, and square-shaped coupons within insulation. CUI monitoring corrosion sensors were installed linearly at 6 and 12 o'clock positions, with a moisture sensor covering insulation thickness. Mineral wool insulation (Rockwool) was chosen and aged at 150°C for 1 hour to reduce hydrophobic properties. Galvanized steel cladding was installed on both sides, and corrosive solutions circulated twice daily. Schematic details of the setup are shown in figure 1. To simulate wetting conditions, we pumped and circulated corrosive solutions inside the cladding twice daily (every 12 hours) from the solution reservoir to the top of the cladding, ensuring a consistent wet environment for the insulation material.

Microscopic observations

The scanning electron microscopic (SEM) observations were carried out in secondary and backscattered modes (Tescan, Vega model). Also, Energy dispersive X-ray analysis was carried out on the samples using the same tool.

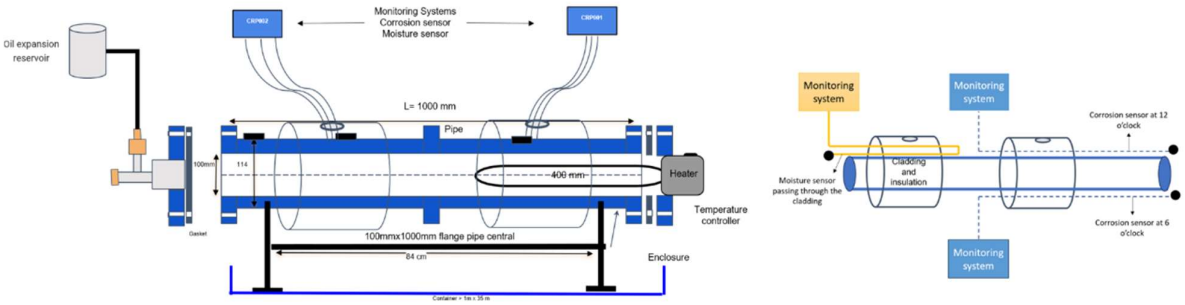

Figure 1 – (left): Schematic diagram of the CUI rig setup and the positions of the cladding used in this study. (right): Configuration of moisture and corrosion sensors within the cladding.

A summary of the tests on the rig and other details are provided in table 1.

Table 1 - Overview of cyclic and constant temperature tests on the CUI test rig.

Test Type	Time (days)	Solution	Temperature (ºC)	Test type	Sensor Type
Cyclic Temp.	Cladding A: 14 Cladding B: 30	0.1 wt.% NaCl (both)	cycled between: 80ºC and room temp.	Cladding A: LPR Cladding B: Weight loss	Moisture
Constant Temp.	Cladding A: 66 Cladding B: 91	Cladding A: Acetic Acid (10% vol.) Cladding B: Acetic Acid (10% vol.) + NaCl (3.5% wt.)	50ºC	Weight Loss	Corrosion

Materials and solutions

Two types of test samples were used for comparison with the corrosion sensor results. The first type comprised 10 mm-wide ring samples cut from a 5" NPS A-106 pipe. These samples underwent cleaning and polishing with progressive sandpaper up to 300 grit, followed by degreasing in a specialized solution. The second type consisted of mild steel coupons, sized at 40 mm x 20 mm, with composition details obtained through EDAX analysis reported in table 2. Similar to the ring samples, the coupons were abraded with sandpaper up to 300 grit. Initial sample weights were determined using a digital balance with 0.001 gr accuracy.

To investigate the effects of cyclic and constant temperature conditions on corrosion rates, two different corrosive solutions were employed. For cyclic temperature rig tests, a 0.1% wt. sodium chloride solution was used. To accelerate corrosion in constant temperature tests, corrosive solutions comprising Acetic acid 10 vol.% and Acetic Acid 10% vol. with 3.5 wt.% sodium chloride were utilized.

The corrosive solutions were carefully prepared using high-purity chemicals, including sodium chloride (99.9% purity, APC Pure, UK), acetic acid (99.9% purity, APC Pure, UK), and distilled water. This stringent use of high-purity chemicals ensured accurate and consistent results in the experimental tests.

Table 2- The chemical composition of the carbon steel coupons used in the study measured by EDAX.

Spectrum Label	Atomic %
C	3.05
O	2.29
Si	0.43
Mn	1.01
Fe	93.22
Total	100.00

Electrochemical tests

The corrosion ring samples behavior was evaluated under CUI conditions using linear polarization resistance during the rig tests. We utilized the EmStat4S potentiostat/galvanostat from Palmsense (Netherlands) for the electrochemical tests.
To measure the linear polarization values of the ring samples inside the cladding during the CUI tests, we employed a potential range of ±15mV for the linear polarization tests, following the ASTM 189 test method for LPR (Linear Polarization Resistance) test during CUI laboratory tests [10]. One ring sample served as the working electrode, while the other acted as the reference and counter electrode.

Monitoring system and sensors

The Corrosion Sensor is a special thin sacrificial cable made from carbon steel that detects wave reflections at locations where corrosion has caused a discontinuity. The Moisture Sensor is another type of cable that operates on the same principle, generating reflections at locations where the sensor comes into contact with moisture. When used in conjunction, these sensors provide valuable insights into the presence of corrosive conditions beneath the insulation. Pictures of the moisture and corrosion sensors are depicted in figure 2. To acquire data, the monitoring systems send electromagnetic waves through these sensors and observe the resulting reflections. These reflections indicate changes in the impedance of the environment caused by water/moisture ingress or progress of corrosion. Monitoring data were collected at 10-minute intervals and stored locally on the device before being transferred to a Cloud system via the internet.

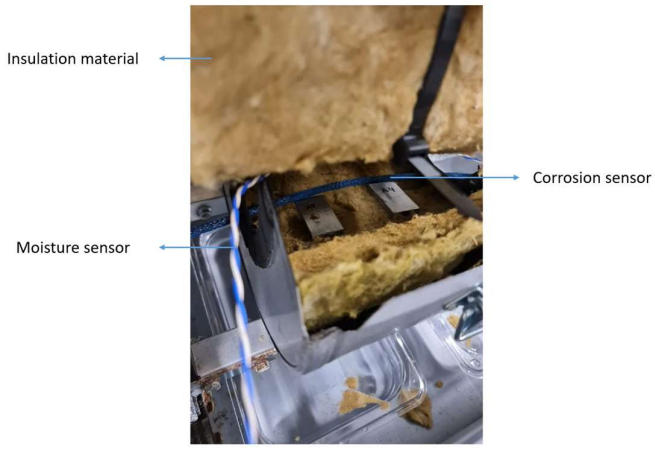

Figure 2 - Photograph showing the positioning of corrosion and moisture sensors within the insulation on the pipe rig. Test coupons are also visible in the picture.

Results and discussion

Cyclic Temperature Rig Tests

Cyclic temperature increases the risk of CUI. Water evaporation and concentration of aggressive ions play an important role in the increase in CUI rate [1,2]. To understand this better, part of this study was allocated to monitor the water/moisture movements inside the insulation using CUI moisture sensor.

In this study, we utilized two claddings, each containing six quarter-ring pipe samples. One cladding was dedicated to conducting LPR tests (located in cladding A in figure 3), while cladding B was used for weight loss tests. Within each cladding, eight quarter-ring samples were deployed as follows: two samples at 12 o'clock, two at 3 o'clock, two at 9 o'clock, and two at 6 o'clock positions. The arrangement of the quarter-ring samples can be seen in figure 3. The cyclic rig tests were conducted with the temperature cycling between 80°C and ambient room temperature. The rig was maintained at 80°C for 12 hours, after which it was turned off and allowed to cool down to room temperature over the next 12 hours. To prevent evaporation, water circulation was initiated during the cooling phase of the tests and continued for 12 hours. Due to water evaporation at the end of the heating cycle, the insulation's resistivity would measure high. As a result, the LPR measurements were performed at three instances in each cycle: first, with the start of water circulation when the temperature is still high, second time after the end of the cooling phase when the system was fully wet and cold, and finally, one hour after the heater reached the temperature of 80°C.

Figure 4 displays the average linear polarization resistance values for the six samples over time. The graph illustrates that in each cycle the lowest resistance values occurred at the start of the heating cycle, while the highest LPR was obtained at the end of the wetting cycle. This observation suggests that the corrosion rate is highest at the starting of the heating phase than anytime during cooling. Additionally, the polarization resistance shows a sharp decline after 24 hours, which can be attributed to the insulation material being wet with saline water and remained wet for the whole duration of the test.

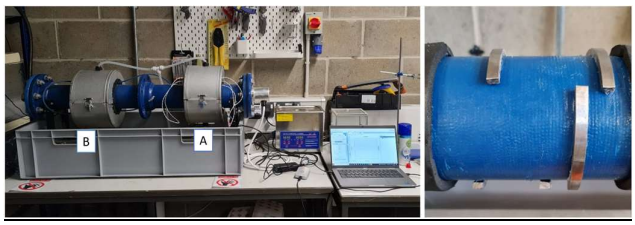

Figure 3- (left): Customized pipe rig setup for cyclic testing: cladding A for LPR samples and cladding B for weight loss samples. (right): the arrangement of quarter ring Samples on the pipe rig

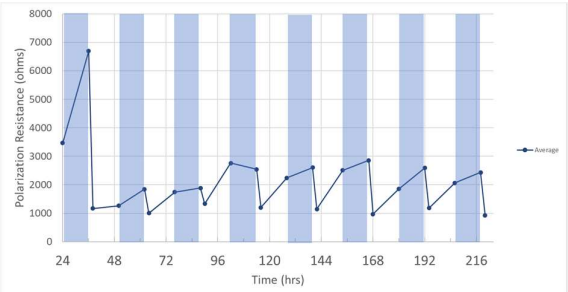

Figure 4- Average LPR values over time during the cyclic test: blue band represents wetting cycle, white represents heating cycles.

Visual Observations and Weight Loss Measurements

As anticipated, the visual examinations of the samples within the cladding dedicated to the weight loss test revealed that the samples positioned at 6 o'clock exhibited more extensive corrosion compared to those at other positions. The images of the as-corroded ring samples and their surfaces after acid washing are depicted in figure 5. A closer examination of the corroded samples' surface reveals the presence of numerous pits, indicating localized corrosion that concentrates at these areas.

Figure 5– The weight loss ring samples after 4 weeks of CUI test on the rig. The first number indicates the o'clock positions of the samples.

When analyzing the weight loss measurements from the samples, no clear trend based on the sample's position was observed. This observation might be attributed, in part, to the localized nature of the corrosion that cannot be measured by weight loss. The weight loss values are presented in figure 6. These findings suggest that the corrosion mechanism involved in the samples' degradation is that of localized corrosion.

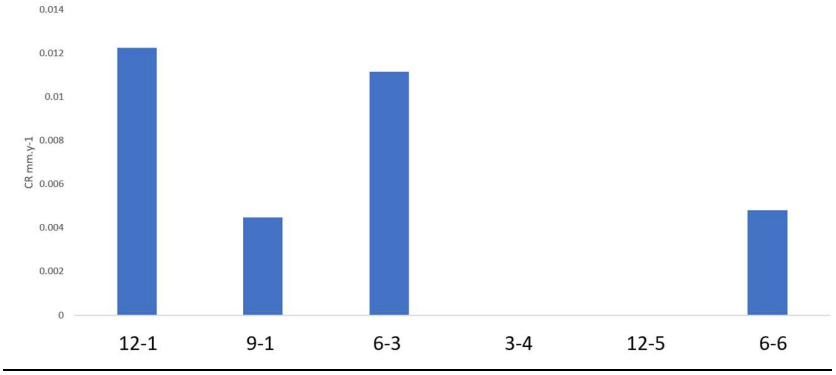

Figure 6- The graph of the corrosion rates for the ring samples measured by weight loss. The first number represents the o'clock position of the sample.

Scanning Electron Microscope Observations

SEM observation was conducted on sample number 6-3, which exhibited significant pitting and was positioned at 6 o'clock. The backscattered mode micrographs supported the macroscopic observations. Figure 8 illustrates the pit site's morphology on the sample surface, using both secondary and backscattered modes in the micrograph. The darker components within the pits represent the remaining oxide. Furthermore, the EDAX data shown in figure 9 from two points at the same location on the surface confirm the detection of chloride inside the pit, indicating the significant role of chloride in driving CUI.

These SEM observations provide valuable evidence of the impact of chloride ions on the pitting corrosion mechanism, further contributing to our understanding of CUI and its implications for the samples.

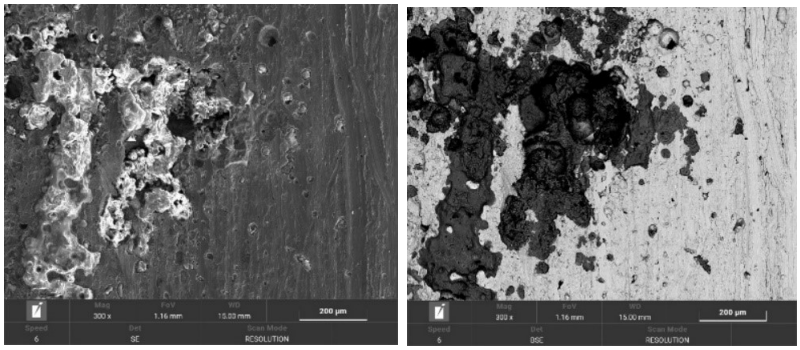

Figure 8- Micrograph of a pitting site on the surface of a ring sample in the secondary mode (left) and backscattered mode (right).

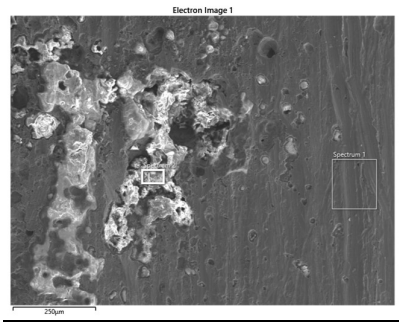

Spectrum Label	Spectrum 1	Spectrum 2
C	3.05	4.62
O	2.29	30.06
Si	0.43	0.31
S		0.18
Cl		1.11
Cr		0.19
Mn	1.01	0.29
Fe	93.22	63.24
Total	100.00	100.00

Figure 9- Micrograph showing a pit on the surface of the samples and the chemical composition from the outside of the pit (Spectrum 1) and from inside the pit (Spectrum 2)

CUI Monitoring Results

Moisture Sensor Data

During the cyclic test, moisture sensor was positioned inside the cladding dedicated to LPR testing, allowing data collection from both the external and internal parts of the insulation. The arrangement of the moisture sensor inside the cladding facilitated the capture of moisture data from two different regions.

Figure 10 presents the heat-map obtained from the moisture sensor during the cyclic test, clearly depicting the cycles of wetting and drying. The left side detections on the heat-map indicates the moisture on the outer layer of the insulation, while weaker signals on the right side are associated with water presence inside the insulation.

The heat map reveals a notable concentration of water on the sides of the claddings, as indicated by the signals from the top and the interior of the insulation. Moreover, the presence of moisture inside the insulation interior suggests water movement towards the cladding sides, a crucial observation concerning water behaviour within the cladding.

Another significant finding from the moisture sensor data is the persistence of wetness in the insulation interior even after the end of 12-hour heating cycles. The moisture pattern on the

external surface of the insulation appears more concentrated, whereas in the middle, it exhibits a more widespread distribution.

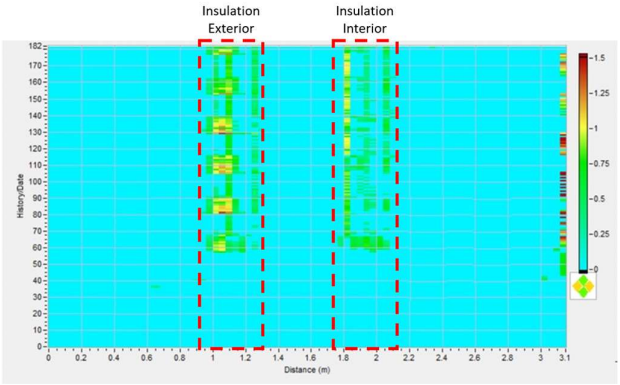

Figure 10- The heat-map obtained from the moisture sensor inside the cladding. The horizontal axis on the heat-map is the length of the sensor and the vertical axis is the number of data acquisitions. The Signal between 1-1.2m is related to the outside of the insulation and the detection from 1.8-2m is from the inside of the insulation.

Constant Temperature CUI rig tests

Constant temperature CUI rig tests are designed to compare the corrosion rates obtained from CUI monitoring systems with the data obtained from weight loss tests. To achieve this, two different claddings were deployed on the CUI test rig, with each cladding containing a different solution as shown earlier in table 1. Throughout the tests, the rig's temperature was maintained at 50°C, and the solutions were regularly circulated inside the cladding and replenished to account for evaporation.

Inside each cladding, two types of samples were deployed: four half-ring samples positioned at 12 o'clock and two at 6 o'clock, along with two coupons placed within the insulation at the bottom of the cladding. These ring samples and coupons were produced using the same materials used in previous rig tests.

A corrosion sensor was positioned inside the cladding, in close proximity to the ring samples at the bottom (6 o'clock). The corrosion rate measurement using the monitoring system was carried out by monitoring the signal from this sensor. The samples inside the cladding containing 10 vol.% acetic acid showed detections after 66 days, while the cladding containing 10 vol.% acetic acid and 3.5% NaCl chloride showed detections after 91 days. These detections allowed the CUI monitoring system to accurately calculate the corrosion rates inside the cladding.

The corrosion rates of both the ring samples and the coupons inside the cladding were also measured through weight loss assessments. The corrosion rates obtained from the sensors and the weight loss measurements for each type of sample are presented in figure 11 and table 3. The standard deviation of the corrosion rates is large compared to the mean value. Large standard deviation hints at the large scatter in the corrosion rates.

As observed in the graph and table, the results obtained from the sensor within the range of the values of corrosion rates for the ring samples and the coupons. The higher corrosion rates of the coupons can be attributed to their positioning inside the insulation, where accumulation of solution led to faster corrosion rates. The ring samples, on the other hand, show lower corrosion rates that can be attributed to their geometry and less water retention on their surfaces. The heat-maps of the corrosion sensor data are also presented in figure 12. The laboratory weight loss results can be used to calibrate the corrosion rates of the sensors to obtain a more accurate estimates.

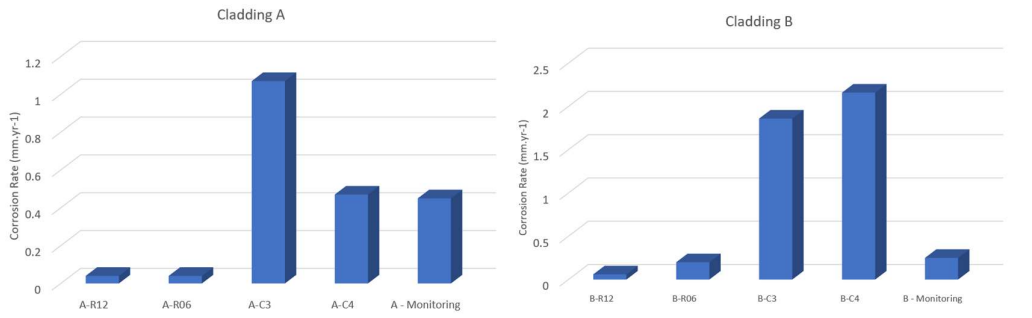

Figure 11- corrosion rates obtained from the ring samples, coupons and the corrosion sensor for cladding A and B in constant temperature tests.

Table 3- Corrosion rates obtained from the CUI constant temperature rig tests and the corrosion sensor data.

	Samples	Corrosion Rate (mmyr-1)	Mean & Standard Deviation (SD)	Description
Cladding A	A-R12	0.04	Mean = 0.41 SD = 0.42	ring at 12 o'clock
	A-R06	0.04		ring at 6 o'clock
	A-C3	1.07		coupon
	A-C4	0.47		coupon
	A - Monitoring	0.45		sensor
Cladding B	B-R12	0.06	Mean = 0.91 SD = 1.01	ring at 12 o'clock
	B-R06	0.2		ring at 6 o'clock
	B-C3	1.86		coupon
	B-C4	2.16		coupon
	B - Monitoring	0.25		sensor

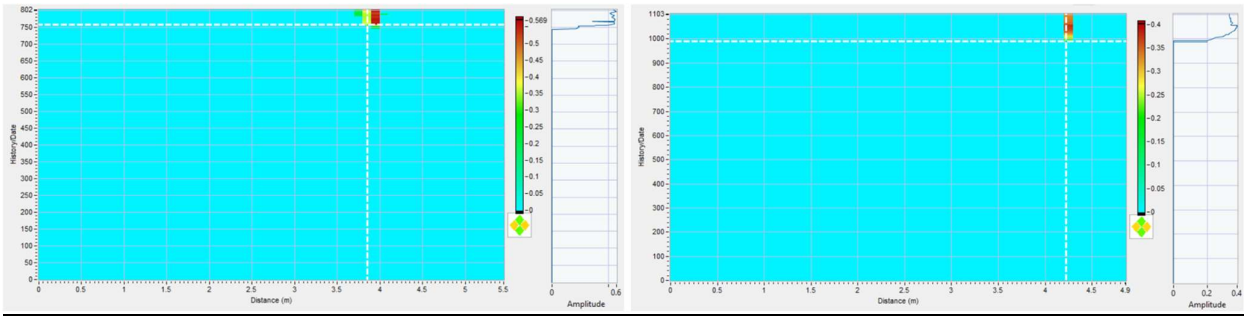

Figure 12- (left): Corrosion sensor heat-map from the sensor installed in the cladding A (acetic acid solution), and (right): the heat-map from cladding B. The cross hair shows the location of corrosion detection on the sensor.

Conclusions

In this study, we conducted CUI tests on a test rig at cyclic and constant temperatures to observe the moisture movement pattern inside the cladding and measure corrosion rates. Additionally, we deployed a novel CUI monitoring system based on EMGR, which provided valuable information regarding the aforementioned aspects. The study's findings revealed that CUI

corrosion on the ring samples exhibited a pitting pattern, that might render weight loss measurements inadequate for assessing the actual weight loss in short testing times. Electrochemical analysis of the LPR values indicated that sample resistance was lowest during the heating phase of the cyclic test, suggesting potentially higher corrosion rates during the initial heating phase. The CUI moisture monitoring yielded invaluable insights into moisture movement inside the insulation, highlighting the non-uniformity in water flow within the cladding and through the insulation material. Notably, water tended to choose the path of least resistance, favouring movement towards the sides of the cladding. This effect should be taken into account when conducting laboratory CUI tests.

Coupon samples displayed higher corrosion rates compared to the values obtained from the ring samples and sensors. Nevertheless, the corrosion sensor successfully detected the occurrence of corrosion. By validating the system against traditional weight loss measurements, we confirmed its reliability to detect corrosion and the potential to calibrate the sensor against the coupon or ring test specimens.

Looking ahead, the implementation of this monitoring system holds enormous potential for CUI research. Also, real-time data empowers proactive and efficient predictive maintenance, reducing downtime, minimizing costs, and enhancing safety.

Acknowledgements

The authors are grateful to Innovate UK for their support and funding throughout the Knowledge Transfer Partnership (KTP) project between Cranfield University and CorrosionRADAR Ltd. Their contribution has been invaluable in the successful completion of this study.

References

1. API, "Corrosion Under Insulation and Fireproofing", API Recommended Practice 583 1st Edition (2014).
2. API, "Damage Mechanisms Affecting Fixed Equipment in the Refining Industry", API Recommended Practice 2nd Edition (2011).
3. S. F. Burch, "HOIS CUI inspection project C43: Phase 1 report", HOIS **13** (2013).
4. Q. Cao et al., "A Review of Corrosion under Insulation: A Critical Issue in the Oil and Gas Industry," Metals (Basel), **12** (2022) 561.
5. E. Bowman, N. Thompson, D. Gi, O. Moghissi, M. Gould, J. Payer, "International Measures of Prevention, Application, and Economics of Corrosion Technologies Study", NACE International (2016).
6. C. Watt, C.-M. Lee, S. Paterson, A. Jopen, "Using industry data to compare performance of different risk-based methods for the management of corrosion under insulation," SPE International Oil field Corrosion Conference and Exhibition, Paper no. SPE-205057-MS (2021).
7. NACE International., "Standard recommended practice: the control of corrosion under thermal insulation and fireproofing materials: a systems approach," NACE International (2004).
8. Technology Leadership Board, Oil and Gas UK (by Lockheed Martin), "Asset Integrity Theme Landscaping Study" (2016).
9. CorrosionRADAR, Detect Monitor Predict CUI, https://www.corrosionradar.com/ (accessed Jul. 25, 2022).
10. ASTM G189-07, "Standard Guide for Laboratory Simulation of Corrosion Under Insulation" (2021).

Reliable prediction of galvanic corrosion at offshore aluminum-steel joints using hybrid computational modelling

Daniel Höche, Helmholtz-Zentrum Hereon, Geesthacht/Germany
Carsten Blawert, Helmholtz-Zentrum Hereon, Geesthacht/Germany
Mohamed El Amine Ben Seghier, Helmholtz-Zentrum Hereon, Geesthacht/Germany
Maria Serdechnova, Helmholtz-Zentrum Hereon, Geesthacht/Germany
Natalia Konchakova, Helmholtz-Zentrum Hereon, Geesthacht/Germany
Mikhail L. Zheludkevich, Helmholtz-Zentrum Hereon, Geesthacht/Germany
Jan Bertram, Muelhan Holding AG, Hamburg/Germany
Andreas Momber, Muelhan Holding AG, Hamburg/Germany
Ole Øystein Knudsen, SINTEF, Trondheim/Norway
Jon Aaby Møretrø, Norsk Hydro ASA, Sunndalsøra/Norway

There are benefits in utilizing aluminum alloys in offshore construction concepts as lightweight. However, the existing corrosion protection concepts for Al-based construction engineering are still not mature and might fail. Often galvanic couples to steel are initiation points of critical damage. Thus, there is a need for improved and adapted design of such joint towards reliable corrosion damage management.

Here, data and its sensing on the entire corrosively loaded system are the key especially within severe and varying environmental conditions which might accelerate the detrimental effect of harsh atmospheric corrosion. Design of the hybrid joint can be improved by computational modelling based on available electrochemical and environmental data. In this regard a combined data- and physics-based approach is shown. Data will be analyzed and e.g., electrolyte film parameters modeled, enabling the reliable prediction of joint-layout-related galvanic corrosion. Washers, spacers etc. and their effects on the corrosion is studied and predicted. Data on relative humidity, electrolyte film thickness or time of wetness are discussed and formulated, towards utilization within the model. Finally, engineering guidelines for aluminum steel couples in offshore applications are formulated.

Acknowledgment: Research project MARINAL (MarTERA: MARINAL, MARINAL - Safe use of aluminium in marine multi-material constructions).

Stainless steel discoloration and Cl^- pitting: Hyperspectral study and analysis

Dimitri Soccol[1], Erik Thomas[2], Wouter Saeys[3],

[1]MTM, KU Leuven, (Ghent Technology Campus)

[2]METALogic NV, member of TÜV Austria Group, (Rotselaar)

[3]MeBioS, KU Leuven, (Leuven, Arenberg)

The stainless steels are the workhorse material in chemical, pharmaceutical and food industry. Their corrosion resistance results in long service lifetime and low contamination of products. They owe this corrosion resistance to the alloying elements, which provide stainless steel with a thin protective oxide layer. Initially, the surface state of stainless steel is well controlled. However, this might change while in service. Discolorations are often observed after prolonged use, which indicates a difference in the protective layer.

Practically, it is not known if and to what extent there is an effect of discoloration on the occurrence of pits. The most reliable estimate of pitting resistance is provided by electrochemical and exposure tests, using industrial standards to ensure reproducibility [1]. During these tests, susceptibility to pitting is quantitatively assessed in the presence of Cl^- in aqueous solution. A large amount of literature reports exist that quantify the link between electrochemical pitting and the specific surface treatment. Unfortunately, no link has been made with discoloration or optical spectra. Nevertheless, stainless steel surface discolorations are of highest concern during visual inspections. A specific example of discoloration is the occurrence of "rouging" in pharmaceutical installations, which appearance initiates costly cleaning procedures [2,3].

In the current work, a hyperspectral methodology will be presented to quantitatively determine stainless steel discoloration and relate the spectral information to pitting behavior. An additional link will be made with the surface chemistry of the oxide layer and the electrochemical exposure history. Therefore, a wide range in discoloration and chemical history was explored:

1. Non-discolored surface pretreatments Three pretreatment variations were selected with a known strong impact on E_{pit}: no treatment after grinding,

passivation in citric acid and passivation in nitric acid. Neither of these samples showed visible discoloration, but served as reference cases.

2. Rouging discoloration 1: 12 weeks exposure to cyclically heated and aerated deionized water (T_{av} of 40 °C).
3. Discoloration 1: Electrochemical simulation of oxidizing environment at pH 14.
4. Discoloration 2: Electrochemical simulation of oxidizing environment with complex-forming medium (1 M Na_3-citrate at pH = 13).

Spectral characterization is performed by optical (using a spectro-photometer) and spectral imaging (using a hyperspectral camera) to quantify the extent of discoloration. The susceptibility to pitting is tested in a Cl^- containing environment by electrochemical pitting potential (E_{pit}) measurements. A few of the more extreme discolored samples and their spectra have been included in Figure 1 and Figure 2.

Figure 1 Three samples prepared for this study: (from left to right) after polishing,- electrochemical blue discoloration- simulated rouge,

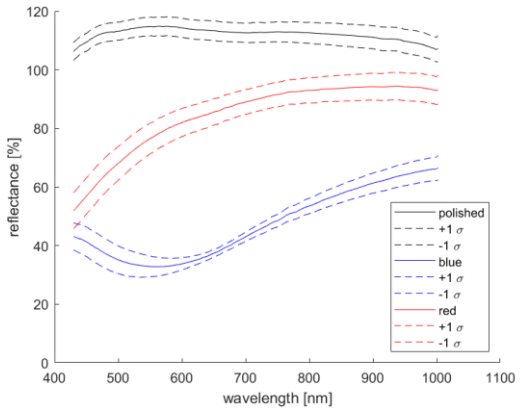

Figure 2: Average spectra of the three examples of Figure 1

[1] ASTM G61-86: Standard Test Method for Conducting Cyclic Potentiodynamic Polarization Measurements for Localized Corrosion Susceptibility of Iron-, Nickel-, or Cobalt-Based Alloys. Standard. West Conshohocken, PA, USA: ASTM International, June 2018

[2] Gonzalez M. M. “Rouge: the Intrinsic Phenomenon in 316L Stainless Steel - a Key Material for Biopharmaceutical Facilities”. In: Pharmaceutical Engineering 32.4 (2012), pp. 1–8

[3] Mathiesen T. and Frantsen J. E. “Rouging of Stainless Steel in WFI Systems -Examples and Present Understanding”. In: NACE Corrosion. Nashville, TN, 2007

High Resolution Respirometric Method – Next Level Corrosion Monitoring for Lab and Field Applications

Michael G. Strebl, Mark P. Bruns, David Hemlein, Sannakaisa Virtanen, Friedrich-Alexander Universität Erlangen-Nürnberg (FAU), Erlangen, Germany

The respirometric method [1,2] is based on quantifying the rates of the main cathodic reactions during aqueous corrosion which are the H_2 evolution reaction (HER) and the O_2 reduction reaction (ORR). With the help of different sensors, this approach indirectly enables monitoring corrosion processes in real-time without interfering with the sample. It is universally applicable both to atmospheric corrosion and immersion conditions.

The experimental setup presented in this work pushes the boundaries of what can be resolved by the respirometric method. A more sensitive version was developed that is suitable to measure corrosion rates of more corrosion resistant materials or materials in weakly corrosive environments. The improvements in resolution are possible due to extremely small chamber volumes, gas tight sealing, improved sensors and better temperature control.

The novel methodology gives new mechanistic insight to the role of cathodic reactions during breakdown of passivity of Al alloys or stainless steels. Furthermore, the high resolution respirometric method provides a monitoring tool to establish the relationship between relevant exposure parameters and accurate corrosion rates. While this approach is certainly promising for laboratory applications, also the applicability to respirometric field measurements will be demonstrated. The idea is to develop a respirometric probe that can be attached to corroding structures in the field.

[1] Strebl, M., Bruns, M., Virtanen, S., Editors' Choice—Respirometric in Situ Methods for Real-Time Monitoring of Corrosion Rates: Part I. Atmospheric Corrosion, J. Electrochem. Soc., 167, 021510 (2020).

[2] Strebl, M.G., Bruns, M.P., Schulze, G., Virtanen, S., Respirometric in Situ Methods for Real-Time Monitoring of Corrosion Rates: Part II. Immersion, J. Electrochem. Soc., 168, 011502 (2021)

Investigating the role of pH on the corrosion rate of construction steel in artificial seawater

Roya Tavangar Rizi[1], Arne Simons[2], Aurélie Laureys[3], Tom Depover[4], Kim Verbeken[5]

[1] *Department of Materials, Textiles and Chemical Engineering, Research group Sustainable Materials Science, Ghent University, Ghent, Belgium, Roya.Tavangarrizi@UGent.be*
[2] *Arne.Simons@UGent.be*
[3] *Aurelie.Laureys@UGent.be*
[4] *Tom.Depover@UGent.be*
[5] *Kim.Verbeken@UGent.be*

Abstract:
A significant portion of the global cost of corrosion originates from offshore applications, where materials are in contact with seawater. For a wide variety of applications, construction steel grade A, is used, although it is highly vulnerable to this marine environment. So far, the strategies to assess corrosion degradation, mostly focus on the ongoing corrosion and do not sufficiently address the future corrosion risk. Therefore, a more innovative and effective approach for this type of degradation is in-situ monitoring of the affecting environmental parameters on the corrosion rate to determine the potential risk. Consequently, the current study aims to investigate how environmental variables such as, temperature, pH, conductivity, and salinity can influence the corrosion rate in a controlled lab environment. For this purpose, Linear polarization resistance (LPR) on grade A steel was performed for a few days using Gamry instruments' potentiostat in artificial seawater, which was prepared based on ASTM Standard D1141. Environmental parameters were simultaneously monitored by water quality sensors. The influence of pH on corrosion rate is further investigated in light of the possible protectiveness of corrosion products/films. Furthermore, the corrosion products' formation rate can differ and consequently influence the corrosion reaction kinetics.

Keywords: Linear polarization resistance; Mild steel; Environmental parameters; pH influence.

Introduction

The necessity of reduction of carbon dioxide emissions leads to move towards using sustainable energy resources. Amongst these fossil-free resources, wind turbines, specifically offshore wind turbines, are an excellent option because of the limited land area to operate and being subjected to higher wind knots [1]. Carbon steel is the most practical material for offshore applications due to its low price along with good mechanical properties. However, these steels are susceptible to corrosive environments such as seawater which can aggravate their mechanical strength and cause catastrophic failures [2]. The corrosivity of seawater is a function of the environmental parameters including temperature, dissolved gases, pH, and salinity. Any change in these parameters can directly or indirectly affect the corrosion rate. Seawater pH is an important factor since it can affect both chemical reactions and biological toxicity [3]. Generally, the pH level of the open surface seawater ranges from 7.5 to 8.3 [4]. The pH variation in seawater can happen due to the dissolution of acidic gases (e.g. CO_2 and H_2S), temperature variation, organic acids, and buffering capacity [5]. The latter causes a relatively constant pH value (between 7.5 and 8.3) which encourages the scale formation. However, it is important to note that onshore areas experience fluctuations in pH because of higher levels of microbial activity [6]. The current work focuses on the influence of pH variations between 7.8 and 9 on the corrosion rate. During the experiments, all environmental parameters were also monitored and data were collected to investigate the impact of pH on other environmental parameters.

Methodology

The artificial seawater (ASW) was made according to ASTM Standard D1141. The standard involves a two-step production process, first making ASW with the composition shown in Table 1. In the second production step, the pH at ambient temperature was adjusted to the desired value by gradually adding specific amounts of 0.1 M NaOH.

Table 1. The composition of artificial seawater made according to ASTM Standard D1141.

NaCl	MgCl	Na_2SO_4	$CaCl_2$	KCl	$NaHCO_3$	KBr	H_3BO_3	$SrCl_2$	NaF
24.53	5.20	4.09	1.16	0.695	0.201	0.101	0.027	0.025	0.003

For variable pH, the tests were performed at 15 °C and 7.8, 8.2, 8.6, and 9 pH by adding variable amounts of 0.1 M NaOH. In addition, the examined construction steel samples with the chemical composition mentioned in Table 2 were prepared by abrading with 80# to 1200# SiC papers. The electrochemical tests were conducted on cold-embedded samples to expose a defined area of mild steel to the solution.

Table 2. The chemical composition (wt%) of the used carbon steel.

Fe	C	Mn	Other
98.210	0.140	0.696	P, S, Si, Al, Cu, Cr, Ni, Mo, V, N, Sn, Ti

The linear polarization resistance (LPR) tests were applied by a potentiostat (Gamry instrument model E potentiostat). For this purpose, the defined area of abraded grade A steel, platinum mesh, and Ag-AgCl electrodes were used as the working, the counter, and the reference electrodes, respectively. Therefore, by running cycles of linear polarization resistance for 99 cycles, the corrosion rate was measured precisely at different pH. In each cycle, which lasted

one hour, LPR was conducted after measuring the open circuit potential and reaching steady state potential.
The polarization resistance results were converted to corrosion current utilizing the Stern-Geary equation (Eq.1).

$$I_{corr} = \frac{\beta_{anodic}\beta_{cathodic}}{2.3R_{pol}(\beta_{anodic} + \beta_{cathodic})} \quad \text{Eq. 1.}$$

Where anodic and cathodic β were later attained by performing potentiodynamic scanning on the samples.
Afterwards, the corrosion current results were converted to corrosion rate by Equation (2). I_{corr}, EW, ρ, A, and K are representing the corrosion current, equivalent weight, density, surface area, and a constant, respectively.

$$Corrosion\ rate(mm/year) = \frac{I_{corr}\,.\,EW\,.\,K}{\rho A} \quad \text{Eq. 2.}$$

All environmental parameters were recorded by a Manta 20, from the company Eijkelkamp. The Manta 20 included temperature, pH, dissolved oxygen, oxygen reduction potential, and conductivity sensors. The temperature measurement was conducted using an electrical resistor (thermistor) whose resistance changed predictably with temperature. The pH was measured as the voltage drop across the glass membrane of a pH electrode. The dissolved oxygen was an optical sensor comprised of a blue-light source, a sensing surface, and a red-light receiver. For determining the water conductivity via the four-electrode method, two pairs of graphite electrodes situated in a stable geometry were utilized. ORP was measured as the voltage drop across the platinum membrane of an ORP electrode. Lastly, a well-maintained reference electrode was devised for reliable pH and ORP measurements and for completing voltage measurements for pH readings.
The temperature was adjusted using a JUBALO thermal bath capable of increasing and decreasing the temperature using a JUBALO heater and cooler. The magnetic stirrer inside the bath rotating at 200 rpm created a homogenous mixture inside the vessel. The vessel was sealed utilizing a Teflon lid with a thickness of 15 mm. An image of the experimental set-up (including environmental probe, reference, working, and counter electrodes) inside the thermal bath can be seen in Fig. 1. After each experiment, the artificial seawater and sample were replaced by fresh ones. Moreover, Manta probes were cleaned with warm soapy water and a soft brush, and calibrated to ensure the sensor response factor was in an acceptable range.

Results and conclusion

The investigation of the corrosion rate shows that in case of pH variation the most influencing factor on corrosion rate will be the pH itself which is inversely correlated to the corrosion rate (i.e. with increasing pH the corrosion rate decreases). Therefore, the influence of varying pH is significant enough to control the corrosion rate, while all other environmental parameters were kept uncontrolled. Interestingly the pH itself is correlated with the dissolved oxygen and oxygen reduction potential. This influence of pH on the corrosion rate despite the small range of variation in pH, which is just in basic region, is highly noticeable.

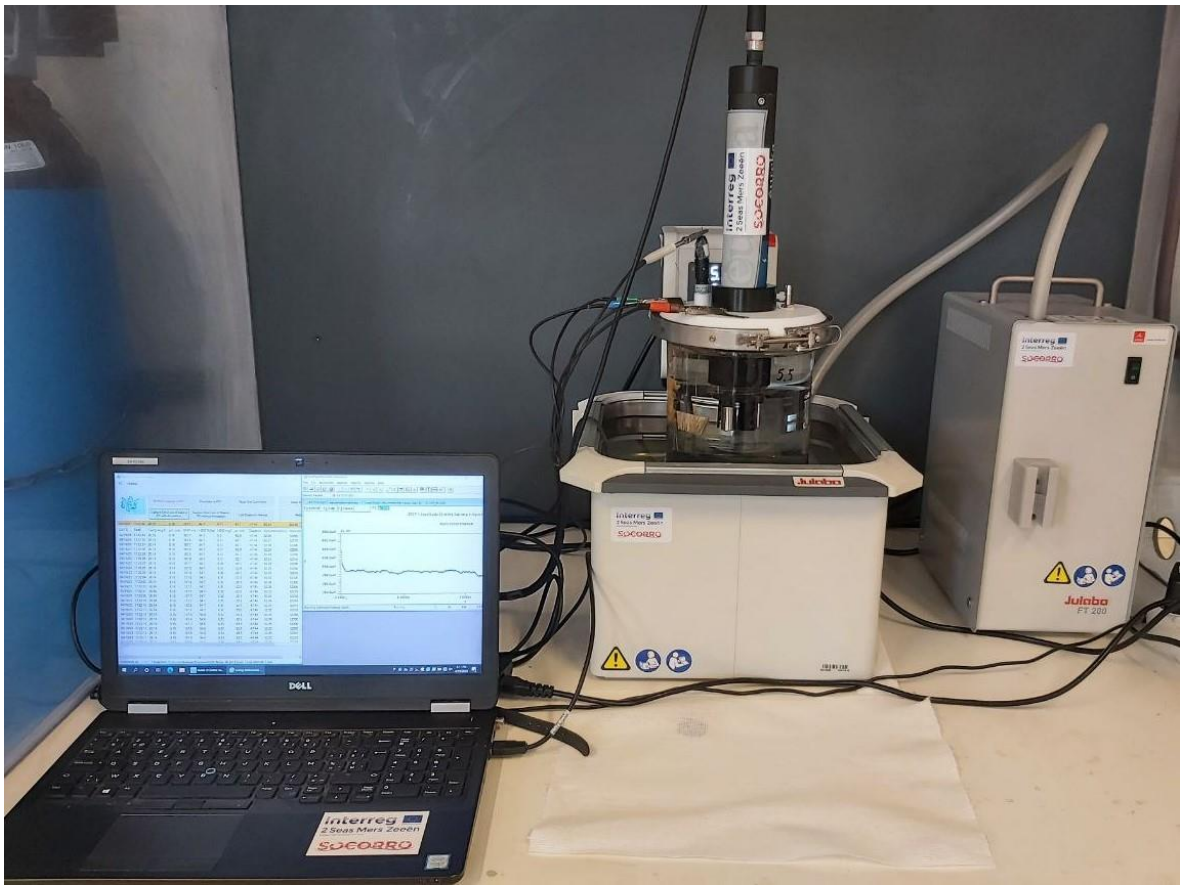

Fig .1. The lab-scaled setup including LPR measurement equipment and environmental probe inside the thermal bath with cooler.

References

[1] S. A. Babatunde and F. T. Najafi, "Overcoming The Challenges of Implementing Offshore Wind Farm Development In The US Through Education and Research," 2018.

[2] P. Refait, A.-M. Grolleau, M. Jeannin, C. Rémazeilles, and R. Sabot, "Corrosion of carbon steel in marine environments: Role of the corrosion product layer," *Corrosion and Materials Degradation*, vol. 1, no. 1, p. 10, 2020.

[3] S. Paul, "Modeling to study the effect of environmental parameters on corrosion of mild steel in seawater using neural network," *Int Sch Res Notices*, vol. 2012, 2012.

[4] C. V Davis, E. B. Rivest, T. M. Hill, B. Gaylord, A. D. Russell, and E. Sanford, "Ocean acidification compromises a planktic calcifier with implications for global carbon cycling," *Sci Rep*, vol. 7, no. 1, p. 2225, 2017.

[5] K. R. Hinga, "Effects of pH on coastal marine phytoplankton," *Mar Ecol Prog Ser*, vol. 238, pp. 281–300, 2002.

[6] K. A. Chandler, "Marine and offshore corrosion," *British Corrosion Journal*, vol. 20, no. 3, p. 106, 1985.

Generation of a controlled fatigue corrosion damage on instrumented steel plates for the Structural Health Monitoring

J. Liegey[1,2], M. El May[1], M. Rebillat[2], O. Devos[1], N. Mechbal[2]

[1] Laboratoire I2M, Arts et métiers Institute of technology, Bordeaux, France

[2] Laboratoire PIMM, Arts et métiers Institue of technology, CNRS, CNAM, HESAM Université, Paris, France

Pitting corrosion is a major concern for the aeronautic industry and providing structures with the intrinsic ability to monitor autonomously their health state is a major actual academic and industrial challenge. One of the objectives of this research is to generate a corrosion pitting on a 316L stainless steel. This pitting will be detected as a geometrical defect by the piezoelectric acoustic sensors positioned in its surrounding. The challenge is to initiate one or more corrosion pits in a controlled manner in size and position in order to follow their propagation kinetics acoustically. We will present the results obtained from the experimental technique developed in the laboratory. The pitting process is initiated by a localized supply of a 3.5% NaCl solution through a micro-capillary. During the corrosion, the electrical charge and the flow rate of the 3.5% NaCl solution are fixed in order to control the size of the pitting on the sample surface. Acoustic sensors positioned around the corroded area record the associated Lamb waves,. A dedicated recording system provided by Cedrat Technologies is used to acquire the Lamb wave data. An SHM algorithm was used to detect, locate and quantify the damage during the pitting corrosion tests. This study will later be used to instrument a fatigue specimen subjected to a corrosive environment to detect and quantify pitting or crack propagation during cyclic stress testing.

Controlling Corrosion on Seawater Plant, Success Story

Abstract

Osamah M. Al-Ghamdi

The seawater plant and its associated piping networks suffers from the multiple causes of corrosion, and one of the most causes, is the Microbial Influenced Corrosion. As the control of corrosion requires deep study of the process/system, through a formal corrosion management program. Sitting robust program requires monitoring the process, collecting and analyzing data, develop action plan and then establish roles and responsibility to each involved individual and/or organization. The journey took long time to finally prove the effectiveness of the program. This paper summarizes a success journey in enhancing the plant reliability and availability through effective corrosion control. The corrosion control program is summarized under 5 pillars:

1- Stakeholder Engagement.
2- Data Analysis.
3- Corrosion Management Program.
4- Processes and Procedures Enhancement.
5- Capital Investments.

Stakeholder Engagement:

Engaging all stakeholder, and in particular the organization's leadership, was a key factor behind this success journey. The higher-level management were involved in most of the technical challenges and as a result all support was obtained in a smoother way, since they are well aware about consequences of the corrosion related failures. Also, the other organizations that are involved with us in the process of the sea water were closely involved with us, through the corrosion management program that was formally concurred by them.

Data Analysis

Starting the real work of developing corrosion management program requires massive work in analyzing all data available, such as process design and actual parameters, design and actual specification of the sea water, costumer input and concerns, lab data, failure analysis, leaks history… etc. After spending enough time in analyzing the available data, the team agreed to enhance the analysis through:

- Installing Additional instruments (analyzers, monitors, transmitters, … etc.).
- Introduce additional sampling location.

Saudi Aramco: Company General Use

- Change the frequency of the sampling.
- Review and adjust the sampling procedures.

Afterward, the team developed a road map to enhance the data analysis. Data were analyzed and corrosion management program was adjusted accordingly as needed.

Corrosion Management Program

Developing the corrosion management is an important step in order to have governance in all efforts being done toward controlling the corrosion. It also insures sustaining the high performance and serves as a good reference for the organization. The corrosion management program was developed by our corrosion engineers, and then reviewed and concurred by the central engineering entity in the corporate.

Processes and Procedure Enhancement

As majority of the corrosion management program items are assigned to operation and maintenance, and in order to ensure they are formally assigned, the corrosion engineers reviewed the current manuals and the formal reference documents in the organization and added items assigned to each unit in the department. These efforts resulted in a better alignment between the corrosion management program and the other operation documents and manuals.

Capital Investment

The corrosion management program, and based on the analysis done by the corrosion engineers, involves short term and long-term action plans to enhance the corrosion control. Action plan were basically considered as multiple projects with different size. The organization built valid and solid convincing case to the corporate Finance team were approval was obtained based on both technical and financial analysis.

Outcomes

As a result of implementing the corrosion management program, the organization successfully achieved the below outcomes:

- Number of water leaks was dropped by more than 70%.
- Enhanced specifications of the processed sea water.
- Enhanced the lab analysis in terms of sample locations, frequency, procedures, etc
- Higher equipment availability % for the corrosion related plant equipment such as hypochlorite generators/pumps.
- Clear road map on the corrosion control presented to the department head, attended by all stake holder, to track the progress of the road map.

Saudi Aramco: Company General Use

Validation of Acoustic Emission Technique for Detection of Corrosion Pit Location

Masoumeh Naghizadeh, Maria Tibbo, Winnie Ying, Hatch. Ltd., Canada

Pitting corrosion, if not adequately mitigated, may cause loss of structural strength and lead to serious incidents. When regular inspection is implemented, it is possible that the pitting corrosion is not detected before the leakage occurs. Thus, to accurately predict the integrity loss due to stable pitting, it is important to have frequent unattended inspections or a continuous corrosion monitoring system. Acoustic Emission (AE) is a real-time non-destructive testing technique can be used for the 3D observation of spherical acousto-elastic waves generated by the rapid release of energy caused by cracking and failure within a material. When this acoustic wavefront signal is received by several dispersed AE sensors, an AE event is recorded and located with mathematical operations.

Implementing a reliable AE system which quantitatively measures pit depth and detects the pit location is challenging. In this study, laboratory testing was performed to validate the capability of AE technology in identification of the onset of stable corrosion pitting and pit location. Electrochemical experiments were performed on a steel surface with small bare area to deliberately form and grow a single corrosion pit. The pitting potential was controlled electrochemically with a potentiostat to accelerate pitting corrosion. An AE sensor location matrix was developed, and sensor attached to the non-exposed side of plate sample, accordingly. AE monitoring was conducted during the experiment to correlate the AE activities with the onset of pitting and the growth rate of the formed pit.

The corroded area was imaged using an optical microscope to confirm pitting corrosion, and the charge density that is transferred during the test was used to approximate the size of the pit. The AE activities, including the arrival times, number, energy and frequency of events, were evaluated during the electrochemical test. The pitting parameters including the pit initiation time, pit growth rate and the location of pits were correlated to the AE activities.

Advanced characterization of biomineralization layer formed on Al-Mg alloy in marine environment.

M. J. F. Marques[a,b], J. Jaume[a], N. Durban[a], D. Mercier[c], A. Seyeux[c], S. Zanna[c], M-L. Delia[a], P. Marcus[c], R. Basseguy[a]

[a]Laboratoire de Génie Chimique, Université de Toulouse, CNRS, INPT, UPS, Toulouse, France.
[b]Laboratório de Materiais e Revestimentos, LNEG – Laboratório Nacional de Energia e Geologia, Lisboa, Portugal.
[C]Institut de Recherche de Chimie Paris, Research Group Physical Chemistry of Surfaces (IRCP), Chimie ParisTech-CNRS, PSL Research University, Paris, France

Concerns about marine pollution and ecological threats caused by traditional corrosion protection technologies have driven the development of new environmentally friendly anti-corrosion solutions. In recent years, it became clear that microorganisms can influence corrosion behaviour in an advantageous way, the so-called MICI (microbiologically influenced corrosion inhibition) [1-3]. Although research on MICI mechanisms is still in the beginning, two main mechanisms have been outlined: direct and indirect inhibition. In the first one, the microorganisms are responsible for the segregation of slow-release inhibitors or surfactants and consume oxygen, which affects the cathodic reaction process. The second one, indirect inhibition mechanism, is associated to the formation of a protective layer on the surface of the material due to metabolic activity of microorganisms. In this context, biomineralization attracted the attention of researchers as a solution to inhibit metal corrosion [4,5].

Until recently, the majority of publications were focused on steel and stainless steel, which have been used for many years in marine constructions. Nevertheless, in recent years, new alternative materials have entered the market as possible options, such as aluminium alloys. In the specific case of the Al-Mg alloy (AA 5083), often used in marine applications, few studies have assessed the influence of biomineralization on its corrosion [6-8]. Being aware of the potential of this microbial induced mineralization phenomenon, the French ANR MICOATEC project (www.micoatec.eu) established a new approach for the development of a bioinspired anticorrosion solution for metal protection based on a biomimetic strategy. Results already presented from the mentioned project, have shown the development of a protective layer on the Al-Mg surface during different immersion times on marine field. The impact of sunlight

exposure and biofouling on the surface modifications were observed [9,10]. The anticorrosive behaviour of this naturally formed layer was also studied [11,12].

Also in the MICOATEC framework, the current work is focused on the chemical and structural characterization of the biomineralization layer formed on the Al-Mg alloy surface during immersion in natural seawater (Genoa Marine Station). Biofilm microbial community analysis and advanced analysis techniques as XPS, GD-OES, ToF-SIMS, SEM/EDX, FIB/TEM and grazing DRX were performed. The aim is to make progress in understanding the formation mechanism of the protective layer.

The first results revealed that the Al-Mg surfaces exposed to the direct sunlight (referred as light side) present no localized corrosion attack. It was observed the formation of a layer with a double structure. Its external surface is highly enriched in magnesium with a significant amount of polysaccharides. In opposition, the Al-Mg surface exposed to the shadow (dark side), show localized corrosion and a lower surface enrichment in magnesium.

A comparison with abiotic conditions (surfaces immersed in sterilized seawater) was performed allowing to demonstrate the corrosion inhibitory effect induced by marine microorganisms on the Al-Mg alloy.

This work was financially supported by the ANR, in the framework of the MICOATEC project (ANR-19-CE08-0018).

[1] N. Kip and J. A. van Veen, “The dual role of microbes in corrosion”, ISME Journal, 9, 542-551 (2015).
[2] Y. Lou et al. “Microbiologically influenced corrosion inhibition mechanisms in corrosion protection: A review”, Bioelectrochemistry, 141 107883 (2021).
[3] J. Wang et al. “ Research progress on microbiological inhibition of corrosion: A review”, Journal of cleaner production, 373, 1336658 (2022).
[4] W. M. Kooli et al, “Bacterial iron reduction and biogenic mineral formation for the stabilisation of corroded iron objects”, Scientific Reports, 8:764 (2018)
[5] N. Guo et al. “Marine bacteria inhibit corrosion of steel via synergistic biomineralization”, Journal of Materials Science & Technology, 66, 82–90 (2021)
[6] Y. Gao et al. “Inhibiting corrosion of aluminum alloy 5083 through Vibrio species biofilm ”, Corros. Sci.,180, 109188 (2021)
[7] J. Jaume et al, “Surface modification of 5083 aluminum-magnesium induced by marine microorganisms ”, Corros. Sci.,194, 109934 (2022)
[8] M.J.F. Marques et al., “Influence of natural seawater variables on the corrosion behaviour of aluminium-magnesium alloy”, Bioelectrochemistry, 149, 108321 (2023).
[9] M.J.F. Marques et al., “Marine Microorganisms and Metal interaction: The Start Point of a New Bio solution for Corrosion Protection”, in: Oral Presentation at virtual EUROCORR Congress 2021, 20-24 sept. (2021)
[10] M.J.F. Marques et al., "Interactions between marine microorganisms and metal: The start point of a new bioinspired solution for corrosion protection”, Matériaux & Techniques, *in press* (2023)
[11] M.J.F. Marques et al., “Effect of marine microbial activity in corrosion inhibition of 5083 aluminium alloy”, in: Oral Presentation at EUROCORR Congress 2022, 28 Aug.- 01sept., Berlin (2022)
[12] C. Nkoua et al, “Corrosion behaviour of the microbially modified surface of 5083 aluminium alloy”, Corros. Sci., 210, 110812 (2023)

A novel high pressure bioelectrochemostat to investigate the impact of microbially influenced corrosion in the deep-sea

Nicolo' Ivanovich, Asian School of Environment, Nanyang Technological University, Singapore;
Pauliina Rajala, Foreign, Commonwealth and Development Office, Finland;
Ruiliang Liu, Singapore Centre for Environmental Life Sciences Engineering, Nanyang Technological University, Singapore. School of Mechanical and Aerospace Engineering, Nanyang Technological University, Singapore;
Yee Phan Yeo, Singapore Centre for Environmental Life Sciences Engineering, Nanyang Technological University, Singapore;
Federico M. Lauro, Asian School of Environment, Nanyang Technological University, Singapore. Singapore Centre for Environmental Life Sciences Engineering, Nanyang Technological University, Singapore, Nanyang Environment & Water Research Institute (NEWRI), Nanyang Technological University Singapore.

Any metallic structure in contact with a conductive liquid is subject to corrosion. This process can be driven solely by abiotic factors, such as chemical composition, pH and dissolved oxygen of the environment, or, in marine environments, may be enhanced by the presence of specific microbial groups responsible for the so called microbially influenced corrosion (MIC). The resulting material degradation has huge economical and environmental impacts.

Although MIC has been studied since the beginning of the last century, the mechanisms related to this phenomenon are still poorly understood and strongly debated in the scientific community. Several mechanisms have been suggested but, due to the vast variety of microbial metabolic potential and the lack of standardized laboratory procedures, none of these have been unequivocally validated.

Moreover, available technologies cannot mimic all chemical and biological factors, typical of maritime settings, in laboratory-based studies. This is particularly true in severe conditions, like the those of the deep sea, which makes up 90% of marine environment. Yet, this is where new installations including pipelines, mining, and exploration are taking place, requiring corrosion-prone metal structures and instruments.

For this purpose, we designed a high pressure electrochemostat able to simulate the effect of high hydrostatic pressure (HHP) up to 60 MPa (equivalent to a depth of 6000 meters) and simultaneously exploit the ability of a common chemostat to constantly supply fresh medium and remove metabolites and by-products.

This novel instrument represents a quantum leap in laboratory-based analysis of MIC as it allows to overcome the limitations related to the commonly used close batch set ups and at the same time targets an almost unknown environment.

We applied the instrument to study the impact of *Pseudesulfovibrio profundus,* a piezophilic member of sulphate reducing bacteria (SRB), a microbial group generally considered within the main responsibles for MIC, at 0.1 MPa and 30 MPa, in presence and absence of medium flow.

Specifically, we merged microbiological, electrochemical and engineering techniques to quantify and characterize the corrosion on common marine grade carbon steel.

Our study revealed that, although HHP doesn't have any effect on abiotic corrosion, it impacts the ability of pressure-adapted bacteria such as *D. profundus* to induce corrosion. Furthermore, the results suggest that the availability of fresh nutrients coupled with the removal of microbial by-products is of paramount importance when trying to reproduce natural processes.

Indeed, the viability of the bacteria highly increases in continuous flow conditions and the accumulation of H_2S, final product of the SRB metabolism, seems to be strongly related to both corrosion rate and type.

As this can be considered as a first step toward more realistic conditions in *in vitro* analysis of MIC, our technology can be applied to study real deep-sea bacterial communities, obtaining representative data on the stress which metallic structures have to face, testing mitigation solutions and clarifying the processes responsible for MIC.

Biofouling and Multidegradation study on metallic piston rods for Wave Energy Converters PTO systems.

Emiliano Pinori, RISE – Research Institutes of Sweden, Borås/Sweden; Johan B. Lindén, RISE – Research Institutes of Sweden, Borås/Sweden; Christian B. von der Ohe, GCE-NODE, Kristiansand/Norway; Troels Vestergaard Lukassen, Wavepiston, Helsingør/Denmark; Antoine Bonel, Corpower Ocean, Stockholm/Sweden; Ross Harnden, Corpower Ocean, Stockholm/Sweden; Guillaume Unique, Corpower Ocean, Stockholm/Sweden.

In the frame of the EU Horizon 2020 project VALID this study focused on develop hybrid testing methodology while improving component and process selection for increased system reliability and reduced LCOE in wave energy converters and other marine renewable energy (MRE) devices involving a power take off (PTO) system in marine environment. Several MRE devices involve a PTO system and scraping systems on the ocean rods to protect the sealers. The action of the scrapers, offshore conditions, and marine biofouling push multi factorial stress on the metallic ocean rods accelerating degradation and corrosion. Instead for testing each factor one by one, a multidegradation test rig (LSMD) (*figure 1*) has been developed.

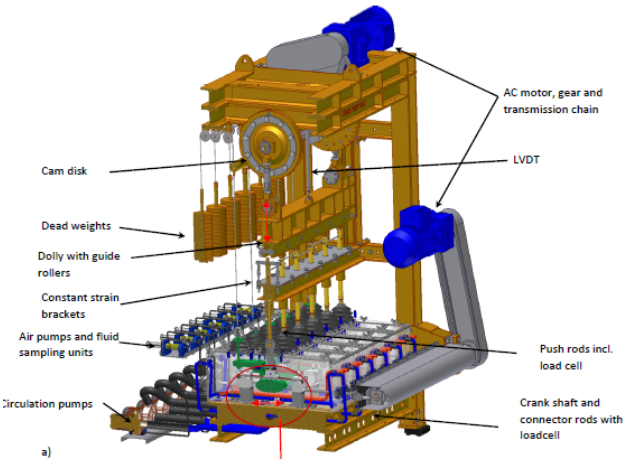

Figure 1: LSMD-Multidegradation rig.

The study put together hardness data from prevalent biofouling organisms at different offshore test bed site's location, experimental and available in scientific literature[1] with the effect of particles with that representative hardness in the multidegradation rig experiment by LSMD. The physical testing of this study involved inclusion of representative particles in the lubrication system to simulate fouling for a particular location. The evolution of seal wear and rod roughness has then be assessed.

[1] Vinagre, Pedro Almeida, Teresa Simas, Erica Cruz, Emiliano Pinori, and Johan Svenson. 2020. "Marine Biofouling: A European Database for the Marine Renewable Energy Sector" *Journal of Marine Science and Engineering* 8, no. 7: 495. https://doi.org/10.3390/jmse8070495

The testing conducted consists of several different stages (*figure 2*). The results of this work suggest a methodology for including biofouling data in hybrid testing for marine environment, as well as a proof-of-concept demonstration with data for one or several particular sites.

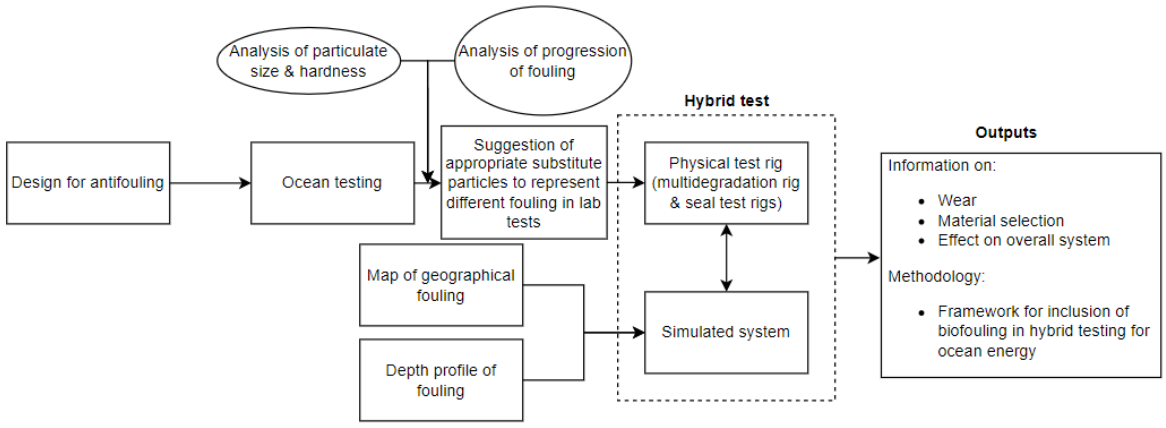

Figure 2: Workflow for biofouling and multidegradation interaction experiments

We will present both the results of the expected prevalent marine biofouling organisms at the sites and depth studied and found in literature, and the influence of the different possibility to use the VALID Hybrid Testing Platform (HTP) to select right material/coatings depending on the depth or location of deployment for the designed PTO or ocean rods systems, in order to keep the goal lifetime of the selected materials.

Microbial Corrosion (WP10)

Pierangela Cristiani (Ricerca sul Sistema Energetico (RSE) SpA, Italy)

Or

Tribocorrosion (WP18)

Dr. Stefano Mischler (École Polytechnique Fédérale de Lausanne (EPFL), Switzerland)

Microbial community analysis of microorganisms on the metal coupons exposed in a deep sea environment

Satoshi WAKAI, JAMSTEC, Yokosuka/Japan; Hirotaka MIZUKAMI, Ayano YASUI, Toshiyuki SUNABA, INPEX CORPORATION, Tokyo/Japan; Yasuyuki MIYANO, Akita Univ., Akita/Japan

Microorganisms in natural and artificial environments frequently influence the deterioration and corrosion of metals, and this phenomenon is referred microbiologically influenced corrosion. In a previous study, significant amounts of slime and corrosion were found in a hydrothermal reactor installed in a deep-sea environment, and accelerated iron dissolution was demonstrated in a laboratory-scale corrosion test using this slime as an inoculum source. In this study, we focused on corrosion in a cold and high-pressure environment in a deep sea.

Seven types of steel and alloys, carbon steel, stainless steels [S30403, S31603, S31703, S31260], and nickel alloys [N06625 and N08825], were tested. Using carbon and stainless steels, plane test pieces (50×20×2 mm) were prepared. Using the coupons excepting carbon steel, crevices (40×25×2 mm and 30×15×2 mm) and U-bend test pieces (75×15×2 mm) were prepared. These coupons were immobilized to a PTFE rod in a metal ladder box, and two metal ladder boxes were deployed in February 2021 at Sagami-bay at 759 and 857 m depth using ROV Kaimei in the research cruise KM21-E02. These metal ladder boxes were recovered in October 2021 using Shinkai 6500 in the research cruise YK21-18C. Biofilm and corrosion products on each coupon were recovered by sterilized cotton swabs. In the crevice test coupons, the outer exposed surface and the inner surface were collected separately. Microbial communities were analyzed by amplicon sequencing.

The carbon steel showed general corrosion with significant amounts of corrosion products, but the plane test pieces of stainless steels didn’t show the visible corrosion. On the other hand, corrosion was observed in the crevice test coupon of S30403 and the U-bend specimen of S30403 and N08825.

The microbial community structure of the carbon steel showed significant enrichment of genera *Sulfurimonas* and *Mariprofundus*. Genus *Sulfurimonas* is a nitrate-reducing sulfur-oxidizing bacterium that has been reported to induce severe corrosion in oil drilling environments. *Mariprofundus ferrooxydans* has been

previously reported as a metal-iron corrosive iron-oxidizing bacterium, which may have preferentially accumulated by acquiring energy through corrosion reactions and oxidation of the resulting divalent iron. Therefore, the enrichment of these microorganisms is reasonable.

On the other hand, on several stainless steel surfaces, enrichment of the genus *Candidatus* Tenderia was observed. In particular, this bacterium accumulated on the outer surface of the S30403 crevice test coupon and in the N08825 U-bend test coupon where corrosion had occurred. A *Candidatus* Tenderia electrophaga is an electrochemically active microorganism and is known to accumulate on the cathodes of electro-cultivation systems. In metal corrosion reactions, an anodic reaction (dissolution of metal ions) and a cathodic reaction (electron consumption) are always paired, and it is possible that this bacterium contributes to the cathodic reaction.

In this study, microorganisms with characteristic metabolic activities were specifically detected in corrosion materials, and microbial functions have been linked to corrosion reactions in deep sea environments with low temperatures and high water pressure. In particular, the characteristic accumulation of electrochemically active microorganism would be expected to contribute to the elucidation of the corrosion mechanism of corrosion-resistant materials such as stainless steel.

Cathodic protection of confined areas under cyclic immersion in sea water

François Henry, Meryll Smith, Anne-Marie Grolleau

Naval Group Cherbourg

Watertight fixation systems are used to maintain equipments and pipings on structures subject to cyclic immersion in sea water. These systems are placed under cathodic protection during the immersion phase.

Some unexpected modifications in a supplier fabrication process led to the use of fixation systems with cavities allowing the penetration of seawater, hence inducing sea water retention in confined areas.

Full scale experiments were carried out in natural sea water to evaluate the possible efficiency of the external cathodic protection system to protect the confined areas during the immersion phase.

The application of the external CP led to the electrolyte modification in the confined areas. The impact of this secondary effect due to CP was studied using potential measurements with miniaturized reference electrodes and RP measurements. These data showed the beneficial effect of CP even on the emersion phases.

Finally, modelling was carried out to determine the impact of the cavities geometry on the efficiency of the cathodic protection in the internal area.

Cathodic protection per ISO 24656:2022 and DNV-RP-B401:2021 – new possibilities for the design?

Dipl.-Ing Lars Lichtenstein
Brooktorkai 18, 20457 Hamburg, Germany, E-mail: Lars.Lichtenstein@dnv.com

DNV – Energy Systems, Renewables Certification

Abstract:

DNV – Energy Systems, Renewables Certification is involved in most of the offshore windfarms worldwide. A very broad overview of the problems arising during the design of corrosion protection systems and the applied solutions and approaches for these issues have been gained over recent years.

Possibilities of finding optimised corrosion protection strategies for different sites conditions and how to deal with the challenges arising from this will be presented.
We will present and discuss the guidance given in the new ISO 24656 Cathodic protection of offshore wind structures, the first ISO explicitly written for this field.

We will compare this with the established recommendations given in the revised DNV-RP-B401:2021 in combination with the revision 7 of Norsok M-501:2022.
Some of the offshore wind farms being developed now are aiming for very long lifetimes of more than 30 years. The design decisions made for the cathodic protection has significant influence on the design.
Corrosion protection is a very long-term topic. Challenges will mainly arise either at the manufacturing and installation phase or at the end of the lifetime of the project of 30+years. There should be a balance between the project risks to be taken and possible mitigation measures, like repair possibilities of coating systems in hard-to-reach areas or retrofit of insufficiently performing cathodic protection systems (ICCP or GACP), for the project to be successful in the long run.

We will provide a comparison between the recommendations given in the different cathodic protection guidelines (ISO and DNV) and show where optimisation can be performed. This will deal with the possibilities of selecting site specific parameters by the designer.
ISO 24656 is providing the opportunity to design the cathodic protection system by trying to limit conservatism on the one hand and allowing to use a model that is closer to reality.

We will show what the impact of the newly introduced frequently wetted areas, seawater flow velocities, indicative design current densities with regards to water velocities and water temperature, internally and externally, and especially the indicative Design current densities in seabed for CP and 'Current Drain' can be.

DNV will present possible solutions for the above given challenges considering the latest available guidelines and standards. We will show how a holistic corrosion protection concept for cathodic protection can be established utilising the latest development and experience from world wind projects.

Investigation of corrosion and cathodic behavior of Aluminium coating in natural seawater

Charles Leballeur[1], Eric Agel[2], Jean-Paul Blanc[2] and Olivier Loukakou[3]

[1]French Corrosion Institute (RISE), Brest, France

[2]TotalEnergies, Pau, France

[3]TotalEnergies Congo, Pointe-Noire, Congo

Aluminium coatings (Thermal spray aluminium or Cold spray Aluminium) can be applied in marine environments or on subsea structure for protecting carbon steel from corrosion. Aluminium acts as a physical barrier and provides galvanic protection. According to several studies, in seawater, even if its corrosion behavior is highly dependent of its composition, Aluminium coating has a low self-corrosion rate and is anodic to carbon steel. For retrofitting of subsea structure, TSA or cold spray can be protected from corrosion using conventional cathodic protection using Zinc or Aluminum-Zinc-Indium anodes for instance. If DNV-RP-B401-2021, gives recommendation regarding the current demand to consider for such material, limited data are available in the literature regarding the actual open circuit potential of Aluminium coatings in seawater and its cathodic behavior.

In this study, the corrosion properties and polarization behavior of cold spray in seawater have been investigated. Cold spray aluminium coupons (99,996%-Al) have been tested in natural seawater during 3 months at open circuit potential, coupled to carbon steel and under potentiostatic and galvanostatic conditions.

Results from this study have shown that after 3 months of exposure, the corrosion rates of cold spray without coupling in seawater were not negligible, higher than some values of the literature. Without coupling, the open-circuit potential of cold spray was measured between -700 and -800 mV/SCE during the first days, then stabilized at about -1050 mV/SCE. Polarization tests confirmed that above -1050 mV/SCE, the cold spray was anodically polarized. Therefore, these results suggest that Aluminium coated surfaces may remain anodic and thus not completely protected.

Urgent retrofitting of heavily damaged heat exchanger with impressed current cathodic protection

Tea Antolović[1], Krešimir Kekez[1], Ivan Stojanović[2],

[1] PA-EL, Veliko Trgovišće, Croatia;

[2] Faculty of mechanical engineering and naval architecture, Zagreb, Croatia;

Abstract

Corrosion rates in the process industry are often hardly predictable. Many facilities operate without particular involvement of corrosion engineering which in turn leads to detrimental corrosion and wall loss. Heat exchanger that exchanges heat between ammonia side and seawater side as a part of blue fish processing factory was found to be heavily damaged by both, corrosion and erosion. Corrosion is enhanced by the colossal water flow rate of about 100 m^3/h which leads to the Reynolds number of up to 14000. In such environment selected coating system did not provide expected protection. In a term of permanent integrity preservation, an impressed current cathodic protection system has been designed and implemented for the remaining life cycle. This paper presents design concepts, installation challenges, cathodic protection parameters and corrosion rates observed by the gravimetric coupons.

Keywords: heat exchanger, cathodic protection, corrosion control, integrity management, corrosion rate, gravimetric coupons.

Cathodic Protection in Power Plants : EDF examples in nuclear and hydropower plants

T. Jaussaud, P. Livolant*, A. Prigent*, A. Mazenc♠ and S. Trevin**

♠ EDF/DIPNN/DI/MCP – Chinon, 37420 AVOINE – France

** EDF/Hydro/DTG/IDM -134 Rue de l'étang, 38950 St MARTIN LE VINOUX - France*

Nuclear and thermal powerplants need coolant as cold source and fresh water or sea water are commonly used with no specific water treatment at EDF in France. Hydropower plants is based on natural water with various technologies and materials.

Ageing management optimization of these power plants is more and more addressed to corrosion to bring onto control long life term of these plants. This consideration of the risk of corrosion on existing installations requires an understanding of any modifications or absence of maintenance of the organs that lead to poorly controlled degradation. The solutions proposed to keep the installations in safe operation for long term are the result of technical and economic optimization. Difficulties in changing working methods and maintaining skills must be taken into account.

Simple and durable are the watchwords for proposing solutions to operators.

The paper deals with some example of Imposed Current Cathodic Protection systems at different stages:

In hydropower field with cathodic protection

- Rivière de l'Est Penstock feedback and the new Project on Frejus Penstock
- 5 years feedback for Run-River Dam of Pizançon

In nuclear power plant

- Benefits and drawbacks for cathodic protection in rotating filter, condenser…

The different facilities are described with their operating parameters and their corrosion protection performance. These systems provide protection either on land or at sea depending on the location of the power plant. Finally, dams require effective cathodic protection design for the freshwater environment.

Investigation of Detrimental Gases Generated from ICCP

X. Zhang

Endures B.V. Den Helder, The Netherlands

Abstract

Applying an impressed current cathodic protection (ICCP) system in a wind monopile or in a seawater tank provides good protection of the steel structures and thereby significantly decreases the maintenance cost. However, applying ICCP to steel may generate detrimental gases like H_2 and Cl_2. Hydrogen evolution at the steel surface may cause hydrogen embrittlement of the steel and Cl_2 generation may result in local pH dropping that accelerates the degradation of the structures and the infield cables. The objective of this work was to measure the H_2 and Cl_2 concentrations generated at the steel surface and anode surface respectively, at different applied potentials and with different MMO anode materials, to help in choosing the right potential level and the right MMO anode materials when applying ICCP.

A two-chamber connected corrosion reactor was used to expose a steel sample in one chamber and an MMO anode in the other chamber, filled with filtered natural seawater. Using this specific set-up, it was possible to separate the gases generated at the anode from H_2 gas generated at the cathode. The ICCP was applied to the steel through the MMO anode at different potential levels vs Ag/AgCl. The H_2 gas volume was measured and compared to the hydrogen volume calculated from the current density assuming that the total charge was consumed by hydrogen evolution. The gases of O_2 and Cl_2 were collected from the MMO anode. The seawater from the anodic chamber was collected after the test and the Cl_2 in the solution was analyzed using titration since the Cl_2 dissolves easily in water and becomes hydrochloric- (HCl) and hypochlorous acids (HClO). The results show that the volume ratio of hydrogen measured (H_2) and calculated (H_2-c) is about 1, when potential was more negative than -1.05 V. Cl_2 generated in the seawater increases when the potential is more negative, which means that caution has to be in place when selecting appropriate potentials for ICCP.

1 Introduction

Steel structures are susceptible to corrosion attack in seawater. Cathodic protection either via sacrificial anodes (such as aluminum and zinc anodes) or via impressed current cathodic protection (ICCP) is widely used to protect steel structures in seawater [1]. Applying an ICCP system in a wind monopile or in a seawater tank provides good protection to the steel structures

and decreases the maintenance cost. However, applying ICCP to steel generates H_2 and Cl_2, which is harmful to the structure and the local environment [2-3]. H_2 is generated at steel/water interface due to cathodic reactions. At the same time, gases of O_2 and Cl_2 are generated at anode/water interface due to anodic (oxidizing) reactions. Hydrogen evolution at the steel surface may cause hydrogen embrittlement of the steel and Cl_2 generation may result in local pH dropping that accelerates the degradation of the structures and the infield cables.

The objective of this work was to measure the H_2 and Cl_2 concentrations generated at the steel surface and anode surface respectively, at different applied potentials and with different MMO anode materials, which would be helpful in choosing the right potential level and the right MMO anode materials when apply the ICCP.

The possible reactions at the cathodic electrode (steel) are oxygen reduction (dissolved oxygen), hydrogen evolution and water reductions, depending on their availability and potential level [4],

$$O_2\,(g) + 2H_2O\,(l) + 4e^- \rightarrow 4OH^-\,(aq) \qquad (E_0 = 0.401\ V\ vs.\ NHE) \qquad (1)$$

$$2H^+ + 2e^- \rightarrow H_2\,(g) \qquad (E_0 = 0\ V\ vs.\ NHE) \qquad (2)$$

$$2H_2O\,(l) + 2e^- \rightarrow H_2\,(g) + 2OH^-\,(aq) \qquad (E_0 = -0.83\ V\ vs.\ NHE) \qquad (3)$$

The H_2 gas was collected from the steel cathode and the H_2 volume was measured. The hydrogen generated in the reaction was also calculated from the current density, assuming that the total charge was consumed by hydrogen evolution.

The reactions at anodes are oxygen evolution and chlorine evolution in acidic solution or oxidation of chloride to become hypochlorite (ClO^-) in alkaline solution [4, 5],

$$4OH^-\,(aq) \rightarrow O_2\,(g) + 2H_2O\,(l) + 4e^- \qquad E_0 = 1.23\ V - 0.059 \times pH \quad (vs.\ NHE) \qquad (4)$$

$$Cl^-\,(aq) + 2e^- \rightarrow Cl_2\,(g) \qquad (E_0 = 1.36\ V\ vs.\ NHE) \qquad (5)$$

$$Cl^-\,(aq) + 2OH^-\,(aq) \rightarrow OCl^-\,(aq) + H_2O\,(l) + 2e^- \qquad (6)$$

$$E_0 = 1.72\ V - 0.059 \times pH \quad (vs.\ NHE)$$

Cl_2 dissolves in water easily to become hypochlorous acid. The concentration of OCl^- in a solution can be determined by reacting to a known mass of KI solution [6, 7].

$$OCl^- (aq) + 2I^-(aq) + 2H^+ \rightarrow I2 (aq) + Cl^- (aq) + H_2O \quad (7)$$

The reaction of OCl^- goes to completion as the I^- is in excess. The amount of I_2 formed is determined by means of titration with sodium thiosulfate ($Na_2S_2O_3$) solution.

$$I_2 (aq) + 2S_2O_3^{2-} (aq) \rightarrow 2I^- (aq) + S_4O_6^{2-} (aq). \quad (8)$$

The gases of O_2 and Cl_2 were collected on the MMO anode side. The Cl_2 generated in the reactions can be in gas phase or dissolve in the seawater and becomes hydrochloric acid (HCl) and hypochlorous acid (HClO). The Cl_2 in gas phase can be measured using a Cl_2 gas sensor. The Cl_2 dissolved in the seawater can be analyzed by means of titration method, using sodium thiosulfate [6].

2 Materials and methods

2.1 Sample preparation

Carbon steel samples were cut from S355 bars in a diameter of 20 mm and in a length of 200 mm. A copper wire cable was connected via a small bolt and a nut at one end of the bar for electrical connection. This end was covered with a short PVC tube and sealed with epoxy resin. The surface to be studied was ground using sandpaper (SiC, P320). The steel surface area to be exposed was 116 cm^2.

Two types of MMO anodes used were MMO Ir-Ta and MMO Ru-Ir-Ti anodes. A copper wire cable was connected with two nuts on the thread side. This end was covered with a PVC tube and sealed with epoxy resin. The MMO surface to be exposed was 8 cm^2 and the remaining surface was covered with Teflon tape plus plastic tape.

A typical steel sample and an MMO anode were shown in Figure 1.

Figure 1. Illustration of a steel sample S355 and an Ir-Ta MMO anode before testing.

2.2 Test set-up

Figure 2 shows a test set-up for a steel sample and an MMO anode exposed to filtered natural seawater. The reactor was composed of two connected glass chambers. The steel as a cathode was set in one chamber and an MMO anode in the other chamber. The reactor was filled with filtered natural seawater (about 2300 ml) and closed with special Teflon plugs. The cathodic cable, a glass tube as an outlet of H_2 gas and a standard KCl saturated Ag/AgCl reference electrode (E_0 = 0.197 V vs. NHE) were inserted through the plug in the chamber on the cathodic side. All potentials presented in the report were referred to this reference electrode. The anode cable and a glass tube as an outlet of gases generated from the anodes were inserted through the plug on the anode side.

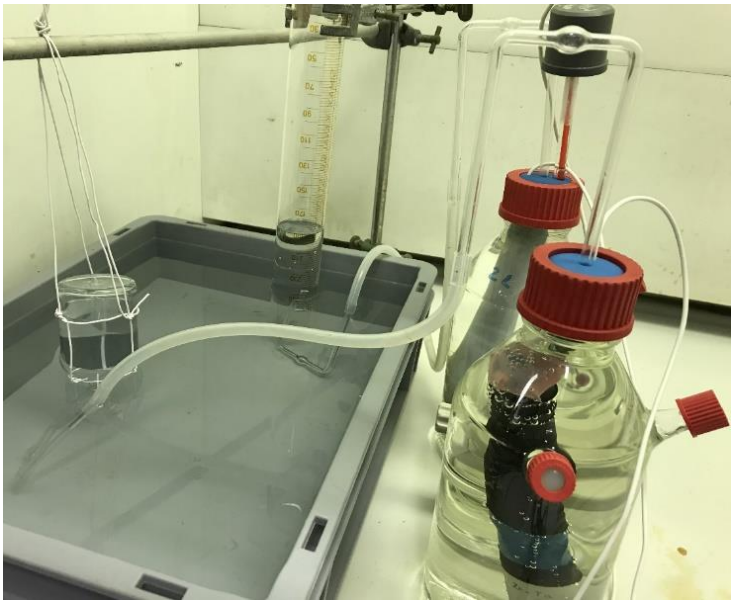

Figure 2. Illustration of a steel sample in one chamber and an MMO anode in the other chamber of a reactor, filled with filtered natural seawater.

The H_2 gas generated from the cathodic electrode was collected in a volume cylinder (250 ml or 500 ml) and gases (O_2 and Cl_2) generated from the anode electrode were collected in a 125 ml glass bottle. The test was run at room temperature (21 ^oC).

2.3 Current density measurements

The three-electrode cell (cathode, anode and reference electrodes) was connected to a potentiostat. Impressed current was applied to the steel at 4 different potential levels: -0.95 V, -1.00 V, -1.05 V and -1.10 V. The current was measured as a function of time and the current density was calculated using current divided by the steel surface area. The test duration varied from 2 hours to 500 hours, depending on the applied potential level.

2.4 H_2 volume and Cl_2 concentration measurements

The volume of H_2 generated from the cathodic reaction was collected and measured using a volume cylinder. After the test, a 100 ml seawater sample from the anodic chamber was taken for pH and Cl_2 measurements.

Chlorine in gas phase was measured using gas detection tubes (Chloor 0.2/a) (Figure 3). The gas detection tube system consists of a pump and glass detection tubes. The tubes are filled with an absorbent material and chemical reagent. The chemical reagent produces a color stain along the tube when chlorine gas is present.

Figure 3. Gas detection tube system for chlorine measurements.

Chlorine dissolved in seawater was measured using an iodometric method using sodium thiosulfate. 50 g seawater sample was taken in a 250 ml Erlenmeyer flask for titration. First, 2 g of KI was added to the seawater sample. Then the seawater sample was stirred and titrated

using 0.01M $Na_2S_2O_3$ solution till the brownish iodine color faded. Finally, 1 ml starch indicator solution was added in the flask and the solution was titrated to a clear endpoint. The volume of $N_2S_2O_3$ solution used in titration was recorded.

The total amount of Cl_2 in the seawater sample was calculated by equation,

$$\text{ppm of } Cl_2 = (\text{volume (ml) of } Na_2S_2O_3) \times 0.01 \times 71 \times 1000/ (2 \times \text{m (seawater)}) \quad (9)$$

where 0.01 is the normality of $N_2S_2O_3$ solution, 71 the molecular mass of Cl_2 (g), 1000 the conversion factor from mg/g to ppm, 2 milliequivalents $S_2O_3^{2-}$ per ClO^-, and m the mass (g) of the seawater sample.

The electrode materials and experimental parameters are given in Table 1.

Table 1. Electrode materials and gases measurements in seawater at 21 °C.

Material	Area (cm^2)	ICCP (V)	Current density i (mA/cm^2)	H_2 (cm^3)	Cl_2 in gas (ppm)	Cl_2 in solution (ppm)	pH
Steel	116	-0.95	√	√			
		-1.00	√	√			
		-1.05	√	√			
		-1.10	√	√			
MMO Ir-Ta	8				√	√	√
MMO Ru-Ir-Ti	8				√	√	√

3 Results

3.1 Current density measurements

Figure 4 shows the current density measured between a steel sample and an MMO Ir-Ta anode as a function of time at -0.95 V in seawater. The current was from anode to steel in seawater and electrons from anode to steel.

The initial current was calculated by choosing an initial period of 48 hours in this case and the average initial current density (Initial i_0) was lower than 50 $\mu A/cm^2$. The current decreased with time due to the deposition of a calcareous layer on the steel surface. Normally, the redox reaction speed at the electrodes/electrolyte increases when a more negative voltage is applied and consequently the speed of calcareous deposition on the cathodes and gases production on the anodes increases. The deposits on the electrode surface may increase the resistance and result in decrease of the current density.

The average current density (i) is about 30 $\mu A/cm^2$ within 20 days in this coupling.

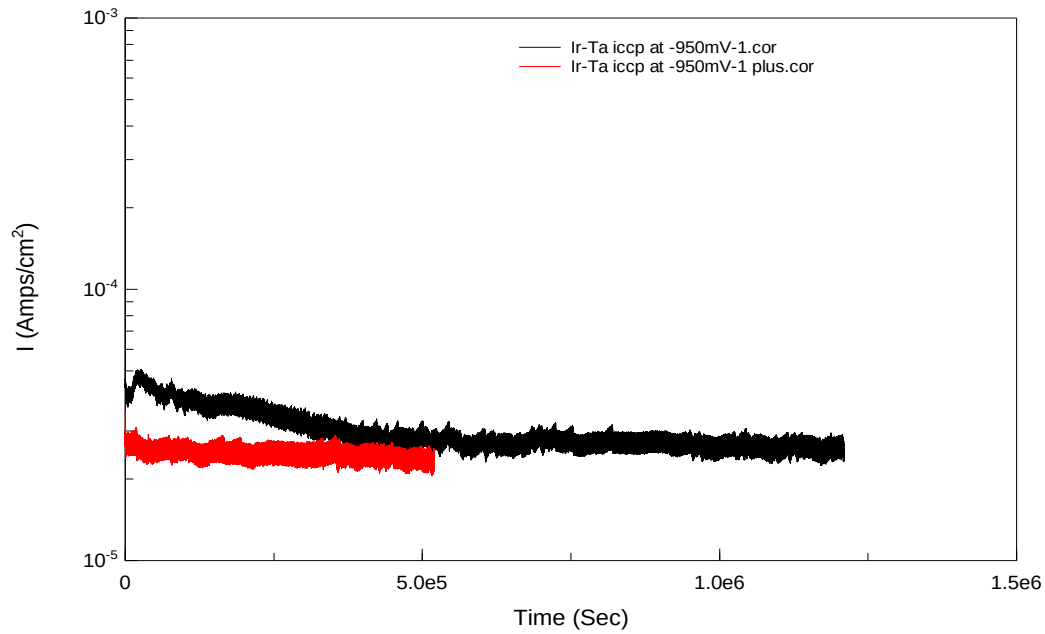

Figure 4. Current density at steel surface at -0.95 V, coupled with MMO Ir-Ta anode in seawater.

Figure 5 shows the current density measured at steel surface via an MMO Ru-Ir-Ti anode as a function of time at -0.95 V in seawater. The initial i_0 and mean current densities (i) in this case are higher than those measured via the MMO Ir-Ta anode. The fluctuation of the current density is attributed to the building up and breaking down of the calcareous layer on the steel surface.

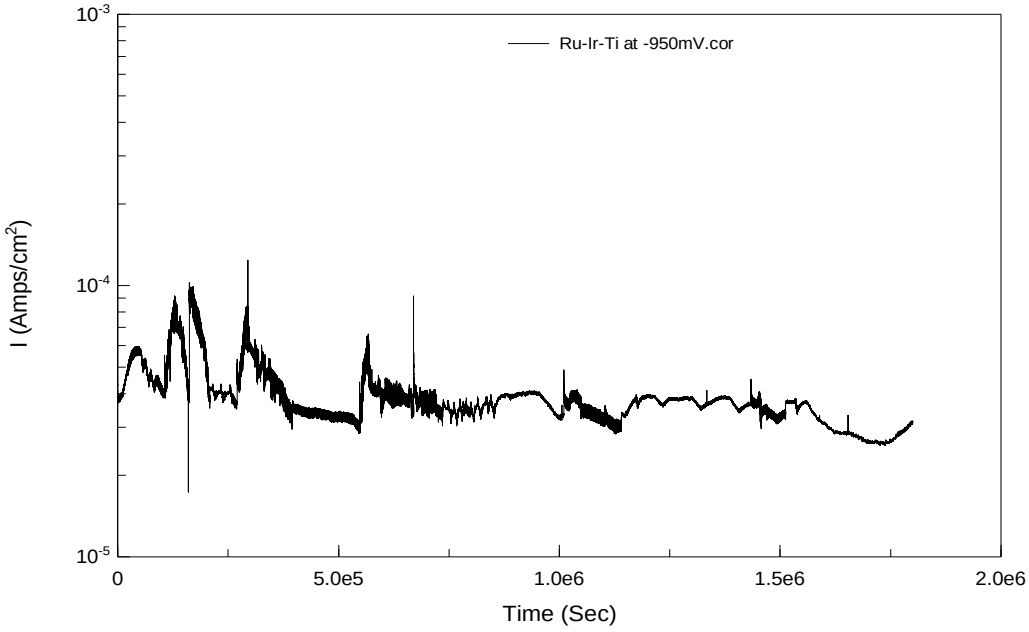

Figure 5. Current density at steel surface at -0.95 V, coupled with MMO Ru-Ir-Ti anode in seawater.

When the applied potential reached a more negative potential at -1.05 V, the current density increased significantly and H_2 evolution became faster. The experimental duration was shortened to a few hours. The initial period of 2 hours was chosen to calculate the initial current in this case. The initial current density, the mean current density at different potentials and the charge transferred at the steel surface, were calculated and presented in Table 2.

Table 2. Current density at steel surface at different potentials, H_2 volume measured and calculated, pH and total Cl_2 measured in seawater.

Anode materials	ICCP (V)	Initial period (h)	Initial i_0 (mA/cm^2)	Test duration (h)	Mean i (mA/cm^2)	Charge ($coul/cm^2$)	H_2 measured (cm^3)	Total Cl_2 (ppm)*	pH (anode side)	H_2-c measured (cm^3)	Ratio H_2/H_2-c
Ir-Ta	-0.95	48	-0.041	480.3	-0.029	-49.49	180	74.6	2.79	668	0.3
	-1.00	48	-0.026	312.5	-0.025	-76.31	494	156.2	2.84	1029	0.5
	-1.05	2	-0.913	4.5	-1.48	-23.96	336	588.6	2.20	323	1.0
	-1.10	2	-4.92	2	-4.92	-35.6	533	617.7	2.27	480	1.1
Ru-Ir-Ti	-0.95	48	-0.055	500	-0.039	-69.28	306	113.6	2.81	934	0.3
	-1.00	48	-0.13	315.3	-0.064	-71.95	603	319.5	2.15	970	0.6
	-1.05	2	-0.83	3.7	-0.92	-12.06	171	344.4	2.66	163	1.1
	-1.10	2	-2.89	2.5	-3.71	-33.33	510	592.9	2.26	450	1.1
* Total Cl_2 in liquid; Cl_2 in gas phase >30ppm.											

3.2 H_2 volume and Cl_2 concentrations

After the tests, the pH of the seawater on the cathodic side (topper part) was about 6.8 for tests at a potential of -0.95 V, and about 11 for tests at other potentials. The relative low pH at -0.95 V is attributed to proton diffusion in a longer test time period than the test at other potentials. The pH of the seawater on the anode side was lower than 3.0 for all the tests (see Table 2).

The volume of H_2 generated on the steel surface at different potentials is presented in Table 2. H_2 evolution speed increased with the applied negative potentials on the steel cathode.

The hydrogen volume was also calculated based on the charge transferred, assuming the electrons were used for reduction of protons in the solution (see Table 2). The volume ratio of hydrogen measured (H_2) and calculated (H_2-c) is about 1, when potentials were more negative than -1.05 V, while it was lower than 0.6 when potential was less negative than -1.05 V. The cathodic reactions first consume dissolve oxygen and then hydrogen evolution takes place when potential becomes more negative. The hydrogen production is following the different steps in hydrogen evolution (reactions (2) and (3)) [8].

Cl_2 gas in the seawater samples was more than 30 ppm measured by the gas detection tubes (Figure 6).

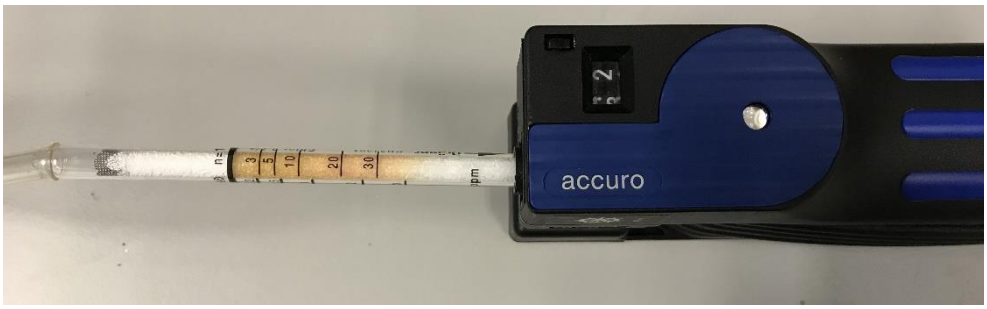

Figure 6. Chlorine in the gas phase detected by gas detection tube (color changed, >30ppm).

The Cl_2 dissolved in seawater became hypochlorous acid which had "bleaching" effect. Figure 7 shows that the blue tape on the MMO Ru-Ir-Ti anode and the red cable were bleached in the sea water.

The total Cl_2 amount in the solution determined by titration is presented in Table 2. The Cl_2 generated increased when a more negative potential was applied, which means that caution has to be in place when selecting appropriate potentials for ICCP.

Figure 7. The blue plastic tape on the MMO Ru-Ir-Ti anode and the red cable were breached by the hypochlorous acid in seawater (at -1.0V).

4 Conclusions

Applying ICCP to protect steel against corrosion in seawater, harmful gases such as H_2 and Cl_2 have to be taken care.

The pH value of the seawater near the anode is lower than 3 because of oxygen and chlorine evolution.

The gases generated on the MMO Ru-Ir-Ti anodes are more than those on the MMO Ir-Ta anodes when the potential is less negative than -1.05 V. When the potential drops to -1.1 V the gases generated on the MMO Ru-Ir-Ti anode are less than those generated on the MMO Ir-Ta anode.

The volume ratio of hydrogen measured (H_2) and calculated (H_2-c) is about 1, when potential is more negative than -1.05 V.

Cl_2 in the gas phase is more than 30 ppm. Cl_2 generated in the seawater increases when the potential is more negative. which means that caution has to be in place when selecting appropriate potentials for ICCP.

5 Acknowledgement

The author acknowledges the Oes Group for financial support and thank Mr. F. Verbruggen for the fruitful discussion.

6 References

[1] DNVGL (2017) Cathodic Protection Design. Recomm Pract DNVGL-RP-B401.

[2] Huizinga S, McLoughlin B, Hannah I, et al (2006) Failure of Subsea Super Duplex Manifold Hub by HISC and Implications for Design, NACE Interbnational, Paper No.06145.

[3] Funahashi M (2013) What You Need to Know About MMO Coated Metal Anodes. NACE International, Paper No. 2107.

[4] Dionigi F, Reier T, Pawolek Z, et al (2016) Design Criteria, Operating Conditions, and Nickel-Iron Hydroxide Catalyst Materials for Selective Seawater Electrolysis. ChemSusChem 9:962–972.

[5] Sun F, Qin J, Wang Z, et al (2021) Energy-Saving Hydrogen Production by Chlorine-free Hybrid Seawater Splitting Coupling Hydrazine Degradation. Nat Commun 12:4182.

[6] HACH (2018) Iodometric Method Using Sodium Thiosulfate.

[7] Ricard (2013) Determining the Concentration of Sodium Hypochrorite (NaClO) in Commercial Bleach Solution.

[8] Gálvez-Vázquez M de J, Grozovski V, Kovács N, et al (2020) Full Model for the Two-Step Polarization Curves of Hydrogen Evolution, Measured on RDEs in Dilute Acid Solutions. J Phys Chem C 124:3988–4000.

Corrosion of carbon steel under calcareous deposit in humid marine environment

R.Palluet[a,b], *Ph.Refait*[a], *M.Jeannin*[a], *A-M.Grolleau*[b]

[a] *Laboratoire des Sciences de l'Ingénieur pour l'Environnement (LaSIE), UMR 7356 CNRS-Univ. La Rochelle, Bât. Marie Curie, Av. Michel Crépeau, F-17042 La Rochelle cedex 01, France.*

[b] *Naval Group, Place Bruat, 50100 Cherbourg-en-Cotentin, France*

Various carbon steel structures are subjected to immersion/emersion cycles in seawater. These structures are commonly protected by an anti-corrosion paint combined with cathodic protection (CP), CP being often achieved using a sacrificial anode. The paint can be damaged, and part of the metal surface is consequently in contact with seawater when the structure is immerged. CP is then the only protection remaining. Depending on the type of sacrificial anode used (aluminium/gallium or zinc) the potential of the steel structure can reach values about -0.850 V/Ag-AgCl-seawater or -1050 V/Ag-Ag-Cl-seawater. Whatever the potential, the cathodic polarization of the steel surface induces the formation of a calcareous deposit. When the structure is emerged, the cathodic protection may not be effective even if the steel surface remains wet (and thus subjected to corrosion), because the electrolytic continuity is interrupted and the CP current cannot flow between anode and steel. The previously formed calcareous deposit may have a protective ability to mitigate the corrosion of the underlying steel surface but the efficiency of this protection is yet to be estimated.

The present study then focusses on the behaviour of carbon steel S355NL coupons covered with a calcareous deposit formed during two months in natural seawater at 10°C as a result of a CP carried out at two different potentials (-0.850 V/Ag-AgCl-seawater and 1050 V/Ag-AgCl-seawater) under atmospheric pressure. XRD analysis of the steel surface after 1 week, 2 weeks, 1 month and 2 months of CP showed that the calcareous deposit formed at -0.850 V/Ag-AgCl-seawater was composed in any case of aragonite. At -1050 V/Ag-AgCl-seawater, brucite formed initially and transformed later to aragonite, in agreement with previous study [1].

The coupons were subsequently left during two weeks in a humid seawater environment, without CP, at room temperature (~20°C). Polarization resistance (R_p) and electrochemical impedance spectroscopy measurements were carried out at different times (0 h, 24 h, 72 h, 168 h and 336 h) for each potential. Visual observation at the end of the experiments revealed in any case the presence of steel corrosion products (orange rust). µ-Raman spectroscopy analysis of the coupons surface however only revealed the presence of aragonite. Corrosion took place actively, as demonstrated by the measured R_p values, leading to the formation of corrosion products between steel surface and aragonite layer.

Reference

[1] D. Nguyen Dang, S. Gascoin, A. Zanibellato, C.G. Da Silva, M. Lemoine, B. Riffault, R. Sabot, M. Jeannin, D. Chateigner, O. Gil., Role of Brucite Dissolution in Calcium Carbonate Precipitation from Artificial and Natural Seawaters, *Cryst. Growth Des.* 17, 4 (2017) 1502-1513.

The effect of calcareous deposits on the hydrogen diffusion and uptake of carbon steel evaluated by permeation experiments

Razieh Tavassolian[1], Kim Verbeken[2], Tom Depover[3]

[1]*Department of Materials, Textiles and Chemical Engineering, Research group Sustainable Materials Science, Ghent, Belgium, Razieh.Tavassolian@Ugent.be*
[2]*Department of Materials, Textiles and Chemical Engineering, Research group Sustainable Materials Science, Ghent, Belgium, Kim.Verbeken@Ugent.be*
[3]*Department of Materials, Textiles and Chemical Engineering, Research group Sustainable Materials Science, Ghent, Belgium, Tom.Depover@Ugent.be*

Abstract

In this research, the effect of calcareous deposits on the hydrogen evolution reaction and hydrogen absorption has been investigated. Therefore, the Devanathan-Stachurski cell has been used to evaluate the hydrogen uptake of a construction steel (S235) which is charged in a NaCl solution containing Ca^{2+} and Mg^{2+} under CP (Cathodic Protection) condition of -1000 mV (Ag/AgCl). On the charging side, calcareous deposits are formed on the steel surface and can influence the cathodic reaction and thus hydrogen uptake. To have a better understanding about the role of calcareous deposits on the hydrogen evolution reaction, electrochemical impedance spectroscopy is used. As such, the deposits surface coverage and resistance to hydrogen evolution reaction are measured during charging time. A NaCl solution (free of Ca^{2+} and Mg^{2+}) is used as reference to avoid these calcareous deposits. Then, the cathodic current density at the charging side, the permeation current density, and hydrogen sub-surface concentration are compared. Furthermore, the deposits formed on the surface are evaluated by scanning electron microscopy and energy dispersive X-ray spectroscopy, obtaining the structure and chemical composition of the deposits. The results elucidate the mechanism of calcareous deposits influence on the hydrogen uptake.

Keywords: calcareous deposits; hydrogen uptake; cathodic protection; Devanathan-Stachurski; electrochemical impedance spectroscopy.

Introduction

Cathodic protection (CP) has been widely used as an effective way to protect steel for submarine applications from corrosion by driving the steel potential to the cathodic region, where corrosion is thermodynamically impossible to occur. However, under CP, OH^- ions can be generated near the surface of the metal as a result of hydrogen evolution reaction, leading to the precipitation of calcareous deposits in seawater. The deposit is mainly a mixture of $CaCO_3$ and $Mg(OH)_2$ which can provide a diffusion barrier to oxygen dissolved diffusion, decreasing corrosion [1, 2].
When the metal is under cathodic protection, depending on the potential, two cathodic reactions occur: dissolved oxygen reduction and water reduction (in more negative potential) [3].

$O_2\ (g) + 2H_2O\ (aq) + 4e^- \rightarrow 4OH^-\ (aq)$
$2H_2O\ (aq) + 2e^- \rightarrow H_2\ (g) + 2OH^-\ (aq)$

In both reduction reactions, hydroxyl ions are released, resulting in an increase in pH at the interface of metal/water. As a result of increasing the interfacial pH, inorganic products such as calcium carbonate and magnesium hydroxide precipitate on the metal surface, as illustrated by the following reactions.

$OH^-\ (aq) + HCO_3^-\ (aq) \rightarrow CO_3^{2-}\ (aq) + H_2O\ (aq)$
$CO_3^{2-}\ (aq) + Ca^{2+}\ (aq) \rightarrow CaCO_3\ (s)$
$Mg^{2+}\ (aq) + 2OH^-\ (aq) \rightarrow Mg(OH)_2\ (s)$

The hydrogen evolution induced by cathodic protection leads to entry of hydrogen atom into the metal lattice, resulting in hydrogen embrittlement of the protected steel. Hydrogen absorption of pipeline steel on which calcareous is formed can be influenced by deposits. Simoni et al. [4] reported that calcareous deposits formed in artificial seawater at -1000 mV was an Mg-rich inner layer and a Ca-rich outer layer, and causes a decrease in the steady state hydrogen flux compared to the solution without Ca^{2+} and Mg^{2+}. Ma et al. [5] showed that the surface of the X70 steel on the charging side after a permeation experiment in a simulated Canadian groundwater (NS4) was covered by a thin $Mg(OH)_2$ layer with a scattered cubic deposit of $CaCO_3$. Besides, hydrogen permeation current and hydrogen concentration on the charging side were much higher in the NS4 solution compared to the modified NS4 solution (without Ca^{2+} and Mg^{2+}). Ou et al. [6] reported that Ca-rich layer on the steel surface under cathodic charging decreases the permeation rate, and a loose deposit of $Mg(OH)_2$ in synthetic seawater without Ca^{2+} and HCO_3^- ions shows higher barrier efficiency and much lower hydrogen absorption. The relation between hydrogen embrittlement and calcareous deposits remains unclear as the results contradict each other and there is no concrete agreement regarding the role of magnesium hydroxide and calcium carbonate on hydrogen uptake. This research is aimed to study the mechanism behind the role of calcium carbonate and magnesium hydroxide on hydrogen uptake of carbon steel. To reach this, electrochemical measurements will be carried out in a controlled condition and the influence of Mg^{2+} will be investigated.

Materials

Materials and electrolytes

S235 construction steel with a diameter of 14 mm and thickness of 1 mm (±0.1) has been used as a working electrode. The chemical composition is given in Table 1. Both surfaces of the specimen were randomly ground down to 500 grit silicon carbide paper and subsequently rinsed with demi water and acetone.

Table 1: chemical composition of the S235 steel grade in wt.%.

Fe	C	Mn	Al	Cr	Cu	Ni	Others
99.37	0.08	0.36	0.03	0.03	0.02	0.02	P+S+O

To study the role of calcareous deposits, three different electrolytes have been used. The chemical composition of the electrolytes is given in Table 2. pH of the electrolytes was adjusted at 8.2 with a 0.1 M NaOH solution.

Table 2: composition of the electrolyte according to ASTM D1141. The concentrations are given in $g.l^{-1}$.

Electrolyte	NaCl	$CaCl_2$	$NaHCO_3$	$MgCl_2$
E1	31.443	1.16	0.201	-
E2	25.073	1.16	0.201	5.20
E3	32.61	-	-	-

Electrochemical measurements

Hydrogen permeation experiments have been done in Devanathan-Stachurski cell. The cell consists of two doubled walled glass cell with the sample in between. The sample was connected to the two potentiostats, under applied of cathodic and anodic potentials. The anodic cell was filled with 0.1 M NaOH while a potential of -500 mV vs. Hg/Hg_2SO_4 was applying to the sample. After the current density reached a steady state value (around 30 $nA.cm^{2-}$), the cathodic cell was filled with one of the electrolytes from Table 2 and simultaneously a potential of -1000 mV vs. Ag/AgCl was applied. After start of charging, the hydrogen permeation current was recorded over time.

While applying CP at the charging side, calcareous deposits are formed and their coverage and thickness are varying over time. To have a better understanding of the role of deposits on the hydrogen permeation, electrochemical impedance spectroscopy (EIS) was performed every two hours during charging. Potentiostatic EIS was applied at -1000 mV vs. Ag/AgCl, at frequency range of 0.1 up to 10000 Hz and at 10 mV amplitude.

Deposits characterisation

After finishing the test, the sample was quickly removed from setup and rinsed with Mili-Q water and acetone. The morphology and composition of the deposits was analysed using scanning electron microscopy and energy dispersive X-ray spectrometry (EDS).

Results and discussion

SEM observations of calcareous deposits from the reduction side is presented in Figure 1. The deposits in Figure 1a are cubic crystals of calcite, one of the crystalline forms of $CaCO_3$ which can be formed in the absence of Mg^{2+}. In the presence of Mg^{2+}, the formation of calcite is inhibited and another morphology with a cauliflower shape, aragonite, is appeared on the surface. The inhibiting effect of Mg^{2+} upon the formation of both calcite and aragonite was reported previously [7]. EDS results confirm that the deposits are $CaCO_3$ with no trace of $Mg(OH)_2$. However, cross-section images demonstrate some small areas of $Mg(OH)_2$ beneath aragonite layer.

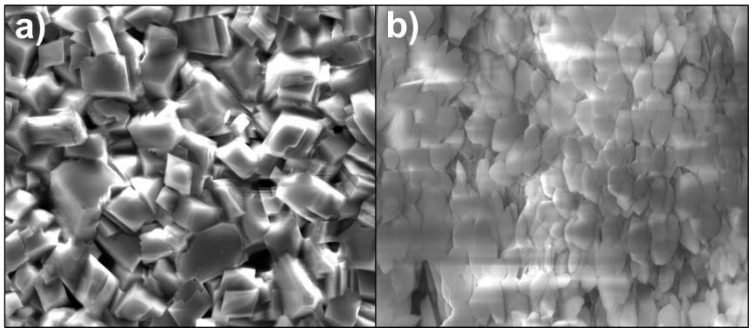

Figure 1: Morphology of $CaCO_3$ deposits after 24 h CP at -1000 mV. a) formed at E1 electrolyte b) formed at E2 electrolyte.

The electrochemical hydrogen permeation technique was used to determine the effect of calcareous deposits on hydrogen permeation of carbon steel. To clarify the role of Ca^{2+} ions, the hydrogen permeation test was performed in NaCl solution containing Ca^{2+} ions instead of artificial seawater to avoid the interference of other ions in seawater. To elucidate the synergistic effects of Mg^{2+} and Ca^{2+} ions on hydrogen uptake, the same experiment was performed in NaCl solution containing Ca^{2+} and Mg^{2+} ions. NaCl solution prepared in Milli-Q water was chose as a reference to compare the results. The effect of different deposits on hydrogen permeation of carbon steel is shown in Figure 2. The hydrogen permeation currents in the electrolytes containing Ca^{2+} and Ca^{2+}+Mg^{2+} are higher than the reference NaCl electrolyte, demonstrating that hydrogen uptake is promoted due to presence of calcareous surface deposits. The amount of hydrogen permeation currents after 24 hours for the electrolytes E1, E2 and E3 are 0.29, 0.37 and 0.23 $\mu A.cm^{-2}$, respectively. SEM images illustrate the change of calcareous morphology from calcite to aragonite, and also the presence of small regions of $Mg(OH)_2$ beneath $CaCO_3$ layer by adding Mg^{2+} ions. It seems that aragonite and/or inner layer of $Mg(OH)_2$ has a promoting role in hydrogen uptake as the hydrogen permeation current is higher in aragonite than in calcite. It was claimed that hydrogen atoms are trapped at the cavity or gap interface of the calcareous layer and not able to diffuse out of the cavity and pores, avoiding hydrogen recombination and promoting absorption of hydrogen into the lattice [8].

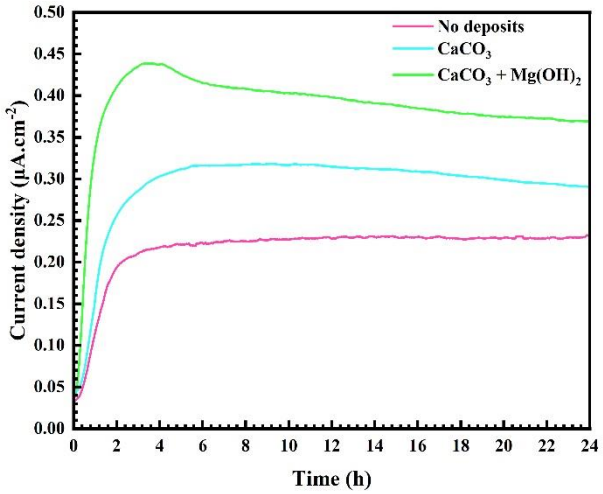

Figure 2: The hydrogen permeation curve of different charging electrolytes. Blue: E1, green: E2, and pink: E3.

Conclusion

The presence of calcareous deposits after charging at -1000 mV was confirmed by SEM and EDS measurements. The morphology of calcareous changed from cubic shape of calcite to aragonite by adding Mg^{2+} ions into the same solution. Hydrogen permeation results showed that calcareous deposits promoted hydrogen uptake, in particular when Mg^{2+} ions are present. The sample without any deposits had the lowest hydrogen permeation current density.

References

1. Hartt, W.H., C.H. Culberson, and S.W. Smith, *Calcareous Deposits on Metal-Surfaces in Seawater - a Critical-Review.* Corrosion, 1984. **40**(11): p. 609-618.
2. Carré, C., et al., *Electrochemical calcareous deposition in seawater. A review.* Environmental Chemistry Letters, 2020. **18**(4): p. 1193-1208.
3. Yang, Y., J. Scantlebury, and E. Koroleva, *A Study of Calcareous Deposits on Cathodically Protected Mild Steel in Artificial Seawater.* Metals, 2015. **5**(1): p. 439-456.
4. Simoni, L., et al., *The influence of calcareous deposits on hydrogen uptake and embrittlement of API 5CT P110 steel.* Corrosion Science, 2017. **118**: p. 178-189.
5. Ma, H., et al., *Influence of iron oxides and calcareous deposits on the hydrogen permeation rate in X65 steel in a simulated groundwater.* International Journal of Hydrogen Energy, 2021. **46**(9): p. 6669-6679.
6. Ou, K.C. and J.K. Wu, *Effect of calcareous deposits formation on the hydrogen absorption of steel.* Materials chemistry and physics, 1997. **48**(1): p. 52-55.
7. Barchiche, C., et al., *Characterization of calcareous deposits in artificial seawater by impedance techniques: 3—Deposit of CaCO3 in the presence of Mg (II).* Electrochimica Acta, 2003. **48**(12): p. 1645-1654.
8. Xing, Y., et al., *Effect of surface calcareous deposits on hydrogen uptake of X80 steel under strong cathodic current.* International Journal of Hydrogen Energy, 2021. **46**(5): p. 4555-4566.

Evaluation of riser-to-platform isolation joints condition over group of gas platforms in the Adriatic Sea

Krešimir Kekez[1], Hrvoje Goreta[2], Zvonimir Štefanović[1]

[1] PA-EL, Dubrovčan 33b, Veliko Trgovišće, Croatia,

[2] INA-Industrija nafte, d.d., Avenija Većeslava Holjevca 10, Zagreb, Croatia;

Abstract

Isolation joints are an important part of a cathodically protected pipeline. Verification of the joints should therefore be a part of the periodic cathodic protection system service control. The purpose of the isolation joint is to prevent detrimental electro-chemical interaction and improve the effectiveness of the cathodic protection system. Isolating joints are also used to ensure effective current distribution for cathodic protection system. A group of gas platforms that are accommodated in Adriatic Sea is interconnected with subsea pipelines from which they are galvanically separated via monolithic isolation joint, installed above the water grade. The paper will present combination of few measurement techniques applied to confirm/disconfirm fitness for service of each tested joint as a mandatory requirement imposed by statutory bodies.

Keywords: cathodic protection, corrosion, gas platforms, subsea pipeline, isolating joint, fitness for service, safety certificate.

Cathodic protection of aluminium alloys in seawater

Ole Øystein Knudsen [1], *Jan Bertram* [2], *Andreas Momber* [2], *Jon Aaby Møretrø* [3], *Waldemar Krieger* [4]

1. SINTEF Industry, Richard Birkelandsvei 2B, N-7465 Trondheim, Norway
2. Muehlhan Ag, Schlinckstrasse 3, 21107 Hamburg, Germany
3. Hydro Aluminium ASA, 6601 Sunndalsøra, Norway
4. Speira GmbH, Aluminiumstraße 1, 41515 Grevenbroich, Germany

Background and motivation

Through an extended use of Al-alloys in subsea structures and equipment, the weight can be significantly reduced. The medium strength Al alloys in the 5000 and 6000 series possess the mechanical advantages of good strength to weight ratio, high corrosion resistance, and product variety. The limited engineering experience with Al alloys and its less noble electrochemical character compared to steel has led to misconceptions and skepticism regarding the use of Al subsea. Al has very different mechanical- and corrosion properties from steel, and Al constructions must be designed with this in mind. Design codes and standards for marine constructions are focused on steel and do not provide the necessary information about how to design with Al. CP design parameters for Al are based on experiences with thermally sprayed aluminium (TSA) and does not take alloy composition into account. The effect of coating on the design parameters and coating breakdown factors are unknown. Coating degradation mechanisms acting on coated Al with CP have not been described. Effect of surface pre-treatments (e.g. blast cleaning) and coating systems (generic types, thickness, etc.) on degradation are not known.

Objectives

The objective with this work was to investigate CP design criteria for aluminium in seawater, i.e. cathodic current density, and degradation mechanisms and rates for coatings on aluminium with CP.

Results

Within the 6000 series of alloys, the cathodic current density initially depended very much on the Cu content in the alloy. An alloy with 0.14 % Cu had a cathodic current density of 110 mA/m². However, the cathodic current density decreased with time, and after 200 days, it was less than 20 mA/m² for all the alloys tested. Probably, noble intermetallic particles had fallen out as previously described by Gundersen et al.[1]. There was still a correlation to Cu content, but the correlation coefficient was smaller, probably because the currents were smaller so that bias in the measurements had a larger relative effect. Among the 5000 alloys, only EN-AW 5083 was tested. However, this alloy deviated from the relationship between Cu content and cathodic current density found for the 6000 alloys. There probably is a similar relationship between Cu content and cathodic current density for 5000 alloys, but quantitatively different from the 6000 alloys. The cathodic current density was higher than the specified design current density recommended for Al in DNV RP-B-401 for several of the alloys tested, i.e. a non-conservative error.

The coatings tested have little or no degradation so far. Epoxy coatings between 50-300 µm were applied on EN-AW 6082 and EN-AW 5083, after various types of pre-treatments, both mechanical and chemical. Hence, coating breakdown factors to be used in CP design for coated aluminium should be small. Much thinner coatings can be used on aluminium, compared to steel.

Conclusions and significance of the work

- Cathodic current density on Al under cathodic protection depends on the alloy composition. The Cu content play a major role, but also other alloying elements.
- The current design codes for CP of aluminium are in many cases wrong and non-conservative
- Coatings on submerged aluminium are little susceptible to degradation and small coating breakdown factors can be used in the CP design. Even 50 µm thick coatings show good performance.

[1] R. Gundersen, K. Nisancioglu, Cathodic Protection of Aluminium in Seawater, CORROSION. 46 (1990) 279–285.

Dimensioning the cathodic protection of high-corroded metallic structure: the case of the in-situ conservation of metallic shipwrecks.

Marine Bayle[1], Justine Vernet[2], Clémentine Caubisens[1], Jean-Bernard Memet[1], Eddy Foy[2], Jean-Paul Gallien[2], Laurent Urios[3], Lila Reboul[4], Nathalie Huet[4], Philippe Dillmann[2], Florence Mercier[2].

[1]A-CORROS Expertise, Arles, France
[2]NIMBE-LAPA CEA Saclay-CNRS (UMR 3685), Gif-Sur-Yvette, France
[3]IPREM CNRS-UPPA (UMR 5254), Pau, France
[4]DRASSM Ministère de la Culture, Marseille, France

The protection of immersed metallic shipwrecks in seawater has been tested by cathodic protection (CP) with galvanic anodes on two shipwrecks: the ocean liner *le Liban* in Mediteranean Sea which was built in 1882 and sunk in 1913 and the ferry boat *HMS Daffodil* built in steel in 1917 and exploded on a mine in 1945 in the Manche.

The main issue is linked to the definition of the surface which must be protected. The shipwreck system is constituted of a network of several materials which can be or not conductive. The corrosion layers is also constituted of isolating and conductive corrosion products and a network of porosities.

The aim of the *Save Our Shipwrecks* (SOS) project is adapting the power supply for cathodic protection on the corrected surface that contribute to the metallic core protection considering the corrosion products contributions and transformations.

The developed methodology consists in linking the corrosion products chemical nature and electronical characteristics with their distribution and proportion in the corrosion layers. For that, SEM-EDX observations and elementary characterizations are coupled with structural global and local analysis by micro-Raman spectroscopy and X-ray diffraction. Moreover, their connectivity with the metallic substrate is tested by C-AFM measurements. These micrometric parameters are linked to the macroscopic behavior by performing potentiodynamic assays on corroded metallic parts sampled from the shipwreck and on simplified coupons left to corrode or protected, appended on the shipwrecks.

The obtained results allow to quantify the contribution of corrosion products and to determine the current range and its duration that should be applied in the beginning of the protection. The rate of current that must then be maintained to ensure sufficient protection of the metallic structure is being tested.

Effect of pressure, temperature and oxygen on the corrosion rate of carbon steel in natural seawater

E. Kassab, Federal University of Rio de Janeiro (UFRJ), Rio de Janeiro/Brazil; E. A. de Souza, Federal University of Rio de Janeiro (UFRJ), Rio de Janeiro/Brazil; J. R. Oliveira, Petrobras, Rio de Janeiro/Brazil, M. S. Rocha, Petrobras, Rio de Janeiro/Brazil, José A. C. Ponciano Gomes, Federal University of Rio de Janeiro (UFRJ), Rio de Janeiro/Brazil.

Carbon steels are widely used in the oil and gas industry due to the association of high mechanical properties and low cost. However, a major concern is the very aggressive marine environment and the low corrosion resistance of carbon steel in seawater. The corrosion of carbon steel in seawater is complex and influenced by many environmental parameters, such as seawater depth, temperature, dissolved oxygen, flow, presence of microorganisms, and pollutants [1]. These environmental parameters may also interact with each other. In this work, the corrosion behavior of carbon steel in natural seawater is investigated in laboratory and the effect of pressure and temperature on the corrosion rates is assessed. Gravimetric tests and conventional electrochemical tests were carried out in autoclaves with pressure ranging from 1 to 100 bar and temperature varying from 4 to 25 ^{o}C, in order to simulate the environmental conditions of three different depths: 0 m, 500 m and 1000 m. The dissolved oxygen content and water velocity were also controlled in the autoclaves and the tests had a duration of approximately 28 days. Flow effects were kept under controlled conditions supported by CFD analysis. The test setup used is shown in Figure 1 and the experimental procedure required was complex. Oxygen content was oscillating and controlled within the range 4 to 7 ppm The results showed that the corrosion rates of carbon steels are strongly influenced by the temperature, with higher corrosion rates measured at 25^{o}C. On the other hand, it was concluded that pressure exerts a minor influence on the corrosion rates of carbon steel in natural seawater.

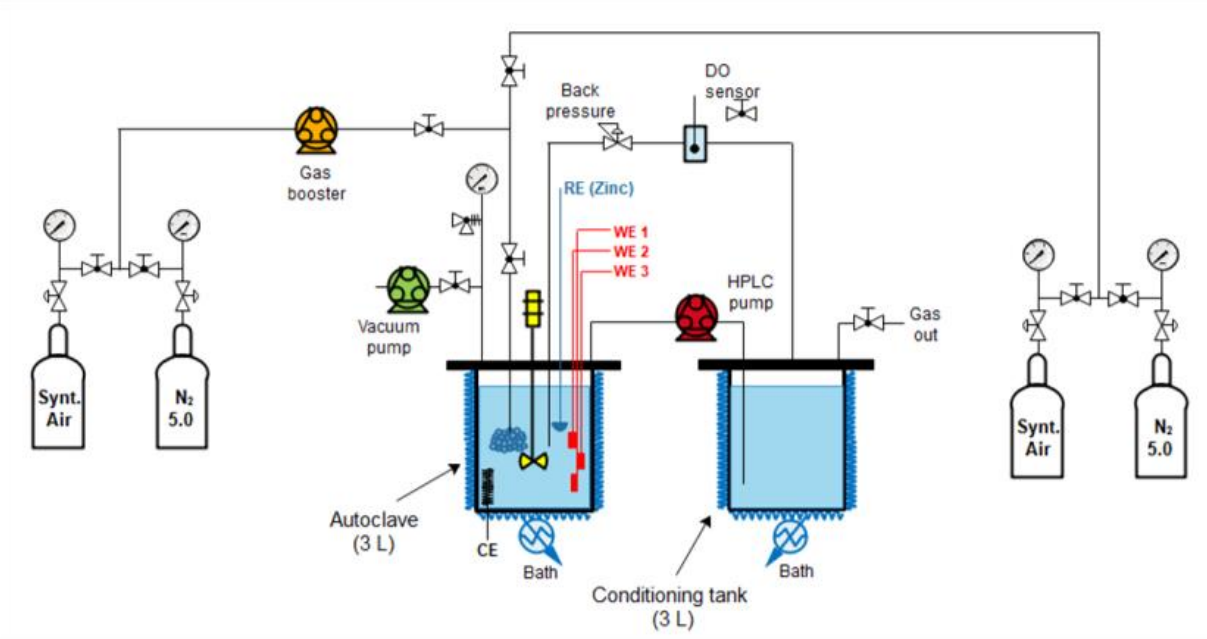

Figure 1. Test set-up of an autoclave.

References:

[1] Guedes Soares, C., Garbatov, Y., Zayed, A. (2011). Effect of environmental factors on steel plate corrosion under marine immersion conditions. Corros. Eng. Sci. Technol. 46(4), 524-541.

Influence of pre-treatments on the corrosion of bare and painted AA6082 aluminium alloys for marine applications

Carsten Blawert[1], Maria Serdechnova[1], Natalia Konchakova[1], Daniel Höche[1], Mikhail L. Zheludkevich[1], Jan Bertram[2], Andreas Momber[2], Ole Øystein Knudsen[3], Jon Aaby Møretrø[4]

[1] *Helmholtz-Zentrum Hereon, Geesthacht/Germany*

[2] *Muelhan AG, Hamburg/Germany*

[3] *SINTEF, Trondheim/Norway*

[4] *Norsk Hydro ASA, Sunndalsøra/Norway*

Aluminium parts for automotive, architecture and aerospace, are typically coated in production lines with chemical pre-treatment and automated paint application or powder coating. In many marine applications under atmospheric and splash zone exposure, no protective coatings will be required for aluminium from the corrosion point of view. However, due to other requirements, e.g. signal colours or uniform appearance, coatings are still applied and should have a high durability. As a consequence, in marine constructions aluminium will often have to be coated under harsher, less controlled conditions in a similar manner to the rest of the construction, i.e. by blast cleaning and spray coating. Such pretreatments can have adverse effects on the corrosion resistance of the substrate due to severe mechanical deformation or transfer of contaminations from the blasting material. The current standard blasting process is using garnet, which is not the most environmentally benign process, as the garnet needs to be disposed after use. Thus the motivation is quite high to identify alternative pretreatment processes with similar or better performance.

In the current work different environmental-friendly surface preparation methods including mechanical blasting (garnet, glass grid and hybrid-blasting (dry-ice + garnet), and alternative repair treatments (rotating corund disc, stainless steel brush and bristle blaster) for use during coating maintenance are applied and the effects on the surface morphology and composition are studied. Iron content and other remains of the blasting and tool materials on the treated surfaces are determined and the influence on the paint adhesion (1 layer Jotamastic, 200 µm) is studied. Additionally, the corrosion properties of the bare alloy surfaces after the pre-treatments will be studied as well as the applied protective coating performance with applied artificial defects in different accelerated laboratory corrosion tests like VDA cyclic climate test 621-415

(DIN EN ISO 11997-1:2006 Zyklus B) with artificial seawater or filiform corrosion test (modified ISO 4623–2). The corrosion performance will be related to the different surface conditions obtained by the different surface pre-treatments and compared to the standard garnet treatment. Options to replace garnet and the performance of possible repair techniques for coated AA6082 will be critically discussed.

Acknowledgment: research project MARINAL, BMWK (MarTERA, Bundesministerium für Wirtschaft und Klimaschutz, under grant 03SX552(b)).

Enhancing the protective performance of polyaniline-induced oxide layer on Al substrate by organic coatings: A strategy for corrosion protection of Al alloys in marine environments

Fandi MENG, Li LIU, Yu CUI, Rui LIU, Fuhui WANG, Northeastern University, Shenyang, 110819, China PR

The application of aluminum alloys in marine environments has been limited since the aggressive seawater and Cl^- often induce serious pitting corrosion on Al alloys. It is widely believed that polyaniline (PANI) can lead to the formation of a protective oxide layer on Al surface due to its passivation ability, and organic coatings with PANI have also been confirmed to have this function. In this work, the growth kinetics of PANI-induced oxide layer beneath marine coatings was tried to established, considering a dense nanocrystalline mixed oxide film was observed between Al alloy and coating. Therefore, a denser and thicker oxide film can be formed based on the calculations of growth kinetics.

Furthermore, to enhance the performance of PANI-induced oxide layer, a zirconium-porphyrin-based organic framework was used as coating fillers. The conductivity and redox capacity of PANI canbe controlled, resulting in a faster growth rate of mixed oxide film. Finally, the good protective performance has benefited from the role of mixed oxide film and organic coating, providing a strategy for long-term protection of Al alloy in marine environments.

Post Corrosion Effects of WC-12%Co - AMDRY 995M/9954 Multi Layered Coatings Used for Marine Applications

***Sultan Mutairi*, Research Center, Saudi Arabia, samotairi9@gmail.com**

***Nayif Rasheedi*, Research Center, Saudi Arabia, Rashna0c@gmail.com**

Keywords: Marine, Corrosion, Micro-sized, Nano-sized, AMDRY.

The work focused on producing coating materials that provides superior mechanical properties. It aimed to identify a single thermal spray method and coating combination capable of producing a multi-layer coating by blending micro and nano tungsten carbide cobalt powders with AMDRY powders deposited by the HVOF and Plasma spray equipment onto carbon steel substrates. This research addresses issues in platforms and marine materials such as material degradation and post corrosion effects. Many techniques were used for assessing the produced coating performance. The results showed enhanced corrosion protective from powder combinations.

Galvanic Anode systems in Concrete structures and their performance part 1

Gino Ebell, Bundesanstalt für Materialforschung und -prüfung (BAM)

Corrosion of reinforcement is one of the major reasons in questioning the sturdiness of building structures. The application of cathodic protection techniques plays a big role in controlling the corrosion process to ensure a longer service life of building structures. This systematic study compares the efficiency and durability of various discrete galvanic zinc anode systems available in the current market using different criteria for measuring efficiencies such as potential measurements, electrolyte resistance measurements and several polarization methods to determine the polarizability of the anodes. Results to validate the performance of long-time exposure of discrete zinc anodes in the concrete medium are already shown in 2021. Now the results of analyzing the phase boundary between mortar and anodes by using 3D computer tomography are shown, as also the field application at large-scale specimens where the potential distribution and the current were investigated.

Keywords: cathodic protection, galvanic anodes, concrete, durability

Interference effect of a bridge concrete foundation structure on buried pipeline

Christophe Baeté[1], [1]Elsyca NV, Wijgmaal/Belgium

CP is an effective method for protecting coating defects on buried pipelines if sufficient current reaches the pipeline surface. In the presence of nearby foundations structures shielding effects may jeopardize the effectiveness of CP and coating surveys.

A case is discussed of a 57 km long 30 inch 3L-PE coated high pressure natural pipeline section with very low CP current demand. Halfway the trajectory a new 420 m long motorway bridge structure is built above the pipeline. In total 498 reinforced concrete foundation piles are aligned along the pipeline causing a potential risk of shielding the low cathodic current. In addition, the pipeline is connected to the bridge structure by an anchoring system for stabilization purposes during settlement of the bridge structure after construction. The anchor positions are susceptible locations where significant coating damage may occur on the short or longer term. The reliability of DCVG survey was therefor questioned as well.

The degree of shielding effect was validated with FEM based computer modeling. The protection level of the pipeline and the DCVG sensitivity was computed for various scenarios. Modeling visualizes the CP current path to the pipeline and through the foundation piles. A local CP design was elaborated for anticipating on the possible coating damages in the future.

Using electroactive bacteria naturally present in marine sediment as a current source for the cathodic prevention of reinforced concrete structures in marine environments

Julie DUBUIT, CORROHM/LMDC-INSA Toulouse/ LGC- INP Labège, Toulouse France; Stéphane LAURENS, LMDC-INSA Toulouse, Toulouse/France; Alexandra BERTRON , LMDC-INSA Toulouse, Toulouse/France; Benjamin ERABLE, LGC-INP Labège/CNRS, Labège/France; David GARCIA, CORROHM, Labège France; Fabrice DEBY, LMDC-INSA Toulouse, Toulouse/France; Luc ETCHEVERRY, LGC-INP Labège/CNRS, Labège/France

In recent years, developing innovative, more efficient, and sustainable anticorrosion approaches has become an environmental challenge. In marine environments, the tidal zone represents the most at-risk area regarding premature corrosion initiation. To address corrosion in reinforced concrete structures, Cathodic Protection and Cathodic Prevention (CP) are today the main solutions implemented. However, the existing CP solutions have significant drawbacks in terms of sustainability more so in marine environments where the ions released by the oxidation of sacrificial anodes can be harmful for marine ecosystems.

This research work explores a new biological technology for the cathodic prevention of reinforced concrete structures in marine environments, labelled BioGalvanic Cathodic Prevention (BGCP). This innovative concept involves a Benthic Microbial Fuel Cell (BMFC) in which the cathode is the steel structure to be protected. The BMFC's anode is buried in marine sediments, where electrons are supplied through the oxidation of various substrates by electro-active microorganisms. BGCP offers three fundamental advantages: autonomous operation (the oxidized organic matter is constantly renewed), a green solution (no environmental impact), and a free current supply. Applying BGCP for the cathodic prevention of semi-immersed structures would thus prevent corrosion initiation without the drawbacks from using sacrificial anodes.

To validate the concept of BGCP, a full scale experimental reinforced concrete element was built replicating the exposure conditions of a pier, semi-immersed in seawater and funded in marine sediments. Steel segments were distributed along the height of the pier. A bioanode was embedded in the sediment layer and connected to the steel segments after activation by electroactive micro-organisms. The current distribution was measured along the height of the pier from the Biogalvanic system, embedded in the sediments. The potential of the different segments was also measured as well as their depolarization to evaluate the

performance of the cathodic prevention system according to the standards. A numerical twin of the experimental specimen was built on the COMSOL Multiphysics® software. Both experimental and numerical results validated the efficiency of the BGCP system in the areas at risk regarding corrosion initiation. In fact, the cathodic prevention of the reinforced concrete element semi immersed in marine sediment was ensured in the tidal zone where the current densities received complied with the European Standard ISO 12696 for they were higher than the lower recommended cathodic prevention bound (-0.2 mA/m^2). The objective is now to extend the application of BGCP for the cathodic protection of formerly built RC structures already undergoing corrosion.

Non-uniform distribution of polarization currents and electric field in reinforced concrete during electrochemical maintenance techniques.

Abdel Razzak EL ZOHBY, Stéphane LAURENS, Raphaëlle POUHET, Laurie LACARRIÈRE, Toulouse University - INSA/UPS civil engineering, Laboratoire Matériaux et Durabilité des Constructions (LMDC), Toulouse/France

Cathodic protection and other electrochemical maintenance techniques, which have become increasingly used in recent years, have proven to be reliable methods for preventing steel corrosion in reinforced concrete. Regardless of the electrochemical technique used, their main concept is to apply a current to the steel reinforcement (through an external anode system) and, thus, to subject the concrete to a stationary electric field. However, when addressing these types of techniques, both literature recommendations and technical implementations focus mainly on the average current density per square meter of steel, while disregarding and unquestioning its non-uniform distribution. This physical problem may lead to significant local electric field values that may cause changes in the cement matrix and the interstitial solution (electrolyte). This non-uniform current distribution and the induced material changes strongly affect the protection level. Therefore, it is important to highlight the latter outcomes and, thus, to consider the 3D character of the physical problem.

In the proposed approach, the main aim consists of studying the spatial distribution of the applied polarization currents and the current concentration zones, which result in high local values of the electric field. In order to apprehend this phenomenon in a relevant way, a 3D simulation campaign based on realistic geometrical shapes (reinforced concrete column and beam) is launched. In this context, different scenarios are simulated using the finite element software Comsol Multiphysics by varying the different parameters (geometry, reinforcement rate, anode type, current density, resistivity, etc…), investigating the effects of the latter's variations.

A realistic range of electric field intensities is then evaluated, and it is noted that this physical quantity can reach in some areas values higher than 1kV/m, although the

overall applied intensity remains moderate (< 1-2 A). Thus, it can be conclusive that the application method of the polarization currents and the geometry of the current lines (depending on the geometry of the anode/concrete/steel system) have a significant effect, perhaps the most profound, in the electrochemical maintenance.

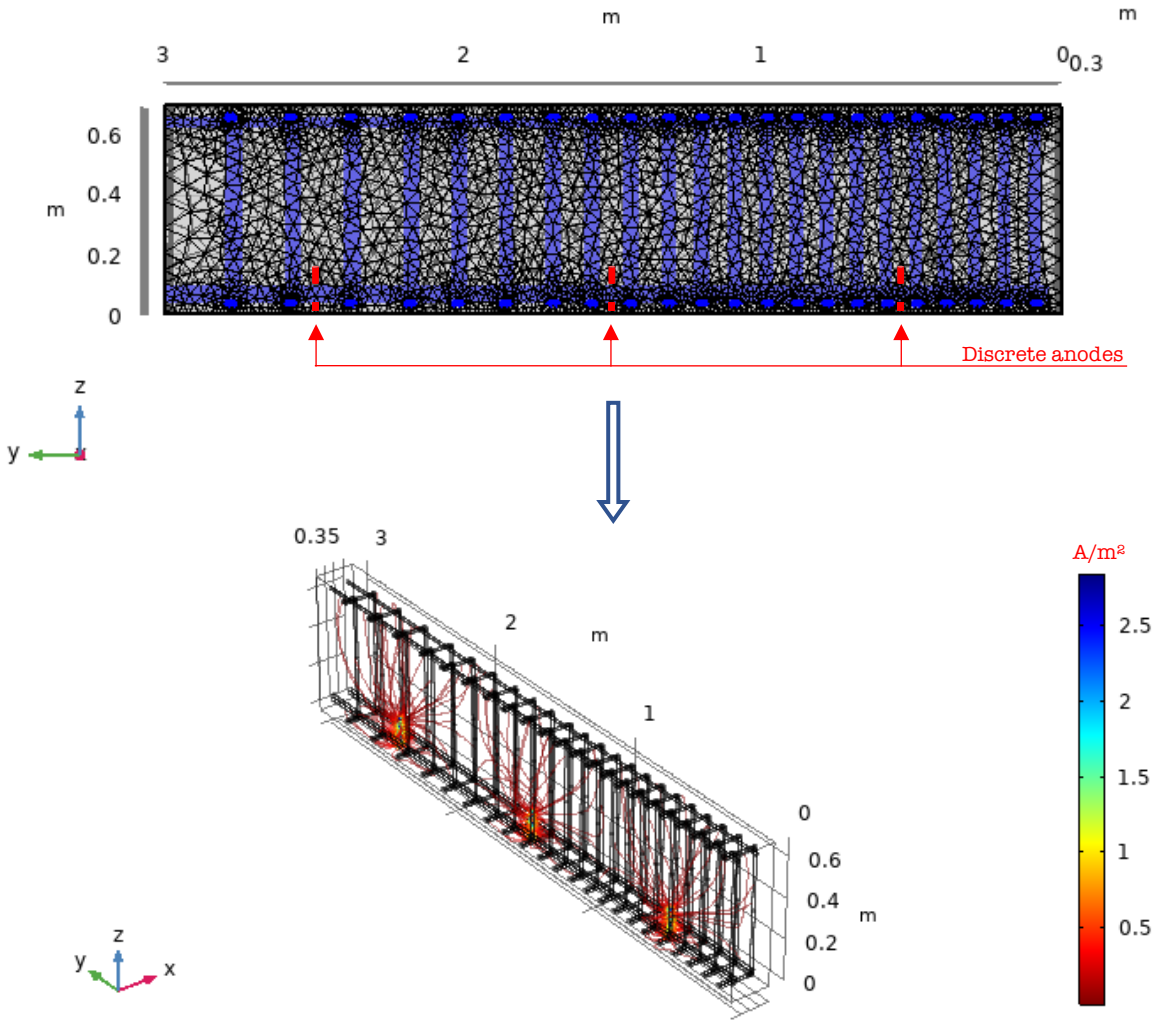

Figure 1 : Geometrical model (1/4 of the beam - symmetry plane (x,z) at y=3m and (y,z) at x=0.35m), meshing and current density distribution.

Coating characterization using hyperspectral imaging technology in near Infrared range

Thomas De Kerf[1], *Zohreh Zahiri*[1], *Simon Verspeek*[1], *Steve Vanlanduit*[1], *Paul Scheunders*[1]
University of Antwerp, Belgium

Coating inspection is a critical task for many industries, as it helps to ensure the performance and longevity of structures. Despite extensive research on coatings, developing accurate and reliable methods for monitoring and analyzing coating condition remains a significant challenge. Hyperspectral imaging (HSI) is a non-destructive imaging technique that has been increasingly used in various fields such as aerospace, automotive, and chemical industries, to inspect the condition of coatings. This technique can provide detailed information about the chemical composition and thickness of coatings, which can be used to identify and quantify the presence of defects or degradation.

The degradation or changes in coating properties may not be immediately apparent with the naked eye. Additionally, traditional quality control methods used for coatings have limitations, including being destructive, time-consuming, only able to be applied to specific points, or requiring direct contact with the surface. A non-destructive, automated monitoring technique that can easily detect changes in coating properties and degradation without causing harm to the coating would be highly beneficial.

In recent years, imaging techniques together with Artificial Intelligent (AI) has obtained substantial attention in many different applications. The imaging techniques are fast, easy, and can be used from different platforms such as drones to take images from the remote or difficult to access areas. However, mentioned above not all coating properties or defects can be seen within the visible range or with RGB (red-green-blue) imaging. In contrast to the RGB images with only 3 wavelengths, hyperspectral images have multiple readings for each pixel by measuring of electromagnetic radiation at more than 100 continuous wavelengths. This results in obtaining a curve so-called “spectrum” for each pixel which changes with respect to the chemical and mineral properties of the material in that pixel. Hence, hyperspectral imaging has been used as a non-destructive non-contact method for identification and characterization of materials in various industries from agriculture to food and heritage monitoring.

In this paper, we investigated the potential of hyperspectral imaging in Near Infrared range for coating characterization. We performed hyperspectral imaging on several case studies from different applications. The coating samples were scanned in the laboratory with an FX17 Specim camera (spectral range of 900-1700nm) and applied different image analysis algorithms (depending on the application) to detect the problems. In Table 1, we summarized the conclusions which were drawn from our observations.

Table1. Potentials of hyperspectral imaging in coating and corrosion characterization

Material	Application	Results
Organic coating	Degradation after corrosion accelerating test	Good
	Curing of water-based coating	Good
	Detecting small coating anomalies (dents, scratches, etc.)	Poor
	Detecting substrate material under coating (average thickness of coating 80µm)	Good
	Differentiating coating thickness (up to 60µm)	Good
	Drying of the coating	Good
	Coating mixtures	Good
	Coating blistering	Poor
Metallic coating	Detecting the change in phosphor content in NiP coating	Good
	Ni coating thickness evaluation (up to 20µm)	Good
	Detecting substrate material under identical NiP coating (coating thickness of 5 µm)	Good
	Quality control of Ni coating on the baskets of PU guns	Good
Powder coating	Curing of powder coating under different temperatures	Fair
	Detecting coating defects such as gassing/ dents/scratches	Poor

In conclusion, this research demonstrates that HSI is a powerful tool for coating inspection that can provide valuable information about the condition of coatings and the progression of corrosion. We propose that HSI has the potential to be widely adopted as a standard method of coating inspection in various industries.

Analysis of internal stresses in organic coatings using digital volume correlation

Kaivalya Borwankar[1], Niek Hijnen[2], Seyedgholamreza Emad[1], Elizabeth Evans[3], Stuart Lyon[1], Xiaorong Zhou[1], Tim L. Burnett[1]

[1]Corrosion and Protection Centre, Department of Materials, The University of Manchester, Oxford Road, Manchester, M13 9PL, U.K.

[2]AkzoNobel, Stoneygate Lane, Felling, Gateshead, U.K.

[3]National X-ray Computed Tomography, Royce Hub Building, The University of Manchester, Oxford Road, Manchester, M13 9PL, U.K.

Subtopic: Coatings

Organic coatings are applied on metallic surface to protect them from corrosion due to exposure to environment. During application on the surface of metals, these coatings undergo shrinkage which can be influenced by the amount of solvent mixed with the paint as well as the paint viscosity. It is believed that paint films undergo shrinkage in direction perpendicular to the paint-environment interface, however the total distribution of internal stresses within the paint film is less understood. Such stresses, if significant, can result in mechanical or environmentally influenced failure in some areas of the coating over others. In this project, we aim to monitor changes in a model epoxy-amine coating system pigmented with barium sulphate filler, at different stages of curing using microscale X-ray computed tomography. The positions of filler particles in the paint are observed at different time intervals and based on the changes in their position, we then use Digital Volume Correlation (DVC) to calculate full-field strains across the 3-dimensional paint network. A map of internal strains can thus be obtained, which can further help understand key microstructural features which can make coatings susceptible to failure.

Relating polymer architecture to water absorption properties in a model waterborne coating

Riccardo Biella[1], Chintankumar Patel[2], Patrick Keil[3], Santiago J. Garcia[1,]*

[1] *Aerospace Structures and Materials Department, Faculty of Aerospace Engineering, Delft University of Technology, 2629HS, Delft, The Netherlands; S.J.GarciaEspallargas@tudelft.nl*

[2] *BASF SE, Carl-Bosch-Strasse 38, 67056 Ludwigshafen am Rhein, Germany*

[3] *BASF Coatings GmbH, Glasuritstrasse 1, 48165 Münster, Germany*

Waterborne polymers show limited emission of harmful volatile organic compounds in anticorrosion coatings. However, current waterborne coatings lack the overall properties necessary for high performance applications. One of the limitations for further improvements is the limited fundamental understanding on the relationships between polymer film heterogeneous architecture, chemical composition and critical performance parameters such as water uptake, adhesion and mechanical properties.

In this work the focus was on establishing a relationship between the the polymer architeccture and the water absorption properties. Polymer architecture was controlled by varying colloid particle size and interparticle cohesion through annealing. Rheology and Positron Annihilation Spectroscopy (PAS) were used to describe the polymer architecture and heterogeneity concentration. Gravimetric measurements were employed to study the water absorption properties and DSC and TGA gave information about polymer properties.

Data obtained from rheology was analysed by deconvoluting the continuous relaxation spectrum. This allowed identifying the individual relaxation mechanisms related to the polymer film architecture: chain relaxation, terminal flow and a third and fourth intermediate relaxation. These last ones were attributed to the contribution of chemical and physical heterogeneities between the particles and the interparticle interdiffusion phase created during the drying process. PAS on the other hand allowed probing the physical structure of the material by studying its defect density and free volume as function of the particle size. Correlation of the obtained data with architectural parameters (relaxation times, S parameter from PAS) and the water absorption properties and polymeric dispersion parameters (e.g. particle size) will be presented.

Water uptake and corrosion protection efficacy of epoxy based composite coatings

*S. S. Ananthapadmanabhan [1], Smrutiranjan Parida[1]**

[1]Indian Institute of Technology Bombay, Mumbai- 400076, India

*Email: 194116008@iitb.ac.in, *paridasm@iitb.ac.in*

Organic coatings on metal substrates serve largely as a corrosion and oxidation barrier. In addition to wet adhesion, water absorption is a crucial factor in determining the endurance of organic coatings. This study assessed the water uptake and corrosion protection efficacy (CPE) of an epoxy-based composite coating. The epoxy composite coating with ethanol treated hollow spheres (THS) (5, 10, 15, and 20 wt%) and nano metal oxide (NM) (3, 5, and 10 wt%) was immersed in 3.5 wt% NaCl solution, and water uptake was calculated using coating capacitance obtained from electrochemical impedance spectroscopy (EIS) analysis using the Basher-Kingsbury equation. The results demonstrated that an epoxy coating containing only THS has greater water uptake (~0.11 @ 20 wt% THS loading) than a bare epoxy coating (~0.077) and that the water uptake increases as the THS loading increases. The composite coating containing THS and NM shows reduced water uptake (~0.029) than bare epoxy and the coating having solely THS. The corrosion protection efficacy (CPE) of the coatings was assessed using an ASTM B117 salt spray test. The THS and NM-containing epoxy coatings are more corrosion resistant (CPE ~89%) than bare epoxy coatings (CPE~49%). The corrosion resistance of the coating only with THS decreases primarily because compact packing is not possible due to the high particle size of the filler, and the empty spaces between them enable the flow of corrosive fluids. The fundamental goal of THS integration is to offer thermal insulation properties to the coating, which can be employed in roofing sheets, external surface constructions, pipelines, and other applications. THS's detrimental influence on corrosion has been mitigated by adding NM into the coating. The presence of NM with smaller particle size seals the gaps between larger THS particles and lowers permeability, creating a tortuous path for corrosive media to penetrate the coating and cause corrosion in the metal substrate, and therefore improves corrosion protection efficacy.

KEYWORDS: *Epoxy, water uptake, EIS, salt spray, protection efficacy*

Glass Transition Temperature of Epoxy Coatings & Their Protective Performance

Muhammad Ahsan Bashir, Vivian Beate Farstad, Performance Coatings, Jotun AS, Sandefjord, Norway.

Glass transition temperature (T_g) of commercial epoxy-amine coatings is an important thermophysical property. There is a lack of open literature showing the important link between protective performance of epoxy coatings & their Tgs. Therefore, we selected 3 commercial epoxy-amine coatings with varying Tgs and tested them in water at different temperatures. The selected water-immersion temperatures (i.e., 40 ◦C & 60 ◦C) were above the T_g of 2 coatings and below the Tg of one commercial coating. In addition to water immersion, sprayed panels of the same coatings were also tested by immersing them in diesel marine oil.

Temperature-Modulated DSC (MDSC), Dynamic Mechanical Analyzer (DMA), & Fourier Transform Infrared (FTIR) Spectroscopy were used to characterize the samples before and after immersion at different time intervals and temperatures.

The obtained results clearly showed that the coating with T_g lower than the immersion temperature of water or diesel marine oil will fail earlier than the coating with a T_g higher than the immersion temperature, as shown in **Figure-1**. The most probable reason for this observation is that the rate (and extent) of ingress of water or diesel marine oil in low T_g coatings will be higher than their respective rate (or extent) in high T_g coatings. Due to differences in the solubility of water and diesel marine oil in the epoxy coatings, one may see differences in the time-to-failure of the coatings. MDSC & DMA results confirmed significant depression in the T_g of the low T_g coating upon immersion while no or insignificant depression in T_g was observed for the high T_g coatings. FTIR results showed that chemical changes might occur in epoxy coatings upon immersion in water at mild temperatures of 40 ◦C to 60 ◦C. A combination of depression in T_g and chemical changes in the polymer network explains the early loss of protective properties of the low T_g epoxy coatings.

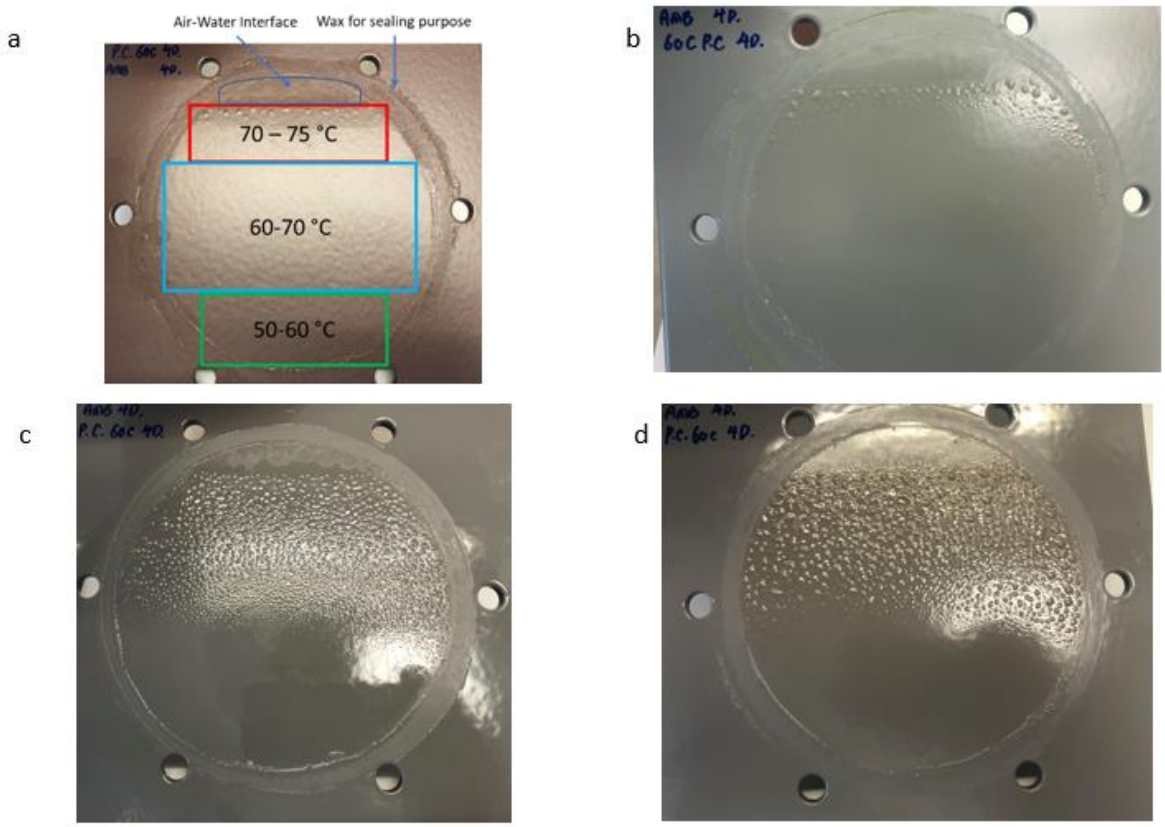

Figure 1. Condition of coated panels after 15 days of immersion in water at 65°C.(a,b) High T_g coatings. (c,d) Low T_g coatings.

Thermal aging and degradation of epoxy coatings at oxidized interfaces

Naomi Farrer, Stuart Lyon, Suzanne Morsch, University of Manchester, UK

Doug Beaumont, Will Edwards, AkzoNobel

Corrosion under insulation (CUI) is a large concern for the petrochemical industry, causing huge costs in both pipe maintenance, and replacement due to damage. To mitigate the risk of CUI, protective coatings are applied to pipes. However, these coatings must be able to withstand various demanding operating conditions, including cycling temperatures, humidity and corrosive leaching from the insulation and plant environment. This research examines the influence of temperature, humidity and pigments on the chemical stability of epoxy-based coatings and their influence on corrosion protection. Insights into the changes in chemistry and physical behaviour of the coating have been determined using various techniques particularly atomic force microscopy infrared spectroscopy (AFM-IR). This technique has allowed for nanoscale differences in polymer chemistry to be investigated within the coating and chemical mapping images to be produced for the degradation of the polymer.

Effect of pigment on the degradation of naturally weathered organic coil coating

D. Persson, RISE Sweden; A. Wärnheim RISE, Sweden; G. Heydari SSAB Sweden; V.Saarimaa Top Analytica, Finland; T.Laihinen Top Analytica, Finland; P. E. Sundell, SSAB, Sweden.

The resistance to degradation of coil coatings is crucial for their lifetime in aggressive atmospheric environments, where the coatings usually are subjected to combined moisture and photo-induced degradation. The weathering-induced degradation of the organic polymer coating is often assessed by accelerated laboratory testing and outdoor field exposures and evaluated by measuring gloss retention and color changes. However, the chemical changes on the micro and nanoscale induced by the degradation processes may alter mechanical and barrier properties of the coating substantially both globally and locally, and may lead to paint delamination, blistering and initiation of corrosion attacks on the substrate. To understand the degradation processes it is important to characterize chemical and physical alterations of coil coatings with techniques which provides information with high lateral and depth resolution.

In this study was a series of polyester melamine coil coatings with different pigment systems naturally weathered after being exposed in a marine atmosphere at Bohus-Malmön at the Swedish west coast for 6 years. Surface and depth resolved analysis of the degradation was performed using FTIR-ATR focal plane array imaging, FTIR-PAS, SEM-EDS / BIB cross sections, AFM and nanoscale AFM-IR. High resolution spectroscopical and imaging techniques, such as FTIR-FPA imaging, SEM/SEM-EDS, AFM and AFM-IR provided information on the degradation process with microscopic and nanoscale lateral resolution. The results show that the degradation effects on the surface and in depth varied considerably between coatings with different colors and pigment systems. It was found that the coating surface morphology, surface chemistry, and chemistry after weathering, was affected by the type, color and concentration of the pigments included in the coating formulation.

Development of water-based paint combining anti-dirt and anti-corrosion properties

A.-P. Romano[1], T. Senechal[1], J. Duchenne[2], P. Merle[3], I. Meziani[4], M. Poelman[1].

[1] Materia Nova Research Center,3, Avenue N. Copernic, Parc Initialis, 7000 Mons, Belgium

[2] RD Coatings- Dothée SA, Rue Ernest Matage, 19, 5330 Assesse, Belgium

[3] Berthier Etude, 990 Chemin de Sauvecanne, 13320 Bouc-Bel-Air, France

[4] SNCF réseau,92, Avenue de France, 75013 Paris 13France

This study is carried out in the frame of a EUROSTARS project “AMPERE” which aims at developing a unique coating system combining an innovative paint and a robotized application system for the maintenance of catenary for railway. The paint system would combine both anti-dirt and anti-corrosion properties in a single layer. The formulation is water-based, does not contain any toxic compound and is able to be applied and dried on site. The selected paint formulation is based on a recently developed, highly durable paint from DOTHEE which currently satisfies the requirements in terms of corrosion and UV-resistance.

In order to obtain an anti-dirt coating, the paint formulation was modified by substitution of a part of the paint by specifics additives. Different types of anti-dirt additives were selected such as commercials additives, additives based on the PDM’s chemistry, modified fillers, modified clays, hydrophobic resin, sol-gel.

The modified and reference paint formulations were applied on steel samples. The mechanicals coating properties were evaluated in terms of visual aspect, thickness, adhesion, and flexibility. The anti-dirt properties prevent the adhesion of compounds or particles. The surface of an anti-dirt coating must be hydrophobic. This property is evaluated by measuring the water contact angle, surface energy and sliding angle. The characterization is carried out by a carbon black test. The corrosion protection was evaluated by EIS on intact samples and by normalized salt spray test on scratched samples (Class C3). The objective of this project is therefore to find the best compromise between anti-dirt properties and durability (corrosion protection mainly).

The Degradation Mechanism of Polyester Powder Coatings Exposed to Cyclic Corrosion Testing (CCT)

Lawrence Coghlan[a], Seyedgholamreza Emad[a], Tim Burnett*[a], Xiaorong Zhou[a], Stuart Lyon[a], Gianfranco D'Ambrosio[b], Niek Hijnen[c]

[a] School of Materials, The University of Manchester, Manchester, M13 9PL, UK

[b] AkzoNobel Coatings S.p.A., Como, Italy

[c] AkzoNobel, Stoneygate Lane, Felling, Gateshead, NE10 0JY, England, UK

Crack initiation and propagation within coatings has been identified as one of the main causes for significant deterioration of organic coatings. This can lead to failure of the coating and even the complete delamination. The exposure of the coatings to the environment is widely known to reduce the coatings impedance over time, a clear sign of coating degradation [1,2]. However, this measurement gives quite a general result and does not give any insight into how the corrosion processes are taking place at a microstructural level.

Any changes to the chemical nature, average particle size and the crystal form of the fillers within the coating will affect the corrosion resistance of the coating [3], highlighting the complex interactions taking place when a coating system is exposed to the environment. The condition, composition and structure of the coating will develop during exposure to the environment and these changes can lead to defects forming, for example within the pigments, the polymer, or at the interfaces between pigment/polymer/substrate. With continued exposure these defects can transition into cracking, with the propagation of these cracks being influenced by the coating microstructure. With continued exposure these defects and cracks can lead to the failure of the coating system.

To better understand the mechanism of crack initiation and subsequent degradation of coatings, powder coated samples have been exposed to cyclic corrosion testing experiments of various lengths to characterize the formation and subsequent development of defects within the coating. These defects, and how they develop into cracks, will be linked with microstructural features within the coating and the substrate surface to better understand the mechanism of initiation and propagation.

[1] C. Le Pen, C. Lacabanne, N. Pébère, Structure of waterborne coatings by electrochemical impedance spectroscopy and a thermostimulated current method: influence of fillers, Progress in Organic Coatings, 39 (2000) 167-175.
[2] D. Wang, E. Sikora, B. Shaw, A study of the effects of filler particles on the degradation mechanisms of powder epoxy novolac coating systems under corrosion and erosion, Progress in Organic Coatings, 121 (2018) 97-104.
[3] V. Gots, O. Lastivka, O. Berdnyk, O. Tomin, P. Shilyuk, Corrosion Resistance of Polyester Powder Coatings Using Fillers of Various Chemical Nature, Key Engineering Materials, 864 (2020) 115-121.

Ageing of 3LPE coating during outdoor storage: providing sound operational answers to pipeline operators

Alexandre Perrot[1], Dominique Gueugnaut[2], Ahmed Fakhry[3], Xavier Campaignolle[4], Eric Parizot[5], Thierry Kerzerho[6]

[1] GRTgaz, Research & Innovation Center for Energy (RICE), Villeneuve-la-Garenne/France, alexandre.perrot@GRTgaz.com
[2] GRTgaz, Research & Innovation Center for Energy (RICE), Villeneuve-la-Garenne/France, dominique.gueugnaut@GRTgaz.com
[3] GRTgaz, Research & Innovation Center for Energy (RICE), Villeneuve-la-Garenne/France, ahmed.fakhry@grtgaz.com
[4] Storengy, Bois Colombes/France, xavier.campaignolle@storengy.com
[5] GRTgaz, Technical Department, Compiègne/France, eric.parizot@grtgaz.com
[6] GRTgaz, Technical Department, Compiègne/France, thierry.kerzerho@grtgaz.com

Abstract: GRTgaz operates a network of gas transportation pipelines of 32 000 km protected against corrosion by cathodic protection and a variety of passive organic coatings, preventing oxidants (O_2, CO_2, H_2O) mass transfer to the metal surface. Among these coatings the 3-layered polyethylene coatings (3LPE) are applied on a significant and growing part of the network since the mid 90's. The study of its ageing is thus of foremost importance for GRTgaz and most European pipeline operators.

Prior to their operational life, 3LPE coated pipes can be stored outdoor for an extended amount of time during which various ageing phenomena take place, including antioxidants loss, photo and thermo-oxidation and cracking of the external polyethylene layer leading to an increased mass transfer and susceptibility to stress cracking. Thus, there is a maximum storage time before which polyethylene weathering induces irreversible damages to the coating, detrimental to its operational functionality. In order to validate sound operational practices, RICE aims at modelling the antioxidants loss in both laboratory and natural conditions at the storage facility of Châteauroux (Figure 1).

Figure 1: Artificial (left) and natural (right) ageing of polyethylene used in this study.

The behaviour law could be then extrapolated to various storage sites with the knowledge of their environmental conditions. In the meantime, chemical modification and microcracking of polyethylene will be followed using FTIR and optical microscopy.

Keywords: OIT; polyethylene; modelization; storage; 3LPE.

Introduction

GRTgaz is a French Transmission System Operator (TSO) operating a network of gas pipelines of 32 000 km protected against corrosion by cathodic protection and a variety of passive organic coatings, preventing oxidants (O_2, CO_2, H_2O) mass transfer to the metal surface. Among these coatings the 3-Layered PolyEthylene (**3LPE**) are applied on a significant and growing part of the network since the mid 90's. The study of its ageing is thus of foremost importance for GRTgaz. They are composed of an epoxy primer, an adhesive layer, and a 2 to 5 mm thick Polyethylene Topcoat (Figure 2).

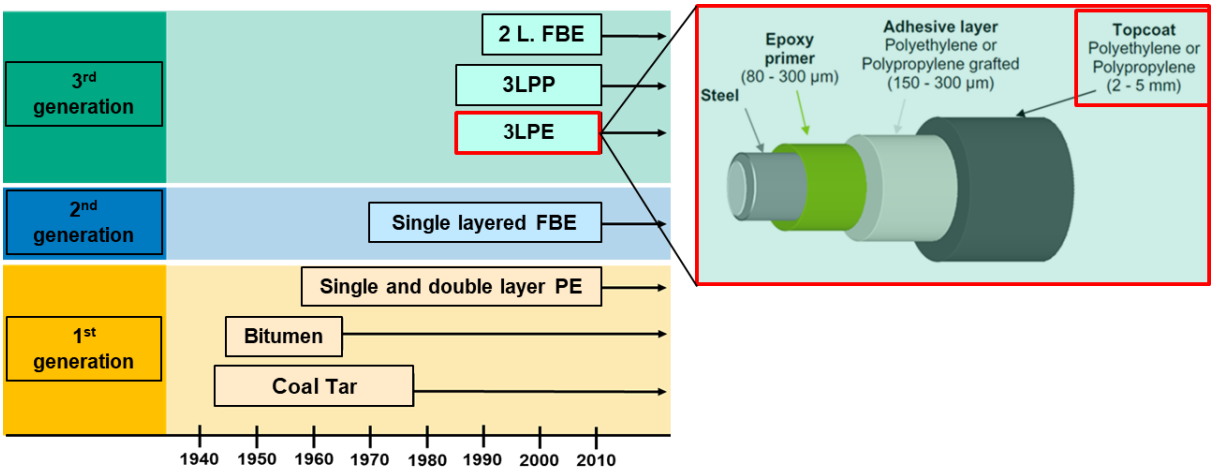

Figure 2 : Evolution of line pipe coating systems in use in France (left) and composition of 3LPE coatings (right).

Due to its thickness and chemical nature, PolyEthylene (**PE**) topcoat is assumed to be the kinetic limiting step in the functionality loss of 3LPE coating systems. In this study, we thus followed the ageing of the two most common PE systems in GRTgaz 3LPE coatings, hereafter named **PE#1** and **PE#2**. Prior to their operational underground life, 3LPE coated pipes can be stored outdoor for an extended amount of time (up to several years). GRTgaz use a single outdoor storage facility located in the French city of Châteauroux[1] (Figure 3).

Figure 3: General view of the Chateauroux storage facility (left), 3LPE coated pipes in storage configuration (right).

During outdoor storage various thermo and photo-activated chemical and physical phenomena affect PE, mainly **antioxidants loss**, **oxidation,** and **cracking,** leading to a mass transfer increase through the coating and susceptibility to stress cracking. Thus, there is a **maximum storage time before which polyethylene alteration induces critical damages to the coating**,

[1]https://www.google.com/maps/place/GRTgaz/@46.8477634,1.7322624,471m/data=!3m2!1e3!4b1!4m6!3m5!1s0x47fb09a5f566bbe3:0xbbc20cf86a7e8f2d!8m2!3d46.8477634!4d1.7344511!16s%2Fg%2F11b7r_s1g9

rendering it unfit for operational duty. This maximum storage time should be defined by TSO's with objective criteria quantifying ageing phenomena.

Methodology

Antioxidant loss can be followed with Oxidation Induction Time (**OIT**), measured by Diffrential Scanning Calorimetry (**DSC**), which is the period during which PE oxidation is inhibited by antioxidants at a given temperature under a flow of pure oxygen. Oxidation and surface cracking can be monitored by Fourier Transformed Infra-Red spectroscopy in Attenuated Total Reflectance mode (ATR **FTIR**) and optical or Scanning Electronic Microscopy (**SEM**) respectively. For long term extrapolation, modelling the drop of PE properties with ageing time is mandatory. Such model already exists for OIT and has been successfully applied in the past by GRTgaz to Distribution System Operators [1] [2] [3] (DSO, PE 63/80, PE100 RC) and water distribution [4] (PE100 RD) PE pipes. It predicts residual OIT (τ) as a function of ageing time (t) as well as various **material** and **environmental** constants:

$$\frac{1}{\tau} - \frac{1}{\tau_0} = \int_0^t k_0 . h_t . exp\left[\frac{-E^{\#}}{R.[T_0' sin(\omega u+\varphi)+T_0'']}\right] . [I_0' sin(\omega' u + \varphi') + I_0'']^{\alpha} . du \qquad (1)$$

With $\mathbf{k_0}$, kinetic constant of antioxidant loss, $\mathbf{E^{\#}}$, Activation energy of antioxidant loss, $\mathbf{h_t}$, water washing constant, $\mathbf{T_0'}$ and $\mathbf{T_0''}$, half substraction and addition of maximal and minimal temperatures, $\mathbf{I_0'}$ and $\mathbf{I_0''}$, half substraction and addition of maximal and minimal UV energy, $\boldsymbol{\alpha}$, radiation attenuation constant.

To validate sound storing practices, we applied this model on 2 PE systems used as 3LPE topcoats (PE#1 and PE#2), in both laboratory and natural conditions at the Chateauroux storage facility and correlated it with PE oxidation and cracking.

Materials

Laboratory ageing of the PE systems was performed on 3 mm thick sheets, obtained through a hot compression of PE pellets sourced directly from coaters. This methodology, described in table 2 of ISO 17855-2, aims at mimicking extrusion process used in the application of 3LPE coatings [5]. Small bands (2*10 cm^2) were then cut from those sheets and sampled at various ageing times with a 5 mm diameter punching tool (Figure 4).

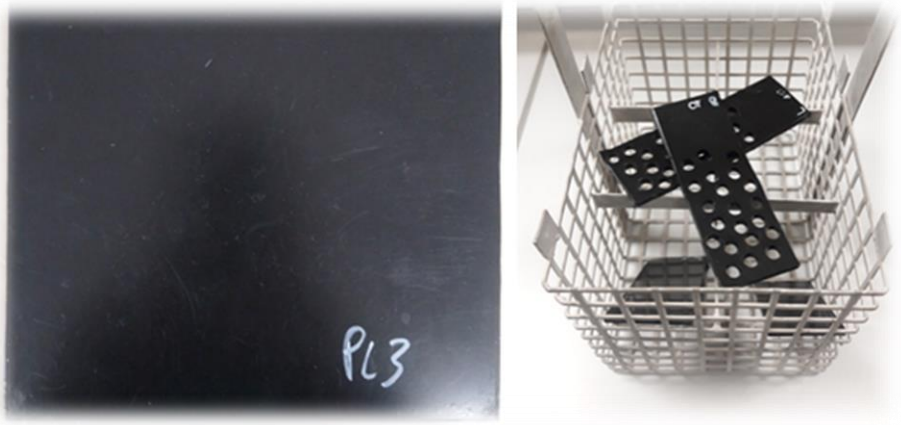

Figure 4: Sheets of PE obtained through ISO 17855-2 process (left) and bands used during laboratory ageing (right).

Weathered PE samples were directly collected on stored pipelines at the Châteauroux facility with a 1 cm diameter punching tool. The pipelines were roughly stored in an east-west direction and the specimens were sampled from the southern face of the pipe at approximately 45° from

the horizontal which is where the most severe ageing is expected to take place (Figure 5). In total, 10 different samples ranging from 1 to 10 year-storage time were collected for PE#2 system and 3 samples ranging from 2 to 4 years were collected for PE#1.

Figure 5: Sampling of the weathered PE samples on the Châteauroux storage site.

Laboratory accelerated ageing

Pure thermo-oxidation was performed at 100, 80, 60 and 40 ± 2 °C in Heraeus thermostated cells for up to 120 days, and photo-thermo oxidation was performed in a SEPAP12/24 environmental cell at 60°C with 4 UV light delivering a total UV surface energy of 27,206 cal.cm^{-2} for up to 3,000 hours (Figure 6).

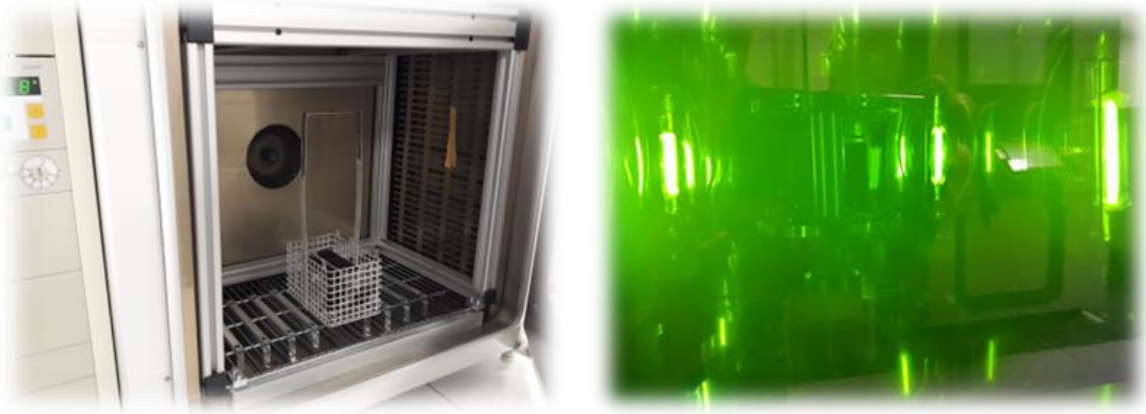

Figure 6: Closed ovens used for accelerated thermo-oxidation (left) and photo-thermo-oxidation (right) of the PE samples.

Results and discussion

Fixing material constants under pure thermo-oxidation

OIT were measured by DSC performed at 200°C under air on a Mettler Toledo DSC1 STAR^{e} apparatus. Prior to all measurements the 5 mm wide and 3 mm thick aged samples were cut in half at roughly 1,5 mm (50%) thickness to measure the OIT in the middle of the sample. Table 1 presents the mean values and standard deviation of OIT measured on thermo-oxidized PE#1 and PE#2 samples at different temperatures and ageing times.

Table 1: Mean values and standard deviation of OIT measured on thermo-oxidized PE samples at different temperatures and ageing times.

	Ageing time (day)	100°C	80°C	60°C	40°C
PE#1	0	156.2 ± 12.5	156.2 ± 12.5	156.2 ± 12.5	156.2 ± 12.5
	15	146.9 ± 0.1	142.3 ± 7.6	/	/
	30	123.6 ± 19.8	135.1 ± 21.2	131.2 ± 2.8	/
	45	121.7 ± 8.1	121.1 ± 7.7	/	/
	60	120.3 ± 6.3	136.9 ± 7.4	154.2 ± 4.3	140.5 ± 13.3
	75	119.2 ± 9.7	140.1 ± 25,3	/	/
	81	107.8 ± 6.2	154.4 ± 3.6	154.1 ± 2.3	146.2 ± 27.2
	90	104.1	144.5 ± 13.5	/	/
	105	74.7 ± 6.8	138.7 ± 4.1	/	/
	120	/	/	/	/
PE#2	Ageing time (days)	100°C	80°C	60°C	40°C
	0	130.4 ± 0.1	130.4 ± 0.1	130.4 ± 0.1	130.4 ± 0.1
	15	113.5 ± 0.8	96.7 ± 13.9	/	/
	30	97.0 ± 2.0	112.8 ± 4.7	116.6 ± 2.8	/
	45	96.3 ± 0.3	113.1 ± 1.1	/	/
	60	88.5 ± 4.7	98.8 ± 9.0	109.7 ± 5.5	117.1 ± 3.4
	75	76.8 ± 8.6	100.2 ± 3.5	/	/
	81	80.9 ± 1.7	95.6 ± 5.2	123.0 ± 4.5	117.5 ± 1.4
	90	85.6 ± 2.8	97.9	121.0 ± 3.0	/
	105	/	95.8 ± 1.4	/	/
	120	77.1 ± 3.4	98.7 ± 4.8	102.2 ± 31.7	122.0 ± 3.7

In the absence of UV irradiation (α = 0), equation 1 can be reduced to equation 2:

$$\frac{1}{\tau} - \frac{1}{\tau_0} = \int_0^t k_0 . exp\left[\frac{-E^{\#}}{RT}\right] . du \leftrightarrow ln\left(\frac{1}{\tau} - \frac{1}{\tau_0}\right) - ln\,(\Delta t) = ln\,(k_0) - \frac{E^{\#}}{RT} \qquad (2)$$

Figure 7 presents the graphical representation of the experimental data of PE#2 - as an example - in the logarithmic form $\ln\left(\frac{1}{\tau} - \frac{1}{\tau_0}\right) = f(\frac{1}{T})$.

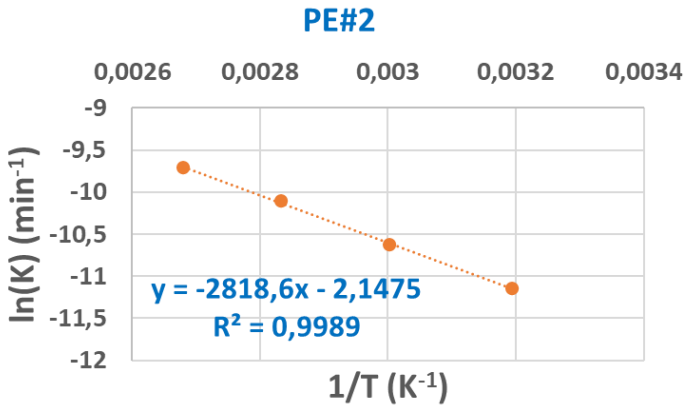

Figure 7: $ln\left(\frac{1}{\tau} - \frac{1}{\tau_0}\right) = f\left(\frac{1}{T}\right)$ graphical representation of the experimental data measured on PE#2 after thermo-oxidative ageing at different temperatures.

As predicted by equation 2 this graphical representation can be fitted with a linear function whose slope and vertical intercept are used to determine the material constants $E^{\#}$ and k_0 of

equation 1 (Table 2). To note is the poor correlation of the data for PE#1, due to experimental scattering on the OIT data, and the best fit for PE#2.

Table 2: Activation energy and kinetic constants measured on PE#1 and PE#2, compared to those of 2 PE used in distribution pipelines in the nineties.

	PE#1	PE#2	PE1-A01	PE2-A02
$E^{\#}$ (kJ/mol)	26,24	23,45	46	47
K_0 (j-1)	0,109	0,118	$7{,}50.10^{2}$	$1{,}15.10^{3}$

Both $E^{\#}$ and k_0 calculated values are close for PE#1 and PE#2 but quite different from the PE systems used in distribution pipelines.

Validation of the model under accelerated photo-thermo-oxidation

Table 3 presents the mean values and standard deviation of OIT measured on photo-thermo-oxidized PE#1 and PE#2 samples at different ageing times in SEPAP12/24.

Table 3: Mean OIT and standard deviation measured on PE#1 and PE#2 in SEPAP12/24 at different ageing times.

PE#1	**Ageing time (hours)**	**0**	**48**	**72**	**144**	**240**	**360**	**505**	**696**	**2850**
	Mean OIT (min)	155.5	151.0	161.6	157.1	131.5	128.9	154.8	155.1	131.5
	Standard deviation (min)	11.5	2.2	7.1	10.1	33.0	14.7	4.1	/	1.2
PE#2	**Ageing time (hours)**	**0**	**48**	**72**	**144**	**240**	**360**	**505**	**696**	**2850**
	Mean OIT (min)	130.4	108.9	125.2	122.2	128.0	118.6	114.4	114.8	76.6
	Standard deviation (min)	0.04	19.5	6.2	8.5	2.98	7.8	11.4	/	6.1

Experimental data were then fitted with equation 3, derived from equation 1, considering $E^{\#}$ and k_0 calculated values, environmental parameters associated with the SEPAP12/24 ageing in static conditions (I_0, T, h_t and α), and an "adjustment" parameter (X), absent from the original model but necessary here for a good fit of the experimental data (Table 4).

$$\frac{1}{\tau} - \frac{1}{\tau_0} = \int_0^t k_0 . h_t . exp\left[\frac{-E^{\#}}{RT}\right] . I_0^{\alpha} . X . du \qquad (3)$$

Table 4: Value of the parameters used for the modelling of the experimental OIT measured on PE#1 and PE#2 during ageing in SEPAP12/24.

PE#1	**Parameter**	k_0 (h^{-1})	$E^{\#}$ (J/mol)	h_t (Ø)	T (K)	I_0 ($cal.cm^{-2}$)	α (Ø)	X (Ø)
	Value	$4.56.10^{-3}$	26242	1	333	27206	0.5	0.015
PE#2	**Parameter**	k_0 (h^{-1})	$E^{\#}$ (J/mol)	h_t (Ø)	T (K)	I_0 ($cal.cm^{-2}$)	α (Ø)	X (Ø)
	Value	$4.90.10^{-3}$	23445	1	333	27206	0.5	0.015

The graphical representation of the experimental data and the models for both PE#1 and PE#2 with the input parameters of Table 4 is presented in Figure 8.

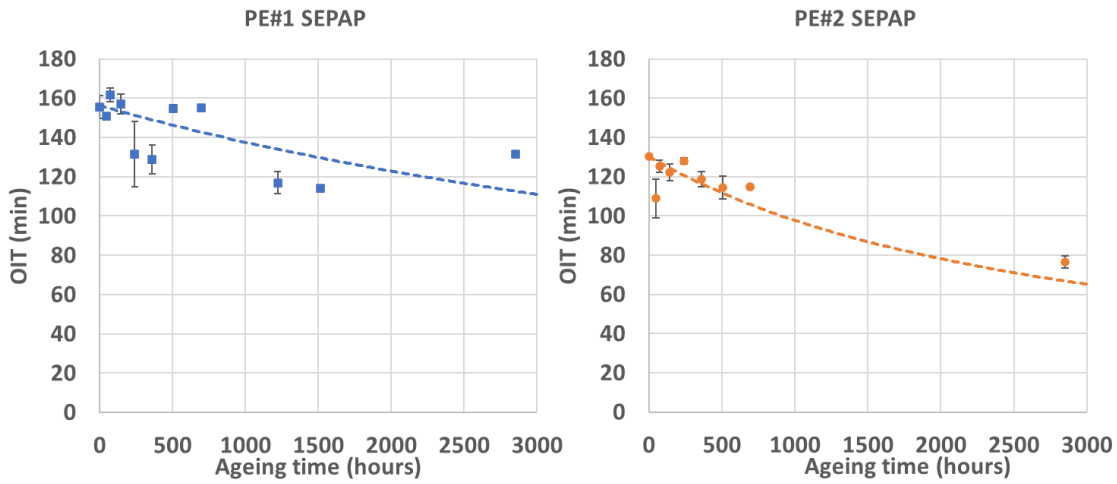

Figure 8: Experimental OIT and model for PE#1 and PE#2 as a function of ageing time in SEPAP12/24.

For both PE systems we obtain a good fit of the experimental data with equation 3 and the input parameters of Table 4. Even though we cannot give a chemical or physical meaning to the adjustment parameter X for the moment, it seems to be associated with the UV irradiation since it was not necessary to use it for the purely thermo-oxidation ageing previously presented.

Extrapolation and validation of the model for Châteauroux storage

Table 5 presents the mean values and standard deviation of OIT measured on photo-thermo-oxidized PE#1 and PE#2 samples collected in the Chateauroux storage facility for different storage times.

Table 5: Mean OIT values and standard deviation for PE#1 and PE#2 sampled on pipelines stored at Châteauroux for different storage times.

PE#1	**Storage time (years)**	2.07	2.26	3.98	/	/	/	/	/	/	/	/
	OIT (min)	122.6	115.6	103.9	/	/	/	/	/	/	/	/
	Standard deviation (min)	1.3	2.4	44.9	/	/	/	/	/	/	/	/
PE#2	**Storage time (years)**	0.26	0.65	0.97	1.35	2.13	2.27	3.05	3.05	3.87	9.45	9.68
	OIT (min)	147.5	126.3	98.4	109.5	119.3	105.7	116.1	98.9	94.5	53.7	86.2
	Standard deviation (min)	27.3	3.3	9.4	3.5	3.5	14.5	3.3	5.8	15.4	13.8	2.1

Experimental data were then fitted with equation 4, considering the same $E^{\#}$ and k_0 calculated values, environmental parameters determined for the Châteauroux storage center in "dynamic" conditions with sine variations (I_0', I_0'', T_0', T_0'', h_t and α), and once again, the same "adjustment" parameter (X) (Table 6).

$$\frac{1}{\tau} - \frac{1}{\tau_0} = \int_0^t k_0 . h_t . exp\left[\frac{-E^{\#}}{R.[T_0' sin(\omega u+\varphi)+T_0'']}\right] . [I_0' sin(\omega' u + \varphi') + I_0'']^{\alpha} . X . du \quad (4)$$

Table 6: Value of the parameters used for the modelling of the experimental OIT measured on PE#1 and PE#2 during storage in Châteauroux.

PE#1	**Parameter**	k_0 **(h^{-1})**	$E^{\#}$ **(J/mol)**	h_t **(Ø)**	**T_0' (K)**	**T_0'' (K)**	**I_0' ($cal.cm^{-2}$)**	**I_0'' ($cal.cm^{-2}$)**	**α (Ø)**	**X (Ø)**
	Value	$4.56.10^{-3}$	26242	1	12.35	286.65	19.32	24.54	0.5	0 .015
PE#2	**Parameter**	k_0 **(h^{-1})**	$E^{\#}$ **(J/mol)**	h_t **(Ø)**	**T_0' (K)**	**T_0'' (K)**	**I_0' ($cal.cm^{-2}$)**	**I_0'' ($cal.cm^{-2}$)**	**α (Ø)**	**X (Ø)**
	Value	$4.90.10^{-3}$	23445	1	12.35	286.65	19.32	24.54	0.5	0 .015

The graphical representation of the experimental data and the models for both PE#1 and PE#2 with the input parameters of Table 6 is presented in Figure 9. Once again there is a good fit of the experimental data with equation 4 and the input parameters of Table 6. The adjustment parameter X keeps the same value for the best fit which confirms its relevance and association with UV irradiation phenomena. Extrapolation of equation 4 to long storage times in Châteauroux shows that antioxidants are still present in significant concentrations up to 40 years after their arrival in both PE systems.

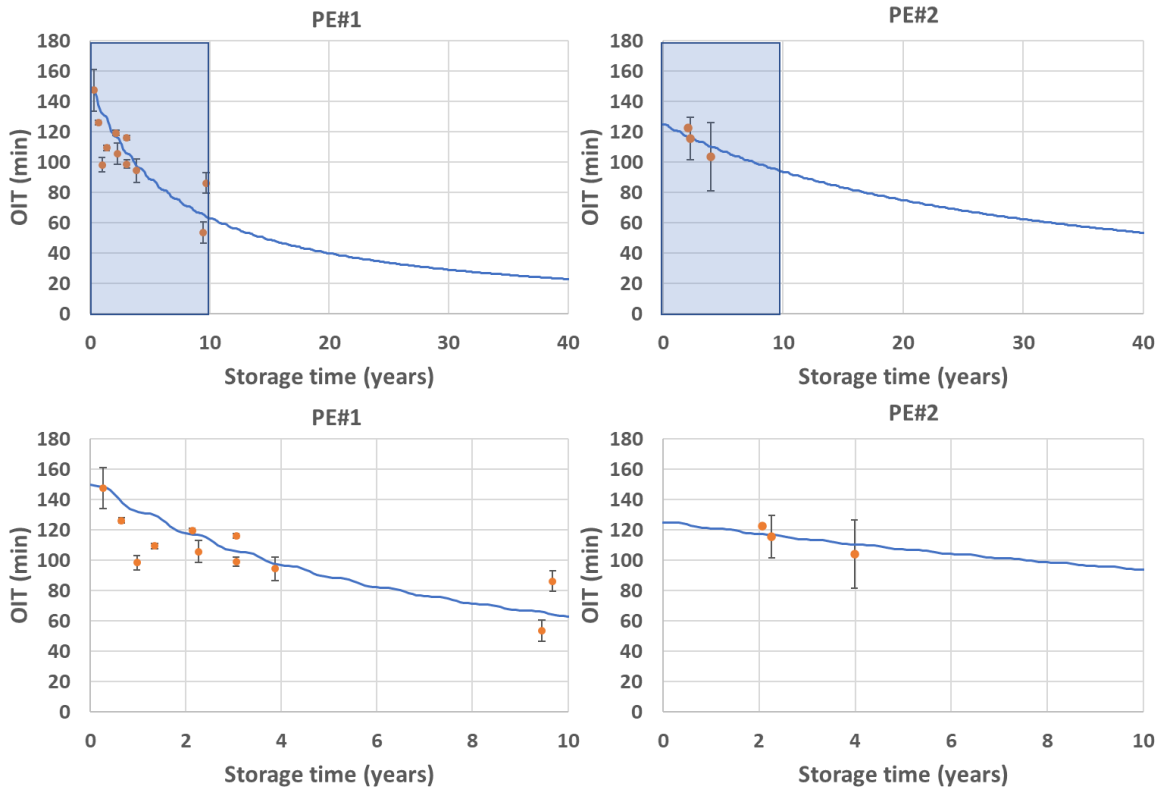

Figure 9: Experimental OIT and model for PE#1 and PE#2 as a function of storage time in Châteauroux.

Oxidation and Cracking

ATR FTIR spectra were measured on the SEPAP12/24 aged samples for the same ageing times as OIT measurements. Figure 10 presents the evolution with ageing times of the baseline-corrected large absorption bands located between [1900-1550] cm^{-1} and [1450-750] cm^{-1}, associated with photo-thermo-oxidation products of PE#2.

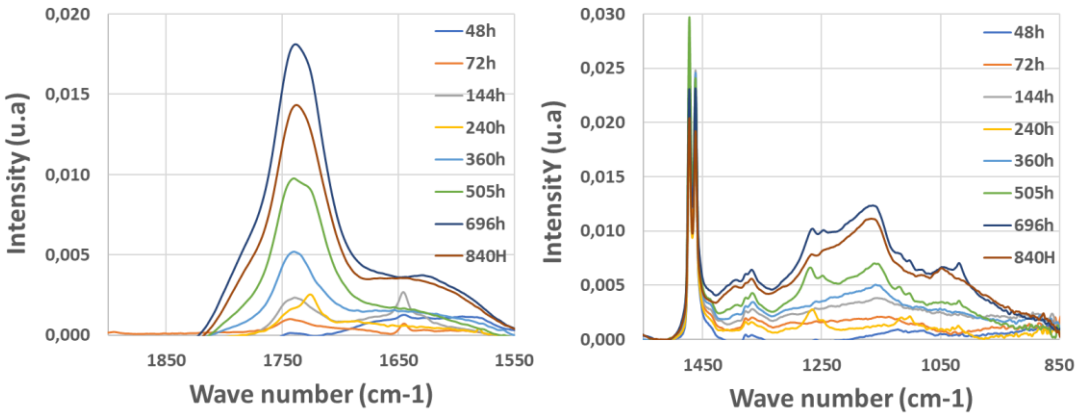

Figure 10: ATR FTIR baseline corrected spectra in the [1900-1550] cm^{-1} and [1450-750] cm^{-1} regions of PE#2 at different ageing times in SEPAP12/24.

From the spectra it is evident that PE#2 is undergoing chemical modifications while its measured OIT is still significant. This is attributed to the fact that OIT are measured in the middle of the samples (1,5 mm) whereas the chemical alteration of the PE systems is characterized in their subsurface region (maximum analysis depth of approximately 5 µm). It is also apparent that the two massifs are composed of dozens different peaks, appearing progressively during the accelerated ageing. To characterize the complex chemical processes taking place during photo-thermo-oxidation of the PE systems, a deconvolution of those massifs with a precise identification of the chemical functions involved is needed. ATR FTIR spectra were integrated according to the procedure previously described and normalized with the peak area of the ωCH_2 triplet absorption band area (Figure 11).

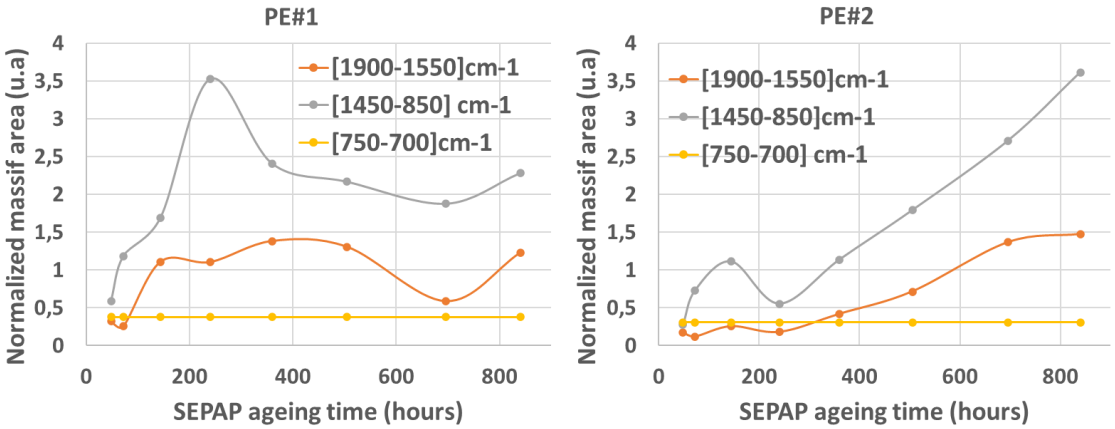

Figure 11: Normalized massif area of PE#1 and PE#2 as a function of SEPAP12/24 ageing time.

Logically, the regions of interest at [1900-1550] cm^{-1} and [1450-750] cm^{-1} present an increase of their normalized surface area with accelerated ageing time. This augmentation is consistent with a global increase of oxidized group concentrations in the subsurface zone. Nevertheless, it is worth noting that the oxidation schemes are different for PE#1 and PE#2, maybe due to different stabilizers packages. This point will be addressed through further investigations.

Finally, optical microscopy was performed on the aged samples after 2850 hours of accelerated ageing time with a Leica MZ12.5 microscope, perpendicular to the surface of the sample. Pictures show an apparent change in aspect between as received and SEPAP12/24 aged PE systems, evidenced by less glossy aspects after ageing. This change in aspect may be linked to the presence of oxidation products or antioxidants on the surface. Further investigations will have to be conducted with SEM to firmly exclude the presence of microcracks.

Conclusions and outlook

A photo-thermo-oxidative model computing the residual OIT as a function of outdoor storage time was successfully applied to 2 PE systems for the Châteauroux storage site. Experimental data collected from 3PLE coatings sampled on this site showed good correlation with the model. Long term extrapolation of OIT with said model shows that antioxidant will still be present in significant concentration after 40 years of storage in the 2 PE systems. ATR FTIR analysis showed that oxidation initiates in the subsurface (up to a 5 µm depth) well before all antioxidants have been chemically or physically consumed.

Deconvolution of the spectra will be performed to investigate the complex chemical processes occurring during the photo-thermo-oxidative ageing, including antioxidants behavior in the studied PE, which will be identified too. Optical microscopy showed a general change in surface aspect that cannot be firmly attributed to physical defaults like microcracks for the moment, pending to further SEM. We will also investigate ISO 21809-1 standard specifications regarding properties of the PE topcoat or the complete 3LPE coating for optimal in-service performances. Such specifications detailed into table 5 and 7 of the standard include PE water intake and various mechanical characterizations (peel strength, Hardness shore D, …).

References

1. Gueugnaut, D., Teygeman, C. and Rousselot, D., "Modellization of the antioxydants loss from the surface of medium density polyethylene gas pipes aged under natural or artificial environmental conditions", in: 17th Annual Conference on Advances in the stabilization and Degradation of Polymers, (1995).
2. Gueugnaut, D., et al. 11émes Journées d'Etudes sur le Vieillissement des Polymères, Bandol (France), (1995).
3. Gueugnaut, D. and Rousselot, D. 13èmes Journées d'Etudes sur le Vieillissement des Polymères, Bandol (France), (1998).
4. Rozental-Evesque, M. and Gueugnaut, D. "A solution for drinking wtaer networks: emerging new generation PE100 pipes with higher chlorine resistance".
5. ISO. ISO 17855-2: Plastics — Polyethylene (PE) moulding and extrusion materials — Part 2: Preparation of test specimens and determination of properties. (2016).

Acknowledgements: Anna-Maria Damiecka for carrying out the measurements campaign.

Renewable Fuels Process Unit Protection Through Thermal Spray Metal Claddings

Matthew MacWatters[1], Iain Hall[2]

[1]*Integrated Global Services, Richmond, U.S., matthew.macwatters@integratedglobal.com*

[2]*Integrated Global Services, Richmond, U.S., iain.hall@integratedglobal.com*

Abstract

Fuels traditionally derived from petroleum sources are increasingly being refined from sustainable carbon feedstocks, including plant oils, animal fats, and waste woods/biomass. Many legacy fuel producers are retrofitting brownfield vessels, or building new vessels, to produce biofuels via feedstock dependent processes such as HEFA-SPK, FT-SPK, pyrolysis, etc. These processes typically involve elevated temperatures/pressures, where normally benign fatty and organic acids, as well as contamainents, can become highly corrosive to typical carbon and low-alloy steel MOCs. Repair and outage costs of these units can be significant, involving complex shell replacement or weld overlay and associated PWHT. High Velocity Thermal Spray (HVTS) cladding technology has a documented history of shell protection in refinery and petrochemical systems where low pH conditions result in material wastage. These modified superalloy systems are resistant to acidic conditions at high temperatures and are effective in providing an impermeable metallurgical barrier without impact to the shell or the need for post thermal processing. Extensive testing was undertaken in corrosion autoclaves using blended biofuel feedstocks at typical vessel conditions. Testing was conducted with and without hydrogen (H_2) saturation. Specific HVTS systems showed high resistance to high temperature organic acid corrosion and are recommended for use as a protective cladding.

Keywords: “High Velocity Thermal Spray”, “Biofuel”, “Renewable Fuel”, “Free Fatty Acid corrosion”, “Sustainable Aviation Fuel (SAF)”

Introduction

Production of renewable biofuels, in the form of biodiesel and sustainable aviation fuel (SAF), has rapidly increased as both private and public entities transition to carbon neutral fuel sources [1]. For SAF, commercially mature processes include synthetic paraffinic kerosene production from Hydroproceessed Esters and Fatty Acids (HEFA-SPK), which typically uses stocks such as vegetable oil, fats, greases, etc., and the Fischer-Tropsch process (FT-SPK), which converts biomass. Pyrolysis, with the pyrolysis oil being upgraded via hydrodeoxygenation, is also promising as it can process a wide range of feedstocks [2,3]. Biodiesel production follows similar pathways, with the focus on converting triglycerides to fatty acid methyl esters (FAME) via transesterification and additional refining [4].

These commercial pathways involve elevated temperatures where common biofuel feedstock components and reaction products, including acetic acid, formic acid, and organic/free fatty acids, can become extremely corrosive, with equivalent TAN numbers of over 100 mgKOH/g. Co-blending with petroleum feedstocks can introduce naphthenic acids and sulfides, which other common contaminants, such as water, chlorine and heavy metals, can pose significant corrosion risks to both new vessels with upgraded stainless steel alloys, as well as retrofitted carbon steel [5,6]. Hydrogen and light hydrocarbons produced during feedstock decomposition can also cause hydrogen embrittlement and blistering [7,8].

High Velocity Thermal Spray Overview

To protect against biofuel corrosion, novel High Velocity Thermal Spray (HVTS) systems were explored as a solution. HVTS is a corrosion mitigation technique where a corrosion resistant metal alloy is atomized and the droplets conveyed at high velocity to a substrate such as carbon steel. This metal coating, commonly based on NiCrMo/Nb/W super-alloys with alloy modifiers to render them suitable for a thermal spray process, forms a corrosion resistant and mechanically superior barrier over the substrate.

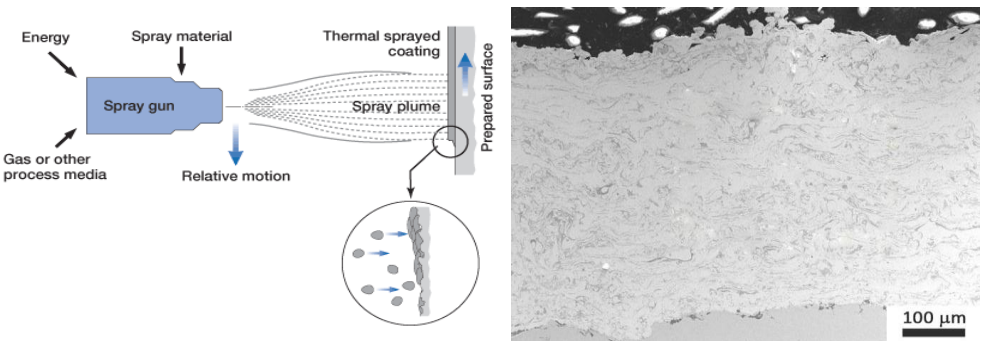

Figure 1 : Example HVTS process diagram (left) and typical HVTS microstructure (right)

Procedure and Design

Equipment and Conditions

A high-pressure/temperature corrosion autoclave with Hastelloy C-22 construction was filled with approximately 1800 ml of renewable feedstock, then saturated and pressurized with gas to reach the required operating pressure and temperature. The Biofuel feedstock employed was sourced from both virgin and used vegetable oils and fats/greases. Two tests were conducted with different gas saturations; Test 1 involved saturation and pressurization

with industrial grade Nitrogen (N_2), while Test 2 utilized Hydrogen (H_2). Pressure/Temperature conditions are based on common biofuel process conditions.

Table 1 : Testing process conditions

Conditions	Test 1	Test 2
Gas Saturation/Pressurization	Nitrogen N_2	Hydrogen H_2
Pressure	13.8 - 15.2 MPa / 2000 - 2200 PSI	
Temperature	343°C / 650°F	
Exposure Time	100 Hours	
Rotational Speed	60 RPM	

A hot tap was used to remove feedstock at set intervals to conduct TAN analysis without disrupting the exposure cycle. Within the autoclave, coupons were fixed to a stirring shaft to provide rotation and maintain homogeneity in the vessel. Coupons were electrically isolated to prevent galvanic corrosion effects. The HVTS test coupons consisted of a carbon steel insert welded into an Inconel 625 (UNS N06625) sheath/picture frame. This coupon design, intended for immersion and autoclave corrosion studies, allows for a carbon steel exposure test area while eliminating edge-effect issues that can lead to non-experimental edge artifacts on small coupons.

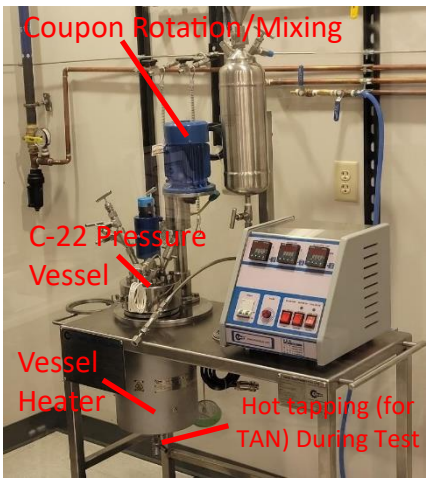

Biofuel feedstock

Figure 2: IGS corrosion autoclave (left)

Materials and Controls

A variety of wrought alloy control coupons and IGS HVTS systems were evaluated. Wrought low-alloy controls included AISI 1010 carbon steel and P22 (ASTM A387 Grade 22) steel, which was used as a representative pressure vessel MOC and features a nominal composition of 2.25Cr -1Mo. 347 Stainless steel was included as a typical liner or weld-overlay material, as was Inconel 625. The Inconel 625 was produced via weld-overlaying, then removing the steel substrate via milling up into the W/O CRA to eliminate any iron. This was verified with a surface chemistry check. For HVTS systems, IGS 5381/5450/5460/5470 were evaluated on both carbon steel and 347 stainless steel substrates. These systems are NiCrTi and NiCrMoNb/W/Al based alloys with strong track records in high temperature and pressure oil/gas environments. IGS 5337, a NiMoX material, was also included. HVTS coupons were prepared using IGS field standard equipment and procedures.

Before application the coupons were profiled with a high specification aluminum oxide blast media. Coating thickness was confirmed using an electromagnetic standoff gauge.

Table 2: Testing materials

Number	Substrate	HVTS	Status
1	347 Stainless Steel	None	Wrought alloy controls
2	P22 (2.25Cr -1Mo)		
4	625 WO		
5	CS	5470	HVTS on a carbon steel substrate
6	CS	5381	
7	CS	5460	
8	CS	5337	
9	CS	5450	
10	347SS	5460	HVTS validation coupons on a 347SS substrate
11	347SS	5450	

Evaluation and Analysis Procedures

Evaluation was performed on both the metallurgical validation samples and the feedstock blend media. The feedstock underwent a biofuel assay consisting of a FAME analysis (EN 14103)), total sulfur and total halide levels (ASTM D4294, Parr Bomb with IC), and basic sediment and water (BS&W) content (ASTM D4007). Additionally, the feedstock Total Acid Number (TAN) was tracked throughout the validation run via hot tapping sample extraction and determined via indicator titration and potentiometric titration (ASTM D664).

All wrought and HVTS coupons were cross-sectionally evaluated and analyzed using a Hitachi 3600N SEM operating at a 30 kV excitation voltage and equipped with Energy-dispersive X-ray spectroscopy (EDS) for elemental analysis. Analysis focused on the condition of the substrate and cladding and presence/composition of any corrosion scale. Additionally, weight changes before and after experimentation were tracked.

Results and Discussion

Feedstock Analysis

A fuels assay revealed chloride levels of approximately 8 ppm, creating a low risk of chloride related corrosion. While the water content is low, the solution starting TAN number was very high, at 95 mg KOH/g. This is due to the high FFA acid composition of the feedstock. For reference, traditional crude oil is considered highly acidic with a TAN greater than 1 mg KOH/g. Approximately 330 ppm levels of sulfur were also found in the feedstock.

Tables 3: Assay results

Assay (Units)	Value
TAN (mg KOH/g)	95
Total Sulfur Content (Mass % / ppm)	0.33 / 330
Water Content - BS&W (% Volume)	<0.025
Sediment - BS&W (% Volume)	0.3
Total halides (Chlorines, Cl) (ppm)	8.1

In addition to a standard assay, the feed also underwent a biofuel-specific FAME (Fatty Acids Methyl Esters) analysis to identify the specific fatty and organic acids present in the feed both before and after testing. A similar analysis was also performed on commercial soybean oil, a common biofuel feedstock. Compared to the soybean oil, the test feedstock had higher levels of Linoleic acid, accounting for over 27% of the FAME composition, which can be typical of blended sources. Traditional vegetable feedstocks are typically higher in palmitic and oleic acids. This is significant as linoleic acid is more corrosive towards specific metals and potentially increases corrosion rates.

Table 4: Feedstock FAME analysis

Compound	C-Number	Soybean Oil (Reference)	Blended Feed (Pre-Test)	Blended Feed (Post-Test H_2)	Blended Feed (Post-Test N_2)
Methyl Palmitate	C16	37%	26%	FAME Analysis still in progress	
Methyl Stearate	C18	3%	3%		
Methyl Oleate/Elaidate	C18:1 cis/trans9	42%	33%		
Methyl Linoleate	C18:2 cis/trans9,12	13%	27%		
Methyl Linolenate	C18:3 cis6-9-12	0%	3%		

Feedstock TAN Analysis

During validation testing, hot feedstock samples were taken at set intervals over each test cycle. During autoclave start-up and initial operation, TAN readings for both tests rapidly increased as free fatty acids were formed from the feedstock components. TAN numbers then slowly decreased over-time, though remained relatively high after 100 hours of run-time. This indicates that the constituent fatty acids are likely being converted into non-acidic esters and soaps. It was noted that the N_2-saturated feedstock peaked at a higher TAN number than the H_2-saturated solution (136 mgKOH/g vs. 125 mgKOH/g) and had a higher end value (63 mgKOH/g vs 48 mgKOH/g), indicating that H_2 saturation could be causing changes in the FFA conversion rates/process.

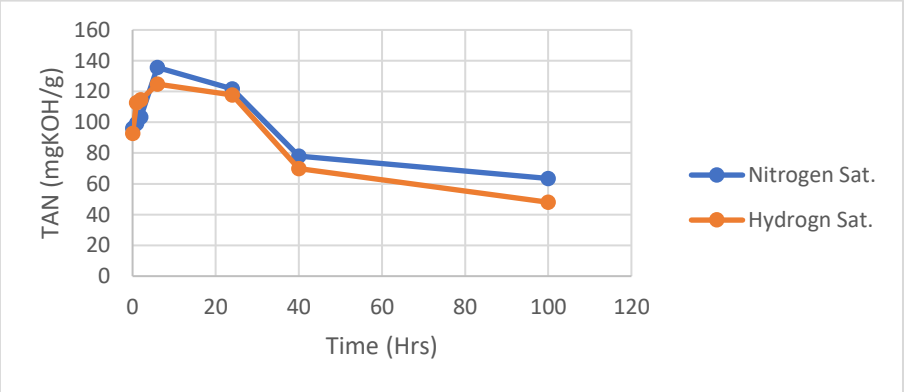

Figure 3: Biofuel solution TAN over time

Metallurgical Analysis – Weight Results

All coupons were weighed before and after testing. Final post-test weights were determined after coupons were lightly cleaned in an acetone solvent to remove any deposited feedstock residue. The carbon steel and P22 wrought alloy (WA) coupon had significant weight loss at over 20% and 6%, respectively. Significantly, for both materials, the nitrogen saturated solution showed a larger weight loss than the hydrogen saturated solution, confirming greater corrosivity of the N_2 solution or a possible inhibition effect with the H_2.

All IGS HVTS coated coupons, as well as the 347SS coupon, experienced negligible weight changes of less than $\pm$ 0.25%. It should be noted that, while minimal, the N_2 test system coupons did experience a net weight gain of 0.18 – 0.23%, while equivalent H_2 coupons experienced close to zero weight change. residue feedstock on the surface that was not fully removed during cleaning. Minor passivation or oxidation effects may also have occurred; typically, these passive films enhance coating corrosion resistance. Weight loss would be indicative of dealloying or an unstable scale formation.

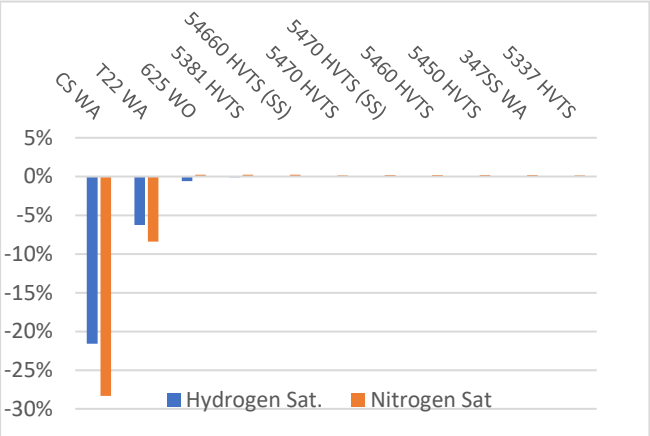

Material	% Change (H_2)	% Change (N_2)
CS WA	-21.57%	-28.33%
P22 WA	-6.23%	-8.39%
625 WO	-0.60%	0.23%
5381 HVTS	-0.09%	0.24%
5460 HVTS (SS)	-0.05%	0.22%
5470 HVTS	-0.05%	0.17%
5470 HVTS (SS)	-0.04%	0.18%
5460 HVTS	0.01%	0.20%
5450 HVTS	0.01%	0.19%
347SS WA	0.02%	0.18%
5337 HVTS	0.06%	0.17%

Figure 4: Coupon weight changes

Metallurgical Analysis – Wrought Alloy SEM Results

SEM Imaging and EDS elemental analysis confirmed weight change results. The carbon steel coupons in the H_2 featured a 150-200 µm corrosion scale and a thinner 50 µm scale in the N_2 testing, primarily iron oxide in composition. Large weight-loss measurements indicate that this scale is not stable and is likely deteriorating in-situ to expose fresh material. The P22 material showed a well-defined scale of approximately 75 – 100 µm, with an iron oxide composition. Small (~ 1% wt.) amounts of chromium are also present. While the P22 H_2 coupon shows general corrosion, the N_2 P22 coupon appears to show the additional formation of pitted areas, which can increase failure risk in pressure vessels, as well as a thinner and less stable scale.

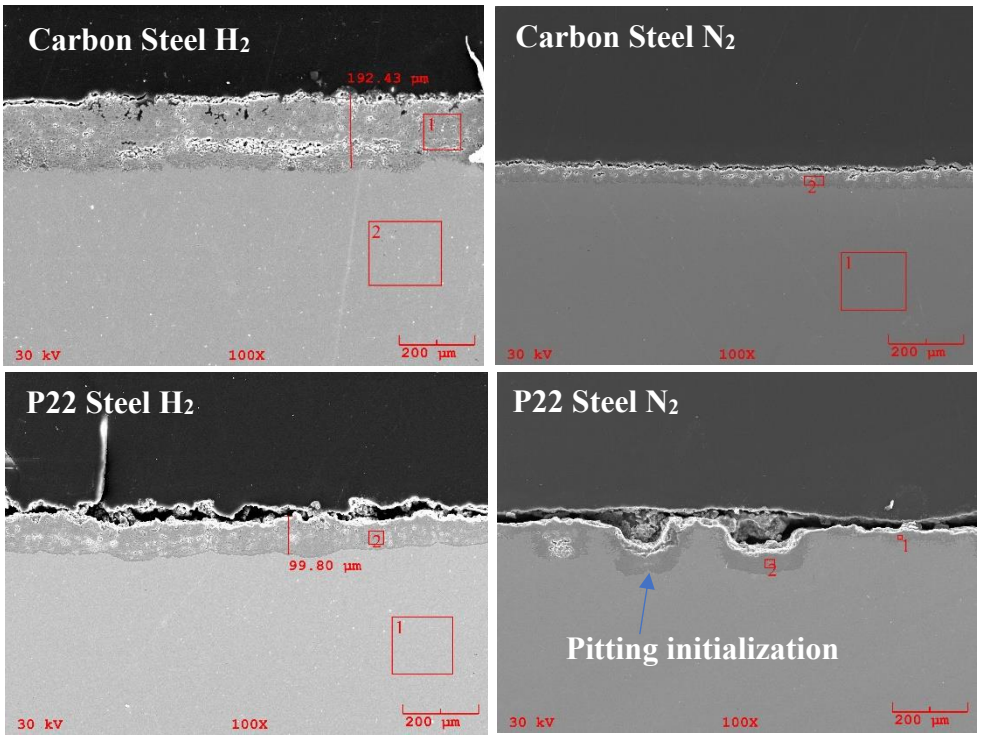

Figure 5: Carbon steel and P22 control coupons

The 347SS control coupons also performed well in testing, showing weight changes equivalent to the HVTS coupons and no significant damage under SEM analysis. It should be noted that the test feedstock was fairly idealized, with low chloride levels. 347SS and other iron chromium materials may experience greater than expected corrosion if the protective oxide layer is compromised. The 625 Weld-overlay also experienced negligible affects, with minimal weight changes. The iron content of the weld-overlay was approximately 3-4%; it should be noted that previous work with 625 WO in biofuel environments has indicated that high levels of iron dilution can compromise the corrosion resistance of this material.

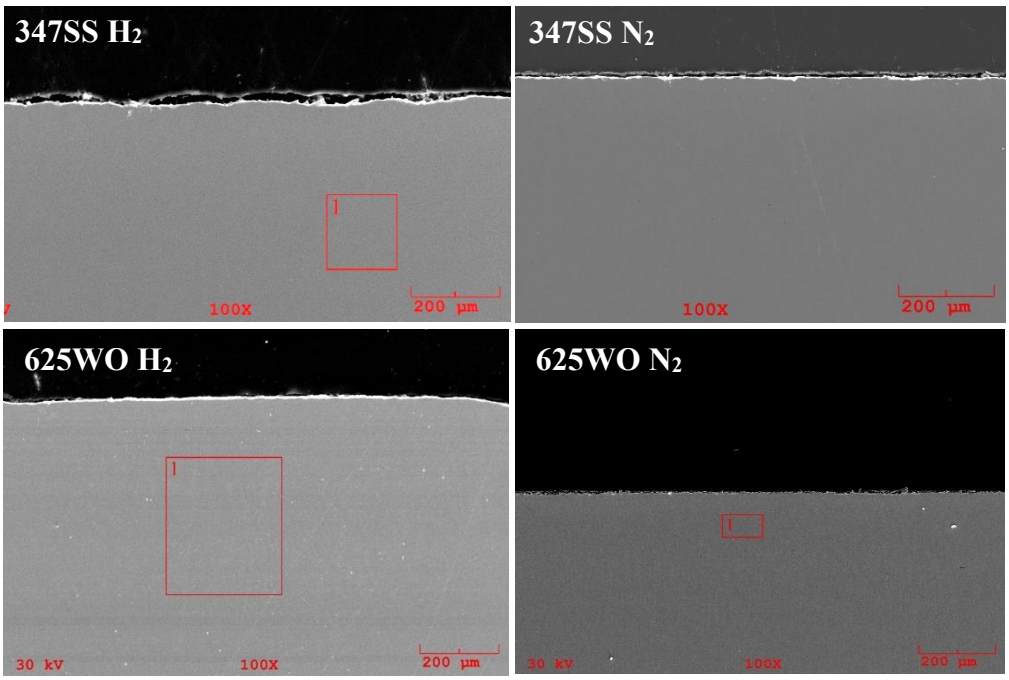

Figure 6: 347SS and Inconel 625 WO control coupons

Metallurgical Analysis – HVTS Results

Overall, the HVTS coupons performed well in both autoclave tests, with SEM imaging confirming weight change results. One coating, 5337, does show some signs of surface attack, with the formation of approx. 20µm of nickel and metal oxides and some degradation of the surface layer. 5337 is a NiMoX coating and may lack the chromium content needed for stable scale formation in a high temperature acidic environment.

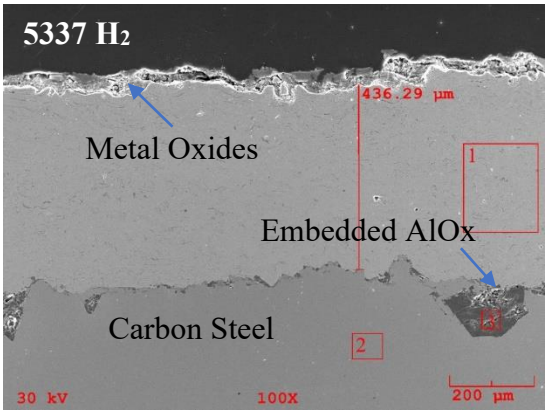

Figure 7: 5337 in H_2 environments

All other HVTS coatings (5381/5450/5460/5470) remained tightly adhered to the underlying carbon steel and prevented any observable penetration of the corrosive organic acids, chlorides, or sulfur. There are no signs of corrosion products at the bond-line between the claddings and substrate. Some embedded aluminum oxide blast media can be seen; however, this is expected and will not compromise bond strength. The claddings themselves show no degradation with no bulk effects. Some surface contamination is noted, as is some separation from the coupon epoxy mount, however this is not coating damage. Finally, no performance differences between the carbon and stainless-steel substrates were noted. Specific alloy selection will depend on specific feedstock needs. For example, 5450/60 are recommended for feeds with high sulfur levels, while 5470 and 5381 are recommended for feeds containing higher chloride levels; all coatings will perform well against FFA attack.

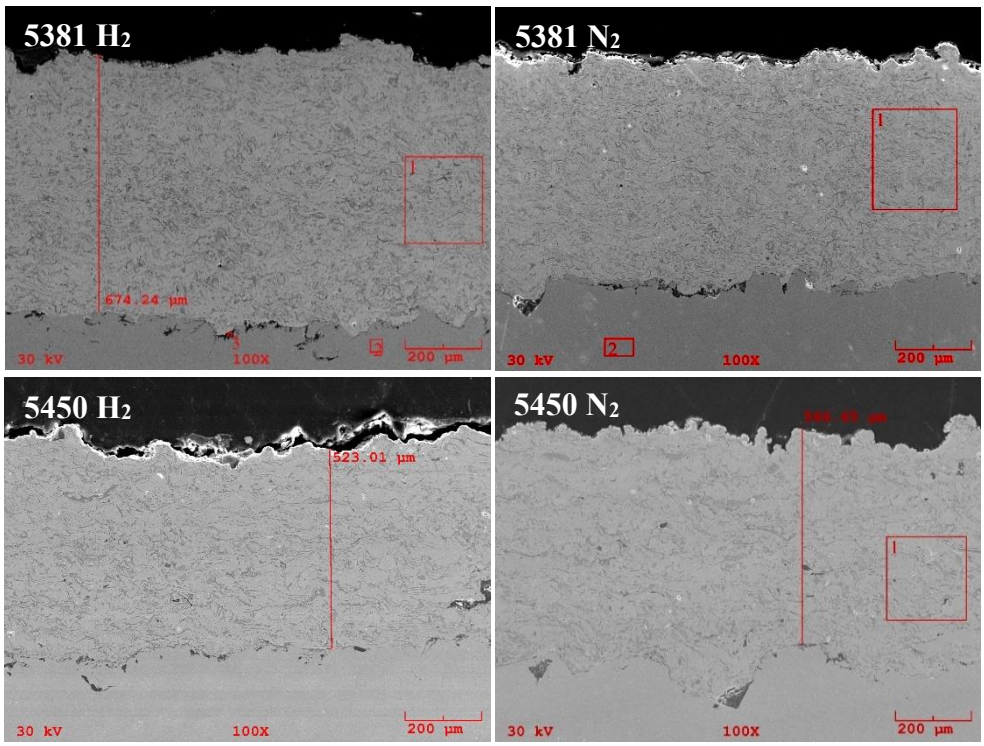

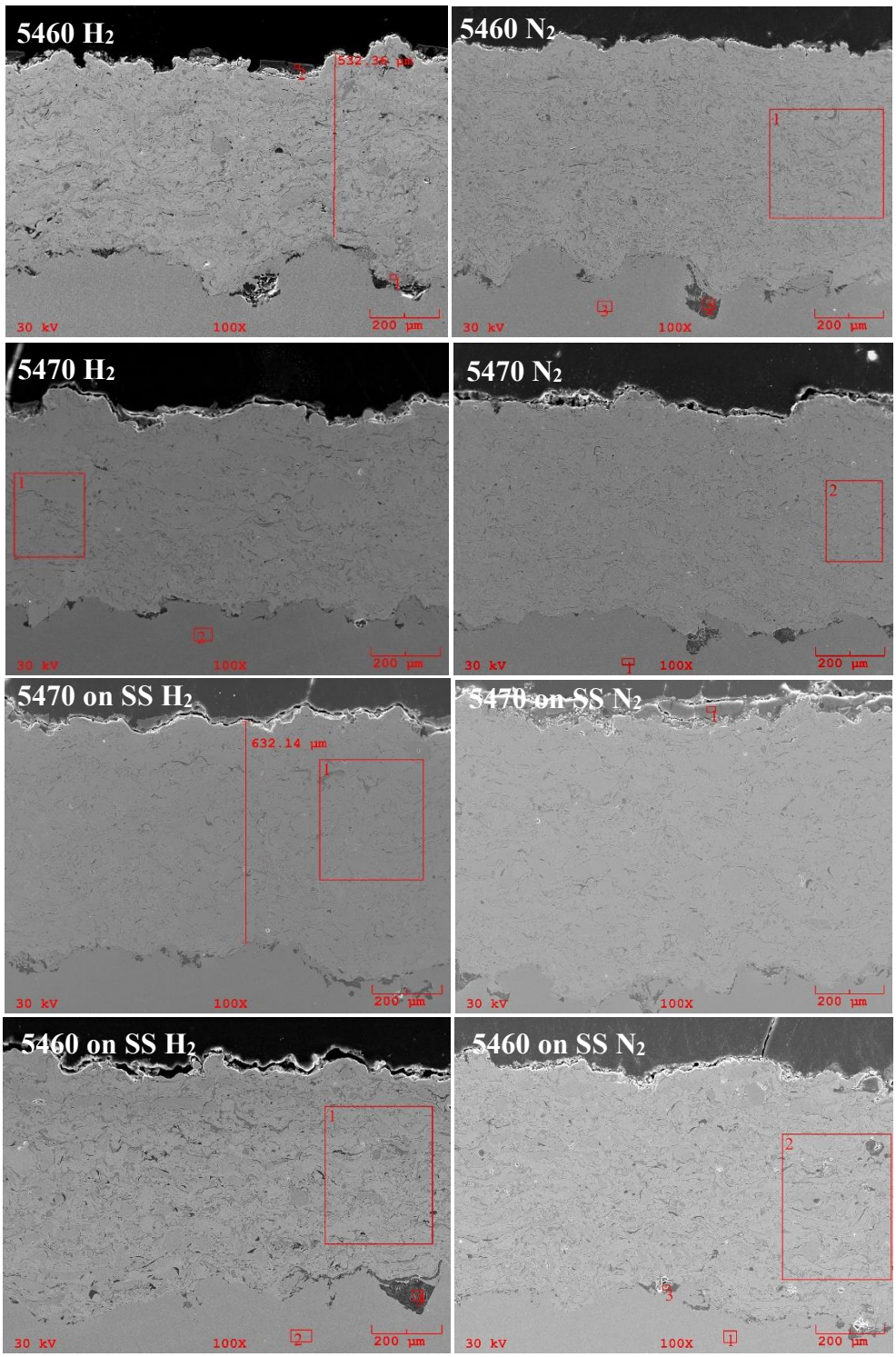

Figure 8: HVTS coupon SEM imaging

Conclusions and Recommendations

Extensive validation testing on the use of engineered HVTS claddings on both carbon steel and stainless steel substates was completed in a biofuel environment. Testing occurred in a C-22 corrosion autoclave at a pressure of 13.8 - 15.2 MPa and temperature of 343°C using a blended biofuel feedstock under both N_2 and H_2 saturation conditions. Prior to testing, the feedstock underwent a standard biofuel assay and FAME analysis to identify corrosion risks. The assay found low levels of chlorides and moisture, but a high TAN (95 mgKOH/g), indicating high levels of organic and free fatty acids. Sampling during operation revealed a rapid increase in TAN readings as temperatures increase, then a decrease over time as FFA are converted to esters and soaps or react with vulnerable metals.

A variety of controls and HVTS coupons were evaluated in this feedstock. Carbon steel and P22 steel both experienced significant weight loss and corrosion from the mixture, with the carbon steel losing over 20% of its weight in 100 hours. Additionally, corrosion appeared to be more aggressive under N_2 saturation conditions. HVTS alloys, including 5450, 5460, 5470, and 5381, were tested on both carbon steel and 347SS substrates. All applied claddings on both CS and SS substrates fully protected the substrate, showed no signs of corrosive penetration, and remained tightly adhered. While specific alloy selections will be made based on local feed chemistry, these HVTS systems are recommended for use in a variety of biofuel environments. While little differentiation was noted in this study, in other biofuel testing work, it was noted that higher chromium content alloys provided better protection in higher sulfur and temperature conditions.

References

1. Maheshwari, P., Haider, M. B., Yusuf, M., Klemeš, J. J., Bokhari, A., Beg, M., Al-Othman, A., Kumar, R., & Jaiswal, A. K. (2022). A review on latest trends in cleaner biodiesel production: Role of feedstock, production methods, and catalysts. *Journal of Cleaner Production*, *355*, 131588.
2. Bauen, A., Bitossi, N., German, L., Harris, A., & Leow, K. "Sustainable Aviation Fuels" Johnson Matthey Technology Review (2020).
3. Ail, S.S.; Dasappa, S. "Biomass to liquid transportation fuel via Fischer Tropsch synthesis – Technology review and current scenario". Energy Rev. 2016, 58, 267–286,
4. J. Van Gerpen, B. Shanks, R. Pruszko, D. Clements, and G. Knothe. "Biodiesel Production Technology". Subcontractor Report NREL/SR-510-36244, Subcontract No. ACO-2-35016-01. National Renewable Energy Laboratory (2004).
5. Goodman, L. R., & Singh, P. M. (2014). CHAPTER 10: CORROSION ISSUES IN BIOFUELS. In *WORLD SCIENTIFIC eBooks* (pp. 267–293).
6. Shehzad, A., Ahmed, A., Quazi, M. M., Jamshaid, M., Rahman, M. S., Hassan, M. R. A., & Javed, H. M. A. (2021). "Current research and development status of corrosion behavior of automotive materials in biofuels." *Energies*, *14*(5), 1440.
7. Palanisamy, S., & Gevert, B. S. (2016). Study of non-catalytic thermal decomposition of triglyceride at hydroprocessing condition. *Applied Thermal Engineering*, *107*, 301–310.
8. Pillot, S.; Chauvy, C.; Corre, S.; Coudreuse, L.; Gingell, A.; Héritier, D. "Effect of temper and hydrogen embrittlement on mechanical properties of 2.25Cr–1Mo steel grades—Application to minimum pressurizing temperature (mpt) issues. Part I: General considerations & materials' properties". *Int. J. Press. Vessel. Pip.* **2013**, *110*, 17–23.

Contribution of analytical techniques in understanding corrosion mechanisms by free fatty acids in vegetable and waste oils

Fouad Andari, Joana Fernandes, Jean Kittel, François Ropital, IFP Energies Nouvelles, Rond-point de l'échangeur de Solaize, BP3, 69360 Solaize (France)

Proposed initiatives and regulations set to combat climate change imposes significant adjustments to the refining industry. Reducing the use of conventional crude oils, which are progressively replaced by biomass based renewable feedstock, is a must. Vegetable and waste oils represent an interesting alternative, since they present many similarities with crude oils and can be processed in existing refinery facilities. However, these feedstock also present specific compositional features that may result in corrosive conditions. For instance, they may contain high levels of free fatty acids, and other corrosive impurities such as water and chlorides.

In this paper, we intend to focus on the impact of free fatty acids on the corrosion of carbon steel. A broad range of analytical techniques is used to better identify the corrosive species and the corrosion mechanisms. ICP-OES measurements is used to determine the concentration of dissolved iron and the results are correlated with the corrosion rate of exposed coupons. Simulated distillation shows better performance than the conventional potentiometric titration method for total acid number (TAN) evaluation (ASTM D664; NF EN ISO 660). It is then used to determine the acid consumption during corrosion tests and to try to find correlations with corrosion rates. Finally, attenuated total reflectance infra-red analysis (ATR-IR) is used to identify metal complexes associated with corrosion reactions. All these methods are applied to corrosion experiments conducted at different temperatures and at different free fatty acid content from near zero (refined vegetable oils) to highly acidic blends.

Corrosion performance of different alloys exposed to HTL conditions

Authors: Daniel Blücher, Torstein Lange (SINTEF Industry) and Judit Sandquist, Inge Saanum (SINTEF Energy) NO-7034 Trondheim, NORWAY
Mikko Uusitalo, Valmet Technologies, Tampere, Finland. Corresponding author: daniel.blucher@sintef.no

This work was financed by the Horizon 2020 project "Black Liquor to Fuel by Efficient Hydrothermal Application integrated to Pulp Mill, BL2F", Grant Agreement 884111[1].

BL2F is a Horizon 2020 project with focus on production of drop-in biofuels for aviation, and shipping, using black liquor, a side stream of the chemical pulping industry as raw material.

Hydrothermal liquefaction (HTL) is a thermochemical conversion process that uses compressed water as reaction medium at temperatures between 200-400 °C and pressures between 10-40 MPa. To make HTL a viable industrial process, especially with black liquor as feedstock, the corrosion resistance of the processing materials is important and must be clarified. There is not much literature, nor experience, available on corrosion in black liquor processing systems operating at supercritical conditions. Available literature data covers temperature ranges of 100-200°C, i.e., not supercritical[2]. Hence, it has been aimed to investigate the behaviour of certain commercial steel qualities at supercritical conditions as basis for construction of a small-scale pilot system. Here, the suitability of different types of alloys as reaction vessel- and process component material was evaluated by testing in simulated- and in real process conditions with focus on resistance to corrosion, inclusive stress corrosion cracking. To simulate the hoop-stress from the high inside pressure in the real process, as well as external loads and residual stresses from e.g., welding, the C-ring test specimens for the different materials were stressed to their respective actual yield strength, $R_{P0.2}$, at the test temperature. Prior to testing in real supercritical HTL conditions, screening testing of the candidates was carried out in simulated water-based black liquor and then examined for corrosion and cracking. Then, to mimic the real conditions, the most promising alloy candidates were exposed in the same electrolyte in SINTEF Energy Research continuous HTL reactor at super critical conditions (both flowing and stagnant).

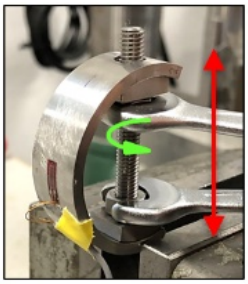

Expanding the C-ring

A selective dissolution (dealloying) of essential alloying elements (Ni, Mo, Fe) has been observed in the supercritical region for certain Ni-based super alloys. A subsequent transformation of metal into scale is accompanied by reduction in the wall thickness. Intergranular grain attack (corrosion) precedes the dissolving of alloying elements and causes sub-surface damage[3].

The corrosion- and materials evaluation study in a) water-based simulated black liquor and b) water-based simulated black liquor at super-critical conditions was successful. The conclusion from the testing program was that the most corrosion resistant alloy for the defined conditions is the chrome-rich carbon steel candidate P91 (UNS K91560). This is a type of creep strength enhanced ferritic (CSEF) alloy, which are steels designed to retain strength at extremely high temperatures. The P91 abbreviation represents the material's chemical composition, i.e., 9% chromium (Cr) and 1% molybdenum (Mo). Further work is required to at conclude on corrosion resistance for the P91 quality at supercritical conditions in the **welded** condition, including the heat affected zone (HAZ), and to better understand caustic corrosion mechanisms for safe design of future full-scale plants.

[1] https://www.bl2f.eu/

[2] https://doi.org/10.1590/1980-5373-MR-2017-0148

[3] DOI 10.1002/xrs.1297

High Temperature Corrosion Prediction in Renewable Diesel and Sustainable Aviation Fuel Applications

Gerrit Buchheim, Sridhar Srinivasan

Becht Inc., Houston, Texas, USA

Abstract

Renewable Diesel (RD) and Sustainable Aviation Fuel (SAF) production from biological sources (natural oils) has seen exponential growth in recent years. Significant, rapid investments have occurred in retrofitting / adapting existing refinery hydroprocessing infrastructure to process natural oils or coprocess natural oils blended with crudes to produce RD and SAF. This stems from the fact that natural oils have the hydrocarbon (HC) structures to fit within the mid-distillate fuel product such as diesel and aviation fuel as well as that these processes are optimized for removal of unwanted Sulfur and Oxygen removal.

In these modified hydroprocessing applications, high temperature decomposition of triglycerides (TRG) leads to production of RD and SAF through hydroprocessing of esters and free fatty acids (FFA). The resulting oxygen free-RD and SAF products are completely fungible with petroleum hydrocarbons and have the added benefit of producing propane as a by-product. Hydro-processing of refined natural oils (degummed, bleached, neutralized, and deodorized) has its own unique corrosion problems. FFA formed in pre-heat trains and off-gases (H_2O, CO_2, CO, H_2) differ from those traditionally found in refinery hydro-processing. While aqueous carbonic acid corrosion due to CO_2 is well understood, high temperature corrosion by transient formation of FFA is not and forms the focus of this paper.

Over the last few years, the authors introduced a molecular mechanistic model to quantify simultaneous high temperature naphthenic acid and sulfidation corrosion (CorrExpert®-Crude) in refinery CDU/VDU operations. That model has been adapted to address high temperature FFA corrosion, given that FFA are carboxylic acids, akin to naphthenic acids found in conventional fossil-fuel based crude unit process streams. Above 540F (280C), TRG generate mixtures of free fatty acids (FFA) that vary in corrosivity and stability as a function of molecular shape / structure and saturation.

Saturated FFA are rigid, tend to align in clumps by self-association and are much less corrosive when compared to conventional HC nap acids. Unsaturated FFA, which leave access for a 2nd acid, are similar to HC nap acids and are equally corrosive. The proposed model facilitates differentiated treatment of unsaturated and saturated FFA to quantify surface reactions sensitive to acid shape and reactivity. Algorithms have been created to predict the “effective TAN” for TRG at temperature as a function of residence time and are designed to be incorporated into the existing corrosion prediction model.
Key words: Corrosion prediction, crude corrosivity, sulfidation, Naphthenic acid corrosion, reactive organic sulfur compounds, simulation and modeling

Corrosion Case Histories in Biorefinery

M. De Marco, C. Casu – Istituto Italiano della Saldatura (IIS), Genoa, Italy

The growing demand for biodiesel created the necessity to have what is called ''drop-in'' renewable fuel, which is completely interchangeable with the fossil origin fuels, without the necessity of blending it in some percentages. Even if most of the reactions to produce this ''new'' biofuel are in some case like the ones very well-known of the fossil fuel industry, the environments can be completely different, due to the change of Raw Materials (RM) and intermediates; this can bring to a change of the corrosive properties of the involved fluids. The widespread presence of aqueous phase, the high oxygen content of the materials, the high TAN, are just some of the corrosion issues of this industry. This work has the aim to illustrate some corrosion case histories, to better understand the differences between the fossil fuel industry corrosion problems and the biorefinery ones.
The cased histories reported try to follow the route of the RM to biofuels, starting with the corrosion in the feedstock tank, following with the pipeline for the transport of the RM, the feed piping to the hydro-processing reactor, the heat exchanger of the stripper section, and ending with unusual damage in reactor effluent pipeline

Keywords: biorefinery, stress corrosion cracking, corrosion resistant alloys, organic acid, organic coating

FOREWORD

The growing demand for biodiesel created the necessity to have what is called ''drop-in'' renewable fuel, which is completely interchangeable with the fossil origin fuels without the necessity of blending it in some percentages.
The production of biodiesel put in scene new problems and challenges for the materials, corrosion, and asset integrity specialists; the variety of raw materials often makes it difficult to predict the criticality of the degradation phenomena of the materials with the aim evaluate likelihood of failure and inspection programs.
Even though, certain reactions and certain processes present in the production of biofuels/renewable fuels are familiar to corrosion and materials engineers working in the refining field (hydrotreatment, hydro-conversion, isomerization, distillation, etc.), everything is not predictable due to raw materials and intermediates changing scenario [1].

- *"Fossil" refinery typical environments*: hydrophobic hydrocarbons with sulfur (sulfides, mercaptans, etc.), nitrogen compounds and small quantities of oxygen.
  By-products from processing: hydrogen sulfide, ammonia, and only small quantities of water.

- *Bio-based fuels typical environments*: species with a high oxygen content (carbohydrates, triglycerides, Free Fatty Acids – FFA, etc.).
  Products and by-products: oxygenated species such as alcohols, CO_2, organic carboxylic acids, and water as a by-product; High Acidity Numbers (TAN)
  Moreover, the presence of water increases corrosion problems.

Considering what above, the transport, storage (raw materials and finished products), production and combustion phases of biofuels/renewable fuels industry could present different corrosion problems than fossil fuels.
The presence of greater quantities of oxygenated species, water, and organic acids (also Free Fatty Acids) entails variable risks of corrosion.
CO_2 and chlorides may also be present which dissolve in the aqueous phase ("low T" corrosion) to increase corrosion risk

Process fluids with organic acids in the aqueous phase can be corrosive to carbon steel and Mo-free stainless steel.
If both chlorides and organic acids are present in significant quantity only Ni-Cr-Mo alloy can offer adequate reliability.
Also, anhydrous streams with organic acids at T> 100 ° C can be associated to corrosion problems in some way similar to naphthenic acid corrosion (NAC).
A specific point that is also under debate is if hydrogen mixing in hydrotreating reactor effluent stream can mitigate corrosion at high T (lowering the TAN) for non-Mo alloys, as happens in fossil refineries for NAC.

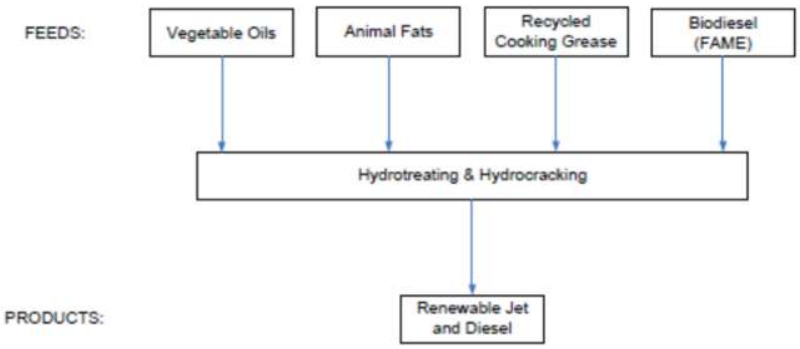

Fig. 1 — Renewable fuel production route

CASE HISTORIES

Case 1 – Coating Failure in a feedstock tank

The firs case is related to an above ground storage tank converted to contain Regenerated Used Cooked Oil (RUCO).
The tank was internally protected by a polyamide cured epoxy coating (60 µm primer; 300 µm topcoat).
The temperature in the tank was increased to 70 °C by heating coil to reduce viscosity of the new product.
Extensive exfoliation of the shell coating occurred (Fig. 2).
The test & analysis carried out permit to conclude that the coating products is thermally more than chemically degraded (max operating temperature for PDS 60 °C); DCS analysis shows a heavily degraded product.
The applied products are not suitable to sustain RUCO temperature maintained in the TANK; no application anomalies can be put in evidence by analysis.

It can be suggested to select an epoxy-phenolic coating products suitable to T> 100 °C.

Fig. 2 – Overall view of detached coating

Fig. 3 – Evaluation of surface profile

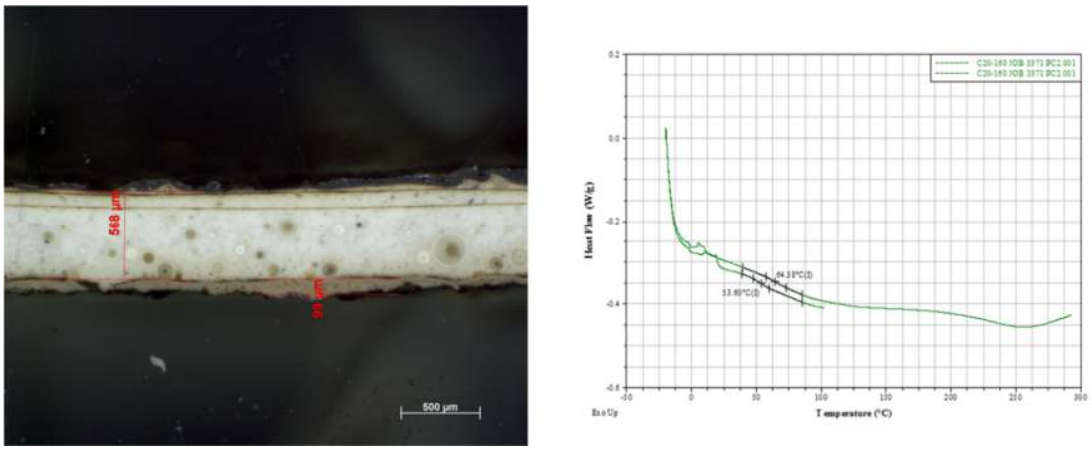

Fig. 4 – Coating layers thickness and DCS analysis

Case 2 – Localized corrosion pipeline – rapeseed/soybean oil

The second case is related to a pipelined used for transport of rapeseed and soybean oils at ambient temperature in a biofuel production site. The pipeline was in intermittent service.
Some localized corrosion phenomena (Fig. 5) occurred at low points in the line (Fig. 6), but at 9 o'clock position (not in the typical 6 o'clock position as in crude oil pipeline).
In the last service period, a higher content of dissolved Fe and TAN was put in evidence in the products.
The laboratory carried-out analysis, among the others, detected the presence of MIC related bacteria (SOB, IRB) in the deposits found in the corroded zones (Fig. 7).
The stagnant fluid in the no-flow period favored MIC corrosion; organic feedstocks reasonably contain a lot of nutrients for MIC related bacteria.
Operating procedures should be changed in order to avoid low(no)-flow periods with product stagnant in the line; the inhibition with biocides could be evaluated.

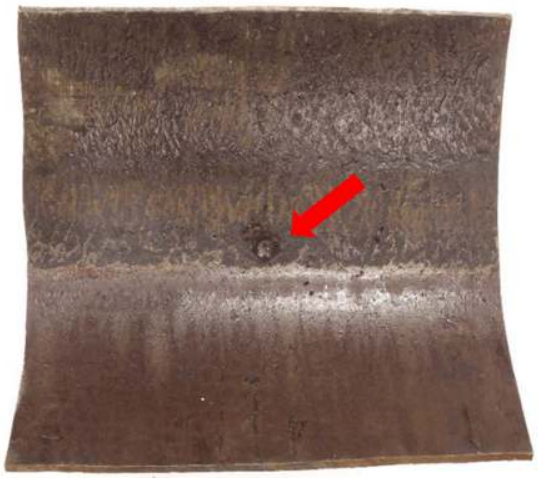

Fig. 5 – Internal view of pipeline sample and position of localized corrosion

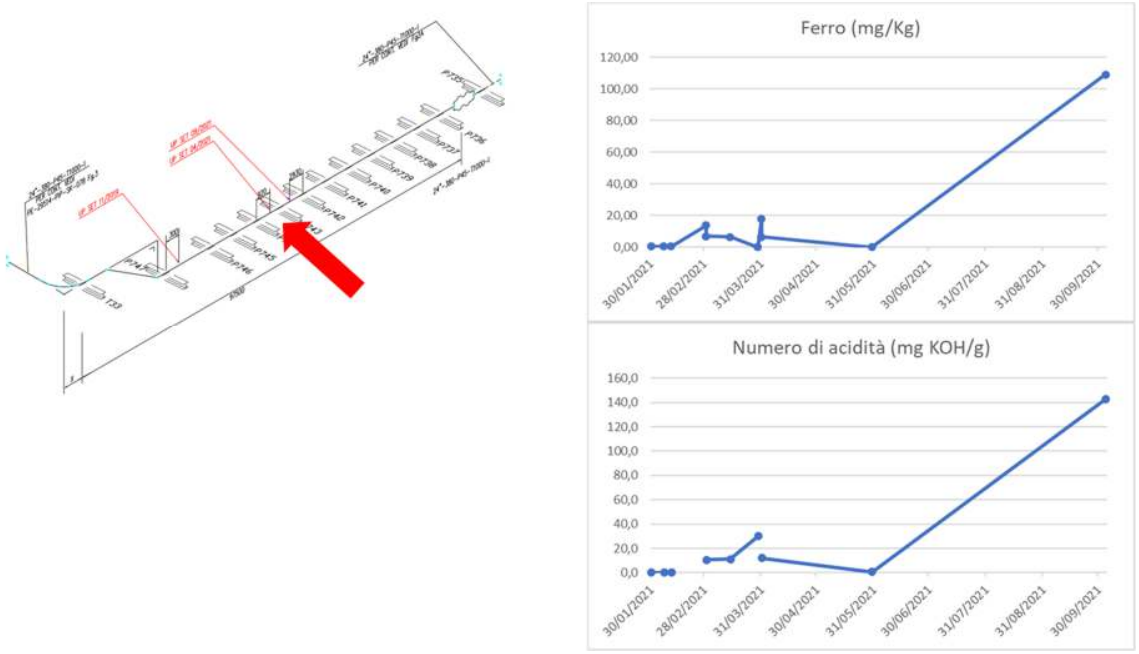

Fig. 6 – Isometric drawings with some data related to dissolved iron (up) and TAN analysis (down).

Sampling code	001 (cells/g)	002 (cells/swab)
Sample specific detection limit	4.9 x10^3	1.7 x10^3
Total Bacteria	9.5x10^6	7.0x10^6
Total Archaea	2.0x10^4	5.4x10^4
Iron oxidizing bacteria (*Gallionella* spp.)	n.d.	n.d.
Iron reducing bacteria (*Geobacter* spp.)	n.d.	1.3x10^4
Sulphate reducing bacteria	n.d.	n.d.
Sulphur oxidizing bacteria	n.d.	4.7x10^5
Sulphur cycling related bacteria	n.d.	n.d.
Methanogene archaea	n.d.	n.d.

Fig. 7 – MIC related bacteria analysis

Case 3 – SCC on piping from pretreatment plants

The third case involve a process piping from phosphoric acid /NaOH treatment Unit. The pipe internal fluid is a biomass (palm oil and waste products) at T= 55-60 °C and P= 1.5 barg; time in service was only 8 months and the construction material is an austenitic stainless steel AISI 304L type.

The performed laboratory analyses (Fig. 9 and Fig. 10) carried out permit to associate the damage phenomena occurred to Stress Corrosion Cracking induced by chlorides (Cl-SCC); entrapped water phase in palm oil and waste products dissolved chloride ions and, at moderate temperature, promoted Cl-SCC on 304 stainless, that is a very susceptible material to this kind of damage.

The material selection shall consider a CRA with greater resistance to Cl-SCC (Duplex/Superduplex SS, Ni-Cr-Mo alloys).

Fig. 8 – Pipe sample internal view; detail of cracks

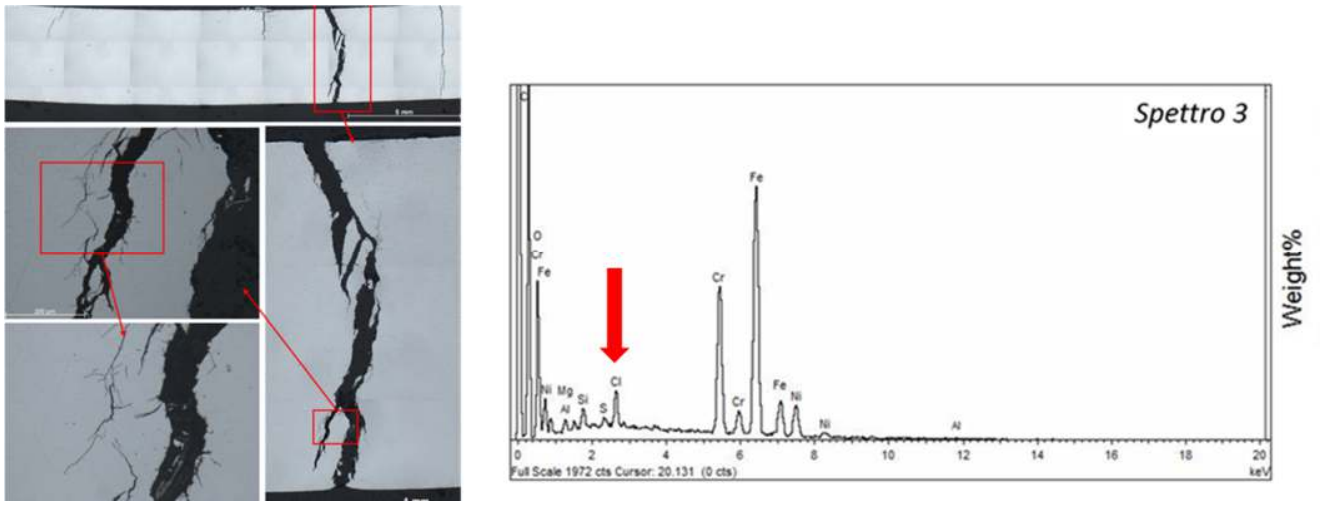

Fig. 9 – Micrographic examination of damaged area and EDS spectra od deposits

Parameter	Value
pH (upH)	6,70
Chlorides (mg/kg)	918
Fluorides (mg/kg)	< 0.5
Phosphates (mg/kg)	< 1
Sulphates(mg/kg)	1671
Nitrates (mg/kg)	9,43
Nitrites(mg/kg)	< 1
Ammonium (mg/kg)	14,5
Calcium (mg/kg)	287
Magnesium(mg/kg)	49
Potassium (mg/kg)	73
Sodium (mg/kg)	370

Fig. 10 –– Water extract analysis from deposits

Case 4 – Selective corrosion of weld in Hydro-processing reactor feed piping

The fourth case is related to a selective internal corrosion of a weld in a hot feed piping from furnace to hydrotreating reactor in a Hydrotreating Unit (Fig. 11). Process fluid is “vegetable oil + hydrogen” (the failure was downstream H_2 injection). Temperature is around 300 °C and pressure 56 barg. The line had been in operation for 3 years and fabricated in AISI 316L type stainless steel.

The damage is in form of a selective local corrosion of weld metal from process side (Fig. 12); chemical analysis performed in corroded weld metal put in evidence the incorrect application of a Mo-free austenitic stainless steel welding consumable (reasonably ER 308 type, related to typical welding consumables for AISI 304 SS).
It is well known that Mo containing Corrosion Resistant Alloys (CRA) offer better resistance to high T corrosion in organic acid and FFA environments (Fig. 13). At the same time, for Biorefinery units it is a matter of debate if the addition of H_2 in feed stream to reactor can inhibit the organic acid and FFA high temperature corrosion for Mo-free SS (as happens in fossil refineries for NAC) [1].
The occurred failure gives practical indication that in HDT Units of biorefinery, H_2 does not inhibit in a significant way the above mentioned corrosion mechanism and, in any case, any selected CRA shall contain Mo.

Fig. 11– Isometric drawing and general view of pipe sample with corroded weld

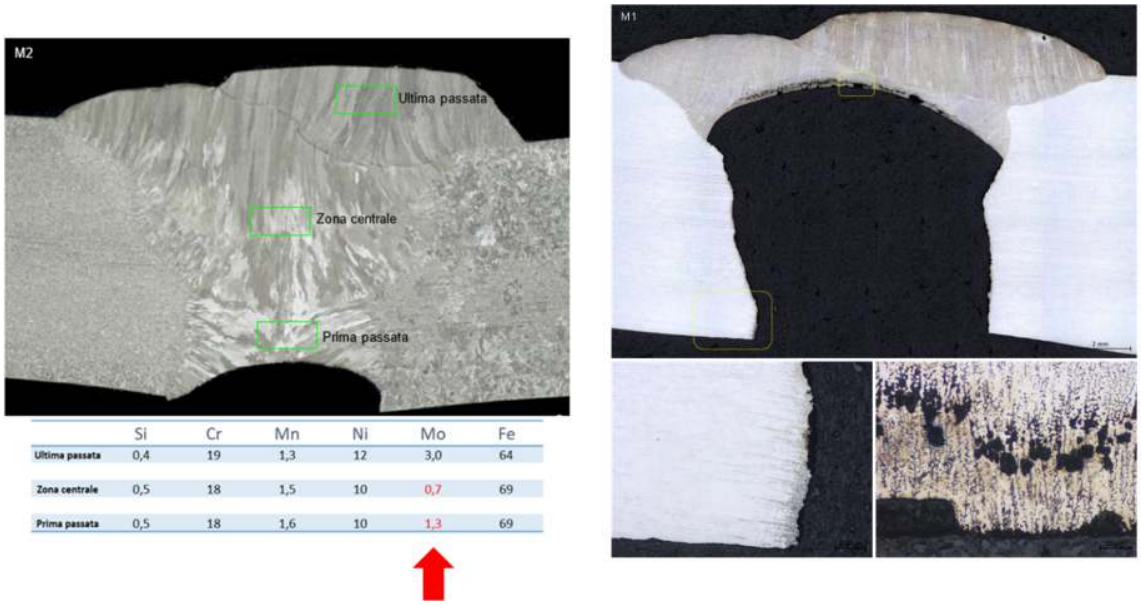

	Si	Cr	Mn	Ni	Mo	Fe
Ultima passata	0,4	19	1,3	12	3,0	64
Zona centrale	0,5	18	1,5	10	0,7	69
Prima passata	0,5	18	1,6	10	1,3	69

Fig. 12 – Micrographic examination and EDS local chemical analysis

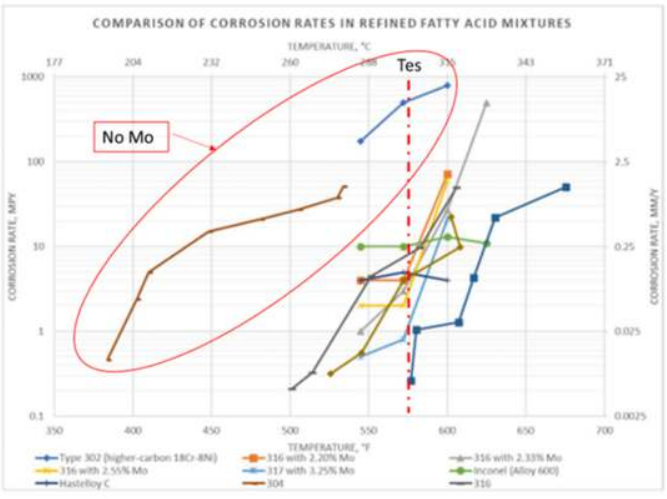

Fig. 13 – Corrosion rate of some CRA in fatty acid environment [2]

Case 6 – Cracking in Alloy 625 reactor effluent line

The present case history is related to the effluent 8" piping from HDT reactor to the first heat exchanger. The piping material is ALLOY 625 Gr. 1 (UNS N06625).
Process fluid is "Hydrocarbon + hydrogen + water", with H_2S and CO_2 present. Temperature is around 355 °C and pressure 32 barg. The piping system had been in service for 18 months.
On some 90° bends, made in ASTM B705 UNS N06625 Cl. 2 Gr. 1, linear through thickness cracks developed in parent metal in any case approximately localized at 7/8 o'clock and oriented at 45° to the longitudinal axis (Fig. 14, 15). Parallel, not-through thickness cracks starting from internal surface are also present (Fig. 16).
For bend with cracks, hardness of parent material was around 350 HV10 and greater.
Cracks are in any case intergranular with little branching (Fig. 17); EDS analysis shows the significant presence of Ni and S (NiS) in the crack (Fig. 18).
The parent material is not sensitized.
The exact damage mechanism at the origin of the cracks is still under investigation. The most likely cause can be associated to stress relaxation phenomena active at service temperature due to residual forming stresses of the bend (hardness is relatively high) and service stress. A similar damage mechanism is reported in literature for air port opening in black liquor recovery boilers (pulp & paper) made in strain hardened 625 alloy with hardness around 36 HRC [3].
The influence of environment can be discussed even though the damage would be eventually high temperature related (sulfur environment) with no liquid water phase present.
Stress relaxation tests in air on strain hardened material specimen is on-going.

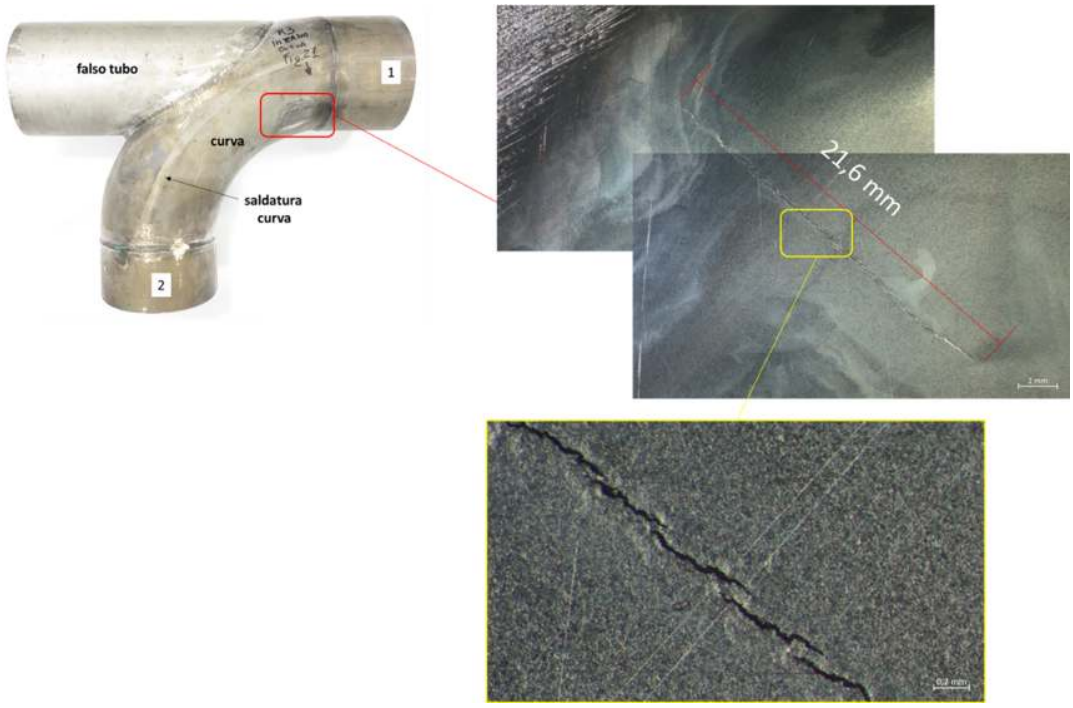

Fig. 14 – View of the pipe sample and position of a crack

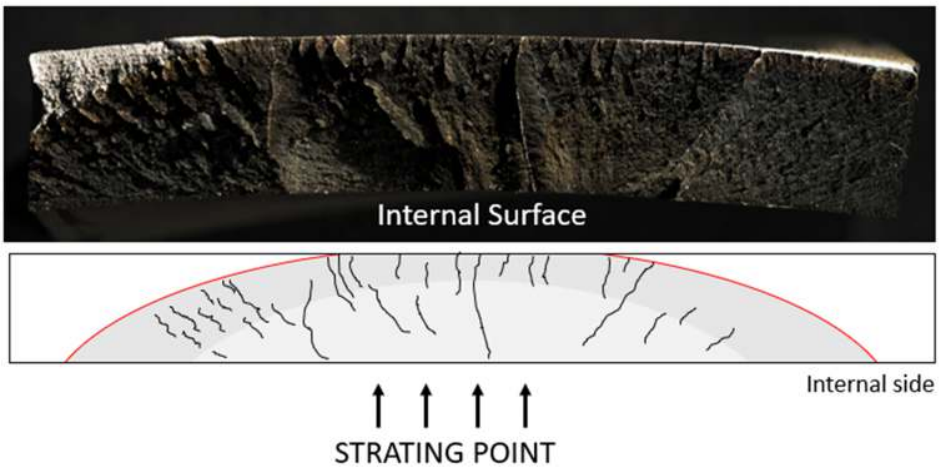

Fig. 15 – Fractographic view of a crack

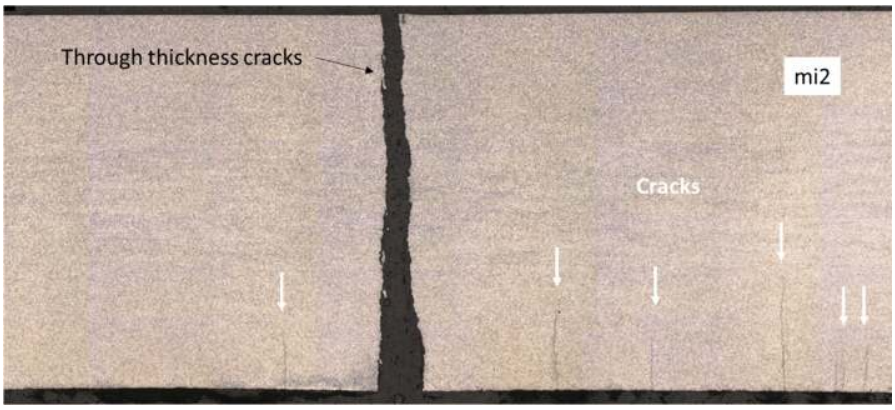

Fig. 16 – Macrographic analysis; details of cracks

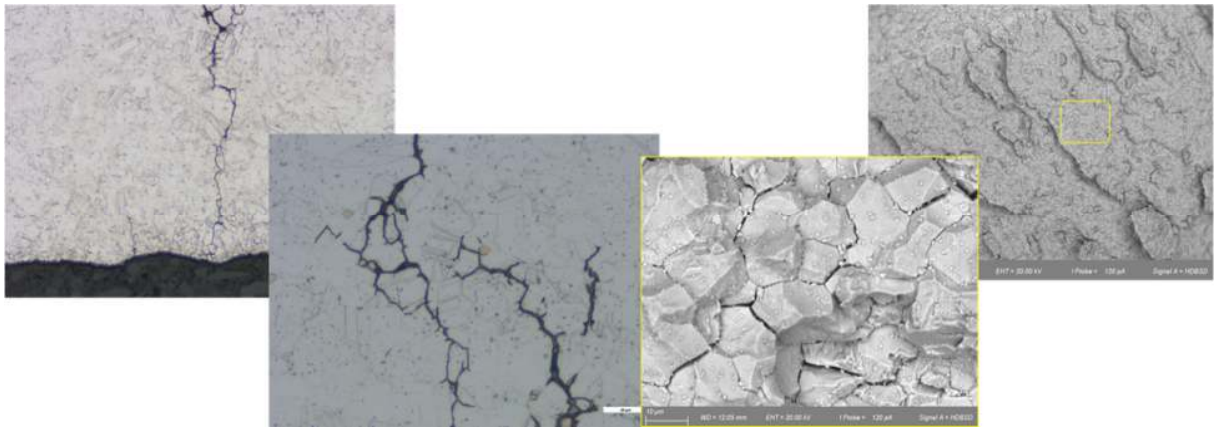

Fig. 17– SEM and micrographic examinations

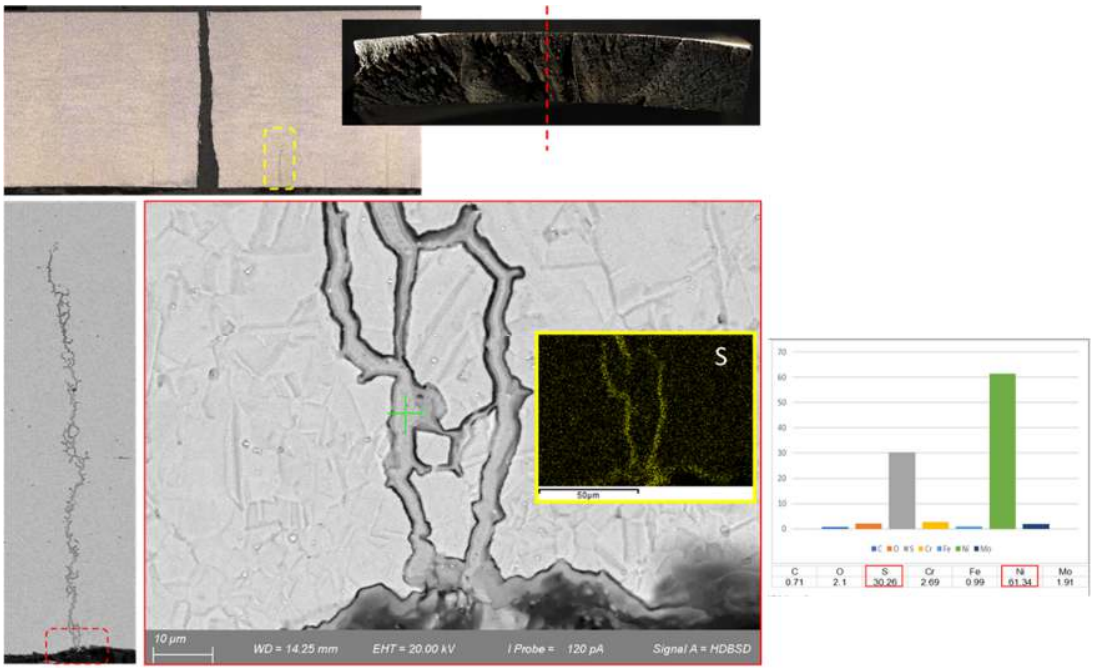

Fig. 18 – EDS analysis of a crack

BIBLIOGRAPHY

[1] Cathleen A. Shargay, Karly Moore and Marty West - Impact of Organic Acid on Materials Selection for Biofuels and Bio-Based Chemical Plants - NACE Corrosion Congress 2014.

[2] Sutton, Kirkham - Converting Hydro-processing Equipment to Produce Renewable Diesel. from Soybean- and Corn Oil: Corrosion and Materials Considerations – AMPP corrosion congress 2022.

[3] G.Y. Lai – High Temperature Corrosion and Materials Applications – ASM International

Evaluation of protective coating for Fuel Cell separator

Caterina Colantoni, Toyota Motor Europe, Zaventem/Belgium;

Stéphane Cotte, Toyota Motor Europe, Zaventem/Belgium;

Corinne Nouvellon, Materia Nova, Mons/Belgium;

Alisson Tromont, Materia Nova, Mons/Belgium;

Thomas Godfroid, Materia Nova, Mons/Belgium;

Purpose:

Method:

Results:

Conclusion:

Aluminum Bipolar Plates in Proton Exchange Membrane Fuel Cells (PEMFCs)

Meisam Dabiri Havigh[1], Kitty Baert[1], Annick Hubin[1], Herman Terryn[1]

1-Vrije Universiteit Brussel, Research Group Electrochemical and Surface Engineering, Pleinlaan 2, 1050 Brussels, Belgium

Fuel cells play a crucial role in the hydrogen based economy since they are considered as a renewable and clean source of energy in different sectors especially transportation systems [1]. One of the big challenges that hinders the wide range application of PEMFCs is their expensive bipolar plates as they are mainly made up of titanium (Ti). To overcome this challenge, aluminum (Al) can be a cost and weight effective alternative. However, the corrosion of Al in harsh working condition of PEMFCs, acidic environment at T≅80 ℃ containing fluoride ions (3 ppm) [2], should be tackled. In the current research, the corrosion barrier properties of bare and multilayer coated AA1050, coated with Ti (on the substrate) and amorphous carbon on top of the Ti layer, is investigated with electrochemical techniques, including Open Circuit Potential (OCP) and Linear Sweep voltammetry (LSV) in the PEMFC working conditions. Surface analysis techniques are also applied to study the morphology of the coating layer before and after electrochemical tests. It is observed that at lower pH values (pH=2 and 3), due to the low activity of fluoride ions, the failure of the coating is because of the acidity of the electrolyte. However, at pH=4, the presence of fluoride ions can interfere and lead to the localized failure of the coating. Aluminum with the present multilayer coating can be a potential alternative for bipolar plates manufacturing if the presence of flaws and defects on the coating is mitigated.

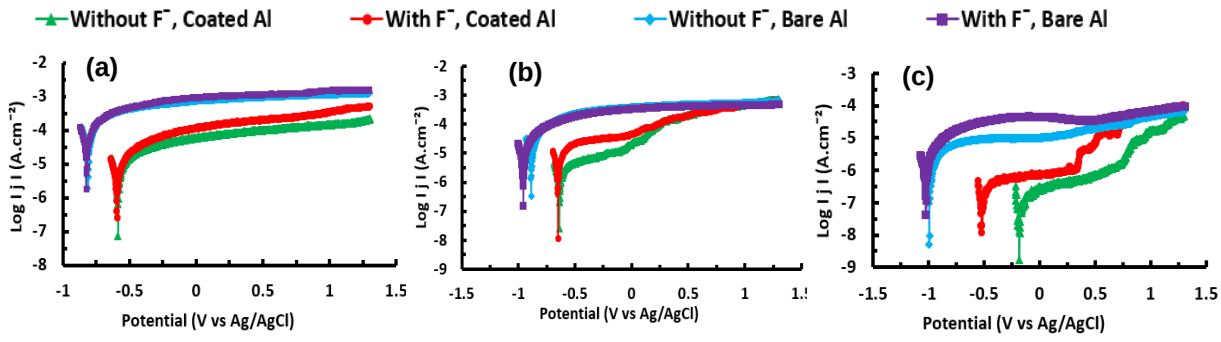

Figure1: LSV measurements for coated and bare AA1050, in the dilute H_2SO_4 electrolytes with a) pH = 2,b) pH = 3 and c) pH = 4, solutions temperature = 80 °C, start potential = 50 mV below OCP, end potential = 1300 mV vs Ag/AgCl, scan rate = 1 mVs^{-1}.

[1] A.-C. Dupuis, Progress in Materials Science, 56 (2011) 289-327.
[2] M.D. Havigh, A. Hubin, H. Terryn, Journal of The Electrochemical Society, 168 (2021) 061503.

Galvanic corrosion of Al-Cu joint bus bars for automotive applications

Rajan Ambat [1,*], Jan Halvor Nordlien [2], Emad Hasan Bartawi [1], Reuben Jacob [1]

[1] Section of Materials and Surface Engineering, Department of Civil and Mechanical Engineering, Technical University of Denmark, Produktionstorvet, Kongens Lyngby, 2800 Denmark

[2] Hydro, Innovation & Technology, Hydrovegen 160, 4265, Håvik, Norway

*Corresponding author: raam@dtu.dk

Abstract

Electrification of automotive requires busbar as an important component for electrical connection between power source to other parts. Due to light weight and high electrical conductivity, Al alloys are most useful for this application, although the bolted end connecting part using aluminium offers high contact resistance due to oxide film. Hence end of the busbars are made of low electrical contact resistance material such as copper especially for high current applications. Therefore, both ends of busbars are usually made of copper welded to aluminium part. Friction stir welding is one possible method used for joining copper to aluminium. However, such joints can be susceptible to galvanic corrosion, while corrosion issues are further enhanced due to electric current passing through the bus bar, which generate a junction potential.

This investigation focus on Al alloy-Copper friction stir welded (FSW) joints mimicking busbars. Busbars are prepared using pure Cu with AA6101 or AA1370 alloys, and effect of FSW microstructure on corrosion performance was investigated. The FSW samples were prepared with various process parameters such as Force, Tool rotation speed, Tool feed rate, and Tool offset. Various corrosion investigations were carried out including Gel test (Agar gel with 0.01M NaCl and universal pH indicator) based on colour development (red for anodic region and blue for cathodic regions), cyclic humidity testing after salt deposition, and electrochemical polarization measurements. For cyclic humidity testing, 50 µg/cm^2 of NaCl was deposited on busbar surface followed by exposure for 72 hours in a climatic chamber using repeated STAGNA Marine condition profile. Electrochemical behavior was studied in 3.5 wt% NaCl solution. Scanning Electron Microscopy (SEM) and Energy Dispersive Spectroscopy (EDS) analysis was used for microstructure and corrosion morphology characterization. Gel test and climatic exposure test showed that corrosion was mainly concentrated on aluminium side of FSW region, while copper acted as cathode. Polarization experiments showed AA6101 is anodically more active than AA1370. Increased force, rotation speed, and tool feed rate during FSW process reduced corrosion of FSW region. Reduction in the tool offset from the aluminium interface also yielded in reduction of anodic activity of the FSW region. Corrosion behaviour was correlated to microstructure produced by the welding process.

Control of corrosion in braking systems of electric (BEV), hybrid (HEV) and plug-in hybrid (PHEV) vehicles

M. Motta[1], M. Zanocco[1], A. Rondinella1, V. Iodice[2], A. Sin[2], L. Fedrizzi[1], F. Andreatta[1]

[1] University of Udine, Polytechnic department of engineering and architecture, Via del Cotonificio 108, 33100 Udine, Italy

[2] ITT Italia S.r.l., Via San Martino 87, 12032 San Martino (CN), Italy

Corresponding author: (M. Motta, E-mail: motta.michele@spes.uniud.it)

Gray cast iron is typically employed for the production of rotors for application in automotive braking systems. Corrosion of the rotors might occur due to exposure of the vehicle to potentially aggressive electrolytes (i.e. wet conditions in the presence of pollutants or exposure to chlorides during winter drive) affecting the efficiency of the braking system. Stiction is an adhesion phenomenon between the friction material of the braking pad and the gray cast iron due to corrosion of the rotor. It typically occurs when the parking brake of a vehicle is activated with an applied static clamping force between the braking pad and the rotor. This might result in damage of the friction material (brake pad), reduced braking performance and even impossibility to drive the vehicle in most severe cases.

The use of corrosion inhibitors is evaluated in this work with the objective of mitigating corrosion attack of gray cast iron rotors in service. In particular, the focus is on the stiction phenomenon, which represents a critical aspect for braking systems of electric (BEV), hybrid (HEV) and plug-in hybrid (PHEV) vehicles.

Complementary electrochemical methods (potentiodynamic polarization and electrochemical impedance spectroscopy), coupled with non-electrochemical methods, are used in order to evaluate effect and inhibition mechanisms of corrosion inhibitors. Moreover, a new electrochemical patented procedure, specifically design to characterize stiction behaviour of non asbestos organic friction materials (NAO), was used in order to characterize the effect of corrosion inhibitors on stiction phenomenon.

Corrosion assessment and composition design of low-electrical conductivity coolants for electric vehicles

L. Sopchenski[1], S. Clerick[2], G. Buytaert[2], S. Lievens[2], A. Hubin[1], H. A. Terryn[1]

[1]Department of Materials and Chemistry, Research Group Electrochemical and Surface Engineering, Vrije Universiteit Brussel, Belgium

[2]Arteco NV, Sint-Denijs-Westrem, Belgium

The thermal management of electric vehicles (EVs) is a complex process that presents extra demands compared to internal combustion engines (ICE). The reduced temperature difference between system and ambient, significant temperature variation during charging, use of new materials in the cooling system, and safety requirements to avoid leak currents from the battery pack are key challenges that must be addressed [1]. For those reasons, the regular anti-freezing coolants used in ICE are being redesigned into low-electrical conductivity coolants to increase electrical safety [2]. Despite the coolant's low conductivity, experimental results reveal that the cooling system remains susceptible to corrosion, asking for the addition of corrosion inhibitors into the coolant composition. The low-conductivity requirement poses constraints both on the selection of corrosion inhibitors and on the corrosion assessments via electrochemical techniques, where the contribution of the ohmic drop cannot be neglected [3,4]. In this study, we present our recent findings on corrosion assessment of reduced/low conductivity coolants. Electrochemical techniques (Potentiodynamic polarization, Linear sweep voltammetry), standard industry tests, and surface analysis techniques were used to investigate the influence of organic/inorganic corrosion inhibitors on the overall conductivity, corrosion protection, and hydrogen evolution in copper and aluminum alloys. Additionally, we discuss the possibility of using cutting-edge electrochemical techniques (odd random phase electrochemical impedance spectroscopy) to unravel the corrosion mechanisms in low-conductive media and push the state-of-the-art of corrosion protection in EVs cooling systems.

1 - Bhosale, A. J., and Vaibhav N. D. “Efficient Ways of Thermal Management of an EV Battery.” Materials Today: Proceedings, September 27, 2022. https://doi.org/10.1016/j.matpr.2022.09.343.

2 - Arteco launches new Coolant for Battery Electric Vehicles Freecor® EV Milli 10. Arteco Coolants. (2022). Retrieved January 11, 2023, from https://www.arteco-coolants.com/en/arteco-launches-new-coolant-battery-electric-vehicles-freecorr-ev-milli-10

3 - Oelßner W, Berthold F, Guth U. “The iR drop - Well-known but often underestimated in electrochemical polarization measurements and corrosion testing.” Mater Corros. (2006), 57(6), 455-466. https://doi.org/10.1002/maco.200603982

4 - Hilbert LR. “Monitoring corrosion rates and localised corrosion in low conductivity water.” Corrosion Science (2006), 48(12), 3907-3923. https://doi.org/10.1016/j.corsci.2006.03.004

FEM to predict corrosion critical conditions in a coating defect on aerospace aluminum alloys

M. Meeusen[1], N. Van den Steen[1], R. Böttcher[2], T. Hack[2], H. Terryn[1]

[1]Vrije Universiteit Brussel (VUB), Research Group Electrochemical and Surface Engineering (SURF), Pleinlaan 2, 1050 Brussels, Belgium
[2]Airbus Central Research and Technology (Airbus CR+T), Willy-Messerschmitt-Straße 1, 82024 Taufkirchen, Germany

Corrosion control of aluminum alloys in the aerospace industry is of high importance to prolongate the service life of aircraft structures. Commonly used high-strength aerospace aluminum alloys such as AA2024 are susceptible to localized corrosion (e.g. pitting corrosion) due to the presence of copper-rich intermetallic particles in the alloy matrix [1]. Therefore, a complex coating system consisting of several (organic) coating layers is usually applied to provide barrier corrosion protection. Dedicated evaluation of these corrosion protective layers is strictly necessary. While laboratory trial procedures and outdoor test programs are personnel and time intensive and accelerated corrosion tests can lead to limited service performance information, predictive modeling of the durability and lifetime of (organic) coated aerospace aluminum alloys under long-term environmental corrosion can provide a promising alternative. Predictive modeling of (organic) coated aerospace aluminum alloys aims to develop a deterministic modeling and simulation concept that allows to forecast the onset of corrosion on relevant micro-defects of a simplified corrosion protection scheme. Furthermore, it allows to generate fundamental understanding of corrosion processes, of important parameters and boundary conditions and constitutes an important first step towards more complex and accurate predictive deterministic and/or hybrid models. The key aspect of this approach is the experimental validation of the predicted conditions in the coating defect.

In this work, a finite element modeling (FEM) approach is employed to model the corrosion critical conditions in a coating defect for coated aerospace aluminum alloys under atmospheric conditions. Hence the heterogeneous microstructure of the aluminum alloy is mimicked into repeated separated homogeneous zones representing the anodic and cathodic surface area spots and as such creating local sources of increased activity. Next to the electrode reactions, relevant homogeneous reactions in the electrolyte are defined. As such the potential and current density distribution in the electrolyte are predicted over time which allows the extraction of relevant corrosion parameters such as the local concentration of corrosive species and pH, to predict corrosion activity. The modeling results are validated by SVET measurements and macroscopic electrochemical techniques.

[1] Visser, P., *Progress in Organic Coatings 99*, 80-90 (2016).

The Needles in the Haystack: An Active Design of Experiments for Accelerated Discovery of Magnesium Corrosion Inhibitors

T. Würger[1], C. Song[1], B. Vaghefinazari[1], A. Lisitsyna[2], P. Fischer[1], G. Wiese[1], M. L. Zheludkevich[1,4,5], S. Albarqouni[2,3], S. V. Lamaka[1], C. Feiler[1,5]

[1]Institute of Surface Science, Helmholtz-Zentrum Hereon, Geesthacht, Germany

[2]Helmholtz AI, Helmholtz Center Munich, Neuherberg, Germany

[3]University Hospital Bonn, University of Bonn, Bonn, Germany

[4]Institute for Materials Science, Faculty of Engineering, Kiel University, Kiel, Germany

[5]Kiel Nano, Surface and Interface Science KiNSIS, Kiel University, Kiel, Germany

As the lightest structural engineering metal, magnesium (Mg) is a promising base material for advanced technology. However, to unlock the full potential of Mg–based materials, precise control over the corrosion rate is important. It was demonstrated that the degradation behaviour can be affected by small organic molecules but identifying such magnesium corrosion inhibitors is not trivial as the size of the chemical space of available compounds is essentially infinite. Hence, identification of novel inhibitors by experimental discovery methods alone is time-, labour- and resource-consuming. Fortunately, computer-assisted methods can be utilised to screen large areas of chemical space with less effort. A fundamental prerequisite to train quantitative structure-property relationship (QSPR) models is the availability of versatile and reliable training data. Here we use small organic molecule corrosion inhibition efficiencies for AZ91 specimen, quantified by a newly developed approach based on profilometer measurements, to train our predictive models. Starting from an initial seed database, we developed an active learning-based workflow to accelerate the discovery of potentially effective compounds. We use the Smooth Overlap of Atomic Positions (SOAP) to encode the molecular structure and to determine the molecular similarities of the compounds in our training dataset. By employing kernel ridge regression (KRR) and kernel principal component analysis (KPCA), the obtained SOAP kernel can be utilized to generate structure-property landscapes that allow to select compounds of interest for further testing from a commercial database of available chemicals. Such test candidates are either selected (i) based on their potential to improve the model performance or (ii) based on their potential to inhibit

corrosion. The compound selection process thereby is complemented by various parameters, such as the prediction uncertainty, solubility and toxicity of the chemical agents. In each iteration of this guided design of experiments approach, yet unknown compounds are predicted by means of KRR, blind tested and then added to the training data for the next iteration whereas the errors and uncertainties of the predictions are used as basis to estimate the impact of active learning. The underlying model becomes exceedingly more accurate with each iteration, while finding potent magnesium corrosion inhibitors in the process. Eventually, the trained model will be able to reliably identify other corrosion inhibitors in the „haystack“ of chemical compounds.

Acknowledgements: All authors gratefully acknowledge financial support from the Helmholtz Artificial Intelligence Cooperation Unit via the AI² project (Grand Agreement ZT-I-PF-5-102). CF and MLZ gratefully acknowledge financial support from the VIPCOAT project (H2020-NMBP-TO-IND-2020, Grant Agreement 952903).

Modeling the Service Life of Corrosion Protection Coatings

Martin van Leeuwen, International Zinc Association, Brussels, Belgium;
Martin Gagné, Zelixir Inc, Toronto, Canada

Life-cycle cost modeling can be used to compare expected performance of corrosion protection systems over the entire life of a steel structure. Life-cycle models consider not only initial application costs, but also future maintenance costs. Critical, however, to the value and validity of the model are the assumptions used for the longevity of various corrosion protection systems and the timing for maintenance interventions. Coating durability guidelines for corrosion protection coatings estimates the time to first maintenance and also provides a schedule for subsequent maintenance actions. Fortunately, many steel structures exist with various corrosion protection coating systems so that cost models can be verified against real-world performance. While guidelines for liquid applied organic coatings compare well with observed real-world performance, estimates for the durability of duplex zinc coatings significantly underestimate the life of the coating, thereby overestimating the life-cycle cost. Real-world performance of organic coatings and duplex zinc coatings will be compared to illustrate the validity and limitations of coating durability guidelines used for life cycle cost modeling.

Key words: Life-Cycle Cost, LCC, Life-Cycle Cost Modelling, Duplex Coating, Zinc Coating

Evaluating organic corrosion inhibitors as chromate replacements through electrochemical experiments

C. Özkan [1], P. Visser [2], A. Cervellera-Dominguez [2], P. Taheri [1], J.M.C. Mol [1]

[1] Department of Materials Science and Engineering, Delft University of Technology, Mekelweg 2, 2628 CD Delft, The Netherlands

[2] AkzoNobel, Rijksstraatweg 31, 2171 AJ, Sassenheim, The Netherlands

The use of chromates in corrosion protective technologies for structural materials in aeronautics is the subject of strict international health and safety regulations since many years. Despite significant progress in this research field, academia and industry are still assessing many different environmentally-friendly and sustainable alternatives to hexavalent chromium: the carcinogenic, mutagenic, reprotoxic, but also the top-performing and well-proven corrosion inhibitor. In our previous work, we have assessed the electrochemical behavior of ~100 small organic molecules using linear polarization resistance, electrochemical impedance spectroscopy and potentiodynamic polarization techniques at different timesteps to obtain a comprehensive electrochemical picture of the first 24 hours of corrosion inhibition for AA2024-T3. In this study, we compare the best performing organic inhibitor candidates from this prior screening with sodium dichromate. 1mM inhibitor - 0.1M NaCl electrolytes demonstrate inhibition efficiencies ~95% for organic inhibitor candidates and 98% for sodium dichromate. Further inhibitor concentration analysis from 0.01 – 10 mM supports this observation, however at higher concentrations chromate outperforms organic inhibitors even more. Increasing concentrations systematically decrease corrosion current densities for sodium dichromate, whereas organic inhibitor protection starts to decrease after 1 mM. Next to the study of direct electrochemical performance, irreversibility of the inhibitor layers is also studied. Initial high performance of an inhibitor does not necessarily lead to long term protection; inhibition must be sustained with an irreversible barrier layer when exposed to aggressive and changing environmental conditions. The results of electrochemical irreversibility experiments suggest that despite the initial inhibition, the majority of the tested organic molecules have reversible bonds that limit their inhibition performance and applicability in dynamic environments. Chromates are also reversible, albeit sustaining a much higher protection compared to the organic compounds.

Acknowledgements

VIPCOAT: H2020-NMBP-TO-IND-2020, Grant Agreement 952903.

Selection of Effective Corrosion Inhibitors for Aluminium Alloys based on Data-Driven Techniques

Lisa Sahlmann[1], Christian Feiler[1, 3], Natalia Konchakova[1], Can Özkan[2], Peyman Taheri[2], J.M.C. Mol[2], Daniel Höche[1], Mikhail L. Zheludkevich[1, 3, 4]

[1]Helmholtz-Zentrum Hereon, Geesthacht/Germany;

[2]Delft University of Technology, Delft/The Netherlands

[3]Kiel Nano, Surface and Interface Science KiNSIS, Kiel University, Kiel/Germany

[4]Institute for Materials Science, Faculty of Engineering, Kiel University, Kiel/Germany

The replacement of highly protective but toxic hexavalent-chromium-based corrosion inhibitors with novel, safer and more cost efficient inhibitor chemistries for aluminum (Al) alloys is urgently required. Fortunately, small organic molecules have emerged as safe and potent alternatives showing promising corrosion inhibition for Al alloys and other materials [1]. Experimental techniques alone can only screen a tiny fraction of the vast chemical space of available compounds (~10^{63}) despite tremendous progress in the screening of potential corrosion inhibitors by efficient high throughput techniques. If a sufficiently large and chemically diverse training dataset is available, quantitative structure-property relationship (QSPR) models offer the opportunity to preselect a short list of promising candidates for experimental testing without in-depth knowledge of the underlying chemical mechanisms.

In this work, we used a set of small organic molecules to develop a data driven model to predict their corrosion response for AA2024-T3. A key step in the development of such models is the generation of molecular descriptors that are used as input features, which can either be derived directly from the molecular structure, from atomistic simulations or be obtained from experimental investigations. The molecular descriptors are analysed for their relevance to the corrosion response of the small organic molecules using recursive feature elimination [2]. Several supervised machine-learning models (e.g., artificial neural networks and random forests), were subsequently developed using the selected molecular descriptors as input. It is noteworthy, that some of the molecular descriptors derived from density functional theory calculations and the available experimental information were determined as relevant to model the target corrosion inhibition metric by the employed sparse feature selection technique.

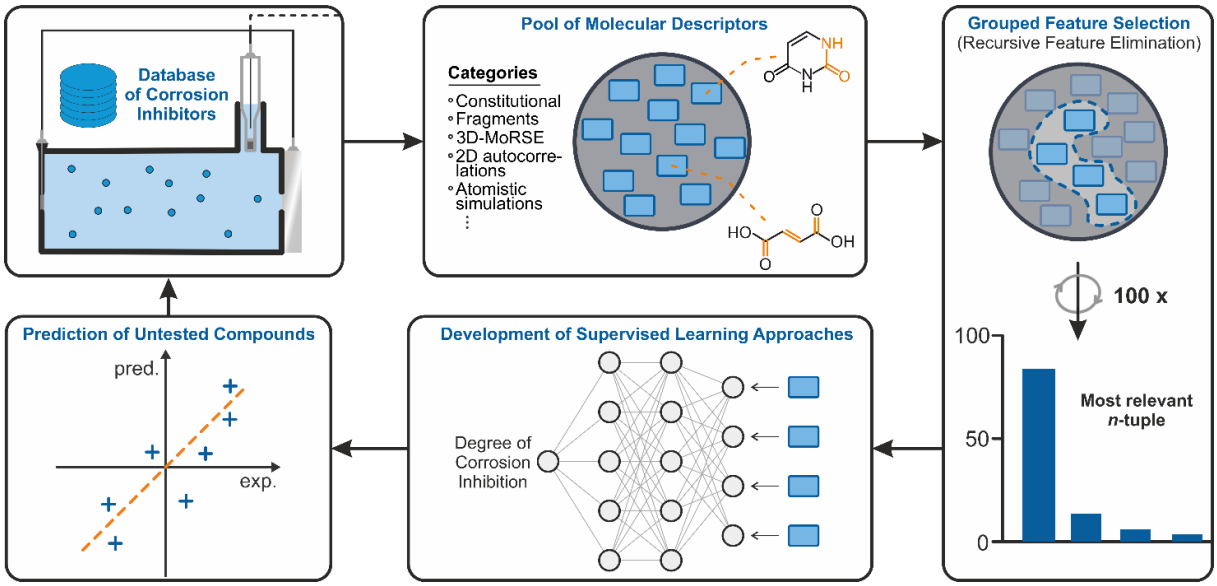

Figure 1: Schematic representation of the used machine learning pipeline.

In this study, we demonstrate that the combination of descriptors that encode the molecular structure with those obtained from atomistic simulations and experiments improves the accuracy of the prediction compared to those models that only use structural input features. Finally, the performance of the trained QSPR models was assessed by predicting the performance of chemicals that have not been used for training of the models and subsequent experimental testing. The additional datapoints obtained from the blind test were subsequently used to augment the training database to probe how active learning affects the robustness and accuracy of the predictions.

Acknowledgements: The VIPCOAT project: H2020-NMBP-TO-IND-2020, Grand Agreement 952903.

[1] D.A. Winkler, M. Breedon, P. White, A.E. Hughes, E.D. Sapper, I. Cole, Using high throughput experimental data and in silico models to discover alternatives to toxic chromate corrosion inhibitors*, Corros. Sci. 106* (**2016**) 229-235.

[2] E.J. Schiessler, T. Würger, S.V. Lamaka, R. H. Meißner, C. J. Cyron, M. L. Zheludkevich, C. Feiler, R. C. Aydin, Predicting the inhibition efficiencies of magnesium dissolution modulators using sparse machine learning models, *npj Comput. Mater. 7* (**2021**) 193.

A modelling approach for the study of aluminum alloy AA2024 corrosion protection through the use of active coatings

N. Abdelrahman[1], P. Meuris[2], N. Van den Steen[1], C. Özkan[3], C. Wang[5], C. Song[5], P. Visser[4], S. V. Lamaka[5], T. Hack[6], P. Taheri[3], J.M.C. Mol[3], B. Van den Bossche[2], H. Terryn[1,3], T. Hauffman[1]

[1] Department of Materials and Chemistry, Research group Electrochemical and Surface Engineering, Vrije Universiteit Brussel, Pleinlaan 2, 1050 Brussel, Belgium

[2]Elsyca NV, Campus Remy, Vaartdijk 3, 3018 Leuven, Belgium

[3]Department of Materials Science and Engineering, Corrosion Technology and Electrochemistry group, Delft University of Technology, Mekelweg 2, 2628 CD Delft, The Netherlands

[4]AkzoNobel, Rijksstraatweg 31, 2171 AJ, Sassenheim, the Netherlands

[5]Institute of Surface Science, Helmholtz-Zentrum Hereon, 21502 Geesthacht, Germany

[6]Airbus Central Research and Technology, Willy-Messerschmitt-Straße 1, 82024, Taufkirchen, Germany

Nowadays, aluminum alloys (AAs) are among the main structural materials in the aeronautical industry. While representing high-strength and low-weight properties, their microstructural complexity and heterogeneity makes them highly susceptible to local corrosion. Therefore, a corrosion protective coating is required. Chromium based inhibitors incorporated in organic coatings have proven to be an efficient solution to protect Aluminum structures. However, given their toxicity and carcinogenic nature, their usage is currently subject to strict international environmental, health and safety legislation. Therefore, the need exists for a safe and efficient replacement. In recent years, multiple corrosion inhibitor types have been shown to be highly promising. Further studies are essential to understand an inhibitor's function and limits in different environments. However, such extensive experiments would be time consuming. Alternatively, modelling has been considered to offer a faster path for insights into an inhibitor's efficiency [1].

This work presents a 2D finite element Multi-Ion Transport and Reaction model [2] simulating the function of active protective coatings. Model geometry is a defect through the protective coatings exposing the metal surface. Electrolyte varying

composition as well as the expected interactions among the inhibitor and the different species within electrolyte are considered. The electro-chemical reactions occurring between the inhibitor and the alloy are suggested. Their kinetic coefficients in the Butler-Volmer equation are fitted using the data obtained from linear sweep voltammetry measurements. The leaching mechanism of the inhibitor within the coating is described. Concentrations of the different species, as well as potential and current changes over the surface, are calculated. Results are validated using surface scanning probe techniques which recorded the changes in species distribution, pH, alloy surface potential and current density.

REFERENCES

[1] Dolgikh, Olga, et al. ”Corrosion protection of steel cut-edges by hot-dip galvanized Al (Zn, Mg) coatings in 1 wt% NaCl: Part II. Numerical simulations.” Materials and Corrosion 70.5 (2019): 780-792

[2] Abodi, Levente-Csaba, et al. ”Modeling localized aluminum alloy corrosion in chloride solutions under non-equilibrium conditions: steps toward understanding pitting initiation.” Electrochimica acta 63 (2012): 169-178

Acknowledgments: VIPCOAT: H2020-NMBP-TO-IND-2020, Grant Agreement 952903

RMIT Classification: Trusted

A state-of-the-art approach to addressing the missing ingredients of molecular modelling applied to corrosion inhibition

Ivan Cole[a], *Jose Maria Castillo-Robles*[a,b], *Ernane F. Martins*[a,b], *and Pablo Ordejón*[b]

[a]RMIT University, Melbourne/Australia; [b]ICN2, Barcelona/Spain

The use of more environmentally friendly small organic molecules to replace the toxic inorganic ones frequently used as corrosion inhibitors has received much attention in the past few years. However, the underlying mechanisms determining their inhibition performance are still far from understood. Molecular modelling can be used to gain atomistic insights into those mechanisms, paving the way for understanding which properties an inhibitor must have to act as a suitable corrosion inhibitor, which allows for the rational design/search of new and more efficient inhibitors [1,2].

When modelling corrosion inhibition (CI), one should consider the following aspects: (1) the inhibitors' structural and electronic properties, (2) the chemistry and adsorption energies of inhibitors on the surface, (3) the surface model, (4) the effect of the anodic and cathodic zones on the surface, (5) the solvent effects, and (6) the electrodes' potential effects and how they shape the inhibitor-inhibitor and the double layer interactions. However, molecular modelling applied to CI is frequently underexplored or follows a standard recipe. The main focus is usually to compute molecular properties (aspects 1 and 2) used in models like the quantitative structure-activity relationship (QSAR).

In that manner, aspects 1-3 are more frequently addressed in the literature. However, most works miss aspects 4-6, which are vital to understanding the inhibitors' CI mechanisms. Here our objective is to use a state-of-the-art approach to tackle precisely those gaps. We combine the non-equilibrium Green's functions (NEGF) formalism [3,4] with the hybrid quantum mechanics/molecular mechanics (QM/MM) method [5] to include the electrode potential effects while fully accounting for the solvent. All that is available in the SIESTA code [6,7], an ab-initio software well-established in materials science that allows for efficiently simulating systems containing thousands of atoms.

In the NEGF approach, an electronic transport setup is used to shift downwards/upwards the electrodes' chemical potential, which approaches the design used experimentally. Accounting for explicit solvent can be prohibitive in terms of

computational cost. In that way, the hybrid QM/MM method allows for cost-effective solvent treatment, where the system is split into QM and MM subsystems. Therefore, the solvent atoms can be described via a classical force field, while a full QM approach is used to the metallic surface and the inhibitors attached to it.

To demonstrate our approach, we have studied the interaction between 2-mercaptobenzoimidazole (MBI) and Cu (111) surfaces under different concentrations and voltages applied to the electrodes using the NEGF formalism. The adsorption energies demonstrate that the system gets more stable as we increase the molecules' concentration, maximizing the surface coverage and forming a self-assembled monolayer. Our results also show that the adsorption energies are sensitive to the voltage we apply, presenting a parabolic dependence. We also assessed the charge redistribution due to the adsorption process and the voltage applied, showing that both lead to significant changes.

We have also investigated the behaviour of water molecules in contact with electrified interfaces via the NEGF-QM/MM approach. We used Au (111) surface as it is widely reported in the literature, allowing us to benchmark our findings. Our results show that the water molecules, especially the interfacial ones, are susceptible to the voltage applied to the electrodes. We observed an increase in the H atoms close to the negatively charged surface, with the OH bond vectors pointing to the surface. Finally, we demonstrate that the new method's performance leads to up to 5 times faster sampling, allowing for more extended MD simulations in systems containing a substantial amount of atoms.

In conclusion, the proposed NEGF-QM/MM approach presented here represents a significant step forward in modelling electrochemistry, which we demonstrate can be successfully applied in CI. This approach will provide us with data that, coupled with artificial intelligence methods, might construct the bridge between the nanoscale CI modelling and the continuum scale of the CI processes.

[1] Chen et al., Materials Design, 112, 410 (2016); [2] Gharbi et al., NPJ Materials Degradation 2, 2 (2018); [3] M. Brandbyge et al., Phys. Rev. B 65, 165401 (2002); [4] N. Papior et al., Computer Physics Communications 212, 8 (2017); [5] C. F. Sanz-Navarro et al., Theoretical Chemistry Accounts 128, 825 (2011); [6] J. M. Soler et al., Journal of Physics Condensed Matter 14, 2745 (2002); [7] A. García et al., The Journal of chemical physics 152, 204108 (2020).

Geometric modelling of the microstructure of active protective coatings: Fitting germ grain models based on SR-nano-CT image data

Katja Schladitz[1], Peter Klein[1], Benedict Grevelhörster[2],

Peter Visser[3], Natalia Konchakova[4]

1 Fraunhofer-Institut für Techno- und Wirtschaftsmathematik ITWM, Kaiserslautern/Germany

2 Rheinland-Pfälzische Technische Universität Kaiserslautern-Landau RPTU, Germany

3 AkzoNobel, Sassenheim/The Netherlands

4 Helmholtz-Zentrum Hereon, Geesthacht/Germany

An effective and commonly applied means of corrosion protection is the use of coatings containing corrosion inhibiting pigments. Damage exposes the coating to the environment, moisture is absorbed, and as a consequence the pigments dissolve releasing inhibiting molecules into the defect. This way, the corrosion protection is renewed. This complex leaching process depends critically on chemical composition and concentration of the inhibitors. The VIPCOAT project aims at creating a platform for facilitating the development of environmentally friendly active protective coating formulations and optimizing them. Numerical simulation of the leaching process within 3D models of the coating microstructure is one way to achieve this. To this end, the morphology and spatial distribution of the corrosion inhibiting particles within the matrix have to be observed and modeled geometrically.

So-called stochastic germ grain models allow to generate real virtual corrosion inhibitor particle populations, driven by just a couple of parameters. A challenge is however, to fit such a model to a real particle system. Proper modeling of the particle shape requires spatial geometric information at the nano-meter scale. Nano-tomography using synchrotron radiation can image complex corrosion inhibitor particle systems spatially. Segmentation of individual particles is however a major challenge. In this contribution, we show how to nevertheless fit a germ grain model with typical grains being cells from a Voronoi tessellation.

Acknowledgment: VIPCOAT: H2020-NMBP-TO-IND-2020, Grant Agreement 952903, and Research Initiative of the Federal State of Rhineland-Palatinate through the priority area Mathematics Applied to Real-World Problems (MathApp)

Following inhibitor dissolution from a coating matrix using in-situ synchrotron radiation nano-tomography

P. Visser[1], K. Schladitz[2], B. Grevelhörster[2,3], P. Klein[2], N. Konchakova[4]

1 AkzoNobel, Sassenheim, The Netherlands

2 Fraunhofer-Institut für Techno- und Wirtschaftsmathematik ITWM, Kaiserslautern/Germany

3 Rheinland-Pfälzische Technische Universität Kaiserslautern-Landau RPTU, Department of Mathematics, Kaiserslautern/Germany

4 Helmholtz-Zentrum Hereon, Geesthacht/ Germany

Active protective coatings act as a reservoir of corrosion inhibitors to provide protection by the release of corrosion inhibitors (leaching) when the coating is damaged. Leaching is a very complicated process and optimization for long-term corrosion protection is labor intensive.

The VIPCOAT project aims to develop a model to simulate and predict the release of corrosion inhibitors from a coating matrix. The model will be based on a combination of stochastic geometry models and numerical simulations of the dissolution of inhibitor particles and diffusion processes. The simulation of the inhibitor release from the coatings will reduce iterations and accelerate the development of active protective coatings with optimal corrosion protection performance.

Understanding the spatial distribution of the inhibitor particles in the coating matrix and changes due to the leaching process are essential for the development and validation of such a model.

In this study, synchrotron radiation nano-tomography was used to capture the coating microstructure and follow the dissolution of corrosion inhibiting particles in-situ. A special cell was designed to place the coating sample in a water flow to study the changing coating microstructure over time.

The results of this study, combined with inhibitor leaching studies, are used as input for the 3D geometric model and numerical simulations to construct a realistic computational model describing the release of corrosion inhibitors from a coating. Such a digital reconstruction of coating matrices and simulating the leaching will provide a new tool to design and optimize novel active protective coating systems.

Acknowledgment: VIPCOAT: H2020-NMBP-TO-IND-2020, Grant Agreement 952903, and Research Initiative of the Federal State of Rhineland-Palatinate through the priority area Mathematics Applied to Real-World Problems (MathApp)

Surrogate modelling of corrosion inhibitor leaching

P. Klein[1], P. Visser[2], K. Schladitz[1], M. Burgard[1,3], B. Grevelhörster[1,3], N.Konchakova[4]

1 Fraunhofer-Institut für Techno- und Wirtschaftsmathematik ITWM, Kaiserslautern/Germany
2 AkzoNobel, Sassenheim, The Netherlands
3 Rheinland-Pfälzische Technische Universität Kaiserslautern-Landau RPTU, Kaiserslautern/Germany
4 Helmholtz-Zentrum Hereon, Geesthacht/ Germany

Active protective coatings contain corrosion inhibiting pigments, which, when in contact with water, release (leach) the corrosion inhibiting species into a defect of a coating. The VIPCOAT project develops a microscale model with the idea to directly simulate the mobilization of the corrosion inhibitors from the pigments using thermodynamically consistent descriptions, and their subsequent diffusion through a coating matrix into a defect area. This microscale simulation model will be initialized by virtually generated microstructures constructed by a stochastic geometry generator, calibrated against 3D images obtained by synchrotron radiation computed tomography (CT).

This simulation approach will get validated against in-situ synchrotron CT leaching experiments on the one hand. On the other hand, a surrogate leaching model with much lower computational complexity will be parametrized and used in system simulations, for example as input in (electro-)chemistry models on metallic surfaces. This approach will allow for a systematic optimization of corrosion inhibition since the influence of tunable coating parameters can get evaluated fast.

This contribution describes the VIPCOAT surrogate leaching model for soluble pigments using dimensional analysis (Buckingham-Π Theorem) in an effective medium approach. The effective transport parameters will be calculated using ether the microstructure simulation or fitted against experiments. The validity of this approach will be demonstrated by fitting in-situ observed leaching and by leaching experiments which do not provide insight into the leaching mechanisms but measure essentially the amount of leached inhibitors from-free standing coatings into water.

Acknowledgment: VIPCOAT: H2020-NMBP-TO-IND-2020, Grant Agreement 952903, and Research Initiative of the Federal State of Rhineland-Palatinate through the priority area Mathematics Applied to Real-World Problems (MathApp).

Epoxy-amine segregation at a solid surface

Kieran Harris, Department of Chemical Engineering, University of Manchester, Manchester UK

Charlie Wand, Lecturer in Natural Sciences, Department of Physics & Astronomy, University of Exeter, UK

Peter Visser, AkzoNobel, Sassenheim, NED

Flor R. Siperstein, Department of Chemical Engineering, University of Manchester, Manchester UK

Epoxy resins are commonly used as anticorrosive coatings and structural components due to their adhesive properties, mechanical strength, as well as their chemical and heat resistance. In general, they are prepared by mixing an epoxy precursor with an amine crosslinker at a stoichiometric ratio. Segregation of the components in the mixture can be observed when applied on a solid surface, leading to inhomogeneities in the coating that can affect its performance. The aim of this work is to understand the molecular level phenomena that leads to segregation of a model epoxy-amine system made of DGEBA (Diglycidyl ether bisphenol A) and MXDA (m-Xylylenediamine) on different iron oxide surfaces (hematite, magnetite and goethite).

Molecular dynamics simulations were performed using the LAMMPS[1] software. DGEBA and MXDA were described using the OPLS-AA force-field[2] and the solids were described using the CLAY-FF[3] with the positions of the atoms taken from crystallographic data. Systems containing 600 molecules were modelled starting from a random configuration and allowing the system to equilibrate.

Density distributions calculated perpendicular to the solid surface showed the formation of a contact layer in all cases, where MXDA is preferentially adsorbed regardless of the composition. For an overall stoichiometric mixture with a MXDA:DGEBA ratio of 0.5 (2 DGEBA molecules per each MXDA molecule), the contact layer has MXDA:DGEBA ratios between 1-1.4, which is a significant excess

---

[1] Thompson, A. P., Aktulga, H. M., Berger, R., *et al.* (2022). *Computer Physics Communications*, *271*, 108171.

[2] Jorgensen, W. L., Maxwell, D. S., & Tirado-Rives, J. (1996). *Journal of the American Chemical Society*, *118*(45), 11225–11236.

[3] Cygan, R. T., Liang, J.-J., & Kalinichev, A. G. (2004). *The Journal of Physical Chemistry B*, *108*(4), 1255–1266.

with respect to the bulk stoichiometric ratio. It was also found that most MXDA molecules adsorb with both amine groups facing the surface in hematite and magnetite, but about a third of the adsorbed MXDA in goethite only adsorbs with one amine group next to the surface and the other facing the bulk (Figure 1). In general, it was found that in a stoichiometric mixture, most DGEBA molecules adsorb only with one epoxy group on the surface, and that the proportion of fully adsorbed DGEBA molecules is larger in hematite and magnetite than in goethite.

Although our simulations do not consider the formation of bonds between the amine group and the metal oxide, the strong preference of the amines to the surface could lead to a reduction in crosslink density near the surface due to stearic hinderance preventing the DGEBA to come sufficiently close to the adsorbed MXDA, which is consistent with experimental observations.[4] The MXDA:DGEBA ratios are very similar at hematite and magnetite surfaces, and slightly larger on goethite, consistent with the difference in the molecular configurations at the surface. The difference in configuration of the adsorbed MXDA in goethite could suggest that a higher crosslink density can be achieved on this surface when compared to hematite or magnetite.

This work provides new insight on the molecular level structure of epoxy-amine films that are used in corrosion protection applications, that can help understanding the differences in performances when a film is applied on different surfaces, or when different filler particles are used.

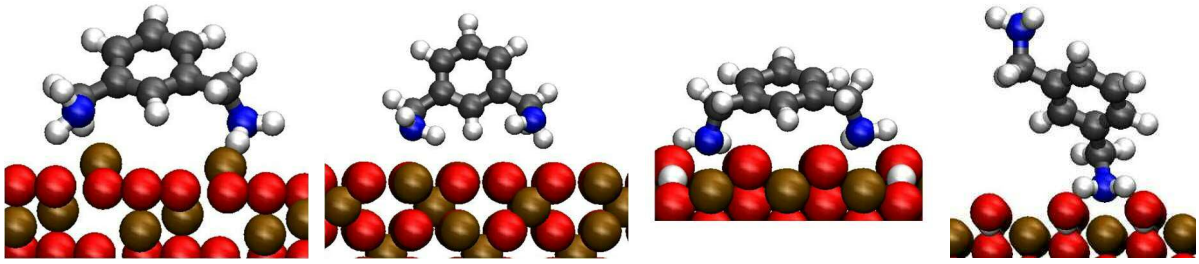

(a) (b) (c) (d)

Figure 1. Sample conformations of MXDA with two amine groups adsorbed on (a) hematite, (b) magnetite, and (c) goethite, and with only one amine group adsorbed on (d) goethite.

[4] Morsch, S., Wand, C. R., Emad, S., *et al.* (2022). *Journal of Colloid and Interface Science*, *613*, 415–425.

Multi-scale modeling for recycled metal pretreatment

Cheng Zhu[1], Krishan Kanhaiya[1], Hendrik Heinz[1], Stephan Koehler[2], Eduard Schreiner[2], Sabine Hirth[2], Tobias Urban[2], Patrick Keil[3], Nawel S. Khelfallah[4], Ratan K. Mishra[2]

[1] Department of Chemical and Biological Engineering, University of Colorado Boulder, Boulder, CO 80303-0596, USA
[2] BASF SE, Carl-Bosch-Strasse 38, 67056 Ludwigshafen am Rhein, Germany
[3] BASF Coatings GmbH, Glasuritstrasse 1, 48165 Muenster, Germany
[4] Chemetall GmbH, Trakehner Strasse 3, 60487 Frankfurt am Main, Germany

Aluminum alloys are very important materials in automotive, aerospace, and construction industries. Major efforts have been devoted to developing corrosion resistance techniques of these materials to extend the lifetime of products and reduce the cost. Multi-scale modeling can provide essential understanding of the mechanisms of corrosion and protection, which has motivated intensive research attempts in the past decades. To perform the multi-scale simulations, inputs from atomistic scale modeling are used as a natural starting point for meso-scale models. Unfortunately, up to now, there is still limited research using molecular dynamics simulations with reliable and flexible models, which hinders the understanding and development of the field. Here, we report the development of atomistic models of Al_2O_3 and related oxyhydroxides using Interface Force Field (IFF). The advantages of IFF lie in the following aspects: (1) non-bonded models with few parameters (charge, bond, and non-bond settings), (2) flexibility and availability to distinct phases of Al_2O_3 and oxyhydroxides with only one set of parameters, (3) high accuracy of estimations of structural and interfacial properties, and (4) considerations of real surface chemistry under various pH conditions.

With the developed models, we realize the estimations of adsorption of corrosion inhibitor molecules on the Al alloys and composite materials, which not only provides insights into the mechanisms of the corrosion process, but also helps screen potential corrosion inhibitors to further improve the current industrial treatment process. This method helps to screen functional groups with recycled alumina for better interactions as well as to understand the interaction mechanisms between corrosion inhibitors and characterized metal oxide surfaces.

The development of modeling capabilities towards metal pretreatment allows us to improve the compatibility of sustainable polymers to recycled metals. For recycled alumina, both surface reactivity and composition could vary significantly. New conversion coatings could compensate for the higher susceptibility towards corrosion. Gain knowledge on recycled alumina surface and the interaction of corrosion inhibitor/polymer with the recycled products will help us to apply in several metal and composite materials. Therefore, a combination of surface analysis methods like X-ray-photoelectron spectroscopy, time-of-flight secondary ion mass spectrometry, and the various types of electron microscopy as well as application data with the modeling methods is required to achieve this goal.

PeriConto -- A knowledge graph-based tool to efficiently look up formulations of coating products

Vinay Gautam and Heinz A. Preisig

Department of Chemical Engineering, NTNU , Trondheim, Norway

VIPCOAT aims to develop a platform for innovating new coated products. Coatings are complex systems consisting of several chemical components and materials, making it challenging to design new coating products. The coating industry mainly depends on the knowledge of experts when it comes to developing new coating formulations. Coating experts and industrial users need help to search for information related to coating ingredients that are primarily available in the form of datasheets from various online and offline sources.

One of the objectives of the VIPCOAT is to solve this issue by developing an ontology-backed information system to aid coating experts and industrial users in efficiently searching information related to coating ingredients, recipes and formulations. The utilised technology is non-traditional as we build the database as a knowledge graph, making it easier to scale up as more data is added. The knowledge graph provides flexibility for adding new taxonomies and relations between terms and subgraphs. It provides a highly-structured interface for the user providing coating information, including coating formulation, properties and performance.

We aim to make the tool available to the coating community, encouraging users to add information to share and provide the capability of seeking new combinations yielding new products that satisfy the ever-changing condition and regulations.

Acknowledgment: VIPCOAT: H2020-NMBP-TO-IND-2020, Grant Agreement 952903.

Data acquisition and transfer using VIPCOAT OIP as a B2B2B Environment

N. Konchakova[1], M. Horvat[2], T. Hagelien[3], H.A. Preisig[4], F. Maia[5], L. Sahlmann[1], C.Feiler[1], C. Özkan[6], A. Mol[6], P.Visser[7], and P. Klein[8]

[1] *Helmholtz-Zentrum Hereon, Geesthacht/ Germany*

[2] *WIKKI LIMITED, London / United Kingdom*

[3] *SINTEF, Trondheim/ Norway*

[4] *NTNU, Trondheim/ Norway*

[5] *Smallmatek - Small Materials and Technologies Lda, Aveiro/ Portugal*

[6] *Delft University of Technology, Delft/ The Netherlands*

[7] *AkzoNobel, Sassenheim/ The Netherlands*

[8] Fraunhofer Institute for Industrial Mathematics, Kaiserslautern/ Germany

The VIPCOAT[1] project aims to establish an interoperable innovation framework, focused on the modeling supported development of novel green active protective coatings. To provide targeted digital services for end-users, an interoperable data & knowledge exchange at the platform should be organized and ensure in an automated way. Proper data documentation facilitates interoperability, management and reusability of material data collected by different experimentalists, used and processed by modelling specialists and transferred through a digital environment like Open Innovation Platforms (OIP).

Design and implementation of a data catalog (DCAT) for active protective coatings support the findability aspect of the FAIR principle. DCAT is an RDF vocabulary for sharing data catalogs on the web. The VIPCOAT consortium applied the technology for the platform implementation and B2B2B relationship utilization at the OIP.

This contribution demonstrates an approach for data documentation needed to facilitate the interoperable sharing of data resources among (industrial) organizations, researchers, government bodies, and society. DCAT handles description of metadata for many data formats using for both modeling and decision support services.

Requirements and the OIP features are demonstrated for use cases of protective additives and inhibitor delivery. The best practice in the DCAT design and utilization, as well as the benefits for the surface science community and industry from the DCAT standardization and B2B2B environment use will be considered and discussed.

Acknowledgment: VIPCOAT: H2020-NMBP-TO-IND-2020, Grant Agreement 952903.

[1] https://cordis.europa.eu/project/id/952903, https://ms.hereon.de/vipcoat/

Determining CO_2 corrosion behavior as well as the mode of corrosion in various steel for CCS applications

Kapil Kumar Gupta[1], Avinash Ingle[1], Sajjad Bahrebar[1], Andreas Christensen[2], Benjamin Lorenzen[2], Rajan Ambat[1]

[1]Section of Materials and Surface Engineering, Department of Civil and Mechanical Engineering, Technical University of Denmark, 2800 Kgs. Lyngby, Denmark

[2]IKM Ocean Team A/S, Vesterhavsgade 56, 6700 Esbjerg

One important method for lowering CO_2 emissions and reducing global warming is carbon capture and storage (CCS). One of the geological structures where the CO_2 stream is considered to be injected is a depleted oil and gas reserve. In addition to wellbore parameters (such as temperature, pressure, and formation water composition) leading to corrosion, the presence of impurities in the CO_2 stream (such as SO_x or NO_x) and water can considerably lower the pH in case of water dropout and further increase corrosivity. Furthermore, impurities like O_2 may introduce an additional cathodic reduction process, which would raise the susceptibility to localized corrosion. Examining the effects of impurities in gas streams on the materials is important to certify that the injection and storage of CO_2 will be secure. Thus, to ensure that the material choice would protect wells' integrity even in worst conditions, it is essential to examine several scenarios for injection and storage.

The goal of this research is to understand the CO_2 corrosion behavior as well as mode of corrosion of various materials under CO_2-saturated brine with impurities. In this thorough study, a wide variety of materials was examined, from low-alloy steels and 13% Cr steels to high-alloy grade materials. Steels were electrochemically exposed to a brine solution that was continuously pumped with carbon dioxide together with impurities such as oxygen, nitrogen dioxide, sulfur dioxide, and humidity (water). The corrosion behavior of the steels was evaluated using conventional electrochemical techniques: DC polarization and AC impedance spectroscopy. The corrosion product scale was characterized using scanning electron microscopy and X-ray Diffraction. Furthermore, the mode of corrosion was evaluated using X-ray (micro-) computed tomography for determining the surface of material underneath corrosion scale and visualizing the scale morphology in 3D.

Corrosion testing of CRAs in simulated CO_2 injection well environment

Gaute Svenningsen, Bjørn Helge Morland, Rolf Nyborg,
Institute for Energy Technology, NO-2027 Kjeller/Norway

Implementation of carbon capture and storage (CCS) will require huge storage sites, which usually will be an underground reservoir with one or several injection wells. The conditions in CO_2 injection wells are somewhat different from conventional oil and gas wells and may therefore require a different approach for corrosion testing. Firstly, because of the high CO_2 pressure (can be up to several hundred bar), which will result in significantly lower pH, particularly for condensed water (pH ≈ 3.0 with 100 bar CO_2). Secondly, because the CO_2 stream may contain additional components at ppm level like H_2S, SOx, NOx and O_2 (impurities). It has been shown experimentally that these impurities can react and create strong acids (sulfuric and nitric acid) or particulate matter (elemental sulphur) [1,2].

Corrosion problems are normally not expected as long as the CO_2 injection is maintained (normal operation). The injected CO_2 will displace any formation water and the well tubing will essentially only be exposed to the CO_2 bulk phase. However, formation water may in certain cases creep back and reach the tubing, for example during a shut-in (no injection). In such cases the tubing will be exposed to high CO_2 pressures, water with chlorides and possibly impurities (H_2S, O_2) or reaction products (strong acids). When injection is restarted after shut-in, it is expected that wet material will dry up with time, but intermittently having a concentrated brine layer on the surface. In combination, all these factors can create a harsh corrosive environment.

A test system with three titanium autoclaves has been made to simulate these conditions with dense phase CO_2 (Figure 1). One autoclave contains the dense phase CO_2 with impurities, and one autoclave contains the formation water. Both these autoclaves are piston-type with nitrogen back pressure, water and high-pressure CO_2 can therefore be transferred to the exposure chamber. It is also possible to simulate alternation in operation mode by moving formation water in and

out of the test chamber, by increasing or decreasing the backpressure above or below the test pressure.

Tailor-made four-point bend holders are used to test for stress corrosion cracking. Pitting/crevice coupons are also used. The set-up allows to place coupons in the CO_2-phase (top), in the CO_2-water interface (mid position) and in the water phase (bottom). Corrosion has been observed in all three positions, but the interface gave clearly the most corrosive condition. It has been observed that the crevice-type environment created between the coupons and the ceramic rollers (used in four-point bend holders) resulted in localised corrosion in several type of materials [3,4].

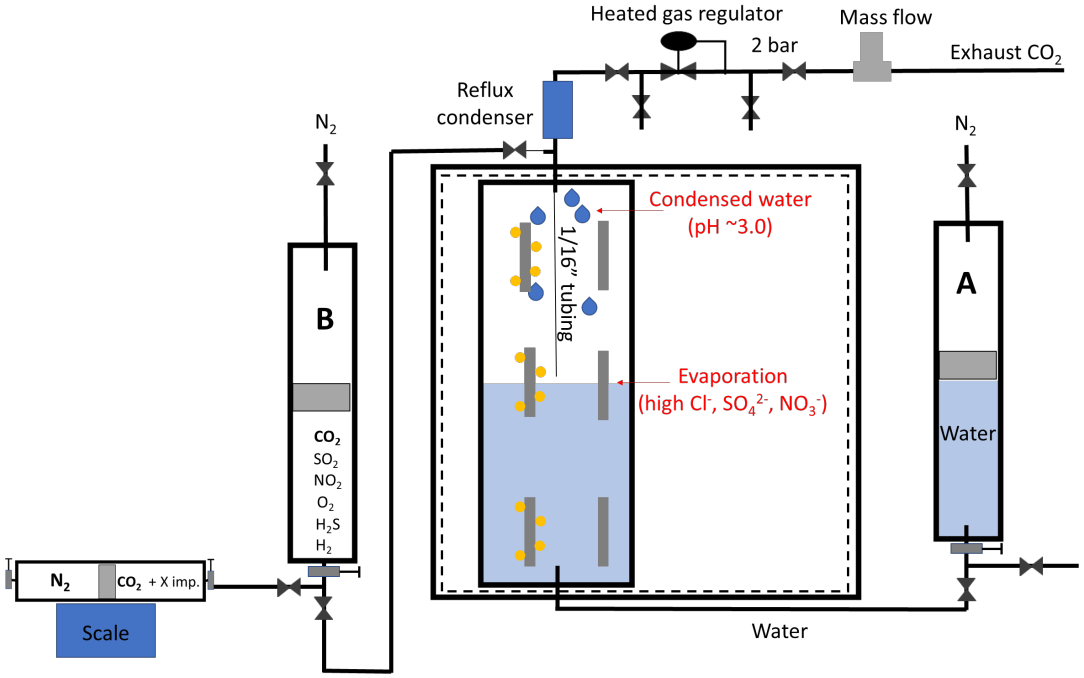

Figure 1: Schematic drawing of the test system.

References

[1] Morland, Dugstad, Svenningsen, *International Journal of Greenhouse Gas Control*, 119, (2022) p. 103697.

[2] Morland, Tjelta, Dugstad, Svenningsen, CORROSION/2018, paper no. 11429 (Houston, TX: NACE International, 2018).

[3] Svenningsen, Morland, Dugstad, Thomas, *Energy Procedia*, (2017).

[4] Svenningsen, Morland, AMPP Annual Conference + Expo, paper no. 18993 (Houston, TX: Association for Materials Protection and Performance, 2023).

Effect of oxygen contamination on the corrosion of carbon and stainless steels in CO2/H2S-containing media

Lou Chevallier[1], Gaurav R. Joshi[1], Jean Kittel[1], Xavier Campaignolle[2], Tiphaine Lutzler[2]

[1]IFP Energies nouvelles, Rond-point de l'échangeur de Solaize, BP 3, 69360 Solaize, France,
lou.chevallier@ifpen.fr, gaurav.joshi@ifpen.fr, jean.kittel@ifpen.fr
[2]Storengy,12 rue Raoul Nordling, 92277 Bois Colombes, France,
xavier.campaignolle@storengy.com, tiphaine.lutzler@storengy.com

Abstract
Carbon and stainless-steel grades are the materials of choice in deep-underground exploitations such as upstream oil and gas installations, storage reservoirs, geothermal wells and those used in carbon capture and storage. These materials are qualified for service at the required strength level as a function of their general resistance to corrosion and cracking at different operating temperatures, water/humidity contents and pressure and acid gas (CO_2 and H_2S) concentrations. In the oil and gas industry, these risks are now generally well controlled and understood because of several decades of industrial experience and appropriate material choices. However, the changing chemistry of produced or stored fluids (e.g., through reservoir souring, oxygen ingress or the presence of impurities in injected fluids) may modify the uniform and localized corrosion resistance of previously acceptable materials. In such a case, a re-evaluation of the materials in the bespoke modified environment is a useful exercise for the operator / steel manufacturer to carry out to better anticipate future risks and select more appropriate grades in future installations. This study focuses on experimentally evaluating the corrosion response of 2 carbon steels (N80 and AISI 4140), 1 CrMo steel (9Cr1Mo) and 1 stainless steel (13Cr) tubing materials exposed to CO_2 and CO_2/H_2S-saturated brines under varying oxygen gas concentrations (ranging from 0–3000 ppmv) at 50°C. The experimental matrix is designed to evaluate the impact of oxygen contamination on uniform and localized corrosion. This study, consisting of short-term electrochemical measurements using open circuit potentiometry, electrochemical impedance spectroscopy and cyclic potentiodynamic polarization, has been conducted to evaluate the mechanistic impact of dissolved oxygen (DO) on the general corrosion response of the selected grades. We report a primary screening of the uniform corrosion and localized corrosion risk through an assessment of the electrochemical data.

Keywords stainless steel; low-alloy steel; localised corrosion; cyclic polarization; oxygen contamination

Introduction

Carbon and stainless-steel grades are used in various applications throughout the oil and gas, geothermal, carbon capture and underground storage sectors. Carbon steel and low-alloy steels provide satisfactory mechanical strength at low cost, although their poor corrosion resistance is known to cause reliability issues. In scenarios where the environment is considered too corrosive, the so-called CRAs (corrosion resistant alloys) and chromium-molybdenum-enriched low alloy steels become interesting prospects. The corrosion resistance of CRAs and Cr-rich low alloy steels is attributed to the formation of a few nm-thick passive films on the surface, comprising iron and chromium oxide and hydroxides depending on the steel composition. This film acts as a barrier with protective properties, isolating the steel surface from solution ions and oxidants.

However, some limitations may arise in the presence of oxygen even at low levels in dissolved CO_2/H_2S-containing media. Previous research has reported that oxygen content greatly alters the passivation features of stainless steels in sodium chloride brine solutions [1,2].

Under sweet (CO_2-containing) conditions, the presence of O_2 could introduce an additional cathodic reaction contribution to the buffered proton reduction reaction [3], and accelerate the corrosion phenomenon:

$$O_2 + 4H^+ + 4\,e^- \rightarrow 2\,H_2O \qquad (1)$$

For instance, electrochemistry tests by Yue *et al* have shown that the stability and protectiveness of the 13Cr passive films were significantly reduced when dissolved oxygen (DO) increased from 10 to 1000 mass ppb under CO_2 and CO_2/H_2S conditions at room temperature [1]. In addition, oxygen was found to increase the passive current density as well as the risk of localized corrosion. Elsewhere, Neville *et al* have demonstrated that the surface film/passive film structure of low carbon and Cr-containing steel is considerably modified in the presence of high oxygen concentrations in CO_2-containing media [4]. Through mass-loss and profilometry studies, these authors report decreasing uniform corrosion rates but increasing localized corrosion rates as the dissolved O_2 content is increased in sweet media. Moreover, in the presence of DO, increasing the chlorinity can significantly alter the surface passive film, increase the corrosion rate and the pitting corrosion [5]. For active ferritic materials, oxygen may modify the formation of protective iron carbonate ($FeCO_3$) by oxidizing ferrous ions to ferric ions, resulting in the formation/incorporation of non-protective iron oxides[4]. Basilico *et al* demonstrated how oxygen contamination of a CO_2-saturated medium encourages localised corrosion in active ferritic steel with a protective $FeCO_3$ film [6]. They demonstrated transient effects through introducing and removing DO, providing insight into the role played by DO in sustaining localised corrosion in the presence of protective corrosion products.

Moving to sour environments, the solution chemistry is complexified well before interfacial and metallurgical aspects are considered. $O_{2(aq)}$ and $H_2S_{(aq)}$ can react together to form new electroactive species, and acidify the solution [7,8]. The formation of elemental sulfur is possible along with other sulfur-oxygen reaction products such as sulfates, thiosulfates and sulfites. For ferritic steels, a loss in the protectiveness of iron sulfide corrosion deposits is also observed, and the corrosion rate is increased [7,8]. On corrosion resistant alloys bearing passive oxides, such as chromium steels the role of these sulfuric species may destabilise the film passivity and render localised corrosion more likely [9,10].

The objective of this work is to study the influence of oxygen concentration on the corrosion behaviour of different steel grades from high-chromium to low-alloy steels in saturated brine exposed to CO_2 and CO_2/H_2S environment. Cyclic potentiodynamic polarization was utilized to evaluate corrosion resistance in sweet and sour environments under different oxygen concentration in saturated brine. The presence of oxygen is expected to induce changes to the cathodic reaction processes and the solution chemistry (CO_2/H_2S). Since the cathodic reaction provides the driving force for anodic oxidation, changes that modify the cathodic reaction kinetics ought to also modify the anodic oxidation behaviour (e.g., the active-passive-transpassive transitions). Questions remain on the impact of the DO content on the modification of the interface structure in passive alloys, one that we aim to initially address using short-term electrochemistry in the present work.

Materials and methods

Materials

For this study, representative materials used in deep-underground installations were chosen: carbon steel N80, Low-alloy steel 42CrMoS4 (AISI 4140), 9% Cr 9Cr1Mo alloy steel (9Cr1Mo), 13% Cr martensitic stainless steel (AISI 410, designated 13Cr in this article).

However, the results for the N80 will not be discussed in this article, since its behaviour was found to be comparable to data acquired from AISI 4140. The chemical compositions of these materials are presented in Table 1, and includes a pitting resistance equivalent number (PREN) calculated using the general formula as follows:

$$PREN = Cr + 3.3\,Mo + 16\,N \quad (2)$$

Table 1: Chemical composition of materials (mass %)

		C	Si	Mn	P	Cu	Cr	Ni	Mo	V	N	Co	PREN
Low alloy	AISI 4140	0.41	0.24	0.82	0.015	0.01	1.02	0.1	0.21				1.7
High Cr	L80 9Cr1Mo	0.125	0.69	0.58	0.016	0.045	8.68	0.16	0.99	0.037	0.048	0.01	12.7
Ferritic-martensitic stainless	AISI 410 (VM80 13Cr)	n.d.	0.22	0.58		0.10	12.9	0.10	0.04			0.17	13.0

The corrosion response of these steel grades has been evaluated in a highly saturated brine. The composition is as follows: 250 g/L NaCl, 0.593 g/L $MgCl_2{,}6H_2O$, 0.156 g/L K_2SO_4, 5.4 g/L $CaCl_2{,}2H_2O$, 4.85 g/L Na_2SO_4. The solution was prepared, deaerated with nitrogen purging and then pre-saturated with the appropriate test gas in a preparation vessel. Since the solution pH and DO were not measured *in situ*, thermodynamic calculations were carried out using PHREEQC (Version 3.0, Database PHREEQC) [11] to simulate the solution chemistry, estimate pH and dissolved gas concentrations and so evaluate the medium severity at t_0. The keywords "Gas phase" and "solution" along with test temperature, pressure, and partial pressure of each gas were used as inputs. Details on the test gas mixtures and PHREEQC outputs are provided in Table 2. It is noted that the estimated pH ~3.75 is as expected for these conditions of CO_2/H_2S partial pressures and DO ranges from 0 – 5000 mass ppb. In practice, the $[O_2]_{aq}$ in the non-O_2 test is expected to be <10 µg/L.

Table 2: Test gas mixtures and solution chemistry obtained by modelling in PHREEQC (V3.0) for a 250 g/L NaCl (4.3M) solution at 50°C.*

Test gas mixtures + absolute pressures			**Dissolved gas concentrations and solution pH at t_0**			
$P(H_2S)$ (mbar)	$P(O_2)$ (mbar)	$P(CO_2)$ (bar)	$[H_2S]_{aq}$ (µg/L)	$[CO_2]_{aq}$ (µg/L)	$[O_2]_{aq}$ (µg/L)	pH
-	0	2	-	464 640	0	3.75
-	20	1.9	-	459 800	159	3.75
-	600	2	-	462 880	4 768	3.75
0.66	0	1.9	327.6	464 200	0	3.75
0.66	20	1.9	327.6	459 800	159	3.75
0.66	600	2.06	327.6	465 960	4 656	3.75

* For simplicity, minority salts were excluded from the calculations.

Electrodes preparation

Electrodes (5×10×3 mm in size) were welded to a connecting wire, mounted in a plastic mould that holds two samples and sealed with an epoxy resin. Precautions were taken to position the carbon steel (N80) and low-alloy steel (AISI 4140) apart from the alloy steel (9Cr1Mo) and stainless steel (13Cr) to avoid possible pollution of the surface of the latter via corrosion products of the former. Before each experiment, working surfaces were abraded to 800-grit, rinsed with deionized water and ethanol, then flushed with N_2. Appropriate care was taken to ensure edge/crevice effects were not observed at resin/sample borders through visual inspections prior to and post-test.

Test cells

The test reactors are presented Figure 1 and consist of a glass cell with a double jacket for temperature control; inlets and outlets for circulation of fluids (gas and liquid); A 3-electrode assembly, comprising a reference electrode (Ag/AgCl), a counter-electrode (Pt gauze) and working electrodes made from the steels to be studied. The pressure in the reactor was controlled using valves set to 2 bar or 2.6 bar (for tests with an O_2 content of 600 mbar corresponding to 3000 ppmv at a total pressure of 200 bar).

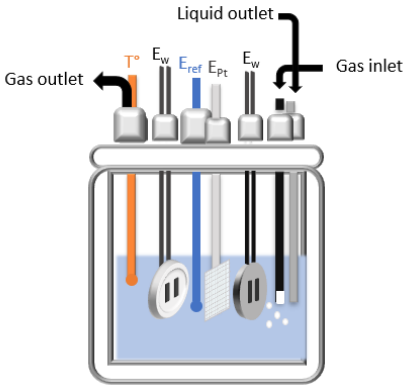

Figure 1: Schematic of test reactor cells

The test matrix is detailed in Table 3. Tests were conducted at 25°C and 50°C, under the partial pressure of CO_2 of 2 bar, with and without presence of 0.66 bar H_2S. To study the influence of O_2 on the corrosion behavior of the steel grades, four concentrations were evaluated: 0, 2, 20, 600 mbar O_2. For simplicity, this article focuses on test results obtained from experiments conducted at 50°C and excludes data at 2 mbar O_2.

Table 3 : Experimental matrix – Temperature: 50°C

Main gas content	Gas O_2 concentration		
	0 ppmv (0 mbar)	**100 ppmv (20 mbar)**	**3000 ppmv (600mbar)**
2 bar CO_2	X	X	X
2 bar CO_2 + 0.66 mbar H_2S	X	X	X

Electrochemical measurements

The test cell containing the different steel electrodes was dry flushed with nitrogen before the solution is transferred. A continuous flow of gas of 20 mL/min was maintained during the test. All electrochemical testing was carried out using a VSP-3e biologic potentiostat. At the beginning of each test, corrosion potential (E_{corr}) was monitored for between 30 to 75 minutes, depending on the steel grade. Even through a steady-state potential is not completely attained for high-chromium alloys, e.g. one to several days [12], the objective was to complete testing at short-enough periods that generally reflect harsh environments. Electrochemical impedance spectroscopy (EIS), ± 10 mV vs OCP, 100 kHz to 10 mHz, 7 points per decade, was carried out. Measurements were performed successively and in this order on VM80 13Cr stainless steel, L80 9Cr1Mo alloy steel, AISI 4140 low-alloy steel, and finally N80 carbon steel. The aim of these measurements is to obtain information on the initial corrosion behaviour of these grades as well as on the electrolyte resistance (R_e) to correct ohmic drop. Subsequently, polarization curves (ASTM G61) were executed for each steel and in the same order using scan rate of 30mV/min from -30 mV to 500 mV vs. E_{corr}, or (generally) until a current density of i_a=5mA/cm² was attained. Once one of these two conditions reached, a return sweep to corrosion potential is performed to assess the steel's ability to repassivate. Only polarization

curves are discussed in this article, however impedance measurements were consistent with the latter.

Results and discussion

Reference conditions

To first examine the behaviour of these alloys in a highly saturated NaCl brine containing no DO, tests were performed under partial pressure of 2 bar CO_2. The polarization curves are shown Figure 2. According to the corrosion current density around the corrosion potential, the corrosion resistance was observed to increase in the order AISI 4140 < 9Cr1Mo < 13Cr, rather as expected.

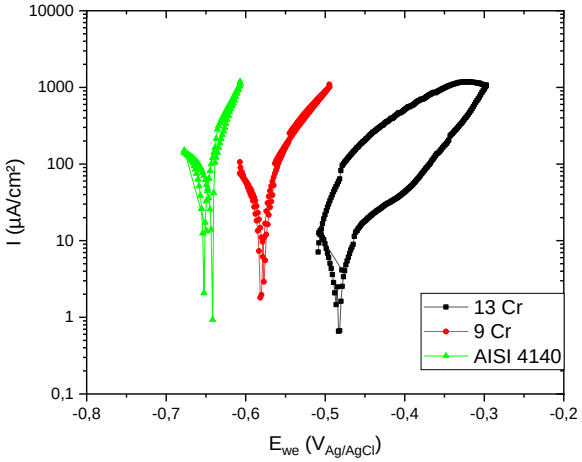

Figure 2: Polarization curves under CO_2 conditions

The evaluated corrosion (E_{corr}), pitting (E_{pit}), repassivation (E_{rep}) potentials and corrosion current (i_{corr}) extracted from the curves are shown in Table 4. The corrosion rate was estimated from corrosion current i_{corr} taken around the intersections of the anodic and cathodic reaction lines. Corrosion rate (CR) was calculated as follows:

$$CR\ (\mu m/y) = i_{corr}\ (\mu A/cm^2) \times MC_{steel} \quad (2)$$

Where MC_{steel} is a steel specific constant (11.7 µm $cm^2.\mu A^{-1}.\ yr^{-1}$) based on Faraday's law and considers the necessary unitary conversions.

Table 4 : E_{corr}, i_{corr}, E_{pit}, E_{rep} and CR values for each steel under CO_2 conditions

	E_{corr} ($V_{Ag/AgCl}$)	i_{corr} (µA/cm²)	E_{pit} ($V_{Ag/AgCl}$)	E_{rep} ($V_{Ag/AgCl}$)	CR (µm/y)
13Cr	- 0.479	9	-	< E_{corr}	105
9Cr1Mo	- 0.578	30	-	-	351
AISI 4140	- 0.649	50	-	-	585

As expected, the AISI 4140 displays activation-controlled kinetics with a shallow anodic slope. The 9Cr1Mo experiences a similar corrosion current density and activation-controlled behaviour, albeit with a steeper slope with respect to the AISI 4140. Nonetheless, its corrosion potential is higher than that of AISI 4140 due to the presence of ennobling elements like Cr and Mo. The 13Cr steel presents a lower i_{corr} of approximately 10 µA/cm². The anodic slope beyond the activation-controlled segment is steeper suggesting some passive film resistance but no true passivation plateau in the anodic regime. At approximately -409 $mV_{Ag/AgCl}$, a slight change in slope is observed, which could tentatively represent the onset of transpassive dissolution.

A hysteresis loop intersects the data below E_{corr}, all of which appears to suggest that 13Cr may have partially depassivated in this low pH, high Cl^- brine. On electrochemical evidence, localized corrosion is possible in 13Cr even in the absence of dissolved O_2.

High-chromium alloys performance with O_2 contamination

The impact of $[O_2]_{aq}$ on high-chromium alloys was investigated under CO_2 and CO_2/H_2S conditions. The polarization curves of 13Cr and 9Cr1Mo under CO_2/O_2 are presented in Figure 3. The corrosion (E_{corr}), pitting (E_{pit}), re-passivation (E_{rep}) potentials and corrosion current (i_{corr}) are summarized in Table 5.

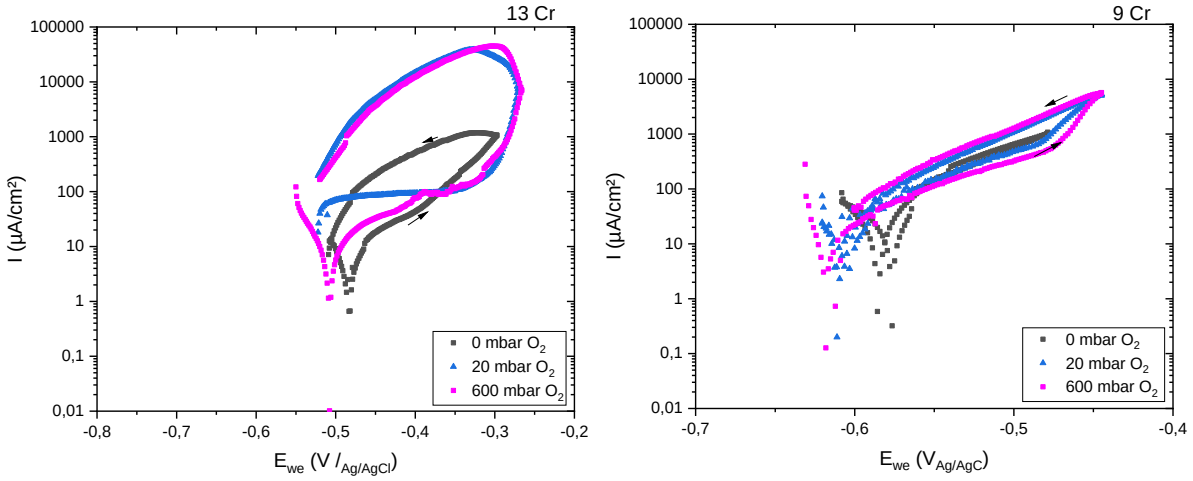

(a) *(b)*

Figure 3 :13Cr (a) and 9Cr1Mo1Mo (b) polarization curves under CO_2/O_2 conditions. O_2 concentrations are 0 mbar (DO<10 ppbv), 20 mbar (DO~160 ppbv) and 600 mbar (DO~4800 ppbv)

Focusing on 13Cr, Fig. 3(a), the introduction of DO leads to a slight increase in i_{corr}, accompanied by a minor shift in corrosion potential. The polarisation curves highlight the presence of a plateau, manifested as a stabilisation of the current density over a small potential range of around 200 mV in the anodic regime. Nevertheless, it is important to note that the observed anodic regime plateau for 13Cr under CO_2 /O_2 conditions has a high current density and a restricted potential range. A good passive film, on a transition metal with protective properties, ought to present current density of around 0.01 to 1 µA/cm² - corresponding to a corrosion rate of around 0.1 - 10 µm/year [13]. Nonetheless, this weak passive plateau was probably unstable and affected by the low pH of the medium. A consistent E_{pit} is observed for the two imposed oxygen concentrations at higher value with respect to the 0 mbar O_2 case (~ -0.3 $V_{Ag/AgCl}$), prior to the sudden increase in current density (attributed to transpassive dissolution / localised corrosion onset). Large, superimposing hysteresis loops are measured, which reflect the difficult and sluggish repassivation kinetics in the presence of oxygen. We deem that no repassivation is observed above E_{corr}, which underlines the instability of the 13Cr passivation behaviour, and localised corrosion is enhanced in the presence of DO, at concentrations as low as 160 µg/L.

Moving to 9Cr1Mo, Fig. 3(b), the corrosion current densities are higher with respect to those of 13Cr. The absence of a steep passive range on these polarisation curves underlines the difference in performance of the 9Cr1Mo compared against that of the 13Cr. However, the appearance of a small hysteresis loop at high potential suggests that the increase in DO favours a clearer onset of localised corrosion. As before, the oxygen content does not seem to produce

any significant difference. Table 5 presents the key polarisation parameters read from the graphs.

Table 5 : E_{corr}, I_{corr}, E_{pit}, E_{rep} and V_{corr} values for high-chromium alloys under CO_2/O_2 conditions

	P(O_2) (mbar)	**E_{corr} ($V_{Ag/AgCl}$)**	**I_{corr} (µA/cm²)**	**E_{pit} ($V_{Ag/AgCl}$)**	**E_{rep} ($V_{Ag/AgCl}$)**	**V_{corr} (µm/an)**
13 Cr	0	- 0.479	9	- 0.409	< E_{corr}	105
	20	- 0.491	n/a	- 0.345	< E_{corr}	n/a
	600	- 0.543	22	- 0.355	< E_{corr}	261
9Cr1 Mo	0	- 0.578	30	-	-	351
	20	- 0.590	25	- 0.481	~ E_{corr}	293
	600	- 0.593	25	- 0.475	~ E_{corr}	281

The anodic polarization curves of 13Cr and 9Cr1Mo under $CO_2/H_2S/O_2$ are presented Figure 4. The corrosion potential (E_{corr}) and corrosion current densities (i_{corr}) extracted from the curves are shown in Table 6.

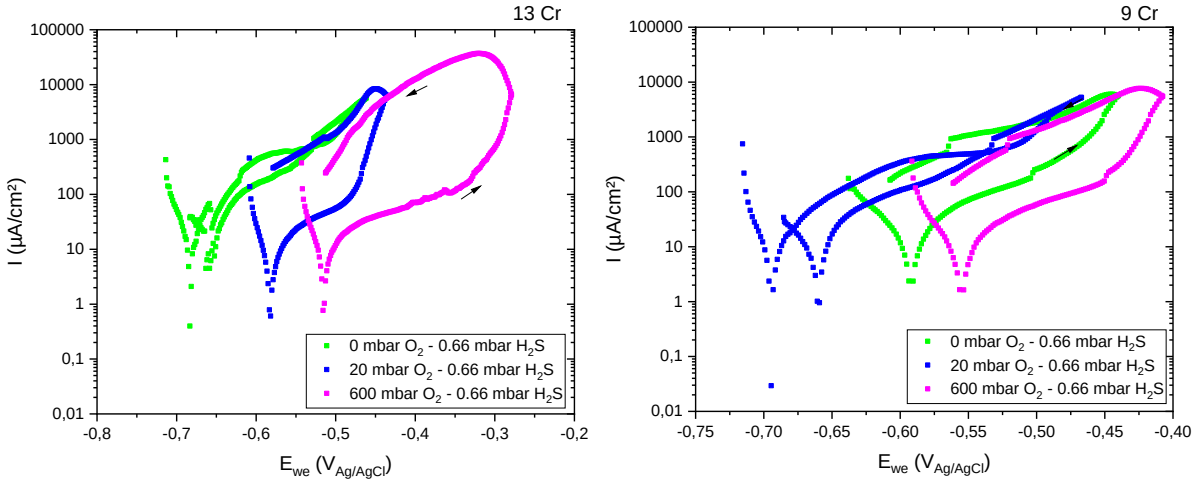

(a) *(b)*

Figure 4:13 Cr (a) and 9Cr1Mo (b) polarization curves under $CO_2/H_2S/O_2$ conditions. O_2 concentrations are 0 mbar (DO<10 ppbv), 20 mbar (DO~160 ppbv) and 600 mbar (DO~4800 ppbv)

For 13Cr, Fig. 4(a), the addition of H_2S shifts the curves towards less noble potentials and slightly increases the current density. This is potentially indicative of the modification played by adsorbed H_2S at the 13Cr interface. The electrochemistry would suggest that the 13Cr presents uniform corrosion behaviour in deaerated CO_2/H_2S conditions. As aforementioned, increasing the $[O_2]_{aq}$ in a CO_2/H_2S containing medium induces the formation of associated sulfur species [7,8]. The introduction of oxygen induces shifts towards higher potentials and ever so slightly decreases i_{corr} around the open circuit potential. However, increasing $[O_2]_{aq}$ appears to increase E_{pit} (which suggests improvements to the modified passive film in this environment) and larger hysteresis loops that do not repassivate above E_{corr}. This suggests a lower pit healing resistance at higher H_2S/O_2 concentrations, possibly due to sulfur species adsorption [10]. It is likely that the chemistry of the solution does not allow the formation of a stable passivation layer. This behaviour is likely a contribution of (i) the presence of sulfur species (induced by $H_2S + O_2$ reactions) adsorbed at the steel interface (ii) the contribution of oxygen/thiosulfates as additional cathodic reagents.

Concerning 9Cr1Mo steel, Fig. 4(b), the presence of H_2S alone decreases the i_{corr} with respect to the pure CO_2 case. The increase in DO concentration does not affect the corrosion current densities (i.e. corrosion rates), which remain equivalent. The linear trend of the 9Cr1Mo curve in a CO_2/O_2 medium is modified in the presence of H_2S, with the appearance of a passive plateau (possibly comprising mixed corrosion products), induced by FeS scale contribution, followed by a hysteresis loop. This is even more apparent in tests at 0 and 600 mbar O_2. Focusing first on the 0 mbar O_2 and 600 mbar O_2 cases, a slight increase in E_{corr} and hysteresis loop sizes are observed. The passive current plateau is slightly improved in the presence of high DO with the slight extension of E_{pit}. However, the increase of the hysteresis loop. The 20 mbar O_2 case is rather peculiar. A decrease in E_{corr} suggests slight surface activation, but a short hysteresis loop is observed that repassivates. It may suggest that the 9Cr1Mo passive film response here presents some improvement against localised corrosion resistance in the presence of low concentrations of oxygen with respect to no oxygen and very high concentrations of oxygen. This aspect merits further evaluation, which is not covered in the present article.

Table 6 : E_{corr}, I_{corr}, E_{pit}, E_{rep} and V_{corr} values for high-chromium alloys under $CO_2/H_2S/O_2$ conditions

	P(O_2) (mbar)	**E_{corr} ($V_{Ag/AgCl}$)**	**I_{corr} (µA/cm²)**	**E_{pit} ($V_{Ag/AgCl}$)**	**E_{rep} ($V_{Ag/AgCl}$)**	**V_{corr} (µm/an)**
13 Cr	0	- 0.644	17	-0.475	-	203
	20	- 0.584	15	- 0.489	< E_{corr}	176
	600	- 0.537	12	- 0.354	< E_{corr}	145
9Cr1 Mo	0	- 0.564	20	- 0.503	< E_{corr}	236
	20	- 0.652	18	- 0.516	> E_{corr}	205
	600	- 0.540	14	- 0.450	< E_{corr}	159

Low alloy steel performance with O_2 contamination

Figure 5 displays the polarisation curves for AISI 4140 under CO_2 (a) and CO_2/H_2S (b) conditions. The corresponding representative values extracted from the polarisation curves are presented in Table 7.

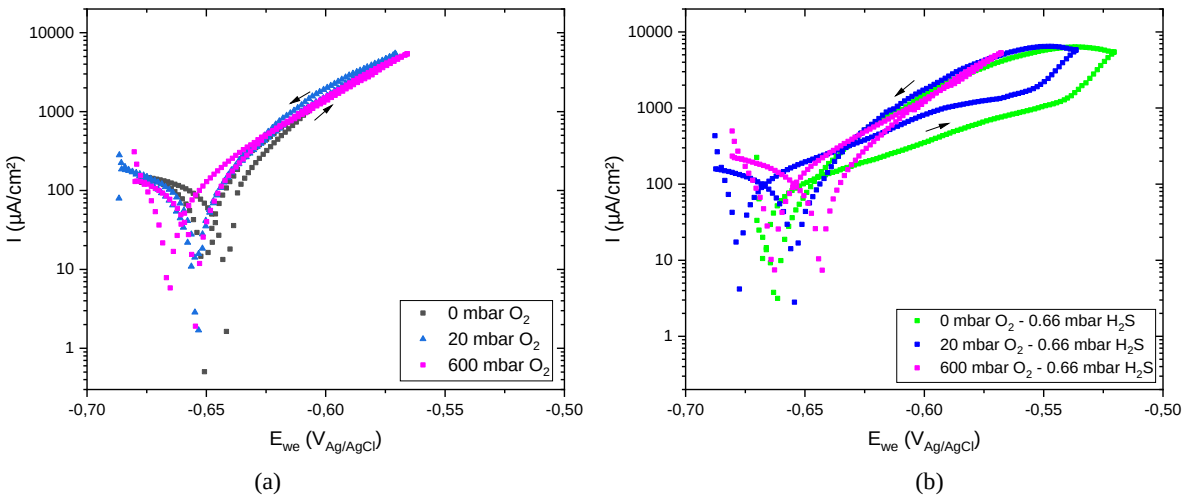

(a) (b)

Figure 5: AISI 4140 polarization curves under (a) CO_2 conditions and (b) CO_2/H_2S conditions. O_2 concentrations are 0 mbar (DO<10 ppbv), 20 mbar (DO~160 ppbv) and 600 mbar (DO~4800 ppbv)

The linear trend of the curves suggests activation-controlled uniform corrosion. In the CO_2-saturated solution, oxygen does not produce a significant effect, regardless of its concentration. The introduction of H_2S modifies the trend, with the appearance of a small hysteresis loop that

suggests an increased likelihood of localised corrosion. This feature is not visible in a pure CO_2 or CO_2/O_2 environment. The slight passivation feature is visible up to 20 mbar, probably due to the formation of a FeS scale, which offers passive film style protectiveness prior to its breakdown at higher potential. At 600 mbar O_2, a linear trend is recovered suggesting that the integrity of iron sulfide films at lower oxygen content is non-existent. This may be a direct effect of solution acidification and the appearance of new species from H_2S-O_2 reactions e.g. elemental sulfur and sulfites/thiosulfates which modify the interface structures/chemistry and the solution chemistry [8].
Corrosion rates appeared to be slightly higher under CO_2/O_2 conditions than in $CO_2/H_2S/O_2$ conditions. Longer tests would certainly confirm or challenge these trends and verify the evolution of deposit protectiveness in presence of oxygen and hydrogen sulfide.

Table 7: E_{corr}, I_{corr}, E_{pit}, E_{rep} and V_{corr} values for low-alloy steel under CO_2/O_2 and $CO_2/H_2S/O_2$ conditions

$P(O_2)$ (mbar)	$P(H_2S)$ (mbar)	E_{corr} ($V_{Ag/AgCl}$)	I_{corr} (µA/cm²)	V_{corr} (µm/an)
0	-	- 0.649	53	620
20	-	- 0.658	136	1591
600	-	- 0.655	94	1100
0	0.66	- 0.641	47	552
20	0.66	- 0.655	71	834
600	0.66	- 0.651	67	785

Conclusions

The short-term corrosion behaviour of low alloy and high chromium steels exposed to CO_2 and CO_2/H_2S-saturated brines under varying oxygen gas concentrations (ranging from 0 – 3000 ppmv) at 50°C, has been evaluated through electrochemical measurements. Despite possessing similar PREN, the 13Cr steel and 9Cr1Mo steels behave in different manners with regards pitting corrosion resistance as evaluated using electrochemical methods.

- Under CO_2/O_2 conditions, the introduction of oxygen does not significantly increase the corrosiveness for such a short time (< 4h). The corrosion response is a function of the metallurgy and composition. High-chromium steels (13Cr and 9Cr1Mo) are much more resistant than low-alloy steel (AISI 4140), due to their chromium content, which enables the formation of a passive film with protective properties. Nevertheless, in the presence of oxygen, significant hysteresis can be observed in the case of 13Cr and 9Cr1Mo, indicating a more complex and slower repassivation after transpassive dissolution compared against deaerated conditions.

- For $CO_2/H_2S/O_2$ conditions, the introduction of H_2S in non-O_2 media slightly increases the corrosion current density of 13Cr steel but decreases that of the 9Cr1Mo and AISI4140 low alloy steel, compared to saturated CO_2 conditions. This is likely a direct role played by a thin, protective iron sulfide film that forms rapidly. However, the addition of increasing oxygen content appears to play a multi-faceted role that complexifies the solution and interfacial chemistry and leads to different responses in the three different grades.
    - *13Cr:* The increases in E_{corr} and E_{pit} suggest an improved passivation response possibly through a combination of modified film structure and visible contribution of O_2 reduction; nonetheless, increasing positive hysteresis as a function of $[O_2]_{aq}$ indicate lower pitting corrosion resistance beyond E_{pit}. High

quantities of DO may be detrimental to the localised corrosion resistance of this 13Cr steel;

- *9Cr1Mo:* Inconsistent responses may indicate different mechanistic regimes. Negligible and high DO reflect a certain tendency for this alloy to form a weak, semi-protective 'passive' film in this medium that could severely break down and not recover; however, at low oxygen concentration (20 mbar), a different interfacial performance is attained possibly combining activation and passive film protection. This low oxygen contamination range merits further attention;
- *AISI 4140:* an initially semi-passive response at low oxygen content, resulting most likely from a passive iron sulfide, becomes activation controlled with greater DO content. The modified solution chemistry (acidification) and its impact on favorably dissolving the protective iron sulfide overlayer are hypothesised as the reasons behind this change in electrochemical response as a function of $[O_2]_{aq}$.

The trends observed over short term ought to be treated with some caution. Longer-term studies may indicate a slowdown or even a reversal of the trend, due to the formation of protective deposits. Further long-term tests in the remit of this experimental evaluation will allow more precise evaluation of steel grade behaviours with regards uniform and localised corrosion.

References

[1] X. Yue, Effect of Traces of Dissolved Oxygen on the Passivation Stability of Super 13Cr Stainless Steel Under High CO2/H2S Conditions, Int. J. Electrochem. Sci. (2017) 7853–7868. https://doi.org/10.20964/2017.08.33.

[2] S.H. Mameng, A. Bergquist, E. Johansson, Corrosion of Stainless Steel in Sodium Chloride Brine Solutions, in: Corrosion 2014, San Antonio, TX (USA), 2014.

[3] E. Remita, B. Tribollet, E. Sutter, V. Vivier, F. Ropital, J. Kittel, Hydrogen evolution in aqueous solutions containing dissolved CO2: Quantitative contribution of the buffering effect, Corrosion Science 50 (2008) 1433–1440. https://doi.org/10.1016/j.corsci.2007.12.007.

[4] Y. Hua, R. Barker, A. Neville, The effect of O2 content on the corrosion behaviour of X65 and 5Cr in water-containing supercritical CO2 environments, Applied Surface Science 356 (2015) 499–511. https://doi.org/10.1016/j.apsusc.2015.08.116.

[5] W. Liu, H. Yang, X. Li, Z. Zhang, Y. Lin, K. Deng, Effect of Chloride and Iodide on the Corrosion Behavior of 13Cr Stainless Steel, Metals 12 (2022) 1833. https://doi.org/10.3390/met12111833.

[6] E. Basilico, S. Marcelin, R. Mingant, J. Kittel, M. Fregonese, R. Barker, J. Owen, A. Neville, F. Ropital, Effect of O2 contamination on carbon steel pseudo-passive scales in CO2 aqueous solutions, Corrosion Science 205 (2022) 110388. https://doi.org/10.1016/j.corsci.2022.110388.

[7] M.D. Deffo Ayagou, G.R. Joshi, T.T. Mai Tran, E. Sutter, B. Tribollet, C. Mendibide, C. Duret-Thual, N. Ferrando, J. Kittel, Corrosion and Hydrogen Permeation in H 2 S Environments with O2 Contamination, Part 2: Impact of H2S Partial Pressure, Corrosion 75 (2019) 389–397. https://doi.org/10.5006/3092.

[8] M.D. Deffo Ayagou, G.R. Joshi, T.T. Mai Tran, B. Tribollet, E. Sutter, C. Mendibide, C. Duret-Thual, J. Kittel, Impact of oxygen contamination on the electrochemical impedance spectroscopy of iron corrosion in H2S solutions, Corrosion Science 164 (2020) 108302. https://doi.org/10.1016/j.corsci.2019.108302.

[9] P.Marcus, E.Protopopoff, Potential-pH diagrams for adsorbed species. Application to sulfur adsorbed on iron in water at 25° and 300°C, J.Chem.Soc. (Journal of the Chemical Society) 137 (1990).

[10] P. Marcus, E. Protopopoff, Thermodynamics of thiosulfate reduction on surfaces of iron, nickel and chromium in water at 25 and 300 degrees C, Corrosion Science 39 (1997) 1741–1752.

[11] Parkhurst, D.L., Appelo, C.A.J., Description of input and examples for PHREEQC version 3—A computer program for speciation, batch-reaction, one-dimensional transport, and inverse geochemical calculations, in: U.S. Geological Survey Techniques and Methods, p. 497.

[12] Marcelin, Sabrina and Pébère, Nadine and Régnier, Sophie, Electrochemical characterisation of a martensitic stainless steel in a neutral chloride solution.

[13] A. Veluchamy, D. Sherwood, B. Emmanuel, I.S. Cole, Critical review on the passive film formation and breakdown on iron electrode and the models for the mechanisms underlying passivity, Journal of Electroanalytical Chemistry 785 (2017) 196–215. https://doi.org/10.1016/j.jelechem.2016.12.020.

Investigation of Cement-Metal barrier performance for ensuring long-term safety of abandoned CO_2 storage wells

Jie Yu [a], *Xinyu Shi* [b], *Min Wu* [b]*, *Rajan Ambat* [a]*

a Technical University of Denmark, Denmark

b Aarhus University, Denmark

Injection and storage of CO_2 into non-producing oil wells is a potential way to mitigate climate change. Generally, several cement plugs are placed in the wellbore to isolate the reservoir and other fluid-bearing formations (*Figure 1*). However, the degradation of cement-metal interface and cement materials with exposure to various states of CO_2 considerably affects the long-term safety of the well by changing mechanical properties, transport properties, and microstructure. This study aims to investigate the cement-metal interface performance, especially under various impurities (H_2O, H_2S, SO_x, NO_x, *etc.*) and different CO_2 conditions. Specimens of cement (class G/class H) - metal (L80 1Cr alloys) were fractured interface analysis via optical microscopy, SEM, FTIR, and TEM and conducted electrochemical tests for interface corrosion level followed by solution chemistry analysis for dissolution level (ICP-OES), combined with in-situ and ex-situ X-ray tomography, synchrotron, post microscopic and spectroscopic investigations. These lab-scale parametric results would be used for the flow loop test facility to simulate actual well conditions and then develop guidelines for the safe operation of cement plugs including the cement-metal interface.

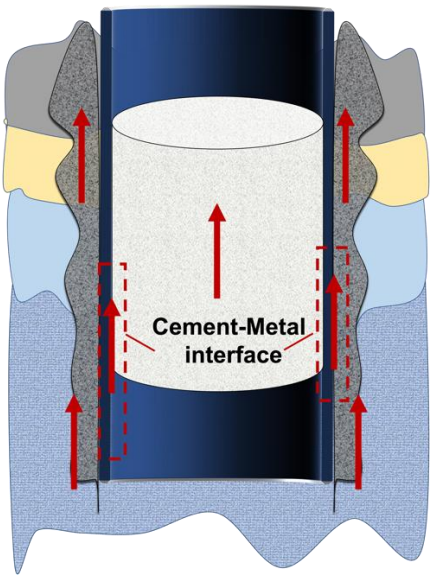

Figure 1: Schematic of a cement plug

Additively manufactured Ti-2Mo for biomedical implants – Corrosion properties, PEO coatings and controlling residual stresses

Julian Fritzen[1], Fabian Haase[2], Stephan Lederer[1], Wolfram Fürbeth[1], Carsten Siemers[2]

[1]DECHEMA-Research Institute, Frankfurt am Main / Germany

[2]Technical University Braunschweig, Braunschweig / Germany

The process of additive manufacturing (AM) e.g., the selective laser melting process (SLM) is more and more accepted and used when it comes to the production of biomedical implants. Benefits of the process are faster production with less material waste, especially for highly complex structures. While on the other hand challenges remain in handling the high residual stresses, pores and rough surfaces, which are the result of the high temperatures and cooling rates of the process.

In this study the newly developed titanium alloy Ti-2Mo, which is free of cytotoxic elements like aluminum and vanadium, is used as a powder base material for the SLM process. Additionally, the effect of elementary boron to Ti-2Mo is investigated.

After surface modifications, like blasting and plasmaelectrolytic polishing (PEP), of the additively manufactured parts, the material is coated by plasmaelectrolytic oxidation for corrosion protection and better osseointegration. The corrosion properties and coating stability are determined regarding the residual stresses.

Residual stresses are measured by the $\sin^2\Psi$-method to compare the different stress tensors of the as built-, annealed- and HIP-state in order to determine the most beneficial stresses for coatings by plasma electrolytic oxidation (PEO).

Influence of the additive manufacturing technologies on the corrosion performances of Ti-6Al-4V for medical implants

M. Cabrini, A. Carrozza, S. Lorenzi, T. Pastore / University of Bergamo, Italy
A. Aversa, D.Manfredi / Politecnico di Torino, Italy

Metal additive manufacturing (AM) technologies are rapidly revolutionizing the biomedical industry, due to the possibility to generate complex shaped parts D.Manfredimost promising field of application of such technologies, that grant a unique surface roughness, thus promoting osseointegration. However, AM-produced implants can provide a wide range of final properties, dependent on several process-dependent factors. Therefore, a full understanding of the impact of these parameters has to be gained. Hence, this work deals with the effect that the AM technologies adopted, heat treatments and surface finishing provide on the corrosion performance of Ti-6Al-4V specimens. Electron beam- and laser-based powder bed fusion techniques were adopted to manufacture the samples, that were investigated in the as-built and heat-treated states, as well as in the untreated, mechanically polished and chemically pickled surface conditions. Initially, a material science-based approach was adopted to investigate the typical microstructures and phases generated by the manufacturing processes and heat treatments. Then, a picking treatment was specifically optimized for these materials via surface roughness measurements via optical confocal imaging. In the end, the corrosion behavior in a physiologic solution at body temperature was assessed via potentiostatic polarizations and electrochemical impedance spectroscopy (EIS) tests. Additionally, an estimation of the total ions release over time was calculated. It was evidenced that surface finishing operations were significantly more impacting on the corrosion performance of the Ti-6Al-4V alloys than the microstructure. The pickled and polished specimens proved to have comparable oxide formation kinetics. However, the former seemed to achieve lower asymptotic current density values, hence ions release rates, proving that the pickled condition is advantageous both in terms of reducing health risks and increasing osseointegration.

Role of precipitation state on the corrosion behavior of MgZnZr alloy selected for robocasting of personalized bioresorbable implant

Julien Moreau, MATEIS/INSA Lyon, Villeurbanne/France ; Benoît Ter-Ovanessian, MATEIS/INSA Lyon, Villeurbanne/France ; Xavier Boulnat, MATEIS/INSA Lyon, Villeurbanne/France; Michel Perez, MATEIS/INSA Lyon, Villeurbanne/France ; Laurent Gremillard, MATEIS/CNRS, Villeurbanne/France; Olivier Dezellus, LMI/UCBL, Villeurbanne/France

Despite the progress made in reconstructing bone defects, many concerns remain to limit pain or the risks of second surgery (including implant removal). These include: implant geometries that are not adapted to the patient's anatomy, unsatisfactory biocompatibility or mechanical properties, and a significant risk of bacterial infections.
Among the technological solutions, the emergence of additive manufacturing makes it possible to produce parts with the desired dimensions and adapted to patients in many different materials. However, the development of certain biomedical materials by additive manufacturing is still at the laboratory scale. This is the case of Mg alloys which are interesting for resorbable implants. Main challenges are: the high flammability of fine Mg-powders, the high vapour pressure of liquid Mg, the great influence of contaminations on the degradation properties (mechanical or corrosion).
To overcome these issues, robocasting, which is a binder-based sintering technology is applied in this work on Mg3Zn0.6Zr (%weight) alloys. The alloying of Zn and Zr aims at increase the mechanical properties by second phase precipitation and grain refinement and reduce the corrosion rate.
In the present work, as a preliminary study, different heat treatments had been applied on dense samples obtained by spark plasma sintering (*500°C/10min/63MPa*) in order to determine an optimized microstructure providing stimulating mechanical properties and corrosion behavior. The precipitation state was monitored by Vickers hardness and thermoelectric power measurements, supplemented by a detailed microscopy analysis. Hardness measurements indicate that two different hardening phases contribute to the enhancement of the mechanical properties. The observation of two different precipitates is in accordance with literature and are identified as β'_1 rod-shaped precipitate (Mg_4Zn_7 + $MgZn_2$) and β'_2 coarse plate precipitate ($MgZn_2$).

Corrosion tests were carried out for the different microstructural states in saline (0.9% NaCl, pH=7.4, 37°C) and simulated physiological (phosphate buffer solution, pH=7.4, 37°C (PBS)) solutions. Mass loss was measured during immersion over 4 weeks and a corrosion rate was estimated. On selected samples, electrochemical impedance spectroscopy (at open circuit potential, frequency range from 100kHz to 0.01mHz, voltage amplitude of 10mV RMS, 9 points per decade) was performed all along the immersion to propose a mechanistic approach of the role of the precipitation state on the corrosion behavior. Evolution of the impedance parameters was discussed regarding the microstructure characterization and the exposed surface analysis. Size and distribution of the precipitates straightforwardly impact the corrosion rate. Well-distributed small precipitates delayed consequently the corrosion degradation in saline solution. Conversely coarse precipitates are prone to galvanic corrosion increasing the corrosion rate. In PBS the corrosion rate is reduced compared to saline solution thanks to the formation of organometallic complex of $Mg_3(PO_4)_2$ which is less soluble than $MgCl_2$ which is produced in saline solution.

Influence of printing parameters on the tribocorrosion behavior of directed energy deposited (DED) stainless steel 316L

Deeparekha Narayanan[1], Maha Messaadi[2], Myriam Dumont[2], Fadlallah Abouhadid[2], Ibrahim Karaman[1], Homero Castaneda[1]

[1]Department of Materials Science and Engineering, Texas A&M University, College Station, TX, USA.
[2]MSMP-EA7350, Arts et métiers ParisTech, 8 Bd de Louis XIV, 59000 Lille, France.

Abstract. The widespread study of additive manufacturing techniques to produce parts made of stainless steel 316L widens the applications this can be used in. In this study, we aim to investigate the use of directed energy deposition (DED) to produce parts such as femoral stems for orthopedic applications. The study compares the effect of processing parameters such as laser power and scan speed on the microstructures of DED stainless steel 316L on the microstructure and electrochemical properties. Four samples were used for this study – a combination of two laser powers (200 W, 300 W) and two scan speeds (10 in/min and 15 in/min). The interfacial behavior of the alloys was studied in phosphate-buffered saline (PBS) solution using electrochemical and alternative sliding friction to quantify their corrosion and tribological properties. Upon comparing the properties obtained in each set of parameters, the optimal values to produce the parts with the best electrochemical properties can be determined. Determination of the optimum parameters and studying techniques to improve them can facilitate these techniques to be put into actual practical applications.

Keywords. Directed energy deposition (DED); stainless steel 316L; tribocorrosion; pitting characteristics; wear;

Introduction

Stainless steel 316L (SS316L) is a commonly used corrosion-resistant material used in various components in structural, marine, biomedical, and oil and gas industries. Additive manufacturing (AM) techniques to processing components for these industries are rapidly gaining popularity due to their ability to produce net shape/ near-net shape parts with very complex shapes with little to no material wastage. This characteristic is very useful in orthopedic components such as parts used in total hip/knee replacements, as they are generally custom-made depending on the specific case and are also extremely complex in geometry. Studying the possible use of AM techniques for such applications is highly favorable to improve the production rate and reduce the number of post-production machining steps necessary before the part is ready. Laser-engineered net shaping (LENS) is a directed energy deposition (DED) technique in which the powder is deposited, and a laser beam is used to melt and fuse it to the substrate. This latter technique is very versatile and can be used to produce large complex shapes and is also capable of in-situ alloying.
In this work, we aimed to study the influence of printing parameters in the DED process, namely laser power and scan speed, on the corrosion and tribological behavior of stainless steel 316L. The localized corrosion behavior, as well as tribological characteristics, were studied in a phosphate-buffered saline (PBS) solution to identify possible mechanisms of local attack and to study their potential use in orthopedic implants based on corrosion properties.

Experimental procedure

Printing parameters

The DED stainless steel 316L samples were manufactured using an Optomec MRS printer with a powder feed rate of 5 rpm, and the scan orientation was ± 45° with a combination of two laser powers – 200W, 300 W, and two scan speeds – 10 and 15 in/min. The samples printed were cubes of 1x1x1 cm^3 and were removed from the substrate using an electric discharge machine (EDM). The edges and top of the samples were either ground or sliced off to reveal a smooth surface for performing the experiments.

Electrochemical experiments

For the corrosion and tribology tests, samples were mounted in a cold setting epoxy resin with wires attached via copper tape to connect the working electrodes. A three-electrode set-up was used; an Ag/AgCl reference electrode (with saturated KCl solution), and a platinum mesh counter electrode, with the sample tested being the working electrode. The samples were polished up to 1200 grit for testing, and the samples were polished extensively after each test. The samples were immersed for an hour in the solution, during which the open circuit potential (OCP) was monitored. Once the potential stabilized, electrochemical impedance spectroscopy (EIS) was performed from 100, 000 Hz to 0.01 Hz with an AC amplitude of 10 mV and 10 points/decade. After the EIS test, cyclic polarization (CP) was performed from -150 mV (vs. OCP) up to 1.5V (vs. OCP) with the reverse scan back to -150 mV (vs. OCP) at a scan rate of 1 mV/s. The test electrolyte used was the PBS solution (pH~7.4) within a comparable composition to synovial fluid and blood serum [1]. All tests were performed on the samples twice to verify the repeatability of the results obtained.

Tribocorrosion experiments

The tribological tests used an adapted pin-on-disc tribometer (Tribotechnic, France) to reproduce alternative motion. A tribocorrosion cell was integrated with a potentiostat/galvanostat Solartron 1287 (Ametek, USA) to record corrosion measurement during the friction test, and using the three-electrode configuration: 316LSS as working electrode (WE), an Ag/AgCl/KClsat as reference electrode (RE) and a platinum mesh electrode (CE)—the surface roughness of 316LSS sample before friction was elevated for each sample. The arithmetic surface roughness was around 0.3 ±0.1. The point contact configuration uses an alumina ball of 6 mm diameter as ca counterpart against the 316L samples as the plane. The tests were carried out at normal loads of 1 N. The sliding distance was 20 m for a sliding speed of 12 mm/s.

During the friction test, the open circuit potential (OCP) was run firstly for 300 s; then, the potential scan was applied (vs. OCP) with a scanning rate of 0.5 mV/s until the end of the test. Based on the CP results, three potentials were selected to evaluate the behavior in the cathodic, passive, and pitting regions. Further details will be provided in the results session.

Surface characterization

The samples were polished up to 1200 grit and fine polished using a 9 μm, 3 μm and 1 μm diamond suspension solution. After final polishing in 0.05 μm SiO_2 suspension, they were etched in aqua regia (3:1 HCl: HNO_3). Microstructural characterization was performed using a

JEOL JCM-6000Plus scanning electron microscope (SEM). Post electrochemical testing, the samples were cleaned and viewed under the SEM to characterize the pits formed. Hardness tests were performed in polished samples using Zwick/Roell Z2.5 hardness machine. The hardness average is estimated from at least five measurements at a load of 1kg/f. A digital microscope (Keyence VHX-7000N) characterized qualitative and quantitative worn surfaces.

Results and discussions

Microstructural characterization

The etched surfaces of the samples tested are shown in Figure 1.

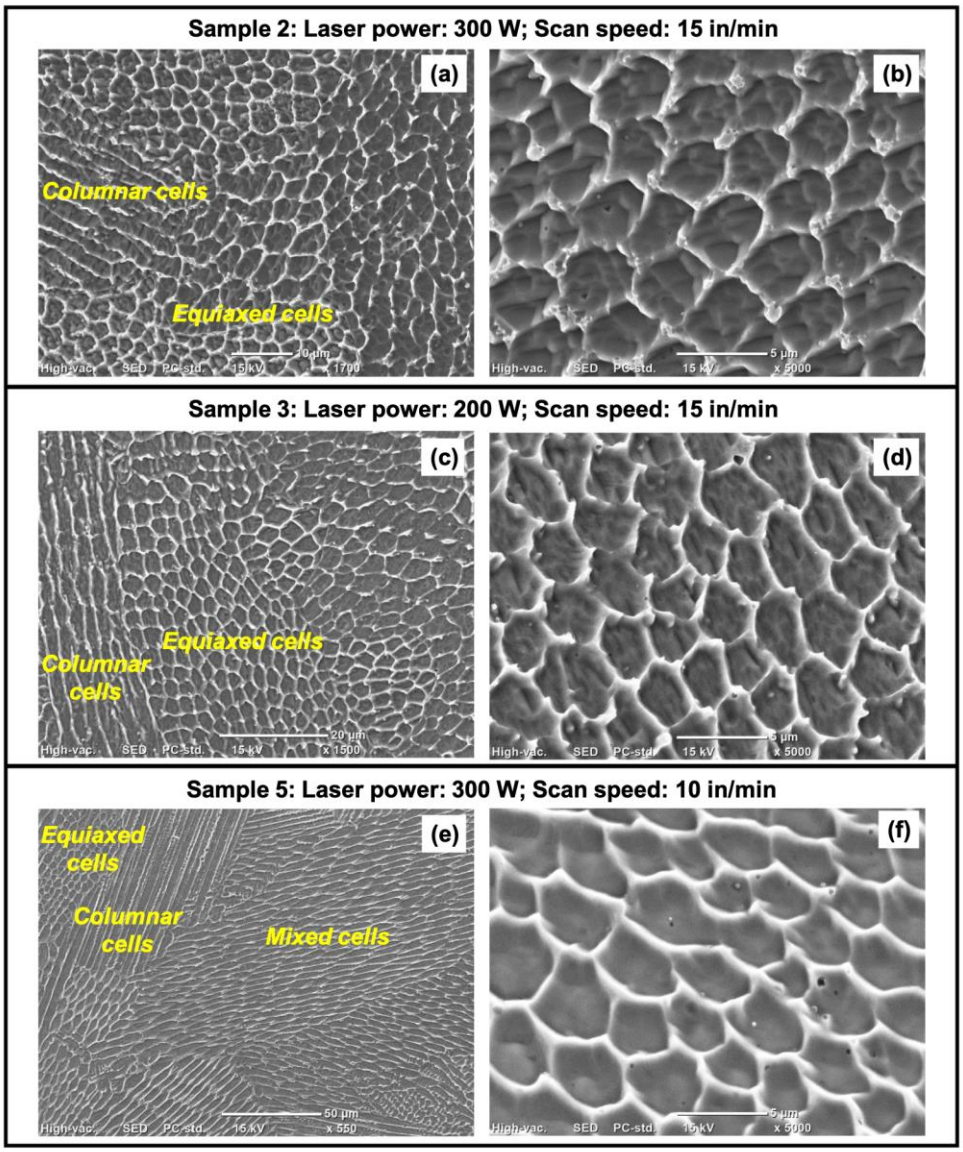

Figure 1. SEM images of (a, b) Sample 2, (c, d) Sample 3 and (e, f) Sample 5 showing the various cell structures formed upon additive manufacturing.

The samples printed with lower laser power showed more surface roughness in the edges due to a lower power density than the higher laser power (300W) samples which had a higher density to melt and fuse metal powders more efficiently. All the samples were relatively defect-free, as determined qualitatively from microstructural observations. Still, detailed studies will have to be performed to quantify any porosity that might be present in the bulk. In samples 3

and 4 (printed with 200 W laser power), some micro-porosities were observed near the edges, which were polished off before testing.
The microstructural features observed on all samples were the typical cellular structures developed upon additive manufacturing. Equiaxed, columnar, and mixed cell morphologies were observed with the cell sizes ranging from 2-5 μm. Using EDS, it was confirmed that the cell boundaries were enriched in Cr, Mo, and Ni while the cell interiors had a higher Fe content.

Cyclic polarization (CP) and electrochemical impedance spectroscopy (EIS) results

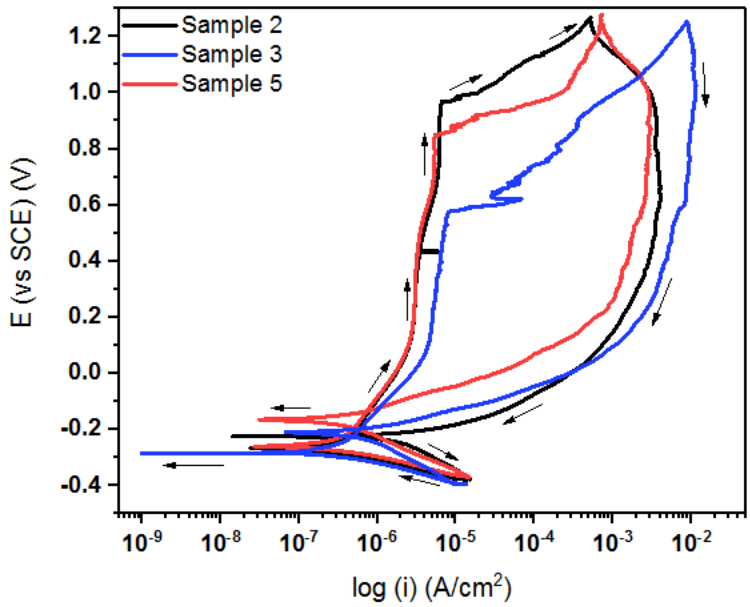

Figure 2. Cyclic polarization (CP) results of the samples tested in PBS solution.

Figure 2 shows the cyclic polarization (CP) results of samples 2, 3, and 5 obtained after immersion in PBS solution. The corrosion potential (E_{corr}) was around -300 mV (vs. SCE reference) for all the samples. They show a wide passive range, with the pitting/ breakdown potentials being around 800 mV and 900 mV (vs SCE) for samples 5 and 2, respectively. Sample 3 showed a significantly lower breakdown potential at about 500 mV (vs. SCE) as well as a higher passive current density (i_{pass}). The repassivation potential for sample 2 and 3 was found to be slightly more negative than that of sample 5, which is indicative that the extent of pitting corrosion was greater in sample 2 despite its higher breakdown potential. Therefore, the samples manufactured using a higher laser power showed a higher resistance to pitting corrosion than Sample 3, which was manufactured using 200 W (lower laser power).

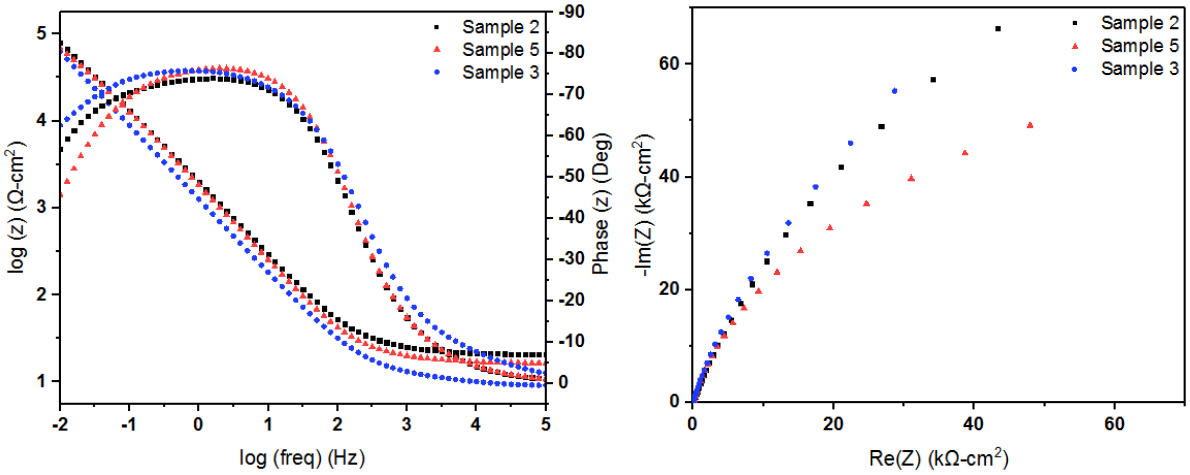

Figure 3. Bode and Nyquist plots of the samples immersed in PBS solution for 1 hour.

The maximum phase angle values from the Bode plots were close to -80° at mid to low frequencies (10^2-10^{-1} Hz) for both the samples. Near the lowest frequencies, the phase angles dropped to slightly lower values which can be indicative of charge transfer processes occurring at the sample/ solution interface. This is further corroborated by the semicircular arcs observed in the Nyquist plot. Sample 2 and 3 had a larger radius of semicircular arc which indicates that the extent of charge transfer occurring at the interface was lower which implies that the films formed were more protective than that of sample 5.

SEM results after cyclic polarization

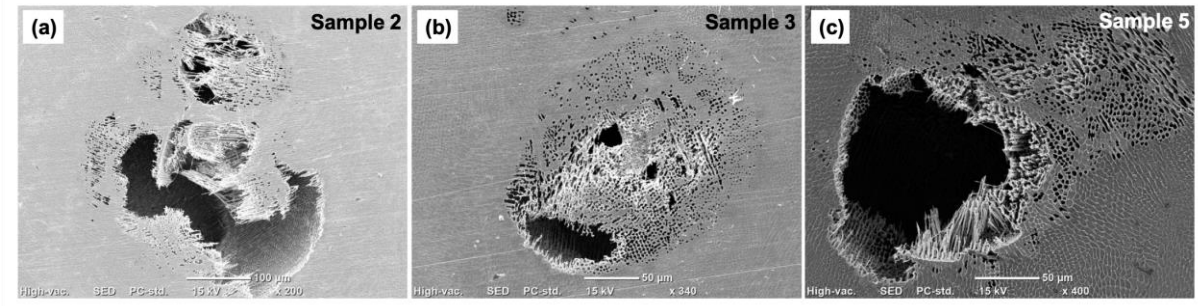

Figure 4. SEM images of samples (a) 2, (b) 3 and (c) 5 after cyclic polarization.

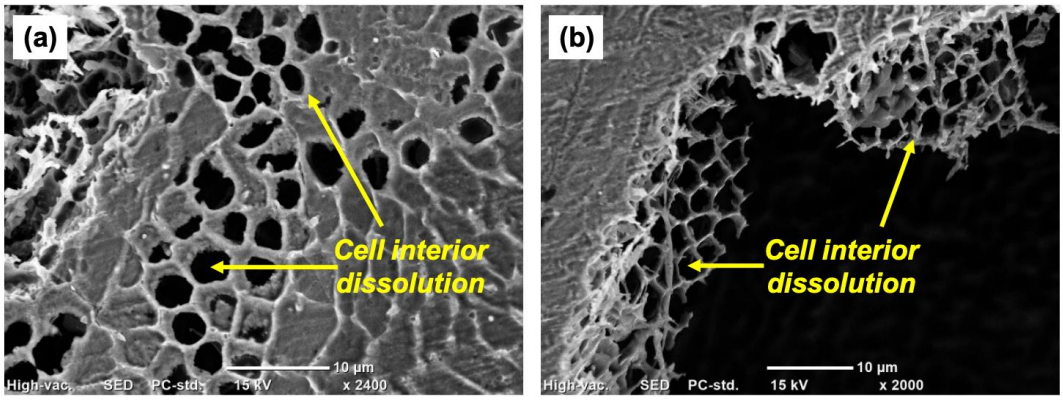

Figure 5. Enlarged images at regions surrounding the pits showing evidence of cell interior dissolution.

The samples were cleaned after the cyclic polarization tests and etched in aqua regia to reveal any microstructural features present around the pits formed. The SEM images of the pits formed in samples 2, 3, and 5 are shown in Figure 4. The pit sizes on all the samples ranged from 20 – 250 µm. As can be observed from the regions surrounding the pits and around the pit interiors (enlarged images in Figure 5), the preferred regions of attack were the cell interiors. It can be observed that the cell interiors had selectively dissolved, leaving behind the cell boundaries.
This has been reported in other works on additively manufactured stainless steel samples as well [2,3].
The micro-segregation of Cr and Mo to the cell boundaries possibly made them more cathodic/ passive compared to the cell interiors, which contained lesser amounts of these passivating elements. Revilla et al. [4] used scanning Kelvin probe force microscopy to map the Volta potential across DED samples and found that the cell boundaries were at a more positive potential than the cell interiors, which could further support this theory. Therefore, it is possible that micro-galvanic cells are developed with the cell interiors serving as anodes and getting selectively attacked.

Evolution of friction coefficient & current

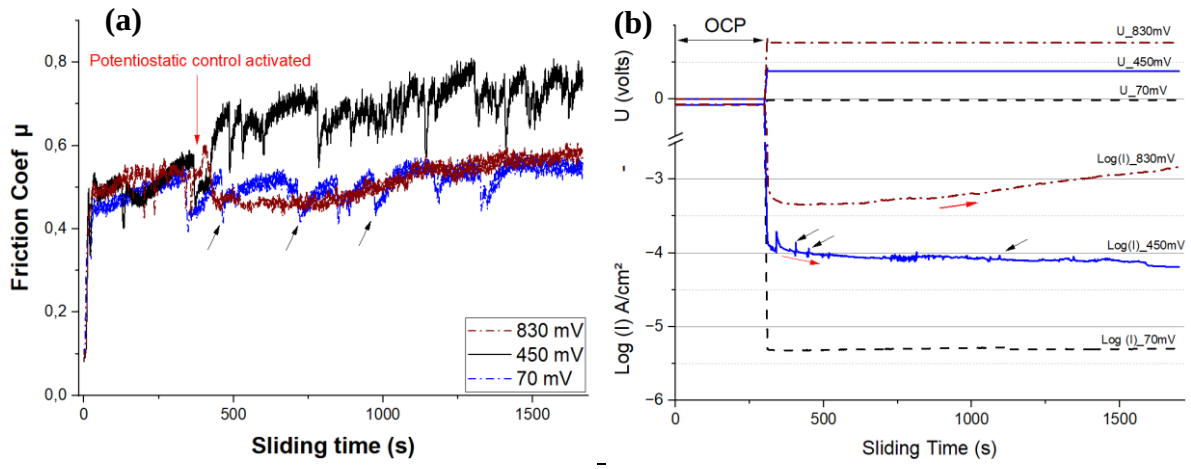

Figure 6. Friction coefficient and corrosion current evolution under potentiostatic control in PBS solution for DED-2 sample.

Figure 6 compares friction coefficients measured during DED-2 friction testing under potentiostatic control at three potentials: 70 mV (OCP) for the cathodic region, +450 mV for the passivation region, and +830 mV for the general pitting region. The friction evolutions are comparable in the first 400s. This suggests that surfaces behave alike during the OCP period. Figure b shows the potential variation and the current in concurrence with rubbing.

Once the potentiostatic is activated, Figure 6 (a) reveals that the friction under passivation potential 450mV is immediately affected, and the friction increases. Meanwhile, for the two other potentials, friction remains almost steady. Although the average is the same, friction evolves dissimilarly; at low potential (70mV), irregular evolution showing a successive decrease/increase (see black arrows in Figure 6 (a)) until the end of the test. For the high potential, above the pitting potential, friction promptly decreases under the potentiostatic control leading to a smooth evolution for 10 min before it rises progressively.

Simultaneously to the friction, in Figure 6 (b), currents drop instantly when the potential is stabilized at the applied value. This is widely attributed to the passivation of the 316LSS

specimens during sliding [5]. The measured currents for both low potentials, 70 mV and 450 mV continue to dimmish. Unusually, the current at passivation potential depicts several pics likely attributed to the metastable pitting [6]. For high potential, at the pitting region, the current increases continuously until the end of the friction test, indicating the general corrosion of the sample. This is in agreement with the literature[6–8].

Friction behaviour and currents evolution recorded with DED-3 samples are reported in Figure 7. It exhibits comparable results to the DED-2; irregular friction evolution at the lowest potential, highest friction occurs at the passivation potential, and at pitting potential, the friction seems to be the smoothest. At low 70 /75mV potentials, the maintained tension is cathodic, indicating the absence of corrosion; then, it is expected that the material loss in the electrolyte is essentially related to the mechanical action. The irregular behaviour might be attributed to the competition between a mechanical-driven passivation of the surface and the destruction of the film [5]. At passivation potential, the passive film is almost instantly formed, which requires a higher tangential load to remove it; further, the successive destruction of the film generated debris that leads to an abrasive and high friction average. At the high pitting potential, the sample is already subjected to a general corrosion, then at the sliding interface, it seems to have the homogenous chemical composition of oxides leading to low friction, again, the increase of friction indicates the development of the abrasive wear due to debris generation.

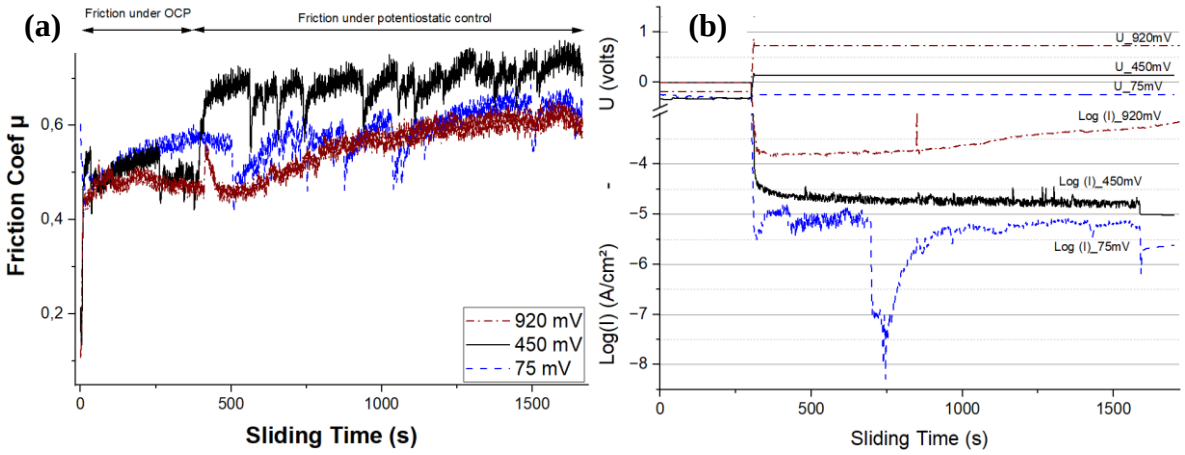

Figure 7. Friction coefficient and corrosion current evolution under potentiostatic control in PBS solution for DED-3 sample.

Recently, Yue et al. showed that the passive film at OCP conditions is formed with a higher proportion of Cr_2O_3 but under potentiostatic control in PBS solution, the passive film would form mainly by hydroxide[9]. This suggested that the tribo-film may change nature at each potential affecting the friction.

Degradation mechanisms

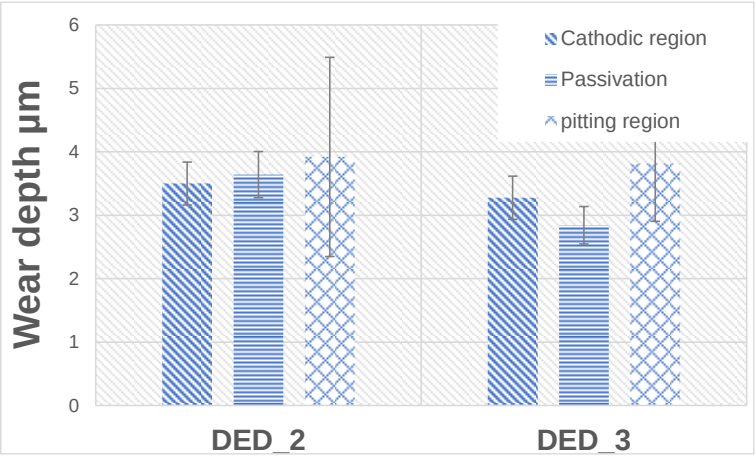

Figure 8. Comparison of wear depth of DED-316L stainless steel samples at the end of tribocorrosion in PBS solution and under different potentials.

The evaluated worn depths at the end of tribocorrosion tests are summarized in Figure 8. In general, the DED-2 is more damaged than the DED-3 at all applied potentials. This is an expected result for mechanical wear; the harder material is supposed to resist sliding wear as suggested by Archard law. Then, it is worth reminding that the sample with higher laser power and scan speed, DED-2, induced harder material with 209±18 Hv_{10} versus 166±13 Hv_{10} for sample DED-3 (200W- 15 in/mm). Additionally, sample DED-2 manifests a proportional increase with the applied potential. This suggests that the dissolution of the metal by the anodic potentials contributes to the acceleration of wear as proposed by the synergic effects of chemical and mechanical wear [5,7,10].

Figure 9 (a, b, c) present optical microscopy images of DED-2 worn surfaces at different potentials. It appears in Figure 9 (a, b) that the wear track is populated with many parallel scratching marks indicating the occurrence of the abrasive mechanism. At the passivation potential, the wear track appears slightly darker, and several small pits seem to be filled in the inter-grooves areas. This is likely attributed to metastable pitting inside the sliding zone below the pitting potential. This was previously reported with the standard manufactured 316LSS in NaCl solutions [7,8]. This agrees with current results presented previously as current pics detects the premature pitting in PBS solution.

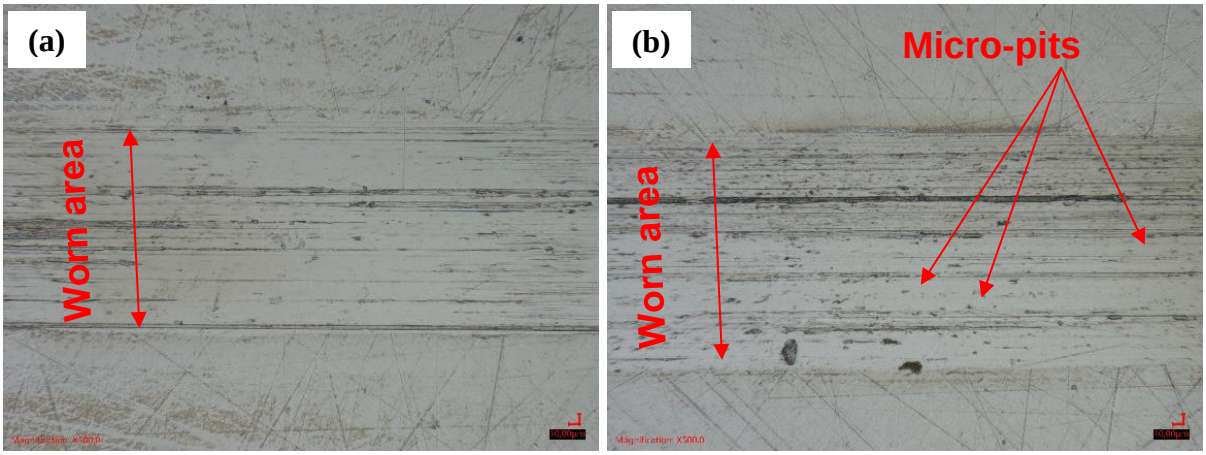

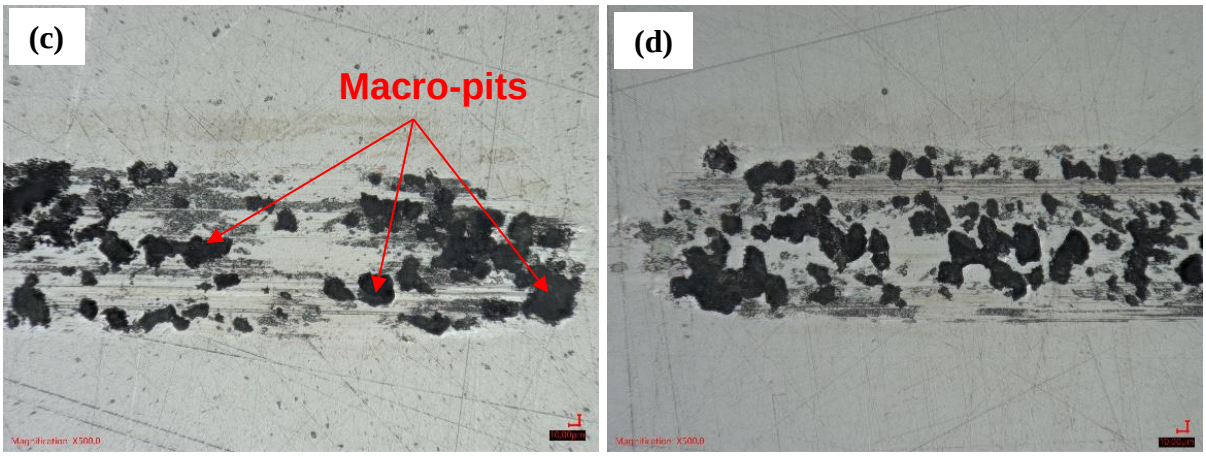

Figure 9. Wear tracks after tribocorrosion tests at different photostatic of DED-2 (a-70mV, b-450mV, c-820mV), d: wear track of DED-3 at pitting potential.

At pitting potential, worn area contains macro-pits appearing in black in Figure 9 (c). The occurrence pitting corrosion pretends the formation of collapsed pits that the size reaches the hundreds of microns [6]. From Figure 9 (d), it can also be seen that the wear track of DED-3 produced a similar degradation mechanism. Regarding wear depth results in the figure, DED-3 shows the lowest degradation at passivation potential when the maximum is obtained for the pitting potential—no synergic effect with the anodic potentials. The satisfactory wear resistance at passivation potential may be explained by generating a relatively soft third body that would not sharply scuff the surface, resulting in a better adhesion of the third body in the rubbing area. Further investigation would be accomplished in the future to characterize the tribo-film and to explain the difference in wear behaviour.

Conclusions

In this work, the corrosion and tribocorrosion behaviours of three additively manufactured 316L SS samples were investigated in PBS solution.
The main conclusions are:
- From the cyclic polarization (CP) results, Sample 2 and 5 (the 300 W samples) showed a lower passive current density and higher breakdown potential in comparison to sample 3 (manufactured using 200 W). Therefore, the pitting corrosion resistance is higher in higher laser power samples.
- Pits after CP tests showed a preferential dissolution of cell interiors in comparison to the cell boundaries due to the depletion of passivating elements (Cr, Mo), which made them more anodic.
-Friction evolution of DED- samples was affected by the applied potential; at the cathodic region, passivation or pitting region.
-The highest friction is obtained at passivation potentiostatic control. The currents assessment detected the presence of pics attributed to the initiation of metastable pits observed by optical microscopy.
- At pitting potential, macros-pitting was observed exclusively in the rubbing area explained by the coalescence of micro-pits and the general corrosion of samples. The currents assessment showed a progressive increase.

Acknowledgments

The authors would like to acknowledge the funding by the National Institute of Standards and Technology; **Federal Award Number: 70NANB21H041**

References

1. S. Karimi, T. Nickchi, A. Alfantazi, Effects of bovine serum albumin on the corrosion behaviour of AISI 316L, Co-28Cr-6Mo, and Ti-6Al-4V alloys in phosphate buffered saline solutions, Corros Sci. 53 (2011) 3262–3272. https://doi.org/10.1016/j.corsci.2011.06.009.
2. D. Narayanan, L. Chen, B. Mansoor, H. Castaneda, A new insight into pitting initiation in selective laser melted 316L stainless steel, Mater Lett. 333 (2023) 133562. https://doi.org/10.1016/J.MATLET.2022.133562.
3. R.I. Revilla, I. De Graeve, Microstructural Features, Defects, and Corrosion Behaviour of 316L Stainless Steel Clads Deposited on Wrought Material by Powder- and Laser-Based Direct Energy Deposition with Relevance to Repair Applications, Materials. 15 (2022). https://doi.org/10.3390/ma15207181.
4. R.I. Revilla, M. Van Calster, M. Raes, G. Arroud, F. Andreatta, L. Pyl, P. Guillaume, I. De Graeve, Microstructure and corrosion behavior of 316L stainless steel prepared using different additive manufacturing methods: A comparative study bringing insights into the impact of microstructure on their passivity, Corros Sci. 176 (2020). https://doi.org/10.1016/j.corsci.2020.108914.
5. Y. Wu, Z. Wang, J. Chen, Y. Ma, Y. Yan, L. Qiao, Effect of frictional frequency on the subsurface evolution of 316L stainless steel in tribocorrosion and its influence on the synergistic effect between corrosion and wear, Tribol Int. 178 (2023) 108026. https://doi.org/10.1016/j.triboint.2022.108026.
6. J. Zou, Z. Wang, Y. Ma, Y. Yan, L. Qiao, Role of gradient nano-structured surface in collapsed pitting corrosion on AISI 316L stainless steel during tribocorrosion, Corros Sci. 197 (2022) 110043. https://doi.org/10.1016/j.corsci.2021.110043.
7. Y. Sun, V. Rana, Tribocorrosion behaviour of AISI 304 stainless steel in 0.5 M NaCl solution, Mater Chem Phys. 129 (2011) 138–147. https://doi.org/10.1016/j.matchemphys.2011.03.063.
8. Y. Sun, R. Bailey, Improvement in tribocorrosion behavior of 304 stainless steel by surface mechanical attrition treatment, Surf Coat Technol. 253 (2014) 284–291. https://doi.org/10.1016/j.surfcoat.2014.05.057.
9. X. Yue, L. Zhang, Y. Hua, J. Wang, N. Dong, X. Li, S. Xu, A. Neville, Revealing the superior corrosion protection of the passive film on selective laser melted 316L SS in a phosphate-buffered saline solution, Appl Surf Sci. 529 (2020) 147170. https://doi.org/10.1016/j.apsusc.2020.147170.
10. P. Ren, H. Meng, Q. Xia, Z. Zhu, M. He, Tribocorrosion of 316L stainless steel by in-situ electrochemical methods under deep-sea high hydrostatic pressure environment, Corros Sci. 202 (2022) 110315. https://doi.org/10.1016/j.corsci.2022.110315.